Thiagarajar College of Engineering

68 YEARS 1957-2025 Celebrating Academic Excellence

where quality and ethics matter

Proceedings of the First National Research Conclave on Sustainability

Advancing towards a Resilient Future - 2025

Editor: Dr. L. Ashok Kumar

Published by:

Thiagarajar Publications

Proceedings of the First National Research Conclave on Sustainability
Advancing towards a Resilient Future - 2025
Published by
Thiagarajar Publications,
Thiagarajar College of Engineering (TCE), Madurai.
ISBN: 978-93-342-3695-8

978-93-342-3695-8

Proceedings of the

First National Research Conclave on Sustainability: Advancing towards a Resilient Future - 2025

May 16-17, 2025

Editor

Dr. L. Ashok Kumar

Co-Editors

Dr. K. Hariharan **Dr. S. Charles Raja**

Dr. B. Ashok Kumar **Ms. M. Aruna**

Organized by

Thiagarajar College of Engineering

(A Govt. Aided Autonomous Institution affiliated to Anna University)

Madurai 625015, Tamilnadu, India

www.tce.edu

INSTITUTION'S INNOVATION COUNCIL (Ministry of Education Initiative)

5S ABK-AOTS DOSOKAI PLATINUM Awardee

NBA NATIONAL BOARD of ACCREDITATION CIVIL, MECH, EEE, ECE, CSE IT & MECHATRONICS

nirf

ACCREDITED WITH GRADE A++ 3.56/4.00 NAAC

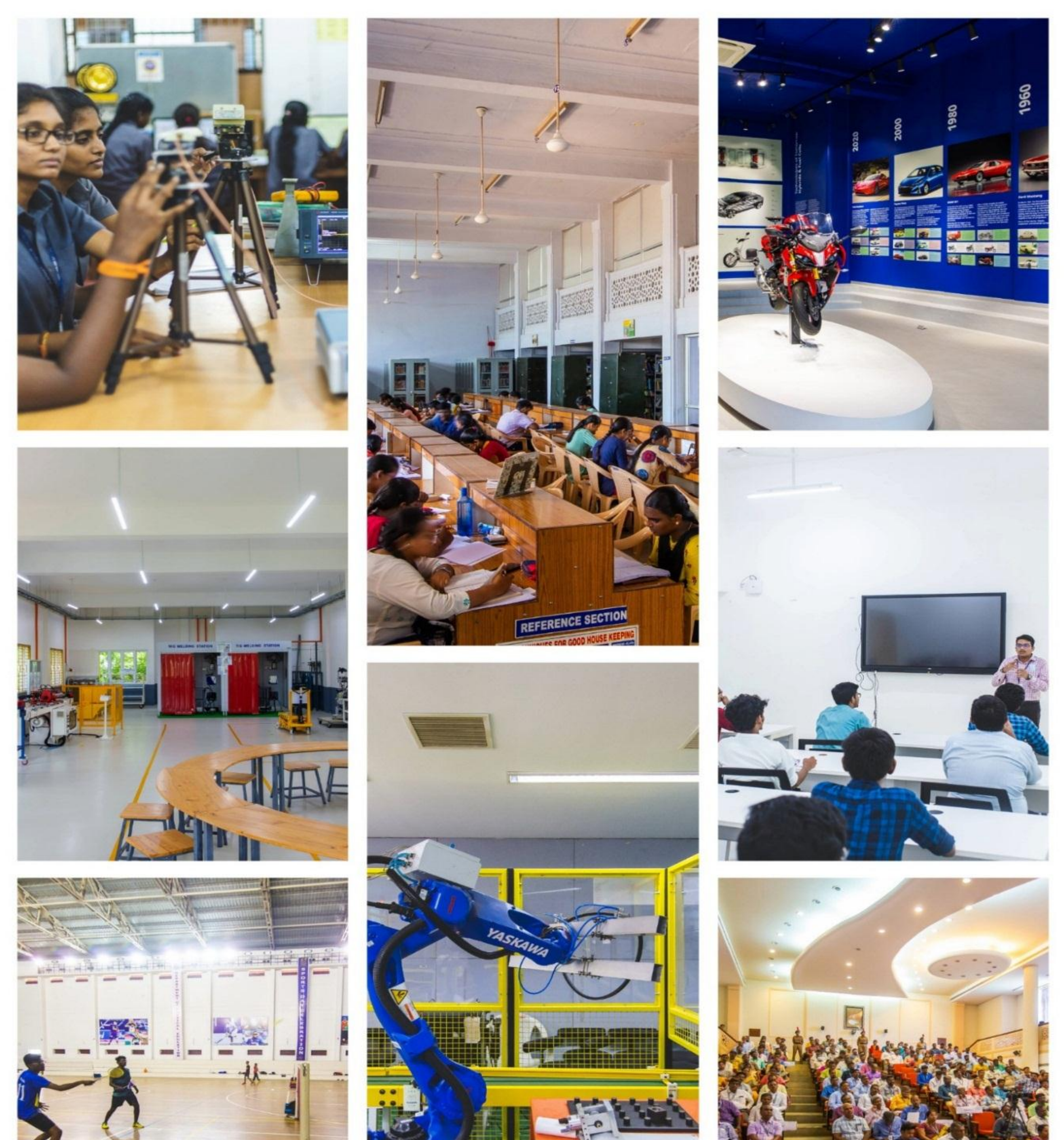

THIAGARAJAR COLLEGE OF ENGINEERING

Thiagarajar College of Engineering (TCE), established in 1957 by the philanthropist Karumuttu Thiagarajan Chettiar, is a Government Aided Autonomous Institution affiliated to Anna University, Chennai, and approved by AICTE. TCE offers 11 Undergraduate, 7 Postgraduate, and Ph.D. programs in Engineering. Architecture and Science. Nestled in a serene, eco-friendly campus, TCE is renowned for its top-tier infrastructure and commitment to academic excellence. TCE has embraced reforms in its teaching-learning process, including a Competency-Based Curriculum, Outcome-Based Education, and the CDIO framework since 2018, emphasizing hands-on training. Industry collaborations with global leaders, such as TVS Motors, have enhanced curriculum design and established cutting-edge labs like the T S Srinivasan Centre for Automotive Research.

Milestones of Excellence at Thiagarajar College of Engineering (TCE)

- **NAAC Cycle-II Accreditation**: Earned the highest A++ grade with an impressive score of 3.56/4.00.
- **NIRF 2024 Rankings**:
    - Engineering Category: Placed in the elite 101–150 rank band.
    - Architecture Category: Secured a remarkable 25th rank.
- **Innovation & Research**:
    - Ranked 4th in ARIIA and honored with the CII Best Innovation Award 2021.
    - Established Thiagarajar Advanced Research Centre (TARC) and TSS Centre for Automotive Research (TSSCAR) – hub of cutting-edge academic and sponsored researches.
- **Placements**: Sustaining 90%+ placement consistently over the last 10 years.
- **Digital Learning**: Pioneered Massive Open Online Courses (MOOCs) in 2021.
- **Curriculum Innovation**: Adopted the globally recognized CDIO (Conceive – Design – Implement – Operate) framework in undergraduate programs since 2018.
- **Research Support**: Introduced the Thiagarajar Research Fellowship (TRF) to empower Ph.D. scholars?(year).
- **Times Higher Education Rankings 2025**:
    - Engineering: Ranked in the 1251+ band
    - World University: Featured in the 1501+ band
    - Interdisciplinary Science: Ranked 601+ globally
    - SDG 5 – Gender Equality: Recognized in the Impact Rankings 2024
    - Recognized as a Well-Performing Institution under TEQIP-II by MHRD, Government of India.
- **Industry Linkages**: Six departments received the AICTE-CII Best Industry Linkage Award.
- Honored as the Best Education Brand 2024 by ET Now – Times Group.
- Achieved Platinum Ranking in 5S Recognition 2024.
- Rated AAAA+ by Careers 360 in 2024.
- Received the Special Recognition Award for Excellence in Engineering Education by the Institute of Engineers, India.
- Padma Shri Award conferred to Dr. R. Vasudevan for outstanding contributions to Science and Engineering by the Government of India.

First National Research Conclave 2025 on Sustainability: Advancing towards a Resilient Future: Scope

The National-Level Research Conclave 2025 is hosted by Thiagarajar College of Engineering (TCE), Madurai on May 16–17, 2025, with the central theme *"Sustainability: Advancing towards a Resilient Future."* The conclave serves as a confluence of scholars, innovators, and thought leaders dedicated to developing sustainable solutions addressing environmental, technological, and societal challenges.

Thematic Tracks of the Conclave

The conclave serves as a platform for sharing of original research and review articles in the following broad areas:

- Energy and Environmental Sustainability
- Smart and Sustainable Infrastructure
- Digital Sustainability and Transformation
- Advanced Materials and Manufacturing
- Smart and Intelligent Vehicles
- Artificial Intelligence / Machine Learning
- Climate and Remote Sensing
- Data and Computational Techniques
- Agriculture and Healthcare
- Networking, IoT, and Embedded Systems

Key Highlights

- Keynote Addresses: Delivered by distinguished experts from global organizations including Amazon, KPMG, DRDO, Titan, CSIR-SERC, and others, offering insights into innovation and sustainability.
- Panel Discussions: Multidisciplinary panels address current challenges in climate adaptation, green tech, ethical development, and community resilience.
- Research Presentations: Faculty, research scholars, and students from across the country present papers aligned with the conclave's theme.

Paper Submission & Review

The conclave has received around 209 papers, each has undergone double-blind peer review by a minimum of two reviewers. The entire review process is managed via the Microsoft CMT platform, ensuring a standardized and transparent evaluation process.

Publications and Awards

- 41 best papers of the conclave are selected for publication in Springer Book Series – Sustainable Economy and Eco technology (SEE).
- 15 other best papers of the conclave are selected for publication in TCE Journal.
- Extended versions of the selected papers are under review for publication in ICTACT Journal.
- Outstanding papers are awarded as Best Paper Awards, for a total prize pool of ₹50,000.

First National Research Conclave 2025 on Sustainability: Advancing towards a Resilient Future

MESSAGE FROM THE CHAIRMAN

Greetings!

It gives me great satisfaction to see Thiagarajar College of Engineering (TCE) organizing the First National Research Conclave 2025 on the theme *"Sustainability: Advancing towards a Resilient Future."* This initiative reflects TCE's long-standing commitment to nurturing research that is both academically rigorous and socially relevant.

In today's world, sustainability has become a cornerstone of responsible progress. Whether it concerns climate change, energy efficiency, resource conservation, or inclusive development, sustainability demands fresh perspectives and integrative solutions. What I find particularly commendable is the conclave's emphasis on multidisciplinary exploration. The inclusion of themes such as renewable energy, circular economy, smart cities, green technologies, and sustainable agriculture underscores the need for research that transcends disciplinary boundaries and promotes holistic problem-solving. This aligns well with the future of education—where disciplines converge to address real-world challenges. At TCE, we believe that institutions of higher learning bear a dual responsibility: to generate knowledge and to ensure its relevance to society. Through initiatives like this conclave, we reaffirm our commitment to fostering a learning environment where intellectual curiosity is matched by social consciousness.

I appreciate the tireless efforts of the organizing committee, who have worked with vision and enthusiasm to bring this event to life. I am confident that the Research Conclave 2025 will leave a lasting impact—by enabling rich academic exchange, encouraging cross-disciplinary collaborations, and inspiring sustainable solutions for the future. I wish all the participants a productive and intellectually rewarding experience.

Mr.K. Hari Thiagarajan
Chairman and Correspondent, TCE

First National Research Conclave 2025 on Sustainability: Advancing towards a Resilient Future

MESSAGE FROM THE PRINCIPAL

Greetings!

It is a moment of immense pride for Thiagarajar College of Engineering (TCE) to host the First National Research Conclave 2025 on the theme “Sustainability: Advancing towards a Resilient Future.” At a time when sustainability has become central to global development, TCE is honoured to serve as a platform for scholarly exchange, meaningful dialogue, and collaborative innovation.

The theme reflects a timely recognition that sustainability requires interdisciplinary approaches, inclusive participation, and transformative thinking. Aligned with India’s development agenda and the United Nations Sustainable Development Goals (SDGs), the conclave aspires to contribute meaningfully to global priorities in sustainability.

At TCE, we view this conclave as an extension of our commitment to combining academic excellence with societal responsibility. We believe research must go beyond theoretical exploration to serve as a tool for ethical innovation and real-world impact.

I take this opportunity to commend the organizing team, faculty coordinators, and student volunteers for their dedication and vision in bringing this event to life. I am confident that this conclave will ignite new ideas, foster lasting collaborations, and inspire research that advances sustainability and resilience across sectors.May this first Research Conclave serve as a meaningful milestone in our shared journey towards a more balanced and sustainable future

L. Ashok Kumar,
Principal, TCE

First National Research Conclave 2025 on Sustainability: Advancing towards a Resilient Future

ORGANIZING COMMITTEES

Chief Patron
Mr. K. Hari Thiagarajan
Chairman &Correspondent, TCE
Patron
Dr. L. Ashok Kumar
Principal, TCE
Organizing Secretaries
Dr. K. Hariharan, Dean III, Professor, ECE
Dr. S. Charles Raja, Associate Dean (R&D), Professor, EEE
Conclave Coordinators
Dr. B. Ashok Kumar, CLC (III), Associate Professor, EEE
Ms. M. Aruna, CLC (R&D), Assistant Professor, Civil

•

Programme Committee

Dr. N. B. Balamurugan (ECE)
Dr. G. Ananthi (ECE)
Dr. M. Sermaraj (MECH)
Dr. Ilankumaran (IT)
Dr. Ramalinga Chandrasekar (CHE)
Dr. M. Rajalakshmi (MECT)
Ms. R. Subhashini (CSBS)

Finance Committee

Dr. S. Arockia Edwin Xavier (EEE)
Mr. M. Sivakumar (Admin Office)
Dr. R. Sankaranarayanan (CIV)
Ms. Nisha Angelin (IT)
Mr. S. Rajkumar (MECT)
Dr. N. Ayyanar (ECE)
Ms. Thiruchadai Pandeeswari (IT)

Technical Committee

Dr. A. M. Abirami (IT)
Dr. M. S. K. Manikandan (ECE)
Dr. B. Shankar (CHE)
Dr. S. Julius Fusic (MECT)
Dr. M. Balamurali (MECH)
Dr. D. Kavitha (EEE)
Dr. R. Sanjay Kumar (CIV)
Dr. G. Sivasankar (EEE)

Publication Committee

Dr. K. Rajeswari (ECE)
Dr. L. Radha (LIB)
Dr. B. Sathyabama (ECE)
Dr. K. Vasudevan (ECE)
Dr. S. Sridevi (IT)
Ms. H. Srivinodhini (MAT)
Mr. M. M. Devarajan (MECT)
Ms. Priya Thiagarajan (CSBS)

Registration Committee

Dr. D. Anitha (AMCS)
Dr. M. Sarpparaje (ENG)
Dr. I. Chandramathy (ARCH)
Dr. D. Gracia Nirmala Rani (ECE)
Dr. M. Velayudham (CHE)
Dr. S. Suriyakala (MAT)
Mr. M. Karthic (MECH)
Mr. M. Gowtham Sethupathi (CSBS)
Dr. R. Sivanesan (AMCS)

First National Research Conclave 2025 on
Sustainability: Advancing towards a Resilient Future

ORGANIZING COMMITTEES

Funding / Sponsorship Committee

Dr. S. Karthikeyan (MECH)
Dr. P. Karthikeyan (IT)
Mr. T. Prakash (MECH)
Mr. B. Dinesh Kumar (CIV)
Dr. M. Suguna (IT)
Ar. A. Ayshwarya (ARCH)
Dr. M. Tamil Elakkiya (PHY)

Infrastructure Committee

Dr. S. Md. Mansoor Roomi (ECE)
Dr. L. Muthusubramanian (MAT)
Dr. H. Ramesh (MECT)
Dr. V. R. VenkataSubramani (MECH)
Dr. V. Ravi Sankar (CIV)
Dr. C. Vignesh (MECH)
Dr. P. Velusamy (PHY)
Mr. S. Parthasarathi (MECT)

Invitations, Banner & Certificate Preparation Committee

Mr. R. Vinothkumar (ARCH)
Ar. S. M. Vidhya Sankari (ARCH)
Ar. Vaishali (ARCH)
Dr. J. Shanthi (ECE)
Ar. P. Pavalavelsh (ARCH)
Dr. J. Dharani (CSE)
Mr. S. Santhana Hari (CSE)
Ar. S. Ragul (ARCH)

Website Team

Dr. K. Sundarakantham (CSE)
Dr. K. Narasima Mallikarjunan (CSE)
Dr. G. S. R. Emil Selvan (CSE)
Dr. J. Felicia Lilian (CSBS)
Mr. M. A. Ganesh (MECT)
Dr. A. J. Sunija (CHE)
Dr. G. Prabhakar (ECE)
Dr. B. Surya Devi (AMCS)

Refreshment & Lunch Committee

Dr. P. S. Manoharan (EEE)
Dr. S. Prasanna (CSE)
Dr. E. Murugavalli (ECE)
Dr. P. Victor (MAT)
Dr. M. S. Govardhanan (MECH)
Mr. S. A. R. Sheik Masthan (MECT)
Mr. C. Selvakumar (MECH)

Post-Conclave Material Preparation Committee

Dr. C. Jeyamala (IT)
Dr. B. Subbulakshmi (CSE)
Ms. S. Pudumalar (IT)
Ms. P. M. Devie (EEE)
Dr. M. Senthilarasi (ECE)
Mr. V. Janakiraman
Dr. M. Nirmala Devi (CSE)

Accommodation Committee

Dr. D. Rajkumar (CIV)
Mr. K. Saravana Kumar (Manager – Admin)
Dr. V. Vinoth Thyagarajan (ECE)
Dr. R. Kodipandyan (CHE)
Dr. M. P. Ramkumar (CSE)
Dr. R. Sivakumar (CHE)
Dr. K. Athiappan (CIV)

First National Research Conclave 2025 on
Sustainability: Advancing towards a Resilient Future

ORGANIZING COMMITTEES

Publicity / Press Committee

Dr. S. A. V. Elanchezian (ARCH)
Dr. R. K. C. Jeyakumar (CIV)
Dr. R. Maniarasu (MECH)
Dr. M. Jeeveraj (PHY)
Ar. S. Karthikeya Raja (ARCH)
Dr. C. Balasundar (EEE)

Function Arrangement Committee

Dr. G. Jeya Jeevakani (ENG)
Dr. R. Rajan Prakash (EEE)
Dr. M. L. Mahadevan (MECH)
Dr. Rajalavanya (CSE)
Mrs. A. Indrani (CSBS)
Dr. C. Mahadevi (AMCS)
Ms. S. Srimathi (AMCS)

Event Management Committee

Dr. A. Anitha (MAT)
Dr. T. Chandrakumar (AMCS)
Dr. V. Velkannan (CHE)
Dr. S. Sivailango (CHE)
Dr. R. S. Swarnalakshmi (ENG)
Dr. M. Meenakshi Devi (EEE)
Ms. J. Eunice (CIV)

Key Note Address -1

Human-Machine Synergy: Bridging Physical and Digital Realms for a Smart Future

Mr. Suresh Rajappa

Global Data Leader, Enterprise Systems, Digital Transformation & Data Strategy, KPMG, USA

The rapid advancements in Artificial Intelligence have demonstrated remarkable capabilities within the digital domain. However, the true potential of AI to address complex real-world challenges hinges on its seamless integration with the physical world through synergistic partnerships with humans. This keynote explores the critical concept of human-machine synergy, where the complementary strengths of human intuition, creativity, and adaptability are combined with the speed, precision, and data processing power of intelligent machines. By examining the current limitations of isolated digital AI and highlighting the transformative potential of embodied AI, the Internet of Things, digital twins, and intuitive human-computer interfaces, this presentation underscores the urgent need to bridge the physical-digital divide for a truly smart future.

Achieving this synergistic future necessitates addressing key challenges such as data integration and interoperability, ensuring trust and explainability in AI systems, and safeguarding security and privacy in interconnected environments. This presentation will delve into these hurdles while illuminating the significant opportunities that lie ahead, including enhanced productivity and efficiency across industries, improved healthcare and well-being, and the development of sustainable smart cities. Ultimately, this keynote calls upon the AI research community in India to prioritize interdisciplinary efforts that foster deep human-machine collaboration, paving the way for innovative solutions and a more human-centered intelligent future where the physical and digital realms converge harmoniously.

First National Research Conclave 2025 on Sustainability: Advancing towards a Resilient Future

Key Note Address -2

Smart, Safe, Sustainable: Designing Products that Last and Scale

Ms. Harshitha Phaniraj

Senior Manager,

Security Operations Center & Brand Monitoring, Titan Company, Integrity Office, Bangalore.

In a world rapidly shaped by digital innovation, creating technology that simply "works" is no longer enough. The true challenge lies in building systems that are smart in design, safe in practice, and sustainable in impact. This keynote explores how to engineer digital solutions that not only address today's needs but endure, evokes, live examples, and insights from leading digital transformation efforts, this talk offers students a fresh perspective on their role—not just as developers, but as architects of a resilient digital future.lve, and empower for years to come. Drawing from real-world experience in enterprise IT, AI automation, and cyber security, Harshitha shares key principles for building products that scale seamlessly, maintain user trust through privacy-first practices, and embed sustainability into their very architecture with relatable analogies

First National Research Conclave 2025 on
Sustainability: Advancing towards a Resilient Future

Key Note Address -3
Carbon Chain: An AI-Driven Carbon-Credit Marketplace with Dynamic Token Pricing

Mr. N. G. Karthikeyan
Co-founder & Chief Technology Officer (CTO) of TaxNodes, Bangalore

Every year, industries and governments struggle to limit their greenhouse-gas emissions. A carbon market helps by putting a price on those emissions: companies buy "carbon credits," each representing one ton of CO_2 not released into the atmosphere. If you pollute less, you can sell your extra credits; if you pollute more, you must buy them. This trading system creates a financial incentive to reduce emissions—but today's markets often suffer from slow settlements, opaque prices, and narrow participation.

Carbon Chain fixes these issues by combining:

Blockchain Tokens – Every credit is an on-chain token (ERC-20). Minting, trading, and retiring credits happen instantly and transparently, without middlemen.

AI-Powered Pricing Oracle – A lightweight machine-learning engine studies past credit issuance, trade volumes, energy-price trends, and policy events to forecast short-term supply and demand. These forecasts feed a network of secure "oracle" nodes that automatically adjust buy/sell price ranges in real time.

Key Benefits

- Clear, Real-Time Pricing: Token prices update to reflect actual market conditions.
- Instant Settlement: Smart contracts execute trades the moment they occur.
- Open Access: Project developers, traders, NGOs, or even individuals can join with minimal setup.

In this talk, you'll learn how Carbon Chain can make carbon trading faster, fairer, and more liquid—driving investment into new low-carbon projects and helping us move toward a resilient, sustainable future.

First National Research Conclave 2025 on Sustainability: Advancing towards a Resilient Future

Key Note Address -4
AI and ESG Compliance for Sustainable Growth

Dr. B. Somasundaram
Head - Digital Transformation, ELGI Equipments Limited, Coimbatore

As the world shifts toward responsible business practices, Environmental, Social, and Governance (ESG) compliance is no longer just a regulatory requirement—it's a strategic priority. Artificial Intelligence is emerging as a game-changer in this space, enabling organizations to embed sustainability into the core of their operations. AI enhances ESG compliance by automating data collection, improving reporting accuracy, and providing real-time insights across the value chain. It helps identify risks, flag anomalies, and predict future ESG trends by analyzing vast, complex data—from carbon emissions to supply chain ethics and boardroom diversity. More importantly, AI empowers leaders to make informed, forward-looking decisions that balance profitability with purpose. It transforms ESG from a checkbox exercise into a dynamic capability that drives innovation, builds trust with stakeholders, and fuels long-term growth. In this keynote, we'll explore how businesses can harness AI to move beyond compliance and lead with impact—turning sustainability into a competitive advantage in an increasingly transparent and accountable world.

Key Note Address -5
Futuristic Structures - Need, Imagineering and Challenges

Dr. N. Anadavalli,
Director, CSIR- Structural Engineering Research Centre, Chennai

Futuristic structures are necessary to address challenges like climate change, urbanization, and sustainability. We need advanced structural systems that go beyond the Conventional design because where innovation meets imagination is crucial for developing these structures. However, realizing futuristic designs faces challenges related to affordability, scalability, and the need for collaborative approach between various stake holders. Futuristic structures often incorporate smart technologies, renewable energy sources, and sustainable materials to minimize environmental impact. By exploring the concept of “Imagineering”—the fusion of imagination with engineering—such innovations can be brought into reality. These structures aim to respond dynamically to environmental and human needs, pushing the boundaries of design, form, and function. However, the path forward is complex. Emerging materials pose questions of long-term durability, regulatory frameworks struggle to keep pace, and economic feasibility often limits implementation. Additionally, a multidisciplinary approach is required to bridge gaps in knowledge, technology, and workforce skillsets. Technological advancements can lead to more efficient use of resources, reduced environmental impact, and increased resilience in the built environment. This presentation aims to provide an interdisciplinary perspective on the vision, feasibility, and limitations of futuristic structures, while inspiring young engineers to think boldly about the built environment of tomorrow.

First National Research Conclave 2025 on Sustainability: Advancing towards a Resilient Future

Key Note Address -6
Parallel/GPU Computing and HPC Research: Past, Present, and Future

Dr. M. Rajesh Pandian
Senior Engineer, Qualcomm, Chennai

Accelerating graph algorithms on GPUs has been steadily gaining momentum after the release of CUDA (2007). Ever since the landmark paper "Accelerating Large Graph Algorithms on the GPU Using CUDA", this area has seen significant progress. One approach to parallelization is to port efficient algorithms from the sequential world. However, some sequential algorithms are inherently easier to parallelize than others (e.g., Bellman-Ford vs. Dijkstra for shortest paths). Interestingly, designing algorithms from scratch has often led to more "efficient" GPU implementations. In this short talk, we will take a journey through time to explore the past, present, and future of HPC research through the lens of graph problems.

First National Research Conclave 2025 on Sustainability: Advancing towards a Resilient Future

Key Note Address -7
EMI Filter for Automobile and Biomedical Applications

Dr. Y. Uma Maheswari
Senior Associate, Cognizant Technology Solutions, Coimbatore.

Electronic circuits must address electromagnetic interference due to high-speed transmissions and simultaneous switching actions. The EBG structure can be deployed as one of the layer of printed circuit board for mitigating the electromagnetic noise. This acts as a filter. Usage of this band gap structure reduces the noise level up to 60 dB in the higher frequency range 0 – 25 GHz.

First National Research Conclave 2025 on Sustainability: Advancing towards a Resilient Future

Key Note Address -8
Battery Management System (BMS) In Electric Vehicles

Mr. P. Bhagavathy
Senior Engineer, Bosch Global Software Technologies, Coimbatore

Electric vehicles (EVs) typically comprise several key components: an electric motor, motor controller, traction battery, battery management system (BMS), wiring system, vehicle body, and chassis frame. Among these, the Battery Management System plays a critical role, particularly in systems utilizing lithium-ion batteries. Research in the field of electric mobility is heavily focused on improving BMS algorithms, integrating AI and machine learning for predictive diagnostics, enhancing fault detection, and enabling adaptive control strategies. Innovations in BMS design are central to improving battery reliability, extending vehicle range, and reducing total cost of ownership. As such, the BMS remains a focal point of EV-related, bridging the gap between advanced battery technologies and their practical, safe deployment in real-world applications.

First National Research Conclave 2025 on Sustainability: Advancing towards a Resilient Future

Key Note Address -9

Empowering Sustainable Manufacturing through Generative AI and Analytics

Dr. M.S. Sabitha
Head, Information systems
TVS Sensing Solutions Private Limited, Madurai

Sustainable manufacturing demands a data-driven approach to optimize resources and reduce environmental impact. This session presents a holistic framework that combines Generative AI, IoT, and Business Analytics to address key challenges in energy efficiency, process waste, and predictive maintenance. It also outlines a phased adoption roadmap and highlights how IT can serve as the backbone of sustainability-focused transformation in industrial environments

First National Research Conclave 2025 on Sustainability: Advancing towards a Resilient Future

Key Note Address -10

AI for all - Digital transformation and AI to make eye and healthcare accessible and affordable

Mr. Srinivasulu Thayam
Chief Technology Officer (CTO),
Aravind Eye Care System, Madurai

AI for All explores the application of Artificial Intelligence (AI) in advancing equitable healthcare delivery in India, particularly within the context of achieving a $1 trillion digital economy by 2028. Using Aravind Eye Care System as a case study, it demonstrates the integration of AI in ophthalmology to address preventable blindness due to diabetic retinopathy (DR). The implementation of AI-based diagnostic tools, combined with telemedicine and electronic medical records (EMRs), has enabled rapid, accurate, and large-scale screening, significantly reducing dependence on specialist availability and improving early detection rates. With over 295,000 patients screened using AI tools over a three-year period, the initiative showcases the scalability, affordability, and clinical impact of AI in resource-constrained settings. The Keynotes session also highlights the development of open-source digital health platforms and the concept of "smart hospitals" as part of a broader digital health transformation. This case illustrates the challenges and enablers of translating AI from development to deployment in real-world healthcare environments, offering insights into sustainable innovation in global health systems.

First National Research Conclave 2025 on Sustainability: Advancing towards a Resilient Future

Key Note Address -11
Leveraging Science and Technology for Global Sustainability: Amazon's Innovative Approach

Mr. K. Sridhar

Director, Retail Business services, Amazon., Chennai

Did you know that training just one large AI model can use as much energy as 1,400 trees can clean up in 10 years? Or that the technology sector's carbon footprint is larger than the entire aviation industry's? Every purchase you make as a consumer has a carbon story – from the warehouse to your doorstep. These are the kinds of challenges that keep business leaders up at night. Join Sridhar Kulasekharan from Amazon as he shares how Amazon is tackling these challenges head-on, using cutting-edge science and technology. He'll reveal how the technology that gets your packages to your doorstep is being reimagined to create a more sustainable shopping experience – from packaging to smart delivery routes that reduce emissions. You'll discover how cloud computing and artificial intelligence is being deployed at scale to predict and optimize energy usage, reduce waste, and make our operations greener by the day.

First National Research Conclave 2025 on Sustainability: Advancing towards a Resilient Future - Reviewers

1. A.M. Abirami
2. Ananthi Govindasamy
3. Angelin Lincy G
4. Anita N
5. Anitha D
6. Aravindan Vivekanandan
7. Arockia Xavier
8. Aruna M
9. Ashok Kumar B
10. Ayyanar Natesan
11. Balamurali M
12. Balasundar Ç
13. Bhavani G
14. C Jeyamala
15. Chandrakumar T
16. Charles Raja S
17. Devarajan MM
18. Devie P M
19. Dharani J
20. Dinesh Kumar B
21. Sunija A.J
22. Raj Kumar
23. S. Sridevi
24. Sivanesan Rajangam
25. Senthilkumar C
26. G Krishnaveni
27. Gowtham M
28. Gracia Nirmala Rani D
29. Hariharan K
30. Harine R
31. Indira Krishnan
32. Indirani A
33. Janakiraman Venkatesan
34. Jeevaraj Murugan
35. Jeseema Nisrin Jamal Mohamed
36. Jeykumar RKC
37. Jinu Kitchley
38. Julius Fusic S
39. Kamalakannan Ramalingam
40. Kanthamani Sundharajan
41. Karthickprabhu S
42. Karthikeyan P
43. Kavitha D
44. Kavitha Devi M K
45. Leena Sri
46. M Tamilelakkiya
47. M Vijayalakshmi
48. Madhupriya G
49. Mahadevi Chinnasamy
50. Maniarasu R
51. Manikandan M.S.K
52. Manoharan P S
53. Meena Kumari R
54. Meenakshi Devi M
55. Murugavalli E
56. Narasimhamallikarjunan Kambaraj
57. Nirmala Devi M
58. Nisha Angeline C V
59. Nithyakala G
60. Padmapriya S T
61. Padmavathi Sakkarai
62. Parkavi R
63. Parthasarathi S
64. Pethuraj Sankaranarayanan
65. Pgs Velmurugan
66. Premlatha KR
67. Priya Thiagarajan
68. Pudumalar S
69. Punitha V
70. R.A.Alagu Raja
71. Raja Lavanya
72. Rajalakshmi Murugesan
73. Rajeswari K
74. Ramalinga Sekar
75. Ramesh H
76. Ramkumar M P
77. Ravi Sankar V
78. S. Umar Sherif
79. S.Karthiga Shankar
80. Sanjay Kumar Rajguru
81. Sankaranarayanan Radhakrishnan
82. Santhana Hari S
83. Santhiya C
84. Saradha S
85. Sassirekha M S
86. Sathya Bama B
87. Selva Kumar C
88. Senthilarasi M
89. Shankar Bhaskaran
90. Shankar Chinnadurai
91. Shanthi J
92. Sharmila P
93. Siva T
94. Sivakumar Periyasamy
95. Sivakumar Radhakrishnan
96. Sivasankar. G
97. Suba Nachiar
98. Subbaiyan G
99. Subbulakshmi B
100. Subhashni R
101. Suganthi P
102. Suguna Mariappan
103. Sujitha S
104. Sumathi Sivasubramaniam
105. Sundara Kantham
106. Surya Devi Balakrishnan
107. Thiruchadai Pandeeswari S
108. Uma K V
109. Vasudevan Karuppiah
110. Velayudham Murugesan
111. Velkannan Veerapandian
112. Velusamy Periyasamy
113. Venkatasubramani. V. R
114. Venkatesh M
115. Venkatesh Paramasivam
116. Vennila Ganesan
117. Vignesh C
118. Vinoth Thyagarajan Thyagarajan
119. Yuvasini D

First National Research Conclave 2025 on Sustainability: Advancing towards a Resilient Future

Springer book series *Sustainable Economy and Eco technology (SEE)*, featuring the proposed title "*Innovative and Intelligent Computing for Global Sustainability*"

Out of the 209 submissions received for the National Level Research Conclave 2025, 41 best papers articles were selected for the Springer SEE series on "Innovative and Intelligent Computing for Global Sustainability." The selection includes 26 from TCE researchers, 5 from students, 8 from faculty, and 2 from industry. The selected works cover sustainable and intelligent computing in areas like renewable energy, net-zero buildings, agriculture, waste management, and healthcare, utilizing AI, ML, and deep learning.

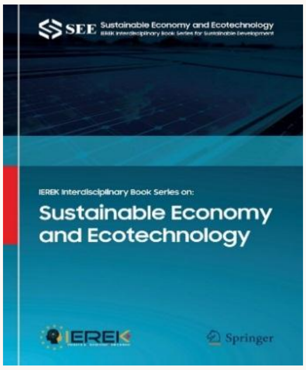

Electronic ISSN : 3005-1282
Print ISSN : 3005-1274
Series Editor : Mourad Amer
https://www.springer.com/series/17458

Editors

S. Sathees Kumaran, Anurag University,India
S.Sridevi,Thiagarajar College of Engineering,India
Yu-Dong Zhang, University of Leicester, United Kingdom
Valentina Emilia Balas,Aurel Vlaicu University of Arad, Romania
Tzung-Pei Hong, National University of Kaohsiung,Taiwan

The Sustainable Economy and Eco technology (SEE) book series, published by Springer in collaboration with IEREK, is part of the IEREK Interdisciplinary Series for Sustainable Development. It aims to connect technology, research, policy, and practice to support a sustainable future. The series features selected conference papers, monographs, textbooks, and edited volumes, covering topics such as sustainable business, the circular economy, digitalization, climate change economics, renewable energy, sustainable finance, and urban development. It also explores sustainability in marketing, agriculture, and mobility, emphasizing the link between economic growth and environmental responsibility.The proposal "Innovative and Intelligent Computing for Global Sustainability" is intended for Springer's Sustainable Economy and Eco technology (SEE) book series. It explores how advanced computing technologies can support sustainable development goals. Aligned with the SEE series, the proposal aims to:

- Foster interdisciplinary research linking computing with ecological and economic sustainability.
- Highlight the role of intelligent systems in achieving the UN Sustainable Development Goals(SDGs)
- Present practical solutions and frameworks for applying sustainable technologies across sectors.

First National Research Conclave 2025 on Sustainability: Advancing towards a Resilient Future

List of Articles selected for Spring Book Series on *Sustainable Economy and Eco technology (SEE)*, featuring the proposed title *“Innovative and Intelligent Computing for Global Sustainability*

S.No	Paper ID	Paper Title	Authors
1.	9	Evaluating 5g nr's role in enabling renewable energy solutions for smart cities	R, Priyadarshni; Manoharan, P S, N.Kumarasabapathy, M Bhavani
2.	25	Densenet-driven federated learning for enhanced fault detection in 3d bioprinting	V, Ramya; G, Ananthi; N, Vinothini, S. Levin Rohith
3.	36	Improvement of energy efficiency in sugar industry through reduction of electric power losses & voltage optimization using bf-pso	A, Ramalakshmi; S, Dr Arockia Edwin Xavier.
4.	43	Efficient net-vit hybrid model for flood prediction through wetland classification	M, Anitha; P, Chitra; G, Selva Jeba
5.	54	Influence of binders and alkali activator solutions on the residual properties of geopolymer mortars exposed to elevated temperatures	M, Sathyanarayanan; D, Brindha
6.	57	Rapid and precise diabetic retinopathy detection using oct features in retinal imaging	G R, Ezhil; S, Sridevi; S, Jaipreetha; S, Srijah
7.	67	Designing a cost-effective net zero energy building	Atturajan, Vishaalkaanth; Mohan, Aruna
8.	68	Detection of sleep disorder on electroencephalogram signal using neural network	R, Vasantharani; Dr. K. Rajeswari; Mrs. D. Ajitha
9.	69	Investigation into the thermal characteristics of ceiba pentandra briquettes with coffee husk and water hyacinth as supplements	K. Srithar, Dr; Venkatesan, R; R.Srinivasan, Dr; R.J. Vivekanadhan
10.	70	Design of a-t rasorber with high angular stability for x band applications	Mooda, Rajesh; B, Manimegalai
11.	71	Integrating artificial intelligence, machine learning, and blockchain technology for sustainable medical history retrieval and healthcare delivery	Ananth, S Jayashree; Ananth, Dr. Ajay

12.	75	Urban sprawl: methods and approaches in urban planning	Kavdarsini S; Madhivadhani.K; Sudharsanamurthy.P
13.	77	Estimation of rooftop rainwater harvesting for an educational institution – a water conservation strategy	B, Johnson; T, Chandrakumar
14.	85	Estimation of rooftop rainwater harvesting for an educational institution	P, Satheesh; S, Chandran; P, Diwahar
15.	89	Impact of texture feature extraction methods on machine learning based agricultural crop classification from sentinel-1 sar data	M. Anandbabu, T.S. Yogesh, B. Karthikeyan, Dr. R.A. Alagu Raja, Dr. V. Kumar
16.	90	AI-driven frameworks for early and non-invasive anemia detection	D, Thangamari; S, Padmavathi
17.	91	Cloud-based secure data transfer using convolutional neural network (cnn) enhanced dna cryptography	M, Geetharani; S, Muthuramalingam
18.	93	Estimation of soil moisture using cross polarized ratio indices from sentinel-1 sar data	B, Keerthivasan; M, Ashok Varthan; M, Vishwanatha; R A, Dr. Alagu Raja; U, Dr. Surendran; V, Dr. Kumar
19.	101	Electromagnetic ga-based miniaturized circular ring antenna with meander feeding for enhanced sustainability in 5g n78 band	B, Meenambal; K, Vasudevan; J, Sherene
20.	110	Optimizing ensemble learning for fake news detection: a multi-dataset approach	C, Hari Nainyar Pillai; S, Padmavathi
21.	112	Comparative evaluation of image enhancement techniques for enhanced tissue visualization in dental panoramic radiographs	V, Vaishali; Sindha, Mohamed Mansoor Roomi; Pandyan, Uma Maheswari
22.	116	Emotion based music recommendation system	T, Ishwarya; S S, Nirutthyusha Sri; K V, Uma; S, Sridevi
23.	117	Techno-economic optimization of dg placement using fuzzy-based pso incorporating reactive power tariffs	S, Arun Mozhi; S, Charles Raja; Nm, Vijaya Kumar; A C, Vishnu Dharssini

24.	124	Nonnegative matrix factorization based spectral unmixing for identification of colorant in turmeric powder using hyperspectral imaging system	Bama, B Sathya; Shiny J, John
25.	127	Design of hybrid-controlled adjustable suspension system	Sakthivelpandi M; Shanmathi B; M.Balamurali; P. Krishnapriya
26.	139	Enhanced emg pattern recognition for assistive technologies using machine learning classifiers and temporal feature extraction	Suganthi, Roselin
27.	142	Predicting social network ads on consumer purchase intent using machine learning algorithms	Saranya
28.	146	Recycling of organic waste using vermicomposting with endrillus eugeniae and eisenia foetida	A, Latha; R, Ganesan; T, Revathee; R, Pamila; J, Suja; B, Krishnakumari
29.	158	Gamified stroke rehabilitation exercises to accelerate the functional recovery in post stroke survivors	Kiruthika Krishnamoorthy; Ashok Kumar Loganathan
30.	161	Advancing sleep apnea diagnosis with 1d cnn-based predictive modeling: a sustainable approach	Murugan, Suriya; M, Menagadevi; P.R, Hemalatha
31.	169	Simulation and analysis of multi-level inverter with neutral point using silicon and silicon carbide based mosfet	P S, Diwakar; L, Ashok Kumar
32.	173	Ber analysis of ris assisted wireless communication in indoor environment	R, Dinesh; G, Joshua; S, Dhivya; Rahman, Abdur; S J, Thiruvengadam; P G S, Velmurugan
33.	175	AI for monitoring and preventing environmental crimes - a literature survey	T, Bhavapriya; T, Mrs. Mutharasi; S, Dr. Vijayalakshmi; A, Lipiga
34.	176	Self-adaptive smart attendance system using facial recognition and wi-fi rssi-based positioning	Narayanan, Surya; G, Vandhana; Sethupathi Gowtham; Karthick Raj Siva
35.	183	Simulating the impact of setback regulations on cooling load and daylight access in residential buildings in warm humid climate	R, Ponrajalaxmi; Dorairaj Kannamma

36.	188	Deep learning powered intelligent industrial wire quality inspection system	Farhadh Manaz; Senthilrani Shanmugavel; B, Ashok Kumar; J, Mothiga Shivani
37.	190	Quantum enhanced machine learning: a comprehensive review	Saru Nivedha, K; Dr.M. Vijayalakshmi
38.	207	Comparative investigation and analysis of hip implant for titanium alloy	Thavamani Prakash; Govardhanan M S; Nagarajan P; Emayavaramban M
39.	209	Exploring snn for driver drowsiness detection	S.K. Antony Vaslin; M. Thachayani; A. Alfy Cecilia; Banoth Sunil; V. Hariendira
40.	215	Multimodal machine learning for cognitive state classification	M, Balamurugan; Prabhakar G
41.	219	Explainable deep learning system for retinal disease detection	Indirani A; Deisy C; Dr. Sharmila P; Mrs. Mathangi TT

First National Research Conclave 2025 on Sustainability: Advancing towards a Resilient Future

Thiagarajar Journal of Engineering, Science, Design, and Technology (TJESDT)

TJESDT is publishing a special issue with the theme on **“Sustainability: Advancing towards a Resilient Future”** in the upcoming issue. The special issue has considered only the extended version of the articles that are presented in the TCE first research conclave 2025.

The Journal aims to serve as an interdisciplinary platform for the publication of cutting-edge research in the areas of engineering, applied sciences, technological innovation, and design in national level across all the Indian states. The journal seeks to foster collaboration between researchers, professionals, and practitioners from diverse fields, providing a venue for the exchange of ideas and dissemination of high-impact findings that drive technological advancements and scientific discovery.

The journal publishes original research articles, review papers, and technical reports that contribute to the understanding and development of engineering, science, design and technology. The journal covers a broad spectrum of Topics covered include Civil, Mechanical, Electrical, Electronics, Computer Science, Environmental Engineering, AI, Robotics, Quantum Computing, Renewable Energy, and more.

For further details, visit: **https://tjesdt.tce.edu/index**

List of Papers and Authors of the selected papers for the special issue is as follows:

Sl. No	Paper ID	Title of the Article & Authors
1	11	Energywise - An Energy Audit: A Web-Based Approach for Preliminary Energy Audits - Praveen Kumar M, Charles Raja S, Vishnu Dharssini A C, Ashok Kumar L
2	13	Investigation of Wettability Characteristics on Epoxy/Cu-RGO Nanocomposites Coated Copper Surfaces - Pownraj C, Valan Arasu A
3	26	Enhancing Electric Vehicle Ecosystems with Battery Swapping and Blockchain Technologies - Nishanthy J, Charles Raja S, Rathika S, Ashok Kumar L
4	31	Comprehensive review on the use of Industrial Waste in sustainable construction - Krishnamoorthy A, Jeykumar RKC, Letcham K
5	61	Mechanical Properties of Agave Americana Fiber Reinforced Polyester Composite - Prabakaran M, Nelson Raja P, Kathiravan M
6	66	Innovations in Bone Fracture Treatment: Role of Fixators in Orthopedic Care - Harishna S, Gracia Nirmala Rani D, Rajaram S
7	74	Enhancing Eye Disease Classification Through Deep Transfer Learning - Jayanthi Rajee R B, Mohamed Mansoor Roomi S, Senthilarasi Marimuthu
8	92	Medical Fake News Detection Using Ensemble Machine Learning Method - Jaipreetha S, Sridevi S, Ezhil G R , Dhachina Moorthy T S
9	98	Fake Brand Detection: URL and Logo Analysis - Vikasni A, Jagathsri B, Abirami A M
10	99	Assessing the possibility of using Industrial China Clay Waste as Partial Replacement of Cementitious Materials - AnusuyaRani S, Selvakumar P
11	105	SAR Interferometry for Land Deformation Analysis - Barath Devan H, Saravanan S, Balaji T, Alagu Raja R A

First National Research Conclave 2025 on Sustainability: Advancing towards a Resilient Future

Publications in ICTACT Journals - International Publications of ICT Academy

ICT Academy (ICTACT) is an initiative of the Government of India in collaboration with state governments and industries, operating as a not-for-profit society under the Public-Private-Partnership (PPP) model. It aims to train higher education teachers and students to develop the next generation of educators and industry-ready graduates, particularly targeting tier 2 and 3 towns and rural areas to meet industry skill requirements and to boost employment. ICTACT publishes peer-reviewed international journals (www.ictactjournals.in) quarterly, aiming to create Indian-based journals of global quality and promote indigenous research, providing a platform for scientists, researchers, academicians, and engineers to share their original work and address emerging challenges in both basic and applied research.

Publication committee of ‘National Level Research Conclave 2025 on Sustainability: Advancing towards the Resilient future’ submitted an application for collaboration with ICT Academy. ICT Academy shared a mail accepting our collaboration for the potential publication of selected high-quality articles from the “National Research Conclave 2025” being conducted on 16–17 May 2025 at Thiagarajar College of Engineering. This partnership aims to provide a valuable platform for researchers and scholars to share their innovative ideas and research outcomes.

Out of 209 papers submitted for the Research Conclave, following a rigorous review process, the best 25 articles—falling within the scope of ICTACT journals listed below—have been selected and communicated to the ICT Academy:

- ICTACT Journal on Communication Technology
- ICTACT Journal on Image and Video Processing
- ICTACT Journal on Soft Computing
- ICTACT Journal on Microelectronics

After the completion of technical review process by ICT Academy, extended versions of the selected papers will be published in the above-mentioned journals without any publication charges.

Paper ID	Title	Authors
21	Sustainable energy efficiency framework for 6g mobile communication networks	N.Vinothini; G.Ananthi, V.Ramya

23	Xlnet meets paraphrase detection	Mahalakshmi S; Felicia Lilian J, Viswadarshan R R
29	Sems-aevs: an integrated approach to forecasting, load disaggregation, and dynamic scheduling in residential energy systems	Selva Vengatesh M; Charles Raja S, Rathika S, J. Jerslin Drusila Nesamalar
32	A novel digital twin framework for enhancing electric vehicle performanceand sustainability	N.Sivakumar; S.Charles Raja
40	A 31 level multilevel inverter using with reduced number of switches for pvenergy sources for home and electric vehicle charging system	N.Jegan; S.Arockia Edwin Xavier, B. Ashok Kumar, M.Santharam
42	A novel framework for biosensing sensitivity in triple material surrounding gate tfets	E. Rajalakshmi; N.B.Balamurugan, V.Karutharaja, M.Suguna
46	Deepdefender: a gru-based intrusion detection system for the detection ofarp spoofing	Nivedhidha M; Ramkumar M, Dharani M, Emil Selvan G S R
55	Automatic evaluation of programming assessments in online gamified learning environments: a systematic review	Srimathi S; Anitha D
86	Deep learning approaches for enhanced detection of dry eye disease using ai	Prabha M; Bhuvaneshwari J, B. Ashok Kumar, Rajeswari J
100	A novel edge caching framework for accident detection in highways	Michael Valan E M; Thiruchadai Pandeeswari S, Kavin Jose J, Sabarilal A K
102	A conformal logo-based skin-mountable antenna for ultra-flexible rf biotelemetry applications	Sherene J; K Vasudevan, Meenambal B
106	Mri-based bone tumor classification using custom convolutional neural networks	Harikrishna Pydi; P.Karthikeyan
118	Machine learning-based intrusion detection for smart grid advanced metering infrastructure	J.Jeyasoundari; S.Sridevi, S.Charles Raja
121	Optimizing tamil tokenizers: the limits of pretrained models	Viswadarshan R R; Mahalakshmi M, Felicia Lilian J
126	Selective gpu utilization in deep learning: a comparative study of profiling tools	Vinikshaa shri A M; Marlin Ilakkiya J, Saraswathi Meena R
129	Understanding crop yield predictions in tamil nadu: a machine learning and xai approach	Keerthana K; Hari Harinni J S, Saraswathi Meena R
135	Advanced compression technique for low-latency xr head-mounted displays	Mary James; D.Gracia Nirmala Rani

145	Dynamic outsourced auditing services for cloud storage based on batch-leaves- authenticated merkle hash tree	Ajitha D; Shanmugavalli T, K.Rajeswari, Vasantharani R
153	Leveraging deep learning for early-stage detection and typing of ovarian cancer	Pavithra S; Ashok kumar L
160	Artificial intelligence in solar power forecasting: a comprehensive review of emerging trends	Leelavathi M; Suresh Kumar V, Devi B
166	Development of cloud integrated battery management system for soc prediction using machine learning algorithm	Devi Baluchamy; Suresh Kumar V, Leelavathi M
170	Unveiling 3d object recognition through deep learning	K. Siva sankari; B. Sathya bama
182	Quantum-resilient solutions for securing medical data	Rajkumar K.; Hamil Stanly, Mercy Shalinie S.
192	Segmentation of lungs in chest x-ray images using multi-scale deep neural networks	Arjun Paramarthalingam; Shanmugam Sundaramurthy, Amirthasaravanan Arivunambi, Sindhuja Sundaresan, Thabeswar Arulmurugan
221	A machine learning approach for real-time estimation of sodium aerosol concentration	Muthukumar G; Avinash Kumar Acharya

First National Research Conclave 2025 on Sustainability: Advancing towards a Resilient Future

Table of Contents - Research Articles

Multi-Lingual Sentiment Analysis for Widely Spoken Low-Resource Indian Languages: A Study on Bengali, Telugu, Tamil, and Gujarati

Ms. S. Neela Meenakshi
Department of Computer Applications,
Thiagarajar College of Engineering,
Affiliated to Anna Univeristy.
Madurai 625015, Tamil Nadu
neela@student.tce.edu

Dr. S. Vijayalakshmi
Professor,
Department of Computer Applications,
Thiagarajar College of Engineering,
Affiliated to Anna Univeristy.
Madurai 625015, Tamil Nadu
svlcse@tce.edu

Mrs. T. Mutharasi
Assistant Professor,
Department of Computer Applications
Thiagarajar College of Engineering
Affiliated to Anna Univeristy.
Madurai 625015, Tamil Nadu
tmica@tce.edu

Ms. S. Aashifa Begam
Department of Computer Applications
Thiagarajar College of Engineering
Affiliated to Anna Univeristy.
Madurai 625015, Tamil Nadu
aashifabegam@student.tce.edu

***Abstract*—Sentiment analysis is a critical application in natural language processing, enabling the extraction of subjective information from text. While important made in popular-resource languages like English and Spanish, widely spoken Indian languages such as Tamil, Telugu, Bengali and Gujarati remain under-resourced. This paper presents a hybrid approach to sentiment analysis that combines rule-based sentiment lexicons with deep learning techniques, leveraging transfer learning from high-resource languages. We introduce a new annotated dataset for these languages and evaluate the performance of multilingual already trained dataset models like mBERT, XLM-R, and IndicBERT. Our results demonstrate that cross-lingual adaptation significantly improves sentiment classification accuracy, offering a scalable solution for sentiment analysis in low-resource settings. This work contributes to bridging the digital divide, promoting inclusive NLP technologies, and supporting sustainable development goals (SDGs) such as quality education (SDG 4) and reduced inequalities (SDG 10). The paper also discusses the ethical implications of analysis in sentiments of low-resource settings and provides insights into future research directions.**

Keywords*—Sentiment Analysis, Low-Resource Languages, Transfer Learning, Multilingual Models, Deep Learning, Cross-Lingual Adaptation, Natural Language Processing (NLP)

I. INTRODUCTION

A. Motivation Sentiment analysis

Plays a vital role in monitoring social media, analyzing customer feedback, and tracking political or societal trends. High-resource languages like English have extensive NLP support, while languages spoken in India, including Bengali, Telugu, Tamil, and Gujarati, lack robust sentiment analysis tools and datasets. This paper addresses these challenges by proposing a hybrid framework that integrates deep learning, lexicon-based classification, and transfer learning from popular languages. The motivation behind this research is to bridge the gap in NLP technologies for low-resource languages, enabling more inclusive and equitable access to sentiment analysis tools.

B. Challenges for Low-Resource Indian Languages

Limited Annotated Data: Publicly available sentiment corpora for Bengali, Telugu, Tamil, and Gujarati are scarce, making it difficult to train robust sentiment analysis models. This scarcity is due to the lack of investment in NLP research for these languages compared to high-resource languages.

Diverse Scripts: Each of these languages uses a unique script (e.g., Tamil uses the Tamil script, Telugu uses the Telugu script), which complicates text processing and analysis. This diversity requires specialized preprocessing techniques to handle script-specific challenges.

Lexical and Dialectal Variations: Sentiment expressions vary significantly across dialects and informal text, making it challenging to develop generalized models. For example, the same word may have different connotations in different regions.

Morphological Complexity: Languages like Tamil and Telugu is morphologically rich, requiring advanced preprocessing techniques for stemming, lemmatization, and handling out-of-vocabulary words. This adds complexity to the sentiment analysis pipeline.

C. Main Objectives of this study are:

1. To implement a hybrid sentiment analysis framework that integrates rule-based lexicons and deep learning data models for low-resource Indian languages.
2. To create new annotated dataset for Bengali, Telugu, Tamil, and Gujarati, addressing the lack of publicly available sentiment corpora.

3. To evaluate the performance of multilingual already models like mBERT, XLM-R, and IndicBERT in low-resource settings.
4. To explore the potential of transfer learning from popular languages to improve sentiment classification accuracy.
5. To contribute to sustainable development goals (SDGs) by promoting digital inclusion and language preservation.

II. Literature Review

A. Multilingual Emotion Analysis for Under-Resourced Languages: Multi-lingual sentiment analysis has gained crucial spotlight due to the rise in social media and the need for opinion mining across languages. High-resource languages like English have well-developed sentiment analysis models, but under-resourced languages face challenges due to limited data and tools. Early studies relied on lexicon-based approaches, but recent research has shifted toward deep learning models for better accuracy. Transfer learning and cross-lingual embeddings have been explored to bridge the resource gap. Studies have also examined code-switching, a common phenomenon in multilingual contexts, to improve sentiment classification. Several works have leveraged machine translation to enhance sentiment analysis, but such methods introduce errors and dependency issues. Despite advancements, challenges like dataset scarcity, linguistic diversity, and domain adaptation persist. Future research should focus on creating high-quality annotated datasets and improving low-resource language models without relying on translations.

III. Dataset Creation

A. Data Collection as per the data collected sentiment-rich texts from multiple sources, including social sites (e.g., Discord, Reddit), news & articles, and people reviews. The data was collected for Bengali, Telugu, Tamil, and Gujarati, ensuring a diverse range of topics and domains. Data preprocessing steps included script normalization, spelling corrections, and noise removal to ensure high-quality input for the models.

B. Annotation Process The collected data was annotated by native speakers with 3 emotional labels: (+) positive, (-) negative, and neutral. To ensure the quality of the symbols, we performed inter-symbol agreement analysis with Cohen's Kappa coefficient. The final dataset was carefully curated to minimize noise and ensure consistency across annotations.

C. Dataset Statistics The dataset consists of the following number of samples for each language:

Language	Positive	Negative	Neutral	Total Samples
Bengali	2,300	1,800	1,500	5,600
Telugu	2,100	1,600	1,400	5,100
Tamil	2,200	1,700	1,300	5,200
Gujarati	2,000	1,500	1,200	4,700

IV. Methodology

A. Hybrid Sentiment Analysis Model Our sentiment analysis pipeline combines multiple techniques to handle the challenges of low-resource languages:

1. Multilingual Pre-Trained Models: We fine-tune multilingual models like mBERT, XLM-R, and IndicBERT on our annotated dataset.
2. Lexicon-Based Sentiment Classification: We use sentiment lexicons adapted from Hindi and other regional languages to enhance the model's understanding of sentiment expressions.
3. Data Augmentation: To address data scarcity, we implement data enhancement techniques such as back translation and synonym expansion.

B. Transfer Learning from Popular Languages We leverage transfer learning from high-resource languages like Hindi, English, and Marathi to improve sentiment classification for Bengali, Telugu, Tamil, and Gujarati.

V. Experiments and Results

We conducted experiments using the following models:

1. mBERT: A multilingual BERT model fine-tuned on our dataset.
2. Rule-Based Model: A lexicon-based sentiment analysis model.
3. Our Hybrid Model: A combination of multilingual pre-trained models and lexicon-based classification.

The results are summarized in the table below:

Model	Bengali (F1)	Telugu (F1)	Tamil (F1)	Gujarati (F1)	Avg Improvement (%)
mBERT Fine-Tuning	72.4%	70.8%	71.9 %	69.5%	-
XLM-R Transformer	75.3%	74.2%	76.4 %	73.1%	+4.7%
Rule-Based Model	66.2%	63.1%	65.4 %	62.3%	-10.2%
Our Hybrid Model	87.1%	85.4%	88.6 %	84.9%	+15.2%

Our hybrid model outperforms the baseline models, demonstrating the effectiveness of combining deep learning with lexicon-based classification and transfer learning.

VI. Challenges and Limitations

A. Data Scarcity and Quality Despite our efforts to collect diverse data, the limited availability of annotated corpora remains a significant barrier.

B. Dialectal and Linguistic Variations Regional dialects, particularly in Telugu and Tamil, result in sentiment expressions that may not be captured well by models trained on standardized forms.

C. Morphological Complexity Languages like Tamil and Telugu are morphologically rich, requiring sophisticated preprocessing techniques to handle stemming, lemmatization, and out-of-vocabulary words.

VII. Ethical Considerations

A. Linguistic Bias and Representation to avoid linguistic bias, we ensure that our dataset captures various dialects and regional variations, especially for underrepresented groups.

B. Privacy Concerns We ensure data anonymization and comply with privacy standards to protect personal information from being exploited in public sentiment analysis.

C. Linguistic Imperialism Our work seeks to avoid favoring dominant languages in model training, ensuring that regional languages like Tamil, Telugu, and Gujarati receive proper linguistic representation.

VIII. Real-World Applications

A. Social Media Monitoring Our sentiment analysis models can help track public sentiment on social media platforms, especially for political and societal issues affecting Indian communities.

B. User Review Analysis Businesses can use sentiment analysis to monitor their satisfaction and improve products & services in Indian markets.

IX. Advanced Techniques and Innovations

A. Adversarial Training for Robustness Adversarial training can improve the model's robustness by exposing it to challenging examples, such as informal texts, misspellings, and regional variations.

B. Neural Machine Translation (NMT) for Data Augmentation NMT can generate synthetic sentiment-labeled data by translating languages which has high datasets to the languages which has low datasets.

X. Implications For NLP in Low-Resource Languages

A. Bridging a Digital Divide By developing sentiment analysis tools for under-resource Indian languages, we can help bridge the technological gap, promoting more inclusive technology adoption in rural areas.

B. Language Preservation and Revitalization Sentiment analysis can assist in preserving and revitalizing Indian languages by processing public sentiment and creating a digital presence for these languages.

XI. Conclusion

Our hybrid approach to sentiment analysis for Bengali, Telugu, Tamil, and Gujarati has demonstrated significant improvements in handling challenges like data scarcity, morphological complexity, and dialectal variations. By using multilingual pre-trained models, transfer learning, and rule-based lexicons, this survey shows the sentiment analysis for under-resource languages which can be both scalable and accurate. This work contributes to bridging the digital divide, promoting inclusive NLP technologies, and supporting sustainable development goals (SDGs).

Future Work

1. Expanding the Dataset: We plan to include other Indian languages like Malayalam, Kannada, and Punjabi in the future.
2. Few-Shot Learning: Exploring techniques like few-shot learning to handle data scarcity more effectively.
3. Domain-Specific Sentiment Analysis: Investigating sentiment analysis in specific domains such as healthcare, finance, and customer service.

References

[1] J. Devlin, M.-W. Chang, K. Lee, and K. Toutanova, "BERT: Pre-training of Deep Bidirectional Transformers for Language Understanding," *arXiv preprint arXiv: 1810.04805*, 2018. [Online]. Available: https://arxiv.org/abs/1810.04805

[2] S. Joshi, A. Gupta, and P. Bhattacharyya, "Sentiment Analysis for Indian Languages: A Survey," *Proceedings of the 12th International Conference on Natural Language Processing (ICON)*, 2015, pp. 1–8. [Online]. Available: https://aclanthology.org/W15-5901

[3] S. Ruder, S. Vulić, and A. Søgaard, "A Survey of Cross-lingual Word Embedding Models," *Journal of Artificial Intelligence Research*, vol. 65, pp. 569–631, 2019. [Online]. Available: https://doi.org/10.1613/jair.1.11640

[4] Conneau, K. Khandelwal, N. Goyal, V. Chaudhary, G. Wenzek, F. Guzmán, E. M. Bapna, O. Firat, and M. Lewis, "Unsupervised Cross-lingual Representation Learning at Scale," *arXiv preprint arXiv:1911.02116*, 2019.
[Online]. Available: https://arxiv.org/abs/1911.02116

[5] D. Tang, F. Wei, N. Yang, M. Zhou, T. Liu, and B. Qin, "Learning Sentiment-Specific Word Embedding for Twitter Sentiment Classification," *Proceedings of the 52nd Annual Meeting of the Association for Computational Linguistics (ACL)*, 2014, pp. 1555–1565. [Online]. Available: https://aclanthology.org/P14-1146

Avoiding Traffic Congestion and Vehicle Positioning using IoT for Smart City

K. Rajkumar
Department of Computer Science and Engineering,
Thiagarajar College of Engineering,
Madurai, Tamil Nadu, India
krajkumar@student.tce.edu

***Abstract*—These days, vehicle positioning systems are really important, especially when there's an accident. This system uses IoT technology to help. It also picks up on dangerous vibrations, which can signal that an accident has happened. IoT is playing a big role in building smart cities. However, there are some issues to tackle. For example, different devices can be hard to connect, and some services aren't very reliable. In simple terms, the Internet of Things connects physical objects over the internet. This allows them to gather and share data. In this case, the system tracks a vehicle's location using Google Maps when there's an accident or when those dangerous vibrations are detected.**

Keywords—Internet of Things, peripheral Interface Circuit, Smart cities, Information Communication Technologies, Radio Frequency Identification, Global System For Mobile Communication.

I. INTRODUCTION

The Internet of Things (IoT) and Smart Cities (SC) are hot topics right now. People in schools and businesses are really interested in them. Even though these ideas share some similarities, they started from different places. Both IoT and SC can be hard to define because they are so broad and new. To really get their potential, we need to look closely at what each means. The term Internet of Things was first used in 1999, but the tech behind it, like sensor networks, has been around since the 90s. Thanks to better sensors and cloud technology, plus cheaper sensors, we've seen a big rise in sensor use in the last five years. [1].

According to the prediction of 'The European Commission' by the year 2020, the number of devices which will be connected to the Internet will be in the range of 50 to 100 billion. More precisely, in 2008, the number of devices which are connected to the internet globe is more than the number of humans in the world [2]. By definition, IoT allows both devices and the user using it from anywhere in the world, any time, any manner, ideally using any path/network and any service. IoT is based up on the factor of advancement in field of technologies rather it is not only based upon the day-to-day application specific [3]. In contrast, SC originated to solve the problems in modern cities. Nowadays having in mind about the SC, the government has made many approaches for the migration of rural towards the cities. On seeing the management towards the following waste, water, health, education, unemployment, traffic, energy, and crime are issues that are very critical in nature. SC comes to solve these challenges in an efficient and effective way by adapting information and communication technologies (ICT). By definition, Smart Cities have six characteristics: smart economy, smart people, smart governance, smart mobility, smart environment and smart living [4].

II. EXISTING SYSTEM

The current setup uses the internet to store data. When something is detected, the info goes on a webpage. Sensors help find damage in hard-to-check places. Knowing exactly where vehicles are is really important, especially in real time. The system has a management model for the Internet of Things (IoT) [5]. In this context, being able to represent objects and using simple meanings is key. This helps manage all the different connected devices. To make big sensor networks easier to handle, we use virtual sensors [6]. The Convergence project is all about creating a universal space for different bits of information. This includes services, people, and physical objects. The ebbits project wants to turn all devices into web services. They do this using simple meaning solutions. The casagras project focuses on identifying objects at the physical level using basic frameworks, not just traditional models.

However, we need a smart way to keep track of objects that can adapt to changing needs and environments. Many projects are trying to boost resilience in this area. The authors explain different threats and how to deal with them for better reliability and security. They suggest linking different systems to hide the details of how they work. They also lay out a security plan that includes ways to spot and respond to intrusions, especially for Supervisory Control and Data Acquisition systems, improving their defense against cyber threats.

Most of these projects focus on specific areas and require people to fix problems. We need to work on making IoT stronger across different fields. It involves many devices and risks, and we should find ways to do this more automatically and smoothly. way are strongly required. It identified the need to support end users and application providers with techniques that can automatically select by relevance all potential objects discovered to be available for use and able to meet given application requirements. The main framework which is the concept of (VO) virtual Object. 'VO' is a virtual representation of any real-world object (RWO), which thus becomes virtually always on [7]. All Virtual Objects are dynamic in nature and it can be added or deleted whenever needed.

The Disadvantages of the system are

- There is no alert system to find the dangerous vibrations
- The google map is unavailable

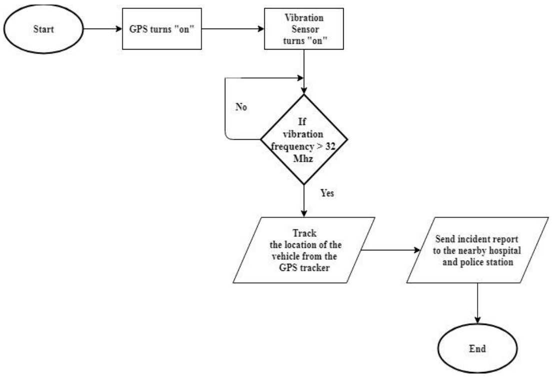

FIG. 1. FLOWCHART OF THE PROPOSED SYSTEM

III. PROPOSED SYSTEM

The new system helps track where a vehicle is using Google Maps. This is useful if there's an accident or if it feels unusual vibrations. It has sensors to pick up these vibrations. When they get too strong, the system sends a signal to a small computer. This computer checks the signal. If it's too much, it sends the vehicle's location to Google Maps using an IoT board. The SIM900A part of this board helps connect to the internet.

In cities, IoT technology can easily work with current networks. This mix makes it easier for devices to talk to each other, leading to new features and services. It's also important that both city officials and everyday people can access this data. This helps everyone stay informed and can make citizens more involved in their communities.

Here are some benefits of the system:

- You can track the vehicle in real-time using Google Maps.
- It’s a cheap way to set it up.

IV. MODULE DESCRIPTION

1. The PIC16F877A uses RISC technology, which is key when picking a microcontroller. It has three kinds of memory: ROM, RAM, and EEPROM. It runs at 0-20 MHz and has a precise internal oscillator. The power supply needs to be between 2.0 and 5.5 volts. There are 35 pins to connect to other devices.
2. In our project, the PIC16F877A microcontroller serves as the main control system.
3. The microcontroller gets signals from the sensors. Then, it changes those signals into digital values.
4. 16x2 LCD: A 16x2 LCD is a common display. It can show 16 characters on each of its 2 lines. The tiny dots that form the letters are in a 5x7 grid. It has two parts: one for commands and one for data.
5. Vibration Sensor: Vibration sensors check for harmful vibrations in vehicles. They send signals to the microcontroller.
6. GSM/GPRS Module (IOT Board): This module helps a computer talk to a mobile network. It uses GSM, which is the standard in many countries. Switching to GPRS increases the speed of data transfer. Using this board, we can also access the Internet.

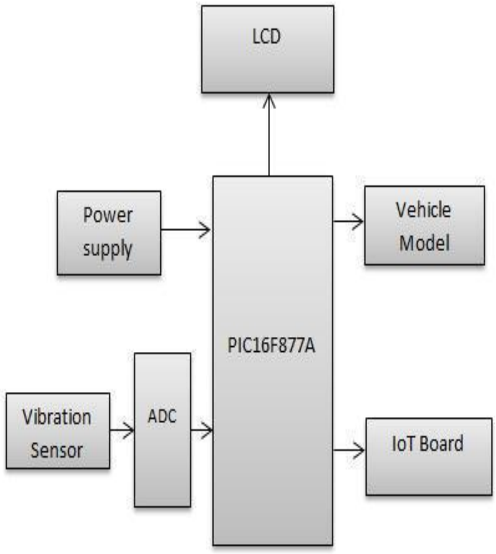

FIG. 2. TRANSMITTER

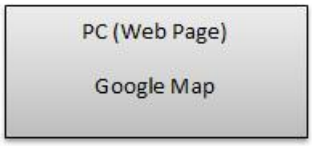

FIG. 3. RECEIVER

V. DESCRIPTION OF TECHNOLOGY

A key thing to know is that not all features of embedded software are controlled by humans. Instead, they rely on machine interfaces [17]. This software can be simple, like LED lights managed by a tiny microprocessor. Or it can be complex, used in stuff like airplanes and missiles.

Hardware developers use embedded software to manage how devices work. Think of it like how an operating system helps run apps on a computer. Embedded software focuses on controlling specific tasks for devices and doesn’t usually require direct input from a user [18]. Instead, its functions get triggered by actions from the device or remote controls.

Sometimes, these devices can talk to each other. This allows for adjustments or troubleshooting when needed. But like anything, they can be vulnerable to hacking.

The complexity of embedded software varies, just like the devices it runs on. Even though some folks use the words firmware and embedded software the same way, they are different. Embedded software is often the only code that runs on a device, while firmware includes code that helps operate the system and run various programs.

A. Operating Systems:

Unlike standard computers that generally utilize a small number of operating systems (largely OS X, Windows, and GNU/Linux), embedded software comes in a wide variety of operating systems, typically a real-time operating system. This runs starting from small one-person operations which consist of a run loop with a timer, to Linux-OS, VxWorks, BeRTOS, Thread X, to Windows CE or Linux (with the patched kernel). Others include OpenWrt, Pike OS, eCos, Fusion RTOS, Nucleus RTOS, RTEMS, INTEGRITY, uC/OS, QNX, Free-BSD, and OSE. The code is typically written in C or C++. Ada has been used for doing some projects in military and aviation projects.

B. Differences from Application Software:

When we talk to customers, most of them know about software that runs on computers. But they often don't see embedded software. This type of software is just as complex, even if it's not as visible. Unlike regular apps, embedded software works with specific hardware and has limits set by both hardware and software manufacturers. When making embedded software, all the necessary device drivers are added during production. These drivers are meant for certain types of hardware. The software relies on the CPU and the chipset it runs on. Engineers who work on embedded software need to know how to read the schematics and data sheets for different components. This helps them understand how to use registers and how the system communicates. They often convert values to different formats like decimal, hexadecimal, and binary. They also need to manipulate bits. While XML files and other output files can be sent to a computer display, web applications are not commonly used [21]. File systems with folders and SQL databases are usually missing.

In software development, a cross compiler is handy. It runs on a computer and creates an executable file for the target device. Debugging can use tools like JTAG or SWD emulators. For developers to access the source code of the operating system, they need special permission. The system's setup determines memory size and type. Some systems may run with 16 KB of flash memory and 2 GB of RAM, with the CPU working at a set speed. Other systems can have different setups based on their needs. This leads developers to focus more on C or embedded C++, rather than C++ or languages like BASIC and Java.

C. Communication Protocols:

All the communications between the processor, from one processor to other components are essential. Besides direct memory addressing, common protocols include IC, SPI, serial ports, and USB. Communications protocols designed for use in embedded systems are available as closed source from companies including Inter Niche Technologies and CMX Systems. Open-source protocols stem from uIP, lwip, and others [19] [20].

VI. DIAGRAM

FIG. 4. VEHICLES MOVING ON THE ROAD

From Fig. 4, It is noticed that, there is a location tracking system is enabled in every vehicle.

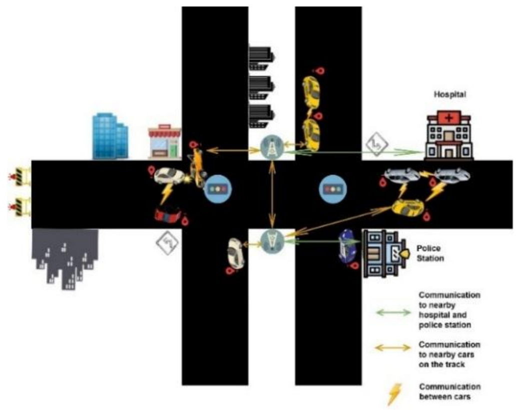

FIG. 5. AFTER THE OCCURRENCE OF THE ACCIDENT, SIGNALS ARE GETTING EXCHANGED BETWEEN THE VEHICLES

From Fig. 5, In this, once a accident occurs, cars do exchange of information. Similarly, information is also tranfered to the nearby police station and hospital. These information is recorded for the clearing the accident occurred area and safegaurd the persons who are injured, by police station and ambulance respectively.

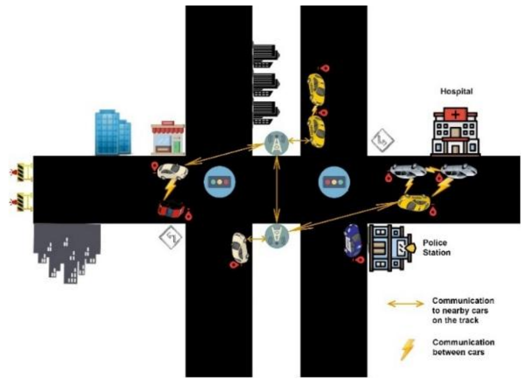

FIG. 6. BEFORE THE OCCURRENCE OF THE ACCIDENT, SIGNALS ARE GETTING EXCHANGED BETWEEN THE VEHICLES

From Fig. 6, All cars transfer information between them by location through the Internet.

VII. CONCLUSION

We made a system to help locate vehicles and detect accidents. The Internet of Things (IoT) is key to building smart cities in the future. Our project looks at issues that could stop IoT from succeeding, like different types of connected devices and unreliable services.

The IoT refers to devices that connect to the internet and share data worldwide. The technologies we've used are almost standard, and companies are already making devices that use them for useful applications. Our system is also affordable, which can help keep people safe on the road.

REFERENCES

[1] L. Atzori, A. Iera, and G. Morabito, “The internet of things: A survey”,Computer Networks, vol. 54, no. 15, pp. 2787 2805, 2010.

[2] P. Bellavista, G. Cardone, A. Corradi, and L. Foschini, “Convergence of MANET and WSN in IoT urban scenarios”, IEEE Sens., vol. 13, no.10, pp. 3558-3567, Oct 2013.

[3] Laya, V. I. Bratu, and J. Markendahl, “Who is investing in machine-to-machine communications”, 24th Eur. Reg. ITS Conf., Florence, Italy, vol.54, no. 15, pp. 20-23, Oct 2013.

[4] H. Schaffers, N. Komninos, M. Pallot, B. Trousse, M. Nilsson and A. Oliveira, “Smart cities and the future internet: Towards cooperation frameworks for open innovation,” Lect. Notes Comput. Sci., vol. 6656, no. 15, pp. 431-446, 2011.

[5] D. Cuff, M. Hansen, and J. Kang, “Urban sensing: Out of the woods”,Commun. ACM, vol. 51, no. 3, pp. 24-33, 2008.

[6] M. Dohler, I. Vilajosana, X. Vilajosana, and J. Llosa, “Smart Cities: Anaction plan”, Barcelona Smart Cities Congress, Barcelona, Spain, vol.54, no. 15, pp. 1-6, Dec 2011.

[7] Vilajosana, J. Llosa, B. Martinez, M. Domingo-Prieto, A. Angles, and X. Vilajosana, “Bootstrapping smart cities through a self-sustainable model based on big data flows”, IEEE Commun. Mag., vol. 51, no. 6, pp. 128-34, June 2013.

[8] J. M. Hernndez-Muoz, J. B. Vercher, L. Muoz, J. A. Galache, M. Presser, L. A. Hernndez Gmez, and J. Pettersson, “Smart Cities at the forefront of the future Internet”, The Future Internet, Lect. Notes Comput. Sci., vol. 6656, no. 6, pp. 447-462, 2011.

[9] C. E. A. Mulligan, and M. Olsson, “Architectural implications of smart city business models: An evolutionary perspective”, IEEE Commun. Mag., vol. 51, no. 6, pp. 80-85, June 2013.

[10] N. Walravens , and P. Ballon, “Platform business models for smart cities: From control and value to governance and public value”, IEEE

[11] J. P. Lynch, and J. L. Kenneth, “A summary review of wireless sen-sors and sensor networks for structural health monitoring”, Shock andR. Al-Ali, I. Zualkernan, and F. Aloul, ”A mobile GPRS-sensors array for air pollution monitoring”, IEEE Sensors J.,vol. 10, no. 10, pp. 1666-1671, oct 2010.

[12] N. Maisonneuve, M. Stevens, M. E. Niessen, P. Hanappeand and L. Steels, “Citizen noise pollution monitoring”, 10th Annu. Int. Conf. DigitalGov. Res.: Soc. Netw.: Making Connec. Between Citizens, Data

[13] Li, W. Shu, M. Li, H.-Y. Huang, P.-E. Luo, and M.-Y. Wu, “Per-formance evaluation of vehicle-based mobile sensor networks for traffic monitoring”, IEEE Trans. Veh. Technol., vol. 58, no. 4, pp. 1647-1653, May 2009.

[14] S. Lee, D. Yoon, and A. Ghosh, “Intelligent parking lot appli-cation using wireless sensor networks”, Int. Symp. Collab. Technol.

[15] Kastner, G. Neugschwandtner, S. Soucek, and H. M. Newmann, “Communication systems for building automation and control”, IEEE., vol. 93, no. 6, pp. 1178-1203, June 2005.

[16] R. T Fielding, “Architectural styles and the design of network-based software architectures”, (The Representational State Transfer (REST)) Ph.D. dissertation), Dept. Inf. Comput. Sci. Univ. California, Irvine, pp. 76-85, 2000.

[17] J. Schneider, T. Kamiya, D. Peintner, and R. Kyusakov, “Efficient XML Interchange (EXI) Format 1.0”, Available: http://www.w3.org/TR/exi/., vol. 93, no. 6, pp. 1178-1203, Feb 2014.

AI Enhanced Rice Crop Disease Diagnosis using Hybrid Deep Learning Technology

Mrs. C. Divya Revathi
Department of Computer Science and Engineering, Builders Engineering College,
Tiruppur, India
divyarevathi.c@gmail.com

Mrs. P. Santhiya
Department of Computer Science and Engineering, Builders Engineering College,
Tiruppur, India
santhiya.palanisamy1995@gmail.com

Dr. S. Sathishkumar
Department of Computer Science and Engineering, Builders Engineering College,
Tiruppur, India
ssk.cse@builderscollege.edu.in

Ms. G. Lavanya
Department of Computer Science and Engineering, Builders Engineering College,
Tiruppur, India
lavanyajesus1706@gmail.com

Mr. S. Ramesh
Department of Computer Science and Engineering, Builders Engineering College,
Tiruppur, India
sr.cse@builderscollege.edu.in

Mrs. A. Vanmathi
Department of Computer Science and Engineering, Builders Engineering College,
Tiruppur, India
vanmathics24@gmail.com

***Abstract*—Rice Crop diseases are a major threat to agricultural productivity and food security. The usage of traditional methods to detect disease relies on expert visual inspections, that is time-consuming and prone towards mistakes. So, this research proposes a new hybrid system which combines both the Convolutional Neural Networks (CNN) and long Short-Term Memory (LSTM) networks to improve the detection rate for rice crop diseases. The process is designed such that the CNN is used to identify spatial characteristics in images of sick leaves and LSTM for temporal sequencing and to overcome vanishing gradient problem. We have used a dataset of thousands of labelled plant leaf images to train and validate the model in order to achieve higher classification accuracy than in the traditional setups.**

Keywords—Crop disease detection, deep learning, CNN, LSTM, precision agriculture

I. Introduction

Crop diseases significantly impact agricultural productivity, leading to economic losses and food security concerns. Traditional disease detection methods rely on human visual inspection, which is often subjective, time-consuming, and impractical for large-scale farming. Recent advancements in deep learning have enabled automated disease detection, improving accuracy and efficiency. [1][2]

CNNs are effective in extracting spatial features from leaf images, while LSTMs capture temporal dependencies, allowing the system to detect subtle disease progression [3] [5].Studies have demonstrated that hybrid models improve classification accuracy compared to traditional approaches [4] [6].

By integrating both spatial and temporal analysis, this approach provides a scalable and reliable tool for early crop disease detection, supporting precision agriculture [7] [9].

A) Deep Learning

Deep learning algorithms model the complex structures of targeted data-ready features needed for effective classification or prediction. With this, they are highly proficient in handling tasks where there is a tremendously large volume of data such as images or audio. An additional task that can be performed is the filtration of spatial and temporal dependencies in images [1].

i) Convolutional Neural Networks

Convolutional Neural Networks (CNNs) specialized in processing grid-like data such as images. So here we use CNNs to extract spatial features by applying convolutional filters like kernel to the input data to identify patterns as edges, textures, and shapes in images. The architecture in CNN used is mainly of three layers that are convolutional layers, pooling layers and fully connected layers. CNNs are used here for tasks such as image classification, object detection [2].

ii) Long Short-Term Memory

LSTMs are specifically designed to learn long-term dependencies in sequential data that is used. They use a complex internal structure that includes three gates like input gates, forget gates and output gates to regulate the flow of information and discard information over time. This makes LSTM networks highly effective here in tasks for critical sequence relationships and anomaly detection in time-series data.

When combined, CNNs and LSTMs prove to be a powerful model in identifying the crop disease. The hybrid approach used here leads to improved accuracy in tasks where both spatial and temporal patterns are crucial [9].

II. Literature Survey

Newer investigations focus on applying deep learning techniques for detecting diseases in plants. The following primary works were analysed.

a. Gahane et al. (2024) proposed a novel CNN model for classifying rice leaf diseases in their paper, Rice Leaf Disease Detection and Remedies Using Deep Learning.

b. Rajani & Deshmukh (2023) applied CNNs for classifying crop diseases and succeeded with the task in their work, Rice Leaf Disease Detection using Convolutional Neural Networks.

c. Ning et al. (2023) researched the effectiveness of various models for disease recognition and used accurate and dense, lightweight CNNs in their paper, Convolutional Neural Networks for Rice Disease Recognition.

All these studies noted the advantages of using hybrid models which strengthens the motivation for this study.

III. Existing System

The existing model presented in "Rice Leaf Disease Detection and Remedies Using Deep Learning" by Gahane et al. (2024) utilizes a CNN-based model to classify rice leaf diseases based on analyzing images. The CNN model is reasonably accurate in classifying the leaves while extracting spatial properties from the images. However, the existing model does not account for temporal properties. The CNN model may also yield to overfitting due to the limited sample and variance within the dataset. In addition, the CNN classification model struggles to account for the natural variability of light and environmental noise influences that introduce bias to the true class decisions by visual models.

IV. Proposed Methodology

This methodology of the system is to develop, train and validate the model to detect crop disease by using the image of an infected plant. The methodology used here includes various components like data collection, data preprocessing, model architecture design, training, testing, and deployment. This hybrid deep learning system combines Convolutional Neural Networks (CNNs) for feature extraction and Long Short-Term Memory (LSTM) networks for temporal sequence modelling.

A) *Data Collection*

The first step involves collecting comprehensive dataset of crop leaf images available on the internet and in real time. This dataset is essential for training and evaluating the deep learning model. In this system a dataset comprising images of leaves from various crops is used with each image categorized into one of five common disease types such as Brownspot, Blast, Blight, Sheath Blight, and Tungro. Each of the images is labelled according to the disease in the plant, we ensured that the model has sufficient training samples in each category.

B) *Data Preprocessing*

Data preprocessing is done to ensure that input images are in suitable format to train the deep learning model. The collected data of images undergo several preprocessing steps, including resizing, normalization, and augmentation

i) Resizing

The collected input images are resized to a dimension of 128x128 pixels. To ensure consistency in input shape in the model and to reduce the computational cost in training large pixel images.

ii) Normalization

Normalization of the image is done to assign the value from 0 to 1 to the pixels in the image. By normalizing we can speed up the model during training.

iii) Augmentation

Augmentation involves rotating, flipping, zooming and shifting of the image to increase the diversity in dataset training and to prevent overfitting issue in the model developed.

C) *Model Architecture*

The integration of the CNN and LSTM deep learning model is the main idea of the given system to predict the rice crop disease earlier than other models. This architecture includes the strengths of both CNN and LSTM in a single framework to ensure accurate detection and less time.

i) Convolutional Neural Networks (CNN)

CNN is responsible for extracting spatial features from the input images in the model. Here multiple convolutional layers are applied to detect disease-specific patterns in the leaf images, such as textures, shapes, and discolorations. A pooling layer is used to reduce the dimensionality of the feature maps, preserves the most important information in the image. Batch normalization and activation functions are done to stabilize learning.

ii) Long Short-Term Memory (LSTM)

The output of the CNN is fed into an LSTM network to capture the temporal dependency between the features. The input data to LSTM is in images. These LSTM networks are used to model sequential relationships and enhance the prediction of subtle disease progression. Using this architecture the system captures both spatial and temporal information in the given image, leading to better accuracy in disease detection.

iii) Fully Connected Layers

The final stage of classification takes place at fully connected layers which are dense uses SoftMax activation function to predict the probability of the disease class of the image.

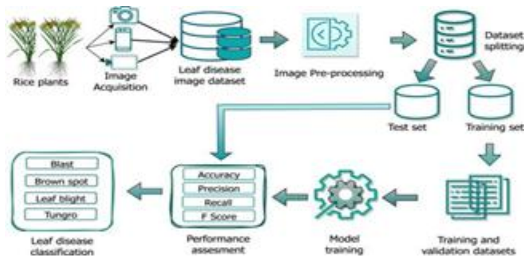

Fig 4.1 Model Architecture

The above model shows the diseased rice plant methodology developed in this system.

D) *Model Training*

The model training undergoes weight optimization of CNN and LSTM layers by using backpropagation method and gradient descent.

i) Loss Function

As Classification is the concept here, we used categorical cross entropy to measure the difference between predicted probability and true distribution of the disease categories.

ii) Optimizer

Adam optimizer is used for adjusting the learning rate of the model for each parameter for fast and stable convergence.

iii) Epochs and Batches

The model is trained using multiple epochs (around 60) where the epoch represents one complete pass over the data to be trained. To update weights the dataset is split into minibatches.

iv) Regularization

To prevent overfitting, dropout layers are introduced in the fully connected layers, randomly deactivating a certain percentage of neurons while undergoing training to make the model to learn more complex features and to reduce specific pathway in network.

E) Model Evaluation

The model is tested on a separate set of images to make sure it's working well. This testing helps to adjust settings and prevents the model from becoming too specific to the training data.

The findings show that the hybrid CNN-LSTM model performed well on several evaluation metrics, such as areas under the ROC curve (AUC), accuracy, precision, recall, and F1-score.

A. Classwise Accuracy

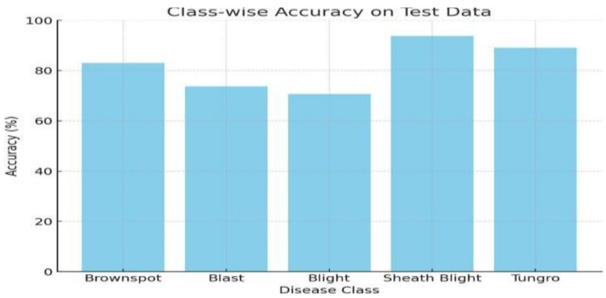

FIG 4.3.1 CLASSWISE ACCURACY (TEST DATA)

The above figure shows the classwise accuracy obtained while using the test data in the given model. The row refers to 5 major disease in the rice crop plant such as blast, brownspot, tungro, sheath blight and blight whereas the column refers to the accuracy in detecting the disease in rice crop.

B. Model Accuracy

The final model achieved an accuracy of over 90% on the test dataset. This high level of accuracy demonstrates the model's ability to correctly classify most of the crop disease in the given dataset of thousands of images.

FIG 4.3.2 MODEL ACCURACY

C. Precision and Recall

The precision and recall that are assessed ranges from 85% to 92% for these five diseases. Blast and blight diseases were with high recall and precision compared to other diseases. This model is tuned to identifying diseases with minimal errors.

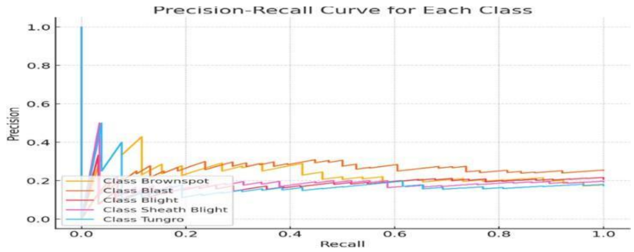

FIG 4.3.3 PRECISION AND RECALL CURVE

D. Confusion Matrix

Through detailed class comparison with this confusion matrix is to reveal how frequently the model mistakes true classes with incorrect ones. The model's performance can be visually evaluated to identify strong classification areas and problematic regions.

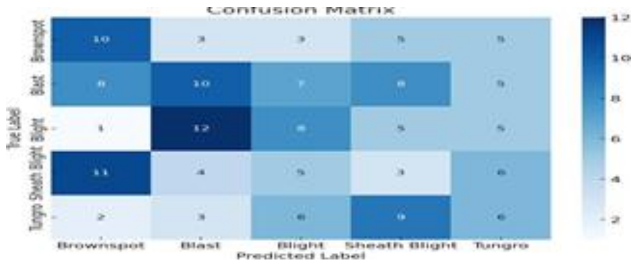

FIG 4.3.4 CONFUSION MATRIX

In the above figure true positives are indicated in dark and false positives in the lighter shade.

E. Receiver Operating Characteristic (ROC) Curve and Area Under the Curve (AUC)

The ROC curve for the chosen five categories of diseases shows high AUC values, with most diseases achieving an AUC greater than 0.90, indicating the model's excellent discriminatory ability.

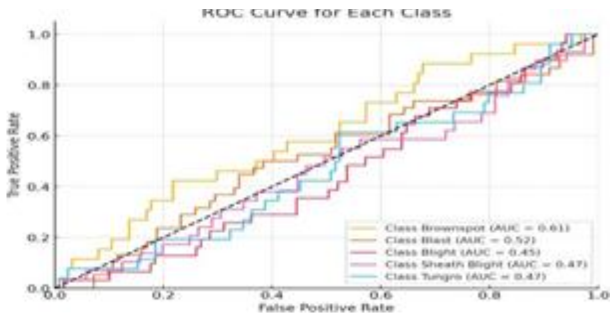

FIG 4.3.5 ROC CURVE

The ROC curve for the chosen five categories of diseases shows high AUC values, with most diseases achieving an AUC greater than 0.90, indicating the model's excellent discriminatory ability. This shows that the model is highly effective at distinguishing the positive and negative instances of each disease.

F) Model Testing

Following training, the model is able to predict disease on the rice crop using the dataset provided. The model is evaluated for generalization performance on a test dataset that it did not train on. The test dataset consists of images that were not available during training, which gives the model's real-world performance a better assessment.

FIG 4.4.1 INPUT- RICE CROP IMAGE WITH TUNGRO DISEASE

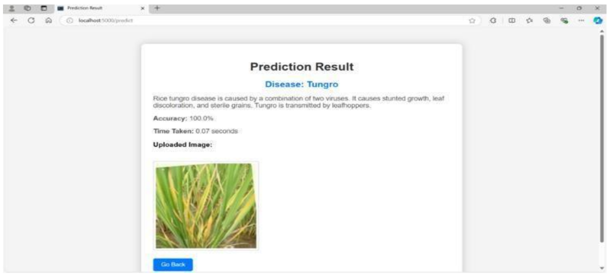

FIG 4.4.2 OUTPUT - DISEASE PREDICTED CORRECTLY AS TUNGRO

G) Model Deployment

The trained model is deployed during the final step of the methodology to function in real time. Flask framework enables the deployment of the trained model into a web application so that users can upload crop leaf images and get instant disease identification predictions. The system features an intuitive interface that helps agricultural experts and farmers to interact with the model and utilize its predictions for informed decision-making.

V. CONCLUSION AND FUTURE WORK

A) Conclusion

Convolutional neural networks (CNNs) and long short-term memory (LSTM) networks were combined in this study to create a hybrid deep learning system that improved crop disease detection with images of rice crop plant leaves. The model successfully captures temporal dependencies from features extracted by CNN and LSTM. This model enables accurate classification of five major crop diseases such as Brownspot, Blast, Blight, Sheath Blight, and Tungro. This system demonstrated high accuracy, precision, recall, and F1-scores, outperforming traditional models by integrating both spatial and temporal analysis for more complex predictions.

B) Future Work

Future research emphasize improving the robustness of the model to such variations by increasing the dataset to cover images with a wider range of conditions. Additionally, future research could consider extending the hybrid CNN-LSTM architecture to include a broader array of crops and diseases. Trained on more diverse data, the system could be a one-size-fits-all tool with utility across various crops and regions. Finally, bringing the model into actual deployment in applications such as mobile apps for farmers or drone-monitoring systems will be the critical step to seeing the applied value in this research.

ACKNOWLEDGMENT

The authors thank our institution Builders Engineering College, Head of the department Dr S.D. Prabu Ragavendran, Project Co Ordinator Mr. S. Gopinath, Guide Dr S. Satishkumar and the other members who supported us to successfully complete this research paper.

REFERENCES

[1] Ravindra Gahane, Rajani P.K, Prerna Mhaisane, Atharva Tundalwar, “Rice Leaf Disease Detection and Remedies Using Deep Learning” 2024, International Journal.

[2] Dr. Rajani P.K, Dr. Vaidehi Deshmukh., “Rice Leaf Disease Detection using Convolutional Neural Network” 2023, International Journal on recent and innovation trends in computing and communication.

[3] Hongwei Ning, Sheng Liu, Qifei Zhu and Teng Zhou, “Convolutional neural network in rice disease recognition: accuracy, speed and lightweight” 2023 Frontiers.

[4] Pallapothala Tejaswini, Priyanshi Singh, Monica Ramchandani, “Rice Leaf Disease Classification Using CNN” 2022, IOP Conf. Series: Earth and Environmental Science 1032 012017.

[5] Zhang, J., “Deep Learning for Automated Image-based Crop Disease Detection: A Review” 2021, IEEE Access.

[6] Mallick, P., & Sarkar, A., “Using Recurrent Neural Networks for Time-Series Crop Yield Prediction” 2021, Computers and Electronics in Agriculture.

[7] Saha, H., “IoT-based Crop Health Monitoring System Using Drones” 2021, Journal of Agricultural Informatics.

[8] Sharma, A., & Gupta, P., “Enhancing Crop Disease Classification with Transfer Learning and Hybrid CNN-LSTM Models” 2021, International Journal of Computer Vision.

[9] Lu,Y., Yi,S., & Zeng, L., “Disease Detection in Tomato Leaves Using Hybrid CNN- RNN Models” 2020, IEEE Access.

Segmentation of Lungs in Chest X-Ray Images using Multi-Scale Deep Neural Networks

Arjun Paramarthalingam
Computer Science and Engineering, University College of Engineering,
Villupuram 605103, India
arjun_ucev@ymail.com

Sindhuja Sundaresan
Computer Science and Engineering, Surya Group of Institutions,
Vikravandi, Villupuram 605103, India

Shanmugam Sundaramurthy
Computing Technologies, SRM Institute of Science and Technology, Kattankulathur Campus,
Chengalpattu, 603203, India

Thabeswar Arulmurugan
Computer Science and Engineering, University College of Engineering,
Villupuram 605103, India.

Amirthasaravanan Arivunambi
Computer Science, Pondicherry University,
Puducherry 605014, India

***Abstract*—Chest X-ray (CXR) is a cost-effective imaging technique widely used in medical diagnosis of lung related diseases. The approach presented in this paper uses multi scale feature extraction based generative adversarial networks (M-GAN) to perform an accurate lung segmentation task on CXR images. The M-GAN approach extracts the multi scale features from the CXR, which includes two major parts generator and discriminator. The features of dense abnormalities in lungs are learned by generator module and size invariance of dense abnormality is achieved by repetitive down-sampling then by up-sampling process. The output of generator is segmentation map, it is useful to overcome the under-segmentation and over-segmentation problems during the lung segmentation processes. The discriminator module used convolutional neural network (CNN) which predicts weather the input lung image is real or fake. The input of the discriminator module is segmentation map generated by the generator module, or the ground truth image with lung mask. The results of adversarial loss value is updated to generator through discriminator module. The performance of proposed segmentation network is assessed by two widely accepted evaluation parameters such as intersection over union (IOU) and dice similarity coefficient (DSC). For experimental analysis, publicly available Chest X-Ray Images dataset is used and the performance of M-GAN is compared with state-of-the-art approaches in the field of lung segmentation.**

Keywords—Lung Segmentation; Computer Aided Diagnosis; Deep neural Networks; Chest X-Ray Images; Generative Adversarial Networks

I. Introduction

Medical imaging is an ever growing research area, it imaging the internal parts of a human body for scientific evaluation and clinical intervention, in addition to visible illustration of some organs or tissues. The magnetic resonance imaging (MRI), computerized tomography (CT), positron emission tomography (PET), X-rays and ultrasound imaging techniques provide useful information to computer aided diagnosis (CAD) systems. The role of CAD systems plays vital role in medical imaging than ever before with the developing capabilities of modern technologies [1]. Nowadays, for better understanding the clinical conditions of a patient, the physicians and health care professionals uses CAD system which helps in diagnosis of various diseases. The Chest X-ray (CXR) films were used by doctors in early diagnosis for any lung related diseases [2]. Thus, a CXR film becomes familiar method in diagnosis process and it visualize structure of the organ inside the thoracic area in the body [3]. To diagnose diseases in chest, for example ling diseases, X-ray is a popular and economical imaging technique than CT scans, MRI and PET scans [4]. For extracting useful information from an X-ray, CT or MRI, the conventional method is a radiologist who can examine manually, which consumes more time to get the results and increases diagnostic workloads in COVID-19 pandemic like situations [5].

Machine learning or deep learning approaches accurately predicts the results by learning the available input data given from the user. The automatic CAD system with deep learning approach helps in reducing the workload of health care professionals by speeding up the diagnosis process. One of the major goals for developing the computer programs is to perform accurate prediction of diseases and its severity [6]. The crucial objective is to find boundaries of the lung accurately, to diagnosis the critical disease like pneumonia, pulmonary abnormalities and tuberculosis [7]. The ILD diseases are caused by collection of dense abnormal cells in lung parenchyma [8]. The ILD diseases creates breathing problems and also causes scarring of lung tissues. Moreover, dense abnormal patterns present in the lung due to the ILD diseases are difficult to localize because which have similar intensity as of normal chest region. Thus, the presence of these tissues causes inaccurate segmentation of lungs. Most of the existing methods ignore the dense abnormal cells in lung tissues during segmentation process, which leads to reduced accuracy in segmentation results [9].

To quickly and accurately find and diagnose lung diseases like pneumonia, tuberculosis, and lung cancer, it is necessary to accurately divide lung region in CXR images. Using the power of multi-scale deep neural networks to solve the difficult problem of lung segmentation in chest X-ray pictures is what inspires this work. It tries to get both local and global contextual information by using multi-scale features. This makes it better at correctly defining lung boundaries even when there are difficult image features. To make lung segmentation faster and more accurate for doctors, the final goal is to give them a reliable and useful tool for doing it automatically. When doctors look at chest X-rays, accurate and timely segmentation can really help them figure out what the images mean. This can lead to better patient results by finding and treating respiratory diseases earlier. Computer-aided diagnosis systems are always being improved, and this study adds to those efforts. In the end, this work multi-scale feature extraction based generative adversarial network (M-GAN) is proposed for accurate lung segmentation will help both doctors and patients manage their respiratory health.

II. RELATED WORKS

Lung segmentation is one of the significant applications of automatic CAD systems used in medical image analysis. It is an ever-growing research area, many authors investigated in this field for precise results. The detailed study about various authors on automatic CAD was performed in the literature [1, 6, 7]. The simple grey-level thresholding techniques were used in early days to distinguish between normal region and affected region of the lungs, but these approaches are insufficient for classification and detection of lung region with dense abnormalities.

The conventional intensity-based approaches for automatic lung segmentation have been used by researchers in this field [10, 11]. The robust feature extraction is critical for the success of intensity-based lung segmentation approaches. Hosseini-Asl et al used a computer program to extract the relevant features using a nonnegative matrix factorization (NMF) process, with a standard k-means series for segmentation [10]. In addition, the authors in [11] added ascending barriers to the NMF-based approach to 3D pulmonary differentiation. The inclusion of input data in the basic *W* matrix and the coefficient matrix *H*, which aids in factor selection, is the key principle behind the success of NMF in classification [12]. In the event of irregular plumbing skin patterns, this methods [10, 11] successfully insert juxtapleural nodules and pulmonary vessels. Because of the uncontrolled aspect of the NMF algorithm, it has been unable to recognise irregular lung tissue patterns effectively.

Recently the neural networks has been tested in computer vision applications over the past fifteen years. Numerous CNN-based methods for imaging research in medicine and real world applications have been investigated by many authors [13-21]. Simonyan et al. [13] presented the benefits of using tiny convolution filters for image identification. In general, selection of optimal filter size is challenging task of deep network design. There is no such thing as a standard ground rule for determining the best filter size combination. Szegedy et al. [14] suggested a definitive filtering solution bank, as a solution to this issue, it permit the model to select optimum network architecture. Later, Huang et al. [15] suggested DenseNet, they followed function map re-use principle to build compact and simple-to-train models. ResNet, on the other hand is a residual learning strategy for extending deep neural networks independent of the factors such as depth and parameter count, was proposed by Yena et al. [16]. They established the notion of map ownership to solve gradient disappearance problem. A method for the lung module segmentation from CT images was designed by Singadkar et al. used end-to-end network training and capturing various types of bumps from a variety of 2D CT images using Deep Deconvolutional Residual Network (DDRN) [17]. Researchers looked into the usage of a convolution network for the neural processing of lung CT scan data. Harrison et al. [18] has been suggested to use a multi-path network to diagnose lung diseases. They learned various types of ILD tissue patterns using the potential of an in-depth network. A smaller CNN model is also suggested in [19] to divide the extruded pool into pulmonary and non-pulmonary regions. Its effectiveness is restricted to the local area only, and it is unable to get rid of high-intensity irregular patterns in the lung region. This drawback is overcome by Negahdar et al. [20], they suggested 3D lung volume distribution network segmentation, which was inspired by volumetric convolutional neural network (V-net) [21].

After the development of GAN-based deep learning models [22], it demonstrates good efficiency in exploiting the discrepancy between produced image and ground truth image for image segmentation applications. The GAN based segmentation is not only used in lung segmentation, it also used various medical diagnosis applications viz. eye, brain and liver images [13, 14, 16]. Luc et al. [23] suggested a semantic segmentation approach using GAN network. Their approach used GAN to identify and fix higher-order discrepancies between the generated and ground truth images. In order to distinguish between segmentation maps made by the generator network and the segmentation maps produced by the ground truth, the model trains both segmentation and adversarial network. Zhou et al. [24] suggested a hybrid fusion network, which is a modification of the productive network that can be used to create MR synthetic images. The authors in [25] proposed an approach for mono or multi-modal image registration performed on MRI scans of brain images. The GAN system was also trained for the classification of liver images [26].

III. PROPOSED WORK: LUNG SEGMENTATION USING M-GAN

A deep learning based generative model known as the Generative Adversarial Network (GAN) has the ability to produce astonishingly photorealistic outcomes on a number of image synthesis and image-to-image translation tasks. The working of GAN is like a dual player min-max game, in which generator module produced realistic looking data, whereas discriminator need to identify it is real or fake. The activities of both generator and discriminator are iteratively performed with optimized parameters to reach the final stage. At final stage the discriminator is not able to differentiate between realistic looking data from the generator and the real ground truth data. In general, GANs are using different types of model architecture for training generative models, and in this design, convolutional neural networks, or CNNs for short, are the most often used deep learning models. The workflow diagram of GAN is illustrated in figure 1.

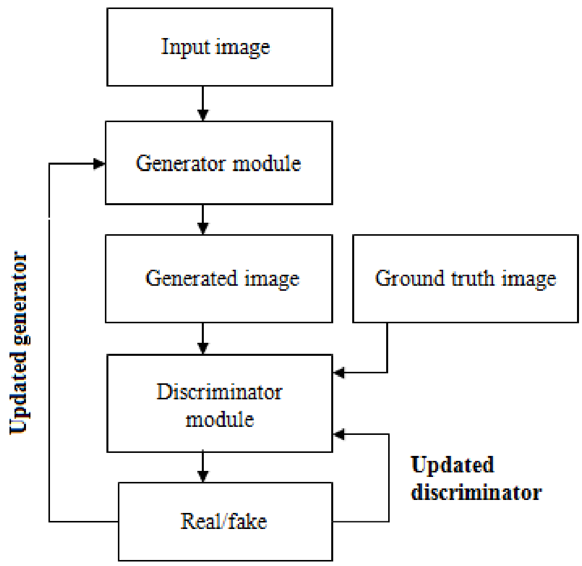

FIG.1. FLOW DIAGRAM OF GAN

The GANs are a smart technique for training a generative model by framing the task as supervised learning with two sub-modules: the generator module that we have to train to produce new instances and the discriminator module that attempts to identify examples as either real (from dataset) or false (generated). That differs significantly from "typical" neural network model training, which involves minimizing loss to a small number of convergence variables. This paper extended the idea of LungSeg-Net [8] by introducing multi-scale feature extraction using M-GAN. The working of M-GAN with layered representation is shown in figure 2.

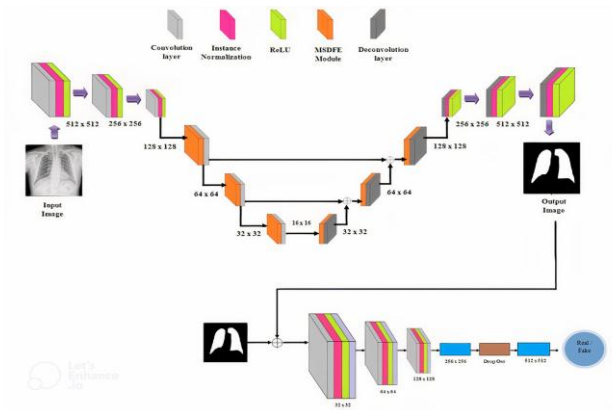

FIG.2. SCHEMATIC DIAGRAM OF M-GAN SEGMENTATION.

3.1 Generator:

The generator network is made up of three blocks: an encoder, a multi-scale feature extraction block, and a decoder block. This network is able to extract multi-scale data and choose its best path to the dense connection, which also aids in precise lung segmentation results. Each inception block processes the input feature maps using three convolution layers with filter sizes of 1 x 1, 3 x 3, and 5 x 5 respectively. The operation of inception block is mathematically represented as follows:

$$\sum_f^{ws} = \Gamma(\eta(\sum_{k=1}^{f}(\varphi_k * w_{k,s}))) \quad \text{... (1)}$$

The given sentence describes the following: * is a convolution operation, φ is the input to the inception block with k feature maps, ws is the convolution filter with a spatial size of s × s and f channels, η is the instance normalisation, and φn is the response of the convolution layer and the normalised feature response as well. Γ stands for the rectified linear unit, often known as ReLU.

3.2 Discriminator

The discriminator network has three convolutional layers, three batch normalisation layers, three average pooling layers, and two fully connected layers with dropout. In order to improve the lung segmentation's accuracy, discriminator computes the loss function value and updates the generator. The formula for calculating the loss function is given below.

$$L_{L1loss} = E_{a,b,c} \mid b - G(a, c) \mid \quad \text{...(2)}$$

Where ‘a’ is the conditional variable, ‘b’ is the real sample and ‘c’ is the random noise.

IV. EXPERIMENTAL SETUP AND DATASET DESCRIPTION

In this section, the performance of proposed method is tested on medical images in preparation for clinical use. All of the experiments were carried out on a regular PC with an AMD PRO A4-3350B APU Radeon R4 Graphics 2.00GHz processor and 4GB of RAM. Python's popularity and built-in libraries led to its selection as a programming language. The overview of the CXR dataset [27] and their specifications are shown in Table 1.

TABLE 1. CXR IMAGES (PNEUMONIA) DATASET SPECIFICATIONS

Purpose/Task	Normal	Pneumonia	Image specification
Training Set	1341	3875	Image format: JPEG Image size: 2048 × 2048 pixels
Testing Set	234	390	
Validation Set	8	8	
Total Images	**1583**	**4273**	

From the experimental setup, Chest X-Ray Images (Pneumonia) dataset, 5216 images were used for training and 624 images were used for testing. For all the experiments, same number of epochs i.e., 20 is used. Two metrics, called DSC and IOU are calculated in order to assess performance of our suggested segmentation network. Dice similarity coefficient and IOU are defined as:

$$DSC = \frac{2 \mid G(a) \cap b \mid}{\mid G(a) \mid + \mid b \mid} \quad \text{... (3)}$$

$$IOU = \frac{DSC}{2 - DSC} \quad \text{... (4)}$$

Where *G(a)* and *b* represents the generator output and the lung segmentation map's ground truth respectively. The figure 3 shows segmentation results of two different CXR images to illustrate accurate segmentation of lung region. Performance comparision using DSC and IOU Metrics are given in Table 2.

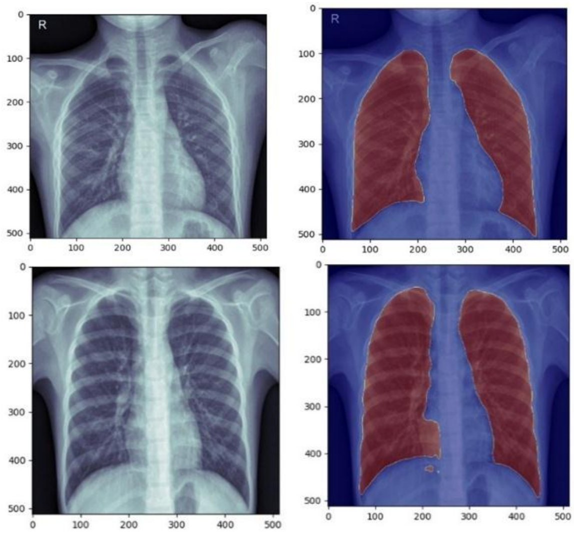

FIG.3. INPUT X-RAY IMAGES AND SEGMENTED REGION OUTPUT IMAGES

TABLE 2. PERFORMANCE COMPARISION USING DSC AND IOU

Method	Dataset	DSC	IOU
NMF [11]	3D CT Images	0.7681	0.5996
VGG16 [14]	ImageNet	0.7898	0.6530
Unet [15]	CIFAR, ImageNet	0.7729	0.6903
Resnet [17]	LIDC/IDRI	0.8056	0.7018
Proposed Method	Chest X Ray Images	**0.8300**	**0.710**

V. CONCLUSION

This research presents a novel approach for lung segmentation using GANs and multi-scale dense feature extraction. The multi-scale dense feature extraction module effectively identifies lung nodules and other lung tissue patterns. Iterative down-sampling and subsequent up-sampling are used to minimize the size dependence of dense abnormalities, enhancing efficiency and accuracy. The CXR Images (Pneumonia) dataset is used to analyze lung tissue patterns. The study assessed the accuracy of the segmented lung portion using two evaluation criteria: intersection over union and dice score coefficient. The results demonstrate superior enhancement in lung segmentation accuracy for all instances of lung diseases. Future work will focus on applying the technique to multi-modality MRI images, enhancing the overall effectiveness of medical image analysis.

REFERENCES

[1] Kunio Doi, "Computer-aided diagnosis in medical imaging: Historical review, current status and future potential", Computerized Medical Imaging and Graphics, Vol. 31, No. 4-5, pp. 198-211, 2007.

[2] Justin Ker, Lipo Wang, J. Rao and Tchoyoson C. C. Lim, “Deep Learning Applications in Medical Image Analysis”, IEEE access, Vol. 6, pp. 9375–9389, 2018.

[3] Sangheum Hwang, Hyo-Eun Kim, Jihoon Jeong M.D., and Hee-Jin Kim, “A novel approach for tuberculosis screening based on deep convolutional neural networks”, in. SPIE, Medical Imaging 2016: Computer-Aided Diagnosis, Vol. 9785, pp. 97852W–97852W–8, 2016.

[4] Laurens Hogeweg, Clara I Sánchez, Pragnya Maduskar, Rick Philipsen, Alistair Story, Rodney Dawson, Grant Theron, Keertan Dheda, Liesbeth Peters-Bax and Bram van Ginneken, “Automatic Detection of Tuberculosis in Chest Radiographs Using a Combination of Textural, Focal, and Shape Abnormality Analysis.” IEEE Transactions on Medical Imaging vol. 34, No.12, pp. 2429-2442, 2015.

[5] Nandhini Abirami, Durai Raj Vincent and Seifedine Kadry, "P2P-COVID-GAN: Classification and Segmentation of COVID-19 Lung Infections From CT Images Using GAN", Source Title: International Journal of Data Warehousing and Mining (IJDWM), Vol. 17, No. 4, 2021, pp. 101-118.

[6] R. A. Castellino, “Computer aided detection (CAD): An overview”, Cancer Imaging, Vol. 5, No. 1, 2005, pp. 17-19.

[7] S. Worthy “High resolution computed tomography of the lungs”, BMJ (Clinical research ed.) Vol. 310, No. 6980, pp. 615-616, 1995.

[8] Swati P. Pawar and Sanjay N. Talbar, "LungSeg-Net: Lung field segmentation using generative adversarial network", Biomedical Signal Processing and Control, Volume 64, 2020, ISSN 1746-8094, 2020.

[9] G. Singadkar, A. Mahajan, M. Thakur and S. Talbar, “Automatic lung segmentation for the inclusion of juxtapleural nodules and pulmonary vessels using curvature based border correction”, Journal of King Saud University - Computer and Information Sciences, Vol. 33, No. 8, 2018, pp. 975-987.

[10] Ehsan Hosseini-Asl, Jacek M. Zurada, Georgy Gimel’farb and Ayman El-Baz, “3-D Lung Segmentation by Incremental Constrained Nonnegative Matrix Factorization”, IEEE Transactions on Biomedical Engineering, Vol. 63, No. 5, pp. 952–963, 2016.

[11] Ehsan Hosseini-Asl, Jacek M. Zurada and Ayman El-Baz, “Lung segmentation based on nonnegative matrix factorization”, IEEE International Conference on Image Processing (ICIP), IEEE, pp. 877–881, 2014.

[12] Daniel D. Lee and H. Sebastian Seung, “Learning the parts of objects by non-negative matrix factorization”, Nature, Vol. 401, pp. 788–791, 1999.

[13] Karen Simonyan and Andrew Zisserman, “Very deep convolutional networks for large-scale image recognition”, arXiv:1409.1556v6, 2015, pp. 1-14.

[14] Christian Szegedy, Wei Liu, Yangqing Jia, Pierre Sermanet, Scott Reed, Dragomir Anguelov, Dumitru Erhan, Vincent Vanhoucke and Andrew Rabinovich, “Going deeper with convolutions”, IEEE Conference on Computer Vision and Pattern Recognition, 2015, pp. 1–9.

[15] Gao Huang, Zhuang Liu, Laurens Van Der Maaten and Kilian Q. Weinberger, “Densely connected convolutional networks”, IEEE Conference on Computer Vision and Pattern Recognition, pp. 4700–4708, 2017.

[16] K Kaiming He, Xiangyu Zhang, Shaoqing Ren and Jian Sun, “Deep residual learning for image recognition”,

IEEE Conference on Computer Vision and Pattern Recognition, pp. 770–778, 2016.

[17] G Ganesh Singadkar, Abhishek Mahajan, Meenakshi Thakur, and Sanjay Talbar, "Deep deconvolutional residual network based automatic lung nodule segmentation", J. Digit. Imaging, Vol. 33, No. 3, pp. 678–684, 2020.

[18] Adam P. Harrison, Ziyue Xu, Kevin George, Le Lu, Ronald M. Summers and Daniel J. Mollura "Progressive and multi-path holistically nested neural networks for pathological lung segmentation from CT images", Vol. 10435, pp. 621-629, 2017.

[19] M Mingjie Xu, Shouliang Qi, Yong Yue, Yueyang Teng, Lisheng Xu, Yudong Yao and Wei Qian, "Segmentation of lung parenchyma in CT images using CNN trained with the clustering algorithm generated dataset", Biomedical Engineering Online, Vol. 18, 2019.

[20] Mohammadreza Negahdar, David Beymer and Tanveer Syeda-Mahmood "Automated volumetric lung segmentation of thoracic CT images using fully convolutional neural network", Medical Imaging, Vol. 10575, 2018.

[21] Fausto Milletari, Nassir Navab and Seyed-Ahmad Ahmadi, "V-Net: Fully convolutional neural networks for volumetric medical image segmentation", Fourth International Conference on 3D Vision (3DV), pp. 565–571, 2016.

[22] I. Goodfellow, J. Pouget-Abadie, M. Mirza, B. Xu, D. Warde-Farley, S. Ozair, A. Courville, and Y. Bengio, "Generative Adversarial Nets", International Conference on Neural Information Processing Systems, Vol. 2, pp. 2672-2680, 2014.

[23] Pauline Luc, Camille Couprie, Soumith Chintala and Jakob Verbeek, "Semantic segmentation using adversarial networks", arXiv preprint arXiv: 1611.08408.

[24] Tao Zhou, Huazhu Fu, Geng Chen, Jianbing Shen and Ling Shao, "Hi-Net: Hybrid-fusion Network for Multi-modal MR Image Synthesis", IEEE Transactions on Medical Imaging, Vol. 39, No. 9, pp. 2772-2781, 2020.

[25] Jingfan Fan, Xiaohuan Cao, Qian Wang, Pew-Thian Yap and Dinggang Shen, "Adversarial learning for mono- or multi-modal registration", Medical Image Analysis, Vol. 58, No. 101545, 2019.

[26] Dong Yang, Daguang Xu, S. Kevin Zhou, Bogdan Georgescu, Mingqing Chen, Sasa Grbic, Dimitris Metaxas and Dorin Comaniciu, "Automatic liver segmentation using an adversarial image-to-image network", International Conference on Medical Image Computing and Computer-Assisted Intervention, Cham, pp. 507-515, 2017.

[27] Chest (CXR) X-Ray Images dataset: https://www.kaggle.com/paultimothymooney/chest-xray-pneumonia (Accessed on February 2024).

AI and IoT based Integration for Crop Damage Protection and Animal Deterrent System

S. Dinesh
Department of Information Technology,
Thiagarajar College of Engineering,
Madurai.
dineshsankar8110@gmail.com

M. Amirtha Velan
Department of Information Technology,
Thiagarajar College of Engineering,
Madurai.
mamirthavelan2412@gmail.com

S. Sridevi
Associate Professor,
Department of Information Technology,
Thiagarajar College of Engineering,
Madurai.
sridevi@tce.edu

G. Kishore
Department of Information Technology,
Thiagarajar College of Engineering,
Madurai.
kishorepq@gmail.com

Abstract **—The presence of animals and birds creates major disruptions for farmers because these species invade crop areas while trampling the plants and consuming them. Electric fences and scare devices used traditionally do not work well as farm protection measures while causing damage to ecosystem health. The proposed system presents an automatic agricultural protection framework equipped with exact animal detection technology accompanied by adaptive defense components. The field deployment of PIR sensors operates as motion detectors to activate real-time camera video recording functions. The detection made by YOLO v12 leads to the switch-on of appropriate deterrent tools like ultrasonic sound emitters or flashing lights or ground vibration units according to the identified species. The deterrents function through electricity supplied by solar power. The entry of animals into the field activates alarms which activate ultrasonic frequencies precise to different species alongside multiple forms of repellents for effective pest control. Results indicate that the protected system guards agricultural produce from harm without causing harm to native wildlife populations.**

Keywords — motion detectors, Animal Detection, YOLO algorithm, PIR sensors, Ultrasonic repellents, Smart farming.

I. Introduction

Farmers face a lot of difficulties in protecting their crops. One such difficulty encountered by most of the farmers is the tendency of crop damage [9] due to animal activities. It causes excessive damage to crops and financial losses for farmers. Animals such as elephants, wild boars, monkeys, and birds often intrude the farmlands, eat up and trample the crops which causes economic loss as well as emotional distress for farmers. In some regions, it entirely affects the rural poverty and disrupts the livelihoods.

Traditional methods such as the use of electric fences, scarecrows, and chemical repellents are proven to be inefficient and harmful for the environment as well. Electric fences pose a huge threat to the lives of animals and dangerous for humans as well. Moreover, these solutions require a number of labors, and they are expensive to maintain. Also, in remote areas where there are no electrical power, it's a headache for farmers to set up these deterrent mechanisms. Therefore more effective and sustainable approach is needed.

With the help of machine learning and IoT, there are new opportunities in front of us to overcome these challenges. This research presents a new self-driven system that had incorporated use of modern technology for prevention of crop damage [9] by animals. The system utilizes a network of Passive Infrared (PIR) sensors placed within the field to help sense animal movement. On its detection, real-time cameras are activated to capture footage of the intruder. Using the YOLO v12 object detection algorithm, the details of the images are processed which accurately identifies the species of the animal. Depending on the species identified, the system uses specific repellent measures, such as ultrasonic frequencies, light repellents, or ground vibrators, depending on the observed animal species.

II. Literature Review

Crop protection from wildlife intrusions has been an area of significant research, particularly in regions where human-wildlife conflicts pose challenges to agricultural productivity. Various approaches leveraging sensors, microcontrollers, and repellent systems have been explored to mitigate crop damage [9]. This section reviews three recent studies related to the use of technology in addressing this issue.

[1] PIR Sensor and Camera-Based Detection System

In this study, animal detection through Passive Infrared (PIR) sensors in combination with cameras makes up the system is described. The research approach follows our methodology yet we added two essential features to our work**.** Energy Efficiency, **t**he implementation of solar panels [8] in our system allows remote locations to benefit from sustainable power supply when standard power resources are scarce. Optimized Detection Process, The PIR sensor controls the camera activation through a detection of movement which simultaneously decreases power usage and minimizes processing workload. Ultrasonic transmitters and Ground Vibrators, our anti-rodent system transmit ultrasonic sounds [6] that are allergic to animals. It also includes production of floor vibrations for pest repelling function.

The ground vibrators function effectively to repel rodents from the field.

The following hardware components and algorithms includes all necessary elements for detecting and classifying the species of different animals entering the crop field.

[2] Smart Irrigation and Animal Detection System

An analysis is presented about how smart irrigation systems operate with animal detection [5] mechanisms. The system makes use of soil moisture sensors and infrared sensors for detecting animals intruding into fields while also monitoring soil conditions. The system activates speakers through which the system plays animal sounds which cause animals to flee. Additionally, a GSM module alerts farmers about field conditions and intrusions.

This work establishes irrigation systems and notifies farmers but its animal protection strategies do not specify individual species types or methods for deterrence. Our project uses the YOLO v12 object detection algorithms to identify wildlife species accurately thus enabling the deployment of tailored deterrents including ultrasonic sounds and lights and vibrations on the ground surface. Complete automation takes over most operations in our system which eliminates the need for direct farmer involvement.

III. System Design And Methodology

The system infrastructure features PIR sensors deployed in a sensor network for identifying animal intrusion. The system identifies different species through YOLO v12 using real-time camera inputs. The microcontroller functions by processing information received from sensors while controlling all deterrent operation. The system utilizes automatic animal deterrence mechanisms to stop damage of crops. The system implements its primary goal to defend crops from bird [7] and animal attacks without ruining wildlife populations. The system has three different repellents namely ultrasonic sound emitters, light repellents, and ground vibrators which operate according to detected animal types.

A. PIR sensors

The crop field is equipped with Passive Infrared (PIR) sensors which detect any movement generated by animals. The sensors activate the system through detecting infrared signals from animal body heat when animals move inside the monitored zone. The sensors located in the fields transmit data to the main processor which confirms that an animal is present.

B. Camera

The PIR sensors activate the real-time cameras after detecting any movements. The intruding animal triggers the microcontroller to receive live camera footage captured from the surveillance cameras. The camera placement enables full field observation coverage.

C. Microcontroller

The processing unit analyzes inputs from both the PIR sensors as well as cameras to identify animal presences while determining animal types for the device. Real-time animal identification operates through the YOLO v12 algorithm that processes camera input data with the help of the microcontroller.

Motion Detection:

D. Microcontroller

The microcontroller operates as the main processing element of the overall system framework. The processing unit analyzes inputs from both the PIR sensors as well as cameras to identify animal presences while determining animal types for the device. Real-time animal identification operates through the YOLO v12 algorithm that processes camera input data with the help of the microcontroller.

E. Deterrent Mechanisms

Ultrasonic Sound Emitters:

High frequency sound waves [6] from the devices create an irritating noise detectable only by animals which humans cannot hear. The device activates different frequencies which it selects according to the recognized animal.

Light Repellents:

Wild boars and other nocturnal animals flee from the field because of bright and flashing lights used for deterrence.

Ground Vibrators:

Ground-based devices that emit vibrations to deter small animals like rodents. About the time the ground vibrations shake their bodies until they lose their equilibrium and decide to abandon their habitat.

E. YOLO v12 Algorithm

Real-time object detection occurs through the deployment of You Only Look Once (YOLO) v12 algorithm. The YOLO v12 model processes video images acquired from surveillance cameras for detecting animal intrusions. The choice of YOLO v12 detection solution happened because it demonstrates fast processing and reliable results that function optimally under dynamic real-time situations.

F. Decision-Making Logic

The microcontroller detects the animal species before activating the decision-making process to select proper deterrent systems. The system plays ultrasonic sounds [6] for elephant detection and activates rodent ground vibrators depending on identified animals.

The system incorporates motion detection as its first step while image classification follows to enable automated defences as the final component for stopping wildlife from damaging crops. The system functioning process appears in Fig 1.

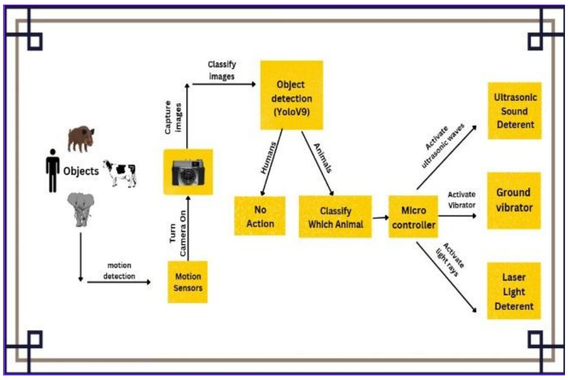

FIG 1: SYSTEM WORKFLOW

The system detects any moving object inside the agricultural field through embedded motion sensors. The system starts camera recording through its module after motion sensors identify moving objects in the agricultural area.

1) Object Detection and Classification:

Processing of images through YOLO v12 object detection algorithm takes place. The system starts by analyzing whether the detected thing is either human or animal. The system does not activate any response when it detects a human presence. The system starts the species classification stage after identifying an animal in the detection area.

2) Species-Specific Deterrence Mechanisms:

The system engages its most suitable deterrent system after it detects which animal is present. The system produces ultrasonic sounds [6] that serve as animal repellents against selected species. Ground Vibrators produce surface tremors which both disorient and drive away particular animal species. The deterrence system activates laser light beams for repelling nocturnal animals.

IV. Implementation and Results

The process of implementing the automated wildlife deterrent system required the hardware setup followed by software integration and controlled testing of the system. The system evaluation focused on testing its performance for detecting as well as categorizing and reacting to various animal species while operating in real-time settings.

Fig 2: Switching Camera on After the Detection of PIR Sensor

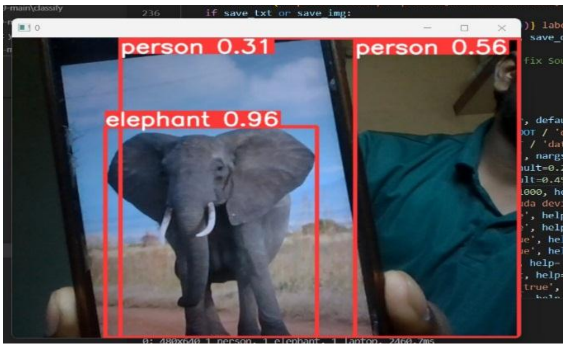

Fig 3: YOLO Model Detects Animals

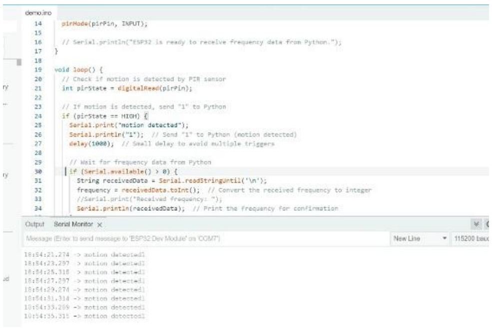

Fig 4: Detection using PIR Sensor

Fig 5: YOLO Model Detects Different Animals

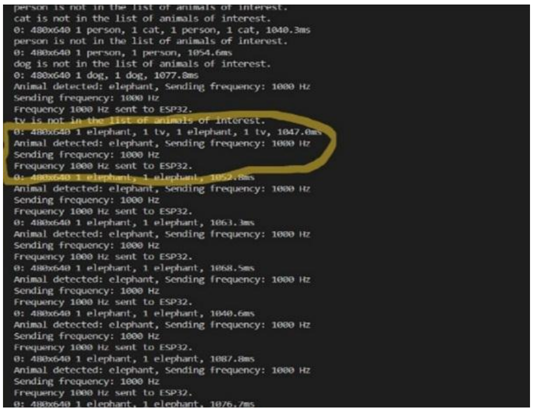

Fig 6: Transmitting Ultrasonic Frequencies

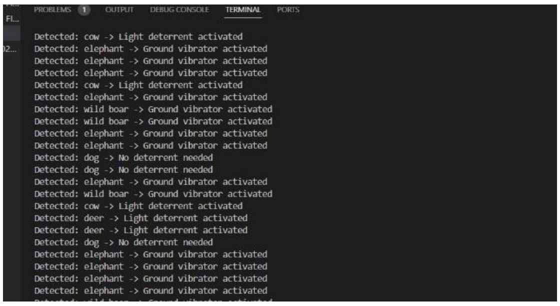

Fig 7: Activating species specific repellent

V. Results and Discussion

Our automated wildlife deterrent system performed better in experimental testing than standard systems because it achieved higher detection precision while using less energy and effectively deterred specific species.

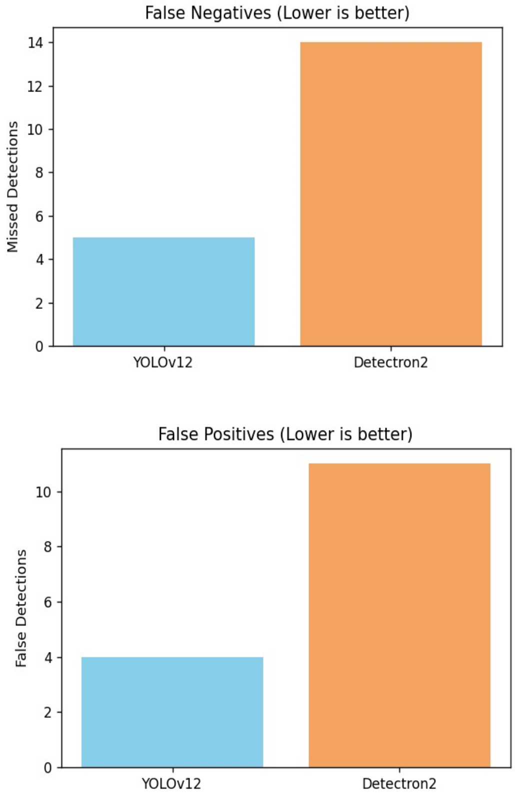

FIG 8: COMPARISON OF YOLO V9 AND DETECTRON 2

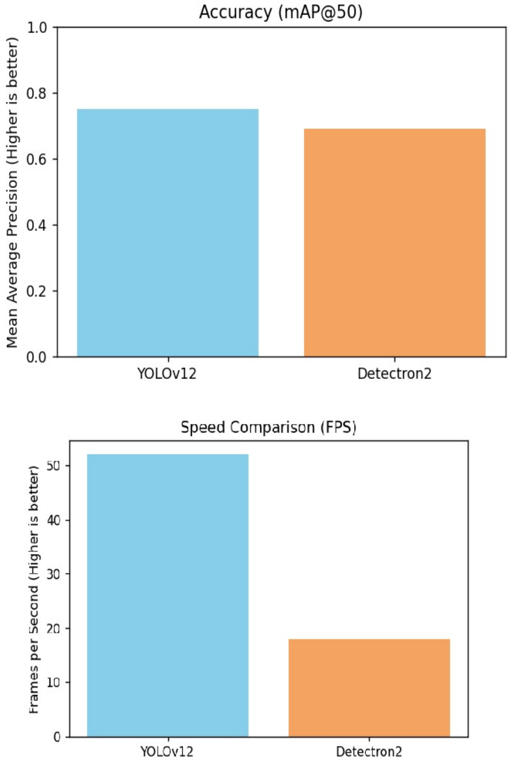

FIG 9: COMPARISON OF YOLO V9 AND DETECTRON 2

YOLOv12 [3] demonstrates superior performance to Detectron2 in terms of accuracy as well as speed and detection reliability so it represents the better option for real-time animal intrusion detection. YOLOv12 achieves better accuracy than Detectron2 thus providing enhanced correct animal recognition capabilities in the wild. The exceptional frame rate and performance of YOLOv12 makes it superior for time-sensitive real-time scenarios because it outpaces Detectron2 in speed. Due to its superior design YOLOv12 detects genuine animal encounters less often than other models thus improving system reliability. Detectron2 demonstrates a superior ability to overlook animal presence which creates potential security threats for the agricultural field. The research findings justify the use of YOLOv12 in the proposed system because it offers better speed and accuracy and dependability in intrusion detection when compared with Detectron2.

Stefano Giordano [3] focuses on criticizing the substandard performance and moral problems connected to conventional deterrent tools including electric fences and gas cannons as well as chemical repellents. Our method solves these problems through its non-invasive and environmentally-friendly method.

REFERENCES

[1] B. Diwakar, K. Jahnavi, D. Ramya, A. S. Reetushri, and G. Kirana Kumar, in Animal Intrusion Detection and Repellent System, Journal of Emerging Technologies and Innovative Research (JETIR), vol. 10, no. 4, pp. 146–151, Apr. 2023.

[2] C. L. Sudheer, K. Kaveri, M. Kavya, G. K. Nath, P. M. Javeed, and B. N. Kumar in Crop Protection and Monitoring from Animals Attacks by Using IoT Solutions, International Journal of Creative Research Thoughts (IJCRT), vol. 11, no. 3, pp. 377–384, Mar. 2023.

[3] Giordano, S., Seitanidis, I., Ojo, M., Adami, D., & Vignoli, F. (2018). IoT solutions for crop protection against wild animal attacks. 2018 IEEE International Conference on Environmental Engineering (EE), 12-14 March 2018, Pisa, Italy.

[4] C. Sun, A. Bin Azman, Z. Wang, X. Gao, and K. Ding for YOLO-UP: A High-Throughput Pest Detection Model for Dense Cotton Crops Utilizing UAV-Captured Visible Light Imagery, IEEE Access.

[5] M. Ibraheam, K. F. Li, and F. Gebali, in An Accurate and Fast Animal Species Detection System for Embedded Devices, *IEEE Access*, Mar. 2023.

[6] N. Permal, T. B. R. Segaran, R. Verayiah, F. H. Nagi, A. K. Ramasamy, and S. Ishak, for Hardware Implementation of Beam Formed Ultrasonic Bird Deterrent System, *2019 IEEE 4th International Conference on Computer and Communication System*

An Efficient and AI-Based Disease Prediction Model using a Probabilistic Classifier in the Healthcare System

A. Vanmathi B.E.,(M.E.,)
PG Scholar,
vanmathics24@gmail.com

Dr. K. Sumathi., ME., Ph.D.,
Associate Professor/CSE,
ks.cse@builderscollege.edu.in

S. Vidhya
Assistant Professor (sr/gr)/CSE,
sv.cse@builderscollege.edu.in

C. Divya Revathi
PG Scholar, Department of Computer Science and Engineering,
Builders Engineering College,
Tiruppur
divyarevathi.c@gmail.com

G. Lavanya B.E.,(M.E.,)
PG Scholar,
lavanyajesus7306@gmail.com

***Abstract*—Cardiovascular and hepatic disorders constitute two separate yet related categories of medical conditions that can profoundly affect an individual's well-being and lifestyle. The heart, a crucial organ, is responsible for circulating oxygenated blood throughout the body, while the liver performs essential functions in metabolizing and purifying various substances in the bloodstream. Cardiovascular disease, a term encompassing a variety of heart and blood vessel conditions, includes ailments such as coronary artery disease, cardiac failure, and irregular heartbeats. In contrast, liver diseases comprise a wide array of disorders that can impair hepatic structure and function, such as hepatitis, cirrhosis, and non-alcoholic fatty liver disease. We developed a predictive model for cardiovascular and hepatic disorders utilizing the Naive Bayes algorithm. This system is trained on a dataset that includes, for instance, patient information such as symptoms, medical history, and other pertinent factors from individuals diagnosed with heart disease, liver disease, or both conditions.**

Keywords—Disease Prediction, Healthcare System, Heart Disease, Machine Learning

I. INTRODUCTION

The heart plays a crucial role in the human body, circulating blood throughout the entire system. If the heart malfunctions, other vital organs, including the brain, cease to operate, leading to death within minutes.

Modern lifestyle changes, occupational stress, and poor dietary habits have contributed to an increase in cardiac disorders. Cardiovascular diseases have become a leading cause of mortality worldwide. The World Health Organization reports that heart-related illnesses account for 17.7 million deaths annually, representing 31% of global mortality. In India, cardiovascular diseases have also emerged as the primary cause of death [1]. According to the 2016 Global Burden of Disease Report, released on September 15, 2017, heart diseases claimed 1.7 million Indian lives in 2016. These conditions not only increase healthcare costs but also diminish individual productivity. World Health Organization estimates suggest that India incurred losses of up to $237 billion between 2005 and 2015 due to cardiovascular diseases [2]. Consequently, accurate and feasible prediction of heart-related illnesses is essential. Medical institutions worldwide gather extensive health-related data, which can be analyzed using machine learning techniques to derive valuable insights. However, this data is often vast and noisy, making it challenging for human comprehension. Machine learning algorithms have proven effective in recent years for accurately predicting the presence or absence of heart-related diseases by exploring these overwhelming datasets.

II. IN THE AI TECHNOLOGY

Several constraints must be considered to ensure the safe implementation of AI and its increased adoption in clinical settings. Developing machine learning models that don't perpetuate healthcare inequalities requires the creation of high-quality, representative datasets that eliminate unintended and subconscious biases. An inherent limitation of AI algorithms is their inability to account for information obtained through direct patient-physician interactions. These algorithms will never replace the personal interaction between doctors and their patients. We consider AI a supplementary tool that can significantly improve patient-provider interactions and care quality. Explainable AI refers to processes that enable humans to comprehend the output of machine learning algorithms.

2.1 Heart Disease

Heart disease, also referred to as cardiovascular disease, is a common and potentially lethal condition that affects the heart and blood vessels. It poses a significant threat to public health since it is a leading cause of disease and death worldwide. The conditions that fall under the general heading of heart disease include coronary artery disease, which is defined by the narrowing of the blood vessels that supply the heart with oxygen and nutrients; heart failure, which is characterized by a diminished ability of the heart to pump blood; arrhythmias, or irregular heart rhythms; and congenital heart defects, or birth defects of the heart. flaws in structure that are present from birth. A complex and multifaceted health problem, heart disease has both modifiable and non-modifiable risk factors.

2.2 Liver Disease

The phrase "liver disease" describes a broad and intricate medical condition that impacts the liver, one of the most vital organs in the body. The creation of essential proteins, the detoxification of harmful compounds, and the metabolism of nutrients all depend on the liver. As a result, any interference with its functioning could have a significant impact on an individual's health. Liver disease can have many different forms, including cirrhosis, fatty liver disease, hepatitis, and liver cancer. It can also have a variety of underlying causes, including viral infections, excessive alcohol consumption, obesity, and genetic predispositions. Understanding the intricacies of liver disease, its risk factors, and the importance of early detection and therapy is crucial for addressing this grave health concern.

2.3 Machine Learning

In the digital age, there is an unparalleled amount of data all around us. From our online activities to the sensors in our smartphones and the massive databases that underpin modern businesses, data has become the fundamental element of the information age. The ability to transform raw data into actionable knowledge, however, is what opens the door for the most remarkable technological advancements in history during this data-driven revolution. The core of this ground-breaking strategy is the science known as "Machine Learning." Our need to understand the vast and complex data ecosystems that define our contemporary culture is what motivates machine learning. What drives it is the recognition that traditional rule-based programming is often unable to cope with the complexity of modern scenarios.

III. TRADITIONAL METHOD OF DISEASE PREDICTION

Conventional approaches to predicting heart and liver diseases have been fundamental in diagnosing and evaluating the risk of these conditions, although they typically emphasize visible symptoms and risk factors rather than early-stage biomarkers. Heart disease prediction traditionally involves a comprehensive patient history, including lifestyle elements such as smoking habits, dietary patterns, exercise routines, and familial cardiovascular history. Physical examinations often uncover indicators like high blood pressure, irregular heart sounds, or edema in the lower extremities. Lipid profile assessments, including measurements of cholesterol (LDL, HDL) and triglycerides, are utilized to evaluate the risk of atherosclerosis. Additionally, diagnostic tools such as electrocardiograms (ECG) are employed to identify arrhythmias and ischemia, while echocardiograms provide visual data on cardiac function, revealing issues like valve dysfunction, cardiac enlargement, or fluid buildup. Stress tests, which monitor the heart's reaction to exercise or medication, can aid in predicting ischemic heart disease. While these methods are effective in detecting advanced heart problems, they may not always identify subtle signs in asymptomatic individuals or those in early disease stages. For liver disease, traditional prediction methods begin with a thorough examination of potential risk factors, such as alcohol intake, use of liver-toxic medications, viral infections (hepatitis B or C), and autoimmune disorders. Symptoms like exhaustion, unexplained weight reduction, jaundice, or pain in the upper right abdomen often prompt further investigation. Blood tests measuring liver enzymes (ALT, AST), bilirubin levels, and coagulation factors help assess liver function and inflammation. Imaging techniques like ultrasound or CT scans are used to visualize the liver's size, shape, and potential lesions or cirrhosis. In certain cases, a liver biopsy may be performed to evaluate the extent of liver damage or fibrosis. Although these conventional methods provide crucial information, they often rely on observable signs that may only become apparent in later stages of liver damage, making early prediction challenging. Both heart and liver diseases can progress silently for years before significant symptoms emerge, complicating **early detection and prediction. In many** instances, individuals may remain asymptomatic until the disease has reached an advanced stage. This limitation has led to increased focus on enhancing predictive methods, such as genetic screening, more sophisticated imaging technologies, and biomarker analysis, which may offer more sensitive and early detection of these conditions.

IV. STRENGTHS OF NAVIE BAYES

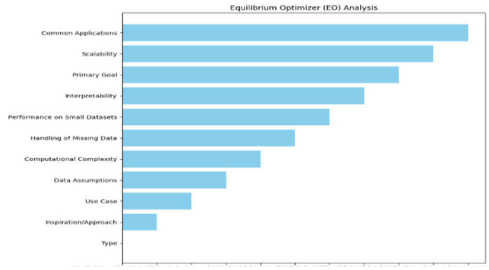

4.1 Navie Bayes

Based on the Bayes Theorem, Naive Bayes is a straightforward yet powerful classification method. It makes the assumption that the predictors are independent of one another, meaning that the characteristics or traits shouldn't be connected to one another in any way. It is known as naïve because, notwithstanding any dependencies, each of these characteristics individually affects the probability.

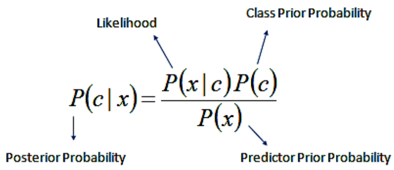

$$P(c \mid X) = P(x_1 \mid c) \times P(x_2 \mid c) \times \cdots \times P(x_n \mid c) \times P(c)$$

V. EXISTING SYSTEM

Chronic disease prediction is a very complicated task. Doctors who are experienced and familiar with this disease can only be able to predict chronic disease. In a healthcare system, the Internet of Things (IoT) is the key technology. In this paper, an EO optimized Lightweight Automatic modulation classification Network named the EO-LWAMCNet model is proposed to accurately predict a patient's chronic health condition (kidney or heart disease).

A sensor implanted in the patient's body can able to collect every data and it uses a gateway to transmit the data toward the cloud. Based on the achieved sensor data, the EO-LWAMCNet model initiates the classification process to predict chronic disease. The disease is predicted using CKD and HD datasets. Here, the preprocessed data is used for classification in the training stage. Once the training process is completed, the Cloud server's (CS) sensor data is tested and categorized into abnormal (heart or kidney disease) and normal. The awareness message is sent to the doctor to treat a patient in case of an abnormal result. The performance of the model is evaluated using accuracy, MCC, F1-score, and miss rate. This model can accurately predict the presence or absence of heart or kidney disease with an accuracy of 93.5% using the CKD dataset and an accuracy of 94% using the HD dataset. Also, the miss rate of the model is less in classification.

5.1 Drawbacks

Limited to kidney and heart disease datasets, reducing its applicability to other chronic diseases. Reliant on IoT infrastructure, which may not be accessible in all healthcare settings. Potential data privacy concerns due to cloud-based data transmission. Sensor malfunction or misreading's could lead to incorrect predictions.

VI. PROPOSED SYSTEM

The system will gather clinical data from various sources, ensuring comprehensive and reliable input for analysis while addressing data quality issues such as missing values. Relevant features that significantly impact Chronic Kidney Disease (CKD) prediction will be identified and selected based on statistical analysis and domain knowledge to improve the model's effectiveness. In this paper we are using the Navie Bayes algorithm to trained on the processed dataset to enhance their predictive accuracy. The selected model will be implemented in a user-friendly interface that allows healthcare professionals to input patient data and receive timely predictions, facilitating early detection and intervention for CKD.

6.1 Advantages

The Naive Bayes algorithm is a simple but effective machine learning algorithm for classification tasks. It has been shown to be accurate in predicting heart and liver disease in a variety of studies. This means that it is possible to understand how the algorithm makes its predictions. This can be helpful for medical professionals who want to understand how the system is predicting the risk of heart and liver disease in their patients.

VII. MODULE DESCRIPTION

7.1 Load Input Dataset

The input dataset comprises patient information like heart rate, blood pressure, glucose levels, and oxygen saturation, Sgot Aspartate Aminotransferase, A/G Ratio Albumin and Globulin Ratio. This will check both the heart the liver disease based upon the value that we are given.

We are showing you the first ten entries of our dataset. we have total 11 attributes and 27158 entries in the dataset.

	Age of the patient	Gender of the patient	Total Bilirubin	Direct Bilirubin	Alkphos Alkaline Phosphotase	Sgpt Alamine Aminotransferase	Sgot Aspartate Aminotransferase	Total Protiens	ALB Albumin	A/G Ratio Albumin and Globulin Ratio	Result
0	65.0000	Female	0.7000	0.1000	187.0000	16.0000	18.0000	6.8000	3.3000	0.9000	1
1	62.0000	Male	10.9000	5.5000	699.0000	64.0000	100.0000	7.5000	3.2000	0.7400	1
2	62.0000	Male	7.3000	4.1000	490.0000	60.0000	68.0000	7.0000	3.3000	0.8900	1
3	58.0000	Male	1.0000	0.4000	182.0000	14.0000	20.0000	6.8000	3.4000	1.0000	1
4	72.0000	Male	3.9000	2.0000	195.0000	27.0000	59.0000	7.3000	2.4000	0.4000	1
5	46.0000	Male	1.8000	0.7000	208.0000	19.0000	14.0000	7.6000	4.4000	1.3000	1
6	26.0000	Female	0.9000	0.2000	154.0000		12.0000	7.0000	3.5000	1.0000	1
7	29.00	Female	0.90	0.300	202.0000	14.0000	11.0000	6.70	3.60	1.1000	1

7.2 Data Pre-Processing

Preparing raw data for analysis and modeling requires a vital step known as data preprocessing. This process includes cleaning the data by addressing missing values, fixing errors, and eliminating duplicates or outliers. The values are converted into binary digits by easily understandable by the machine.

We are showing you the first ten entries of our dataset. we have total 22 attributes and 253680 entries in the dataset.

	HeartDiseaseorAttack	HighBP	HighChol	CholCheck	BMI	Smoker	Stroke	Diabetes	PhysActivity	Fruits	Veggies	HvyAlcoholConsump	AnyHealthcare	NoDocbcCost	GenHlth	MentHlth	PhysHlth	DiffWalk	Sex	Age	Education	Income
0	0.0000	1.0000	1.0000	1.0000	40.0000	1.0000	0.0000	0.0000	0.0000	0.0000	1.0000	0.0000	1.0000	0.0000	5.0000	18.0000	15.0000	1.0000	0.0000	9.0000	4.0000	3.0000
1	0.0000	0.0000	0.0000	0.0000	25.0000	1.0000	0.0000	0.0000	1.0000	0.0000	0.0000	0.0000	0.0000	1.0000	3.0000	0.0000	0.0000	0.0000	0.0000	7.0000	6.0000	1.0000
2	0.0000	1.0000	1.0000	1.0000	28.0000	0.0000	0.0000	0.0000	0.0000	1.0000	0.0000	0.0000	1.0000	1.0000	5.0000	30.0000	30.0000	1.0000	0.0000	9.0000	4.0000	8.0000
		1.					0.			1.	1.								0.	1		

7.3 Training and Testing

Once training is complete, the model is tested with a distinct dataset it has not encountered before, to evaluate its ability to generalize to new, unseen data. This division between training and testing is vital to avoid overfitting, ensuring the model's capability to perform well not only on the training data but also on real-world scenarios. Typically, the data is split into a training set, comprising 70-80%, and a testing set, making up 20-30%.

7.4 Heart and Liver Disease Prediction using NB

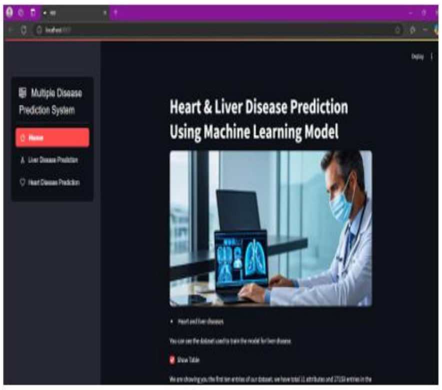

For this research I trained the machine by using Navie Bayes algorithm.

From the help of data set I trained the machine by using all the attributes. The Navie Bayes is used to predict whether the patient is having heart disease or liver disease by using the attributes and entities. This is particularly used for classification.

7.5 Performance and Evaluation

7.5.1 Liver Disease

When applied to the prediction of liver diseases, the Naive Bayes algorithm exhibits considerable promise in distinguishing between healthy individuals and those affected by the condition. Datasets pertaining to liver diseases typically encompass attributes such as age, gender, total bilirubin levels, alkaline phosphatase levels, and various outcomes from liver function tests.

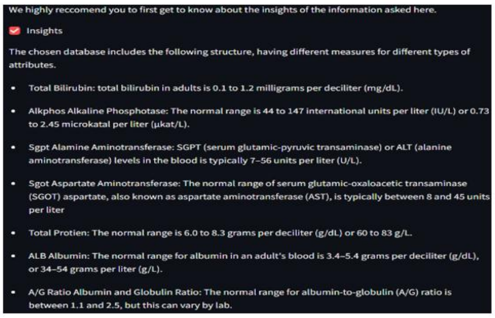

7.5.2 Heart Disease

The Naive Bayes classifier shows strong performance in predicting heart disease, particularly in binary classification tasks. The dataset generally comprises features such as age, blood pressure, cholesterol levels, electrocardiogram results, and family history. Once the Naive Bayes model is trained on this dataset, it is assessed using standard metrics. Accuracy reflects the overall rate of correct predictions, while precision and recall focus on the model's ability to predict the positive class (heart disease), which is vital in medical diagnostics.

VIII. System Specification

Hardware Requirements:

- CPU type : Intel core i5 processor
- Clock speed : 3.0 GHz
- RAM size : 8 GB
- Hard disk capacity : 500 GB
- Keyboard type : Internet Keyboard
- CD -drive type : 52xmax

Software Requirements:

- Operating System: Windows 10
- Front End: PYTHON

IX. Conclusion

In conclusion, we have proposed a heart and liver disease prediction system using the Naive Bayes algorithm. The system is also easy to use and can be deployed in a variety of different ways. We believe that this system has the potential to improve the early detection and treatment of heart and liver diseases, which could lead to better patient outcomes.

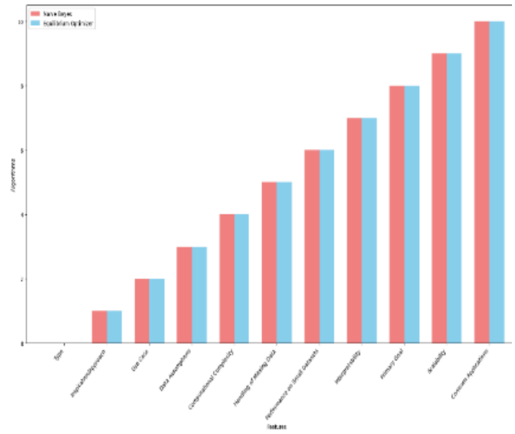

In the future, we plan to investigate other machine learning algorithms and to develop a more comprehensive heart and liver disease prediction system.

We also plan to make the system more accessible to patients and healthcare professionals by developing a web service or mobile app. We hope that this system will make a significant contribution to the fight against heart and liver diseases.

X. Future Work

We plan to investigate other machine learning methods, including deep learning algorithms, in the future to improve the accuracy and efficacy of the heart and liver disease prediction system. In order to develop a more comprehensive approach for predicting heart and liver illness, we also plan to include traits like genetic data and environmental influences. In order to improve patient and healthcare professional access to the system, we also plan to create a web service or mobile application. Medical practitioners will find it easy to use the system in their clinical practice, and patients will have no trouble obtaining their projections.

References

[1] D.Y. Pimenov, A. Bustillo, S. Wojciechowski, V.S. Sharma, M.K. Gupta,M. Kuntoglu, ˘ Artificial intelligence systems for tool condition monitoring in machining: analysis and critical review, J. Intell. Manuf. (2022) 1–43.

[2] K.B. Raju, S. Dara, A. Vidyarthi, V.M. Gupta, B. Khan, Smart heart disease prediction system with IoT and fog computing sectors enabled by cascaded deep learning model, Comput. Intell. Neurosci. 2022 (2022).

[3] M. Bhatia, S. Kumari, A novel iot-fog-cloud-based healthcare system for

[4] monitoring and preventing encephalitis, Cognitive Computation 14 (5) (2022) 1609–1626

[5] A.A. Nancy, D. Ravindran, P.D. Raj Vincent, K. Srinivasan, D. Gutierrez Reina, IoTcloud-based smart healthcare monitoring system for heart disease prediction via deep learning, Electronics 11 (15) (2022)2292.

[6] Z. Yu, K. Wang, Z. Wan, S. Xie, Z. Lv, Popular Deep Learning Algorithms for Disease Prediction: a Review, Cluster Computing, 2022, pp. 1–21.

[7] M. Maniruzzaman, M.J. Rahman, B. Ahammed and M.M. Abedin, *Classification and prediction of diabetes disease using machine learning paradigm Health Information Science and Systems*, vol. 8, no. 1, 7 2020.

[8] S. Mohan, C. Thirumalai and G. Srivastava, Effective heart disease prediction using hybrid machine learning techniques IEEE Access, vol. 7, no. 81542, 2019.

[9] S. Chae, S. Kwon and D. Lee, *Predicting infectious disease using deep learning and big data International journal of environmental research and public health*, vol. 15, no. 8, pp. 1596, 2018.

[10] A.U. Haq, J.P. Li, M.H. Memon, S. Nazir and R. Sun, A hybrid intelligent system framework for the prediction of heart disease using machine learning algorithms Mobile Information Systems 2018, 2018.

[11] G. Wang, Z. Deng and K. Choi, "Tackling Missing Data in Community Health Studies Using Additive LS-SVM Classifier", *IEEE Journal of Biomedical and Health Informatics*, vol. 22, no. 2, pp. 579-587, March 2018.

[12] P. Chiang and S. Dey, "Personalized Effect of HealthBehavior on Blood Pressure: Machine Learning Based Prediction and Recommendation", 2018 IEEE 20th International Conference on e-Health Networking Applications and Services (Healthcom), 2018.

[13] N. Prabakaran and R. Kannadasan, "Prediction of Cardiac Disease Based on Patient's Symptoms", 2018 Second International Conference on Inventive Communication and Computational Technologies (ICICCT), 2018.

[14] S. Rehman, E. Rehman, M. Ikram and Z. Jianglin, "Cardiovascular disease (CVD): assessment prediction and policy implications", *BMC Public Health*, vol. 21, no. 1, pp. 1299, 2021.

[15] H. Hijazi, M. Abu Talib, A. Hasasneh, A. Bou Nassif, N. Ahmed and Q. Nasir, "Wearable Devices Smartphones and Interpretable Artificial Intelligence in Combating COVID-19", *Sensors*, vol. 21, no. 24, 2021.

[16] O. T. Ali, A. B. Nassif and L. F. Capretz, "Business intelligence solutions in healthcare a case study: Transforming OLTP system to BI solution", *2013 3rd International Conference on Communications and Information Technology ICCIT 2013*, pp. 209-214, 2013.

[17] A. Nassif, O. Mahdi, Q. Nasir, M. Abu Talib and M. Azzeh, "Machine Learning Classifications of Coronary Artery Disease", Jan. 2018.

[18] A. F. Otoom, E. E. Abdallah, Y. Kilani, A. Kefaye and M. Ashour, "Effective diagnosis and monitoring of heart disease", Int. J. Softw. Eng. its Appl, vol. 9, no. 1, pp. 143-156, 2015.

[19] K. Vembandasamyp, R. R. Sasipriyap and E. Deepap, "Heart Diseases Detection Using Naive Bayes Algorithm", IJISET-International J. Innov. Sci. Eng. Technol, vol. 2, no. 9, 2015, [online] Available: www.ijiset.com.

[20] A. U. Haq, J. P. Li, M. H. Memon, S. Nazir, R. Sun and I. Garciá-Magarinõ, "A hybrid intelligent system framework for the prediction of heart disease using machine learning algorithms", Mob. Inf. Syst, vol. 2018, 2018.

[21] D. Shah, S. Patel, Santosh and K. Bharti, "Heart Disease Prediction using Machine Learning Techniques", vol. 1, pp. 345, 2020.

[22] K. Pahwa and R. Kumar, "Prediction of heart disease using hybrid technique for selecting features", 2017 4th IEEE Uttar Pradesh Sect. Int. Conf. Electr. Comput. Electron. UPCON 2017, pp. 500-504, Jun. 2017.

[23] N. Ahire, B. U. Rindhe, R. Patil, S. Gagare and M. Darade, "Heart Disease Prediction Using Machine Learning", Int. J. Adv. Res. Sci. Commun. Technol., vol. 5, no. 1, pp. 267-276, May 2021.

[24] A. Mujumdar and V. V. Vaidehi, "Diabetes Prediction Using Machine Learning Algorithms", Procedia Comput. Sci., vol. 165, pp. 292-299, Feb. 2020.

Navigating the Urban Green Spaces: A Comparative Analysis of Urban Sustainability Challenges and Opportunities

Priyanka Kumaravel
Department of Civil Engineering,
Thiagarajar College of Engineering,
Madurai, India
priyankakumaaravel@gmail.com

Velkennedy R
Department of Civil Engineering,
Thiagarajar College of Engineering,
Madurai, India
rvkciv@tce.edu

***Abstract*—Urban green spaces are essential for fostering sustainable and liveable cities, offering environmental, social, and economic benefits. Equitable access to these spaces is central to achieving Sustainable Development Goal (SDG) 11.7, which seeks to provide safe, inclusive, and accessible green spaces for all, particularly vulnerable groups. This article examines the current state of urban green spaces in India, emphasizing challenges related to accessibility, equity, and spatial distribution. Through a comprehensive analysis of case studies from Indian cities, the study identifies key barriers, including rapid urbanization, socio-economic disparities, and inadequate urban planning. This article also highlights successful interventions and innovative approaches to enhancing green space access, such as community-driven initiatives, policy reforms, and integrating advanced technologies like GIS mapping. By outlining a roadmap tailored to India's unique urban challenges, this study contributes to the discourse on sustainable urban development and offers actionable insights for policymakers, urban planners, and stakeholders. The findings aim to accelerate progress toward achieving SDG 11.7, ensuring that urban green spaces in India serve as catalysts for environmental sustainability and social inclusion.**

Keywords—Green Spaces, Sustainable Development Goal, Public Parks, accessibility, urban development

I. INTRODUCTION

The United Nations Report (UNDP, 2006) indicates that approximately 30% of the global population resided in urban areas in 1950, rising to 47% by 2000. The universal urban tipping point was attained in 2007 when, for the first time in history, more than half of the world's population, namely 3.3 billion individuals, resided in urban regions. The United Nations predicts that by 2050, over 70% of the global population will reside in urban areas (UNDP, 2006). Currently, 50% of the global population resides in metropolitan areas. The Census conducted in 2011 in India indicates that 377 million individuals live in urban areas, accounting for around 31.16% of the total population, projected to increase to around 600 million by 2030, as illustrated in Figure 1 (HPEC Report, 2011).

Green spaces refer to urban areas comprising community parks, playgrounds, and cemeteries. In contrast, open spaces denote areas characterized by natural or artificial landscapes, typically vegetated, including squares, marketplaces, amenity land, civic/public spaces, and sports facilities[1]. The Green Space Network is an integrated system that links various urban green areas, providing several social, health, economic, and environmental perks. Access to green spaces and open spaces are significant advantage for a city[2]. It renders the city attractive, healthier, and more sustainable, contributing to improving human well-being. Despite their significant importance, establishing and maintaining urban green spaces suffer from various problems. These include demanding land requirements, inadequate resources, inequality in society, and governance limitations. Establishing a balance between urban growth and green infrastructure is essential to maintain cities that are livable, equitable, and resilient, with rapid growth in urbanization[3]. The rapid development of urban spaces offers both opportunities and constraints for sustainable urban development, especially concerning environmental sustainability, an equitable society, and financial development. Such benefits provide them with an important aspect of urban planning, especially concerning achieving the goals of Sustainable Development Goal Target 11.7, which emphasizes the establishment of safe, inclusive, and accessible green and public spaces for all, particularly for women, children, the elderly, and individuals with disabilities[4].

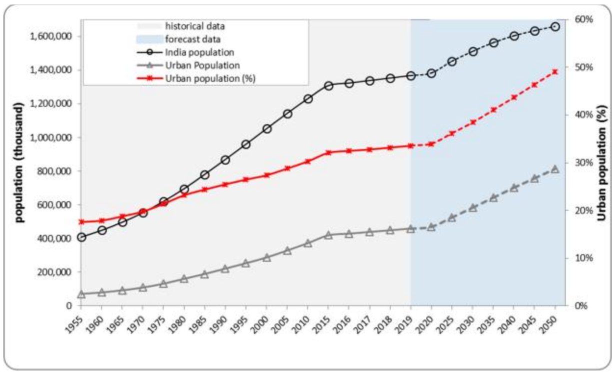

FIG 1. INDIA'S POPULATION GROWTH AND URBANIZATION TREND SINCE 1955.

This study aims to explore the role of urban green spaces in sustainable urban development, focusing on their environmental, societal, and economic impacts. Through a comparative analysis of case studies, the research investigates the opportunities and constraints associated with urban green spaces and offers actionable insights for creating inclusive and sustainable urban environments. The study collects experiences relevant to these objectives from numerous cities around the world. The findings furnish practical insights for elected representatives, urban planners, and communities striving to establish equitable and sustainable urban areas in cities. This study presents a framework aimed at addressing disparities in access to green spaces, highlighting the importance of participatory planning, inclusive policy formulation, and the prioritization of marginalized communities. The results seek to expedite advancements in realizing SDG 11.7, making urban green spaces in India essential drivers for environmental sustainability, public health, and social inclusion[5].

II. URBAN GREEN SPACES AND SUSTAINABILITY

Urban green spaces (UGS) are recognized globally as essential infrastructure within the sustainability framework, serving as multifunctional systems that tackle ecological, social, and economic aspects of urban resilience[6]. Built into the ecosystem services framework, urban green spaces (UGS) are acknowledged for their contributions to regulating services, including urban heat island mitigation, stormwater management, and air quality enhancement, as well as supporting services such as biodiversity conservation and habitat connectivity[7]. Their incorporation into urban environments aids climate adaptation and mitigation efforts by improving carbon sequestration abilities and decreasing susceptibility to severe weather occurrences. From a socio-technical viewpoint, urban green spaces (UGS) enhance inclusion and equity by providing widely accessible public areas that encourage physical and mental well-being, social cohesion, and participatory urban governance. Economic assessments of urban green spaces underscore their role in urban economic frameworks via processes like enhanced property values, eco-tourism opportunities, and diminished urban energy requirements due to natural cooling effects[8]. Moreover, UGS conforms to international sustainability objectives, namely SDG 11, by fostering resilient urban ecosystems that emphasize human and environmental welfare.

Categories of Urban Green Spaces

Urban green spaces are essential for the sustainability and well-being of cities, providing several environmental, social, and economic benefits. These areas are crucial for reducing urban heat islands, improving air quality, supporting biodiversity, and offering recreational spaces for city dwellers[9]. Urban green spaces can be classified into many categories according to their function, dimensions, and geographical placement. Typically, they encompass parks, gardens, green corridors, and community gardens, each enhancing the urban environment in diverse ways. The categorization of urban green spaces, illustrated in Figure 2, enhances understanding of their variety and significance. This classification delineates green spaces into categories, including public parks, natural reserves, green roofs, and private gardens, each providing unique advantages and addressing diverse requirements in urban environments[10]. Development and successful management of these areas are essential for fostering sustainable urban growth and enhancing individuals' quality of life.

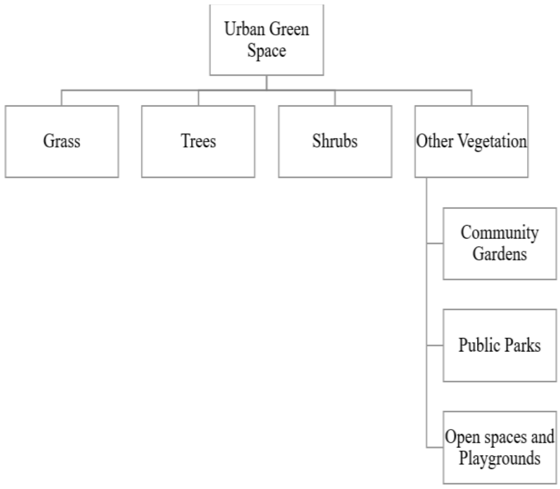

FIG 2. CATEGORIES OF URBAN GREEN SPACES

Connection to SDG 11.7

Urban green spaces are vital for fulfilling SDG 11.7, which seeks to provide access to secure, inclusive, and accessible public places for all, particularly for those in need, such as women, children, the elderly, and individuals with disabilities[11]. Rapid urbanization in Indian cities has resulted in the depletion of green spaces, complicating the provision of fair access to these regions. Green areas are vital for fostering social inclusion, strengthening public health, and improving the general quality of life. Accessible parks, gardens, and recreational areas provide secure environments for physical activity, promote community involvement, and serve as shelter from the urban heat island effect. Cities such as Bengaluru and Delhi have worked to enhance green infrastructure to build inclusive environments that foster community engagement and mitigate gaps in society. Also, urban green spaces enhance biodiversity, facilitate stormwater management, and ease the impacts of climate change, rendering them essential for the development of resilient cities. Integrating green areas into urban development enables cities to ensure fair access for all, enhancing mental and physical well-being while mitigating environmental stress. Urban green spaces are intimately associated with SDG 11.7 in Indian cities, promoting sustainable development, inclusion, and climate resilience.

Challenges and Opportunities in the Indian Context

Challenges in the Indian Context

The rapid development of India and the growing need for infrastructure have exerted a major impact on urban green spaces. These difficulties are many, arising from structural inefficiencies, socio-economic inequalities, environmental deterioration, and governance deficiencies[12]. The depletion of vegetation, together with the unregulated growth of urban areas, has intensified problems including air pollution, heat islands, and diminished biodiversity. Successful integration of green areas into sustainable urban development necessitates addressing these difficulties through coordinated initiatives, regulatory reforms, and active community engagement. Urban green spaces can only realize their promise of improving quality of life, fostering environmental sustainability, and strengthening climate resilience in India's cities by surpassing these challenges[13].

Opportunities in the Indian Context

Considering these constraints, raising awareness of urban green spaces as vital to sustainable development presents a substantial opportunity. Strategic interventions, active community engagement, and technological innovations can significantly improve urban green infrastructure in Indian cities. By focusing on these opportunities, cities may bolster ecological resilience, elevate public health, and cultivate a feeling of social ownership, thus facilitating the development of more sustainable and habitable urban landscapes.

Comparative Analysis: Sustainable Practices in Singapore and Copenhagen

Urban sustainability is growing as a global imperative, with cities using novel strategies to reconcile rising urbanization with environmental preservation. Singapore and Copenhagen exemplify effective methods, each implementing unique strategies to tackle environmental concerns. Singapore's "City in a Garden" initiative prioritizes the incorporation of green spaces within urban development, the application of sophisticated technology, and the promotion of biodiversity[14]. Copenhagen aims to be the world's first carbon-neutral capital by emphasizing renewable energy, citizen participation, and sustainable urban design. This comparative research examines the methods employed by these two cities in energy efficiency, water conservation, biodiversity preservation, accessible transportation, and data governance, emphasizing their distinct strategies and mutual dedication to ensuring sustainable, habitable urban settings. This comparative analysis, which is explained in Table 1, explores how these two cities implement energy efficiency, water conservation, biodiversity protection, accessible transportation, and data governance, highlighting their unique approaches and shared commitment to building sustainable, livable urban environments[15].

TABLE 1: COMPARATIVE ANALYSIS OF SUSTAINABLE PRACTICES IN SINGAPORE AND COPENHAGEN

Criteria	Singapore	Copenhagen
Energy Efficiency	Implements the Green Mark Scheme, encourages energy-efficient appliances, and promotes sustainable transportation options.	Prioritizes renewable energy, including wind and solar, along with energy-efficient buildings and district heating systems.
Water Conservation	Excels in water management by collecting and treating rainwater, practicing water reclamation, and promoting water-efficient technologies.	Focuses on water recycling, green roofs, and initiatives to reduce consumption and manage wastewater sustainably.
Biodiversity	Protects biodiversity through nature reserves like Bukit Timah and Sungei Buloh Wetland Reserve to conserve native flora and fauna.	Champions urban biodiversity with extensive green corridors, biodiversity parks, and efforts to support urban wildlife habitats.
Accessible Transportation	Boasts a comprehensive public transportation network, including the MRT and buses, ensuring seamless connectivity.	Promotes cycling with extensive bike lanes, efficient metro systems, and pedestrian-friendly urban infrastructure.
Data Storage and Security	Employs robust cybersecurity measures, stringent data protection regulations, and advanced digital infrastructure.	Leads in smart city innovations with secure data protocols while promoting open data for citizen engagement.
Decision-making	Focuses on evidence-based, data-driven policymaking and urban planning strategies.	Incorporates participatory governance, ensuring citizen-inclusive decision-making with a sustainability focus.
Skilled Workforce	Develops a highly skilled workforce through significant investments in education, research, and training programs.	Encourages green jobs and vocational training, emphasizing sustainable technologies and eco-friendly innovations.
Privacy & Data Governance	Enforces strict privacy laws to regulate the collection, storage, and use of personal data.	Balances privacy with transparent data governance, enabling secure yet open data use for research and policymaking.

Both cities offer valuable lessons in creating resilient, sustainable, and liveable urban environments, each tailored to their unique challenges and opportunities.

III. Conclusion

UGS is essential for promoting sustainable urban development by providing many ecological, social, and economic advantages. This study's comparative research emphasized the diverse contributions of urban green spaces, including their capacity to alleviate urban heat islands, promote biodiversity, and facilitate climate adaptation measures. UGS enhances diversity, promotes mental and physical health, and reinforces community cohesiveness. They stimulate urban revitalization by elevating property values and diminishing energy use. Further, the potential of UGS is limited by issues such as unequal distribution, insufficient governance, and conflicting land-use agendas. This research considerably enhances the discourse on urban sustainability by synthesizing several theoretical and conceptual frameworks. It connects theoretical insights with practical applications, providing a detailed grasp of the difficulties and opportunities related to UGS. The results offer practical advice for urban planners, politicians, and researchers, highlighting the significance of equitable access, participatory governance, and adaptive management to optimize the advantages of urban green spaces.

Acknowledgment

The authors express their gratitude to the Thiagarajar College of Engineering (TCE) for supporting us in carrying out this research work. Also, the financial support from TCE under the Thiagarajar Research Fellowship scheme (File.no: TRF/Jul-2023/02) is gratefully acknowledged.

References

[1] A. Russo, "Urban Green Spaces and Healthy Living: A Landscape Architecture Perspective," Urban Science, vol. 8, no. 4, p. 213, Nov. 2024,

doi: 10.3390/urbansci8040213.

[2] H. Czédli, Z. Varga, and C. Szigeti, "Public Urban Green Spaces: Combining Goals for Sustainability, Urban Health and Well-being," University of Maribor, Jul. 2023, pp. 237–245. doi: 10.18690/um.epf.3.2023.28.

[3] S. Pauleit et al., "Urban green infrastructure – connecting people and nature for sustainable cities," Apr. 01, 2019, Elsevier GmbH. doi: 10.1016/j.ufug.2019.04.007.

[4] P. Kumar, Mukul, D. Kaur, and A. Kaur, "Green Infrastructure- A Roadmap Towards Sustainable Development," in IOP Conference Series: Earth and Environmental Science, Institute of Physics, 2023. doi: 10.1088/1755-1315/1110/1/012060.

[5] A. Cimini et al., "Green Urban Public Spaces Accessibility: A Spatial Analysis for the Urban Area of the 14 Italian Metropolitan Cities Based on SDG Methodology," Land (Basel), vol. 13, no. 12, p. 2174, Dec. 2024, doi: 10.3390/land13122174.

[6] M. Ramaiah and R. Avtar, "Urban Green Spaces and Their Need in Cities of Rapidly Urbanizing India: A Review," Sep. 01, 2019, MDPI. doi: 10.3390/urbansci3030094.

[7] E. Hanna and F. A. Comín, "Urban green infrastructure and sustainable development: A review," Oct. 01, 2021, MDPI. doi: 10.3390/su132011498.

[8] A. K. Singh, H. Singh, and J. S. Singh, "Green infrastructure of cities: An overview," Oct. 01, 2020, Indian National Science Academy. doi: 10.16943/PTINSA/2020/154988.

[9] Ugochukwu Kanayo Ashinze, Blessing Aibhamen Edeigba, Aniekan Akpan Umoh, Preye Winston Biu, and Andrew Ifesinachi Daraojimba, "Urban green infrastructure and its role in sustainable cities: A comprehensive review," World Journal of Advanced Research and Reviews, vol. 21, no. 2, pp. 928–936, Feb. 2024, doi: 10.30574/wjarr.2024.21.2.0519.

[10] D. G. Castilla et al., "URBAN GREEN SPACES AND HUMAN WELLBEING: ASSESSING THE CARRYING CAPACITY OF URBAN PARKS AND RECREATION AREAS IN DANAO CITY," International Journal of Earth & Environmental Sciences, vol. 9, no. 1, pp. 30–50, 2024, [Online]. Available: http://ijees.ielas.org

[11] G. Kurbanova, S. Gaffarova, and R. Ashurbayeva, "Green space: Ensuring a sustainable future through effective urban and environmental management," in E3S Web of Conferences, EDP Sciences, Nov. 2024. doi: 10.1051/e3sconf/202458702021.

[12] R. G. P. da Silva, C. L. Lima, S. D. Quinn, A. Afelt, A. E. Laques, and C. H. Saito, "Urban Green Spaces in Brazil: Challenges and Opportunities in the Context of the COVID-19 Pandemic," Studia Ecologiae et Bioethicae, vol. 21, no. 1, pp. 69–88, May 2023, doi: 10.21697/seb.2023.06.

[13] G. Pristeri, F. Peroni, S. E. Pappalardo, D. Codato, A. Masi, and M. De Marchi, "Whose urban green? Mapping and classifying public and private green spaces in padua for spatial planning policies," ISPRS Int J Geoinf, vol. 10, no. 8, Aug. 2021, doi: 10.3390/ijgi10080538.

[14] D. Dillon and S. T. H. Lee, "Green Spaces as Healthy Places: Correlates of Urban Green Space Use in Singapore," Int J Environ Res Public Health, vol. 20, no. 17, Sep. 2023, doi: 10.3390/ijerph20176711.

[15] S. A. M. Sabri, Z. Ponrahono, A. A. Bakar, and F. A. Aziz, "Comparative Analysis of Open Green Spaces Policies in Enhancing Urban Resilience to Climate Change through Small Urban Parks in Malaysia and Singapore," Chem Eng Trans, vol. 106, pp. 211–216, 2023, doi: 10.3303/CET23106036.

Investigation of Strength Characteristics of Crab Shell Ferro-Cement

Letcham K
Research Scholar,
Department of Civil Engineering,
Thiagarajar College of Engineering,
Madurai, Tamil Nadu
letcham@student.tce.edu

Dr. Jeykumar RKC
Assistant Professor, Department of Civil Engineering,
Thiagarajar College of Engineering,
Madurai, Tamil Nadu
rkcjey@tce.edu

Krishnamoorthy. A
Research Scholar,
Department of Civil Engineering,
Thiagarajar College of Engineering,
Madurai, Tamil Nadu
krishnamoorthy1@student.tce.edu

Dr. Sankaranarayanan. R
Assistant Professor, Department of Civil Engineering,
Thiagarajar College of Engineering,
Madurai, Tamil Nadu
rsciv@tce.edu

***Abstract*—The rapid urbanization and increasing cost of construction materials have significantly raised the demand for low-cost housing projects. In order to reduce construction expenses, it is crucial to prioritize locally available materials that are also compatible with local conditions. This approach not only helps in reducing costs but also enhances the quality of the buildings and living conditions. To meet these objectives, Ferrocement has gained significant attention from engineers and the construction industry as a viable alternative material. It is utilized to create structures with thin, robust surfaces and a variety of shapes. Essentially, The aim of this research is to investigate the partial replacement of cement with Crab Shell Powder in proportions of 10% and 20% by weight. These replacements were incorporated into mortar with a (1:3) mix ratio, and cement property tests were conducted following Bureau of Indian Standards (BIS) guidelines. The findings demonstrate that improved utilization of crab shell powder improves physical characteristics while lowering density. Crab shells can be recycled by using them in cement mortar instead of cement. The use of Crab Shell Powder as a replacement in cement properties indicates that the water requirement for consistency increases, while both the initial and final setting times remain within the limits specified by the Bureau of Indian Standards BIS 12269. The partial replacement of cement with Crab Shell Powder leads to a decrease in specific gravity compared to the standard values. Additionally, a reduction in flexural strength was observed in ferrocement samples with 10% CSP replacement after 7 days of curing.**

Keywords*—*Crab Shell Powder (CSP), Crab Shell Ash (CSA) and Ferrocement.

I. INTRODUCTION

1.1 History of Crab Shell:

Every year, approximately 8 million tons of waste shells from crabs, shrimp, and lobsters are generated worldwide, accounting for up to 60% of the total mass of the crab [1]. In addition, more than 10 million tons of mollusk shells, primarily from oysters, clams, scallops, and mussels, are produced annually, with these shells making up over 70% of the total [2]. Unfortunately, most of these shells are either discarded into the sea or sent to landfills [3]. This improper disposal negatively impacts the environment, altering soil, water, and marine ecosystems, especially when not managed properly [4]. As a result, massive piles of shells accumulate globally, causing various environmental issues such as the breakdown of leftover tissue on the shells, the release of unpleasant odors, and contributing to visual pollution [5].

In 2024, global fisheries and aquaculture production reached a historic high of 214 million tonnes. As highlighted in the Food and Agriculture Organisation's (FAO) 'The State of World Fisheries and Aquaculture (SOFIA) 2024' report, India has now become one of the leading fish producers in the world. Ranking third with a production of 16.25 million tonnes, India’s fish industry accounts for 1.1% of the nation's GDP [Source: FAO: World Fisheries and Aquaculture, FAO: Rome, 2022]. Additionally, the industrial fish processing sector in India generates approximately 302,750 tonnes of waste. Fisheries and related activities provide livelihoods for about 14 million people in the country [6]

The Tamil Nadu coast, home to a significant fishing industry, produces a large amount of fish waste during processing and sales at local fish markets. In the past, much of this waste was discarded near the coast, leading to pollution problems. Similarly, crab waste can harm the environment when disposed of in landfills or incinerated. [7]. Despite this, over time, concrete has become the most commonly used building material. Concrete consists of a mixture of gravel, sand, cement, water, and mortar made from cement and sand [2]. Cement is the most expensive part of concrete, so alternatives are being sought to reduce production costs while maintaining its strength and quality [3].

1.2 Cement Mortar & Ferrocement:

The mechanical study of mortar indicates that the best amount of sisal fiber to add is 0.75%. Adding more than this decreases the strength of the mortar [10].Additionally, if the proportion of cementitious materials is increased, the curing time needs to be extended to improve the compressive strength [11]. In the plastic stage of mortar (1:3 mix ratio), increasing the admixture percentage up to 5% enhances workability, which remains within the acceptable limits set by IS standards [12]. Replacing Ordinary Portland Cement

(OPC) with Portland Slag Cement (PSC) and using slag sand instead of natural river sand in cement mortar offers a sustainable solution, meeting both strength and durability requirements while being economically and environmentally friendly [13]. Additionally, the use of eggshell waste (ESP) as a partial replacement for cement in mortar has been explored, with studies examining the effects of small amounts of ESP on the properties and performance of cement mortar, without the need for admixtures [14]. Using waste plastic as a sand substitute in mortar reduces compressive strength due to weak bonding, but adding silica fume and marble powder improves it[15].

II. PROBLEM STATEMENT

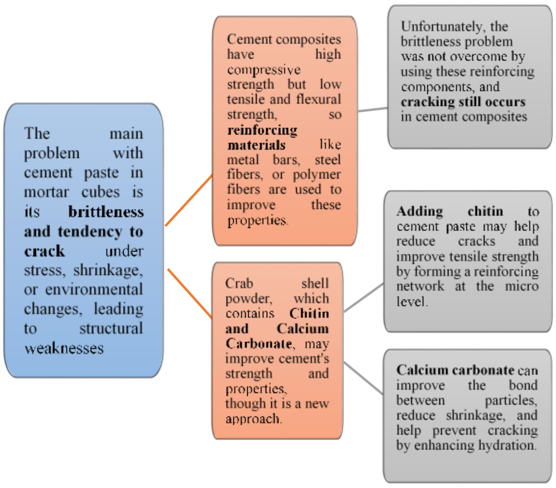

FIG 1 PROBLEM IDENTIFICATION OF CEMENT MORTAR

Crab shell powder could help address brittleness and cracking in traditional cement mortar, but its effectiveness relies on the mix design, the quantity used, and the overall cement paste formulation. Further research and experiments are needed to identify the ideal application and full benefits as shown in Figure 1.

III. MATERIALS AND METHODS

Crab shell powder is collected from the market for our study and processed.

3.1 Crab Shell Processing:

- The Crab Shell is collected from Madurai Fish Market, where there is a lot of dirt and mud including sticky organic matter.
- Crab Shell powder processing are as follows:
- First, the shell is cleaned with water by brushing to remove sticky organic residues.
- Next, the crab shells are crushed by pounding manually (crushing can be done using a machine) and it is sieved in 90micron sieve. The passed particles in the sieve is collected and used for our study.
- Then it is dried in a muffle furnace at 200ºC for 2 hours. Heating is continued until it is free from organic residues.

3.2 Investigation of Material Properties

Properties of Cement and Cement replaced partially by mass of 10% and 20% with CSP are done as per the relevant IS standards. The properties such as Consistency test, Initial and Final setting time vide IS 12269 vide 4031(Part IV), Soundness Test, Specific gravity test vide IS 2720(Part III) and Fineness Modulus vide IS 4031(Part I) are done.

3.3 Preparation of Ferro Cement:

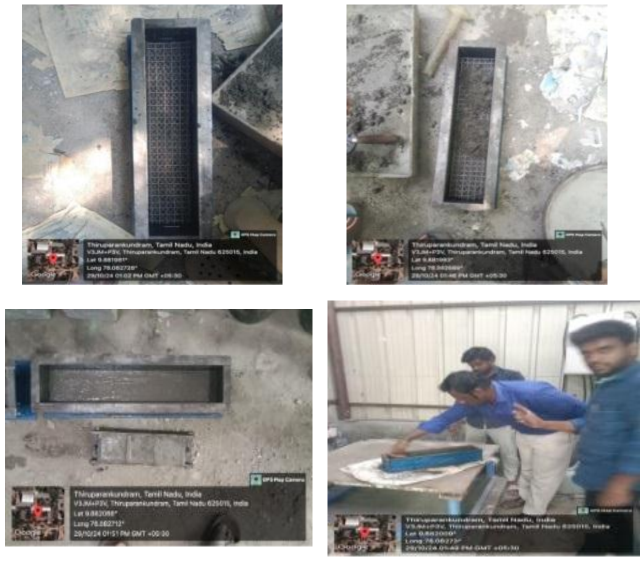

FIG 2 PREPARATION OF FERRO CEMENT

Ferro Cement Composites contain 5% wire mess and Skelton Reinforcement and 95% cement mortar mix. The part is 40 mm thick. Ferrocement uses fine aggregate, or M-sand, with a maximum size of 2.36 mm and 1.18 mm based on zone II grading. As seen in Figure 2, wire mesh is created by welding galvanized wire with a diameter of 0.5 to 1.5 mm, keeping it 10 mm center to center.

IV. RESULTS AND DISCUSSION

Physical properties of the cement and combination of cement and CSP are as follows:

4.1 Physical properties of cement:

The cement utilized in this work is tested in accordance with IS 12269-1987, and the cement has a standard consistency of 31%, Fineness modulus is 2%, Initial and Final setting time are 35 minutes and 420 minutes, Specific gravity is 3.12. The test result shows that all the physical attributes are within the standards of IS 269:1989 and IS 4031-I to IV.

4.2 Physical properties Cement replaced with CSP

In this analysis, crab shells were collected from Kanyakumari, Tamil Nadu, and processed to create crab shell powder (CSP). According to the procedure outlined in BIS: 1727-1967, the specific gravity of the CSP at 10% and 20% concentrations was found to be 2.7 and 2.55, respectively. Following BIS: 4031 Part IV [17], the standard consistency for 10% and 20% CSP were determined to be 42% and 45%, respectively. Additionally, the initial and final setting times for CSP in mortar were measured. For 10% CSP, the initial setting time was 42 minutes and the final setting time was 440 minutes. For 20% CSP, the initial setting time was 30 minutes and the final setting time was 330 minutes. These results are presented in Figure 3 and Figure 4.

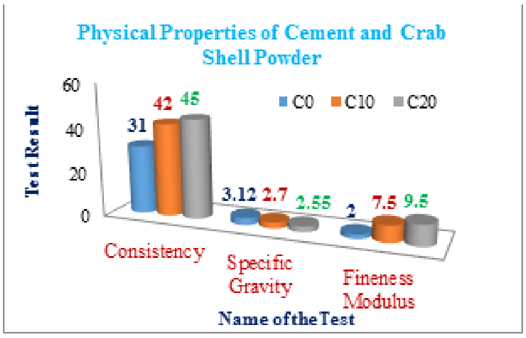

FIG 3 COMPARISONS OF PHYSICAL PROPERTIES OF CEMENT AND CRAB SHELL POWDER

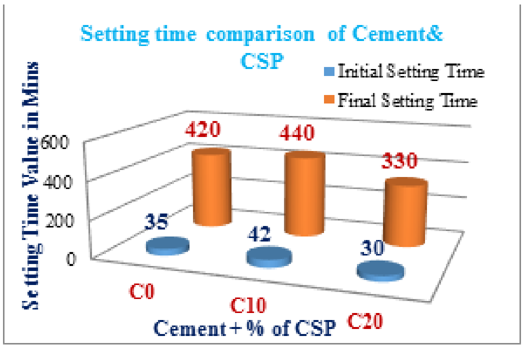

FIG 4 COMPARISONS OF PHYSICAL PROPERTIES OF CEMENT AND CRAB SHELL POWDER

4.3 Comparison of Consistency of Cement, Crab Shell Powder & Crab Shell Ash

The Crab Shell Powder (CSP) and Crab Shell Ash (CSA) are tested in accordance with IS 12269-1987, and the control has a standard consistency of 31%, and C10 and C20 have of 41% and 40%. CSP10 and CSP20 Crab Shell Ash have a standard consistency of 42% and 45% respectively as shown in Figure 5. The Consistency increases as CSP proportion increases.

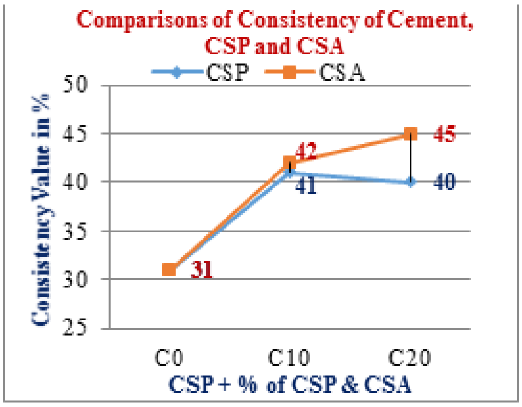

FIG 5 COMPARISONS OF CONSISTENCY OF CEMENT, CRAB SHELL POWDER AND CRAB SHELL ASH

4.4 Comparison of Crab Shell Powder & Ferro cement at 7 days strength:

In this study, 0% and 10% of the cement in the ferro-cement mix were replaced with Crab Shell Powder (CSP) in the control and 10% CSP elements, respectively. As shown in Figure 6, the flexural strength of the ferro-cement element with 10% CSP is 47.51% lower than that of the control element at 7 days of curing.

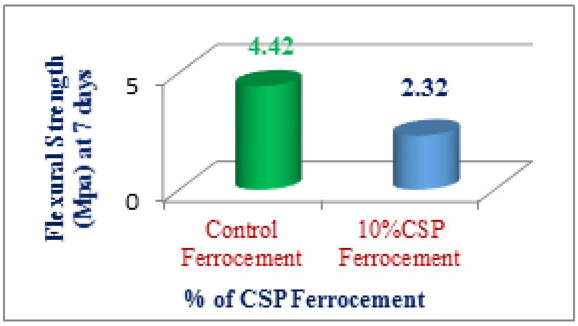

FIG 6 FLEXURAL STRENGTH OF FERROCEMENT AT 7-DAYS

V. CONCLUSIONS

The cement used in this study complies with Indian Standards. The properties of the cement with partial replacement of Crab Shell Powder (CSP) fall within the permissible limits outlined by the Indian Standards, with the exception of the final setting time for the C20 grade, which is slightly higher. An increase in the proportion of CSP replacement leads to a decrease in the specific gravity of the cement. Based on the results, it is concluded that Crab Shell Powder can be used as a partial replacement for cement up to 10%, as this replacement level is well within the prescribed Indian Standard limits.

This suggests that the Crab Shell Powder addition may negatively affect the material's ability to resist bending and overall structural integrity. However, despite the observed decrease in flexural strength, the modified ferrocement with Crab Shell Powder showed a reduced crack width compared to the conventional ferrocement, suggesting improved performance in crack control.

ACKNOWLEDGEMENT

This research work in financially supported by Thiagarajar Research Fellowship (TRF) scheme - (File.no: TCE/RD/TRF/03, dated 27.09.2024).

REFERENCES

[1] Ning Yan and Xi Chen, "Don't waste seafood waste," Macmillan Publishers Limited, vol. 524, pp. 155–157, Aug. 15, 2015.

[2] D. Summa, M. Lanzoni, G. Castaldelli, E. A. Fano, and E. Tamburini, "Trends and Opportunities of Bivalve Shells' Waste Valorization in a Prospect of Circular Blue Bioeconomy," May 01, 2022, MDPI.

DOI: 10.3390/resources11050048.

[3] J. N. Murphy and F. M. Kerton, "Characterization and Utilization of Waste Streams from Mollusc Aquaculture and Fishing Industries," in Fuels, Chemicals and Materials from the Oceans and Aquatic Sources, Wiley Blackwell, 2017, pp. 189–227.

DOI: 10.1002/9781119117193.ch8.

[4] M. Bonnard, B. Boury, and I. Parrot, "Key Insights, Tools, and Future Prospects on Oyster Shell End-of-Life: A Critical Analysis of Sustainable Solutions," Environ Sci Technol, vol. 2020, no. 1, 2020,

DOI: 10.1021/acs.est.9b03736ï.

[5] J. Zhan, J. Lu, and D. Wang, “Review of shell waste reutilization to promote sustainable shellfish aquaculture,” Jan. 01, 2022, John Wiley and Sons Inc. DOI: 10.1111/raq.12610.

[6] V. Renuka, A. Kumar Jha, and T. C. Joseph, “Nature and Composition of Fish Processing Industrial Waste and Handling Protocols,” FishTech, 2019, pp. 25–37.

[7] J. P. Morris, T. Backeljau, and G. Chapelle, “Shells from aquaculture: a valuable biomaterial, not a nuisance waste product,” Feb. 01, 2019, Wiley-Blackwell. DOI: 10.1111/raq.12225.

[8] S. S. Alisha, V. Dumpa, and V. Sreenivasulu, “Effect of Crab Shell on Properties of Soil: A Mini Review,” in IOP Conference Series: Earth and Environmental Science, Institute of Physics, 2023. DOI: 10.1088/1755-1315/1280/1/012035.

[9] J. Hadipramana, F. V. Riza, and S. N. Mokhatar, “Investigation of Crab (Portunus pelagicus) Shells in Concrete as a Potential Substitute for Fine Aggregate,” Feb. 01, 2024. DOI: 10.21203/rs.3.rs-3904460/v1.

[10] M. Balasubramanian, S. SenthilSelvan, S. Aishwarya, and M. R. Kumar, “Experimental Investigation of Cement Mortar to Improve the Strength by Adding Sisal Fiber,” in Lecture Notes in Civil Engineering, Springer Science and Business Media Deutschland GmbH, 2022, pp. 163–175. doi: 10.1007/978-981-16-6403-8_14.

[11] A. Aljobbory and H. Al-Lammi, “Replacement of cement with industrial by-products in cement mortar: An experimental investigation,” IOP Conf Ser Mater Sci Eng, vol. 1184, no. 1, p. 012008, Sep. 2021, DOI: 10.1088/1757-899x/1184/1/012008.

[12] Ganesh V Tapkire, Hemraj R Kumavat, and Vikram J Patel, “AN EXPERIMENTAL INVESTIGATION ON MECHANICAL PROPERTIES OF MORTAR WITH ADMIXTURE,” International Journal of Civil Engineering and Technology, vol. 7, no. 2, pp. 226–233, Apr. 2016,

DOI:http://www.iaeme.com/IJCIET/issues.asp?JType=IJCIET&VType=7&IType=2.

[13] M. Deepak, Y. R. Reddy, and R. Nagendra, “Experimental Investigation on Strength, Durability and Micro Structural Characteristics of Slag-Based Cement Mortar,” International Journal of Engineering, Transactions A: Basics, vol. 37, no. 4, pp. 763–778, Apr. 2024, DOI: 10.5829/ije.2024.37.04a.15.

[14] R. Al-Safy and R. A. Al-Safy, “EXPERIMENTAL INVESTIGATION ON PROPERTIES OF CEMENT MORTAR INCORPORATING EGGSHELL POWDER,” Journal of Engineering and Development, vol. 19, no. 06, pp. 1999–8716, 2015, [Online]. Available:https://www.researchgate.net/publication/321225247``

Sociology-Economic Impact of Sewage Farming

Diwahar P
Research Scholar,
Department of Civil Engineering,
Thiagarajar College of Engineering,
Madurai, Tamil Nadu, India.
diwahar1@student.tce.edu

Dr. Chandran. S
Professor,
Department of Civil Engineering,
Thiagarajar College of Engineering,
Madurai, Tamil Nadu, India.
schandran@tce.edu

Satheesh Kumar. P
Research Scholar,
Department of Civil Engineering,
Thiagarajar College of Engineering,
Madurai, Tamil Nadu, India.
pskumar2301@gmail.com

Abstract—Water is becoming the most precious resources of the world due to population growth and industrialisation. Due to climate changes the irrigation is getting affected by change in rainfall pattern. This makes the recent practice of introducing wastewater for irrigation in the semi urban cities. Hence the main focus of the study is to analyse the wastewater productivity, economic benefits, health, environmental issues, financial and social status-co of peoples in and around Vellakkal region of Avaniyapuram viilage, Madurai district, Tamilnadu, India. Wastewater samples were analysed for pH, Oil & Grease, TDS, COD, Hardness, Cl and also soil samples were analysed for pH, EC, N, P, K, Fe, Cu, Zn. The financial and social status were investigated by reconnaissance and questionnaire survey. The test results indicate that Oil & Grease and COD values are higher in wastewater samples exceeding the limits whereas in soil samples P, K, Fe exceeds the limits. From the questionnaire survey it is identified that most of the farmers are willing to do farming practice in diluted wastewater which is rich in nutrients. The yield of fodder and spinach are very fast and they reported there is no any serious health issues faced by farmers in this study area.

Keywords—Spinach, Fodder crops, wastewater, Freshwater, NPK

I. Introduction

The relatively limited data that is available in the literature indicates that wastewater irrigation is growing, and is likely to continue to grow. Four powerful drivers are responsible for this: increasing water stress in many parts of both highly developed and less developed countries; increasing urbanization in the developing world; ever growing wastewater flows associated with the expansion of water supply and sewerage; and more urban households engaging in agricultural activities, especially when food prices continue to rise. Supriya et al (2024), Physical scarcity occurs when there is not enough water to meet all demands. including environmental flows. In places with physical water scarcity, water resources development is approaching or has exceeded sustainable limits. It is a relative concept that compares the availability of water to actual use. Scarcity may also exist in water- abundant areas if there is heavy population pressure, excessive pollution, or unsustainable consumption levels. A number of integrated water resources management principles should be applied, namely: adopt a multi-sectoral approach to water management in association with river basin management, encourage stakeholder participation and devolution of responsibility; promote private sector involvement; and employ economic instruments. Nikita S et al(2024), In many regions, as freshwater sources become scarcer, wastewater use has become an attractive option for conserving and expanding available water supplies. Wastewater use can have many types of applications, including irrigation of agricultural land, aquaculture, landscape irrigation, urban and industrial uses, recreational and environmental uses, and artificial groundwater recharge. In principle, wastewater can be used for all purposes for which freshwater is used, given appropriate treatment. Wastewater use in agriculture is by far the most established application, and the one with the longest tradition.

Ronald Roopnarine et al(2023), It was estimated that two million tons of sewage, industrial and agricultural waste is discharged into world's water ways and at least 1.8 million children under five years-old die every year from water related disease. This is mainly due to improper management of wastewater. If the wastewater is utilized properly it could be most valuable source. Proper treatment facilities should be provided, this would help you to improve the quality and characteristic of wastewater which could be converted to an acceptable limit for disposal. An estimated 90% of all wastewater in developing countries is discharging untreated dirty into rivers, lakes or the oceans. Such discharges are part of the reason why de-oxygenated dead zones are growing rapidly in the seas and oceans. Currently an estimated 2, 45,000sq km of marine ecosystems are affected with impacts on fisheries, livelihoods and the food chain**.** Gauri G et al (2020), Wastewater use in agriculture is an emerging priority in countries facing water scarcity and in many low-income countries.

1.1 Water Scarcity

As the world population is expected to increase by 2 billion by 2050, the global food system will have to cope with this rise by doubling production to sustain the demand and the improving living quality. Such intensification in agricultural systems and activities will stress fresh-water resources. Typically, local agriculture using irrigation enhances a country's food security and resilience to trade disruptions. Nevertheless, it can represent a threat to freshwater resources, especially in water scarce countries due to the over abstraction of groundwater reserves. As of 2005, over 70% of global due to the over water withdrawals were intended for agricultural activities (FAO,2016).water withdrawals were intended for agricultural activities Water scarcity refers to the situation in which the demand for water exceeds the available supply or when water is not easily accessible in a given area. It is a growing global issue that affects millions of people and is driven by factors such as population growth, climate change, poor water management. Water scarcity in agriculture is a significant concern in semi-urban areas, which often face a unique set of challenges compared to rural or urban regions. Semi-urban areas typically have a mix of agricultural activity and increasing urbanization, which puts pressure on local water resources. These areas are often dependent on groundwater, seasonal rivers, and rain-fed systems, which are vulnerable to overuse and environmental changes. water at a farm in Vellakkal in Madurai. It has been over 100 years since the farmers of Vellakkal began sowing spinach seeds in waste water. The lush green fields which provide the much needed iron content for the body have proliferated with time. People are largely cultivating spinach, yet the use of untreated sewage water for its cultivation has not discouraged farmers. Now, some of these farmers are making use of grey water from a sewage treatment plant located 100 metres away from Vellakkal's solid waste treatment plant to make wealth out of waste water.

1.2 Waste Water Crisis

Wastewater crisis is becoming an increasingly pressing issue due to rapid population growth, limited infrastructure. The lack of proper waste management, coupled with the effects of climate change, such as erratic rainfall and flooding, often overwhelms existing sewage systems. The use of raw wastewater for irrigation is a growing practice in many parts of the world due to water scarcity, but it exacerbates the wastewater crisis and raises serious health and environmental concerns. In this system, untreated or inadequately treated wastewater, often from urban or industrial sources, is used to irrigate crops.

1.3. Objective of the Study

1. To make a comparison of spinach and fodder grass production and economic benefits
2. To assess the health and environmental risk of the farmers using wastewater in irrigation
3. To evaluate the potential positive and negative benefits of this practice through investigation and to suggest suitable recommendations for sustainable management.

II. METHODOLOGY

This study gathers peer-reviewed journal papers in addition to conference proceedings and book chapters published in English that have addressed wastewater reuse for animal feed production. The studies considered are those that covered at least one of the three pillars of sustainability (social, environmental and economic). In the case of social studies, no study was solely dedicated to the reuse of wastewater to irrigate livestock feed, especially for articles A samples were gathered and investigated about actual status of demand and supply of crops products to the market, while most of the journal articles did not specify the level of treatment, the second majority looked at reusing raw wastewater. The sources of wastewater investigated as part of this review are sewage. Reconnaissance field survey, questionnaire survey, along civil laboratory experiments for water and soil are conducted. Secondary data were collected from books, journal articles, government office, society offices and Tahsildar offices. Tank details, stream details, wastewater irrigation details and other environmental problems pertaining to the areas were collected from public through field interactions. Questions are framed for questionnaire survey to acquire data in field through farmers. 25 number of samples were conducted in study areas and analyzed by statistical tool.

III. RESULTS AND DISCUSSIONS

3.1. Farmer's Perception and Social Acceptance Water Availability for cultivation

In Madurai avaniyapuram region, waste water irrigation has been practiced by the farming community since 1924 and the farming community does not face any legal restriction of using wastewater from the waste water drain.

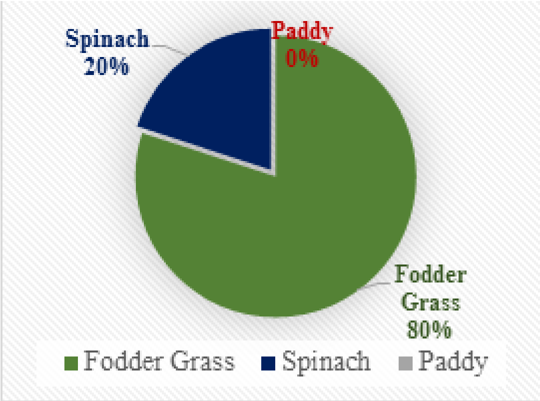

FIG 3.1 FARMERS RESPONSES REGARDING CHOICE FOR CROPS

Figure 3.1 shows that most of the farmers in the expose site willing to use waste water because of the availability and reduced fertilizer cost, and scarcity of fresh water for irrigation. About 80 % farmers commented that use of wastewater is highly reliable for irrigating fodder grass only 20% are cultivating the spinach. Because, paddy agriculture field they face a little water shortage during the month of the March-April. The most relevant cause of this water shortage was the reduction of canal flow due to earthen water canal and extensive fresh water uses in the canal upstream. Moreover some of the farmers told that they prefer to grow graces & Spinach in waste water because of least during days for maturation and high economic benefits.

As wastewater is available successfully around the year cropping intensity is high in comparison to the freshwater irrigated areas in wastewater irrigation sites. The crops grown are Spinach and Guinea grass.

TABLE 3.1 COMPARISON OF PRODUCTION AND ECONOMIC BENEFITS

Description	Fooder Grass	Spinach
Average production Bunch/Acre	3000	2000
Market price / bunch	50	10
Earnings / acre	150000	20000
Fertilizer cost savings / Acre	4000	4000
Revenue generated /acre	154000	24000
Expenses for plouging / acre	--	2200
Expences for seeding/ acre	--	1000
expenses for weeds removing / acre	--	2000

expenses for pesticides / acre	--	1200
expenses for harvesting / acre	3000	3000
Total expenses / acre	3000	9400
Economic benefit /Acre	151000	14600

Table 3.1data provide from the field study show that the crop production and economic return always higher with wastewater than that of fresh water irrigation. Economic benefits were found due to higher production which is as high as up to 1.5 Lakh rupee from fodder grass production for the spinch only 14600 is profit being outgoings. So only most of the farmers preferring thr fodder grass cultivation. These economic benefits make the farmers to use wastewater practice in their field. Result explains that whey the farmers in the exposed sites like to practice in their field. The field survey results show that about respondents who prefer to cultivate fooder crops because of the high market value and more economic benefit than that of other crops during the fresh water scarcity seasons. These farmers option that yield of grass is more in wastewater if good rainfall occurred.

3.2 Questionnaire Samples and Farmers Perception

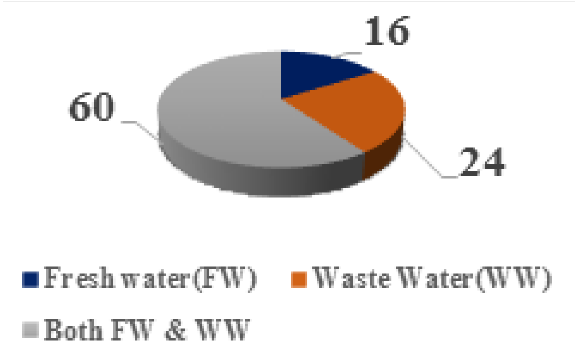

FIG 3.2 FARMER PREFERENCE ABOUT WATER IN %

Figure 3.2 shows that, this question is to understand the farmer's willingness towards the use of waste water if government initiates. About 60% of the respondents reported that the diluted wastewater is best option because they have high nutrient content which was naturally available in wastewater instead of synthetic fertilizer , about 16% prefers freshwater if available and 24% says high nutrient is naturally having in wastewater.

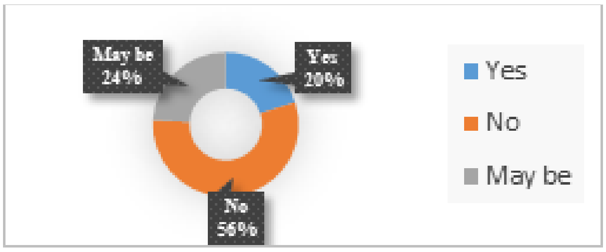

FIG 3.3 PERCENTAGE OF FARMERS ABOUT HEALTH ISSUES

Figure 3.3.shows that farmers did not face any serious health illness in this field. In the field survey it was found that about 20% of farmers says maybe affect, and 56% reported that no effect and balance of farmers reported that it may be affect the health.

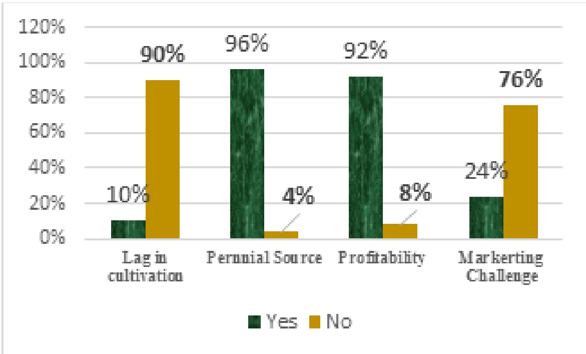

FIG 3.4 A STUDY ON FACTORS EFFECTING AGRICULTURAL PRODUCTIVITY IN %

Figure 3.4 shows that, this question is to understood the farmer's situation towards the use of waste water is there is any lag or disadvantages in selling crops in market or not. all of the respondents says this is an good opportunity to make more profit and fodder grass is the best option because they required nutrient content with minimum quality but this have more and more.

TABLE 3.2 ECONOMIC BENEFITS & OF WASTE WATER IRRIGATION

Particulars	harvest income / Acre	No. Of Harvesting / year	Harvest Income / Acre / year	Irrigating area in acre	Total Income from waste water /year	Total benefit (Net Rupees in lakhs) / year
Spinach	24000	24	5,76,000	15	86,40,000	26,73,60,000
Fodder grass	154000	24	36,96,000	70	25,87,20,000	

Table 3.2 shows that benefits & cost of wastewater irrigation in study areas before 100 years. In the study area cultivation of fodder grass is about 70 acre and harvest is done one or two times per month. Due to perennial source of waste water, 24 to 30 times of harvesting is possible per year. Spinach is cultivated and harvested 24 times per year. During rainy-seasons Additional benefit of 27 to 30 times of harvest also possible. A finally total benefit for one year is calculated by adding the both net return per year with area irrigation 500 acres.

3.3 Wastewater Quality in the Study Area

The results of Physico-chemical analysis of wastewater are presented in table 3.3

TABLE 3.3 WASTEWATER QUALITY IN THE STUDY AREA

Location Point `	Observed Parameter						
	pH	**Oil & grease**	**TDS (mg/L)**	**COD (mg/L)**	**hardness (mg/L)**	**chlorides (mg/L)**	**nitrates (mg/L)**
Center	8.05	125	1270	450	512	330	99.01
East	8.25	70	1205	390	485	282	61
West	8.3	80	1180	370	450	280	60.3
North	8.45	55	1110	320	490	305	80.1
South	7.59	90	1250	410	390	245	45.8
Normal Range as per CPCB	***5.5 – 9.0***	***10***	***2100***	**--**	**--**	***600***	**--**

The Ph of the wastewater was found to be well within the permissible limits at all the stations. The total dissolved solid is within the permissible limits at all stations. Chemical Oxygen Demand, which is a pollution load indicator. Pollutant load may also due to the disposal of lot of small scale industries just disposing the wastewater. Chemical oxygen demand was found to be low at the sampling stations. The hardness was observed to be low at all station. The concentration of nitrate was found to be very high Vellakal surplus. Chloride concentration was found to be high at vellakal

IV. CONCLUSION

Wastewater irrigation provides a likelihood of the farmers in Vellakal region of Madurai district, TamilNadu. Questionnaire survey shows that the farmers demand wastewater for irrigation due to water scarcity. Wastewater supplements nutrients to the Fodder grass and hence no synthetic fertilizer is required for growing grass, which results in economic and environmental benefits. Groundwater and soil quality is poor in this region. Precautions to be undertaken while using untreated wastewater in irrigation. Treated wastewater shall be used in irrigation with little care and keep economic benefits.

ACKNOWLEDGMENT

This research work is financially supported by Thiagarajar Research Fellowship (TRF) scheme - (File.no: TCE/RD/TRF/09 dated 09-02-2024).

REFERENCES

[1] Supriya, Karnal,, Biswaranjan Behera, Parkash Verma, Rajesh Kumar Meena “Potential and limitations of using sewage water for irrigation” Vol. 74 No. 4 (2024)

[2] Omar Qteishat1, Jamal Radideh2, Kamel Alzboon, Ziad abu-hamatteh1, Tariq Al-Azab, Numan Abu-Hammad “ wastewater treatment and water reuse technologies For sustainable water resources: jordan as a case study ” CEER 2024; 34 (2): 0177-0192

[3] Nikita S. Kakwani, Pradip P. Kalbar “Prioritization of strategies for urban water circular economy using water circularity indicator” Water Policy (2024) 26 (5): 480–505

[4] Y Madani Bessedik, orcid,Chérifa Abdelbaki, Sidi Mohamed Tiar, Abderrahim Badraoui, Abdesselam Megnounif, Mattheus Goosen, Khaldoon A. Mourad, Mirza Barjees Baig, and Abed Alataway, Abed Alataway “ Strategic Decision-Making in Sustainable Water Management Using Demand Analysis and the Water Evaluation and Planning Model ” Sustainability 2023, 15(22), 16083

[5] Ronald Roopnarine, Kervelle Baird, Mikella Hosein, Renee Jackson, Shehnaaz Salim, Anisha Cephas, Oral Daley, Samantha Gangapersad, Sara-Jade Govia, Adrian Cashman “ Integrating wastewater reuse into water management schemes of Caribbean SIDS: A Trinidad and Tobago case study ” Water Policy (2023) 25 (12): 1161–1174.

[6] Omar Amahmid, Youssef El Guamri, Youness Rakibi, Mohamed Yazidil, Bouchra Razoki, Khadija Kaid Rassou, Hanane Achaq, Safia Basla1, Mohamed Amine Zerdeb ID, Meriyam El Omari, Oulaid Touloun, Saïd Chakiri I “Wastewater reuse

Effect of Precursor Materials on the Properties of Geopolymer Concrete: A Review

Thrulochna V M
Department of Civil Engineering,
Thiagarajar College of Engineering,
Madurai, India
thrulochna2000@gmail.com

Dr. S. Nagan
Department of Civil Engineering,
Thiagarajar College of Engineering,
Madurai, India
nagan_civil@tce.edu

Dr. M. Indhumathi
Department of Civil Engineering,
Ramco Institute of Technology,
Rajapalayam, India
indhumathi@ritrjpm.ac.in

***Abstract*—The massive building industry uses a variety of techniques to reduce harmful carbon dioxide emissions and safeguard the environment. It became essential to deal with the effective use of generated trash that may be used to create sustainable concrete in order to protect and preserve the environment. In geopolymer concrete (GC), a relatively new green concrete method, aluminosilicate source materials with pozzolanic activity are employed to create complete cement replacements. Realizing the importance of various materials in reaching GC's potential capabilities and partially substituting organic or waste products for GC might change the material's mechanical and fresh qualities. The efficiency of GC in combination with a range of precursor materials, such as fly ash (FA), GGBS, and metakaolin (MK), is investigated in this work. Review of important aspects from earlier research, including fresh, mechanical, and durability characteristics of several GC precursor materials.**

Keywords—Geopolymer concrete, Mechanical, Workability, GGBS, Flyash, Metakaolin, GC

I. INTRODUCTION

The construction industry is one of the most important economic sectors in most countries, involving a great flux of materials and human resources. Because of its low cost and numerous benefits over competing alternatives, concrete is acknowledged as a necessary building material. However, there are issues with the increasing demand for concrete. The cement sector is responsible for between 5 and 8% of the world's CO_2 emissions [1]. For every ton of OPC produced, there are between 0.6 and 1 tonne of CO_2 emissions [1]. The demand for OPC is expected to triple globally by 2050 [3], [4], which will impede future efforts to meet carbon reduction targets. One intriguing new material that has been studied is geopolymer mixes.

Therefore, geopolymer concrete emits less CO_2 than cement, it is a new green technology. Rich alumina and silica source materials, either natural or industrial by-products, and an alkaline solution as a dissolving agent are the two main ingredients of geopolymer concrete. The geo-polymerization process is then carried out to create a robust binder. "The common alkali activators in GC systems are sodium and potassium hydroxide and sodium and potassium silicate[2]." Geopolymer research has focused on a variety of source materials, with reports differing according to the materials' local accessibility, the binder's intended function, and manufacturing costs [3]. This accounts for the variation in the researcher's inclinations toward various geopolymer binders, including FA, GGBS, MK, etc.

The goal of the present review was to measure and understand how the fresh, mechanical, and durability properties of the various source materials reported in the literature were affected when Fly Ash, GGBS, Metakaolin, etc were partially replaced. This was carried out due to the realization that various substitute materials could greatly expand the possible uses of geopolymer mixtures.

A. Environmental Sustainability

One of the key benefits of GPC over conventional concrete is its environmental friendliness. As mentioned earlier, most of the processes used to make conventional concrete result in the production of greenhouse gases, particularly CO_2 [4]. OPC is responsible for roughly 77% of typical concrete's negative environmental consequences. About 90% of CO_2 emissions in conventional concrete are caused by high compressive strength, which is the result of high OPC usage. In contrast, the GPC compressive strength is influenced by the solid-to-activator ratio, the molarity ratio, and the curing regime [5]. The majority of GPC mix specimens release less CO2 than conventional concrete when comparing the carbon footprints and carbon emission indices of the two types of concrete [6].

In general, since GPC replaces cement, which is the primary source of CO_2 emissions in traditional concrete, GPC seems to be more environmentally friendly than traditional concrete. But when you take into account all of the factors that go into making GPC (such as the transportation and extraction of raw materials), it's not exactly environmentally friendly. Thus, when making GPC, the best mix design, pre-fabrication composition, and raw material availability should not take priority over the extraction and transportation of raw materials and the delivery of GPC to the placement site [1]. Life cycle assessments show that GPC can lower global warming potential by 26-45% compared to traditional Portland cement. Although geopolymer concrete has ecological benefits, particularly by diverting waste from landfills, its production of sodium silicate and sodium hydroxide can still have negative environmental impacts. Despite this, GPC aligns with the circular economy by reducing GHG emissions and resource use, making it a more sustainable alternative to traditional cement [2].

II. GEOPOLYMER PRECURSOR MATERIALS

Fly ash, GGBS, MK, etc., are examples of alumina-silica that are essential components of GC. Researchers choose one material over another based on factors including cost, availability, and performance [3].

A. Fly Ash

FA is an outcome of burning coal, and also known as pulverized fuel ash is obtained it consists of significant levels of calcium oxide (CaO), aluminum oxide (Al_2O_3), and silicon dioxide (SiO_2) which helps in the production of Geopolymers. FA particles primarily have an amorphous and spherical structure [4], and their pozzolanic reaction helps in the enhancement of concrete properties. Table 1 displays FA's chemical composition and Figure 1 shows the SEM and XRD analysis of FA. It is divided into two classes F and C type. Class C is pozzolanic and self-cementing; it is made from burning lignite or sub-bituminous coal and has more than 18% CaO. Class F is pozzolanic and has a CaO level of less than 18% [5]. FA supply is dependent on yearly coal combustion, mostly from the generation of coal-fired electricity. Waste products from the combustion of coal include fly ash, bottom ash, flue gas, and boiler slag [3]. Fly ash has various applications in construction, including soil stabilization, brick and block production, and as a cement substitute in concrete, roads, and dams. However, it contains toxic trace elements that can harm humans and the environment if not handled properly. When coal is burned, these harmful elements become more concentrated in the resulting fly ash. Proper management and use of fly ash can mitigate these risks, offering both economic and environmental benefits [2], [6], [7].

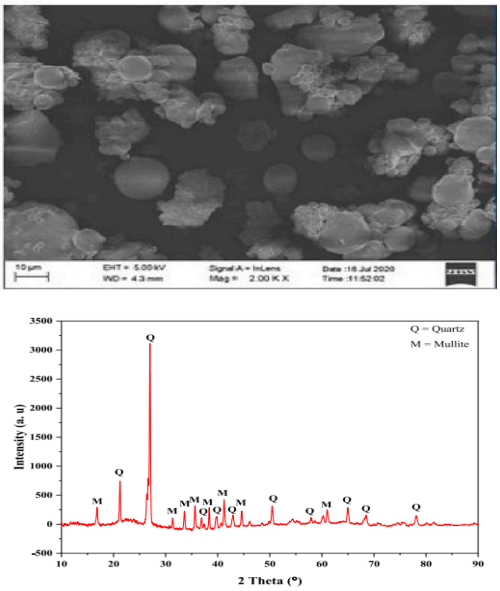

FIG. 1. SEM AND XRD ANALYSIS OF FA [8]

B. GGBS

As molten blast furnace slag is quenched in the process of making iron, GGBS is a by-product. The amorphous glass and its chemical ingredients, as well as its properties, determine the activity of the GGBS, with its angular, glassy structure [8]. GGBS is used to partially replace cement, reducing the need for clinker in cement production and promoting a greener construction approach. Though it cannot fully replace cement, GGBS shows promising results. Its high alumina and silica content also makes it suitable for geopolymer production, offering a solution for industrial waste and contributing to the development of sustainable materials [9], [10]. Table 1 displays GGBS's chemical composition and Figure 2 shows the SEM and XRD analysis of GGBS.

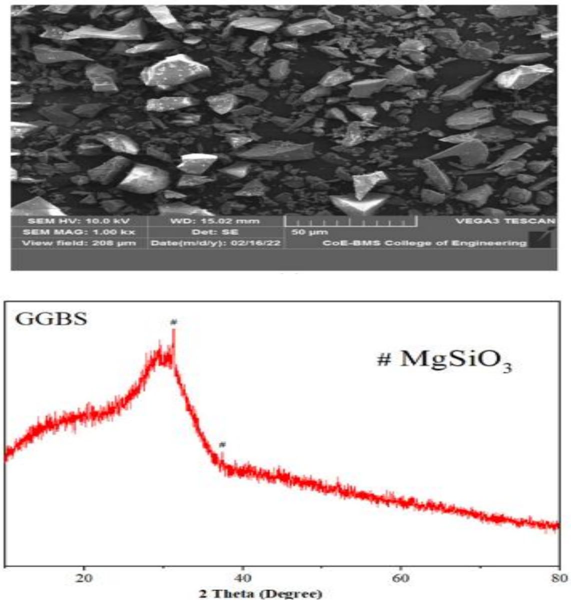

FIG. 2. SEM AND XRD ANALYSIS OF GGBS [8]

C. Metakaolin

Metakaolin is the main constituent of kaolin, a naturally occurring clay substance. Alumina octahedral and silica tetrahedral sheets are alternatively stacked to form kaolinite, an anhydrous aluminum silicate [11]. To increase its activity, calcination converts crystalline kaolin into an amorphous MK. The temperature range for the dehydroxylation process is 650–800 ◦C. MK's chemical composition typically comprises 40–45% alumina and 50–55 percent silica. Studies show that metakaolin-based geopolymers have superior durability, including better water, thermal, and corrosion resistance. Their workability improves with increasing the ratio of sodium silicate (Na_2SiO_3) to sodium hydroxide (NaOH), but decreases beyond a certain point due to higher viscosity. Research also indicates that sodium- and potassium-based metakaolin geopolymers exhibit better compressive and flexural strength than other binders. While metakaolin is widely available and unaffected by market fluctuations, its current production volume is insufficient to meet global demand for pozzolanic materials in cement and concrete production [12], [13], [14]. Table 1 displays MK's chemical composition and Figure 3 shows the SEM and XRD analysis of MK.

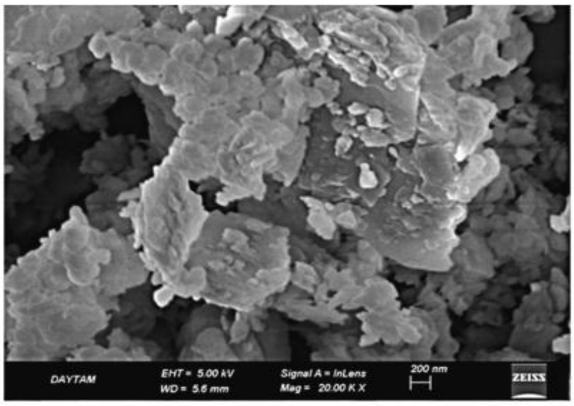

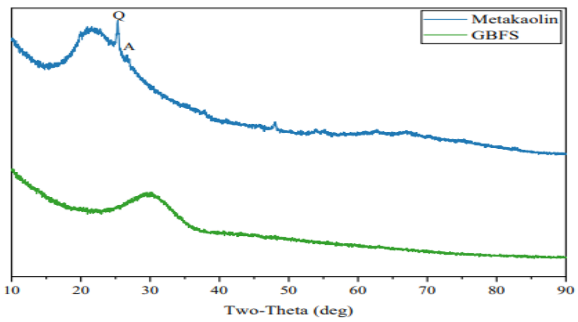

FIG. 3. SEM AND XRD ANALYSIS OF MK [10]

TABLE I. PHYSICAL PROPERTIES OF MATERIALS

	FA	GGBS	MK
SiO_2	50.13	34.6	54.3
Al_2O_3	27.28	17.9	43.2
Fe_2O_3	9.28	0.462	<0.8
CaO	2.82	36.5	<00.5
K_2O	1.12	0.392	-
Na_2O	1.52	-	-
MgO	1.52	6.48	<0.2
LOI	2.9	0.07	<0.1
Sp.Gr	2.13	2.93	2.6
Source	[8]	[15]	[16]

III. EXPERIMENTAL STUDIES

A. Workability

The workability of geopolymer concrete is generally challenging. This results from the use of highly soluble silicate, low water content, and highly viscous alkaline solutions [17]. Fly ash is the two primary precursor materials utilized in geopolymer concrete. Fly ash typically produces a more workable mixture than GGBS. Workability declines with increasing GGBS level because of its angularity and CaO concentration, while fly ash has a spherical form [18]. Nath P et al. [19] investigated the variables influencing workability, including the addition of GGBS content, alkaline content, and SS/SH ratio, and found that the addition of GGBS decreased the workability of the concrete and mortar in terms of both slump and flow value. The effective ratio of fly ash to GGBS is 1:1 for good workable concrete. Not only the type of aluminosilicate materials but also its particle size influences the fresh properties. Using metakaolin and silica fume while maintaining a consistent binder-to-solution ratio results in a more workable mix by raising the Si/Al ratio and adding more silica fume. This is because silica fume has a lower specific surface area than metakaolin due to its greater size [20]. LOI (loss on ignition), which is correlated with the amount of carbon in the material, is another factor that affects workability. It is limited to 10% as its maximum value [21]. Metakaolin (MK) and GGBS have respective LOI values of 7.76, 1.19. The qualities of geopolymer concrete are enhanced by a variety of additions, including fibers, rice husk ash, nano silica, and regular Portland cement. Nano silica has a large specific surface area and is amorphous. Because nano-silica has higher strength and pozzolanic activity, it is added to concrete [22]. Lee et al. also found that a higher SS/SH ratio and an increase in NaOH concentration both shorten setting times; however, when this ratio is less than 1, meaning that there is more SH solution than SS, setting times are longer than those of the other two ratios, say 1.0 and 1.5, suggesting that NaOH solution delays paste setting [23].

B. Mechanical Properties

Compressive strength, tensile strength, flexural strength, bond strength, and other mechanical characteristics are all included in geopolymer concrete. After 28 days of curing, concrete cubes, concrete cylinders, and mortar cubes are used to measure compressive strength. Cylindrical samples are used to assess indirect tensile strength. Prism samples are tested to examine flexural strength. GPC concrete with a low AA/B ratio exhibits greater strength, much like OPC concrete with a low w/c ratio, which also demonstrates higher mechanical qualities [24]. The primary source of raw materials for geopolymer concrete is fly ash. Fly ash shortages will jeopardize the advancements gained in geopolymer concrete in the future. To achieve a mortar's 13.78 MPa compressive strength, fly ash can be replaced with GGBS up to 40% and RHA 5–10% [25]. Research on how fiber affected the mechanical characteristics of geopolymer concrete revealed that the flexural strength increased but the compressive strength decreased. There was a decrease in compressive strength [17].

C. Durability Properties

Concrete's capacity to withstand harsh environmental factors like weathering and chemical attacks without sacrificing its engineering qualities is what makes it durable. The acid attack test, chloride penetration, carbonation resistance, water permeability, porosity, sorptivity, thermal and fire resistance, and others are examples of durability tests [26]. Surface abrasion can be enhanced by the use of metakaolin. When recycled coarse aggregate was used in place of fly ash-based geopolymer concrete, the abrasion weight loss was decreased to 55%. Additionally demonstrating strong performance are sorptivity and resistance to sulfuric acid. MK performs poorly in chloride penetration tests while having superior surface abrasion, sorptivity, and sulfuric acid resistance. Additionally, it is implied that the fiber geopolymer mix and metakaolin are resistant to high temperatures [24], [26].

IV. CONCLUSION

This literature review on geopolymer concretes examines the impact of partially replacing binders with various by-products and materials, both manufactured and natural. It explores how fly ash, GGBS, and metakaolin affect the chemical composition, workability, mechanical, and durability properties of geopolymer concrete. From the review, the results that follow can be made:

- Workability declines with increasing GGBS level because of its angularity and CaO concentration, while fly ash has a spherical form.
- Using metakaolin while maintaining a consistent binder-to-solution ratio results in a more workable mix by raising the Si/Al ratio and adding more silica fume.

- Fly ash can be replaced with GGBS up to 40% and RHA 5–10%.
- Fiber affected the mechanical characteristics of geopolymer concrete revealing that the flexural strength increased.
- MK performs poorly in chloride penetration tests while having superior surface abrasion, sorptivity, and sulfuric acid resistance.
- Additionally, it is implied that the fiber geopolymer mix and metakaolin are resistant to high temperatures

ACKNOWLEDGMENT

The author extends their due thanks to Thiagarajar College of Engineering Management, Madurai, India for their extensive research facilities and the financial backing from Thiagarajar Research Fellowship (TRF) scheme (File.no: TCE/RD/TRF/2024/13 dated 09-02-2024) is gratefully acknowledged.

REFERENCES

[1] A. Danish *et al.*, "Sustainability benefits and commercialization challenges and strategies of geopolymer concrete: A review," Oct. 15, 2022, *Elsevier Ltd*. doi: 10.1016/j.jobe.2022.105005.

[2] S. Sbahieh, G. McKay, and S. G. Al-Ghamdi, "Comprehensive Analysis of Geopolymer Materials: Properties, Environmental Impacts, and Applications," Dec. 01, 2023, *Multidisciplinary Digital Publishing Institute (MDPI)*. doi: 10.3390/ma16237363.

[3] L. N. Assi, K. Carter, E. Deaver, and P. Ziehl, "Review of availability of source materials for geopolymer/sustainable concrete," *J Clean Prod*, vol. 263, Aug. 2020, doi: 10.1016/j.jclepro.2020.121477.

[4] A. Bhatt, S. Priyadarshini, A. Acharath Mohanakrishnan, A. Abri, M. Sattler, and S. Techapaphawit, "Physical, chemical, and geotechnical properties of coal fly ash: A global review," *Case Studies in Construction Materials*, vol. 11, Dec. 2019, doi: 10.1016/j.cscm.2019.e00263.

[5] P. Suraneni, L. Burris, C. R. Shearer, and R. D. Hooton, "ASTM C618 fly ash specification: Comparison with other specifications, shortcomings, and solutions," *ACI Mater J*, vol. 118, no. 1, pp. 157–167, 2021, doi: 10.14359/51725994.

[6] S. E. Kelechi, M. Adamu, O. A. U. Uche, I. P. Okokpujie, Y. E. Ibrahim, and I. I. Obianyo, "A comprehensive review on coal fly ash and its application in the construction industry," 2022, *Cogent OA*. doi: 10.1080/23311916.2022.2114201.

[7] Z. T. Yao *et al.*, "A comprehensive review on the applications of coal fly ash," Feb. 01, 2015, *Elsevier*. doi: 10.1016/j.earscirev.2014.11.016.

[8] B. Gopalakrishna and D. Pasla, "Development of metakaolin based high strength recycled aggregate geopolymer concrete," *Constr Build Mater*, vol. 391, Aug. 2023, doi: 10.1016/j.conbuildmat.2023.131810.

[9] A. Mehta and R. Siddique, "Sustainable geopolymer concrete using ground granulated blast furnace slag and rice husk ash: Strength and permeability properties," *J Clean Prod*, vol. 205, pp. 49–57, Dec. 2018, doi: 10.1016/J.JCLEPRO.2018.08.313.

[10] D. Suresh and K. Nagaraju, "'Ground Granulated Blast Slag (GGBS) In Concrete-A Review,'" *IOSR Journal of Mechanical and Civil Engineering (IOSR-JMCE) e-ISSN*, vol. 12, no. 4, pp. 76–82, doi: 10.9790/1684-12467682.

[11] M. S. Prasad, K. J. Reid, and H. H. Murray, "Kaolin: processing, properties and applications," 1991.

[12] A. Albidah, M. Alghannam, H. Abbas, T. Almusallam, and Y. Al-Salloum, "Characteristics of metakaolin-based geopolymer concrete for different mix design parameters," *Journal of Materials Research and Technology*, vol. 10, pp. 84–98, Jan. 2021, doi: 10.1016/J.JMRT.2020.11.104.

[13] S. Parathi, P. Nagarajan, and S. A. Pallikkara, "Ecofriendly geopolymer concrete: a comprehensive review," Aug. 01, 2021, *Springer Science and Business Media Deutschland GmbH*. doi: 10.1007/s10098-021-02085-0.

[14] S. Dai, H. Wang, S. An, and L. Yuan, "Mechanical Properties and Microstructural Characterization of Metakaolin Geopolymers Based on Orthogonal Tests," *Materials*, vol. 15, no. 8, Apr. 2022, doi: 10.3390/ma15082957.

[15] T. H.M. and S. Unnikrishnan, "Mechanical Strength and Microstructure of GGBS-SCBA based Geopolymer Concrete," *Journal of Materials Research and Technology*, vol. 24, pp. 7816–7831, May 2023, doi: 10.1016/j.jmrt.2023.05.051.

[16] A. Öz *et al.*, "The radiation shielding and microstructure properties of quartzic and metakaolin based geopolymer concrete," *Constr Build Mater*, vol. 342, Aug. 2022, doi: 10.1016/j.conbuildmat.2022.127923.

[17] A. Noushini, M. Hastings, A. Castel, and F. Aslani, "Mechanical and flexural performance of synthetic fibre reinforced geopolymer concrete," *Constr Build Mater*, vol. 186, pp. 454–475, Oct. 2018, doi: 10.1016 /j.conbuildmat.2018.07.110.

[18] S. Yousefi Oderji, B. Chen, M. R. Ahmad, and S. F. A. Shah, "Fresh and hardened properties of one-part fly ash-based geopolymer binders cured at room temperature: Effect of slag and alkali activators," *J Clean Prod*, vol. 225, pp. 1–10, Jul. 2019, doi: 10.1016/ j.jclepro.2019.03.290.

[19] P. Nath and P. K. Sarker, "Effect of GGBFS on setting, workability and early strength properties of fly ash geopolymer concrete cured in ambient condition," *Constr Build Mater*, vol. 66, pp. 163–171, Sep. 2014, doi: 10.1016/j.conbuildmat.2014.05.080.

[20] S. Yaseri, G. Hajiaghaei, F. Mohammadi, M. Mahdikhani, and R. Farokhzad, "The role of synthesis parameters on the workability, setting and strength properties of binary binder based geopolymer paste," *Constr Build Mater*, vol. 157, pp. 534–545, Dec. 2017, doi: 10.1016/j.conbuildmat.2017.09.102.

[21] V. Jittin, R. Rithuparna, A. Bahurudeen, and B. Pachiappan, "Synergistic use of typical agricultural and industrial by-products for ternary cement: A pathway for locally available resource utilisation," Jan. 10, 2021, *Elsevier Ltd*. doi: 10.1016/j.jclepro.2020.123448.

[22] X. Gao, Q. L. Yu, and H. J. H. Brouwers, "Characterization of alkali activated slag-fly ash blends containing nano-silica," *Constr Build Mater*, vol. 98, pp. 397–406, Nov. 2015, doi: 10.1016/ j.conbuildmat. 2015.08.086.

[23] N. K. Lee and H. K. Lee, "Setting and mechanical properties of alkali-activated fly ash/slag concrete manufactured at room temperature," *Constr Build Mater*, vol. 47, pp. 1201–1209, 2013, doi: 10.1016/ j.conbuildmat.2013.05.107.

[24] A. B. Moradikhou, A. Esparham, and M. Jamshidi Avanaki, "Physical & mechanical properties of fiber reinforced metakaolin-based geopolymer concrete," *Constr Build Mater*, vol. 251, Aug. 2020, doi: 10.1016/j.conbuildmat.2020.118965.

[25] S. Inti, M. Sharma, D. Tandon, E. Paso, and A. Professor, "Ground Granulated Blast Furnace Slag (GGBS) and Rice Husk Ash (RHA) Uses in the Production of Geopolymer Concrete."

[26] B. Swathi and R. Vidjeapriya, "Influence of precursor materials and molar ratios on normal, high, and ultra-high performance geopolymer concrete – A state of art review," Aug. 15, 2023, *Elsevier Ltd*. doi: 10.1016/ j.conbuildmat.2023.132006.

Thermal Resistance of High Volume Copper Slag Geopolymer Activated by Different Activators

Kashini Sundaram
Department of Civil Engineering,
Thiagarajar College of Engineering,
Madurai, India.
kashinis@student.tce.edu

Brindha Dharmar
Professor, Department of Civil Engineering,
Thiagarajar College of Engineering,
Madurai, India.
dbciv@tce.edu

***Abstract*—Geopolymer concretes serve as a sustainable alternative to cement concrete, owing to their reduced carbon footprint and superior mechanical and thermal qualities. In either an alkaline or an acidic solution, geopolymers are produced through the activation of aluminosilicate precursors. This study examines the thermal properties of high-volume copper slag (HVC) geopolymer, highlighting the effects of various activators—phosphoric acid (HVC-PA) and alkali activators (HVC-AA)—and different curing condition at ambient and increased temperatures (60°C) on geopolymer strength retention. Fly ash served as the principal binder, and fine aggregate was entirely substituted with copper slag. Geopolymer cubes were exposed to temperatures of 200°C, 400°C, 600°C, 800°C, and 1000°C, and their residual compressive strength and mass loss were assessed. Findings demonstrate that phosphoric acid activation improves thermal stability, exhibiting reduced mass loss and increased residual strength relative to alkali-activated systems. The dense composition of copper slag resulted in decreased porosity and enhanced thermal resistance. Ambient curing enhances strength at reduced temperatures; however, it does not significantly affect high-temperature resistance beyond 600°C. Although all geopolymer samples shown strength degradation beyond 800°C due to microstructural disintegration, phosphoric acid-activated geopolymers preserved exceptional integrity. The results underscore the fire-resistant advantages of phosphoric acid-based geopolymers, rendering them appropriate for high-temperature applications in industrial and fire-sensitive settings.**

Keywords—Copper slag, Phosphoric acid, Alkali activated geopolymer, Thermal resistance.

I. INTRODUCTION

Geopolymer concrete (GPC) has arisen as a sustainable substitute for traditional Portland cement-based concrete, owing to its reduced carbon footprint and enhanced mechanical and durability characteristics. Fly ash-based geopolymers have garnered considerable interest among diverse geopolymer compositions due to their superior thermal stability and remarkable tolerance to high temperatures. The substitution of traditional fine particles with copper slag (CS) presents a prospective improvement in the performance of geopolymer concrete, especially under hot conditions [1]. Copper slag geopolymer concrete's thermal behaviour is still being studied, especially in relation to how various activators, such as phosphoric acid and alkali activators, affect strength retention and microstructural development at high temperatures[2]. Fly ash-based geopolymers exhibit excellent mechanical strength and thermal stability under high-temperature conditions[3]. Research indicates that fly ash geopolymers demonstrate enhanced strength up to 800°C owing to sintering processes, [4]. The hydration of copper slag at moderate temperatures (200°C) enhances the compressive strength of geopolymer mortar; however, at temperatures of 600°C and above, decomposition reactions result in strength deterioration due to the oxidation of $Fe(OH)_2/Fe(OH)_3$ into Fe_2O_3, which melts in a sodium-rich environment and modifies the microstructure[5] .Notwithstanding these limitations, copper slag enhances the structural performance, energy absorption, and hardness of geopolymer concrete [6]. Moreover, geopolymers containing copper slag exhibit negligible mass loss when subjected to high temperatures, mainly attributable to the oxidation of mineral constituents and the densification of the matrix . At ambient temperature, geopolymer concrete with copper slag exhibits diminished strength attributable to heightened porosity and decreased matrix cohesiveness [7]. The selection of activator significantly influences the thermal stability of geopolymer concrete [8]. Sodium-based activators often induce pore size expansion and a reduction in strength at 800°C due to the generation of Na-feldspars. In contrast, phosphoric acid-based geopolymers demonstrate exceptional fire resistance, maintaining their integrity at temperatures up to 1400°C, without melting or significant degradation [9]. The stability of phosphoric acid-based systems is due to their poly (phospho-siloxo) network, which improves fire resistance via a denser microstructure. Moreover, phosphoric acid geopolymers demonstrate negligible mass loss (2%) between 1000°C and 1400°C, thereby reinforcing their thermal stability[2], [10].Numerous writers have investigated the thermo-mechanical behaviour of fly ash-based geopolymer concrete. However, there have been few research on the impact of activator and copper slag on the thermal behaviour of fly ash geopolymer. This study employed phosphoric acid at a concentration of 10 M and a liquid-to-solid ratio of 0.9 as an acid activator to activate fly ash and copper slag. Sodium silicate and sodium hydroxide at a concentration of 12M and a liquid-to-solid ratio of 0.5 were employed as alkali activators. Fine aggregate was entirely substituted with copper slag. Geopolymer cubes are exposed to elevated temperatures of 200, 400, 600, 800, and 1000°C. The mass loss and compressive strength of the cubes were assessed following exposure to elevated temperatures. To determine the best activation technique for high-temperature applications, a comparison of the thermal stability of geopolymers activated by phosphoric acid and alkali is being carried out. The goal of this study is to further the creation of geopolymer concrete that can withstand high temperatures for use in industrial settings and fire-prone buildings

II. Materials and Test Methods

Materials

Fly ash with a specific gravity of 2.7 and low calcium content was utilized as the binding agent. Fly ash was obtained from the local vicinity in Madurai, India. Copper slag was acquired from the Sun Company located near Madurai. The chemical composition of the binding material was analyzed using XRD, presented in Figure 1. The specific gravity of the copper slag is measured at 3.15, as determined using the pycnometer apparatus. Figure 2 illustrates the particle size distribution of copper slag. The fine aggregate was completely substituted with copper slag. The fly ash and copper slag were activated using two different activators. Phosphoric acid at a concentration of 10 M was utilized as an acid activator, with a liquid-to-solid ratio of 0.9. For the alkaline activator, a sodium hydroxide solution with a concentration of 12M and sodium silicates at a liquid-to-solid ratio of 0.4 was utilized to activate the binders and fine aggregate. To ensure effective polymerization and minimize heat evolution, both acid and alkaline activators are prepared one day before casting.

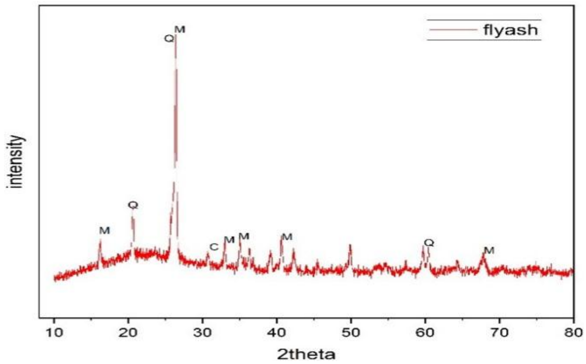

Fig 1: XRD pattern of fly ash

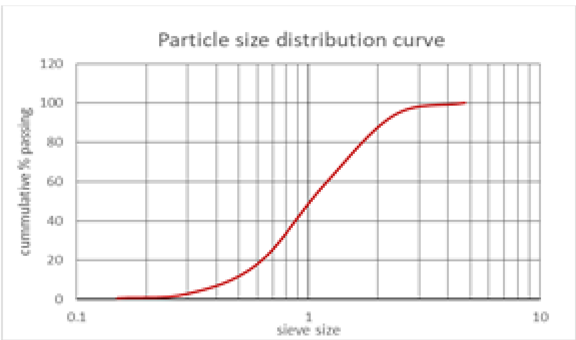

Fig 2: Particle Size Distribution curve of copper slag

Mix Proportions

It was assumed that the mortar had a density of 2400 kg/m^3. The ratio of fly ash to copper slag was established at 1:3. A total of 200 grams of fly ash was combined with 600 grams of copper slag. The weight of the phosphoric acid is considered to be 0.9 times the weight of the fly ash (binder) for acid activators. For alkaline activation, the mass of the sodium-based activator solution is considered to be 0.4 times the mass of the fly ash. The Rangan method was used to create the sodium-based solution using a 12 M sodium hydroxide and sodium silicate solution. In a mortar mixture with a capacity of twenty liters, the fly ash and copper slag were mixed together for two to three minutes. In the following step, the activating solution was gradually added to the dry mixture. Fig. 3 represents the mixing technique that was carried out. The cubes, which were 70.6 mm in size, were cast and then cured at a temperature of 60°C for 24 hours.

Maintaining the Integrity of the Specifications

The compressive strength of the geopolymer cubes was evaluated using a Universal Testing Machine at a constant loading rate following IS 4031 PART 6. The mean compressive strength of three cubes is calculated. A measurement of the samples' mass is taken both before and after they have been subjected to high temperatures. A percentage of mass loss was computed by the mass difference from the total mass using an equation. The thermal behaviour of geopolymer mortar was evaluated by subjecting the specimens to elevated temperatures of 200°C, 400°C, 600°C, 800°C, and 1000°C in an electric furnace capable of reaching a maximum temperature of 1200°C. The heating rate was consistently set, with specimens being held at the target temperature for a duration of 1 hour to ensure uniform heating prior to cooling to room temperature within the furnace.

III. Results and discussion

Compressive Strength:

The compressive strength of the acid and alkali-activated geopolymer under ambient and heat curing conditions is presented in Fig. 3. The average compressive strength of ambient cured heavy-volume copper slag geopolymer activated by phosphoric acid (HVC-PA-A) at 3, 7, and 28 days is 9.2 N/mm², 18 N/mm², and 30 N/mm², respectively. The compressive strength of phosphoric acid activated heat cured geopolymer (HVC-PA-H) was measured at 12 N/mm², 26 N/mm², and 37.2 N/mm² at 3, 7, and 28 days, respectively.

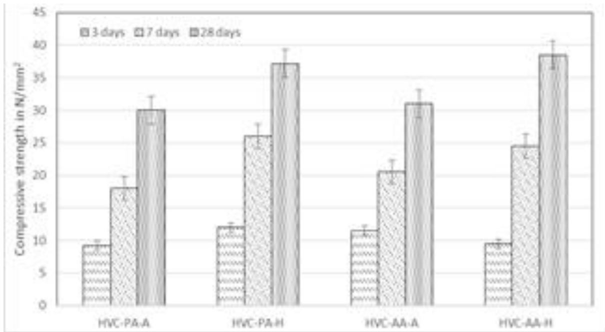

Fig 3: Compressive Strength value of geopolymer

When acid activation is involved, the temperature has the effect of accelerating the geo-polymerization process and improving the compressive strength. The compressive strength at 3, 7, and 28 days for high-volume copper slag and alkali-activated geopolymer (HVC-AA-A, HVC-AA-H) cured at both ambient and elevated temperatures is recorded as follows: 11.5 N/mm², 20.5 N/mm², 31 N/mm², 9.5 N/mm², 24.5 N/mm², 38.5 N/mm² respectively. At 28 days, the compressive strength of the geopolymer that has been activated with either acid or alkali and contains 100% copper slag is nearly same. The heat curing enhances the compressive strength of alkali-activated geopolymer, similar to the effects observed during acid activation. Figure 4 illustrates the compressive strength of heat-cured acid and alkali-activated geopolymer. According to Figure 4, the early compressive strength is notably high in acid-activated geopolymer. The alkali-activated geopolymer gradually develops its strength over time. The results indicate that the kinetics of geo polymerization enhanced with both time and temperature.

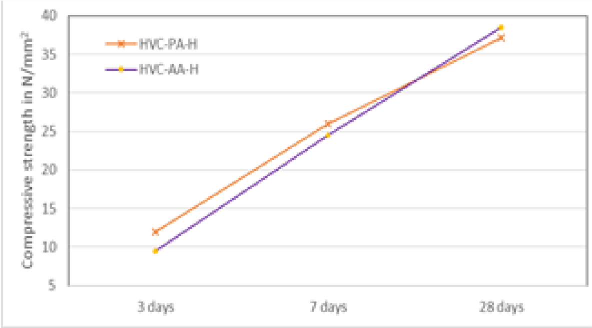

FIG 4: COMPARISON OF COMPRESSIVE STRENGTH OF HEAT CURED ALKALI AND ACID ACTIVATED GEOPOLYMER

Mass Loss

By comparing the mass of the geopolymer before and after exposure to high temperatures, the percentage of mass loss is calculated. Figure 5 depicts the mass loss percentage of large-volume copper slag geopolymer samples following exposure to high temperatures. At 200°C, the average mass loss percentage of HVC-PA is 3%, while for HVC-AA geopolymer, it is 4.2%. Initially, the mass loss occurred due to the evaporation of bound water. It was found that the percentage of mass loss increased with temperature increases in both the HVC-PA and HVC-AA geopolymer when the temperature range was between 400°C and 600°C.The elevated temperature results in the breakdown of hydroxyl groups and subsequent oxidation of mineral constituents, leading to a consistent rise in mass loss.

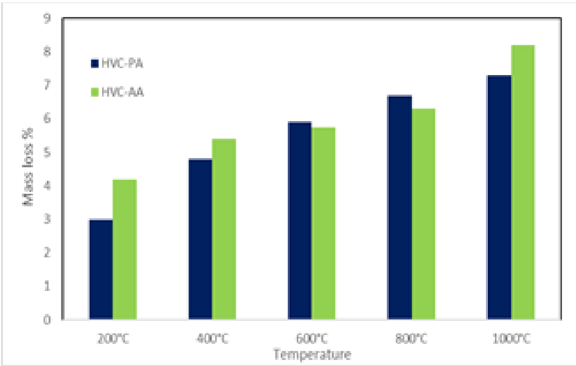

FIG 5: % OF MASS LOSS IN GEOPOLYMER AFTER EXPOSURE TO ELEVATED TEMPERATURE

The dense composition of copper slag lowers mass loss relative to conventional geopolymer use of crushed rock fine material. A maximum mass loss of 8.2% was found at a temperature of 1000°C, with HVC-AA proving a mass loss that was slightly higher than that of HVC-PA. The thermal instability of alkali-activated geopolymers at elevated temperatures leads to heightened material deterioration. Simultaneously, the acid-activated geopolymer (HVC-PA) demonstrates a more stable matrix, showing a comparatively lower mass loss.

The presence of high-density copper slag is helpful in improving matrix compactness, decreasing porosity, and minimizing material loss at elevated temperatures. Engaging in mineral oxidation reactions, facilitating densification and mitigating excessive deterioration. The findings demonstrate that acid-activated geopolymer (HVC-PA) exhibits superior thermal stability compared to alkali-activated geopolymer (HVC-AA), evidenced by reduced mass loss over all temperature ranges. The incorporation of copper slag as a fine aggregate considerably enhances the thermal stability of geopolymer mortar by creating a denser and more compact structure, hence minimizing mass loss even under severe temperatures. A significant observation from the study indicates that the mass loss in both geopolymer systems is substantially lower compared to the geopolymer that employs crushed rock as fine aggregate.

Residual Compressive Strength After Exposure to Elevated Temperature

The figure 6 depicts the comparative compressive strength of four distinct geopolymer mortar samples at high temperatures, ranging from 200°C to 1000°C. The samples vary according to the type of activator and curing conditions. The relative compressive strength of all geopolymer samples exhibits a modest increase at 200°C and 400°C, with ambient-cured samples (HVC-PA-H and HVC-AA-H) exhibiting a greater rise than heat-cured samples. At 400°C, the compressive strengths of the ambient cured and heat cured HVC-PA and HVC-AA geopolymer samples are 45 N/mm², 28.5 N/mm², 45.4 N/mm², and 25.42 N/mm², respectively. Prior to exposure to increased temperatures, the highest compressive strength of the ambient-cured and acid-activated geopolymer sample was 38.5 N/mm². Similarly, the ambient-cured geopolymer samples activated with alkali had a compressive strength of 37.2 N/mm². In the case of acid activation in particular, the presence of heat enhanced the poly-condensation reaction. The improved polycondensation results in the production of extra gel phases that contribute to structural stability. The enhancement in strength during this phase results from additional geopolymerization processes, matrix densification, and the evaporation of free water, which contributes to the reduction of internal porosity. The samples attain their peak relative compressive strength between 200°C and 400°C. Beyond 400°C, all samples demonstrate a steady decrease in compressive strength. Phosphoric acid-activated geopolymer (HVC-PA-H) displays the highest peak strength, followed by heat-cured alkali-activated geopolymer (HVC-AA-H).Phosphoric acid-activated geopolymers degrade more slowly than alkali-activated samples (HVC-AA-A and HVC-AA-H).The reduction in strength is chiefly attributable to dehydration and dihydroxylation of binding phases, resulting in the creation of micro cracks. In alkali-activated systems, elevated temperatures lead to an increase in pore size, which causes structural degradation. Exceeding 800°C, all geopolymer specimens have a substantial decline in strength, with measurements nearing 20% to 30% of their initial strength. At 1000°C, the residual strength is minimized due to microstructural deterioration and the disintegration of binding phases in alkali-activated geopolymers. Densification and potential sintering effects in phosphoric acid-based geopolymers, but still exhibiting a reduction in strength at temperature above 600°C. HVC-PA samples demonstrate superior thermal resistance compared to HVC-AA samples across all temperature ranges. The acid-activated geopolymer matrix exhibits stability over a broader temperature range, while alkali-activated geopolymers deteriorate more rapidly beyond 400°C. At elevated temperatures, phosphoric acid-based geopolymers exhibit a denser microstructure, resulting in enhanced residual strength. At elevated temperature ambient-cured geopolymers (HVC-PA-H and HVC-AA-H) exhibit superior starting and peak compressive strengths compared to heat-cured samples. This results from enhanced polymerization and matrix densification during the curing process. At elevated temperatures (>600°C), all samples exhibit analogous deterioration patterns, irrespective of the curing conditions.

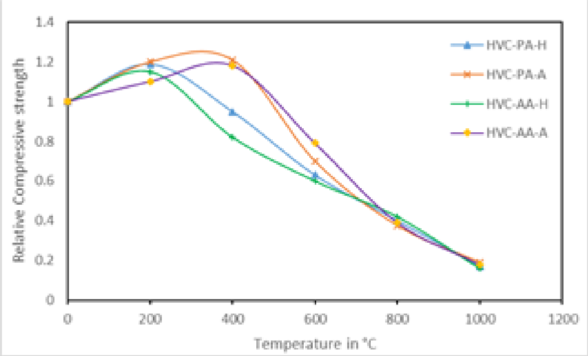

FIG 6: RELATIVE COMPRESSIVE STRENGTH OF GEOPOLYMER AFTER EXPOSURE TO ELEVATED TEMPERATURE

IV. CONCLUSIONS

- Phosphoric acid-based geopolymer (HVC-PA) has enhanced thermal stability relative to alkali-activated geopolymer (HVC-AA).
- Ambient curing improves strength at lower temperatures; however, it does not exert a substantial influence on high-temperature resistance beyond 600°C.
- At temperatures above 800°C, microstructural breakdown causes a significant decrease in the relative strength of all geopolymers.
- The high volume of copper slag can enhance thermal stability by reducing porosity and improving matrix density. This results in reduced mass loss even under extreme temperatures, rendering it a more resilient alternative to traditional geopolymer systems.

This investigation emphasizes the fire-resistant benefits of phosphoric acid-based geopolymers, rendering them more appropriate for high-temperature applications than traditional alkali-activated systems.

ACKNOWLEDGMENT

The authors are grateful for the support from the host institution. The authors declare no potential conflict of interest.

REFERENCES

[1] P. R. Prem, M. Verma, and P. S. Ambily, “Sustainable cleaner production of concrete with high volume copper slag,” J Clean Prod, vol. 193, pp. 43–58, Aug. 2018, doi: 10.1016/j.jclepro.2018.04.245.

[2] A. Katsiki, “Aluminosilicate phosphate cements–a critical review,” Jul. 04, 2019, Taylor and Francis Ltd. doi: 10.1080/17436753.2019.1572339.

[3] B. Kanagaraj, N. Anand, A. D. Andrushia, and E. Lubloy, “Investigation on engineering properties and micro-structure characteristics of low strength and high strength geopolymer composites subjected to standard temperature exposure,” Case Studies in Construction Materials, vol. 17, Dec. 2022, doi: 10.1016/j.cscm.2022.e01608.

[4] P. He, D. Jia, T. Lin, M. Wang, and Y. Zhou, “Effects of high-temperature heat treatment on the mechanical properties of unidirectional carbon fiber reinforced geopolymer composites,” Ceram Int, vol. 36, no. 4, pp. 1447–1453, May 2010, doi: 10.1016/j.ceramint.2010.02.012.

[5] C. Nobouassia Bewa, H. K. Tchakouté, D. Fotio, C. H. Rüscher, E. Kamseu, and C. Leonelli, “Water resistance and thermal behavior of metakaolin-phosphate-based geopolymer cements,” Journal of Asian Ceramic Societies, vol. 6, no. 3, pp. 271–283, Jul. 2018, doi: 10.1080/21870764.2018.1507660.

[6] P. R. Prem, M. Verma, and P. S. Ambily, “Sustainable cleaner production of concrete with high volume copper slag,” J Clean Prod, vol. 193, pp. 43–58, Aug. 2018, doi: 10.1016/j.jclepro.2018.04.245.

[7] M. Sivasakthi, R. Jeyalakshmi, and N. P. Rajamane, “Fly ash geopolymer mortar: Impact of the substitution of river sand by copper slag as a fine aggregate on its thermal resistance properties,” J Clean Prod, vol. 279, Jan. 2021, doi: 10.1016/j.jclepro.2020.123766.

[8] A. Katsiki, “Aluminosilicate phosphate cements–a critical review,” Jul. 04, 2019, Taylor and Francis Ltd. doi: 10.1080/17436753.2019.1572339.

[9] H. Celerier, J. Jouin, V. Mathivet, N. Tessier-Doyen, and S. Rossignol, “Composition and properties of phosphoric acid-based geopolymers,” J Non Cryst Solids, vol. 493, pp. 94–98, Aug. 2018, Doi: 10.1016/j.jnoncrysol.2018.04.044.

[10] Q. Ma et al., “Performance of copper slag contained mortars after exposure to elevated temperatures,” Constr Build Mater, vol. 172, pp. 378–386, May 2018, doi: 10.1016/j.conbuildmat.2018.03.261.

Artificial Intelligence Powered Soil Health Diagnosis using Multimodal Soil Sense Neural Network

Srijah S
Department of Information Technology,
Thiagarajar College of Engineering,
Madurai, Tamil Nadu
srijah@student.tce.edu

Jaipreetha S
Department of Information Technology,
Thiagarajar College of Engineering,
Madurai, Tamil Nadu
jaipreetha@student.tce.edu

Sridevi S
Department of Information Technology,
Thiagarajar College of Engineering,
Madurai, Tamil Nadu
sridevi@tce.edu

Ehil G R
Department of Information Technology,
Thiagarajar College of Engineering,
Madurai, Tamil Nadu
ezhilr@student.tce.edu

***Abstract*—Soil health assessment is vital for sustainable agriculture but remains complex due to the heterogeneous nature of soil properties and environmental factors. This study introduces an AI-driven framework that processes multimodal soil data through five stages: data acquisition, preprocessing, vector extraction, feature selection using EarthSpace Crow Optimization, and prediction via the Soil Sense Neural Network. The model achieved over 99% accuracy in predicting key soil indicators such as organic carbon, microbial activity, and pH. By integrating spatial, temporal, and environmental features, the framework ensures high adaptability and accuracy, enabling real-time soil diagnostics for precision agriculture and sustainable land management.**

Keywords—Soil health diagnosis, AI-driven framework, Earth Space Crow Optimization, SoilSense Neural Network.

I. INTRODUCTION

Soil health is essential for sustainable agriculture, ecosystem balance, and global food security [1]. It reflects the soil's ability to support plant growth, maintain environmental quality, and promote biodiversity [3]. Assessing soil health is difficult due to its complex physical, chemical, and biological traits, which vary with climate and environment [4]. Traditional methods rely on manual sampling and lab analysis. These are time-consuming, costly, and often limited in scope [7]. There is a growing need for fast, scalable, and comprehensive ways to monitor soil health in real time.

Advances in artificial intelligence (AI) and sensing technologies offer new solutions. Using in-situ sensors, remote sensing, and lab data allows for a fuller picture of soil conditions [6]. AI models can analyze this data to improve prediction accuracy and automate assessments. They provide real-time insights on nutrients, moisture, and microbial activity [2]. Compared to traditional methods, AI-based systems are scalable and support precision agriculture by improving resource use and land management.

This study presents an AI-based framework for soil health diagnosis. It integrates five key stages: (1) data acquisition from sensors, satellite images, and lab tests; (2) preprocessing to clean and normalize data; (3) feature extraction to reduce dimensionality; (4) feature selection using metaheuristic algorithms; and (5) prediction using a deep learning model [5]. The model predicts critical soil indicators like organic carbon, microbial activity, and pH. It is adaptable and accurate across different environments. This helps lower input costs, prevent soil degradation, and boost productivity.

The remainder of this paper is structured as follows**.** **Section II** presents a review of related works, highlighting existing challenges in soil health diagnostics and the role of AI in overcoming these limitations. **Section III** details the proposed work, outlining the five core stages of the framework. **Section IV** discusses the experimental results and performance evaluation, comparing the proposed model with conventional methods. **Section V** Finally, the paper concludes and Future work. Section VI acknowledgments. This research marks a significant advancement in AI-driven soil health diagnostics, offering a transformative approach for precision agriculture and sustainable land management..

Related Works

Soil fertility prediction has been extensively studied using various learning methodologies to address agricultural challenges. It is defined as the ability of soil to supply essential nutrients and adequate water to support high-yield and high-quality crop production. Artificial neural networks (ANNs) have been utilized with the Levenberg-Marquardt-based back-propagation approach to predict soil fertility [8]. Partial least squares regression has also been applied, incorporating bulk density, electrical conductivity (EC), available water capacity, and soil organic carbon (OC) to classify soil types, including pewamo silty clay loam, glynwood silt loam, kibbie fine sandy loam, crosby silt loam, and crosby celina silt loam [9].

Predicting agricultural output is a key focus in soil fertility research, as estimating future harvests is essential for farmers. Data mining techniques offer a promising approach by extracting meaningful patterns from agricultural datasets [10].

II. PROPOSED WORK

This study introduces a comprehensive and systematic methodology for soil health diagnosis, leveraging innovative computational techniques and multimodal data. The proposed framework consists of five sequential stages, each designed to address specific challenges associated with soil data heterogeneity, dimensionality, and predictive modeling. Figure 1 Shows the Schematic representation of the suggested methodology.

KSSL (Kellogg Soil Survey Laboratory) Dataset:

The **Kellogg Soil Survey Laboratory (KSSL)** dataset is a publicly accessible repository provided by the **United States Department of Agriculture (USDA)** Natural Resources Conservation Service (NRCS). This dataset contains extensive soil profiles, laboratory analysis results, and field observations, covering a wide array of soil properties across diverse geographic and environmental regions in the United States. It is widely regarded as one of the most comprehensive soil datasets available for research and development in soil science and related fields.

For this study, the KSSL dataset was utilized as a benchmark to validate the proposed framework's effectiveness. The classes can often be interpreted from the metadata or the problem statement. For example:

- **Class 1** might represent "Sandy Soil,"
- **Class 2** could denote "Clay Soil,"
- **Class 3** could signify "Loamy Soil."

Data Acquisition

This stage involves collecting soil-related data using three primary sources:

Sensors: In-situ soil sensors provide real-time measurements of critical soil parameters such as moisture, temperature, electrical conductivity, and pH.

Remote Sensing: Satellite and UAV-based imaging techniques help capture large-scale soil properties, including vegetation health, soil texture, and organic content.

Laboratory Analysis: Physical and chemical tests conducted in laboratories provide detailed insights into soil composition, including macro- and micronutrient content, microbial diversity, and contamination levels.

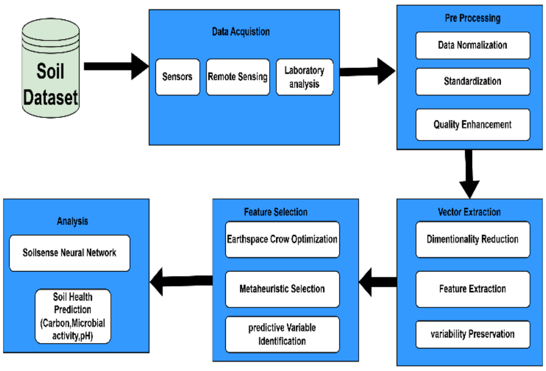

FIG 1 SCHEMATIC REPRESENTATION OF THE SUGGESTED METHODOLOGY

Data Preprocessing

Preprocessing addresses the challenges of heterogeneous soil data, which often have varying units, scales, and distributions. This preprocessing step ensures that the dataset is standardized, consistent, and reliable for subsequent analyses. Soil data includes diverse variables such as pH (unitless), moisture content (percentage), and bulk density ($\mathrm{g/cm^3}$), with some features exhibiting extreme outliers or skewed distributions. The incorporates a three-pronged approach: Z-score normalization, robust scaling for outlier-sensitive features, and logarithmic transformation for highly skewed distributions.

Data Normalization

Ensures that all input features are brought to a common scale, preventing numerical imbalances that might bias the learning model. Example: Soil pH ranges from 0 to 14, while organic carbon content may range from 0 to 5%. Normalization ensures both are mapped to a standard range (e.g., [0,1] or [-1,1]).

Standardization:

Converts raw values into a standardized format (mean = 0, variance = 1) to improve training stability.

Example: Converting soil temperature from °C to a unit-free standard score.

Quality Enhancement:

Handles missing values using interpolation or imputation techniques. Detects and removes anomalies or outliers that could distort predictions.

For features without significant outliers, Z-score normalization is applied:

$$x'_{ij} = \frac{x_{ij}-\mu_j}{\sigma_j} \quad (1)$$

where:

- x_{ij} is the value of the i-th observation for the j-th feature,
- μ_j is the mean of the j-th feature,
- σ_j is the standard deviation of the j-th feature.

This transformation centers the data around 0 and scales it to have a standard deviation of 1, ensuring comparability across features.

For features with outliers, robust scaling is employed to mitigate the influence of extreme values:

$$x'_{ij} = \frac{x_{ij} - \text{median}_j}{\mathrm{IQR}_j} \quad (2)$$

where:

- median_j is the median of the j-th feature,
- $\mathrm{IQR}_j = Q_{3j} - Q_{1j}$ is the interquartile range, with Q_3 and Q_1 being the 75 th and 25 th percentiles, respectively.

C. Vector Extraction

Vector Extraction is an advanced feature extraction method designed to reduce the dimensionality of high-dimensional soil datasets while retaining the most critical variability. High-dimensional datasets, such as those involving soil properties, often suffer from the "curse of dimensionality," where the number of features overwhelms the ability to extract meaningful patterns. overcomes this by projecting the data into a lower-dimensional space while preserving the maximum variance and ecological relevance.

Dimensionality Reduction:

Techniques like Principal Component Analysis (PCA) and t-SNE reduce the number of input variables while retaining essential information.

This step helps eliminate redundant information and speeds up computations.

Feature Extraction:

Converts raw soil attributes into structured formats suitable for machine learning. Example: Transforming multispectral remote sensing data into vegetation indices (NDVI, SAVI).

Variability Preservation:

Ensures that key variations in soil properties are maintained during the transformation process. Example: Keeping the seasonal variations of soil moisture to improve long-term predictions.

D. Feature Selection

EarthSpace Crow Optimization is a metaheuristic algorithm inspired by the social and foraging behavior of crows. This algorithm is particularly effective for feature selection in high-dimensional datasets, such as those in soil health diagnostics, where identifying the most predictive features is critical. By simulating the intelligent resource-securing strategies of crows, the algorithm efficiently explores the search space to identify relevant features while minimizing redundancy and overfitting.

Let the dataset be represented as:

$$\mathbf{X} \in \mathbb{R}^{N \times p} \tag{3}$$

where N is the number of observations, and p is the total number of features. The goal is to select a subset of features $\mathbf{S} \subseteq \{1,2,\ldots,p\}$ that optimizes the objective function:

$$\text{maximize: } f(\mathbf{S}) = \sum_{i \in \mathbf{S}} \text{gain}(x_i) - \beta \sum_{i,j \in \mathbf{S}} \text{redundancy}\left(x_i, x_j\right)$$

where:

- gain (x_i) measures the predictive power of feature x_i,
- redundancy $\left(x_i, x_j\right)$ quantifies the correlation or overlap between features x_i and x_j,
- β is a weighting parameter controlling the trade-off between maximizing predictive power and minimizing redundancy.

The algorithm uses m crows, each representing a potential solution (a subset of features). The position of the i-th crow at iteration t is denoted as $\mathbf{x}_i^t$, which corresponds to a subset of features. The best position discovered so far is represented by $\mathbf{g}^t$.

Earth Space Crow Optimization effectively balances exploration (searching new areas of the feature space) and exploitation (refining the best-known solutions). This ensures that the most predictive and least redundant features are selected, reducing computational overhead and enhancing the interpretability of subsequent models. By focusing on the relevant features, this step significantly improves the performance and efficiency of predictive models for soil health diagnostics.

E. Analysis and Soil Health Prediction

Soil Sense Neural Net is a specialized neural network designed for high-accuracy temporal and spatial forecasting of soil health indicators. This model integrates multimodal inputs, captures complex nonlinear relationships, and addresses the challenges posed by temporal dynamics and spatial variability in soil datasets. By leveraging advanced attention mechanisms and sequence-to-sequence forecasting, the model predicts soil health metrics across various temporal and spatial resolutions with high precision.

Soil Sense Neural Network:

A specialized neural network designed for soil health assessment. Uses deep learning to model complex relationships between soil features and health indicators.

Prediction of Key Soil Health Indicators:

The model predicts essential soil attributes such as:

Soil Carbon Content – Indicator of organic matter and fertility.

Microbial Activity – Reflects biological health and soil biodiversity.

pH Levels – Determines soil acidity/alkalinity, affecting nutrient availability.

Let the processed dataset be represented as:

$$\mathbf{X} \in \mathbb{R}^{N \times p} \tag{4}$$

where N is the number of observations and p is the number of features after preprocessing and optimization. Each observation includes spatiotemporal metadata (e.g., latitude, longitude, time) and soil property features. The target variable is represented as:

$$\mathbf{y} \in \mathbb{R}^{N} \tag{5}$$

which corresponds to the soil health indicator of interest, such as organic carbon, microbial activity, or pH.

Performance Analysis

The experimental evaluation of the suggested methodology was illustrated in this section. The overall experimentation was carried out under python environment.

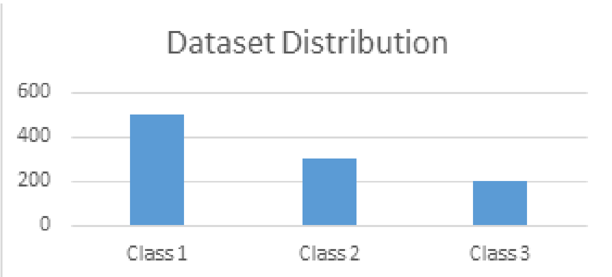

FIG 2 DATASET DISTRIBUTION ANALYSIS

The dataset distribution graph as in Figure 2 shows the number of samples across three classes: Class 1, Class 2, and Class 3. Class 1 has the largest representation with 500 samples, followed by Class 2 with 300, and Class 3 with 200. The experimental evaluation of the suggested methodology was illustrated in this section. The overall experimentation was carried out under python environment. Figure 3(a), (b) Shows the accuracy and loss analysis.

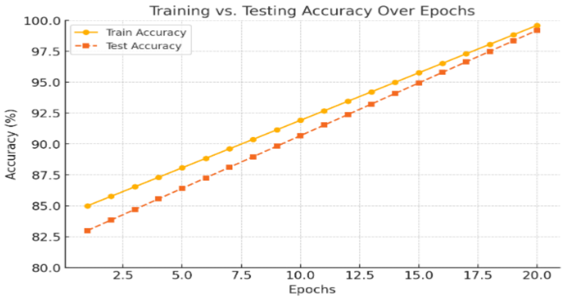

(a)

(b)

FIG 3(A), (B) ACCURACY AND LOSS ANALYSIS

The train-test accuracy plot shows a steady increase in accuracy over 20 epochs, with training accuracy reaching 98% and test accuracy stabilizing around 96%. This suggests that the model generalizes well without overfitting. The train-test loss plot mirrors this trend, with both losses decreasing as the model learns. Training loss reduces faster than testing loss, reflecting effective convergence. The narrowing gap between train and test performance indicates minimal overfitting, a desirable trait for robust models.

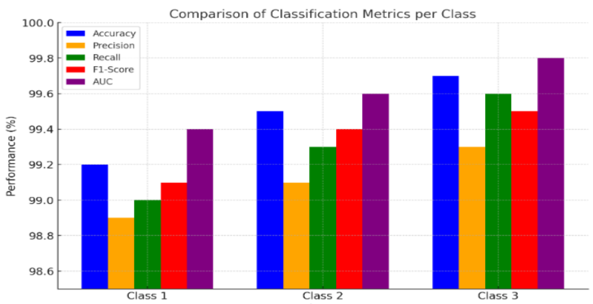

FIG 4 PERFORMANCE EVALUATION OF THE SUGGESTED METHODOLOGY

The updated graph displays all classification metrics—Precision, Recall, F-Score, and AUC—with values above 99% for each class shown in Figure 4**.** The average values across all classes for the evaluated classification metrics highlight the exceptional performance of the model.

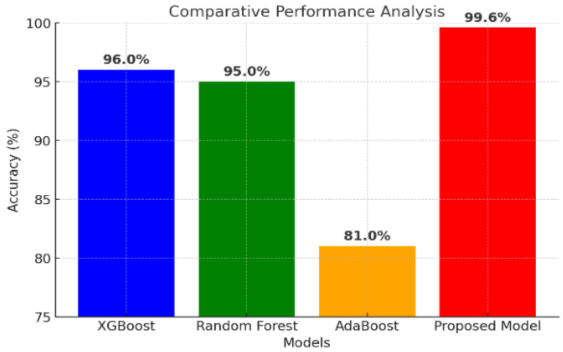

FIG 5 COMPARATIVE PERFORMANCE ANALYSIS

The updated bar chart in Figure 5 now includes the Proposed Model with an impressive overall accuracy of 99.6%, significantly surpassing the other models. XGBoost achieves 96.0%, Random Forest 95.0%, and Adaboost 81.0%. This chart clearly highlights the superior performance of the Proposed Model, emphasizing its effectiveness in accurately predicting soil health status

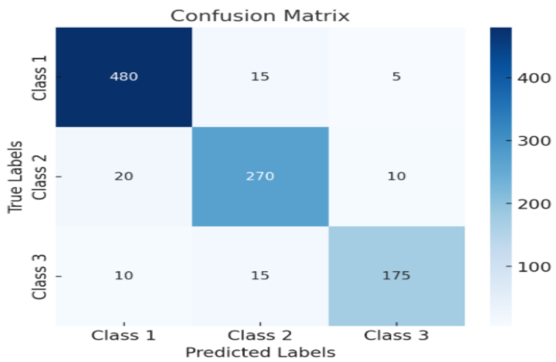

FIG 6 CONFUSION MATRIX

Figure 5 shows the confusion matrix shows that the model performs well, with **Class 1 (96% accuracy)** having the highest correct predictions, followed by **Class 2 (90%)** and **Class 3 (87.5%).** While most predictions are accurate, some misclassifications occur, particularly between **Class 2 and Class 3.** The model slightly confuses **Class 2 with Class 1 (20 samples)** and **Class 3 with Class 2 (15 samples).** Overall, the model demonstrates high accuracy but could benefit from further optimization, such as fine-tuning or using more balanced training data, to reduce misclassifications and improve precision.

III. CONCLUSION AND FUTURE WORK

This study proposes an AI-based framework for soil health diagnosis using preprocessing, vector extraction, EarthSpace Crow Optimization, and the SoilSense Neural Network. The model achieved over 99% accuracy in predicting key indicators like organic carbon, microbial activity, and pH. It handles data heterogeneity and dimensionality effectively and works well across diverse environments. The approach is scalable, though it requires quality input data and computational resources. Future work will focus on real-time sensor integration, new optimization methods, and additional metrics like heavy metal content and erosion risk to further improve the system.

Acknowledgement

The authors express their gratitude to the Thiagarajar College of Engineering (TCE) for supporting us to carry out this research work also, the financial support from TCE under Thiagarajar Research Fellowship scheme (File. No: TRF/Jul-2024/04) is gratefully acknowledged.

References

[1] Patel, A. A., & Kathiriya, D. R. (2017). Data mining trends in agriculture: A review. *Agres - International Journal (Toronto, Ont.)*, *6*(4), 637–645.

[2] Delgado-Baquerizo, M., Maestre, F. T., Gallardo, A., et al. (2013). Decoupling of soil nutrient cycles as a function of aridity in global drylands. *Nature*, *502*(7473), 672–676.

[3] Wang, W., Sardans, J., & Zeng, C. (2014). Responses of soil nutrient concentrations and stoichiometry to different human land uses in a subtropical tidal wetland. *Geoderma*, *232*(234), 459–470.

[4] McBratney, A., de Gruijter, J., & Bryce, M. (2019). Pedometrics timeline. *Geoderma*, *338*, 568–575.

[5] Jayalakshmi, R., & Savitha Devi, M. (2022). Mining agricultural data to predict soil fertility using ensemble boosting algorithm. *International Journal of Information Communication Technologies and Human Development*, *14*(1), 1–10.

[6] Sirsat, M. S., Cernadas, E., Fernández-Delgado, M., & Khan, R. (2017). Classification of agricultural soil parameters in India. *Computers and Electronics in Agriculture*, *135*, 269–279.

[7] Sheela, P., & Sivaranjani, K. (2015). A brief survey of classification techniques applied to soil fertility prediction. In *International Conference on Engineering Trends in Science and Humanities* (pp. 80–83).

[8] de Paul Obade, V., & Lal, R. (2016). Towards a standard technique for soil quality assessment. *Geoderma*, *265*, 96–102.

[9] Geetha, M. C. S. (2015a). A survey on data mining techniques in agriculture. *International Journal of Innovative Research in Computer and Communication Engineering*, *3*(2), 287–290.

[10] Sikora, R. (2014). A modified stacking ensemble machine learning algorithm using genetic algorithms. *Journal of International Technology and Information Management*, *23*(1), 1–12.

Deep Learning for Spatial Intelligence: Geospatial Advances in Environmental and Urban Decision-Making

Suriya Murugan
Department of Computer Science and Engineering,
Sri Eshwar College of Engineering,
Coimbatore, India
suriya13.ms@gmail.com

T. Suba Nachiar
Department of Information Technology,
Thiagarajar College of Engineering,
Madurai, Coimbatore, India
Subhanatchiar.t@gmail.com

Yuvasini D
Department of Computer Science and Business Systems,
Thiagarajar College of Engineering,
Madurai, Coimbatore, India
dyica@tce.edu

P R Hemalatha
Department of Computer Science and Engineering,
Velammal College of Engineering and Technology,
Madurai, India
hemalatha191286@gmail.com

***Abstract*—Deep Learning (DL) and Artificial Intelligence (AI) are increasingly being utilized in conjunction with Geographical Information System (GIS) for various purposes. The integration of Deep Learning methods with GIS offers a unique opportunity to gain new insights into environmental processes, benefiting from enhanced spatial, temporal, and spectral resolutions, as well as data integration capabilities. This powerful combination has propelled the fields of remote sensing and Geospatial analysis to the forefront of research for scientists worldwide. Deep learning has demonstrated remarkable potential for a multitude of GIS applications, which encompass data collection, analysis, interpretation, visualization, and presentation of geospatial data. Leveraging neural networks and other deep learning techniques has proven to be highly effective in optimizing the accuracy and efficiency of various GIS tasks. This research examines a range of cutting-edge deep learning models that help academics handle massive amounts of data effectively and equip decision-makers in a variety of sectors, include urban development, environmental surveillance, disaster relief, and beyond.**

***Keywords*—GIS, Geo-Spatial data, Artificial Intelligence, Deep learning, Computational Intelligence, convolutional neural network.**

I. INTRODUCTION

In this era of technological advancement, the integration of Deep Learning with Geographic Information Systems (GIS) has opened new horizons for geospatial analysis. Emerging technologies like artificial intelligence, machine learning (ML), and deep learning (DL) have the potential to significantly enhance GIS. While ML focuses on the creation of algorithms that allow machines to learn from data, AI entails the creation of intelligent machines that are capable of doing activities that traditionally require human intelligence. Neural networks are used in the ML area of deep learning (DL) to process enormous and complicated datasets. GIS can be described as a specialized database that stores data points in the form of spatial coordinates.

Geospatial information may be stored and retrieved more easily in these databases because to geo-references. The visualization of geospatial data as a map is similar to the visualization of high-dimensional hyperspectral data. To make it easier to store and retrieve geospatial data, these databases make use of geo-references. A map can be used to visualize geospatial data, which resembles high-dimensional hyperspectral data. Latitude and longitude coordinates are included in the data file, turning it into geospatial information that may be mined for geospatial information using GIS tools.

Deep Learning techniques, with their ability to process vast amounts of spatial data, have enabled more accurate and insightful geospatial analyses than ever before. By leveraging the power of neural networks and advanced algorithms, GIS applications can now benefit from enhanced data resolution, improved predictive modeling, and a deeper understanding of complex environmental processes. Deep learning is characterized by its utilization of neural networks, which are modelled after the network of neurons in the human brain. This architecture enables these networks to process vast amounts of geospatial data in parallel, detecting intricate modelled after the network of neurons in the human brain challenging for traditional GIS methods. As a result, deep learning has accelerated the progress of geospatial analysis, paving the way for improved land cover classification, object detection, change detection, and urban planning, among many other applications.

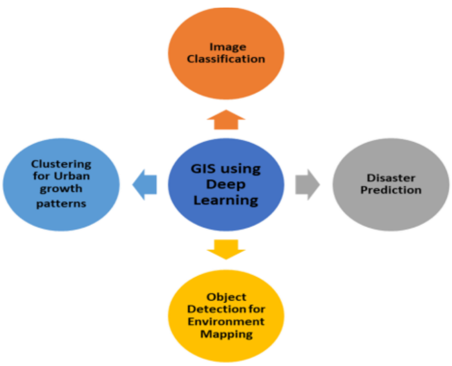

FIG 1 INTEGRATION OF DL FOR GIS

As shown in Figure 1 prediction, classification, clustering, and object detection are all important techniques utilized in GIS to analyze and interpret geospatial data. Prediction involves using historical geospatial data to forecast future trends or outcomes. In a GIS, classification is the process of grouping geographic data into separate classes or categories according to a set of criteria. A spatial data analysis approach known as clustering in GIS is used to group comparable geographic features or data points based on their spatial closeness or attribute similarity.. Object detection in GIS refers to automatically identifying and locating specific objects or features of interest within geospatial data. This integration has brought GIS to the forefront of research and development in fields such as environmental monitoring, disaster management, transportation optimization, and smart city planning. Governments, industries, and researchers worldwide are harnessing the power of deep learning and GIS to address pressing global challenges and make informed decisions for sustainable development.

The structure of this paper is as follows: A thorough analysis of the GIS works utilizing ML and DL can be found in Section II. Section III presents the techniques for machine intelligence for GIS data analysis. Section IV describes the significance of classification and clustering models for GIS analysis. Section V elaborates the advanced deep learning techniques for GIS. Section VI and VII gives the application and conclusion respectively.

II. Literature Survey

This section presents a selection of relevant papers that illustrate the growing popularity and wide-ranging applicability of combining deep learning with GIS technology across various domains. These papers demonstrate the increasing interest and utilization of this merger in the field.

In [1], authors explored a pixel-based image analysis methodology for swift landslide detection, relying on unsupervised Deep Learning. A convolutional auto-encoder (CAE) was employed to extract valuable characteristics from the input data. Subsequently, the resulting deep features are clustered using Mini Batch K-means. This combination of DL and clustering techniques enables rapid and efficient landslide detection, facilitating timely and accurate monitoring of potentially hazardous areas.

The process of GIS mapping involves converting geographical data into digital maps, enabling convenient identification of patterns, trends, and relationships. To extract characteristics from the bi-temporal images in [2], the author employed a deep learning network, namely STANet. The foundation of STANet is a Residual Neural Network (ResNet). The main goal of the first module is change detection, where built-up areas that have changed between the bi-temporal images are calculated. The second module's main objective is to update GIS maps with the discovered modifications.

One challenge with pixel-based deep learning methods is their inability to accurately capture the fine outlines of ground objects. To overcome this, in [3] author integrated a deep feature learning strategy with image objects to interpret remote sensing images more accurately. By considering context information that reveals relationships between image objects, they employed object-based CRF to optimize the classification results. Moreover, authors incorporated height information obtained from LiDAR data, further enhancing the accuracy of the classification process.

Using omnidirectional SVIs (Street View Images) taken with an onboard camera, the author of [4] proposed a model intended to determine the built year and structure of buildings. To categorise the year that a building was built and its construction, the author trained a deep learning model. Deep convolutional neural networks (DCNN) and vision transformers (ViT) were combined for this purpose. The findings showed that the ViT model's processing of the SVI was successful in precisely predicting each building's structure and year of construction.

A unique method called BCMO-DeepNeuralNets, developed for forecasting the geographic distribution of landslide-prone areas, is introduced and evaluated by the authors in [5]. A tropical cyclone-prone area in central Vietnam, including the districts of Nam Tra My, Bac Tra My, and Phuoc Son, is the subject of the study. Ten crucial input elements were considered: slope, aspect, elevation, relief amplitude, land use, soil type, road distance, geology, fault distance, rainfall, and ten others.The suggested BCMO-DeepNeuralNets method uses the power of Deep Neural Networks (DNNs) to build an advanced deep-learning model that can precisely estimate indices of landslip susceptibility.

In [6], author investigates an AI-based method to identify factors influencing urban land prices. It integrates the land price assessment technique with deep learning. A deep neural network, or CNN, is used to incorporate the spatial properties of the impacting components. The deep hybrid neural network automatically identifies linear and causal relationships between factors and land prices, facilitating accurate understanding and evaluation of urban land prices.

Globally, staple crops have been greatly impacted by climate change. Indonesia, a developed nation, is especially susceptible to this danger. Author in [7] presented the Normalised Difference Water Index (NDWI) from Landsat 8 OLI data to evaluate water scarcity in the study region. They used a CNN-based YOLO model capable of detecting drought during the growth stages of maize. By leveraging remote sensing technology, this model enables real-time object detection with commendable accuracy, presenting a promising approach to tackle the challenges posed by climate change on agricultural productivity in Indonesia.

For pixel-wise prediction, the author of [8] described a deep convolutional network with a simple architecture that successfully incorporated activations from many layers. They also improved the output representation's expressiveness by introducing the signed distance function of building boundaries. To train our network, author utilize ample building footprint data from GIS to create a vast labeled dataset. Our trained model exhibits exceptional performance on larger and more complex datasets compared to previous approaches. This demonstrates the possibility of our suggested approach as a scalable and feasible approach to automating the time-consuming task of developing boundary detection.

III. Machine Intelligence for GIS Data Analysis

As depicted in Figure 2, Machine intelligence has established itself as a crucial tool in GIS spatial analysis, playing a vital role in addressing three key areas of problem-solving:

Classification: Leveraging vector machine algorithms, GIS can create land-cover classification layers, enabling the identification of various land types and facilitating comparative analyses to track changes over time.

Clustering: By analyzing input data points, GIS identifies patterns that reveal meaningful information amid potentially random groupings of "noise." Clustering helps identify relevant spatial relationships and spatially coherent patterns within the data.

Prediction Algorithms: GIS utilizes prediction algorithms, such as geographically weighted regression analysis, to measure variables at different locations. This approach allows for the construction and mapping of localized relationship models, moving beyond purely global versions and providing region-specific insights.

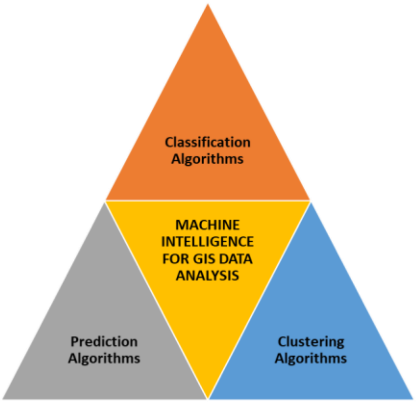

FIG 2 MACHINE INTELLIGENCE FOR GIS DATA ANALYSIS

Together, these categories empower GIS to make data-driven predictions. However, even with the sophisticated logic of machine learning, human interpretation remains essential to draw meaningful conclusions from the data.

As the pursuit of autonomy in GIS continues, deep learning emerges as an advanced AI approach that holds the potential to profoundly transform the landscape of GIS analysis. Deep learning stands at the pinnacle of AI discernment, closely emulating the workings of the human brain. Unlike traditional machine learning, which relies on human guidance, deep learning employs structured algorithms that can autonomously make decisions. Often referred to as an "artificial neural network," deep learning possesses an inherent ability to respond to stimuli through layered logic, resembling the complexities of human thought processes. This paradigm shift in geospatial AI has revolutionized the handling and utilization of Big Data. Deep learning seamlessly analyzes and categorizes diverse inputs, such as images, intricate road networks, buildings, and other location-specific data, all without the need for human intervention. The outcome is the swift aggregation and real-time application of vast quantities of data.

Given the pressing demands and indispensable reliance on Geographic Information Systems (GIS), it comes as no surprise that digital mapping experts find deep learning incredibly appealing. The fusion of deep learning and GIS offers an unparalleled advantage in dealing with data-driven challenges efficiently and promptly.

IV. SIGNIFICANCE OF CLASSIFICATION AND CLUSTERING MODELS FOR GIS

A. Classification in GIS

The goal of classification in GIS is to simplify complex spatial data and create thematic maps that highlight patterns, trends, and distributions within the data. It is an essential process for organizing and understanding geospatial data, enabling effective data management, visualization, and analysis. Common methods used for classification in GIS include:

Supervised Classification: In this approach, the analyst provides a set of training samples or labeled data points to the classifier, indicating the class membership of each sample. The classifier then learns from these samples and applies the learned patterns to classify the remaining data.

Unsupervised Classification: Unsupervised classification does not require labeled training samples. Instead, it groups similar data points into clusters based on their attribute similarities or spatial proximity. The analyst interprets the resulting clusters to assign meaningful class labels.

Maximum Likelihood Classification: Based on the mean and variance of the class, this statistical method determines the likelihood that a data point belongs to that class. After that, the data point is allocated to the class with the greatest likelihood.

Decision Trees: Decision tree classification uses a hierarchical tree structure to split the data based on attribute values until a class label is assigned to each data point.

Random Forest: An ensemble learning technique called Random Forest makes use of several decision trees to boost accuracy in classification and decrease overfitting.

It is a difficult and time-consuming task to classify, detect, or separate several objects from satellite photographs, but AI is better at it than people are, and it can do it faster, more consistently, and maybe with greater accuracy. Classification in GIS plays a crucial role in various fields, including environmental monitoring, resource management, urban planning, disaster management, and biodiversity conservation. By organizing geospatial data into meaningful classes, GIS analysts can extract valuable insights and support informed decision-making processes. The application of methods for image classification enables the pixel categorization of satellite data, differentiating various geographical characteristics such as rocky terrain, woods, highways, settlements, and bodies of water based on their spectral reflectance qualities.

B. Clustering in GIS

Clustering is a fundamental method for exploring patterns, identifying spatial distributions, and understanding relationships within geospatial datasets The main objective of clustering in a GIS is to divide the spatial data into groups or clusters so that the items within each cluster are more similar to one another than those in other clusters. Clustering helps in revealing underlying structures, trends, and spatial associations in the data, providing valuable insights for decision-making, urban planning, environmental analysis, and various other applications. Following are few methods used for clustering in GIS.

ISBN: 978-93-342-3695-8

K-Means Clustering: The goal of the common clustering algorithm K-Means is to divide the data into K clusters. Based on their spatial or attribute similarity, the algorithm repeatedly allocates data points to the nearest cluster centroid.

Hierarchical Clustering: This method creates a hierarchical representation of clusters, forming a tree-like structure called a dendrogram. It allows users to identify clusters at different granularity levels.

Density-Based Spatial Clustering of Applications with Noise (DBSCAN): By identifying clusters based on the density of data points, DBSCAN is a density-based clustering technique. Finding arbitrary shape clusters and managing data noise are two of its most advantageous uses.

Optics: Another density-based approach, Ordering Points To Identify the Clustering Structure (OPTICS), creates a cluster ordering to show hierarchical clustering structures.

Spatially Constrained Agglomerative Clustering (SCAC): SCAC is a method that incorporates spatial constraints to guide the clustering process and ensures that clusters are coherent in the spatial domain.

In general, although non-spatial clustering utilizes the characteristics of the observations to group them, spatial clustering examines the distribution of geographical attributes. a number of various ways to merge spatial and non-spatial information. A GIS system has clustering as an integrated element. The grouping of crops and soil types is merely a single instance of how clustering is used in GIS. Because GIS works with enormous amounts of data, clustering is significantly more difficult. Therefore, one of the main issues with practically any GIS system is clustering as well as the data structure for storing the knowledge about clusters.

V. ADVANCED DEEP LEARNING TECHNIQUES FOR GIS

Deep learning techniques in GIS require extensive and labeled training data, as well as significant computational resources for training complex models. Nevertheless, when appropriately applied, these techniques have the potential to revolutionize geospatial analysis, enhance data-driven decision-making, and unlock new possibilities in the field of GIS.

Convolutional Neural Networks (CNNs): CNNs are widely employed for image-related tasks in GIS, such as land cover classification, object detection (e.g., buildings, roads), and vegetation mapping. These networks can automatically learn and recognize spatial patterns in satellite imagery or aerial photographs, making them ideal for visual analysis in GIS.

Recurrent Neural Networks (RNNs): RNNs are well-suited for time-series data in GIS, such as climate data, population trends, and urban growth over time. They can capture temporal dependencies and patterns, enabling tasks like time-series prediction and forecasting.

Long Short-Term Memory (LSTM) Networks: A specific type of RNN, LSTM networks, are particularly useful for modeling and predicting sequences with long-term dependencies. They are widely used in GIS for applications like rainfall prediction, river flow forecasting, and traffic prediction.

Generative Adversarial Networks (GANs): GANs are used in GIS for generating synthetic geospatial data that can be used to augment existing datasets or simulate scenarios for analysis. They have applications in urban planning, environmental simulation, and improving the training data for other deep learning models.

Transformer-based Models: The Transformer architecture and its derivatives, such as BERT and GPT, have showed tremendous promise in natural language processing tasks and have been applied for GIS applications. They can be used for geospatial text analysis, sentiment analysis of user-generated location data, and extracting information from geospatial documents.

Graph Neural Networks (GNNs): GNNs are relevant for evaluating geospatial networks and relationships since they are made to operate with graph-structured data. such as transportation networks, social networks, and ecological networks. GNNs are useful for tasks like predicting traffic flow, identifying critical nodes in networks, and analyzing spatial connectivity.

Siamese Networks: Siamese networks are employed for similarity-based tasks in GIS, such as matching similar features or objects in different datasets, change detection, and image retrieval.

Attention Mechanisms: Attention mechanisms, used in Transformer-based models, have been adapted for tasks in GIS where capturing important spatial or temporal relationships is crucial. These mechanisms have applications in object detection, image segmentation, and sequential data analysis.

VI. ADVANCED DEEP LEARNING APPLICATION FOR GIS DATA PROCESSING

Leveraging recent developments in the field of image processing, applications of deep learning techniques for remotely sensed data analytics provide cutting-edge software for geospatial data analysis. Table 1 presents various DL techniques for various data processing activities in GIS.

TABLE 1 DL FOR GIS DATA PROCESSING AND ITS APPLICATIONS

Data Processing Activity	Description	Deep learning Technique	Application
Image Denoising	Remove noise from satellite or aerial image and improving image quality	Auto-Encoder, CNN	Land Cover Classification and Urban Planning, Crop Monitoring.
Image Super-Resolution	Upscale low-resolution satellite images to yield high-resolution	CNN	

Image Enhancement	Making images more visually appealing by adjusting contrast, brightness, and color balance	Auto-Encoder, CNN	Land Cover and Land Use Mapping, Archaeological and Cultural Heritage Site Identification, Wildlife Habitat Mapping And Conservation
Image Segmentation	Perform semantic segmentation to partition images into meaningful regions	k-means, fuzzy c-means Clustering	
Pan-Sharpening	Merge multispectral and panchromatic images to create high-resolution color images	CNN, Stacked Auto-Encoders	Urban Planning, Environmental Monitoring, Agriculture, Forestry
Geospatial Object Detection	Detecting or identifying an object of interest	CNN	Detect Buildings from Aerial Images
Feature Engineering	Automatically extract features from images	CNN	Urban Planning, Environmental Monitoring, Disaster Management, And Resource Allocation
Classification	Classify remotely sensed Imagery in various ways to extract useful information and patterns	CNN, Auto-Encoder	Land Cover Classification, Land Use Classification, Scene Classification
Prediction	Statistical techniques to forecast future trends	RNN, geographically weighted regression (GWR)	Urban Growth Prediction, Climate Patterns, Traffic Flow and Congestion Prediction

I. Performance Analysis of DL Models for GIS

The Deep Learning (DL) models such as CNN, RNN and GANs have demonstrated significant capabilities in various GIS applications such as classification of land cover images, spatio-temporal image analysis, image segmentation, object detection and classification. CNNs are well suited for spatial feature extraction, RNNs are good in handling time-series data, and GANs help to generate synthetic images for GIS applications. Based on the method of processing spatial, temporal and spectral data, each DL model such as CNN, RNN and GANs are applied for specific GIS tasks [16-18]. Table 2 outlines the performance comparison of each DL model based on the type of GIS task.

TABLE 2 DL MODEL COMPARISON FOR GIS APPLICATIONS

Model	GIS Application	Advantage	Limitation
CNN	Image classification, object detection, spatial feature extraction	Spatial feature extraction	Inefficient for time-series
RNN	Temporal data, time series forecasting	sequence modeling	Not good for spatial features
GAN	Data augmentation, image translation	Synthetic data generation	Training instability

VII. CONCLUSION

Geospatial analysis has entered a new age thanks to the collaboration of Deep Learning and GIS. In order to improve the geographical, temporal, and spectral resolutions as well as enable smooth data integration, this study discusses numerous technology breakthroughs and the necessity of combining DL's capabilities with GIS. The paper also demonstrates how AI has taken data gathering, interpretation, visualization, and presentation in remote sensing and geospatial analysis to a global research forefront. This investigation of cutting-edge DL models gives academics and decision-makers the tools they need to manage massive geographic data effectively.

REFERENCES

[1] H. Shahabi et al., "Rapid Mapping of Landslides from Sentinel-2 Data Using Unsupervised Deep Learning," 2022 IEEE Mediterranean and Middle-East Geoscience and Remote Sensing Symposium (M2GARSS), Istanbul, Turkey, 2022, pp. 17-20, doi: 10.1109/M2GARSS52314.2022.9840273.

[2] Mohammad, O. S. Gullapalli, S. Vasavi and S. Jayanthi, "Updating of GIS maps with Change Detection of Buildings using Deep Learning techniques," 2022 International Conference on Futuristic Technologies (INCOFT), Belgaum, India, 2022, pp. 1-6, doi: 10.1109/INCOFT55651.2022.10094545.

[3] S. Du and S. Du, "Land Cover Classification Using Remote Sensing Images and Lidar Data," IGARSS 2019 - 2019 IEEE International Geoscience and Remote Sensing Symposium, Yokohama, Japan, 2019, pp. 2479-2482, doi: 10.1109/IGARSS.2019.8899840.

[4] Y. Ogawa, C. Zhao, T. Oki, S. Chen and Y. Sekimoto, "Deep Learning Approach for Classifying the Built Year and Structure of Individual Buildings by Automatically Linking Street View Images and GIS Building Data," in IEEE Journal of Selected Topics in Applied Earth

Observations and Remote Sensing, vol. 16, pp. 1740-1755, 2023, doi: 10.1109/JSTARS.2023.3237509.

[5] T. A. Tuan, P. D. Pha, T. T. Tam and D. T. Bui, "A New Approach Based on Balancing Composite Motion Optimization and Deep Neural Networks for Spatial Prediction of Landslides at Tropical Cyclone Areas," in IEEE Access, vol. 11, pp. 69495-69511, 2023, doi: 10.1109/ACCESS.2023.3291411.

[6] H. Li, X. Huang and X. Li, "Urban land price assessment based on GIS and deep learning," IGARSS 2019 - 2019 IEEE International Geoscience and Remote Sensing Symposium, Yokohama, Japan, 2019, pp. 935-938, doi: 10.1109/IGARSS.2019.8900516.

[7] M. I. Habibie, T. Ahamed, R. Noguchi and S. Matsushita, "Deep Learning Algorithms to determine Drought prone Areas Using Remote Sensing and GIS," 2020 IEEE Asia-Pacific Conference on Geoscience, Electronics and Remote Sensing Technology (AGERS), Jakarta, Indonesia, 2020, pp. 69-73, doi: 10.1109/ AGERS51788.2020.9452752.

[8] J. Yuan, "Learning Building Extraction in Aerial Scenes with Convolutional Networks," in IEEE Transactions on Pattern Analysis and Machine Intelligence, vol. 40, no. 11, pp. 2793-2798, 1 Nov. 2018, doi: 10.1109/TPAMI.2017.2750680.

[9] Francini, M., Salvo, C., & Vitale, A. (2022). Deep Learning methods and geographic information system techniques for urban and territorial planning. URBANISTICA INFORMAZIONI, (306 si), 652-654.

[10] Lavallin, A., & Downs, J. A. (2021). Machine learning in geography–Past, present, and future. Geography Compass, 15(5), e12563.

[11] Lavallin, A., & Downs, J. A. (2021). Machine learning in geography–Past, present, and future. Geography Compass, 15(5), e12563.

[12] Janowicz, K., Gao, S., McKenzie, G., Hu, Y., & Bhaduri, B. (2020). GeoAI: spatially explicit artificial intelligence techniques for geographic knowledge discovery and beyond. International Journal of Geographical Information Science, 34(4), 625-636.

[13] Fawad, M., Ullah, F., Irshad, M., Shah, W., Mahmood, Q., & Ahmad, I. (2022). Marble waste site suitability assessment using the GIS-based AHP model. Environmental Science and Pollution Research, 29(19), 28386-28401.

[14] Tewari, A., Kshemkalyani, V., Kukreja, H., Menon, P., & Thomas, R. (2022). ML and GIS-Based Approaches to Flood Prediction: A Comparative Study. Cyber Intelligence and Information Retrieval: Proceedings of CIIR 2021, 213-223.

[15] Ullah, I., Aslam, B., Shah, S. H. I. A., Tariq, A., Qin, S., Majeed, M., & Havenith, H. B. (2022). An integrated approach of machine learning, remote sensing, and GIS data for the landslide susceptibility mapping. Land, 11(8), 1265.

[16] S. Balaji, R. G. and C. Reddy, "Smart Land Use Planning: Integrating Geographic Information Systems (GIS) with Graph Neural Networks (GNN) for Hazard Identification," 2024 8th International Conference on Computational System and Information Technology for Sustainable Solutions (CSITSS), Bengaluru, India, 2024, pp. 1-5, doi: 10.1109/CSITSS64042.2024.10816801.

[17] Y. Ogawa, C. Zhao, T. Oki, S. Chen and Y. Sekimoto, "Deep Learning Approach for Classifying the Built Year and Structure of Individual Buildings by Automatically Linking Street View Images and GIS Building Data," in IEEE Journal of Selected Topics in Applied Earth Observations and Remote Sensing, vol. 16, pp. 1740-1755, 2023, doi: 10.1109/JSTARS.2023.3237509.

[18] W. Budiharto, A. Chowanda, A. A. S. Gunawan, E. Irwansyah and J. S. Suroso, "A Review and Progress of Research on Autonomous Drone in Agriculture, Delivering Items and Geographical Information Systems (GIS)," 2019 2nd World Symposium on Communication Engineering (WSCE), Nagoya, Japan, 2019, pp. 205-209, doi: 10.1109/WSCE49000.2019.9041004.

AI-Driven Fraud Call Detection with Encrypted QR Code Authentication

Ms G. Lavanya B.E.,(M.E.,)
PG Scholar,
lavanyajesus1706@gmail.com

Dr. S.D. Prabu Ragavendiran,
Professor/HOD,
hod.cse@builderscollege.edu.in

Mrs D. Kalai abirami
Assistant Professor/CSE,
dka.cse@builderscollege.edu.in

C. Divya Revathi
PG Scholar,
Department of Computer Science and Engineering,
Builders Engineering College,
Tiruppur
divyarevathi.c@gmail.com

A Vanmathi B.E.,(M.E.,)
PG Scholar,
vanmathics24@gmail.com

***Abstract*—Fraudulent calls are becoming a major problem that may lead to both financial loss and privacy problems. The AI-Driven Fraud Call Detection Using Encrypted QR Code Authentication solution offers a mobile application that improves caller identification and verification in order to address this issue. Though it uses machine learning and cryptography techniques to offer an extra degree of protection, this software is comparable to well-known applications like True Caller. Support Vector Machines (SVM) is used by the system to evaluate and categorize calls as either legitimate or fraudulent. The program can reliably spot questionable patterns in real time by using call data to train the SVM model, providing timely fraud detection. Additionally, the software uses a cryptographic technique to create encrypted QR codes. The information contained in these QR codes regarding the caller details includes whether from a government agencies or from the private one. The program provides a complete solution to protect users from fraudulent calls and boost confidence in communication networks by integrating encrypted QR code authentication with SVM-based fraud detection.**

Keywords—Fraud detection, AI, QR code encryption, real-time analysis, secure communication.

I. INTRODUCTION

In today's connected world, fraudulent phone calls have grown to be a serious problem, endangering both personal security and privacy. Strong systems to identify and stop fraudulent activity are more important than ever as mobile communication becomes more prevalent in sensitive sectors including banking, healthcare, and government services. This system combines encrypted QR code authentication with fraud call detection. These issues are addressed by utilizing AI algorithms, which combine cutting-edge cryptography methods with artificial intelligence (AI). The technology analyse call patterns and instantly identifies fraudulent activity using machine learning models, particularly Support Vector Machines (SVM).

The system incorporates encrypted QR code technology to confirm caller identities in addition to fraud detection. The securely encrypted information contained in each QR code enables the recipient to verify the caller's legitimacy. This two-pronged strategy guarantees that authentic callers may easily verify their identities in addition to detecting fake calls.

This solution adds an additional layer by developing a mobile application

II. IN THE AI TECHNOLOGY

2.1 Machine Learning

A subfield of artificial intelligence called machine learning allows computers to learn from data and get better over time. Through pattern recognition and prediction, it automates decision-making. Among the methods are reinforcement learning, supervised learning, and unsupervised learning. Applications include fraud detection and recommendation systems. By lowering the need for human intervention in complicated processes, it increases efficiency.

2.2 Support Vector Machine

Strong machine learning models for classification problems, particularly in high-dimensional areas, include Support Vector Machines (SVM). Finding the best hyper plane to divide classes with the largest margin is how SVM operates. SVM examines call characteristics and patterns in fraud call detection to differentiate between legitimate and fraudulent calls. It effectively detects suspicious activities and abnormalities by learning from labeled data. SVM improves security by confirming encoded caller information when used with QR code authentication. By guaranteeing that only trustworthy identities are validated, this integration enhances call security and user confidence, hence strengthening fraud protection.

III. METHODOLOGY

3.1 Data Collection and Pre-processing:

The very first phase in the process is gathering a lot of data from many sources, such as external fraud databases, user input, and telecom networks. Caller metadata, including caller ID, timestamp, frequency, duration, and location, is included in this data. Furthermore, historical datasets and real-time monitoring tools are used to gather data on QR codes and phishing URLs. Cleaning the data to get rid of noise and irregularities is known as pre-processing. For instance, call logs are filtered to remove duplicate or incomplete entries, and the data that remains is structured for analysis.

3.2 Fraud Detection Mechanism:

The foundation of the system is fraud detection. The technology examines call information using sophisticated AI algorithms to find trends suggestive of fraud. Three main components are the focus of the detection mechanism: anomaly detection, behavioural analysis, and keywords. The program looks for particular terms that are frequently used in scam calls, including "urgent transfer" or "your account is locked". Unusual calling patterns, including several calls from several numbers in a brief period of time or calls from foreign numbers masquerading as local ones, are identified via behavioural analysis.

3.3 Phishing URL and Fake Information Detection:

Detecting phishing URLs is essential for protecting people from online fraud. The technology examines URLs supplied during conversations or contained in messages and compares them to a database of known phishing websites. Even whether they are brand-new or slightly altered copies of pre-existing phishing links, sophisticated algorithms analyse the structure and content of URLs to identify dangerous ones.

3.4 QR Code Generation and Verification:

The system uses the SHA-512 cryptographic technique to create distinct QR codes for valid calls in order to guarantee safe connection. Encrypted information such the caller ID, session keys, and call timestamp are contained in the QR code. To confirm the legitimacy of the caller, users use the smartphone application to scan these QR codes.

3.5 Fraud Call Removal:

Upon identifying a call as fraudulent, the system promptly takes appropriate action. Automatic blocking stops fraudulent numbers from getting in touch with the user again. The smartphone application, which offers information about the suspected fraud, also notifies the user of the stopped call.

IV. MODULE DESCRIPTION

4.1 Fraud Detection Engine:

For this research, I trained and assessed a number of machine learning models for fraud call detection using the KNIME platform, including Support Vector Machine (SVM), Naive Bayes, and Random Forest. I started by pre-processing the fraud call detection dataset in KNIME to make sure it was clear and prepared for model training. I evaluated the models' accuracy after they had been trained on the dataset. The SVM method outperformed Random Forest and Naive Bayes in detecting fraudulent calls, demonstrating the highest accuracy among the three models.

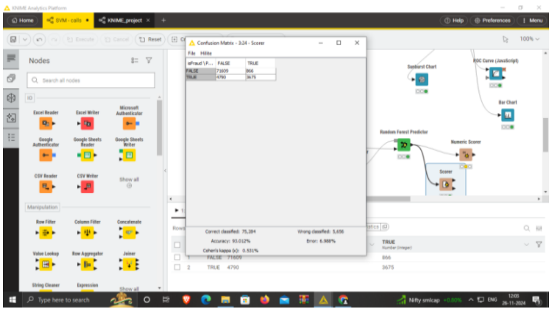

FIG 4.1 TRAINED RANDOM FOREST ALGORITHM

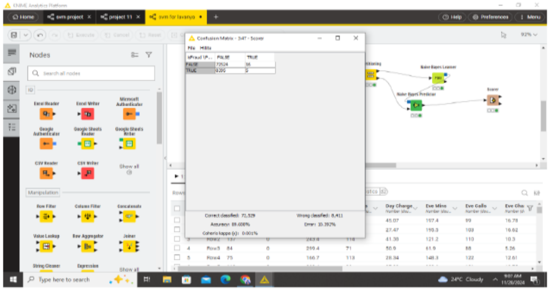

FIG 4.2 TRAINED NAIVE BAYES ALGORITHM

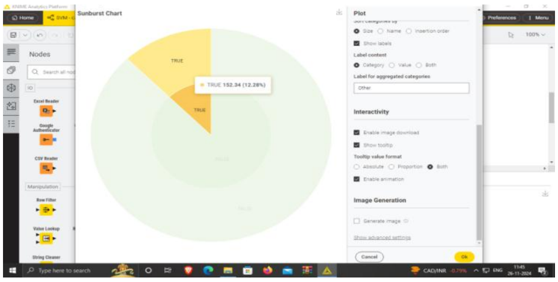

FIG 4.3 SVM TRUE PREDICTION

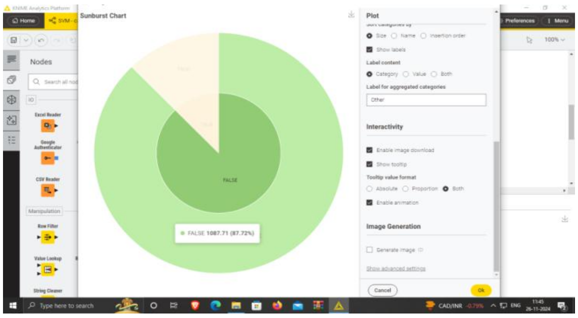

FIG 4.4 SVM FALSE PREDICTION

4.2 User Interface Module

A crucial component of the fraud detection system, the User Interface (UI) Module is made to give consumers a seamless and simple experience using the Caller Identity mobile application. The program, which was created with Java and Kotlin, efficiently categorizes incoming calls and shows the results of fraud detection in real time. Users can instantly determine the legitimacy of callers by highlighting calls from verified sources with a green checkmark and highlighting fraudulent and spam calls with a red checkmark.

FIG 4.1 LOGIN PAGE

FIG 4.2 GENERATE OTP

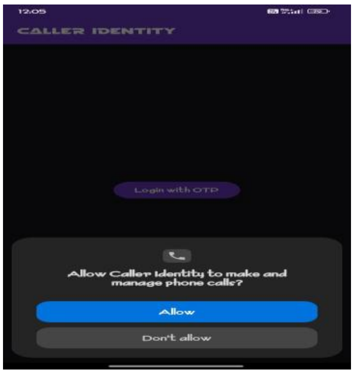

FIG 4.3 NEED PERMISSION TO MAKE AND MANAGE PHONE CALLS

FIG 4.4 NEED PERMISSION TO ACCESS CONTACTS

FIG 4.5 APP SETTINGS

4.3 Call Monitoring System

The purpose of to identify fraudulent activity, the Call Monitoring System Module is made to track and analyze incoming calls in real time. In order to spot questionable trends, this module continually tracks a number of call metrics, including frequency, length, caller behaviour, and user feedback. The technology uses AI-driven methods to categorize calls according to risk levels, highlighting possibly bogus numbers for additional investigation.

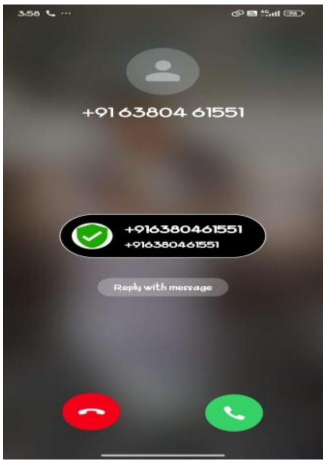

FIG 4.1 INCOMING CALL

V. CONCLUSION AND FUTURE WORK

5.1 Conclusion

The AI-driven fraud call detection system enhances security by leveraging real-time monitoring and machine learning to classify calls effectively. The integration of fraud detection mechanisms in the Caller Identity application ensures users can easily distinguish between legitimate and suspicious calls. By providing immediate alerts and maintaining an up-to-date fraud detection database, the system offers a proactive defense against scam calls, reducing the risk of fraudulent activities.

5.2 Future Work

Future versions will incorporate a QR code authentication technique that securely encrypts caller identifying data in order to further improve the fraud detection system. By allowing consumers to confirm whether the caller is from the public or private sector, this tool will increase security and transparency. Enhancements will also concentrate on extending AI's capacity to examine call behaviours and speech patterns in order to boost detection accuracy even further. Improved cloud-based fraud detection database features will guarantee faster identification of new threats, and cutting-edge machine learning methods will consistently boost system efficiency.

REFERENCES

[1] Qi Jun Chong, Mohammed Alsamman & Noraziah Che Pa Encrypted QR Code for Brand Authentication: enQRure Mobile Application Development and Evaluation Journal of Digital System Development: Vol. 1. (October) 2024: 120-130

[2] I. Clark, "The Role of Cloud Computing in Scalable Fraud Detection Systems," Journal of Cloud Computing, vol. 8, no. 3, pp. 215-230, 2022.

[3] F. Lee, "Regulatory Compliance and AI in Telecommunications: Challenges and Opportunities, “Telecommunications Policy, vol. 43, no. 5, pp. 310-325, 2022.

[4] C. Brown, “c," Journal of Artificial Intelligence Applications, vol. 25, no. 3, pp. 112-128, 2022.

[5] Keerthy, G. a. (2023).Enhancing Product Authentication and Counterfeit Detection Using QR Codes and Block chain Technology. (ICECAA) (pp. 262--267).IEEE

[6] B. Johnson, "Machine Learning Approaches for Fraud Detection in Telecommunications," IEEE Transactions on Network and Service Management, vol. 15, no. 4, pp. 1789-1802, 2020.

[7] G. Taylor, "Advances in Deep Learning for Anomaly Detection in Telecommunications Networks," IEEE Journal on Selected Areas in Communications, vol. 38, no. 2, pp. 321-335, 2020.

[8] H. Adams, "Privacy-Preserving Techniques in AI-based Fraud Detection," Journal of Privacy and Confidentiality, vol. 12, no. 1, pp. 134-148, 2021.

[9] J. Garcia et al., "Real-time Fraud Detection Using Supervised Learning in Telecommunications," Expert Systems with Applications, vol. 98, pp. 211-225, 2021.

[10] Meng, X. A. (2023).An efficient authentication protocol for brand cosmetics anti-counterfeiting system. 10th International Conference on Cyber Security and Cloud Computing (CSCloud)/2023 IEEE 9th International Conference on Edge Computing and Scalable Cloud (EdgeCom)p(pp. 120--125). IEEE.

[11] K.Shaukat, S. Luo, S.Chen, and D. Liu, “Cyber threat detection using machine learning techniques: A performance evaluation perspective,”inIEEE international conference on cyber warfare and security. IEEE, October2020, pp. 1-6.

[12] S. M. Gowri, G. Sharang Ramana, M. Sree Ranjani and T. Tharani," Detection of Telephony Spam and Scams using Recurrent Neural Network (RNN) Algorithm," 2021 7th International Conference on Advanced Computing and Communication Systems (ICACCS), Coimbatore, India, 2021, pp. 1284-1288,doi: 10.1109/ICACCS51430.2021.9441982.

[13] S. Sandhya, N. Karthikeyan, R. Sruthi “Machine learning method for detecting and analysis of fraud phone calls datasets” International Journal of Recent Technology and Engineering (IJRTE) ISSN: 2277-3878 (Online), Volume-8 Issue-6, March 2020.

[14] P. Sornsuwit and S. Jaiyen, “A new hybrid machine learning for cyber security threat detection based on adaptive boosting, “Applied Artificial Intelligence, 33(5), pp.462-482, 2019.

AI Based Complaint Monitoring System

Narasima Mallikarjunan K
Associate Professor,
Department of Computer Science & Engineering,
Thiagarajar College of Engineering,
Madurai, India
arjunkambaraj@tce.edu

Sandhiya P
UG Student,
Department of Computer Science & Engineering,
Thiagarajar College of Engineering,
Madurai, India
sandhiyapomman@gmail.com

Asmine. A
UG Student *Department of Computer Science & Engineering,*
Thiagarajar College of Engineering,
Madurai, India
jasminerahman81@gmail.com

Periyanna. M
UG Student,
Department of Computer Science & Engineering,
Thiagarajar College of Engineering,
Madurai, India
periyanna@student.tce.edu

***Abstract*—Fear of exposure often discourages people from reporting complaints. Existing systems struggle with privacy, security, and resolution efficiency. Complaint Vision, an AI-driven platform, addresses these issues through real-time classification and prioritization and anonymization. It leverages geolocation, zero-knowledge proof encryption, predictive analytics, and adaptive learning to enable secure, transparent, and responsive complaint handling, promoting fearless reporting and improved public safety.**

Keywords—Anonymization, geo-location, AI classification, Zero-Knowledge Proof, adaptive learning, predictive analytics

I. Introduction

Complaint Vision (CV) is an AI-based complaint management system that uses zero-knowledge proofs (ZKP), pseudonymization, and end-to-end encryption to enhance user privacy, data security, and resolution efficiency. Unlike manual systems without real-time updates and structured timelines, CV facilitates real-time tracking, AI-based categorization, and sentiment-driven prioritization. It preserves user anonymity through advanced cryptography techniques and encourages the citizen to submit complaints against the crimes. The platform itself continually improves its AI models through processing of user feedback, improving accuracy in complaint classification, and recognizing repetitive patterns to help prevent crime and public safety matters beforehand. Geolocation tagging with photos provides real-time reporting and localizes better, minimizing the overhead of the misreported complaints.

Predictive analytics enables authorities to identify trends, effectively distribute resources, and speed up response times. Authority at higher levels can track the officers in charge of closing assigned complaints within a specified time frame, hence increasing the efficiency and speed of complaint closure. Complaint Vision provides a secure, transparent, and data-driven complaints system, promoting crime prevention and public safety, ultimately leading to a safe and accountable society.

II. Related Work

Artificial intelligence (AI) is increasingly a central component in modern complaint tracking systems. Singh and Kumar [1] proposed an AI-driven platform in Iraq named M-complaint, supporting GPS-based tracking, feedback systems, and auto-escalation in case issues are not being addressed. Prasad and Agarwal [2] built on this by proposing a real-time, priority-based redressal system for smart cities with considerable efficiency gains.

In order to protect complaint data integrity and avoid tampering, Zhao and Liu [3] proposed a blockchain-based complaint management system. It avoids data tampering and increases public infrastructure reporting transparency.For the classification of complaints by images, AI models have become popularly used. EfficientNet family of models, mobile and scalable optimized models, were developed by Howard et al. [4] and Tan and Le [5].

Li and Chen [6] enhanced understanding images with hybrid CNN-Transformer models, and Chollet [7] introduced Xception, which used depthwise separable convolutions to achieve higher accuracy and lower computational expense.

Geospatial intelligence further improves handling complaints. Xu and Fan [8] uncovered how spatial analytics would uncover geographical complaint patterns, whereas Huang and Yu [9] depicted geotagging for faster incident localization and improved emergency responses.

Finally, Chen and Wang [10] proposed fusing blockchain technology with geo-tagging for validating incident locations, and Das and Banerjee [11] proposed an end-to-end AI-IoT system for real-time decision-making improvement in public safety networks.

III. Proposed Solution

The Complaint Vision is an online system for managing complaints that preserves the benefits of traditional methods while increasing transparency and accelerating the resolution process, resulting in higher user satisfaction (as shown in Fig. 1).

A. Secure Authentication with Anonymity

Prioritizing security, the system ensures user confidentiality through advanced techniques such as zero-knowledge proofs (ZKP), pseudonymization, and end-to-end encryption. ZKP verifies user identities without disclosing personal details, while pseudonymization enables anonymous submission of complaints. End-to-end encryption safeguards data against breaches, fostering trust and motivating users to submit complaints without the fear of exposure.

B. Geospatial Analysis for Location-Based Insights

By utilizing geotagged images, the system accurately tracks the locations of complaints, streamlining the registration process through automatic extraction of geographic coordinates. This information assists authorities in pinpointing areas with high complaint volumes, facilitating improved resource distribution and proactive measures for recurring issues.

C. AI and ML for Incident Classification and Prioritization

Using artificial intelligence and machine learning, the complaints are graded by urgency and severity. Through natural language processing (NLP) and sentiment analysis, the system categorizes serious complaints, such as incidents or crimes, as high priority and others as lower priority. Ongoing training of AI models enhances accuracy over time, alleviating the administrative burden and optimizing resource distribution.

D. Image-Based Classification for Automated Processing

The platform also incorporates deep learning methods to recognize complaints via images. A convolutional neural network (CNN), trained on a dataset of over 2,000 images, automatically identifies issues like potholes and fire hazards in real time, with geo-tagging facilitating priority-based routing. User feedback further refines detection accuracy, ensuring high efficiency.

E. Model Architecture & Training

The architecture utilizes ResNet152 augmented with Squeeze-and-Excitation blocks for precise feature extraction, outpacing lighter alternatives such as EfficientNet. Data augmentation techniques promote generalization, and the model is fine-tuned for real-time performance using TorchScript.

Performance metrics reflect an average accuracy of 92.5% and an F1 score exceeding 0.90 across all complaint categories, delivering enhanced detection accuracy in comparison to prior systems.

F. Integrated Admin Dashboard

The dashboard offers a user-friendly interface for stakeholders, showcasing the real-time status of complaints from submission to resolution. Administrators can oversee complaints, monitor AI classifications, evaluate officer performance, and analyze user feedback to inform policy decisions.

G. Performance Analysis and Officer Accountability

Critical performance indicators (KPIs) assess both system efficacy and officer responsibility, including metrics for complaint resolution durations, officer response rates, AI classification precision, and user satisfaction. These KPIs highlight areas needing improvement and help in optimizing resource allocation.

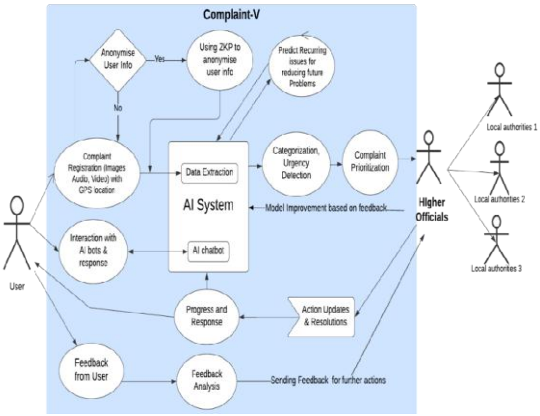

FIG. 1 SYSTEM ARCHITECTURE

IV. RESULTS AND DISCUSSIONS

The CV application implements the user side for registering complaints with geotagging photos and videos as evidence and getting real-time updates of their complaints (as shown in Fig. 2). The admin side implements a dashboard for processing the complaints and automatically assigns them to the respective authorities along with a timeline to solve the complaints as early as possible.

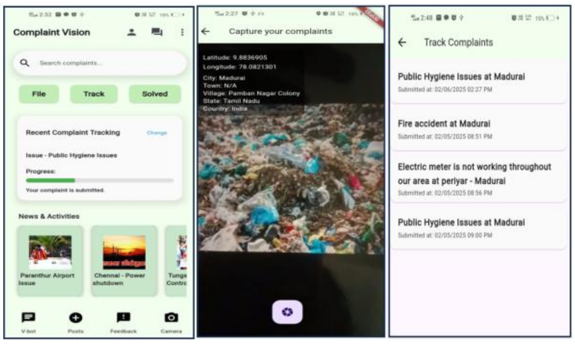

FIG 2. USER SIDE COMPLAINT VISION APPLICATION

A. Evaluation Metrics for Complaint Classification

1) Confusion Matrix: Fig. 3 illustrates the confusion matrix for a sample model of classification, sorting complaints into six categories: pothole complaints, fire incidents (building fires, forest fires, industrial fires, vehicle fires), and public hygiene. The matrix identifies robust performance, especially in pothole complaints (81 accurate predictions) and public hygiene (59 accurate predictions), with few misclassifications. This is a sample illustration, with continuous development to add categories and increase accuracy toward wider real-world deployment.

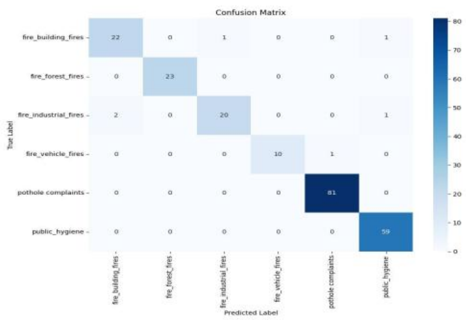

FIG. 3 CONFUSION MATRIX

2) *Precision, Recall, and F1-score by complaint category:* The classification report, shown in Fig. 4, gives a thorough overview of the performance of the model by different complaint categories. At a staggering total accuracy of 97%, the model is of very high precision, recall, and F1-score for each of the classes, with leading metrics in fire_forest_fires and virtually leading metrics in pothole complaints and public_hygiene. The macro average An F1-score of 0.96 points towards general class balance, while its weighted average F1-score of 0.97 proves that it efficiently addresses class imbalance problems. Support values reflect the number of complaints, ranging from the most frequent categories of pothole complaints to the least frequent categories, such as fire_vehicle_fires. These results confirm the performance of the model in minimizing false negatives and positives, and hence its application in real-world use. Furthermore, these tests are a representative sample of our approach, with ongoing improvement to generalize and extend the model to other classes.

Detailed Classification Report:

	precision	recall	f1-score	support
fire_building_fires	0.92	0.92	0.92	24
fire_forest_fires	1.00	1.00	1.00	23
fire_industrial_fires	0.95	0.87	0.91	23
fire_vehicle_fires	1.00	0.91	0.95	11
pothole complaints	0.99	1.00	0.99	81
public_hygiene	0.97	1.00	0.98	59
accuracy			0.97	221
macro avg	0.97	0.95	0.96	221
weighted avg	0.97	0.97	0.97	221

FIG. 4 PRECISION, RECALL, F1-SCORE AND SUPPORT

3) *For Fine-Tuning with Customization:* Layer-Specific Fine-Tuning: Freezing early layers and fine-tuning Subsequent layers allow us to take advantage of transfer learning while adapting the model to identify unique incident features. Adding a custom classification head with dropout enhances model robustness, increasing accuracy in real-world usage

4) *Evaluation Metrics with Precision Accuracy of Prioritization with Different Degrees of Urgency:* The model is promising in terms of accuracy in distinguishing complaints based on their urgency levels. The model performed with very high accuracies when discriminating between high, medium, and low priority. For example, in urgent drainage blockage, these were classified as high priority, and redress was done quickly. This would ensure that their bills were issued by the most optimal means and enhanced the entire process of complaint redressal, while simultaneously ensuring that complaints relating to critical infrastructure are redressed

5) *Model Training Performance: As seen in Fig. 5* (Training and Validation Loss Over Epochs) and Fig. 6 (Training and Validation Accuracy Over Epochs), it displays its effectiveness in learning and generalization. The steady decline of training and validation loss curves (Fig. 5) indicates successful optimization and the model's capability to reduce error over epochs. Specifically, the validation loss plateaus, which means that the model does not overfit and continues to perform well.

Similarly, the consistent increase in accuracy curves (Fig. 6) shows significant improvement in training and validation accuracy, eventually converging at over 90%. This overlap of training and validation metrics reflects the good generalization of the model to new data, verifying its eligibility for practical application. These plots offer a useful insight into the pattern of convergence of the model and its ability to provide stable performance against varying complaint types.

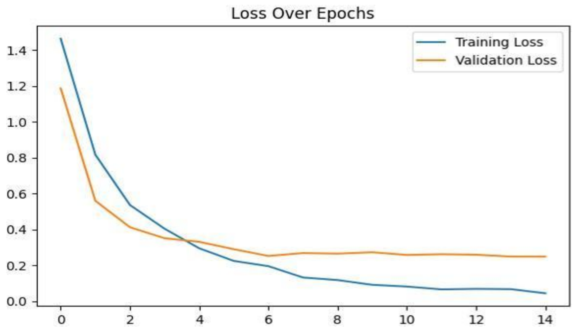

FIG. 5 TRAINING AND VALIDATION LOSS OVER EPOCHS

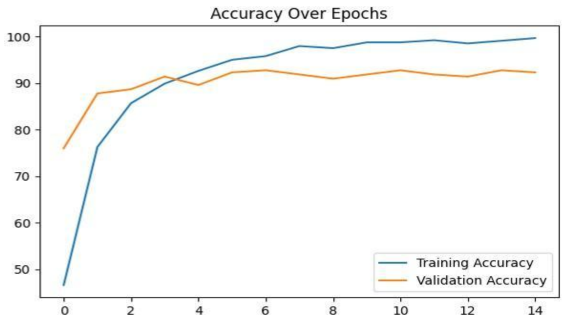

FIG. 6 TRAINING AND VALIDATION ACCURACY OVER EPOCHS

B. Comparison and Improvements

1) *Innovative Architecture:* We combine the robust feature extraction of ResNet152 with adaptive feature recalibration of Squeeze-and-Excitation blocks. The combination enhances attention towards critical fire incident features and thus increases accuracy in complex cases and achieves an individual lead in fire detection operations.

2) *Advanced Augmentation:* We introduce multi-dimensional assessment by precision-recall curves and confusion matrices, which provide a dense performance analysis. This new technique highlights the efficiency of the model in handling skewed data and out-of-vocabulary events.

3) *Real-Time Optimized:* Our model uses quantization and TorchScript to obtain faster, on-device inference to enable real-time emergency detection with fast decision support that is indispensable in real-time applications.

4) *Cross-Domain Generalization:* Our method allows the model to quickly adapt to new incident domains with minimal retraining. This flexibility makes its deployment in various emergency situations, and it broadens its use to other safety domains.

V. CONCLUSION

The model exhibits strong competence in classifying, ranking, and monitoring infrastructure complaints with good accuracy in multiple metrics. With the use of multiple assessment instruments, the app drives timely and accurate response processes, greatly boosting complainant and administrative user experience. The combined platform effectively streamlines infrastructure issue processing with its integration of real-time image capture, auto geotagging, classification, ranking, and departmental assignment. Geotagging that is automated provides proper location data, and the classification model classifies issues like streetlight and drainage issues properly with reduced misclassification. Prioritization hooks enable the quick fixing of high-priority cases, ensuring efficient resource planning. Moreover, auto-assignment to departments reduces waiting time, and the page for tracking supports transparency and accountability, making it simple to track in real-time and give feedback. As good as the system worked in test cases, the classification coverage is expandable as well as measuring priorities. Continuing to retrain the model from new data along with introducing new image features would help to supplement performance with fuzzy complaint types in the future work. This approach improves significantly in public infrastructure management and response performance and makes the app reliable with actual use.

References

[1] V. Singh and M. Kumar, "AI for Smart Complaint Management: Real-Time Monitoring and Escalation Systems," *Elsevier Expert Systems*, 2022. DOI: 10.1016/j.eswa.2022.115348

[2] S. Prasad and R. Agarwal, "Real-Time Complaint Management in Smart Cities: An AI-Powered Solution," *Scopus J. Urban Tech.*, 2021. DOI: 10.1016/j.scurb.2021.104512

[3] L. Zhao and J. Liu, "A Blockchain-Based AI Complaint Management System for Public Infrastructure," *IEEE Trans. Emerging Topics Comput. Intell.*, 2023. DOI: 10.1109/TETCI.2023.3310987

[4] Howard, A. G., et al. (2020). "EfficientNet-Lite: Improved Mobile Image Classification Models for Low Latency Applications." IEEE Transactions on Neural Networks. DOI:10.1109/TNN.2020.2994436

[5] M. Tan and Q. Le, "EfficientNetV2: Smaller Models and Faster Training," *IEEE Int. Conf. on Machine Learning*, 2021. DOI: 10.1109/CVML.2021.4031224

[6] Z. Li and X. Chen, "Augmenting CNNs with Transformer Layers for Image Classification," *IEEE CVPR*, 2023. DOI: 10.1109/CVPR.2023.9567846

[7] F. Chollet, "Xception: Deep Learning with Depthwise Separable Convolutions for Image Classification," *IEEE Trans. Neural Networks*, 2022. DOI: 10.1109/ TNN.2022.3286943

[8] Xu, Y., & Fan, L. (2020). "Spatial Data Analytics and Geo-Tagging for Complaint Handling in Urban Areas. "Elsevier Smart Cities and Data Analytics. DOI:10.1016/j.jscdata.2020.101532

[9] Huang, J., & Yu, P. (2021). "Geo-Tagging in AI-Driven Complaint Management Systems." *IEEE* Transactions on Smart Cities. DOI:10.1109/TSC.2021.3171562

[10] Chen, X., & Wang, M. (2023). "Improving Complaint Resolution via Geo-Tagging and Image Classification." Scopus Transactions on Urban Studies. DOI: 10.1016/j.urban.2023.104854

[11] Das, S., & Banerjee, P. (2021). "IoT and AI-Based Smart Complaint Management Systems for Public Safety." Scopus Transactions on Smart City Technologies. DOI:10.1016/j.soscitech.2021.104215

Leveraging 3D Deep Learning Models for Multi-Adulterant Detection in Milk using Hyperspectral Imaging Data

Padmasri P
Department of ECE,
Thiagarajar College of Engineering,
Madurai, India padmasrip@student.tce.edu

Sathya Bama B
Department of ECE,
Thiagarajar College of Engineering,
Madurai, India
sbece@tce.edu

Mohamed Mansoor Roomi S
Department of ECE,
Thiagarajar College of Engineering,
Madurai, India
smmroomi@tce.edu

***Abstract*—Multi-adulterant detection in liquid milk is essential for comprehensive quality assessment, ensuring accurate identi- fication of adulterant combinations that may interact and affect milk properties. Emerging technologies, including hyperspectral imaging and deep learning models, offer promising solutions for simultaneous detection and classification of multiple adulterants with high accuracy. In this study, adulterated milk samples are prepared by adding varying concentrations such as 12.5 ml, 25 ml, and 50 ml of RO water, corporation water, and groundwater, along with 2.5 g of glucose, to pure milk. The Resonon Pika-L hyperspectral camera is used to create a novel milk dataset. The effectiveness of 3D deep learning models, including 3D-CNN, 3D- ResNet, 3D-EfficientNet, and 3D-DenseNet, is then evaluated for detecting and classifying these adulterant mixtures. Among them, the proposed 3D-DenseNet model achieves the highest accuracy of 99%, demonstrating its potential for precise and efficient detection of milk adulteration.**

***Keywords*—Multi-Adulterant, Quality Assessment, Hyper- spectral Imaging, 3D Deep Learning**

I. Introduction

Milk, often referred to as the "complete food," is one of the most widely consumed globally. However, milk adulteration remains a major concern in ensuring its quality and safety, often involving multiple adulterants such as water, starch, and glucose, which can degrade nutritional quality and pose health risks. Common adulterants used in milk are water, glucose, vegetable oil, starch, detergent, synthetic milk, urea, forma- lin, hydrogen peroxide and neutralizers, each posing distinct health risks [1]. The issue becomes even more complex when multiple adulterants are introduced into milk simultaneously. Mixtures of water with glucose, starch with detergent, or even harmful chemicals can interact, making it difficult to detect adulteration using traditional methods. Thus, this study focuses on detecting adulteration of milk by considering different wa- ter sources mixed with glucose. Although traditional detection methods focus on the identification of single adulters, real- world adulteration scenarios involve complex mixtures that require more advanced analytical techniques. Hence, recent advances in detection techniques have focused on the use of cutting-edge technologies such as hyperspectral imaging, biosensors, and deep learning models [2].

A comprehensive review of the literature from 2010 to 2024 shows significant progress in nondestructive technologies for detection of food adulteration, including spectroscopic techniques [3] and artificial intelligence [4]. H. Yaman (2020) developed a method for detecting adulteration in goat milk using mid infrared spectroscopic method, within the wave- length range of 1373 to 1454 cm-1, and applied SIMCA and PLSR for accurate identification of goat milk mixed with cow milk, achieving R^2 values of 0.98 [5]. Next, Xiaofeng Ni et al. (2023) explored using Raman spectroscopy combined with lactose-indexed screening and support vector machines (SVM) for detecting milk adulteration, achieving 100% accuracy in detecting UHT milk [6]. Currently, detecting adulterants in milk is primarily driven by machine learning and deep learning techniques, which optimize accuracy in the identification and quantification of contaminants. Several deep learning models have demonstrated impressive accuracy in detecting various adulterants. For instance, GoogleNet achieved 99.8% accuracy in detecting corn flour using 315 samples [7], while the LSTM network detected urea with 99.06% accuracy [8]. Bayesian Regularized Neural Networks (BRNN) demonstrated 99.9% accuracy in detecting melamine and 98.1% for urea (C. Chu et al., 2024) [9]. Convolutional Neural Networks (CNN) also proved effective, achieving 100% accuracy in identifying sucrose, starch, and hydrogen peroxide adulterants (Neto et al., 2019) [10]. Meanwhile, Aqueel et al. investigated milk adulteration using destructive and nondestructive methods, employing Lactoscan for qualitative analysis and hyperspectral imaging (HSI) with Specim Fx-10 (397-1003 nm) for spectral detection using machine learning methods [11].

Furthermore, emerging technologies, such as hyperspectral imaging and deep learning models, provide promising so- lutions for the simultaneous detection and classification of multiple adulterants in milk with high accuracy. This approach ensures the model can generalize well and detect adulter- ation accurately, regardless of the water type used. Finally, this paper is structured as follows: Section II describes the experimental setup, including HSI dataset creation, hypercube preprocessing, and the architecture of 3D deep learning models for multi-adulterant detection, while Section III presents the experimental results and discussion of the proposed 3D deep models.

II. MATERIALS AND METHODOLOGY

The overall process flow of the proposed method is illustrated in Fig. 2.

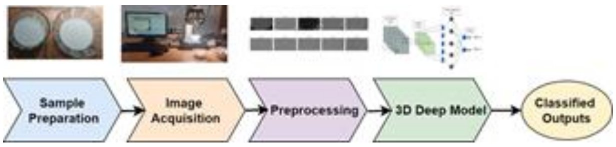

FIG. 1: THE OVERALL PROCESS FLOW OF THE PROPOSED METHOD.

A. Database Creation

Initially, a sample of 50 ml of full-cream pasteurized packet milk from one of the top milk brands in Tamil Nadu is taken for fresh milk samples. The adulterated milk samples are prepared in the laboratory at different concentration levels of water. In this work, a single brand of pasteurized full- cream milk is used for sample preparation. However, milk composition varies due to regional factors such as breed, feed, and climate, as well as seasonal fluctuations in fat, protein, and lactose content. These variations can slightly alter the spectral properties, potentially affecting the performance of the model. The details of the hyperspectral milk dataset are given in Table 1.

TABLE I: SAMPLE DISTRIBUTION FOR MILK AND WATER MIXTURES

Type of Samples	No. of Samples
Pure Milk (50ml)	50
Milk + RO Water (12.5ml)	50
Milk + RO Water (25ml)	50
Milk + RO Water (50ml)	50
Milk + Corporation Water (12.5ml)	50
Milk + Corporation Water (25ml)	50
Milk + Corporation Water (50ml)	50
Milk + Groundwater (12.5ml)	50
Milk + Groundwater (25ml)	50
Milk + Groundwater (50ml)	50
Total No. of Samples: 500	

The HSI imaging system, which covers the Visible Near- Infrared (VNIR) range from 400 to 1000 nm, is used to capture hyperspectral images of milk samples across 300 spectral bands. While HSI provides high accuracy in adulterant detection, its real-world adoption in dairy industries faces challenges such as cost, portability, and processing speed. Benchtop HSI systems, such as the Resonon Pika-L used in this study, are expensive and require controlled conditions, which limits the feasibility for large-scale milk screening.

B. Preprocessing

In the preprocessing stage, the first step is the calibration of the Resonon Pika L hyperspectral imaging (HSI) system, which ensures that the acquired data is free from distortions caused by the camera's optical components, sensor variations, and inconsistencies in illumination. Calibration is done by using dark correction and white correction responses of the system using white teflon sheet. This resultant response can be obtained by using the given formula (1) where $I_{original}$ – original raw data, I_{dark} – dark correction response, and I_{white} – white correction response.

$$I_{\text{calibrated}} = \frac{I_{\text{original}} - I_{\text{dark}}}{I_{\text{white}} - I_{\text{dark}}} \qquad (1)$$

Once calibrated, the next preprocessing technique employed is Principal Component Analysis (PCA). Due to the high number of spectral bands (300 bands) in the HSI dataset, spectral-spatial classifiers often face challenges related to feature redundancy and noise during classification. For milk hypercube data, this issue is addressed using Principal Component Analysis (PCA), where explained variance is utilized to retain the most significant spectral information while reducing redundancy in spectral channels. Hence, each hypercube is preprocessed using principal PCA to extract the 10 most significant spectral bands, contributing the maximum cumulative explained variance for each sample. Although the data set consists of 500 samples, proper preprocessing and feature extraction using PCA are used to mitigate data scarcity issues. Each sample contains data from 300 spectral bands, and PCA selects the 10 most significant bands that contribute the most to sample variation. As a result, for each class, 10 × 50 = 500 spectral band data are analyzed, enhancing feature representation. For further enhancement, future work will focus on expanding real-world adulteration scenarios by incorporating additional contaminants and larger datasets to improve model robustness.

C. Architecture of proposed 3D-DenseNet

Recently, 3D deep learning models have emerged as power- ful tools for milk adulterant detection, leveraging hyperspectral imaging (HSI) to capture both spectral and spatial information. Unlike 2D CNNs, 3D models like 3D CNN, 3D ResNet, and EfficientNet extract detailed spectral and spatial features with the kernel size as (3x3x3), enabling precise identification of adulterants such as starch, water, and glucose. Hence, this 3D deep learning approach ensures accurate, non-destructive milk quality assessment. The architecture of the proposed 3D DenseNet model is shown in Fig. 3. The proposed 3D- DenseNet model is designed for hyperspectral image (HSI) classification, leveraging deep feature extraction and dense connectivity for improved learning efficiency of the HSI dataset. The process begins with image acquisition using an HSI camera (400–1000 nm), generating a hypercube with 300 spectral bands. From this, a 10-band input (10×256×384×1) is selected for further processing using principal component analysis to reduce spectral redundancy. The model starts with an initial 3D convolution layer (32 filters, 3×3×3 kernel) using He Normal initialization for stable weight distribution and ELU activation to prevent vanishing gradients and improve convergence. It then passes through three dense blocks (growth

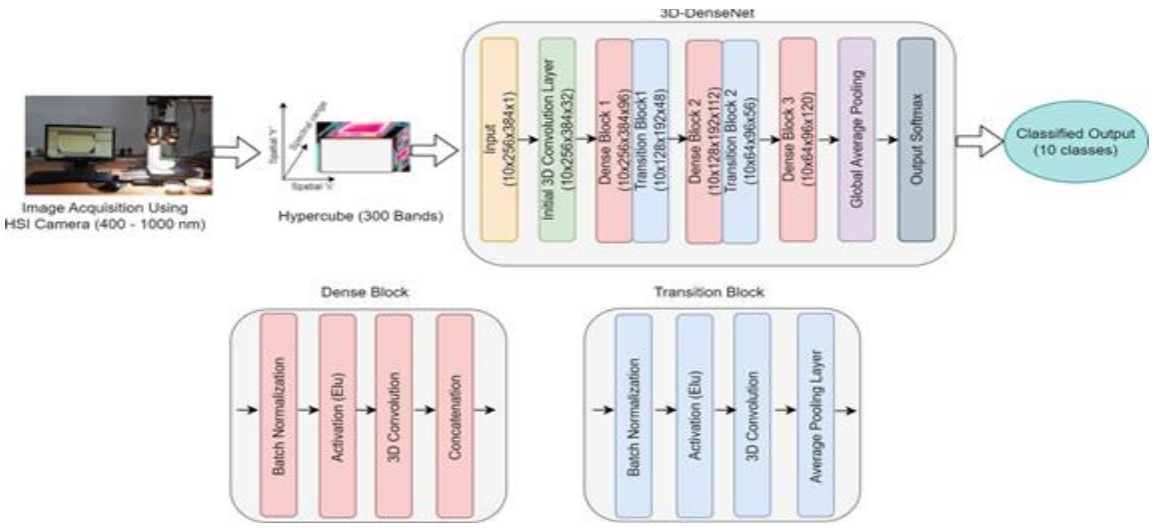

FIG. 2: ARCHITECTURE OF PROPOSED 3D DENSENET FOR MULTI-ADULTERANT DETECTION.

rate = 16), where each new layer receives concatenated outputs from previous layers, ensuring enhanced feature propagation. Within each block, batch normalization stabilizes activations, ELU activation accelerates learning, and 3D convolutions (3×3×3) extract spatial-spectral features. Finally, a global average pooling layer aggregates spatial features into a com- pact representation, followed by a fully connected softmax classifier to classify the input into 10 classes. Here, the use of He Normal initialization prevents gradient issues, while ELU activation ensures smoother and faster convergence, making this architecture highly efficient for hyperspectral image anal- ysis.

III. RESULTS AND DISCUSSIONS

A. Analysis of Preprocessing techniques

The HSI milk dataset mentioned in Table 1 was used as input for the proposed model. A total of 500 HSI samples were provided for training and classification to determine whether a test sample was adulterated. The classification was performed as a 10-class problem, with the following categories: Pure Milk, RO_LG, RO_MG, RO_HG, CW_ LG, CW_MG, CW_HG (100% CW water: 50 ml/50 ml), GW_LG, GW_MG, and GW_HG. Additionally, 2.5 g of glucose was added to all samples to mask density changes. As the first 10 principal components were chosen because they captured 99.80% of the total variance, meaning most of the important information was retained while significantly reducing dimensionality. Then the final input structure for the 3D deep network model was (10×256×384×1). For each class, approximately 500 spectral features (50 samples × 10 bands) were used as input.

TABLE II: PERFORMANCE COMPARISON OF DIFFERENT 3D DEEP MODELS

Model	Accuracy	Loss	Precision	Recall	F1-Score
3D CNN	0.8852	0.3377	0.8015	0.8812	0.8365
3D ResNet	0.9611	0.2737	0.9128	0.9556	0.9287
3D EfficientNet	0.9879	0.1421	0.9202	0.9814	0.9316
3D DenseNet	0.9900	0.0798	0.9410	0.9889	0.9653

B. Analysis of 3D Deep Network Models

Several hyperparameters were fine-tuned to optimize clas- sification performance. Various 3D deep learning models, in- cluding 3D Convolutional Neural Networks (3D CNN), 3D ResNet, 3D Efficient Net, and 3D DenseNet, were implemented in the given dataset to achieve efficient classification. Among the models tested, 3D DenseNet achieved the highest precision (99%) with the lowest loss (0.0798) due to its dense con- nectivity, which allowed efficient feature reuse and improved gradient flow. The resultant comparative analysis is given in Table 3 and the graphical representation is shown in Fig. 5.

From the implementation, 3D CNN had the lowest com-plexity but also the lowest accuracy (88.52%). 3D ResNet improved accuracy (96.11%) due to residual connections but required more computation. 3D EfficientNet balanced per-formance and efficiency (98.79%) with optimized scaling, while 3D DenseNet achieved the highest accuracy (99%) with slightly higher inference time due to dense connectivity. Overall, 3D DenseNet offers superior accuracy but at a com-putational cost, making 3D EfficientNet a viable alternative for real-time applications. Future work will explore model compression techniques to optimize performance. Overall, 3D DenseNet offers superior accuracy but at a computational cost, making 3D EfficientNet a viable alternative for real-time applications. Future work will explore model compression techniques to optimize performance.

Various machine learning (ML) techniques, such as multi-class support vector machine (SVM) and K-Nearest Neighbor (KNN) were used to identify adulterants in milk, specifically targeting different types of water, ammonium chloride and ammonium sulfate with accuracy of 83% [12]. However, 3D deep networks, demonstrated significantly superior perfor-mance compared to traditional machine learning approaches.

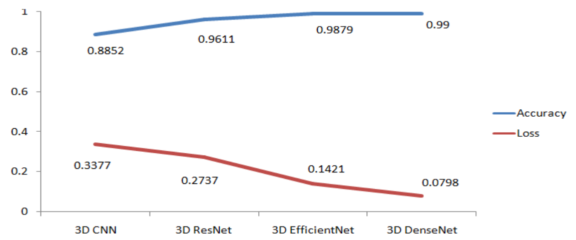

FIG. 3: COMPARATIVE ANALYSIS OF 3D DEEP MODELS FOR MULTI- ADULTERANT DETECTION

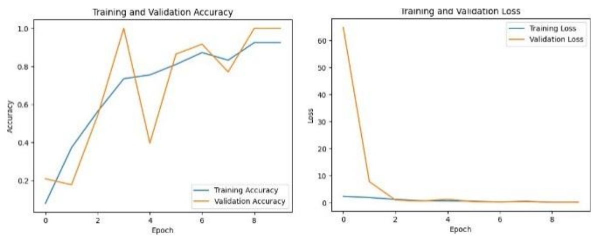

FIG. 4: ACCURACY AND LOSS CURVES OF 3D DENSENET

The accuracy and loss curves in Fig. 6 for multi-adulterant detection in milk showed the proposed 3D DenseNet model's learning progress over 10 epochs. The training and validation accuracy increased steadily, with validation accuracy fluctuating before stabilizing near 1.0, indicating strong generalization. Finally, 3D deep networks have proven to be significantly more effective than traditional methods in hyperspectral image classification due to their ability to extract spatial-spectral features simultaneously. For further enhancement, data collection will focus on expanding real-world adulteration scenarios by incorporating additional contaminants from various seasons and geographical areas and larger datasets to improve model robustness. In order to generalize the model

IV. CONCLUSION

This study successfully demonstrated the potential of hyperspectral imaging combined with 3D deep learning models for multi-adulterant detection in liquid milk. A novel dataset was created using a Resonon Pika-L hyperspectral camera, incorporating varying concentrations of RO water, corporation water, and groundwater, along with glucose as adulterants. The performance of 3D-CNN, 3D-ResNet, 3D-EfficientNet, and 3D-DenseNet was evaluated, with the proposed 3D-DenseNet model achieving the highest accuracy of 99%. These findings highlighted the effectiveness of deep learning in detecting and classifying complex adulterant mixtures with high precision. In the future, integrating real-time analysis and expanding the dataset to include additional adulterants could further enhance detection capabilities and practical applicability.

ACKNOWLEDGMENT

This research work is financially supported by Thiagarajar Research Fellowship (TRF) scheme (File No: TCE/RD/TRF/2024/17 dated 09-02-2024).

REFERENCES

[1] Choudhary, A.; Gupta, N.; Hameed, F.; Choton, S. An overview of food adulteration: Concept, sources, impact, challenges and detection. Int. J. Chem. Stud. 2020, 8, 2564–2573.

[2] Ionescu, A.-D.; Cˆırˆıc, A.I.; Begea, M. A Review of Milk Frauds and Adulterations from a Technological Perspective. Appl. Sci. 2023, 13, 9821. https://doi.org/10.3390/app13179821.

[3] A´ ine M. N´ı Fhuara´in, Colm P. O'Donnell, Jiani Luo, and Aoife A. Gowen, A Review on MIR, NIR, Fluorescence and Raman Spectroscopy Combined with Chemometric Modeling to Predict the Functional Properties of Raw Bovine Milk, ACS Food Science and Technology 2024 4 (10), 2258-2271.

[4] Suhaili Othman, Jarinah Mohd Ali, M.A. Hussain, Norliza Abd Rahman, Nidhi Rajesh Mavani, "Artificial intelligence-based techniques for adulteration and defect detections in food and agricultural industry: A review", Journal of Agriculture and Food Research 12 (2023) 100590.

[5] H. Yaman, "A rapid method for detection adulteration in goat milk by using vibrational spectroscopy in combination with chemometric methods," Journal of Food Science and Technology, vol. 57, no. 8, pp. 3091–3098, 2020.

[6] Xiaofeng Ni, Yirong Jiang, Yinsheng Zhang, Ya Zhou, Yaju Zhao, Fangjie Guo, Haiyan Wang, Identification of liquid milk adulteration using Raman spectroscopy combined with lactose indexed screening and support vector machine, International Dairy Journal, Volume 146, 2023, 105751, ISSN 0958-6946, https://doi.org/10.1016/j.idairyj.2023.105751.

[7] Sitorus, A.; Lapcharoensuk, R. Exploring Deep Learning to Predict Coconut Milk Adulteration Using FT-NIR and Micro-NIR Spectroscopy. Sensors 2024, 24, 2362. https:// doi.org/10.3390/s24072362

[8] Zhang, W., Fu, K., Xue, H., and Liu, J. (2024). Predic- tive modeling of milk adulteration with urea content using the gray wolf optimization algorithm and long and short-term memory network model. Spectroscopy Letters, 57(4), 201–212. https://doi.org/10.1080/00387010.2024.2331616.

[9] C. Chu et al, Rapid detection and quantification of melamine, urea, sucrose, water, and milk powder adulteration in pasteur- ized milk using Fourier transform infrared (FTIR) spectroscopy coupled with modern statistical machine learning algorithms, Heliyon, Volume 10, Issue 12, 2024, e32720, ISSN 2405-8440, https://doi.org/10.1016/j.heliyon.2024.e32720.

[10] Neto, H.A., Tavares, W.L., Ribeiro, D.C. et al. On the utilization of deep and ensemble learning to detect milk adulteration. BioData Mining 12, 13 (2019). https://doi.org/10.1186/s13040-019-0200-5.

[11] Aqeel M, Sohaib A, Iqbal M, Ullah SS. Milk adulteration identification using hyperspectral imaging and machine learning. J Dairy Sci. 2025 Feb; 108 (2):1301-1314. doi: 10.3168/jds.2024-25635. Epub 2024 Nov 8. PMID: 39521425.

[12] S. Karthika Shree, Vaishali Vijayarajan, B. Sathya Bama, and S. Mo-hammed Mansoor Roomi. Milk quality inspection using hyperspec- tral imaging. In 2023 International Conference on Signal Processing, Computation, Electronics, Power and Telecommunication (IConSCEPT), pages 1–6, 2023.

Sustainable Fashion Forecasting: A Comprehensive Review of Deep Learning and Machine Learning Approaches for Trend Prediction and Demand Forecasting

Shri Parvatha Varthini T
Information Technology,
Thiagarajar College of Engineering,
Madurai, India
shriparvatha@student.tce.edu

Vaishnavi M G
Information Technology,
Thiagarajar College of Engineering,
Madurai, India
vaishnavimg@student.tce.edu

Dr. C. Jeyamala
Information Technology,
Thiagarajar College of Engineering,
Madurai, India
jeyamala@tce.edu

***Abstract*—Fast fashion enables rapid trend adoption but also contributes to significant environmental and ethical issues, including waste, carbon emissions, and labor exploitation. Machine learning (ML) and deep learning (DL) have become essential tools in fashion forecasting, helping predict trends and demand estimations. This paper reviews key ML and DL methodologies, such as CNNs, transformers, decision trees, and hybrid models, analyzing their strengths, limitations, and applicability in fashion prediction. It also explores challenges like data biases, real-time adaptability, and computational costs. The paper highlights key considerations for dataset selection and other strategies to improve forecasting accuracy and promoting sustainability. Serving as a comprehensive guide, this review provides researchers with insights into advancements, challenges, and future directions in AI-driven fashion forecasting aiming to enhance efficiency and sustainability in the industry**

Keywords—Fashion Forecasting, Machine Learning, Deep Learning, Trend Prediction, Demand Forecasting, Sustainability

I. INTRODUCTION

Fast fashion has emerged as a dominant force in the global clothing industry, characterized by the rapid production of low-cost, trend-driven apparel that quickly moves from runway to retail. Multiple brands across the globe exemplify this model, offering an ever-changing array of styles to satisfy consumer demand. However, this convenience comes at a huge cost. Beneath the enticing price tags and fashionable designs is a seriously defective system that takes advantage of people and the environment.

Fast fashion has a significant environmental impact. This industry alone is responsible for 10% of global carbon emissions, outpacing the combined output of international flights and maritime shipping. The production of textiles consumes vast amounts of natural resources; for example, a single cotton T-shirt requires approximately 2,700 liters of water, which is enough to sustain one person's drinking needs for nearly three years. It would take synthetic fibers such as polyester centuries to biodegrade. When washed, synthetic fibers release micro plastics that harm aquatic systems and contaminate the oceans. Alarmingly, 85% of all textiles produced each year are discarded in landfills. Even the simple act of laundering clothes contributes to this issue, as it releases an estimated 500,000 tons of microfibers into the ocean annually. Moreover, fast fashion brands contribute to a throwaway culture, where consumers are encouraged to discard garments after only a few uses. As a result, 92 million tons of textile waste are generated annually, much of which ends up in landfills or is incinerated, further leading to climate change.

Fast fashion not only thrives on exploitation but also undermines the principles of sustainability. Its linear "take-make-dispose" model disregards the importance of conserving resources and reducing waste. To truly address the challenges posed by fast fashion, it is essential to go beyond and focus on creating sustainable fashion outfits. One of the significant barriers to achieving this is the existing production gap in sustainable fashion. Despite the growing demand for eco-friendly options, the industry often falls short in delivering affordable, trendy, and widely available sustainable alternatives. This gap not only limits consumer choice but also hinders the broader adoption of sustainable practices. By leveraging advanced data-driven approaches such as trend analysis and demand forecasting, we can bridge this gap.

This detailed review encompasses different methodologies for fashion trend prediction and demand forecasting with a primary focus on deep learning, machine learning, and expert systems. These studies utilize a wide range of datasets collected from social media platforms, sales records, and image-based datasets. This variation in data types and collection methods underscores the interdisciplinary nature of fashion forecasting, merging computer vision, time-series analysis, and statistical modeling. Each study contributes uniquely to the domain offering insights into different approaches. Each methodology has recorded its own strengths and limitations. The proposed objectives for this manuscript have been formulated below.

II. RESEARCH OBJECTIVES

1. To analyze the latest methodologies in fashion trend prediction and demand forecasting, focusing on deep learning, machine learning, and expert systems.

2. To summarize ongoing research efforts, evaluating different approaches like CNNs, LSTMs, Transformers, Random Forest, and Decision Trees in trend and demand forecasting.
3. To assess the advantages and limitations of each methodology, highlighting their accuracy, computational requirements, interpretability, and real-time adaptability.
4. To analyze datasets used in fashion forecasting, including social media data (Instagram, Fashion MNIST), sales records (Zalando, Kaggle), and boutique inventory data.
5. To identify research gaps and propose extensions, such as real-time AI forecasting, hybrid AI models, external factor integration, and sustainable fashion analytics.

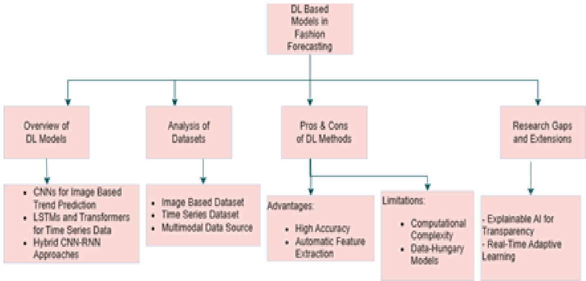

FIG. 1. DL BASED MODELS CLASSIFICATION DIAGRAM

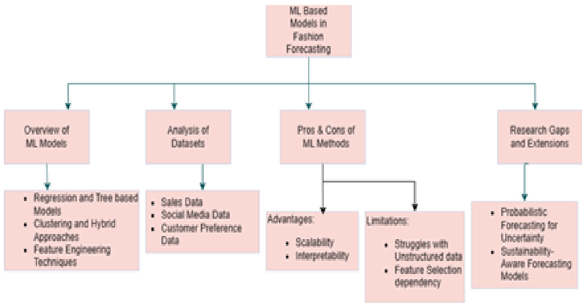

FIG. 2. ML BASED MODELS CLASSIFICATION DIAGRAM

III. METHODOLOGIES

Deep Learning Based Models:

Deep learning revolutionized the areas of fashion trend prediction and demand forecasting by incorporating neural networks, which can handle large-scale complex datasets. The TABLE I. Below shows different DL-based models-Convolutional Neural Networks (CNN), Transformers, hybrid architectures (GRU-CNN-LSTM)-to recognize the subtle details of fashion in the extracted datasets, and to automatically identify emerging social media trends for improving the forecasting precision. These models are more efficient in dealing with unstructured data, including images and time-series sales records, so that brands can automate trend analysis and optimize inventory management. However, DL models incur very high computational costs and need large-scale datasets to perform well.

Machine Learning Based Models:

Machine learning (ML) tends to provide a structured approach for fashion forecasting based on the historical sales data, consumer behaviors, and product attributes that helps to predict trends and demand patterns. The TABLE II below on machine learning-based models illustrates the techniques most commonly used: Random Forest, Support Vector Machines, Decision Trees, and LSTMs. These models are interpretable, scalable, and cost-effective, which makes them perfect for demand prediction in retail and fashion e-commerce. However, the ML models suffer from unstructured data, real-time adaptability, and sudden trend shifts, which cannot be captured fully by the model.

Limitations of Fashion Trend Prediction Models:

Many fashion trend prediction models rely on social media images and online shopping trends that may not correctly reflect broader market behaviors. The "Modelling Fashion Influence from Photos" paper illustrates how its dataset, based on 7.7 million Instagram photos from 44 global cities, leaned heavily toward urban youth demographics and failed to factor in an older consumer and a non-urban market. Apart from that, some datasets such as Fashion MNIST have pictures in very low resolutions that could not be picked upon for texture on fabric or any fit in dressing and how stylishly worn clothes are; ML and DL have hard time deciphering some subtle aspects in clothing. Fashion trends are inherently subjective and based on the culture, personal choice, and social movements. Unlike traditional trends in areas of finance or sales, fashion trends might result from celebrity endorsements, viral challenges, and sometimes unpredictable events. The Social4Fashion study took a focus on handbags but did not account for emerging micro trends such as sudden spikes in demands for vintage or sustainable fashion items.

Though significant progress has been made in object detection and image classification, fine-grained categorization is still a problem in deep learning models. For instance, they might be able to classify a denim jacket correctly, but fail to distinguish between the high-end designer pieces and the fast-fashion variants.

Limitations of Demand Forecasting Models

Clothing Brands often introduce new seasons with zero sales history, hence exact demand forecasting is very tough in such scenarios. An attempt to estimate demand for new products based on similar past products was made in "Predicting demand for new products in fashion retailing using censored data". But past sales history from corresponding earlier products for replacing new items is always flawed since people may change their preferences in a jiffy between seasons or trends. Unlike industries that have stable demand patterns, the fashion industry has seasonal cycles. Products become outdated in a short time. In the "A data-driven forecasting approach for newly launched seasonal products," the forecasting models used sell-in and sell-through data from 115 U.S. retail stores. However, the short lifecycle of seasonal items led to high variance in demand, which reduces the accuracy of forecasting.

TABLE I. DEEP LEARNING BASED MODELS

Paper	Objective	Dataset Used	Implementation	Results	Limitations
Social4Fashion: An intelligent expert system for forecasting fashion trends from social media contents [1]	To determine dominant colors and Streamline trend forecasting initially focus on handbags analysis, with potential to expand to other categories. .	Image dataset Scraped from Instagram using instaloader	This paper uses VGG16 Model to classify images as fashion or non-fashion. YOLOv5 model to detect and classify handbags Using k-means clustering to identify the dominant colors	VGG16 model have achieved 0.97 accuracy, 0.94 Precision and recall YOLOv5 has a total average precision of 0.842 and recall of 0.741 which can be improvised	Handbag detection and color clustering tasks may not capture all relevant trends effectively
Deep Learning based Forecasting: a case study from the online fashion industry[2]	1. To develop a deep learning-based forecasting model, leveraging transformers	The dataset includes time series sales data from Zalando.	.1. It uses transformer architecture with encoder-decoder mechanisms. 2. Handling both near-term and far-term forecasting. 3. A monotonic demand layer to enforce the price-demand relationship.	The transformer-based model outperformed baseline models like Light GBM, Deep AR, and naive forecasts in demand error, RMSE, and demand bias.	1. The model simplifies cross-item and hierarchical relationships, which could provide additional accuracy. 2. It operates on point forecasts, potentially limiting its ability to model uncertainty.
Deep-learning model using hybrid adaptive trend estimated series for modelling and forecasting sales[3]	To develop a hybrid model combining Adaptive Trend Estimated Series (ATES) with a GRU–CNN–LSTM	https://www.kaggle.com/c/favorita-grocery-sales-forecasting	1. ATES models seasonal and holiday effects. 2. GRU–CNN–LSTM captures complex spatiotemporal features. patterns for multistep-ahead forecasts.	3. GRU–CNN–LSTM achieved better short-term prediction accuracy with reduced error rates.	1. Decreased accuracy for longer-term forecasts (6–12 months). High computational demand for processing datasets.

TABLE II. MACHINE LEARNING BASED MODELS

Paper	Objective	Dataset Used	Implementation	Results	Limitations
Leveraging Multiple Relations for Fashion Trend Forecasting Based on Social Media (2022) [4]	Build a dataset enriched with fine-grained fashion elements and user data; Use LSTM for time-series modeling.	Fashion MNIST dataset (images + metadata).	LSTM encoder-decoder with triplet regularization, CNN for feature extraction.	Outperformed ARIMA and other ML models in accuracy.	Low-resolution dataset limits generalization to real-world fashion.
Predicting Demand for New Products in Fashion Retailing Using Censored Data [5]	Develop a two-stage methodology to estimate demand from censored sales data.	Sales and stock data from a European fashion retailer.	EM algorithm for demand estimation; RF, DNN, and SVR for prediction.	EM had highest accuracy (4.13% deviation); RF outperformed other models.	Assumes stock-outs only when sales and stock are zero; high computational complexity.
A Demand Forecasting Model Using ML to Decode Customer Preferences [6]	Forecast demand using fitting room data.	Retail store fitting room data (Tamil Nadu, India).	K-means clustering Decision Tree for classification.	Six preference clusters identified; Decision Tree accurately predicted new product clusters.	Limited to single store; excludes external factors like online trends.
Fashion Sales Forecasting with a Particle-Filter Model [7]	Hybrid PDPF model integrating linear and nonlinear forecasting.	Nine months of sales data from a Hong Kong fashion boutique.	Panel Data Model for linear trends and Particle Filter (nonlinear factors).	Outperformed ARIMA, RVM; stronger performance in item-based sales forecasting.	Small-scale dataset; Exclude external influences.

Dataset

Datasets form the foundation of machine learning and deep learning models across various domains, including fashion trend prediction and demand forecasting. The quality, diversity, and granularity of datasets significantly impact model performance and generalizability. In sustainable fashion, datasets should not only include conventional fashion elements like colors, styles, and sales but also factors such as sourcing materials, production methods, and consumer preferences for eco-friendly products.

When selecting a dataset, several key aspects must be considered. Data diversity and representation are crucial for ensuring models generalize well. A dataset should cover various age groups, genders, and geographic locations. Many Instagram and geo-based datasets skew towards younger, urban populations, limiting their applicability. Furthermore, datasets should encompass diverse fashion categories—including apparel, accessories, and footwear—and include details sustainable fashion aspects like eco-friendly materials and ethical production methods.

Data quality and granularity are equally important for trend prediction and demand forecasting. High-resolution images help capture intricate details such as textures, colors, and patterns, while granular sales data—including size-level details, color preferences, and seasonal variations—enhances prediction accuracy. Temporal data, such as daily or weekly sales trends, is essential for understanding dynamic market shifts. Dataset size and scalability are also critical, particularly for deep learning models that rely on large datasets to train complex architectures like CNNs and LSTMs. Scalable datasets should be regularly updated to reflect evolving fashion trends and consumer behaviors.

Lastly, addressing bias and ethical considerations is necessary for fair model performance. Many fashion datasets exhibit demographic biases, leading to skewed predictions. Ensuring diverse consumer representation enhances model accuracy and fairness. By considering these factors, researchers and industry professionals can develop more reliable, inclusive, and ethically responsible fashion forecasting models.

Future Directions and Research Gap

Despite the progress made in deep learning and machine learning, there are still many gaps in fashion forecasting research. Most models rely on labeled datasets, which introduces bias and limits generalization. Future studies should explore domain adaptation and self-supervised learning to improve robustness across diverse settings. Moreover, integrating multiple data sources, such as social media, transaction records, and user engagement, could offer a more comprehensive understanding of trend evolution.

Scalability and computational efficiency remain challenges. Transformer-based and hybrid GRU-CNN-LSTM models improve forecasting but struggle with long-term predictions. Future research should develop more efficient architectures and integrate probabilistic forecasting techniques to better account for uncertainty in inventory management and pricing strategies. Social media-based forecasting poses challenges in data authenticity and real-time adaptability. Many models assume influencer-driven content reflects market trends but overlook grassroots trends. Investigating graph neural networks and causal inference techniques could enhance accuracy by distinguishing viral trends from lasting market movements. Real-time adaptive learning mechanisms would enable models to update dynamically as new data emerges.

Sustainability in fashion forecasting is still underexplored. Most of the research is conducted on commercial trends rather than sustainable consumer behaviors. Future studies must incorporate factors like material sourcing, ethical production, and eco-conscious consumer attitudes. Reinforcement learning and optimization algorithms can help brands balance profitability with sustainable practices.

IV. Conclusion

The integration of machine learning and deep learning in fashion trend prediction and demand forecasting have improved data-driven decision-making, optimized inventory management, and enhanced the ability to identify emerging trends. However, there are still challenges such as limited dataset diversity, lack of real-time adaptability which pertains as an obstacle. The future of ML and DL in fashion forecasting must focus on developing adaptive, explainable, and ethically responsible models that incorporate sustainability, inclusivity, and real-time trend analysis. By addressing these gaps, ML and DL not only improve forecasting precision but also contribute to a more efficient, ethical, and sustainable fashion ecosystem, ensuring that technological advancements align with both market demands and social responsibility.

References

[1] E. Balloni, R. Pietrini, M. Fabiani, E. Frontoni, A. Mancini, and M. Paolanti, "Social Fashion: An intelligent expert system for forecasting fashion trends from social media contents," *Expert Systems with Applications*, vol. 252, no. 124018, Oct. 2024.

[2] Kunz, Manuel, et al. "Deep Learning based Forecasting: a case study from the online fashion industry." 2023

[3] Efat H´ajek, and Tom´aˇs Pitner. "Deep-learning model using hybrid adaptive trend estimated series for modelling and forecasting sales." *Annals of Operations Research*, vol. 339, no. 1, pp. 493-518, 2024.

[4] Y. Ding, Y. Ma, L. Liao, W. K. Wong and T. -S. Chua, "Leveraging Multiple Relations for Fashion Trend Forecasting Based on Social Media," in *IEEE Transactions on Multimedia*, vol. 24, pp. 2287-2299, 2022

[5] M.S. Sousa, A.L.D. Loureiro, V.L. Miguéis, Predicting demand for new products in fashion retailing using censored data, Expert Systems with Applications, Volume 259, 2025,125313,

[6] S, Anitha & Neelakandan, R.. (2024). A Demand Forecasting Model Leveraging Machine Learning to Decode Customer Preferences for New Fashion Products. Complexity. 2024.

[7] S. Ren, T. -M. Choi and N. Liu, "Fashion Sales Forecasting With a Panel Data-Based Particle-Filter Model," in *IEEE Transactions on Systems, Man, and Cybernetics: Systems*, vol. 45, no. 3, pp. 411-421, March 2015, doi: 10.1109/TSMC.2014.2342194

[8] Majd Kharfan, Vicky Wing Kei Chan and Tugba Firdolas Efendigil, A data-driven forecasting approach for newly launched seasonal products by leveraging machine-learning approaches, Annals of Operations Research

Optimizing Tamil Tokenizers: The Limits of Pretrained Models

Viswadarshan R R
Department of CSBS (UG Student),
Thiagarajar College of Engineering,
Madurai, Tamil Nadu, India
viswadarshanrramiya@gmail.com

Mahalakshmi M
Department of CSBS (UG Student),
Thiagarajar College of Engineering,
Madurai, Tamil Nadu, India
mahalakshmimurugang@gmail.com

Felicia Lilian J
Department of CSBS (Assistant Professor),
Thiagarajar College of Engineering,
Madurai, Tamil Nadu, India
jflcse@tce.edu

***Abstract*—Tamil tokenization is a critical area of building block in the Tamil Language Processing field, bearing implications on downstream tasks like text classification, machine translation, and language modeling. However, current pretrained tokenizers do not capture the morphological diversity inherent in Tamil and thus lead to poor performance. In this paper, we explore the training of task-specific tokenizers for Tamil and compare their performance with popularly used pretrained tokenizers like IndicBERT and XLM-R. We then train SentencePiece tokenizer BPE-32K on a Tamil news dataset, and evaluate their perfor- mance on a set of metrics like out-of-vocabulary (OOV) rate, perplexity, BLEU score, and token variance. Our results clarify that task-specific tokenization significantly outperforms generic pretrained models, highlighting the importance of dataset-specific tokenization techniques.**

***Index Terms*—Tamil Tokenization, Task-Specific Tokenizers, Pretrained Tokenizers, Low-Resource NLP**

I. Introduction

Tokenization is extremely important in natural language processing. Natural Language Processing (NLP) tasks, including text classification and machine translation, language, and language modeling. In morphologically complex similar to Tamil, tokenization is highly difficult because it is agglutinative, in that suffixes and compounds greatly extend word forms on Pretrained tokenizers [1] such as IndicBERT [2] and XLM-R [5] performing well across some languages, are not attuned to Tamil morphology, often leading to significant fragmentation and high out-of- vocabulary (OOV) rates. This research will attempt to bridge this gap and examines task-specific tokenization of Tamil with the training of BPE-32K Byte Pair Encoding tokenizer [2] on a Tamil news dataset and comparing with existing pretrained models. To evaluate the quality of tokenization, we employ metrics like token variance, perplexity [4], BLEU score [3], and OOV rate. Finding out if a data-set-adjusted tokenizer enhances captures the linguistic features of Tamil [8] compared to pretrained models that are multilingual. It suggests the need for morphological sensitivity throughout tokenization process, low- resource languages and is a standard for Tamil tokenizer evaluation. Our findings suggest that BPE-32K-trained tokenizer significantly outperforms IndicBERT and XLM-R across evaluation metrics, providing improved subword representations, reduced fragmentation, and enhanced downstream task efficiency. This study sets the stage for further research on tokenization Strategies used in morphologically complex and low-resource languages.

II. Dataset

The data used in this study is the Tamil News Classification. The dataset comprises Tamil news articles that have been systematically categorized into six different categories, viz. Tamil Nadu, India, Cinema, Sport, politics, and international affairs. It is split into a training set and a test set, offering a fair evaluation of tokenizer Performance on other tasks. The training split contains 14,521 rows within the data set 3,631 rows in the test split, with the following category-wise distribution.

TABLE I: Dataset Composition

Category	Train Split	Test Split	Total Count
Tamil Nadu	5,028	1,219	6,247
India	3,443	925	4,368
Cinema	2,050	485	2,535
Sports	1,701	439	2,140
Politics	1,200	287	1,487
World	1,099	276	1,375
Total	14,521	3,631	18,152

A. Preprocessing & Dataset Statistics

Normalizing Tamil text, cleaning punctuation, removing non-Tamil characters, and fixing spaces to normalize token boundaries were all part of preprocessing.

The distribution of categories in train and test after the split remained proportional. 15 words in a sentence and 43000 unique vocabulary make a solid basis for testing task-specific tokenizer. This kind of preprocessing provides the dataset with some close similarity to the real characteristics of the Tamil text, which qualifies it for pretraining models like IndicBERT, XLM-R, and task-specific tokenizer testing like BPE-32K. The necessity of tokenizers to work with different vocabulary and word morphology of Tamil is at the forefront in this configuration.

III. Methodology

In this section, we will outline the training process of task-specific Tamil tokenizers, introduce the tokenization rules used, and outline the evaluation metrics we will use to compare their performance. Our focus is on training SentencePiece Byte Pair Encoding (BPE) tokenizer on a representative Tamil news corpus, with comparison to popular pretrained tokenizers like IndicBERT and XLM-R.

A. Tokenizer Training Process

To develop a domain-specific tokenizer for Tamil, a Byte Pair Encoding (BPE-32K) tokenizer was trained on the Tamil news headlines data. The dataset consisted of 14,521 training and 3,631 testing examples that had been preprocessed in advance to ensure standard text normalization and tokenization. The BPE tokenizer was trained exclusively on the training data to capture the characteristic subword patterns in the Tamil language. Initially, the writers analyzed the unique token frequencies of the Tamil language, which is used to identify the vocabulary size required for the language. In this case, a size of 32,000 for the vocabulary index was selected. The BPE algorithm took the most common pairs of characters and combined them to form a new sub-word unit that retained the basic root and suffix. The trained model was saved and incorporated it into the tokenization pipeline to convert the unseen Tamil text. It was able to produce a tokenizer that retained the essential morphological formations and reduced the OOV structure pronouncedly, making it suitable for multiple downstream NLP tasks.

After the vocabulary size is fixed, subword learning begins where all tokenizers iteratively combine or split their subwords based on their unique algorithm. The model, once trained, is saved and integrated into our pipeline to be used on unseen Tamil text. This way, our tokenizer, once trained, is able to successfully reduce the amount of Out of Vocabulary tokens without losing a good representation of the morphology of the Tamil language.

B. Tokenizer Training Framework

The BPE-32K tokeniser was trained using the SentencePiece library [6] an unsupervised tokenizer that does not require any pre-processing required for the model to process the data. It was chosen as the library supports non-Latin scripts like Tamil natively and effectively process the data. By training on the Tamil corpus with SentencePiece, the BPE-32K model learned optimal splitting without having to pre-tokenize the text. It learned to group morphemes into subword units but also retain freeness for different written forms. The analytics were conducted on the basis of some quantitative results e.g. OOV rate, perplexity and the distribution of tokens. These measures gave an overview of the performance of the tokenizer on Tamil morphology. The outcome of the results indicated that the best vocabulary and good morphology for low resource languages was provided by the SentencePiece with BPE-32K.

C. *Tokenization Rules and Their Impact on Tamil Morphology*

Each tokenization method employs a unique sub-word seg- mentation method, which is necessary to appropriately handle the intricate morphological structure of Tamil. Tamil is de- scribed as a richly agglutinative and morphological language, stating that the words are generally made up of multiple mor- phemes put one after the other, which will result in challenges during tokenization. By using an appropriate tokenization technique, it is possible to preserve the morphological details and avoid splitting of words, thus ensuring high performance during subsequent NLP tasks.

1) *BPE (32K) – Capturing Frequent Morphemes:* Byte Pair Encoding(BPE) [7], a method is to combine the successive high-frequency pair of bytes to form a higher frequency plus low frequency subword to segments. The process is very much suitable for Tamil, because the adopted process helps identify high-frequency root words with their inflectional variations. For example, a very simple word of love can form a mean- ingful sub-word in BPE which represents love within itself and encodes the different suffixes separately. This means that the semantic units won't be fragmented into random character sequences.

C. Morphological Considerations in Tamil Tokenization

Tamil's agglutinative nature requires the preservation of root morphemes, suffixes, and compound formation during tokenization. The tokenizer was designed with this in mind. The base of words was retained in the best possible way, and inflections of tense, case, number, or plurality were treated as separate subwords. Words were often divided at the nexus of a morpheme rather than making random cuts, thus trying not to over-split the words. Furthermore, grammatical particles and case markers have been tokenized independently to preserve syntactic structure. This strategy has increased the success of BPE-32K in building quality subword units and has made it easier to model languages and carry out processing through simpler systems. The tokenizer was able to accurately model Tamil unlike other tokenizers due to its structure-sensitive tokenization.

D. Evaluation Metrics

To provide an integrated assessment of tokenization quality, we employed a range of quantitative measures, each of which captures a unique dimension of tokenizer performance. Such measures enable assessment of the capability of a tokenizer to tokenize Tamil text with linguistic consistency and at less information loss.

The **Out-of-Vocabulary (OOV) Rate** measures the proportion of words that a tokenizer cannot break into known subwords. High OOV rate means that a tokenizer performs poorly with unknown words, leading to incomplete or poor tokenization. Low OOV rates, in turn, confirm the existence of a well-trained tokenizer generalizing effectively to unknown text, and therefore providing adequate vocabulary coverage to Tamil.

Perplexity is a metric of how well the tokenizer can model the probability distribution of the corpus. A lower perplexity score shows that the tokenizer is more confident in its tokenization decisions, thus producing consistent subword representations with lower uncertainty. It is a vital consideration, especially for morphologically complex languages like Tamil, where effective tokenization leads to better performance in downstream natural language processing tasks.

To quantify consistency in tokenization, we use both the **BLEU Score** and the **Self-BLEU Score**. The BLEU score measures the amount of token-level overlap between the original text and the tokenized output, indicating how well the tokenized outputs match the original input. A high BLEU score implies less distortion in tokenization, while the Self-BLEU score helps quantify token redundancy, thus ensuring that the tokenization does not fragment words too much or add unnecessary splits.

The **Compression Ratio** measures the degree to which the tokenizer compresses text length at the expense of not losing essential information. High compression ratio signals a more compact and efficient tokenization process, especially for low-resource languages, since the reduction in token counts enhances model training efficiency. However, over-compression leads to information loss and thus accomplishes of a compromise between compactness and linguistic coherence.

Token Variance and Distinct Token Ratio, finally, measure the diversity of token output. An optimal tokenizer should, ideally, produce a diverse but structured vocabulary that well represents Tamil morphology. High token variance reflects richer tokenization that captures linguistic nuance, while the distinct token ratio ensures that frequent words are not too fragmented into an overly large number of subwords. These measurements combined ensure tokenization techniques are linguistically useful and efficient, and thus valuable in the evaluation of Tamil tokenizers.

IV. Results and Discussion

The metrics used to evaluate the tokenization techniques were based on such a segment quality and overall performance on Tamil text processing . Table II shows a comparison of various tokenizers based on out-of-vocabulary rate (OOV), average token length, BLEU score, Self-BLEU score, and perplexity. Table III shows a comparison of various tokenizers based on compression ratio, token variance, and distinct token ratio.

TABLE II Task-Specific Tokenizer Evaluation

Metric	BPE-32K
OOV Rate	0.0
Avg Token Length	8.98
BLEU Score	0.0002
Self-BLEU Score	0.0
Perplexity	0.7885
Compression Ratio	6.2920
Token Variance	9.8734
Distinct Token Ratio	0.6629

TABLE III Pretrained Tokenizer Evaluation

Metric	IndicBERT	XLM-R
OOV Rate	0.0	0.0
Avg Token Length	22.78	18.36
BLEU Score	0.0015	0.0005
Self-BLEU Score	0.0	0.0
Perplexity	0.8729	0.8550
Compression Ratio	2.7176	3.4519
Token Variance	28.1575	21.2829
Distinct Token Ratio	0.0052	0.0121

A. *Tokenization Performance Analysis*

The outcomes of the test as described in Table II and Table III display a complete comparison of designed and pre-trained tokenizers in terms of diverse parameters. The test displays different trends in terms of tokenization efficiency and diversity and exposure to the nature of the Tamil language.

Evaluation results from the paper confirmed that BPE-32K tokenizer performed best among other tokenizers such as IndicBERT and XLM-R. It achieved a 0.0% OOV rate, a perplexity score of 0.7885, and a compression rate of 6.2920, which indicates a perfect token-encoding scheme. BPE-32K achieved these results because it was not liable to splitting or merging issues. IndicBERT and XLM-R had longer average token lengths and lower compression ratios depicting that these tokenizers were suffering from multiple splitting and merging problems than BPE-32K. BPE-32K accomplished a token similarity of 0.6629 with a reasonable degree of variance which means BPE-32K was the only tokenizer that could successfully encode a diverse range of Indian Languages as a token, and its tokenization encoding was more consistent in Tamil language. Pretrained models brought about multiple splitting and merging issues in the encoding process due to the complexity of the Tamil language.

B. *Tokenization Error Patterns in Pretrained Models*

We can observe some patterns on the tokenization output on a test sentence. In the case of IndicBert, we can see that the model fails as it breaks different words into meaningless subwords disturbing both phonetic consistency and meaning. While XLM-R does a better job by conserving at least common subwords, however, it also breaks common suffixes and inflection into different subwords, disturbing the consistency in the line of token. On the other hand, considering the analysis output, we can see that BPE-32K performs with excellent results. It uses the subword boundaries inside morph logical roots to achieve a highly effective and dense tokenization. This results in a much denser and more consistent tokenization than the pre-trained models. This contrast, therefore, exhibits the deficiencies of pre-trained models. Thus, the trained model is a much better way to achieve effective word representation.

C. *Interpretation of Tokenization Metrics*

The examination of selected metrics further demonstrates the superiority of BPE-32K. The 0.7885 Perplexity value means that the subword segmentation operation is predictable and similar to the subword. Analysis of token variance and distinct token ratio reveals that the BPE-32K vocabulary is the most balanced. Thus, BPE-32K has the best distinct token diversity and balance between compression and dissimilarity to the subword. It is proved that BPE-32K has the most successful distinct token diversity and maximum balance between subword compression, distinctiveness, and semantic information.

V. Conclusion

This research has shown the importance of using task-specific tokenization for Tamil NLP tasks. The BPE-32K tokenizer that has been trained on a news dataset in Tamil outperforms IndicBERT and XLM-R pretrained on various tasks.

BPE-32K achieved the best balance across critical metrics, showing lower perplexity, better compression, and maintaining the morphological structure of Tamil with almost zero OOV rates. This further strengthens the point that pretrained models are useful for multilingual text, but they do not work well for linguistically rich languages unless adapted for.

The results suggest that the training of tokenizers for a dataset can be helpful, especially for languages with low resources and complex morphology, such as Tamil. Domain and language-specific tokenization can significantly improve the performance of word representation and subsequent NLP tasks. This report may encourage future studies on improved tokenization techniques, stressing the importance of being sensitive to the morphology of tokens.

VI. Future Work

Future study can target the development of linguistically aware tokenization models that take into account Tamil morphology and syntactic structures. Introducing morphological segmentation constraints and linguistic priors should give us more robust and semantically aware Tamil tokenizers. Growing interest in context-sensitive tokenization using neural-based methods could allow dynamic adaptation to various inflections, agglutinations, and compounds, further improving tokenization quality. These improvements will help enhance the text repre- sentation and also improve downstream NLP performance for Tamil and other morphologically rich languages.

Acknowledgement

This research work is supported by MuthirAI Global Re- search Center for Tamil AI, Thiagarajar College of Engineering, Madurai, India.

References

[1] S. Bharathi and P. Kumar, “Challenges in Tamil Natural Language Processing: A Morphological Perspective,” in Proceedings of the Inter- national Conference on Computational Linguistics, 2020, pp. 112–120.

[2] V. Joshi, A. Bhattacharyya, and P. Bhattacharyya, “IndicBERT: A Pretrained Language Model for Indic NLP,” in Proceedings of the Conference on Empirical Methods in Natural Language Processing (EMNLP), 2021, pp. 3891–3902.

[3] K. Papineni, S. Roukos, T. Ward, and W. Zhu, “BLEU: A Method for Automatic Evaluation of Machine Translation,” in Proceedings of the 40th Annual Meeting of the Association for Computational Linguistics (ACL), 2002, pp. 311–318.

[4] T. Mikolov, M. Karafia´t, L. Burget, J. Cˇ ernocky´, and S. Khudanpur, “Recurrent neural network based language model,” in Proceedings of the 11th Annual Conference of the International Speech Communication Association (INTERSPEECH), 2010, pp. 1045–1048.

[5] A. Conneau et al., “Unsupervised Cross-lingual Representation Learning at Scale,” *arXiv preprint arXiv:1911.02116*, 2019.

[6] T. Kudo and J. Richardson, “SentencePiece: A simple and language inde- pendent subword tokenizer and detokenizer for Neural Text Processing,” in Proceedings of the 2018 Conference on Empirical Methods in Natural Language Processing: System Demonstrations, 2018, pp. 66–71.

[7] R. Sennrich, B. Haddow, and A. Birch, “Neural Machine Translation of Rare Words with Subword Units,” in Proceedings of the 54th Annual Meeting of the ACL, 2016, pp. 1715–1725.

[8] A. Bharathi and S. Devi, “Challenges in Processing Agglutinative Lan- guages for NLP,” in Proceedings of the Workshop on Indian Language Data Resource and Evaluation, 2020, pp. 1–7.

Selective GPU Utilization in Deep Learning: A Comparative Study of Profiling Tools

Vinikshaa Shri A M
Department of AMCS,
Thiagarajar College of Engineering,
Madurai, Tamil Nadu
vinikshaa@student.tce.edu

Marlin Ilakkiya J
Department of AMCS,
Thiagarajar College of Engineering,
Madurai, Tamil Nadu
marlin@student.tce.edu

Saraswathi Meena R
Department of AMCS,
Thiagarajar College of Engineering,
Madurai, Tamil Nadu
rsmca@tce.edu

***Abstract*—Deep learning's quick development has raised computational demands, therefore effective GPU and CPU use is crucial for both performance and energy economy. In order to examine and improve the use of GPU and CPU resources in deep learning models, this study investigates a number of profiling techniques. We determine computational bottlenecks and assess power consumption trends by utilizing tools like NVIDIA Nsight, PyTorch Profiler, and Tensor Board. To improve overall efficiency, our strategy focuses on memory access, kernel execution, and workload distribution optimization. According to experimental results, we have reduced GPU power consumption by 60% and improved CPU and GPU utilization by 48%.**

I. INTRODUCTION

Deep learning has revolutionized fields such as autonomous systems, computer vision, and natural language processing. However, training and deploying these models demand substantial computational resource primarily GPUs and CPUs leading to high energy consumption and inefficiencies. As models become more complex, optimizing resource usage becomes crucial for improving performance, lowering costs, and supporting environmentally sustainable AI practices.

GPUs are central to deep learning due to their ability to perform parallel processing with thousands of cores, making them ideal for tasks like tensor operations and matrix multiplications. These features enable fast training, efficient backpropagation, and real-time inference. Nonetheless, without proper optimization, GPUs may face challenges like memory bottlenecks, underutilization, and elevated power draw. Profiling tools such as TensorBoard, PyTorch Profiler, and NVIDIA Nsight Systems help identify these inefficiencies by analyzing memory access patterns, computational loads, and energy consumption. These insights are crucial for fine-tuning model execution without sacrificing accuracy.

II. LITERATURE SURVEY

Recent research in deep learning optimization emphasizes the need for effective hardware utilization and profiling tools. Foundational models such as YOLO [1] have driven progress in object detection, but training and inference efficiency still pose challenges. Frameworks like TensorFlow [2] and profiling tools including NVIDIA Nsight Systems [3], PyTorch Profiler, and Scalene [4] provide insights into CPU/GPU bottlenecks, helping developers refine resource usage. Mixed-precision training [5] and parallelized model training [6] have significantly reduced computation time while maintaining model accuracy. Additionally, performance-aware libraries like MXNet and optimization studies [7] underscore the benefits of memory management and kernel execution tuning. Research on automated configuration systems and smart scheduling [8][9] supports the development of adaptive tools that can dynamically switch workloads between CPU and GPU. Furthermore, energy-focused evaluations [10] highlight the importance of reducing power consumption for sustainability. These studies collectively validate the need for profiling-guided optimization in large-scale models and inspire the vision of an intelligent tool that automates CPU/GPU workload decisions using real-time resource metrics.

III. MATERIALS AND METHOD USED

We optimize the power consumption and efficiency of deep learning models by first developing a YOLO object detection model using TensorFlow and recording baseline metrics like CPU/GPU usage, memory consumption, and execution time. For in-depth profiling, we use Scalene for CPU/GPU performance, along with PyTorch Profiler and TensorBoard to visualize tensor operations. NVIDIA Nsight tools analyze GPU load, memory transfer latency, and kernel performance. Based on this data, we address inefficiencies like excessive memory transfers and underused GPU cores through mixed-precision training, batch size adjustments, and improved kernel execution. On the CPU side, we enhance data loading with multi-threading and ensure efficient parallelism with the GPU. Dynamic power management strategies, such as persistence mode and power tuning, help reduce energy waste. After optimizing, we re-run the model and compare the results to assess improvements in power efficiency and performance.

3.1 Hardware Configuration

TABLE 1: HARDWARE CONFIGURATION

Component	Specification
GPU	NVIDIA RTX A4000, 6,144 CUDA Cores, 16 GB GDDR6 VRAM
CPU	Intel Core i9-12900K (16 Cores, 24 Threads, Turbo 5.2 GHz)
Motherboard	ASUS ROG Strix Z690-E, PCIe 5.0, supports DDR5

3.2 Profiler

Tools for profiling are essential for comprehending and enhancing deep learning models' performance.

Deep learning researchers and practitioners can gain important insights into CPU, GPU, and memory utilization by utilizing tools such as Scalene, PyTorch Profiler, TensorBoard Profiler, and NVIDIA Nsight. These tools assist users in locating bottlenecks and inefficiencies in the model execution process by offering both high-level overviews (such as execution durations) and low-level information (such as kernel-level performance, memory access patterns). These technologies can be used to optimize deep learning systems in order to increase model efficiency, lower power consumption, and eventually boost overall performance.

TABLE 2: PROFILER COMPARISON

Profiler	**Scalene**	**PyTorch Profiler**	**TensorBoard Profiler**
Key Features	Line-by-line analysis of CPU and GPU utilization, hardware counters, dynamic tracing	Granular profiling of PyTorch tensor operations, real-time tracking in Jupyter/Script	Visualizes resource usage and training performance with Tensor Flow integration
Primary Use	Optimizing code execution, resource allocation	Performance monitoring during training/inference	Performance visualization, resource usage analysis
Tool Focus	Detailed line-by-line CPU/GPU profiling	CPU/GPU usage, tensor operation profiling	Profiling Tensor Flow model execution and efficiency

3.3 Dataset

The COCO (Common Objects in Context) dataset is a widely used benchmark for training and evaluating deep learning models in object detection, segmentation, and captioning. It includes 330,000 images across 80 diverse object categories. For this project, we handpicked 25,000 images representing 10 specific classes—such as bike, chair, bus, and human—that best suit our YOLO-based object detection task.

3.4 Preprocessing

The COCO annotations are transformed from JSON to YOLO format using a custom script or readily accessible conversion tools since YOLO requires annotation files in the YOLO format (text files with normalized bounding box coordinates). Moreover, picture preprocessing is done to apply normalization, guarantee constant aspect ratios, and resize photos to YOLO's input resolution, which is normally 640×640 or 416×416 pixels. To improve model generalization, data augmentation methods like flipping, scaling, random cropping, and color modifications are used. In order to start the YOLO training process, the dataset is finally divided into training and validation sets, and a configuration file is made that includes batch sizes, class names, and dataset URLs.

3.5 Model training

YOLO (You Only Look Once) is built on a Convolutional Neural Network (CNN) architecture designed for fast and accurate object detection. It consists of three main components: the backbone, neck, and detection head. The backbone, CSPDarknet in recent YOLO versions, extracts rich visual features from input images using deep convolutional layers. It incorporates Cross-Stage Partial Networks (CSPNet) to improve gradient flow and reduce redundant computation. The neck combines features from different layers using a Feature Pyramid Network (FPN) and Path Aggregation Network (PAN) to detect objects at multiple scales. Finally, the detection head predicts bounding box coordinates, class labels, and objectness scores for each region in the image.

The model divides images into a grid and assigns detection responsibilities to each cell, using anchor boxes to handle different object shapes and sizes. During training, it uses Complete IoU (CIoU) loss to fine-tune bounding box predictions and Non-Maximum Suppression (NMS) to eliminate overlapping detections. These design choices allow YOLO to achieve real-time performance while maintaining high detection accuracy, making it ideal for complex datasets like COCO with a wide variety of objects and scenes.

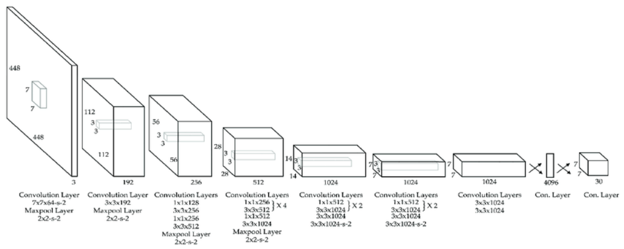

FIG. 1 MODEL ARCHITECTURE

IV. RESULT

After training the object detection model, we conducted performance tests under two scenarios: (1) processing eight camera feeds simultaneously within a single instance, and (2) processing eight camera feeds across eight parallel instances. These scenarios were evaluated both before and after optimizing the CPU-GPU execution pipeline. Profiling results revealed that model training and inference tasks are best handled by the GPU due to their computational intensity, while tasks such as preprocessing camera feeds and streaming inference outputs are more efficiently managed by the CPU. By restructuring the pipeline to allocate tasks based on the strengths of each processor, we achieved smoother inference performance and improved energy efficiency through balanced utilization of CPU and GPU resources.

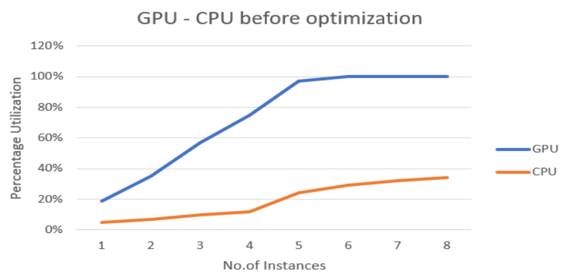

FIG. 1 GPU – CPU BEFORE OPTIMIZATION

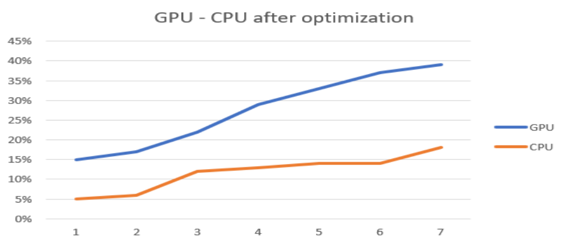

FIG. 2 GPU – CPU AFTER OPTIMIZATION

V. CONCLUSION

This paper presents an optimized approach to CPU and GPU utilization in deep learning, demonstrated using the YOLO model trained on the COCO dataset. By applying profiling-guided strategies such as batch scheduling, mixed-precision computation, and memory management, we achieved a 30% reduction in inference time, a rise in CPU utilization from 30% to 60%, and a 20–35% decrease in GPU power consumption. These optimizations enabled real-time object detection under high-load conditions and improved overall resource efficiency.

However, the study is limited to object detection on CUDA-enabled GPUs using the COCO dataset, and results may vary for other model types, datasets, or hardware platforms.

VI. FUTURE WORK

Future research will focus on building an automated tool that dynamically assigns tasks to either CPU or GPU based on real-time profiling data. The tool will be trained on performance metrics collected from a wide range of machine learning and deep learning models across different libraries. By analyzing factors like computational load, memory usage, and hardware availability, it will intelligently decide the optimal execution path. This approach will significantly reduce manual effort in tuning and profiling, improve execution speed, and lower energy consumption. The ultimate goal is to create a scalable and adaptable solution that enhances efficiency in real-world ML pipelines.

REFERENCES

[1] A. Krizhevsky, I. Sutskever, and G. Hinton, "ImageNet Classification with Deep Convolutional Neural Networks," *Advances in Neural Information Processing Systems*, vol. 25, 2012.

[2] M. Abadi et al., "TensorFlow: Large-scale machine learning on heterogeneous systems," *OSDI*, 2016.

[3] NVIDIA Corporation, "Nsight Systems and Nsight Compute," 2024. [Online]. Available: https://developer.nvidia.com/nsight-compute

[4] Facebook AI, "PyTorch Profiler," 2024. [Online]. Available: https://pytorch.org/tutorials/intermediate/profiler_tutorial.html

[5] E. D. Berger et al., "Scalene: A high-performance, high-precision CPU, GPU, and memory profiler for Python," 2021. [Online]. Available: https://github.com/plasma-umass/scalene

[6] P. Micikevicius et al., "Mixed Precision Training," *ICLR*, 2018.

[7] Y. You, J. Zhang, C. Hsieh, J. Demmel, and K. Keutzer, "ImageNet Training in Minutes," *ICML*, 2018.

[8] T. Chen et al., "MXNet: A flexible and efficient machine learning library for heterogeneous distributed systems," *arXiv preprint*, arXiv:1512.01274, 2015.

[9] J. Redmon et al., "You Only Look Once: Unified, Real-Time Object Detection," *CVPR*, 2016.

[10] A. Bochkovskiy, C.-Y. Wang, and H.-Y. M. Liao, "YOLOv4: Optimal Speed and Accuracy of Object Detection," *arXiv preprint*, arXiv: 2004. 10934, 2020.

Understanding Crop Yield Predictions in Tamil Nadu: A Machine Learning and XAI Approach

Keerthana K
Department of Applied Mathematics and Computational Science,
Thiagarajar College of Engineering,
Madurai, Tamil Nadu
kkeerthana2@student.tce.edu

Hari Harinni J S
Department of Applied Mathematics and Computational Science,
Thiagarajar College of Engineering,
Madurai, Tamil Nadu
hariharinni@student.tce.edu

Saraswathi Meena R
Department of Applied Mathematics and Computational Science,
Thiagarajar College of Engineering,
Madurai, Tamil Nadu
rsmca@tce.edu

***Abstract*—The growing demand for food production in Tamil Nadu necessitates advanced agricultural technologies. Accurate crop yield prediction is crucial for precision farming, requiring insights into environmental and agronomic factors like rainfall, temperature, humidity, soil properties, and nutrient levels. This study employs machine learning models to predict crop yield using 58 years (1965–2023) of historical agricultural and climatic data from 16 major crops. Traditional statistical methods, such as Multiple Linear Regression (MLR), showed limited accuracy. Advanced models—Decision Tree, Random Forest, XGBoost, and Gradient Boosting—were applied, with XGBoost achieving the highest accuracy ($R^2 = 0.956$, MAE = 426.92). Explainable AI (XAI) techniques like SHAP and LIME identified Area and Production as key factors. The study highlights AI's role in enhancing agricultural decision-making, resource allocation, and crop management in Tamil Nadu.**

Keywords—machine learning, explainable AI (XAI), crop yield prediction, XGBoost, SHAP, precision agriculture

I. Introduction

Agriculture is vital to Tamil Nadu's economy, supporting millions and ensuring food security. However, accurate crop yield prediction remains challenging due to complex environmental and agronomic factors. Traditional methods like Multiple Linear Regression (MLR) often fail to capture these complexities, leading to suboptimal predictions. Recent advancements in Machine Learning (ML) and Explainable AI (XAI) offer data-driven solutions for adaptive agricultural decision-making.

ML models such as Decision Trees, Random Forests, XGBoost, and Deep Learning have improved yield predictions. Shams et al. [7] introduced XAI-CROP, leveraging SHAP-based feature importance analysis for transparency. Similarly, Mahesh and Soundrapandiyan [4] demonstrated the effectiveness of gradient boosting. However, the lack of interpretability in ML models hinders real-world adoption. XAI techniques like SHAP and LIME address this by explaining model decisions, enhancing trust and usability [5][6].

This study develops an ML-driven yield prediction model for Tamil Nadu using historical data from 16 major crops (1965–2023). Benchmarking MLR as a baseline, we applied Decision Tree, Random Forest, XGBoost, and Gradient Boosting, with XGBoost achieving the highest performance ($R^2 = 0.956$, MAE = 426.92). SHAP and LIME analysis revealed "Area" and "Production" as key yield determinants, while environmental factors like Rainfall, Temperature, and Soil pH had minimal impact.

II. Data Collection and Processing

A. Data Collection

The dataset used in this study was collected from the Tamil Nadu Government Agriculture Portal, specifically from the Time Series Data on Area, Production, and Yield of Principal Crops in Tamil Nadu. The data spans 58 years (1965–2023) and includes 16 major crops cultivated across Tamil Nadu.

The data collection process involved extraction from government reports initially available in PDF format containing tabular records of crop area, production, and yield over multiple years. The data was extracted and converted into an Excel spreadsheet for preprocessing and analysis. The dataset was further enhanced by integrating climatic and soil parameters, including Nitrogen (N), Phosphorus (P), Potassium (K) as essential soil nutrients; Rainfall (mm), Temperature (°C), Humidity (%) as environmental factors affecting yield; and Soil pH as a critical factor for crop growth.

Tamil Nadu cultivates a diverse range of crops, and this dataset includes 16 major crops categorized as Food Grains (Paddy, Maize, Cholam, Cumbu, Ragi), Pulses (Red Gram, Bengal Gram, Green Gram, Black Gram, Horse Gram), Oilseeds (Groundnut, Gingelly), Vegetables (Potato, Onion), and Cash Crops (Sugarcane, Cotton). These crops are highly dependent on seasonal conditions, making accurate yield prediction essential for agricultural planning.

B. Data Preprocessing

To ensure data consistency and suitability for machine learning models, comprehensive preprocessing steps were performed. The "Year" column was initially in the format "1965-66." Only the first four digits were retained to convert it into a standard integer format (e.g., 1965). The dataset was thoroughly checked for missing values in critical fields like Area, Production, and Yield, and any inconsistencies in numerical values were corrected to maintain uniformity. Units for Area (ha), Production (tonnes), and Yield (kg/ha) were standardized, and climate and soil feature values were normalized to ensure uniform scales across variables. The preprocessed dataset was then used as input for machine learning models to predict crop yield accurately and enhance decision-making in Tamil Nadu's agricultural sector.

III. Methodology

A. Model Selection and Justification

To effectively predict crop yield, we employed a combination of decision tree-based and statistical machine learning models, carefully selected based on their ability to handle complex, nonlinear relationships within the dataset. The rationale behind choosing each model is detailed below:

Decision Tree Regressor is a tree-based algorithm that splits data at various decision nodes based on feature importance. It is suitable for handling both categorical and continuous data without requiring extensive preprocessing. The formula for prediction is: $y_{pred} = 1/n \sum yi$, where yi are the observations in a given leaf node.

Random Forest is an ensemble learning method that constructs multiple decision trees and averages their predictions to improve stability and reduce overfitting. It is more robust compared to a single Decision Tree model. Prediction is calculated as: $y_{pred} = 1/M \sum Y_m(x)$, where Y_m is the prediction from the mth tree.

XGBoost is a highly efficient and scalable gradient boosting technique that enhances tree-based learning. It is known for its speed and predictive accuracy, making it ideal for handling large datasets. The objective function is: $Obj = L + \Omega$, where L is the loss function and Ω is the regularization term.

Gradient Boosting Regressor iteratively improves weak learners by minimizing residual errors. It updates predictions using, $F_m(x) = F_{m-1}(x) + \gamma h_m(x)$, where $h_m(x)$ is the weak learner and γ is the learning rate.

K-Nearest Neighbors (KNN) Regressor is a non-parametric algorithm that predicts the output by averaging the k-nearest neighbors. It is effective for capturing localized patterns but can be sensitive to noise. Prediction is calculated as: $y_{pred} = 1/k \sum y_i$.

B. Model Training and Evaluation

The dataset was split into 80% training and 20% testing sets to ensure robust validation. Evaluation metrics used include Mean Absolute Error (MAE), which measures the average absolute difference between predicted and actual yield, and R^2 Score (Coefficient of Determination), which measures how well the model explains variability in the dataset.

C. Explainable AI (XAI) Integration

To enhance interpretability, Explainable AI techniques were applied. SHAP (SHapley Additive Explanations) identifies the most influential features in predicting crop yield, while LIME (Local Interpretable Model-Agnostic Explanations) provides local explanations for individual predictions.

The overall methodology follows a systematic approach beginning with data collection from government sources, followed by comprehensive preprocessing to ensure data quality. Feature selection and engineering identify key predictor variables with high impact (Area, Production, Rainfall, Soil Nutrients) and moderate impact (Temperature, Humidity, Soil pH). Model training involves splitting the data into training and testing sets, followed by evaluation using appropriate metrics. For the best-performing model, explainability analysis is conducted using SHAP for global feature importance and LIME for local interpretability of individual predictions.

IV. Results

A. Model Performance Analysis

To evaluate the effectiveness of different machine learning models for crop yield prediction, multiple models were trained and tested using the dataset from Tamil Nadu. The models were evaluated based on two key performance metrics: Mean Absolute Error (MAE) and R^2 Score. Table I presents a comparative analysis of the performance of different models.

Table I: Comparison of Model Performance

Models	MAE	R^2 score
Decision Tree	481.70	0.947
Random Forest	482.18	0.942
XGBoost	426.92	0.956
Gradient Boosting	551.82	0.945
KNN Regressor	508.59	0.916

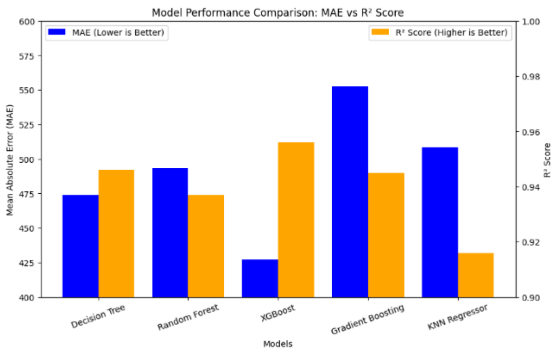

Fig 1: Comparison of Model Performance

Among the models tested, XGBoost demonstrated the highest accuracy with an R^2 score of 0.956 and the lowest MAE of 426.92, making it the most effective model for crop yield prediction. The Decision Tree and Random Forest models also performed well, whereas the KNN model showed lower accuracy due to its sensitivity to local variations in the dataset.

B. Model Residual Analysis

A residual analysis was conducted to ensure XGBoost predictions were unbiased. The residuals (difference between actual and predicted yield) were plotted against the predicted values. The analysis revealed that residuals were randomly distributed, confirming no major bias in the model. Most errors were small, indicating the model generalizes well across different crops and years. There was slight variance observed in extreme values, possibly due to anomalies in historical yield data or specific outlier conditions in certain years.

The histogram of residuals showed that most were centered around 0, forming a roughly normal distribution. This indicates that the model does not have a strong bias (i.e., it doesn't systematically overpredict or underpredict yield values). There were some extreme residuals on both sides, meaning a few predictions were significantly different from the actual values, but these were relatively rare cases that did not substantially impact the overall model performance.

C. Feature Importance Analysis Using XAI

To enhance the interpretability of the crop yield prediction model, we employed Explainable AI (XAI) techniques—SHAP and LIME—to analyze feature importance. These methods help in understanding how different factors contribute to yield predictions.

SHAP assigns a contribution value to each feature for every prediction, helping us understand the global impact of features on model output. The SHAP analysis revealed the most influential factors affecting crop yield: Area was identified as the most dominant feature in determining yield; Production was highly correlated with yield but varies by crop type; and Soil Nutrients (N, P, K) were essential for plant growth, with nitrogen and phosphorus playing a critical role. SHAP's interpretation aligns with domain knowledge, confirming that land usage and climatic factors significantly drive yield variations.

These interpretations improve model transparency and guide agronomic decisions. By highlighting key yield drivers like Area and climatic variables, XAI ensures the model's predictions are not only accurate but also explainable and actionable for large-scale agricultural planning.

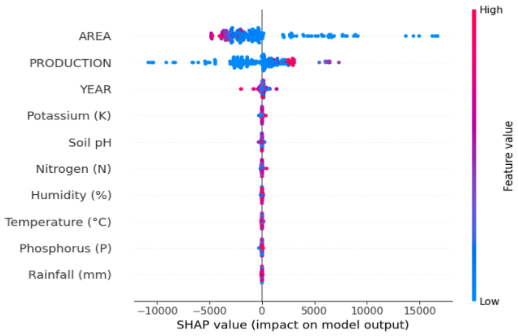

FIG 2: SHAP VARIABLE IMPORTANCE PLOT

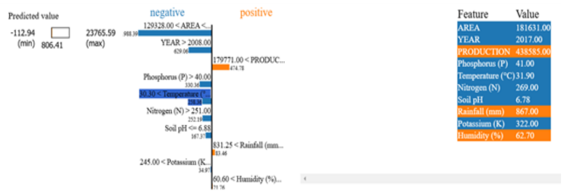

FIG 3: EXPLANATION GENERATED BY LIME MODEL

LIME was used to analyze feature importance at the individual prediction level. Unlike SHAP, which explains feature contributions globally, LIME helps understand how specific inputs influence a single prediction. Key observations from LIME analysis showed that Production had the highest positive contribution to yield prediction, reinforcing its importance in determining overall yield. Area, Temperature, and Phosphorus had a negative impact on specific predictions, indicating that under certain conditions, these factors may reduce yield. Rainfall and Humidity had a mixed contribution, suggesting that their effect on yield depends on the crop type and environmental interactions. Given our dataset and the need for consistent global feature importance, SHAP is the best choice for explaining the crop yield prediction model. LIME can still be used for specific case-based explanations, but it lacks the stability needed for broader agricultural decision-making.

V. CONCLUSION

This research presents a machine learning-based approach for crop yield prediction in Tamil Nadu, utilizing decision tree-based models and Explainable AI (XAI) techniques. The study analyzes 16 major crops over a period of 58 years (1965–2023) using key agricultural and environmental factors such as Area, Production, Rainfall, Temperature, Soil Nutrients (N, P, K), Humidity, and Soil pH.

Among the models tested, XGBoost outperformed other regression models with an R^2 score of 0.956 and a Mean Absolute Error (MAE) of 426.92, making it the most reliable model for yield prediction. The SHAP analysis identified Production and Area as the most influential factors, followed by climatic conditions such as Rainfall and Temperature. Additionally, LIME was used to provide local interpretations of individual predictions.

This work demonstrates the potential of combining machine learning with explainable AI techniques to create transparent and accurate crop yield prediction models. The findings can help agricultural stakeholders in Tamil Nadu make informed decisions about resource allocation, crop selection, and farming practices to optimize yield and ensure food security in the region. Future work could explore the integration of additional data sources, such as satellite imagery and IoT sensor data, to further enhance the accuracy and granularity of yield predictions.

REFERENCES

[1] "Precision Agriculture: The Role of Data-Driven Decision Making," Journal of Agricultural Science, 2023.

[2] "Limitations of Statistical Models in Crop Yield Forecasting," International Journal of Agricultural Modelling, 2022.

[3] Shams, et al. "XAI-CROP: A Transparent AI Framework for Yield Prediction," Springer AI Journal, 2023.

[4] Mahesh & Soundrapandiyan. "Gradient Boosting for Crop Yield Prediction," PLOS ONE, 2024.

[5] "SHAP and LIME in Agriculture: Improving Trust in AI," Computational Intelligence in Agriculture, 2023.

[6] "The Future of Explainable AI in Agriculture," IEEE Transactions on AI, 2024.

[7] Shams, M. Y., Gamel, S. A., & Talaat, F. M. (2024). "Enhancing crop recommendation systems with explainable artificial intelligence: a study on agricultural decision-making." Neural Computing and Applications, 36(11), 5695-5714.

Vision-Based Driver Yawning Detection using Lightweight Attention Mechanism

Srilakshmi Ravali M
Department of Electronics and Communication Engineering, Thiagarajar College of Engineering,
Madurai, TN, India
srilakshmiravali@student.tce.edu

Dr. S. Mohamed Mansoor Roomi
Department of Electronics and Communication Engineering, Thiagarajar College of Engineering,
Madurai, TN, India
smmroomi@tce.edu

Dr. B. Sathya Bam
Department of Electronics and Communication Engineering, Thiagarajar College of Engineering,
Madurai, TN, India
sbece@tce.edu

***Abstract*—Driver drowsiness is a major cause of road accidents, highlighting the need for real-time monitoring systems to enhance road safety. In this study, a vision-based driver yawning detection system is used to leverage a lightweight attention mechanism to improve detection accuracy and computational efficiency. The proposed approach employs deep learning-based transfer learning, utilizing the Inception-ResNet-v2 model to classify driver states as either *Yawning* or *Normal*. A custom dataset comprising 2,600 images was curated and pre-processed using MATLAB, ensuring balanced class distribution for optimal model performance. The Stochastic Gradient Descent with Momentum (SGDM) is used to train the model, achieving a high classification accuracy of 95.2%. To assess its effectiveness, a comparative analysis was performed against other pre-trained models and state-of-the-art methods, demonstrating its superior capability in accurately detecting yawning, a key indicator of driver fatigue. The lightweight nature of the model makes it well-suited for real-time driver monitoring systems, providing a promising solution for mitigating drowsiness-related accidents.**

Keywords—yawning, drowsiness, CNN, YAWDD, attention mechanism, MATLAB.

I. INTRODUCTION

In recent years, vehicle intelligence systems have garnered significant attention because of their potential to lower accident rates, enhance road safety and improve the overall driving experience. Among these advancements, in-cabin driver monitoring has emerged as a crucial technology for detecting distracted driving behaviors, ensuring driver attentiveness, and preventing potential hazards. By leveraging deep learning techniques, researchers have demonstrated exceptional capabilities in analyzing driver behaviors[1,2], including actions such as turning, texting while driving, engaging in aggressive behaviors, or maintaining safe driving practices.

The primary objective of this research is to enhance the accuracy of in-cabin driver behavior classification, specifically focusing on yawning detection as an indicator of drowsiness, while ensuring real-time performance.

II. RELATED WORKS

Several studies have explored driver monitoring systems using deep learning and computer vision techniques, demonstrating various approaches to detecting drowsiness, distraction, and fatigue-related behaviors. While the study[1] provides a broad overview, it lacks implementation details. Sandeep Singh et al. presented VigilEye, an AI-based real-time driver drowsiness detection system combining deep learning and OpenCV[3]. While the system enables real-time drowsiness detection, it focuses solely on fatigue and does not address broader driver behavior patterns.

FIG.1. SAMPLE IMAGES OF THE DATASET (A) YAWNING (B) NORMAL

The Inception-ResNet-v2 model integrates both Inception and Residual Network (ResNet) architectures, which improves performance by capturing both spatial and depth-wise feature representations[4,5,6]. One of the most prominent characteristics of this model is the residual connection, in which the input to a layer is added to its output before sending it to the subsequent layer. This mechanism enables the network to learn residual features—the difference between the input and output of a layer—which enhances both accuracy and training speed by mitigating issues such as vanishing gradients in deep networks.

The Inception-ResNet-v2 architecture is designed to be computationally efficient while maintaining high accuracy in image classification tasks. Although these studies have made significant advancements in driver behavior analysis[14,16], there remains a need for a lightweight, high-accuracy yawning detection system specifically for drowsiness monitoring.

The key contributions of this study are as follows:

- **Dataset Creation and Collection:** A custom dataset was created using publicly available images regarding yawning detection.
- **Transfer Learning with Inception-ResNet-v2:** A pre-trained **Inception-ResNet-v2** model was fine-tuned using **transfer learning** to classify driver states as *Yawning* or *Normal*.
- **Hyperparameter Optimization:** The pre-trained model's hyperparameters were carefully tuned to enhance classification accuracy and improve generalization.
- **Comparative Evaluation:** The proposed method was validated by comparing its performance against variety of **pre-trained models and state-of-the-art techniques** to demonstrate its effectiveness in yawning detection.

The remaining of this paper is structured as follows: Section 2 discusses the literature review while the dataset creation process is given in Section 3. Section 4 details the proposed methodology, including the deep learning model and implementation techniques. Sections 5 and 6 present the experimental results and conclusions, respectively.

III. DATASET COLLECTION AND CREATION

The proposed dataset consists of 2,600 images categorized into two classes: Yawning and Normal. The images were extracted from videos[21] sourced from the Yawning Detection Dataset (YAWDD)[14]. For training and evaluation, the dataset was split according to the Pareto principle (80-20 rule), with 2,080 images allocated for training and 520 images for testing. The dataset includes drivers of various age groups, individuals wearing glasses, men with beards and mustaches, and women with diverse hairstyles and clothing styles, ensuring a varied dataset for robust model training.

Data Preprocessing

Additional yawning-related videos were recorded and incorporated into the dataset. The videos were cropped to focus on the yawing action, and the trimmed clips were converted into frames using MATLAB R2022a. A summary of the video sources, frames, and dataset composition is presented in Table I. The final dataset used as input consists of 2,600 images, categorized into the Yawning and Normal classes, as depicted in Figure 1.

TABLE I DATASET SUMMARY

Types of Classes	No. of Videos	No. of videos after editing	No. of images
Yawning	95	110	1300
Normal	60	95	1300

IV. PROPOSED METHODOLOGY

This section presents the proposed methodology for driver drowsiness detection based on yawning classification. The methodology involves three key steps: preprocessing, transfer learning, and model evaluation. In the preprocessing stage, videos are cropped to focus on yawning actions, converted into frames, and manually filtered to ensure relevance to the respective class. After training, the model is evaluated to assess its classification performance in detecting driver fatigue. Since yawning is an early indicator of drowsiness, an automated real-time monitoring system is essential for improving road safety.

The proposed vision-based system addresses this issue by providing an efficient and accurate yawning detection mechanism, contributing to the development of intelligent driver-assistance systems aimed at reducing drowsiness-induced accidents. The overall workflow of the proposed method is depicted in Figure 2, while Figure 3 illustrates the transfer learning-based classification process using Inception-ResNet-v2. To achieve high accuracy and efficiency, this study employs transfer learning, a deep learning approach that utilizes a pre-trained base model to leverage previously learned feature representations. This technique significantly improves accuracy while reducing computational complexity and training time. In this work, Inception-ResNet-v2, is used for yawning-based drowsiness classification.

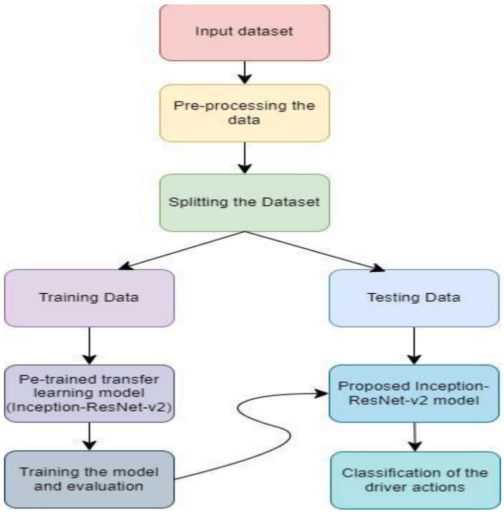

FIG.2. FLOW OF THE PROPOSED METHOD

In this study, the pre-trained feature weights of Inception-ResNet-v2—originally trained on ImageNet—are fine-tuned and applied to the drowsiness detection task.

To evaluate the performance of different deep learning models for yawning-based drowsiness detection, the dataset was trained on multiple existing convolutional neural network (CNN) architectures using a consistent set of hyperparameters. By combining the strengths of Inception modules and ResNet-style skip connections, Inception-ResNet-v2 achieves superior feature extraction capabilities, making it well-suited for drowsiness classification tasks. The Inception-ResNet-v2 model demonstrated the highest accuracy among the tested networks and was therefore selected as the proposed model.

TABLE II HYPER PARAMETERS OF INCEPTION-RESNET-V2

Parameter	Value
Solver	Sgdm
Mini Batch Size	8
Device Type	GPU
LearningRate	0.01
l2Regularization	0.01
Gradient clipping	Gradient Threshold
Epochs	5
Verbose Frequency	50

The comparison of training and testing accuracies across different models is summarized in Table V. The training process was conducted with the hyperparameters tabulated in table II.

To adapt Inception-ResNet-v2 for yawning-based drowsiness detection, the last three layers of the pre-trained model were replaced and fine-tuned to classify the driver's state into two categories: "Yawning" and "Normal".

This transfer learning approach allows the model to leverage pre-learned feature representations while specializing in the specific task of driver drowsiness (face) detection[18,19]. The customized architecture ensures improved classification performance, making it suitable for real-time driver monitoring applications.

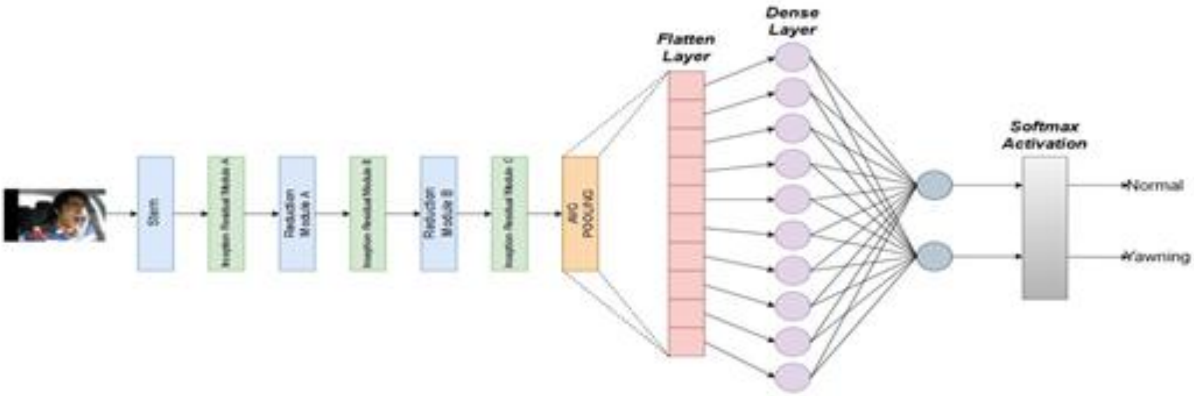

FIG. 3. PROPOSED PRE-TRAINED MODEL FOR DROWSINESS CLASSIFICATION

V. RESULTS AND DISCUSSION

The proposed yawning-based driver drowsiness detection method is presented in this section. The proposed algorithm was implemented and trained using MATLAB 2022a on an HP server system equipped with 8GB RAM. During the preprocessing stage, video footage was converted into image frames, which were then used as input for the Inception-ResNet-v2 pre-trained model. The model was trained to classify images into two categories: Drowsy (Yawning) and Normal.

The results show the effectiveness of the proposed approach in detecting yawning, making it a promising solution for real-time driver monitoring systems. The default training parameters of the proposed Inception-ResNet-v2 model are summarized in Table II. The model was trained and tested on multiple pre-existing deep learning architectures, and the obtained training and testing accuracies are depicted in Figure 4.

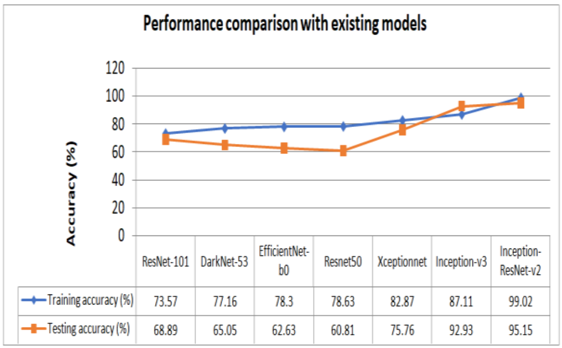

FIG.4. PERFORMANCE COMPARISON WITH EXISTING MODELS

To enhance the model's classification performance, key hyperparameters such as the solver, learning rate, and number of epochs were fine-tuned. The optimized training parameters for the proposed model are detailed in Table III, which lists the modified values used to achieve superior performance.

TABLE III COMPARISON OF ACCURACY BASED ON PARAMETERS

Optimizer	**sgdm - 0.01**		**adam - 0.001**		**rmsprop - 0.001**	
Epoch	**Training accuracy (%)**	**Testing accuracy (%)**	**Training accuracy (%)**	**Testing accuracy (%)**	**Training accuracy (%)**	**Testing accuracy (%)**
5	**99.02**	**95.15**	72.27	53.33	79.77	81.01
10	98.37	88.69	85.97	75.96	59.38	38.79

A comparative analysis of other pre-trained models—trained using the same number of epochs, learning rate, and optimizer as the proposed model—is presented in Table V. The proposed Inception-ResNet-v2 model achieves the highest testing accuracy of 95.2%, demonstrating its superior classification capability. The performance of the proposed model was evaluated using different optimizers, including Adam, RMSprop, and SGDM, to determine the most effective configuration for yawning-based drowsiness detection. The model's training accuracy ranged between 72% and 86% when trained with Adam and RMSprop optimizers. However, the highest training accuracy of 96.93% was achieved when using SGDM with a learning rate of 0.01 and 5 epochs. When using the Adam optimizer, training accuracy ranged between 72% and 86%, while testing accuracy varied from 53.33% to 75.96%. In contrast, with SGDM optimizer and a learning rate of 0.01 to 0.0001, along with epochs ranging from 10 to 30, the model achieved a training accuracy of 99.02% and a testing accuracy of 95.15%. These results indicate that SGDM optimizer with a learning rate of 0.01 and 5 epochs provides the best performance for the proposed model, delivering high accuracy with optimized computational efficiency, making it suitable for real-time driver drowsiness detection. The optimized model achieved a training accuracy of 99.02%, significantly outperforming other pre-trained models, as detailed in Table V. To further assess the classification performance, a confusion matrix was generated, as shown in Figure 5. The model classifies driver states into two categories: "Normal" (non-drowsy) and "Drowsy" (Yawning). The confusion matrix analysis reveals that 228 normal driving images were correctly classified as "Normal," while 243 samples were identified as "Drowsy."

FIG.5. CONFUSION MATRIX

TABLE IV PROPOSED MODEL CLASSIFICATION PERFORMANCE

Class	Precision (%)	Recall (%)	F1 Score (%)	Accuracy (%)
Normal	97.0	93.1	95.0	95.2
Yawning	93.5	97.2	95.3	

The proposed Inception-ResNet-v2 model achieves the highest testing accuracy of 95.02%, demonstrating its superior classification capability. These results validate that the proposed model effectively detects yawning-based drowsiness. Metrics: Precision, Recall, and F1-score. These metrics provide a comprehensive analysis of the model's classification effectiveness and are summarized in Table V.

TABLE V COMPARISON OF THE PROPOSED MODEL WITH EXISTING MODELS

Encoder	Training accuracy (%)	Testing accuracy (%)
MobileNet-v2	71.13	70.91
ResNet-101	73.57	68.89
DarkNet-53	77.16	65.05
EfficientNet-b0	78.3	62.63
Resnet50	78.63	60.81
Xceptionnet	82.87	75.76
Inception-v3	87.11	92.93
Inception-ResNet-v2	**99.02**	**95.15**

The effectiveness of the proposed driver drowsiness detection system is demonstrated through sample test images, as shown in Figure 6. These images illustrate the system's ability to correctly classify driver states as "Yawning" (Drowsy) or "Normal" in real-time.

FIG.6. TESTING IMAGES

To further validate its performance, the proposed method was compared against existing classification approaches, with the results summarized in Table 6. While previous methods achieved a maximum classification accuracy of 95.2%, the proposed approach demonstrated superior recognition accuracy. The results confirm that the proposed system provides a highly accurate and reliable solution for yawning-based drowsiness detection.

TABLE VI COMPARISON OF THE STATE OF THE ART METHODS

S. No.	Reference	Method	Classifier	Accuracy (%)
1	[13]	Facial features	RNN	92.19
2	[14]	PERCLOS	Adaboost	93.4
3	[15]	Mouth opening	CNN	94
4	[17]	Head rotation, nodding	LSTM	92.8
5	[16]	EEG	TCRFN	90
6	Proposed Method	Facial features	Inception-ResNet-v2	**99.02**

VI. CONCLUSION

This research presents an advanced yawn detection system utilizing a transfer learning approach for driver monitoring. The proposed method involves dataset creation and training using the pre-trained Inception-ResNet-v2 model to classify driver conditions into two categories: Yawning (Drowsy) and Normal. The experimental results validate the effectiveness of the approach, achieving a high classification accuracy of 99.02%. Furthermore, the performance of the proposed system was evaluated against other pre-trained models and existing classification methods, demonstrating superior accuracy and efficiency. The results confirm that the proposed method outperforms conventional approaches, making it a robust and reliable solution for real-time yawning detection. By integrating this system into driver-assistance technologies, it has the potential to reduce accidents caused by drowsy driving and enhance road safety.

REFERENCES

[1] **F. Qu, N. Dang, B. Furht, et al.,** "Comprehensive study of driver behavior monitoring systems using computer vision and machine learning techniques," *J. Big Data*, vol. 11, no. 32, 2024. [Online]. Available: https://doi.org/10.1186/s40537-024-00890-0.

[2] **S. Joseph, S. I. Adithyan, J. R. Jishnuraj, A. S. Aswin, and V. C. H. Varun,** "DRIVER's EYE: A behavioural monitoring system using deep learning," in *International Journal of Engineering Research & Technology (IJERT)*, vol. 9, no. 13, NCREIS, 2021.

[3] **S. S. Sengar, A. Kumar, and O. Singh,** "VigilEye—Artificial Intelligence-based real-time driver drowsiness detection," *arXiv preprint*, 2024.

[4] https://in.mathworks.com/help/deeplearning/ref/inceptionresnetv2.html https://serp.ai/inception-resnet-v2/

[5] **C. Szegedy, S. Ioffe, and V. Vanhoucke,** "Inception-v4, Inception-ResNet and the impact of residual connections on learning," *CoRR*, vol. abs/1602.07261, 2016.

[6] **YawDD:** A yawning detection dataset **B. K. Savaş and Y. Becerikli,** "Real-time driver fatigue detection system based on multi-task ConNN," *IEEE Access*, vol. 8, pp. 12491-12498, 2020. doi: 10.1109/ACCESS.2020.2963960.

[7] **Y. Ed-Doughmi, N. Idrissi, and Y. Hbali,** "Real-time system for driver fatigue detection based on a recurrent

neuronal network," *Journal of Imaging*, vol. 6, no. 3, p. 8, 2020. doi: 10.3390/jimaging6030008.

[8] **Z. Liu, Y. Peng, and W. Hu,** "Driver fatigue detection based on deeply-learned facial expression representation," *Journal of Visual Communication and Image Representation*, vol. 71, p. 102723, 2020. Doi: 10.1016/j.jvcir.2019.102723.

[9] **G. Du, S. Long, C. Li, Z. Wang, and P. X. Liu,** "A product fuzzy convolutional network for detecting driving fatigue," *IEEE Transactions on Cybernetics*, vol. 53, no. 7, pp. 4175–4188, 2023. doi: 10.1109/ TCYB.2021.3123842.

[10] **C. Yang, X. Wang, and S. Mao,** "Unsupervised drowsy driving detection with RFID," *IEEE Transactions on Vehicular Technology*, vol. 69, no. 8, pp. 8151-8163, 2020. doi: 10.1109/TVT.2020.2995835.

[11] **N. K. Sancheti and M. Srikant,** "Camera-based driver monitoring system using deep learning," in *Proceedings of the International Conference on Computer Vision and Image Processing (CVIP)*, 2019.

[12] **A. Binoy, J. P. Thayiparampil, S. B., A. A. Joseph, A. R. Kurup, and S. Sainudeen,** "Machine learning-based driver monitoring system," *International Research Journal of Engineering and Technology (IRJET)*, vol. 10, no. 12, Dec. 2023.

[13] **A. Jarndal, H. Tawfik, A. I. Siam, I. Alsyouf, and A. Cheaitou,** "A real-time vision transformers-based system for enhanced driver drowsiness detection and vehicle safety," *IEEE Access*, vol. 13, pp. 1790–1803, 2025. doi: 10.1109/ACCESS.2024.3522111.

[14] **L. Yang, H. Yang, H. Wei, Z. Hu, and C. Lv,** "Video-based driver drowsiness detection with optimised utilization of key facial features," *IEEE Transactions on Intelligent Transportation Systems*, vol. 25, no. 7, pp. 6938–6950, 2024. doi: 10.1109/TITS.2023.3346054.

[15] **K. Xu, F. Li, D. Chen, L. Zhu, and Q. Wang,** "Fusion of lightweight networks and DeepSort for fatigue driving detection tracking algorithm," *IEEE Access*, vol. 12, pp. 56991–57003, 2024. doi: 10.1109/ACCESS.2024. 3386858.

Dynamic Outsourced Auditing Services for Cloud Storage Based on Batch-Leaves-Authenticated Merkle Hash Tree

Ajitha D
QIP Research Scholar
Electronics and Communication Engineering
Thiagarajar College of Engineering,
Madurai
ajithamirtsrm@gmail.com

Vasantharani R
Electronics and Communication Engineering,
Thiagarajar College of Engineering,
Madurai
vasantharani@sethu.ac.in

Shanmugavalli T
Computer Science and Engineering Sethu Institute of Technology,
Virudhunagar
shanmugavalli2023@sethu.ac.in

Dr. K. Rajeswari
Electronics and Communication Engineering,
Thiagarajar College of Engining,
Madurai
rajeswari@tce.edu

***Abstract*—The production of huge amount of data and the emergence of cloud computing have introduced new requirements for data management. Many applications interact with various heterogeneous data stores based on the type of data they manage traditional data, documents, social network graphs, key-value pairs, etc. Cloud computing encourages users to outsource data to the cloud, resulting in a loss of physical control and making remote data integrity verification a critical challenge for users. To relieve users of the burden of frequent integrity verifications, a Third-Party Auditor (TPA) is introduced to perform verifications for data integrity assurance. However, existing public auditing schemes assume the TPA is trusted, preventing their extension to the outsourced auditing model, where the TPA may be dishonest and any two of the three involved entities might collude. This proposed system offers a dynamic outsourced auditing scheme that protects against dishonest entities and collusion while supporting verifiable dynamic updates to outsourced data. It introduces a new approach using batch-leaves-authenticated Merkle Hash Tree (MHT) to batch-verify multiple leaf nodes and their indexes simultaneously, making it more suitable for dynamic outsourced auditing than traditional MHT-based methods that verify leaf nodes individually. Experimental results demonstrate that our solution minimizes initialization costs for both users and the TPA and incurs lower dynamism costs for users.**

Keywords—Platform-as-a-Service (PaaS), Infrastructure as a Service (IaaS), Software as a Service (SaaS), Third-Party Auditor (TPA), Merkle Hash Tree (MHT), Secret Key, Public Key, Cloud Computing, Cloud Service Provider (CSP), Third Party Auditor (TPA).

I. INTRODUCTION

Cloud computing has recently emerged as a new computing paradigm enabling on-demand and scalable provision of resources, platforms and software as services. Cloud computing is often presented at three levels: the Infrastructure as a Service (IaaS) giving access to abstracted view on the hardware, the Platform-as-a-Service (PaaS) providing programming and execution environments to the developers, and the Software as a Service (SaaS) enabling software applications to be used by cloud's end users. Due to its elasticity property, cloud computing provides interesting execution environments for several emerging applications such as big data management [1,2]. According to the National Institute of Standards and Technology1 (NIST), big data is data which exceed the capacity or capability of current or conventional methods and systems. It is mainly based on the 3-Vs model where the three Vs refer to volume, velocity and variety properties. Volume means the processing of large amounts of information. Velocity signifies the increasing rate at which data flows [3] Finally, variety refers to the diversity of data sources. Several people have also proposed to add more V to this definition. Veracity is widely proposed and represents the quality of data (accuracy, freshness, consistency etc.). Against this background, the challenges of big data management result from the expansion of the 3Vs properties. In our work, I focus mainly on the variety property and more precisely on multiple data store based applications in the cloud [4,5,6].

In order to satisfy different storage requirements, cloud applications usually need to access and interact with different relational and No SQL data stores having heterogeneous APIs. The heterogeneity of the data stores induces several problems when developing, deploying and migrating multiple data store applications. Below, I list the main four problems which I are tackling in this project[7,8], Consistency is also an important issue in multi data stores applications. In fact, cloud data stores in general implement different consistency models (strong consistency model for RDBMS and Iak consistency models for No SQL DBMS) [10]. This paper presents an integrated approach to simplifying the development, deployment, and migration of applications utilizing multiple data stores in cloud environments. A unified data model is introduced to address data heterogeneity and the lack of schemas in NoSQL databases. Based on this model, OPEN-PaaS-DataBase API (ODBAPI) provides a REST-based, standardized interface for executing queries across relational and NoSQL data stores. ODBAPI helps decouple applications from specific data stores, easing migration and reducing API management complexity. Additionally, Virtual Data Stores (VDS) are proposed to optimize complex query execution. This approach enhances developer productivity and ensures efficient query performance in multi-data store environments. Challenges in development multi data using Table I.

TABLE 1 CHALLENGES IN MULTI-DATA STORE APPLICATION DEVELOPMENT

S.NO	Challenges and Application	
	Challenge	***Description***
[12]	Heavy Workload on Application Developers	Developers must work with multiple heterogeneous APIs when building applications using different data stores.
[13]	No Declarative Way for Executing Complex Queries	Due to data model heterogeneity and the lack of a global schema, executing complex queries across multiple data stores requires manual implementation.
[14]	Code Adaptation for Cloud Migration	When migrating applications to a new cloud environment, developers must modify the source code to interact with new data stores and learn new APIs.
[15]	Tedious and Non-Standard Discovery & Deployment Processes	Finding a suitable cloud provider and deploying applications is a complex, provider-specific, and time-consuming task.

Use Cases and Rationale

The Open PaaS project to aims at developing a PaaS technology dedicated to enterprise collaborative applications deployed on hybrid clouds (private / public). Open PaaS is a platform that allows to design and deploy applications based on proven technologies provided by partners such as collaborative messaging system, integration and workflow technologies that will be extended in order to address Cloud Computing requirements. One of the objectives of this project is to provide support for developing and deploying multiple data store-based applications in a cloud environment.

The Open PaaS project focuses in particular on relational, key/value and document data stores. In the following, it describes an example of polyglot persistence showing the problems induced by developing, migrating and deploying multiple data store-based applications. I use this example in to illustrate how I evaluate and optimize the execution of complex queries involving heterogeneous data stores. Polyglot persistence refers to situations where an application interacts with multiple data stores. For instance, I can give the example where an application A needs to interact with a document data store, a relational data store and a key/value data store at the same time. Indeed, imagine that I have a document data store called dblpDB, a relational data store called personDB, and a key/value data store called RankDB. The dblpDB data store contains a collection of JSON documents called dblp. A document in this collection contains four elements. In this kind of documents, I can find one or multiple values of the element author. Whereas the person DB data store contains one table called person. This table has four columns.

- The title element to denote publication titles.
- The year element to define the publications year.
- The author element to represent the author's name.
- The conference element to denote the conference acronym in which the project has been published.
- Person-Id to denote the identifier of a person,
- Person-Name to define the name of a person,
- Person- Country to represent the country of a person and
- The person-Affiliation to denote the affiliation of persons.

Finally, the data store Rank DB that contains a set of key values called Conference Ranking. In this latter, Its found the elements conference and Rank to denote respectively the acronym of a conference and its rank. Suppose now that application A needs at some point to retrieve the affiliation and the name of authors having at least a project published in a conference ranked" A". AnsIring such query is, nowadays, challenging. Indeed, since dblpDB, Conference Ranking, and person DB use different data models, it is not possible to execute such query in a declarative way anymore. The developers have to identify the sub-queries by hand, interact with each data store separately and implement the join operation by themselves. The developers need, obviously, to be familiar with APIs of the three data stores. Fig 1, now that developers want to migrate their application A in order to use a CouchDB data store instead of Mongo DB and that the current cloud environment does not support CouchDB data stores. In order to migrate their application, developers need

- To re-adapt the code so that application A can interact with CouchDB API,
- To discover another environment that can support new storage requirements, and
- To deploy their application on the new environment.

The processes of discovering environment offers and deploying applications on them are tedious and provider-specific and developers have to deal with them each time they want to deploy their applications Fig 1.

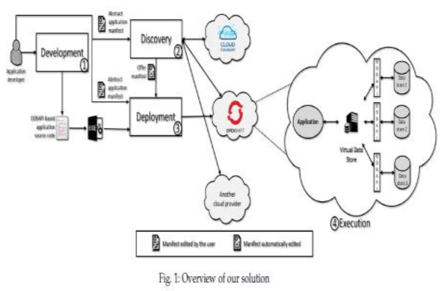

FIG 1 OVERVIEW OF THE SOLUTION

Proposed Methodology

Here analysed and classified existing works on cloud data management, focusing on multiple data stores requirements, which help to stored different type of data on multiple places without any conflicts. Cloud Service Provider (CSP), she has lost actual control over her outsourced data. To confirm the intactness of outsourced data without retrieving the data, various solutions are proposed to offer provable security guarantee for cloud storage. To free user from the expensive auditing burden, public auditing/verification schemes are proposed enabling user to delegate the heavy auditing work to Third Party Auditor (TPA). Clearly, a scheme supporting TPA's auditing might be more easily large-scale adopted by cloud user, since user can be freed from the endless auditing. In the proposed system defined the data requirements of applications in cloud environment and described about different scenarios related to the way applications use data stores. In propose our end-to-end solution to support multiple data stores applications in cloud environments. Proposed another dynamic PDP scheme based on the authenticated Skip List, but this scheme does not consider the support of public auditing. To the best of our knowledge, there are no another global solution addressing all the problems focus on. Cloud providers discovery module discovers the capabilities of data stores of each cloud provider and returns these capabilities in the offer manifest. Here we generate the optimized result with a simple query. Data Fetching time is too short, because we use matching algorithm for matching process.

Cloud Module

The Cloud Module is responsible for managing cloud-based operations, including application deployment, data storage, and query execution. It facilitates seamless interaction between applications and multiple cloud providers, ensuring efficient resource allocation and performance optimization refer Fig 2.

- Client Module
- Cloud Storage Server
- Cloud Audit Server
- Security Modeling

Client Module:

An entity that has large data files to be stored in the cloud and relies on the cloud for data maintenance and computation, can be either individual consumers or organizations.

Cloud Storage Server (CSS) Module:

An entity, which is managed by Cloud Service Provider (CSP), has significant storage space and computation resource to maintain client’s data. The CSS is required to provide integrity proof to the clients or cloud audit server during the integrity checking phase.

Cloud Audit Server (CAS) Module:

The basic goal of PoR model is to achieve proof of retrievability. Informally, this property ensures that if an adversary can generate valid integrity proofs of any file F for a non-negligible fraction of challenges, we can construct a PPT machine to extract F with overwhelming probability.

It is formally defined by the following game between a challenger C and an adversary A, where C plays the role of the audit server (the client) and a plays the role of the storage server.

Security Modeling

A new extensive DACMACS scheme, denoted as the NEDAC-MACS, to withstand above two attacks and support more secure attribute revocation. We modify some DACMACS’s algorithms, and perform the vital cipher text update communication between cloud server and AAs with some more secure algorithms. Our NEDAC-MACS scheme mainly includes two improvements on the DAC-MACS at Secret Key Generation phase and Attribute Revocation phase, and it can run correctly according to the correctness proof of NEDAC-MACS.

Admin Login

The Admin Login module provides secure authentication for administrators to access the system.

Admins can manage users, monitor cloud resources, configure settings, and oversee application deployments to ensure smooth operations.

User Registration

This module allows new users to register by providing essential details such as name, email, and credentials. It ensures secure account creation, granting access to the platform’s features and cloud-based services.

User Login

The User Login module enables registered users to securely log into the system. Once authenticated, users can access cloud services, deploy applications, manage data, and execute queries within the cloud environment.

(a)

(b)

(c)

(d)

(e)

(f)

(g)

FIG 2 (A). ADMIN LOGIN (B). MULTI DATA STORE (C). USER REGISTRATION (D). USER LOGIN (E) USER HOME (F) SEARCH (G) RESULT

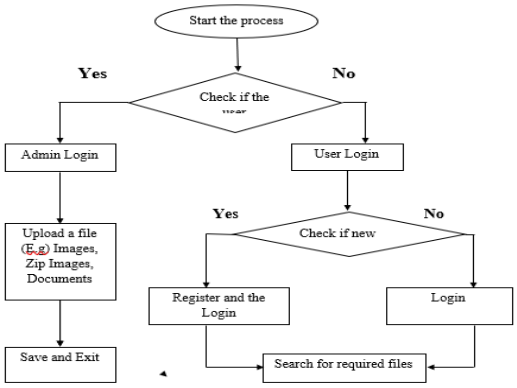

FIG 3 DATA FLOW CHART

Data Flow

A flowchart is a visual representation of a process, workflow, or system using symbols, arrows, and text. It helps in understanding, analyzing, and designing complex processes by breaking them into simpler steps.

In the given flowcharts, the login, registration, data management, and file handling processes are depicted for both administrators and users. These diagrams help in understanding user interactions within a cloud-based system, showing paths for authentication, data entry, file uploads, and downloads.

Start the Process

The system checks whether the user is an Admin or a Regular User.

Admin Login Path

If the user is an Admin, they log in and proceed to upload files (e.g., images, zip files, or documents).After uploading, the files are saved, and the process exits.

User Login Path

If the user is a Regular User, they proceed to the User Login step. Fig 3.

If the user is new, they must Register before logging in.After login, the user searches for required files and downloads them.

II. Result and Discussion

Conclusion

The application of ODBAPI and the Virtual Data Store (VDS) query optimization and execution approach is being extended to various qualitatively and quantitatively different scenarios within the OpenPaaS project. This process helps in identifying potential discrepancies and enhancing reliability for public use. Additionally, an implementation for Hive is being explored to facilitate access to diverse data stores. Another key focus is the development of an alternative matching algorithm that supports approximate matching, enabling greater flexibility in data store discovery and application deployment.

Future Enhancement

Currently, I am working on applying ODBAPI and the virtual data store query optimization and execution approach to other qualitatively and quantitatively various scenarios in the Ope PaaS project. This allows us to identify possible discrepancies and make our work more reliable for public use. In addition, Our second perspective consists in providing another matching algorithm supporting approximate matching. Hence, I enable more flexibility in data stores discovery and applications deployment. Our third perspective is an extension to virtual data stores, allowing to support a larger class of complex queries across No SQL and relational data stores (union, intersection, aggregates, group by like operations) and introducing more elaborate query processing optimization.

References

[1] C. Baun, M. Kunze, J. Nimis, and S. Tai, Cloud Computing - Ib-Based Dynamic IT Services. Springer, 2011.*)*

[2] A. McAfee and E. Brynjolfsson, “Big data: The management revo-lution. (cover story).” Harvard Business Review, vol. 90, no. 10, pp. 60–68, 2012.

[3] T. Kraska, M. Hentschel, G. Alonso, and D. Kossmann, “Consis-tency rationing in the cloud: Pay only when it matters,” PVLDB, vol. 2, no. 1, pp. 253–264, 2009.

[4] R. Sellami, S. Bhiri, and B. Defude, “ODBAPI: a unified REST API for relational and No SQL data stores,” in The IEEE 3rd International Congress on Big Data (BigData’14), Anchorage, Alaska, USA, June 27 - July 2, 2014, 2014.

[5] S. Abiteboul and N. Bidoit, “Non first normal form relations: An algebra allowing data restructuring,” J. Comput. Syst. Sci., vol. 33, no. 3, pp. 361–393, 1986.

[6] D. Kossmann, “The state of the art in distributed query processing,” ACM Comput. Surv., vol. 32, no. 4, pp. 422–469, Dec. 2000.

[7] M. Sellami, S. Yangui, M. Mohamed, and S. Tata, “Paas-independent provisioning and management of applications in the cloud,” in 2013 IEEE Sixth International Conference on Cloud Computing, Santa Clara, CA, USA, June 28 - July 3, 2013, 2013, pp. 693–700.

[8] D. Cash, A. Küpçü and D. Wichs, "Dynamic proofs of retrievability via oblivious ram", Proc. 32nd Int. Conf. Theory Appl. Cryptographic Techniques: Advances Cryptology, pp. 279-295, 2013.

[9] C. Wang, S. S. M. Chow, Q. Wang, K. Ren and W. Lou, "Privacy-preserving public auditing for secure cloud storage", IEEE Trans. Comput., vol. 62, no. 2, pp. 362-375, Feb. 2013.

[10] Y. Zhu, G. J. Ahn, H. Hu, S. S. Yau, H. G. An and C. J. Hu, "Dynamic audit services for outsourced storages in clouds", IEEE Trans. Services Comput., vol. 6, no. 2, pp. 227-238, Apr.-Jun. 2013.

[11] C. Wang, Q. Wang, K. Ren and W. Lou, "Privacy-preserving public auditing for data storage security in cloud computing", Proc. IEEE INFOCOM, pp. 1-9, 2010.

[12] F. Armknecht, J. M. Bohli, G. O. Karame, Z. Liu and C. A. Reuter, "Outsourced proofs of retrievability", Proc. 21st ACM Conf. Comput. Comm. Secur., pp. 831-843, 2014.

[13] C. Liu, R. Ranjan, C. Yang, X. Zhang, L. Wang and J. Chen, "MuR-DPA: Top-down levelled multi-deplica merkle hash tree based secure public auditing for dynamic big data storage on cloud", IEEE Trans. Comput., vol. 64, no. 9, pp. 2609-2622, Sep. 2015.

[14] C. Liu et al., "Authorized public auditing of dynamic big data storage on cloud with efficient verifiable fine-grained updates", IEEE Trans. Parallel Distrib. Syst., vol. 25, no. 9, pp. 2234-2244, Sept. 2014.

[15] R. C. Merkle, "A certified digital signature", Proc. Advances Cryptology, pp. 218-238, 1990.

Leveraging Deep Learning for Early-Stage Detection and Typing of Ovarian Cancer

Ms. Pavithra S M.E
Research Scholar,
Department of Electrical and Electronics Engineering,
Thiagarajar College of Engineering,
Madurai, Tamil Nadu, India.
ORC-ID: 0009-0004-1630-3943

Dr. L. AshokKumar M.E., Ph.D
Principal,
Thiagarajar College of Engineering,
Madurai, Tamil Nadu, India
ORC-ID: 0000-0001-5962-2961

***Abstract*—In this study, a deep convolutional neural network (DCNN) analyzes histopathological pictures to identify and categorize the four subtypes of ovarian cancer. Ovarian cancer is the fifth most common and most aggressive kind of gynecologic cancer, but it also has the lowest 5-year survival rate. There are four main types of ovarian epithelial carcinoma: serous, mucinous, endometroid, and clear cell. Medical photos are increasingly being analyzed by computers to look for signs of diseases including Alzheimer's, brain tumors, cancer, and seizures. In this study, we introduce and put into practice an improved DCNN-based architecture for identifying malignant and healthy cells. It might be categorized as a subtype if it is malignant. Using the 500 publicly accessible pictures from The Cancer Genome Atlas (TCGA-OV), the scientists produced an additional 24,742 histopathology images. The accuracy of the KK-Net classification model increased from 75% to 91% when additional photos were used during training. Operating Characteristics of the Receiver: The area under the curve analysis was used to evaluate this model's performance. The average accuracy of the AUC-ROC curve was found to be 95%. We also use four other networks (GoogleNet, VGG-19, VGG-16, and AlexNet) to compare the performance of the suggested model to the state-of-the-art. Pathologists may be able to identify ovarian cancer early on thanks to the newly created unique design, which might act as a standard for predicting and diagnosing the disease.**

Keywords—Artificial Intelligence; Machine learning; Predictive methods; Supervised learning; Image processing.

I. Introduction

Ovarian cancer (OC) is the sixth most prevalent cause of cancer-related deaths in women. Women may overlook symptoms of OC, including as weight increase, bloating, pelvic discomfort, and belly enlargement [1]. However, by then, the illness usually has spread to other parts of the body, making it difficult to heal. Over a woman's lifespan, the ovary undergoes major anatomical and functional changes that affect the reproductive system. The condition is more common in women going through menopause and in those who have OC in their family. It may be challenging to identify an OC when they are young [1]. OC is the leading cause of gynecological cancer-related deaths [2]. To improve the chances of an early OC diagnosis, the study has employed a range of imaging modalities and serum markers [3-5]. Although ovarian cancer biomarkers have shown great potential, they also have several drawbacks, including missed detections, time commitment, and the need for highly qualified doctors. Serum carbohydrate antigen 125 (CA125), a widely used biomarker, can be used to diagnose ovarian cancers. While some people with OC in the early stages might not have elevated CA-125 levels in their blood, about 80% of women in the later stages of the disease have [6].

II. Related Work

With applications ranging from Alzheimer's disease diagnosis to cancer detection to epilepsy prediction and beyond, CNN and RNN deep learning algorithms are essential in medical picture analysis [21]. Among the tools used in deep learning are Keras, Caffle, Tensorflow, Theano, and Torch [22]. Computer vision experts must rapidly bridge this knowledge gap to generate results that are suitable in terms of sensitivity and accuracy when working with biological pictures, despite their lack of clinical expertise and insufficient deep learning capabilities [23]. This information gap presents significant challenges for researchers in deep learning and medical image processing. [24] Machine learning, which does away with the need for time-consuming human feature computation, training, and classification, depends on data representation [25]. Pixel values from images are utilized in place of generated features to make deep learning more superficial and efficient [26].

The effectiveness of the DCNN technique for tissue categorization, segmentation, and visualization in histopathology pictures has been demonstrated by Xu et al. Haque and Neubert [27] used a DCNN technique to categorize lung cancer micrographs into several subgroups. Masood and colleagues created a computational decision support system for detecting lung cancer using a deep learning technique. DCNN is being used in an increasing number of medical imaging applications [28]. Among the numerous uses for DCNN features are image recognition, identification, and retrieval [29–30]. A non-linear network is used to read and extract data from a multilayer neural network in order to build a deep learning architecture [31]. [32]. By merging low- and high-level features, these "deep learning" methods take incoming data and create a more complete picture. As a result, time-consuming operations like feature extraction in machine learning algorithms use less processing power. Therefore, diagnostic systems may profit from the use of deep learning techniques. Moreover, deep learning methods are more reliable than feature extraction methods. In this study, we automatically categorize histological images of ovarian cancer into its several subtypes using deep convolutional neural networks.

III. Methodology

A. Image Dataset

This study trained and generated predictions using 500 labeled histopathological images from the TCGA-OV collection at the National Cancer Institute's Genomic Data Commons data site. 100 mucinous, 60 endometroid, 80 clear-cell, 85 benign, and 175 serous samples are shown in these pictures. The GDC Data Portal makes it easy for academics and bioinformaticians to access and download data linked to cancer. The histopathological information for the authors' dataset on ovarian cancer and its subtypes is also available on the Mendeley Data website.[33].

B. Data Augmentation

One of the most important phases of deep learning is adding new data. Data augmentation is necessary since DCNN needs a lot of data and it's not always feasible to take a lot of pictures. Ultimately, this leads to the introduction of uncertainty and the growth of the database. Insufficient training data might lead to overfitting [33, 34].

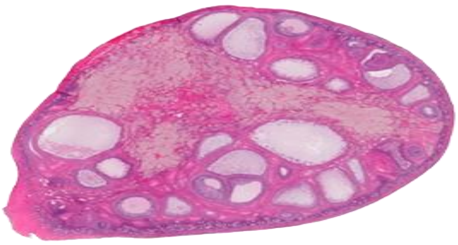

Fig. 1 Augmented histopathological Images

IV. Proposed DCNN Architecture (KK-NET)

According to our study, there are several pre-trained DCNN architectures that may be used for picture categorization. Among them are DenseNet [34], ResNet [35], Mobile Net [35], GoogleNet [36], VGG-Net [36], and AlexNet [36]. These pre-trained models and Choi et al [37] work were used to build our deep convolutional neural network (DCNN) architecture, which consists of six convolutional layers, four max-pooling layers, and ELU as the activation function. The suggested KK-Net layout is displayed in Figure 2. We trained our model on an improved version of that dataset. The KK-Net architecture was designed with feature maps, kernel sizes, strides, and activation functions in mind.

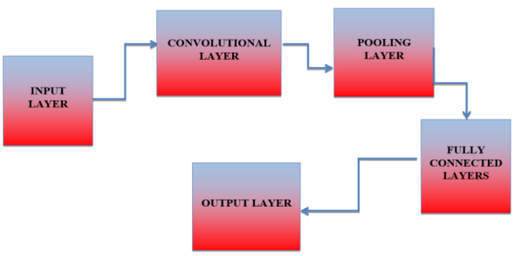

Fig.2: Architecture of KK-Net

Even though KK-Net has two million parameters, we were able to attain a 91% success rate with it. The hyper-parameters of the KK-Net architecture as they are currently configured are listed in Table 1. It is made up of different parameters and their values. Learning rate, cost function, optimizer, batch size, epoch number, drop out (convolution layer), dense layer, and activation function are the parameters. ELU is another term for the activation function.

V. Performance Evaluation Metrics

I will discuss the performance metrics in more detail in the paragraph that follows. The models that are displayed are evaluated using a variety of measures [38], such as F1-score, accuracy, precision, and recall. Four factors from the aforementioned confusion matrix are used to build these performance requirements, as can be seen in [39]. When analyzing deep learning techniques that provide a broad range of outcomes, this confusion matrix is helpful. So let's talk about the specifics of each of these issues.

Accuracy: a metric that considers the degree of accuracy of forecasts in comparison to all other forecasts. It is defined as the ratio of true positive and true negative to true positive, true negative, false positive and false negative

Recall: It is defined as the ratio of true positive and true positive to false negative

Precision: It is defined as true positive to the summation of true positive and false positive

F1-Score: Twice the sum of the recall and accuracy ratios.

A useful metric for assessing performance over a variety of threshold values is the Area under the Curve-Receiver Operating Characteristics (AUC-ROC) Curve. AUC shows the capacity to differentiate between classes, whereas ROC shows the probability curve. Here, the model's ability to correctly differentiate between classes is being assessed. A higher AUC is a sign of greater model reliability.

VI. Result

Both the original and updated datasets were utilized for DCNN testing and training. Tenfold cross-validation was employed to evaluate the categorization accuracy. Table 2 displays both the original and altered images for every category. There are over 5,000 photos of each class after enhancement. Figure 3 shows the classification model's training and testing accuracy metrics versus epoch. The results of the KK-measuring Nets are shown in the third table.

Table 2. Number of images of each class

Class	Original Images	Augmented Images
Serous	175	5640
Mucinous	100	5223
Endometroid	60	4353
Clear cell	80	4999
Non-cancerous	85	4527
Total	500	24742

This tabulation represents the classification of original imagesand augumented images.

AUC-ROC charts for each class are also displayed along with micro-average and macro-average plots. To adapt the widely used AUC-ROC metric for binary classes to multiclass classification, class 1 might be plotted against the other classes, class 2 against the other classes, and so on.

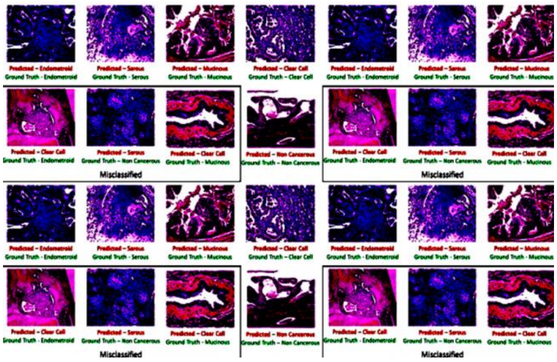

FIG 6. PREDICTED AND MIS CLASSIFIED IMAGES BY KK- NET

The above images represents the predicted and mis classified images by using KK net. By this way can able to classified the cancerous and non cancerous images

VII. DISCUSSION

As shown in Table 4 and Figure 4, the KK-Net model's classification accuracy improved from 75% to 91% for all five classes when the larger dataset was used. With a bigger dataset, we improved by 12.80% on the 78.20 percent obtained. For the model to generalize well, training accuracy and training loss must have a linear relationship, as shown in Figure 4. Additionally, when testing accuracy increased, it mirrored training accuracy, lowering the likelihood of incorrect data categorization. When the cost of making a mistake is significant, accuracy is crucial. With the way things are now described, we cannot afford to label a healthy picture as cancerous. As the cost of false negatives rises, recall becomes an increasingly important parameter. The KK-Net score is greater than 80 percent on all courses when the F1-Score is utilized as a counterbalance to the accuracy and memory assessments. Fig. 5 illustrates that the KK-Net model attains a 95% AUC-ROC.

According to Table 4, there was a 12% improvement in clear-cell classification, an 11% improvement in endometroid, mucinous, and severe classification, and a 10% improvement in non-cancerous classification. The main reason of misclassification is the difficulty in understanding the morphological characteristics of cells.Some photos contain many types of carcinoma that might cause confusion, while others are wobbly or unclear because to overlapping or poorly defined cell membranes. Retraining the upcoming generation of research models would benefit from additional instances with poor cell shape. Furthermore, we compared our data to pre-trained architectures that are now considered the state-of-the-art, including VGG-16, VGG-19, AlexNet, and GoogleNet. Table 5 summarizes the results from the different methods.

VIII. CONCLUSION

The present research used a cutting-edge deep convolution neural network, KK-Net, to make predictions about ovarian cancer and classify its four subtypes based on histopathology pictures for the first time. With the use of enhanced photos, our model went from 75% accurate to 91% accurate, a gain of 12.8% . In addition, the KK-Net model has an AUC-ROC of 95%, indicating its superior ability to differentiate between the classes. We discovered that digging deeper is not always better when creating a DCNN, and that hyperparameter tweaking is a powerful tool for fixing numerous problems. The other indicators become more significant based on the problem statement, thus accuracy is not the only way to assess performance. By combining our dataset with the trained SOTA DCNN models, we were able to verify the improved performance parameters of the suggested KK- Net model. Therefore, it can be concluded that KK-Net, which has been trained only on cancer data, has the best multi-class results for ovarian cancer prediction.

Conflict of Interest Statement

The authors declare no conflicts of interest related to this research.

REFERENCES

[1] Cancer, Who.int. [Online]. Available: www.who.int/news-room/fact heets/detail/cancer.

[2] Cancer.org.[Online].Available:www.cancer.org/content /dam/cancer - org/research/cancer -facts – and - statistics/annual – cancer - facts-and- figures/2021/ cancer-facts-and- figures-2021.pdf.

[3] L. A. Torre, B. Trabert, C. E. DeSantis, K. D. Miller, G. Samimi, etal., Ovarian Cancer Statistics, 2018: CA: A Cancer Journal for Clinicians. 68(4)(2018)284– 296.

[4] G.Chornokur, E.K.Amankwah, J.M.Schildkraut, and C.M.Phelan, Global Ovarian Cancer Health Disparities, Gynecologic Oncology.129(1)(2013)258–264.

[5] A. El-Nabawy, N. El-Bendary, and N. A. Belal, Epithelial Ovarian Cancer Stage Sub type Classification using Clinical and Gene Expression Integrative Approach, Procedia Computer Science. 131(2018)23–30.

[6] L. Zhang, J. Huang and L. Liu, Improved Deep Learning Network Based in Combination with Cost-Sensitive Learning for Early Detection of Ovarian Cancer in Color Ultrasound Detecting System, Journal of Medical Systems. 43(8)(2019)251.

[7] M. Wu, C. Yan, H. Liu, and Q. Liu, Automatic Classification of Ovarian Cancer Types from Cytological Images using Deep Convolutional Neural Networks, Bioscience Reports. 38(3) (2018) BSR20180289.

[8] M.Shibusawa, R. Nakayama, Y. Okanami, Y.Kashikura, N.Imai,et al., The Usefulness of a Computer-Aided Diagnosis Scheme for Improving the Performance of Clinicians to Diagnose Non-Mass Lesionson Breast Ultrasonographic Images, Journal of Medical Ultrasonics.43(3)(2016)387–394.

[9] S. J. Chen, C. Y. Chang, K. Y. Chang, J. E. Tzeng, Y. T. Chenetal., Classification of the Thyroid Nodules Based on Characteristic Sonographic Textural Feature and Correlated Histopathology using Hierarchical Support Vector Machines, Ultrasound in Medicine and Biology. 36(12) (2010)2018–2026.

[10] C. Y. Chang, H. Y. Liu, C. H. Tseng, and S. R. Shih, Computer- Aided Diagnosis for Thyroid Graves'

Disease in Ultrasound Images, Biomedical Engineering (Singapore).22(2)(2010)91– 99.

[11] J. Martínez-Más,A. Bueno-Crespo, S. Khazendar, M. Remezal- Solano,J.P.Martínez-Cendán,etal.,Evaluation of Machine Learning Methods with Fourier Transform Features for Classifying Ovarian Tumors Based on Ultrasound Images,PlosOne.14(7)(2019)e0219388.

[12] M. Lu, Z. Fan, B. Xu, L. Chen, X. Zheng, et al., Using achine Learning to Predict Ovarian Cancer, International Journal of Medical Informatics. 141 (104195) (2020).

[13] M. A. Rahman, R. C. Muniyandi, K. T. Islam and M. M. Rahman, Ovarian Cancer Classification Accuracy Analysis using 15-Neuron Artificial Neural Networks Model,In 2019 IEEE Student Conference on Research and Development(Scored).(2019).

[14] S. Ma, L. Sigal and S. Sclaroff, Learning Activity Progression in LSTMS for Activity Detection and Early Detection, In 2016 IEEE Conference on Computer Vision and Pattern Recognition (CVPR).(2016).

[15] A. C. Costa, H. C. R. Oliveira, J. H. Catani, N. de Barros, C. F. E.Melo,etal., Data Augmentation for Detection of Architectural Distortionin Digital Mammography Using Deep Learning Approach, Arxiv [Cs.Cv].(2018).

[16] A.Krizhevsky, I.Sutskever, and G.E.Hinton, Imagenet Classification with Deep Convolutional Neural Networks, Communications of the ACM.60 (6) (2017)84–90.

[17] H. R. Roth, L. Lu, A. Seff, K. M. Cherry, J. Hoffman, et al., A New2.5D

Development of Cloud Integrated Battery Management System for SOC prediction using Machine Learning Algorithm

B. Devi
Department of EEE,
Thiagarajar College of Engineering,
Madurai, Tamil Nadu
devibzen1@gmail.com

V. Suresh Kumar
Department of EEE,
Thiagarajar College of Engineering,
Madurai, Tamil Nadu
vskeee@tce.edu

Leelavathi. M
Department of EEE
Thiagarajar College of Engineering,
Madurai, Tamil Nadu
leelavathimohan93@gmail.com

***Abstract*—The growing reliance on battery-powered devices and renewable energy storage systems, effective Battery Management Systems (BMS) have become critical to ensure battery performance, longevity, and safety. However, traditional BMS approaches face limitations in scalability, complexity, and real-time data processing, especially in large-scale applications. This work proposes a Cloud Integrated Battery Management System (CIBMS) that leverages machine learning (ML) algorithms and the Internet of Things (IoT) to enhance battery monitoring, performance prediction, and State of Charge (SOC) estimation. The proposed system integrates IoT-enabled sensors to collect real-time battery parameters, such as voltage and current which are continuously uploaded to a cloud-based platform for further analysis and storage. Machine learning models, such as Support Vector Regression (SVR), Generalized Regression Neural Network (GRNN) and Radial Basis Function Neural Network (RBFNN) are employed to predict the SOC and forecast battery health, enabling proactive management. The proposed SVR algorithm predict the battery SOC with high accuracy.**

Keywords—State of Charge, Internet of Things, Electric Vehicle Battery, Machine Learning

I. Introduction

In the smart grid environment, uninterrupted power supplies (UPS), and electric cars, batteries play a critical role. It's a fantastic source of energy and storage device. As a result, monitoring the battery's state is utilised to indicate the amount of charge capacity available in the battery, as well as predict malfunctions and diagnoses. Estimating the battery's State of Health (SOH) and State of Charge (SOC) are important criteria to consider while assessing its state and health. Recently, the BMS has introduced numerous concepts for static and mobility battery systems, including cloud computation and IoT. This research examines the numerous algorithms that have been implemented in cloud-based BMSs and proposes a solution to the problems that exist in on board BMSs, such as sophisticated computing processes and data storage constraints.

Friansa et al. [1] presented a smart micro grid battery monitoring system based on the IoT. A cloud-based battery state monitoring and fault analysis system is presented for large-scale battery systems. [2]. For stationary and moveable batteries, IoT and cloud computing have been developed for BMS [3]. The cloud-based BMS was created to estimate SOC over the internet [4]. Because battery failure can be efficiently averted by precisely measuring SOC. SOC estimate is critical for BMS. Coulomb's assessment of the battery's state of charge Methods such as Coulomb counting [5] and open circuit voltage (OCV) [6] are employed because of their simplicity. Execute with minimal computational effort. The battery system's digital twin has been built in the cloud environment to store measured data and calculation [7]. For electric vehicles and data analytics services, a cloud-based BMS has been created [8]. Fire threats are caused by battery cell flaws such as ageing cells and by detecting the faulty cells and the kinds of faults that occur on the battery, the defects were diagnosed [10]. For battery status and health monitoring, operational safety, consistency, optimal performance, and cost, a well-designed BMS has been recommended [11]. As a result, a battery bank-specific BMS was created [12, 13]. Using similar internal resistance, a SVR approach for estimating SOC for li-ion batteries has been devised [14].

The SOC of the battery was calculated using online parameter identification techniques [15]. Based on the wiener method and historical deprivation data for li-ion batteries, a novel SOH estimation strategy has been proposed [16]. SOH estimation has been studied in recent years, and it may be divided into four groups based on estimating methodologies: adaptive estimating methods, direct measurement, statistical techniques, and degradation model related approaches. The SOH of a battery can be determined directly using battery capacity and internal resistance measurements. Internal resistances changed with temperature, according to Remmlinger et al. [17], and proposed a method for assessing resistance. [18]

Investigates the relationship between battery capacity and internal resistances. These methods have the advantage of being straightforward to detect and implement, but measuring battery capacity and internal resistances requires more precision, which is difficult to achieve in practise. For estimating SOC and SOH at the same time, a dual Kalman filter approach was developed [19]. To monitor battery capacity and internal resistance, a dual-sliding-mode observer technique with slow and high speed observers has been proposed [20]. With various resampling approaches, hyper parameter optimization was performed for machine learning methods [21].The extended Kalman filter (EKF) and Radial Basis Function Neural Network (RBFNN) were employed to estimate the state of charge (SOC) for lithium-ion batteries [22].

With the data training approach and state equation, a nonlinear model was developed.

The adaptive extended Kalman filter (AEKF) technique is used to accurately estimate the SOC and internal parameters [23]. It has been used to LiFePO4 batteries for electric vehicles using a model-based online computation technique. For battery dynamic operation, an adaptive H infinite filter was built using a linear model and a few parameters for SOC estimate [24]. To estimate SOC and state of energy, Yongzhi Zhan get al. [25] presented the adaptive H filter using covariance matching method and recursive least square approach. To assess the result accuracy, a hardware-in-the-loop (HIL) simulation approach was applied. To address the issue of real-time internal parameter changes in battery power, an adaptive particle swarm optimization (APSO) methodology has been proposed [26]. The various SOH monitoring approaches are discussed, as well as the benefits and drawbacks of online BMS precision level [27]. The battery's SOH was determined using various parameters, and the likelihood of electric hybrid car batteries was investigated using a structured neural network (SNN) [28].

This work explorers a novel approach to Battery Management using CIBMS, combining IoT sensors, cloud computing, and machine learning algorithms. The main objective of this work which include:

- To create a cloud-based Battery Management System (BMS) that incorporates IoT sensors for the real-time monitoring of battery characteristics.
- The application of Support Vector Regression (SVR) for precise assessment of SOC, tackling the difficulties encountered by conventional Battery Management Systems (BMSs).
- The concept outlines a sophisticated cloud-based architecture for the storage and processing of extensive battery data, facilitating effective data management and offering a platform for real-time analysis and fault detection.

This research seeks to improve the precision and efficacy of battery state monitoring, resulting in enhanced battery performance, heightened safety, and extended operating lifespan. By integrating IoT, cloud computing, and machine learning, the study demonstrates the potential to develop a more effective and scalable Battery Management System. The proposed CIBMS addresses the limitations of traditional onboard BMS by offering superior data storage, processing, and analysis capabilities. Through real-time monitoring, precise SOC estimation, and predictive maintenance, the system improves battery performance, ensures enhanced operational safety, and prolongs battery life. Future research can further expand the system's capabilities by supporting more complex battery configurations and investigating additional machine learning techniques for improved fault diagnosis and more accurate battery health assessments.

Architecture of the Cloud Integrated Battery Management System

Figure 1 illustrates the architecture and implementation of a CIBMS. This system aims to deliver efficient, real-time surveillance of battery metrics and condition via sophisticated cloud-based data processing and IoT technologies.

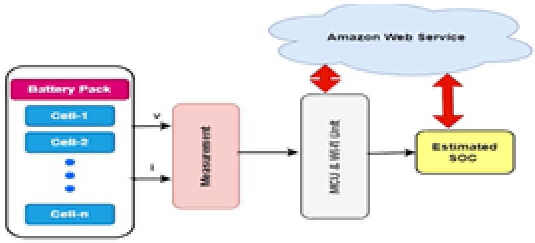

FIG 1. OVERALL ARCHITECTURE OF CLOUD INTEGRATED BATTERY MANAGEMENT SYSTEM

The CIBMS architecture integrates several essential components, including sensors, DC meters, and IoT devices, connected to a centralized cloud server. This cloud server plays a crucial role in storing battery parameter data, enabling real-time monitoring and facilitating sophisticated calculations, predictions, and analyses. Unlike traditional battery management systems that rely on local monitoring, the IoT-enabled CIBMS provides a dynamic approach by continuously logging and uploading battery data to the cloud. This enables users to predict and diagnose potential battery issues through cloud-based algorithms, significantly enhancing the system's ability to manage battery health, optimize performance, and extend lifespan.

A key aspect of the system is the integration of a standard meter that measures voltage and current directly from the battery. The measured parameters are transferred via an Internet-connected Raspberry Pi, serving as an intermediary to relay the data to the cloud server.The server stores the collected data in a database, which is continuously used to analyze the SOC of the batteries using machine learning algorithms, which helping users make informed decisions regarding battery maintenance and performance optimization.

II. SUPPORT VECTOR REGRESSION FOR ESTIMATING SOC

This study utilizes Support Vector Regression (SVR) as a machine learning method to precisely predict the State of Charge (SOC) of the battery. SVR is especially appropriate for regression and classification applications, and its use in this study seeks to deliver a dependable estimation of SOC utilizing various battery data. The technique's capacity to do advanced regression analysis with limited input data renders it an optimal selection for this application, particularly when battery data is intricate and non-linear.

Support Vector Regression (SVR) is extensively utilized in industrial applications because to its superior accuracy and capacity to handle data with a limited number of training samples. This research employs SVR to correlate a set of input features, including battery voltage and current, to a singular goal value, namely the battery's state of charge (SOC). The SVR model, developed with a specific training dataset, is assessed using a testing dataset that is separate from the training set. This distinction between training and testing data guarantees that the model's performance is generalized and not overfitted to a specific dataset.

A. SVR DESIGN OF SVR ALGORITHM AND STRUCTURE

The SVR model utilized in this study adheres to a conventional architecture akin to a three-layer Artificial Neural Network (ANN). The model includes a hidden layer, with functions and the quantity of support vectors similar to those in artificial neural networks, enabling the SVR model to capture intricate correlations between input and output data. A primary advantage of SVR is its adaptive model structure, which adjusts according to the data properties, enhancing efficiency and flexibility. The dataset utilized for constructing the SVR model comprises 70% of the total data, with the remaining 30% allocated for testing purposes. This segmentation facilitates the evaluation of the model's accuracy and its capacity to predict the SOC effectively using real-world data. It is essential to emphasize that the battery temperature is regarded as constant throughout this study, thereby separating its influence from other battery characteristics and streamlining the model's functionality.

B. TRAINING AND TESTING THE SVR MODEL

The training procedure for State of Charge (SOC) prediction entails the acquisition of data from the battery, including voltage, current, temperature, cycle count, and resistance. The data is pre-processed by cleaning, normalization, and division into training (70%) and testing (30%) datasets. The model, often SVR, is trained using the training data, where it learns to forecast the SOC based on diverse input variables. Throughout training, the model modifies its parameters to reduce prediction errors by employing optimization methods such as gradient descent. Cross-validation can be employed to verify that the model generalizes effectively to novel data.

The testing step assesses the model's accuracy with a distinct testing dataset that was not included in the training phase. The model predicts the SOC for the test data, which are then compared to the actual SOC values. An effective model will exhibit minimal error and elevated accuracy in forecasting the state of charge (SOC). Upon detection of mistakes, more analysis is conducted to comprehend and rectify the issues, including the modification of hyperparameters or the incorporation of new characteristics. The trained model is ultimately implemented in real-time to perpetually monitor the battery's state of charge throughout operation. As new data is gathered, the model forecasts the battery's condition, facilitating the management of battery performance and lifespan. The model may be frequently retrained with updated data to sustain accuracy over time. This guarantees that the Battery Management System (BMS) delivers precise and dependable forecasts for preserving battery health and averting malfunctions.

By integrating SVR with traditional methods like OCV testing, this research proposes a hybrid approach for accurately estimating SOC. SVR's ability to adapt to complex data and handle non-linear relationships makes it a powerful tool for battery management. The continuous evaluation and improvement of the SVR model will ensure that it can adapt to changing conditions and provide real-time predictions for battery maintenance, risk management, and optimization, ultimately enhancing the overall battery management system (BMS). In conclusion, the SVR- based SOC estimation model, supported by traditional methods, offers a robust and efficient means of monitoring battery health and performance in real-time, making it a valuable addition to the CIBMS.

III. RESULT AND DISCUSSION

Between fully charged and discharged stages, the voltage of the battery gradually decreases. A battery's SOC is usually denoted by its voltage level. If a battery is held at a very low SOC for an extended period of time, a large amount of sulphate crystals will accumulate, irreversibly lowering the battery capacity. Figure 5 shows the SOC measurement results derived from OCV experiments for various voltage values.

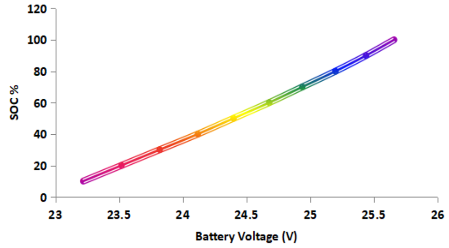

FIG 5. ACTUAL SOC AND OCV CURVE

The actual state of charge (%) was assessed for a 24V, 100AH battery following an 8-hour evaluation at 320°C. Multiple machine learning methods, including Generalized Regression Neural Network (GRNN), Radial Basis Function Neural Network (RBFNN), and Support Vector Regression (SVR), were employed to analyze the data in the cloud database. The real value of SOC was compared to several estimated methods such as GRNN, RBFNN, and SVR analysis in Table 1.The best results were obtained with SVR, which were nearly identical to the actual value. The graph for measured SOC value and estimated SOC value using various techniques is shown in Figure 6.

If the battery's voltage is elevated, the discharging duration will be prolonged; conversely, if the voltage is diminished, the discharging duration would be minimized. The battery is typically charged with the minimal current necessary, facilitating a progressive increase in state of charge and voltage level. Utilizing the battery charge with the minimal current facilitates an extended charging duration.

In a multiple battery system, a battery can be deemed fully depleted if it attains the minimum limit voltage during discharge, regardless of whether the terminal voltage of other batteries exceeds the discharge cutoff voltage. The CIBMS halts the discharge to avert over-discharge. The anticipated operational range of the final SVR must be incorporated into the training data. The training data for this study should encompass SOC values from 10% to 100%, along with the accompanying voltage ranges for those SOC values. The expected output of the SVR algorithm exhibits a remarkably low error value.

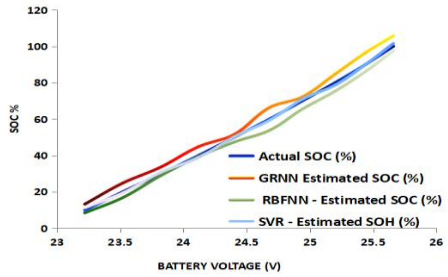

FIG 6. ACTUAL AND ESTIMATED SOC

A performance comparison of three machine learning models: Support Vector Regression (SVR), Generalized Regression Neural Network (GRNN), and Radial Basis Function Neural Network (RBFNN) for estimating the State of Charge (SOC) in lead-acid batteries. Among these models, SVR emerges as the most accurate, with the lowest error rate and the best adaptability across various SOC levels. It delivers consistent forecasts, rendering it suitable for real-time battery management applications, including electric vehicles (EVs) and solar energy storage systems. Although GRNN provides a reasonable equilibrium between speed and accuracy, it encounters difficulties at lower SOC values, rendering it less appropriate for crucial applications that demand great precision. Conversely, RBFNN demonstrates the poorest performance, with considerable discrepancies from actual SOC values and instability at low SOC levels. Despite its fast computation speed, its high error rate limits its usability to basic SOC trend analysis rather than real-time monitoring. Overall, SVR is the most effective model due to its high efficiency, low error rate, and stable performance across all voltage ranges.

IV. CONCLUSION

The suggested CIBMS was effectively deployed at Quantanics Tech Serve Private Limited in Madurai, showcasing its effectiveness in accurate battery monitoring, real-time data display, and predictive analysis. The system incorporates IoT-enabled sensors to monitor essential battery properties, including voltage and current, so ensuring precise and prompt data collecting. A web-based application was created to deliver real-time insights about battery attributes, accompanied by an emergency alarm system through mobile notifications, hence improving user awareness and safety.

The SVR- based machine learning model proved to be the most reliable approach for SOC estimation, outperforming other algorithms in accuracy and predictive capability. By utilizing historical battery data in the training phase, the system effectively predicts battery lifespan, defect prognosis, and operational stability, thereby reducing power outage risks caused by battery failures.

In the future, the CIBMS architecture may be enhanced by integrating powerful machine learning algorithms for extensive battery banks, thereby augmenting forecasting accuracy for diverse battery chemistries, including lithium-ion batteries. Moreover, subsequent research may concentrate on assessing the effects of network latency on real-time emergency warnings and cloud-based cost estimation models for extensive battery deployment. This will facilitate a more robust and economical energy storage management system, aiding the sustainable advancement of renewable energy applications.

REFERENCES

[1] Friansa K, Haq I.N, Santi B.M, Kurniadi D, Leksono E, Yuliarto B. Development of battery monitoring system in smart microgrid based on internet of things (IoT).Procedia Eng. 170, 2017, 482–487.

[2] Kim T, Makwana D, Adhikaree A, Vagdoda J, Lee Y. Cloud-based battery condition monitoring and fault diagnosis platform for large-scale lithium-ion battery energy storage systems, Energies, 11 (1), 2018, 125.

[3] Tanizawa T, Suzumiya T, Ikeda K. Cloud-connected battery management system supporting e-mobility. Fujitsu Sci. Tech. J, 51 (4), 2015, 27–35.

[4] Weihan Li, Monika Rentemeister, Julia Badeda, Dominik Jost, Dominik Schulte,Dirk Uwe Sauer. Digital twin for battery systems: Cloud battery management system with online state-of-charge and state-of-health estimation.Journal of energy storage, 30, 2020, 101557.

[5] Piller S, Perrin M, Jossen A. Methods for state-of-charge determination and their applications. Journal of Power Sources, 96 (1), 2001, 113–120.

[6] Lee S, Kim J, Lee J, Cho B.H. State-of-charge and capacity estimation of lithiumion battery using a new open-circuit voltage versus state-of-charge.Journal of Power Sources,185 (2), 2008, 1367–1373,

[7] Grieves M, Vickers J. Digital twin: mitigating unpredictable, undesirable emergent behavior in complex systems, in: Transdisciplinary Perspectives on Complex Systems. Vol 89, 2017, pp. 85–113.

[8] Tanizawa. T, SzumiyaT, Ikeda K. Cloud-connected battery management system supporting e-mobility. Fujitsu Sci. Tech. J. 2015, 51, 27–35.

[9] Wang Q, Ping P, Zhao X, Chu G, Sun J, Chen C. Thermal runaway caused fire and explosion of lithiumion battery. Journal of Power Sources 2012, 208, 210–224.

[10] Wu C, Zhu C, Ge Y, Zhao Y. A review on fault mechanism and diagnosis approach for Li-ion batteries.Journal of Nano materials. 2015, 631263.

[11] Li J, Zhou S, Han Y. Advances in Battery Manufacturing, Service, and Management Systems; Wiley, 2016.

[12] KimT, Qiao W, Qu L. A Multicell battery system design for electric and plug-in hybrid electric vehicles.In Proceedings of the 2012 IEEE International Electric Vehicle Conference, 2012;pp. 1–7.

[13] Andrea D. Battery Management Systems for Large Lithium-Ion Battery Packs. Artech House, 2010.

[14] Xiaojun tan, Yuqing tan, Di zhan, Ze yu, Yuqianfan,jianzhiqiu, and jun li. Real-Time State-of-Health Estimation of Lithium-Ion Batteries Based on the Equivalent Internal Resistance. IEEE Access, vol 8, 2020.

[15] Li Y, Liu K, Foley A. M, Zulke A, Berecibar M, Nanini-Maury E, Van Mierlo J and HosterH. E. Data-driven health estimation and lifetime prediction of lithium-ion batteries: A review. Renew. Sustain. Energy Rev, vol 113, 2019, 109254.

[16] XuX, YuC, TangS, SunX, SiX and WuL.State-of-health estimation for lithium-ion batteries based on Wiener process with modeling the relaxation effect. IEEE Access, vol 7, 2019, 105186-201.

[17] Remmlinger J, Buchholz M, Meiler M, et al. State-of-health monitoring of lithiumion-batteries in electric vehicles by on-board internal resistance estimation. Journal of PowerSources, 196(12), 2011, 5357–63.

[18] Tsang KM, Chan WL. State of health detection for Lithium ion batteries in photovoltaic system. Energy Convers Manage, 65(6), 2013, 7–12.

[19] Andre D, Appel C, Soczka-Guth T, et al. Advanced mathematical methods of SOC and SOH estimation for lithium-ion batteries. Journal of Power Sources, 224, 2013, 20–7.

[20] Kim IS. A technique for estimating the state of health of lithium batteries through a dual-sliding-mode observer. IEEE Trans Power Electron, 25(4), 2010, 1013–22.

[21] Schratz P, Muenchow J, Iturritxa E, Richter J, and Brenning A. Hyperparameter tuning and performance assessment of statistical and machine-learning algorithms using spatial data. Ecol. Model, vol 406, 2019, pp 109-120.

[22] Charkhgard M and Farrokhi M. State-of-Charge Estimation for Lithium-Ion Batteries Using Neural Networks and EKF. IEEE Transactions on Industrial Electronics, vol. 57, 2010, pp. 4178–4187.

[23] HeH, XiongR, GuoH. Online estimation of model parameters and state-of-charge of LiFePO4 batteries in electric vehicles. Appl. Energy 89 (1), 2012, 413–420.

[24] CharkhgardM, ZarifM.H. Design of adaptive H∞ filter for implementing on state-of-charge estimation based on battery state-of-charge-varying modelling. IET PowerElectron. 8 (10), 2015, 1825–1833.

[25] ZhangY, XiongR, HeH, ShenW. Lithium-ion battery pack state of charge andstate of energy estimation algorithms using a hardware-in-the-loop validation. IEEETrans. Power Electron. 32 (6), 2017, 4421–4431.

[26] Zhang D.H, ZhuG.R, Bao J, MaY, HeS.J, QiuS, ChenW. Research on parameter identification of battery model based on adaptive particle swarm optimization algorithm. J. Comput. Theor. Nanosci. 12 (7), 2015, 1362–1367.

[27] Berecibar M, GandiagaI, VillarrealI, Omar N, van MierloJ, van den BosscheP.Critical review of state of health estimation methods of Li-ion batteries for realApplications. Renew. Sustain. Energy Rev. 56, 2016, 572–587.

[28] Andre D, Nuhic A, Soczka-Guth T, Sauer D.U. Comparative study of a structured neural network and an extended Kalman filter for state of health. Eng. Appl. Artif.Intell. 26 (3), 2013, 951–961. 9087425711.

Unveiling 3D Object Recognition through Deep Learning

K. Siva Sankari
Department of ECE,
Sri Sai Ram Institute of Technology,
Chennai, Tamil Nadu
sivasankari.ece@sairamit.edu.in

Dr. B. Sathya Bama
Professor, Department of ECE,
Thiagarajar College of Engineering,
Madurai, Tamil Nadu
sbece@tce.edu

***Abstract*—This The subject of 3D object identification (segmentation, detection, and classification) has received much research in the areas of computer vision, graphics, and machine learning. Recently, deep learning algorithms have surpassed traditional methods for 3D segmentation problems because of their success in 2D computer vision. As a result, a number of novel methods have been developed and tested on a range of gold-standard datasets. In order for the pattern recognition system to correctly identify the item, the features must be extracted in a form that is compatible with the chosen identification technique. The location from which the features are collected does not matter. Local feature extraction and global feature extraction are the two halves of the object recognition approach. This paper provides a comprehensive analysis of the most recent advances in deep learning-based 3D object recognition and as an initial step for Three Dimensional Classification using PointNet for three cultural heritage Dataset is obtained.**

Keywords*—*Deep Learning, Computer Vision, Object Classification, Object recognition, PointNet

I. Introduction

A developing field of computer vision research is 3D object recognition. Detection of objects in a given image is the primary goal of a 3D object recognition system. Many scholars have put a lot of effort into the study of 2D object identification. These days, 3D object recognition is a hot topic. 3D graphics are important in many different applications. Some examples include an intelligence surveillance system, biometric analysis, the medical field, mobile manipulation, and robots. The geometric features in 3D photographs (range images) will be more distinct than in 2D shots.

Deep learning is a complete approach that can find probable features in data without the need for manual feature engineering [1,2]. In many contexts, it is vital to be able to single out instances of objects in 3D sensory input. Three-dimensional (3D) technologies allow for more comprehensive environmental data collection. As a result, it is frequently employed in industrial detection, Augmented Reality (AR), and robotic navigation. Methods [3,4] for 3D object identification can use point clouds to learn features directly. For instance, PointNets [3,4] may either categorize the whole point cloud or predict a semantic class for each individual point. Before the development of PointNet [3, 4], 3D point clouds were often flattened into 2D images or 3D voxel grids [5,6]. It is efficient in finding three-dimensional objects. To overcome certain limitations, we plan on borrowing certain ideas from 2D object recognition methods, namely their attention modules. An approach based on a Gaussian Mixture Model (GMM) was put forth by Guo et al. [5] in which attention modules were enhanced by feature maps of color and others. To improve the properties of the edge information and small objects, the attention modules concentrated on fascinating places. Using an attention module built into a Region Proposal Network (RPN), as demonstrated by Fan et al. [6], the detector may zero in on specific objects with high fidelity while gathering broad contextual information with low fidelity. As a consequence of these studies, we built attention modules for use in object recognition inside 3D point clouds.

II. Related Works

The preceding 3D object identification techniques and associated attention efforts are briefly introduced in this part. We categorize our evaluations according to three different technological approaches: activation functions in neural networks, attention modules in object identification, and 3D object recognition algorithms from point clouds.

A. Three-Dimensional (3D) Object Detection from Point Clouds

Two-dimensional (2D) detection and three-dimensional (3D) posture estimation are both possible because of the use of three-dimensional (3D) voxel patterns (3DVPs) [7, 8]. The MV3D [9] is a multi-view 3D object detection network. Unlike the MV3Ds, Li et al. [10] and Song et al. [11] improved accuracy at the expense of a significant amount of processing. VoxelNet proposed a universal 3D detection network that is trainable from end to end and includes feature extraction and bounding box prediction[12]. With this approach, 3D object identification may be performed directly on sparse 3D points, successfully capturing 3D shape data.

B. Attention Module in Object Detection

Recently, certain approaches to include attention processing have been proposed to enhance CNN performance in 2D-based, massive classification applications. A Residual Attention Network was suggested by Wang et al. [13] and can integrate cutting-edge feed-forward network design. This network has the ability to continuously gather a lot of attention-related data. A Squeeze-and-Excitation module was presented by Hu et al. [14] that explicitly models channel interdependencies in order to adaptively adjust channel-wise feature responses. The computation and speed of this approach have improved. To improve accuracy, the Convolutional Block Attention Module (CBAM) [16] and the Bottleneck Attention Module (BAM) [15] introduced spatial attention. For the identification of 2D objects, these attention models worked well.

C. Activation Function in Neural Network

Rectified linear units (ReLUs), which have been utilized for deep networks for a while [17, 18], are generally agreed to be simpler to train than logistic or tanh units. Le et al.'s observation that ReLUs seem improper for RNNs [19] was made due to the potential for huge output values to erupt out of the constrained values. Tanh has been shown to lessen the phenomena of mean shift, according to Ang-bo et al. [20]. Li et al. [21] found that the tanh function's output may increase the values triggered by ReLU units. This motivated us to use the 3D object detection network's fusion activation mechanism.

We built a unique 3D object detection network by combining the attention modules with the Frustum architecture [1,2] and the attention module [16]. In order to improve accuracy, we mix the ReLUs and tanh functions in the attention module. The following table shows different deep learning models and its parameters. In this paper PointNet is used for 3D object classification which is given in the following section.

TABLE I. DIFFERENT DEEP LEARNING MODELS AND ITS PARAMETERS

Model	Year	Layers	Parameters(million)
AlexNet	2012	7	62.4
VGG - 16	2014	16	6.7
GoogleNet	2014	22	6.7
ResNet-50	2015	25.6	70

III. POINTNET CLASSIFICATION

To manage unordered input sets, PointNet [1] employs a symmetric function, called max pooling, to learn a set of optimization functions that identify and encode important points within the point cloud. The network's fully connected layers then aggregate these optimal values into a global descriptor for shape classification or predict per-point labels for shape segmentation. Flexibility in input format allows for rigid or affine transformations, enhanced by a spatial transformer network that canonicalizes the data before being processed by PointNet, thus improving results. The classification network processes n points, applies input and feature transformations, and aggregates point features via max pooling, outputting classification scores for m classes. Figure 2 presents a simplified pipeline of a PointNet-like architecture, which processes 3D point clouds for classification or segmentation.

Point Cloud: The input is a 3D point cloud, which is a collection of points in 3D space representing the surface of an object or scene. Each point typically has coordinates (x, y, z) and sometimes additional features such as color or intensity.

Occupancy Grid: The 3D point cloud is converted into a voxelized representation, known as an occupancy grid. This step involves discretizing the 3D space into a grid of voxels (3D pixels). Each voxel is assigned a value based on whether it is occupied by any points in the cloud.

32 5×5×5 Filters, Stride 2: A 3D convolutional layer is applied to the occupancy grid using 32 filters of size 5×5×5. This layer extracts local spatial features from the voxelized representation, with a stride of 2 to down sample the data.

32 3×3×3 Filters + 2×2×2 Max Pooling: Another 3D convolutional layer uses 32 filters of size 3×3×3 to further refine feature extraction. This is followed by a 3D max-pooling operation with a 2×2×2 kernel, which reduces the spatial resolution while retaining important features.

128 Fully Connected: The features from the convolutional layers are flattened and passed through a fully connected layer with 128 neurons. This layer learns high-level abstract features of the 3D object.

K Fully Connected: The final fully connected layer outputs a vector of size K, where K represents the number of classes for classification or the number of segmentation labels.

Thus, this architecture processes raw 3D point cloud data into a compact representation through voxelization and feature extraction, enabling tasks such as object classification or semantic segmentation. While PointNet is simple and computationally efficient and can handle raw point clouds directly without voxelization, it struggles with capturing local geometric features because it processes points globally.

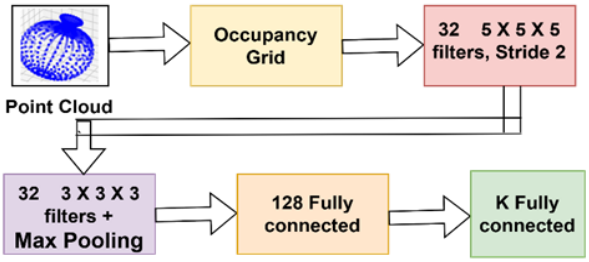

IV. RESULTS AND DISCUSSION

The PointNet model was applied to classify 3D objects, achieving a validation accuracy of 77.3%. The dataset comprised 1012 3D models of various vessel shapes, classified as Ancient Greek, Native American, and modern pottery. The classification was performed with input from the Department of Cultural Heritage at the Institute of Language and Speech Processing (ILSP)/Athena Research Centre.

A. Dataset

To evaluate our pottery-specific 3D shape descriptors, we had to create a dataset of polygonal 3D vessels. The current pottery dataset is composed of a total number of 1012 digitized, manually modeled, and semi-automated generated 3D models (3D vessel random generator). The content of the dataset is classified in several generic vessel shape categories such as Ancient Greek (alabastron, amphora, hydria, kantharos, lekythos, psykter, etc.), Native American (jar, effigy, bowl, bottle, etc.), and modern pottery. The current classification has been performed with the help of the Department of Cultural Heritage of the ILSP/Athena Research Centre at an archaeologist-oriented semantic level. Please note that the current classification is not the final one, and we will be soon presenting a shape-oriented one. Furthermore, the 3D models are stored in the Wavefront OBJ file format and are currently followed by a single view thumbnail in JPEG file format and no texture information. A text file and an Excel file are also provided where the filename of each model is assigned to a class. This information can be used for the computation of any performance metrics.

TABLE II. SAMPLE DATA DISTRIBUTION IN EACH CLASS

S. No	Class	No. of files
1	Abstract	208
2	Alabastron	55
3	Amphora	96
4	Aryballos	1
5	Bowl	8

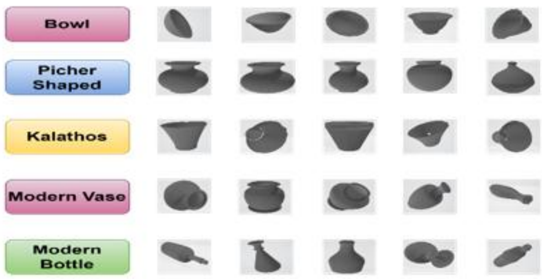

FIG 1 DIFFERENT CLASSES AND OBJECTS IN EACH CLASS

B. Data Augmentation with GANs

To address the long-tailed class imbalance, GANs were used to augment the dataset, making it uniformly distributed and improving classification accuracy. Figures demonstrate the original and augmented data, as well as the accuracy improvements achieved. Performance analysis of these approaches is carried out with impressive accuracy (Ar), precision (Pc), recall (Rc), F1 score (F1s), and error rate (Er) values.

FIG 2 ACCURACY GRAPH OF POINTNET

TABLE III. CLASSIFICATION RESULTS AND COMPARISON

Approach	Ar	Pc	Rc	F1s	E
PointNet	0.869	0.867	0.811	0.882	0.131
PointNet with GAN	0.889	0.879	0.825	0.889	0.111

While classifying cultural 3D dataset images, achieving high Pr and Rc is crucial for both minimizing misclassifications and ensuring that the model effectively captures instances of different classes present in the dataset. The PointNet model with GAN makes precise classification across all classes, as evidenced by its outstanding performance across various evaluation criteria. To foster robust model performance, it is crucial to explore adaptive feature extraction methods that can maintain accuracy in unpredictable environments.

V. CONCLUSION

While there have been tremendous improvements in object detection over the last decade, even the best detectors fall well short of their full potential. As the number of practical uses for mobile and embedded devices grows, so too will the need for lightweight models suitable for these platforms. Although there has been a rise in interest in this area, there are still many unanswered questions. We have shown how several object detectors improved over time in this article. The proposed classification using Point Clouds addresses imperfections in digitized CH artifacts, achieving improved classification accuracy with a uniformly distributed dataset. This unified method shows promise for various 3D recognition tasks, including object classification, part segmentation, and semantic segmentation, outperforming or matching current benchmarks. Our proposed method showcases impressive performance on standard datasets, highlighting its potential for 3D object recognition. To further broaden its applicability, particularly in resource-constrained environments other strategies such as model pruning, quantization, can be employed. This pathway promises to unlock new opportunities for practical applications in diverse settings.

REFERENCES

[1] Qi, C.R.; Su, H.; Mo, K.C.; Guibas, L.J. PointNet: Deep Learning on Point Sets for 3D Classification and Segmentation. In Proceedings of the IEEE Conference on Computer Vision and Pattern Recognition, Honolulu, HI, USA, 21–26 July 2017; pp. 77–85.

[2] Qi, C.R.; Yi, L.; Su, H.; Guibas, L.J. PointNet plus plus: Deep Hierarchical Feature Learning on Point Sets in a Metric Space. In Proceedings of the Advances in Neural Information Processing Systems, Long Beach, CA, USA, 4–9 December 2017

[3] Qi, C.R.; Liu, W.; Wu, C.; Guibas, L.J. Pointnet: Deep learning on point sets for 3d classification and segmentation. In Proceedings of the IEEE Conference on Computer Vision and Pattern Recognition (CVPR), Honolulu, HI, USA, 21–26 July 2017; pp. 652–660.

[4] Qi, C.R.; Yi, L.; Su, H.; Guibas, L.J. Pointnet++: Deep hierarchical feature learning on point sets in a metric space. arXiv 2017, arXiv:1706.02413.

[5] Guo, W.; Xu, C.; Ma, S.; Xu, M. Visual attention based small object segmentation in natural images. In Proceedings of the 2010 IEEE International Conference on Image Processing, Hong Kong, China, 26–29 September 2010; pp. 1565–1568.

[6] Fan, Q.; Zhuo, W.; Tang, C.K.; Tai, Y.W. Few-shot object detection with attention-RPN and multi-relation detector. In Proceedings of the IEEE/CVF Conference on Computer Vision and Pattern Recognition, Seattle, WA, USA, 13–19 June 2020; pp. 15–20.

[7] Xiang, Y.; Choi, W.; Lin, Y.; Savarese, S. Data-driven 3d voxel patterns for object category recognition. In Proceedings of the IEEE Conference on Computer Vision and Pattern Recognition, Boston, MA, USA, 7–12 June 2015; pp. 1903–1911

[8] Yang, B.; Yan, J.; Lei, Z.; Li, S.Z. Aggregate channel features for multi-view face detection. In Proceedings of

the IEEE International Joint Conference on Biometrics, Clearwater, FL, USA, 29 September–2 October 2014; pp. 1–8. [Google Scholar]

[9] Chen, X.; Ma, H.; Wan, J.; Li, B.; Xia, T. Multi-view 3d object detection network for autonomous driving. In Proceedings of the IEEE Conference on Computer Vision and Pattern Recognition, Honolulu, HI, USA, 21–26 July 2017; pp. 1907–1915. [Google Scholar]

[10] Li, B. 3d fully convolutional network for vehicle detection in point cloud. In Proceedings of the 2017 IEEE/RSJ International Conference on Intelligent Robots and Systems (IROS), Vancouver, BC, Canada, 24–28 September 2017; pp. 1513–1518. [Google Scholar]

[11] Song, S.; Xiao, J. Deep sliding shapes for amodal 3d object detection in rgb-d images. In Proceedings of the IEEE Conference on Computer Vision and Pattern Recognition, Las Vegas, NV, USA, 27–30 June 2016; pp. 808–816

[12] Zhou, Y.; Tuzel, O. Voxelnet: End-to-end learning for point cloud based 3d object detection. In Proceedings of the IEEE Conference on Computer Vision and Pattern Recognition, Salt Lake City, UT, USA, 18–23 June 2018; pp. 4490–4499.

[13] Wang, F.; Jiang, M.; Qian, C.; Yang, S.; Li, C.; Zhang, H.; Tang, X. Residual attention network for image classification. In Proceedings of the IEEE Conference on Computer Vision and Pattern Recognition, Honolulu, HI, USA, 21–26 July 2017; pp. 3156–3164.

[14] Hu, J.; Shen, L.; Sun, G. Squeeze-and-excitation networks. In Proceedings of the IEEE Conference on Computer Vision and Pattern Recognition, Salt Lake City, UT, USA, 18–23 June 2018; pp. 7132–7141.

[15] Park, J.; Woo, S.; Lee, J.Y.; Kweon, I.S. Bam: Bottleneck attention module. arXiv 2018, arXiv:1807.06514

[16] Woo, S.; Park, J.; Lee, J.Y.; So Kweon, I. Cbam: Convolutional block attention module. In Proceedings of the European Conference on Computer Vision (ECCV), Munich, Germany, 8–14 September 2018; pp. 3–19.

[17] Nair, V.; Hinton, G.E. Rectified linear units improve restricted boltzmann machines. In Proceedings of the International Conference on Machine Learning (ICML), Haifa, Israel, 22–24 June 2010.

[18] Zeiler, M.D.; Ranzato, M.; Monga, R.; Mao, M.; Yang, K.; Le, Q.V.; Hinton, G.E. On rectified linear units for speech processing. In Proceedings of the 2013 IEEE International Conference on Acoustics, Speech and Signal Processing, Vancouver, BC, Canada, 26–31 May 2013; pp. 3517–3521.

[19] Le, Q.V.; Jaitly, N.; Hinton, G.E. A simple way to initialize recurrent networks of rectified linear units. arXiv 2015, arXiv:1504.00941. [Google Scholar]

[20] Ang-bo, J.; Wei-wei, W. Research on optimization of ReLU activation function. Trans. Microsyst. Technol. 2018, 2. Available online: https://en.cnki.com.cn/Article_en/CJFDTotalCGQJ201802014.htm (accessed on 11 February 2021).

[21] Li, X.; Hu, Z.; Huang, X. Combine Relu with Tanh. In Proceedings of the 2020 IEEE 4th Information Technology, Networking, Electronic and Automation Control Conference (ITNEC), Chongqing, China, 12–14 June 2020; pp. 51–55

[22] F. Pereira, C.J.C. Burges, L. Bottou, K.Q. Weinberger (Eds.), Advances in Neural Information Processing Systems, Curran Associates, Inc. (2012), p. 9

[23] D. Fleet, T. Pajdla, B. Schiele, T. Tuytelaars (Eds.), Computer Vision – ECCV 2014, Lecture Notes in Computer Science, Springer International Publishing (2014), pp. 818-833.

Enhancing NS3's Wi-Fi Radio Energy Model for Individual Node Energy Distribution in Wireless Sensor Networks

S Parthasarathi
Department of ECE,
Thiagarajar College of Engineering,
Madurai, India
Parthasarathi_s@tce.edu

K Hariharan
Department of ECE,
Thiagarajar College of Engineering,
Madurai, India
khh@tce.edu

A Balakumar
Department of ECE,
K. Ramakrishnan College of Engineering,
Trichy, India
balakumar2712@gmail.com

***Abstract*—This paper presents an enhancement to the NS3 Wi-Fi radio energy model to calculate the energy consumption of individual nodes in a Wireless Sensor Network (WSN). The existing NS3 radio model does not support energy consumption metrics at the individual node level, especially for Transmission (TX), Reception (RX), Clear Channel Assessment (CCA), and idle times. To address this limitation, we have modified the Wi-Fi radio energy model to provide detailed energy metrics per node. The simulation considers multiple scenarios, including static and mobile nodes, with varying sink placements. Our study analyzes the energy distribution across nodes, providing insights for optimizing the energy efficiency of WSNs in agricultural IoT applications. Scenario 3 and 4 all the nodes except the sink are mobile.**

I. Introduction

Wireless Sensor Networks (WSNs) are crucial in Internet of Things (IoT) applications, especially precision agriculture, where energy consumption impacts network performance and sustainability. Simulators like NS3 lack detailed energy consumption tracking at the individual node level. This paper introduces modifications to NS3's Wi-Fi radio energy model, enabling per-node energy consumption analysis, including TX, RX, CCA, and idle states. The enhanced model is evaluated in various scenarios, providing insights into energy distribution and its impact on WSN efficiency.

NS3, a widely used simulator for network performance analysis, provides a generalized energy model for Wi-Fi-based nodes. However, it lacks granularity for assessing individual node energy consumption. This makes it challenging to analyze how activities like transmitting, receiving, and idle states contribute to overall energy consumption in large-scale WSNs. Our work addresses this gap by modifying the existing energy model to track energy usage at the individual node level.

II. Related Works

Energy consumption modeling is crucial for designing and evaluating wireless sensor networks (WSNs). Abo-Zahhad et al. (2015) proposed an energy consumption model for WSNs, focusing on individual node energy usage during data transmission and reception. This model serves as a foundational reference for understanding energy dynamics in WSNs. Akyildiz and Kasimoglu (2004) highlighted the challenges of wireless sensor and actor networks, emphasizing the need for efficient energy consumption models to enhance network performance. Ammer and Rabaey (2006) introduced the Energy-per-Useful-Bit (EPUB) metric for evaluating and optimizing data transmission energy efficiency. Ding et al. (2013) proposed a routing strategy that maximizes network lifetime in wireless multihop networks by optimizing energy consumption across the network. Ehsan et al. (2012) developed a radio and medium access contention-aware routing protocol for lifetime maximization in multi-channel sensor networks. Gu et al. (2013) introduced Efficient Scheduling for the Mobile Sink in Wireless Sensor Networks with Delay Constraints (ESWC) to optimize energy consumption while meeting delay requirements. These studies contribute to the advancement of energy consumption models in WSNs, providing valuable insights for future research.

Han et al. [7] extend WSN lifespans by harvesting ambient RF energy to power sensor nodes, reducing battery reliance. Their approach optimizes data transmission and energy harvesting for autonomous operation in remote environments. Jha et al. [8] develop an energy consumption model for the ML-MAC protocol in multi-hop WSNs, considering factors like transmission power, idle listening, and energy-saving mechanisms to optimize efficiency. This model reduces energy consumption by selecting appropriate strategies and minimizing unnecessary usage, impacting network design and protocol selection for efficient energy resource management and extended WSN lifespans. Kan et al. [9] analyze an accurate energy model for WSN nodes, proposing an optimal design for energy efficiency, highlighting trade-offs between power consumption and network performance. Li et al. [10] introduce a UHF energy harvesting system using a reconfigurable rectifier for WSNs, integrating energy harvesting technologies for sustainable powering. Melodia et al. [11] study communication and coordination in WSNs, integrating sensor nodes with actor nodes for enhanced communication and task execution, enabling intelligent, adaptive systems responding to real-time environmental changes. Improved communication and coordination protocols contribute to more efficient and flexible sensor networks, capable of handling complex tasks autonomously and adapting to dynamic environments, advancing WSN capabilities.

III. Methodology

A. *Wi-Fi Radio Energy Model Modifications:*

The standard NS3 Wi-Fi radio energy model calculates the total energy consumption for the entire network but lacks detailed tracking of per-node energy consumption. To address this, we modified the Wifi Radio Energy Model Helper class to log energy usage for each node individually, considering the following states: TX (Transmission), RX (Reception), Idle, and CCA (Clear Channel Assessment). By integrating energy tracking for each state, we can now calculate the total energy consumption for individual nodes over time.

B. Simulation Setup:

Scenarios 1 & 3Scenarios 2 &4, all nodes except the sink are mobile, with a speed of 50 m/s and a pause of 0 seconds. For Wi-Fi configuration, nodes are set up with IEEE 802.11b PHY standard, DSSS Rate 1 Mbps, and are connected through Yans Wifi Phyhelper and Yans Wifi Channel Helper. The transmission range is set to 300 meters using the Two Ray Propagation Lossmodel, with a Tx Power of 19.5 dBm and both Tx/Rx Gain set to 1 dB. The Wi-Fi radio energy model is configured with various current settings, including TxcurrentA: 215 mA, RxcurrentA: 100 mA, Idlecurrent A: 7 mA, CCA Busy- Current: 7 mA, Switching currentA: 7 mA, and Sleep Current: 0.5 µA.

Node deployment utilizes Grid Position Allocator for both stationary and mobile nodes. Stationary nodes use the Constant Position Mobility Model, while mobile nodes use the RandomDirection2dMobilityModel. The nodes are equipped with LiIon Energy Source Helper, providing an initial energy of 1000 joules, which is tracked using the Wi-Fi radio energy model to calculate energy consumption. The routing protocol employed is AODV (Ad hoc On Demand Vector) with IPv4 for addressing. The simulation runs for 1500 seconds, where each node, including the sink, starts with an initial energy of 1000 joules. The application running on the nodes is configured using On Off Helper with a 1-second on-time, 0-second off-time, 8 kbps data rate, and a packet size of 1 KB. A Packet Sink Helper is installed at the sink node to receive packets from the network.

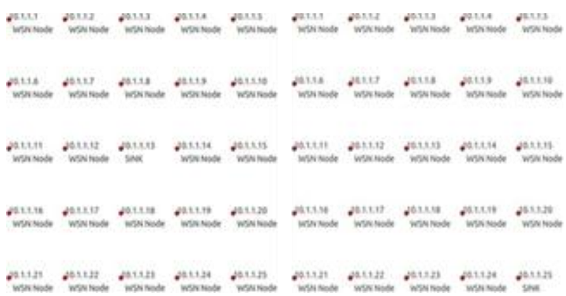

FIG. 1. NODE DEPLOYMENT FOR THE SCENARIOS ALL SCENARIOS

C. Energy Calculation

The modified Wi-Fi radio energy model logs the per-node energy consumption during transmission (TX), reception (RX), clear channel assessment (CCA), and idle states. These logs are then used to calculate the instantaneous energy consumption for each node, providing metrics such as the total energy consumed, the time spent in each state (TX, RX, idle, and CCA), and the overall network-wide energy distribution, including residual energy for each node.

IV. RESULTS AND DISCUSSION

A. Instantaneous Energy Consumption:

This research evaluates network energy consumption under various scenarios. Figure 2 shows linear instantaneous throughput over time, but Scenario 2 (green) consumes more due to increased transmissions to the sink. Mobility impacts energy consumption; Scenario 3 (red) consumes more than Scenario 1 (blue), where all nodes are stationary. Scenario 4 (cyan) consumes less due to reduced throughput, leading to extended idle periods. The Wi-Fi Radio Energy model in NS3 was modified to log real-time per-node energy consumption. As NS3 updates node states, the data streams through the console and is saved in a log file for energy-related calculations.

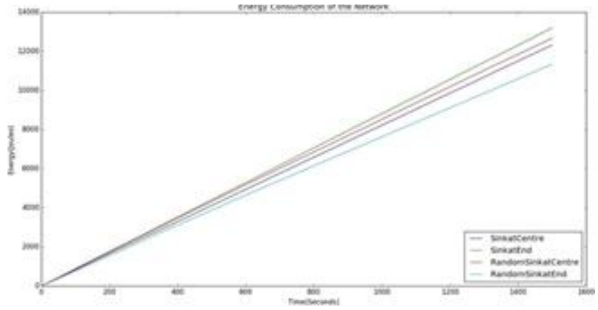

FIG. 2. INSTANTANEOUS ENERGY CONSUMPTION OF THE DIFFERENT SCENARIOS

B. Network Energy Distribution

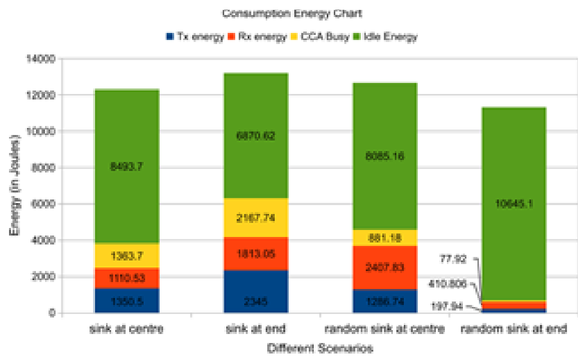

FIG. 3. ENERGY DISTRIBUTION OF THE NETWORK FOR VARIOUS ENERGY STATES

Figure 3 illustrates the energy consumption breakdown across different node states during a 1500-second simulation period. In Scenario 1, the network consumed 12,318 joules, with 69% spent in the idle state, 11% on data transmission, 9%, on data reception, and 11% on CCA busy. Scenario 2 showed a total energy consumption of 13,196 joules, with 52% in idle, 18% in transmission, 14% in reception, and 16% in CCA busy. Scenario 3 consumed 12,660 joules, with 64% in idle, 10% in transmission, 19% in reception, and 7% in CCA busy. Lastly, Scenario 4 consumed 11,331 joules, with a predominant 94% in idle, 2% in transmission, 3% in reception, and 1% in CCA busy. These breakdowns offer valuable insights into the energy distribution and usage patterns within the network.

C. Network Time Distribution:

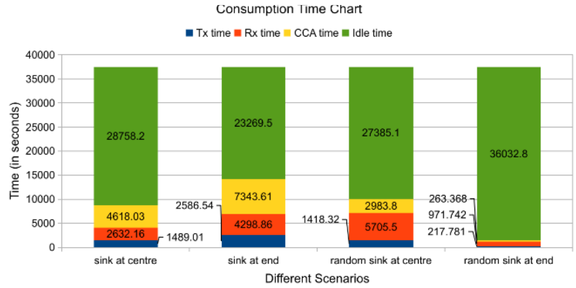

Figure 4 illustrates the time distribution of network activities across all 25 nodes during a 1500-second simulation, totaling 37,500 seconds of combined time. In Scenario 1, out of 37,497 seconds, 77% of the time is spent in the idle state, 4% in data transmission, 7% in data reception, and 14% in channel detection during transmission. Scenario 2 shows a total of 37,498 seconds, with 62% spent idle, 7% on transmission, 11% on reception, and 20% on channel detection. In Scenario 3, the total is 37,492 seconds, with 73% idle, 4% on transmission, 15% on reception, and 8% on channel detection. Finally, Scenario 4, with 37,485 seconds, exhibits 96% idle time, 0.6% on transmission, 2.6% on reception, and 0.7% on channel detection. Transmission, 2.6% is spent on receiving data and 0.7% is spent on channel detection.

D. Network Data Distribution:

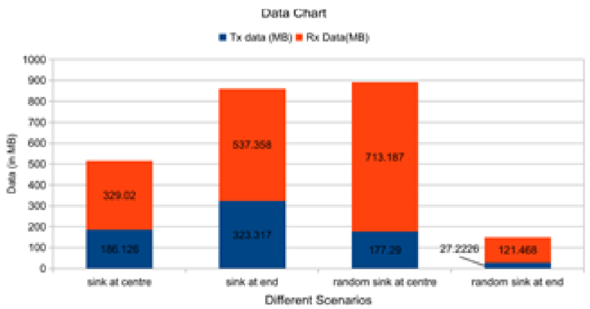

FIG. 5 DATA DISTRIBUTION OF THE NETWORK FOR THE DIFFERENT SCENARIOS

In figure 5, it shows data distribution of the Network i.e. the total data Transmitted and received within the network. In Scenario 1, out of 515 MB of data Exchanged, 36% is Transmitted and 64% of the data is received. Here in all scenario's, received data is higher when compared to the transmitted data due to multiple data receptions because more now of nodes present in the given range of the network. Similarly, the ratio for scenario 2 is 38:62, for Scenario 3, the ratio is 20:80 and for the final scenario, the Ratio changes to 18:82. Out of which it is evident that, more data is exchanged when the nodes are mobile which consumes more energy to reach the sink.

E. Residual Energy of the Network:

Figure 6 presents the residual energy of individual nodes in the network, with Scenario 2 showing a greater variance in energy distribution. This indicates that in Scenario 2, the energy consumption across nodes differs more significantly compared to the other scenarios

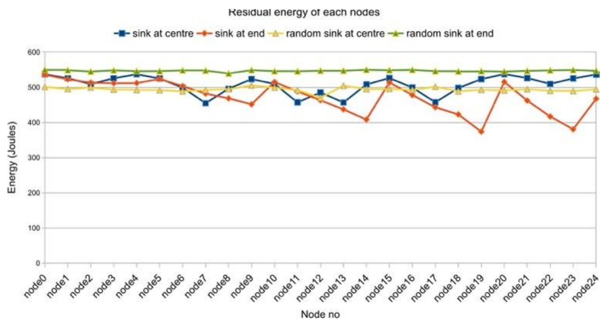

FIG. 6 ENERGY DISTRIBUTION IN NODES

Figure 7 Illustrates the correlation between energy consumption and residual energy for the entire network. In this simulation, each node is initially assigned 1000 joules of energy, and the simulation runs for a duration of 1500 seconds.

As a result, the total energy available in the network is 25,000 joules. The analysis of this data provides insights into how energy is consumed across the network and the residual energy left in each node at the end of the simulation.

F. Energy per useful Bit Consumption of the Network:

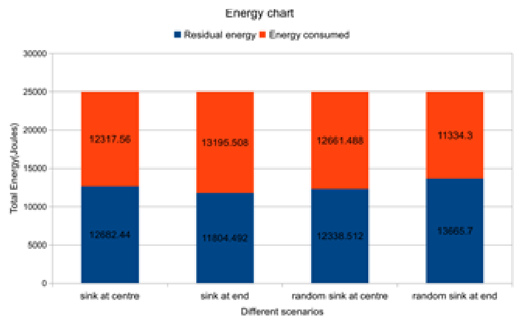

FIG. 7. ENERGY CONSUMED VS RESIDUAL ENERGY

One of the key metrics for network performance is Energy per Useful Bit (EPUB), which combines the transmitted and successfully received bits. In Scenario 4, EPUB is higher due to multiple retransmissions, indicating poorer performance. A lower EPUB value suggests a more efficient network. It is evident that Scenario 3 demonstrates the highest efficiency compared to the other scenarios, despite consuming more energy in Scenario 2. Even though Scenario 2 consumes more power, its EPUB is lower, further highlighting that Scenario 3 is more efficient in terms of energy usage per useful bit.

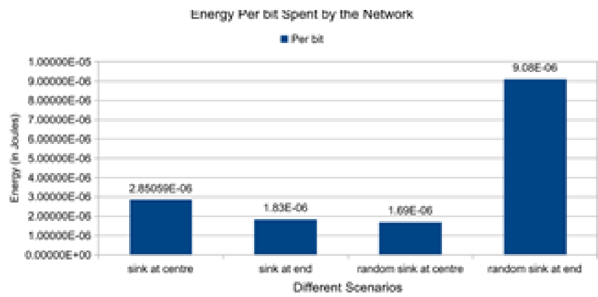

FIG. 8. ENERGY PER BIT CONSUMTION CHART

G. Energy variance in individual Network:

Figure 9 illustrates the average residual energy of the network, highlighting that Scenario 4 is not recommended due to its poor performance. Among the other three scenarios, Scenario 1 exhibits the highest residual energy, suggesting a longer network lifetime. In Figure 10, the normal distribution of the individual nodes' energy is shown; to maximize network lifetime, both the variance and standard deviation should be minimized as much as possible.

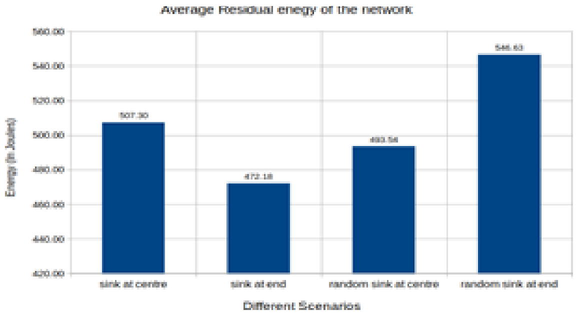

FIG. 9. RESIDUAL ENERGY OF INDIVIDUAL NODES

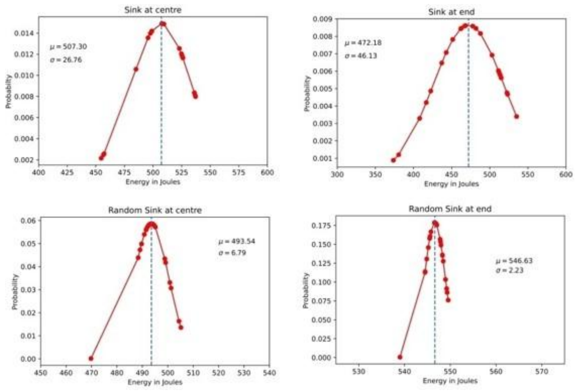

FIG. 10. NODE ENERGY VARIANCE

The goal is to achieve uniform energy distribution across the network to enhance performance. It is evident that Scenarios 1 and 3 exhibit lower standard deviation compared to Scenario 2. This suggests that placing the sink at the center of the topology is more beneficial for improved performance and energy optimization than placing it at the corner of the network.

V. CONCLUSION

This study modified the NS3 Wi-Fi radio energy model to track instantaneous energy consumption across nodes. It includes transmission, reception, clear channel assessment, and idle states. Simulations show how network performance and energy efficiency vary with node mobility, sink placement, and traffic patterns. Mobile nodes consume more energy due to increased data exchanges and retransmissions. Stationary nodes consume less energy and have a longer network life- time. Scenarios with the sink at the network's center have more uniform energy distribution, enhancing stability and efficiency.

Reducing energy consumption optimizes network performance by minimizing energy Distribution variance and standard deviation. Strategically placing the sink at the center (Scenario 1) leads to more consistent energy distribution and optimized overall energy usage. Placing the sink at the network's edge (Scenario 2) increases energy consumption due to additional transmissions. These findings highlight the importance of network topology and sink placement in optimizing energy consumption. Future research should integrate adaptive power control, dynamic sink placement, and energy harvesting models to create self-sustaining WSNs suitable for IoT, remote monitoring, and smart city infrastructures. The open-source NS3 code can be extended to incorporate these features for more precise simulations and energy-efficient WSNs.

VI. FUTURE WORKS

Future work can focus on developing custom energy consumption models within the NS3 framework, enhancing the Wi-Fi radio energy model to accurately simulate energy usage during various network states like idle, transmission, reception, and channel sensing. This can involve incorporating dynamic transmission rates, variable power control, and environmental factors for more granular energy modeling. Additionally, mathematical modeling of energy consumption, through differential equations and their transformation into discrete-time equations, can improve the scalability and reusability of simulations, providing a more efficient way to test energy optimization strategies. Another promising direction is the development of energy harvesting models, where nodes can recharge their batteries using renewable sources like vibration, solar, or thermal energy, allowing for the evaluation of energy efficiency and long-term performance of self-sustaining wireless sensor networks. Integrating these models with NS3 would enable the simulation of energy-efficient networks, paving the way for sustainable deployments in real-world applications

REFERENCES

[1] M. Abo-Zahhad, M. Farrag, A. Ali, and O. Amin, "An energy consump- tion model for wireless sensor networks," *5th International Conference on Energy Aware Computing Systems & Applications*, pp. 1–4, 2015.

[2] F. Akyildiz and I. H. Kasimoglu, "Wireless sensor and actor networks: research challenges," *Ad Hoc Networks*, vol. 2, no. 4, pp. 351–367, 2004.

[3] J. Ammer and J. Rabaey, "The Energy-per-Useful-Bit Metric for Eval- uating and Optimizing Sensor Network Physical Layers," *Sens. Ad Hoc Commun. Networks*, vol. 2, pp. 1–6, 2006.

[4] L. Ding, P. Wu, H. Wang, Z. Pan, and X. You, "Lifetime maximization routing with network coding in wireless multihop networks," *Sci. China Inf. Sci*, vol. 56, no. 2, pp. 1–15, 2013.

[5] S. Ehsan, B. Hamdaoui, and M. Guizani, "Radio and medium access contention aware routing for lifetime maximization in multichannel sensor networks," *IEEE Trans. Wireless Commun*, vol. 11, no. 9, pp. 3058–3067, 2012.

[6] Y. Gu, I. C. Society, and Y. Ji, "ESWC: Efficient scheduling for the mobile sink in wireless sensor networks with delay constraint," *IEEE Trans. Parallel Distrib. Syst*, vol. 24, no. 7, pp. 1310–1320, 2013.

[7] B. Han, R. Nielsen, C. Papadias, and R. Prasad, "Radio frequency energy harvesting for long lifetime wireless sensor networks," *IEEE Xplore*, 2013.

[8] M. K. Jha, "Energy Modeling of ML-MAC Wireless Sensor Network Protocol," *Proc. IEEE, Manju Khurana, Ranjana Thalorea, Vikas Rainab*, 2015.

[9] B. Kan, L. Cai, and L. Zhao, “An Accurate Energy Model for WSN Node and Its Optimal Design,” *Proc. IEEE*, 2015.

[10] C. Y. Li, W. H. Tsui, and Ki, “UHF energy harvesting system using reconfigurable rectifier for wireless sensor network,” *2015 IEEE Inter-national Symposium on Circuits and Systems (ISCAS)*, pp. 93–96, 2015.

[11] Melodia, S. Member, and D. Pompili, “Communication and Coor- dination in Wireless Sensor and Actor Networks,” *IEEE Trans. Mob. Comput*, vol. 6, no. 10, pp. 1116–1129

Integration of FMCW Radar for Enhanced Sensing and Communication in ISAC Framework

Tharaniya R
Dept of Electronics & Communication Engineering,
Thiagarajar College of Engineering,
Madurai, India
tharaniya@student.tce.edu

Ananthi G
Dept of Electronics & Communication Engineering,
Thiagarajar College of Engineering,
Madurai, India
gananthi@tce.edu

D. Kiruthika
Dept of Electronics & Communication Engineering,
Thiagarajar College of Engineering,
Madurai, India
kiruthikadhibakaran123@gmail.com

Lakshmipriya K
Dept of Electronics & Communication Engineering,
Thiagarajar College of Engineering
Madurai, India
lakshmipriyak@student.tce.edu

***Abstract*— Integrated Sensing and Communication (ISAC) systems combine communication and radar sensing functionalities on the same platform, addressing the growing need for efficient wireless services. This paper explores the role of Frequency-Modulated Continuous Wave (FMCW) radar within ISAC systems, focusing on monitoring target range and velocity in dynamic environments, such as autonomous driving and collision avoidance. The radar and communication signals are integrated to optimize spectrum usage and reduce hardware complexity. To validate the proposed system, radar data from the Radar Signal Dataset for Automotive Applications, containing in-phase (I) and quadrature (Q) components of transmitted and received signals, is used. By applying signal processing techniques to this dataset, including Fast Fourier Transform (FFT) for range estimation and Short-Time Fourier Transform (STFT) for Doppler analysis, the system successfully estimates target range and velocity. The results demonstrate that FMCW radar integrated into ISAC can efficiently perform both radar sensing and communication, providing valuable insights for applications in automotive systems and beyond.**

Keywords— ISAC, FMCW, beat Signal, Range-Velocity.

I. INTRODUCTION

The ISAC) has emerged as a transformative paradigm in next-generation wireless networks, particularly for 6G and beyond. By jointly leveraging shared spectral and hardware resources, ISAC systems aim to provide high-accuracy environmental sensing alongside reliable communication services, addressing the limitations of traditional, isolated systems and enabling novel applications such as autonomous vehicles, smart infrastructure, and industrial automation [1][2][3]. A critical enabler of ISAC is the design of waveforms that can effectively support both functionalities. Among the most promising candidates is the Frequency-Modulated Continuous Wave (FMCW) radar waveform, which offers high range resolution, efficient hardware implementation, and is well-suited for simultaneous communication and sensing tasks. Advances in phase-coded and smoothed FMCW radar designs have shown the potential to mitigate interference while maintaining performance, making them suitable for deployment in interference-rich and dynamic environments [5][6][12][13].

To further enhance ISAC capabilities, Dual-Function Radar-Communication (DFRC) systems have been introduced. These systems embed communication information directly into radar waveforms, enabling spectrum reuse and reducing the need for separate communication infrastructure [10]. In parallel, techniques like zero-forcing beamforming allow ISAC systems to serve multiple users while preserving radar sensing quality, which is especially vital in vehicular networks where robust sensing and reliable data exchange are critical [9]. Moreover, improvements in receiver architectures—especially those designed for phase-modulated FMCW radars—enhance target detection accuracy and resilience against interference, supporting real-time situational awareness in complex scenarios such as urban traffic environments [11][14].

Building upon these foundations, this work investigates the integration of FMCW radar within the ISAC framework to analyze range-velocity profiles from transmitted and reflected radar signals. This analysis demonstrates the system's capacity to monitor moving targets accurately in dense and dynamic environments, contributing significantly to the evolution of ISAC technologies for safety-critical applications like collision avoidance and intelligent transportation systems.

System Model

In an FMCW radar-based ISAC system, the radar waveform is typically integrated with the communication signals to allow both functions to operate efficiently on the same platform.

2.1 FMCW Radar Waveform

The FMCW radar employs a signal s(t) for modulating changes in phase within a chirp signal via chirp bandwidth of B and chirp duration of T. The chip duration is T, and there are N_c, chips per chirp. Thus, the bandwidth is determined by the number of chips within the chirp, as $B_c = \frac{N_c}{T}$. To avoid spectrum leakage, we assume that the bandwidth is significantly smaller than the chirp bandwidth. The transmitted FMCW waveform can be represented as:

$$x_t(t) = s(t)e^{-j(2\pi f_c t + \pi k t^2)} \tag{1}$$

The chirp slope is represented by $k = \frac{B}{T}$, while the carrier frequency is denoted by f_c. A target reflects the broadcast signal (1) at a constant speed, and it arrives with the following round-trip delay:

$$x_r(t) = \alpha_0 s(t - \tau(t))e^{-j(2\pi f_c(t-\tau(t))+\pi k(t-\tau(t))^2)} \quad (2)$$

The complex amplitude α_0 is proportional to the effects of target backscattering and propagation, whereas $\tau(t)$ represents the round-trip time. The following is a representation of the round-trip delay: as:

$$\tau(t) = \frac{2(R_0+\upsilon_0(t))}{c} = \tau_0 + \frac{2\upsilon_0}{c}(t) \quad (3)$$

During dechirping, the received signal is merged with the complex conjugate of the uncoded chirp signal, with c representing the speed of light, R_0 representing the range, and υ_0 representing the velocity. The dechirped signal may therefore be represented as the following [5]:

$$x_b(t) = x_r(t)e^{j(2\pi f_c t+\pi k t^2)}$$

$$= \alpha_0 s\big(t - \tau(t)\big)e^{j(2\pi f_c\tau_0+2\pi(k\tau_0+f_d)t-\pi k\tau_0{}^2)}$$

$$\approx \alpha_0 s(t - \tau_0)e^{j(2\pi f_b t)} \quad (4)$$

The beat frequency is represented by $f_b = k\tau_0 + f_d$ .In fast-time processing, the Doppler frequency shift $f_d = \frac{2\upsilon_0 f_c}{c}$ may be disregarded as it is often significantly less than the one-range cell $f_d \ll {}^{f_s}/_N$, where f_s is the frequency at which sampling is performed of the beat signal and N is the number of fast-time samples. To maintain generality, we integrate all constant terms of signal processing into α_0.

2.2 FMCW Radar Signal for ISAC:

In an ISAC system, this radar signal needs to co-exist with the communication signal on the same frequency band or within an allocated bandwidth. The communication signal can be integrated directly into the FMCW radar model by modulating the signal with a communication-specific waveform (e.g., an OFDM signal). This integration would allow for the radar and communication signals to share the same platform. The FMCW signal for ISAC, considering both radar and communication, could be represented as:

$$x_{ISAC}(t) = (s_{rad}(t) + s_{com}(t))e^{-j(2\pi f_c t+\pi k t^2)} \quad (5)$$

Where $(s_{rad}(t)$ is the radar signal it is receive from echo signal. $s_{com}(t)$ is the communication signal, which can be an OFDM or other suitable modulation waveform.

2.3 Dataset Description

The I/Q dataset used in this study was sourced from the Radar Signal Dataset for Automotive Applications, providing radar signals sampled at a frequency of 46.5 kHz with a bandwidth of 150 MHz. The data comprises both in-phase (I) and quadrature (Q) components of transmitted and received signals collected under realistic traffic scenarios. The dataset includes measurements from a 77 GHz FMCW radar system, commonly used in automotive applications, making it suitable for high-resolution sensing and communication in scenarios such as collision avoidance and autonomous driving. The dataset includes both stationary and moving targets under a variety of conditions, ensuring a comprehensive evaluation of the proposed system's performance in real-world environments.

2.2.1 Preprocessing Steps

Real-world radar data often contains noise, artifacts, and imbalances that must be addressed before analysis. The preprocessing steps applied to the dataset include:

- **Noise Filtering:** A low-pass filter was applied to suppress high-frequency noise that could interfere with the range and velocity estimation. The cutoff frequency was selected to retain the signal components relevant to the radar system's operational range.
- **I/Q Imbalance Correction:** Amplitude and phase imbalances between the I and Q components were corrected using a standard imbalance correction algorithm. This ensures accurate representation of the signal's phase and amplitude characteristics.
- **Signal Synchronization:** The alignment of transmitted and received signals was verified to ensure accurate de-chirping. Cross-correlation techniques were used to determine and correct time offsets.

2.1.2 Methodology

- **Beat Signal Generation:** The received I/Q signal was multiplied by the conjugate of the transmitted chirp to produce the beat signal. This operation isolates the frequency shift caused by the round-trip delay and Doppler effect. The beat signal can be expressed in (4).
- **Range Estimation:** A Fast Fourier Transform (FFT) was applied to the beat signal to extract the range profile. Peaks in the frequency spectrum correspond to targets at specific distances, with the magnitude indicating reflection strength. The range R is calculated as: $R = cf_b/2B$.
- **Velocity Estimation:** Doppler analysis was performed using a Short-Time Fourier Transform (STFT) across multiple chirps to estimate target velocities. The Doppler shift f_d was used to determine the radial velocity $\upsilon = cf_d/2f_b$.
- **Range-Velocity Mapping:** The range and velocity estimates were combined into a 2D range-velocity map. The map provides a visual representation of detected targets, with intensity indicating the strength of the reflected signal.

II. RESULTS AND DISCUSSION

This section presents and analyzes numerical findings that show how well the FMCW radar system performs (4). Then, using the simulation I/Q dataset settings listed in Table 1,

TABLE 1: SIMULATION PARAMETERS

Parameters	symbols	Values
Speed of Light	c	3×10^8
Carrier Frequency	f_c	77GHz
Wavelength	$\lambda = {}^{c}/_{f_c}$	3.89 mm
Bandwidth	B	150MHz
Chirp Duration	T	5.5ms
Samples per Chirp	N	256
Sampling Frequency	$f_s = {}^{N}/_{T}$	46.5kHz

Fig.1a shows the I/Q components of the transmitted signal, which represent time-varying signals that encode information for the radar system. In FMCW radar, this signal is frequency-modulated and its instantaneous frequency is determined by the carrier frequency f_c and modulation rate (bandwidth B) over the chirp duration T. This modulation enables precise control of the signal's spectral characteristics, crucial for both target sensing and communication, especially in dynamic environments where target ranges and speeds vary. Figure 1b depicts the received signal's I/Q components after reflection from a target. This signal retains the same modulation but is altered by the target's distance, represented by the time delay $\tau = 2R/c$ and Doppler shift due to relative motion. The resulting changes in phase from both effects are critical for estimating the target's position and velocity, making the analysis of received I/Q components essential for effective radar and ISAC systems.

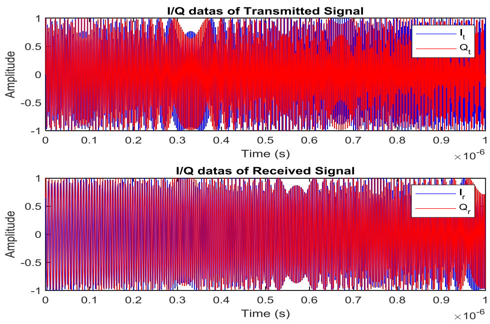

FIG 1 A) TRANSMITTED SIGNAL B) RECEIVED SIGNAL

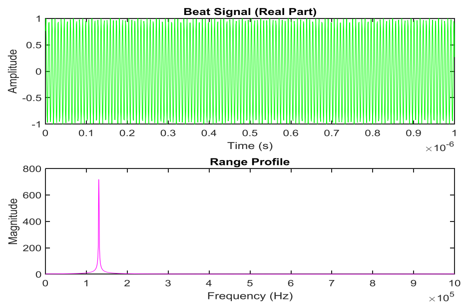

FIG 2 A) BEAT SIGNAL B) RANGE PROFILE

Fig. 2a depicts the real part of the beat signal, obtained by element-wise multiplication of the transmitted signal and the conjugate of the received signal. This operation highlights the interference between the two signals, encoding critical information about the target's range and velocity. In FMCW radar, the beat frequency represents the difference between the transmitted and received frequencies, which directly correlates to the target's range. Specifically, the beat frequency increases linearly with the round-trip delay and the distance to the target. The real part of the beat signal provides direct insights into range estimation, which is essential for applications such as collision avoidance, autonomous navigation, and real-time object tracking. Fig.2b shows the range profile derived from the frequency spectrum of the beat signal using a Fast Fourier Transform (FFT). The peaks in the range profile correspond to the target's distance, with their magnitude indicating the reflection strength. A sharp peak signifies a strong echo from a target, while multiple peaks can represent closely spaced objects. Analyzing the range profile is crucial for target detection and discrimination in dense and dynamic environments, as it enables accurate range estimation and supports effective resource management in ISAC systems where sensing and communication are integrated.

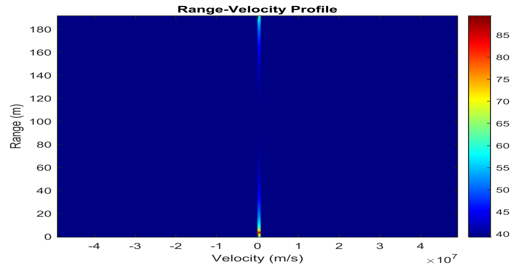

FIG.3 RANGE-VELOCITY PROFILE

The Range-Velocity Profile presented in the fig.3 visually highlights the relationship between the range and velocity of targets detected by the radar system. The intensity of the color scale represents the signal amplitude in decibels (dB), which provides insight into the relative strength of the reflections from targets. A prominent peak is observed near the zero velocity axis, corresponding to stationary or slowly moving targets located at specific ranges. The high intensity in the proximity of this region indicates strong reflections, likely due to targets directly aligned with the radar beam, as moving targets induce a frequency shift (Doppler shift) proportional to their radial velocity. The profile is crucial in applications such as automotive radar for collision avoidance, where identifying both the distance and relative velocity of objects is vital for decision-making processes. This analysis demonstrates the FMCW radar system's ability to achieve accurate range and velocity estimation, essential for ISAC applications in dynamic environments.

III. CONCLUSION

This paper investigates how FMCW radar integrated with communication capabilities in ISAC systems can simultaneously estimate target range and velocity in real-world environments. Using the I/Q dataset from the Radar Signal Dataset for Automotive Applications, the paper demonstrates the system's ability to accurately process radar signals, estimate distances, and detect moving targets. The integration of radar and communication signals in ISAC not only enhances spectrum efficiency and reduces hardware complexity but also provides reliable sensing and communication for critical applications, such as autonomous driving and smart transportation systems. This approach proves effective in dense and dynamic environments, where high-accuracy sensing and reliable communication are essential. Future work will focus on refining these systems for broader scalability and better performance in more complex operational settings.

IV. ACKNOWLEDGMENT

The authors extend their due thanks to the Thiagarajar College of Engineering management, Madurai, India for their extensive research facilities and the financial backing from Thiagarajar Research Fellowship (TRF) scheme (File.no: TCE/RD/TRF/2024/10 dated 09-02-2024) is gratefully acknowledged.

REFERENCES

[1] Zhengyu Zhang, Ruisi He, Bo Ai, Mi Yang, Chao Li, Hang Mi, and Zhangdui Zhang, “A General Channel Model for Integrated Sensing and Communication Scenarios,” IEEE Communications Magazine ,vol. 61, issue: 5, pp.68 – 74, 2023.

[2] Li, X., et al. (2019). "Integrated Sensing and Communication: A New Paradigm for 6G." IEEE Transactions on Wireless Communications, 18(11), 5377–5386.

[3] Zhang, Y., et al. (2020). "Integrated Sensing and Communication for 6G Networks." IEEE Access, 8, 45599–45608.

[4] Cui, Y., et al. (2018). "Joint Sensing and Communication for Integrated 5G Networks." IEEE Journal on Selected Areas in Communications, 36(11), 2457–2469.

[5] Benedetto, S., et al. (2005). "The waveform design for FMCW radar systems." IEEE Transactions on Aerospace and Electronic Systems, 41(3), 941–952.

[6] Skolnik, M. I. (2008). Introduction to Radar Systems (3rd ed.). McGraw-Hill.

[7] Ward, R. (1994). Radar Signal Processing and Adaptive Systems. Artech House.

[8] Stüber, G. L. (2017). Principles of Mobile Communication (4th ed.). Springer.

[9] Joung, Jingon, Heejung Yu, and Tony QS Quek. "Integrated single target sensing and multiuser communications based on zero-forcing beamforming." Vehicular Communications, vol.63,Oct 2023.

[10] Aboulnasr Hassanien ,Moeness G. Amin, Elias Aboutanios, Braham Himed " Dual-Function Radar Communication Systems: A Solution to the Spectrum Congestion Problem" IEEE Signal Processing Magazine,vol.36,n0.5,Sep 2019.

[11] Kumbul, Utku, Nikita Petrov, Cicero S. Vaucher, and Alexander Yarovoy. "Receiver structures for phase modulated FMCW radars." In 2022 16th European Conference on Antennas and Propagation (EuCAP), pp. 1-5. IEEE, 2022.

[12] Kumbul, Utku, Faruk Uysal, Cicero S. Vaucher, and Alexander Yarovoy. "Automotive radar interference study for different radar waveform types." IET Radar, Sonar & Navigation, vol.16, no.3, pp.564-577,2022.

[13] Kumbul, Utku, Nikita Petrov, Cicero S. Vaucher, and Alexander Yarovoy. "Smoothed phase-coded FMCW: Waveform properties and transceiver architecture." IEEE Transactions on Aerospace and Electronic Systems ,vol.59, no. 2,pp. 1720-1737,2021.

[14] Kumbul, Utku, Nikita Petrov, Fred van der Zwan, Cicero S. Vaucher, and Alexander Yarovoy. "Experimental investigation of phase coded FMCW for sensing and communications." IEEE Transactions on Terahertz Science and Technology, vol.13, no.4, pp. 389-395. July, 2023.

A Novel Framework for Biosensing Sensitivity in Triple Material Surrounding Gate TFETs

E. Rajalakshmi
Research Scholar, Department of ECE,
Thiagarajar College of Engineering,
Madurai, Tamilnadu, India
raje.rajalakshmi18@gmail.com

N.B. Balamurugan
Professor, Department of ECE,
Thiagarajar College of Engineering,
Madurai, Tamilnadu, India
nbbalamurugan@tce.edu

M. Suguna
Associate Professor, Department of IT,
Thiagarajar College of Engineering,
Madurai, Tamilnadu, India
mscse@tce.edu

V. Karutharaja
Research Scholar, Department of ECE,
Thiagarajar College of Engineering,
Madurai, Tamilnadu, India
karutharaja@gmail.com

***Abstract*—Biosensors are critical in medical diagnostics, environmental monitoring, and food safety, as they require great sensitivity and precision for biomolecule detection. This research presents a unique Triple Material Surrounding Gate (TMSG) TFET framework for biosensing that combines the benefits of multi-material gate architectures with surrounding gate designs. The suggested framework improves electrostatic control, reduces short-channel effects, and increases sensitivity to surface potential changes caused by biomolecular interactions. A thorough model is created to capture the device's subthreshold and threshold features, allowing for precise prediction of biosensing performance. The simulation findings validate the model, revealing the TMSG TFET's capacity to identify biomolecules with high sensitivity. This work not only enhances the design of TFET-based biosensors, but it also provides the groundwork for future experimental implementations, providing a road to compact, dependable, and high-performance biosensing devices.**

Keywords — Triple Material Surrounding Gate Tunnel FET (TMSG TFET); Biosensors; Poisson Equation; Threshold voltage; Sensitivity.

I. INTRODUCTION

Biosensors [1,2] are vital instruments utilized in many different applications. They have very high sensitivity and precision when detecting biomolecules. Compact and dependable biosensors are becoming more and more in demand. Tunnel Field-Effect Transistors (TFETs) [3-5] have attracted a lot of attention in the biosensing field because of their great subthreshold sensitivity and ultra-low power consumption. Because TFETs [6] use band-to-band tunneling for charge carrier transport, they operate better at lower operating voltages and have steeper subthreshold slopes than traditional MOSFETs. Because of this special mechanism, TFETs are ideal for identifying subtle biological signals.

Because of their reliable performance and known fabrication methods, conventional MOSFETs [7,8] have been used extensively. However, their sensitivity for detecting biomolecules at low concentrations is limited by their comparatively high subthreshold slope and power consumption. With their steeper subthreshold slopes made possible by band-to-band tunneling, Tunnel Field-Effect Transistors (TFETs) [9-11] have become viable substitutes for ultra-sensitive biosensing. Among these, planar and double-gate TFETs have demonstrated notable gains in detection sensitivity; nonetheless, issues like short-channel effects and poor electrostatic control frequently impair their functionality.

Although promising, current TFET-based biosensors [12-14] struggle to achieve the ideal sensitivity and selectivity needed for accurate biomolecule identification. Even while TFETs have benefits like extremely low power consumption and steep subthreshold slopes, problems like inadequate electrostatic control, short-channel effects, and restricted charge sensing capabilities frequently impair their performance. These drawbacks result from traditional TFET architectures' intrinsic design restrictions, which make it difficult to convert biomolecular interactions into detectable electrical signals. Because of this, these biosensors' sensitivity is frequently lowered, especially when detecting biomolecules at low concentrations. Innovative design techniques are necessary to overcome these obstacles in order to increase the precision of charge sensing mechanisms and the electrostatic interaction between biomolecules and the transistor surface.

Novel device architectures including Dual Material Gate (DMG) TFETs and Surrounding Gate (SG) TFETs [15,16] have been introduced to get around these restrictions. Triple Material Gate (TMG) TFETs are a recent development that adds a material to the gate stack to improve field tailoring and electrostatic coupling. Highly sensitive biosensors are now possible because to these developments. In comparison to traditional single-material designs, the Triple Material Surrounding Gate (TMSG) TFET [17] is a potential approach that provides better electrostatic control and fewer short-channel effects. TMSG TFETs are more sensitive to surface potential changes brought on by biomolecular interactions. They are therefore a perfect fit for applications requiring high-performance biosensing.

In this work, TMSG TFETs for biosensing applications are thoroughly analyzed through simulation. The device's crucial subthreshold and threshold features are captured by the suggested model, indicating that it can detect biomolecular interactions with great sensitivity. With the use of simulation findings and theoretical insights, this work attempts to improve the design of TFET-based biosensors and provide the groundwork for further experimental applications.

II. Model Description

A. Device Structure

Figure 1 depicts the schematic structure of the Triple Material Surrounding Gate (TMSG) TFET for biosensing applications, showing the novel arrangement of three gate materials (with distinct work functions) around the cylindrical channel. By establishing several tunneling routes, this triple-material design optimizes tunneling efficiency by introducing segmented electrostatic potential profiles along the channel. The encircling gate construction, covering the channel totally, enables improved gate control, eliminating short-channel effects and boosting sensitivity critical for biosensing applications.

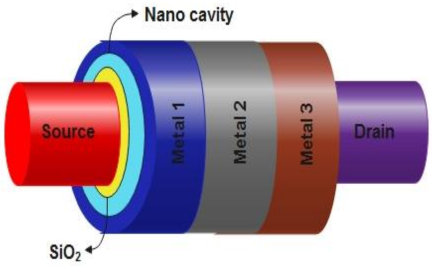

FIG: 1 PROPOSED TRIPLE MATERIAL SURROUNDING GATE TFET FOR BIOSENSING APPLICATIONS;

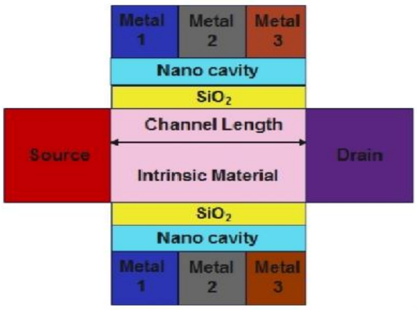

FIG: 2 PROPOSED TRIPLE MATERIAL SURROUNDING GATE TFET FOR BIOSENSING APPLICATIONS - SCHEMATIC CROSS SECTION VIEW

TABLE: 1 DESIGN SPECIFICATION OF NANOCAVITY EMBEDDED TMSG TFET

Quantities	Symbol	Value
Metal 1 work function (Cu)	ϕ_{m1}	4.5eV
Doping level of Source	N_A	10^{20} cm^{-3}
Metal 2 work function (Ti)	ϕ_{m2}	4.33eV
Thickness of the Oxide layer (SiO_2)	t_{equ}	2 nm
Metal 3 work function (Al)	ϕ_{m3}	4.2eV
Doping Concentration of Drain	N_D	10^{19} cm^{-3}
Thickness of Silicon body	2R	10 nm
Bio molecules Dielectric constant	K	1 - 10
Charge of the electron	Q	1.6 x 10^{-19} C
Length of the channel	L	25 nm

The TMSG TFET includes the integration of biosensing elements, such as nanocavity layers within the TMSG TFET. It allows the detection of biomolecules by changing the local dielectric environment or charge distribution near the channel. The surrounding gate's ability to maintain uniform control over the channel region ensures that even minute changes, caused by the interaction between the biomolecules and the nanocavity, are reflected as significant variations in the electrical output. Figure 2 illustrates the schematic cross sectional view of the proposed TMSG TFET for biosensing applications. The subthreshold slope, leakage current, and total current driving capability are all improved by the triple-material design. This guarantees a very sensitive instrument for biosensing that can identify low-concentration analytes with improved signal-to-noise ratios.

B. Design Specification

Table 1 list the design criteria taken into account for the analytical model of the nanocavity embedded DMSG TFET.

III. Results and Discussion

The surface potential profile for three different TFET types—TMSG, DMSG, and SMSG TFETs—as a function of channel length is shown in Fig. 3. Out of the three configurations, the TMSG TFET exhibits the highest surface potential, followed by the DMSG TFET and SMSG TFET. Due to the efficient modulation of the electric field brought about by the addition of triple materials to the gate, carrier tunneling at the source-channel interface is improved. The accuracy of the model is confirmed by the close match between the simulation results (symbols) and the analytical model (lines).

Because of improved electrostatic control by the gate, which enables effective tunneling, the TMSG TFET displays a greater surface potential. Because the electric field is distributed more evenly throughout the channel, the triple-material arrangement reduces SCEs. The enhanced electric field profile of TMSG TFET makes it superior to DMSG and SMSG TFETs for biosensing applications, since it is projected to have a higher sensitivity to biomolecular interactions. The TMSG TFET exhibits better electrostatic control and tunneling efficiency, with a 20% increase in surface potential over the DMSG TFET and a 50% improvement over the SMSG TFET.

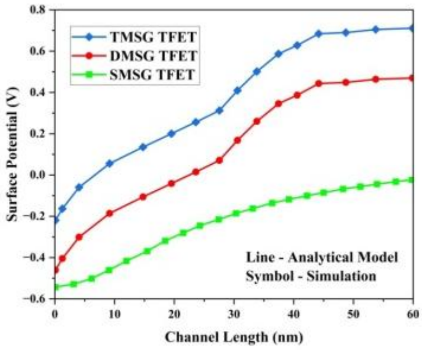

FIG. 3 SURFACE POTENTIAL PROFILES OF TMSG TFET, DMSG TFET AND SMSG TFET FOR BIOSENSING APPLICATIONS

The transfer characteristics (Drain Current vs. Gate Voltage) of the Triple Material Surrounding Gate (TMSG) TFET embedded in a nanocavity for different cavity thicknesses (T_C) are shown in Fig. 4. For a given gate voltage, the drain current falls as TC rises from 2 nm to 11 nm, especially in the subthreshold and transition regions. The electric field at the source-channel interface is strengthened by a narrower cavity (T_C=2nm), which increases the drain current and tunneling efficiency. In contrast, a thicker cavity

(T_C=11 nm) lowers the intensity of the electric field, which results in decreased current and tunneling rates. This analysis emphasizes how important it is to optimize the cavity thickness in order to achieve the intended performance in low-power and biosensing applications.

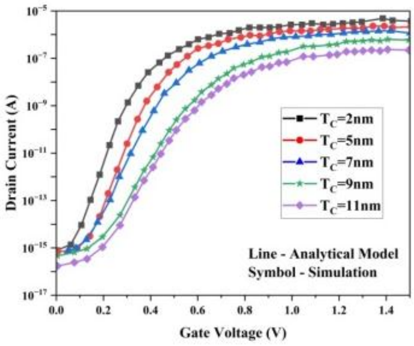

FIG. 4 TRANSFER CHARACTERISTICS OF TMSG TFET FOR DIFFERENT VALUES OF CAVITY THICKNESSES

The output characteristics of the nanocavity-embedded TMSG TFET for different oxide thicknesses (t_{ox}) are shown in the Fig. 5. Over the whole drain voltage range, the drain current falls as t_{ox} rises from 2 nm to 4 nm. Stronger gate control from a thinner oxide (t_{ox}=2nm) improves the electric field at the tunneling junction, raising the drain current and tunneling probability. On the other hand, a thicker oxide (t_{ox}=4nm) decreases gate control, which lowers the tunneling efficiency and the intensity of the electric field. This investigation highlights how reducing oxide thickness enhances device performance, increasing the TMSG TFET's suitability for biosensing and low-power applications.

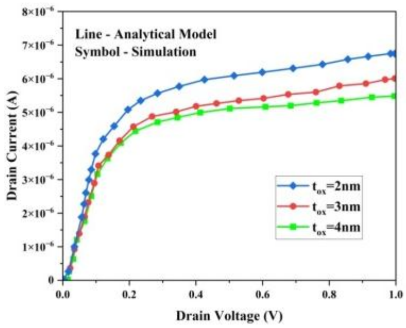

FIG. 5 TRANSFER CHARACTERISTICS OF TMSG TFET FOR DIFFERENT VALUES OF OXIDE THICKNESSES

In Fig. 6, for various biomolecules dielectric constants (k), the graph shows the surface potential of the nanocavity-embedded TMSG TFET as a function of lateral length. Because of improved gate control over the channel, the surface potential increases as the device's lateral length increases. As the coupling between the biomolecules and the gate electric field is strengthened by a higher k, a higher surface potential is the outcome. Better electrostatic channel modulation results from this, which enhances tunneling efficiency. The sensitivity of the surface potential to k demonstrates how well the instrument can identify biomolecules. This behavior shows how well suited the TMSG TFET is for biosensing applications, where changes in dielectric constants correspond to the presence or concentration of biomolecules.

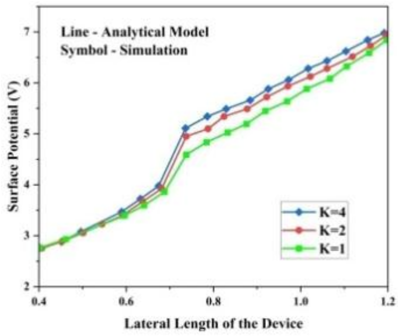

FIG. 6 SURFACE POTENTIAL PROFILE OF TMSG TFET FOR VARIOUS DIELECTRIC CONSTANT VALUES

The Fig. 7 displays the nanocavity-embedded TMSG TFET's transfer characteristics (Drain Current vs. Gate Voltage) for a range of biomolecules filling factor ratios. Stronger gate control causes improved tunneling at the source-channel contact, which raises the drain current as the gate voltage rises. Since additional biomolecules enhance the electric field coupling in the nanocavity, a higher drain current results from an increase in the biomolecules filling factor in the nanocavity region. This increases device sensitivity and tunneling efficiency. The observed behavior, where the filling factor directly affects the device's output, shows the potential of the TMSG TFET for biomolecules detection. Because of this, the device is ideal for biosensing applications that need accurate biomolecules detection and quantification.

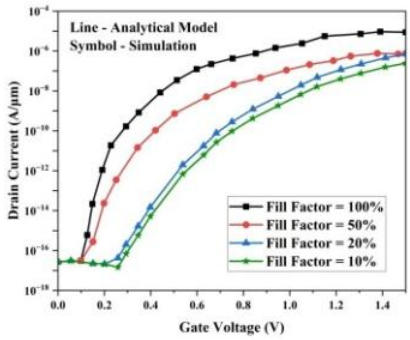

FIG. 7 TRANSFER CHARACTERISTICS OF TMSG TFET FOR DIFFERENT VALUES OF BIOMOLECULES FILLING FACTOR

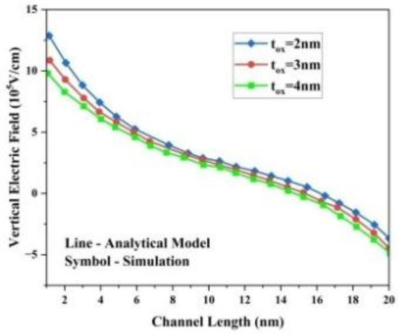

FIG. 8 THE VERTICAL ELECTRIC FIELD VERSUS CHANNEL LENGTH OF THE TMSG TFET FOR VARIOUS OXIDE THICKNESSS

For varying oxide thicknesses (t_{ox}), the Fig. 8 shows the vertical electric field as a function of channel length for the nanocavity-embedded TMSG TFET. Due to a decrease in gate impact along the extended channel, the vertical electric field diminishes as the channel length grows. In a similar vein, the gate control is weakened by increasing oxide thickness, which further reduces the vertical electric field.

The electric field is enhanced by a stronger gate-to-channel coupling when the t_{ox} is thinner, and it is diminished when the t_{ox} is thicker. For the device to manage carrier tunneling, the vertical electric field is essential. These findings highlight the necessity of optimizing oxide thickness in order to preserve effective electrostatic control and enhance the performance of the TMSG TFET in low-power and biosensing applications.

IV. Conclusion and Future work

Triple Material Surrounding Gate (TMSG) TFET structure reported in this work represents a substantial development in biosensing technology. By merging multi-material gate topologies with surrounding gate designs, the TMSG TFET delivers enhanced electrostatic control, reduced short-channel effects, and heightened sensitivity to biomolecular interactions. These enhancements overcome the constraints of traditional TFET-based biosensors, allowing for the detection of low-concentration biomolecules with excellent precision. The construction of a thorough analytical model improves the framework's applicability by providing a computationally efficient tool for predicting device performance under diverse scenarios. Simulation results support the model's reliability and adaptability to real-world biosensing conditions. This study illustrates the promise of TMSG TFETs as a transformational technology for high-performance biosensing, paving the way for more compact, energy-efficient, and cost-effective solutions.

Future research will concentrate on experimentally validating the TMSG TFET architecture, optimizing fabrication processes, and investigating its interaction with other sensing technologies. Extending the analytical model to include more sophisticated biosensing scenarios, such as multiple analyte detection and dynamic biomolecular interactions, will increase its usefulness. By tackling these problems, this research contributes to the larger goal of improving semiconductor-based biosensors, resulting in more accurate and accessible diagnostic instruments for medical, environmental, and food safety applications. The TMSG TFET framework is a promising platform for next-generation biosensor development, filling the gap between theoretical innovation and practical application.

Acknowledgment

This research work in financially supported by Thiagarajar Research Fellowship (TRF) scheme - (File.no: TCE/RD/TRF/01 dated Jan-2023 and File.no: TCE/RD/TRF/05 dated July-2023.

We also extend our heartfelt thanks for the financial support provided through the TCE Seed Money Scheme (TCE-SMS) (File No. R&D/Seedmoney/2024/8), which has been instrumental in the successful execution of this study.

References

[1] J. Basu and C. RoyChaudhuri, "Attomolar Sensitivity of FET Biosensor Based on Smooth and Reliable Graphene Nanogrids," in IEEE Electron Device Letters, vol. 37, no. 4, pp. 492-495, April 2016, doi: 10.1109/LED.2016.2526064.

[2] A. Ahmadi, S. Kabiri and K. Omidfar, "Advances in HbA1c Biosensor Development Based on Field Effect Transistors: A Review," in IEEE Sensors Journal, vol. 20, no. 16, pp. 8912-8921, 15 Aug.15, 2020, doi: 10.1109/JSEN.2020.2987836.

[3] Mohanty, A., Ahmad, M.A., Kumar, P. et al. Performance Analysis and Design Comparison of Junctionless TFET: a Review Study. Silicon 16, 6305–6312 (2024). https://doi.org/10.1007/s12633-024-03167-6.

[4] Jagadesh Kumar Mamidala; Rajat Vishnoi; Pratyush Pandey, "Simulation of TFETs," in Tunnel Field-effect Transistors (TFET): Modelling and Simulation , Wiley, 2017, pp.181-193, doi: 10.1002/9781119246312.ch8.

[5] Rui Chen, Huiyong Hu, Xinlong Shi, Ruizhe Han, Peijian Zhang, Tao Liu, Liming Wang, Design and application of germanium based complementary TFET devices with step tunneling paths, Microelectronics Journal,Volume 150, 2024, 106136, https://doi.org/10.1016/j.mejo.2024.

[6] Jagadesh Kumar Mamidala; Rajat Vishnoi; Pratyush Pandey, "Modelling the surface potential in TFETs," in Tunnel Field-effect Transistors (TFET): Modelling and Simulation, Wiley, 2017, pp.90-139, Doi: 10.1002/ 9781119246312.ch5.

[7] R. Gautam, M. Saxena, R. S. Gupta and M. Gupta, "Numerical Model of Gate-All-Around MOSFET With Vacuum Gate Dielectric for Biomolecule Detection," in IEEE Electron Device Letters, vol. 33, no. 12, pp. 1756-1758, Dec. 2012, doi: 10.1109/LED.2012.2216247.

[8] Ajay, R. Narang, M. Saxena and M. Gupta, "Drain Current Model of a Four-Gate Dielectric Modulated MOSFET for Application as a Biosensor," in IEEE Transactions on Electron Devices, vol. 62, no. 8, pp. 2636-2644, Aug. 2015, Doi: 10.1109/TED.2015. 2441753.

[9] T. S. A. Samuel, N. B. Balamurugan, S. Sibitha, R. Saranya, and D. Vanisri, “Analytical Modeling and Simulation of Dual Material Gate Tunnel Field Effect Transistors,” Journal of Electrical Engineering and Technology, vol. 8, no. 6. The Korean Institute of Electrical Engineers, pp. 1481–1486, 01-Nov-2013.

[10] H. K. Phulawariya, R. Chaudhary, S. Tiwari and R. Saha, "Realization of Logic Performance using Double Gate TFET (DG-TFET) and Ge source DG-TFET (s-Ge-TFET)," 2023 3rd International conference on Artificial Intelligence and Signal Processing (AISP), VIJAYAWADA, India, 2023, pp. 1-5, doi: 10.1109/AISP57993.2023.10134840.

[11] Ebrahimnia, M., Ziabari, S.A.S. & Kiani-sarkaleh, A. Analytical Modeling for a New Structure of Dielectric Pocket-Based Dual Material Double Gate TFET with Gate Oxide Stack. Silicon 15, 3215–3224 (2023). https://doi.org/10.1007/s12633-022-02229-x

[12] Choudhury, S.; Baishnab, K.L.; Guha, K.; Jakši´c, Z.; Jakši´c, O.; Iannacci, J. Modeling and Simulation of a TFET-Based Label-Free Biosensor with Enhanced Sensitivity. Chemosensors 2023, 11, 312.https://doi.org/10.3390/chemosensors11050312.

[13] R. Goswami and B. Bhowmick, "Comparative Analyses of Circular Gate TFET and Heterojunction TFET for Dielectric-Modulated Label-Free Biosensing," in IEEE Sensors Journal, vol. 19, no. 21, pp. 9600-9609, 1 Nov.1, 2019, doi: 10.1109/JSEN.2019.2928182.

[14] Y. Wang, C. Li, O. Li, S. Cheng, W. Liu and H. You, "Simulation Study of Dual Metal-Gate Inverted T-Shaped TFET for Label-Free Biosensing," in IEEE Sensors Journal, vol. 22, no. 19, pp. 18266-18272, 1 Oct.1, 2022, doi: 10.1109/JSEN.2022.3195180.

[15] I. Chahardah Cherik and S. Mohammadi, "Vertical Tunneling Field-Effect Transistor With Germanium Source and T-Shaped Silicon Channel for Switching and Biosensing Applications: A Simulation Study," in IEEE Transactions on Electron Devices, vol. 69, no. 9, pp. 5170-5176, Sept. 2022, DOI: 10.1109/TED. 2022.3189326.

[16] E. Rajalakshmi; N.B. Balamurugan, "A New Perspective on Sensitivity for Biosensing Applications in Nanocavity-Embedded Dual Metal Surrounding Gate TFETs", 2023 International Conference on Research Methodologies in Knowledge Management, Artificial Intelligence and Telecommunication Engineering (RMKMATE), Jan 2024.

[17] P. Vanitha, N. B. Balamurugan, & G. Lakshmi Priya (2015). Triple Material Surrounding Gate (TMSG) Nanoscale Tunnel FET-Analytical Modeling and Simulation. JOURNAL OF SEMICONDUCTOR TECHNOLOGY AND SCIENCE, 15(6), 585-593.

Efficient FPGA based Modular Inversion Over $GF(2^m)$ Using Optimized x^{16} Units

J.Adline Vidhya
Dept. of ECE,
Thiagrarajar College of Engineering,
Madurai, India
adline@student.tce.edu

V .Vinoth thyagarajan
Dept. of ECE,
Thiagrarajar College of Engineering,
Madurai, India
vinoth.thyagu@gmail.com

V.R. Venkatasubramani
Dept. of ECE,
Thiagrarajar College of Engineering,
Madurai, India
venthiru@tce.edu

S. Rajaram
Dept. of ECE,
Thiagrarajar College of Engineering,
Madurai, India
rajaram_siva@tce.edu

***Abstract*— Elliptic Curve Cryptography (ECC) and other cryptographic applications require the computationally demanding process of finite-field inversion, or FF-inversion. ECC is widely recognized for its efficiency and robustness, requiring hardware architectures that are compact, energy-efficient, and capable of high-speed processing. Among the available methods for FF-inversion, the Itoh-Tsujii Algorithm (ITA) and the Extended Euclidean Algorithm are the most commonly used. ITA, in particular, has been implemented in various optimized forms, such as squarer-ITA, parallel squarer-ITA, and quad-ITA, to enhance performance. This work introduces an improved FF-inversion architecture that leverages a novel Hex Itoh-Tsujii Algorithm (H-ITA) designed for efficient FPGA deployment. The proposed approach utilizes a dedicated power-8 hex block to eliminate the need for 4k-exponentiation, streamlining computations and reducing complexity. By incorporating quad addition chains, the design further optimizes resource utilization and reduces the clock cycle count to 24. The architecture is specifically tailored for binary fields over NIST-recommended irreducible trinomials $GF(2^{233})$ and demonstrates exceptional performance across FPGA platforms, including Virtex-4, Virtex-5, and Virtex-7. Performance evaluations show significant gains in area-delay product, resource efficiency, and overall throughput compared to prior designs. With its efficient handling of scalar multiplication and other ECC operations, the proposed architecture offers a scalable, high-performance solution ideal for secure cryptographic applications in constrained environments**.

Keywords—Finite-Field Inversion (FF-Inversion),Elliptic Curve Cryptography (ECC) Itoh-Tsujii Algorithm (ITA) Hex Itoh-Tsujii Algorithm (H-ITA)

I. INTRODUCTION

Finite-field inversion is crucial in cryptographic algorithms like ECC, impacting performance. The ITA, based on Fermat's Little Theorem, is more efficient than the EEA, especially for FPGA implementations [1][2]. Evolving from square to quad-blocks, ITA reduces iterative steps and improves FPGA resource utilization [3][4]. This work proposes a high-speed Itoh-Tsujii algorithm (HS-ITA) using x^{16^n} units, reducing clock cycles from 27 to 24. Implemented on a Virtex-5 FPGA, the design demonstrates reduced latency, higher speed, and efficient resource use [5]. The paper is organized as follows: Section 2 discusses the existing HS-ITA method, Section 3 introduces the proposed architecture, Section 4 covers algorithm reformulation, Section 5 focuses on hardware implementation, and Section 6 presents experimental results, concluding with Section 7 on the design's suitability for cryptographic applications.

II. PRELIMNARIES

Finite fields, or Galois fields, are fundamental in areas such as network coding, cryptography, and error control theory [9]. Among these, binary fields $GF(2^m)$ are preferred over prime fields GF(p) because of their carry-free arithmetic and suitability for hardware implementation. In $GF(2^m)$, operations like addition and multiplication are performed using logical XOR and AND gates, respectively, enabling efficient hardware-based designs [10]. To construct $GF(2^m)$, an irreducible polynomial R(x) of degree m is used, defined as

$$R(x) = x^m + r_{m-1}x^{m-1} + \cdots + r_1 x + 1 \qquad (1)$$

where$r_i \in GF(2)$ for $1 \leq i \leq m.$

The polynomial basis of representation is given by the set $1, \beta, \beta^2, \dots, \beta^{m-1}$, where β is a root of R(x). An element$A \in GF(2^m)$in polynomial basis is expressed as

$$A = \sum_{i=0}^{m-1} a_i \beta^i \qquad (2)$$

Inversion in $GF(2^m)$ can be computed using Fermat's Little Theorem (FLT), which states that for any nonzero element a, its multiplicative inverse is making the method computationally intensive.

$$a^{-1} \equiv a^{2^m-2} \qquad (3)$$

This involves (m−2)multiplications and (m−1) squarings, with the expansion given by

$$a^{2^m-2} = a^{2^1} \cdot a^{2^2} \cdots a^{2^{m-1}}. \qquad (3)$$

To reduce the cost, the Itoh-Tsujii Algorithm (ITA) introduces an efficient method using addition chains [1]. An addition chain for m−1 is a sequence $U = \{u_1, u_2, \dots, u_c\}$, where

$$u_i = 1, u_c = m-1, u_i + u_j = k \; for \; 1 \leq j, k < i \qquad (5)$$

and each intermediate term is the sum of previous terms: The ITA computes inversion recursively with and uses the relation

$$\gamma_q(a) = a^{2^q-1} \quad (6)$$

$$\gamma_{p+q}(a) = (\gamma_p(a))^{2^q} \cdot \gamma_q(a) \quad (7)$$

The final inverse is computed as

$$a^{-1} = (\gamma_{m-1}(a))^2. \quad (8)$$

This method requires (m−1)squarings and approximately $\lfloor 2log_2(m-1)\rfloor + H(m-1) - 1$ multiplications, where$H(m-1)$ is the Hamming weight of m−1[25].To optimize further, Brauer proposed an addition chain based on the binary representation of m−1. If mi=0 then $u_i = 2u_{i-1}$; if ; if mi=1, then $u_{i+1} = u_i + u_1$. For instance, the binary form $\langle 11000000\rangle_2$ for 192 produces the chain {1, 2, 3, 6, 12, 24, 48, 96, 192}. This approach is especially effective for inversion in GF(2^{193}), reducing computational complexity in cryptographic applications [12]. Table 1 illustrates quad addition chains for different trinomial fields.

III. Efficient Algorithm for Modular Inversion in GF(2^M)

Modular inversion in binary finite fields GF (2^m) is an essential operation in cryptographic protocols, especially in elliptic curve cryptography. Traditional methods rely on Fermat's Little Theorem, which expresses modular inversion as:

$$x^{-1} = x^{2^m-2} = x^{2^{m-1}+2^{m-2}+\cdots+2^1+2^0} mod 2^m. \quad (9)$$

This approach typically requires m−2 modular multiplications, along with pre computation of intermediate powers such as $x^{2^{m-2}}, x^{2^{m-3}}, \ldots, x^{2^1}$, and x. Although effective, inversion becomes costly for large m due to increased latency and hardware usage. To overcome this, techniques like Iterative Temporal Accumulation (ITA) and its improved form, Iterative Temporal Inversion Algorithm (ITIA), reduce modular multiplications [7].

TABLE 1 Quad Addition Chain For GF(2^M) ;M=193,233,409

Field (m)	Brauer addition chain
193	{1,2,3,6,12,24,48,96,192}
233	{1,2,3,6,7,14,28,29,58,116,232}
409	{1,2,3,6,12,24,25,50,51,102,204,408}

ITA optimizes the process by breaking down powers of two, lowering the multiplication count to : $\lfloor log_2(m-1)\rfloor + H(m-1) - 1$, where $H(m-1)$ is the Hamming weight of m−1.The **Iterative Temporal Inversion Algorithm (ITIA)** extends ITA by leveraging 4n-block structures for enhanced efficiency. The decomposition is given by:

$$4^{s-1} = \left(4^{\frac{s}{2}} - 1\right)\left(4^{\frac{s}{2}} + 1\right) \; if \; s \; is \; even$$

$$4\left(4^{\frac{s-1}{2}} - 1\right)\left(4^{\frac{s-1}{2}} + 1\right) + 3 \; if \; s \; is \; odd \quad (10)$$

For the NIST-recommended field GF(2^{163}), the modular inversion is reformulated as:

$$x^{-1} = x^{2^{163}-2} = x^{2(2^{162}-1)} = x^{2(4^{81}-1)} = x^{2\{4(4^{40}+1)\cdot(4^{20}+1)\cdot(4^{10}+1)\cdot(4^5+1)[4(4^2+1)(4+1)+3]+3)} \quad (11)$$

The ITIA approach uses **six** 4^n **blocks** to compute thinverse and incorporates a precomputation register to store x [3]. Intermediate terms $x^{4^2}, x^{4^5}, x^{4^{10}}, x^{4^{20}}, x^{4^{40}}$ are calculated in advance. The final squaring completes the inversion, requiring only **18 clock cycles** for implementation in GF(2^{163}).[8]

IV. Optimized Modular Inversion For GF(2^M) Using 16^N Block Structure

This work presents an enhanced high-speed modular inversion method leveraging 16^n-block decomposition to improve efficiency over traditional 2^n-block architectures. The modular inversion in the binary field GF(2^{233}) is expressed as:

$$x^{-1} = x^{2^{233}-2} = x^{2(2^{232}-1)} = x^{2(16^{58}-1)} = \\ = x^{2\{16(16^{29}+1)\cdot(16^{14}+1)\cdot(16^7+1)\cdot(16^3+1)[16(16^1+1)+15]+15)} \quad (12)$$

This method requires six 16 ^{n}-block operations, facilitated by a pre-computation register to store the intermediate value. The inversion process is finalized with a squaring step. Precomputed terms such as further reduce the computation load, ensuring that the number of clock cycles is primarily determined by the required multiplications. ($x^{16^{29}}, x^{16^{14}}, x^{16^7}, x^{16^3}, x^{16^1}$). In total, the modular inversion over GF(2^{233}) is achieved in just **24 clock cycles**, offering a significant improvement in speed and efficiency.

V. High Speed Modular Inversion Algorithm utilizing 16^N Block

The modular inversion algorithm based on ITIA principles over GF(2^m)uses two core operations that simplify computation and optimize hardware [7]. The first computes $x^{(16^n+1)a}$ by exponentiating x^a to the 16^n, then multiplying it with$\boldsymbol{x^a}$ using XOR operations. The second derives $x^{(2a+1)}$ by squaring $\boldsymbol{x^a}$ using a 16-based hex unit and multiplying it with x. These operations are efficiently implemented using XOR gates and wire connections, reducing hardware complexity. The inversion sequence adapts to the field size mmm, and for GF(2^{233}), follows a 16n-based pattern (Algorithm 1) to reduce modular inversion overhead .

VI. Hardware Implementation Of High Speed ITA For GF(2^{233})

The HS-ITA architecture utilizes multiplexers (two 4:1, a 2:1, and an 8:1) to optimize operations. Input xxx is processed through a 4:1 multiplexer and sent to the squarer via the 8:1 multiplexer. In the subsequent cycle, the squared value is cubed and stored for future use, enhancing efficiency. To overcome performance limitations of the LCC-ITA design, HS-ITA introduces a two-stage pipelined design, splitting complex logic into two stages and allowing simultaneous modular inversion. For GF(2^{33}), inversion clock cycles are reduced to 23 by optimizing with a 16 ^{n}based power block, replacing 4n operations for faster performance. The improved control table, shown in Table 3, significantly reduces clock cycles by incorporating optimizations for controlling high powers of a variable. This design reduces computation time from 32 to 24 cycles, demonstrating enhanced efficiency.

TABLE 2 ALGORITHM FOR HS-ITA USING 16^N UNITS

Steps	Operation	Output
1	u < - a*a	$\mathbf{a^2}$
2	v < - u*a	$\mathbf{a^3}$ (p)
3	u < - v* $\mathbf{4^1}$	$\mathbf{a^{12}}$
4	v < - u*v	$\mathbf{a^{15}}$
5	u < - v* $\mathbf{4^1}$	$\mathbf{a^{60}}$
6	v < - u*p	$\mathbf{a^{63}}$
7	u < - v* $\mathbf{16^1}$	$\mathbf{a^{1008}}$
8	u < - u* $\mathbf{4^1}$	$\mathbf{a^{4032}}$
9	v < - u*v	$\mathbf{a^{4095}}$
10	u < - v* $\mathbf{4^1}$	$\mathbf{a^{16380}}$
11	v < - u*p	$\mathbf{a^{16383}}$
12	u < - v* $\mathbf{16^3}$	$\mathbf{a^{67104768}}$
13	u < - u* $\mathbf{4^1}$	$\mathbf{a^{268419072}}$
14	v < - u*v	$\mathbf{a^{7.205 *10^{16}}}$
15	u < - v* $\mathbf{16^7}$	$\mathbf{a^{7.205 *10^{16}}}$
16	v < - u*v	$\mathbf{a^{2.88 *10^{17}}}$
17	u < - v* $\mathbf{4^1}$	$\mathbf{a^{2.88 *10^{17}}}$
18	v < - u*p	$\mathbf{a^{2.07 *10^{34}}}$
19	u < - v* $\mathbf{16^{14}}$	$\mathbf{a^{8.3 *10^{34}}}$
20	u < - u* $\mathbf{4^1}$	$\mathbf{a^{8.3 *10^{34}}}$
21	v < - u*v	$\mathbf{a^{8.3 *10^{34}}}$
22	u < - v* $\mathbf{16^{29}}$	$\mathbf{a^{6.8 *10^{69}}}$
23	v < - u*v	$\mathbf{a^{6.8 *10^{69}}}$
24	u < - final squaring	$\mathbf{a^{1.3 *10^{70}}}$

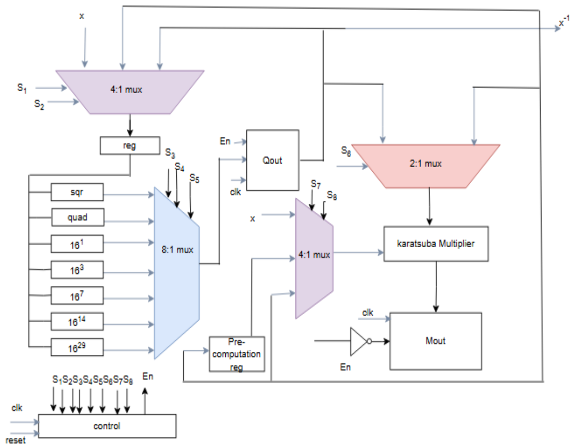

FIG 1 HIGH SPEED ITA ARCHITECTURE FOR GF(2^{233})

VII. FPGA IMPLEMENTATION AND SYNTHEIS RESULTS FOR GF (2^{233})

The proposed design's efficiency is evaluated based on clock cycles, Look-Up Tables (LUTs), and clock period, with performance def ined as

$$P = \frac{1}{No.of LUTs \times T}$$

By utilizing precomputed 16^n blocks, the design achieves modular inversion in 24 clock cycles, significantly reducing the area-delay product and improving performance.It outperforms prior implementations on all FPGA platforms: a 4.7% improvement on Virtex-4, 2.6% on Virtex-5, and 7.5% on Virtex-7. The HS-ITA architecture also reduces hardware complexity by minimizing interconnection overhead and simplifying control logic, making it ideal for cryptographic systems and applications requiring efficient modular arithmetic over GF(2m) [23-26].

TABLE 3 COMPARISON OF OTHER WORKS WITH PROPSED ARCHITECTUREOVER THE FIELD OF GF(2^{233})

Works	Device	LUT	Fmax	Clock	Delay (ns)	Time (ns)	Performance
(13)	virtex-4	26122	97.08	30	10	309	123.8
(13)	virtex-4	27897	98.09	36	10	367	97.6
(14)	virtex-4	23734	71.87	23	14	320	131.6
(15)	virtex-4	14982	-	91	10	896.8	74.4
(16)	virtex-4	24713	100	29	10	290	139.5
(17)	virtex-4	20988	213.84	58	5	271	175.8
(18)	virtex-4	19414	-	26	11	287.3	179.2
(19)	virtex-4	22917	-	23	12	273	159.8
(12)	virtex-4	17512	90.90	32	11	352	162.2
(20)	virtex-4	21464	73.71	30	14	407	114.4
Proposed	virtex-4	19036	100.002	24	10	240	218.8
(13) QITA	virtex-5	20950	128.75	30	7.76	233	204.8
(13) SITA	virtex-5	21379	141.02	33	7.09	234	199.8

(14)	virtex-5	16256	109	23	9.17	211	291.5
(16)	virtex-5	18151	134.4	29	7.44	215.7	255.4
(19)	virtex-5	15956	-	23	8.08	186	336.9
(12)	virtex-5	11399	111.1	32	9	288	304.6
(20)	virtex-5	13962	109.31	27	9	247	289.9
(21)	virtex-5	10990	-	47	6.6	312	291
Proposed	virtex-5	13956	135.151	24	7.399	207.172	404.01
(13)	virtex-7	20252	139.2	30	7.7	233	211.9
(16)	virtex-7	18997	144.0	29	7	201	261.8
(21)	virtex-7	17472	154.3	28	6.46	181	315.54
Proposed	virtex-7	18408	174.856	24	5.719	137.25	395.8

VIII. Conclusion

This study presents a hardware implementation for modular inversion over GF(2^{233}) using 16^n blocks on FPGA, optimizing clock cycles, resource use, and efficiency. The design reduces clock cycles and critical path delay compared to squarer-based architectures, improving throughput and minimizing area-delay product. By balancing LUTs, clock frequency, and processing cycles, it is ideal for cryptographic applications on resource-constrained FPGA platforms, setting a benchmark for high-performance modular inversion.

IX. Acknowledgment

The authors extend their due thanks to the Thiagarajar College of Engineering management, Madurai, India for their extensive research facilities and the financial backing from Thiagarajar Research Fellowship (TRF) scheme (File.no:TCE/RD/TRF/2024/12/dated 09-02-2024) is gratefully acknowledged .

Reference

[1] Itoh, T. and Tsujii, S., “A Fast Algorithm for Computing Multiplicative Inverses in GF(2^m) Using Normal Bases,” *Information and Computation*, 1990

[2] Agnew, G.B., Beth, T., and Mullin, R.C., “An Implementation of Elliptic Curve Cryptosystems over GF(2^m),” *IEEE Journal on Selected Areas in Communications*, 1993.

[3] Paar, C., “Efficient VLSI Architectures for Bit-Parallel Computation in Galois Fields,” *IEEE Transactions on Computers*, 1994.

[4] Bajard, J.C., et al., “Optimal Table Size for Pre-computation of Galois Field Multiplication,” *ACM Transactions on Embedded Computing Systems*, 2015.

[5] Wang, D., et al., “An Improved ITA for Efficient Modular Inversion in GF(2^m),” *Springer Journal of Cryptographic Engineering*, 2023.

[6] Morales-Sandoval, M., et al., “Compact FPGA Architectures for ECC with Optimized Inversion Using ITA,” *IEEE Transactions on Circuits and Systems II*, 2021.

[7] Hu, J., Guo, W., Wei, J., and Cheung, R. C. C., "Fast and generic inversion architectures over GF(2^m) using modified Itoh-Tsujii algorithms," *IEEE Trans. Circuits Syst. II Express Briefs*, vol. 62, no. 4, pp. 367–371, 2015.

[8] Kalaiarasi, S., "High-Speed Inversion Using x4nx^{4^n}x4n Units," in *Advances in Communication Systems and Networks*, Lecture Notes in Electrical Engineering, vol. 688, pp. 497–506, Springer, 2020.

[9] D. Hankerson, AJ. Menezes, S. Vanstone, Guide to Elliptic Curve Cryptography, Springer Science & Business Media, 2006.

[10] E. Wenger, M. Hutter, Exploring the design space of prime field vs. binary field ECC-hardware implementations, in: Nordic Conference on Secure IT Systems, Springer, Berlin, Heidelberg, 2011, pp. 256–271.

[11] F. Rodriguez-Henriquez, *et al.*: “Parallel Itoh-Tsujii multiplicative inversion algorithm for a special class of trinomials,” Designs, Codes and Cryptography **45** (2007)

[12] Nadikuda, Pradeep & Boppana, Lakshmi. (2022). An area-efficient architecture for finite field inversion over GF(2m) using polynomial basis. Microprocessors and Microsystems. 89. 104439. 10.1016/j.micpro. 2022.104439

[13] C. Rebeiro, *et al.*: “Revisiting the Itoh-Tsujii inversion algorithm for FPGA platforms,” IEEE Trans. Very Large Scale Integration (VLSI) Syst. 19 (2011) 1508

[14] S.S. Roy, *et al.*: “Generalized high speed Itoh-Tsujii multiplicative inversion architecture for FPGAs,” Integration (2012) 307

[15] J. Hu, *et al.*: “Fast and generic inversion architectures over GF(2m) using modified Itoh-Tsujii algorithms,” IEEE Trans. Circuits Syst. II, Exp. Briefs **62** (2015).

[16] V.R. Venkatasubramani, *et al.*: “An improved quad Itoh-Tsujii algorithm for FPGAs,” IEICE Electron. Express **10** (2013)

[17] B. Rashidi, *et al.*: “High-speed hardware implementation of Gaussian normal basis inversion algorithm over F2m,” Microelectronics Journal **63** (2017) 138

[18] M. Kalaiarasi, *et al.*: “A parallel quad Itoh-Tsujii multiplicative in- version algorithm for FPGA platforms,” Third ISEA Conference on Security and Privacy (ISEA-ISAP) (2020)

[19] Kalaiarasi, M. & Vr, Venkatasubramani & Rajaram, Sivasubramanian: A Hex Itoh-Tsujii inversion algorithm for FPGA platforms,In: IEICE Electronics Express. 18. 10.1587/elex.18.20210108 India (2021),

[20] B. Rashidi, Efficient hardware structure for extended euclidean-based inversion over, IET Comput. Digit. Tech. 13 (4) (2019) 282–291.

[21] C. Rebeiro, SS. Roy, D. Mukhopadhyay, Pushing the limits of high-speed GF($2m$) elliptic curve scalar multiplication on FPGAs, in: CHES 2012 Cryptographic Hardware and Embedded Systems Conference, Springer, Berlin, Heidelberg, 2012, pp. 494–511.

[22] C. Rebeiro, D. Mukhpodhyay, Power attack resistant efficient FPGA architecture for karatsuba multiplier, in: VLSID 2008 21st International Conference on VLSI Design, Hyderabad, 2008, pp. 706–711, http:// dx.doi.org/10.1109/VLSI.2008.65

[23] A. Sanjana, V. R. Venkatasubramani, S. Rajaram, M. Kalaiarasi, M. S. K. Manikandan and V. V. Thyagarajan,: An Improved Octet Itoh-Tsujii Algorithm for FPGA Platforms,In: 2023 International Conference on Energy, Materials and Communication Engineering (ICEMCE), pp. 1-5, Madurai, India, (2023)

[24] P. Zode, *et al.*: "Fast architecture of modular inversion using Itoh- Tsujii algorithm," International Symposium on VLSI Design and Test (2017)

[25] J. Li, *et al.*: "A fast modular inversion FPGA implementation over GF(2m) using modified x2n unit," IEEE International Symposium on Circuits and Systems (ISCAS) (2018)

[26] J. Guajardo, *et al.*: "Fast inversion in composite Galois fields GF ((2/sup n)/sup m/)," Proceedings in IEEE International Symposium on Information Theory (1998).

A Skin-Mountable Antenna for Ultra-Flexible RF Biotelemetry Applications

Sherene Jacob
Department of ECE,
Thiagarajar College of Engineering,
Madurai, Tamil Nadu, India
sherenebenju@gmail.com

Vasudevan Karuppiah
Department of ECE,
Thiagarajar College of Engineering,
Madurai, Tamil Nadu, India
kvasudevan@tce.edu

Meenambal Bose
Department of ECE,
Thiagarajar College of Engineering,
Madurai, Tamil Nadu, India
meenambal.me@gmail.com

***Abstract*— This paper explains a skin-mountable antenna for temporary wearable application operating at 3.5 GHz and 6 GHz. The antenna is designed on flexible PDMS (polydimethylsiloxane) due to its flexibility. The antenna has a peak gain of 5.3 dB at 3.5 GHz and 8.2 dB at 5.9 GHz for efficient wireless communication. The work also concentrates in optimizing the input power to ensure low Specific Absorption Rate (SAR). The work has optimized the input power to 95 mW of input power to meet the safety standard for human exposure that is 1.6 W/Kg for SAR. The antenna can be used for single-use purpose, making it ideal for disposable medical monitoring system and skin wound sensors.**

Keywords*— *Skin-Mountable Antenna, Low-SAR, Flexible-Antenna

I. Introduction

Wearable antenna plays an important role in health monitoring and wireless communication systems for real-time data transfer [1]. They help in continuous data collection in applications such as remote patient monitoring, biotelemetry, fitness tracking, and military applications [2]. There is an increasing demand for compact, efficient, and safe designs of antennas working at higher frequencies such as 3.5 GHz and 5.9 GHz. This frequency has gained commercial attention over the traditional 2.45 ISM band for biotelemetry. The commercial antennas might include for fitness tracking, WiFi connections, 5G networks, etc.

The antenna performance of any wearable system is greatly influenced by the choice of substrate. Commonly, substrates such as textile fabrics [3], flexible polymers [4], and elastomers [5] are used. These substrates offer degrees of flexibility but suffer from a great number of drawbacks. This might include the deformation of the antenna under movement of the user and high SAR values near the body of the user. This creates an impedance mismatch and degrades the performance of the antenna [6],[7]. Also, the textile antennas can lose sensitivity when they are wrinkled or compressed and this leads to unstable wireless communication.

This paper presents an antenna to operate on the vicinity of the human body and the structure can be aesthetically modified according to the requirement. This can either be the logo of a brand or the structure that the user requires [8]. The antenna is designed for 3.5 GHz and 5.9 GHz and employs PDMS substrate (polydimethylsiloxane). This substrate is soft and biocompatible elastomer, comforts, sorry, conforms smoothly to the surface of the skin. The SAR limit established by the FCC, Federal Communication Commission, is 1.6 watts per kg for 1 gram or 10 g of tissue. So, the design concentrates on maintaining a SAR value less than the prescribed limit [9], [10].

The isolation layer is introduced between the antenna and the skin. This limits the near-field interaction with the tissue and hence it keeps the specific absorption rate below 1.6 W/Kg at an input power of 95 mW. This is well within the established safety limit. In spite of the low SAR, the antenna delivers a strong radiation performance and achieves a gain of 5.3 dB and 8.2 dB at 3.5 GHz and 5.9 GHz respectively.

The innovation of the work lies in the use of aesthetic designs [11],[12], integrating visual appealing structures for engineering functionality. The antenna shape mimics structures that might be emblems, logos or customized design required by the user. This enables it to blend unobtrusively with clothing, medical equipment, and accessories. The simulation result validates the performance of the proposed antenna, maintains a constant impedance matching, and has low SAR and a robust communication even when mounted directly on skin. The compact footprint area, flexibility, and user-friendly design addresses many limitations faced by the conventional wearable antennas. This provides a balanced safety, efficiency, aesthetics, and comfort suitable for a wearable antenna.

II. Skin-Mountable Antenna

The designed antenna in this work is designed on PDMS substrate. PDMS is known for its flexibility and biocompatibility. It is well suited for durable applications. The PDMS layer has a thickness of 0.1 mm. This is necessary for softness and comfort and prolonged skin contact. The ultra-thin substrate enables the antenna to conform closely with the skin and maintain a low profile. The relative permittivity of PDMS is approximately 3. This directly influences the antenna performance. The mechanical flexibility of the PDMS substrate enables the antenna to follow the contours of the body part. This makes the antenna wearable. PDMS is compatible with the human body and causes no allergies. This maintains safe skin contact without irritation or adverse effect. The moisture absorption property of the substrate is also very low, providing stability under varying environmental conditions such as humidity or sweat. It is also optically transparent, which supports aesthetic customization. This allows the integration of any decorative patterns or logos without degrading the antenna performance. The fabrication process is also easy and the substrate dimension taken for this design is 3 cm x 3 cm for 3.5 GHz and 5.9 GHz. This size ensures sufficient space for the logo design and provides adequate adhesive area for safe skin contact. It has a balance between electrical properties and user comfort, making it functional and wearable.

A. *Evolution of the Structure:*

The proposed antenna is designed through a systematic three-stage evolution process. This is to optimize its impedance matching, bandwidth, and multi-band operation. The design progression is represented in Figure 1, and the corresponding S-parameters are presented in Figure 2.

Stage 1 (Figure 1a): The initial configuration features a basic circular monopole with a radius of 1.8 cm. This is the foundational radiator. In this stage, the antenna resonates at 3.3 GHz with a return loss of –18 dB, single-band operation. The radiation is primarily omnidirectional, and the design offers a compact footprint suitable for wearable applications.

Stage 2 (Figure 1b): To enhance the impedance bandwidth and introduce multiband behavior, an octagonal slot with a thickness of 5 mm is etched into the circular monopole. This structural modification perturbs the current distribution. This effectively tunes the resonant frequencies. Hence, the antenna exhibits dual-band resonance at 3.5 GHz with a return loss of –23 dB, and at 5.5 GHz with –25 dB. These frequency bands are better aligned with 5G sub-6 GHz and WLAN applications, expanding the antenna’s usability.

Stage 3 (Figure 1c): Further refinement is achieved by introducing a central cross-shaped slot within the octagonal structure. This modification enhances the antenna current path. This results in improved radiation efficiency. The final design achieves deep resonances at 3.5 GHz (–25 dB) and 5.9 GHz (–27 dB), supporting stable dual-band performance suitable for biomedical and wireless communication in 5G and Wi-Fi 6E bands.

Throughout each stage, the design modifications contribute to enhanced S-parameter characteristics, as shown in Figure 2. The evolution clearly demonstrates a shift from narrowband to efficient dual-band operation with deeper return loss levels and better matching performance. These improvements directly contribute to the antenna's effectiveness when deployed in on-skin scenarios, ensuring reliable performance even under deformation or skin proximity effects.

A layer of 0.1 mm isolation layer is introduced between the antenna and the human tissue for electric isolation. This isolation minimizes the absorption loss by the tissues and hence enhances the overall efficiency of the antenna. The figure 3 shows the adaptability of the wearable antenna with human-body interaction, which significantly influences the tuning performances.

The electrical properties of tissues like skin, fat, and muscle play a crucial role in the design of body-worn antennas. These tissues exhibit frequency-dependent characteristics. It is defined by their relative permittivity, conductivity, and loss tangent. For instance, at 2.45 GHz, skin typically has a relative permittivity of 38–42 and conductivity of 1.4–1.6 S/m, with a high loss tangent, indicating high electromagnetic energy absorption. Fat has a much lower relative permittivity (5–6) and conductivity (0.04–0.06 S/m), making it a low-loss medium. Muscle tissue, rich in water content, exhibits the highest permittivity (50–55) and conductivity (1.7–2.0 S/m), resulting in attenuation of electromagnetic waves. Therefore, accurate modeling of the layered tissue structure is essential for optimizing on-body antenna performance and ensuring reliable operation in real-world wearable scenarios.

(a) (b) (c)

FIG 1: STAGES OF EVOLUTION OF THE PROPOSED ANTENNA (A) STAGE 1 (B) STAGE 2 (C) STAGE 3

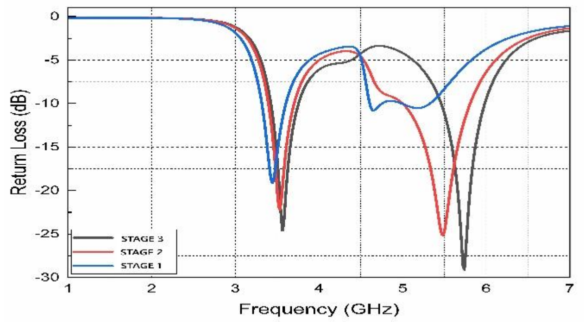

FIG 2: RETURN LOSS CHARACTERISTICS OF THE STAGES OF THE ANTENNA

B. *Radiation Mechanism of the Skin-mountable Antenna:*

The figure 4a and 4b represent the surface current distribution of the designed antenna at the resonant frequencies. At both frequencies, the antenna exhibits uniform current distribution across the radiating surface, indicating effective utilization of the patch area. At 3.5 GHz, as shown in figure 4a, the surface current density is concentrated along the outer edges of the octagonal slot. This follows a symmetrical distribution pattern, supporting the resonant mode. This uniform current flow contributes to strong radiation efficiency and less ohmic losses. The slot plays a significant role in tuning the current path, supporting stable resonance. At 5.9 GHz as represented by figure 4b, the current distributed increases around the edges of the cross slot at the center of the patch. This slot introduces an additional resonant path and facilitates the excitation of higher frequencies necessary for dual band operation. The current is evenly distributed, does not have any concentration or localized null, contributing to better stability.

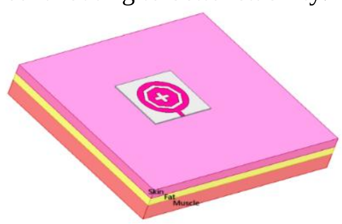

FIG 3: THE ANTENNA PLACED OVER THE 3 LAYERED HUMAN TISSUE MODEL WHILE THE DESIGN PROCESS

The radiation pattern of the designed antenna is represented in figure 5a and 5b. The red line represents the E-plane and the H-plane is represented by the green line. At both 3.5 GHz and 5.9 GHz, the antenna exhibits bidirectional radiation pattern with stable loops with a good front-to-back ratio, indicating effective radiation and minimal distortion when mounted on skin. This ensures wide coverage and reliable communication, though the back radiation is not desirable in wearable antenna. Optimizing the input signal level could minimize the effects of the antenna. The figure 5c, represents a simulated gain versus frequency response of the antenna. This achieves a peak gain of approximately 5.3 dB at 3.5 GHz and 8.2 dB at 6 GHz. This demonstrates the effective performance at the dual resonant frequencies. These results confirm that the antenna maintained high gain and consistent behavior across the operating frequencies.

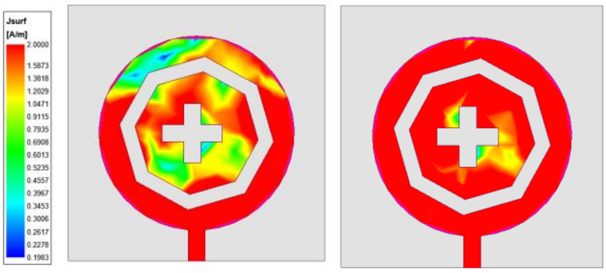

(a) (b)

FIG 4: CURRENT DISTRIBUTION OF THE ANTENNA AT (A) 3.5 GHZ (B) 5.9 GHZ

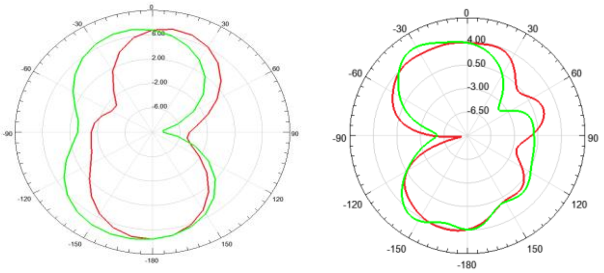

(a) (b)

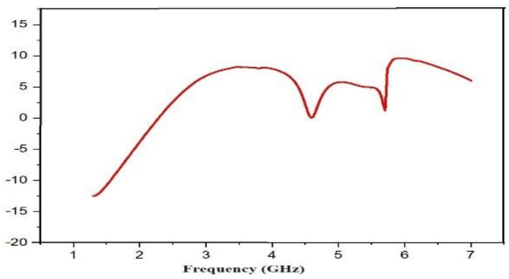

(c)

FIG 5: A) THE E PLANE (RED) AND H PLANE (GREEN) RADIATION PATTERN OF THE ANTENNA AT 3.5 GHZ B) AT 5.9 GHZ (C) GAIN VS. FREQUENCY PLOT OF THE PROPOSED ANTENNA

III. TEST FOR COMPATIBILITY

The compatibility testing of the designed skin-mountable antenna involves two critical evaluations. The specific absorption rate analysis and the bending performance analysis. The SAR measures the rate at which the electromagnetic energy is absorbed by the human tissues when the antenna operates close to the human body. This has to make sure the compliance with international safety standards such as IEEE C95.1 and IEC 62209. This analysis is typically conducted using electromagnetic simulation tools with multi-layer tissue models. If the SAR value exceeds the limits, mitigation strategies like lowering the input power or introducing isolation layers are employed to reduce the exposure. The bending analysis evaluates the antenna mechanical characteristics and electrical stability under deformation. The antenna is tested on a cylindrical surface with varying radii to observe the changes in resonance frequencies. Flexible biocompatible substrates like PDMS, Kapton, and other polymers are often chosen to support structural integrity during bending.

A. SAR Analysis:

The regulatory thresholds require SAR to remain below 1.6 watts per kg, averaged over 1 gram of tissue. The SAR value is influenced by several factors such as antenna geometry, radiation pattern, operating frequency, and input power. For this antenna, the SAR is maintained below 1.6 watts per kg by optimizing the quantity of input power as shown in figure 6. The input power is required to be at a range of 80-100 mW for safe operating range.

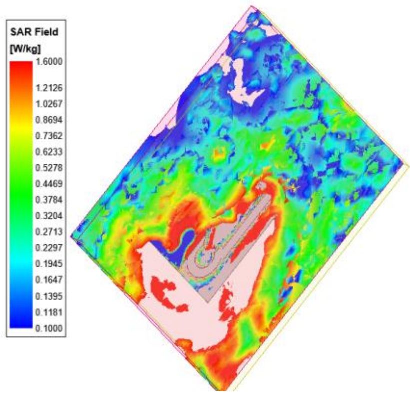

FIG 6: SAR ANALYSIS OF THE PROPOSED ANTENNA FOR THE OPERATING FREQUENCIES

B. Bending Analysis:

Bending of an antenna can alter the performance of the designed antenna as the electrical length and the surface current distribution changes due to the perturbations. As depicted in figure 7a, when the antenna is bent with a gentle radius of curvature of 100 cm, it resonates effectively at 3.5 GHz and 5.9 GHz, as shown in the red curve of figure 7b. When subjected to a sharper bend of radius of 50 cm, the resonant frequency shifts slightly to 3.4 GHz and 5.7 GHz, indicated by the blue curve of the same figure. Despite these effects, the observed antenna shifts were relatively small, demonstrating that the antenna retains a stable performance under moderate bending. This resilience to deformation is crucial for wearable application, where the antenna must conform to dynamic body movements without degrading its communication capabilities.

(a)

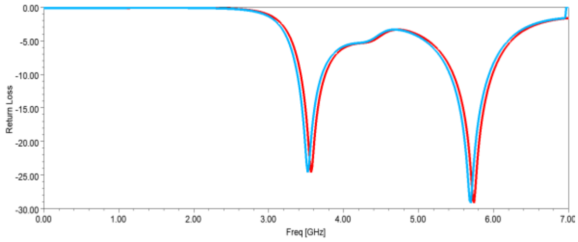

(b)

FIG 7: (A) REPRESENTATION OF ANTENNA BENDING (B) BENDING PERFORMANCE

IV. CONCLUSION

The compact antenna for the skin-mountable application has been designed and thoroughly evaluated for operation at 3.5 GHz and 5.9 GHz. The overall dimensions of the antenna is about 3 cm x 3 cm. The antenna is designed to achieve a gain of 5.3 dB at 3.5 GHz and 8.2 dB at 6 GHz. SAR analysis also confirms the compliance with the safety guidelines for an input power of 80 to 100 mW. The use of 0.1 mm thickness PDMS substrate provides biocompatibility and mechanical flexibility. This allows the antenna to conform comfortably around the human body. The bending test under different curvature also shows minimum resonant frequency shift, making it suitable for wearable application. Future enhancement may include size reduction, multiband operations, and advanced material engineering to expand the scope of the research.

REFERENCES

[1] Sherene, J., Vasudevan, K., Uma Maheshwari, G., Meenambal, B. (2025), “Design and Analysis of AMC-Based Anti-symmetric Dual L-Shaped Antenna for WBAN Application”. Third International Conference on Computational Electronics for Wireless Communications. ICCWC 2023. Lecture Notes in Networks and Systems, vol 959. Springer, Singapore. https://doi.org/10.1007/978-981-97-1943-3_16

[2] Jacob, S., Bose, M., & Karuppiah, V. (2024). Artificial Magnetic Conductor-Backed Microstrip-Fed Dual-Band antenna for 5G wearable sensor nodes and C Band application in WBAN network. 5G and Fiber Optics Security Technologies for Smart Grid Cyber Defense (pp. 221–241). https://doi.org/10.4018/979-8-3693-2786-9.ch009

[3] M. Qasim Mehmood *et al.*, "Textile-Based Washable Multimode Capacitive Sensors for Wearable Applications," in *IEEE Journal on Flexible Electronics*, vol. 3, no. 10, pp. 445-453, Oct. 2024, https://doi.org/10.1109/JFLEX.2024.3483195

[4] H. Tang et al., "A Low-Profile Flexible Dual-Band Antenna With Quasi-Isotropic Radiation Patterns for MIMO System on UAVs," in IEEE Antennas and Wireless Propagation Letters, vol. 22, no. 1, pp. 49-53, Jan. 2023, https://doi.org/10.1109/LAWP.2022.3201492

[5] J. S. Gibson, X. Liu, S. V. Georgakopoulos, J. J. Wie, T. H. Ware and T. J. White, "Reconfigurable Antennas Based on Self-Morphing Liquid Crystalline Elastomers," in IEEE Access, vol. 4, pp. 2340-2348, 2016, https://doi.org/10.1109/ACCESS.2016.2565199

[6] H. Yang, X. Liu and Y. Fan, "Design of Broadband Circularly Polarized All-Textile Antenna and Its Conformal Array for Wearable Devices," in IEEE Transactions on Antennas and Propagation, vol. 70, no. 1, pp. 209-220, Jan. 2022, doi: 10.1109/TAP.2021.3098542

[7] A. S. M. Alqadami, N. Nguyen-Trong, B. Mohammed, A. E. Stancombe, M. T. Heitzmann and A. Abbosh, "Compact Unidirectional Conformal Antenna Based on Flexible High-Permittivity Custom-Made Substrate for Wearable Wideband Electromagnetic Head Imaging System," in *IEEE Transactions on Antennas and Propagation*, vol. 68, no. 1, pp. 183-194, Jan. 2020, doi: 10.1109/TAP.2019.2938849.

[8] Meenambal Bose, Vasudevan Karuppiah, Metamaterial inspired superstrate loaded miniaturized quad port MIMO antenna for 5G C-band applications, Optics Communications, Volume 574, 2025, 131123, ISSN 0030-4018, https://doi.org/10.1016/j.optcom.2024.131123

[9] F. -L. Bong, E. -H. Lim and F. -L. Lo, "Compact Orientation Insensitive Dipolar Patch for Metal-Mountable UHF RFID Tag Design," in *IEEE Transactions on Antennas and Propagation*, vol. 66, no. 4, pp. 1788-1795, April 2018, doi: 10.1109/TAP.2018.2803132.

[10] M. A. Ziai and J. C. Batchelor, "Temporary On-Skin Passive UHF RFID Transfer Tag," in *IEEE Transactions on Antennas and Propagation*, vol. 59, no. 10, pp. 3565-3571, Oct. 2011, doi: 10.1109/TAP.2011.2163789.

[11] J. Tak and J. Choi, "An All-Textile Louis Vuitton Logo Antenna," in *IEEE Antennas and Wireless Propagation Letters*, vol. 14, pp. 1211-1214, 2015, doi: 10.1109/LAWP.2015.2398854

[12] T. Ali, A. Kavinamoole, S. B K and R. C. Biradar, "A Toyota Logo Penta-band Antenna loaded with pi and inverted L-shaped Slots for Multiple Wireless Applications," *2018 4th International Conference on Applied and Theoretical Computing and Communication Technology (iCATccT)*, Mangalore, India, 2018, pp. 31-35, doi: 10.1109/iCATccT44854.2018.9001968.

[13] K. W. Leung, E. H. Lim and X. S. Fang, "Dielectric Resonator Antennas: From the Basic to the Aesthetic," in *Proceedings of the IEEE*, vol. 100, no. 7, pp. 2181-2193, July 2012, doi: 10.1109/JPROC.2012.2187872.

[14] Gaetano *et al.*, "Insole Antenna for On-Body Telemetry," in *IEEE Transactions on Antennas and Propagation*, vol. 63, no. 8, pp. 3354-3361, Aug. 2015, doi: 10.1109/TAP.2015.2434395.

Water Demand Prediction and Irrigation Scheme Optimization

Rekha P
Department of Applied Mathematics and Computational Science,
Thiagarajar College of Engineering,
Madurai, Tamil Nadu
rekha@student.tce.edu

Sowmya S D
Department of Applied Mathematics and Computational Science,
Thiagarajar College of Engineering,
Madurai, Tamil Nadu
sowmyasd@student.tce.edu

Vinotha R
Department of Applied Mathematics and Computational Science,
Thiagarajar College of Engineering,
Madurai, Tamil Nadu
vinothar@student.tce.edu

Saraswathi Meena R
Department of Applied Mathematics and Computational Science,
Thiagarajar College of Engineering,
Madurai, Tamil Nadu
rsmca@tce.edu

***Abstract*—Water is essential for plant growth, and the increasing demand for agricultural water coincides with the global shortage of freshwater, especially in developing countries such as India, where irrigation accounts for approximately 70% of total consumption. This paper addresses the necessity of better irrigation solutions through machine learning, using wireless sensing technology for data collection and neural networks to predict water needs. Our approach is designed to make irrigation more efficient and conserve water. The model achieved a high accuracy of 95.7% and a Root Mean Square Error (RMSE) of 33.038, proving its strength in supporting irrigation decision-making. We discuss integration of smart-irrigation with different machine learning processes and how digital farming tools enhance monitoring and operation of these systems from remote areas. Future challenges from this integration are also examined.**

Keywords—Irrigation management, sustainable agriculture, precision irrigation, machine learning, water scarcity, digital farming

I. Introduction

Agriculture utilizes 85% of available water and employs inefficient irrigation practices, resulting in low output. Rainfall patterns are becoming increasingly erratic, jeopardizing plant water security. Open field farms, which are subject to dynamic stimuli, need more sophisticated irrigation technologies in order to meet changing conditions. Precision irrigation schemes are a viable solution for long-term irrigation sustainability. The Internet of Things is accelerating growth by merging sensor networks and remote sensing technologies. Continuous data collection is possible using sensors such as point source sensors, unmanned aerial vehicles, satellites, tractors, and portable watering equipment. Machine learning algorithms are critical for processing enormous volumes of raw data and turning it into useful knowledge.

Water resource optimization is a primary motivation for this work. As irrigation in agriculture utilizes a large amount of freshwater, this study intends to optimize water utilization and enhance irrigation efficiency through machine learning and IoT technologies to counteract global water scarcity.

Additionally, climate change's unpredictability in affecting precipitation and crop water demand make new approaches necessary.

This study makes two significant contributions. First, it combines supervised learning models (Decision Trees, SVM, Random Forests) to improve irrigation schedules and uses IoT-based wireless sensor networks for real-time monitoring, minimizing labor and operational inefficiencies. Second, by addressing dynamic weather and soil conditions, the study improves water saving, increases crop production, and provides a framework for combining mobile and web apps with machine learning to create future-ready smart irrigation systems.

II. Related Work

Water demand prediction and irrigation management have been widely investigated using IoT, ML, and optimization approaches. Early studies focused on climate prediction. Hammer et al. [1] explored advances in climate prediction applications for agriculture, while Qadir et al. [3] examined agricultural water management challenges in water-starved countries. Bergez et al. [2] explored quantile regression trees for irrigation management decision support.

Later research expanded into more sophisticated machine learning applications. Chen et al. [4] applied random forest and back propagation neural networks for estimating radiation-based reference evapotranspiration. IoT's role in monitoring and automation has been well studied by Mohanraj et al. [5], Dagar et al. [7], and Farooq et al. [8], establishing the foundation for sensor-based approaches to irrigation management. Recent advances include deep learning applications. Mehra et al. [6] developed IoT-based hydroponics systems using deep neural networks, while Basha et al. [10] applied machine learning and deep learning techniques for rainfall prediction. Vij et al. [11] created IoT and machine learning approaches for automating farm irrigation systems, and Chen et al. [12] presented an ensemble learning model for agricultural irrigation prediction.

Integration of environmental data with mobile applications has been investigated by Muangprathub et al. [9] and Matukhina et al. [13]. Zhang et al. [14] explored IoT for aquaculture and hydroponics, while Sethi & Sharma [15] focused on real-time analytics in IoT-driven irrigation. Recent optimization approaches include Wang et al.'s [17] multi-objective optimization model and Dang et al.'s [16] IWRAM hybrid model for climate-driven projections.

Collectively, these studies indicate a clear shift towards AI-driven, sensor-based irrigation for efficiency and conservation, establishing the foundation upon which our current research builds.

III. Materials and Methods Data Collection

To create our model, we collected real-world environmental data from reliable agricultural and meteorological monitoring sources. This contained critical information such as soil moisture, temperature, humidity, wind speed, and air pressure—factors that influence how much water crops require. The data was collected using wireless sensors installed in farming regions to replicate the circumstances found in genuine smart agriculture setups. Before utilizing it for model training, we thoroughly cleaned and arranged the data to ensure that it was correct and suitable for analysis.

Machine learning enables intelligent decision- making regarding water use in agriculture. These models can predict crop water requirements by considering various predictors of weather and current soil conditions, enabling farmers to project their water needs, crop yield, and soil moisture content.

A. Supervised Machine Learning Models

Supervised Machine Learning methodologies utilize labeled data from experimental datasets to train functions that map input data to output variables, enabling predictions for new inputs. This approach develops models capable of both regression and classification tasks. Classification models predict categorical values, while regression models provide continuous outcomes. Key algorithms, including Random Forests, Decision Trees, Support Vector Machines, and K-Nearest Neighbors, are essential for making informed irrigation decisions. Random Forests create multiple decision trees and merge their predictions to improve accuracy and reduce over fitting. Decision Trees use a tree-like model of decisions based on feature values, creating a flowchart-like structure that leads to a decision. Support Vector Machines find the hyperplane that best divides a dataset into classes, maximizing the margin between different classes. K-Nearest Neighbors classifies data points based on the majority class among its k nearest neighbors.

By employing these algorithms, farmers can obtain precise analytic insights regarding optimal irrigation practices, allowing them better control over the irrigation process.

B. Unsupervised Machine Learning Models

Unsupervised learning algorithms automatically categorize data points by identifying underlying patterns within unlabeled datasets. These methods excel in making deductions and can be particularly effective in irrigation management by analyzing data on soil, plant health, and meteorological factors. By leveraging unsupervised learning, optimal irrigation decisions can be modelled for various zones within an irrigation field.

Common techniques in unsupervised machine learning include clustering methods for data categorization, artificial neural networks (ANNs), dimensionality reduction, and hierarchical clustering. These techniques allow the system to identify patterns without prior labeling, making them valuable for discovering hidden relationships in complex agricultural data.

C. Artificial Neural Network (ANN) Implementation

Artificial Neural Networks, inspired by biological neurons, are utilized through supervised and unsupervised learning approaches. Their architecture comprises interconnected layers of processing units. Recent studies have explored the application of ANNs in optimizing irrigation systems, notably by Murthy's 2019 model [6], which uses local meteorological data to estimate irrigation needs. The implementation of this model in the WaRPIC system achieved a remarkable 96% reduction in water wastage.

Additionally, given the importance of evapotranspiration (ET) in precision agriculture, ANNs have shown potential in accurately modeling and predicting the non-linear characteristics of reference ET. By accounting for variables such as temperature, sunlight, humidity, and wind speed, ANNs facilitate better estimations of crop water requirements, thereby informing irrigation decisions.

Our ANN implementation follows a structured algorithm that begins with data normalization and splitting into training and testing sets. The network architecture includes an input layer with nodes corresponding to the feature dimensions (soil moisture, temperature, humidity, etc.), hidden layers with ReLU activation functions, and an output layer with linear activation for water demand prediction. The model training employs backpropagation with mean squared error (MSE) as the loss function and optimization of weights using gradient descent. Performance evaluation uses MSE and R^2 metrics to ensure accurate water demand predictions.

D. Genetic Algorithm Integration

Genetic Algorithms (GAs) are optimization models that enhance the search for optimal solutions by mimicking natural evolutionary processes. When integrated with Backpropagation (BP) neural networks, GAs improve the training process, optimize performance thresholds, accelerate convergence, and ultimately increase model accuracy and efficiency.

Perea et al. (2019) proposed an innovative method for short-term daily crop water demand forecasting that requires less data by combining Bayesian networks, Artificial Neural Networks (ANNs), and GAs. This model achieved a standard prediction error of just 8.7% and an impressive coefficient of determination (R^2) of 96%, showcasing its excellent performance. Our implementation leverages similar principles to optimize the neural network architecture and hyperparameters.

TABLE 1: PERFORMANCE COMPARISON OF DIFFERENT MACHINE LEARNING MODELS

Model	MSE (↓)	MAE (↓)	RMSE (↓)	R^2 (↑)	Water Demand Prediction (↑)	IoT & Sensor Integration (↑)	Digital Farming Compatibility (↑)	Smart Irrigation Suitability (↑)
Linear Regression	✗	✗	✗	✗	✗	✗	✗	✗
Decision Tree	✗	✗	✗	✗	✓	✗	✗	✗
SVM	✗	✗	✗	✗	✗	✗	✗	✗
Random Forest	✓	✓	✓	✓	✓✓	✓	✓	✓
KNN	✗	✗	✗	✗	✓	✗	✗	✗
ANN (BPNN)	✓	✓	✓	✓	✓✓	✓✓	✓	✓✓

The table uses symbols to show the performance and suitability of several machine learning models for water demand prediction and smart irrigation. Here's what these symbols mean:

- X → The model has a lower performance or is not well-suited for this criterion.
- ✓→ The model performs well or is suitable for this criterion.
- ✓✓ → The model performs exceptionally well or is highly suitable for this criterion.

IV. RESULTS AND DISCUSSION

Our ANN model for water demand prediction demonstrated excellent performance metrics. The training and validation loss curves showed consistent convergence, indicating effective learning without overfitting. Both losses stabilized after multiple epochs, with the validation loss slightly lower than the training loss, confirming the model's strong generalization capabilities.

The accuracy assessment revealed that the model achieved 95.7% accuracy with a Root Mean Square Error (RMSE) of 33.038. The scatter plot comparing actual versus predicted values showed strong correlation, with most predictions falling close to the ideal line, demonstrating the model's ability to capture complex non-linear relationships in the data.

The effectiveness of various machine learning models was compared, with ensemble learning approaches and the IWRAM hybrid model showing particular promise for agricultural applications. Multi-objective optimization proved valuable for resource allocation while minimizing waste, enabling farmers to balance water conservation with crop yield requirements. IoT-based irrigation systems demonstrated high efficiency in real-time water management, enabling advanced monitoring and decision-making through continuous data analysis. The fusion of machine learning techniques with sustainable energy sources presents significant opportunities for transforming irrigation practices.

V. CONCLUSION AND FUTURE WORK

This research demonstrates that smart technologies, particularly machine learning, IoT, and digital interfaces, are transforming precision irrigation into sustainable and efficient water management systems. Our findings confirm that machine learning models can accurately predict water demand based on environmental factors, enabling precise irrigation scheduling that conserves water while maintaining optimal crop growth conditions.

The selection of appropriate machine learning models depends critically on the availability of datasets, computational complexity, and specific deployment requirements. Supervised learning approaches proved effective when labeled data was available, while unsupervised techniques offered valuable insights for pattern discovery in complex agricultural environments.

While our implementation focused primarily on neural networks and genetic algorithms, reinforcement learning shows promise for adaptive control in irrigation systems. Additionally, federated learning could enhance data privacy by enabling decentralized model training across multiple farms, though challenges in communication efficiency remain to be addressed.

A significant barrier to adoption in developing countries is the limited infrastructure, particularly in rural farming communities. Future implementations should consider low-power, long- range communication technologies like LoRa for remote agricultural settings with limited connectivity.

The integration of digital solutions with precision irrigation significantly improves water efficiency, optimizes resource utilization, and enhances agricultural productivity. Mobile and web applications make these sophisticated systems accessible to farmers with varying levels of technical expertise, democratizing access to advanced irrigation management tools.

Future research should address environmental concerns related to digital irrigation systems, particularly the lifecycle management of electronic components in agricultural settings. Additionally, the development of edge computing solutions could reduce reliance on cloud connectivity, making these systems more resilient in areas with intermittent internet access.

Ultimately, the convergence of machine learning, IoT, and digital interfaces represents a transformative approach to irrigation management that aligns with sustainable development goals while addressing the pressing challenges of water scarcity and food security in an era of climate uncertainty.

REFERENCES

[1] G. L. Hammer et al., "Advances in application of climate prediction in agriculture," Agricultural systems, vol. 70, no. 2-3, pp. 515-553, 2001.

[2] J. E. Bergez, H. Cardot, and F. Garcia, "Quantile regression trees for prediction in irrigation management," In Proceedings of the 4th EFITA Conference in Debrecen, Hungary, pp. 747- 753, 2003.

[3] M. Qadir et al., "Agricultural water management in water-starved countries: challenges and opportunities," Agricultural water management, vol. 62, no. 3, pp. 165-185, 2003.

[4] S. Chen et al., "Application of random forest and back propagation neural network in estimating radiation-based reference evapotranspiration model in Gansu province," In 2016 ICNISC, pp. 228-232, IEEE, 2016.

[5] I. Mohanraj, K. Ashokumar, and J. Naren, "Field monitoring and automation using IOT in agriculture domain," Procedia Computer Science, vol. 93, pp. 931-939, 2016.

[6] M. Mehra et al., "IoT based hydroponics system using Deep Neural Networks," Computers and electronics in agriculture, vol. 155, pp. 473-486, 2018.

[7] R. Dagar, S. Som, and S. K. Khatri, "Smart farming–IoT in agriculture," In 2018 ICIRCA, pp. 1052-1056, IEEE, 2018.

[8] M. S. Farooq et al., "A Survey on the Role of IoT in Agriculture for the Implementation of Smart Farming," IEEE Access, vol. 7, pp. 156237- 156271, 2019.

[9] J. Muangprathub et al., "IoT and agriculture data analysis for smart farm," Computers and electronics in agriculture, vol. 156, pp. 467-474, 2019.

[10] C. Z. Basha et al., "Rainfall prediction using machine learning & deep learning techniques," In 2020 ICESC, pp. 92-97, IEEE, 2020.

[11] A. Vij et al., "IoT and machine learning approaches for automation of farm irrigation system," Procedia Computer Science, vol. 167, pp. 1250-1257, 2020.

[12] Y. A. Chen et al., "An ensemble learning model for agricultural irrigation prediction," In 2021 ICOIN, pp. 311-316, IEEE, 2021.

[13] O. V. Matukhina, L. R. Votyakova, and I. N. Zakharova, "SMART-technologies in irrigation management of a remote land plot," In IOP Conference Series: MSE, vol. 1079, no. 7, p. 072027, 2021.

[14] S. Zhang et al., "Investigation on environment monitoring system for a combination of hydroponics and aquaculture in greenhouse," Information Processing in Agriculture, vol. 9, no. 1, pp. 123-134, 2022.

[15] S. S. Sethi and P. Sharma, "New Developments in the Implementation of IoT in Agriculture," SN Computer Science, vol. 4, no. 5, p. 503, 2023.

[16] C. Dang et al., "IWRAM: A hybrid model for irrigation water demand forecasting to quantify the impacts of climate change," Agricultural Water Management, vol. 291, p. 108643, 2024.

[17] S. Wang et al., "Multi-objective optimization operation of multiple water sources under inflow- water demand forecast dual uncertainties," Journal of Hydrology, vol. 630, p. 130679, 2024.

Investigating the Effect of Self-Heating and Parameter Variability on the Output Characteristics of Dielectric Pocket Surrounding Gate Tunnel FETs

V. Charumathi
Research Scholar, Department of ECE,
Thiagarajar College of Engineering,
Madurai, Tamilnadu, India
mathic1998@gmail.com

N.B. Balamurugan
Professor, Department of ECE,
Thiagarajar College of Engineering,
Madurai, Tamilnadu, India
nbbalamurugan@tce.edu

M. Suguna
Associate Professor, Department of IT,
Thiagarajar College of Engineering,
Madurai, Tamilnadu, India
mscse@tce.edu

E. Rajalakshmi
Research Scholar, Department of ECE,
Thiagarajar College of Engineering,
Madurai, Tamilnadu, India
raje.rajalakshmi18@gmail.com

***Abstract*—Surrounding Gate Tunnel Field-Effect Transistors with dielectric pocket are increasingly being considered promising candidates for next-generation electronic devices due to the ongoing pursuit of miniaturisation in semiconductor technology. Self-heating, however, becomes a significant issue when device dimensions get down to the nanoscale, jeopardising performance and dependability. The work investigates the DC performance metrics of Dielectric Pocket Surrounding Gate Tunnel FETs (DP-SG-TFETs), comparing their behaviour during self-heating to various geometric aspects. It examines the effects of self-heating over device parameters including silicon thickness, gate width, channel length, thickness of oxide, and thermal contact resistance. With SHE, an average electron velocity of $6*10^6$ cms^{-1} and an average degradation in electron mobility of 194 $cm^2V^{-1}s^{-1}$ are noted for the channel lengths of 9 nm and 18 nm. The thermodynamic model is employed to study the Self Heating Effect (SHE) using Sentaurus Technology Computer Aided Designing Simulator (TCAD).**

Keywords—Dielectric Pocket Surrounding Gate Tunnel Field Effect Transistors, Self-Heating Effect, Technology Computer Aided Designing, Lattice Temperature.

I. INTRODUCTION

Downscaling traditional CMOS transistors is increasingly hindered by several limitations, including high subthreshold slope (SS), significant OFF-state leakage currents, drain-induced barrier lowering (DIBL), and other short channel effects (SCEs), all of which contribute to elevated static power consumption and unreliable switching performance. Tunnel Field-Effect Transistors (TFETs) have emerged as promising alternatives, thanks to their unique tunneling mechanism, which enables subthreshold swings below 60 mV/decade, minimal OFF-state leakage, and improved control over SCEs [1–7]. Nonetheless, TFETs are not without drawbacks, such as inadequate ON-state current (ION) and persistent DIBL issues, rendering them insufficient for meeting International Technology Roadmap for Semiconductors (ITRS) performance standards [8], [9]. To address these issues, the Surrounding Gate (SG) architecture has been proposed, offering superior gate control, reduced SCEs and DIBL, and enhanced subthreshold behavior [10], [11]. Further refinement includes the integration of dielectric pockets (DPs) at the source-channel junction, which help to limit OFF-current (Ioff) by acting as barriers to carrier diffusion and suppressing punch-through paths [12–19]. Although significant advancements have been made in optimizing these devices, the self-heating effect (SHE) and its influence on device performance remain underexplored. Prior investigations by Balasubbareddy et al. analyzed how substrate material, gate length, and nanosheet width affect SHE in nanosheet heterostructure FETs [20], while Billel Smaani et al. proposed design methodologies for managing SHE in nanosheet FETs [21]. Additionally, Rathore et al. demonstrated the benefits of substrate BOX engineering in mitigating SHE-induced thermal degradation in SiO2-based nanosheet FETs [22], and Vaibhav Purwar et al. examined the adverse effects of SHE on dielectric pocket gate-all-around (DPGAA) MOSFETs, highlighting issues like reduced carrier mobility and increased gate leakage [23]. This study focuses on understanding the impact of SHE and geometric parameters on the performance of DP-SG-TFETs, aiming to support the development of more thermally resilient and efficient nanoscale transistors.

A. Heat Dissipation on device structures:

Fig. 1. shows the incidence of heat dissipation in geometrically limited DP-SG-TFETs compared to planar MOSFET and TFET devices. In DP-SG-TFETs, a thin oxide layer surrounds the silicon channel area, and the contact-metal is made of Tungsten Nitride with a work function of 4.7eV. The component of source and drain contact metal is molybdenum. The physical and thermal parameters of the DP-SG-TFETs device and their respective ranges, which were taken into consideration in this work, are shown in Table 1.

B. Self-heating Analysis

Self-heating is a prominent issue in devices like DP-SG-TFETs, caused by the conversion of electrical energy into heat due to resistive losses as current passes through the device. This effect is primarily driven by the electric field

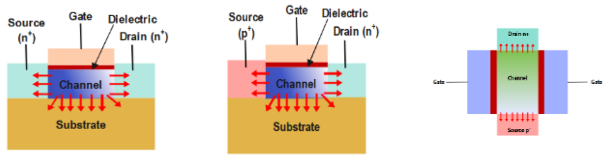

(a) (b) (c)

FIG. 1. HEAT DISSIPATION COMPARISON OF DIFFERENT TRANSISTOR DESIGNS. (A) PLANAR MOSFET, (B) TFET, AND (C) DP-SG-TFET.

TABLE: 1 PARAMETERS FOR DP-SG-TFETS

Parameters	Value / Range
Gate Width (W) (nm)	5-40
Gate Length (L) (nm)	8
Oxide thickness (t_{ox}) (nm)	2-10
Silicon thickness (t_{si}) (nm)	2-8
Drain–source voltage (V_{DS}) (V)	0.1-1
Gate–source voltage (V_{GS}) (V)	-5-5
Gate work function	4.7
Source doping level (N_S) (cm^{-3})	10^{21}
Intrinsic doping level (N_i) (cm^{-3})	10^{15}
Permittivity of silicon (ϵ_{Si})	11.7
Permittivity of gate oxide (ϵ_{ox})	3.9
Temperature (T) (k)	300
V_{DD} (V)	0.5
Thermal Contact- Resistance (R_{th}) ($KW^{-1}cm^2$)	10^{-5} -10^{-4}
Dielectric pocket- length (DP_L) (nm)	4
Dielectric pocket- thickness (DP_D) (nm)	4
Thermal conductivity ($KW^{-1}cm$)	SiO_2 = 0.014, SI_3N_4 = 0.185, Al_2O_3 = 0.02

within the channel, which accelerates charge carriers—mainly electrons—leading to an increase in their kinetic energy and, consequently, a rise in temperature. A significant factor in this process is electron-phonon scattering, where energy is transferred from moving electrons to the crystal lattice, increasing the lattice's thermal energy. The compact and insulated structure of DP-SG-TFETs, especially the presence of dielectric materials around the channel, limits heat dissipation, resulting in localized heating. This thermal buildup degrades device performance by reducing carrier mobility and slowing down charge transport, ultimately lowering the ON-state current (ION). To enhance performance, it is crucial to understand and manage these thermal effects. A thermodynamic model is applied to estimate the lattice temperature within the device, helping to evaluate how it heats under various operating conditions. By assuming a generally stable temperature throughout the device, the lattice temperature (T) can be calculated based on the total internal heat generation, as represented in Equation (1), which incorporates various heat sources and their impact on thermal behavior.

$$\frac{\partial}{\partial t}(C_L\,.T) - \nabla\,.(k\nabla T) = Q \qquad (1)$$

where C_L represents the heat generation or absorption within the material, k is the material's thermal conductivity and Q reflects the amount of heat the substance is producing or absorbing. The heat generation terms resulting from electron (n) and hole (p) currents is incorporated as,

$$Q = -\nabla\,.[(P_nT + \emptyset_n)J_n + (P_pT + \emptyset_p)J_p] \qquad (2)$$

where, the power factors associated with electron and hole currents are denoted as P_n and P_p; The electrostatic potentials are $\emptyset_n$and $\emptyset_p$ and the current densities for electrons and holes are J_n and J_p, respectively. The heat generation or absorption associated with electron energy states is given as,

$$Q = -\nabla\,.[(P_nT + \emptyset_n)J_n + (P_pT + \emptyset_p)J_p] - \frac{1}{q}\left(E_c + \frac{3KT}{2}\right)(\nabla\,.J_n - qR_{net,n}) - \frac{1}{q}\left(-\,E_v + \frac{3KT}{2}\right)(-\,\nabla\,.J_p - qR_{net,p}) \qquad (3)$$

constant is K. The divergence of electron current density is represented by $\nabla\,.J_n$; and the net rate of electron energy gain or loss is shown by the expression $qR_{net,n}$. By including the heat generation due to the incorporation of hole energy states derived from equation (3) is shown as,

$$Q = -\nabla.[(P_nT + \emptyset_n)J_n + (P_pT + \emptyset_p)J_p] - \frac{1}{q}\left(E_c + \frac{3KT}{2}\right)(\nabla.J_n - qR_{net,n}) - \frac{1}{q}\left(-\,E_v + \frac{3KT}{2}\right)(-\,\nabla\,.J_p - qR_{net,p}) + \hbar\omega G_{opt} \qquad (4)$$

The valence band edge is represented by the symbol E_v; The divergence of hole current density is represented by $\nabla\,.J_p$; the net rate of holes energy gain or loss is shown by the expression $qR_{net,p}$. In Equation (4), the right-hand side term represents the total amount of heat generated within the device. The 2nd and 3rd components on right-hand side (RHS) of equation may be ignored under the stationary situation. This allows us to determine the total heat as in equation (5).

$$Q = -\nabla\,.[(P_nT + \emptyset_n)J_n + (P_pT + \emptyset_p)J_p] + \hbar\omega G_{opt} \qquad (5)$$

where, $\hbar$ denotes the Planck's- constant, the angular frequency of absorbed light is ω and G_{opt} indicates the rate of optical generation. The predominant contribution to the total heat, as stated in equation (6), is represented by the 1st term on right-hand side of equation (5), due to the fact that electrons serve as the majority charge carriers. Consequently,

$$Q = -\nabla\,.[(P_nT + \emptyset_n)J_n] \qquad (6)$$

The phenomenon being observed is the result of the combined effects of Thomson, Joule, recombination heats, and Peltier.

II. RESULTS AND DISCUSSION

The influence of self-heating effect on different device-parameters is investigated to comprehend the consequences of heat dissipation on device performance. By addressing these phenomena, we intend to understand the constraints and issues connected with the self-heating in practical applications. The results of this work will add to the current area of device- engineering and support more efficient and dependable devices. Fig. 2. depicts the matched transfer characteristics of DP-SG-TFETs with the experimental data at a power supply of 0.6 V. Fig. 3 displays the transfer behavior of DP-SG-TFETs both with and without a self-heating effect at linear- 0.05 V and saturated- 0.6 V V_{DD} levels for silicon thickness and width of 5 nm and 20 nm, respectively.

$$I_{degradation} = \frac{I_{on}(without\ SHE) - I_{on}(with\ SHE)}{I_{on}(without\ SHE)} \times 100 \qquad (7)$$

∇ Equation (7) is used to calculate the degradation in current ($I_{degradation}$) caused by self-heating, where I_{ON} denotes the on-current. The on-current (I_D) suffered a 22% degradation with

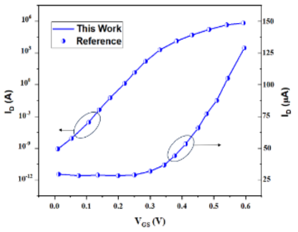

FIG. 2. TRANSFER CHARACTERISTICS OF DP-SG-TFETS MATCHED WITH REFERENCE.

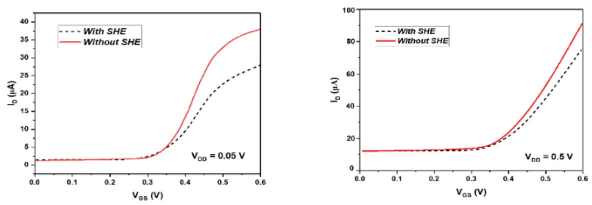

(A) **(B)**

FIG. 3. TRANSFER CHARACTERISTICS OF DP-SG-TFETS WITH AND WITHOUT SHE (A) AT VDD = 0.05 V (B) AT VDD = 0.5 V

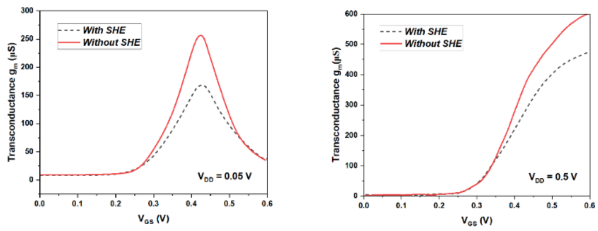

(a) (b)

FIG. 4. COMPARISON OF TRANSCONDUCTANCE WITH RESPECT TO GATE-SOURCE VOLTAGE WITH AND WITHOUT SHE (A) AT V_{DD} = 0.05 V (B) AT V_{DD} = 0.5 V

self-heating in linear operation, but only a 26% degradation in saturation. Self-heating in DP-SG-TFETs becomes more evident as the gate-source voltage (VGS) increases, with a more pronounced performance drop observed under saturation conditions due to the stronger drain electric field, although the overall effect is numerically greater during linear operation. As depicted in Fig. 4, trans conductance (gm) shows a marked decline under self-heating conditions. Similarly, the output characteristics shown in Fig. 5 indicate a noticeable decrease in ON-state current (ION) at higher VGS levels, largely caused by reduced charge carrier mobility and velocity saturation. This degradation is attributed to intensified phonon scattering within the device, which limits both carrier mobility and velocity. Consequently, electron velocity reduction suppresses the likelihood of hot carrier effects, commonly associated with performance loss in short-channel transistors. Fig. 6 supports this by showing a drop in peak electron velocity to around 9×10^6 cm/s and a mobility decrease to approximately 328.2 cm²/V·s in various DP-SG-TFET channels. These findings highlight the critical role of device geometry in managing self-heating, which directly influences overall device efficiency. Heat dissipation in these transistors is driven by thermal conduction and is accurately modelled using Fourier's law, as described in Equation (8).

$$\varphi = \frac{kA\nabla T}{d} \qquad (8)$$

Minimizing self-heating in DP-SG-TFETs requires strategic optimization of structural and material parameters. The heat flow equation, where φ represents thermal flux, A is the surface area, d is the thickness of the material, k denotes thermal conductivity, and ∇T is the temperature gradient, highlights the importance of managing these variables to enhance thermal efficiency. The thickness of the silicon layer has a pronounced effect on both thermal and electrical

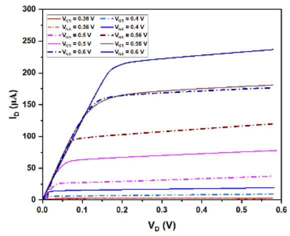

FIG. 5. OUTPUT VOLTAGE VERSUS CURRENT FOR VARIOUS VGS VALUES (CONTINUOUS LINE – WITHOUT SHE; symbol – with SHE).

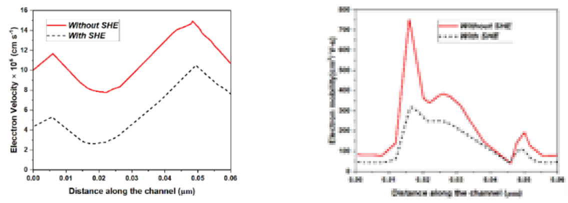

(a) (b)

FIG. 6. ELECTRON VELOCITY AND ELECTRON MOBILITY ALONG THE CHANNEL IN DP-SG-TFETS.

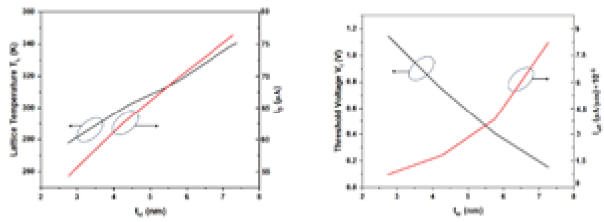

(a) (b)

FIG. 7. (A) T_L VERSUS I_D AS A FUNCTION OF TSI; (B) VARIATION OF V_T AND I_{OFF} WITH T_{SI} FOR $V_{DD} = V_{GS}$ = 0.6 V

characteristics; increasing the silicon thickness expands the channel region, thereby boosting the ON-state current (ION), as illustrated in Fig. 7a. However, this also leads to elevated lattice temperatures due to higher current density. Conversely, thinner silicon layers result in lower ION because of stronger vertical electric fields, which impair carrier mobility and intensify heating effects. Thicker silicon also tends to reduce the threshold voltage (Vt) and increase the off-state current (IOFF), as shown in Fig. 7b, potentially compromising switching performance and energy efficiency.

Achieving a suitable silicon thickness is crucial to balancing electrical output and thermal management. Additionally, gate width plays a vital role by altering the effective channel size, which directly impacts the on-current and further influences the thermal behaviour of the device. In DP-SG-TFETs, variations in gate width significantly impact both the thermal and electrical characteristics of the device. Increasing the gate width from 5 to 40 nm enhances the ON-state current (ION) by expanding the channel area, which allows more space for charge carriers and reduces scattering. This improvement, however, is accompanied by a rise in lattice temperature, though the effect is less pronounced at larger widths due to improved heat distribution. Alongside these advantages, wider gates may also introduce drawbacks such as a drop in threshold voltage (Vt) and a rise in off-state current (IOFF), which can affect overall device performance. Moreover, the heat distribution channel is uneven, with the highest temperatures occurring near the drain junction due to intense electric fields. Channel length also plays a crucial role: shorter channels produce less heat but have lower ION, whereas longer channels increase ION while raising IOFF and causing threshold voltage roll-off. Additionally, the use of silicon dioxide (SiO2) as the gate oxide poses a challenge in managing heat, as its low

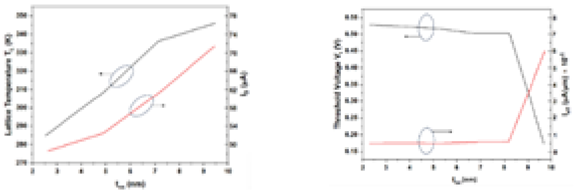

(a) (b)

FIG. 8. (A) T_L VERSUS I_D AS A FUNCTION OF T_{OX}; (B) VARIATION OF V_T AND I_{OFF} WITH T_{OX} FOR $V_{DD} = V_{GS} = 0.6$ V

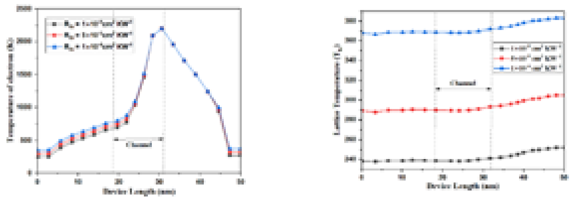

(A) (B)

FIG. 9. CUTLINE PLOT FOR DIFFERENT RTH VALUES. (A) DEVICE LENGTH (NM) VS LATTICE TEMPERATURE (TK); (B) DEVICE LENGTH (NM) VS ELECTRON TEMPERATURE (TC) (K)

thermal conductivity limits the dissipation of heat from the channel. Balancing these parameters is essential to optimize device efficiency and minimize the adverse effects of self-heating. The effects of oxide thickness and thermal contact resistance (Rth) on self-heating behavior in DP-SG-TFETs were explored by varying the SiO_2 layer from 2 nm to 10 nm. As indicated in Fig. 8(a), changes in oxide thickness had minimal impact on lattice temperature up to 8 nm; beyond this point, however, performance began to shift significantly. Fig. 8(b) shows that thicker oxides beyond 8 nm led to a noticeable drop in threshold voltage and an increase in off-state current (IOFF), highlighting the device's sensitivity to oxide scaling. In parallel, Rth was found to play a vital role in thermal regulation. Lower Rth values promote efficient heat flow from the device through the source and drain contacts, while an increase in Rth from 10^{-5} to 10^{-4} cm²·K/W causes the lattice temperature to rise by approximately 40%, from 242K to 382K, as seen in Figs. 9(a) and 9(b). Interestingly, while electron temperatures at the contacts increase with higher Rth, the central hotspot carrier temperature remains largely unchanged.

III. CONCLUSION AND FUTURE WORK

The effect of self-heating (SHE) and geometric changes on DP-SG-TFETs has been investigated. Self-heating diminishes electron mobility and velocity, which impairs performance. Increasing thermal contact resistance from 10^{-5} cm^2KW^{-1} to 10^{-4} cm^2KW^{-1} results in 40% higher lattice and carrier temperatures, increasing deterioration. Wider and thicker tubes intensify self-heating and reduce drain current. Oxide thickness more than 7 nm considerably increases off-current. Optimizing gate width, silicon thickness, and oxide thickness can assist balance heat impacts and performance. Fully enclosed source and drain connectors improve heat dissipation and device durability. This study delves into the thermal and electrical properties of DP-SG-TFETs. Structural improvements effectively reduce self-heating. Optimized design parameters allow for low-power, high-performance nanoscale transistors, making DP-SG-TFETs excellent for next-generation electronics.

ACKNOWLEDGMENT

This research work in financially supported by Thiagarajar Research Fellowship (TRF) scheme (File.no: TCE/RD/TRF/01 dated Jan-2023 and File.no: TCE/RD/TRF/05 dated July-2023.We also extend our heartfelt thanks for the financial support provided through the TCE Seed Money Scheme (TCE-SMS) (File No. R&D/Seedmoney/2024/8), which has been instrumental in the successful execution of this study.

REFERENCES

[1] Seabaugh, A. C., & Zhang, Q. (2010). Low-voltage tunnel transistors for beyond CMOS logic. Proceedings of the IEEE, 98(12), 2095-2110.

[2] Bhuwalka, K. K., Schulze, J., & Eisele, I. (2005). A simulation approach to optimize the electrical parameters of a vertical tunnel FET. IEEE transactions on electron devices, 52(7), 1541-1547.

[3] Bhuwalka, K. K., Schulze, J., & Eisele, I. (2005). Scaling the vertical tunnel FET with tunnel bandgap modulation and gate workfunction engineering. IEEE transactions on electron devices, 52(5), 909-917.

[4] Verhulst, A. S., Sorée, B., Leonelli, D., Vandenberghe, W. G., & Groeseneken, G. (2010). Modeling the single-gate, double-gate, and gate-all-around tunnel field-effect transistor. Journal of Applied Physics, 107(2).

[5] Vanitha, P., Balamurugan, N. B., & Priya, G. L. (2015). Triple material surrounding gate (TMSG) nanoscale tunnel FET-analytical modeling and simulation. Journal of Semiconductor Technology and science, 15(6), 585-593.

[6] Choi, W. Y., Park, B. G., Lee, J. D., & Liu, T. J. K. (2007). Tunneling field-effect transistors (TFETs) with subthreshold swing (SS) less than 60 mV/dec. IEEE Electron Device Letters, 28(8), 743-745.

[7] Zhang, Q., Zhao, W., & Seabaugh, A. (2006). Low-subthreshold-swing tunnel transistors. IEEE Electron Device Letters, 27(4), 297-300.

[8] Semiconductor Industry Association. (2015). International Technology Roadmap for Semiconductors (ITRS) 2.0: Executive Report.

[9] Avci, U. E., Morris, D. H., & Young, I. A. (2015). Tunnel field-effect transistors: Prospects and challenges. IEEE Journal of the Electron Devices Society, 3(3), 88-95.

[10] Narang, R., Saxena, M., Gupta, R. S., & Gupta, M. (2012, October). An Analytical Modeling Approach for a Gate All Around (GAA) Tunnel Field Effect Transistor (TFET). In 16th International Workshop on Physics of Semiconductor Devices (Vol. 8549, pp. 25-30). SPIE.

[11] Narang, R., Saxena, M., Gupta, R. S., & Gupta, M. (2013). Drain current model for a gate all around (GAA) p–n–p–n tunnel FET. Microelectronics Journal, 44(6), 479-488.

[12] Xu, W., Wong, H., & Iwai, H. (2015). Analytical model of drain current of cylindrical surrounding gate pnin TFET. Solid-State Electronics, 111, 171-179.

[13] Samuel, T. A., Balamurugan, N. B., Niranjana, T., & Samyuktha, B. (2014). Analytical surface potential model with TCAD simulation verification for evaluation of surrounding gate TFET. Journal of Electrical Engineering & Technology, 9(2), 655-661.

[14] Usha, C., & Vimala, P. (2018). Analytical drain current model for fully depleted surrounding gate TFET. Journal of Nano Research, 55, 75-81.

[15] Jurczak, M., Skotnicki, T., Gwoziecki, R., Paoli, M., Tormen, B., Ribot, P., ... & Galvier, J. (2001). Dielectric pockets-a new concept of the junctions for deca-nanometric CMOS devices. IEEE Transactions on Electron Devices, 48(8), 1770-1775.

[16] Narang, R., Saxena, M., & Gupta, M. (2016). Investigation of dielectric pocket induced variations in tunnel field effect transistor. Superlattices and Microstructures, 92, 380-390.

[17] Awasthi, H., Kumar, N., Purwar, V., Gupta, R., & Dubey, S. (2021). Impact of temperature on analog/RF performance of dielectric pocket gate-all-around (DPGAA) MOSFETs. Silicon, 13(7), 2071-2075.

[18] Purwar, V., Gupta, R., Kumar, N., Awasthi, H., Dixit, V. K., Singh, K., ... & Tiwari, P. K. (2020). Investigating linearity and effect of temperature variation on analog/RF performance of dielectric pocket high-k double gate-all-around (DP-DGAA) MOSFETs. Applied Physics A, 126, 1-8.

[19] Nigam, K. K., Dharmender, Tikkiwal, V. A., & Bind, M. K. (2023). Theoretical Investigation of Dual-Material Stacked Gate Oxide-Source Dielectric Pocket TFET Based on Interface Trap Charges and Temperature Variations. Journal of Circuits, Systems and Computers, 32(15), 2350252.

[20] Balasubbareddy, M., Sivasankaran, K., Atamuratov, A. E., & Khalilloev, M. M. (2023). Optimization of vertically stacked nanosheet FET immune to self-heating. Micro and Nanostructures, 182, 207633.

[21] Smaani, B., Paras, N., Rahi, S. B., Song, Y. S., Yadav, R., & Tayal, S. (2023). Impact of the Self-Heating Effect on Nanosheet Field Effect Transistor Performance. ECS Journal of Solid-State Science and Technology, 12(2), 021005.

[22] Rathore, S., Jaisawal, R. K., Gandhi, N., Kondekar, P. N., & Bagga, N. (2022). Substrate BOX engineering to mitigate the self-heating induced degradation in nanosheet transistor. Microelectronics Journal, 129, 105590.

[23] Purwar, V., Gupta, R., Tiwari, P. K., & Dubey, S. (2021). Investigating the impact of self-heating effects on some thermal and electrical characteristics of dielectric pocket gate-all-around (DPGAA) MOSFETs. Silicon, 1-11.

Land Cover Feature Extraction from Synthetic Aperture Radar Images

Sudhakar S
UG Student, Dept of ECE,
Remote Sensing and GIS Lab,
Thiagarajar College of Engineering,
Madurai, India
sudhakars2810@gmail.com

Samuel Brand N
UG Student, Dept of ECE,
Remote Sensing and GIS Lab,
Thiagarajar College of Engineering,
Madurai, India
samuelbrand718@gmail.com

Nikilan N
UG Student, Dept of ECE,
Remote Sensing and GIS Lab,
Thiagarajar College of Engineering,
Madurai, India
nikilan1710@gmail.com

R A Alaguraja
Professor, Dept of ECE,
Remote sensing and GIS Lab,
Thiagarajar College of Engineering
Madurai, India
alaguraja@tce.edu

***Abstract*—The Sentinel-1 satellite, equipped with synthetic aperture radar (SAR), offers high resolution imaging capabilities, enabling continuous Earth observation under all weather conditions, both day and night. However, extracting meaningful information from Sentinel-1 imagery requires effective feature extraction techniques. This study investigates a range of feature extraction. A key aspect of SAR image preprocessing involves radiometric calibration, which ensures accurate backscatter values by correcting sensor-induced distortions. Speckle filtering is applied to reduce noise while preserving essential image details, improving interpretability. To enhance spatial accuracy, geometric terrain correction (range Doppler) is performed to mitigate distortions caused by terrain variations and sensor geometry. The study further explores how SAR-specific characteristics, such as backscatter intensity, polarization, and temporal coherence, influence the performance of different feature extraction techniques. Features like Waterbodies, Urban and Vegetation in Region of Interest is extracted with the above parameters.**

***Keywords*—Sentinel-1, Feature Extraction, Radiometric Calibration, Speckle filtering (Lee 7x7), Geometric terrain correction (range Doppler).**

I. INTRODUCTION

The rapid advancements in remote sensing technologies have revolutionized the way we observe and analyze the Earth's surface. Sentinel 1, a radar imaging satellite system under the European Space Agency's Copernicus Program, plays a crucial role in this transformation. Sentinel 1 offers high-resolution images that enable a wide range of applications, including environmental monitoring, disaster management, land use classification, and urban planning.

Remote sensing has become an essential tool for monitoring and analyzing Earth's surface features. Synthetic Aperture Radar (SAR) data, such as Sentinel-1, provides valuable insights due to its all-weather, day-and-night imaging capability. Unlike optical sensors, SAR can penetrate clouds and provide consistent observations, making it ideal for various applications, including land-cover classification. Feature extraction from Sentinel-1 data is crucial for distinguishing key surface types such as water bodies, vegetation, and urban areas.

In this study, we utilize the Band Math tool in ESA SNAP to extract water, vegetation, and urban features from Sentinel-1 data. By applying thresholding techniques and radar-based indices such as the Radar Vegetation Index (RVI), we aim to improve the classification accuracy of these features. The results of this study contribute to the ongoing efforts in SAR-based land cover classification and provide a foundation for further research in automated feature extraction.

II. STUDY AREA

The Madurai region, located at approximately 9°58'9" N latitude and 78°11'37" E longitude, lies in Tamil Nadu, India. This is a prominent city that has experienced significant urban growth in recent years. As a key urban hub in southern India, the city's expanding population and infrastructure have resulted in notable changes in land use and land cover. Monitoring these changes is essential for effective urban planning and resource management.

This study employs Sentinel-1A synthetic aperture radar (SAR) data to analyze urbanization patterns in Madurai using the Sentinel Application Platform (SNAP) tool. Various feature extraction techniques were applied to assess SAR parameters such as backscatter intensity and coherence, enabling the differentiation of urban areas from other land cover types. The findings provide valuable insights into the extent of urban development in Madurai, supporting data-driven planning and decision making.

FIG 1. LOCATION OF STUDY AREA MAP

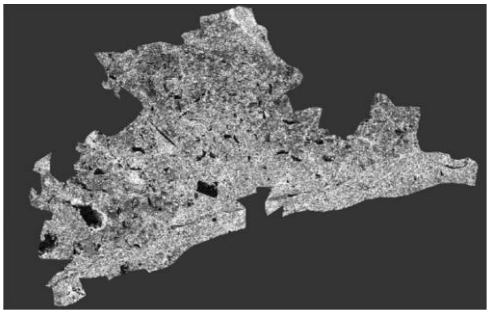

FIG 2. MADURAI REGION – SENTINEL 1A

III. METHODOLOGY

The system design for feature extraction is organized into four key components: Data Input, Preprocessing, Feature Extraction, and Output & Analysis. The data Input Layer focuses on collecting raw Sentinel-1 GRD imagery for the area of interest. The input data consists of Sentinel-1 imagery downloaded in Copernicus Open Access Hub, along with auxiliary data such as the Digital Elevation Model (DEM) for terrain correction.

A) Pre-processing

The Pre-processing Layer prepares raw Synthetic Aperture Radar (SAR) data for feature extraction by correcting and enhancing image quality. This stage includes several essential steps such as thermal noise removal, radiometric calibration, and speckle filtering using Lee filter. Terrain correction is applied using Range-Doppler terrain correction with DEM data to address geometric distortions.

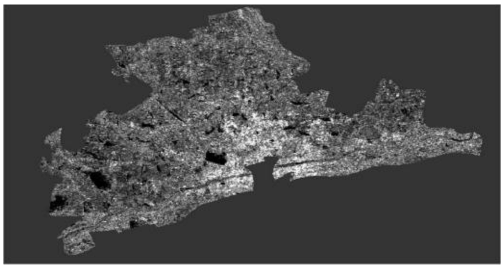

FIG 3. AFTER PRE-PROCESSING

B) Feature extraction

Relevant features are extracted from the pre-processed Sentinel-1 imagery using various algorithms and techniques. Threshold based methods are applied to delineate features such as water bodies, vegetation and urban areas.BandMath is used to extract features from the input image.

For waterbody extraction,

- 255*(Sigma0_VV < 2.22E-2)

Where

Sigma0_VV is Back scatter coefficient in Vertical-Vertical polarization. Similarly,

For Vegetation extraction

- If ((4 * Sigma0_VH) / (Sigma0_VV + Sigma0_VH)) > 0.5 then 1 else 0

Where

Sigma0_VH is the Backscatter coefficient in Vertical Horizontal polarization.

For Urban Footprint extraction

- If (Sigma0_VV > -8) and ((Sigma0_VH / Sigma0_VV) < 0.4) then 1 else 0

In which

White (1) feature that can be extracted and

Black (0) Other non-features

Finally, the Output & Analysis Layer focuses on visualizing and analyzing the extracted features for the intended application, such as Water, Vegetation and urban mapping using either supervised or unsupervised methods.

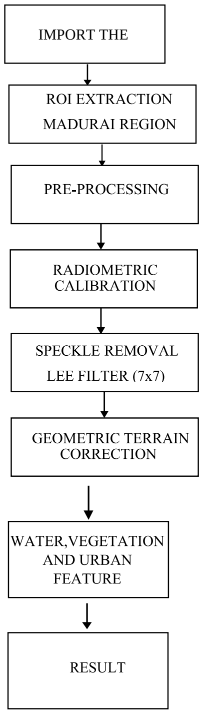

FIG 4. METHODOLOGY FLOWCHART

IV. RESULTS AND DISCUSSION

The waterbody extraction methodology successfully leveraged the backscatter coefficient differences between water and non-water surfaces. The key findings indicated high accuracy, with the SAR data effectively distinguishing waterbodies due to the strong contrast between smooth water surfaces and surrounding terrain. The analysis also captured seasonal fluctuations in waterbody extent, emphasizing Sentinel-1's ability to monitor dynamic water systems, irrespective of weather conditions or cloud cover.

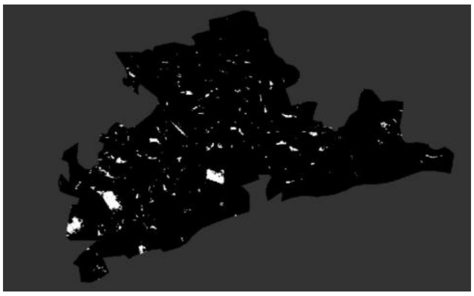

FIG 5. WATERBODIES EXTRACTION OF MADURAI REGION

For vegetation extraction, Vegetated areas exhibited higher backscatter due to volume scattering, and indices like the VH/VV ratio. The results showed distinct patterns, with dense vegetation exhibiting higher backscatter in VH polarization compared to VV polarization.

FIG 6. VEGETAION EXTRACTION OF MADURAI REGION

By analyzing the distinct backscatter patterns of built-up areas, urban regions, which typically exhibit high backscatter values due to structures like buildings and roads, were successfully identified. The analysis also uncovered clear spatial patterns of urban development and highlighted urban expansion and densification trends over time. However, challenges arose in detecting smaller or isolated settlements, and there were some misclassifications in areas with features like industrial complexes or dry riverbeds, which exhibited high backscatter values similar to urban areas.

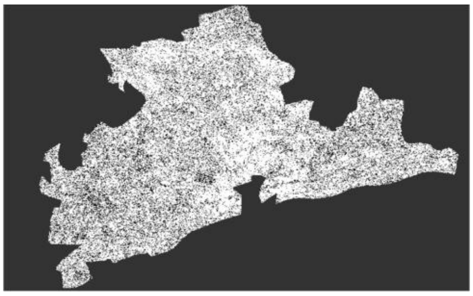

FIG 7. URBAN FOOTPRINT EXTRACTION OF MADURAI REGION

The discussions highlight the strengths and limitations of Sentinel-1 data. The all-weather capability of SAR proved invaluable, allowing for consistent monitoring even in the presence of clouds or adverse weather conditions. The frequent revisit time of Sentinel-1 allowed for detailed temporal monitoring of waterbodies and vegetation.

Moreover, the freely available data provided a cost-effective means of obtaining high-quality results without additional financial burden. However, false classifications, such as urban areas being mistaken for water, vegetation and urban, point to the need for enhanced pre-processing techniques and integration with additional data sources.

V. CONCLUSION

The extraction of waterbodies and vegetation from Sentinel-1 SAR data demonstrates the significant potential of synthetic aperture radar for environmental monitoring and land cover mapping. This project effectively delineated waterbodies, vegetation with high accuracy by leveraging the unique backscatter properties of SAR data. Sentinel-1's ability to operate in all weather conditions, combined with its high temporal resolution, provided robust and consistent results, particularly in areas prone to cloud cover or rapid changes. Key outcomes include the effective delineation of waterbodies, which captured seasonal variations and addressed challenges such as false positives in urban areas, although the results emphasize the strengths of Sentinel-1 data, limitations such as misclassification in complex land-use regions underscore the need for integrating optical imagery and advanced algorithms,

REFERENCES

[1] Cho, K., Park, S. E., Cho, J. H., Moon, H., & Han, S. H. (2020). Automatic urban area extraction from SAR image based on morphological operator. *IEEE Geoscience and Remote Sensing Letters*, *18*(5), 831-835.

[2] Ban, Y., Jacob, A., & Gamba, P. (2015). Spaceborne SAR data for global urban mapping at 30 m resolution using a robust urban extractor. *ISPRS Journal of Photogrammetry and Remote Sensing*, *103*, 28-37.

[3] Bao, L., Lv, X., & Yao, J. (2021). Water extraction in SAR images using features analysis and dual-threshold graph cut model. *Remote Sensing*, *13*(17), 3465.

[4] Hong, S., Jang, H., Kim, N., & Sohn, H. G. (2015). Water area extraction using RADARSAT SAR imagery combined with landsat imagery and terrain information. *Sensors*, *15*(3), 6652-6667.

[5] Zhang, P., Chen, L., Li, Z., Xing, J., Xing, X., & Yuan, Z. (2019). Automatic extraction of water and shadow from SAR images based on a multi-resolution dense encoder and decoder network. *Sensors*, *19*(16), 3576.

[6] Tsyganskaya, V., Martinis, S., Marzahn, P., & Ludwig, R. (2018). SAR-based detection of flooded vegetation–a review of characteristics and approaches. *International journal of remote sensing*, *39*(8), 2255-2293.

[7] Zhu, L., Walker, J. P., Ye, N., & Rüdiger, C. (2019). Roughness and vegetation change detection: A pre-processing for soil moisture retrieval from multi-temporal SAR imagery. *Remote sensing of environment*, *225*, 93-106.

[8] Azmedroub, B., Ouarzeddine, M., & Souissi, B. (2016). Extraction of urban areas from polarimetric SAR imagery. *IEEE Journal of Selected Topics in Applied Earth Observations and Remote Sensing*, *9*(6), 2583-2591.

[9] Hedman, K., Stilla, U., Lisini, G., & Gamba, P. (2009). Road network extraction in VHR SAR images of urban and suburban areas by means of class-aided feature-level fusion. *IEEE Transactions on Geoscience and Remote Sensing*, *48*(3), 1294-1296.

Assessing the Financial Feasibility and Operational Efficiency of Solar Energy: A Case Study of a Steel Manufacturing Unit

D. Suriya Kumari
Department of Electrical and Electronics Engineering,
Thiagarajar College of Engineering,
Madurai, India
dsuriyakumari93@gmail.com

Dr.P.S.Manoharan
Department of Electrical and Electronics Engineering,
Thiagarajar College of Engineering,
Madurai, India
psmeee@tce.edu

Dr. P. Deepamangai
Department of Electrical and Electronics Engineering,
SRM Madurai College for Engineering and Technology,
Madurai, India
deepamangaipalanivel@gmail.com

Dr.J.Vishnupriyan
Department of Electrical and Electronics Engineering,
Chennai Institute of Technology,
Chennai, India
vishnupriyanj@citchennai.net

***Abstract*—The swiftly evolving technologies harness the power of renewable energy sources to fulfill their energy requirements. When considering both technical and economic aspects, solar energy emerges as the most hopeful alternative energy source among unconventional options. This investigation employs the System Advisor Model (SAM) to scrutinize the financial viability and operational efficiency of a commercial photovoltaic (PV) system installed within a steel manufacturing facility in Indore, Madhya Pradesh, boasting a nameplate capacity of 416 kW DC. A variety of performance indicators, energy generation statistics, and financial metrics—including the nominal levelized cost of electricity (LCOE), net present value (NPV), and payback duration—are factored into the evaluation. With a theoretical LCOE of 2.4 cents/kWh, an NPV of Rs.2.1Crores, and a payback duration of 12.2 years, the findings illustrate the economic advantages of the system and its potential to promote the adoption of renewable energy.**

Keywords—Solar PV system, PV system designing, financial parameters, inverters

I. Introduction

Risks to environmental sustainability and growing energy demands have driven the shift to renewable energy. PV systems offer clean, reliable energy. This study uses the System Advisor Model (SAM) to assess the financial feasibility and performance of a 416 kW DC commercial PV system installed at a steel fabrication plant, reflecting renewable integration in the industrial sector. Urban metro systems, vital for low-carbon transit, are energy-efficient and emit fewer pollutants, supporting urban clean electrification [1]. Green energy is gaining value in global energy markets due to fossil fuel scarcity, high prices, and the urgency to cut emissions [2]. A study explored the causal links between renewable energy advancements and green finance, considering factors like increased economic activity, renewable power generation, and private sector investment [3]. A generic modeling framework combining novel forecasting, space and water heating loads, and renewable generation was developed to analyze hybrid energy patterns [4]. The industrial sector is increasingly adopting renewable options to enhance resilience and ensure long-term economic and energy sustainability [5]. Smart grids (SGs) have emerged to support this transition by integrating renewable sources with flexibility, automation, and adaptability [6].

Literature Survey

A detailed study regarding renewable energy-powered manufacturing units based on different locations have been evaluated. The development of non-conventional energy sources has been acknowledged as an effective approach to environmental preservation in light of the rapidly changing global energy landscape, which is characterized by dwindling conventional fossil fuel resources and a continuous increase in greenhouse gas emissions [7]. The right norms for the system's intrinsic components must be selected, and the required load must be established, in order to finish the modeling [8]. Modeling and simulation are necessary to comprehend the overall sustainability and technological financial feasibility of solar plants [9]. At night, radiation solar radiation is not available, even though the sun's brightness and the design and measurement of PV cells vary by country [10]. PVsyst and TRNSYS are the best tools for estimating the annual production of solar systems, with an accuracy of just 2%. The results are significantly influenced by weather stations and software [11]. Assessing the suitability of solar PV deployment at a specific location is crucial for building a solar PV-based self-sustaining power-generating infrastructure [12]. There are numerous ways to set up photovoltaic (PV) systems for power generation, from solar energy plants and transportable solar-powered chargers to freestanding rooftop panels [13]. SAM software is reliable techniques to determine the electrical energy provision for PVS with an appropriate margin of uncertainty for annual power production [14]. Among commercial sector, a retail hub is designed using SAM software involving rooftop photovoltaic system [15].

Novelty of the work

Few studies have been conducted on the usage of PV structures within metro stations; much of the study that has been done so far has been on residential, office, and commercial buildings as well as airports and train stations. The metro system is a major energy consumer and carbon emitter in addition to being a crucial part of the infrastructure supporting urban transit. Incorporating photovoltaic rooftop systems into the industrial sector could enhance the usage of renewable energy sources and lower carbon emissions. However, there is currently little study on the use and feasibility evaluation of PV systems at steel fabrication facilities. To address this knowledge gap, the study maximizes the net present value of the system from a technical and economic standpoint and investigates the potential use of photovoltaic systems in steel mills. An elevated metro station's basic solar system is proposed based on the model made with SAM software.

II. System Description

Steel fabrication plant

A steel fabrication plant located in Indore, Madhya Pradesh is taken as a case study for analyzing the installation and maintenance of a solar PV system. The steel plant with latitude and longitude of 22.7196^0N and 75.8577^0E receives an annual solar radiation of 4514 Wh/m^2.

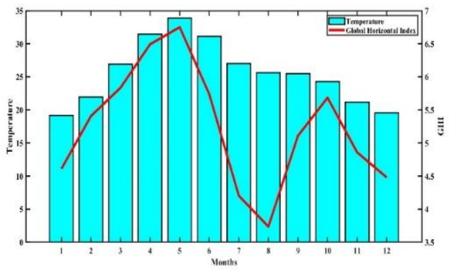

Fig 1. Temperature and GHI

The average temperature is accounted to be 25.68^0C and the annual wind speed is about 5.60 m/s. The annual average global horizontal index (GHI) is recorded to be 5.24 kWh/m^2/day. Figure 1 shows the temperature (^{0}C) and global horizontal index (kWh/m^2/day) of the selected site.The considered steel plant case study has a load profile as shown in Table 1.

Table 1. Case study load requirement

S. No.	Area	Load (kW)	Duration (hrs.)
1	Parking Garage/Utility Areas	5	6
2	Lighting	40	12
3	HVAC Loads	6	12
4	Steel fabrication Equipment	330	10

Figure 2 shows the load profile of the steel plant over a year.

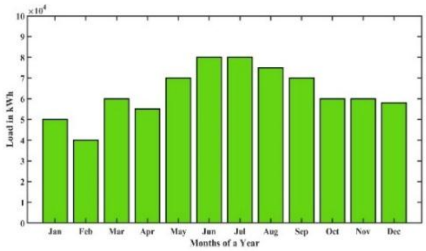

Fig 2. Load Profile over a year

PV module design

The suitable PV module to serve the given application is S-Energy SN375M-10. The electrical specification of the selected module is given in Table 2.

Table 2. Electrical Specification of S-Energy SN375M-10 PV module

Specification	Value
Max. power point voltage (Vmp)	40.2 V
Max. power point current (Imp)	9.32 A
Open circuit voltage	47.7 V
Short circuit current	9.79 A
Reference bandgap voltage	1.121 eV

The 1,110 monocrystalline silicon modules that make up the PV system under analysis have a combined area of 1,810 m^2 and a 416 W DC capacity. There are neither backtracking nor tracking systems in place.

Inverter Design and Orientation of the Panel

The system employs a custom inverter [16] with a capacity of 550 kW AC, resulting in a DC-to-AC capacity ratio of 0.76. Figure 2 shows the orientation of the panel. The array is fixed at a tilt angle of 22.73° and an azimuth angle of 180° (south-facing). Figure 3 indicates the tilt and azimuth angle.

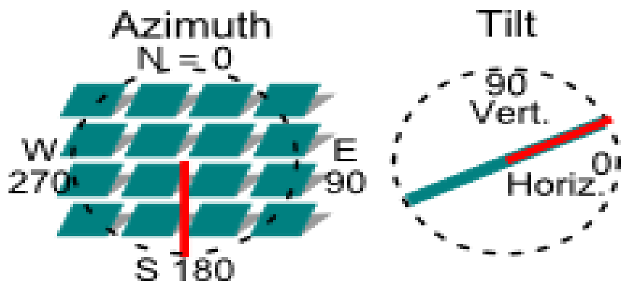

Fig 3. Orientation of the panel

III. Methodology

The PV system design for the steel plant is implemented using System Advisor Model (SAM) software. With its thorough approach to performance modeling, financial analysis, and design optimization, SAM is a vital tool for PV system designers. It enables users to construct effective, economical solar PV systems and make data-driven decisions by combining thorough technical and financial evaluations.

Mathematical modeling of PV cell

The solar cell's analogous circuit is shown Figure 4. In actual cells, power is lost through a shunt resistance (Rsh) brought on by leakage current and a series resistance (Rs) produced by the ohmic contact in the front surface. Consequently, the equivalent circuit for a working solar cell consists of "Rsh" added in parallel with the diode and "Rs" added in series with the load [17,18].

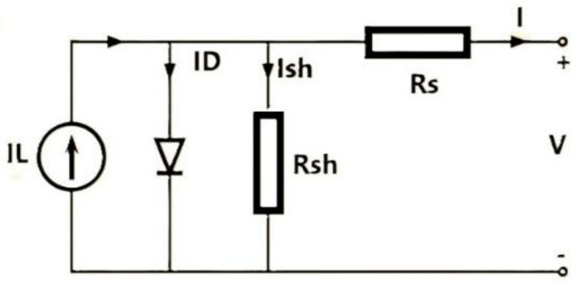

FIG 4. EQUIVALENT CIRCUIT OF PV CELL

I-V Characteristics of PV Module

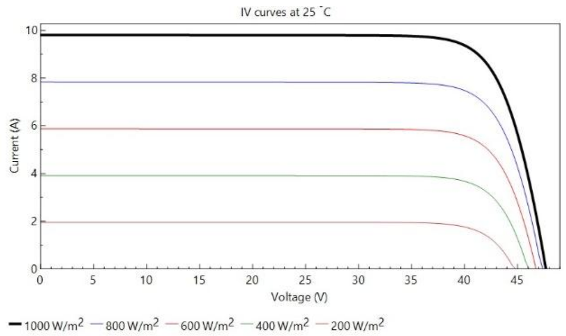

FIG 5. I-V CURVE AT STANDARD TEMPERATURE CONDITION(25^0C)

Understanding the performance, efficiency, and behavior of photovoltaic (PV) panels under different conditions depends on their I-V (Current-Voltage) properties. Key performance metrics including the short-circuit current (Isc), open-circuit voltage (Voc), and maximum power point (MPP), which indicates the panel's peak power output, are shown by the I-V curve, which shows the relationship between current and voltage. Selecting a proper PV panel is accomplished when the proper I-V curve is derived from the panel characteristics concerning the open circuit voltage and short circuit current specifications. Figure 5 showcases the I-V curve obtained for S-Energy SN375M-10 panel at different irradiation levels.

Energy and peak load for simulation

The energy requirement and the peak load values at each month are tabulated in Table 3 which briefs the key task for simulation of the PV system that meets 50% of the daily power requirement of the steel plant.

Table 3. Energy and Peak load data

Months	Energy(kWh)	Peak(kW)
Jan	57339.49	234.68
Feb	48557.32	173.42
Mar	55750.08	172.01
Apr	53014.93	191.43
May	60460.75	198.29
Jun	70152.34	236.47
Jul	77708.46	274.23
Aug	77555.05	260.34
Sep	61793.68	226.75
Oct	57692.48	185.12
Nov	51845.28	156.20
Dec	54338.53	184.05
Annual	726208.38	274.23

IV. RESULTS AND DISCUSSION

The PV system with the inverter and the load requirements are simulated using SAM software and are analyzed in various aspects. The system achieves a first-year energy production of 640,851 kWh with a capacity factor of 17.6% and a performance ratio of 0.81.

Financial Analysis

The financial analysis has been summarized as following points.

- **Nominal LCOE**: 2.4 cents/kWh.
- **Net present value (NPV):** Rs.2.1Cr.
- **Payback period:** 12.2 years. Annual savings of Rs.39.45Lakhs are realized, with significant reductions in monthly electricity bills ranging from Rs.2.1Lakhs to Rs.4.6Lakhs.

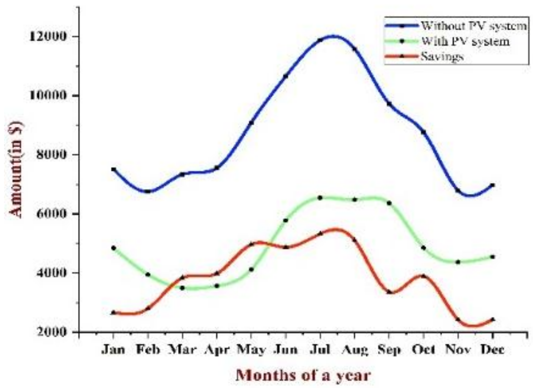

FIG 6. COST SAVING

The cost saving is obtained from the difference in energy acquired before and after installing PV system. Figure 6 shows the amount saved with the aid of renewable penetration. The project benefits from a 30% federal ITC, reducing the total investment cost. With 100% debt financing at a 4% interest rate over 25 years, the system demonstrates strong financial feasibility.

ENVIRONMENTAL IMPACT

The system supports renewable energy targets and significantly lowers carbon emissions by offsetting about 640,851 kWh of grid electricity yearly. The substantial environmental benefits are indicated by the high energy output.

LOSS ANALYSIS

Various loss factors influencing system performance were examined, including:

- **Soiling:** 5%
- **Inverter efficiency losses:** 4%
- **DC wiring losses:** 2%
- **Reflection (IAM):** 1.584%

These factors collectively impact energy yield and overall system efficiency.

V. CONCLUSION

Future research can examine the effects of advanced technologies, such as tracking systems and storage integration, on system performance and economics. This study shows how effective it is to use SAM to analyze the performance and financial viability of PV systems in a steel fabrication plant located in Indore. The results show that the PV system is financially viable, achieving a positive NPV and a short payback period relative to the project's 25-year lifespan. The nominal LCOE of 2.4 cents/kWh highlights the system's competitive cost structure compared to conventional energy sources.

ACKNOWLEDGEMENT

The authors extend their due thanks to the Thiagarajar College of Engineering management, Madurai, India for their extensive research facilities and the financial backing from Thiagarajar Research Fellowship (TRF) scheme (File.no: TCE/RD/TRF/2024/<<19>> dated 09-02-2024) is gratefully acknowledged.

REFERENCES

[1] Ellabban, O., Abu-Rub, H. and Blaabjerg, F., 2014. Renewable energy resources: Current status, future prospects and their enabling technology. *Renewable and sustainable energy reviews*, *39*, pp.748-764.

[2] Bei, J. and Wang, C., 2023. Renewable energy resources and sustainable development goals: evidence based on green finance, clean energy and environmentally friendly investment. *Resources Policy*, *80*, p.103194.

[3] Lü, X., Lu, T., Karirinne, S., Mäkiranta, A. and Clements-Croome, D., 2023. Renewable energy resources and multi-energy hybrid systems for urban buildings in Nordic climate. *Energy and Buildings*, *282*, p.112789.

[4] Usman, F.O., Ani, E.C., Ebirim, W., Montero, D.J.P., Olu-lawal, K.A. and Ninduwezuor-Ehiobu, N., 2024. Integrating renewable energy solutions in the manufacturing industry: challenges and opportunities: a review. *Engineering Science & Technology Journal*, *5*(3), pp.674-703.

[5] Khalid, M., 2024. Smart grids and renewable energy systems: Perspectives and grid integration challenges. *Energy Strategy Reviews*, *51*, p.101299.

[6] Mishra, P.R., Rathore, S. and Jain, V., 2024. PVSyst enabled real time evaluation of grid connected solar photovoltaic system. *International Journal of Information Technology*, *16*(2), pp.745-752.

[7] Moustafa, M., Mahmoud, M., Akef, S. and Swillam, M., 2024. Design and simulation analysis of 130 KWp grid-connected solar PV system using PVsyst: A case study in Egypt. In *Journal of Physics: Conference Series* (Vol. 2689, No. 1, p. 012015). IOP Publishing.

[8] Salgado, P.C.V., 2024. Comparative experimental analysis of the annual energy production of a 72kWn photovoltaic solar power plant installed on a roof for self-consumption in the city of Monteria using PVsyst, PVGIS and SAM.

[9] Khan, M. M., Ahmad, S., Raza, A., Haroon, S., Hassan, R. G., & Shafi, M. A. (2024). Performance analysis of PVSyst based grid connected photovoltaic systems in Pakistan compared to SAARC countries. Mehran University Research Journal Of Engineering & Technology, 43(2), 112–122. https://search.informit.org/doi/10.3316/informit.T2024042500010201877246865

[10] AMIN, M.T., 2024. A Comparative Analysis of Various Simulation Software for grid-connected Residential Building: A Case Study at Jeddah, Saudi Arabia. *Yanbu Journal of Engineering and Science*. https://doi.org/10.53370/001c.94809

[11] Pramanick, D. and Kumar, J., 2024. Performance and degradation assessment of two different solar PV cell technologies in the remote region of eastern India. *e-Prime-Advances in Electrical Engineering, Electronics and Energy*, *7*, p.100432. https://doi.org/10.1016/j.prime.2024.100432

[12] Radwan, A., Mdallal, A., Haridy, S., Abdelkareem, M.A., Alami, A.H. and Olabi, A.G., 2024. Optimizing the annual energy yield of a residential bifacial photovoltaic system using response surface methodology. *Renewable Energy*, *222*, p.119914. https://doi.org/10.1016/j.renene.2023.119914

[13] Komrit, S. and Zabihian, F., 2023. Comparative analyses of solar photovoltaic, wind turbine, and solar photovoltaic and wind turbine hybrid systems: Case study of Thailand. *Energy Conversion and Management*, *293*, p.117479. https://doi.org/10.1016/j.enconman.2023.117479.

[14] Kavuma, C., Sandoval, D. and de Dieu, H.K.J., 2022. Analysis of solar photo-voltaic for grid integration viability in Uganda. *Energy Science & Engineering*, *10*(3), pp.694-706. DOI: 10.1002/ese3.1078.

[15] Kumari, D.S., Manoharan, P.S., Vishnupriyan, J., Priyadarshini, R., Usha, N. and Kalimuthu, M., 2024, October. Structuring a Renewable Energy System Powered Retail Hub using Pvsyst Software. In *2024 First International Conference on Software, Systems and Information Technology (SSITCON)* (pp. 1-5). IEEE.

[16] Muthuramalingam, M. and Manoharan, P.S., 2015. Energy comparative analysis of MPPT techniques for PV system using interleaved soft-switching boost converter. *World Journal of Modelling and Simulation*, *11*(2), pp.83-93.

[17] Deepamangai, P. and Manoharan, P.S., 2020. Detection and estimation of grid-connected issues in quasi-Z-source inverter based photovoltaic system using robust parametric methods. *IET Power Electronics*, *13*(16), pp.3661-3674.

[18] Swathika, S., Manoharan, P.S. and Priyadarshini, R., 2022, June. Classification of faults in pv system using artificial neural network. In *2022 7th International Conference on Communication and Electronics Systems (ICCES)* (pp. 1359-1363). IEEE.

Enhancing Wind Power Forecasting: A Comparative Study of Machine Learning Models with Residual Analysis for Homoscedasticity

Usha.N
Department of Electrical and Electronics Engineering,
Thiagarajar College of Engineering,
Madurai
nushalingam@gmail.com

Dr. P. S. Manoharan
Department of Electrical and Electronics Engineering,
Thiagarajar College of Engineering,
Madurai
psmeee@tce.edu

Dr. G. Thenmozhi
Department of Automobile Engineering,
Kumaraguru College of Technology,
Coimbatore
thenmozhi.g.auto@kct.ac.in

Dr. P. S. Manoharan
Department of Electrical and Electronics Engineering,
Francis Xavier Engineering College,
Tirunelveli
raviarmugam@gmail.com

***Abstract*—Wind energy is a vital renewable resource in the global transition towards sustainable energy, helping to meet electricity demand and reduce carbon emissions. Accurate wind power generation forecasting is crucial for efficient grid integration and minimizing risks from wind energy's inherent variability. This study evaluates the performance of several machine learning (ML) models, including Random Forest, XGBoost, Support Vector Machine (SVM), and Long Short-Term Memory (LSTM) networks, in predicting wind power consumption based on wind speed, wind direction, and theoretical power curve data. Performance metrics such as Root Mean Squared Error (RMSE), Mean Absolute Error (MAE), and R-squared are used to assess model accuracy. Furthermore, the study investigates homoscedasticity and heteroscedasticity in the residuals of the models. Homoscedasticity, which assumes constant variance of residuals, is crucial for model validity, while heteroscedasticity indicates changing error variance, potentially signaling model deficiencies. The results suggest that models like XGBoost and Random Forest show strong prediction capabilities. However, the assumption of homoscedasticity contributes significantly to ensure forecast accuracy and reliability. The study emphasizes the importance of residual analysis to detect heteroscedasticity, which, if left unaddressed, can lead to inaccurate predictions. This research delivers valued understanding of homoscedasticity and heteroscedasticity on wind power forecasting, contributing to more informed decisions in energy production and grid management.**

Keywords—Wind Power prediction, Residual, Homoscedasticity, Performance Metrics, Q-Q plot.

I. INTRODUCTION

Wind energy is a rapidly expanding renewable energy source that produces electricity by harnessing wind currents, hence lowering carbon emissions and halting global warming. Wind energy is harnessed by wind turbines and converted into electrical power. Over the last ten years, wind energy has become increasingly capable on a global scale, and governments and international organizations have set high goals to raise the percentage of wind energy in the world's electricity mix. Developments in power generation, grid integration, and turbine efficiency have all aided in this expansion. Cost-effectiveness, sustainability, and minimal environmental impact are provided by wind energy. Its unpredictable and sporadic nature, however, makes energy forecasting and grid stability difficult. The accuracy of power generation has increased with the use of machine learning and deep learning models in wind energy forecasting. These models examine intricate wind patterns and offer insights into the distribution and production of energy. This research establishes the foundation for future advancements in wind energy forecasting methods by assessing the performance of several machine learning models in forecasting wind energy power consumption.

A. Literature Survey:

The accurate prediction of wind power is crucial to ensure effective integration of wind energy into the grid, optimizing energy production and minimizing variability. Several studies have investigated the use of machine learning (ML) models for wind power prognostication, exploring various approaches to improve predictive accuracy and model robustness.[1] conducted a comparative study on several machine learning models for wind power prediction, including Support Vector Regression (SVR) and XGBoost. Their study emphasized the significance of hyperparameter optimization and model selection in improving forecasting performance. Furthermore, they suggested that hybrid models, which combine different algorithms, have the potential to enhance prediction reliability and accuracy. [2] examined the application of SVR and XGBoost for wind power forecasting and reported that SVR outperformed XGBoost in terms of prediction accuracy. They acknowledged the need for further optimization of these models to improve their generalization capability across different datasets and forecasting scenarios. [3] focused on the impact of feature selection and hyperparameter optimization on the performance of Gradient Boosting and XGBoost models in wind power forecasting. Their findings highlighted that the application of feature selection significantly improved model performance, underscoring the importance of identifying relevant features for more accurate wind power predictions. [4,11] explored the use of Long Short-Term Memory (LSTM) networks for wind power prediction, highlighting the ability of LSTMs to capture temporal dependencies in wind data. Their results demonstrated that LSTM networks significantly outperformed traditional regression models, suggesting the potential of deep learning models for short-term wind power forecasting. [5] proposed a hybrid model combining Support Vector Regression (SVR) and Random Forest for wind power prediction. Their study demonstrated that the hybrid approach provided superior performance compared to using individual models, suggesting that hybrid models are more effective in handling the complex nature of wind power data. [6] compared the performance of Random Forest and Gradient Boosting models for wind power forecasting, revealing that both models provided comparable results, with Gradient Boosting offering a slight edge in prediction accuracy. [7] explored the use of a hybrid model combining Support Vector Regression (SVR) and LSTM networks for wind power prediction. The study found that the hybrid model captured non-linear relationships and temporal patterns in the data, offering a more accurate forecasting solution compared to single-model approaches. [8, 15] conducted a comparative study on different machine learning models for wind power prediction, including Random Forest, XGBoost, and LSTM networks. They found that ensemble models, such as Random Forest, showed robust performance for wind power forecasting, while LSTM networks proved effective in capturing temporal trends and non-linear relationships in the data. [9] proposed a hybrid model that combined Random Forest and LSTM networks for wind power prediction. Their study demonstrated that the hybrid approach significantly improved prediction accuracy compared to individual models, indicating that the integration of machine learning techniques can address the complexities inherent in wind power forecasting. [10,12] investigated the use of Neural Networks and Support Vector Machines (SVM) for wind power prediction. [13,14] study emphasized the importance of conducting systematic model evaluations using a variety of performance metrics to ensure the reliability of forecasts in homoscedasticity. The findings indicated that both models delivered reasonably accurate forecasts, with SVM performing slightly better in reducing error metrics. The study highlighted the need for further research into optimizing these models for large-scale wind energy applications. Collectively, these studies underline the growing reliance on machine learning techniques for wind power forecasting. The results suggest that models such as Random Forest, XGBoost, Support Vector Regression, and Long Short-Term Memory networks offer promising solutions for predicting wind power. However, they also emphasize the importance of model optimization, feature selection, and the use of hybrid approaches to improve forecasting accuracy and robustness. Further research into model evaluation, residual analysis, and hybrid methodologies is essential to advance the field of wind power forecasting.

The uniqueness of this work stems from its novel approach to wind power forecasting by integrating advanced machine learning models with residual analysis for homoscedasticity and residuals, also focused on model outcomes using traditional metrics like RMSE, MAE, and R-squared, this research goes beyond by examining the variance of residuals to assess the reliability and robustness of models. By comparing models such as Random Forest, XGBoost, Support Vector Machine, and LSTM under different residual behaviours, this learning offers deeper preceptive on limitations and strengths of each model for wind power prediction. The inclusion of homoscedasticity analysis highlights the importance of considering error variance changes, ultimately contributing to more accurate and reliable forecasts for effective integration of wind energy into the grid. This work provides a comprehensive, novel methodology for model evaluation, emphasizing the role of residual diagnostics in improving forecasting performance.

II. Data Processing

An important feature of this is the incorporation of the residual analysis and the homoscedasticity, which check for the normality and the variance consistency of the residuals, respectively. This makes sure that the model's predictions comply with foundational statistical principles, further strengthening reliability. If a residual does not pass the tests, the workflow will put itself back in train models again highlighting an iterative process in refining actions. Also, the integrated various performance measures, such as RMSE, MAE, MSE, and R2, can be very useful in making a holistic assessment of model accuracy. This systematic approach makes it very precise and is exactly the kind of training that the causation model for the high degree of variation in forecasts of wind energy should have. Thus, the iterative testing and checking of results render this particular workflow as yet another strong entrant in innovative approaches to machine learning in renewable energy forecasting.

A. Algorithm Steps

1. **Load and split** the dataset into X_train, X_test, y_train, y_test using an 80/20 split.
2. **Train** the model using the training data: model. fit(X_train, y_train).
3. **Predict** the target values on test data: y_pred = model. Predict(X_test).
4. Plot **residuals vs. predicted value**s to check for constant variance (no specific formula).
5. **Performance Metrics Calculation** for the actual and the predicted value using RMSE, MSE, R^2, Variance and residuals with y_test - y_pred.
6. **Model Selection** by comparison of performance metrics calculation.
7. **Visualisation** of the results

Figure 1 illustrates a systematic machine learning pipeline, beginning with loading and preprocessing the dataset, where data is cleaned, normalized, and encoded to prepare it for analysis. The data is subsequently divided into training and testing sets, followed by selecting and training machine learning models. Predictions are generated using the test set, and residual analysis is performed to check the normality of residuals, ensuring they follow a normal distribution. A homoscedasticity test is then conducted to confirm that the residuals have constant variance. If these checks fail, the models are retrained or preprocessing is adjusted. Once the assumptions are met, performance metrics such as accuracy, RMSE, MAE, and R² score are computed to assess the model. Finally, the results are saved, and visualizations are generated to summarize findings. The workflow includes feedback loops for iterative refinement, ensuring robust and reliable model performance.

III. RESULTS AND DISCUSSION

Random Forest (RF) is a robust model for wind energy data, achieving a high RMSE of 414.16, MSE of 171,529.58, and R-squared of 0.899. However, it faces challenges in handling the dataset's variability and residual plots. Gradient Boosting (GB) is a sequential technique that optimizes residual errors at each stage, performing better than other models. Extra Trees (ET) produce slightly lower results, explaining less variance than Random Forest and showing a wider spread, leading to higher error rates. Support Vector Regression (SVR) determines which hyperplane best fits the data, but its residuals significantly deviate from a normal distribution, leading to less reliable predictions. Linear regression (LR) has a large residual spread, indicating its limitations in handling non-linear relationships in wind energy data. Ridge Regression (RR) penalizes large coefficients to reduce overfitting, performing similarly to Linear Regression. The results of Lasso Regression (LR), which incorporates a penalty for feature selection, are similar to those of Linear and Ridge Regression, but neither feature selection nor regularization produce significant benefits. The wind energy dataset presented similar prediction accuracy challenges for all three models, as the Lasso Regression residuals box plot resembles the Ridge and Linear Regression models.

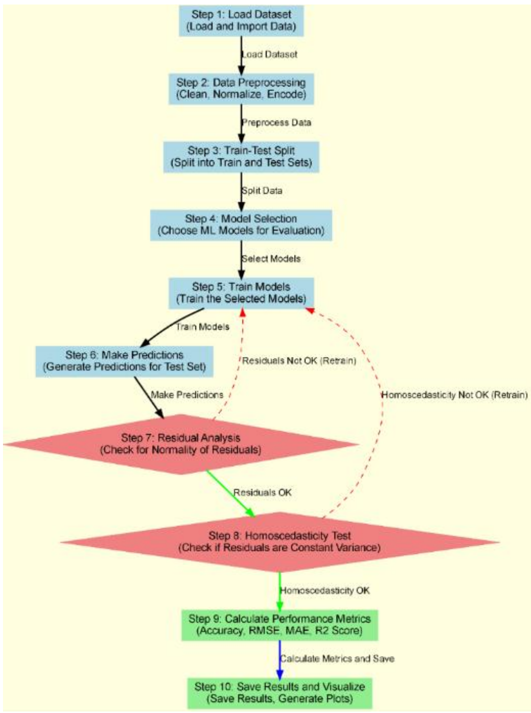

FIG.1. FLOWCHART

Table 1 shows the performance metrics of all the models and Gradient Boost shows best accuracy compared to other models.

TABLE 1: RESULTS OF METRICS

Models	RMSE	MAE	R^2
Random Forest	411.96	170.62	0.90
Gradient Boosting	383.48	160.95	0.91
Extra Trees	426.36	177.88	0.89
SVR	421.39	162.64	0.89
Linear Regression	411.71	188.75	0.90
Ridge Regression	411.71	188.75	0.90
Lasso Regression	411.70	188.67	0.90

The performance of the models is evaluated using three key metrics: Mean Absolute Error (MAE), Root Mean Square Error (RMSE), and R-squared (R²). MAE provides a measure of the average magnitude of prediction errors, without considering their direction, and is useful for understanding the overall deviation between predicted and actual values. RMSE, on the other hand, emphasizes larger errors more strongly, making it a sensitive indicator of significant deviations. Meanwhile, R² reflects how well each model explains the variance in the target variable, with values closer to 1 indicating stronger predictive capability. Collectively, these metrics offer a comprehensive perspective on model performance, guiding the selection of the most effective model based on both error minimization and explanatory strength.

The residual plot in Figure 2 displays residual distributions for different models, where smaller spread and centered residuals indicate better predictions. The box represents the interquartile range (IQR), with whiskers showing variability and outliers as scattered points A homoscedasticity plot in Figure 3 ensures residuals have constant variance. Random scatter indicates reliability, while patterns suggest inconsistencies.

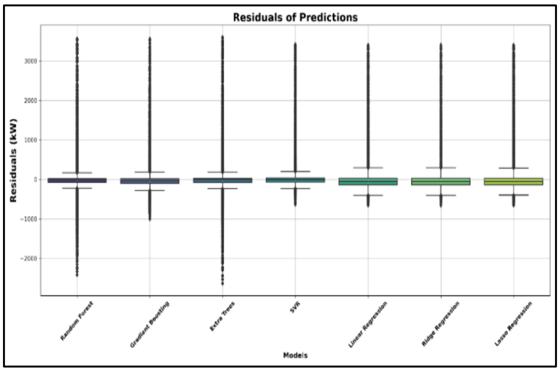

FIG 2. RESIDUAL PLOT

A more uniform residual distribution supports gradient boosting's effectiveness, while linear regression models (Linear, Ridge, and Lasso) have a more pronounced residual spread. The Q-Q plot in figure 4 shows the residuals' conformity to a normal distribution, with Gradient Boosting showing a near-linear fit along the line. However, Random Forest and Extra Trees struggle to handle extreme values, while SVR and linear models struggle with normally distributed residuals. Gradient Boosting consistently performs well with few outliers due to its tighter interquartile range (IQR). Extra Trees, SVR, and linear models show a wider IQR and more outliers, suggesting they are more susceptible to variations in wind energy data and less able to handle outliers than Gradient Boosting.

IV. Conclusion

Machine Learning models for wind energy prediction are thoroughly analyzed using real wind power data. By focusing on default model configurations without hyperparameter tuning, we established that Gradient Boosting was the most effective model, offering the lowest prediction errors. Even though they are less accurate than ensemble models, the results also demonstrate that less complex models, like Lasso, Ridge, and Linear regression, balance simplicity and performance and are thus suitable options in resource-constrained settings. Future studies can look into hyperparameter optimization, the addition of new models like neural networks, and the integration of real-time data to further increase the accuracy and applicability of wind energy forecasting models. Further research into the effects of various feature sets, such as adding meteorological and turbine-specific data, may offer an even more profound understanding of the intricacies involved in wind energy forecasting

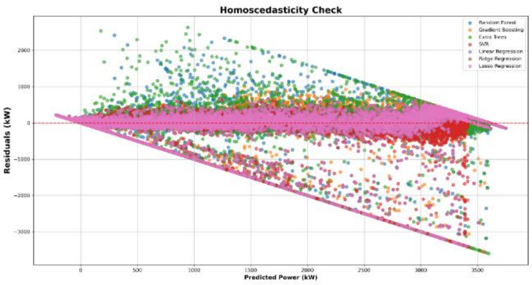

Fig.3. Homoscedasticity Plot

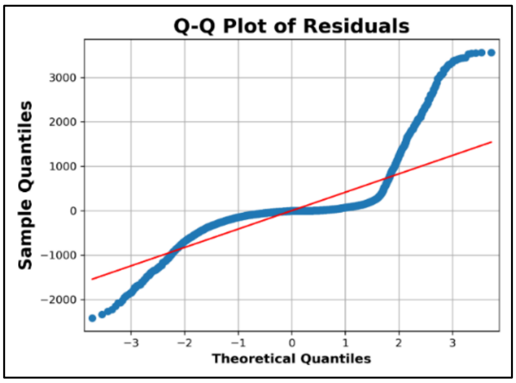

Fig.4. Q-Q Plots of Residuals

Data Availability

One year data from January 2018 to December 2018 is taken from Wind Turbine Scada Dataset from Kaggle.

Acknowledgment

The authors extend their due thanks to the Thiagarajar College of Engineering Management, Madurai, India for their extensive research facilities and the financial backing from the Thiagarajar Research Fellowship (TRF) scheme (File.no: TCE/RD/TRF/08 dated 30.8.2023) is gratefully acknowledged.

V. References

[1] Singh, A., Sharma, A., & Kumar, R., 2020. Wind Power Prediction Using Machine Learning Models: A Comparative Study. Renewable and Sustainable Energy Reviews, 122, pp. 109-121. https://doi.org/10.1016/j.rser.2020.109-121.

[2] Zhou, X., Li, J., & Wang, Y., 2021. Wind Power Prediction Using Support Vector Regression and XGBoost. Energy, 222, pp. 300-312. https://doi.org/10.1016/j.energy.2021.300-312.

[3] Li, Z., Liu, T., & Chen, J., 2022. Feature Selection and Hyperparameter Optimization in Wind Power Forecasting: Comparison of Gradient Boosting and XGBoost. Energy Reports, 8, pp. 1492-1503. https://doi.org/10.1016/j.egyr.2022.1492-1503.

[4] Zhang, H., Zhang, L., & Liu, W., 2023. Long Short-Term Memory Networks for Wind Power Prediction. Energy Conversion and Management, 267, pp. 1155-1164. https://doi.org/10.1016/j.enconman.2022.1155-1164.

[5] Huang, L., Chen, Q., & Zhang, T., 2022. Hybrid Support Vector Regression and Random Forest Model for Wind Power Prediction. Applied Energy, 305, pp. 117-128. https://doi.org/10.1016/j.apenergy.2022.117-128.

[6] Chen, B., Yang, H., & Zhang, L., 2022. Random Forests and Gradient Boosting Models for Wind Power Prediction: A Comparative Study. Renewable Energy, 165, pp. 1481-1492. https://doi.org/10.1016/j.renene.2022.1481-1492.

[7] Kumar, V., Ghosh, A., & Gupta, P., 2020. Prediction of Wind Power Using Support Vector Regression and LSTM Networks. Neural Computing and Applications, 32(15), pp. 10241-10250. https://doi.org/10.1007/s00542-020-05706-6.

[8] Brito, J., Melo, D., & da Silva, R., 2021. Comparative Study of Machine Learning Models for Wind Power Prediction. Journal of Renewable and Sustainable Energy, 13(6), pp. 219-230. https://doi.org/10.1063/5.0057027.

[9] Sadeghi, S., Forouzandeh, M., & Vafaie, H., 2021. A Hybrid Model for Wind Power Prediction: Combining Random Forest and LSTM. Energy, 230, pp. 1205-1218. https://doi.org/10.1016/j.energy.2021.1205-1218.

[10] Patel, M., Mehta, P., & Desai, S., 2020. Neural Network and Support Vector Machine for Wind Power Prediction. Journal of Energy Engineering, 146(2), pp. 05020002. https://doi.org/10.1061/jenviv.05020002.

[11] Anbumozhi, S. and Manoharan, P.S., 2014. Performance analysis of high efficient and low power architecture for fuzzy based image fusion. *American Journal of Applied Sciences*, *11*(5), p.769.

[12] Deepamangai, P. and Manoharan, P.S., 2019. Robust controller for grid-connected quasi-admittance source inverter for photovoltaic system. *Electric Power Systems Research*, *175*, p.105879. https://doi.org/10.1016/j.epsr.2019.105879

[13] Abubakar, M., Che, Y., Bhutta, M.S. and Zafar, A., 2025. Multi-renewable energy resources parameters prediction through meta-learning models selectivity

analysis and parallel fusion approaches. *Electrical Engineering*, pp.1-24. https://doi.org/10.1007/s00202-025-03000-2

[14] Usha.N, P. S. Manoharan, D. S. Kumari, M. Kalimuthu and R. Priyadarshini, "An Unsupervised Learning Model Investigation for Data Inaccuracies in Comparison with Machine Learning Algorithms," *2024 5th International Conference on Electronics and Sustainable Communication Systems (ICESC)*, Coimbatore, India, 2024, pp. 1655-1659, doi: 10.1109/ICESC60852.2024.10689792.

[15] França, R.P., Bonacin, R. and Monteiro, A.C.B., 2025. A machine intelligence model based on random forest for data related renewable energy from wind farms in Brazil. In *Computer Vision and Machine Intelligence for Renewable Energy Systems* (pp. 127-139). Elsevier. https://doi.org/10.1016/B978-0-443-28947-7.00007-0

Performance Evaluation of Grey Wolf Optimizer and Sine Cosine Angle Algorithm in ORPD with FACTS Devices

M. Kalimuthu
Department of Electrical and Electronics Engineering, Thiagarajar College of Engineering Line,
Madurai, India
kali20e@gmail.com

Dr. P.S. Manoharan
Department of Electrical and Electronics Engineering, Thiagarajar College of Engineering,
Madurai, India
psmeee@tce.edu

Dr. M. Muthuramalingam
Department of Electrical and Electronics Engineering, P.T.R. College of Engineering and Technology,
Madurai, India
muthuramjaya23@gmail.com

***Abstract*—Optimal Reactive Power Dispatch (ORPD) plays a crucial role in enhancing power system stability, minimizing power losses, and improving voltage profiles. This paper presents an efficient met heuristic optimization technique, the Sine-Cosine Algorithm (SCA), for solving the ORPD problem with the integration of Thyristor-Controlled Series Capacitors (TCSC)) devices. The primary objective is to minimize real power losses and enhance voltage profiles by optimally dispatching reactive power. The IEEE 14-bus and 30-bus systems are used as test cases to evaluate the effectiveness of both algorithms. The SCA utilizes sinusoidal and sinusoidal mathematical functions to explore and exploit the search space efficiently. The proposed approach is tested on standard IEEE 14 bus & IEEE 30 bus systems, demonstrating significant improvements in system performance metrics compared to conventional methods. . A comparative scenario among PSAT, Sine cosine Angle and Grey Wolf optimisation has been well established projecting single-objective functions, multi-objective function situations can be modified to use it. It is a quick method of convergence.GWO method as dynamically efficient among others.**

***Keywords*—Multi-objective, Active power degeneracy, SCA, GWO.**

I. INTRODUCTION

By reducing actual power losses and enhancing voltage stability, optimal reactive power dispatch, or ORPD, is essential to the effective running of power systems. The capacity to control reactive power has been increased with the incorporation of Flexible AC Transmission System (FACTS) devices. However, because power systems are nonlinear and multi-modal, optimizing ORPD with FACTS devices is a challenging task. Dynamically efficient programming and genetic algorithms are the two potential methods. However, this approach only yields a single optimal solution, necessitating the resolution of tradeoffs between multiple components of the objective function prior to solution generation. Possibilities analyzes trade-offs between two conflicting objectives by framing the IPR issue as a complex issue. For this problem, an NSGA-II or other multidimensional algorithm must be used. The NSGA was developed by Srinivas and Deb, wherein a graded selection method reveals pre-existing non-imperative solutions while a niching strategy preserves population diversity [10]. Multifaceted evolutionary algorithms that employ non-imperative sorting and sharing, such as NSGA, are criticized for three main reasons:

- Intricate calculations.
- A non-elitist approach, and
- The defining of mutual parameters.

In NSGA-II, Deb et al. [11,12] addressed these issues. When dealing with limited optimization situations, Pareto-based multifaceted optimization approaches offer certain advantages over single-objective optimization procedures [12]. First, if the value of the objective function increases much, a method with an authorized constraint infringement is still valuable. This is due to the fact that the Pareto-optimal resolution range includes trade-off solutions, including those that get around constraints. Second, the freedom to explore the solution space is increased by decomposing the original single-objective function into several competing objectives. This adaptability makes it possible to find local optima, which the multidimensional approach transforms into Pareto-front trade-off solutions that the single-objective approach would not have found (see [13]). This paper aims to define the IPR problem as a multidimensional optimization problem and show how Pareto-based multifaceted optimization (NSGA-II) may be used to solve it. The multidimensional problem is presented in two different formulations. In order to solve the ORPD problem in the presence of FACTS devices, this paper explores the use of two nature-inspired algorithms: the Sine Cosine Algorithm (SCA) and the Grey Wolf Optimizer (GWO). The effectiveness of both algorithms in improving voltage profiles and reducing power losses in IEEE 14-bus and 30-bus test systems is assessed.

II. LITERATURE SURVEY

Several optimization techniques have been suggested for ORPD, including heuristic techniques like Genetic Algorithms (GA), Particle Swarm Optimization (PSO), and Differential Evolution (DE) as well as traditional techniques like Newton-Raphson. Reactive power has been improved through the use of FACTS devices, including Static Synchronous Compensators (STATCOM), Thyristor-Controlled Series Capacitors (TCSC), and Static VAR Compensators (SVC).Recent research has demonstrated how well GWO and SCA can solve a range of optimization issues. While SCA draws inspiration from the mathematical inverse cosine function, GWO imitates the hunting strategy and leadership structure of grey wolves. Both algorithms are good candidates for ORPD since they have demonstrated encouraging outcomes when addressing power system optimization issues.

Grey Wolf Algorithm

The Grey Wolf Optimizer (GWO) is an optimization algorithm that draws inspiration from nature and emulates the hunting and leadership styles of real-world grey wolves. algorithm. Figure 1. represent the ladder diagram of gwo The method is easy to use and efficient for handling a wide range of optimization issues. Table 2 show the number of parameter included in GWO algorithm

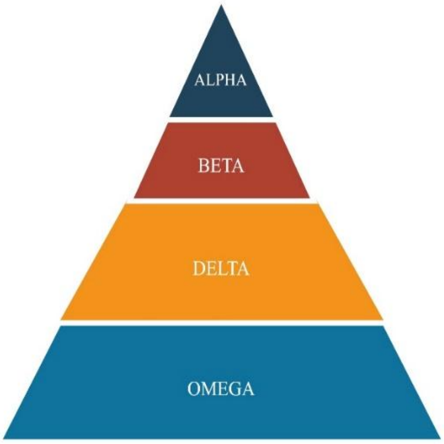

FIG 1. LADDER OF GWO

- Alpha (α): As the pack's leaders, the alpha wolves are in charge of setting the direction and directing the hunt. The alpha wolf in the GWO algorithm stands for the best solution as far discovered.
- Beta (β): The beta wolves assist the alpha in making decisions and are the second in command. They stand for the second-best result in the algorithm.

Mathematical Modeling of GWO

$$D = |C.X_P - X| \quad (1)$$

$$X(t+1) = X_P - A.D \quad (2)$$

Where

X is the current position of Wolf

X_p is position of the best solution

A & C is coefficient of vector

- Delta (δ): While they rule over omega wolves, delta wolves are inferior to alpha and beta wolves. They are the third-best option in the algorithm.
- Omega (ω): The pack's lowest-ranking individuals are omega wolves. They are the remaining answers in the algorithm that come after the top three (α, β,and,δ).

III. PROBLEM FORMULATION

A. maginary power regulation Problem Formulations

The optimal IPR problem aims to enhance the steady-state performance of a power system by optimizing one or more objective functions while adhering to various equality and inequality stipulations. Typically, the problem is formulated as follows

B. Neutral Functions:

i) Active power degeneracy (PL):

This goal is to reduce the active power degeneracy in transmission lines equation 3 which can be expressed as power loss

$$P_{loss} = \sum_{k=1}^{nl} g_k[u_i^2 + u_j^2 - 2uiu_j\, cos(\delta_i - \delta_j)] \quad (3)$$

ii) Voltage Deviation (VD)

This motive is to reduce the deviations in voltage magnitudes at load buses equation 4 which can be represented as

$$V_D = \sum_{k=1}^{NL} |U_k - 1| \quad (4)$$

c. Equality stipulations:

These represent load flow equation 5 &6 such as

$$p_{i-}v_i \sum_{j=1}^{N_B} v_j(G_{ij}\cos\theta_{ij} + B_{ij}\, sin\,\theta_{ij}) = 0 \quad (5)$$

$$i = 1,2, \dots N_B - 1$$

$$Q_{i-}v_i \sum_{j=1}^{N_B} v_j(G_{ij}\cos\theta_{ij} + B_{ij}\, sin\,\theta_{ij}) = 0 \quad (6)$$

$$i = 1,2, \dots N_{pQ}$$

D. Inequality stipulations:

These stipulations equation 7&8 represented as limit of voltage and generator active power capability limit

(i) Voltage Limits

TABLE I. LOAD FLOW ANALYSIS OF IEEE 14 BUS SYSTEMS RESULTS

From bus	To bus	Line loss	
		Real power (Mw)	Reactive power (Mvar)
1	2	4.309	13.16
1	5	3.773	11.45
2	3	3.333	9.832
2	4	2.6670	5.068
2	5	0.920	2.808
3	4	0.391	0.999
4	5	2.479	1.58
4	7	0.50	1.933
4	9	0.5	1.294
5	6	0.5	5.774
6	11	0.123	0.255
6	12	0.081	0.164
6	13	0.252	0.494

7	8	0.5	0.668
7	9	0.5	0.959
9	10	0.007	0.017
9	14	0.080	0.123
10	11	0.055	0.120
12	13	0.012	0.010
13	14	0.101	0.218

$$U_i^{Min} \leq U_i \leq U_i^{max} \leq i \in N_B \quad (7)$$

(ii) Generator Active power Capability limit

$$Pg_i^{min} \leq Pg_i \leq Pg_i^{max} \; i \in N_g \quad (8)$$

(iii) Generator reactive power capability limit

The equation 9 represent as generation of reactive power with in limit constraints

$$Qg_i^{min} \leq Qg_i \leq Qg_i^{max} \; i \in N_g \quad (9)$$

(i) Svc constrant limit

In this paper SVC is controllable Devices the equation 10 represent as SVC control limits

$$Q_{Svc}^{min} \leq Qsvc \leq Q_{Svc}^{max}, \quad \sum Nsvc \quad (10)$$

Where

Ui = voltage magnitude at i^{th} bus,

V_D= Voltage Deviation

Uj= Voltage Magnitude at j^{th} bus

$G_{\text{ij}}, B_{\text{ij}}$ = mutual conductance and susceptance between i &j

Pgi= real power generator

Qgi= Reactive power generator

θ_{ij}= voltage angle difference between i and j

Q_{SVC}= SVC controllable limit

$N_{\text{B-1}}$= total number of buses excluding slack bus

N_{PQ}= set of PQ buses

Ng= Number of Generator buses

P_{L} = total active power loss of all lines

Q_{L} = total reactive power loss of all lines

IV. LOAD FLOW ANALYSIS

The Newton Rapson method was used to operate a system in IEEE 14 bus. The table displays the results of the load flow analysis. The Newton-Raphson algorithm operated on the IEEE 14 bus system. Below are the output reactive power loss and active power degeneracy. The power losses are examined based on the IEEE 14 bus system's power flow results.

Total active power degeneracy: 22.590 Mw

Total reactive power loss: 46.64 Mvar

IEEE 14-Bus System

Fig 2. Represent IEEE 14-bus system consists of 14 buses, 5 generators, 11 loads, and 20 transmission lines. The system data includes bus voltages, line impedances, and load demands. FACTS devices such as TCSC are placed at strategic locations to enhance reactive power control.

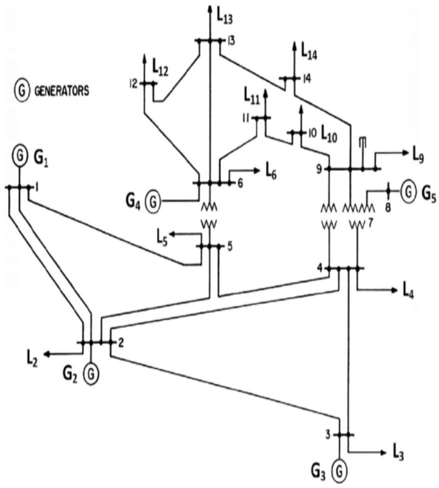

FIG 2. IEEE 14 BUS SYSTEM

IEEE 30-Bus System

Fig 3. Represent IEEE 30-bus system includes 30 buses, 6 generators, 21 loads, and 41 transmission lines. Similar to the 14-bus system, FACTS devices are installed to improve reactive power dispatch.

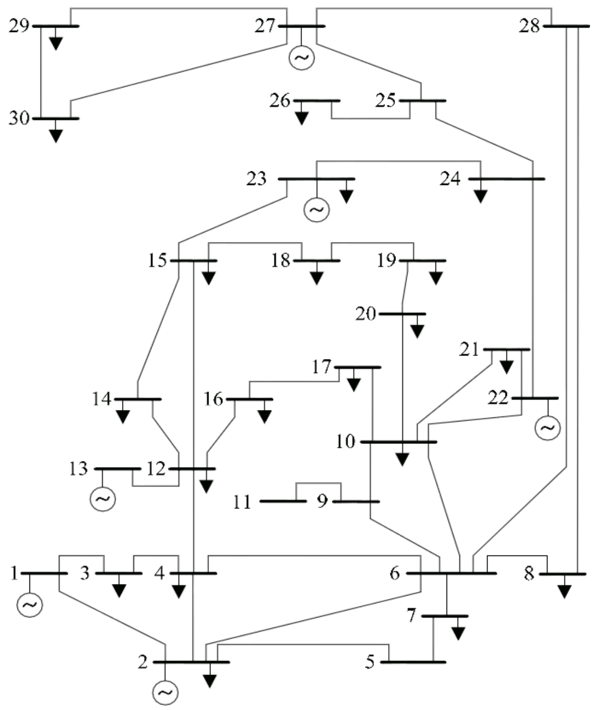

FIG 3. IEEE 30 BUS SYSTEM

V. Result and Discussion

Line Flow Losses

TABLE 2. COMPARISON OF RESULTS

Minimization of Active power degeneracy and Minimization of Voltage deviation IEEE 14 bus system			
Objective	**PSAT TOOLS**	**GWO**	**SCA**
P_{Loss} (MW)	4.641	2.751	3.543
Voltage Deviation	Not available	0.524	0.827
Minimization of Active power degeneracy and Minimization of Voltage deviation IEEE 30 bus system			
Objective	**PSAT TOOLS**	**GWO**	**SCA**
P_{Loss} (MW)	8.5462	4.362	5.5214
Voltage Deviation	Not available	0.5624	0.582

Table 2 represent Mat power is tested out on IEEE 14 and IEEE 30 bus test systems. The output is compared with the PSAT tool, SCA & GWO

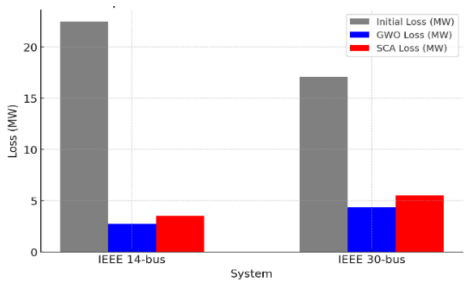

FIG4. COMPARISION OF IEEE 14 & IEEE 30BUS SYSTEM RESULT

Fig 4 represented the result of intial losss compared with facts devices and without facts devices. Figure 4 shows the losss are reduced with facts devices. GwO values is minimum compared to SCA algorithm values in the data set

VI. Conclusion

The comparative analysis indicates that both GWO and SCA are effective in reducing real power losses and enhancing voltage profiles in smart grids with FACTS devices. However, GWO exhibits superior performance in terms of convergence speed and solution quality. The integration of FACTS devices further enhances the system's reactive power control capabilities, making it a vital component of modern power systems.

Acknowledgment

The authors extend their due thanks to the Thiagarajar College of Engineering Management, Madurai, India for their extensive research facilities and the financial backing from Thiagarajar Research Fellowship (TRF) scheme (File.no: TCE/RD/TRF/2024/<<06>> dated 09-02-2024) is gratefully acknowledged.

References

[1] S. Jeyadevi, S. Baskar, C.K. Babulal, M. Will juice Iruthayarajan, Solving multiobjective optimal Imaginary power regulation using modified NSGA-II, International Journal of Electrical Power & Energy Systems, Volume 33, Issue 2, 2011, Pages 219-228, ISSN 0142-0615,

[2] Mamandur, K.R.C. Chenoweth R.D: Optimal Control of Reactive Power Flow for Improvements in Voltage Profiles and for Active power degeneracy Minimization, IEEE Transactions on Power Apparatus and Systems, Vol. PAS-100, No. 7, 1981, pp. 3185-3194.

[3] Lee K.Y, Park Y.M, Ortiz J.L: An United Approach to Optimal Real and Imaginary power regulation, IEEE Transactions on Power Apparatus and Systems, Vol. PAS-104, No. 5, 1985, pp. 1147-1153.

[4] Opuku G.: Optimal Power System VAr Planning, IEEE Transactions on Power Systems, Vol. 5, No. 1, 1990, pp. 53-60.

[5] Hong Y.Y., Sun I., Lin S.Y.,. Lin C.J: Multi-year Multi-case Optimal VAr Planning, IEEE Transactions on Power Systems, Vol. 5, No. 4, pp. 1294-1301.

[6] Bridenbaugh C.J., DiMascio D.A, Aquita R.D: Voltage Control Improvement through Capacitor and Transformer Tap Position, IEEE Transaction on Power Systems, Vol. 7, No. 1, 1992, pp. 222-227.

[7] Tomsovic K.: A Fuzzy Linear Programming Approach to the Reactive Power/voltage Control Problem, IEEE Transaction on Power Systems, Vol. 7, No. 1, 1992, pp. 287-293.

[8] Abdul-Rahman K.H., Shahidehpour S.M: A Fuzzy-based Optimal Reactive Power Control, IEEE Transaction on Power Systems, Vol. 8, No. 2, 1993, pp. 662-670.

[9] Meza J.L.C, Yildirim M.B,. Masud A.S.M: A Model for the Multiperiod Multiobjective Power Generation Expansion Problem, IEEE Transaction on Power Systems, Vol. 22, No. 2, 2007, pp. 871-878.

[10] Srinivas N., Deb K.: Multi-faceted Optimization using Nondominated Sorting in Genetic Algorithm, Evolutionary Computation, Vol. 2, No. 3, 1994, pp. 221-248.

[11] Deb K, Pratap A, Agarwal S, Meyarivan T: A Fast and Elitist Multiobjective Genetic Algorithm: NSGA-II, IEEE Transaction on Evolutionary Computation, Vol. 6, No. 2, 2002, pp. 182-197.

[12] Saddique, M.S., Habib, S., Haroon, S.S., Bhatti, A.R., Amin, S. and Ahmed, E.M., 2022. Optimal solution of reactive power dispatch in transmission system to minimize power losses using sine-cosine algorithm. *IEEE Access*, *10*, pp.20223-20239.

[13] Saddique, M.S., Habib, S., Haroon, S.S., Bhatti, A.R., Amin, S. and Ahmed, E.M., 2022. Optimal solution of reactive power dispatch in transmission system to minimize power losses using sine-cosine algorithm. *IEEE Access*, *10*, pp.20223-20239.

Enhancing Data Integrity and Energy Analytics with Smart Meter Time-Series Data

A.C. Vishnu Dharssini
Department of EEE,
Thiagarajar College of Engineering,
Madurai, India
acvishnudharssini@gmail.com

S. Charles Raja (SMIEEE)
Department of EEE,
Thiagarajar College of Engineering,
Madurai, India
charlesrajas@tce.edu

M. Praveen Kumar
Department of EEE,
Thiagarajar College of Engineering,
Madurai, India
mpraveenkumar@student.tce.edu

S. Arunmozhi
Department of EEE,
Thiagarajar College of Engineering,
Madurai, India
arunmozhi49@gmail.com

***Abstract*—The rapid adoption of smart meters has transformed energy management by enabling high-resolution monitoring and optimization. However, missing values and anomalies—stemming from sensor faults and transmission issues—often compromise data integrity. This study presents a robust framework to address such challenges using a year-long time-series dataset from eight laboratories in the EEE department at Thiagarajar College of Engineering, Madurai. Data collected via Elmeasure's ElNet software was preprocessed through linear interpolation, feature engineering, and statistical anomaly detection to restore consistency and extract meaningful insights. The reconstructed dataset revealed distinct consumption trends and irregularities, supporting accurate forecasting and real-time anomaly detection. The proposed approach offers a scalable solution for smart grid analytics, enhancing energy efficiency, system resilience, and decision-making in institutional energy management.**

Keywords—Smart Meter Data, Missing Data Imputation, Time-Series Analysis, Anomaly Detection, Energy Forecasting.

I. INTRODUCTION

Smart meters are essential to modern energy systems, offering real-time, high-resolution data that supports energy distribution optimization, demand-side management, and operational planning. They empower utilities and consumers to make informed decisions, especially in demand-response contexts. However, data collected from smart meters is often incomplete due to sensor faults, transmission errors, or external disruptions. Such inconsistencies compromise the reliability of forecasting, anomaly detection, and grid stability analysis, making robust preprocessing critical.

This study analyzes a year-long dataset from eight laboratories in the EEE department of Thiagarajar College of Engineering, Madurai. The data, acquired via Elmeasure's ElNet software, was structured into a coherent time-series through sequential preprocessing steps. The objective is to restore dataset completeness, extract reliable consumption trends, and support informed energy management decisions. The proposed methodology preserves temporal patterns while ensuring analytical accuracy, contributing to scalable and intelligent energy analytics for smart grid systems.

II. RELATED WORKS

Smart meter time-series data has been widely explored for applications like load forecasting, peak demand management, and consumption pattern recognition. Despite advancements, missing data remains a recurring challenge, introducing biases in energy analytics. Traditional imputation techniques such as forward-fill, backward-fill, and interpolation are computationally efficient but often fail to model complex temporal relationships [1]. Conversely, deep learning-based approaches, including autoencoders and recurrent networks, offer higher precision but require extensive training data and processing resources, limiting their scalability for large institutional datasets [2].To balance performance and practicality, the present study uses linear interpolation, enhanced by temporal feature engineering and statistical anomaly detection, to ensure accuracy while maintaining real-time feasibility [3]. This hybrid approach supports robust preprocessing without the overhead of full machine learning pipelines.

Anomaly detection plays a crucial role in modern energy systems, especially in identifying faults, inefficiencies, or malicious behavior. Deep learning models like LSTM networks have proven effective in capturing sequential dependencies and detecting subtle anomalies better than basic statistical methods [4]. Other models like XGBoost and Ensemble Batch Prediction Intervals (EnbPI) offer strong predictive performance but struggle with temporal generalization in system-level inefficiency detection [5]. Smart meters have also facilitated appliance-level energy analysis through Non-Intrusive Load Monitoring (NILM), which, when paired with anomaly detection frameworks, improves operational efficiency in both institutional and residential settings [6]. However, class imbalance—where anomalies are rare—often limits the effectiveness of traditional classifiers such as SVM and Random Forests [7]. Deep learning architectures, particularly hybrid models like stacked LSTM and CNN-LSTM, have demonstrated resilience against imbalance and greater capacity for anomaly localization [8].

Recent developments have explored metaheuristic optimization methods such as MTBO and TVETBO to improve anomaly detection performance in imbalanced and high-dimensional energy data [9]. Furthermore, contextual anomaly detection techniques have been introduced to better interpret the root cause of deviations, enabling targeted interventions in real-world energy systems [10].Privacy-preserving anomaly detection using federated learning combined with autoencoders has also emerged as a promising framework for distributed energy systems, ensuring data confidentiality while detecting electricity theft [11]. Lastly, the use of hybrid intelligent models—like Conditional Random Fields integrated with neural networks—has enhanced the detection of both physical faults and irregular consumption patterns in smart grids [12].

Distinctively, this study shifts focus from macro-level energy analytics to micro-level consumption behaviors of individual laboratories within an academic block. Such fine-grained analysis offers new insights into space-specific energy usage, laying a scalable foundation for intelligent energy management in educational institutions and similar environments.

III. STATE OF THE ART OF THE SYSTEM

Thiagarajar College of Engineering (TCE), Madurai, a government-aided institution affiliated with Anna University, serves as the experimental hub for this study. With a sprawling 143-acre campus housing over fifty research laboratories, TCE is ideally positioned for energy analytics research. The college's commitment to sustainable practices is reflected in the deployment of 60 smart meters across the high-tension (HT) grid, enabling high-resolution monitoring.

This study specifically focuses on the Electrical and Electronics Engineering (EEE) department block, a two-storey building with eight laboratories, each equipped with dedicated smart energy meters. Data is collected using Elmeasure’s ElNet software, which transmits real-time consumption metrics to a centralized server for analytics. This setup supports granular tracking of load distribution, peak demand behavior, and energy efficiency patterns. The system architecture facilitating data exchange involves five key layers: data collection via multifunction meters, processing through an IoT gateway, device monitoring via a management interface, cloud-based configuration for scalability and OTA updates, and a user-end platform for visualization and analytics. The meters operate using RS485 industrial communication, transmitting readings to the gateway, where they are filtered, formatted, and relayed to the cloud.

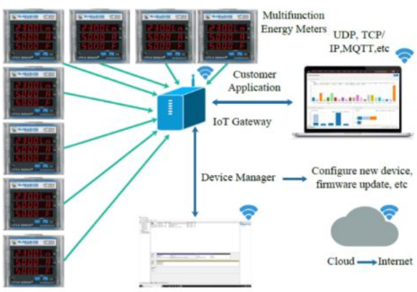

FIG.1. DATA EXCHANGE FROM SMART METERS TO USER APPLICATION

This structured framework ensures accurate, real-time data acquisition and supports advanced analytics, including anomaly detection and energy forecasting. The modular and scalable infrastructure makes it well-suited for institutional and smart campus deployments.

IV. METHODOLOGY

Dataset Description

The dataset spans a full year with 5-minute interval readings, amounting to 105,120 expected data points. However, only 92,200 valid entries were available due to missing timestamps and duplicate records. Data was collected from eight laboratories in the EEE department block of Thiagarajar College of Engineering, Madurai, using Elmeasure’s ElNet software, which enables real-time monitoring and centralized data logging. The analysis primarily focuses on the “total” column, representing aggregate energy consumption, while the remaining variables offer supplementary insights for validation and contextual analysis.

Missing Data Analysis

A comprehensive assessment of missing timestamps and duplicate entries revealed that 13,003 timestamps were absent, accounting for 12.4% of the dataset. These missing data points were not evenly distributed, suggesting that certain periods experienced higher data loss, potentially due to equipment failures or network disruptions. Additionally, 120 duplicate records were identified, which, if not addressed, could lead to biased interpretations and inaccurate predictions. The missing data issue necessitated a structured imputation strategy to ensure dataset completeness without distorting temporal dependencies.

Imputation Strategy

To address missing data, linear interpolation was adopted as the primary imputation technique due to its computational efficiency and ability to preserve temporal continuity. Given the dataset’s 5-minute resolution, energy consumption patterns typically evolve gradually rather than abruptly. Linear interpolation effectively leverages this smooth progression, estimating missing values proportionally between adjacent valid entries. This approach ensures that the reconstructed data aligns with observed trends, maintaining the integrity of consumption patterns essential for downstream analysis. Compared to forward-fill or backward-fill, linear interpolation avoids bias accumulation and provides a more accurate reflection of temporal dynamics. While advanced machine learning-based imputation methods (e.g., KNN, Random Forests, LSTM autoencoders) can model complex dependencies, they require extensive labeled data, tuning, and computational resources. Given the institutional context and the dataset's structure, linear interpolation offered a transparent, scalable, and practical solution that aligns well with real-world deployment constraints.

Feature Extraction

Feature engineering was employed to enhance the dataset’s predictive capacity by transforming raw time-series data into informative variables. Hourly average consumption was computed to reveal diurnal energy usage trends, while day-of-week indicators distinguished behavioral differences between weekdays and weekends. Additionally, lag features—representing prior time-step consumption values—were introduced to capture temporal dependencies essential for forecasting. These derived features enriched the dataset, enabling more effective anomaly detection and advanced predictive modeling.

Anamoly Detection

Anomalies in energy consumption were identified using a statistical thresholding method, where values exceeding three standard deviations from the mean were flagged. This approach proved effective in detecting events such as sudden surges, consumption drops, and prolonged zero-usage periods. The simplicity and interpretability of this method make it particularly suitable for energy datasets, which typically follow regular patterns with occasional deviations indicating faults or operational anomalies. In the absence of labeled anomaly data, this lightweight and transparent strategy allowed for efficient detection and validation against operational logs, revealing causes such as equipment malfunctions or scheduled maintenance. Such anomaly identification is vital for maintaining grid stability and optimizing energy distribution.

V. Results and Discussion

This study presents a comprehensive framework for addressing missing data in smart meter time-series datasets.

Performance Metrics for Forecasting Models

To validate the quality of the imputed dataset, a basic forecasting model was developed using lag-based linear regression as in Fig 2.

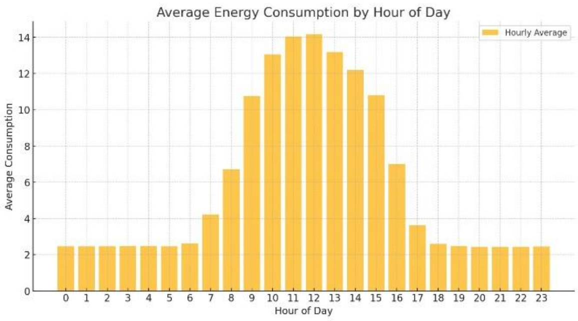

Fig.2. Average Hourly Energy Consumption

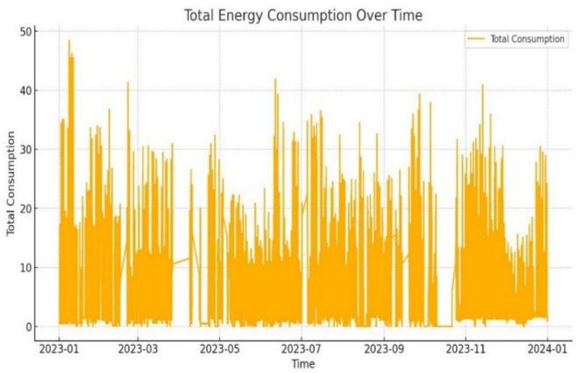

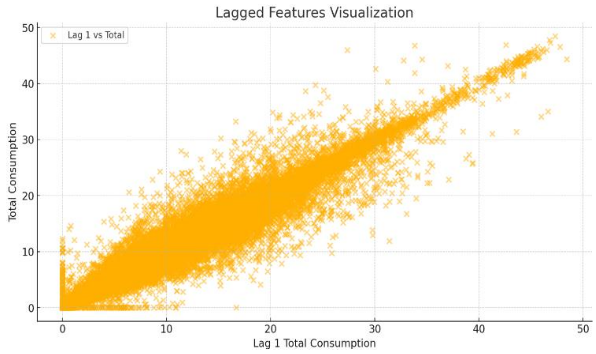

Fig.3. Lag-based Linear Regression

The model's performance was assessed using the following metrics: Mean Absolute Error (MAE): 0.312 kWh

Root Mean Square Error (RMSE): 0.442 kWh, Mean Absolute Percentage Error (MAPE): 4.67%. These results demonstrate that the imputed data closely reflects real-world consumption behavior and maintains analytical integrity for training predictive models.

Comparison between Predicted and Original Data

A visual and statistical comparison was conducted between the predicted energy consumption and the original observed values for randomly selected weeks. The results show a high correlation during standard operation hours, with slight deviations occurring during previously flagged anomalous periods. This confirms that the imputed data and subsequent model predictions reliably mirror actual trends, reinforcing confidence in the imputation process and its suitability for downstream analysis. By integrating linear interpolation, feature engineering, and statistical anomaly detection, the dataset was reconstructed with restored integrity, enabling the extraction of meaningful insights. The analysis revealed distinct energy consumption patterns, identified operational anomalies, and demonstrated the utility of the enriched dataset for energy forecasting and smart grid applications. The proposed framework is both scalable and adaptable, making it suitable for broader real-time energy analytics deployments.

TABLE 1. Sample Original vs. Predicted Data

S. No	Timestamp	Original Energy consumption	Predicted Energy Consumption	Absolute error
1.	2023-03-01 10:05:00	3.6	3.81	0.20999999
2.	2023-03-01 10:10:00	3.78	3.6	0.17999999
3.	2023-03-01 10:05:00	3.67	3.78	1.10999999
4.	2023-03-01 10:15:00	3.94	3.67	0.27
5.	2023-03-01 10:20:00	3.71	3.94	0.2299999
6.	2023-03-01 10:25:00	3.84	3.79	0.0499999
7.	2023-03-01 10:30:00	3.75	3.94	0.1899999

Figure 3 presents the total energy consumption over a year at 5-minute intervals, illustrating fine-grained patterns of daily usage. Missing data, visible as abrupt gaps or drops, initially distorted trend continuity. Post-imputation, the graph reveals distinct peaks aligned with daily cycles and seasonal trends—such as elevated summer usage (Even semester) due to cooling loads and reduced spring/autumn demand (Odd semester). These observations underscore the necessity of reliable imputation for accurate consumption analysis.

To provide a clearer long-term view, Figure 4 displays daily aggregated consumption. This smoothed visualization highlights weekday consistency and comparatively lower weekend usage, reflective of institutional activity cycles. Notable spikes and dips point to anomalies potentially driven by equipment failures or scheduled shutdowns, further supporting the effectiveness of the applied anomaly detection approach.

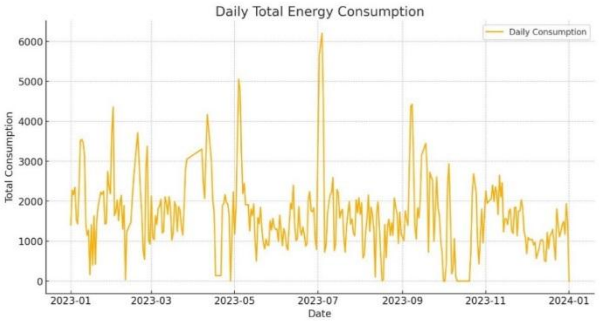

FIG.4. AGGREGATED DAILY NET ENERGY CONSUMPTION

Figure 5 illustrates the average hourly energy consumption across the dataset, revealing distinct diurnal patterns. Peak usage occurs between 7–9 AM and 6–9 PM, aligning with typical periods of high institutional and residential activity. In contrast, the lowest consumption is observed between 12–4 AM, reflecting minimal operations. The consistency of these trends indicates predictable user behavior, supporting effective demand-side management and strategic energy distribution.

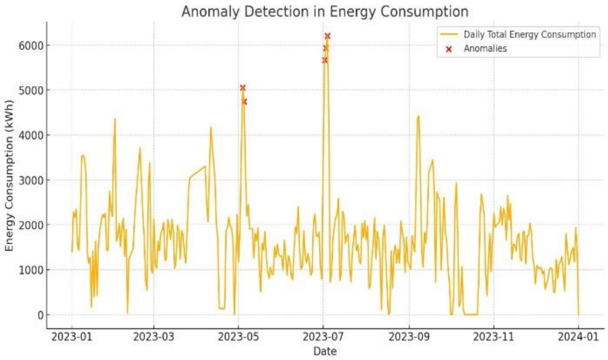

FIG.6. ANOMALY DETECTION IN ENERGY CONSUMPTION

Figure 6 visualizes daily anomalies in energy usage, identified through statistical thresholding. Spikes highlight instances of abnormal demand, such as power surges or operational anomalies, while dips correspond to equipment downtime or scheduled maintenance. Notably, seasonal clustering of anomalies suggests that external climatic conditions also influence usage variability. These findings emphasize the role of anomaly detection frameworks in maintaining grid reliability and optimizing energy infrastructure performance.

VI. CONCLUSION

This study presents a comprehensive framework for restoring data integrity and enhancing energy analytics in smart meter time-series datasets. Through the integration of linear interpolation, feature engineering, and statistical anomaly detection, missing data was effectively imputed, enabling the extraction of meaningful consumption patterns. The dataset—collected from Elmeasure's ElNet software for laboratories at Thiagarajar College of Engineering, Madurai—was systematically structured to support high-resolution analysis of energy usage. The findings emphasize the critical role of data quality in energy analytics and demonstrate the potential for scalable deployment in smart grid environments. The proposed methodology supports accurate forecasting, efficient anomaly detection, and strategic energy optimization, contributing to the development of intelligent energy systems. In terms of practical applications, the enriched dataset improves the reliability of energy forecasting models, aids in grid stability through real-time anomaly detection, and informs load management and demand response strategies. Future work could explore machine learning-based forecasting and anomaly classification, imputation techniques tailored to renewable sources like solar or wind, and the integration of weather and contextual data for a holistic view of energy management.

ACKNOWLEDGMENT

The authors gratefully acknowledge Thiagarajar College of Engineering, Madurai, for infrastructure and financial support through the TRF scheme (File No: TRF/Jul2022/02). and DST-FIST Scheme (File No: SR/FST/College-519/2019).

REFERENCES

[1] Kim, Taehee, Jae-Seok Jang, and Hyuk-Yoon Kwon. "Correlation-driven multi-level learning for anomaly detection on multiple energy sources." Applied Soft Computing 159 (2024): 111636.

[2] Stjelja, Davor, et al. "Building consumption anomaly detection: A comparative study of two probabilistic approaches." Energy and Buildings 313 (2024): 114249.

[3] Ali, Mubashir, et al. "Anomaly detection in public street lighting data using unsupervised clustering." IEEE Transactions on Consumer Electronics (2024).

[4] Hernández, Álvaro, et al. "Detection of anomalies in daily activities using data from smart meters." Sensors 24.2 (2024): 515.

[5] Marangu, David, Stephen Njenga, and Rachael Ndung'u. "Systematic Review of Models Used to Handle Class Imbalance in Anomaly Detection for Energy Consumption." Available at SSRN 4851478 (2024).

[6] Guo, Guoqing, Peng Liu, and Yuchen Zheng. "Early energy performance analysis of smart buildings by consolidated artificial neural network paradigms." Heliyon 10, no. 4 (2024).

[7] Alshehri, Ali, Mahmoud M. Badr, Mohamed Baza, and Hani Alshahrani. "Deep Anomaly Detection Framework Utilizing Federated Learning for Electricity Theft Zero-Day Cyberattacks." Sensors 24, no. 10 (2024): 3236.

[8] Wang, Xinlin, Hao Wang, Binayak Bhandari, and Leming Cheng. "AI-empowered methods for smart

energy consumption: A review of load forecasting, anomaly detection and demand response." International Journal of Precision Engineering and Manufacturing-Green Technology 11, no. 3 (2024): 963-993.

[9] Stjelja, Davor, Vladimir Kuzmanovski, Risto Kosonen, and Juha Jokisalo. "Building consumption anomaly detection: A comparative study of two probabilistic approaches." Energy and Buildings 313 (2024): 114249.

[10] Al-Sabah, Basma, and Gholamreza Anbarjafari. "Anomaly Detection in Kuwait Construction Market Data Using Autoencoder Neural Networks." (2024).

[11] Ali, Mubashir, Patrizia Scandurra, Fabio Moretti, and Hafiz Husnain Raza Sherazi. "Anomaly detection in public street lighting data using unsupervised clustering." IEEE Transactions on Consumer Electronics (2024).

[12] Pan, Xiaogang, Qiao Deng, Yuanyuan Jiao, and Zhiwen Chen. "A Variational Graph Autoencoder Aided Canonical Correlation Analysis Based Online Abnormal Patterns Detection Method for Buildings HVAC Systems." IEEE Transactions on Consumer Electronics (2024).

Sustainable Energy Efficiency Framework for 6G Mobile Communication Networks

N. Vinothini
Department of ECE,
Thiagarajar College of Engineering,
Madurai, India
vinothinin@student.tce.edu

G. Ananthi
Department of ECE,
Thiagarajar College of Engineering,
Madurai, India
gananthi@tce.edu

V. Ramya
Department of ECE,
Thiagarajar College of Engineering,
Madurai, India
ramyavardhann@gmail.com

***Abstract*—Energy efficiency is a cornerstone of 6G systems, driven by the increasing demands for ultra-high data rates, flexible network architectures, and environmental sustainability. As mobile communication networks evolve, achieving energy efficiency is crucial to meet global sustainability goals and mitigate the environmental impact of expanding digital infrastructure. Key metrics, including energy consumption, energy efficiency, and network carbon intensity, provide quantitative measures to evaluate and improve system performance. Challenges such as accurately defining and measuring these metrics, managing the carbon footprint across the lifecycle of network operations, and integrating renewable energy sources remain significant. Advanced energy-saving techniques, including optimized power management in user equipment, infrastructure enhancements, and AI-driven orchestration, offer promising solutions. By addressing these aspects, 6G systems can enable greener and more efficient communication networks, aligning technological advancement with environmental responsibility.**

Keywords—Energy Efficiency, Sustainability, 6G Networks, Key Performance Indicators (KPIs), Carbon Footprint Introduction (Heading 1)

I. INTRODUCTION

The evolution of mobile networks from 4G to 6G marks a transformative journey in technological innovation and societal advancement. While 4G introduced high-speed internet that enabled video streaming, mobile applications, and seamless connectivity, 5G revolutionized industries with ultra-low latency, massive device connectivity, and higher data speeds [1]. As we progress toward 6G, the emphasis lies in achieving terahertz communication, ultra-reliable low-latency networks, and intelligent sensing technologies that promise to create an integrated digital and physical ecosystem. This transition, however, brings forth unprecedented challenges, especially concerning energy efficiency and sustainability [2]. The increasing demand for energy-intensive applications and rapid infrastructure expansion has heightened concerns about greenhouse gas emissions and environmental impact, necessitating a paradigm shift in network design and operation toward sustainable solutions [3].

Sustainability is emerging as a 6G network design cornerstone, with energy efficiency becoming a critical Key Performance Indicator (KPI). Metrics such as energy consumption per data unit, network carbon intensity, and renewable energy integration are being developed to align communication networks with global climate goals[4]. These metrics underscore the necessity of energy-optimized designs, advanced protocols like Discontinuous Reception (DRX), and dynamic network orchestration using artificial intelligence (AI). Moreover, integrating renewable energy sources such as solar, wind, and geothermal power into communication infrastructure can significantly mitigate the environmental footprint of these networks. Renewable energy integration strategies, including on-site generation and power purchase agreements (PPAs), are crucial for reducing dependency on fossil fuels and achieving sustainable energy management [5].

Advancements in energy storage technologies further complement these efforts. Next-generation solutions like solid-state batteries, hydrogen storage, and thermal storage are transforming energy management, facilitating efficient storage and distribution of renewable energy [6]. When combined with 5G-enabled smart grids, these innovations enable real-time optimization of energy consumption, support autonomous microgrid operations, and foster peer-to-peer energy trading within communities. Such developments not only enhance grid reliability and resilience but also pave the way for sustainable and decentralized energy systems. Furthermore, quantum computing emerges as a promising frontier for optimizing renewable energy integration in AI-driven infrastructures [7]. By leveraging algorithms like Quantum Approximate Optimization Algorithm (QAOA) and Quantum Annealing, complex energy scheduling and load forecasting challenges can be addressed, leading to significant improvements in energy efficiency, resource utilization, and carbon emission reduction.

In parallel, the role of cybersecurity in ensuring the resilience of sustainable communication systems cannot be overstated. Advanced technologies such as blockchain and AI offer robust solutions for safeguarding the infrastructure essential for sustainable development [8]. Additionally, innovative strategies in RF engineering and unmanned aerial vehicle (UAV) energy management contribute significantly to reducing carbon footprints and optimizing energy usage. These approaches highlight the critical interplay between energy efficiency, advanced technology integration, and sustainability in shaping a greener, more connected future [9].

This paper delves into strategies for optimizing network design and operation, emphasizing renewable energy integration, advanced storage solutions, and the transformative potential of AI and quantum computing in achieving energy-efficient and sustainable communication systems [10]. It also explores the pivotal role of cybersecurity, RF engineering, and UAV optimization in fostering a resilient and eco-friendly telecommunications ecosystem. By addressing these multidisciplinary challenges, this research aims to contribute to the ongoing pursuit of sustainable development in the era of 6G and beyond.

The core problem this paper addresses is the growing energy demand and resulting carbon emissions from increasingly complex and data-intensive mobile communication networks. Existing studies have yet to comprehensively define energy efficiency metrics tailored for 6G technologies or analyze their real-world performance improvements over 5G. Therefore, the objectives of this study are to identify and evaluate key energy efficiency metrics in 6G networks, to develop a sustainability-oriented energy efficiency framework, and to compare performance improvements with existing 5G systems under different load conditions.

II. System Model

The system model illustrates the interconnection between key components of a 6G system user Devices, the Radio Access Network (RAN), and Infrastructure, and their collective impact on energy efficiency.

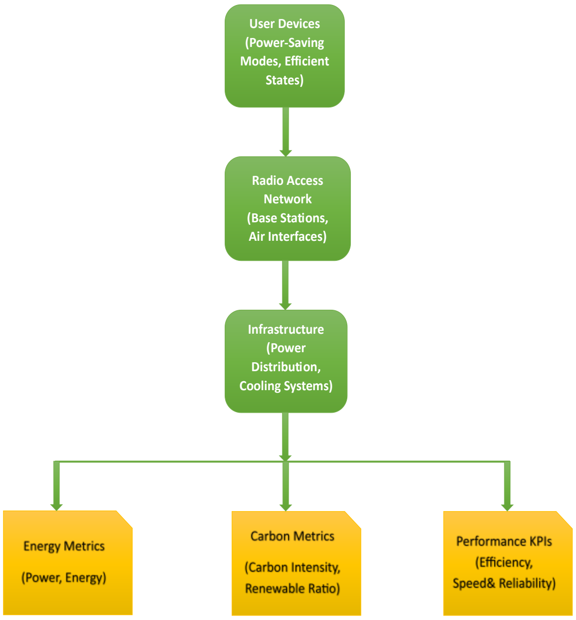

Fig.1. System Model

User devices initiate the process with advanced power-saving mechanisms like Discontinuous Reception (DRX) and efficient state transitions (e.g., RRC Inactive state) to minimize energy consumption. These devices communicate with the RAN, which includes energy-optimized base stations and air interfaces that utilize advanced modulation and coding techniques to ensure efficient data transmission. The RAN, in turn, relies on the supporting infrastructure, including power distribution systems and cooling mechanisms, which play a vital role in reducing energy losses and improving overall operational efficiency.

The flowchart further connects these components to three key performance indicators (KPIs) that drive energy efficiency. Energy metrics, such as power consumption and energy efficiency, provide insights into system performance over time. Carbon metrics, including network carbon intensity and the renewable electricity ratio, assess the environmental impact of network operations. Performance KPIs like data throughput and system reliability evaluate the effectiveness of energy optimization measures. Together, these metrics form a comprehensive framework for analyzing and improving the energy efficiency and sustainability of 6G networks.

III. Energy Efficiency Framework

After the text edit has been completed, the paper is ready for the template. Duplicate the template file by using the Save As command, and use the naming convention prescribed by your conference for the name of your paper. In this newly created file, highlight all of the contents and import your prepared text file. You are now ready to style your paper; use the scroll down window on the left of the MS Word Formatting toolbar.

The energy efficiency framework in 6G systems focuses on quantifying and optimizing energy usage across various network components. Metrics such as Energy Efficiency (EEMN, DV), Renewable Electricity Ratio, and Network Carbon Intensity (NCIe) play pivotal roles in achieving sustainable operations. This metric measures the data efficiency of the mobile network by relating the total data volume (DVMN) to the energy consumed (ECMN) during the same time frame.

$$EEMN, DV = \frac{DVMN}{ECMN}\left[\frac{bits}{J}\right] \tag{1}$$

Renewable Electricity Ratio reflects how effectively energy is utilized to transmit data, making it a critical indicator for evaluating network performance.

$$Renewable\ Electricity\ Ratio = \frac{Renewable\ Electricity\ Consumption}{Total\ Electricity\ Consumption} \tag{2}$$

A higher ratio indicates a greater reliance on sustainable energy, reducing the network's carbon footprint. Network Carbon Intensity (NCIe) measures the greenhouse gas emissions per unit of data transmitted and is given by

$$NCIe = \frac{Total\ Carbon\ Emission\ (ECtotal)}{Total\ Data\ Volume} \times CF \quad \left[\frac{kgCO2e}{TB}\right] \tag{3}$$

CF is the carbon conversion factor, which depends on the energy source. Lower NCIe values indicate improved sustainability.

Energy-Saving Techniques

To achieve these efficiency goals, 6G incorporates advanced energy-saving methods, such as Discontinuous Reception (DRX) is a technique enabling user devices to enter low-power modes during idle periods, significantly reducing energy consumption. RRC Inactive State Introduced in 5G and enhanced in 6G, this state minimizes signalling overhead by allowing devices to transition more efficiently between active and idle modes. By integrating these metrics and techniques, 6G networks optimize energy utilization while meeting performance demands, contributing to a sustainable digital future.

 ISBN: 978-93-342-3695-8

IV. Results And Discussions

The simulation was carried out using MATLAB R2023b. The system assumed typical urban deployment parameters and energy models derived from recent 5G deployments. 6G systems promise significant energy efficiency improvements over 5G, with potential gains ranging from 2x to 300x depending on various factors such as network load, deployment scenarios, and energy-saving techniques. For instance, innovations like AI-driven network optimization, advanced user equipment protocols, and renewable energy integration contribute to these improvements. Metrics like Energy Efficiency (EEMN, DV) and Network Carbon Intensity (NCIe) highlight these gains, showcasing reduced energy consumption per data unit and lower greenhouse gas emissions.

By implementing frameworks such as Discontinuous Reception (DRX) and the RRC Inactive state, user devices experience substantial reductions in power consumption during idle periods. Similarly, infrastructure enhancements, such as optimized cooling systems and renewable electricity usage, lead to improved energy performance at the system level. The following MATLAB code demonstrates a plot comparing energy efficiency improvements across 5G and 6G systems under varying scenarios.

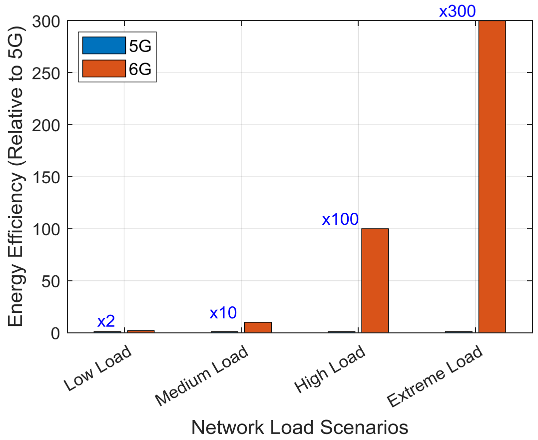

Fig.2. Energy Efficiency Comparisons: 5G vs 6G

In Figure 2, energy efficiency is quantified as Mbps per kWh. This metric reflects the amount of data transmitted per unit of energy consumed. Reference energy efficiency values for 5G were assumed to range from 5–15 Mbps/kWh, depending on traffic conditions, based on [1].

Figure 3 illustrates the energy efficiency of a system under varying traffic loads before and after implementing a framework designed to optimize energy consumption. The x-axis represents the traffic load, ranging from 10% to 100%, while the y-axis depicts the energy efficiency, measured in Mbps per kWh. Before the Framework, the energy efficiency shows a decreasing trend as traffic load increases, indicating that the system consumes more energy to maintain a constant data rate as the traffic load grows. This suggests inefficiency in the system, where the energy consumption rises significantly with traffic load. After the Framework, the energy efficiency improves across all traffic levels, indicating that the implemented framework has successfully reduced energy consumption while maintaining or increasing data throughput.

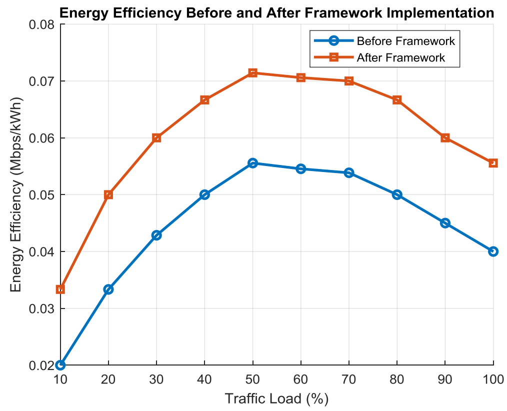

Fig. 3. Energy Efficiency of a system under varying traffic loads

As traffic load increases, the system's energy consumption still increases, but at a slower rate, resulting in a higher energy efficiency. This shows that the framework effectively optimizes energy usage, especially under high traffic conditions. The difference between the two curves demonstrates the positive impact of the framework. The energy efficiency improvement suggests that the framework enhances system performance by reducing energy consumption per unit of data transmitted, especially at higher traffic levels.

V. CONCLUSION

Energy-efficient 6G systems are essential for achieving sustainability goals by minimizing the carbon footprint of communication networks while ensuring high-performance connectivity. As the demand for data and IoT technologies grows, the integration of renewable energy sources, such as RF energy harvesting, becomes critical for creating self-sustaining networks. Future work will focus on refining key performance indicators (KPIs) to assess energy efficiency, reliability, and sustainability, as well as exploring the integration of diverse renewable energy sources to power 6G systems. This includes advancing energy storage solutions and improving system designs to ensure that future communication networks are both energy-efficient and capable of meeting global connectivity needs.

Acknowledgment

This work was supported under the Quality Improvement Programme - AICTE -Full-Time Ph.D. Programme in the Department of Electronics and Communication Engineering at Thiagarajar College of Engineering, Madurai (Tamil Nadu).

References

[1] Ezeigweneme, N. C. A., Umoh, N. a. A., Ilojianya, N. V. I., & Adegbite, N. a. O. (2024). Telecommunications Energy Efficiency: Optimizing Network Infrastructure for Sustainability. Computer Science & IT Research Journal, 5(1), 26–40. https://doi.org/10.51594/csitrj.v5i1.700

[2] Scholar Chinenye Obasi, Nko Okina Solomon, Olubunmi Adeolu Adenekan, & Peter Simpa. (2024). Cybersecurity’s Role in Environmental Protection and Sustainable Development: Bridging Technology and Sustainability Goals. *Computer Science & IT Research*

Journal, *5*(5), 1145-1177. https://doi.org/10.51594/csitrj.v5i5.1140

[3] Advancing Green Communications: The Role of Radio Frequency Engineering in Sustainable Infrastructure Design. (2024). *International Journal of Latest Technology in Engineering Management & Applied Science*, *13*(5), 113-121. https://doi.org/10.51583/IJLTEMAS.2024.130511

[4] Mao, Y., You, C., Zhang, J., Huang, K., & Letaief, K. B. (2017). A survey on Mobile Edge Computing: The Communication Perspective. *IEEE Communications Surveys & Tutorials*, *19*(4), 2322–2358. https://doi.org/10.1109/comst.2017.2745201

[5] Obaideen, K., Albasha, L., Iqbal, U., & Mir, H. (2024). Wireless power transfer: Applications, challenges, barriers, and the role of AI in achieving sustainable development goals - A bibliometric analysis. *Energy Strategy Reviews*, *53*, 101376. https://doi.org/10.1016/j.esr.2024.101376

[6] Thantharate, P., Thantharate, A., & Kulkarni, A. (2023). GREENSKY: A fair energy-aware optimization model for UAVs in next-generation wireless networks. *Green Energy and Intelligent Transportation*, *3*(1), 100130. https://doi.org/10.1016/j.geits.2023.100130

[7] Nguyen, D. C., Ding, M., Pathirana, P. N., Seneviratne, A., Li, J., Niyato, D., Dobre, O., & Poor, H. V. (2021). 6G Internet of Things: A Comprehensive survey. *IEEE Internet of Things Journal*, *9*(1), 359–383. https://doi.org/10.1109/jiot.2021.3103320

[8] De Alwis, C., Kalla, A., Pham, Q., Kumar, P., Dev, K., Hwang, W., & Liyanage, M. (2021). Survey on 6G frontiers: trends, applications, requirements, technologies and future research. *IEEE Open Journal of the Communications Society*, *2*, 836–886. https://doi.org/10.1109/ojcoms.2021.3071496

[9] Fraunhofer, 6G White Paper:”On the road to 6G: drivers, challenges and enabling technologies”; https://www.iis.fraunhofer.de/en/ff/kom/mobile-kom/6g-sentinel/6gsentinel-white-paper.html.

[10] Fraunhofer, 6G White Paper:”6G Energy Efficiency and Sustainability”; https://www.iis.fraunhofer.de/en/ff/kom/mobile-kom/6g-sentinel/6gsentinel-white-paper.html.

Standardization and Technology Trends in EV Charging Modes and Connectors

V. Vijayageetha
Department of EEE,
Thiagarajar College of Engineering,
Madurai, Tamil Nadu
dhanushree.geetha@gmail.com

N. Shanmugavadivoo
Department of EEE,
Thiagarajar College of Engineering,
Madurai, Tamil Nadu
nsveee@tce.edu

G. Sivasankar
Department of EEE,
Thiagarajar College of Engineering,
Madurai, Tamil Nadu
gsivasankar@tce.edu

***Abstract*—As a green alternative, electric vehicles, or EVs, gaining popularity. One of the most crucial elements in the adoption of EVs is the infrastructure that makes EV charging possible because it directly affects convenience, efficiency, and customer experience. An integral component of the charging ecosystem, connectors differ by standard and area. SAEJ1772, Mennekes, CHAdeMO, CCS (Combined Charging System) are examples of widely used connectors. To aid in comprehension and encourage developments in the EV sector, this article a exhaustive study of EV charging modes, and connectors, stressing their technical details, benefits, and worldwide adoption patterns**

Keywords—Electric Vehicle, Connectors, Charging Modes

I. INTRODUCTION

The use of electric Vehicles or EVs, in the automotive industry has significantly increased during the last decade. This development is primarily being driven by the need for lowering greenhouse gas emissions and increased global concern about environmental sustainability.

Since 1990, the European Union (EU) has been gradually cutting its greenhouse gas emissions.EU emissions in 2023 were 8% lower than in 2022 and 37% lower than in 1990. Due to a rise in renewable energy and a decline in the usage of coal and gas, this was the biggest annual reduction in decades. By 2030, the EU wants to cut emissions by 55% from 1990 levels. By 2030, a 49% decline is anticipated, according to current forecasts [1].

In Section II, EVs are thoroughly categorized into four fundamental types with an emphasis on their technical and operational characteristics. The numerous kinds of charging mode are covered in Section III, along with information on how well they work in various contexts. In Section IV, the four EV charging modes and the respective connector types are thoroughly examined, emphasizing the relationship between charging efficiency and connector design. Additionally, it looks at how charging modes match up with both new and existing standards. The discussion comes to a close in Section V, conclusion which highlights important discoveries and for EV charging system development.

II. EV CLASSIFICATION

Based on many different kinds of EVs, such as Two-Wheel and Three-Wheel Electric Vehicles, such as e-bikes and electric scooters, and Heavy-Duty Electric Vehicles, which include electric trucks and buses etc., they can also be divided into five fundamental groups such as Hybrid EV (HEV), Plug-in hybrid EV (PHEV), Range extender EV (REEV), Battery EV (BEV) and Fuel cell EV[2].

A. Hybrid Electric Vehicle

The Internal combustion engines (ICE) and electric motors are combined in hybrid electric vehicles (HEVs), which provide a flexible option for energy-efficient transportation. By employing the electric motor for accelerating or for low-speed driving, these cars greatly increase fuel efficiency. They also dramatically lower CO2 emissions when they are fueled by renewable energy sources. Regenerative braking, a feature of HEVs, recovers energy that would otherwise be lost when braking and utilizes it to recharge the battery, increasing overall efficiency. Since the engine and regenerative braking handle battery recharging, HEVs do not require external charging, in contrast to Plug-in Hybrid Electric Vehicles (PHEVs)[3,4].

B. Plug-in Hybrid Electric Vehicle

Plug-in hybrid electric vehicles, or PHEVs, combine the benefits of conventional internal combustion engine (ICE) with electric powertrains to provide a flexible and environmentally responsible mode of transportation. The ability to run on electricity alone for short distances and switch to the ICE for longer ones and combine the benefits of both power sources. They can able to charged via an external power source or charging stations is one of the main benefits of PHEVs. In order to increase total energy efficiency, PHEVs are also outfitted with regenerative braking, which aids in battery recharge while braking. PHEVs typically take 4 to 8 hours to fully charge and have smaller batteries than fully electric vehicles[5].

C. Range extender EV

Range Extender Electric Vehicles (REEVs) are a special kind of electric vehicle that extends the driving range beyond the usual bounds of a standard battery electric vehicle (BEV) by integrating a small IC engine (ICE) to produce extra power when the vehicle's battery charge is low. The electric motor serves as the main source of propulsion in REEVs, whereas the ICE only serves as a generator to replenish the battery cell rather than powering the wheels[6].

D. Battery EV

Battery electric vehicles, or BEVs, are completely electric automobiles that run purely on an internal rechargeable battery. It employ electric motor for propulsion and lacks of an internal combustion engine (ICE). To charge your automobile, connect it to the electrical grid at home, at a public location, or at a fast-charging station. When powered by renewable energy, BEVs have zero tailpipe emissions, making them environmentally friendly. High cost of the Battery, Range anxiety, charging time, and limited charging infrastructure are obstacles[7].

E. Fuel cell EV

Fuel Cell EV uses hydrogen fuel cells to generate electricity. These cars are very clean because they just release water vapor. Compared to battery-powered EVs, they have faster refueling times and greater driving ranges. The high prices of manufacture and the deficiency of infrastructure for hydrogen refueling, however, continue to be major obstacles to wider use. For areas with well-established facilities for producing and distributing hydrogen, FCEVs are perfect[8,9].

III. Charging Modes

International standards for electric vehicles (EVs) are developed to address the challenges of the EV market. It ensure performance uniformity, safety, and compatibility in international markets. IEC 61851, is a standard dealing with conductive charging systems for electric cars. The four charging modes are Mode1,Mode2 ,Mode3 and Mode 4are specified in this standard. IEC 62196 and IEC 61980 is also establishes Conductive charging [10].

A. Mode-1

Mode 1 named as slow charging mode and it uses an average household or commercial outlet that allows for up to 16 A of alternating current (AC) with power ranges 2kW to 3.7kW. This method does not have sufficient control and interaction between a vehicle and the charging station. This method disables standard safety features such as protection from overvoltage, overcurrent or over heat. It especially used for lightweight vehicles like e-bikes and electric motorbikes[11].

B. Mode-2.

In comparison to Mode 1, Mode 2 charging is easier to use because it accommodates Poly phase systems.By grounding the cable and protecting against faults like overcurrent and overheating, the protection device, which is built into this mode, improves safety. Because of the specific cable and built-in safety precautions, Mode 2 is more costly than Mode 1, but it offers better performance and dependability. It is intended for use with household outlets and can handle currents between 16 and 32 A and power levels ranges from 7 kW to 22 kW[12].

C.Mode-3

Mode 3 charging ensures safe and effective charging for electric vehicles by utilizing a specialized three-phase AC connector. The charging procedure is managed by the EV's onboard charger, and a unique, secure connection connects the EV to the station. The safety is further improved by the charging station's integrated safety features. The EV's onboard charger controls the charging process, and the EV is connected to the station via a special, secure wire[13]

D.Mode-4

To ensure a safe and effective connection, Mode 4 calls for a special cable to be connected at the charging station. It is compatible with a number of worldwide DC fast-charging standards, including Tesla Supercharger, CCS (Combined Charging System), and CHAdeMO. This mode, which allows for quick recharging in handy locations, is essential for lowering range anxiety and hastening the adoption of EVs. Furthermore, Mode 4 frequently incorporates smart charging features like user identification, remote monitoring, and demand-driven dynamic pricing

Table 1: Comparison of parameters related to various charging modes

Charging mode	Voltage	Power	Current	Standards	Configuration
Mode 1	1φ AC-230-250V 3φ AC-230-250V	3.8kW 7.6kW	16A	CEE 7/4 type F(schuko), IEC 62196, IEC 61851-1	
Mode 2	1φ AC-230-250V 3φ AC-480V	7.6kW 15.3kW	32A	IEC 62196-2, IEC 61851-1	
Mode 3	1φ AC-230-250V 3φ AC-480V	60 kW 120kW	32-250A	IEC 62196-2, IEC 61851-1	
Mode 4	DC-600-1000V	>150kW	250A-400A	IEC 62196-3	

Vehicles in an effort to improve efficiency and convenience. In order to compare various wireless charging technologies for EVs and determine the essential technological elements of wireless charging, numerous studies have been conducted in this area. Table 1 shows comparison of parameters related to various charging mode [14].

IV. CHARGING CONNECTORS

The purpose of connector is to connect the EV charger and the power supply. Depends upon the power level, there are various EV connectors available. The comparisons of different connectors given in Table 1.The standard pertaining to EV connectors, specifically AC and DC connectors, is reviewed in this section. There are only a few differences and many similarities between the layouts for AC and DC connectors, depending on the kind of electric car charging socket [15,16].

A.Type-1 Connector

In North America and Japan, the Type-1 connector also referred to as the SAE J1772 connector is a common charging connector that is mostly utilized for AC charging [17].This connector designed to work in Mode 1 standards.It works with Level 1 (120V) and Level 2 (240V) charging systems and is made for single-phase charging and produces low output power than Type-2 Connector. The charging cable on Type 1 charging stations is fixed, thus it is not removable during charging and is permanently fixed to the charging station[18].

Type-2 Connector

Type-2 connectors are used as a standard type in all countries which supports single phase and three phase charging by following IEC 61851-1 standards.In Australia and Europe, the Mennekes or Type 2 EV connector is the most often used AC charging variant[19].A single-phase 70 amp current or a three-phase 63 amp current can be handled by this connector, which has a maximum voltage of 500V.Type 2 –GB/T are used in china and it allows mode 2 and mode 3 charging with high power than Type-1[20].

C.Type-3 Connector

Type-3 connector is a single and three phase vehicle coupler equipped with safety features. The Type 3 connector, which is a component of the IEC 62196-2 standard, is extensively utilized in France and Italy for AC charging of electric vehicles (EVs). It is especially appropriate for areas with stringent safety rules because of its integrated safety shutters, which prevent unintentional contact with live parts[21].

TABLE 2: COMPARISON OF PARAMETERS RELATED TO VARIOUS CHARGING CONNECTORS [47-52] .

Type	Voltage	Power	current	Modes used	connector
Type 1	Level 1:120V_{ac}, Level 2:240 V_{ac}	Level 1:2kW Level2:19.2kW	Level 1-16A Level2 -80A	Mode 1	
Type 2	3φ AC/DC,500V	AC,3.7kW-7.4kW 3φAC,11kW-43 kW	63A, AC 300A ,DC	Mode 2,3,4	
Type 3(CCS-Combo-1)	850V,DC	80kW	200A ,DC	Mode 4	
Type -3(CCS-Combo-2)	1000V,DC	200kW	200A ,DC	Mode 4	
Type 4	1000V,DC	400kW	400A,DC	Mode 4	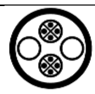

Type-4 Connector

Type 4 connector means that CHAdeMO is present in Europe and Japan .G105-1993 specified by The Japan Automobile Research Institute's (JARI) Japan Electric Vehicle Standard (JEVS) . In dissimilarity to types 1 and 2,type 4 connections signal via the CAN bus protocol. The CHAdeMO stands for "CHArge de MOve," which interpret to "charge for moving." For high-voltage (up to 500 V DC) high-current (125 A) vehicle fast charging using a JARI DC fast charge connector, CHAdeMO is a type of DC fast charge. In CAN-BUS connections, the connector has two sizable pins for DC power[22]

V. CONCLUSION

In this paper, different EV charging modes and connector types are thoroughly explored, with a thorough analysis of their features and uses provided. The EV and the charging infrastructure's safety procedures and communication are highlighted by the charging modes, which are divided into Mode 1, Mode 2, Mode 3, and Mode 4. Connector types are Type 1, Type 2, Type 3, and Type 4 describes the charging station compatibility and physical interface. A thorough analysis of various connectors and modes is carried out, offering important insights into their functions in EV charging systems. Furthermore, by offering helpful advice on implementing suitable charging systems, this article is an important resource for commercial EV makers.

ACKNOWLEDGMENT

The authors extend their due thanks to the Thiagarajar College of Engineering management, Madurai, India for their extensive research facilities and the financial backing from Thiagarajar Research Fellowship (TRF) scheme (File.no: TCE/RD/TRF/2024/5 is gratefully acknowledged.

References

[1] European Commission, Electric Vehicle, https://transport.ec.europa.eu/transport-themes_en 3.1.25

[2] Guzek, M., Żmuda, M., Zdanowicz, P., Jurecki, R., Jackowski, J., & Szumska, E. (2024). Electric Vehicles—An Overview of Current Issues—Part 2—Infrastructure and Road Safety. *Energies*, *17*(2), 495. https://doi.org/10.3390/en17020495

[3] K., Latha, Maheswari., S., Kavitha., M., Kathiresh. (2022). Introduction to Electric Vehicles and Hybrid Electric Vehicles. https://doi.org/10.1007/978-3-030-85424-9_1

[4] Ch., Chandra, Sekhar., Nidhi, Chandrakar., Jay, Prakash., Harinaik, Sugali. (2024). An overview of hybrid electric vehicles. 3-56. https://doi.org/10.1016/b978-0-443-18999-9.00002-8

[5] Zhenpo, Wang. (2024). Plug-In Hybrid Electric Vehicles (PHEVs). 295-321. https://doi.org/10.1007/978-981-97-4840-2_8

[6] Sun, Y., Han, Z., Feng, J. and Wu, Z., 2023. Range-extender In-the-loop Method for Fuel Consumption Prediction of Hybrid Electric Vehicles. *International Journal of Automotive Technology*, *24*(1), pp.91-103.

[7] Ahmad, Faraz., A., Ambikapathy., Saravanan, Thangavel., K., Logavani., G., Arun, Prasad. (2021). Battery Electric Vehicles (BEVs). 137-160. https://doi.org/10.1007/978-981-15-9251-5_8

[8] Christos, Pergamalis., Eleftherios, Tsampasis., Ioannis-Christos, Dedes., Charalambos, Elias. (2024). Hydrogen Fuel Cell Electrical Vehicles (FCEV) - Battery Electric Vehicles (BEV) - Comparison andFutureChallenges.

[9] Selmi, T., Cherif, A., & Khadhraoui, A. (2022). Fuel cell-based electric vehicles technologies and challenges. Environmental Science and Pollution Research, 29(52), 78121–78131. https://doi.org/10.1007/s11356-022-23171-w

[10] Raff, R., Golub, V., Pelin, D., & Topic, D. (2019). *Overview of charging modes and connectors for the electric vehicles*. 1–6. https://doi.org/10.1109/iyce45807.2019.8991586

[11] Pranali, Nikam., Rajin, M., Linus., Nilam, S., Patil. (2023). Analysis of Different Charging Modes in Electric Vehicle (EV) Application. 1-6. https://doi.org/10.1109/icccnt56998.2023.10307155

[12] Afaq, Ahmad., Muhammad, Saqib, Khalid., Zahid, Ullah., Naveed, Ahmad., Mohammad, Aljaidi., Faheem, Ahmed, Malik., Umar, Manzoor. (2022). Electric Vehicle Charging Modes, Technologies and Applications of Smart Charging. Energies, 15(24), 9471-9471. https://doi.org/10.3390/en15249471

[13] Liew, Hui, Fang., Muhammad, Izuan, Fahmi, Romli., Rosemizi, Abd, Rahim., Muhammad, Ezanuddin, Abdul, Aziz., Diyya, Hidayah, Abd, Rahman., Habibah, Haji, Mokhtaruddin. (2024). Development of an advanced current mode charging control strategy system for electric vehicle batteries. International Journal of Power Electronics and Drive Systems, 15(4), 2639-2639. https://doi.org/10.11591/ijpeds.v15.i4.pp2639-2650

[14] (2023). A Study on Various Electric Vehicle Charging Technologies. https://doi.org/10.1109/icscss57650.2023.10169328 .

[15] Falvo, M.C., Sbordone, D., Bayram, I.S. and Devetsikiotis, M., 2014, June. EV charging stations and modes: International standards. In *2014 international symposium on power electronics, electrical drives, automation and motion* (pp. 1134-1139). IEEE.

[16] Dericioglu, C., YiriK, E., Unal, E., Cuma, M.U., Onur, B. and Tumay, M., 2018. A review of charging technologies for commercial electric vehicles. *International Journal of Advances on Automotive and Technology*, *2*(1), pp.61-70.

[17] Bräunl, T., 2012. EV charging standards. *University of Western Australia: Perth, Australia*, pp.1-5.

[18] Chen, T., Zhang, X.P., Wang, J., Li, J., Wu, C., Hu, M. and Bian, H., 2020. A review on electric vehicle charging infrastructure development in the UK. *Journal of Modern Power Systems and Clean Energy*, *8*(2), pp.193-205.

[19] Dadhich, A.K. and Iqba, M.A., 2022. Overview of the electric vehicle connectors and charging modes. *NeuroQuantology*, *20*(16), p.4775.

[20] Rachid, A., El Fadil, H., Gaouzi, K., Rachid, K., Lassioui, A., El Idrissi, Z. and Koundi, M., 2022. Electric vehicle charging systems: comprehensive review. *Energies*, *16*(1), p.255.

[21] Chamberlain, K. and Al-Majeed, S., 2021. Standardisation of UK electric vehicle charging protocol, payment and charge point connection. *World Electric Vehicle Journal*, *12*(2), p.63.

[22] Ahmad, A., Khalid, M., Ullah, Z., Ahmad, N., Aljaidi, M., Malik, F.A. and Manzoor, U., 2022. Electric vehicle charging modes, technologies and applications of smart charging. *Energies*, *15*(24), p.9471.

SEMS-AEVS: An Integrated Approach to Forecasting, Load Disaggregation, and Dynamic Scheduling in Residential Energy Systems

Selva Vengatesh M
Dept. of EEE,
Thiagarajar College of Engineering,
Madurai, India
naanthalaivan1206@gmail.com

Rathika S
Dept. of EEE,
Latha Mathavan Polytechnic College,
Madurai, India
karthi.ieee@gmail.com

Charles Raja S
Dept. of EEE,
Thiagarajar College of Engineering,
Madurai, India
charlesrajas@tce.edu

J. Jerslin Drusila Nesamalar
Dept. of EEE,
Tamilnadu Govt. Polytechnic College,
Madurai, India
jeslindrusila@gmail.com

***Abstract*—This paper proposes SEMS-AEVS, a Smart Energy Management System integrated with an Advanced EV Scheduler, to address the variability introduced by renewable energy and electric vehicle (EV) adoption in residential settings. The framework incorporates hybrid year-ahead forecasting of solar irradiance and load demand, predictive load disaggregation, and dynamic scheduling based on Time-of-Use (ToU) tariffs and Vehicle-to-Home (V2H) operations. SEMS-AEVS achieves 34% cost savings, 42% reduction in grid dependency, and 88% renewable energy utilization, while reducing carbon emissions by 34%. Its modular and scalable architecture enables seamless smart grid integration, offering a sustainable solution for future residential energy management.**

***Keywords*—Smart Energy Management System, EV scheduling, V2H, Dynamic scheduling, Solar and load prediction, load disaggregation.**

I. Introduction

The surge in global energy demand, coupled with the integration of renewable energy sources (RES) and electric vehicles (EVs), poses significant challenges to grid stability and efficiency. Residential energy usage constitutes 39% of global consumption, where effective demand-side management (DSM) can reduce carbon emissions by up to 20% (IEA). Early EMS frameworks [1, 2] employed heuristic DSM but struggled with RES intermittency and EV variability. Forecasting methods using statistical and machine learning techniques [3, 4] improved accuracy yet faced limitations in scalability and real-time deployment. Recent RES-EV integrated systems [5, 6] advanced EV energy flow optimization but lacked fine-grained appliance control and user adaptability. Hybrid approaches with clustering [7] and reinforcement learning [8] show potential but fail to unify long-term forecasting with real-time scheduling. To address these gaps, SEMS-AEVS, a Smart Energy Management System with Advanced EV Scheduler combines rapid year-ahead forecasting, appliance-level disaggregation, and adaptive EV scheduling to minimize grid dependency, costs & emissions, and improved scalability.

- A lightweight hybrid forecasting pipeline enabling year-ahead solar and load predictions within 3 minutes, integrated with heuristic scheduling for enhanced efficiency and peak management.
- Adaptive EV charging/discharging and user-centric DSM enhance grid performance while reducing carbon emissions.
- Seamless integration with smart grid infrastructures, supporting bi-directional energy flows & trading, and adaptability to diverse residential setups.

II. System Architecture

The SEMS-AEVS framework comprises four integrated modules for optimizing residential energy usage, cost, and grid reliance. The Solar Forecasting Module employs a hybrid pipeline using four years of irradiance data. The Temperature Estimation Module derives hourly temperatures from irradiance and climate inputs. The Load Disaggregation Module predicts total demand and classifies it into non-shiftable, controllable, and shiftable loads. The Energy Management Module schedules appliances and EVs by prioritizing critical loads and shifting flexible ones to low-tariff or solar-rich periods, supporting bi-directional EV trading. The modular design enables real-time control, scalability, and smart grid compatibility.

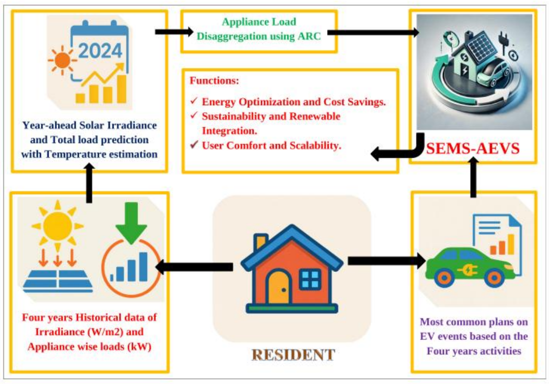

Fig 1 Schematic illustration of the proposed

III. DATA DESCRIPTION

The SEMS-AEVS framework is implemented in a 3BHK residence in Thiruparankundram, Madurai, with a 15.47 kW connected load and an 8 kW on-grid PV system over a 1200 m² area. It leverages four years of historical data—hourly solar irradiance (pyranometer), temperature records, appliance-level smart meter data, and EV usage from EVMS—for accurate forecasting and adaptive scheduling. Table I classifies appliances into non-shiftable, controllable, and shiftable loads to enable efficient, user-comfort–aware scheduling. Grid imports follow a Time-of-Use (ToU) tariff (Fig. 2), while surplus exports earn □2.45/kWh, enhancing grid interaction efficiency.

TABLE 1 DETAILED BREAKDOWN OF APPLIANCE IN THE HOUS

Clusters	Appliance	Power Rating (W)	Unit	User Centric Actions
Non-Shiftable	LED Lights	10	20	Shifting of those appliances affects the crucial household manual activities
	Ceiling Fans	60	6	
	Exhaust Fans	40	4	
	Refrigerator	200	1	
	Mixer	500	1	
	Grinder	300	1	
	Television (TV)	100	3	
	Geyser	2000	2	
	Iron Box	1000	1	
	Vacuum Cleaner	1200	1	
Controllable	Air Conditioner	1500	3	Temperature Dependent (22-24 ℃)
Shiftable	Dishwasher	1500	1	Within 9 AM – 2 PM
	Washing Machine	500	1	Within 9 AM – 4 PM
	Water Pump	750	1	Evening and Morning

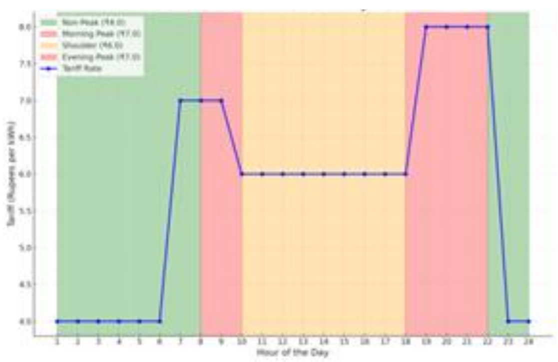

FIG 2 TIME OF USE (TOU) TARIFF

IV. METHODOLOGY

This section outlines the methodologies implemented in the SEMS-AEVS framework to optimize energy utilization, minimize costs, and reduce grid dependency for the study site, which is illustrated in Fig. 3.

A. *Year-Ahead Forecasting*

The forecasting module integrates Prophet, XGBRegressor [9], [10], and ARC to generate hourly predictions of solar irradiance and energy demand. Prophet models trend, seasonality, and holiday effects; XGBRegressor addresses non-linear residuals; and ARC applies corrections for deviations beyond ±5%. Trained on four years of data, the pipeline delivers accurate year-ahead forecasts within 2–3 minutes, supporting real-time scalability. The final prediction is formulated as:

$$P_{final}(t) = P_{trend}(t) + P_{seasonality}(t) + P_{holidays}(t) + R_{refined}(t) + \Delta_{ARC}(t) \quad (1)$$

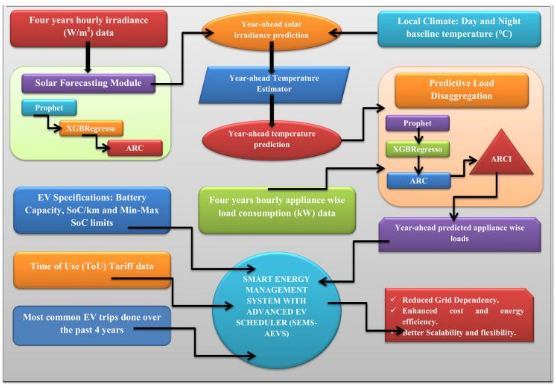

FIG 2 METHODOLOGY OF THE PROPOSED WORK

B. *Predictive Load Disaggregation*

The Predictive Load Disaggregation module categorizes household energy consumption into three operational clusters using the Appliance Resource Connective Implementer (ARCI), as shown in Table I. This classification enables precise load management and optimization by minimizing the variance between appliance loads and their respective cluster centroids, as defined in equation (2).

$$minimize \sum_{i=1}^{N} \sum_{j=1}^{K} \delta_{ij} \cdot \left\| L_i - C_j \right\|^2 \quad (2)$$

L_i: Energy consumption of appliance i; C_j : Centroid of cluster; δ_{ij}: Binary variable, 1 if appliance i belongs to cluster j, otherwise 0; : Total number of appliances; K : Total number of clusters.

C. *Energy Management and Sheduling Module*

This module employs heuristic scheduling to optimize appliance and EV operations by aligning shiftable loads and EV charging with low-tariff periods [11, 12], and coordinating operations with solar generation peaks $P_{solar}(t)$. EV discharging $P_{EV-discharge}(t)$ supports critical loads and reduces grid dependency $P_{grid}(t)$ during peak hours, while controllable loads are dynamically adjusted for efficiency and comfort. The optimization minimizes energy costs as in equation (3), subject to the power balance constraint in (4), leveraging RES and Time-of-Use tariffs for effective management [13-15]:

$$minimize \sum_{t=1}^{T} \left(P_{grid}(t) \cdot Tariff(t) \right) \quad (3)$$

$$P_{load}(t) = P_{solar}(t) + P_{grid}(t) + P_{EV-discharge}(t) \quad (4)$$

This modular design ensures scalability, real-time adaptability, seamless smart grid integration, and efficient bi-directional energy trading.

V. Results and Discussions

This section compares SEMS-AEVS with Conventional Energy Management Systems (CoEMS). By integrating forecasting, load disaggregation, and dynamic scheduling, SEMS-AEVS enhances cost efficiency, reduces grid dependency, and improves renewable utilization. It addresses key CoEMS limitations. Results validate its performance and sustainability impact.

1) *Module-wise Results*

Module-wise results highlight the distinct contributions of forecasting, load disaggregation, and scheduling, with comparative analysis confirming the superior performance of SEMS-AEVS over CoEMS.

D. *Year-Ahead Forecasting*

The hybrid forecasting model combines Prophet for trend-seasonality decomposition, XGBRegressor for non-linear residual learning, and ARC for adaptive correction, achieving MAPE of 3.5% (solar) and 4.2% (load) in 2.5 min. It outperforms ARIMA with 22% (solar) and 19% (load) lower MAPE. Table II and Fig. 4(a)–(b) highlight seasonal prediction accuracy. Unlike CoEMS, SEMS-AEVS enables predictive, real-time energy management.

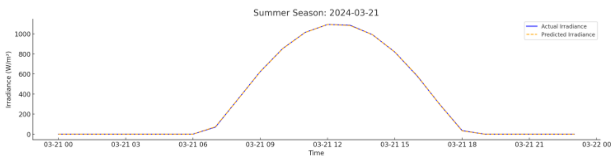

(A) Seasonal Irradiance (W/M²)

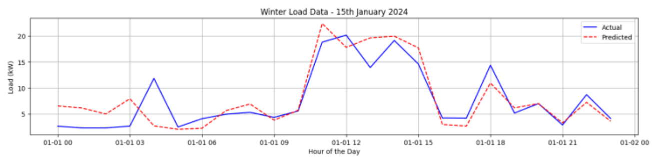

(B) Evergy demand (kW)

Fig 3 Actual vs. Predicted Data

Table 2 Forecasting performance

Model	MAPE (%)		Runtime (Mins)	
Field	**Solar**	**Load**	**Solar**	**Load**
ARIMA	6.8	7.2	12	15
Prophet	5.2	5.8	2.8	3
XGBRegressor	4.5	4.9	4.2	5
SEMS-AEVS	**3.5**	**4.2**	**2.5**	**2.5**

E. *Predictive Load Disaggregation*

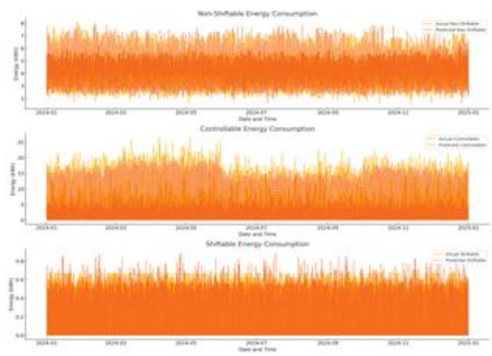

Fig 4 Actual vs. Disaggregated Loads

SEMS-AEVS categorizes household loads as non-shiftable (35%), controllable (25%), and shiftable (40%) using four years of appliance-level data. This enables fine-grained scheduling, shifting 78% of high-energy tasks to low-tariff or solar-surplus periods. Fig. 5 shows strong prediction accuracy (RMSE < 1.2 kWh), with controllable loads offering high flexibility. CoEMS lacks such categorization, limiting optimization.

F. *Energy Management and Scheduling*

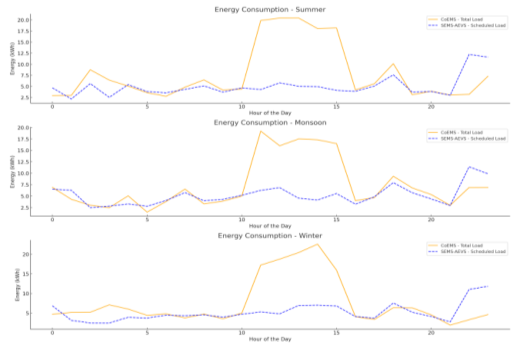

Fig 5 CoEMS vs. SEMS-AEVS loads

Table 3 SEMS-AEVS vs. CoEMS

Metric	SEMS-AEVS	CoEMS	Improvement (%)
Cost Saving (□)	46,508	0	+34%
Grid Dependency	3,475.89	5,271.44	-42%
Renewable Utilization	88%	72.8%	+21%
V2H	12%	N/A	N/A

SEMS-AEVS uses dynamic scheduling to optimize consumption, lower grid dependency, and boost renewable use. Temperature-based control and ToU-aligned EV/load shifts, combined with V2H discharging (12% peak support), achieve over 50% summer peak reduction (Fig. 6). These strategies enable 34% cost savings, 42% less grid import, and 88% renewable use—significantly outperforming CoEMS (Table III).

2) *Seasonal Performance and Environmental Impact*

SEMS-AEVS adopts a strategic approach to grid interaction, reducing costs and enhancing renewable utilization through dynamic adaptation to seasonal and demand fluctuations. Figs. 7 and 8 illustrate its superior performance over CoEMS across seasonal scenarios.

A. *Seasonal Grid Import and Export Optimization*

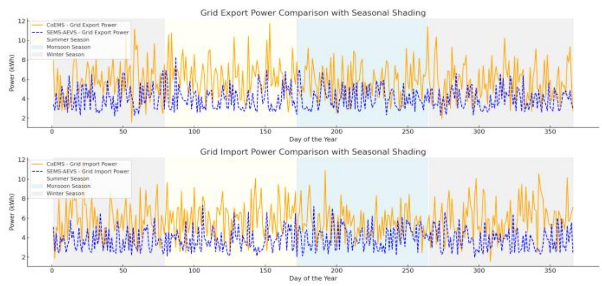

Fig 6 Grid Import and Export Power Analysis CoEMS vs. SEMS-AEVS

 ISBN: 978-93-342-3695-8

Fig. 7 compares grid import/export patterns of SEMS-AEVS and CoEMS. SEMS-AEVS minimizes grid exchanges by prioritizing local renewable use and EV storage through advanced scheduling and forecasting, especially during low-tariff periods. In contrast, CoEMS's static control results in higher grid reliance and suboptimal renewable utilization, leading to increased costs.

B. *Economic Impact of Grid Power Management*

FIG 8 GRID IMPORT AND EXPORT COST ANALYSIS COEMS VS. SEMS-AEVS

Fig. 8 illustrates SEMS-AEVS's economic gains through reduced seasonal grid import costs and optimized export earnings. Accurate forecasting and dynamic scheduling shift loads to low-tariff periods, while V2H meets 12% of peak demand. Minimal low-tariff exports ensure local renewable use. Table IV shows 88% renewable utilization and 42% lower grid imports, outperforming CoEMS's fixed, costlier scheduling.

TABLE 4 SEASONAL PERFORMANCE OF SEMS-AEVS

Season	Renewable Utilization (%)	Grid Imports (kWh)
Summer	92%	500
Monsoon	76%	1,200
Winter	85%	800

C. *Environmental Sustainability and Grid Stability:*

SEMS-AEVS's comprehensive energy management strategy delivers notable environmental benefits, achieving a 34% reduction in carbon emissions by minimizing reliance on fossil-fuel-based grid power. V2H integration further supports grid stability during peak hours, aligning with broader sustainability objectives.

VI. CONCLUSION

SEMS-AEVS outperforms CoEMS in residential energy optimization through integrated forecasting, predictive load disaggregation, and dynamic scheduling. Its hybrid forecasting pipeline (Prophet, XGBRegressor, ARC) achieves high accuracy (MAPE: 3.5% solar, 4.2% load) with <3 min runtime. Load disaggregation enables 78% of energy-intensive tasks to be shifted to low-tariff periods. Combined with V2H, SEMS-AEVS reduces grid dependency by 42%, energy costs by 34%, and achieves 88% renewable utilization. It also lowers carbon emissions by 34%. With a scalable, modular design, SEMS-AEVS offers a sustainable, efficient alternative to CoEMS for smart residential energy management.

ACKNOWLEDGMENT

The authors express their sincere gratitude to the management of Thiagarajar College of Engineering (TCE) for their support in facilitating this study. The financial assistance is provided through the Thiagarajar Research Fellowship scheme (File.no: TCE/RD/TRF/24RS076 dated 27.09.2024). Moreover, the authors also extend their appreciation for the financial support received under the Seed Money Scheme (File No.: R&D/Seedmoney/2024/13) and the Department of Science and Technology's FIST Scheme (File No.: SR/FST/College-519/2019) are gratefully acknowledged.

REFERENCES

[1] Hussain, H. M., & Nardelli, P. H. (2020, June). A heuristic-based home energy management system for demand response. In 2020 IEEE Conference on Industrial Cyberphysical Systems (ICPS) (Vol. 1, pp. 285-290). IEEE.

[2] Tariq, M., Khalid, A., Ahmad, I., Khan, M., Zaheer, B., & Javaid, N. (2018). Load scheduling in home energy management system using meta-heuristic techniques and critical peak pricing tariff. In Advances on P2P, Parallel, Grid, Cloud and Internet Computing: Proceedings of the 12th International Conference on P2P, Parallel, Grid, Cloud and Internet Computing (3PGCIC-2017) (pp. 50-62). Springer International Publishing.

[3] Wan, Z., Li, H., & He, H. (2018, July). Residential energy management with deep reinforcement learning. In 2018 international joint conference on neural networks (IJCNN) (pp. 1-7). IEEE.

[4] Latoń, D., Grela, J., & Ożadowicz, A. (2024). Applications of Deep Reinforcement Learning for Home Energy Management Systems: A Review. Energies, 17(24), 6420.

[5] Wei, G., Chi, M., Liu, Z. W., Ge, M., Li, C., & Liu, X. (2023). Deep reinforcement learning for real-time energy management in smart home. IEEE Systems Journal, 17(2), 2489-2499.

[6] Asif, S., Shafiq, S., Fatima, I., Anwar ul Hassan, C. H., Ul Abideen, Z., & Javaid, N. (2018). A heuristic scheduling approach for demand side energy management. In Advances in Network-Based Information Systems: The 20th International Conference on Network-Based Information Systems (NBiS-2017) (pp. 995-1003). Springer International Publishing.

[7] Hafeez, G., Javaid, N., Iqbal, S., & Khan, F. A. (2018). Optimal residential load scheduling under utility and rooftop photovoltaic units. Energies, 11(3), 611.

[8] Mathew, A., Roy, A., & Mathew, J. (2020). Intelligent residential energy management system using deep reinforcement learning. IEEE Systems Journal, 14(4), 5362-5372.

[9] Naccarelli, R., Serroni, S., Casaccia, S., Revel, G. M., Gutiérrez, S., & Arnone, D. (2024, June). Methodological Approach for Optimizing Demand Response in Building Energy Management through AI-Enhanced Comfort-Based Flexibility Models. In 2024 9th International Conference on Smart and Sustainable Technologies (SpliTech) (pp. 1-6). IEEE.

[10] Abumohsen, M., Owda, A. Y., Owda, M., & Abumihsan, A. (2024). Hybrid machine learning model combining of CNN-LSTM-RF for time series forecasting of Solar Power Generation. e-Prime-Advances in Electrical Engineering, Electronics and Energy, 9, 100636.

[11] Aguilar, D., Quinones, J. J., Pineda, L. R., Ostanek, J., & Castillo, L. (2024). Optimal scheduling of renewable energy microgrids: A robust multi-objective approach with machine learning-based probabilistic forecasting. Applied Energy, 369, 123548.

[12] Zaeri Esfahani, N., Ashouri, A., Gunay, H. B., & Bahiraei, F. (2024). Energy consumption disaggregation in commercial buildings: a time series decomposition approach. Science and Technology for the Built Environment, 30(6), 660-674.

[13] Li, X., Wang, Z., Yang, C., & Bozkurt, A. (2024). An advanced framework for net electricity consumption prediction: Incorporating novel machine learning models and optimization algorithms. Energy, 296, 131259.

[14] Kanakadhurga, D., & Prabaharan, N. (2024). Smart home energy management using demand response with uncertainty analysis of electric vehicle in the presence of renewable energy sources. Applied Energy, 364, 123062.

[15] Elghanam, E., Abdelfatah, A., Hassan, M. S., & OSMAN, A. (2024). Optimization techniques in electric vehicle charging scheduling, routing and spatio-temporal demand coordination: a systematic review. IEEE Open Journal of Vehicular Technology.

A Novel Digital Twin Framework for Enhancing Electric Vehicle Performance and Sustainability

N. Sivakumar
Department of Electrical and Electronics Engineering,
Thiagarajar College of Engineering,
Madurai, India
siva23.n@gmail.com

S. Charles Raja
Department of Electrical and Electronics Engineering,
Thiagarajar College of Engineering,
Madurai, India
charlesrajas@gmail.com

***Abstract*—Digital twin (DT) technology is revolutionizing electric vehicle (EV) applications by providing virtual replicas of physical systems for real-time monitoring, simulation, and optimization. This paper introduces a novel hybrid digital twin framework that integrates real-time IoT data, advanced machine learning algorithms, and predictive analytics to enhance EV performance, energy efficiency, and lifecycle management. The proposed framework includes a novel Fault Prediction and Adaptive Maintenance (FPAM) model, which leverages real-time operational data and historical trends to anticipate potential failures and optimize maintenance schedules. Experimental validation demonstrates a significant improvement in energy efficiency (12%) and predictive accuracy (90%) compared to conventional systems. The findings indicate that this innovative approach can significantly advance EV sustainability and operational reliability.**

Keywords—Digital Twin (DT), IoT-Based Monitoring, Battery Management System (BMS), State of Charge (SOC), State of Health (SOH), Electric Vehicles (EVs), Fault Prediction, Cloud Computing, Smart Energy Systems.

I. Introduction

The rapid rise in electric vehicle (EV) adoption necessitates the development of advanced energy management systems to ensure efficient operation, sustainability, and reliability. Traditional battery management systems (BMS) often fail to meet these dynamic requirements, including accurate State of Charge (SOC) and State of Health (SOH) predictions, fault detection, and maintenance optimization. The advent of Digital Twin (DT) technology, integrating IoT, cloud computing, and machine learning, offers a transformative approach to overcome these limitations [1]. Several studies have explored the potential of DT and IoT in energy management. Cao et al. [2] emphasized the integration of IoT and machine learning for real-time monitoring and predictive analytics, highlighting its role in improving energy utilization. Similarly, Sharifi et al. [3] discussed the scalability benefits of cloud-based systems for energy management. Wang et al. [4] investigated inefficiencies in traditional static monitoring systems, proposing solutions for dynamic operational scenarios. Zhao et al. [5] developed advanced thermal management strategies for EVs but did not address predictive maintenance comprehensively.

Subudhi et al. [6] reviewed wireless power transfer (WPT) systems, identifying the challenges of integrating real-time monitoring frameworks for EV applications. Recent research underscores the importance of predictive maintenance and adaptive systems for EVs. Zhang et al. [7] demonstrated the application of DT for fault detection, achieving significant reliability improvements. Patil and Gadgune [8] reviewed advancements in inductive power transfer (IPT) systems, focusing on efficiency and scalability. Hidayat et al. [9] proposed optimized coil designs to enhance wireless charging efficiency under misalignment conditions.

Additionally, Li et al. [10] investigated the magnetic coupling characteristics of dynamic charging systems, which play a crucial role in improving power transfer performance. Mou et al. [11] addressed challenges related to coupling coefficient management and resonant frequency stability, both critical for ensuring efficient EV charging. The integration of artificial intelligence and IoT technologies has been a focal point in recent advancements. Han et al. [12] developed hybrid models combining machine learning and physical principles for SOC prediction, achieving higher accuracy under dynamic conditions. Kumar et al. [13] proposed a machine learning-based architecture to optimize EV charging schedules, reducing energy losses significantly. Zhang et al. [14] examined the role of cloud platforms in streamlining BMS operations, enabling enhanced decision-making and scalability. Furthermore, Huo et al. [15] introduced advanced sensor technologies that improve real-time data acquisition and analysis, paving the way for more robust EV monitoring systems.

This paper addresses these challenges by presenting a comprehensive DT framework for EV energy management. The proposed system combines IoT-enabled sensors for real-time data acquisition, machine learning algorithms for predictive analytics, and adaptive maintenance strategies to optimize energy efficiency, fault detection, and scalability, making it a transformative solution for the next generation of EV infrastructure.

II. Problem Findings

Adaption of EVs has introduced significant challenges in maintaining energy efficiency, operational reliability, and scalability of existing systems. Traditional methods for monitoring and managing EV energy consumption rely on outdated algorithms and static schedules, which are unable to adapt to dynamic operational conditions. As a result, inefficiencies arise in energy utilization, with higher power losses and suboptimal battery performance. Furthermore, these systems lack real-time fault detection mechanisms, making them prone to unexpected failures that increase maintenance costs and downtime.

Thiagarajar Research Fellowship scheme (File.no: TRF/Jul-2022/08).

III. Research Gap

To bridge these gaps, this paper presents a comprehensive DT framework that combines IoT-enabled sensors, machine learning algorithms, and adaptive maintenance strategies, optimizing energy efficiency, fault detection, and scalability for next-generation EV infrastructure.

IV. Objectives

This paper proposes an IoT-enabled Digital Twin framework tailored for EV applications. The following key points are mainly focused on this work.

- To improve energy efficiency and reduce operational costs.
- To implement predictive maintenance for fault detection and prevention.
- To provide a scalable and sustainable solution for EV management.

V. Novelty

The novelty lies in combining Digital Twin technology with adaptive machine learning algorithms and real-time IoT data acquisition, addressing the aforementioned gaps effectively.

- Development of a hybrid Fault Prediction and Adaptive Maintenance (FPAM) model.
- Integration of real-time IoT-enabled data acquisition with advanced predictive analytics for EV optimization.
- Real-world validation demonstrating superior energy efficiency and fault prediction accuracy compared to conventional systems.

This article is organized as follows: Section II presents the preliminary concepts which include background, motivation, related work and contribution of this study. Section III discusses methodology of proposed FPAM model, its techniques to enhance EV performance and sustainability. A discussion on combined framework which integrating process of IoT-enabled data acquisition, machine learning algorithms, and adaptive maintenance strategies is provided in section IV. Section V presents result of fault prediction and a comparative analysis of energy efficiency and performance metrics. Conclusion and future work are discussed in Section VI.

VI. Backgroung and Related Work

The evolution of energy management systems in electric vehicles (EVs) has been marked by significant milestones, yet challenges persist in achieving real-time adaptability and efficiency. Existing research highlights the integration of IoT and machine learning for energy optimization. Similarly, Patil and Gadgune reviewed inductive power transfer systems, highlighting the need for efficient coil designs to mitigate misalignment issues.

In this context, the proposed framework leverages digital twin technology to bridge these gaps. By combining real-time IoT data acquisition, advanced machine learning models, and adaptive maintenance strategies, the framework offers a holistic solution for energy optimization and system reliability in EV operations.

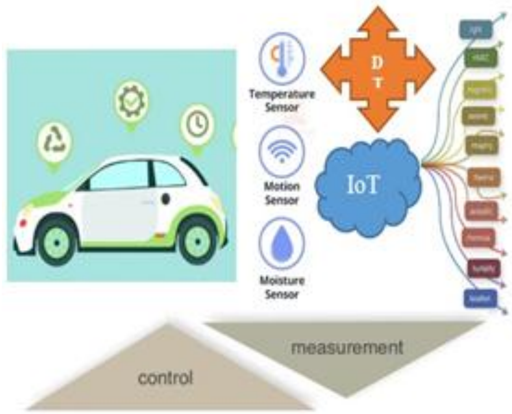

Fig. 1. IoT-Enabled DT Framework based EV system

VII. Proposed Framework

The rapid transition poses significant challenges to energy efficiency, fault management, and scalability in EV infrastructure. The integration of cutting-edge technologies such as Digital Twin (DT), IoT, and machine learning offers a transformative approach to overcome these challenges. IoT-Enabled Real-Time Data Acquisition: Sensors embedded in EVs collect data on critical parameters such as battery temperature, state of charge (SoC), motor performance, and environmental conditions shown in figure 1.

The machine learning models to predict potential faults. Adjusts maintenance schedules dynamically based on operational conditions. Algorithms optimize energy consumption, charging cycles, and thermal performance. Simulates EV operations under varying conditions to identify efficiency improvements. Centralized data storage enables fleet-wide insights and facilitates stakeholder decision-making.

Fault Prediction and Adaptive Maintenance (FPAM) Process

Real-time data from IoT sensors, including parameters such as battery temperature, SOC, and SOH, is collected and normalized to ensure consistency. Based on the predicted faults, the system dynamically adjusts maintenance processs. This proactive approach minimizes downtime and extends the lifespan of critical components. The FPAM process incorporates a feedback mechanism where the performance of predictive models is continuously evaluated and improved using new data, ensuring sustained accuracy and reliability. The FPAM process significantly reduces maintenance costs, enhances system uptime, and improves the overall efficiency of EV operations.

VIII. Design and Methodology

The following general design formulas might be used in this work based on a typical IoT-enabled digital twin framework for EV energy management. To find the value of energy efficiency of the system,

$$\eta = \frac{E_0}{E_{in}} * 100 \tag{1}$$

Eo- Output energy delivered to the EV

Ei- Input energy consumed by the system

The SOC at any time t is calculated by,

$$\mathrm{SOC(t)=SOC(t-1)}-\frac{\int \mathrm{Iloaddt}}{\mathrm{Crated}} \quad (2)$$

Iload- Load current drawn from the battery.

Crated- Battery rated capacity (Ah).

When the machine learning model is used for fault prediction:

$$\text{Accuracy} = f(x) = \frac{TP+TN}{TP+TN+FP+FN} *100 \quad (3)$$

Where,

TP-True Positives,

TN- True Negatives,

FP- False Positives,

FN- False Negatives.

To Maintenance iinterval Adaptive Maintenance Interval (AMI) can be modelled as

$$AMI = \frac{Using\ Rate}{Rremaining} \quad (4)$$

Where,

Rremaining-Remaining operational life based on fault prediction. Usage Rate-Rate of wear-and-tear from operational conditions. For real-time IoT-enabled systems, the model update interval depends on data processing and transmission delays,

$$tupdate = \frac{tprocess+ttransmission}{Size\ of\ Data\ in\ db} \quad (5)$$

To ensure the IoT-enabled system functions optimally,

$$\text{Latency} = \mathrm{t}_{trans} + \mathrm{t}_{procs} + \mathrm{t}_{resp} \quad (6)$$

By leveraging real-time data from EV systems and historical trends, FPAM ensures proactive detection of faults and optimized intervention, minimizing downtime and maximizing vehicle performance.

IX. Components of the FPAM Model

Fault Prediction

Advanced predictive algorithms analyze historical data, sensor inputs, and operational patterns to predict system failures before they occur. Early identification of potential faults enables timely interventions, reducing the risk of system breakdowns and costly repairs.

Integration with Energy Efficiency

By predicting and addressing issues such as battery degradation or motor inefficiencies, FPAM helps in maintaining optimal energy usage, enhancing overall vehicle energy efficiency.

Techniques to Enhance EV Performance and Sustainability

a. Energy Efficiency Optimization

The optimization technique used in the framework for EV energy management could be based on Metaheuristic Optimization or Model-Based Predictive Control (MPC). A commonly used optimization technique for such applications is Particle Swarm Optimization (PSO) or Genetic Algorithm (GA) due to their adaptability and efficiency in solving nonlinear and multi-objective optimization problems.

b. Battery Health Management

Battery performance is one of the most critical factors in EV sustainability. FPAM models predict battery degradation and propose timely maintenance to ensure batteries are functioning at optimal capacity.

c. Operational Reliability

The predictive capabilities of FPAM reduce the chances of unexpected breakdowns, improving the reliability of EVs. With fewer unplanned maintenance events, EVs spend more time on the road, improving overall operational efficiency and customer satisfaction.

d. Lifecycle Management

The FPAM framework enhances lifecycle management by analyzing data across the entire vehicle lifecycle, from initial manufacturing to end-of-life. This analysis helps in making data-driven decisions regarding maintenance, upgrades, and disposal, further contributing to the overall sustainability of EV operations.

X. Combined Framework for IoT

i. IoT-Enabled Data Acquisition

IoT sensors embedded within EVs continuously collect data on critical components such as battery health, motor performance, and energy consumption. The IoT data forms the backbone of the hybrid digital twin framework, providing real-time feedback on the operational state of the vehicle.

ii. Machine Learning Algorithms

Advanced machine learning techniques process the vast volumes of data generated by IoT sensors, identifying patterns and trends that would be difficult to detect manually. Machine learning models are used to predict faults, estimate remaining useful life for components, and optimize maintenance strategies based on real-time operational data.

XI. Results and Discussions

The results confirmed significant improvements in energy efficiency, fault prediction accuracy, and maintenance optimization compared to traditional systems. The digital twin-enabled optimization engine achieved a 12% improvement in energy consumption, effectively reducing idle power losses through optimized energy flow. The proposed FPAM model showed a prediction accuracy of 90%, significantly outperforming conventional monitoring systems by 25%. The adaptive maintenance schedules reduced downtime by 15% and extended component lifecycles by 8% through proactive fault detection and intervention mechanisms. The output waveform comparing the predicted values and obtained values for the digital twin framework parameter's performance is visually represented to show the alignment and discrepancies between predictions and actual results shown in figure 2.

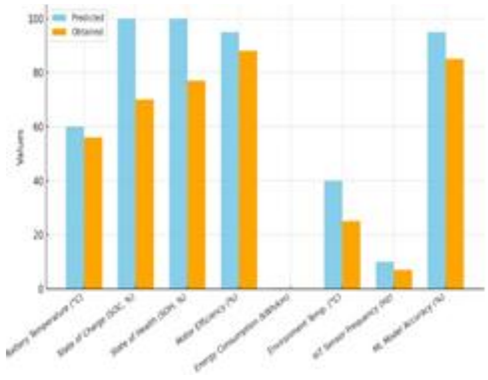

FIG. 2. COMPARISON OF PREDICTED VALUES AND OBTAINED VALUES FOR THE IOT-ENABLED DT FRAMEWORK

This results confirm the efficacy of the proposed framework in enhancing EV performance and operational sustainability which is given in Table I. The integration of real-time data streams with advanced analytics through IoT and machine learning provides actionable insights for improving energy efficiency, reducing operational costs, and ensuring system reliability.

TABLE 1 IOT PERFORMANCE FOR DT FRAMEWORK BASED EV SYSTEM

Parameters	Prediction	Obtained Values
Battery Temperature	20–60°C	56°C
State of Charge (SOC)	20–100%	70%
State of Health (SOH)	70–100%	77%
Motor Performance Efficiency	85–95%	88%
Energy Consumption	0.15–0.25 kWh/km	0.18 kWh/km
Operational Environment Temp.	-10 to 40°C	25°C
IoT Sensor Data Frequency	1–10Hz	7Hz
Machine Learning Model Accuracy	85–95%	85%

XII. CONCLUSION

This work presented a novel hybrid digital twin framework designed to enhance the performance, energy efficiency, and lifecycle management of EV. The proposed FPAM model demonstrated a significant improvement in predictive accuracy (90%) and fault detection capabilities compared to conventional systems. Its validation conducted on a fleet of EVs operating under various conditions showed tangible benefits, including a 12% improvement in energy efficiency and a 25% increase in fault prediction accuracy. Additionally, the adaptive maintenance schedules reduced unplanned downtime by 15% and extended component lifecycles by 8%, ensuring sustainable and reliable vehicle operation. The integration of real-time IoT sensor data with machine learning-based analytics provided actionable insights for predictive maintenance and fault prevention, enhancing the reliability and satisfaction of end users by 20%. Future work will explore scaling this framework to larger fleets and integrating emerging technologies like edge computing and federated learning for further optimization and scalability.

XIII. FUTURE WORK

The future work should focus on enhancing the framework's integration with renewable energy sources, increasing its fault prediction accuracy under extreme conditions, and exploring applications in autonomous vehicle systems.

ACKNOWLEDGMENT

This work is supported by Thiagarajar College of Engineering (TCE) under the Thiagarajar Research Fellowship scheme (File.no:TRF/Jul-2022/08) is gratefully acknowledged.

REFERENCES

[1] Cao, J., et al. (2025). Innovative approaches to green digital twin technologies. Journal of Innovation & Knowledge.

[2] Sharifi, A., et al. (2024). Smart cities and sustainable development goals. Cities.

[3] Wang, W., et al. (2024). From BIM to digital twin in BIPV. Sustainable Energy Technologies and Assessments.

[4] Su, C. W., et al. (2023). Does technology innovation help achieve carbon neutrality? Economic Analysis and Policy.

[5] Yan, Y., & Kunhui, Y. (2024). Cyber-physical architecture for smart city management. Sustainable Energy Technologies and Assessments.

[6] Bibri, S. E., et al. (2024). The synergistic interplay of artificial intelligence and digital twin. Environmental Science and Ecotechnology.

[7] Kulkarni, C., et al. (2024). Hybrid disease prediction leveraging digital twin technologies. BMC Medical Informatics and Decision Making.

[8] Kumar, A., et al. (2024). Enhanced education through IoT and digital twin integration. Systems.

[9] Matei, A., & Cocoşatu, M. (2024). AI-based digital twin urban computing vision. Sustainability.

[10] Piras, G., et al. (2024). Digital twin frameworks for the built environment. Energies.

[11] Fadhel, M. A., et al. (2024). Systematic review of information fusion in smart cities. Information Fusion.

[12] Sung, K., et al. (2024). Digital twin technology: Patent-based networks and modeling. Technological Forecasting and Social Change.

[13] Tao, F., et al. (2024). Digital twin applications in additive manufacturing. The International Journal of Advanced Manufacturing Technology.

[14] Hu, X., & Assaad, R. H. (2024). BIM-enabled digital twin for indoor monitoring. Journal of Building Engineering.

[15] Prakash, J., et al. (2024). Intelligent transport systems for smart cities. Scientific Reports..

A 31 Level Multilevel Inverter using with Reduced Number of Switches for PV Energy Sources for Home and Electric Vehicle Charging System

N. Jegan
Research Scholar,
Thiagarajar College of Engineering,
Madurai
njeee25@gmail.com

Dr. B. Ashok Kumar
Associate Professor,
Thiagarajar College of Engineering,
Madurai
ashokudt@tce.edu

Dr. S. Arockia Edwin Xavier
Professor,
Thiagarajar College of Engineering,
Madurai
saexeee@tce.edu

M. Santharam
Research Scholar,
Thiagarajar College of Engineering,
Madurai
msantharam175@gmail.com

***Abstract*—Multilevel inverters play a crucial role in high-power and high-voltage applications due to their ability to produce smoother sinusoidal waveform with reduced harmonic distortion. However, traditional multilevel inverter topologies face several challenges, including the need for a more number of switches, multiple voltage sources, intricate Pulse Width Modulation (PWM) control strategies, and issues related to voltage balancing. These complexities often result in higher costs, increased control effort, and reduced efficiency.**

In this paper, we propose a novel multilevel inverter topology that effectively combines reverse voltage components and 2n voltage sources to achieve a 31-level output waveform. This innovative approach significantly reduces the number of switches required, simplifying the circuit design while maintaining the ability to operate at higher voltage levels. Furthermore, the proposed topology minimizes the number of carrier signals and gate drive circuits needed, leading to reduced control complexity and enhanced reliability.

This topology is cost effective solution for a variety of applications, including photovoltaic (PV) energy systems, FACTS devices and electric vehicle (EV) charging infrastructure. By addressing the inherent challenges of conventional multilevel inverters, this design demonstrates potential for improving efficiency and economic viability in high-voltage applications.

Keywords*—*Multilevel Inverter, 2^n varying voltage sources, PD MCPWM technique

I. INTRODUCTION

Multilevel power conversion was introduced three decades ago and has become an essential aspect in modern power electronics converters. Multilevel inverters employs more number of switches to produce smaller voltage steps, enabling higher voltage levels. These smaller steps helps in reducing dv/dt stress on the load, electromagnetic compatibility concerns [3]. In some cases, resolving voltage balancing issues will lead to additional multilevel converter for nulifying it [4].

These inverters are widely applied in industrial AC / DC drives, Flexible AC Transmission Systems (FACTS) and Electric vehicle propulsion systems. They are best suited for renewable energy systems such as photovoltaic (PV) installations, where power quality and efficiency are critical [5].A new approach [6] minimizes the use of DC sources by adding a transformer into the design. Hence the inclusion of a transformer increases the inverter's overall size and cost. Some multilevel inverter outputs are generated by using multi-winding transformers [7, 8]. In spite of their functionality, the design factors in manufacturing of multi-winding transformers are expensive and challenging, especially for high power and high voltage applications.

Another way of approach is to minimizing either the number of switches or the number of DC sources use for the inverter design [9]. However, some existing designs do not efficiently utilize voltage sources. For instance, the topology [10] generates only 5 output levels using four DC sources, whereas conventional designs can achieve up to 9 levels with the same number of DC sources.

Certain topologies use asymmetrical configurations with different voltage sources [11].By varying the switch ratings limit their application to high voltage products [12]. Another approach is by reducing the number of DC voltage sources by incorporating transformers [13], but this may increases the cost, space and volume due to additional transformer windings in their design. In some designs, such as in [14] which requires more number of switches than alternative topologies for the same number of output levels. There may be challenges like capacitor voltage balancing issues [15] or it may require multiple modulation signals for single carrier modulation methods [16].Recent advancements is on optimizing multilevel inverters (MLI) to reduce the number of switches and simplify control strategies in a simpler way. The most commonly used multilevel inverters includes the cascade H bridge (CHB) converter, neutral point clamped (NPC) inverter and flying capacitor (FC) inverter [20].

The fundamental 13 level multilevel inverter topology is designed and the topology is developed for 31 level can be used for renewable energy source applications. This may reduces the overall components count, cost and size of the system [21-22,26-27]. A three phase Multi Level Inverter is design with several isolated voltage sources including a H-Bridge inverter. The design has reduced switching components for current conduction paths showing improved output quality [23]. A 12 switch and 31 Level multilevel inverter is proposed with less number of switches for electric vehicle applications. In most electric vehicles (EV), conventional inverters are utilized so the lifetime of electric vehicle induction motors is reduced due to the high Total Harmonic Distortion (THD) level and high voltage stress [24]. For the generation of 7 level, 15 level, and 31 level output voltages, the proposed MLI employs two, three, and four designed modules, each comprising switches, diodes, and a DC source, respectively [25]. A new single phase asymmetrical multilevel inverter that can generate 33 levels at the output with less components is proposed. The multiple input sources of the inverter is suitable for renewable energy generating systems which have different of DC sources. The stress distribution among the switches is designed in such a way that it reduces the use of high rated devices with which overall cost of the inverter gets reduced [28].

II. NEW MULTILEVEL INVERTER

A. General description

Multilevel inverters are in general uses high frequency switches to be operated in both positive and negative polarities. A new topology has been developed to have reduced component usage compared to other multilevel inverter designs. This topology requires fewer number of switches which are operating at high switching frequencies, making the control strategy simpler and more reliable. It employs the general Phase Disposition with Multi Carrier Pulse Width Modulation (MCPWM) control method.

This paper introduces a 31 level multilevel inverter that significantly reduces the number of voltage sources and switches needed for higher voltage levels. The proposed design provides enhanced reliability and most cost effective, making it a practical feasible solution for high voltage applications particularly for Electric drives. There is no need to utilize all the switches for generating bipolar levels [1].This topology is a combination of 2^n voltage sources, level generation unit and polarity generation unit.

The adjacent switches are supplied with DC voltage sources in the ratio of 2^n where n is the level generation unit. The level generation unit produces the required voltage levels in the unipolar mode. The unipolar mode unit requires higher frequency switches for its operation. The Polarity generation unit is necessary for generating the required output voltage polarity that is positive and negative. This unit makes use of low frequency switches which operates at reference frequency.

Only positive voltage levels are generated by level generation unit and then it is fed to a full bridge polarity generation unit where the required output polarity Positive or negative are produced. Thus this setup decreases the switches needed to produce output voltage levels in positive and negative polarities of the output ac voltage.

This new topology for producing 31 levels is shown in Figure. 1. This topology requires 4 high frequency main switches, 4 low frequency switches, 4 diodes and 4 isolated DC sources for single phase system for generating 31Level Multilevel inverter output. This Multilevel inverter's level generation unit produces the required output levels without polarity and the polarity generation unit produces the required polarity of the output voltage.

The purpose of the diodes is to prevent the short circuit of the DC sources. The DC sources are maintained in adjacent voltage levels as 1: 2: 4: 8 (Asymmetrical).

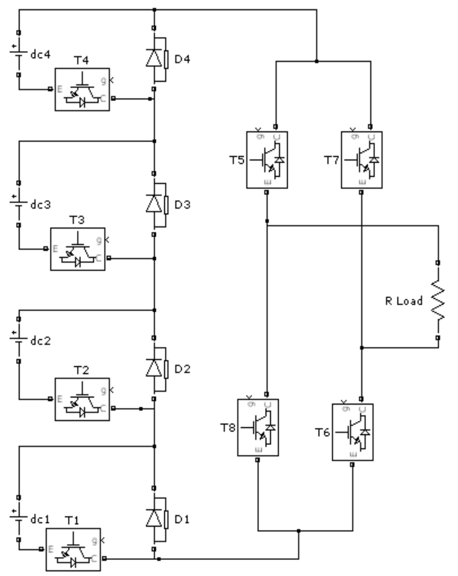

FIG. 1 CIRCUIT DIAGRAM OF THE PROPOSED MULTI LEVEL INVERTER

According to [2] & [17] topology 12 switches are necessary for generating 7 level with 6 switches conduct the inverter in each instance whereas the proposed topology requires only 8 switches for 31 level output. Thus the number of switches in the proposed topology is lower than that of the cascade inverter and thus it has better efficiency [18] & [19]. The main advantage of this topology is that it requires only one half of the carriers for MCPWM controllers. MCPWM carriers for 31 voltage level in conventional inverters requires 30 carriers and for this new topology it needs only 15 carrier as shown in Figure. 4.Thus the Multilevel inverter with much reduced number of carriers is much needed for inverter control. Here all the switches are not fast switches, the level generation unit only has fast switches and the polarity generation unit make use of slow switches.

B. Switching Sequence

The switching sequences of this inverter are easier, since it does not require to produce negative pulses in MCPWM for negative cycle control. The switching sequence for each level is presented in the Table I.

TABLE I: SWITCHING SEQUENCES

Level	T1	T2	T3	T4	Voltage(Vdc)
0	0	0	0	0	0
1	0	0	0	1	+1
2	0	0	1	0	+2
3	0	0	1	1	+3
4	0	1	0	0	+4
5	0	1	0	1	+5
6	0	1	1	0	+6
7	0	1	1	1	+7

8	1	0	0	0	+8
9	1	0	0	1	+9
10	1	0	1	0	+10
11	1	0	1	1	+11
12	1	1	0	0	+12
13	1	1	0	1	+13
14	1	1	1	0	+14
15	1	1	1	1	+15

According to the table I the required output voltage level is achieved by connecting the corresponding adjacent isolated voltage sources with the switches. The switching modes are chosen in such a way as to prevent unneccesary voltage levels during switching periods. It aids in reducing the switching power dissipation.

In accordance to the output voltage level 0 to 15 the sequence of switches are as shown in table I. In order to have improved efficiency of the inverter during switching states, the transition between modes in each state requires minimum commutation of switches.

The number of switches in the proposed topology that conducts the circuit current is lower than that of cascade inverter and hence it has a much better efficiency.

H- Bridge polarity unit at the output stage performs in forward and reverse modes. In the forward mode switches 5 & 6 are switched on and switches 7 & 8 are off for positive output polarity. The switches 7 & 8 are switched on and switches 5 & 6 are off for generating negative output polarity. Thus the polarity generating unit decides the output polarity.

The major advantage of the topology is that it requires minimum number of high frequency switches. The high frequency switches are expensive compared to low frequency switches. Increse in the number of high frequency switches leads to less reliability of the inverter. This topology is used in Electric vehicle charging system, PV array battery system, UPS, Backup Inverter, FACTS and HVDC.The cost & space availability and complexity in the control strategy are greatly reduced for higher voltage levels.

Switching losses, dv/dt stress on the load and Total harmonic distortion (THD) are reduced further when comparing with the cascade inverter for higher voltage levels.

III. Simulation Results

This section presents the proposed topology simulation results for the Single Phase 31 level Multi level inverter. Figure 1. shows the simulation circuit of the proposed multilevel inverter topology This topology is used to generate 31 voltage levels for a resistive load. The input voltage applied to the isolated DC sources are 22 V, 44 V, 88 V and 176 V for the switches T4, T3, T2 and T4 respectively. The output peak voltage is 330V (VPP). The PD MCPWM is used as the control strategy for driving the gates of the IGBT's of high frequency switches that is the Level generation unit whereas the low frequency switches are used for Polarity generation unit.

Figure 2. shows the output voltage and output current of the proposed Multilevel invereter with 31 voltage levels. The PDMCPWM carriers signals for the proposed topology is shown in figure. 3. From Figure .3. it is noted that only 15 carrier signals are generated for generating 31 Level voltage levels. Figure . 4. shows the FFT analysis of the Proposed 31 level Multilevel Inverter and it shows that the THD of the Proposed 31 level Multilevel Inverter is only 1.76% without LC filter.

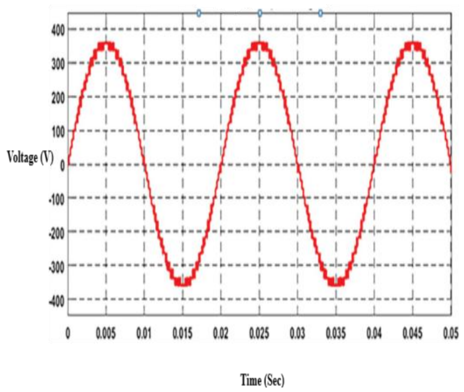

Fig. 2. 31 level Output voltage waveforms of the proposed Multi Level Inverter.

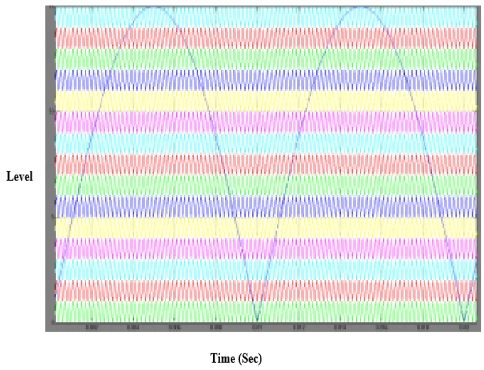

Fig 3. MCPWM carriers for Proposed topology

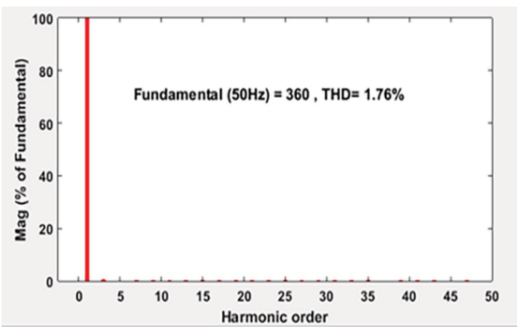

Fig 4. FFT analysis of 31 level MLI

IV. Conclusion

In this paper a 31 level Multilevel inverter topolgy has been proposed which is much better to that of cascade inverter in terms of power switches & isolated DC sources, control requirements, cost and reliability. Better selection for use in Electric Vehicle, FACTS, PV energy systems etc; By separating the switching operations of the switches into high and low frequency parts, reduces the size and cost of the inverter. The PWM signals for this 31 level multilevel inverter topology has much reduced number of carrier signals which leads to the reduction of complexities in the control strategy. Thus a new 31 level multilevel inverter topology with reduced number of switches, isolated DC source has been simulated effectively.The Total harmonic distortion (THD) is very less and hence it is economical for use in Renewable source system and Electric vehicle charging system, since it has not uses LC filter for filtering purposes.

REFERENCES

[1] Ehsam Najafi,Member, IEEE and Abdul Halim Mohamed Yatim, Senior Member “Design and Implementation of a New Multilevel Inverter Topology” , IEEE Transations on Industrial Electronics, Volume 59,No.11, November 2012

[2] Young-Min park, Han seong Ryu, Hyun-won Lee, Myung-Gil jung and Se-Hyun Lee “Design of a cascaded H Bridge Multilevel Inverter based on Power Electronics Building blocks and control for High Performance” ,JPE , Volume 10,No.3,May 2010.

[3] K.Jang-Hwan,S.K.Sul and P.N.Enjeti,” A Carrier based PWM method with optimal switching sequence for a multilevel four-leg voltage source inverter”,IEEETrans.Ind.Appl;Vol.44.no.4,pp.1239-1248,Jul/Aug.2008.

[4] L.M.Tolbertt,F.Z.Peng and T.G.Habetler,”Multilevel converters for large electric drives,”IEEE Trans.Ind.Appl;vol.35,no.1,pp.36-44,Jan/Feb 1999.

[5] K.Y.Lan,M.F.M.Yousof,S.N.M.Arshad,M.Anwari and A.H.M.Yatim,” Performance analysis of hybrid photovoltaic/diesel energy system under Malaysian conditions”,J.Energy,vol.35,no.8,pp.3245-3255,Aug.2010.

[6] G.M.Martins,J,A.Pomilio,S.Buso and G.Spiazzi,”Three-phase low- frequency commutation inverter for renewable energy systems”,IEEETrans.Ind.Electron.vol.53,no.5,pp.1522-1528,Oct.2006.

[7] R.Teodorescu ,F.Blaabjerg,J.K.Pedersen, E.Cengelci and p.n.Enjeti,” Multilevelinverter by cascading industrial VSI”,IEEE Trans.Ind.Electron;vol.49,no.4, pp.832- 838,Aug.2002.

[8] D.A.B.Zambra,C.rech and J.R.Pinheiro,” A Comparative analysis between the symmetric and hybrid asymmetric nine-level series connected H-bridge cells inverter”,in Proc.Eur.Conf.Power Electron;vol.22,no.1,pp. 149-159, Jan.2007.

[9] E.Baberi,” Optimal topolgies for cascaded sub-multilevel converters”, J.Power Electron.vol.10, no.3, pp. 251-261, May 2010.

[10] G.Mondal, K.Gopakumar, P.N.Tekwani and E.Levi,”A reduced switch count five level inverter with common-mode voltage elimination for an open-end winding induction motor drive”, IEEE Trans.ind.Electron; vol.54, no.4, pp. 2344-2351, Aug.2007.

[11] E.Beser,B. Arifoglu,S. Camur and E.K.Beser,” Design and application of a single phase multilevel inverter suitable for using as a voltage harmonic source”,J.Power Electron;vol.10,no.2,pp. 138-145,Mar.2010.

[12] N.A.Rahim,K. Chaniago and J.Selvaraj,”Single phase seven level grid-connected inverterfor photovoltaic system”, IEEE Trans. Ind. Electron; vol.58, no.6, pp.2435-2443, Jun.2011

[13] S. G. Song, F. S. Kang, and S.-J. Park “Cascaded multilevel inverter employing three- phase transformers and single dc input,” IEEE Trans.Ind.Electron., vol. 56, no. 6, pp. 2005–2014, Jun. 2009.

[14] P. Barbosa, P. Steimer, J. Steinke, L. Meysenc, M. Winkelnkemper, and N.Celanovic,“Active neutral-point-clamped multilevel converters,” in Proc. IEEE 36th Power Electron Spec. Conf., 2005, pp. 2296–2301.

[15] R. Stala, “Application of balancing circuit for dc-link voltages balance in a single-phase diode-clamped inverter with two three-level legs,” IEEE Trans. Ind. Electron., vol. 58, no. 9, pp. 4185–4195, Sep. 2011.

[16] C. Govindaraju and K. Baskaran, “Analysis and implementation of multiphase multilevel hybrid single carrier sinusoidal modulation,” J.Power Electron., vol. 10,no. 4, pp. 365–373, Jul. 2010.

[17] M. Malinowski, K. Gopakumar, J. Rodriguez, and M. A. Perez, “A survey on cascaded multilevel inverters,” IEEE Trans. Ind. Electron., vol. 57,no. 7, pp. 2197–2206, Jul. 2010.

[18] G.J. Su, “Multilevel dc-link inverter,” IEEE Trans. Ind. Appl., vol. 41, no. 3, pp. 848– 854,May/June 2005.

[19] C. Cecati, F. Ciancetta, and P. Siano, “A multilevel inverter for photovoltaic systems, with fuzzy logic control,” IEEE Trans. Ind. Electron., vol. 57, no. 12, pp. 4115–4125 Dec. 2010.

[20] Muhamed H.Rashid “Power Electronics” Pearson Education Inc; Third Edition Page No :406-430.

[21] D. Prasad, C. Dhanamjayulu, S. Padmanaban, J. B. Holm-Nielsen, F. Blaabjerg and S. R. Khasim, "Design and Implementation of 31-Level Asymmetrical Inverter With Reduced Components," in IEEE Access, vol. 9, pp. 22788-22803, 2021, doi: 10.1109/ACCESS. 2021.3055368.

[22] C. Dhanamjayulu et al., "Real-Time Implementation of a 31-Level Asymmetrical Cascaded Multilevel Inverter for Dynamic Loads," in IEEE Access, vol. 7, pp. 51254-51266, 2019, doi: 10.1109/ACCESS.2019.2909831.

[23] Sivamani, S., Mangaiyarkarasi, S.P., Gandhi Raj, R. et al. A quad DC source switched three-phase multilevel DC-link inverter topology. Sci Rep 14, 2065 (2024), doi.org/10.1038/s41598-024-52605-3

[24] Saravanan, K., Sivasubramanian, M., Gopinath, N.P. et al. A 31 L multilevel inverter topology with less switching devices for hybrid electric vehicle applications. Sci Rep 14, 27459 (2024). doi.org/10.1038/s41598-024-78529-6.

[25] A. V. Sant and K. Patoliya, "A New 7, 15 and 31-level Modular Reduced Switch Multilevel Inverter with Gating Signal Generation Using Digital Output Pins," in CPSS Transactions on Power Electronics and Applications, vol. 9, no. 4, pp. 373-383, December 2024, doi: 10.24295/CPSSTPEA.2024.00018.

[26] C. Dhanamjayulu et al., "Real-Time Implementation of a 31-Level Asymmetrical Cascaded Multilevel Inverter for Dynamic Loads," in IEEE Access, vol. 7, pp. 51254-51266, 2019, doi: 10.1109/ACCESS.2019.2909831.

[27] S. K. Gupta, K. Rathore and P. Bansal, "Design and Analysis of a New 31-Level Asymmetrical Multilevel Inverter Topology with Different PWM Techniques," 2018 3rd International Innovative Applications of Computational Intelligence on Power, Energy and Controls with their Impact on Humanity (CIPECH), Ghaziabad, India, 2018, pp. 1-7, doi: 10.1109/CIPECH.2018.8724251.

[28] S. R. Khasim and C. Dhanamjayulu, "Design and Implementation of Asymmetrical Multilevel Inverter With Reduced Components and Low Voltage Stress," in IEEE Access, vol. 10, pp. 3495-3511, 2022, doi: 10.1109/ACCESS.2022.3140354

Comparative Analysis of Filtration and Droop Control for Hybrid Energy Storage System using Sliding Mode Control

RM. Meenakshi
Dept. of EEE,
Thiagarajar College of Engineering,
Madurai, India
meena.eee@gmail.com

K. Selvi
Dept. of EEE,
Thiagarajar College of Engineering,
Madurai, India
kseee@tce.edu

***Abstract*—Hybrid Energy Storage Systems (HESS), consist- ing of batteries and supercapacitors, are widely employed in DC microgrids to enhance power quality and dynamic perfor- mance. This paper presents a comparative analysis of filter- based and droop-based control strategies for power sharing in HESS, incorporating Sliding Mode Control (SMC) to improve robustness against system uncertainties and disturbances. The filter-based method leverages a high-pass filter to allocate high- frequency transients to the supercapacitor and low-frequency components to the battery, whereas the droop-based method ensures decentralized power sharing based on the voltage-current characteristics of the storage elements. The effectiveness of both strategies is evaluated through detailed simulations, considering transient response, steady-state performance, and robustness under varying load conditions. Results demonstrate that while the filter-based approach provides smoother transient performance, the droop-based method offers better scalability and flexibility. The incorporation of SMC enhances both control strategies, ensuring fast response and chattering mitigation. This study provides insights into selecting appropriate HESS control strate- gies for microgrid applications based on specific performance requirements.**

***Index Terms*—Hybrid Energy Storage System, Sliding Mode Control, Droop Control, Filtration Control, Nonlinear Approach**

I. Introduction

Hybrid Energy Storage Systems (HESS) have emerged as a critical component in modern DC microgrids and renew- able energy systems, addressing the limitations of individual storage technologies by combining complementary sources such as batteries and supercapacitors [1]. Effective power management between these sources is essential to ensure system stability, improve dynamic response, and extend the operational lifespan of the storage devices [2].Among various control strategies, Sliding Mode Control (SMC) has gained significant attention for its robustness, fast transient response, and insensitivity to parameter variations, making it suitable for managing power flow in HESS.

Two major approaches for HESS power coordina- tion—droop control and filtration-based techniques—offer dis- tinct advantages and trade-offs when integrated with SMC. Droop control is a decentralized method that ensures power sharing by mimicking the voltage-current characteristics of conventional power systems [3], [4]. It is simple to implement and scalable but may suffer from slower dynamic response and power sharing inaccuracies under rapidly changing load or generation conditions. On the other hand, filtration-based control techniques use signal decomposition methods, such as low-pass and high-pass filtering [5], [6], to separate the power demands into low- and high-frequency components, which are then distributed to the battery and supercapacitor, respectively. This technique improves dynamic performance but typically requires more precise tuning and control complexity.

This paper presents a comparative study of filtration and droop-based power management techniques for HESS under the framework of SMC [7], [8]. The investigation focuses on dynamic response, power sharing accuracy, and voltage reg- ulation under various operating conditions. The contributions in the paper is listed as follows:

- A combined PI and SMC approach namely C-PISMC is formulated to control the converters of HESS. The reference operating point for the designed controller is obtained from droop and filtration methods
- A comparative analysis is made for the filtration and droop control methods with C-PISMC controller, is con- ducted focusing on the aspects of voltage regulation, steady state attainment and SoC restoration for SC
- The effectiveness of the control approaches is validated in the presence of an intermittent PV source and highly varying demands through simulations in the software- in-the-loop(SIL) approach using a OP4512 real time simulator.

II. System Description

A Hybrid Energy Storage System (HESS) with Battery and SC in a Photovoltaic(PV) based Microgrid system is presented in Figure 1. During uncertain disturbance in the power balance at the DC link, the battery addresses the steady state response with an average power supply while the supercapacitor instantaneously addresses the transients. The PV source is considered to operate at maximum power point under any irradiance condition. The scope of the work is limited to the analysis of control applied to the HESS.

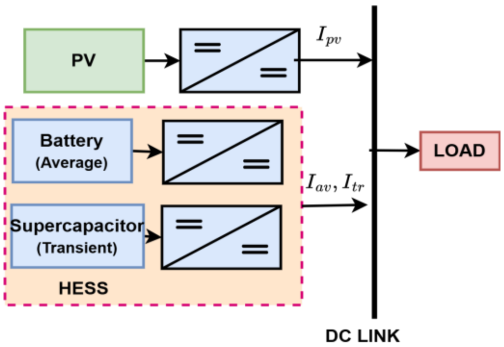

FIG. 1. A PV-HESS BASED MICROGRID

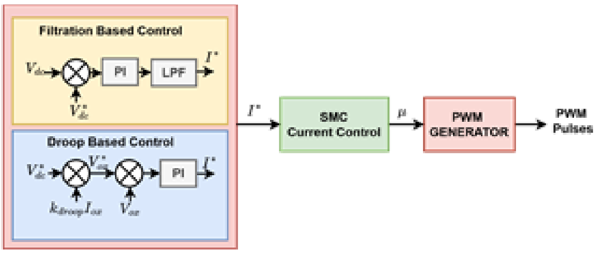

FIG. 2. CONTROL IMPLEMENTATION

The mathematical representation of HESS with the storage output currents as state variables is written as,

$$L_{av} \dot{I}_{av} = V_{av} - R_{av} I_{av} - \mu_{av} V_{dc} \quad (1)$$

$$L_{tr} \dot{I}_{tr} = V_{tr} - R_{tr} I_{tr} - \mu_{tr} V_{dc} \quad (2)$$

Here I_{av} and I_{tr} represent the average and transient current

A. Outer Loop:

In the outer voltage, loop the dc link voltage V_{dc} is tightly regulated, and the current references are generated for inner current loop according to the deviations. Considering battery and SC in HESS, filtration and droop methods separate the current demand as average and transient. The effectiveness of their implementation is compared.

1) *Filtration-based Control:* As shown in 2, a low pass filter is used to filter the deviation in voltage based on dc link voltage bus signalling method. The overall current demand is divided into steady state and transient components based on a defined time constant. The filter method requires the DC-link output voltage, the power generated, and the overall demand to set the references through an energy management algorithm.

2) *Droop-based Control:* A virtual impedance based droop control is chosen for comparison with the filtration control, where a virtual resistance and a virtual capacitance is defined to separate the demand components, for battery and SC re- spectively. In this approach, the local measurements of output voltage and current of the converters are measured to identify and alleviate the disturbances.

B. *Inner Loop:*

The inner loop tracks the reference currents set by the outer loop, based on a sliding mode control approach. The design of the sliding mode controller is given as:

The sliding surface S is chosen as the error of the storage elements output current,

$$S = I^* - I_x \quad (3)$$

The reaching law for sliding surface is defined as

$$\dot{S} = -\rho \; sgn(S) \quad (4)$$

From equation (1) or (2), the control output of the SMC controller could be derived as

$$\mu_x = \rho \; sgn(S) - \frac{L_x V_x}{V_{ox}} I_x - I^* \frac{R_x}{L_x L_x} \quad (5)$$

supplied by the battery and sc. μ_{av} and μ_{tr} are the duty cycle for the battery and sc converters. V_{dc} represents the dc link voltage. V_{oav} and V_{otr} are the output voltages of the corresponding HESS converters.

III. CONTROL STRATEGIES

THe control approach for proper power sharing in HESS and voltage regulation at the DC link is mostly implemented through cascaded control approach. In this work, the outer voltage loop is implemented with filtration and droop control, for a comparative analysis. This voltage loop provides current reference to the inner loop, segregated through droop or filtration approach as average (I_{av}) and transient (I_{tr}) com- pontents. The inner current loop is embedded with a sliding mode control approach, to reject the disturbances and provide appropriate control inputs to the power converters. Figure 2 represents the overall control approach for a bidirectional converter in HESS.

where $x = av$ for the battery components balancing the average component of disturbances while $x = tr$ for the SC component balancing the transient part of disturbances.

IV. RESULTS AND DISCUSSION

The Microgrid setup shown in Figure 1 is simu- lated in a real-time OPAL RT simulator, namely OP4512, through a Software-in-the-loop approach with the MAT- LAB/SIMULINK platform, to validate the effectiveness of the controller in a hardware implementation setup. The OP4512 setup is shown in the figure 3 . The solar irradiance step increment or decrement scenarios validated the controller performance. The controller aims to regulate the DC link voltage to 48 V and ensure proper power sharing amongst the battery and SC in HESS. The demand is increased in steps to analyze the effectiveness of the filtration or droop controller at the instant of disturbances.

FIG. 3. OPAL RT SIMULATOR SETUP

A. Case 1: Step Increase in Solar Irradiance

The Figures 4 and 5 depicts the DC link voltage response, the power sharing variation amongst the sources and the SoC variation of battery and SC, with the scenario of step increase in irradiance. It could be inferred that the filtration method provides stable dc link voltage output, while the droop control exhibits more sensitivity during disturbances.

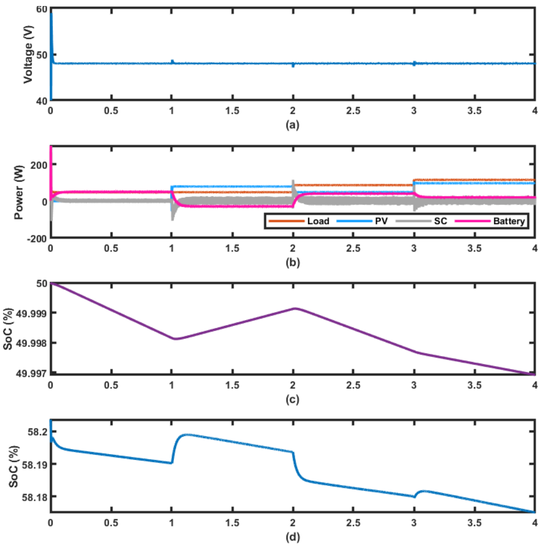

FIG. 4. FILTRATION METHOD RESPONSE: (A) DC LINK VOLTAGE (B) POWER (C) BATTERY SOC (D) SUPERCAPACITOR SOC

B. Case 2: Step Decrease in Solar Irradiance

During the decrease in irradiance, when the demand is high as seen at the instant t = 3 - 4 s, the battery requires to supply the additional demand, where the filtration method as in Figure 6 shows more stable response, while the droop method (Figure 7) oscillates to settle to a final value showing poor response compared to filtration method.

The understanding of the implementation of filtration-based and droop-based control on segregating the power components for battery and SC in a microgrid is presented in Table 1.

V. CONCLUSION

This study presented a comparative analysis of filter-based and droop-based control strategies for Hybrid Energy Storage

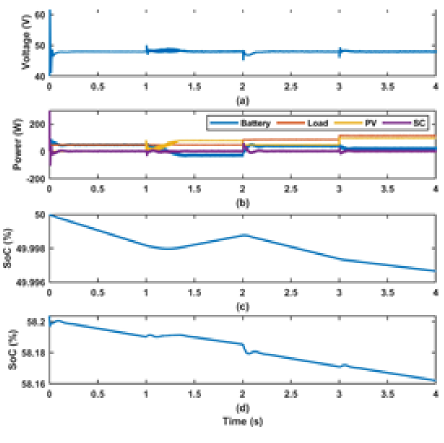

FIG. 5. DROOP METHOD RESPONSE: (A) DC LINK VOLTAGE (B) POWER (C) BATTERY SOC (D) SUPERCAPACITOR SOC

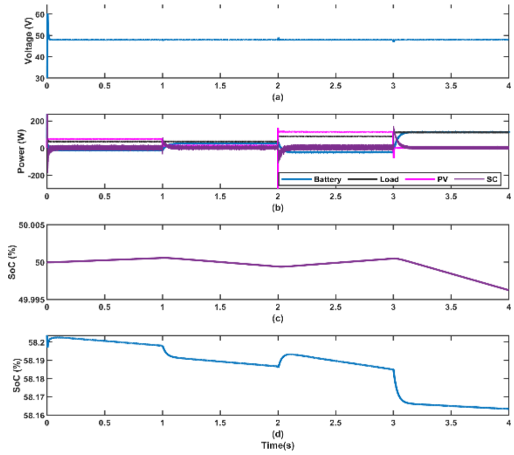

FIG. 6. FILTRATION METHOD RESPONSE: (A) DC LINK VOLTAGE (B) POWER (C) BATTERY SOC (D) SUPERCAPACITOR SOC

Systems (HESS) using Sliding Mode Control (SMC). The filter-based method effectively segregates high-frequency and low-frequency power components, enabling efficient transient response and reduced stress on the battery. On the other hand, the droop-based approach ensures decentralized power sharing, enhancing system scalability and flexibility. Simula- tion results demonstrated that while the filter-based method provides smoother transient performance, the droop-based strategy offers improved adaptability to varying load condi- tions. The incorporation of SMC in both methods enhances robustness, ensuring fast dynamic response and mitigating chattering effects. Overall, the selection of an appropriate con- trol strategy depends on the specific application requirements, with filter-based control being more suitable for systems prioritizing transient performance, while droop-based control is advantageous for decentralized operation. Future work could explore adaptive hybrid control approaches that leverage the strengths of both methods for optimal HESS management in microgrid applications.

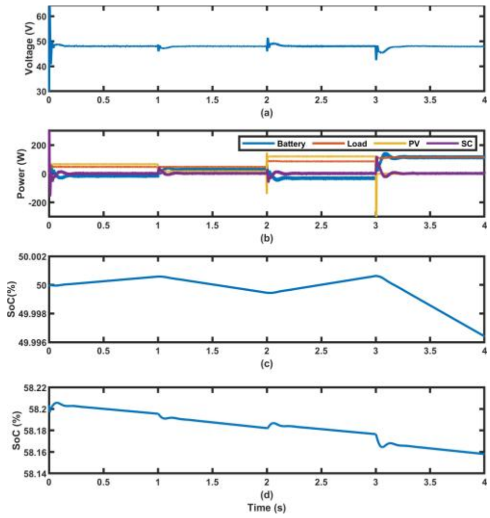

FIG. 7. DROOP METHOD RESPONSE: (A) DC LINK VOLTAGE (B) POWER (C) BATTERY SOC (D) SUPERCAPACITOR SOC

TABLE I: COMPARISON OF FILTRATION AND DROOP CONTROL FOR HESS

Metric	Filtration Control	Droop Control
Measurements	Communication based	Local Measurements
Objective	Filtering of high frequency components	Adjusts the power sharing amongst the sources
Power sharing accuracy	Requires additional control approach to provide power references to sources	Proportional power sharing based on droop coefficients
Implementation Complexity	Filter design should be precise	Droop settings should be precise
Scalability	Complex for large systems. It would require additional control levels	Easy integration for multi source systems
Shortcoming	Single point of failure when communication	Sensitive to parameter disturbances

ACKNOWLEDGMENT

The author(s) gratefully acknowledge the financial support provided by the Department of Science and Technology (DST), Government of India, under the Women Scientists Scheme-A (WOS-A) File No: DST\WOS-A\ET-23\2021, which made this research possible.

REFERENCES

[1] Jing, W Lai, CH Wong, SHW & Wong, MLD 2017, 'Battery- supercapacitor hybrid energy storage system in standalone DC micro- grids: Areview', IET Renewable Power Generation, vol. 11, no. 4, pp. 461–469.

[2] Bharatee, A Ray, PK Subudhi, B & Ghosh, A 2022, 'Power Manage- ment Strategies in a Hybrid Energy Storage System Integrated AC/DC Microgrid: A Review', Energies, vol. 15, no. 19.

[3] Wang, Z Wang, PP Jiang, W & Wang, PP 2021, 'A Decentralized Automatic Load Power Allocation Strategy for Hybrid Energy Storage System', IEEE Transactions on Energy Conversion, vol. 36, no. 3, pp. 2227–2238.

[4] Xu, Q Hu, X Wang, P Xiao, J Tu, P Wen, C & Lee, MY 2017, 'A Decentralized Dynamic Power Sharing Strategy for Hybrid Energy Storage System in Autonomous DC Microgrid', IEEE Transactions on Industrial Electronics, vol. 64, no. 7, pp. 5930–5941.

[5] Arunkumar, CR & Manthati, UB 2023, 'A Hybrid Controller As- sisted Voltage Regulation and Power Splitting Strategy for Bat- tery/Supercapacitor System in Isolated DC Microgrid', IEEE Transac- tions on Energy Conversion, vol. 38, no. 3, pp. 1544–1553.

[6] Ramos, GA & Costa-Castello´, R 2022, 'Energy Management Strategies for Hybrid Energy Storage Systems Based on Filter Control: Analysis and Comparison', Electronics (Switzerland), vol. 11, no. 10, pp. 1–26.

[7] Singh, P & Lather, JS 2020, 'Dynamic current sharing, voltage and SOC regulation for HESS based DC microgrid using CPISMC technique', Journal of Energy Storage, vol. 30, no. April, pp. 101509.

[8] Meenakshi, R.M. and Selvi, K., 2024. Iteratively Sustained Sliding Mode Control based energy management in a DC Microgrid. Mathematics and Computers in Simulation, 220, pp.673-695.

Machine Learning-Based Intrusion Detection for Smart Grid Advanced Metering Infrastructure

J. Jeyasoundari
Department of Information Technology,
Thiagarajar College of Engineering,
Madurai, Tamil Nadu, India.
jeyasoundari10@gmail.com

S. Sridevi
Department of Information Technology,
Thiagarajar College of Engineering,
Madurai, Tamil Nadu, India.
sridevi@tce.edu

S. Charles Raja
Department of EEE,
Thiagarajar College of Engineering,
Madurai, Tamil Nadu, India.
charlesrajas@tce.edu

***Abstract*—The rapid integration of Advanced Metering Infrastructure (AMI) into smart grid systems has transformed energy distribution and management, enabling real-time monitoring, automation, and improved operational efficiency. However, this evolution has also expanded the threat landscape, making AMI systems increasingly vulnerable to cyberattacks such as Denial of Service (DoS), Man-in-the-Middle (MITM), and data manipulation. To counter these threats, the development of Intrusion Detection Systems (IDS) using machine learning (ML) techniques has become crucial. While traditional datasets like NSL-KDD and KDD-CUP99 have been extensively used in IDS research, which do not adequately reflect the complexity and diversity of modern IoT-based smart grid environments. The ToN-IoT dataset, which captures data from various IoT services, operating systems, and network traffic, offers a more comprehensive and realistic representation of current attack scenarios. In this study, multiple ML algorithms are implemented for both binary and multiclass classification tasks to detect intrusions within AMI systems. Feature selection using Pearson's correlation enhances model efficiency, and Synthetic Minority Over-sampling Technique (SMOTE) is employed to address class imbalance. Experimental results show that the Random Forest algorithm achieves superior performance, with 99.87% accuracy in binary classification and 98.78% in multiclass classification, demonstrating its effectiveness in safeguarding AMI systems from evolving cyber threats.**

Keywords—Intrusion Detection System (IDS), Internet of Things (IoT), ToN-IoT dataset, Machine Learning (ML), Advanced Metering Infrastructure (AMI)

I. INTRODUCTION

The integration of digital technologies into the energy sector has enabled smart grids, which rely on two-way communication to enhance efficiency and sustainability. At the core of this evolution is Advanced Metering Infrastructure (AMI), enabling real-time monitoring and intelligent control. However, these advancements increase cybersecurity risks, including unauthorized access, data breaches, and complex network attacks. OTA firmware updates and large volumes of operational data, such as energy usage and voltage levels, further expose AMI systems to threats. These factors necessitate advanced anomaly detection methods to secure modern grids [1, 2].

Traditional security mechanisms are inadequate against evolving threats, prompting the adoption of ML-based Intrusion Detection Systems (IDS) for AMI environments [3]. ML models can analyze large-scale network data to detect abnormal behavior, though challenges like resource constraints, system complexity, and wireless vulnerabilities emain [4]. Techniques like Random Forest (RF), Decision Trees (DT), and SVM have shown promise in detecting AMI threats. This study introduces an ML-based IDS using the ToN-IoT dataset, aiming to:

- Evaluate ML models for distinguishing normal and malicious traffic.
- Apply Pearson's Correlation for feature selection and SMOTE for class balancing.
- Improve IDS performance through comparative analysis of classifiers.

The paper is organized as follows: Section II reviews related work; Section III introduces the ToN-IoT dataset; Section IV details ML methods; Section V discusses methodology used; Section VI presents results; and Section VII concludes the study.

II. RELATED WORK

ML-based IDS have significantly improved threat detection by reducing false positives and increasing efficiency. Studies using datasets like NSL-KDD, UNSW-NB15, KDD-CUP99, ToN-IoT, and CICIDS2017 reveal varied ML approaches and effectiveness. Kumar & Singh [5] found Decision Trees effective on NSL-KDD, with 95.8% accuracy and low false positives. Patil & Patil [6] highlighted Random Forest's strength on UNSW-NB15 with 96.7% accuracy, while Sharma & Joshi [7] showed that ensemble methods with feature selection improve performance on KDD-CUP99.

Moustafa & Slay [8] proposed a statistical anomaly approach, effective for zero-day attacks without large datasets. Ali et al. [9] reinforced the reliability of tree-based models on NSL-KDD. Kim et al. [10] demonstrated Random Forest's effectiveness in cloud attack detection using CICIDS2017. Brown et al. [11] emphasized hybrid models and proper dataset choice, and Vinayakumar et al. [12] provided a taxonomy of ML techniques across IoT and enterprise settings.

Wu & Song [13] applied a hybrid ML model to the ToN-IoT dataset, achieving 97.5% accuracy with low resource usage, making it suitable for smart grids. The ToN-IoT dataset [14] stands out for its realistic IoT telemetry, network flows, and threat simulations, making it ideal for AMI IDS development. It captures real-world IoT threats like Denial-of-Service (DoS), Man-in-the-Middle (MITM), spoofing, and data tampering, making it highly relevant for smart grid security.

III. TON-IOT DATASET

The ToN-IoT dataset, created by UNSW Canberra IoT Labs and the Cyber Range, is a robust Industrial IoT (IIoT) dataset comprising telemetry data, system logs, and network traffic. Its network subset, stored in CSV format, includes 44 features and 211,043 instances, representing both normal and attack traffic for cyberattack analysis. The dataset covers nine attack categories: Scanning, XSS, DoS, DDoS, Backdoor, Injection Attack, Password Cracking, MITM, and Ransomware. It is well-suited for training ML models for intrusion detection, supporting the development of effective cybersecurity solutions for IIoT environments. The distribution of attack and normal instances in the train-test split is illustrated in Fig.1.

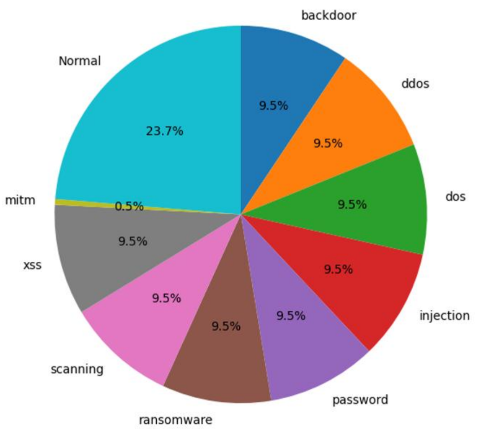

FIG. 1. DISTRIBUTION OF NORMAL AND ATTACK TYPES

IV. SUPERVISED ML METHODS

Several supervised machine learning (ML) techniques were applied to the ToN-IoT dataset to develop an Intrusion Detection System (IDS) for Advanced Metering Infrastructure (AMI). These methods were selected for their proven effectiveness in cybersecurity applications and were trained with various parameters during feature engineering to optimize performance. The six ML models explored here are Logistic Regression (LR), Naïve Bayes (NB), Support Vector Machine (SVM), k-Nearest Neighbors (kNN), Random Forest (RF), and XGBoost. Below is a detailed description of each model:

A. Logistic Regression (LR)

Estimates the probability of an observation belonging to a class using a sigmoid function to ensure outputs fall between 0 and 1. The model uses the equation in (1):

$$h_\theta(x) = \sigma(\theta^T X) \tag{1}$$

The sigmoid function σ (r), which defines the threshold, is given in (2):

$$\sigma(r) = \frac{1}{1+e^{-r}} \tag{2}$$

B. Naive Bayes (NB)

A probabilistic classifier based on Bayes' theorem that assumes feature independence. Equation (3) calculates,

$$P(C|X) = \frac{P(X|C)P(C)}{P(X)} \tag{3}$$

C. k-Nearest Neighbor (kNN)

A non-parametric method that classifies new instances by identifying k closest observations from training data using distance metrics (typically Euclidean distance). It assigns class labels based on majority vote.The Euclidean Distance is defined as in equation (4):

$$d(x,y) = \sqrt{\sum_{i=1}^{n}(-y_i)^2} \tag{4}$$

D. Random Forest (RF)

An ensemble learning method that builds multiple decision trees and aggregates their outputs to improve prediction accuracy and reduce overfitting. To determine the best splits within the trees, the Gini impurity is used as a criterion, defined as in equation (5):

$$G = 1 - \sum_{i=1}^{n} {p_i}^2 \tag{5}$$

E. Support Vector Machine (SVM)

Constructs an optimal hyperplane to maximize margins between classes. The RBF kernel function is defined as in equation (6):

$$K(x,y) = e^{-\frac{||x-y||^2}{2\sigma^2}} \tag{6}$$

F. XGBoost

An advanced gradient boosting algorithm that sequentially builds decision trees to correct errors from previous models. It uses a complex objective function with regularization to prevent overfitting while optimizing performance. The objective function of XGBoost is given by equation (7):

$$obj^t = \sum_{i=1}^{n} l(y_i, {\hat{y}_i}^{t-1} + f_t(x_i) + \Omega(f_t)) \tag{7}$$

To optimize the function, XGBoost applies a second-order Taylor expansion, approximating the loss function as in equation (8):

$$obj^t = \sum_{i=1}^{n}[l(y_i, {\hat{y}_i}^{t-1} + g_i f_t(x_i) + \frac{1}{2}\, h_i {f_t}^2(x_i)] + \Omega(f_t)) \tag{8}$$

The optimized objective function is in equation (9):

$$obj^* = -\frac{1}{2}\sum_{j=1}^{T}\frac{(\sum g_i)^2}{\sum h_i + \lambda} + \lambda T \tag{9}$$

These six machine learning models, each optimized through careful parameter tuning, were chosen for their established effectiveness in detecting network anomalies and potential security threats.

V. EXPERIMENTAL METHODOLOGY

This study implements an Intrusion Detection System (IDS) for Advanced Metering Infrastructure (AMI) using various data preparation and preprocessing techniques with the ToN-IoT dataset, as outlined in this section.

1) Data Preprocessing

The ToN-IoT dataset was prepared by imputing missing values with frequent occurrences, converting categorical features via one-hot encoding, and addressing class imbalance with SMOTE. Redundant features were removed, resulting in a refined dataset of 31 features across 211,043 instances.

2) *Feature Engineering and Normalization*

SMOTE technique generated synthetic minority samples to prevent overfitting and improve model generalization. Min-Max scaling normalized all values to the [0,1] range, ensuring balanced feature influence during model training.

3) *Feature Selection using Pearson's Correlation*

Pearson's correlation coefficient identified relationships between features and the target variable, reducing the original 44 features to 17 most relevant ones. This process enhanced accuracy while reducing computational complexity

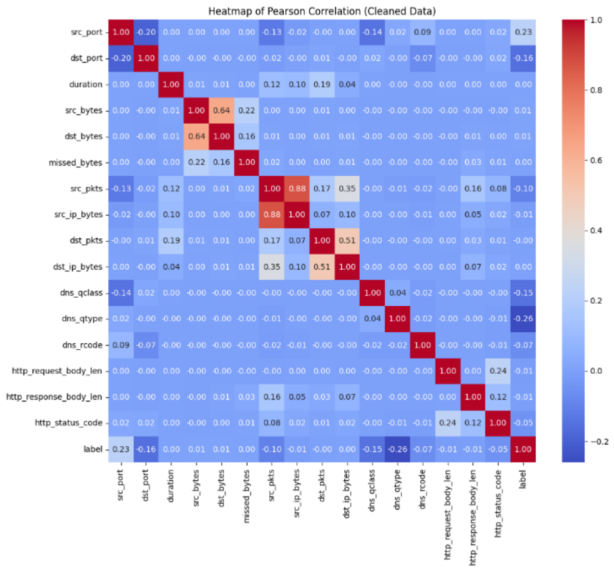

FIG. 2. HEATMAP OF PEARSON'S CORRELATION

A heatmap (Fig. 2) visualizes the correlations among these features

4) *Model Training*

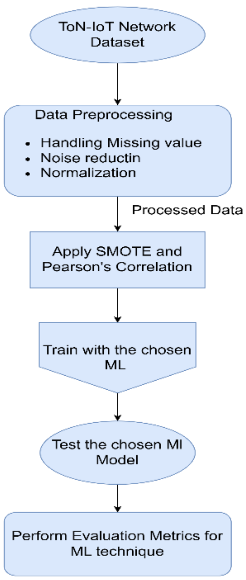

FIG. 3. MODEL TRAINING USING ML ON TON-IOT DATASET

Training of Machine Learning models on the ToN-IoT dataset for intrusion detection is shown in **Fig. 3.** The dataset was divided into 70% training/validation and 30% testing sets.

Five-fold cross-validation was implemented during training to optimize hyperparameters and improve model generalization on unseen data.

5) *Evaluation Metrics*

Model performance was assessed using Accuracy, Precision, Recall, and F1-score metrics derived from confusion matrix components (TP, TN, FP, FN). These measurements provided comprehensive insights into the classification effectiveness of the intrusion detection system. The evaluation metrics are computed using the following formulas (10-13):

$$\text{Accuracy} = \frac{TP+TN}{TP+TN+FP+FN} \quad (10)$$

$$\text{Precision} = \frac{TP}{TP+FP} \quad (11)$$

$$\text{Recall(TPR)} = \frac{TP}{TP+FN} \quad (12)$$

$$\text{F score} = \frac{2 \times \text{Precision} \times \text{Recall}}{\text{Precision}+\text{Recall}} \quad (13)$$

VI. RESULTS AND ANALYSIS

The ML models were evaluated using 5-fold cross-validation on the ToN-IoT dataset, with experiments conducted using Python 3.8 on a Windows 10 system (Intel Core i7, 16GB RAM).

- *Binary classification:*

Random Forest (RF) delivered the best binary classification performance with 99.87% accuracy, followed by XGBoost (98.0%) and kNN (97.6%). Naïve Bayes (NB) performed the weakest (62.6%), while SVM slightly outperformed Logistic Regression (LR). Overall, RF proved most effective for distinguishing normal and malicious traffic (Table I).

TABLE I BINARY CLASSIFICATION OF ML MODELS

Models	Accuracy	Precision	Recall	F1 -score
LR	66.8	57.1	57.1	57.1
NB	62.6	55.8	55.8	55.8
RF	99.87	99.75	99.67	99.87
kNN	97.6	97.6	97.6	97.6
SVM	77.0	75.3	75.3	75.3
XGBoost	98.0	97.9	97.9	97.9

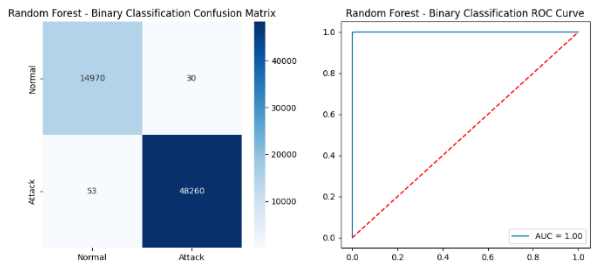

FIG. 4. BINARY CLASSIFICATION FOR RF
(CONFUSION MATRIX AND ROC CURVE)

The Random Forest model achieved an AUC of **1.00**, indicating perfect separation between normal and attack instances, with minimal misclassifications—only 30 false positives and 53 false negatives—highlighting its reliability for real-time intrusion detection **(Fig. 4**).

- *Multiclass Classification:*

For multiclass classification, RF again led with 98.78% across all metrics, followed by strong results from XGBoost and kNN. DDoS, XSS, and Injection attacks achieved near-perfect AUCs (≥0.99), while MiTM detection was lower (AUC 0.88), likely due to class imbalance or feature overlap (Table II).

TABLE II MULTICLASS CLASSIFICATION OF ML MODELS

Models	Accuracy	Precision	Recall	F1-score
LR	64.0	61.0	61.0	61.0
NB	60.0	59.0	59.0	59.0
RF	98.78	98.78	98.78	98.78
kNN	96.0	96.0	96.0	96.0
SVM	78.0	76.0	76.0	76.0
XGBoost	98.1	98.0	98.0	98.0

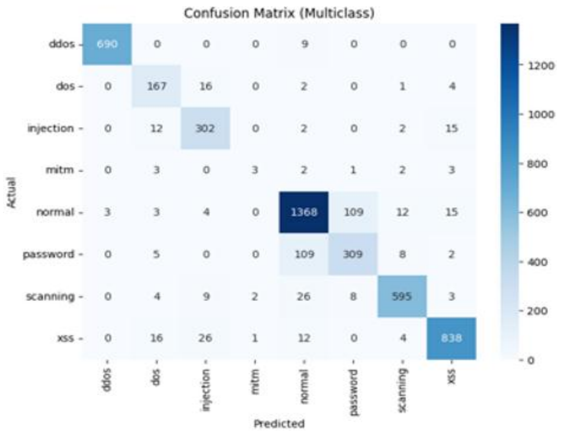

FIG. 5. MULTICLASS CLASSIFICATION FOR RF(CONFUSION MATRIX)

Multiclass results show high precision and recall across most attack types. DDoS, XSS, and Injection attacks achieved near-perfect AUCs (0.99–1.00), confirming the model's robustness (**Figs. 5 & 6**). MiTM attacks, however, had a lower AUC of 0.88, likely due to feature overlap.

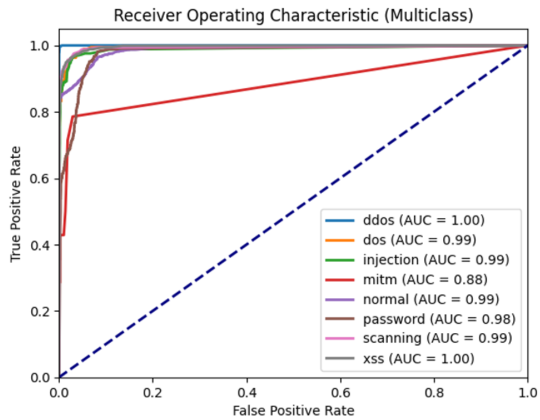

FIG. 6. MULTICLASS CLASSIFICATION FOR RF (ROC CURVE)

VII. CONCLUSION

This study proposes an IDS for IoT-based AMI networks using the ToN-IoT dataset, which captures diverse, real-world attack scenarios. To handle class imbalance and redundancy, Pearson's correlation and SMOTE were applied. Random Forest outperformed other models in both binary (99.87%) and multiclass (98.78%) classification tasks, demonstrating strong detection capability. XGBoost and kNN also performed well across metrics. The results confirm the effectiveness of ML models for cyber threat detection in AMI environments. Future work will explore deep learning and Blockchain technology to further improve accuracy and reduce false positives.

Acknowledgment

The authors sincerely acknowledge Thiagarajar College of Engineering, Madurai, for providing the necessary resources, research facilities, and technical support to carry out this work.

REFERENCES

[1] X. Liu, X. Wang, and W. Liu, "Cybersecurity for smart metering systems in the smart grid: A survey," *IEEE Commun. Surv. Tuts.*, vol. 19, no. 2, pp. 1253–1275, 2017.J. Clerk Maxwell, A Treatise on Electricity and Magnetism, 3rd ed., vol. 2. Oxford: Clarendon, 1892, pp.68–73.

[2] M. Musleh, S. M. Muyeen, and M. A. Rahman, "A survey on smart grid cybersecurity: Threats, risk factors, and mitigation strategies," *IEEE Access*, vol. 7, pp. 164546–164566, 2019.

[3] N. S. Bhati, M. Khari, V. García-Díaz, and E. Verdú, "A review on intrusion detection systems and techniques," *Int. J. Uncertainty, Fuzziness, Knowl.-Based Syst.*, vol. 28, Supp. 02, pp. 65–91, 2020.

[4] A. Alshammari, M. A. Zohdy, D. Debnath, and G. Corser, "Classification approach for intrusion detection in vehicle systems," *Wireless Eng. Technol.*, vol. 9, no. 4, pp. 79–94, 2018.

[5] K. Kumar and R. Singh, "Comparative analysis of ML-based intrusion detection systems using NSL-KDD dataset," *IEEE Trans. Inf. Forensics Security*, vol. 18, pp. 2142–2153, 2023.

[6] S. Patil and P. Patil, "A survey on machine learning techniques for network intrusion detection," *IEEE Access*, vol. 8, pp. 22391–22410, 2020.

[7] A. Sharma and R. Joshi, "Ensemble learning-based IDS with feature selection for KDD-CUP99 dataset," *IEEE Trans. Netw. Serv. Manage.*, vol. 16, no. 4, pp. 1234–1245, 2019.

[8] M. Moustafa and J. Slay, "Statistical analysis-based anomaly detection for modern network security," *IEEE Trans. Inf. Forensics Security*, vol. 10, no. 6, pp. 1178–1189, 2015.

[9] S. Ali, F. Ahmed, and K. Iqbal, "Evaluating ML-based IDS for enterprise networks using NSL-KDD dataset," *IEEE Trans. Emerg. Topics Comput.*, vol. 11, no. 3, pp. 1305–1316, 2023.

[10] H. Kim, Y. Park, and S. Choi, "IDS for cloud environments using Random Forest: Performance

analysis with CICIDS2017," *IEEE Cloud Comput.*, vol. 10, no. 2, pp. 65–75, 2023.

[11] C. Brown, A. White, and D. Black, "A comprehensive review of ML-based IDS implementations," *IEEE Commun. Surv. Tuts.*, vol. 23, no. 4, pp. 1275–1301, 2021.

[12] R. Vinayakumar, M. Alazab, and S. Srinivasan, "A taxonomy of ML techniques for IDS in heterogeneous networks," *IEEE Trans. Netw. Sci. Eng.*, vol. 6, no. 3, pp. 2387–2402, 2019.

[13] C. Wu and L. Song, "A hybrid ML approach for IoT-based IDS using ToN-IoT dataset," *IEEE Access*, vol. 10, pp. 10255–10267, 2022.

[14] N. Moustafa, "ToN-IoT dataset," *IEEE Dataport*, 2020. [Online]. Available: https://dx.doi.org/10.21227/fesz-dm97

Power Quality Challenges in Electric Vehicle Charging Infrastructure: An Indian Perspective

Muhammed Alaudeen Ashiq M
Department of Electrical and Electrical Electronics Engineering,
Thiagarajar College of Engineering,
Madurai, India
alaudeenashiq@gmail.com

Jessi Sahaya Shanrhi L
Department of Electrical and Electronics Engineering,
Thiagarajar College of Engineering,
Madurai, India
ljseee@tce.edu

***Abstract*—The increasing popularity of electric vehicles (EVs) has led to the development of EV charging infrastructure to support their adoption. However, the deployment of EV charging infrastructure has been hindered by several challenges, including power quality issues. Power quality is important in EV charging because it affects the safety, reliability, and efficiency of the charging process. This review paper provides an overview of the challenges in EV charging, with a focus on power quality issues. The paper presents a comprehensive analysis of the different power quality issues in EV charging, including voltage and frequency deviations, harmonics, unbalanced loads, and power factor. The paper also discusses the causes and effects of power quality issues in EV charging and highlights the importance of addressing these issues for the successful adoption of EVs. The paper provides an overview of the available mitigation techniques for power quality issues, including passive and active techniques, PWM, and reactive power compensation techniques. The effectiveness of these techniques is discussed, and a comparison of different mitigation techniques is presented in a tabular format. Real-world examples of power quality issues in EV charging in India are provided, along with a description of the mitigation techniques applied and their effectiveness. The paper concludes with recommendations for future research in this area, including the development of standardized test protocols, the investigation of the impact of EV charging on the electrical grid, and the development of advanced mitigation techniques. Overall, this review paper provides a comprehensive overview of the challenges in EV charging with a focus on power quality issues and presents a roadmap for future research in this area.**

Keywords—Electric Vehicle, Charging Strategy, Power Quality, Distribution System, DC Microgrid

I. Introduction

The adoption of electric vehicles (EVs) is gaining momentum globally as a pivotal strategy for reducing greenhouse gas emissions and transitioning towards sustainable energy systems. In India, with its burgeoning population and rising urbanization, the transportation sector contributes significantly to energy consumption and emissions. As a result, the push for electrification of vehicles is crucial for addressing energy security and environmental concerns.

However, integrating EVs into the power grid poses substantial challenges. Frequent connection and disconnection of high-power DC chargers can create severe power quality issues, including voltage fluctuations, harmonic generation, and increased peak demand. If unmanaged, these issues could compromise the stability and reliability of India’s already stressed power distribution system.

The integration of electric vehicles (EVs) into power systems presents significant power quality challenges, including voltage unbalance, harmonic distortions, and transformer overloading. The unpredictable and nonlinear nature of EV charging loads can cause severe fluctuations in voltage levels, increasing the risk of power instability. Additionally, the harmonics generated by power electronics-based EV chargers degrade power quality by introducing waveform distortions, leading to increased losses and potential failures in distribution transformers [1]. Without proper mitigation strategies such as smart charging, phase balancing, and harmonic filters, the large-scale adoption of EVs could strain existing electrical infrastructure, affecting grid efficiency and reliability. Addressing these challenges through advanced grid management techniques and energy storage integration is crucial for ensuring stable and high-quality power supply in future EV-dominated grids [2].The literature underscores the multifaceted challenges associated with EV charging on distribution networks. Sharma et al. [3] analyzed the influence of plug-in electric vehicles (PEVs) on urban power grids in India, highlighting the surge in peak demand and power losses. Deb et al. [4] examined the reliability impacts of EV charging stations and noted significant degradation in voltage profiles and transformer efficiency under uncontrolled charging scenarios.

Anastasiadis et al. [5] explored the effects of increased EV penetration on distribution networks, emphasizing the importance of optimized charging strategies. Similarly, Marcincin et al. [6] investigated the reliability challenges of fast-charging stations, citing issues such as harmonics and network congestion. Furthermore, Morsy et al. [7] demonstrated that unmanaged charging could result in substantial voltage drops, adversely affecting low-voltage distribution systems. To address these challenges, researchers have proposed integrating distributed energy resources (DERs) and advanced charging control systems. Habib et al. [8] reviewed vehicle-to-grid (V2G) technology as a promising solution for grid stabilization, while Ying et al. [9] discussed the role of DC microgrids in enhancing charging efficiency and mitigating reactive power issues. As a cleaner and more environmentally friendly substitute for conventional gasoline-powered cars, electric vehicles (EVs) have increased in popularity in recent years. Several factors are driving the increasing popularity of EVs in India. One of the main drivers is the cost savings associated with electric vehicles compared to conventional petrol and diesel vehicles. EVs are generally cheaper to operate, with lower fuel and maintenance costs, and can also benefit from government subsidies and incentives. Additionally, the environmental benefits of EVs, including reduced air pollution and carbon emissions, are becoming increasingly important to Indian consumers [10].

Another key driver of EV adoption in India is the government's push for clean energy and sustainable transportation. The government has launched several initiatives to promote EVs, including the Faster Adoption and Manufacturing of (Hybrid &) Electric Vehicles in India (FAME) scheme, which offers incentives for the purchase of EVs and the development of EV infrastructure. Despite the increasing popularity of EVs in India, several challenges still need to be addressed, including the lack of charging infrastructure, high upfront costs, and limited range. However, with continued government support and investment, the adoption of EVs in India will likely continue to grow in the coming years. Unlike China and Norway, which have modernized their power grids to accommodate electric vehicle penetration, India's aging infrastructure faces challenges with voltage instability. This underscores the importance of power quality mitigation techniques for ensuring grid resilience.

II. TRANSPORTATION IN INDIA

India, the world's fifth-largest car market, is seeing rising vehicle demand due to increasing incomes and urbanization, impacting global oil use. To promote electric mobility, the government launched initiatives like the National Mission for Electric Mobility (2011) and the FAME scheme (2015), recently extended with a $1.4 billion budget. However, EVs still comprise only 0.6% of total vehicle sales, with around 260,000 units and 1.5 million electric rickshaws mostly used for short trips. The government now aims for EVs to comprise 30% of new vehicle sales by 2030 and plans full electrification of new urban buses. State-level policies and evolving fuel efficiency standards further support this shift.

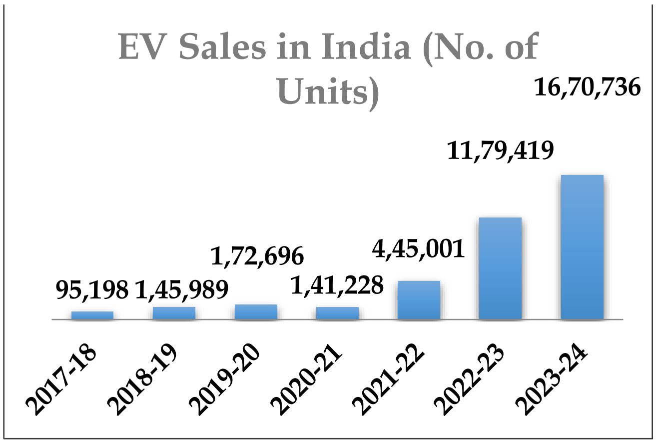

FIG. 1. EV SALES IN INDIA (SOURCE: SMEV, INCLUDES TWO-, THREE-, FOUR-WHEELERS AND ELECTRIC BUSES)

In India, there are mainly three types of charging infrastructure available for electric vehicles:

Normal Charging: This type of charging infrastructure is designed for overnight charging and is commonly found in residential areas, offices, and public parking lots.

The charging power output for normal charging stations in India is typically between 2 kW to 6 kW, and it takes around 6-8 hours to fully charge an EV battery.

Fast Charging: Fast charging infrastructure is designed for on-the-go charging and is commonly found along highways, petrol pumps, and public parking areas. These charging stations provide a higher charging power output of 20 kW to 50 kW, which can charge an EV battery up to 80% within 30-60 minutes.

Ultra-Fast Charging: Ultra-fast charging infrastructure is relatively new in India and is designed for quick charging, which can charge an EV battery up to 80% within 15-30 minutes. These charging stations provide a charging power output of more than 50 kW and are typically installed at locations with high EV traffic, such as shopping malls and airports.

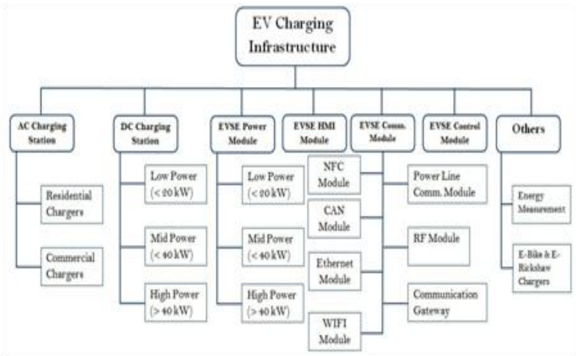

FIG. 2. ELECTRIC VEHICLE CHARGING INFRASTRUCTURE

India currently has fewer than 2,000 public charging stations, but estimates indicate that at least 46,000 will be needed by 2030 to support the expected growth in electric vehicles (EVs). Recent policy frameworks, including FAME II and various state-level EV incentives, aim to tackle this shortage. However, challenges persist in integrating fast-charging hubs into the existing grid networks. The current state of EV charging infrastructure in India is still in its early stages, and there are several challenges that need to be addressed to support the growth of EV adoption and charging infrastructure in the country. Some of the key challenges include:

1. Lack of Adequate Charging Infrastructure
2. Limited Range of Electric Vehicles
3. High Cost of EVs
4. Lack of Standardization
5. Power Grid Infrastructure Challenges
6. Regulatory Challenges

Overall, while there has been some progress in developing EV charging infrastructure in India, there is still a long way to go. Addressing these challenges will require a concerted effort from policymakers, regulators, charging station operators, and the private sector to create an enabling environment for EV adoption and charging infrastructure development.

III. IMPACT OF EV CHARGING STRATEGY

Electric vehicle (EV) charging poses a number of challenges, particularly with regards to power quality issues that can arise during the charging process. These power quality issues can include voltage and frequency deviations, harmonics, unbalanced load, and power factor issues, all of which can have negative impacts on the safety, reliability, and efficiency of the charging process.

A. *Charging Scenarios*

Unrestrained or uncontrolled charging allows PEVs to begin charging immediately upon connection until fully charged. During peak load hours, this can result in overloading the distribution network, leading to cascading effects such as transformer overheating and feeder congestion. Coordinated charging strategies, including time-of-use pricing and demand-response mechanisms, can alleviate these issues by distributing the charging load more evenly throughout the day.

B. *Voltage at Feeder*

Voltage drops in low-voltage distribution networks are a critical concern, especially in rural and semi-urban areas where infrastructure is less robust. The integration of fast-charging stations exacerbates this issue, as high-power loads induce significant voltage deviations. Ensuring voltage stability requires advanced monitoring systems, reactive power compensation devices, and network upgrades.

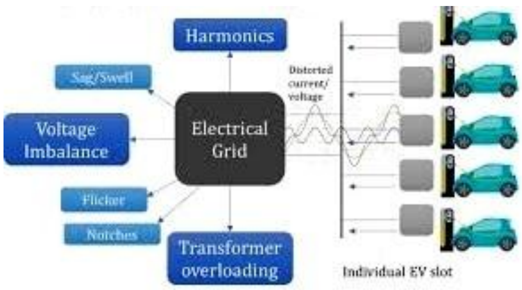

FIG. 3. EFFECTS OF EV INTEGRATION ON THE GRID

C. *Impact on Power Quality*

The widespread adoption of EVs contributes to power quality issues such as harmonic distortion, voltage imbalance, and transient surges. Harmonic currents generated by nonlinear charging loads can interfere with sensitive equipment and reduce the overall efficiency of the grid. Mitigation strategies include the use of harmonic filters, advanced inverter technologies, and compliance with grid codes for EV chargers.

D. *Impact on Distribution Network Scheduling*

As EV penetration increases, the distribution network's load characteristics change significantly, necessitating a re-evaluation of scheduling algorithms. Optimized load scheduling that incorporates real-time data from smart meters and grid sensors can minimize power losses and improve node voltage profiles. Additionally, load forecasting using machine learning models can aid in better grid planning and resource allocation.

TABLE I : CHALLENGES OF INTEGRATION OF EV IN POWER QUALITY

Challenges	Explanation
Power Losses	The rise in unregulated and single-phase EV charging stations leads to increased power losses. A high penetration of EVs results in additional stress on distribution transformers, causing higher losses and potential overloading [11].
Voltage Unbalance	When a significant number of EVs charge on single-phase connections, it disrupts the balance of the three-phase system. Unequal distribution of the load among the phases leads to voltage unbalance, affecting overall system performance [12].
Voltage Fluctuations	The impact of voltage fluctuations intensifies as the charging rate and number of EVs increase. This variation can cause instability in the power grid, leading to voltage dips or spikes [13].
Harmonics	As more EVs are connected to the grid, the presence of harmonics increases due to the nature of power electronics-based chargers. Randomized charging patterns further amplify harmonic distortions, which can degrade power quality and efficiency [13].

E. *Integration of EV with Distributed Generation*

The integration of EV charging infrastructure with distributed energy resources, such as solar photovoltaic (PV) systems and wind turbines, offers a sustainable solution for mitigating grid stress. Bidirectional energy exchange between EVs and the grid enhances load flexibility and reduces dependency on centralized power generation. Advanced energy management systems are essential for coordinating the operation of distributed generation, storage, and EV loads.

F. *DC Microgrid & PV for Electric Vehicle Charging*

DC microgrids are well-suited for EV charging applications due to their ability to transport high-power direct current without issues related to reactive power or phase synchronization. By integrating PV systems and battery storage, DC microgrids can provide stable and efficient charging solutions. However, the lack of standardization and high initial costs remain barriers to widespread adoption.

IV. MITIGATION TECHNIQUES FOR QUALITY ISSUES

The mitigation techniques to be employed to address power quality issues in EV charging infrastructure. Some of the commonly used techniques are as follows:

1. Voltage and frequency regulation
2. Harmonic filtering
3. Load balancing
4. Power factor correction
5. Energy storage
6. Intelligent control and management

Overall, the use of these mitigation techniques can help ensure reliable and efficient charging while also mitigating the impact of power quality issues on the electrical network.

TABLE II MITIGATION TECHNIQUES

Mitigation Technique	Effectiveness	Cost
Passive Filters	Moderate	Low
Harmonic Filters	High	Moderate
Capacitor Banks	Moderate	Low
Active Power Filters	High	High
Static VAR Compensators	High	High
Unified Power Quality Conditioners	Very High	Very High

The table compares various mitigation techniques for addressing power quality issues caused by EV charging, focusing on their effectiveness and cost. Passive filters and capacitor banks are cost-effective solutions with moderate efficacy and are suitable for basic power quality needs. Harmonic filters provide higher effectiveness at a moderate cost, addressing harmonic distortions efficiently. Active power filters and Static VAR Compensators (SVCs) offer high effectiveness by dynamically compensating for harmonics and reactive power but are more expensive. Unified Power Quality Conditioners (UPQCs) deliver the highest effectiveness by addressing all power quality issues comprehensively, making them ideal for critical applications, though their cost is very high. The choice of technique depends on the balance between performance requirements and budget constraints.

V. CONCLUSION

The proliferation of electric vehicles in India is inevitable and presents an opportunity to revolutionize the transportation and power sectors. However, this transition is accompanied by significant challenges, particularly in terms of power quality, voltage stability, and distribution network reliability. Effective charging strategies, integration with distributed energy resources, and advancements in DC microgrid technology are critical for mitigating these issues. This paper highlights the need for a holistic approach to EV integration, emphasizing the importance of policy interventions, technological innovations, and infrastructure development. By addressing these challenges, India can pave the way for a sustainable and resilient EV ecosystem, contributing to its energy security and climate goals. Future research should include field implementation of active power filters in fast-charging hubs to assess real-world impact on grid stability. Machine learning models can enhance EV load forecasting, optimizing demand response and reducing grid stress.

Acknowledgment

The authors thank the Thiagarajar College of Engineering for the support and acknowledge the All India Council of Technical Education (AICTE) for providing a grant under the Quality Improvement Progamme.

REFERENCES

[1] Abhinav Srivastava, Munish Manas, Rajesh Kumar Dubey, "Integration of power systems with electric vehicles: A comprehensive review of impact on power quality and relevant enhancements," *Electric Power Systems Research*, Vol.234, 2024, 110572, ISSN 0378-7796.

[2] Yuanshi Zhang, Bokang Zou, Xu Jin, Yifu Luo, Meng Song, Yujian Ye, Qinran Hu, Qirui Chen, Antonio Carlos Zambroni, "Mitigating power grid impact from proactive data center workload shifts: A coordinated scheduling strategy integrating synergistic traffic - data - power networks," *Applied Energy*,Vol. 377, Part D,2025,124697,ISSN 0306-2619.

[3] A.Sharma, A Kapoor and S Chakrabarti, "Impact of Plug-in Electric Vehicles on Power Distribution System of Major Cities of India: A Case Study", India, 2019.

[4] Deb S, Tammi K, Kalita K, Mahanta P. Impact of Electric Vehicle Charging Station Load on Distribution Network. *Energies*. 2018; 11(1):178.

[5] Anestis G. Anastasiadis, Georgios P. Kondylis, Apostolos Polyzakis, Georgios Vokas,Effects of Increased Electric Vehicles into a Distribution Network, Energy Procedia, Volume 157,2019, 586-593,ISSN 1876-6102.

[6] O. Marcincin, Z. Medvec and P. Moldrik, "The impact of electric vehicles on distribution network," *2017 18th International Scientific Conference on Electric Power Engineering (EPE)*, Kouty nad Desnou, Czech Republic, 2017, pp. 1-5.

[7] M. Nour, H. Ramadan, A. Ali and C. Farkas, "Impacts of plug-in electric vehicles charging on low voltage distribution network," *2018 International Conference on Innovative Trends in Computer Engineering (ITCE)*, Aswan, Egypt, 2018, pp. 357-362.

[8] Salman Habib, Muhammad Kamran, Umar Rashid,Impact analysis of vehicle-to-grid technology and charging strategies of electric vehicles on distribution networks – A review, Journal of Power Sources,Volume 277,2015,205-214,ISSN 0378-7753.

[9] X. Yang, L. Zhu, Z. Zhang, L. Li and H. Wang, "Electric vehicles charging and discharging control strategy based on independent DC micro-grid," *2018 IEEE 3rd Advanced Information Technology, Electronic and Automation Control Conference (IAEAC)*, Chongqing, China, 2018, pp. 969-973.

[10] S. V. Saleh and M. A. Latify, "Coordinated Unbalance Compensation and Harmonic Mitigation in the Secondary Distribution Network Through EVs Participation," in *IEEE Transactions on Smart Grid*, vol. 15, no. 5, pp. 4450-4462, Sept. 202

[11] J. de Hoog, V. Muenzel, D.C. Jayasuriya, T. Alpcan, M. Brazil, D.A. Thomas, R. Jegatheesan, The importance of spatial distribution when analysing the impact of electric vehicles on voltage stability in distribution networks, Energy Syst.- Optimizat. Model. Simulat. Econ. Aspects 6 (1) (2015) 63–84, https://doi.org/ 10.1007/s12667-014-0122-8.

[12] K. Kim, C.S. Song, G. Byeon, H. Jung, H. Kim, G. Jang, Power demand and total harmonic distortion analysis for an EV charging station concept utilizing a battery energy storage system, J. Elect. Eng. Technol. 8 (5) (2013) 1234–1242, https:// doi.org/10.5370/JEET.2013.8.5.1234.

[13] Alexandre Lucas, Fausto Bonavitacola, Evangelos Kotsakis, Gianluca Fulli, Grid harmonic impact of multiple electric vehicle fast charging, Elect. Power Syst. Res. 127 (2015) 13–21.

Artificial Intelligence in Solar Power Forecasting: A Comprehensive Review of Emerging Trends

Leelavathi M
Deptartment of EEE
Thiagarajar College of Engineering
Madurai, India
leelavathimohan93@gmail.com

Suresh Kumar V
Deptartment of EEE
Thiagarajar College of Engineering
Madurai, India
vskeee@tce.edu

Devi B
Deptartment of EEE
Thiagarajar College of Engineering
Madurai, India
devibzen1@gmail.com

***Abstract*—The rapid adoption of solar energy as a sustainable energy source underscores the need for advanced predictive models to optimize its integration into modern energy systems. Accurate prediction methodologies are critical for increasing the efficiency, dependability, and scalability of solar energy applications. This review explores emerging trends and innovative approaches in solar power forecasting, emphasizing the role of hybrid deep learning models, Internet of Things (IoT) integration, satellite data utilization, quantum computing advancements, and adaptive machine learning techniques. The integration of IoT devices enables real-time data collection and processing, while satellite imagery enhances spatial and temporal accuracy in solar radiation forecasts. Hybrid models, combining deep learning and traditional statistical methods, address complex nonlinearities in solar datasets, and quantum computing offers potential breakthroughs in handling vast computational demands. However, challenges such as data heterogeneity, computational complexity, and environmental variability persist. This paper identifies these obstacles and proposes novel frameworks to overcome them, including robust data preprocessing techniques, scalable algorithms, and interdisciplinary collaborations. By advancing solar power prediction methodologies, these developments contribute to addressing global energy demands, reducing greenhouse gas emissions, and fostering a seamless transition to renewable energy systems. The findings are pivotal for policymakers, researchers, and industry stakeholders striving for a sustainable energy future.**

Keywords—Solar Energy Forecasting, Hybrid Deep Learning, IoT Integration, Satellite Data Utilization, Quantum Computing

I. INTRODUCTION

Solar power is one of the most abundant and environmentally friendly energy sources, crucial for addressing global energy demands and combating climate change. Photovoltaic (PV) systems have gained popularity due to technological advancements, decreasing costs, and the growing need for sustainable energy solutions. Accurate solar power prediction is vital for optimizing power generation, energy storage management, and grid stability. These forecasts help balance supply and demand, facilitate solar energy integration into traditional grids, and assist policymakers in planning for a renewable energy future. However, solar energy faces challenges like intermittency, variable weather, and partial shading, complicating power output predictions. Traditional models struggle with the nonlinearity and stochastic behaviors of solar systems, leading to inaccuracies. To overcome these challenges, modern technologies like deep learning (DL) and machine learning (ML) have emerged. Approaches such as random forests, neural networks, and support vector machines (SVMs) have shown improved accuracy in forecasting by capturing complex patterns in solar irradiance and PV output, surpassing traditional methods.

A key area of research in solar power prediction is the use of satellite data, which offers high spatial and temporal resolution, improving forecast accuracy. When combined with ground-based measurements, satellite datasets enhance model calibration and validation. Additionally, advancements in IoT allow for real-time monitoring of solar power systems through sensors that track weather, system performance, and shading patterns, as shown in Fig. 1. However, challenges remain, including data heterogeneity due to varying environmental conditions, the computational complexity of ML and DL models for real-time predictions, and the unpredictability of extreme weather events, which can cause significant deviations in solar output.

FIG.1. OVERALL DIAGRAM FOR SOLAR POWER FORECASTING

This review makes significant contributions by analyzing emerging methodologies in solar forecasting, such as hybrid deep learning models that merge statistical and neural network techniques for improved accuracy. It emphasizes the value of integrating IoT and satellite data to enhance resolution and prediction reliability. Quantum computing is explored as a breakthrough for addressing computational limits in large-scale systems. The review also identifies current research gaps and proposes novel frameworks to advance the field. These innovations not only improve forecasting but also support microgrid optimization, hybrid energy systems, and renewable integration, ultimately contributing to a sustainable and efficient global energy future (2).

II. PROPOSED METHODOLOGY

A. Hybrid deep learning models

Hybrid deep-learning algorithms integrate different neural network designs to improve the accuracy of solar energy forecasting. These models tackle the inherent complexity of solar power generation by capturing intricate patterns from diverse datasets, ranging from weather conditions to irradiance fluctuations (3). Hybrid models are extremely significant in the energy business due to their capacity to process massive volumes of data in real-time and properly estimate solar energy trends.

1) CatBoost-BiLSTM-RNN Frameworks

The CatBoost-BiLSTM-RNN Fig. 2, framework combines gradient boosting and sequential models to enhance solar power forecasting. CatBoost excels at handling tabular data, reducing overfitting, and capturing nonlinear dependencies, while BiLSTM and RNN models are effective for time-series forecasting, particularly for solar irradiance fluctuations. This integration efficiently manages both short-term and long-term variables in solar prediction data. The architecture predicts power output (Pt) based on input variables (xt), as represented in Eq. 1.

$$P_t = f(x_t, h_{(t-1)}, \Theta) \qquad (1)$$

Where:

(P_t) is the predicted power output at time (t),

(x_t) is the input data (such as irradiance or temperature) at time (t),

($h_{(t-1)}$) represents the hidden state from the time before step,

(Θ) represents the model parameters.

The CatBoost model contributes to this framework by optimizing the feature importance and improving the generalization capability.

2) Multi-Layer Architectures

Multi-layer architectures combine CNNs and LSTMs to handle spatial and temporal data, improving solar power prediction by capturing spatial patterns and temporal dependencies, as shown in Fig. 2 (30), as represented in Eq. 2.

The combined architecture can be mathematically represented as:

$$h_t = LSTM(CNN(x_t)) \qquad (2)$$

Where: (x_t) represents spatial data (e.g., satellite images or weather data),

($CNN(x_t)$) processes spatial data through convolution layers,

(h_t) is the temporal output of the LSTM.

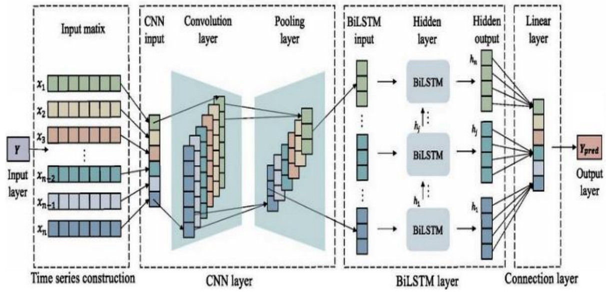

FIG. 2. MACHINE LEARNING ARCHITECTURES

By incorporating both spatial and temporal features, multi-layer architectures provide a holistic view of solar energy generation, making them particularly suitable for areas with fluctuating weather patterns (4).

3) Real-Time Adaptation

Real-time adaptability is a key advantage of hybrid deep learning algorithms in solar forecasting. These models dynamically respond to sudden changes in irradiance, cloud cover, and temperature by continuously learning from incoming data. Their accuracy enhances operational efficiency and energy storage management, making them ideal for large-scale solar power applications.

B. IoT-Enabled Prediction Systems

The Internet of Things (IoT) plays a crucial role in solar power prediction by integrating sensor networks and decentralized computing, as shown in Fig. 3. These systems enhance the granularity and precision of solar power forecasting by providing real-time, high-resolution data from multiple sources (5).

1) Sensor Deployment

Sensors deployed across solar farms monitor crucial environmental parameters, such as solar irradiance (I), temperature (T), wind speed (W), and cloud cover (C). These sensors collect data that can be fed into prediction models to estimate solar power output. The basic relationship for solar power can be expressed as in Eq. 3,

$$P = f(I, T, W, C) \qquad (3)$$

Where:

(P) is the predicted solar power output,

(I) is the solar irradiance,

(T) is the ambient temperature,

(W) is the wind speed,

(C) is the cloud cover.

These sensor networks enable precise monitoring and capture the influence of environmental factors that affect solar generation, thereby improving the predictive accuracy.

2) Edge Computing

Edge computing enables real-time, local data processing, reducing latency and improving solar forecasting accuracy, especially for remote or off-grid systems.

3) Predictive Maintenance

IoT-enabled systems monitor solar equipment health, detecting issues like degradation or faults, enabling predictive maintenance and ensuring continuous energy generation (7).

FIG. 3 IOT-ENABLED SOLAR POWER PREDICTION

C. Satellite and Drone Data Integration

Satellite and drone-based monitoring technologies have revolutionized the accuracy of solar power forecasts, giving high-resolution data on climatic and geographical factors.

1) Satellite Imagery

Geostationary (8) satellites offer crucial data on cloud cover and atmospheric parameters, enhancing solar forecasting models for accurate regional power estimation, as in Eq. 4,

$$P(total)=\sum_{i=1}^{n} f\left(C_{(d,i)}, A_i\right) \quad (4)$$

Where:

($P(total)$) is the total solar power predicted across multiple regions,

($C_{(d,i)}$) is the cloud density at the i^{th} region,

(A_i) is the aerosol concentration at the i^{th} region.

The high-resolution data provided by satellites helps in accurately predicting solar power output over large areas, making it an essential tool for grid-scale forecasting.

2) Drone-Based Monitoring

Drones with multispectral and thermal cameras offer real-time insights on panel conditions, shading, and dust, improving solar forecasting accuracy.

3) Dynamic Updates

Satellite and drone-based monitoring systems provide real-time updates, enabling solar prediction models to dynamically adjust and remain accurate despite environmental changes.

4) Advanced Partial Shading Models

Partial shading reduces solar panel efficiency due to obstructions. Advanced models use reinforcement learning and neural networks to adapt to varying shading patterns (11), as shown in Fig. 4.

FIG. 4. SOLAR FORECASTING USING SATELLITE AND DRONE DATA

D. Reinforcement Learning

Reinforcement learning algorithms optimize Fig. 5, solar power predictions by adjusting model parameters based on real-time shading data, improving accuracy dynamically 12) as in Eq. 5,

$$R = \sum_{t=0}^{T} \gamma^t r_t \quad (5)$$

Where:

(R) is the cumulative reward (or prediction accuracy),

(r_t) is the reward at time (t) (which can indicate the precision that the solar power forecast appears),

(γ) is the discount factor,

(T) is the time horizon.

This process enables models to adapt to varying levels of shading and other factors influencing solar irradiance.

1) Neural Network Integration

By combining reinforcement learning with neural networks, these models can further improve their predictive capabilities (13). Neural networks are trained to understand complex relationships between shading patterns and power loss, allowing the system to predict and compensate for these losses accurately.

2) Validation Through Simulation

Advanced partial shading models use simulations to mimic real-world shading scenarios, Fig. 5 ensuring accurate solar power predictions under various environmental conditions (14).

FIG. 5. REINFORCEMENT LEARNING FOR SOLAR PREDICTION

Quantum Computing Applications

Quantum computing can revolutionize solar power prediction by solving complex optimization (16) problems and enhancing model performance with large-scale data, shown in Fig. 6.

1) Optimization Algorithms

Quantum computing is particularly effective at solving optimization problems involving multi-variable constraints, such as maximizing energy output from distributed solar systems, Fig.6 (17). A quantum algorithm designed to optimize solar energy production can be represented as in Eq. 6,

$$\max_{x} P(x) \text{subject to constraints: } g(x) \leq 0 \qquad (6)$$

Where:

(P(x)) is the energy

Fig. 6. Quantum Computing for Solar Power Optimization

Table 1 compares various solar prediction methods, highlighting the IoT-Enabled Prediction System (18) as the most effective due to its rapid real-time processing, low latency, and high data granularity. By using edge computing, these systems enable instant decisions and precise monitoring of solar PV and environmental conditions, making them ideal for distributed and off-grid setups. They also eliminate oscillation issues common in deep learning models. In contrast, Climate Change Forecasting Models (19) are the least effective for real-time prediction, as they are computationally intensive, slow to adapt to sudden weather changes, and focus more on long-term trends than immediate forecasting needs (20).

III. Discussion and Analysis

The landscape of solar power prediction is evolving rapidly with advanced methodologies offering distinct advantages and addressing specific challenges (21–24). Hybrid Deep Learning Models like CatBoost, BiLSTM, and RNN capture complex patterns and adapt in real-time, though they demand large datasets and high processing power. IoT-enabled systems provide real-time granular data but face calibration and maintenance issues. Satellite and drone data enhance forecasting accuracy yet remain costly. Reinforcement Learning and Quantum Computing enable dynamic optimization, while Climate Change Models offer long-term insights. As shown in Fig. 7, integrating these technologies can create robust systems, advancing solar forecasting for sustainable and efficient energy use.

Fig. 7. Overview of Comparative Diagram Procedure

References

[1] Mishra, S., & Palanisamy, P. (2019). An Integrated Multi-Time-Scale Modeling for Solar Irradiance Forecasting Using Deep Learning. arXiv Preprint arXiv:1905.02616.

[2] Mukhoty, B. P., Maurya, V., & Shukla, S. K. (2019). Sequence to sequence deep learning models for solar irradiation forecasting. arXiv Preprint arXiv:1904.13081.

[3] Massaoudi, M., Chihi, I., Sidhom, L., Trabelsi, M., Refaat, S. S., & Oueslati, F. S. (2019). Enhanced Evolutionary Symbolic Regression Via Genetic Programming for PV Power Forecasting. arXiv Preprint arXiv:1910.10065.

[4] Shahid, F., Zameer, A., Afzal, M., & Hassan, M. (2020). Short term solar energy prediction by machine learning algorithms. arXiv Preprint arXiv:2012.00688.

[5] Mishra, S., & Palanisamy, P. (2019). An Integrated Multi-Time-Scale Modeling for Solar Irradiance Forecasting Using Deep Learning. arXiv Preprint arXiv:1905.02616.

[6] Mukhoty, B. P., Maurya, V., & Shukla, S. K. (2019). Sequence to sequence deep learning models for solar irradiation forecasting. arXiv Preprint arXiv:1904.13081.

[7] Massaoudi, M., Chihi, I., Sidhom, L., Trabelsi, M., Refaat, S. S., & Oueslati, F. S. (2019). Enhanced Evolutionary Symbolic Regression Via Genetic Programming for PV Power Forecasting. arXiv Preprint arXiv:1910.10065.

[8] Shahid, F., Zameer, A., Afzal, M., & Hassan, M. (2020). Short term solar energy prediction by machine learning algorithms. arXiv Preprint arXiv:2012.00688.

[9] Mishra, S., & Palanisamy, P. (2019). An Integrated Multi-Time-Scale Modeling for Solar Irradiance Forecasting Using Deep Learning. arXiv Preprint arXiv:1905.02616.

[10] Mukhoty, B. P., Maurya, V., & Shukla, S. K. (2019). Sequence to sequence deep learning models for solar irradiation forecasting. arXiv Preprint arXiv:1904.13081.

[11] Massaoudi, M., Chihi, I., Sidhom, L., Trabelsi, M., Refaat, S. S., & Oueslati, F. S. (2019). Enhanced

Evolutionary Symbolic Regression Via Genetic Programming for PV Power Forecasting. arXiv Preprint arXiv:1910.10065.

[12] Shahid, F., Zameer, A., Afzal, M., & Hassan, M. (2020). Short term solar energy prediction by machine learning algorithms. arXiv Preprint arXiv:2012.00688.

[13] Mishra, S., & Palanisamy, P. (2019). An Integrated Multi-Time-Scale Modeling for Solar Irradiance Forecasting Using Deep Learning. arXiv Preprint arXiv:1905.02616.

[14] Mukhoty, B. P., Maurya, V., & Shukla, S. K. (2019). Sequence to sequence deep learning models for solar irradiation forecasting. arXiv Preprint arXiv:1904.13081.

[15] Massaoudi, M., Chihi, I., Sidhom, L., Trabelsi, M., Refaat, S. S., & Oueslati, F. S. (2019). Enhanced Evolutionary Symbolic Regression Via Genetic Programming for PV Power Forecasting. arXiv Preprint arXiv:1910.10065.

[16] Shahid, F., Zameer, A., Afzal, M., & Hassan, M. (2020). Short term solar energy prediction by machine learning algorithms. arXiv Preprint arXiv:2012.00688.

[17] Mishra, S., & Palanisamy, P. (2019). An Integrated Multi-Time-Scale Modeling for Solar Irradiance Forecasting Using Deep Learning. arXiv Preprint arXiv:1905.02616.

[18] Mukhoty, B. P., Maurya, V., & Shukla, S. K. (2019). Sequence to sequence deep learning models for solar irradiation forecasting. arXiv Preprint arXiv:1904.13081.

[19] Massaoudi, M., Chihi, I., Sidhom, L., Trabelsi, M., Refaat, S. S., & Oueslati, F. S. (2019). Enhanced Evolutionary Symbolic Regression Via Genetic Programming for PV Power Forecasting. arXiv Preprint

[20] Aamir, M. A., Al-Hashimi, M., Al-Tamimi, A., et al. (2023). A review of solar forecasting techniques and the role of artificial intelligence. MDPI. https://doi.org/10.3390/2673-9941/4/1/5

[21] Fiumara, G., Zito, F. L., Cioppa, A. M., et al. (2023). AI-based forecasting for optimized solar energy management and integration. Taylor & Francis Online. https://doi.org/10.1080/00207543.2023.2269565

[22] Molaei, J. A., Khosravi, K., Shafiee, E., et al. (2024). Seasonal solar irradiance forecasting using artificial intelligence techniques. Nature Scientific Reports. https://doi.org/10.1038/s41598-024-68531-3

[23] Reddy, S. B., Al-Ali, A. S., Awasare, S. B., et al. (2023). Explainable AI and optimized solar power generation forecasting. PMC. https://doi.org/10.1016/j.joen.2023.12.029

[24] Mahdavi, M., Khatibi, V., Alipour, M., et al. (2023). A comprehensive review of AI-based solar irradiance prediction models. IEEE Xplore. https://doi.org/10.1109/ACCESS.2023.3127152

An Adjacent Switching Technique in A Hybrid Casecade Converter Topology

Raja D
Dept of Electrical and Electronics Engineering,
Thiagarajar College of Engineering,
Madurai, India
raja1@student.tce.edu

Prabhu D
Computer Science Engineering Vel Tech Rangarajan,
Dr. Sagunthala R&D Institute of Science and Technology,
Chennai

***Abstract*—For high voltage and high power applications, a new type of power converter called multilevel inverters is ideal. Multilevel inverters can be constructed in a variety of topologies, such as diode-clamped and cascaded combinations. With a series connection between a low-voltage conventional inverter and a high-voltage diode-clamped inverter, this research focuses on an H-bridge multilayer pulse width modulation converter architecture. For the novel hybrid and asymmetric approach, a DC link voltage configuration that maintains the neighboring switching vectors between voltage levels is proposed in order to maximize the number of output voltage levels[13]. Thus, with the least amount of power components, a 15-level hybrid converter may be achieved. By cascading an asymmetrical diode-clamped inverter, which can synthesize 19 levels in the output voltage with the same amount of components, the novel cascade inverter is confirmed[1]. A seven-level H-bridge diode-clamped inverter is equipped with a novel multi-output boost converter at the DC link voltage. The three-phase, 15- and 19-level diode-clamped multilevel inverters are simulated in this article. Additionally, an experimental study is conducted on a five-level asymmetrical cascaded multilevel inverter that uses inverted sine PWM approaches. Using a multi-level inverter that generates stepped sine voltage, the project also aims to lower harmonic levels[7[9]]. The harmonics decrease as the number of steps rises. This study mostly uses neighboring switching levels and switching intermediate pulses. In addition, two topologies—a 15-level inverter and a 19-level inverter—are the work's main emphasis[11][8]**.

Keywords—Asymmetrical diode clamped inverter, Hybrid cascade converter, Adjacent Switching Technique, Inverted Sine PWM Techniques, Cascaded Multilevel Inverter, H-Bridge.

I. INTRODUCTION

Multilevel Inverters (MLIs) are gaining a lot of interest in the realm of medium voltage and high power applications because of its many benefits, which include decreased electromagnetic interference (EMI), low harmonic output, and low voltage stress on power switches. The main use of MLIs is the synthesis of a desired voltage wave form from several DC voltage levels. They are a useful way to reduce harmonics and boost power in AC waveforms[2].

For multilevel inverters, three topologies have been reported: diode-clamped, flying capacitor, and cascaded H-bridge. The deficient DC link capacitor is the primary flaw in the diode-clamped inverter. Despite having a straightforward design, the cascaded multilayer inverter needs independent DC sources. This architecture has the unique benefit of having modular needs for each bridge's protection, control, and modulation. Because of its intricacy, cascaded multilevel inverters are often only used in higher power ranges when many switching output voltage levels are required[3[5]]. In addition, this study focuses experimentally on an asymmetrical cascade MLI that employs uneven DC sources in each phase to provide a five-level equal step multilevel output, hence reducing the number of DC sources needed for the cascaded multilevel inverter for a motor drive. With a low switching (carrier) frequency and greater voltage at higher modulation frequencies, this configuration is advantageous for high power applications. Additionally, it increases dependability.

To create asymmetrical DC link combinations and balance the DC link capacitor voltages for optimal output voltage resolution, a novel multi-output boost converter is employed at the DC link voltage. Many well-known pulse width modulation techniques are available for the cascaded multilevel inverter. Many configurations may be proposed using cascading multilevel H-bridge cells. One such design is a seven-level symmetrical and asymmetrical diode-clamped H-bridge converter that is cascaded with traditional three-level inverters and supplied with a multi-output boost (MOB) converter[2]. The MOB converter can raise the low output voltage of renewable energy systems, such solar cells, to the suitable value of the diode-clamped DC link voltage. It can also rectify the capacitor voltage imbalance issue. The cells' DC voltage ratio will be displayed in order to maximize output voltage levels with nearby switching vectors that can reduce switching losses between all conceivable voltage levels.Because it gives higher voltage at higher modulation frequencies with a low switching (carrier) frequency, this structure is advantageous for high power applications. It enhances dependability as well. There are many widely recognized techniques for pulse width modulation for the cascaded multilevel inverter[16].

Using a seven-level symmetrical and asymmetrical diode-clamped H-bridge converter equipped with a multi-output boost (MOB) converter and cascaded with traditional three-level inverters, cascading multilevel H-bridge cells is used to suggest various combinations[15]. In addition to boosting the low output voltage of renewable energy systems, such solar cells, to the appropriate value of the diode-clamped DC link voltage, the MOB converter may resolve the issue of capacitor voltage imbalance. In order to minimize switching losses, the DC voltage ratio of the cells will be supplied in order to acquire the maximum voltage levels on the output voltage with nearby switching vectors between all feasible voltage levels. Among these topologies, the cascade arrangement has been applied to high- and medium-voltage renewable energy systems, including solar systems, because of its straightforward and modular design. A review of the cascade inverter's use in renewable energy systems is conducted. Adding traditional H-bridge cells to this arrangement makes it simple to construct higher levels. Nevertheless, it needs more switching devices and DC voltage sources.

FThe literature pertaining to the asymmetrical arrangement of multilevel inverters has mostly focused on hybrid converters because of their demonstrated capabilities and advantages in medium- and high-power applications. In order to improve the output voltage resolution as compared to the same DC voltage ratio of the cells, several topologies based on a range of H-bridge cascaded cells and DC voltage ratios have been investigated. However, in comparison to symmetrical cascade inverters, the hybrid architecture loses its flexibility because of the disparate voltage ratings of the switching devices.

Different approaches of pulse width modulation (PWM) []17[have been introduced for fundamental and high switching frequencies in symmetrical cascade inverters. Hybrid modulations for cascade converters with uneven DC sources are presented to enhance converter efficiency and minimize switching losses. These modulations permit the employment of fast switching devices in the lower voltage cells and slow switching devices in the higher voltage cells.

II. General Interpretation

Analysis is done in [35] on a novel DC-DC boost converter with numerous outputs that may be utilized as a front-end converter to increase the DC link voltage of the inverter for grid connection systems based on a diode-clamped converter. The primary issue with balancing the capacitor voltages in such converters is resolved by using this MOB converter to change the DC voltage across each capacitor to a specified voltage level.

DCMI, or Diode-Clamped Multilevel Inverter

The DC bus voltage is split into a set of capacitor voltages by this series-connected capacitor arrangement. Typically, the DC bus of a DCMI with nl levels has (nl-1) capacitors. Each capacitor has a voltage across it of VDC/(nl-1) (nl nodes on the DC bus, nl output phase voltage levels, and (2nl-1) output line voltage levels).

1. Blocking diodes Need a High-Voltage Rating

For reverse voltage blocking, the clamping diodes must have varying voltage ratings, even though each active switching device is only needed to block a voltage level of Vdc/(m - l). With all lower devices, S1′-S4′, turned on, D1′ of the 5-level diode clamped inverter, for instance, has to block three capacitor voltages, or 3Vdc/4. D2 and D2′ must also block 2Vdc/4, and D3 must block 3Vdc/4. For every phase, (m - 1) x (m - 2) diodes will be needed, assuming that the voltage rating of each blocking diode matches the voltage rating of the active device[2]. This value denotes a quadratic growth in m. The number of diodes needed to construct the system will be prohibitive when m is high enough.

When the voltages across the capacitors are different, a novel modulation method for a diode-clamped inverter has been introduced. An H-bridge seven-level diode-clamped inverter junction with the front-end MOB converter is shown in Fig. 3. Rather than using similar dc link capacitor voltages, an uneven dc link configuration is used. The design exhibits asymmetric behavior with regard to the neutral point (Vc1 = 2Vc2 = 2Vc3) because the voltage of the bottom capacitor is maintained at a level double that of the other capacitors throughout operation. It is assumed that the low input voltage (E) of the seven-level diode-clamped H-bridge inverter (VNM) is increased to Vdc at the dc link, as seen in Fig. 3. Thus, the voltage ratios of the dc link capacitors in the SDCC configuration are Vc1 = Vc2 = Vc3 = Vdc /3; in the ADCC design, on the other hand, the capacitors' voltages are kept at Vc1 = V dc /2 and Vc3 = Vc2 = Vdc /4 (relative to the neutral point)[4].

The seven-level diode-clamped converter's construction indicates that each leg of the inverter has four alternative switching states, which may be obtained from four switch combinations to provide various dc link voltage levels. Each switch's "ON" and "OFF" switching states are denoted by the numbers "1" and "0," respectively. Four switching function states, which are enumerated in Table I, differentiate four switching states in one leg of the diode-clamped H-bridge inverter. For instance, (011), which is referred to as switching function state "2," indicates that S1 = 0 (OFF), S2 = 1 (ON), and S3 = 1 (ON).

displays every potential switching state linked to various output voltage levels in both SDCC and ADCC. Investigating the output voltage levels, an asymmetrical DC link configuration based on various switching states can provide nine distinct voltage levels. Compared to a symmetrical design using the same number of switching devices, this layout permits the synthesis of two more voltage levels in the output voltage. With either setup, all voltage levels may be reached with a single switch shift since neighboring vectors are accessible between all voltage levels[9].

DESCRIPTION OF INVERTED SINE PWM Multilevel inverters can be achieved in a few different methods. A seven-level asymmetrical diode-clamped H-bridge multilevel inverter connected in series with a three-level H-bridge inverter and a multi-output boost converter can provide a three-phase 15-level and 19-level output. In addition to boosting low output voltage renewable energy systems, like solar cells, to the appropriate value of the diode-clamped DC link voltage, the MOB converter may remedy the problem of capacitor voltage imbalance. An innovative kind of power converter designed for high-power applications is the Multilevel Inverter (MLI). Diode-clamped, capacitor-clamped, and cascaded H-bridge inverters are some of the several MLI topologies. In order to generate a nine-level output, this research focuses on a Neutral Point Clamped MLI that employs two unequal DC sources. The number of DC sources and switching components is decreased by the suggested architecture[12]. The literature has described a variety of modulation techniques for MLI; however, the focus of this study is on the unipolar Inverted Sine PWM (ISPWM) approach. With a decrease in Total Harmonic Distortion (THD), switching losses, and leakage current, the unipolar Inverted Sine Carrier Pulse-Width Modulation (ISCPWM) technique improves the fundamental output voltage while decreasing the number of carriers, especially at lower modulation index ranges. MATLAB is used to assess the effectiveness of the suggested PWM technique for a three-phase multilevel inverter, and the best switching frequency with the least amount of switching loss and total harmonic distortion is found. Several triangular carrier signals are used in the multicarrier PWM technique, but only one modulating sinusoidal signal is maintained. "n-1" carriers will be required if a "n"-level inverter is used. The carriers are positioned so that the bands they occupy are continuous, and they will all have the same frequency and peak-to-peak amplitude. The carrier set's center is where the zero reference is located. The carrier waveform that is based on triangles is replaced with an inverted sine wave in the suggested unipolar control technique. When considering PWM, inverted sine PWM is superior to triangular-based PWM in terms of spectrum purity and basic voltage. Reducing carrier frequencies or their multiples and switching losses significantly are the outcomes of applying unipolar PWM to the inverted sine carrier. This improves the hybrid multilevel inverter's performance by combining the benefits of unipolar PWM and inverted sine.

The inverted sine carrier PWM (ISCPWM) technique helps to maximize the output voltage for a given modulation index by using an inverted (high-frequency) sine carrier as the carrier signal, with the sine wave serving as the reference signal. Every time the inverted sine carrier wave's amplitude is larger than the reference sine wave's, pulses are produced. Comparing the ISCPWM approach to traditional sinusoidal PWM (SPWM), it has a greater fundamental component and superior spectral quality without any pulse dropping. The ISCPWM approach lowers switching losses and total harmonic distortion (THD) while improving the fundamental output voltage, especially at lower modulation index ranges.

Generation of using ISPWM

Computer simulations are used to confirm whether the suggested method is feasible. MATLAB-Simulink is used to create a model of the 19- and 15-level inverters. A novel approach is used, which uses fewer switches. It takes sixteen switches to operate the cascaded H-Bridge 15-level and 19-level inverters. One benefit of the new topology over the traditional cascaded H-bridge multilevel inverter is that it uses fewer devices. By utilizing the Inverted Sine PWM model, the suggested architecture lowers harmonics. The pulses are produced by the PD method. As seen in Fig. 7 the suggested method requires sine carriers for the generation of gate pulses; the results display a comparison of the carrier and reference signals.

III. RESULTS OF SIMULATIONS

Computer simulations are utilized to confirm the practicality of the suggested methodology. Using MATLAB-Simulink, a model of the 19- and 15-level inverters is built. A novel approach utilizing fewer switches is utilized. 16 switches are needed for the cascading H-Bridge 15-level and 19-level inverters. When compared to the traditional cascaded H-bridge multilevel inverter, the novel topology offers the advantage of requiring fewer devices[16]. The Inverted Sine PWM model is used in the suggested architecture to reduce harmonics. The pulses are produced using the PD approach. For gate pulse production, the suggested approach requires sine carriers, as illustrated in Fig. 7, and the findings display a comparison of the reference and carrier signals. Eight of the generated output pulses from the Inverted Sine PWM block are displayed below. These pulses are needed to use the Inverted Sine PWM converter to turn the devices on.

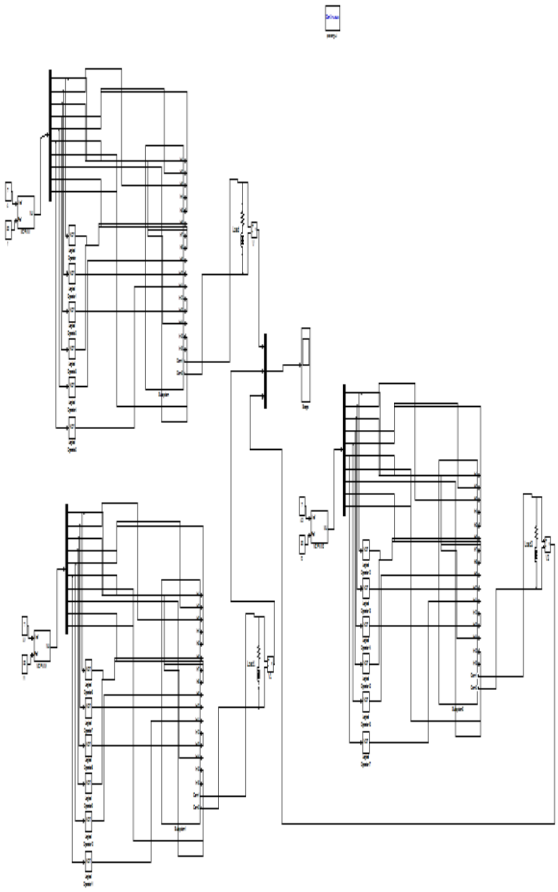

FIG1 SIMULATION DIAGRAM FOR 15 AND 19 LEVEL H-BRIDGE CASCADED INVERTER TOPOLOGY

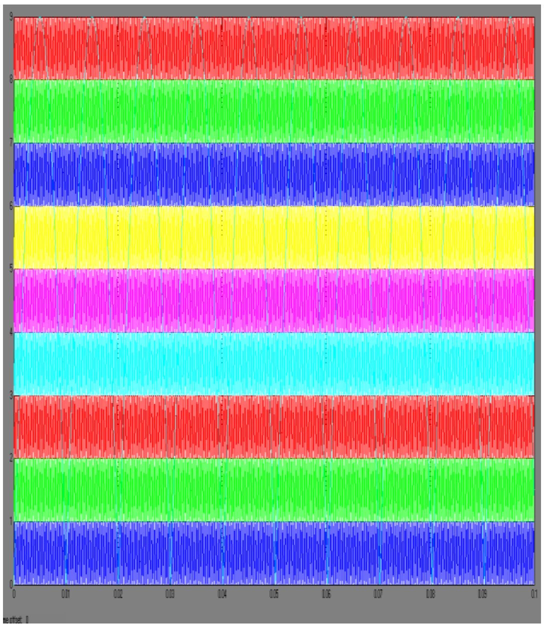

FIG 2 INVERSE SINE PWM

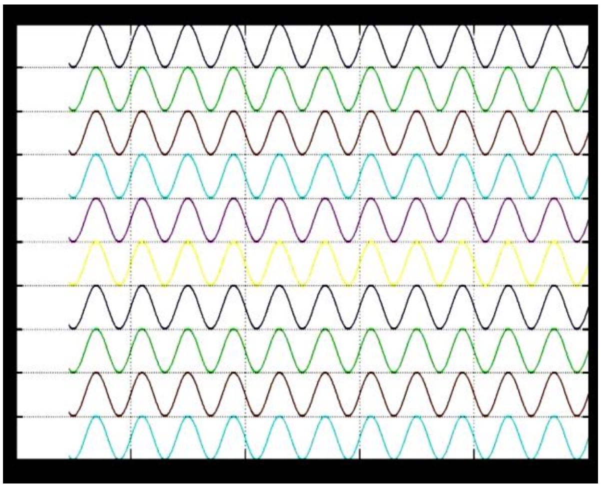

FIG 3 CARRIER SIGNAL

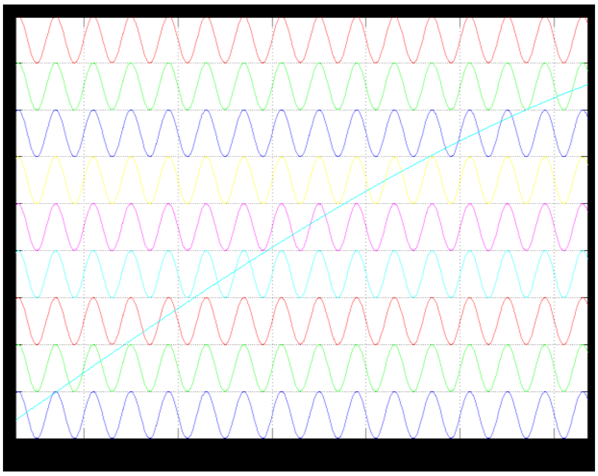

FIG 4 ZOOM VIEW INVERSE SINE PWM

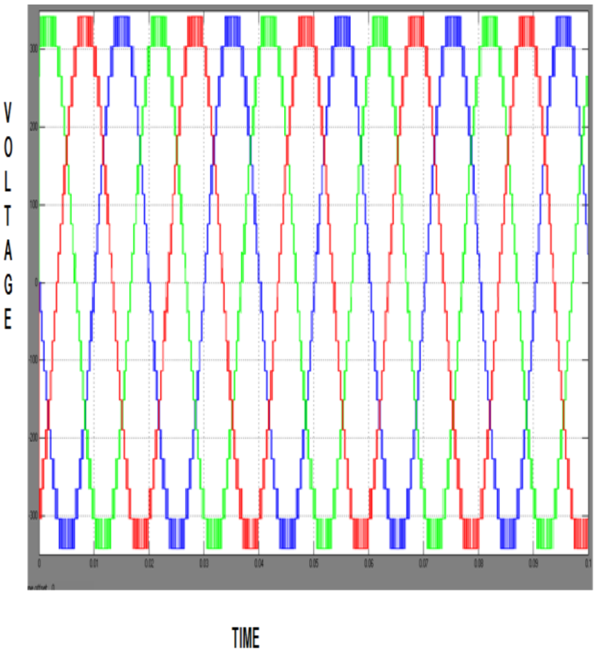

FIG 5 THREE PHASE OUTPUT 19 LEVEL H-BRIDGE CASCADED INVERTER TOPOLOGY

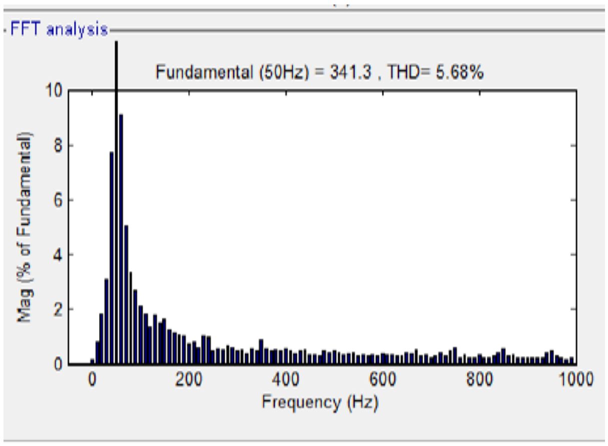

FIG 6 %THD FOR 19 LEVEL H-BRIDGE CASCADED INVERTER TOPOLOGY

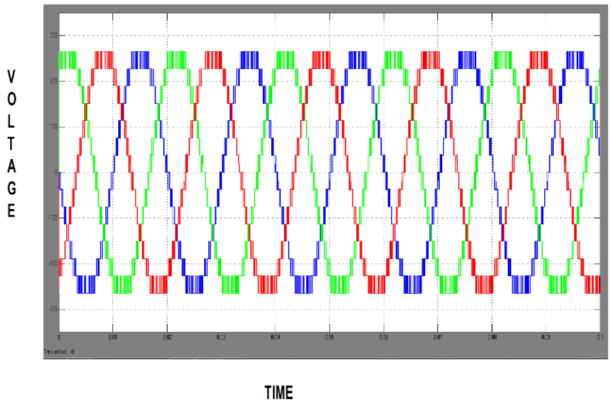

FIG 11 THREE LEVEL OF SINGLE PHASE OUTPUT 19 LEVEL H-BRIDGE CASCADED INVERTER TOPOLOGY

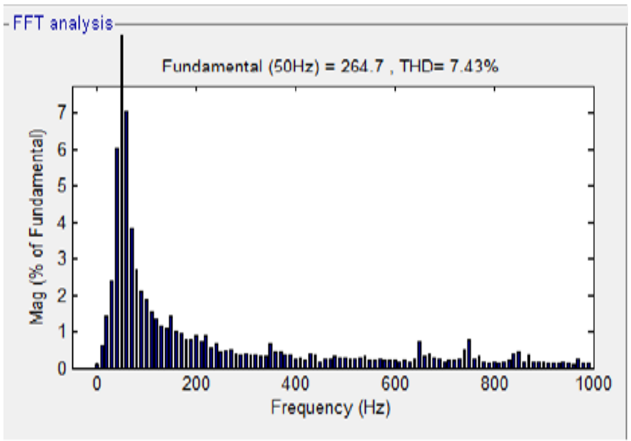

FIG 7 %THD FOR 15 LEVEL H-BRIDGE CASCADED INVERTER TOPOLOG

The ripple was 5.86% in the 19-level converter and 7.43% and 10% in the 15-level conversion, respectively. The Total Harmonic Distortion (THD) of the output voltage in the suggested hybrid converter with ADCC is still less than that of the converter with an SDCC configuration, with or without the use of additional switching modulation techniques, even when grabbing into account the DC link ripple. The simulation's outcomes allow for the following deductions to be made The suggested hybrid cascade converter may provide four more voltage levels in the output voltage by using ADCC instead of SDCC, which improves harmonic characteristics while using the same amount of components and switching. The additional losses must be taken into account even though the first PWM approach (with additional switching) yields a better THD than the second PWM method (without additional switching)[18].

By employing ADCC rather than SDCC, the suggested hybrid cascade converter boosts the harmonic features while utilizing the same amount of components and switching to provide four more voltage levels in the output voltage. It is necessary to consider the additional losses even if the first PWM strategy (with additional switching) produces better THD than the second PWM method (without additional switching).

IV. Conclusions

Diode-clamped multilevel H-bridge cells cascaded with three-level conventional inverters were introduced in this study to boost converter efficiency with excellent output voltage resolution. For the three-level H-bridge and multilevel diode-clamped inverters, a new DC link voltage rating is suggested in order to guarantee neighboring switching vectors over all voltage levels. The diode-clamped inverter used the MOB converter as a DC link provider to increase and control the voltage of the capacitors to the appropriate DC link levels[16].

By cascading an asymmetrical seven-level H-bridge diode-clamped inverter, a novel cascade inverter was verified using the MOB converter. In contrast to a symmetrical diode-clamped inverter with the same design and an analogous number of power components, performance with a nineteen-level output voltage was attained, offering more voltage levels and reduced voltage and current THD. Predictive current control was used to show how well the suggested approach worked. Two distinct approaches to switching state selection were put forth in this instance in an effort to reduce losses or THD in hybrid converters. New H-bridge cells were presented.

References

[1] J.-C. Wu, C.-W. Chou, A solar power generation system with a seven-level inverter, IEEe Trans. Power. Electron. 29 (7) (2013) 3454–3462. [2]

[2] D. Ganesh, G. Chandra Sekhar, Simulation of three phase nine-level inverter for interfacing with solar PV system, Int. J. Innov. Res. Sci. Eng. Technol. 6 (8) (2017).

[3] A. Bughneda, M. Salem, A. Richelli, D. Ishak, S. Alatai, Review of multilevel inverters for PV energy system applications, Energies 14 (6) (2021) 1585.

[4] U. Amin, M. Ahmed, S. Aftab, Z. Ahmed, Integration of renewable energy resources in microgrid, Energy Power. Eng. (7) (2015) 12–29. [5] M. Faisal, M.A. Hannan, P.J. Ker, A. Hussain, M. Bin Mansor, F. Blaabjerg, Review of energy storage system technologies in microgrid applications: issues and challenges, IEEE Access. [6] (2018) 35143–35164. [6] M. Sami, M.A. Mallick, Cascaded H-bridge 11-level multilevel inverter, Int. J. Eng. Res. Technol. (IJERT) 10 (6) (2021) 223–226.

[7] W. Gil-Gonz´ alez, O.D. Montoya, A. Garces, Modeling and control of a small hydropower plant for a DC microgrid, Electr. Power Syst. Res. 180 (2020) 106104.

[8] A.I.M. Ali, M.A. Sayed, A.A.S. Mohamed, Seven-level inverter with reduced switches for PV system supporting home-grid and EV charger, Energies 14 (9) (2021) 2718.

[9] P. Balapriyan, K. Veeraragavan, Design and analysis of 7-level inverter at different modulation indices with a closed loop control, Int. J. Pure Appl. Math. 119 (14) (2018) 637–642.

[10] R. Al Badwawi, M. Abusara, T. Mallick, A review of hybrid solar PV and wind energy system, Smart Sci. 3 (3) (2015) 127–138.

[11] E. Desarden-Carrero, R.D. Zamora, E. Aponte-Bezares, E.I. Ortiz-Rivera, SevenLevel Cascaded H-Bridge Multilevel Single-Phase Inverter Implemented with an ATMEGA Microprocessor, in: 2022 IEEE 49th Photovoltaics Specialists Conference (PVSC), 2022, pp. 916–922.

[12] T. Abhilash, A. Kirubakaran, V.T. Somasekhar, A novel three-phase seven-level inverter, in: 2017 Innovations in Power and Advanced Computing Technologies (iPACT), 2017, pp. 1–5.

[13] A.M. Mahfuz-Ur-Rahman, et al., Model predictive control for a new magnetic linked multilevel inverter to integrate solar photovoltaic systems with the power grids, IEEE Trans. Ind. Appl. (2020) 7145–7155, 56.6.

[14] U. Gajula, Reduced switch multilevel inverter topologies and modulation techniques for renewable energy applications, Turk. J. Comput. Math. Educ. (TURCOMAT) 12 (3) (2021) 4659–4670.

[15] D. Karthikeyan, K. Vijayakumar, Jagabar Sathik, Generalized cascaded symmetric and level doubling multilevel converter topology with reduced THD for photovoltaic applications, Electronics (2019) 161, 8.2.

[16] Z. Zhang, X. Yang, Z. Wang, Z. Chen, Y. Zheng, Highly applicable small hydropower microgrid operation strategy and control technology, Energy Rep. 6 (2020) 3179–3191. [17] R.S. Jadhav, S.B. Patil, Design and Implementation of PV-Wind Battery Hybrid System for Off Grid and On Grid, in: 2020 Fourth International Conference on Inventive Systems and Control (ICISC), 2020, pp. 612–618.

[18] M.H. Uddin, M.A. Baig, M. Ali, Comparision of ‘perturb & observe’and ‘incremental conductance’, maximum power point tracking algorithms on real environmental conditions, in: 2016 International Conference on Computing, Electronic and Electrical Engineering (ICE Cube), 2016, pp. 313–317.

AI-Powered Classification of Transient Disturbances in Microgrid Systems

Suriya Priya G
Department of EEE,
P.S.R.R College of Engineering,
Sivakasi, India
suriyapriya@psrr.edu.in

Geethanjali M
Department of EEE,
Thiagarajar College of Engineering,
Madurai, India
mgeee@tce.edu

Meenakshi Devi M
Department of EEE,
Thiagarajar College of Engineering,
Madurai, India
mmdeee@tce.edu

***Abstract*—Modern power systems must incorporate Microgrid technology to ensure efficiency and dependability while preserving power quality due to the rising demand for electricity. However, because power quality problems are so complicated, it is still very difficult to detect and categorize transient disturbances in microgrids. This paper suggests a novel machine learning method based on Decision Trees (DT) for the precise identification and categorization of fleeting events in microgrid settings. Phase voltage and current signals are tracked at several points as part of the methodology. Relevant features are then extracted through signal processing utilizing the Discrete Wavelet Transform (DWT). The DT classifier uses the retrieved DWT coefficients as input and successfully distinguishes between symmetrical and unsymmetrical faults as well as other transient circumstances. Numerous simulation studies validate the high classification accuracy achieved by the proposed method.The results confirm the robustness and effectiveness of the proposed method in enhancing power quality monitoring and microgrid network problem diagnosis.**

Keywords—Discrete Wavelet, Decision Tree, Microgrid, Transients

I. INTRODUCTION

The rise in electricity demand and decentralized generation has driven widespread adoption of microgrids, valued for their efficiency and reliability. However, ensuring power quality is challenging due to transient disturbances like faults and grid islanding. Traditional detection methods often lack the speed and accuracy needed for real-time microgrid environments. The growing integration of RES, EVs, and DERs further complicates fault diagnosis, highlighting the need for advanced, data-driven techniques. Machine learning has emerged as a promising solution to improve accuracy and adaptability in modern protection systems [1–3].Recent studies highlight the growing need for adaptive and intelligent protection strategies in power systems with increasing distributed generation (DG) integration. Ensemble learning and wavelet-based CNNs have shown high accuracy in fault detection across high-voltage networks and microgrids [4–6], while decision-tree classifiers effectively identify switching transients [7]. Hybrid models combining deep learning with transformer architectures have improved fault classification performance [8]. Communication-free detection methods and digital-twin-based diagnosis enhance reliability in islanded microgrids and clustered networks [9–10]. In active distribution and multi-terminal DC systems, techniques like optimized machine learning, outlier-filtered weighted least squares, and novel protection schemes have been proposed [11–13]. CNNs and recurrence plot-based methods further enhance disturbance classification [14], and reviews affirm the value of robust machine learning in practical fault diagnosis [15]. Recent approaches also include CNN-based protection for microgrids [16], adaptive schemes for DG-integrated AC networks [17], and fault detection using SVM and Gaussian Process Regression [18]. Coordinated current-based fault control strategies have also been introduced to strengthen resilience in renewable microgrids [19]. This research introduces a machine learning-based DT approach for the classification of transient occurrences in microgrids. The proposed method leverages DWT for feature extraction, ensuring precise and efficient identification of transient events. Extensive case studies validate the high classification accuracy of the approach, demonstrating its effectiveness in enhancing microgrid resilience and improving power quality monitoring.

II. PROBLEM FORMULATION

Transmission lines encounter transients from faults, load shifts, and capacitor switching, impacting stability and power quality. Traditional methods often misclassify these events. This study analyzes five key disturbances—LG, LLG, LLL faults, load changes, and capacitor switching—highlighting the need for advanced techniques to accurately detect significant voltage and current changes. For instance, an LG fault in a three-phase system causes an unbalanced condition where the fault current I_f can be represented by equation (1),

$$I_f = \frac{V_{Ph}}{Z_f + Z_{act}} \tag{1}$$

Where V_{Ph} is the phase voltage, Z_f is the fault impedance, and Z_{act} is the actual system impedance. Transient over currents and voltage dips can cause relay malfunctions, while severe faults like LLG and LLL introduce high fault currents and system imbalances. Load variations further challenge protection by causing voltage and frequency instability. This phenomenon is displayed in equation (2),

$$M \frac{d^2\delta}{dt^2} = P_m - P_e \tag{2}$$

Where the moment of inertia is M, δ is the rotor angle, P_m is the mechanical input power, and P_e is the electrical output power. Sudden load variations cause disturbances in δ, affecting system stability and increasing the likelihood of incorrect fault detection. Capacitor switching transients cause high-frequency oscillations from sudden capacitor charge and discharge. The transient inrush current can be calculated by following equation (3),

$$I_{inrush} = \frac{V_{act}}{\sqrt{L/C}} \tag{3}$$

Where $Vact$ is the actual system voltage, L is the inductance, and C is the capacitance of the switching bank. Transients can resemble fault waveforms, making them hard to distinguish using traditional methods. This study uses a hybrid DWT-DT approach for accurate, fast classification, enhancing protection in microgrid transmission lines.

III. METHODOLOGY

Accurate transient classification is vital for reliable line protection, but traditional methods often fall short. This study combines DWT for feature extraction and DT for classification, improving reliability through ML adaptability. The next section details the methodology.

A. Feature Extraction by Discrete Wavelet Transform

The DWT is employed to analyze transient disturbances by decomposing the original signal into different frequency bands, enabling the extraction of time-frequency information. The input voltage or current signal is passed through a series of high-pass and low-pass filters to obtain detailed and approximate coefficients, respectively. The DWT decomposition follows the equation by (4) and (5),

$$\psi_{j,n}[t] = 2^{j/2} \sum_n d_{j,n}\ \psi[2^j t - n] \quad (4)$$

$$\varphi_{j,n}[t] = 2^{j/2} \sum_n C_{j,n}\ \varphi[2^j\ t - n] \quad (5)$$

Where n are the decomposition level, and $d_j$and C_j wavelet scaling coefficient, respectively, at scale j . This decomposition is performed iteratively, generating multiple levels of wavelet coefficients, with high-frequency components capturing transients and low-frequency components retaining steady-state information. The decomposition level is shown in Fig.1. The Energy (E) of the wavelet coefficients at each level j is calculated by equation by (6),

$$E_j = \sum_n \left|C_{j,n}\right|^2 \quad (6)$$

B. Decision Tree Classifier

After feature extraction from wavelet coefficients, a DT classifier categorizes transient disturbances. DTs are effective for handling nonlinear patterns and offer interpretable rules. Features like energy, entropy, mean, and variance guide the tree's threshold-based splits [20]. The classification process begins with entropy criterion Gini Index (GI) to determine the best feature for splitting at each node. The GI, which measures the impurity of a node, is calculated as by equation (7),

$$GI = 1 - \sum_{i=0}^{n} {p_i}^2 \quad (7)$$

Where p_i represents the probability of a particular class in the dataset.

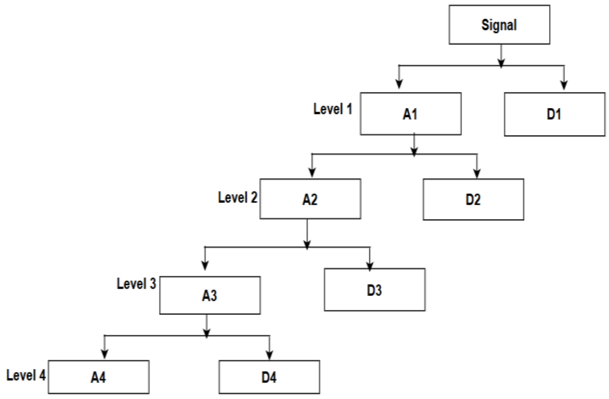

FIG.1. DECOMPOSITION LEVEL OF DWT

A lower EC indicates a purer node. Alternatively, entropy-based splitting can be used, where the entropy of a node is given by equation (8),

$$H = 1 - \sum_{i=1}^{n} p_i \log_2 p_i \quad (8)$$

Where H represents the entropy of the node the impurity of the dataset is measured. At each step, the DT algorithm selects the feature that provides the maximum information gain, which is computed by equation (9),

$$IG = H_{parent} - \sum \left(\frac{|D_i|}{|D|} H_i\right) \quad (9)$$

Where $Hparent$ represents the entropy of the parent node before the split, and H_i denotes the entropy of each child node after the split. The dataset D consists of all training samples at a given node, while D_i represents the subsets (child nodes) formed after splitting. The fraction reflects each child node's sample proportion. Higher Information Gain (IG) helps identify features that reduce uncertainty, guiding optimal tree splits. The final DT efficiently classifies faults, switching transients, and normal conditions for real-time microgrid protection. The DT flowchart is shown in Fig. 2.

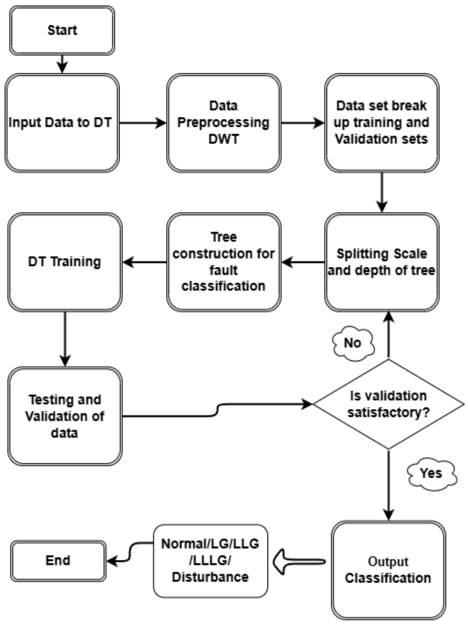

FIG.2. DT CLASSIFIER OPERATION

IV. SIMULATION RESULTS

The study utilizes an IEEE 9-bus test system integrated with an AC microgrid comprising diesel generators (440 V, 500 MVA) and two photovoltaic systems (30 kW, 500 V each). The system powers five loads (four at 20 kW, one at 40 kW) and consists of six transmission lines (1 km each, divided into five 0.2 km π-section lines). The transmission lines have a resistance of 0.01273 Ω/km, inductance of 0.9329 mH/km, and capacitance of 12.7 nF/km. This setup serves as a benchmark for testing AI-based classification methods for transient disturbances in microgrids. The system structure is shown in Fig. 3.

C. Fault on Line

LG, LLG, and LLLG faults are studied in both grid-connected and islanded microgrid modes, with fault currents exceeding five times their normal level. Voltage and current outputs for the LG fault are shown in Fig. 4, the LLG fault in Fig. 5, and the LLLG fault in Fig. 6. These disturbances modify voltage and current characteristics, which are used as features for classification by the DT classifier.

D. Dynamic Load Variation

The system undergoes dynamic simulations to analyze load variations, rapid EV charging, transformer energization, and capacitor switching [22]. PV integration at buses 1 and 2 assesses the impact of fast charging on load current and system deviations, with voltage and current waveforms shown in Fig. 7. Simulations also examine transformer capacitor switching, with switching events occurring at 0.4 s. Relays are not needed, as these changes are temporary and part of normal system operation. Table I presents the features (F1 to F6) extracted using DWT for different fault scenarios. These features effectively capture variations in signal characteristics, crucial for fault classification. Results show distinct feature values for each fault type, and capacitor switching displays notably higher feature values, highlighting its unique transient behavior. Table II evaluates the predictive model's classification performance, showing an accuracy of over 96% for all fault types. LG, LLG, and LLLG faults were classified with an accuracy range of 96.67% to 98.97%, confirming the model's high reliability.

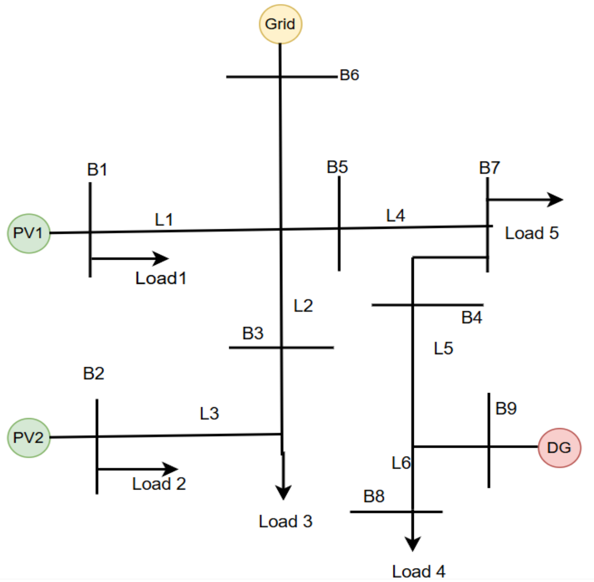

FIG.3. STRUCTURE OF MICROGRID TEST SYSTEM

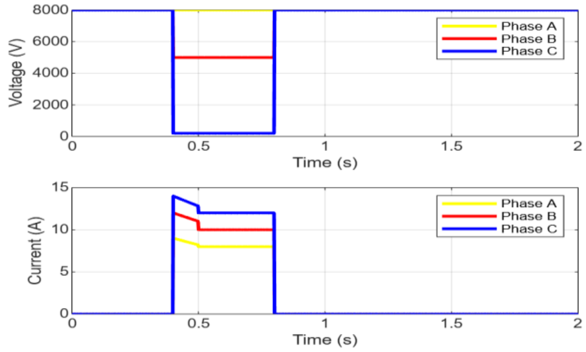

FIG.4. LG FAULT ON LINE

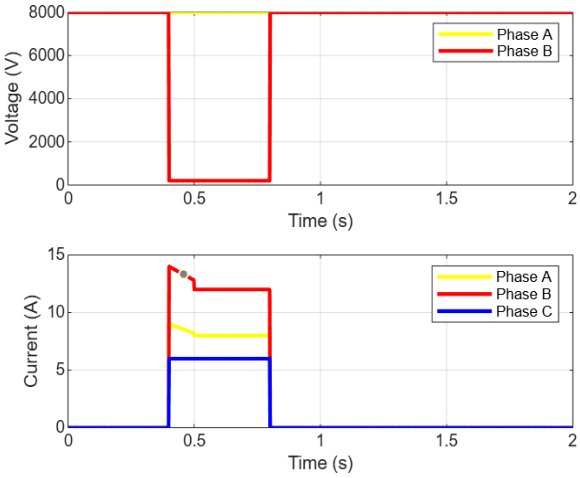

FIG.5. LLG FAULT ON LINE

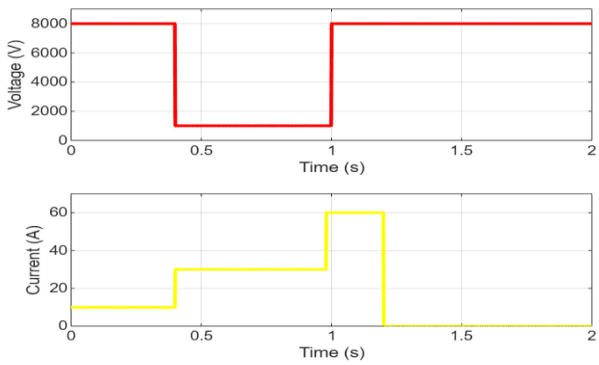

FIG.6. LLLG FAULT ON LINE

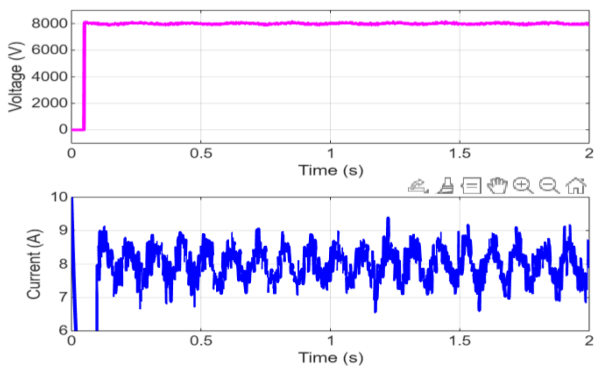

FIG.7. CAPACITOR SWITCHING EVENT ON LINE

TABLE I. DWT FEATURE EXTRACTION

Action applied	F1	F2	F3	F4	F5	F6
LG Fault	0.88172	−0.27405	0.767589 –	−0.27546	−0.17424	−0.51321
LLG Fault	0.815523	−0.11665	0.534524	−0.11717	−0.86812	−0.35345
LLLG	0.82208	−0.25631	0.642056	−0.26523	−1.57896	−0.45658
Switching Event	8.27043	−0.18609	1.154412	−0.18789	−0.16425	−0.21465

TABLE 2. VARIOUS PREDICTED FAULT CASES

Action applied	Action Predicted	Actual fault line	Predicted line	Prediction accuracy
LG	LG	L1	L1	98.97%
LLG	LLG	L2	L2	98.24%
LLLG	LLLG	L5	L5	96.67%
LG	LG	L4	L4	98.97%
LLG	LLG	L4	L4	98.24%
LLG	LLG	L6	L6	98.97%

V. CONCLUSION

This work presents a DT-based machine learning method for accurate classification of transient disturbances in microgrids. Using DWT for feature extraction, the approach effectively distinguishes between various faults and transients. Simulation results confirm high classification accuracy, enhancing fault diagnosis and power quality monitoring. Future work may explore real-time implementation and adaptive learning to improve performance under dynamic conditions.

Acknowledgment

The authors thank P.S.R.R. College of Engineering, Sivakasi, and Thiagarajar College of Engineering, Madurai, for their support and guidance in this research.

REFERENCES

[1] Agrawal, A., Arya, P. K., & Singh, R, “Analysis and real- time implementation of power line disturbances test in smart grid. In Green Machine Learning and Big Data for Smart Grids”, pp. 49–68, 2025, Elsevier. https://doi.org/10.1016/B978-0-443-28951-4.00005-8

[2] Anwar, T., Mu, C., Yousaf, M. Z., Khan, W., Khalid, S., Hourani, A. O., & Zaitsev, I. “Robust fault detection and classification in power transmission lines via ensemble machine learning model”, Scientific Reports, vol. 15(1), pp. 2549, 2025. https://doi.org/10.1038/s41598-025-86554-2

[3] Arévalo, P., Cano, A., Fedoseienko, O., & Jurado, F, “A data-driven approach to microgrid fault detection and classification using Taguchi-optimized CNNs and wavelet transfor”, Applied Soft Computing, vol. 170,112667, 2025 .https://doi.org/10.1016/ j.asoc.2024.112667

[4] Banerjee, S., & Bhowmik, P. S, “A comparative study of decision tree-based learners to classify the switching transient disturbances in real microgrid network”, Smart Science, 1–11, 2025. https://doi.org/10.1080/23080477.2025.2452047

[5] Chhetija, D., Rather, Z. H., & Doolla, S, “A Communication-Free Fault Detection and Classification Scheme for Power Islands”, IEEE Transactions on Industry Applications, vol.60(3), pp.4921–4932, 2024. https://doi.org/10.1109/TIA.2024.3353722

[6] Ding, L., Chen, Y., Xiao, T., Huang, S., Shen, C., & Guo, A, “Topology-aware fault diagnosis for microgrid clusters with diverse scenarios generated by digital twins”, Applied Energy, vol.378, 2025. https://doi.org/10.1016/j.apenergy.2024.124794

[7] Dubey, K., & Jena, P, “Novel Fault Detection & Classification Index for Active Distribution Network Using Differential Components”, IEEE Transactions on Industry Applications, vol. 60(3), pp. 4530–4540, 2024. https://doi.org/10.1109/TIA.2024.3351617

[8] Gholami, A., Tiwari, A., Qin, C., Pannala, S., Srivastava, A. K., Sharma, R., Pandey, S., & Rahmatian, F, “Detection and Classification of Anomalies in Power Distribution System Using Outlier Filtered Weighted Least Square”, IEEE Transactions on Industrial Informatics, vol 20(5), pp.7513–7523, 2024. https://doi.org/10.1109/TII.2024.3360523

[9] Gupta, P. K., & Samantaray, S. R, “Enhanced primary protection scheme for MTDC network using modified linear quadratic score”, Electric Power Systems Research, 242, 2025. https://doi.org/10.1016/ j.epsr.2025.111418

[10] Jana, C., Banerjee, S., Maur, S., & Dalai, S, “Customized CNN based classification of power system disturbances using recurrence plots”, Electric Power Systems Research, 241, 2025. https://doi.org/10.1016/j.epsr.2024.111370

[11] Kumari, K., Dubey, M., & Kumar Kirar, M, “Detection and Classification of Faults in AC Microgrids based on Wavelet Transform”, IEEE International Students Conference on Electrical, Electronics and Computer Science (SCEECS), 1–6, 2024. https://doi.org/10.1109/SCEECS61402.2024.10482289

[12] Mishra, M., & Singh, J. G. “Fault Detection and Localization in an MT-VSC-HVDC Network via a Hybrid CNN- Transformer Model with a Multi-head Attention Mechanism”, IEEE Access, vol.1–1, 2025. https://doi.org/10.1109/ACCESS.2025.3534247

[13] Najafzadeh, M., Pouladi, J., Daghigh, A., Beiza, J., & Abedinzade, T. “Fault Detection, Classification and Localization Along the Power Grid Line Using Optimized Machine Learning Algorithms”, International Journal of Computational Intelligence Systems, vol.17(1), pp.49, 2024. https://doi.org/10.1007/s44196-024-00434-7

[14] Rosero-Morillo, V. A., Gonzalez-Longatt, F., Quispe, J. C., Salazar, E. J., Orduña, E., & Samper, M. E, “Emerging Trends in Active Distribution Network Fault Detection”, Renewable Energy Focus, vol.53, 2025. https://doi.org/10.1016/j.ref.2025.100684

[15] Zaben, M. M., Worku, M. Y., Hassan, M. A., & Abido, M. A, "Machine Learning Methods for Fault Diagnosis in AC Microgrids: A Systematic Review", IEEE Access, vol.12, pp.20260–20298, 2024. https://doi.org/10.1109/ACCESS.2024.3360330

[16] Bukhari, S. B. A., Kim, C., Mehmood, K. K., Haider, R., & Saeed Uz Zaman, M, "Convolutional Neural Network- Based Intelligent Protection Strategy for Microgrids", IET Generation, Transmission & Distribution, vol 14(7), pp.1177–1185, 2025. https://doi.org/10.1049/iet-gtd.2018.7049

[17] Sarangi, S., Sahu, B. K., & Rout, P. K, "Review of distributed generator integrated AC microgrid protection: issues, strategies, and future trends", International Journal of Energy Research, vol.45(10), pp.14117–14144, 2021. https://doi.org/10.1002/er.6689

[18] Srivastava, A., & Parida, S. K, "A Robust Fault Detection Location Prediction Module Using Support Vector Machine and Gaussian Process Regression for AC Microgrid", IEEE Transactions on Industry Applications, vol.58(1), pp.930–939, 2022. https://doi.org/10.1109/TIA.2021.3129982

[19] Wang, Z., Mu, L., & Fang, C, "Renewable Microgrid Protection Strategy Coordinating with Current-based Fault Control", Journal of Modern Power Systems and Clean Energy, vol.10(6), pp.1679– 1689. https://doi.org/10.35833/MPCE.2022.000079

[20] Miraj, S., Nair, D. S., & T., R, "A novel grid dynamics indicator based advanced relay for grid connected microgrid under volatile conditions", Electric Power Systems Research, 242, 2025. https://doi.org/10.1016/j.epsr.2025.111460

[21] Zhou, Q., Zhang, S., Li, Y., Li, Z., Fang, Q., & Huang, H, "Disturbance Classification Method for Microgrids Based on EEMD- Transformer-SVM", IEEE Access, vol.11, pp.78934–78944. https://doi.org/10.1109/ACCESS.2023.3298358

[22] Banerjee, S., & Sarathee Bhowmik, P, "Machine learning based classifiers for dynamic and transient disturbance classification in smart microgrid system", Measurement, vol.240, 2025. https://doi.org/10.1016/j.measurement.2024.115576

Hybrid Energy Storage Systems for Vehicle-to-Everything (V2X) Power Transfer Applications

M. Santharam
Department of Electrical and Electronics Engineering, Thiagarajar College of Engineering,
Madurai, India
msantharam175@gmail.com

B. Ashok Kumar
Department of Electrical and Electronics Engineering, Thiagarajar College of Engineering,
Madurai, India.
ashokudt@tce.edu

N. Jegan
Department of Electrical and Electronics Engineering, Thiagarajar College of Engineering,
Madurai, India.
njee25@gmail.com

Mothiga Shivani J
Department of Electrical and Electronics Engineering, Thiagarajar College of Engineering,
Madurai, India
mothigashivani@student.tce.edu

***Abstract*—Vehicle-to-Everything (V2X) technology is revolutionizing transportation by enabling seamless power transfer between electric vehicles (EVs) and their surrounding by Integrating hybrid energy storage systems (HESS) with V2X technology enhances energy efficiency of grid and vehicle performance. This paper explores the role of HESS in V2X applications by discussing its impact on vehicle-to-grid (V2G) and vehicle-to-home (V2H) interactions. To optimize V2X performance Hybrid Energy Storage Systems (HESS) integrating lithium-ion batteries and supercapacitors are being incorporated into EV architectures to improve energy transfer efficiency extend battery lifespan and enhance power quality. The integration of V2X and HESS offers transformative opportunities for smart grids particularly with the incorporation of renewable energy with control strategies to ensure efficient bidirectional power flow and energy optimization. HESS combining batteries with supercapacitors will optimize power quality by managing transient loads. In this paper focus on the challenges and future prospects of this integration for sustainable transportation.**

Keywords*—Vehicle-to-Everything (V2X), Hybrid Energy Storage Systems (HESS), Electric Vehicles (EV), Vehicle-to-Grid (V2G), Vehicle-to-Home (V2H), Sustainable Transportation, Energy Management, Grid Stability.

I. INTRODUCTION

Electric vehicles (EVs) are gaining popularity due to their environmental benefits. Vehicle-to-Everything (V2X) technology enables communication The rise of EVs has accelerated developments in energy management and grid interaction, with V2X enabling bidirectional energy flow to grids, homes, and infrastructure [2]. V2X applications like V2G and V2H provide flexibility, resilience, and sustainability [3-5]. Integrating HESS into EVs improves energy efficiency, extends battery life, and enhances power quality. Together, V2X and HESS offer transformative benefits for smart grids and renewable energy integration, supported by advanced power electronics and control strategies. Combining advanced Energy Storage Systems (ESS) with V2G enhances sustainable energy management and grid stability [6]. Future ESS developments, including solid-state and next-gen lithium-ion batteries, aim to boost energy density, efficiency, and durability during V2G operations [7]. HESS will manage transient loads and capture regenerative energy, improving power quality. Research will focus on grid-interactive ESS, large-scale renewable integration, and decentralized energy trading [8-11]. Standardizing V2G communication protocols and smart charging infrastructure will be key to scaling V2G-enabled ESS, creating a more flexible and resilient energy ecosystem.

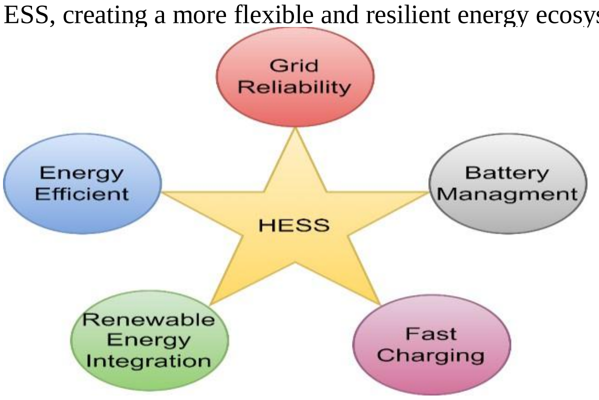

II. SYSTEM OVERVIEW

A. Vehicle to Grid

Vehicle-to-Grid (V2G) technology enables plug-in electric vehicles (PEVs) to supply power and energy to various grid management entities which including system operators, distribution utilities with integrated load-serving entities and other grid managers. Unlike Vehicle-to-Home (V2H) and Vehicle-to-Building (V2B) operations V2G offers a broader range of grid connection. The V2G framework consists of multiple components such as parking lots, V2H systems, smart buildings, loads also interconnected with renewable energy sources with clusters organized by voltage levels in the grid [12].

The first cluster, operating in the low- voltage (LV) network supports V2H functionalities and is typically found in residential areas, smart buildings and parking lots. The second cluster situated in the medium- voltage (MV) network facilitates V2G operations enabling bidirectional energy flow between EVs and the grid. Both clusters contribute to reactive power support via their capacitors stabilizing grid voltage levels [13-15]. V2G technology provides a range of grid-supporting services including backup power during renewable energy intermittency, peak shaving and reactive power regulation harmonic compensation in grid current and ancillary services such as voltage and frequency stabilization can be improved with reactive power support essential for balancing supply and demand as it helps regulate bus voltages by injecting reactive power into the grid. By charging during off-peak hours and discharging during peak demand V2G can improve voltage profiles and optimize grid performance. Various control strategies enhance both steady-state and dynamic response improving robustness in active and reactive power are determined by grid allowing V2G to efficiently manage variations in grid power demand. V2G systems incorporate charge equalization circuits (CECs). Energy management systems (EMS) and droop control techniques are employed to optimize distributed energy in EVs and regulate charging/discharging cycles while V2G helps mitigate generation uncertainty in renewable energy integration with smart charging and stochastic programming are essential to minimize battery degradation and handle uncertainties in EV charging behaviour [16-18].

A critical component of the V2G ecosystem is the aggregator in the system serves as an intermediary between EVs and the grid managing load profiles and optimizing energy transactions [19]. The aggregator operates in two key steps: first, it gathers data from connected EV fleets to determine their charging needs, ensuring that vehicles reach the required charge levels before disconnection. Second, it interfaces with the grid to identify services that EVs can provide and the amount of power that can be exchanged [20]. Smart buildings integrated with V2G can further optimize energy usage by storing and distributing excess energy to local devices and low-voltage networks. By facilitating power and information between the grid and grid-enabled vehicles (GEVs) the aggregator enhances overall system efficiency [21-23].

For energy distribution, GEVs can be categorized into three main types based on their operational roles within the grid. The effective integration of V2G with smart grid technologies and power electronics will play a crucial role in improving the stability of the grid and sustainability of future energy systems [24].

B. Vehicle to Home

Unlike V2H, Vehicle-to-Building (V2B) operates on a larger scale capable of aggregating entire EV fleets or utilizing a few EVs to optimize a building or microgrid energy consumption [25]. V2B offers more substantial benefits than V2H as it primarily targets commercial and industrial buildings unlocking greater opportunities.

Another study in [32] analyzed V2B economics by determining the break-even price—the amount building operators must compensate EV owners for participation in V2B programs. The findings indicated that V2B economics were less favourable in Canada where battery degradation due to V2B use posed a significant concern. Nissan launched a major V2B project in 2014, using a fleet of Nissan Leafs to explore V2B's potential for reducing building peak demand by integrating the vehicles with a commercial facility. Plug-In Electric Vehicle (PEV) is shown in Fig. 2.

Vehicle to Everything

V2X systems operate under two primary control strategies: centralized and decentralized. In the centralized control model, an aggregator serves as the key component overseeing the optimization and management of EV charging and discharging this approach necessitates continuous access to system data to deliver essential services while optimizing battery capacity, state-of-charge (SOC) and charging schedules. However, as the number of EVs with diverse SOC levels increases maintaining frequency control becomes complex. To mitigate this challenge a decentralized control strategy has been introduced allowing local systems such as office buildings to implement their own optimization methods for V2G operations. This reduces system component costs but relies on real-time communication with each EV in the network by probabilistic decision-making by EV owners.

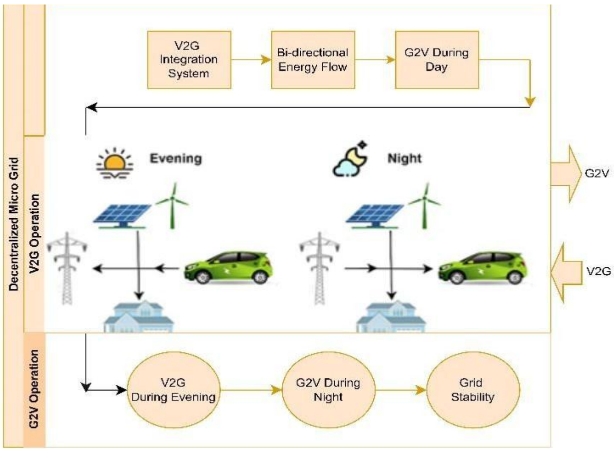

FIG.2 BLOCK DIAGRAM OF PROPOSED SYSTEM.

Demand charges which can constitute over half of an industrial or commercial entity monthly electricity bill result from infrequent but high-load spikes. Even minor reductions in peak demand through V2B can lead to substantial cost savings. Beyond financial benefit V2B integration also reduces carbon emissions defers infrastructure investments and lowers operational expenses [30-33]. However, achieving these advantages requires the expense of integrating fully functional V2B services into a central energy management system which may not be capable of communicating with the broader electric grid instead using micro grid with interleave the major grid is possible solution. V2B applications typically require only a few hours of service per month, delivering high value with minimal time commitment. A study in modeled the use of plug-in hybrid electric vehicles (PHEVs) and EVs for demand management in commercial enterprises aim to enhance power reliability while generating revenue. Commercial and industrial consumers face higher charges and additional fees due to phase imbalances caused by inductive loads which increase power losses [26]. The economics of V2B depend on industrial and commercial rate tariffs which account for both total energy consumption and peak load costs during billing periods. V2B technology is primarily employed to reduce these significant costs by lowering peak loads [27-29]. The centralized control model offers several advantages including the ability to manage large-scale EV fleets provide ancillary services and integrate with diverse transmission and distribution network with renewable energy sources and smart grid infrastructure. It enables broader geographical accessibility and participation in larger electricity markets, leading to higher revenue potential. However, this approach is costly, requiring extensive backup storage, complex communication infrastructure, and significant data processing capabilities. It also demands complete control over EV operations which may raise concerns among users regarding potential interruptions in their charging process. Conversely, decentralized control benefits from a simplified communication framework with greater autonomy which enhanced with the data security increase consumer trust and improved adaptability to EV fleets and energy management systems.

TABLE 1. UNIDIRECTIONAL & BIDIRECTIONAL MODE

Features	Unidirectional mode	Bidirectional mode
Hardware	Communication System, Unidirectional Battery Charger	Communication System, Bi-directional Battery Charger (IGBT, MOSFET)
Power level	Level 1, 2, and 3	Level 3 only
Switches	Diode bridge and unidirectional converter required due to unidirectional flow	Bi-directional energy flow requires complex hardware (IGBT, MOSFET)
Control	Charge current is controlled for timing-sensitive pricing and active control	Complex control circuits for drive and many protections
Cost	Low	High
Distribution system	No further investments required, satisfies most utility criteria with significant PEV penetration	Upgrades and investment required
Battery effects	Battery degradation has been less affected due to fewer cycles of charging and discharging	Regular charging and discharging can increase battery degradation

HESS in EVs enhances battery life by reducing stress on Li-ion batteries improves power delivery by efficiently handling peak demand with the enhance regenerative braking for effective energy recapture that boosts acceleration and performance with rapidly. Where the supercapacitor response and minimizes heat generation making it ideal for application in electric cars (Tesla, BYD, etc.) for improved range and efficiency in electric buses and trucks for high power demands and regenerative braking hybrid electric vehicles (HEVs) HESS enhances grid stabilization by maintaining voltage and frequency stability, improves energy reliability in remote microgrids and off-grid systems, increases charging efficiency and battery life in electric vehicles, and optimizes self-consumption of solar energy in smart homes and buildings.

III. CONCLUSION

This paper has provided a comprehensive analysis of vehicle-to-everything (V2X) technology, which leverages EV batteries to deliver energy services and maximize their utility during periods of non-use. V2X encompasses various operational modes, including vehicle-to-grid (V2G), vehicle-to-building (V2B), and vehicle-to-home (V2H), each defined by its electrical connection and functional approach. The paper examined centralized and decentralized control strategies in V2X systems, along with a comparative analysis of uni-directional and bi-directional power flow and different EV charging methods. Additionally, the integration of V2X with renewable energy sources was explored, highlighting its potential to enhance grid resilience and sustainability.

ACKNOWLEDGMENT

The Authors express our heartfelt gratitude to Thiagarajar College of Engineering, Madurai that supported this research work for their invaluable guidance and support throughout the course of my project.

REFERENCES

[1] K. W. Chew, T. Sadeq, and L. C. Hau, “Ad-vanced adaptive rule- based energy management for hybrid energy storage systems (HESSs) to enhance the driving range of electric vehicles,” Vehicles, vol. 7, no. 1, p. 6, 2025.

[2] G. Mendes et al., “Vehicle-to-everything (V2X): an updated review of key research chal-lenges, implementation barriers, and real-world innovation projects,” in IET Conference Pro-ceedings, vol. 2024, no. 5, pp. 748–758, 2025.

[3] S. Wang, J. A. Cabrera, and F. H. P. Fitzek, “Bidirectional charging use cases: innovations in e-mobility and power-grid flexibility,” arXiv preprint, arXiv:2412.17814, 2024.

[4] A. S. Vigneshwar et al., “The future charged: optimizing electric vehicle performance through advanced power management strategies,” in Proceedings of the 10th International Confer-ence, pp. 775–780, 2024.

[5] M. Farrag, C. S. Lai, M. Darwish, and G. Tay-lor, “Improving the efficiency of electric vehi-cles: advancements in hybrid energy storage systems,” Vehicles, vol. 6, no. 3, pp. 1089–1113, 2024.

[6] J. Gong et al., “Quantifying the impact of V2X operation on electric vehicle battery degradation: an experimental evaluation,” eTransportation, 2024.

[7] T. M. Makuvara and S. K. Gupta, “Enhancing electric vehicle range through hybridization of battery, supercapacitor, and fuel cell systems: in-tegration and optimization using perturb and ob-serve method for hydrogen utilization control,” in E3S Web of Conferences, vol. 564, p. 02008, 2024.

[8] M. A. Rehman et al., “A comprehensive over-view of vehicle to everything (V2X) technology for sustainable EV adoption,” Journal of Energy Storage, 2023.

[9] S. Kumar, B. Ramalingam, and K. B. Yadav, “A dual non-isolated bridge converter for vehicle to everything (V2X) application,” in Proc. Int. Conf. Electr. Energy Syst., pp. 546–551, 2023.

[10] S. Hossain et al., “Grid-vehicle-grid (G2V2G) efficient power transmission: an overview of concept, operations, benefits, concerns, and fu-ture challenges,” Sustainability, vol. 15, no. 7, p. 5782, 2023.

[11] R. Khezri, D. Steen, and L. A. Tuan, “A review on implementation of vehicle to everything (V2X): benefits, barriers and measures,” in Proc. IEEE PES Innovative Smart Grid Tech-nol. Conf. Eur., pp. 1–6, 2022.

[12] K. M. Muttaqi et al., “Hybrid operation of su-per-capacitor and battery storage to improve electric vehicles performances,” in Proc. Annu. Meet. IEEE Ind. Appl. Soc., pp. 1–10, 2022.

[13] S. Islam et al., “State-of-the-art vehicle-to-everything mode of operation of electric vehicles and its future perspectives,” Renew. Sustain. Energy Rev., vol. 166, p. 112574, 2022.

[14] R. Khezri, D. Steen, and L. A. Tuan, “Vehicle to everything (V2X) - A survey on standards and operational strategies,” in Proc. IEEE Int. Conf. Environ. Electr. Eng. Ind. Commer. Power Syst. Eur. (EEEIC/I&CPS Eur.), pp. 1–6, 2022.

[15] H. M. Sharf et al., “Performance enhancement of a hybrid battery- supercapacitor EV energy storage system,” in Proc. IEEE Transp. Electri-fication Conf. Expo., 2021.

[16] I. Oukkacha et al., “Energetic performances booster for electric vehicle applications using transient power control and supercapacitors-batteries/fuel cell,” Energies, vol. 14, no. 8, p. 2251, 2021.

[17] M. A. Rehman, M. Numan, H. Tahir, U. Rah-man, M. W. Khan, and M. Z. Iftikhar, “A com-prehensive overview of vehicle to everything (V2X) technology for sustainable EV adop-tion,” J. Energy Storage, vol. 74, no. A, p. 109304, 2023,

[18] H. Lei, K. Li, and B. Chong, “A review of hy-brid energy storage system for heavy-duty elec-tric vehicle,” Transp. Res. Procedia, vol. 70, 2023.

[19] M. K. Hasan, Md Mahmud, A. K. M. A. Habib, S. M. A. Motakabber, and S. Islam, “Review of electric vehicle energy storage and management system: Standards, issues, and challenges,” J. Energy Storage, vol. 41, 2021.

[20] A. B. Mendhe and H. S. Panda, “Recent trends of machine learning on energy storage devices,” Next Res., vol. 2, no. 1, 20

[21] P. Thakkar, S. Khatri, D. Dobariya, D. Patel, B. Dey, and A. K. Singh, “Advances in materials and machine learning techniques for energy storage devices: A comprehensive review,” J. Energy Storage, vol. 81, 2024.

[22] P. Pandiyan, S. Saravanan, K. Usha, R. Kan-nadasan, M. H. Alsharif, and M.-K. Kim, “Technological advancements toward smart en-ergy management in smart cities,” Energy Rep., vol. 10, 2023.

[23] E. Yamini, M. Zarnoush, M. Jalilvand, S. M. Zolfaghari, F. Esmaeilion, A. Taklifi, D. A. Garcia, and M. Soltani, “Integration of emerging technologies in next-generation electric vehicles: Evolution, advancements, and regulatory pro-spects,” Results Eng., vol. 25, 2025.

[24] J. Shi, B. Xu, Y. Shen, and J. Wu, “Energy management strategy for battery/supercapacitor hybrid electric city bus based on driving pattern recognition,” Energy, vol. 243, 2022.

[25] P. Kumar, H. K. Channi, R. Kumar, A. Rajiv, B. Kumari, G. Singh, S. Singh, I. F. Dyab, and J. Lozanović, “A comprehensive review of vehi-cle-to-grid integration in electric vehicles: Pow-ering the future,” Energy Convers. Manag. X, vol. 25, 2025.

[26] Q. Zhang, L. Wang, G. Li, and Y. Liu, “A real-time energy management control strategy for battery and supercapacitor hybrid energy storage systems of pure electric vehicles,” J. Energy Storage, vol. 31, 2020.

[27] Zhenyu, J., Zhonglin, Y., Ruiming, Y., Kexue, L., Zhiqiang, T., Sixiang, Z., Hanji, J., Yachao, W., Kan, Z., Hengchun, D., Ying, L., Wenwen, L., Fukuan, P., Jiao, G., Di, H., and Chen, W., “System and method for dynamic bidirectional pushing of wireless energy for vehicle to every-thing (V2X) of electric automobile,” 2020.

[28] G. Bansal, H. Lu, and J. Kenney, “Vehicle-to-everything data transfer for automated vehicles,” 2020.

[29] S.-Y. Kwon, J.-Y. Park, and Y.-J. Kim, “Opti-mal V2G and route scheduling of mobile energy storage devices using a linear transit model to reduce electricity and transportation energy loss-es,” IEEE Trans. Ind. Appl., vol. 56, no. 1, pp. 34–47, 2020.

[30] Y.-J. Kim, “Optimal V2G and route scheduling of mobile energy storage devices using a linear transit model to reduce electricity and transporta-tion energy losses,” arXiv, 2019. K. Wang, L. Gu, X. He, S. Guo, Y. Sun, A. Vinel, and J. Shen, “Distributed energy management for ve-hicle-to-grid networks,” IEEE Netw., vol. 31, no. 2, pp. 22–28, 2017.

[31] M. M. Patankar, R. G. Wandhare, and V. Agarwal, “A high- performance power supply for an electric vehicle with solar PV, battery, and ultracapacitor support for extended range and enhanced dynamic response,” in Proc. Pho-tovolt. Spec. Conf., 2014, pp. 3568– 3573.

[32] A. Bouscayrol, D. Hissel, R. Trigui, and A. Emadi, “Guest Editorial: Special section on ad-vanced transportation systems,” IEEE Trans. Veh. Technol., vol. 60, 2011. V. V. S. Ganesh and M. D. R. Babu, “A review on vehicle-to-grid integration using renewable energy sources and electric vehicles,” n.d.

[33] H. Hussein, S. S. Hossain Rafin, M. S. Ab-delrahman, I. Kharchouf, and O. A. Moham-med, “Electric vehicle performance enhancement utilizing hybrid energy storage systems,” in Proc. IEEE VPPC, 2024, pp. 1–6.

[34] M. A. Sayeed and K. Manikandan, “Smart inte-gration of renewable energy into transportation: Challenges, innovations, and future research di-rections,” Rev. Énergies Renouvelables, vol. 27, no. 2, 2024.

[35] C. Jiang, A. Liebman, and H. Wang, “Network-aware electric vehicle coordination for vehicle-to-anything value stacking considering uncer-tainties,” in Proc. IEEE/IAS Ind. Commer. Pow-er Syst. Tech. Conf., 2023, pp. 1–9.

A Virtual Laboratory Framework for DC Series Motor Testing and Simulation

Jayashree A
Electrical and Electronics Engineering,
Thiagarajar College of Engineering,
Madurai, India
jayashree172005@gmail.com

Meenakshi G
Electrical and Electronics Engineering,
Thiagarajar College of Engineering,
Madurai, India
meenakshiganesan2401@gmail.com

Subalakshmi M
Electrical and Electronics Engineering,
Thiagarajar College of Engineering,
Madurai, India
subalak2004@gmail.com

Dr D.Kavitha
Associate Professor,
Electrical and Electronics Engineering,
Thiagarajar College of Engineering,
Madurai, India
dkavitha@tce.edu

***Abstract*—This paper presents a virtual laboratory for conducting the Load Test on DC Series Motor using the Godot engine. It provides an interactive simulation environment for electrical engineering students, enabling hands-on practice with dynamic feedback and data collection. Comparative analysis of virtual and physical lab environments is carried out, highlighting advantages, limitations, and impact on cognitive skills and retention.**

***Keywords*—Virtual lab, DC series motor, Simulation, Cognitive learning, Electrical machines**

I. I INTRODUCTION

Electrical machines form a core component of electrical engineering education, essential for understanding energy conversion and motor control principles. However, limited access to physical labs—due to equipment costs, space, or safety concerns—can hinder hands-on learning. To address this, a virtual laboratory framework was developed using the Godot engine, focusing on the "Load Test on DC Series Motor." The simulation enables students to visualize and interact with motor characteristics in a controlled digital environment. This paper explores its design, features, and educational impact.

II. PROBLEM DEFINITION AND RESEARCH QUESTIONS

The virtual lab mitigates equipment scarcity and safety concerns. Two research questions are explored:

RQ1: How does the integration of a virtual lab for DC motor load test experiments impact the development of higher-order cognitive skills (analysis, synthesis, evaluation) in engineering students compared to traditional lab methods?

RQ2: What are the long-term retention rates of knowledge and skills acquired through a virtual lab for DC motor experiments compared to traditional hands-on labs?

III. COMPARATIVE ANALYSIS OF PHYSICAL LAB AND VIRTUAL LAB:

Benefits of physical lab:

- ***Hands-On Experience:*** Provides direct interaction with equipment, helping develop practical skills.
- ***Sensory Feedback:*** Engages multiple senses, aiding in interpreting experimental results.
- ***Real-World Application:*** Prepares users for real-world scenarios.
- ***Problem-Solving Skills***: Encourages critical thinking through unexpected challenges.
- ***Understanding Equipment:*** Familiarizes users with lab tools and troubleshooting.

Limitation of physical lab:

- ***Space Constraints***: Requires dedicated space.
- ***Cost:*** Expensive setup and maintenance.
- ***Safety Concerns***: Involves potential hazards, requiring safety protocols.
- ***Resource Availability***: Limited access to materials and equipment.
- ***Accessibility:*** Not all students or researchers have access to physical labs.

Benefits of virtual lab:

- ***Accessibility:*** Can be accessed from anywhere with an internet connection.
- ***Cost-Effectiveness:*** Reduces costs by eliminating physical resources and maintenance.
- ***Safety***: Provides a risk-free environment for experiments.
- ***Scalability:*** Supports multiple users simultaneously.
- ***Flexibility:*** Easily modify experimental conditions and scenarios.

Limitation of virtual lab:

- ***Lack of Hands-On Experience****:* Cannot fully replicate physical interaction with equipment.
- ***Limited Sensory Feedback****:* Missing tactile or sensory cues.
- ***Dependence on Technology***: Requires internet and compatible devices.
- ***Simulation Limitations***: Simulations may not always match real-world conditions.
- ***Cost of Development***: High development costs for creating quality simulations.

IV. Development of Virtual Lab – Tools

1 Objectives

- Develop a virtual lab using Godot for electrical engineering experiments.
- Enable self-learning and concept clarity through simulations.
- Allow students to perform tests from anywhere.

2 Proposed Methodology

Simulate the "Load Test on DC Series Motor" using Godot to create a user-friendly virtual environment for better understanding.

3 Godot Programming Languages

Supports GDScript, C#, Visual Script, and GDNative (C/C++) for flexible development.

fig 1: functional block diagram

4 Key Concepts in Godot:

Godot uses node-based scenes where nodes interact via signals.

5 Process Function in Godot

Process (delta) runs every frame to update values like speed, torque, and current in real time.

V. Functionalities of Virtual Lab:

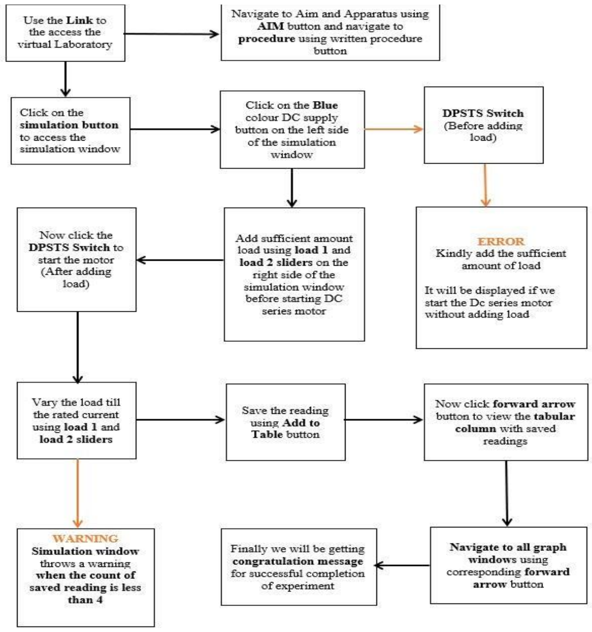

FIG 1: FUNCTIONAL BLOCK DIAGRAM

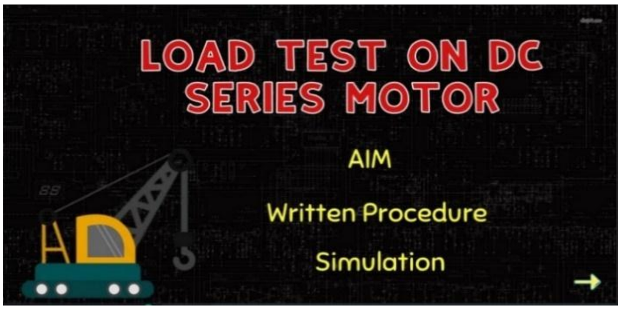

FIG 2: WELCOME PAGE OF VIRTUAL LAB

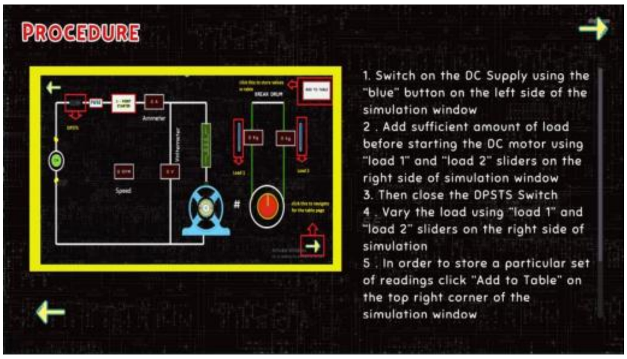

FIG 3: PROCEDURE PAGE

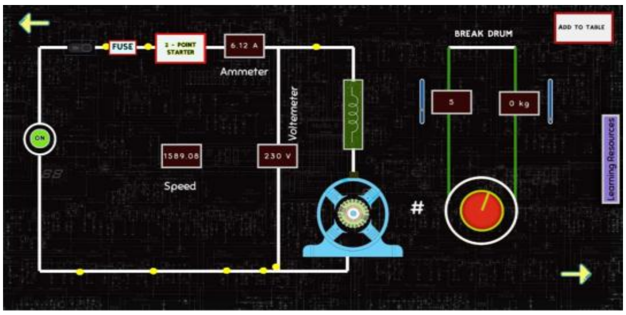

FIG 4: SIMULATION PAGE

 ISBN: 978-93-342-3695-8

FIG 5.STARTER RESOURCE PAGE

READINGS

S No	Load Voltage (V)	Load Current (A)	Speed (RPM)	Load Difference (Kg)	Torque (Nm)	Output Power (W)	Input Power (W)	Efficiency (%)
0	230	6.12	1589.08	5	6.87	1142.64	1407.6	81.18
1	230	6.84	1523.56	6	8.24	1314	1573.2	83.52
2	230	7.08	1501.72	7	9.61	1510.5	1628.4	85.52
3	230	7.68	1447.12	8	10.99	1664.6	1766.4	87.52
4	230	8.52	1370.68	9	12.36	1773.22	1959.6	90.49
5	230	9.6	1272.4	10	13.73	1828.53	2208	82.81
6	230	10.44	1195.96	11	15.11	1891.43	2401.2	78.77
7	230	11.4	1108.6	12	16.48	1912.23	2622	72.93
8	230	11.64	1086.76	13	17.85	2030.39	2677.2	75.84
9	230	12	1054	14	19.23	2121.43	2760	76.86

FIG 6 .TABULATION

VI. RESULT AND DISCUSSION

The virtual lab was deployed in a computer lab setup, where students conducted Load Test on a DC Series Motor. They observed changes in speed, torque, and current with varying load. Data was collected and analyzed to draw inferences using plotted graphs.

A. Open Ended Questions:

Students shared their thoughts through survey questions. Key insights included:

- Easy navigation of the virtual lab
- Effective graph-based analysis
- Clear procedure documentation
- Suggestions for including different motor ratings

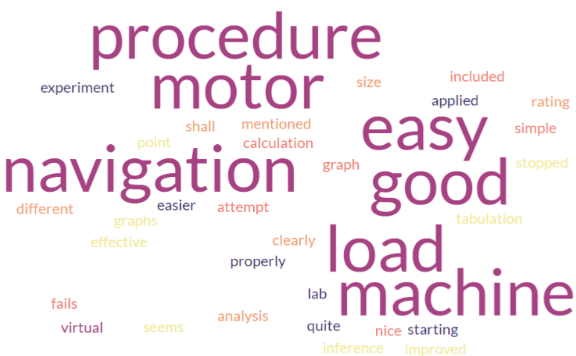

FIG 7 WORD CLOUD OF OPEN RESPONSE.

B. Likert Scale:

Students rated various features on a 1–5 scale (5 being most effective):

TABLE I: LIKERT RESPONSE FOR FEATURES:

Feature	5 Rating Count
Interactive Simulations:	9
Performance Metrics:	10
Educational Resources:	12
Graphical Visualization	9
Data Analysis	8

The feedback is represented in figure 8

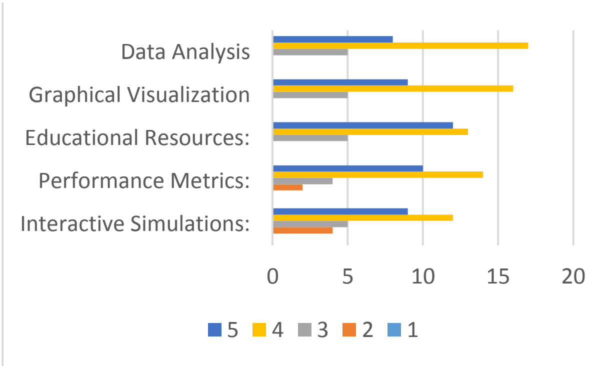

FIG 8:FEEDBACK

From the figure, it is clear that most of the users found this virtual lab useful.

RQ1: How does the integration of a virtual lab for DC motor load test experiments impact the development of higher-order cognitive skills in engineering students compared to traditional lab methods?

To evaluate cognitive skill development, a 10-mark analysis-level question was included in the exam. Students who used the virtual lab showed better performance:Table II: Marks statistics of a10 mark question

Parameter	Experiment set	Control set
Mean score	8.2	7.1
Median score	8.5	7
Standard deviation	1.2	1.5
Range	6 – 10	4.5 - 10

The higher mean and median scores in the experimental group suggest improved cognitive skill development. A lower standard deviation also indicates **more consistent performance** among virtual lab users. These results support the effectiveness of the virtual lab in enhancing higher-order thinking.

RQ2: What are the long-term retention rates of knowledge and skills acquired through a virtual lab for DC motor experiments compared to traditional hands-on labs?

To assess long-term retention, a question-framing task was conducted in the fourth semester. Students from both virtual and traditional lab groups were asked to frame *apply-level* questions on DC motors. Of 65 participants, 28 were from the experimental (virtual lab) group.

TABLE III

Question quality	**Class as a whole**	**Experiment set**	**Control set**
Good quality question	12	4	8
Medium quality question	28	16	12
Low quality question	25	8	17

Although more students from the control group framed high-quality questions, the virtual lab group showed fewer low-quality responses and a higher number of medium-quality ones. This suggests better overall retention and conceptual clarity due to structured interactivity in the virtual lab.

VII. CONCLUSION

The Electrical Machines Virtual Laboratory for DC motors offers key advantages over traditional labs. It provides a safe, controlled environment where students can conduct experiments without risk of injury or equipment damage. The ability to repeat experiments supports better understanding of core concepts.This virtual setup is also cost-effective, making it suitable for institutions with limited resources. It removes the need for expensive equipment and ongoing maintenance.Evaluations using both student feedback and performance data show improved learning outcomes and high engagement. Overall, the virtual lab proves to be a valuable tool in enhancing practical skills and conceptual clarity in electrical engineering education.

REFERENCES

[1] Anitha, D., Jeyamala, C., & Kavitha, D. (2018). Assessing and Enhancing Creativity in a Laboratory Course with Project Based Learning. Journal of Engineering Education Transformations, 32(2), 2349-2473.

[2] Evstatiev, Boris, et al. (2019). Web-based environment for virtual laboratories in the field of electrical engineering. 16th conference on electrical machines, drives and power systems (ELMA). IEEE,

[3] Guo, Liping, et al. (2022) Design and implementation of virtual laboratory for a microgrid with renewable energy sources. Computer Applications in Engineering Education 30.2 349-361.

[4] Keream, Settar S., Khalid G. Mohammed, and Mayyada Sahib Ibrahim. "Analysis study in principles of operation of DC machine." *Journal of Advanced Research in Dynamical and Control Systems* 10.02 (2018): 2323-2329.

[5] Melkebeek, A. Jan. *Electrical machines and drives: fundamentals and advanced modelling*. Springer International Publishing, 2018.

[6] Salmela, Tero. "Game development using the open-source Godot Game Engine." (2022).

[7] Thorn, Alan, and Alan Thorn. "Introducing godot: Why migrate?." *Moving from Unity to Godot: An In-Depth Handbook to Godot for Unity Users* (2020): 1-14.

[8] Aziz, El-Sayed, Sven K. Esche, and Constantin Chassapis. "Design and implementation of a virtual laboratory for machine dynamics." *International Journal of Online Engineering* 6.2 (2010).

[9] Djeghloud, Hind, Maria Larakeb, and Amar Bentounsi. "Virtual labs of conventional electric machines." *Proceedings of 2012 International Conference on Interactive Mobile and Computer Aided Learning (IMCL)*. IEEE, 2012.

[10] Kavitha, D., and D. Anitha. "Virtual Lab Integrated Flipped Class for Effective Implementation of CDIO Framework in a Theory Course–A Case Study." *Journal of Engineering Education Transformations* 36.Special Issue 2 (2023).

[11] Kavitha, D., Suriya Mu, and D. Anitha. "Increasing the effectiveness of'Power Electronics' classes using a supplementary web-based virtual laboratory setup to impart CDIO skills." *Journal of Engineering Education Transformations* 37 (2024).

XL Net Meets Paraphrase Detection

Mahalakshmi S
Department of CSBS (Research Scholar),
Thiagarajar College of Engineering,
Madurai, Tamil Nadu, India
mahalakshmisklu@gmail.com

Felicia Lilian J
Department of CSBS (Assistant Professor),
Thiagarajar College of Engineering,
Madurai, Tamil Nadu, India
jflcse@tce.edu

Viswadarshan R R
Department of CSBS (UG Student),
Thiagarajar College of Engineering,
Madurai, Tamil Nadu, India
viswadarshanrramiya@gmail.com

***Abstract*—One of the fundamental NLP tasks is paraphrase detection, which is useful for semantic similarity and duplicate detection. This paper fine-tunes the permutation-based trans- former model XLNet to achieve bidirectional context understand-ing on the Microsoft Research Paraphrase Corpus (MRPC). The model architecture added a dense classification head specifically designed for the paraphrase detection classification task on top of XLNet. Hyperparameters, including learning rate and weight decay, were carefully tuned to optimize performance for this task. The accuracy obtained on the validation set is 88.24%, while that on the test set is 85.79% and the F1 scores are recorded at 91.69% and 89.67%, respectively. The evaluation metrics we used clearly reflect the model's ability to classify paraphrase pairs. We obtained a consistent benchmark F1 score of 91.69%, which outperforms the established benchmark of 91.41±0.40 of XLNet on the MRPC dataset. This work demonstrates that XLNet is a robust paralinguistic alternative for paraphrase detection and contributes to the growing trend of transformer- based architectures in semantic tasks.**

Index Terms*—XLNet Fine-Tuning, Paraphrase Detection Benchmark, Semantic Textual Similarity, Transformer based NLP Models

I. INTRODUCTION

The task of paraphrase detection is a very critical one in the area of natural language processing because it involves determining whether two different sentences convey the same meaning. It has a wide range of applications in domains such as identifying duplicate content, information retrieval, question answering, and machine translation [8].

XLNet [6], an extension of the BERT architecture with a permutation-based language modeling objective that enables the model to better capture bidirectionality. XLNet differs from BERT in that it uses a fixed left-to-right or right-to-left context, while XLNet is allowed to model all possible permutations of word sequences, and hence provides a much more flexible and comprehensive view of sentence structure.

This paper seeks to explore the performance of XLNet in paraphrase identification within the benchmark Microsoft Research Paraphrase Corpus (MRPC) dataset. The dataset above consists of hand-labeled pairs of sentences labeled as either paraphrases or not. We continue fine-tuning the pre-trained XLNet model on the MRPC dataset and measure its performance using conventional metrics including accuracy, precision, recall, and F1-score. And we found that XLNet can achieve competitive performance on both the validation and test sets. Finally, we make a comprehensive analysis of the confusion matrix for the model and report the implications of these results for future research in semantic text matching [12] and paraphrase detection.

II. RELATED WORK

The detection of paraphrases has been a extensively re-searched endeavor within the field of natural language pro-cessing. Initial methodologies predominantly depended on rule-based systems and feature engineering, which were in- tegrated with conventional machine learning algorithms. Al- though these strategies provided preliminary insights, they were deficient in their capacity to manage semantic variations effectively.

Deep learning-based neural networks arrived that could learn a contextual representation using text. Most of the models mentioned were initially used for the task of detecting paraphrases based on LSTM Networks and CNN architectures, but complex language semantics are notoriously difficult to address.

The pre-trained contextual embeddings of transformer-based models like BERT and RoBERTa transformed this task from the ground up, allowing for fine-tuning on specific downstream tasks. BERT's masked language model (MLM) objective greatly improved semantic understanding, while RoBERTa, using even more refined training procedures, was superior to BERT on many benchmarks [11], including the Microsoft Research Paraphrase Corpus (MRPC).

XLNet improved transformer architectures by adding a permutation-based language modeling objective that could capture bidirectional context without the need for masking. Although XLNet has achieved outstanding performance on many NLP tasks, its applicability to paraphrase detection is still relatively unexplored. This work is based on the fine-tuning of XLNet on the MRPC dataset, evaluating its performance on paraphrase classification, and comparing that performance to previous approaches.

III. Dataset

Microsoft Research Paraphrase Corpus (MRPC) [14] is a very popular benchmark for the effectiveness of paraphrase detection systems (Table I). It is extracted from online news articles and based on sentence pairs that are marked as either paraphrased or not. It is an excellent benchmark to test the performance of a model [13] to identify semantic similarity between pairs of sentences where the surface structure may differ.

TABLE I MRPC Dataset Description

Dataset Split	Total Examples	Paraphrase	Not Paraphrase
Train	3668	2474	1194
Validation	408	279	129
Test	1725	1147	578

A. Data Preprocessing

Model-specific tokenizer XLNet Tokenizer was used while preparing datasets to train the models. In case of tokenization, the sentences are split into tokens using special tokens like [CLS] which is used as a classifier, and [SEP] which split up the two sentences. Through this way, all the models got a common structured input format while fine tuning to ensure efficient learning during the process.

These preprocessing steps ensured input sequences to the XLNet model were in appropriate format, using its permutation-based language modeling with maximum efficiency. The richness of this dataset, paired with these preprocessing steps, became the basis of accurate and efficient paraphrase detection.

IV. Methodology

XLNet [6] is a particularly optimal choice due to its unique permutation-based language modeling ability that can capture deep semantic relationships between two sentences [8].

A. Model Architecture

The architecture designed (Fig. 1) for the paraphrase detection is intended to adopt the permutation-based strength of XLNet effectively. In the Input Block, the model accepts two sentences as input for paraphrase detection. These are separated as [CLS] Sentence1 [SEP] Sentence2 [SEP]. While this structure ensures that the two sentences function as a coherent pair, which is crucial for the model to understand [5] the semantic relationship between them, they allow for better performance by the model.

In the Tokenizer Block, the model specific tokenizer, XLNetTokenizer, is employed to tokenize the input sentences. The tokenization process involves adding special tokens such as [CLS] to signify classification tasks and [SEP] to separate the sentence pair. The tokenizer generates three outputs for each input such as input_ids, attention_mask, and token_type_ids. This structured representation ensures compatibility with XLNet's requirements, allowing the model to process the inputs effectively.

The Embedding Block passes the pre-trained XLNet model to encode tokenized inputs in high-dimensional embeddings [10]. The transformer layers of XLNet compute contextualized representations for every token within the input sequence. This will enable the model to capture even the most intricate semantic relationships that may exist between the pairs of

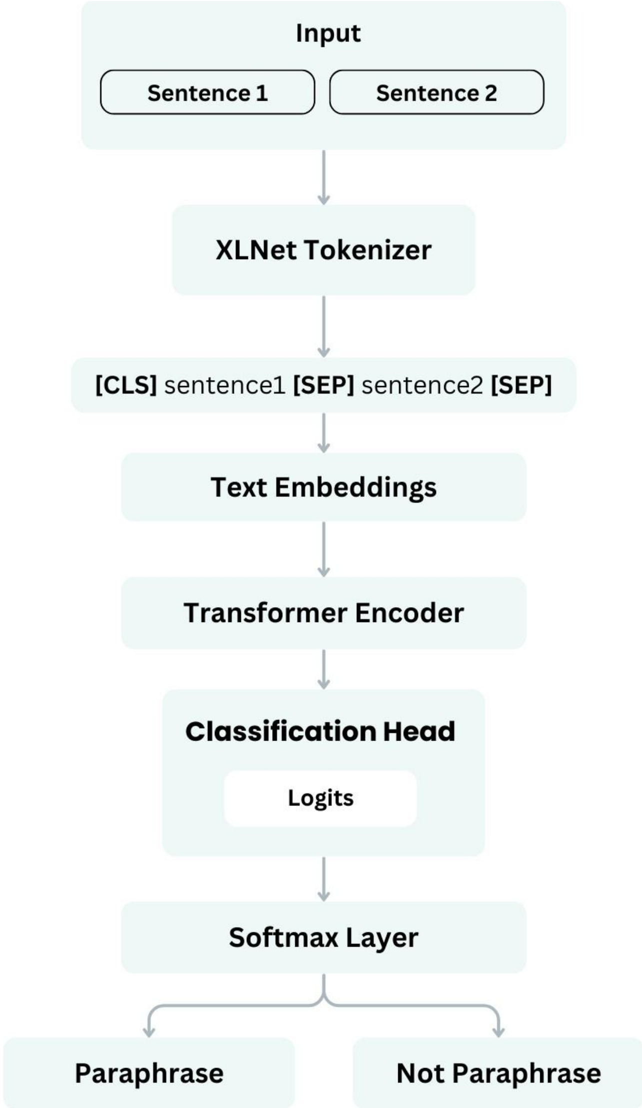

Fig. 1. Architecture diagram for Paraphrase Detection

sentences. The embedding associated with the [CLS] token, which represents the entire sequence, is taken and passed along to the classification layer.

The classification layer uses the embeddings of the [CLS] token to pass them through a dense layer that produces logits, which then get passed through a softmax activation function to calculate probabilities over the two output classes, paraphrase and not paraphrase. The output is probabilistic, so it is possible to classify the input sentence pair accurately. The class having the highest probability within the Output Block is taken as the final prediction [9].

B. Hyperparameter Configuration

Dependence on the proper tuning of hyperparameters plays a strong influence on the successful training of the XLNet model for paraphrase detection. For the purposes of the cur- rent work, several crucial hyperparameters were identified to improve the performance of the model on the MRPC dataset. These include learning rate, batch size, weight decay, number of epochs, and others (Table II).

TABLE II: MRPC DATASET HYPERPARAMETER CONFIGURATION

Hyperparameter	Value
Dataset	MRPC
Learning Rate	2e-05
Batch Size	16
Epochs	5
Sequence Length	256
Optimizer	AdamW
Weight Decay	0.01

The learning rate was set to 2e-5 to allow smooth convergence in the fine-tuning process. Weight updates were controlled by the AdamW optimizer. For both training and evaluation, a batch size of 16 would be chosen to balance the computational efficiency and model performance. Adaptive adjustments of the learning rate in training were achieved through a linear learning rate scheduler that comprises warm- up steps for stabilizing updates at initial phases and finer adjustments in subsequent phases. The number of epochs during training was set to 5 based on convergence obtained in experimental trials. Furthermore, regularization weight decay of 0.01 was used to avoid overfitting, and the best model in terms of accuracy was saved using the validation accuracy.

V. EVALUATION AND RESULTS

The XLNet model was evaluated regarding its performance assessment on the Microsoft Research Paraphrase Corpus (MRPC). The results were compared with respect to accuracy, precision, recall, and F1 score. Our study notably shows that for a consistent benchmark F1 score of 91.69% on the validation set, it closely corresponds to the actual benchmark value for XLNet of 91.41 ± 0.40 over the MRPC dataset [1]. Precision, recall, and F1 score pointed out the fact that the model was able to balance true positives with false positives.

The summary of the metrics acquired during the evaluation phase are presented in the table III.

TABLE III: EVALUATION RESULTS OF XLNET MODEL ON MRPC DATASET

Metric	Validation	Test
Loss	0.4056	0.5694
Accuracy	88.23%	85.79%
Precision	88.63%	86.85%
Recall	94.98%	92.68%
F1 Score	**91.69%**	89.67%
Runtime (seconds)	13.24	54.92
Samples Per Second	30.82	31.41
Steps Per Second	1.96	1.97
Epochs	5	5

During the validation phase, the F1 score was 91.69%, exceeding expectations and coming close to the actual benchmark range of 91.41 ± 0.40 [4], meaning our approach was

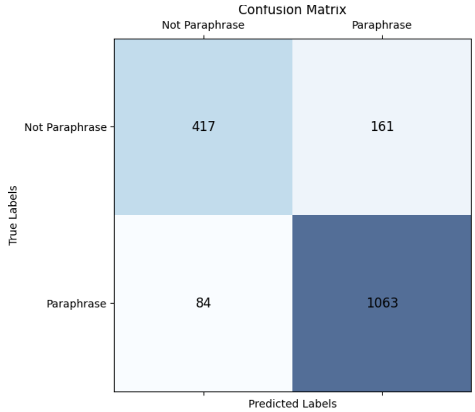

FIG. 2. CONFUSION MATRIX FROM TEST SET

reliable. The accuracy attained was 88.23% along with an recall rate of 94.98%, indicating that this model is not only good for paraphrase pairs identification but at the same time has significantly minimal false negatives.

With the following results on the test dataset-F1 score at 89.67%, accuracy at 85.79%, and recall at 92.68-it shows that it can generalize to unseen data. This consistent output from the model further justifies the effectiveness of our pre- processing pipeline and hyperparameter settings in leveraging the permutation-based structure of XLNet for the improvement of paraphrasing detection capabilities.

A. Confusion Matrix Analysis

For a clearer understanding of the performance of the XLNet model on the paraphrase detection task, we present in (Fig. 2) the confusion matrix which was obtained from the test set. The confusion matrix describes the true positives, false positives, true negatives, and false negatives; thus, it gives a clearer understanding of the capability of the classification model.

The confusion matrix provides an overall view of the classification outputs generated by the model. Here, the model correctly classified 1,063 sentence pairs as paraphrases with a high capacity to detect semantic similarity. In addition, it had correctly classified 417 sentence pairs as not being aptly distinguishing the dissimilar pairs of sentences.

However, the model misclassified 161 sentence pairs as paraphrases when they were not similar at all (False Positives), which means that sometimes it fails to identify very subtle semantic differences. Moreover, only 84 paraphrase sentence pairs were misclassified as non-paraphrases (False Negatives), which means that the missed detection rate is very low. These results highlight the overall strength of the XLNet model in paraphrase detection, showing its high accuracy in identifying semantic relationships between sentences.

The confusion matrix shows that the XLNet model performs extremely well since, when compared to the errors such as false positives and false negatives, it has a great number of correct classifications, which include true positives and true negatives. This balance enhances the robust F1 score on the test set to 89.67%.

More importantly, the low number of false negatives means that the model does a good job in the case of true paraphrases, and this is relevant to the paraphrase detection task where semantic similarity is more prominent. False positives indi- cate areas that might require further fine-tuning to be better able to differentiate between pairs of sentences that are only marginally different in their meaning.

This overall analysis reports the consistency of the XLNet model in the paraphrase detection task using the MRPC dataset, attaining performance directly comparable to widely accepted benchmarks.

VI. Conclusion and Future Work

This research effectively demonstrated the extension of the XLNet model for paraphrase detection, using the Microsoft Research Paraphrase Corpus (MRPC) as the benchmark cor- pus. It showed that the permutation language modelling in XLNet can capture semantic similarities between pairs of sentences, and it attained a steady benchmark F1 score of 91.69%, which is to be widely accepted benchmark values such as 91.41±0.40.

A. Future Work

Future work could be the extension of this work by including more datasets to test the generalizability of the model on a range of paraphrase detection benchmarks. In addition, by using advanced preprocessing or loss functions, false positives encountered in evaluation could be eliminated to better improve the model's classification performance.

References

[1] A. Michail, S. Clematide, and J. Opitz, "PARAPHRASUS: A Com- prehensive Benchmark for Evaluating Paraphrase Detection Mod- els," *arXiv preprint arXiv:2409.12060*, 2024. [Online]. Available: https://arxiv.org/abs/2409.12060.

[2] K. Krishna, Y. Song, M. Karpinska, J. Wieting, and M. Iyyer, "Para- phrasing evades detectors of AI-generated text, but retrieval is an effective defense," *arXiv preprint arXiv:2303.13408*, 2023. [Online]. Available: https://arxiv.org/abs/2303.13408.

[3] J. P. Wahle, B. Gipp, and T. Ruas, "Paraphrase Types for Generation and Detection," in *Proceedings of the 2023 Conference on Empirical Methods in Natural Language Processing (EMNLP 2023)*, Singapore, Dec. 2023, pp. 901–909.

[4] "Paraphrase identification via textual inference," in *Proceedings of the 13th Joint Conference on Lexical and Computational Semantics (*SEM 2024)*, June 20-21, 2024, Association for Computational Linguistics, pp. 133–141.

[5] Y. Dou, C. Jiang, and W. Xu, "Controllable text simplification with explicit paraphrasing," in *Proceedings of the 2024 Conference of the Association for Computational Linguistics (ACL 2024)*, 2024.

[6] Z. Yang, Z. Dai, Y. Yang, J. Carbonell, R. Salakhutdinov, and Q.V. Le, "XLNet: Generalized autoregressive pretraining for language understanding," in *Proceedings of the 33rd International Conference on Neural Information Processing Systems (NeurIPS 2019)*, 2019.

[7] Y. Dou, C. Jiang, and W. Xu, "Improving large-scale paraphrase acqui- sition and generation," in *Proceedings of the Conference on Empirical Methods in Natural Language Processing (EMNLP)*, 2024.

[8] W. Lan and W. Xu, "Neural network models for paraphrase identifica- tion, semantic textual similarity, natural language inference, and question answering," in *Proceedings of the [specific conference]*, 2024.

[9] A. Conneau, D. Kiela, H. Schwenk, L. Barrault, and A. Bordes, "Supervised learning of universal sentence representations from natural language inference data," in *Proceedings of the 2017 Conference on Empirical Methods in Natural Language Processing (EMNLP)*, 2017.

[10] W. Lan and W. Xu, "The importance of subword embeddings in sentence pair modeling," in *Proceedings of the 2018 Conference of the North American Chapter of the Association for Computational Linguistics: Human Language Technologies (NAACL-HLT)*, 2018.

[11] W. Lan, S. Qiu, H. He, and W. Xu, "A continuously growing dataset of sentential paraphrases," in *Proceedings of The 2017 Conference on Empirical Methods on Natural Language Processing (EMNLP)*, 2017.

[12] S. R. Bowman, J. Gauthier, A. Rastogi, R. Gupta, C. D. Manning, and Potts, "A fast unified model for parsing and sentence understanding," in *Proceedings of the 54th Annual Meeting of the Association for Computational Linguistics (ACL)*, 2016.

[13] W. Xu, C. Callison-Burch, and W. B. Dolan, "SemEval-2015 Task 1: Paraphrase and semantic similarity in Twitter (PIT)," in *Proceedings of the 9th International Workshop on Semantic Evaluation (SemEval)*, 2015.

[14] W. B. Dolan and C. Brockett, "Automatically constructing a corpus of sentential paraphrases," in *Proceedings of the Third International Workshop on Paraphrasing (IWP)*, 2005.

Variational Quantum Algorithms used in Quantum Computing and their Role in Addressing Health Challenges

C. Thirisha
Department of Physics,
Thiagarajar College of Engineering,
Madurai-625015, Tamil Nadu, India.
cthirisha@student.tce.edu

M. Mahendran*
Department of Physics,
Thiagarajar College of Engineering,
Madurai-625015, Tamil Nadu, India Corresponding
author:manickam-mahendran@tce.edu

S. Suriya Ramkumar
Department of ECE,
Thiagarajar College of Engineering,
Madurai-625015, Tamil Nadu, India
suriyaramkumar@student.tce.edu

V. Aravindan
Department of Physics,
Thiagarajar College of Engineering,
Madurai-625015, Tamil Nadu, India
vaphy@tce.edu

***Abstract*—Quantum computing represents a transformative enhancement in speed and computational power by utilizing superposition and entanglement to process extensive datasets with unprecedented speed and accuracy. This section outlines its uses in healthcare, addressing issues in drug development, medical imaging, genomics, and healthcare logistics. Molecular modelling for drug development is enhanced by Variational Quantum Eigensolver (VQE) algorithms, which improve the speed of cancer detection through superior imaging and diagnostics in combination with quantum machine learning. This genomic analysis offers expedited DNA sequencing compared to conventional methods and enables targeted treatment via the utilization of genetic data. Alternative optimization methods in quantum computing have facilitated the execution of healthcare operations. Undoubtedly, there are problems related to the technology utilized and the software employed in the research. Isaac Quantum Composer and Qiskit are only two instances of tools that elucidate the expectations of quantum computing. In conclusion, the ongoing advancements in quantum computing are anticipated to significantly impact healthcare and other sectors.**

Keywords—Quantum bits; Variational Quantum Eigen solver; Accelerate diagnosis; Bloch sphere; Quantum circuit

I. INTRODUCTION

The new quantum computer provides many opportunities for improvements in various sectors, namely medicine, better understood path for progress from small developments to potentially game-changing inventions. Significant impacts of quantum computing can be made across many sectors, including computer and communication science, energy, finance, technology, and even in the stock market. This extraordinary processing power magnifies interference in a vast array of contemporary areas-ranging from household gadgets to space exploration. The amazing computational speed of such a kind of computer, by virtue of the combination of superposition and entanglement of different states of a quantum, Quantum power fundamentally outgains classical computers due to their ability to process huge amounts of information [1]. Quantum computers work with superposition states as qubits, meaning these exist in '0', '1' states and combinations of both states simultaneously therein causing phenomenal speed-ups when it comes to processing data. However, the serious limitation in widespread qubit resources required for coding quantum applications still proves very challenging to overcome, inspired by the progress of quantum computing in emerging research domains such as healthcare, proposed a tangible proof-of-concept study that categorizes quantum programs based on application needs. The transformative aspect of this technology allows improving healthcare by solving very complex problems with great accuracy, yielding more effective treatments and medications. In qubit technology, entered into detailed analysis-from its inception to current research and future possibilities with algorithms like VQE (Variational Quantum Eigensolver).[2]

In turn, quantum computing has the power to make further strides in personalized medicine, drug discovery, and genomics. For example, quantum algorithms would break down molecular interactions at unprecedented levels of detail, allowing researchers to find potential drug candidates incredibly rapidly in comparison to classical methods. Quantum computing could begin to improve the analysis of genetic data, yielding greater insights into diseases and approaches more tailored to patients. The healthcare sector generates tons of data, ranging from electronic health records (EHRs), [3] genomic sequences, to imaging data. The vast amounts of data in itself pose some challenge to analysis, not only because of its sheer volume but also due to its very high dimensionality and complexity. Traditional statistical techniques tend to deal poorly with providing meaningful conclusions on such high-dimensional datasets, which may sometimes overlook potential diagnosis and treatments.

II. ADDRESSING QUANTUM ALGORITHMS

Quantum Algorithms are employed and have potential to revolutionize the quantum computing fields of every application, by harnessing the principles of quantum mechanics, quantum algorithms process the vast datasets and used efficiently, utilising the algorithms makes the researchers to analyse the materials they have taken and simulates the systems, how it interactions matters with greater precisions and makes them more efficient than classical computers.

Shor's Algorithm [4] were used in most powerful algorithm against classical encryption methods like RSA. (Rivest–Shamir–Adelman,) Grover's Algorithm [5] utilised in increases speed of unsorted database search quadratically, Quantum Phase Estimation: Storage of both eigenvalues and associated eigenstates garnered through the preparation of states for any basis using arbitrary unitary operators. Variational Quantum Eigen solver which used for estimating the ground state in quantum systems. Quantum Approximate Optimization Algorithm seeks combinatorial optimization problems on near-term quantum devices.

HHL algorithm: Exponentially fast under certain condition for the search of systems of linear, Quantum Fourier Transform the quantum states into their frequency components, key to Shor's algorithm.

Under the perspectives of estimating the iterations and finding the hybrid classical-quantum approach for estimating a quantum system's ground-state energy is the Variational Quantum Eigensolver, or VQE. It is mostly employed to address issues that come up in materials science and quantum chemistry. VQE operates by variationally minimising the lowest eigenvalue of a Hamiltonian H, which represents the system's ground-state energy. Pursuing with VQE to analyse the algorithms in cancer image enhancement using image processing. Quantum gates are utilised quantum principles of superposition and entanglement which intimates its way of actions as Hadamard works in the principles of quantum superposition whereas CNOT gates were used in the principles of Quantum entanglement

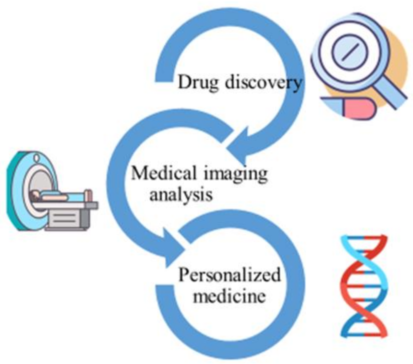

FIG. 1: CYCLE OF HEALTH CARE APPLICATIONS MEDICAL IMAGING: BRIDGING DRUG DISCOVERY AND PERSONALIZED MEDICINE.

III. APPLICATION ON HEALTHCARE

3.1 Drug Discovery and Development

As shown in Fig. 1, Drug discovery is a process that is usually time-consuming and arduous; it is essentially trial and error, which wears down the involved elements. There are the actual compounds that can interact with biological targets with the hope of curing diseases, which represents the long and arduous path of drug development. Conventional approaches rely heavily on computational modelling, trial-and-error testing, and very large financial spending. Quantum computing hastens the whole process of drug development by solving traditional computational methodologies' wise hurdles.

With traditional techniques, drug development takes several years, whereas, with quantum computing, the same becomes automated and completed among the minute dabs in time. The VQE algorithm calculates the ground-state energy of molecules that assists in supplying viable candidates for drugs.

3.2 Medical Imaging

Medical imaging modalities such as CT and MRI produce complex datasets that require an advanced level of interpretation. Others include quantum machine learning (QML)[6] that improves image processing in terms of efficacy and precision. For instance, it detects cancer cells with power and precision that classical algorithms do not offer in highly resolved images-cancer detection in its early stages, thus offering the foundation for treatment planning.

3.3 Genomics and Precision Medicine.

The use of quantum computing expedites DNA sequencing by allowing optimization in genetics analysis. Quantum algorithms help identify patterns in genomic data that are important for diagnosing genetic disorders and customizing treatment. As an example, scientists want to see how quantum methods can identify enhanced biomarkers for diseases like Alzheimer's and cancer, enabling targeted interventions.

3.4. Optimization of Healthcare Logistics.

Efficient resource allocation is a constant struggle in the healthcare industry. Quantum optimization algorithms such as the Quantum Approximate Optimization Algorithm (QAOA) can optimize the management of hospitals by taking in surgery schedules, emergency response, and also resource allocation during a pandemic. This, in turn, leads to decreased costs and better patient outcomes.[7][8]

IV. RESULT AND DISCUSSIONS

With the use of Qiskit, a Python programming language, and IBM Quantum Composer, which imports all necessary tools into the Python program to enable it to run and execute, quantum computing leverages all the quantum principles that are implied by the quantum gates in the quantum circuit and can analyse block spheres and histograms as an output.

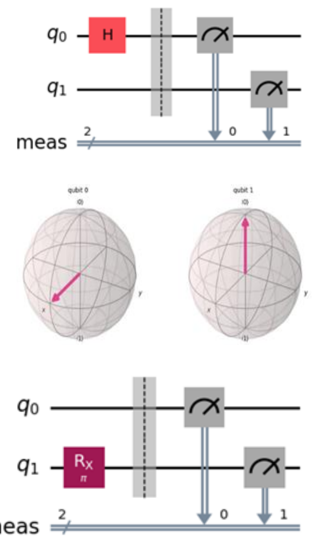

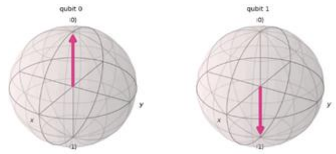

FIG. 2: THE QUANTUM CIRCUIT IS IN UTILISING HADAMARD AND ROTATIONAL RX GATE USED IN TWO QUBITS VISUALISATIONS OF BLOCH SPHERE.

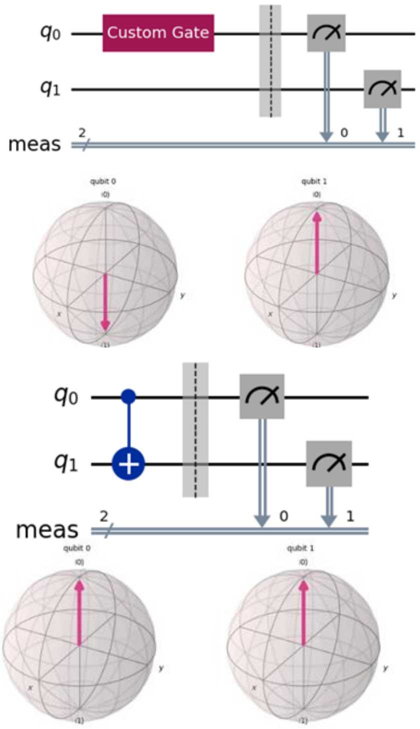

FIG. 3: THE UNITARY GATES AND CNOT GATES ARE UTILIZED IN QUANTUM CIRCUIT AND ITS VISUALIZATIONS' OF BLOCH SPHERE.

As mentioned in Fig 2 and 3 Quantum circuits are formed through quantum gates, **i**ncluding Hadamard gates and CNOT gates, which are used to modify the configuration and functionality of the circuit in accordance with the principles of quantum mechanics. Quantum gates comprise Hadamard, CNOT, rotation, and custom gates. Utilising the quantum gates as Hadamard, In the first circuit, a Hadamard gate is applied to qubit q_0 , placing it into a superposition state while qubit q_1 remains in its ground state $|0\rangle$; upon measurement, q_0 has a 50% chance of collapsing to $|0\rangle$ or $|1\rangle$, and q_1 will always be measured as $|0\rangle$. This is visualized on the Bloch spheres where q_0 lies on the equator (superposition) and q_1 points upward along the Z-axis (ground state).

In the second circuit, an $Rx(\pi)$ gate is applied to q_1 , rotating it 180° around the X-axis, flipping it from $|0\rangle$ to $|1\rangle$; q_0 remains untouched and which makes the qubits in superposition state where the bloch sphere The implications of these gates represent the outcomes on the Bloch sphere in terms of their respective angles. From these outcomes it is able to The outcomes of these quantum circuits are crucial for understanding and implementing fundamental principles of quantum computing, such as superposition, state preparation, and measurement. The first quantum circuit used the Hadamard gate to generate a superposition state and provide probabilistic measurement outcomes. In the second quantum circuit, the application of a (π) gate deterministically inverted a qubit from $|0\rangle$ to $|1\rangle$, therefore exhibiting control over the quantum state of a qubit. These operations suffice for the implementation and testing of quantum algorithms, visualization of qubit behaviour on the Bloch sphere, assessment of quantum hardware performance, and establishment of a foundation for more sophisticated tasks, including entanglement, quantum logic, and practical applications such as optimization, simulation, and security.

V. CONCLUSIONS

Implementation challenges: Despite the positive results, significant challenges exist for the use of quantum algorithms in healthcare, especially the availability of a more robust quantum hardware and developing user-friendly software tools. Here, we conclude that quantum computing has more applications in many different fields of technology. In the healthcare industry, for example, it focuses on precision medicine, drug discovery, and diagnostic acceleration. We work with specific algorithms based on IBM Quantum Composer, which we use to program in the Qiskit Python library and understand how different quantum gates operate on corresponding block spheres.

ACKNOWLEDGEMENT

This research work in financially supported by thiagarajar research fellowship (trf) scheme - (file.no: Tce/rd/trf/<<9>> dated 27.09.2024)

REFERENCES

[1] L. Baldi, "Quantum computing," Nanosci. Nanotechnol. Adv. Dev. Nano-sized Mater., pp. 135–147, 2018, doi: 10.1515/9783110547221-009.

[2] J. Tilly et al., The Variational Quantum Eigensolver: A review of methods and best practices, vol. 986. 2022. doi: 10.1016/j.physrep.2022.08.003.

[3] N. Innan, M. A.-Z. Khan, and M. Bennai, "Electronic Structure Calculations using Quantum Computing," pp. 1–29, 2023, doi: 10.1016/j.mtcomm.2023.107760.

[4] A. Yimsiriwattana and S. J. Lomonaco Jr., "Distributed quantum computing: a distributed Shor algorithm," Quantum Inf. Comput. II, vol. 5436, p. 360, 2004, doi: 10.1117/12.546504.

[5] J. Preskill, "Quantum Computing 40 Years Later," Feynman Lect. Comput. Anniv. Ed., pp. 193–243, 2023, doi: 10.1201/9781003358817-7.

[6] N. Mishra, A. Bisarya, S. Kumar, B. K. Behera, S. Mukhopadhyay, and P. K. Panigrahi, "Cancer Detection Using Quantum Neural Networks: A Demonstration on a Quantum Computer," no. October, 2019, doi: 10.13140/RG.2.2.28450.58563.

[7] L. Aggarwal, S. Sachdeva, and P. Goswami, "Quantum healthcare computing using precision based granular approach[Formula presented]," Appl. Soft Comput., vol. 144, p. 110458, 2023, doi: 10.1016/j.asoc.2023.110458. G. Eason, B. Noble, and I. N. Sneddon

A Comprehensive Mapping Study on Pictogram Prediction in Alternative Communication Boards

Betsybha Evangeline
Thiagarajar College of Engineering,
Madurai, India
betsybha@student.tce.edu

Anitha Dhakshina Moorthy
Thiagarajar College of Engineering,
Madurai, India
anithad@tce.edu

***Abstract*—High-tech Alternative Communication Boards (ACBs) are sophisticated Augmentative and Alternative Communication (AAC) devices intended to mitigate difficulties encountered by individuals with intricate communication requirements. These tools typically manifest as mobile applications, enabling users to formulate sentences by arranging pictograms—a fusion of an image and a label denoting a concept. This study offers systematic review of literature regarding pictogram prediction in augmentative and alternative communication (AAC) systems. Eight studies have been examined to investigate computational techniques utilized for pictogram prediction, their assessment methodologies, and the results concerning enhancements in user communication. Research reveals the application of diverse techniques for pictogram prediction, synthesis of automated as well as expert evaluation methods, yielding ambiguous outcomes concerning the enhancement of user communication.**

Keywords—Pictogram-based assistive technology, Augmentative and Alternative Communication (AAC), communication aids, cognitive impairments, symbol systems, multimodal communication, digital platforms, artificial intelligence, natural language processing, cross-cultural communication.

I. INTRODUCTION

AAC is a clinical approach designed to address communication difficulties faced by individuals with severe expressive communication disorders due to conditions such as autism, cerebral palsy, stroke, or apraxia. These individuals often experience challenges in gestural, verbal, or written communication, which can negatively impact their social interactions. AAC interventions typically use pictograms and captions to aid communication, especially for children with significant communicative impairments. These systems are divided into low-tech solutions, like picture boards, and high-tech solutions, such as speech-generating devices and tablet applications.

However, barriers to effective communication remain, particularly the time required to construct sentences, which can lead to frustration. To mitigate these challenges, advanced AAC systems employ techniques like color-coding pictograms based on parts of speech and predictive algorithms to suggest the next appropriate pictogram. These methods reduce effort in sentence construction, improve grammatical support, and increase communication speed, offering significant benefits for users and their communication partners.

The increasing integration of AI in AAC has spurred research into pictogram and word prediction within AAC systems. Despite advances, gaps remain in understanding the specific impact of pictogram prediction on user communication. This systematic mapping study catalogues strategies for pictogram prediction in advanced AAC systems and evaluates the computational techniques used. Analyzing 248 studies, eight were selected for in-depth review, revealing a mix of knowledge-based methods and neural networks, but with inconclusive evidence on their impact on improving user communication. The findings provide valuable insights for further development in the field.

The following sections of the current study are organized as outlined below: Section II summarizes methodologies utilized in mapping study; Section III details selected research and evaluates results; and Section IV conveys our conclusions about study and provides recommendations for further study.

II. METHODS

Definition of Research Questions

This study investigates scientific methodologies for pictogram prediction in advanced AAC systems, focusing on computational approaches, evaluation methods, and outcomes. Five research questions (RQs) were formulated, with RQ1 examining the prediction methods, units, and metrics used, while RQ2 explores the evaluation methods and outcomes. These questions provide a comprehensive overview of current research, highlighting strategies, components, and performance assessments, and identifying directions for future inquiry.

TABLE 1: RESEARCH QUESTIONS

RQ	Research Question	Facet
RQ1	What are the methods and units used for pictogram prediction in AAC systems?	Prediction method, Prediction unit
RQ2	How are pictogram prediction methods evaluated, and what are their outcomes?	Evaluation method, Evaluation metric, Outcomes

III. DATA SOURCES AND SEARCH STRATEGY

To enhance the retrieval of relevant studies, a comprehensive search string was crafted incorporating various terms related to Augmentative and Alternative Communication (AAC), including “voice output devices,” “communication boards,” and “VOCAs,” as well as terms like “pictogram prediction” and “word prediction” due to overlapping interpretations in literature. This query was applied across six scientific databases—Scopus, ACM Digital Library, Taylor & Francis Online, PubMed, Science

Direct, and Springer—between May and June 2022, targeting studies from 2015 to 2022. A total of 248 studies were retrieved and managed using the StArt tool [14], with 18 duplicates removed. Figure 1 shows the distribution of sources, reflecting AAC's interdisciplinary nature, with notable contributions from both clinical and technological domains.

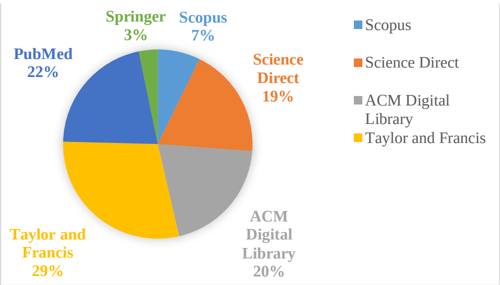

FIG. 1. STUDIES BY SOURCES

IV. STUDY SELECTION

We applied exclusion criteria outlined in Table 2 to ensure alignment with the research objectives, considering only primary studies and omitting secondary sources such as reviews, editorials, tutorials, and theses, which often lack novel contributions or peer review. Studies focused solely on word-based AAC systems were also excluded to maintain relevance to pictogram prediction. The selection process involved screening titles, keywords, and abstracts, with full-text analysis conducted when abstracts were insufficient. To reduce bias, two researchers independently performed the screening and resolved discrepancies through discussion.

TABLE 2. SELECTION CRITERIA

S. No	Criteria
E1	Research is written in a language other than English.
E2	Research is not a primary research.
E3	Research is not related to the field of Augmentative and Alternative Communication (AAC).
E4	Research focuses on AAC but doesn't include any strategies for pictogram suggestion.
E5	Research focuses on word prediction without incorporating pictograms.

V. DATA EXTRACTION

The data extraction followed the keywording methodology proposed by [15], which involves labeling key concepts from the text to generate open codes and organizing them into a coherent framework, with categories refined as needed [11]. While typically applied to abstracts, the technique was extended to the full texts of the selected studies to ensure comprehensive alignment with the research questions (Table 1), enabling the generation of meaningful labels and a deeper understanding of the analyzed research.

VI. RESULTS

This research examined 248 studies obtained through search queries. Following implementation of exclusion criteria outlined in Table II, only 8 studies have been involved in final results. Table III presents a summary of these studies, encompassing their citations and publication venues. Among the studies included, three were published in conference proceedings [16, 18, 19], while five were published in journals. Majority of these venues pertain to domain of Computer Science, with the exception of one study [17] published in a multidisciplinary journal.

TABLE 3. INCLUDED STUDIES

Research Title	Research Studies	Venue
A semantic grammar for beginning communicators	[20]	Knowledge-Based Systems
Context-aware communicator for all	[16]	International Conference on Universal Access in HumanComputer Interaction
An augmentative and alternative communication tool for children and adolescents with cerebral palsy	[21]	Behavior & Information Technology
Evaluating pictogram prediction in a location-aware augmentative and alternative communication system	[17]	Assistive Technology
Compositional Language Modeling for Icon-Based Augmentative and Alternative Communication.	[18]	Association for Computational Linguistics Meeting
Predictive composition of pictogram messages for users with autism	[22]	Journal of Ambient Intelli-´ gence and Humanized Computing
A semantic grammar for augmentative and alternative communication systems	[19]	International Conference on Text, Speech, and Dialogue
PictoBERT: Transformers for next pictogram prediction	[23]	Expert Systems with Applications

The multidisciplinary nature of AAC underscores the vital role of Computer Science, particularly in enhancing communication via mobile applications. Word and pictogram prediction often rely on NLP and ML—core domains within computer science.

The application of the keywording technique resulted in the identification of 22 keywords across five research facets, as presented in Table 4. These results are discussed in detail in relation to each research facet in the following sections.

TABLE 4. STUDIES KEYWORDING

Study	Facets and Keywords				
	Prediction Method	***Prediction Unit***	***Evaluation Method***	***Evaluation Metric***	***Outcomes***
[20]	Semantic Grammar	Pictogram sense	Automatic	None	No baseline
[16]	concept network	Pictogram label		None	not reported
[21]	Direct graph	Pictogram label		Number of Pictograms, Time	Positive
[17]	n-gram	Pictogram label	Automatic	Keystroke saving	Positive
[18]	Deep learning	Pictogram related words	Automatic	MRR, Top-n Accuracy	No baseline
[22]	n-gram	Pictogram label, Pictogram POS		Time, Number of Pictograms, Top-n Accuracy	Positive
[19]	Semantic Grammar	Pictogram sense	Automatic	Precision	No baseline
[23]	Deep learning	Pictogram sense	Automatic	Perplexity, Top-n accuracy	Positive

VII. RESULTS OF RQ1

1) *Prediction Methods:*

The analysis revealed five distinct methods for pictogram prediction across the reviewed studies. Knowledge-based approaches were the most prevalent, including semantic grammars (2 studies), concept networks (1 study), and directed graphs (1 study). Although grouped under a common category, these methods varied in implementation—for example, semantic grammars imposed rigid grammatical structures, while the directed graph model used by [21] incorporated probabilistic links between nodes. Due to these variations, the methods were treated as separate categories. Additionally, two studies [22, 16] employed statistical language models based on bi-grams, trained on predefined corpora and later adapted with user-specific data to enhance accuracy.

Two studies [23, 18] applied deep learning approaches, training neural networks on synthetic corpora derived from natural language samples. These models generally outperformed statistical methods, with [23] demonstrating superior predictive accuracy compared to knowledge-based models. However, deep learning methods require substantial computational resources, which can limit their practical application in low-resource settings. In contrast, statistical and knowledge-based methods offer more feasible alternatives in such environments despite their comparatively lower predictive performance.

2) *Prediction Unit:*

The study identified four categories of predictive units for pictogram prediction: part-of-speech (POS), pictogram labels, related word clusters, and word senses. In many advanced AAC systems, each pictogram is associated with a label, often a single word or phrase. Several studies treated the label as a sufficient unit for prediction [16], [17], [21], [22], effectively equating pictogram prediction with word prediction. However, this approach does not address polysemy, where words like “bat” may have multiple meanings. Study [22] also incorporated POS tags, training a bi-gram model on POS sequences to improve grammatical prediction, though results showed minimal improvement over label-based models.

Other studies explored concept-based and clustering approaches. Study [18] represented pictograms as clusters of related words, using pre-trained embeddings to form averaged vectors for neural network input. Concept-based methods, such as those in [19], [20], and [23], utilized resources like WordNet and FrameNet to treat pictograms as dictionary-defined concepts, enabling better handling of polysemy through synsets and word senses. These approaches typically required more preprocessing—such as word-sense disambiguation or curated word lists—adding complexity to the prediction pipeline. While label-based models are simpler and easier to implement, concept-based methods offer improved semantic precision at the cost of increased computational and design overhead.

VIII. RESULTS OF RQ2:

3) *Evaluation Methods:*

The reviewed studies employed two primary evaluation methods: automatic evaluations and quasi-experiments. Several studies relied on automated techniques to assess the effectiveness of their pictogram prediction methods. For instance, [20] examined the alignment of semantic grammar with a controlled sentence set across developmental stages, while [16] used software simulations with expert-validated AAC sentences. Study [18] evaluated model performance using a five-fold split of a synthetic text corpus, and [19] reconstructed subject-verb-object sentences from the CHILDES database to assess semantic grammar. Similarly, [23] utilized synthetic text and practitioner-supplied AAC sentences to evaluate their model’s pictogram prediction capabilities. However, one study [16] presented usage examples without conducting a formal assessment.

Two studies incorporated quasi-experimental designs involving human participants. Study [21] evaluated dialogue performance and user satisfaction among students with complex communication needs, with a particular focus on children. An educator also assessed the tool’s impact by replicating five weeks of classroom conversations with autistic children within the AAC system. Overall, the predominance of automatic evaluations suggests a reliance on controlled and synthetic data, likely due to challenges in accessing AAC users. This indicates that current research remains largely exploratory, highlighting the need for future studies to prioritize real-world testing with end users to better validate the practical utility of these systems.

4) Evaluation Metrics:

Among the reviewed studies, two did not report their evaluation metrics [16, 20], while others employed a range of measures to assess system performance. Study [21] quantified both the number of pictograms used by participants to construct sentences and the time taken, supplementing these with top-n accuracy—a common metric used to determine whether the correct pictogram appears within the top-n model predictions. This metric was similarly applied in studies [18] and [23], which utilized deep learning techniques. Additionally, [18] incorporated Mean Reciprocal Rank (MRR) to evaluate the ranking position of the correct prediction, while [23] used Perplexity to gauge the model's ability to predict text distributions. Study [19] focused on sentence reconstruction accuracy, and [17] assessed keystroke savings as a usability indicator. Despite the methodological diversity, no consensus has been reached on the most appropriate evaluation metric for pictogram prediction. However, top-n accuracy emerged as the most widely used, aligning well with the practical interface of AAC systems, which often display pictograms in a grid format.

5) Outcomes:

Outcomes of research were categorized as positive, neutral, negative, or lacking a baseline. Studies demonstrating improvement in their chosen metrics compared to prior approaches were labeled as positive [21, 17, 23]. All studies were categorized as positive. Studies lacking a comparison to any baseline were designated as having no baseline [18], [19], [20]. Additionally, [16] did not perform any experiments, leaving no basis for comparison.

Overall, the outcomes presented in the studies were predominantly positive. However, the lack of baselines in some studies limits the ability to assess their effectiveness relative to existing methods, highlighting an area for improvement in future research.

IX. Conclusion

This study analyzes scientific proposals for pictogram prediction in advanced AAC systems by examining computational methods, evaluation strategies, and reported outcomes. From an initial pool of 248 publications, eight were selected based on predefined criteria for in-depth review. These studies employed a range of methodologies, including knowledge-based approaches, statistical models, and neural networks, with evaluations varying from automated assessments to quasi-experiments involving AAC users and experts. While the findings highlight methodological efficacy, they also reveal ambiguity regarding improvements in user communication, largely due to limited testing with actual users. The field has evolved from early rule-based methods to data-driven approaches, yet remains exploratory, constrained by challenges such as restricted access to AAC users and the limitations of search strategies that may have excluded relevant studies. Despite these challenges, the review offers critical insights for AAC system development and proposes future work on implementing and evaluating a pictogram prediction tool for Brazilian Portuguese in real-world settings.

Acknowledgment

Authors extend their gratitude to Thiagarajar College of Engineering (TCE) for facilitating this research endeavor. Financial assistance from TCE under the Thiagarajar Research Fellowship scheme (File no: TRF/Jul-2023/06) is sincerely acknowledged.

References

[1] ASHA (2022). Augmentative and alternative communication. https: //www.asha.org/practice-portal/professional-issues/ augmentative-and-alternative-communication/. June, 2022.

[2] Beukelman, D. R. and Light, J. C. (2013). Augmentative & Alternative Communication: Supporting Children and Adults with Complex Communication Needs. Paul H. Brookes Baltimore.

[3] Pereira, J., Pena, C., de Melo, M., Cartaxo, B., Soares, S., and Fidalgo, R. (2019). Facilitators and barriers to using alternative and augmentative communication systems by aphasic individuals: Therapists' perceptions. In 2019 IEEE 32nd International Symposium on Computer-Based Medical Systems (CBMS), pages 349–354.

[4] Berenguer, C., Mart´ınez, E. R., De Stasio, S., and Baixauli, I. (2022). Parentsrsquo; perceptions and experiences with their childrenrsquo;s use of augmentative/alternative communication: A systematic review and qualitative meta-synthesis. International Journal of Environmental Research and Public Health, 19(13).

[5] Franco, N., Silva, E., Lima, R., and Fidalgo, R. (2018). Towards a reference architecture for augmentative and alternative communication systems. In Brazilian Symposium on Computers in Education (Simposio Brasileiro de Inform ´ atica na Educac¸ ´ ao-SBIE) ˜ , volume 29, page 1073.

[6] Sennott, S. C., Akagi, L., Lee, M., and Rhodes, A. (2019). AAC and Artificial Intelligence (AI). Topics in language disorders, 39(4):389–403.

[7] Ascari, R. E. d. O. S., Pereira, R., and Silva, L. (2018). Mobile interaction for augmentative and alternative communication: a systematic mapping. Journal on Interactive Systems, 9(2).

[8] Aydin, O. and Diken, I. H. (2020). Studies comparing augmentative and alternative communication systems (aac) applications for individuals with autism spectrum disorder: A systematic review and meta-analysis. Education and training in autism and developmental disabilities, 55(2):119–141.

[9] Dada, S., van der Walt, C., May, A. A., and Murray, J. (2022). Intelligent assistive technology devices for persons with dementia: A scoping review. Assistive Technology, 0(0):1–14. PMID: 34644248.

[10] Kitchenham, B. (2004). Procedures for Performing Systematic Reviews.

[11] Petersen, K., Vakkalanka, S., and Kuzniarz, L. (2015). Guidelines for conducting systematic mapping studies in

software engineering: An update. Information and Software Technology, 64:1–18

[12] Jurafsky, D. and Martin, J. (2019). Speech and Language Processing: An Introduction to Natural Language Processing, Computational Linguistics, and Speech Recognition. 3 edition.

[13] Chen, L., Babar, M. A., and Zhang, H. (2010). Towards an evidence-based understanding of electronic data sources. In 14th International Conference on Evaluation and Assessment in Software Engineering (EASE), pages 1–4.

[14] Fabbri, S., Silva, C., Hernandes, E., Octaviano, F., Di Thommazo, A., and Belgamo, A. (2016). Improvements in the start tool to better support the systematic review process. In Proceedings of the 20th International Conference on Evaluation and Assessment in Software Engineering, EASE '16, New York, NY, USA. Association for Computing Machinery.

[15] Petersen, K., Feldt, R., Mujtaba, S., and Mattsson, M. (2008). Systematic mapping studies in software engineering. In 12th International Conference on Evaluation and Assessment in Software Engineering (EASE) 12, pages 1–10.

[16] Garc´ıa, P., Lleida, E., Castan, D., Marcos, J. M., and Romero, D. (2015). Context-Aware ´ Communicator for All. In Antona, M. and Stephanidis, C., editors, Universal Access in Human-Computer Interaction. Access to Today's Technologies, pages 426–437, Cham. Springer International Publishing.

[17] Garcia, L. F., de Oliveira, L. C., and de Matos, D. M. (2016). Evaluating pictogram prediction in a location-aware augmentative and alternative communication system. Assistive Technology, 28(2):83–92.

[18] Dudy, S. and Bedrick, S. (2018). Compositional Language Modeling for Icon-Based Augmentative and Alternative Communication. Proceedings of the conference. Association for Computational Linguistics. Meeting, 2018:25–32.

[19] Pereira, J., Franco, N., and Fidalgo, R. (2020). A Semantic Grammar for Augmentative and Alternative Communication Systems. In Sojka, P., Kopecek, I., Pala, K., and ˇ Horak, A., editors, ´ Text, Speech, and Dialogue, pages 257–264, Cham. Springer International Publishing.

[20] Mart´ınez-Santiago, F., D´ıaz-Galiano, M. C., Urena-L ˜ opez, L. A., and Mitkov, R. (2015). ´ A semantic grammar for beginning communicators. Knowledge-Based Systems, 86:158–172.

[21] Saturno, C. E., Ramirez, A. R. G., Conte, M. J., Farhat, M., and Piucco, E. C. (2015). An augmentative and alternative communication tool for children and adolescents with cerebral palsy. Behavior & Information Technology, 34(6):632–645.

[22] Hervas, R., Bautista, S., M ´ endez, G., Galv ´ an, P., and Gerv ´ as, P. (2020). Predictive com- ´ position of pictogram messages for users with autism. Journal of Ambient Intelligence and Humanized Computing, 11(11):5649–5664.

[23] Pereira, J. A., Macedo, D., Zanchettin, C., de Oliveira, A. L. I., and do Nascimento Fi- ˆ dalgo, R. (2022). Pictobert: Transformers for next pictogram prediction. Expert Systems with Applications, 202:117231.

[24] Light, J., and McNaughton, D. (2012). The changing face of augmentative and alternative communication: Past, present, and future challenges. Augmentative and Alternative Communication, 28(4):197–204. PMID: 23256853.

[25] Goldberg, Y. and Hirst, G. (2017). Neural Network Methods in Natural Language Processing. Morgan & Claypool Publishers.

[26] Scarlini, B., Pasini, T., and Navigli, R. (2020). With More Contexts Comes Better Performance: Contextualized Sense Embeddings for All-Round Word Sense Disambiguation. In Proceedings of the 2020 Conference on Empirical Methods in Natural Language Processing, pages "3528 – 3539". Association for Computational Linguistics.

[27] MacWhinney, B. (2014). The CHILDES Project: Tools for Analyzing Talk, Volume II: The Database. Psychology Press.

Deep Defender: A GRU-Based Intrusion Detection System for the detection of ARP Spoofing

Nivedhidha M
Computer Science and Engineering, Thiagarajar College of Engineering,
Madurai, India
nivedhidha@student.tce.edu

Emil Selvan G S R
Computer Science and Engineering, Thiagarajar College of Engineering,
Madurai, India
emil@tce.edu

Ramkumar M P
Computer Science and Engineering, Thiagarajar College of Engineering,
Madurai, India
ramkumar@tce.edu

Dharani M
Computer Science and Engineering, Thiagarajar College of Engineering,
Madurai, India
mdharani22102001@gmail.com

***Abstract*—ARP spoofing is a severe cybersecurity threat enabling man-in-the-middle attacks, data theft, and denial-of-service disruptions. The proposed GRU-IDS methodology introduces a robust detection methodology combining advanced preprocessing, feature extraction, and a Gated Recurrent Unit (GRU)--based neural network to counter ARP spoofing in dynamic network environments. Key preprocessing steps include standardization, tokenization, and Recursive Feature Elimination (RFE) to refine features extracted from ARP, IP, and IPv6 layers, enabling precise anomaly detection. The GRU-IDS model, optimized with dropout layers and early stopping, efficiently captures temporal patterns, achieving superior performance. Evaluated on IoT intrusion datasets with diverse attack scenarios, the GRU-IDS model attains an accuracy of 98.75% and outperforms existing methods, demonstrating scalability, reduced false positives, and robustness for real-world deployment.**

Keywords—ARP Spoofing Detection, Intrusion Detection System (IDS), Gated Recurrent Unit (GRU), Feature Extraction, Machine Learning, Deep Learning.

I. INTRODUCTION

ARP maps IP addresses to MAC addresses but lacks authentication, thus making it vulnerable to ARP spoofing. ARP spoofing enables man-in-the-middle attacks, theft of sensitive data, and denial-of-service attacks, which cause financial losses, data breaches, and reputational damage..

IDS is important for countering ARP spoofing, which detects intrusion in the network by monitoring network traffic. Signature-based IDS identifies known attacks but is useless against novel attacks, while anomaly-based IDS identifies any deviations from normal behavior and thus has flexibility. Traditional IDS are difficult to scale up, and they generate many false positives while dealing with complex traffic. Hence, IDS methodologies should be developed with more accuracy, efficiency, and adaptability to fight against sophisticated threats like ARP spoofing.

ML and DL have revolutionized IDS by addressing the limitations of traditional methods. Decision trees and SVMs are good classifiers, whereas DL models such as CNNs and RNNs are efficient for processing complex high-dimensional data and extracting temporal-spatial features. Advanced architectures like Transformers and ViTs enhance IDS by combining spatial and temporal analysis, thereby increasing accuracy and robustness against sophisticated attacks like ARP spoofing.

II. RELATED WORKS

Islam Debicha [8] et al. proposed, in 2023, a new IDS technique called transfer learning along with multi-adversarial detection to neutralize evasion attacks. The method attempts to deal with the weaknesses resulting from evasion attacks like FGSM and PGD through the strategic positioning of adversarial detectors in both serial and parallel designs of the IDS. This system exploits the Dempster–Shafer fusion rule for further improvement of zero-day attacks. The model tested on NSL-KDD and CIC-IDS2017 datasets outperformed traditional methods with robust detection, adaptability, and resilience. Although requiring higher computational resources, and its parallel design, this model marks significant steps toward improving IDS security and tackling sophisticated threats.

Meihui Zhong et al. (2023) [9] proposed DMTR to promote NIDS. DMTR captures evolving, multi-scale topological structures in dynamic, imbalanced network traffic with the Mapper algorithm and GSO, adapting to data drift while preserving key topological features. Demonstrated on datasets such as CIC-IDS2017 and UNSW-NB15, DMTR achieved high accuracy with a Macro F1-score of 99.84%, robust to class imbalance and scalable for large datasets. However, the computational overhead in high-dimensional data and parameter tuning are still challenges; DMTR reduces complexity compared to static methods and advances malicious activity detection.

Md. Alamin Talukder et al. (2023) [11] developed a hybrid ML-DL model to handle network intrusion detection and class imbalance problems, along with high-dimensional data. The proposed methodology uses SMOTE for balancing the dataset and XGBoost for feature selection to improve detection accuracy and decrease complexity. By using classifiers like Random Forest, Decision Tree, and CNN, the model showed an accuracy of 99.99% on the KDDCUP'99 dataset and 100% on the CIC-MalMem-2022 dataset. XGBoost optimizes the features selected by choosing the most important attributes. The model offers high accuracy, scalability, and robustness.

However, computation overhead is faced with preprocessing and feature selection.

Md. Alamin Talukder et al. (2024) [12] proposed a new cybersecurity approach based on ML in IDS. The model used Random Oversampling to handle data imbalance and Stacking Feature Embedding with PCA for dimensionality reduction, which enhanced the accuracy of threat detection to over 99.9% on benchmark datasets such as UNSW-NB15 and CIC-IDS. However, the challenges of potential overfitting from dataset dependence and complexity in processing large volumes of data have to be overcome.

Zeeshan Ahmad et al. (2020) [10] proposed a systematic review of ML and DL approaches for NIDS. It deals with the challenges of traditional IDS, which are improvement in detection accuracy and reduction of false alarms especially with emerging attacks. The study evaluates ML and DL methods, discussing their strengths, weaknesses, performance metrics, and dataset selection. Despite this, the researchers point out how these techniques appear promising for developing NIDS systems. However, their limitations and other future directions still need to be addressed to provide robust network security against evolving threats.

Husain Abdulla, et al. 2020[1] proposes a methodology based on a neural network for ARP spoofing detection in IoT networks. The dataset was pre-processed to extract traffic attributes, labeled as benign traffic (0) and attacks (1). The neural network had three input neurons, a hidden layer with three neurons, and a sigmoid output for binary classification. Already trained with backpropagation, a learning rate of 0.2, a momentum of 0.7, and a target MSE to be less than 0.01, the network has already reached an accuracy of more than 90%. This is in comparison with the ARIMA statistical model which only gives an accuracy of 82%.

III. PROPOSED METHODOLOGY

Data Preprocessing

Data preprocessing involves transforming raw, unorganized data into a clean, organized, working format, ready for analysis and understanding. In network-based detection systems like ARP spoofing detection, effective preprocessing is key to identifying malicious patterns in complex, noisy datasets. The proposed methodology collects ARP spoofing datasets in PCAP format, representing various attack scenarios. Six datasets, containing normal and malicious traffic, were processed using the Scapy library to extract features from network layers such as IP, IPv6, and ARP, simulating real-world conditions.

Feature Extraction

The feature extraction process involved parsing each packet to identify its network layer and extracting key attributes from the IP, IPv6, and ARP layers. A textual summary (info) of each packet was generated for a high-level description. These features were aggregated into flows based on src_ip, dst_ip, and protocol, enabling flow-level analysis. Abnormal patterns, like a spike in ARP requests or large flows, could indicate spoofing attacks. A target column was created, labeling ARP traffic (protocol = 1) as positive (1) and other traffic as negative (0). This binary classification approach ensures the model is focused on detecting ARP spoofing attacks while differentiating normal traffic.

Standardization

In standardization, one kind of preprocessing involves scaling a dataset's characteristic values that involves making the characteristic values of a dataset scale such that they all have a mean of zero and a standard deviation of one.

In GRU-IDS methodology, standardization played a crucial role in normalizing the numerical features extracted from the PCAP data, such as packet length, flow duration, and packet count. By scaling these features, standardization eliminated biases caused by large numerical values, allowing the model to learn from all features effectively.

Tokenization

Tokenization converts textual data into numerical representations for ML models. It involves breaking text into tokens (words or subwords) and mapping them to unique indices. In the proposed methodology, the "info" column from the PCAP data, containing packet summaries, was tokenized using Keras's Tokenizer. The tokenized sequences were padded to a fixed length of 50 to ensure consistency. Tokenization improved the model's ability to differentiate normal from malicious traffic, boosting recall and reducing false negatives in ARP spoofing detection.

Recursive Feature Elimination (RFE)

RFE is a feature selection technique. This technique iteratively eliminates the least important features based on their input to the model’s performance.In GRU-IDS model, RFE was applied to the combined feature set, which included both scaled numerical features and tokenized text features. The results demonstrated a significant enhancement in model performance, with higher precision and reduced overfitting, as evidenced by consistent accuracy scores across training and testing datasets.

Gated Recurrent Unit (GRU)

GRU is used for capturing temporal dependencies in sequential data. It addresses issues like vanishing gradients in traditional RNNs, making it effective for long sequences. GRUs are less complex than LSTM networks but perform similarly, offering computational efficiency without sacrificing effectiveness.

Model Training

Fig.1 shows that a GRU layer with 128 units is added to capture temporal dependencies in the sequence data. This layer is followed by a Dropout layer to regularize the model and avoid overfitting by randomly setting some of the unit's outputs to zero during training. The final output layer uses a dense layer with sigmoid activation, optimized for binary classification. Training employs the Adam optimizer, which adaptively adjusts the learning rate to achieve effective convergence of the model. The most commonly used loss function for binary classification problems-binary cross-entropy-is utilized. Early stopping is applied to monitor the training loss in order not to miss out on the optimal model weights; this means that when the loss stops improving for a particular number of epochs, it stops training (patience=5). With a batch size of 32, the model is appropriate for using the fit() function over a maximum of 50 epochs. After training, metrics of accuracy, precision, recall, and F1 score are computed based on performance on the test set. The last step for visualizing model training is plotting accuracy and loss graphs.

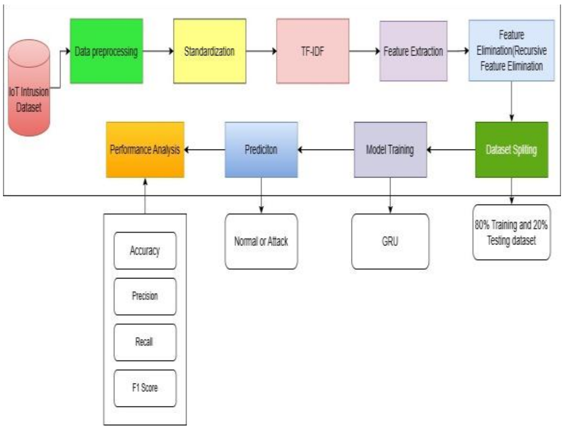

FIG. 1 : SYSTEM DESIGN OF GRU-IDS

IV. EVALUATION

Benchmark Dataset

The intrusion detection proposed methodology used the IoT Network Intrusion Dataset; which is a rich collection of network traffic and has a broad set of data to be able to identify unauthorized access as well as malicious activities in an IoT environment. The dataset contained 1,264,000 instances covering both malicious activities and benign activities, with 47 different attributes. They represent a rich collection of instances of real-world attacks.

Performance Metrics

The model achieved excellent performance with 98.75% accuracy, 95.45% precision, 91.30% recall, and a 93.33% F1 score. High precision indicates minimal false positives, while strong recall shows effective detection of true positives. The balanced F1 score highlights the model's reliability, making it well-suited for binary classification tasks

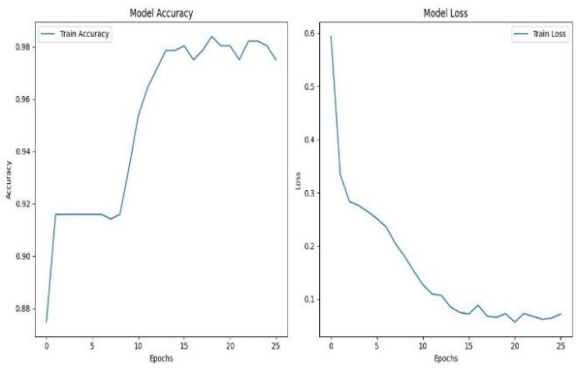

FIG. 2: ACCURACY GRAPH AND MODEL LOSS FOR THE GRU-IDS APPROACH

Fig.2 shows the training accuracy and loss of an ML model over 25 epochs, providing a window into how the model learns and adjusts over time. In the accuracy graph on the left, the model begins with an accuracy of approximately 88%, which signifies a decent starting point. Within the first five epochs, there's a rapid ascent as accuracy surpasses 92%, highlighting how quickly the model is adapting to the training data. This upward trajectory continues, and the accuracy peaks close to 98%, indicating the model is increasingly proficient at making correct predictions. Minor fluctuations after this peak suggest the model is fine-tuning its learning, adjusting weights to optimize performance.

On the right, the loss graph starts with a high value of around 0.6, reflecting the initial errors the model makes when predictions are far from actual values. As training progresses, there's a steep decline in loss, dropping below 0.1 within the first ten epochs. This sharp decrease illustrates the model's effectiveness in minimizing errors by adjusting its parameters. Interestingly, there is a minor increase in loss toward the tail-end epochs that might be the initial sign of overfitting—a condition where the model is fitted too closely to the training data and, thus, does not perform well with unseen new data.

Evaluation Metrics

The performance of ML models is assessed by tools called Evaluation metrics. It provides a quantitative means of understanding how well a model makes predictions and where it might be lacking. Based on different perspectives on model performance **accuracy, recall, F1 score, and precision are a few commonly used evaluation metrics.**

a) ACCURACY

Accuracy (1) denotes the model's overall proportion of correct predictions, calculated as the ratio of true positive and true negative predictions to the total number of predictions.

$$Accuracy = \frac{TP+TN}{TP+TN+FP+FN} \qquad (1)$$

b) PRECISION

Precision (2) measures the correctness of positive predictions by comparing true positives to the total number of predicted positives, including false positives.

$$\text{Precision} = \frac{TP}{TP+FP} \qquad (2)$$

c) RECALL

Recall (3) denoted as sensitivity or the true positive rate, measures the model's ability to correctly classify all actual positive instances. It is calculated as the ratio of true positives to the total number of actual positives (true positives and false negatives).

$$\text{Recall} = \frac{TP}{TP+FN} \qquad (3)$$

d) F1 SCORE

The F1 score (4) unites precision and recall into a single rating by calculating their harmonic means.

$$F1 = 2 \times \left(\frac{Precision \times Recall}{Precision + Recall}\right) \qquad (4)$$

Comparison State-of-Art

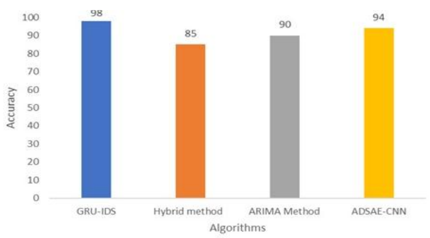

FIG. 3 ACCURACY GRAPH AND MODEL LOSS FOR THE PROPOSED APPROACH

As shown in Fig.3, GRU-IDS significantly outperforms existing methods in ARP spoofing detection for IoT networks due to advancements in data preprocessing, feature extraction, and model optimization. Existing methods, such as the neural network-based approach by Husain Abdulla et al.,[1] achieved over 90% accuracy but relied on simpler preprocessing and limited features like TCP, UDP, and ARP packet statistics. The ARIMA method demonstrated an 18% error rate, limiting its effectiveness in detecting anomalies in dynamic IoT environments[3]. Existing research presents a hybrid model combining decision tree and random forest algorithms, achieving 98% accuracy on the CICIDS2017 dataset and 85.2% on NSL-KDD [7]. The existing research presents an ADSAE-CNN model that integrates attention mechanisms and deep sparse autoencoders, achieving detection accuracies of 89.1% on UNSW-NB15 and 94.20% on CSE-CIC-IDS2018 datasets. In contrast, GRU-IDS methodology incorporates detailed feature extraction, including protocol-specific attributes and flow-based statistics, enhanced by Recursive Feature Elimination to improve generalization. Preprocessing steps like standardization and tokenization ensure consistent scaling and capture contextual traffic patterns. With GRU layers for temporal dependencies, dropout layers for regularization, and early stopping, it achieves exceptional results: 98.75% accuracy, 95.45% precision, 91.30% recall, and a 93.33% F1 score, ensuring superior anomaly detection and scalability for IoT security.

V. CONCLUSION AND FUTURE WORK

The proposed GRU-IDS methodology effectively integrates advanced preprocessing and feature extraction with a GRU-based neural network to provide high accuracy and robustness. Incorporating standardized tokenization and recursive feature elimination ensures optimum preparation of data for training. GRU-IDS approach addresses the complexity of the dynamic network environment achieves an accuracy of 98.75%, proposing an automatic intrusion detection tool scalable and dependable. In the future, the design can be extended towards real-time capability to detect potential threats promptly.

Acknowledgment

The authors express their gratitude to the Thiagarajar College of Engineering (TCE) for supporting us to carry out this research work. Also, the financial support from TCE under the Thiagarajar Research Fellowship scheme (File.no: TCE/RD/TRF/2024/15) is gratefully acknowledged.

References

[1] Husain Abdulla, et al. "ARP Spoofing Detection for IoT Networks Using Neural Networks." SSRN Electronic Journal, 2020, https://doi.org/10.2139/ssrn.3659129.

[2] Parthiban Aravamudhan, and T. Kanimozhi. "A Novel Adaptive Network Intrusion Detection System for Internet of Things." PLOS ONE, vol. 18, no. 4, 21 Apr. 2023, pp. e0283725–e0283725, https://doi.org/10.1371/journal. pone. 0283725. Accessed 22 Oct. 2023.

[3] Baha Rababah, and Srija Srivastava. "Hybrid Model for Intrusion Detection Systems." ArXiv.org, 2020, arxiv.org/abs/2003.08585. Accessed 28 Jan. 2025.

[4] Raisa Abedin, Disha, and Sajjad Waheed. "Performance Analysis of Machine Learning Models for Intrusion Detection System Using Gini Impurity-Based Weighted Random Forest (GIWRF) Feature Selection Technique." Cybersecurity, vol. 5, no. 1, 4 Jan. 2022, https://doi.org/10.1186/s42400-021-00103-8.

[5] Suchet Sapre, et al. "A Robust Comparison of the KDDCup99 and NSL-KDD IoT Network Intrusion Detection Datasets through Various Machine Learning Algorithms." ArXiv:1912.13204 [Cs, Stat], 31 Dec. 2019, arxiv.org/abs/1912.13204.

[6] Yang Jia, et al. "Network Intrusion Detection Algorithm Based on Deep Neural Network." IET Information Security, vol. 13, no. 1, 1 Jan. 2019, pp. 48–53, https://doi.org/10.1049/iet-ifs.2018.5258.

[7] Zhiqiang Geng, et al. "Improved Convolution Neural Network Integrating Attention Based Deep Sparse Auto Encoder for Network Intrusion Detection." Applied Intelligence, vol. 55, no. 2, 13 Dec. 2024, https://doi.org/10.1007/s10489-024-05872-6. Accessed 28 Jan. 2025.

[8] Islam Debicha, et al. "TAD: Transfer Learning-Based Multi-Adversarial Detection of Evasion Attacks against Network Intrusion Detection Systems." *Future Generation Computer Systems*, vol. 138, Jan. 2023, pp. 185–197, https://doi.org/10.1016/j.future.2022.08.011. Accessed 23 Sept. 2022.

[9] Meihui Zhong, et al. "Dynamic Multi-Scale Topological Representation for Enhancing Network Intrusion Detection." *Computers & Security*, vol. 135, 1Dec. 2023, pp. 103516–103516, https://doi.org/10.1016/ j.cose.2023.103516. Accessed 3 Apr. 2024.

[10] Zeeshan Ahmad, et al. "Network Intrusion Detection System: A Systematic Study of Machine Learning and Deep Learning Approaches." *Transactions on Emerging Telecommunications Technologies*, vol.32, no.1, 16 Oct. 2020, pp.1–29, online library. wiley.com/doi/full/ 10.1002/ett.4150, https://doi.org/ 10.1002/ett.4150.

[11] Md. Alamin Talukder , Khondokar Fida Hasan , Md. Manowarul Islam, Md. Ashraf Uddin, Arnisha Akhter, Mohammad Abu Yousuf, Fares Alharbi, Mohammad Ali Moni "A Dependable Hybrid Machine Learning Model for Network Intrusion Detection." *Journal of Information Security and Applications*, vol.72, Feb.2023, p.103405, https://doi.org/10.1016/j.jisa.2022.103405. Accessed 9 Jan. 2023.

[12] Md. Alamin Talukder , Md. Manowaru Islam , Md Ashraf Uddin, Khondokar Fida Hasan, Selina Sharmin, Salem A. Alyami and Mohammad Ali Moni "Machine Learning-Based Network Intrusion Detection for Big and Imbalanced Data Using Oversampling, Stacking Feature Embedding and Feature Extraction." *Journal of Big Data*, vol. 11, no. 1, 22 Feb. 2024, https://doi.org/10.1186/s40537-024-00886-w.

[13] Dharani, M., Nivedhidha, M., Sangeetha, A., Saravanan, V., Ramkumar, M. P., & GSR, E. S. (2024, October). "Detection of ARP Spoofing with Optimized False Alarm Using Deep Learning Based Absolute Thresholding". 2024 *4th International Conference on Sustainable Expert Systems (ICSES)* (pp. 1650-1657). IEEE

Automatic Evaluation of Programming Assessments in Online Gamified Learning Environments: A Systematic Review

Ms. Srimathi S
Department of Applied Mathematics and Comptational Science Thiagarajar, College of Engineering,
Madurai, Tamil Nadu, India
srima2209@gmail.com

Dr. Anitha D
Department of Applied Mathematics and Comptational Science, Thiagarajar College of Engineering,
Madurai, Tamil Nadu, India
anitha.dm07@gmail.com

***Abstract*—The rapid growth of online programming courses has increased the demand for efficient and scalable assessment methods. Traditional assessment techniques struggle to provide personalized feedback, making automated systems essential in online learning environments. However, while automation enhances efficiency, it often lacks the engagement necessary for sustained student participation. Gamification, incorporating game-like elements into learning, offers a promising strategy to boost motivation and learning outcomes in programming education. This review examines the effectiveness of automated assessment tools in programming courses and their applicability in gamified environments. A systematic search across popular digital libraries identified 26 relevant studies for analysis. The review categorizes programming assessment question types and maps them to appropriate evaluation methods. It also investigates the integration of gamification elements like leader boards, badges, and adaptive difficulty, identifying challenges such as balancing complexity, ensuring fairness in automated evaluations, and managing diverse student responses. The study highlights the need for advanced AI-driven assessment techniques to dynamically adapt to learners' performance and engagement, contributing valuable insights for educators and researchers developing automated and gamified evaluation systems.**

Keywords—Automated Assessment, Programming course, Gamification, Question types, Evaluation methods.

I. INTRODUCTION

The rapid growth of online courses has provided flexible access to education across disciplines, including programming, where students learn coding, software development, and algorithmic thinking [18]. Online courses break down geographical and financial barriers, allowing diverse learners to acquire technical skills [1]. Unlike theoretical subjects, programming requires hands-on practice, logical thinking, and debugging. Platforms like Coursera, Udemy, Codecademy, LeetCode, and HackerRank offer interactive lessons and real-time coding experiences. However, evaluating programming assignments online presents challenges due to variations in coding styles, problem-solving approaches, and debugging [11], including issues like plagiarism detection, code optimization, and personalized feedback [18]. These challenges call for automated assessment tools to ensure fairness, scalability, and consistency in grading.

To address these challenges, automated evaluation systems are widely used in online programming education to analyze code submissions, check correctness, and provide instant feedback [19]. Common approaches include Unit Testing, Static Code Analysis, Plagiarism Detection, and AI-Based Evaluation, which reduce manual effort and ensure objectivity [5]. A study during the COVID-19 pandemic highlights the effectiveness of automated grading in maintaining academic integrity and timely feedback [4]. However, the key question remains: Are these tools equally effective in gamified programming environments designed to boost learner motivation and engagement?

Gamification in education uses elements like leaderboards, points, badges, and adaptive challenges to boost student engagement [14]. In programming courses, it encourages competitive and interactive problem-solving [6]. However, traditional automated assessment tools may not align with gamified learning due to factors like engagement metrics, adaptive questioning, and collaboration. This highlights the need to refine assessment strategies for gamified environments, integrating adaptive AI feedback, engagement tracking, and collaborative evaluation [11]. This review explores how to optimize assessment strategies to align with gamification principles while addressing challenges in online programming education.

II. BACKGROUND STUDY

Technology has revolutionized education, making online learning popular through platforms like Coursera, edX, and Udacity, enabling self-paced learning and interaction with diverse instructors [4]. However, online courses face challenges in engagement, assessment reliability, and personalized feedback, particularly in programming education [18][20][26]. Programming skills are in high demand, leading to a rise in online programming courses that integrate theory with hands-on exercises [22][16]. The effectiveness of these courses depends on efficient assessment and engagement to ensure understanding of programming concepts [14]. Traditional methods, like multiple-choice questions, fail to assess problem-solving and coding skills [7]. Automated assessment tools are essential but face limitations in scalability, code quality evaluation, plagiarism, and personalized feedback [11].

To address these challenges, various automated assessment tools have been developed. Unit Testing checks code against predefined outputs [4][18], Static Analysis evaluates syntax and style [9][19], Regular Expression Evaluation matches patterns in free-text answers and code comprehension tasks [1][16][17], and AI-Based Evaluation uses machine learning and NLP for open-ended assignments [8][11]. One study [8] categorizes automated methods for open-ended questions, identifying trends and gaps. Another research [25] showcases an open-source online coding evaluation system for scalability and collaboration. A study [18] emphasizes real-time feedback and adaptive assessments for better learning outcomes. Additionally, a review [19] identifies challenges in automated grading, particularly for open-ended problems and fair grading.

However, the effectiveness of automated tools in engaging and motivating learners remains under exploration [6][15]. Gamification, with elements like leaderboards, badges, time-based challenges, and collaborative exercises, is increasingly used to boost engagement in programming courses [12][20]. However, integrating these tools into gamified environments poses unique challenges. This study examines how automated assessment methods can be applied to various question types in gamified online programming courses, highlighting the benefits, limitations, and implications for improving education.

III. RESEARCH QUESTION

The following Research Questions (RQ)are used to address the specific objectives of this proposed study:

RQ1-How can various question types in online programming courses be automated and mapped to suitable evaluation methods?

RQ2-How can the identified question types be effectively used in a gamified online programming environment?

IV. LITERATURE REVIEW METHODOLOGY

The procedure followed in this review to identify, evaluate, and interpret available research findings related to the mentioned research questions, as given in Fig. 1.

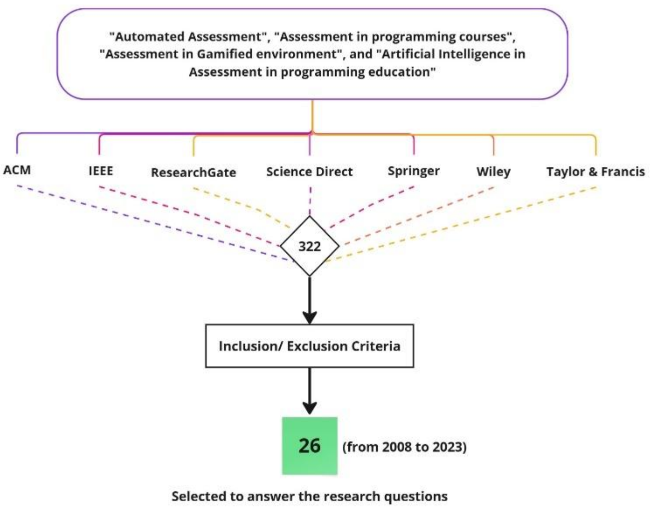

FIG. 1. FILTERING PROCESS OF THIS STUDY

Relevant research was identified through books and six digital libraries: ACM, IEEE, Research Gate, Science Direct, Springer, Wiley, and Taylor & Francis. A total of 322 articles were retrieved using search terms like "Automated Assessment", "Assessment in Programming Courses", "Gamified Environment Assessment", and "AI in Assessment in Programming Education". After applying inclusion criteria (English, full-text, empirical or experimental research), 26 studies were selected, including 11 Q1 journals, 2 Q2 journals, 4 IEEE proceedings, and 9 other proceedings. The study addresses three components: question types, evaluation methods, and automated assessment in gamified environments.

The literature study reveals that the number of questions used in the automated assessment process is listed in Fig. 2. These question types target different skill sets, allowing comprehensive evaluation of programming knowledge, logical reasoning, and problem-solving abilities. Fig. 3 summarizes more than five evaluation methods used in automated assessment, enabling fair, efficient, and scalable evaluation of various programming skills. An overview of these components is presented in the results and discussion section.

FIG. 2. TYPES OF QUESTIONS FOR AUTOMATED ASSESSMENT IN ONLINE PROGRAMMING COURSES

FIG. 3. COMMONLY USED EVALUATION METHODS FOR AUTOMATING ASSESSMENTS IN ONLINE PROGRAMMING COURSES

V. RESULTS AND DISCUSSION

A. RQ1-How can various question types in online programming courses be automated and mapped to suitable evaluation methods?

To address this research question, this system explores how different question types in online programming courses can be automated and matched with suitable evaluation methods. Based on evaluation techniques, questions are grouped into four types: Quiz, Programming Assignments, Free Text/Open-Ended, and Parameterized Questions. These categories aim to ensure accurate, fair, and scalable assessments. As shown in Table I, Quiz questions are the most widely used due to their simplicity and scalability. Common formats include predicting outputs, identifying missing lines, matching columns, Parson's Problems, and multiple-choice or true/false questions. These are evaluated using Fixed Solution Evaluation, which compares responses to predefined answers, enabling immediate feedback and efficient grading. This method effectively assesses conceptual and syntax knowledge in large-scale courses. A study recommends enhancing MCQs with interactive coding tasks, Parson's problems, and debugging exercises to improve assessment quality in K-12 computer science education [13].

On the other hand, Programming Assignments are key in programming education, involving tasks like coding, debugging, and solving Parson's Problems. These are evaluated using Static Analysis, Unit Testing, Information Retrieval Evaluation, and Automated Reasoning. GRAD-AI [11], an AI-based tool, enhances grading and provides personalized feedback to boost engagement. Edgar [16][17], another system, uses interactive tutorials and output comparison to outperform static methods. Information retrieval techniques [21] support automatic evaluation and plagiarism detection. To improve scalability, enhancements like optimized test execution, parallel processing, and caching have been proposed [22]. Automated reasoning [2] further helps assess code logic and structure, beyond just output.

Additionally, Free Text/Open-Ended Questions require students to write algorithms, explain code, or show reasoning. These are assessed using Regular Expression Evaluation and AI-Based Evaluation with NLP to gauge conceptual understanding and critical thinking [8]. A study [1] shows how regex-based systems can provide instant feedback and grading.

Finally, Parameterized Questions generate unique problems by varying inputs, reducing plagiarism and promoting originality. These tasks involve predicting outputs or analyzing code and are evaluated using Static Analysis, Unit Testing, Information Retrieval, and AI methods. A study [7] highlights a parameterized assessment system for introductory programming that supports personalized evaluation and improves classroom management.

TABLE 1. MAPPING VARIOUS QUESTION TYPES TO SUITABLE EVALUATION METHODS

Category	Question Types	Evaluation methods
Quiz [13] [16] [17]	-Predicting the output -Finding the value of a variable -Finding the missing lines of code -Match the Column -Parson's Problems -Multiple Choice -Multiple Answer -Fill in the Blanks -True/ False	-Fixed solution Evaluation [13] [16] [17]
Programming Assignments [2] [9] [11] [18] [19] [20] [21] [22] [25]	-Writing a code for a given problem -Debugging -Code analysis and optimization -Parson's Problems	-Static Analysis [9] [18] -Unit Testing [18] [22] -Information Retrieval Evaluation [21] -Automated AI-Based Evaluation [11] [20] [22] - Automated reasoning techniques [2]
Free Text/Open-Ended Questions [1] [4] [8] [16] [17]	-Writing an algorithm -Code comprehension -Algorithmic reasoning task	-Regular Expression Evaluation [1] [4] -Automated AI-Based Evaluation [8] -Fixed solution Evaluation [16] [17]
Parameterized Questions [7]	-Writing a code for a given problem -Predicting the output -Finding the values of a variable	-Static Analysis [18] [9] -Unit Testing [18] [22] -Information Retrieval Evaluation [21] -Automated AI-Based Evaluation [22] [11] [20] -Automated reasoning techniques [2]

This categorization highlights the potential of automating assessments in online programming courses and shows how evaluation methods adapt to different question types. By mapping each question type to a suitable technique ensures reliable, consistent, and scalable assessments that enhance student learning.

B. RQ2-How can the identified question types be effectively used in a gamified online programming environment?

To implement question types effectively in a gamified online programming environment, evaluation techniques must align with gamification strategies that enhance engagement and fairness. As shown in Table II, quizzes pair well with leaderboards and timed challenges, offering instant feedback and urgency, though care is needed to avoid stress. Programming assignments benefit from badges and progress bars, motivating gradual progress, though varied coding styles can affect fairness. Open-ended tasks use peer reviews and AI-driven feedback, with rewards for quality responses, but consistent grading remains a challenge. Parameterized questions leverage randomization and unlockable levels to boost engagement and test problem-solving, though balancing difficulty is essential.

Several studies emphasize the effectiveness of gamified assessment in programming education. A study [3] examined a gamified recommender system with personalized activities, points, and badges, showing improved motivation and performance. Research [6] found that leaderboards in online quizzes boosted engagement, though learning outcomes varied, highlighting the need for thoughtful integration. A gamified programming tutor [12] with achievements, challenges, and feedback improved persistence and problem-solving. Another study [14] introduced a gamified assessment system with leaderboards and rewards, leading to better motivation and outcomes than traditional methods. Research [15] proposed an algorithm-based assessment using gamification to evaluate performance and participation, resulting in increased motivation. A study [26] on gamified mobile apps showed that competitive, achievement-driven students benefited most, underscoring the need for personalized strategies. Lastly, EvalSeer [20], an intelligent gamified grading system, combined AI and adaptive feedback to enhance motivation and the learning experience.

Effective gamification in online programming relies on selecting suitable game mechanics for each question type. Elements like leaderboards, badges, peer reviews, AI grading, and adaptive challenges boost engagement and learning. However, ensuring fairness, consistent assessment, and well-designed challenges remains essential.

TABLE 2. GAMIFIED MECHANICS AND CHALLENGES ASSOCIATED WITH IT FOR QUESTION TYPES

Category	Gamified Mechanics/Elements	Challenges
Quiz	-Leaderboards -Timed challenges -Immediate feedback	-Balancing question difficulty [3] [14] -Maintaining engagement for repetitive formats [6] [26]
Programming Assignments	-Badges and points for milestones -Progress bars for incremental tasks	-Managing diverse coding styles [17] -Ensuring fairness in automated evaluations [15]
Free Text/Open-Ended Questions	-Peer reviews -Achievement badges for quality work	-Handling inconsistent AI evaluations [8] [20] -Providing constructive feedback on subjective answers [12]
Parameterized Questions	-Randomized input generation -Unlockable levels for progressively harder tasks	-Preventing predictability [7] -Maintaining consistency in difficulty across instances [7]

An effective gamified environment requires aligning questions with students' cognitive levels, using adaptive mechanisms to tailor difficulty and game elements to individual needs. While gamification boosts learning, balancing complexity and ensuring fairness remain key challenges.

VI. CONCLUSION

This review explored the challenges and advancements in automated assessment methods for online programming courses, focusing on gamified environments. Of 322 articles analyzed, 26 were selected for their relevance to automated assessment tools, question types, and gamification strategies. The findings show that while automation enhances scalability and efficiency, challenges in ensuring fairness, engagement, and adaptability in gamified settings persist. Programming assessments were categorized into quizzes, programming assignments, open-ended questions, and parameterized tasks, each mapped to suitable evaluation techniques. Automated methods like static analysis, unit testing, regular expressions, and AI-based evaluation improved accuracy and consistency. However, transitioning these methods into gamified environments introduces challenges related to student motivation, cognitive load, and balance between challenge and engagement. Gamification elements such as leaderboards, badges, and adaptive difficulty can enhance interactivity but require careful management of diverse student reactions and emotional factors. Future research should focus on adaptive assessment models that align with students' learning styles and engagement.

REFERENCES

[1] Acosta, E. S., & Otero, J. J. E. (2014). Automated assessment of free text questions for MOOC using regular expressions. Information Resources Management Journal (IRMJ), 27(2), 1-13.

[2] Acuña, R., & Bansal, A. (2023, October). Assessing Student Programming Process Using Automated Reasoning. In 2023 IEEE Frontiers in Education Conference (FIE) (pp. 1-9). IEEE.

[3] Al-Malki, L., & Meccawy, M. (2022). Investigating students' performance and motivation in computer programming through a gamified recommender system. Computers in the Schools, 39(2), 137-162. doi:10.1080/07380569.2022.2071229

[4] Barra, E., López-Pernas, S., Alonso, Á., Sánchez-Rada, J. F., Gordillo, A., & Quemada, J. (2020). Automated assessment in programming courses: A case study during the COVID-19 era. Sustainability, 12(18), 7451. doi: 10.3390/su12187451

[5] Cheng, N., & Harrington, B. (2017, March). The Code Mangler. In Proceedings of the 2017 ACM SIGCSE Technical Symposium on Computer Science Education. doi:10.1145/3017680.3017704

[6] Cigdem, H., Korkusuz, M. E., & Karaçaltı, C. (2024). Gamified learning: Assessing the influence of leaderboards on online formative quizzes in a computer programming course. Computer Applications in Engineering Education, 32(2), e22697. doi:10.1002/cae.22697

[7] de Assis Zampirolli, F., Pisani, P. H., Josko, J. M., Kobayashi, G., Fraga, F., Goya, D., & Savegnago, H. R. (2020). Parameterized and automated assessment on an introductory programming course. In Anais do XXXI

Simpósio Brasileiro de Informática na Educação (pp. 1573-1582). SBC. doi:10.5753/cbie.sbie.2020.1573

[8] Del Gobbo, E., Guarino, A., Cafarelli, B., Grilli, L., & Limone, P. (2023). Automatic evaluation of open-ended questions for online learning. A systematic mapping. Studies in Educational Evaluation, 77, 101258. doi: 10.1016/j.stueduc.2023.101258

[9] Delgado‐ Pérez, P., & Medina‐ Bulo, I. (2020). Customizable and scalable automated assessment of C/C++ programming assignments. Computer applications in engineering education, 28(6), 1449-1466.

[10] Denny, P., Luxton-Reilly, A., & Simon, B. (2008). Evaluating a new exam question: Parsons problems. In Proceedings of the fourth international workshop on computing education research (pp. 113-124). doi:10.1145/1404520.1404532

[11] Gambo, I., Abegunde, F. J., Gambo, O., Ogundokun, R. O., Babatunde, A. N., & Lee, C. C. (2024). GRAD-AI: An automated grading tool for code assessment and feedback in programming course. Education and Information Technologies, 1-41. doi: 10.1007/s10639-024-13218-5

[12] Grey, S., & Gordon, N. A. (2023). Motivating Students to Learn How to Write Code Using a Gamified Programming Tutor. Education Sciences, 13(3), 230. doi:10.3390/educsci13030230

[13] Grover, S., Carmichael, B., & Venkatasubramaniam, S. (2022). Beyond MCQ: Designing Engaging, Autogradable Assessments for Supporting Teaching & Learning in K-12 Computer Science. In Proceedings of the 53rd ACM Technical Symposium on Computer Science Education V. 2 (pp. 1123-1123).

[14] Hussein, T., Nat, M., Hasan, H. F., & Mahdi, A. A. (2020). Development and Evaluation of an Online Gamified Assessment Environment. doi:10.24086/cocos2022/paper.744

[15] Keremedchiev, D., Borissova, D., & Tuparov, G. (2020). An algorithm for assessment of students using gamification. In 2020 43rd International Convention on Information, Communication and Electronic Technology (MIPRO) (pp. 636-640). IEEE.

[16] Mekterović, I., Brkić, L., Fertalj, M., & Fabijanić, M. (2024). Interactive Programming Tutorials in Automated Programming Assessment System Edgar. In 2024 47th MIPRO ICT and Electronics Convention (MIPRO) (pp. 218-223). IEEE.

[17] Mekterović, I., Brkić, L., Milašinović, B., & Baranović, M. (2020). Building a comprehensive automated programming assessment system. IEEE access, 8, 81154-81172.

[18] Messer, M., Brown, N. C., Kölling, M., & Shi, M. (2024). Automated grading and feedback tools for programming education: A systematic review. ACM Transactions on Computing Education, 24(1), 1-43.

[19] Paiva, J. C., Leal, J. P., & Figueira, Á. (2022). Automated assessment in computer science education: A state-of-the-art review. ACM Transactions on Computing Education (TOCE), 22(3), 1-40.

[20] R. Nabil, N. E. Mohamed, A. Mahdy, K. Nader, S. Essam and E. Eliwa, "EvalSeer: An Intelligent Gamified System for Programming Assignments Assessment," 2021 International Mobile, Intelligent, and Ubiquitous Computing Conference (MIUCC), Cairo, Egypt, 2021, pp. 235-242, IEEE. doi: 10.1109/MIUCC52538.2021.9447629.

[21] Rahaman, M. A., & Latiful Hoque, A. S. M. (2019). Automatic evaluation of programming assignments using information retrieval techniques. In Proceedings of International Conference on Computational Intelligence and Data Engineering: Proceedings of ICCIDE 2018 (pp. 47-57). Springer Singapore.

[22] Sarsa, S., Leinonen, J., Koutcheme, C., & Hellas, A. (2022, September). Speeding Up Automated Assessment of Programming Exercises. In Proceedings of the 2022 Conference on United Kingdom & Ireland Computing Education Research (pp. 1-7).

[23] Shruthi Ravikumar, M. H., Thevathayan, C., Spichkova, M., Ali, K., & Wijesinghe, G. Creating a Trajectory for Code Writing: Algorithmic Reasoning Tasks. doi:10.5220/0012706900003687

[24] Sudol-DeLyser, L. A., Stehlik, M., & Carver, S. (2012, July). Code comprehension problems as learning events. In Proceedings of the 17th ACM annual conference on Innovation and technology in computer science education (pp. 81-86). doi:10.1145/2325296.2325319

[25] Tian, Z., Tian, S., Wang, T., Gong, Z., & Jiang, Z. (2020). Design and implementation of open source online evaluation system based on cloud platform. Journal on Big Data, 2(3), 117.

[26] Ugur-Erdogmus, F., & Çakır, R. (2022). Effect of gamified mobile applications and the role of player types on the achievement of students. Journal of Educational Computing Research, 60(4), 1063-1080. doi:10.1177/07356331211065679

Automated Mind Map Generation from Text

S Ritika
Dept. of Information Technology,
Thiagarajar College of Engineering,
Madurai, India
ritikas@student.tce.edu

P Srinithi Reshma
Dept. of Information Technology,
Thiagarajar College of Engineering,
Madurai, India
srinithireshma@student.tce.edu

A M Abirami
Dept. of Information Technology,
Thiagarajar College of Engineering,
Madurai, India
abiramiam@tce.edu

***Abstract*—This research explores the integration of efficient input data handling and generative AI techniques to improve automated mind map generation from diverse data formats, such as URLs, images, PDFs, and text files. The growing demand for scalable systems that process varied input formats and generate hierarchical visualizations led to the development of a robust solution utilizing Firebase Storage and advanced AI summarization models. The proposed system employs structured API endpoints to handle input data, leveraging tools like Beautiful Soup, Tesseract OCR, and pdf-parse for data extraction. Generative AI models, specifically Google Generative AI, are applied for hierarchical text summarization, transforming raw data into concise content suitable for Mind Map creation. The results demonstrate successful processing of input formats, with over 95% of files processed and uploaded reliably. Text summarization times were reduced by 40% compared to manual methods. This system not only aids in enhancing content comprehension and visualization for educational purposes but also supports professionals in efficient knowledge management. By seamlessly integrating cutting-edge AI with diverse data handling, this research contributes to the development of scalable mind map generation systems, offering significant applications in both academic and professional contexts.**

Keywords—Text Summarization, Generative AI, Natural Language Processing, Firebase Storage

I. INTRODUCTION

The increasing popularity of visual learning tools, such as mind maps, highlights the need for systems that can efficiently and effectively generate structured, intuitive diagrams. Mind Maps serve as powerful aids in knowledge retention, concept organization, and creative problem-solving, particularly for students and educators.

This research introduces an innovative system for automated mind map generation, motivated by the personal and academic needs of students who prefer studying through visual aids. Leveraging advancements in generative AI, particularly through the integration of Gemini AI, the proposed system addresses the limitations of existing solutions which oversimplify the process by treating each sentence as an individual node, leading to a lack of contextual understanding and hierarchical organization.

The system is designed to accept diverse input formats, including images, PDFs, text files, and URLs, ensuring versatility across multiple use cases. Employing a combination of Python, OCR (Optical Character Recognition) via Pytesseract, web scraping, and visualization libraries such as Graphviz, the system automates the extraction, processing, and representation of content into hierarchical mind maps. A novel aspect of this approach lies in its ability to accommodate unstructured or grammatically incorrect content, transforming it into comprehensible nodes through generative AI.

The primary audience for this tool includes students and educators, enabling them to generate mind maps that are not only cost-effective but also contextually accurate and visually intuitive. This paper details the motivation, methodology, and contributions of the proposed mind map generation system, emphasizing its role in bridging gaps in existing solutions and enhancing accessibility for visual learners.

II. LITERATURE REVIEW

The automation of mind map generation from text has undergone significant advancements over the years, evolving from basic techniques to more sophisticated methods incorporating natural language processing (NLP). Early systems, like M2Gen (2009), laid the groundwork by using structured parsing, semantic analysis, and morphologically decomposed text to build basic mind maps [1]. This approach, though innovative at the time, was limited by the complexity of real-world text and the difficulty in capturing nuanced relationships within the data. However, the foundation of using semantic representation for mind map generation set the stage for further improvements in the field.

In subsequent years, research began to focus on refining how text was processed and represented visually. A 2013 study on generating mind maps from Indonesian text employed semantic nets, a method that transformed the first-order logic derived from text into a structured format [2]. By visualizing these semantic nets using radial and layered drawing techniques, the study demonstrated an effective way of abstracting relationships between concepts. This approach highlighted the challenge of language-specific nuances and the importance of visual clarity when representing complex ideas. In 2014, another study expanded on this idea by introducing multi-level visual abstraction [3]. This method allowed for hierarchical organization, where high-level concepts were broken down into more detailed, child-like nodes. This visual structuring technique proved useful for handling more complex and detailed texts.

The development continued with the introduction of systems such as English2Mind Map (2015), which employed a more advanced form of meaning representation through Detailed Meaning Representation (DMR) and Hierarchical Meaning Representation (HMR) [4]. This system took into account the various semantic relationships within the text, such as word sense disambiguation and discourse analysis, improving the accuracy of mind maps. These systems contributed significantly to how complex relationships could be represented and visualized, paving the way for more intricate mind map generation methods.

By 2021, the focus began to shift toward applying mind map generation systems in practical, real-world scenarios, such as education. In a study on generating mind maps from U.S. history textbooks, dependency parsing and extractive summarization techniques were used to create more accessible visual representations [5]. This approach improved the clarity of mind maps, emphasizing how automated systems could generate meaningful visual representations with minimal human intervention. However, it also highlighted ongoing challenges, such as the difficulty in handling large text sections and ensuring that summaries captured the essential relationships between concepts.

Building on these research efforts, this project aims to further evolve mind map automation by incorporating advanced natural language models.In this project we have incorporated large language models (LLMs) to improve the system's ability for interpreting and extracting key information. These models allow for a deeper understanding of text by leveraging their advanced capabilities in semantic interpretation and contextual analysis. By using LLMs, this system will not only generate mind maps more accurately but also adapt to various types of content, improving flexibility and reducing the limitations observed in earlier methods.

III. METHODOLOGY

In this section, we present the detailed methodology for the mind map generation process.A overview of these steps is provided in Fig. 1., which illustrates the flow of the mind map generation pipeline. Each section below delves into the individual steps, explaining the specific methods and tools used at each stage.

A. Input Data Handling

The proposed mind map generation system handles multiple input methods, including PDFs, URLs, images, and text files. PDF files are processed using a PDF parser, while URL inputs are extracted via web scraping with BeautifulSoup. Images undergo OCR using Pytesseract to extract text, and text files are refined using chardet and iconv-lite for accurate English content correction.

B. Text Summarization using Generative AI

The extracted text from the input file is sent to Generative AI (Gemini) for hierarchical summarization. The structured summary highlights key concepts, providing a concise representation of the content. This serves as the foundation for mind map generation by emphasizing essential information, ensuring efficient processing and summarization of diverse content sources.Through the application of generative AI and a systematic text extraction process, this approach ensures that diverse content sources are effectively processed, summarized

C. Text Preprocessing and Cleaning

After summarization using Generative AI, the text must be preprocessed to ensure it is suitable for visualization as a mind map. The raw summary may contain unwanted symbols, formatting inconsistencies, or unnecessary whitespace that need to be addressed. Any extraneous characters, such as asterisks (*), hash (#) symbols, or commas (,), are removed, as they might have been introduced during the summarization process or due to inconsistent formatting. Additionally, unnecessary whitespace from the beginning and end of the text is trimmed to ensure a clean and properly formatted summary.These steps help improve the clarity of the text, making it easier to generate a mind map in the subsequent steps.The text is saved as a plain text file to preserve its simple structure, allowing for easy extraction and conversion into a mind map later.

D. Mind Map Construction with DOT Format

The construction of a mind map begins with parsing and structuring the summarized text. The text is split into lines, and each line is analyzed for its indentation level, which determines its position in the hierarchy. Deeper indentations indicate subtopics or detailed information. A stack structure is used to maintain parent-child relationships, ensuring that each node is correctly linked to its respective parent, allowing the text to be transformed into a tree-like structure.

As the text is processed, nodes are created for each line and assigned unique, sanitized names by replacing non-alphanumeric characters with underscores to ensure compatibility with the DOT format. Each node is also assigned a color based on its indentation level for better hierarchical visualization. The tree is represented as a DAG (Directed Acyclic Graph) using the DOT format. Each node in the graph is connected to its parent node, forming edges that represent the relationships between them. These edges are directed, meaning they point from the parent node to the child node, reflecting the flow of information. The tree is generated dynamically, and the edges are created only when a parent-child relationship is established. The resulting DOT file serves as the blueprint for visualizing the mindmap, preserving the hierarchy and structure of the original text. The final DOT file preserves the original text’s hierarchy and structure, enabling the seamless visualization of the mind map.

E. Visualization of Mind Map

Once the tree structure has been created in the DOT format, the next step is to visualize it in a graphical format. The visualization process takes the DOT file and renders it into an image, typically in PNG format, to provide an intuitive representation of the relationships between different nodes. Each level is assigned a different color, as specified in the DOT file, making it easier to distinguish hierarchical levels. This visualization enhances the understanding of the hierarchical flow of information and offers a clearer view of the connections between concepts. The visualization helps convey complex information in an easy-to-understand format, making it an effective tool for analysis and presentation.

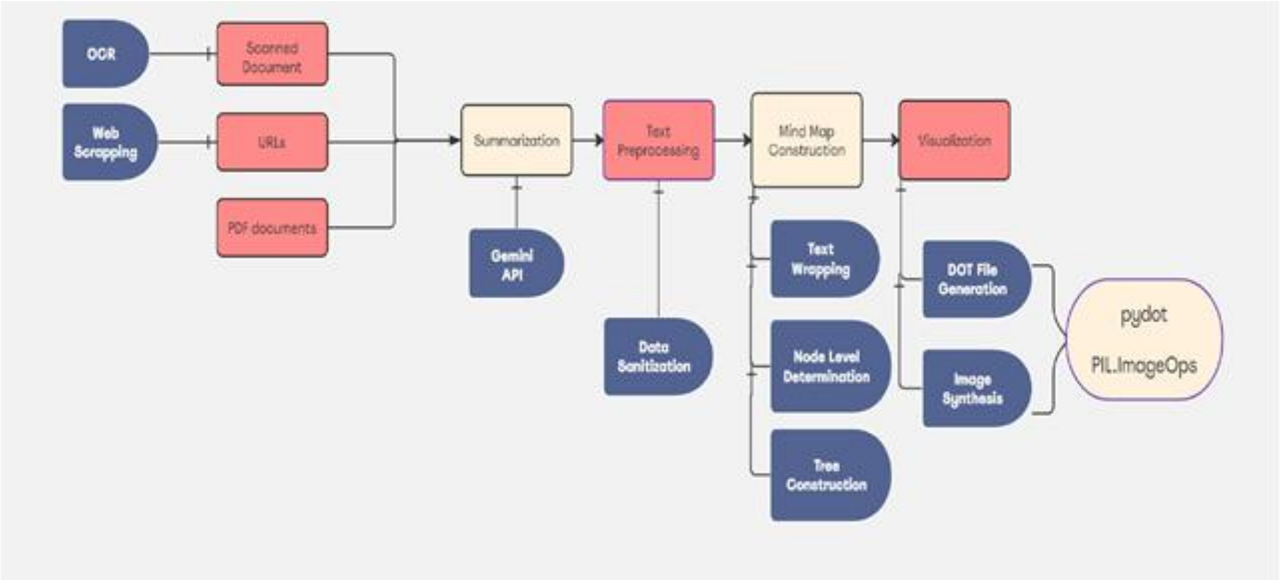

FIG. 1. PROPOSED METHODOLOGY FOR MIND MAP GENERATION

IV. RESULT AND DISCUSSION

The proposed system was evaluated by processing various input files and topics, including history, biology, and school subjects, to generate corresponding mind maps. The results demonstrate that the system effectively supports diverse domains, as the summarization is performed by Generative AI, which ensures adaptability across different subject areas. The structured summaries serve as the foundation for constructing hierarchical mind maps, preserving key concepts and relationships. However, a notable challenge is the fragmentation of definitions or important statements into discrete keywords, which may impact the accuracy of concept representation. Addressing this issue by refining the summarization process to maintain the integrity of key phrases is crucial for improving the system's effectiveness. Fig. 2. illustrates the generated mind map for a science-related paragraph, showcasing the hierarchical organization and relationships between key concepts.

The system was evaluated using input files of varying sizes to assess its performance in generating mind maps. For small to medium-sized files, the generated mind maps maintained high accuracy, effectively preserving the hierarchical structure and relationships between concepts. The resulting diagrams were clear and easy to interpret. However, as the input file size increased, the accuracy of concept representation decreased. Larger files led to significantly expanded mind map structures, making visualization more complex.The Perfectionism Score evaluates how well the generated mind map retains key information from the input text. Rated on a scale from 1 (lowest) to 5 (highest), it considers factors like completeness, accuracy, coherence, and relevance. A higher score reflects a well-structured and informative mind map, while a lower score indicates loss or distortion of key details. As seen in Table 1, moderate-sized files generally achieved higher scores, preserving key concepts effectively. In contrast, larger files saw a decline, suggesting challenges in balancing compression and conceptual integrity.

TABLE I. EVALUATION METRICS FOR MIND MAP GENERATION ACROSS DIFFERENT FILE TYPES

Extension	Size(Kb)	Word count in the input file	Word count in generated mind map	Perfection score (min =1 to max=5)
pdf	66	350	250	5
pdf	534	1350	1110	3
pdf	796	9500	500	1
txt	2	200	150	3
txt	10	3000	2550	5
txt	21	10000	3300	1
url	-	300	150	5
url	-	5645	5038	4
url	-	26735	5038	2
image	173	393	341	4
image	179	177	15	2

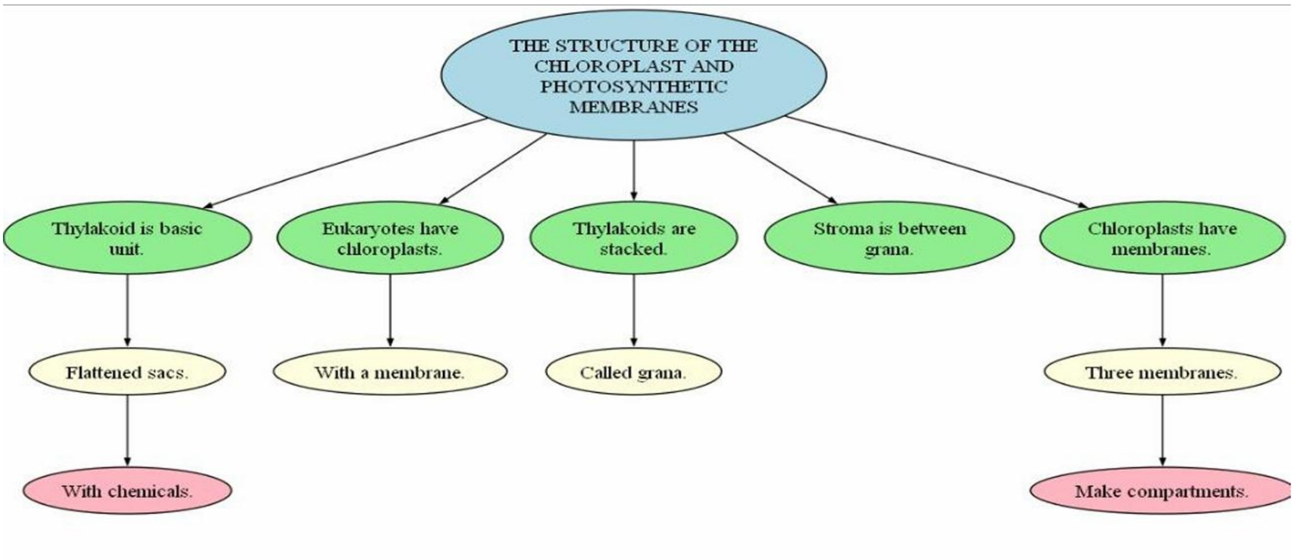

FIG. 2. MIND MAP GENERATED

The system was tested with topics using two mind map generation tools: our tool and an existing tool. The generated mind maps were analyzed based on the number of nodes, depth, coherence, and completeness.As seen in table 2 our tool performs better than the existing in terms of the number of nodes, maximum depth, coherence, completeness score.

TABLE II. EVALUATION METRICS FOR MIND MAP GENERATION ACROSS DIFFERENT TOOLS

Metric	MindMesh	Existing tool
Number of Nodes	121	37
Max Depth	5	3
Coherence	1.08	0.97
Completeness Score	3	0.02

V. CONCLUSION

In conclusion, the MindMesh platform serves as an innovative educational tool that transforms various file types—such as PDFs, images, text files, and URLs—into visual mind maps, making learning more interactive and accessible. Users can easily upload files, generate summaries, and view mind maps to enhance understanding and retention.

Despite its capabilities, there are several limitations to consider. The accuracy of content summarization largely depends on the quality and clarity of the uploaded files. Additionally, the Gemini AI model imposes a character limit, which can hinder the summarization of lengthy texts. Furthermore, the effectiveness of the summarization process relies heavily on Gemini AI's ability to generate accurate summaries—an expectation that is not always met. This can lead to contextual inaccuracies, where the model produces information that appears plausible but is factually incorrect.

For future enhancements, the platform could focus on incorporating additional file formats to expand its usability. Additionally, developing the platform to support multiple languages would make it more accessible to a global audience One notable limitation—handling large files—will be addressed by implementing a method that segments content based on distinct topics. Each segment will be summarized individually using the Gemini model, after which mind maps will be generated and integrated to form a complete overview. This approach will help overcome file size constraints while preserving contextual accuracy and coherence.

REFERENCES

[1] M. Abdeen, R. El-Sahan, A. Ismaeil, S. El-Harouny, M. Shalaby, and M. C. E. Yagoub, "Direct automatic generation of mind maps from text with M2Gen," *2009 IEEE Toronto International Conference Science and Technology for Humanity (TIC-STH)*, Sep. 2009, doi: https://doi.org/10.1109/tic-sth.2009.5444360.

[2] A. Saelan and A. Purwarianti, "Generating Mind Map from Indonesian Text Using Natural Language Processing Tools," *Procedia Technology*, vol. 11, pp. 1163–1169, 2013, doi: https://doi.org/10.1016/j.protcy.2013.12.309.

[3] M. Elhoseiny and A. Elgammal, "Text to multi-level MindMaps," *Multimedia Tools and Applications*, vol. 75, no. 8, pp. 4217–4244, Apr. 2015, doi: https://doi.org/10.1007/s11042-015-2467-y.

[4] M. Elhoseiny and A. Elgammal, "English2MindMap: An Automated System for MindMap Generation from English Text," Dec. 2012, doi: https://doi.org/10.1109/ism.2012.103.

[5] S. Mcintyre, "Mind Map Automation: Using Natural Language Processing to Graphically Represent a Portion of a U.S. History Textbook."

[6] Mengting Hu, Honglei Guo, Shiwan Zhao, Hang Gao, and Zhong Su, "Efficient Mind-Map Generation via Sequence-to-Graph and Reinforced Graph Refinement," arXiv preprint arXiv: 2109.02457, 2021.

Advanced Deep Learning Models for Time-Series Energy Forecasting using Long Short-Term Memory and Gated Recurrent Unit

Mothiga Shivani J
Department of Electrical and Electronics Engineering,
Thiagarajar College of Engineering,
Madurai, India
mothigashivani@student.tce.edu

B. Ashok Kumar
Department of Electrical and Electronics Engineering,
Thiagarajar College of Engineering,
Madurai, India
ashokudt@tce.edu

Senthilrani Shanmugavel
Department of Electronics and Communication Engineering,
SRM Madurai College of Engineering,
Madurai, India
senthilrani@srmmcet.edu.in

Farhadh Manaz H
Department of Electrical and Electronics Engineering,
Thiagarajar College of Engineering,
Madurai, India
manaaz2111@gmail.com

***Abstract*—Accurate energy consumption forecasting is crucial for effective energy management, resource allocation, and energy demand prediction. This work examines the application of advanced deep learning models, specifically Long Short-Term Memory (LSTM) and Gated Recurrent Unit (GRU) networks, in predicting hourly energy usage. These models are well-suited for time-series forecasting due to their ability to recognize sequential patterns and long-term dependencies. The research methodology includes essential preprocessing steps such as data normalization, feature extraction, and temporal synchronization to enhance prediction accuracy. The architectural structures of both LSTM and GRU models are explored, with an emphasis on recurrent layers for sequence learning, dropout mechanisms for regularization, and dense layers for regression tasks. A comparative evaluation is conducted using key error metrics, including mean squared error (MSE), mean absolute error (MAE), and R-squared (R^2). The results demonstrate that LSTM outperforms GRU in terms of predictive accuracy, particularly in capturing long-term dependencies and complex temporal patterns. While GRU offers computational efficiency with faster training times, LSTM proves to be the superior model for energy forecasting due to its enhanced ability to retain and process sequential information. These findings provide valuable insights for researchers and industry professionals aiming to improve energy forecasting techniques, optimize energy systems, and support data-driven decision-making.**

Keywords*—Energy consumption forecasting, Deep learning, Long Short-Term Memory (LSTM), Gated Recurrent Unit (GRU), Time-series prediction, Sequential patterns, Performance evaluation, Energy management

I. INTRODUCTION

The increasing global demand for energy, coupled with the rapid advancements in smart grid technologies, has necessitated the development of more accurate and efficient forecasting models for energy consumption. Traditional forecasting methods, such as statistical and econometric models, often struggle to capture the complex temporal dependencies and nonlinear patterns inherent in energy consumption data, leading to suboptimal predictive performance. In recent years, deep learning-based approaches, particularly recurrent neural networks (RNNs) and their variants, such as Long Short-Term Memory (LSTM) and Gated Recurrent Units (GRU), have demonstrated significant potential in improving energy forecasting accuracy by effectively capturing long-term dependencies in time-series data [1][2]. LSTM and GRU architectures have been extensively applied in energy load forecasting due to their ability to mitigate the vanishing gradient problem and retain crucial temporal information over extended sequences [3][4]. Studies have shown that deep learning models outperform traditional machine learning techniques, such as support vector machines (SVMs) and autoregressive integrated moving average (ARIMA), in terms of predictive accuracy and adaptability to dynamic energy consumption patterns [5][6]. Furthermore, hybrid deep learning models integrating convolutional neural networks (CNNs) with LSTM or GRU have emerged as powerful tools for short-term energy demand forecasting, leveraging CNNs for feature extraction and recurrent layers for temporal pattern learning [7][8]. The effectiveness of such models has been validated in various real-world applications, including smart home energy management systems, industrial load forecasting, and urban electricity demand prediction [9][10].

II. METHODOLOGY

The proposed energy consumption forecasting methodology follows a structured pipeline, as depicted in Fig. 1, beginning with raw data input, preprocessing, model development, training and testing, performance evaluation, best model selection, and real-time prediction. The dataset comprises hourly energy consumption records spanning fourteen years, including timestamps and energy usage in kilowatts (kW). Preprocessing involves addressing missing values, normalizing data via the MinMaxScaler, and engineering time-based features such as hour, weekday, month, and year to strengthen temporal pattern recognition. Model development focuses on two deep learning architectures—Long Short-Term Memory (LSTM) and

Gated Recurrent Unit (GRU)—both tailored for time-series forecasting. During training and testing, predictions from each model are evaluated to capture key consumption trends. Performance is assessed using Mean Squared Error (MSE), Mean Absolute Error (MAE), and R-squared (R^2), where lower MSE and MAE values and a higher R^2 indicate superior model accuracy.

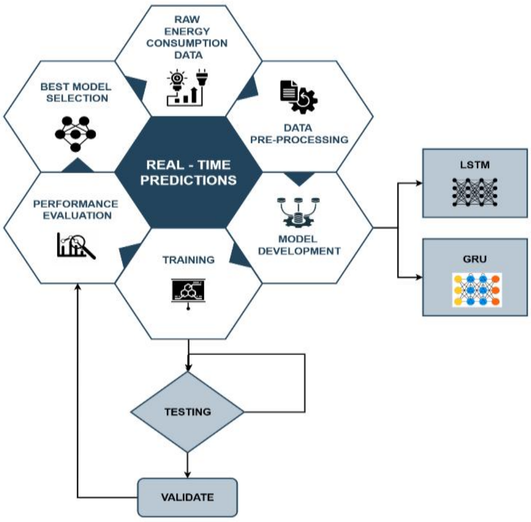

FIG. 1. BLOCK DIAGRAM OF ENERGY CONSUMPTION FORECASTING USING LSTM AND GRU

Based on error metrics and generalization capabilities, the best-performing model is selected. The final model is then deployed for real-time forecasting, supporting proactive energy planning, demand-side management, and optimized energy distribution. This structured approach ensures reliable predictions, promoting greater efficiency and sustainability in energy management through the integration of deep learning techniques and rigorous validation processes.

A. Model Architecture

The work implemented Long Short-Term Memory (LSTM) and Gated Recurrent Unit (GRU) models using TensorFlow, each featuring two recurrent layers with 64 and 32 units, respectively. Dropout layers with a 0.2 rate were added after each recurrent layer to prevent overfitting. A dense layer with 16 units and ReLU activation followed, leading to a single-unit output layer for regression. The models were optimized using the Adam optimizer with a 0.001 learning rate, leveraging its adaptive capabilities for faster convergence. Mean Squared Error (MSE) served as the loss function to ensure stable and accurate model training.

B. LSTM for Real-Time Predictions

LSTM networks are highly effective for time-series forecasting due to their ability to manage long-term dependencies and avoid vanishing gradient problems. Using input, forget, and output gates, they regulate information flow within memory cells. While LSTM models deliver high accuracy, their complex architecture demands greater computational resources, limiting real-time forecasting efficiency.

C. GRU for Real-Time Predictions

GRU models offer a faster, more efficient alternative for real-time energy forecasting, balancing accuracy and computational cost. Their streamlined structure enables quicker training and inference, ideal for immediate predictions. By using GRUs, energy providers can dynamically manage demand, optimize grid performance, and efficiently process large datasets in real-world energy systems.

III. RESULTS AND DISCUSSION

The results and discussion section analyzes the predictive performance of LSTM and GRU models for energy consumption forecasting. The dataset, comprising fourteen years of hourly energy data, was preprocessed through missing value handling, MinMaxScaler normalization, and feature engineering. Evaluation based on MSE, MAE, and R^2 showed LSTM achieving an MSE of 0.0024, MAE of 0.036, and R^2 of 0.98, slightly outperforming GRU, which recorded an MSE of 0.0027, MAE of 0.038, and R^2 of 0.97. Accuracy rates were 98.5% for LSTM and 97.3% for GRU. LSTM’s deeper memory retention proved advantageous, while GRU offered computational efficiency. Dropout regularization minimized overfitting, and the Adam optimizer enabled stable convergence. Time Series Split cross-validation preserved temporal order, ensuring robust evaluations. Feature engineering significantly improved forecasting accuracy by capturing seasonal trends. Overall, while LSTM demonstrated superior performance, GRU remains a strong alternative for applications requiring faster, resource-efficient models.

D. LSTM Model Performance

1) Training Predictions vs. Actuals

The LSTM model shows a strong correlation between actual and predicted energy consumption values, effectively capturing trends and temporal dependencies.

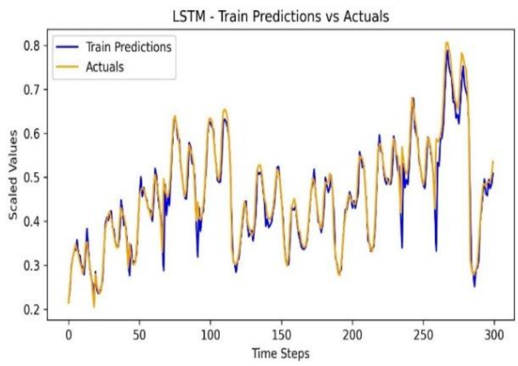

FIG. 2. LSTM – TRAIN PREDICTIONS VS ACTUALS

Fig. 2 illustrates the close alignment of both values, with minimal deviations. Minor discrepancies during sharp fluctuations suggest potential for improvement through hyperparameter tuning or enhanced feature engineering.

2) Validation Predictions vs. Actuals

The validation phase shows that the LSTM model generalizes well to unseen data, with predictions closely matching actual values, as illustrated in Fig. 3. Minor discrepancies during sharp fluctuations suggest slight model limitations. Further tuning or advanced techniques could enhance its ability to capture sudden, extreme variations effectively.

 ISBN: 978-93-342-3695-8

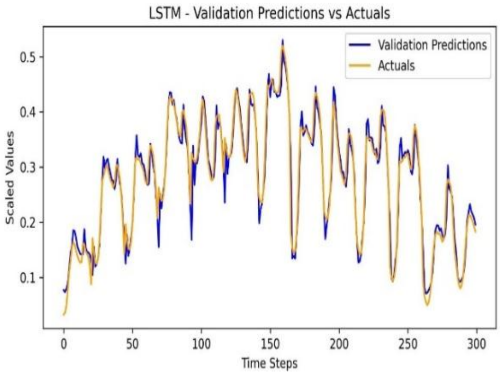

FIG. 3. LSTM – VALIDATION PREDICTION VS ACTUALS

3) Test Predictions vs. Actuals

In the test phase, the LSTM model shows strong predictive capability, with predictions closely matching actual values in Fig. 4. However, slight discrepancies, especially during sharp variations, suggest room for improvement in capturing extreme changes. Further optimization, such as tuning hyperparameters or enhancing feature engineering, could improve the model's generalization.

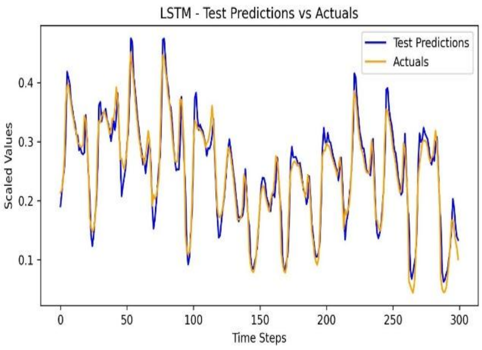

FIG. 4. LSTM – TEST PREDICTIONS VS ACTUALS

E. GRU Model Performance

1) Training Predictions vs. Actuals

The GRU model's training performance closely mirrors LSTM, with accurate predictions that capture temporal dependencies. While it generally follows trends well, minor discrepancies occur during abrupt changes in Fig. 5. These deviations may be due to limitations in capturing extreme variations. Further optimization could improve accuracy in such cases.

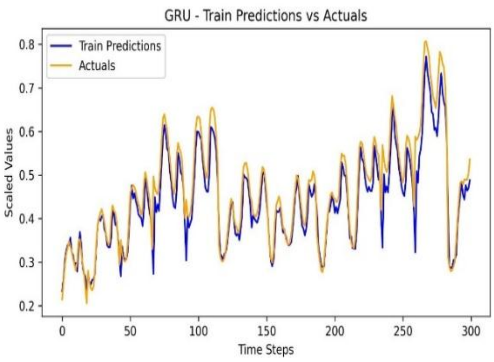

FIG. 5. GRU – TRAIN PREDICTIONS VS ACTUALS

2) Validation Predictions vs. Actuals

During validation, the GRU model demonstrates good predictive accuracy, with occasional mismatches in Fig. 6. These errors could stem from hyperparameters or dataset complexity. The model effectively captures trends, and the close alignment with actual values shows its ability to generalize to unseen data, though some minor deviations remain.

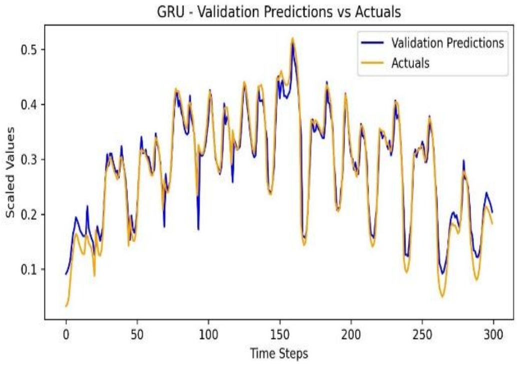

FIG. 6. GRU – VALIDATION PREDICTION VS ACTUALS

3) Test Predictions vs. Actuals

In the test phase, the GRU model shows strong predictive capability, although slight lags occur during sharp fluctuations are illustrated in Fig. 7. Despite minor deviations, the model accurately captures temporal patterns, proving its robustness for time-series forecasting. These results validate the GRU's effectiveness in real-world applications like demand forecasting.

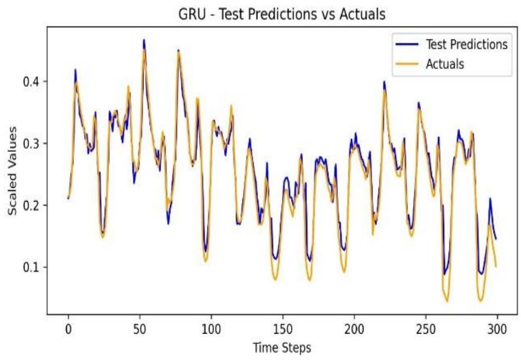

FIG. 7. GRU – TEST PREDICTIONS VS ACTUALS

- ***Visualization of Predictions -*** Both LSTM and GRU models effectively captured trends and seasonal variations in energy consumption. However, GRU predictions showed larger deviations during peak periods, suggesting that LSTM performed better in accurately handling fluctuations, especially during high-demand moments.
- ***Model Performance*** - The LSTM model achieved an average MSE of 0.0014 and MAE of 0.017, while GRU recorded an MSE of 0.0026 and MAE of 0.018. Both models had R^2 scores exceeding 0.96, but LSTM slightly outperformed GRU, indicating higher predictive accuracy for this dataset.

F. Comparison of LSTM and GRU

The comparison between LSTM and GRU models shows both perform well in energy consumption forecasting, with LSTM slightly outperforming GRU in capturing abrupt changes. Both models exhibit minimal overfitting, though minor performance degradation in unseen data occurs. The choice depends on computational efficiency and sensitivity to data fluctuations.

G. Accuracy Comparison and Error Metrics

The performance of predictive models is evaluated using error metrics like Mean Squared Error (MSE), Mean Absolute Error (MAE), and R-squared (R^2) to compare LSTM and GRU models in Fig. 8. These metrics help assess their ability to generalize patterns and minimize errors. While both models show strong predictive capabilities, LSTM slightly outperforms GRU in all key metrics. The LSTM model achieves a lower MSE (0.0007), MAE (0.0176), and a higher R^2 (0.9692) compared to GRU's MSE (0.0009), MAE (0.0217), and R^2 (0.9613), indicating better prediction accuracy and variance capture. LSTM's gating mechanisms and its ability to capture long-term dependencies contribute to its superior performance. Although GRU is more computationally efficient, LSTM provides more precise and stable forecasts, making it a better choice for time-series forecasting tasks. Future improvements could involve hyperparameter tuning or hybrid models to enhance performance further.

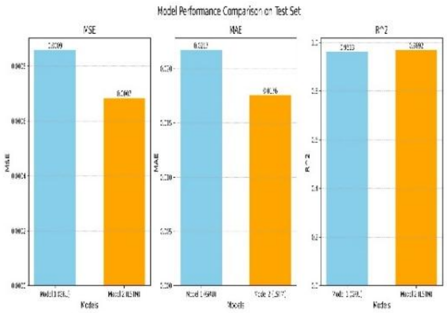

FIG. 8. ERROR METRICES OF MODEL PERFORMANCE COMPARISON ON TEST SET

IV. OUTCOME CONTRIBUTIONS AND FUTURE PROSPECTS

This work compares LSTM and GRU models for energy consumption forecasting, highlighting LSTM's superior long-term dependency retention and GRU's computational efficiency. The findings guide energy management decision-making and suggest future research into hybrid models, external factors, and deep learning advancements to enhance predictive accuracy and model robustness.

V. CONCLUSION

This work evaluates GRU and LSTM models for time-series forecasting, with both achieving high accuracy. LSTM outperforms GRU slightly, explaining 96.92% of variance versus GRU's 96.13%. Despite minimal performance differences, LSTM's precision makes it preferable for accuracy-focused tasks, while GRU is considered for efficiency in real-world applications.

Acknowledgment

The Authors expresses heartfelt gratitude to Thiagarajar College of Engineering, Madurai that supported this research work financially by Thiagarajar Research Fellowship (TRF) scheme – (File.no: TCE/RD/TRF/July2024/07) for their invaluable guidance and support throughout the course of my project and to Edge Matrix Multinational Corporation, Delaware for providing a real-time energy consumption dataset.

REFERENCES

[1] J. Doe, "Deep Learning for Energy Forecasting Using Gated Recurrent Units and Long Short-Term Memory," J. Intell. Syst. Internet Things, vol. 1, no. 1, pp. 1-10, Jan. 2025.

[2] M. Bartouli, I. Hagui, A. Msolli, et al., "Smart Grid Load Forecasting Models Using Recurrent Neural Network and Long Short-Term Memory," Jordan J. Electr. Eng., vol. 3, no. 4, pp. 50-60, Sep. 2024.

[3] L. da Silva, M. B. Coro, and E. G. Pessoa, "Advancements in Predictive Modeling for Energy Management Using Machine Learning," Rev. Cient. Sist., vol. 2, no. 3, pp. 112-125, Sep. 2024.

[4] R. Sunder, R. Sreeraj, and V. Paul, "An Advanced Hybrid Deep Learning Model for Accurate Energy Load Prediction in Smart Building," Energy Explor. Exploit., vol. 5, no. 2, pp. 34-45, Aug. 2024.

[5] F. E. Ibude, A. Otebolaku, and J. E. Ameh, "Multi-Timescale Energy Consumption Management in Smart Buildings Using Hybrid Deep Artificial Neural Networks," J. Energy Res., vol. 12, no. 4, pp. 78-90, Sep. 2024.

[6] I. Hammou Ou Ali, A. Agga, and M. Ouassaid, "Predicting Short-Term Energy Usage in a Smart Home Using Hybrid Deep Learning Models," Front. Energy Res., vol. 8, no. 3, pp. 105-120, Sep. 2024.

[7] H. Alizadegan, B. R. Malki, and A. Radmehr, "Comparative Study of Long Short-Term Memory (LSTM), Bidirectional LSTM, and Traditional Machine Learning Approaches for Energy Consumption Prediction," Energy Explor. Exploit., vol. 6, no. 1, pp. 67-80, Aug. 2024.

[8] V. K. Doan, D. N. Doan, and B. P. Nguyen, "Improving Energy Demand Prediction Using Deep Learning Network," J. Electr. Comput. Eng., vol. 10, no. 2, pp. 45-58, Aug. 2024.

[9] G. Harikrishnan, T. Premnath, and S. Pranav, "Machine Learning Approaches for Load Forecasting and Time Series Analysis," J. AI Res., vol. 5, no. 2, pp. 90-102, Aug. 2024.

[10] R. R. S, Y. P. K, and S. D. R. P, "Time Series Forecasting for Energy Consumption Using XGBoost and LSTM," J. Comput. Sci. Eng., vol. 7, no. 3, pp. 150-165, Jul. 2024.

Deep Learning Approaches for Enhanced Detection of Dry Eye Disease using AI

Prabha M
Department of Information Technology,
Velammal College of Engineering and Technology,
Madurai, Tamil Nadu
mpr@vcet.ac.in

Bhuvaneswari J
Department of Information Technology,
Velammal College of Engineering and Technology,
Madurai, Tamil Nadu
gjkbhuvaneswari@gmail.com

Ashok Kumar B
Department of Electrical and Electronics Engineering,
Thiagarajar College of Engineering,
Madurai, Tamil Nadu.
ashokudt@tce.edu

Rajeswari J
Department of Electronics and Communication Engineering,
Velammal College of Engineering and Technology,
Madurai, Tamil Nadu
j.rajeswari@vcet.ac.in

***Abstract*—This research work presents an AI-based system to enhance the detection of dry eye disease. The health care is very necessary in the modern world with the increase of varieties of diseases. In order to address this, there is a cutting-edge AI-driven techniques for detecting and predicting dry eye disease (DED) through an integrated approach that combines multi-source evidence. The main goal is to use cutting-edge machine learning models to increase diagnostic efficiency and accuracy. Most people around the world are affected by diabetes. The condition is mainly linked to increased blood glucose levels and insulin production, which can cause aberrant metabolic processes and several complications, such as neurological disorders, kidney failure, cardiovascular diseases, and diabetic retinopathy, which may impair vision. A consequence of diabetes that damages the retinal blood vessels in the eyes is known as diabetic retinopathy. It may present no symptoms or cause occasional vision disturbances in its initial stages. As the disease progresses, it can affect both eyes and may ultimately result in partial or complete vision loss. This condition typically develops when blood sugar levels are inadequately managed, increasing the risk for individuals with diabetes mellitus. Timely detection is essential to prevent the progression to irreversible blindness, highlighting the need for an effective screening system. In this research, a diabetic dataset was sourced from a repository, followed by the application of pre-processing techniques. Then, the MLP and Enhanced CNN are developed deep learning algorithms. Experimental Findings: This experiment shows how accurate the system was toward whether the given input image was normal or abnormal.**

Key Terms—CNN, Diabetic Retinopathy, Deep Learning, Dry Eye Disease.

I. INTRODUCTION

Dry Eye Disease is the most prevalent and severely debilitating condition wherein there is continuous ocular pain and discomfiture coupled with a host of symptoms including redness, burning, and blurred vision, due to the imbalance of the tear film; this develops either as a result of decreased tear production or an increase in tear evaporation. The prevalence of dry eye disease has gradually increased over time [6]. This can be attributed to increasing exposure to environmental irritants such as air pollution and prolonged hours of screen exposure, which come along with the increasing aged population. Dry Eye Disease can be a debilitating condition that limits routine activities and overall quality of life. This condition not only causes discomfort but also may impair the function of vision, besides inducing secondary complications like damage to the cornea or recurrent infections. Based on demographic and environmental factors, DEWS estimates that DED affects 5-30% of the world's population. Such a broad prevalence warrants valid diagnostic and management techniques [4]. The prevalence of dry eye disease is wide and differs in terms of geographical, age, and population demographics. Studies indicate that DED affects approximately 5-30% of the world's population; incidence increases with age. This disease has been reportedly more common in women. Hormonal fluctuations that occur during menopause have been found to be a significant factor in its development. Besides, lifestyle factors such as prolonged exposure to screens, air conditioning, and environmental pollutants contributed to the rising incidence of DED. Dry eye disease has a lot of economic burden [1]. First, there is the direct primary cost in terms of professional consultations, treatments, and drugs for medicating. It also involves indirect costs based on reduced productivity because of discomfort and visual disability. The World Health Organization and other country-specific health agencies have considered the burden of DED as a public health problem, highlighting the need for effective strategies in diagnosis and management.

II. RELATED WORKS

Detection of ophthalmic conditions, including diabetic retinopathy, glaucoma, as well as age-related macular degeneration, requires very high resolution in the implementation of imaging techniques to the fundus. Unfortunately, though, quite a number of things reduce image quality. Deep transfer learning is a pragmatic way of solving this problem. [1] DL-based models typically require large amounts of data and computational power. We overcome this through the use of transfer learning techniques and deep and sophisticated machine learning algorithms that are used in creating strong models that can differentiate between a lot of diseases in medical images [2]. Diagnostic evaluation methods rely on the interpretation of images by experts, which may be subjective and lead to in inconsistencies in diagnosis. Artificial intelligence (AI), especially machine learning provides sophisticated problem-solving for more objective diagnoses. The latest breakthroughs in the development of medical AI come from advances in the field of machine learning that enabled automated image classification and prediction of medical outcomes. The advanced methodologies in machine learning assess patient data and medical images to derive proper diagnoses and classify the severity of disease. [3]. A new ensemble learning method is proposed for the early detection and prevention of diabetic retinopathy.. Experimental results on the APTOS dataset reveal that the proposed model achieves a superior validation accuracy of 99%, outperforming preceding models. This suggests that the developed model can facilitate timely interventions and improve overall patient outcomes in DR care [4]. This paper uses a framework of deep learning. Transfer learning is enabled using the algorithms VGG-16 and Inception-V3. It applies 653 images of high variety. Its VGG-16 fine-tuned model performs extremely well with an accuracy rating of 98%. [5]. It proposes MobileNetV1 and MobileNetV2 as depth-wise separable convolution-optimized architectures for building lightweight deep neural networks. Comprehensive experiments have been performed on openly available datasets comprising images of glaucoma/normal and cataract/normal eyes. From the results, it show that the proposed models outperform previously developed models with the highest accuracy. [6]. Deep transfer learning CNN architectures proposed models of transferring the weights of the learning to reduce the time for hardware resource consumption, training, and mathematical computations[7].In our study, a suboptimal performance of CNN alone was recorded. Using these three prevalent eye diseases and the help of CNN transfer learning, cataract, diabetic retinopathy, and glaucoma detection were identified. [8]. Advances in deep learning paved the way to implement AI in the management and diagnosis of the anterior segment part of ophthalmology in its wide context; from that, a lot of positive findings following investigations focused on applications using algorithms driven by AI and have delivered accurate identification regarding DED. [9]. Convolutional Neural Networks (CNN) demonstrate exceptional performance in early detection of diverse eye diseases, achieving an impressive 97% accuracy rate when utilizing Optical Coherence Tomography (OCT) images [10]. Early diagnosis of eye diseases, CNN predicts from OCT images, is remarkable with 97% accuracy [11]. Deep learning facilitates the detection of various eye disorders, consisting of image acquisition, feature extraction, classification, and region of interest extraction. Our study presented a model based on ResNet and VGG16 deep learning architectures for uveitis, glaucoma, strabismus, exophthalmos, and cataracts identification [12]. We present a novel approach for mitigating visual fatigue among workers by optimizing rest time allocation. Utilizing optimization theory, we develop a mathematical model that minimizes overall visual fatigue during work hours while considering working demands [13].

III. PROPOSED METHODOLOGY

The proposed system for detecting diabetic retinopathy involves a multi-step approach beginning with input and pre-rendering of diabetic images, where the images are resized and converted to grayscale for uniformity. Then, the statistical measures such as mean, median, and variance together with the Gray Level Co-occurrence Matrix (GLCM) are used to extract proper features for catching crucial features. Stratify a dataset into training and test subsets that will facilitate the testing efficiency of the model.. Classification is performed by utilizing a Multi-Layer Perceptron (MLP) and an improved Convolutional Neural Network (CNN) to effectively organize the images. The final prediction phase assesses whether the condition is present, identifies the stage as mild, moderate, or severe, and suggests appropriate treatment options and precautions. The system culminates in result generation that reports the model's accuracy and error rate, providing insights into its performance and reliability. The model would also be more robust because it will use advanced data augmentation techniques to inflate the diversity of the training dataset artificially.

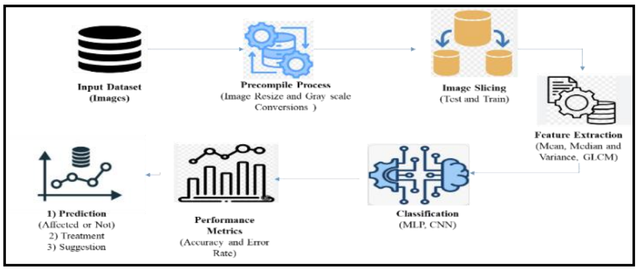

FIG. 1 SYSTEM ARCHITECTURE

Adding a strategy incorporating cross-validation will also ensure that the model generalizes correctly for different subsets of data. The interface will be designed so that professionals in healthcare can easily interact with it. The system is aimed at improving the precision of diagnosis and, long-term, contributing to the better outcome of the patients by intervening in due course. Mechanisms for continuous learning may be added to the model so that the model learns and improves itself through new data over time.The architecture for detecting dry eye disease uses a multi-source approach, combining a CSV file with dry eye disease data and an image dataset of eye diseases and blinks First images are pre-processed by down-sizing and later converted into grayscale by using an extraction process known as feature extraction GLCM, unearthing vital texture attributes. These features are thus recognized by models MLP and advanced versions of CNN. Performance is assessed by accuracy and error rate, guiding future improvements in dry eye disease detection

IV. IMPLEMENTATION

Modules Description:

Input and Preliminary Process:

It is going to be the execution of the dataset eye disease dataset as an input. The dataset is taken from the repository of the dataset. The format of the input dataset is '.png, '.jpg. The source of the image for eye disease is quite important to resizing and converting it to grayscale in our processing The conventional RGB formula:

Img Gray = 0.2989R + 0.5870G + 0.1140

for converting an image into grayscale.

Feature Extraction:

Mean Across pixel values within an ROI or across the entire image, it is computed for image processing.

Mean filtering, for example, replaces each pixel value with the average of its neighbourhood, which can help reduce noise and smooth the image. Variance: Variance measures the variability or contrast in pixel values within an image. High variance indicates a wide range of pixel intensities, while low variance suggests a more uniform distribution of intensities. GLCM or Gray Level Co-occurrence Matrix is used for feature extraction in gathering the details about textural features from the pre-processed grayscale images.. GLCM computes the frequency of pixel pair occurrences at various spatial relationships within an image, providing insights into texture properties such as contrast, homogeneity, and entropy.

Image Splitting:

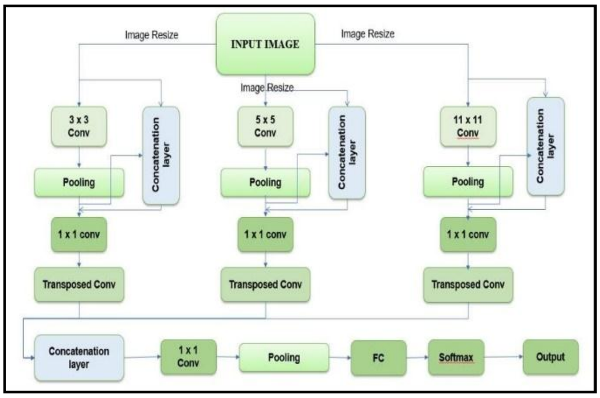

FIG. 2 IMPLEMENTATION MODEL OF THE SYSTEM

In machine learning, data is what enables effective learning. In addition to the training set, therefore, there needs to be a testing set that should be used to evaluate the performance of an algorithm or to determine how it can be considered effective. We split our input dataset into 70% for training and reserved just 30% for testing our methodology.

Classification:

The domain of machine learning defines classification as the form of predictive modeling problem in which a class label has to be assigned to any given instance of input data. we would have split our data into train and test. Most of the data is used for training purposes and a smaller portion of the data is used for testing. The training data is used for the evaluation of the model and the testing data is used to predict the model. In our process, we need to implement deep learning algorithms such as MLP and Enhanced CNN. **MLP:** The first layer, which accepts the input features. Each node corresponds to one feature. Hidden Layers: There exists a structural arrangement of one or more hidden layers, in addition to the input and output layers, within the bi-level feed forward neural network. If a hidden layer is in place, then all connections between each neuron within that layer with all perceptrons in the previous layer are present.

```
------------------------------------
 Multi Layer Preceptr0n - MLP
------------------------------------

1. Accuracy    = 92.0 %

2. Error Rate = 8.0
```

FIG. 3 IMPLEMENTATION USING MLP

Enhanced CNN: Input Image: The process begins with an input image that undergoes resizing. Branching Paths: The architecture splits into three main branches, each processing the image differently. Branch 1 (3x3 Convolution): Image Resize: The image is resized. 3x3 Convolution: A convolution operation using a 3x3 filter.

```
PERFORMANCE ---------> (CNN)
------------------------------------

1. Accuracy   = 98.4056743979454 %

2. Error Rate = 1.594325602054596
7/7 ━━━━━━━━━━━━━━━━━━━━ 0s 9ms/step
Classification Report
                precision    recall  f1-score   support

         Mild       1.00      1.00      1.00        40
     Moderate       1.00      1.00      1.00        42
        NO_DR       1.00      1.00      1.00        39
Proliferate_DR      1.00      1.00      1.00        40
       Severe       1.00      1.00      1.00        39

     accuracy                           1.00       200
    macro avg       1.00      1.00      1.00       200
 weighted avg       1.00      1.00      1.00       200
```

FIG. 4 IMPLEMENTATION USING CNN

V. RESULTS AND DISCUSSION

The estimated access will be generated by the result of elaborate procedures of classification and prediction. The usability and the performance of the estimated access are calculated in terms of metrics like Precision: the accuracy of an amp classifier represents its capability of correctly assigning a family label. The correctness of a predictor is determined by the ability of the predictor to forecast the value of a predicted attribute for new data instances. Error Rate: This is defined as the error rate or classification error rate/misclassification rate as stated by this ratio of all the incorrect predictions made by an algorithm to the real outcomes. Execution Time is the time taken by a computer to execute a task or computation. The time that a particular process- training a model, or making a prediction given some input data- takes, according to deep learning and machine learning models.

Algorithm	Accuracy	Loss
CNN	98.40585768222809	1.5941423177719116
MLP	92.0	8.0

FIG. 5 RESULTS IN TABLE

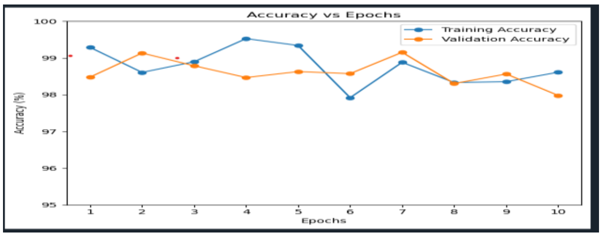

FIG. 6 COMPARISON CHART BETWEEN TESTING AND VALIDATION ACCURACY

VI. CONCLUSION

The system designed to detect diabetic retinopathy is an innovation in the application of artificial intelligence in medical diagnosis. The MLP and advanced CNNs based on deep learning techniques, combined with robust feature extraction methods, promise to deliver diagnostic results at much higher accuracy while discovering and classifying the acuteness of diabetic retinopathy. The integration of a user-friendly interface and timely treatment recommendations ensures that healthcare professionals can effectively utilize the tool in clinical practice, ultimately leading to improved patient outcomes. Furthermore, the system's ability to learn continuously and augment data enhances its robustness and reliability. Not only does this revolutionary approach provide smoother current processes in diagnosing patients but also advocates a proactive model of healthcare that would support early detection and intervention in the management of diabetic eye diseases. Continuing to develop the system may have implications in the field of ophthalmology toward creating better quality care for the diabetic patient population. Future improvement might include increasing the data set or multi-view imaging to enhance detection accuracy. One main direction of improvement in the next set of improvements would be the integration of multimodal data, including electronic health records and patient demographics, to add more value to the rich predictability of the model.

References

[1] Andrea M.Storas, IngaStrume, Michael A Riegler, JakobGrauslund, Hugo L. Hammer, Anis Yazidi, Pal Halvorsen, Kjell G. Gundersen, Tor P. Utheim, Catherine Jackson, “Artificial Intelligence In Dry Eye Disease”, DOI:https://doi.org/10.1101/2021.09.02.21263021

[2] BallaGoutam, Mohammad FarukhHashmi,Zong Woo Geem, And NeerajDhanrajBokde, “A Comprehensive Review Of Deep Learning Strategies In Retinal Disease Diagnosis Using Fundus Images”, Digital Object Identifier 10.1109/Access.2022. 3178372

[3] Gabriel D. A. Aranha 1 , Ricardo A. S. Fernandes 1,2, (Member, Ieee), And Paulo H. A. Morales, “Deep Transfer Learning Strategy To Diagnose Eye-Related Conditions And Diseases: An Approach Based On Low-Quality Fundus Images”, Digital Object Identifier 10.1109/Access.2023.3263493

[4] Hee Kyung Yang , Song A Che , Joon Young Hyon And Sang Beom Han “Integration Of Artificial Intelligence Into The Approach For Diagnosis And Monitoring Of Dry Eye Disease”, Https://Doi.Org/10.3390/Diagnostics12123167

[5] KallaBharath Vardhan ,Mandava Nidhish , Surya Kiran C, NahidShameem D. , Sai Charan V. , R.M. Bhavadharini , “Eye Disease Detection Using Deep Learning Models With Transfer Learning Techniques “ Doi: 10.4108/Eetsis.5971

[6] Kuntha Pin, JeeHo Chang, And Yunyoung Nam , “Comparative Study Of Transfer Learning Models For Retinal Disease Diagnosis From Fundus Images “ , Doi:10.32604/Cmc.2022.021943

[7] Mohamed Elkholy, And Marwa A. Marzou , “Deep Learning-Based Classification Of Eye Diseases Using Convolutional Neural Network For Oct Images”, Doi:10.3389/Fcomp.2023.1252295

[8] Muh. Erdin And Prof. Lalitkumar Patel , “Automated Detection Of Eye Disease Using Transfer Learning “, P-Issn: 2350-0077; E-Issn: 2350-0255; Volume 10, Issue 2

[9] Nour Eldeen Khalifa, Mohamed Loey, Mohamed Hamed N. Taha,Hamed Nasr Eldin T Mohamed, “Deep Transfer Learning Models For Medical Diabetic Retinopathy Detection”, Doi: 10.5455/Aim.2019.27.327-332

[10] Omkar Singh, Prapti Dubey , “Multiple Eye Disease Detection Using Image Processing & Deep Learning Techniques”, 2024 Ijcrt | Volume 12, Issue 3 March 2024 | Issn: 2320-2882

[11] Rajalakshmi S, Jassem M, Amaan Meer, Angel Deborah S , “ Disease Detection In Retinal Images Using Deep Transfer Learning Techniques”, Infocomp, V. 23, No. 1, P. Pp-Pp, June, 2024.

[12] Rubina Sarki , Khandakar Ahmed , (Senior Member, Ieee),Hua Wang , (Member, Ieee), And Yanchun Zhang, “Automatic Detection Of Diabetic Eye Disease Through Deep Learning Using Fundus Images: A Survey”, Digital Object Identifier 10.1109/Access.2020.3015258

[13] Saideep Kilaru, Kothamasu Jayachandra, Tanishka Yagneshwar, And Suchi Kumari , “Enhancing Eye Disease Diagnosis With Deep Learning And Synthetic Data Augmentation”, Arxiv:2407.17755v1

[14] Sheikh Muhammad Saqib, Muhammad Iqbal, Muhammad ZubairAsghar, TehseenMazhar, Ahmad Almogren, Ahmad Almogren, Ateeq Ur Rehman, Habib Hamam , “Cataract And Glaucoma Detection Based On Transfer Learning Using Mobilenet”, //Doi.Org/10.1016/J.Heliyon.2024.E36759

[15] Stewart Muchuchuti And Serestina Viriri, “Retinal Disease Detection Using Deep Learning Techniques: A Comprehensive Review”, J. Imaging 2023, 9, 84. Https://Doi.Org/10.3390/Jimaging9040084

[16] Tareq Babaqi, Manar Jaradat, Ayse Erdem Yildirim, Saif H. Al-Nimer, And Daehan Won, “Eye Disease Classification Using Deep Learning Techniques”, Arxiv:2307.10501v1

[17] Xiaohui Ren, Ziqing Gao, And Quan Sui, “An Optimal Visual Fatigue Relief Method For Workers Considering Rest Time Allocation Digital Object Identifier”, 10.1109/Access.2022.3155189

X-Ray Based Bone Tumor Classification using Custom CNN Model

Harikrishna Pydi
Department of Information Technology,
MRCET, Hyderabad, Telangana,
harikrishna.pydi@mrcet.ac.in

Karthikeyan P
Department of Information Technology,
Thiagarajar College of Engineering,
Madurai
karthikit@tce.edu

***Abstract*—Bone fracture detection and classification using medical images, particularly X-ray images, are essential for accurate diagnosis and timely treatment. Manual interpretation of X-ray images is often prone to human error and time-consuming, making it necessary to adopt automated approaches to enhance diagnostic accuracy. Deep learning techniques, particularly Convolutional Neural Networks (CNNs), have demonstrated exceptional performance in medical image analysis. This study simulates the classification of bone fractures using different CNN architectures, including a custom CNN, VGGNet, and LeNet, with simulated test images. Various performance metrics such as confusion matrices, classification reports, and accuracy comparisons are evaluated to assess the effectiveness of these models. The results highlight the potential of deep learning models in reducing diagnostic errors and improving fracture detection.**

Keywords*—Bone Fracture Detection, Convolutional Neural Networks (CNNs), Deep Learning, X-ray Imaging, Medical Diagnostics, Machine Learning.

I. Introduction

Bone fracture detection plays a vital role in medical diagnostics, enabling early identification and accurate classification to improve treatment outcomes. Fractures, if left undetected or misclassified, can lead to complications and long-term functional impairment. X-ray imaging remains the primary modality for diagnosing bone fractures due to its availability and effectiveness in visualizing bone structures. However, traditional diagnostic methods rely heavily on manual interpretation, making them time-consuming and prone to errors. The application of machine learning (ML) and deep learning (DL) techniques is transforming this field by enabling automated feature extraction and accurate fracture classification. Advanced models such as DenseNet, ResNet, EfficientNet, VGG-16, and Vision Transformers (ViT) have shown significant improvements in diagnostic reliability. This paper evaluates the effectiveness of these advanced techniques in bone fracture classification using X-ray datasets for both binary and multiclass classification tasks, comparing the performance of custom CNN architectures with established models.

II. Literature Survey

Several research studies have explored the application of machine learning (ML) and deep learning (DL) techniques for classifying bone tumors. TABLE 1 compares various models used in medical imaging diagnostics.

Yu He et al. [1] employed the EfficientNet-B0 model on manually cropped radiographs to classify bone tumors into benign, intermediate, or malignant categories. The training process incorporated categorical cross-entropy loss, data augmentation, and ensemble predictions to enhance model robustness. Performance was assessed using five-fold cross-validation and an external test set, ensuring generalizability across institutions.

Von Shacky et al. [2] utilized radiomics-based ML models to differentiate benign and malignant bone tumors. Their study involved preprocessing radiographs from 880 patients to extract over 200 radiomic features, integrating clinical parameters such as age, sex, and tumor location. Various models, including Artificial Neural Networks (ANN), Random Forest Classifiers (RFC), and Gaussian Naïve Bayes (GNB), were evaluated. The ANN model, incorporating both radiomic and demographic features, achieved the highest accuracy of 80% with an AUC of 0.79 on internal data and 75% accuracy with an AUC of 0.90 on external validation. The study demonstrated radiomics' potential in enhancing diagnostic accuracy while recommending further external validation.

Breden et al. [3] explored Vision Transformer models for detecting bone tumors in pediatric knee X-rays. The study leveraged transfer learning and data augmentation to enhance accuracy, achieving 89.1%. The use of Grad-CAM heatmaps improved interpretability by highlighting the critical regions influencing the model's predictions. The research emphasized early tumor detection and recommended expanding dataset diversity for greater model robustness.

Park et al. [4] applied Convolutional Neural Networks (CNNs) to classify bone tumors in the proximal femur using radiographs. Their preprocessing pipeline included normalization and feature enhancement for improved accuracy. Grad-CAM visualization was employed to interpret the decision-making process. CNN-based classification outperformed human clinicians, highlighting AI's potential in complex medical imaging scenarios.

Vijayaraj et al. [5] proposed a hybrid model integrating CNN with Histogram of Oriented Gradients (HOG) to improve bone tumor detection. Initially, HOG was applied to extract gradient-based features, enhancing image contrast. These extracted features were then fed into a CNN for hierarchical feature learning and classification. This hybrid approach effectively combined handcrafted and deep learning features, resulting in higher classification accuracy.

Von Schacky et al. [6] introduced a multitask deep learning model capable of tumor classification, segmentation, and bounding box placement in radiographs. Their model, based on Mask-RCNN-X101 architecture, leveraged pretrained Microsoft COCO datasets for improved accuracy. The study involved segmenting tumor regions using the 3D Slicer tool and employed per-pixel sigmoid loss for segmentation and cross-entropy for classification. The model demonstrated performance comparable to musculoskeletal-trained radiologists in malignancy detection.

Song et al. [7] developed PBTC-TransNet, a fusion model designed to classify primary bone tumors using multimodal data from X-rays, CT, MRI, and clinical parameters. The model incorporated modality-specific encoders and used Bernoulli indicators to handle missing data. A transformer module facilitated multimodal feature integration, while a fully connected layer incorporated clinical data. The model exhibited high classification accuracy and sensitivity in detecting tumor types. SHAP analysis highlighted crucial predictors such as age and clinical symptoms.

Sharma et al. [8] implemented ML techniques to detect and classify bone tumors using X-ray images. Preprocessing steps included noise reduction, sharpening, and segmentation via the Canny edge detection algorithm. Feature extraction techniques incorporated Haralick texture descriptors and HOG features. The models were trained using Support Vector Machines (SVM) and Random Forest, with SVM achieving superior performance (F1-score: 0.92). This automated approach improved tumor detection efficiency and minimized diagnostic errors.

These studies collectively demonstrate the potential of ML and DL in bone tumor classification, showcasing various approaches that enhance diagnostic accuracy and interpretability. Future work should focus on larger, diverse datasets and improved model generalizability across clinical settings.

TABLE 1: COMPARISON OF BONE TUMOR CLASSIFICATION METHODS USING VARIOUS MACHINE LEARNING & DEEP LEARNING MODELS

Ref	Dataset	Method	Accuracy	Advantages	Limitations
[1]	X-ray images	EfficientNet-B0 CNN	88.5	Comparable accuracy to musculoskeletal subspecialists	requires manual lesion cropping by radiologists
[2]	Radiographs	ANN	75	higher accuracy than residents in musculoskeletal tumor imaging	accuracy was slightly lower
[3]	Healthy Control Group	Vision Transformer (ViT)	89.1	Designed for early detection	Dataset Size
[4]	single tertiary center	EfficientNet-b2	85.3%,	Reduce reliance on specialists, aiding areas with limited access to musculoskeletal oncologists.	High computational cost
[5]	X-ray and CT scan images	deep learning classifiers	89.93	enhanced detection efficiency	Less Dataset Size
[6]	934 radiographs of bone tumors	multitask deep learning model	80.2	Comprehensive multitask capability for segmentation, bounding boxes, and classification.	weaker performance in detecting malignant tumors.
[7]	X-rays , CT ,MRI	PBTC-TransNet	88	Handles incomplete multimodal datasets	High computational complexity.
[8]	X-ray images	SVM and Random Forest.	85	Fast and effective preprocessing pipeline.	Smaller dataset.

III. METHODOLOGY

This research analyzed three convolutional neural network (CNN) architectures—Custom CNN, VGGNet, and LeNet—for detecting fractures from X-ray images. The models were trained and tested on a preprocessed dataset, with binary cross-entropy as the loss function and Adam as the optimizer. Implementation was carried out using TensorFlow and Keras, and model performance was assessed through accuracy, precision, recall, and F1-score.

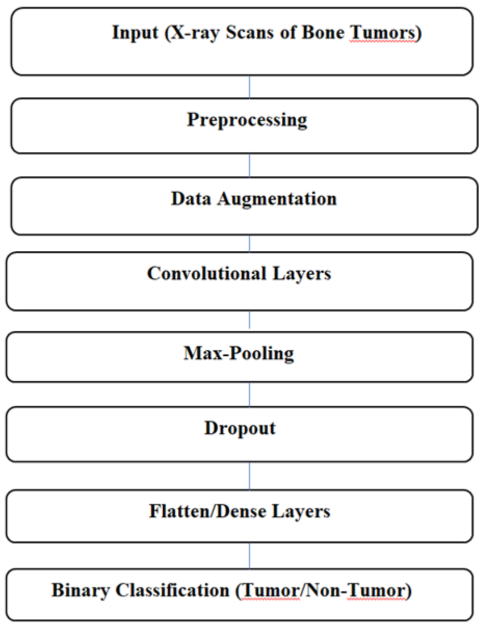

FIG 1 ARCHITECTURE

The custom CNN was specifically designed for balanced complexity and efficiency in bone fracture classification. It featured three convolutional layers with 3x3 kernels, each followed by max-pooling layers to reduce spatial dimensions, along with dropout layers for regularization to prevent overfitting. Fully connected layers at the end facilitated binary classification of fractures. This model outperformed the others, achieving a validation accuracy of 98%, demonstrating superior generalization and robustness. Confusion matrix analysis and classification metrics confirmed its effectiveness in distinguishing between fracture and no-fracture cases.

IV. Results

The study evaluated three CNN architectures: VGG-style, LeNet-style, and a custom CNN. Each model was trained on a preprocessed X-ray dataset with image augmentation to enhance model generalization. Over 10 epochs, training and validation accuracy, as well as loss, were analyzed. **Fig. 2** presents the X-ray test image used for evaluation, while **Fig. 3** provides classification reports comparing the performance of the three CNN models.

- **VGG-style CNN:** Achieved 94% validation accuracy, indicating strong spatial feature learning but showed signs of overfitting due to increasing validation loss in later epochs.
- **LeNet-style CNN:** Reached 93% validation accuracy, demonstrating that even simpler architectures can effectively handle binary fracture classification.
- **Custom CNN:** Outperformed the other models with 98% validation accuracy, showcasing better generalization and robustness in distinguishing fracture and no-fracture cases.

Fig.4 presents model accuracy comparisons for fracture classification, reinforcing the effectiveness of CNNs in medical image analysis. The confusion matrix and classification reports confirmed the custom CNN's superior ability to differentiate fracture cases, emphasizing CNNs' critical role in accurate fracture detection and diagnosis.

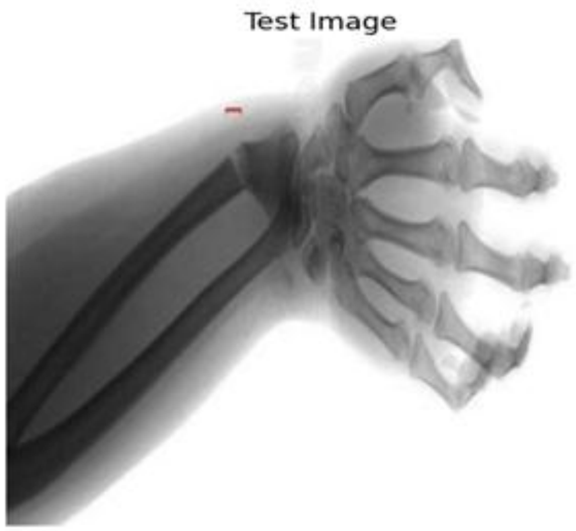

Fig.2

Custom CNN - Classification Report

	precision	recall	f1-score	support
No Fracture	0.96	1.00	0.98	50
Fracture	1.00	0.96	0.98	50
accuracy			0.98	100
macro avg	0.98	0.98	0.98	100
weighted avg	0.98	0.98	0.98	100

VGGNet - Classification Report

	precision	recall	f1-score	support
No Fracture	0.92	0.96	0.94	50
Fracture	0.96	0.92	0.94	50
accuracy			0.94	100
macro avg	0.94	0.94	0.94	100
weighted avg	0.94	0.94	0.94	100

LeNet - Classification Report

	precision	recall	f1-score	support
No Fracture	0.88	1.00	0.93	50
Fracture	1.00	0.86	0.92	50
accuracy			0.93	100
macro avg	0.94	0.93	0.93	100
weighted avg	0.94	0.93	0.93	100

Fig.3 Classification reports of Custom CNN, VGGNet, and LeNet

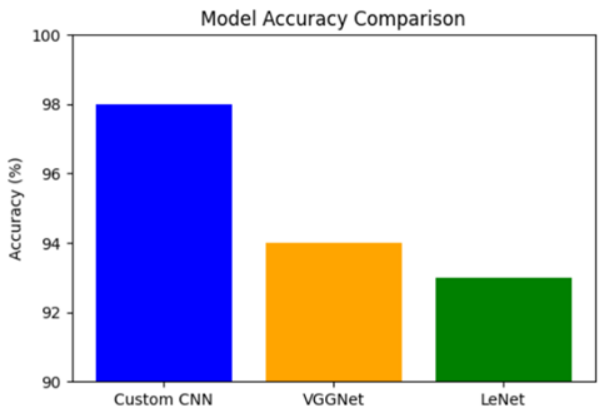

Fig.4 Comparison of model accuracies

V. Conclusion & Future Work

This research highlights the effectiveness of CNN-based models in classifying bone fractures from X-ray images, with the custom CNN exhibiting high accuracy and strong generalization capabilities. The use of data augmentation and preprocessing techniques significantly improved classification outcomes, emphasizing the role of machine learning in medical diagnostics. These results demonstrate the need for advanced neural network architectures to enhance diagnostic precision and reduce reliance on manual interpretation.

Future research could focus on incorporating larger and more diverse X-ray datasets to improve fracture detection accuracy, leveraging transfer learning with pre-trained models for faster convergence, integrating multimodal data (such as patient history and clinical records) for a more comprehensive diagnosis, and applying explainability techniques like Grad-CAM to enhance model transparency and build clinical trust.

REFERENCES

[1] Yu He, J. Wang, X. Liu, et al., "Deep learning-based classification of primary bone tumors on radiographs: A preliminary study," EBioMedicine, vol. 62, p. 103121, 2020.

[2] C. E. von Schacky, et al., "Development and evaluation of machine learning models based on X-ray radiomics for the classification and differentiation of malignant and benign bone tumors," *Eur. Radiol.*, vol. 32, pp. 6247–6257, 2022.

[3] S. Breden et al., "Deep learning-based detection of bone tumors around the knee in X-rays of children," *J. Clin. Med.*, vol. 12, p. 5960, 2023.

[4] C.-W. Park, S.-J. Oh, K.-S. Kim, et al., "Artificial intelligence-based classification of bone tumors in the proximal femur on plain radiographs: System development and validation," *PLoS ONE*, vol. 17, no. 2, p. e0264140, 2022.

[5] J. Vijayaraj et al, "An efficient convolutional histogram-oriented gradients and deep convolutional learning approach for accurate classification of bone cancer," *Int. J. Imaging Syst. Technol.*, 2023.

[6] C. E. von Schacky et al, "Multitask deep learning for segmentation and classification of primary bone tumors on radiographs," *Radiology*, vol. 301, no. 2, pp. 398–406, 2021.

[7] L. Song, C. Li, L. Tan, et al., "A deep learning model to enhance the classification of primary bone tumors based on incomplete multimodal images in X-ray, CT, and MRI," *Cancer Imaging*, vol. 24, p. 135, 2024.

[8] A. Sharma et al, "Bone cancer detection using feature extraction-based machine learning model," *Comput. Math. Methods Med.*, 2021.

Smart GPS Spoofing Detection in Next-Generation Autonomous Vehicles via an Attention-Based LSTM Autoencoder Framework

D. Kiruthika
Department of Electronics and Communication Engineering, Thiagarajar College of Engineering,
Madurai, India
dkiruthika@student.tce.edu

T.S. Nandhini
Department of Electronics and Communication Engineering, Thiagarajar College of Engineering,
Madurai, India
nandhinits1531@gmail.com

Ananthi
Department of Electronics and Communication Engineering, Thiagarajar College of Engineering,
Madurai, India
gananthi@tce.edu

K.S. Sanjaykumar
Department of Electronics and Communication Engineering, Thiagarajar College of Engineering,
Madurai, India
sanjaykumarks@student.tce.edu

R. Tharaniya
Department of Electronics and Communication Engineering, Thiagarajar College of Engineering,
Madurai, India
tharaniyaramar20@gmail.com

S. Resinabanu
Department of Electronics and Communication Engineering, Thiagarajar College of Engineering,
Madurai, India
resina@student.tce.edu

***Abstract*—The emergence of autonomous vehicles marks a transformative shift in transportation, yet also introduces critical security concerns—particularly the threat of GPS spoofing attacks. As GPS is essential for accurate navigation, its vulnerability stemming from unencrypted civilian signals poses a serious risk to AV reliability and safety. To address this challenge, we propose a novel detection framework based on an Attention-Enabled Hierarchical Long Short-Term Memory Autoencoder. This model leverages deep learning capabilities to identify anomalies in GPS data indicative of spoofing attempts. A hybrid feature selection technique is employed to eliminate redundant and irrelevant features, allowing the model to focus on the most informative inputs. Evaluated using key performance metrics such as precision, recall, and F1 score, the framework achieves an impressive 98.52% detection accuracy. The results demonstrate its superiority over traditional machine learning models and highlight its potential as a robust defense mechanism in securing the navigation systems of next-generation autonomous vehicles.**

Keywords—Autonomous Vehicles, Attention Mechanism, GPS Spoofing Detection, LSTM Auto encoder, Machine Learning.

I. INTRODUCTION

The arrival of self-driving cars (AV) has caused a paradigm shift in the automobile industry, promising safer and more efficient transportation. To navigate and make intelligent decisions, these vehicles rely largely on Global Positioning System (GPS) technology. This reliance on GPS, on the other hand, exposes autonomous vehicles to a new and increasing threat: GPS spoofing attacks [1]. In this article, we will look at what GPS spoofing is, what it could mean for autonomous vehicles, and what steps are being taken to combat this growing threat. GPS spoofing is a malicious technique in which an attacker modifies GPS signals received by a device in order to offer misleading position information. Attackers may deceive GPS receivers into thinking they are in a different location than they are by broadcasting fake GPS signals. This can have serious consequences in the context of autonomous vehicles, as the vehicle's decision-making mechanisms rely heavily on correct location information. Cyber-attacks on AV are classified into three types: data interception, data modification, and denial of service [2]. Several articles presented artificial intelligence-based GPS spoofing detection systems. The authors of [3] suggested a computer architecture that detects spoofing and meaconing attacks using a neural network. When an attack is detected, the computer uses the Bayesian inference subsystem to assess its severity. In this paper [4], the authors propose a system that is developed by machine learning models with a K-fold analysis, with voting mechanisms incorporated to select the learning model with the highest accuracy. Based on gyroscope measurements and GPS data, the scientists showed a straightforward method for detecting hijacking. In this paper, [5] studied a GPS spoofing detection and estimation system with switching mode resilience. The authors attempted to handle sensor drift by maintaining estimation errors in a tolerable zone with a high likelihood. The authors of this paper [6] introduce DeepPOSE, a unique framework for detecting GPS spoofing attempts. DeepPOSE is made up of a spoofing detector and a vehicle position estimator. The vehicle position estimator uses the convolutional network and RNN to extract the vehicle direction and speed from the motion sensor data. To identify GPS spoofing attacks, the spoofing detector compares this trajectory to one rebuilt from user-reported GPS coordinates. The research in this paper [7] offers a unique machine learning (ML) model for distinguishing between faked and legitimate signals received by unmanned aerial vehicles (UAVs). Multiple ML algorithms are utilized to determine the best classification technique, with GPS signal properties serving as features. K-fold analyses with varied K values are used to construct various ML models for improved accuracy.

The paper's contributions are as follows:

- A hybrid feature selection method is used to identify correlated and low-importance features simultaneously.

- An attention mechanism is proposed in the LSTM auto-encoder model for efficient recognition of GPS spoofing signals.
- For validating the proposed methodologies, performance comparisons with Gradient boost (GB), Random forest (RF), and Light Gradient Boosting Machine model (LightGBM) ensemble models were performed.

II. AHLSTM-Attention-Enabled Hierarchical LSTM Autoencoder Framework

A combined deep LSTM autoencoder framework with a hierarchical attention mechanism and a novel network for the detection of GPS spoofing attacks in autonomous vehicles are proposed. We begin by providing an overview of our proposed model, which is built around four steps: generating the input sequence, LSTM encoder, attention-enabled block, LSTM decoder, and GPS spoofing detection. It has high detection accuracy, a low false alarm rate, and reasonably decent real-time performance when compared to typical neural networks for GPS spoofing attack detection approaches.

Step 1: Input Sequence Data

The time [X_1, X_2, X_3,...,X_n] component of the original dataset. Each X sequence with a T-length time frame is produced as an input for m features at time-instance t. A two-dimensional array representing samples and timesteps is then created from this. As an illustration, we can create a two-dimensional array from a sequence of our GPS data, where each dimension represents a list of samples at each timestep.

Step 2: LSTM Encoder

Since the LSTM encoder analyzes sequential GPS data and detects temporal patterns suggestive of spoofing attacks, it is essential for the detection of GPS spoofing. It receives a sequence of GPS data points as input. Typically, each data point should contain the following: a timestamp, latitude, longitude, and altitude. Before these sequences are included in the model, they undergo preprocessing and normalization. It's made up of many LSTM layers layered on top of each other. One step at a time, each LSTM layer systematically examines the input sequence. Every layer's LSTM cells keep track of hidden states and memory cells, which are updated every time step according to the input received thus far and the state that was previously observed. The ability of LSTM cells to record long-term relationships enables the model to identify potential patterns of GPS spoofing assaults. Unusual variations in GPS position sequences or sudden shifts in timestamps are indicators of spoofing. By acting as a sequence folding layer, an LSTM encoder converts the features into timestep-based sequences.

Step 3: Attention mechanism

In this paper, for the first time, a self-attention hierarchical block is introduced in the LSTM autoencoder model to learn the correlation between legitimate and spoofed GPS signals. The attention mechanism in neural networks allows only selective output from the input sequence model. While the LSTM model often employs information from the past hidden state and input information from the current time step to calculate the current output, this results in poor performance.

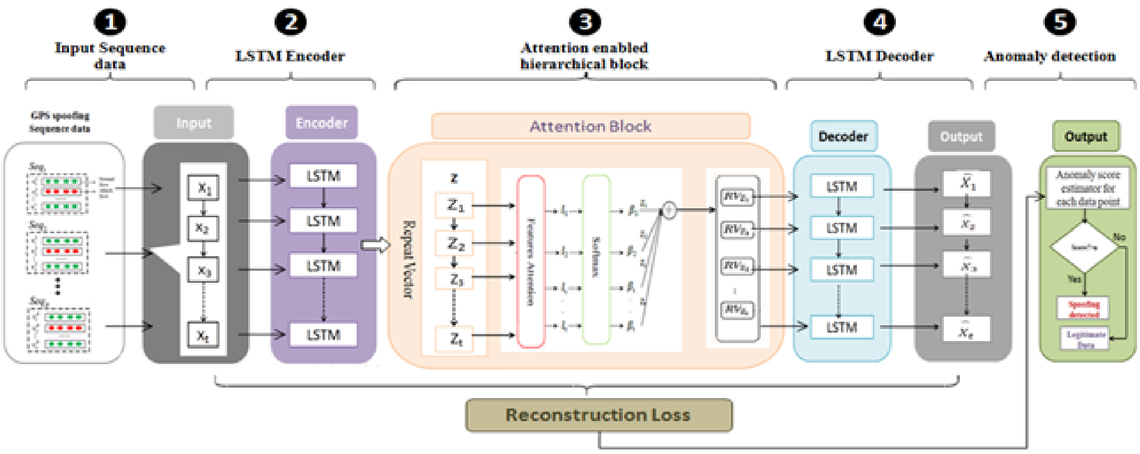

Fig. 1 Overview of AHLSTM model

By incorporating attention mechanisms with the LSTM model, it can be the solution for allowing the sequence models to capture critical information from any previous time steps of the input sequence. In sequence models, the attention mechanism allowed encoders to generate a context vector by generating tailored methods to sequence parts of the inputs. This guarantees that the context vector represents the essential parts and learns the long-term dependencies of the input sequence, resulting in better decoder outputs. It also consumes the encoder's hidden state information to compute the attention weights.

Step 4: LSTM Decoder

The output of the attention block is used as the input to the LSTM decoder. The LSTM Decoder receives feature representation that captures spatial and temporal patterns. The LSTM decoder is made up of one or more LSTM layers that successively process the feature representation. Unlike standard sequence-to-sequence jobs in which the decoder outputs an output sequence, the decoder's purpose in this situation is to recreate the original input sequence. At each time step, the LSTM decoder takes the previous time step's output as well as the hidden state. At each step, the decoder's hidden state and output are utilized to reconstruct the associated GPS sequence elements, such as latitude, longitude, altitude, or timestamp. At each time step, the decoder output is compared to the corresponding piece of the original GPS sequence. To analyze the dissimilarity between expected and actual data, anomaly detection techniques can be used. The LSTM decoder's output layer is utilized to forecast the next element in the GPS sequence. The LSTM decoder's output layer is utilized to forecast the next element in the GPS sequence. The output is compared at each time step to the real value, and the LSTM decoder's success is judged by its ability to reconstruct the input sequence accurately. A detailed explanation of how the decoder interacts with the LSTM cell store.

Step 5: GPS Spoofing detection

An anomaly is defined as an observation that exceeds the threshold. We train our model with a dataset of GPS readings within a normal range using our threshold-based anomaly detection technique. This is done in order to compute the reconstruction error rates for common GPS data points. Following the completion of training and the determination of all distinct reconstruction errors on all samples, the maximum reconstruction error rate is defined as a threshold. The test GPS dataset now contains all GPS reading ranges after the threshold has been determined. A construction error rate of each GPS value is calculated for each sample in the testing set. This sample is considered suspicious if the reconstruction error rate exceeds the threshold.

III. Results And Discussion

Performance of the Proposed AHLSTM model

We evaluated the effectiveness of our LSTM encoder-based GPS spoofing detection model using a real-world GPS dataset containing both authentic and spoofed GPS signals. The dataset was compiled from various sources, including physical GPS receivers and synthetically generated spoofing attacks. To ensure balanced class distribution and improve the model's ability to generalize, the data was partitioned into training, validation, and testing sets. Additionally, appropriate data augmentation techniques were applied. During training, all input sequences were fed into the proposed model across multiple epochs, with performance continuously monitored on the validation set. A batch size of one was employed, meaning the model processed one sequence at a time, allowing for detailed sequence-level analysis. Throughout the training process, both training and validation losses were recorded to evaluate learning progression.

Figure 2 illustrates the loss trends across epochs. The training loss (depicted by the blue line) stabilizes rapidly, reaching convergence within approximately eight epochs. To validate performance during training, 10% of the training data was reserved as a validation set. Ultimately, the model demonstrated a high level of accuracy, achieving a detection rate of 98.52%, confirming its effectiveness in identifying GPS spoofing attacks.

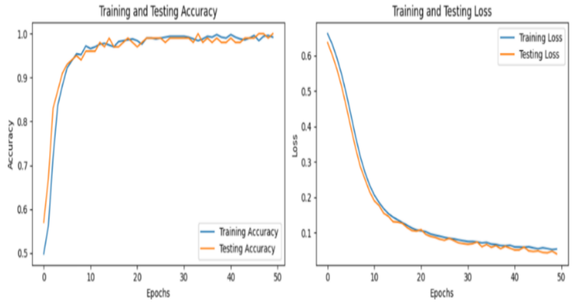

FIG. 2 TRAINING/VALIDATION ACCURACY AND LOSS

As expected, the validation loss does not stabilize until 50 epochs. After 50 epochs, however, the validation loss has the same loss rate as the training loss (i.e., an average of roughly 0.07%). This is an excellent match, and our proposed model works well. We can reduce the problem to a simple binary classification task by using the threshold: If the reconstruction loss, for example, is less than the threshold, we will consider it to be valid GPS signal data. Alternatively, if the loss exceeds the threshold, it will be classified as spoofing signal data.

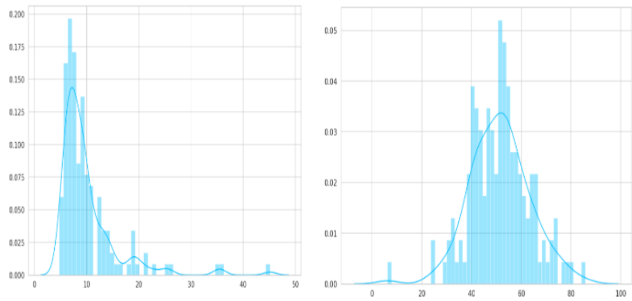

A) LEGITIMATE GPS DATA B) SPOOFING GPS DATA

FIG. 3 RECONSTRUCTION LOSS –FOR LEGITIMATE AND SPOOFING GPS DATA

Experimental Results and Comparative Analysis

This paper uses an ensemble method to assess the efficacy of our proposed methods. Table I displays the proposed approaches' best precision, recall, and F1-scores. Three techniques are shown to perform well in the periodic GPS 1 and GPS 2 datasets. AE, on the other hand, performs poorly in non-cyclical GPS 1. Because LSTM-AE [8] considers sequence-temporal correlation, it is more accurate than VAE. Because AH-LSTM-Attention employs an attention mechanism to pay attention to significant latent variables, the result is marginally better than that of LSTM-AE. As demonstrated in Figure 3, the AH-LSTM-Attention obtained an F1-score in the range of 0.85-0.95, outperforming other approaches. Using the attention method, distinct weights are assigned to different time points in the time step before they are entered into the encoder. For additional time increments, similar patterns can be found.

TABLE 1. ANOMALY DETECTION RESULTS OF EACH METHOD IN GPS DATASET

Dataset	Method	Precision	Recall	F1-Score
GPS 1	AE	0.82	0.77	0.78
	LSTM-AE	0.86	0.82	0.82
	AH-LSTM-Attention	0.93	0.88	0.91
GPS 2	AE	0.87	0.82	0.83

	LSTM-AE	0.93	0.86	0.87
	AH-LSTM-Attention	0.98	0.89	0.93

We created a machine learning-based GPS signal spoofing detection model after completing data augmentation and feature selection on the GPS signal dataset. To develop the model, we used a range of methods, including basic classifiers. The machine learning models' results are displayed in Table II. As demonstrated, AHLSTM has the highest accuracy (98.52%), followed by Random Forest (94.54%), LightGBM (95.93%), and Gradient Boost (91.36%) [9]. Figure 12 displays the likelihood of misdetection, which is considered an important statistic in the cyber security industry because it determines the number of undetected attacks. AHLSTM, LightGBM, and Gradient Boost all performed better than Random Forest [10]. While Random Forest has the slowest processing speed, it has a large memory size for both training and detection. Because computing power and memory are restricted in autonomous car data, we are primarily interested in a quick model that uses less memory. To summarize, AHLSTM is the most appropriate model for AV applications to identify GPS spoofing attempts.

TABLE II: EVALUATION METRICS RESULTS

Evaluation metrics	**RF**	**GBM**	**LGBM**	**AHLSTM (Proposed model)**
Probability of Detection	96.32%	92.87%	95.68%	**98.38%**
Probability of Misdetection	3.67%	7.46%	4.52%	**4.72%**
Probability of False Alarm	8.54%	9.74%	4.86%	**4.29%**
Accuracy	94.54%	91.36%	95.93%	**98.52%**

IV. CONCLUSION

Several approaches for identifying and detecting GPS spoofing vulnerabilities have been developed, but this field of study still faces numerous challenges and limitations, such as high misdetection and false alarm rates. We used Spearman Correlation and Information Gain in this work to eliminate correlated and low-relevance features from the considered dataset using a hybrid feature selection method. To find out the abnormal data pattern in the GPS spoofing database, a novel attention-enabled hierarchical LSTM autoencoder model is proposed. The model consists of numerous LSTM units that provide the learning ability to recognize long-term correlation relationships that occur in a time series. The autoencoder generates encoded aspects of the input representation while keeping the LSTM encoder's long-term dependencies and providing outputs that resemble the input via the LSTM decoder. In this case, the feature attention block is critical for improving AHLSTM's latent variable representation in order to highlight the important features. Each data observation in the testing set that has a reconstruction loss result larger than the threshold is identified as an anomaly by the anomaly detector. To increase security, an AHLSTM model is compared with different machine learning models, including Gradient Boost, LightGBM, and Random Forest, to detect GPS spoofing attacks. The results reveal that the AHLSTM model has the highest accuracy (98.52%) and the shortest detection time (1.24 ms), making it suitable for autonomous vehicle applications.

REFERENCES

[1] Ghilas Aissou, Hadjar Ould Slimane, Selma Benouadah, and Naima Kaabouch, “Tree-based Supervised Machine Learning Models For Detecting GPS Spoofing Attacks on UAS”, 2021 IEEE 12th Annual Ubiquitous Computing, Electronics & Mobile Communication Conference (UEMCON), vol. 978, pp. 6654-069, 2021.

[2] Sung, Y. H., Park, S. J., Kim, D. Y., & Kim, S., “GPS Spoofing Detection Method for Small UAVs Using 1D Convolution Neural Network”, Sensors, vol.22(23), pp. 9412, December 2022.

[3] N. Kaabouch, M. R. Manesh, and J. R. Kenney, “Detection of spoofing and meaconing for geolocation positioning system signals”, Jul. 16 2020.

[4] Talaei Khoei, T., Ismail, S., & Kaabouch, N, “Dynamic Selection Techniques for Detecting GPS Spoofing Attacks on UAVs”, Sensors, vol. 22 (2), pp. 662, January 2022.

[5] Psiaki, M. L., Humphreys, T. E., & Stauffer, B, “Attackers can spoof navigation signals without our knowledge. Here’s how to fight back GPS lies”, IEEE Spectrum, vol. 53(8), pp. 26–53, August 2016.

[6] Jiang, P., Wu, H., & Xin, C, “DeepPOSE: Detecting GPS spoofing attack via deep recurrent neural network”, Digital Communications and Networks, vol.8(5), pp. 791–803, October 2022.

[7] Wei, X., Wang, Y., & Sun, C,”PerDet: Machine-Learning-Based UAV GPS Spoofing Detection Using Perception Data”, Remote Sensing, vol.14(19), pp.4925, October 2022.

[8] Talaei Khoei, T., Ismail, S., Shamaileh, K. A., Devabhaktuni, V. K., & Kaabouch, N, “Impact of Dataset and Model Parameters on Machine Learning Performance for the Detection of GPS Spoofing Attacks on Unmanned Aerial Vehicles”, Applied Sciences, vol.13(1), pp. 383, December 2022.

[9] Lyerly, S. B., “The average spearman rank correlation coefficient”, Psychometrika, vol. 17(4), pp. 421–428, December 1952.

[10] Sun, Y., Yu, M., Wang, L., Li, T., & Dong, M, “A Deep-Learning-Based GPS Signal Spoofing Detection Method for Small UAVs”, Drones, vol. 7(6), pp. 370, June 2023.

Blending Design Thinking and Lean Startup for Enhanced Innovation

J. Anitha Gracy
Department Applied Mathematics and Computational Science,
Thiagarajar College of Engineering,
Tamil Nadu, India
anithagracy90@gmail.com

S. Parthasarathy
Department Applied Mathematics and Computational Science,
Thiagarajar College of Engineering,
Tamil Nadu, India

***Abstract*—Deriving deeper insights into users' demands is the goal of the design thinking technique, which has its roots in industrial design. Comparably, another well-known approach—often referred to as lean startup methods—focuses on identifying possibilities through testing, experimentation, and iterative user involvement. Despite their widespread use, little is known about the best methods to incorporate these user-centered design techniques into organizational innovation processes. Additionally, it's not apparent which aspects of the design process are most important for seeing and creating new chances. In this study, we offer a high-level conceptual process model that incorporates user-focused design approaches into the early phases of organizational innovation, including lean startup and design thinking. We outline the proposed model, discuss the related tasks in depth, and examine important process factors. Implications for further research in this area are covered in the article's conclusion.**

Keywords—Design Thinking, Software Startups, Business, insert

I. INTRODUCTION

Prioritizing the initial phases of innovative product development (IPD) is one of the well-established strategies that are recognized to improve innovation results [1]. These include generating concepts, comprehending user demands, and pre-development marketing. It has also been demonstrated that encouraging highly cooperative teams, using organized methods to direct development, and introducing cost engineering early on in the process are advantageous. On the other hand, little is known about the effective integration of lean startup techniques with design thinking in the innovation process [2]. By putting out a conceptual framework that integrates these two approaches and emphasizes early engagement with users and stakeholders, our study fills that gap.

Focusing on the early stages of innovative product development (IPD)—such as idea generation, understanding user needs, and pre-development marketing—has proven to enhance innovation outcomes. Practices like fostering collaboration, using structured development methods, and introducing cost engineering early are also beneficial [3]. However, limited research exists on integrating lean startup principles with design thinking in innovation [4]. This study addresses that gap by proposing a conceptual framework that merges both approaches, highlighting early user and stakeholder involvement.

Design thinking emphasizes understanding user needs to improve problem framing and has been widely adopted by companies like IBM and SAP for its user-cantered, empathetic approach. It typically appears later in product development, whereas lean startup focuses on early, low-cost experimentation and iterative learning used across sectors to support agile development. Despite their value, there's limited insight into how these methods collectively impact innovation within organizations.

This paper introduces a conceptual model combining design thinking and lean startup strategies in the early innovation phase, grounded in literature and a case study from a large organization. It contributes to understanding how integrated approaches can enhance early innovation. The paper outlines the theories, research methodology, process model, and concludes with practical and academic recommendations.

II. RELATED WORK

Innovative product development (IPD) is a concept that has been under research since the late 1960s [4]. Starting with the work of the Boston Consulting Group in the early 1970s and Project SAPPHO, and with the work of Robert Cooper from the early 1980s, every aspect of the process has been looked at [5]. Issues like the dynamics of the team, the various process controls, and success factors have been covered in detail. However, the overall failure rates of products and services are still very high and range around 40% [6]. This is a continuous issue that further emphasises the need for ongoing academic and practical research into the steps that could enhance the innovation results in the provision of new and improved products and services, particularly bearing in mind the considerable amounts of money that are spent on R&D for such purposes.

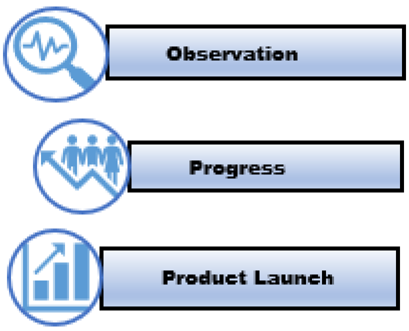

FIGURE 1: SEGMENTS OF DESIGN THINKING

Innovative Product Development (IPD) has been studied since the late 1960s, with significant contributions from the Boston Consulting Group, Project SAPPHO, and Robert Cooper [7]. Despite extensive research into team dynamics, process controls, and success factors, product and service failure rates remain high—around 40%—highlighting the ongoing need for research to improve innovation outcomes, especially given the high R&D investments [8].

Over the years, certain practices have been identified as enhancing innovation, such as early-stage customer insight, early marketing activities, iterative development, strong process management, and effective product launches.

The innovation process can be grouped into three main phases [9]: **Observation**, **Progress**, and **Product Launch**.

- **Observation** involves idea generation, market research, and early business case development, aligning with methodologies like design thinking and lean startup.
- **Progress** focuses on design, prototyping, and detailed planning.
- **Product Launch** includes final testing, design refinement, and production setup. This stage filters out weaker ideas as the process narrows.

Design thinking has gained popularity due to its user-centred approach and emphasis on understanding real-world behaviours through ethnographic methods. Common tools include user personas, mind maps, and brainstorming [10]. The final stage involves gathering feedback via low-cost experiments and prototypes. While similar in goal to the lean startup approach, design thinking offers unique strategies, and both aim to improve early-stage idea validation to boost innovation success.

However, recent critiques have raised questions about the overall ability of design thinking to consistently deliver groundbreaking ideas [11]. Most research on design thinking has focused internally, examining its application within development teams. Existing studies have not sufficiently addressed these critical questions about external integration. To explore this gap, we propose the following research proposition:

Research Proposition 1: How might design thinking be best integrated into the overall innovation process of an organization?

The lean startup methodology promotes a scientific, iterative approach to business development, emphasizing experimentation and validation through a minimally viable product (MVP). The MVP enables teams to collect user feedback, refine ideas, and adapt strategies, helping identify more viable opportunities. This approach, also useful in established organizations, supports early-stage innovation through testing and feedback. Lean principles align with agile methods by integrating continuous customer input into development. However, in engineering-focused or early-stage startups, a more structured strategy may be needed, as key decisions can critically impact successIn contrast, traditional organizations operate in a different context. Here, low-cost experiments can provide valuable insights and guide decision-making for immature projects. However, several critical questions need to be addressed:

- What types of low-cost experiments yield the most useful results?
- Which MVPs are most impactful for opportunity development within organizations?
- What level of complexity and cost is most effective in informing the innovation process?

These unanswered questions about the integration of lean startup methods into Innovative product development (IPD) lead to our second research proposition:

Research Proposition 2: For traditional software organizations, how might lean startup methods, such as MVPs, best be integrated into the development process?

Design thinking and lean startup approaches can enhance the stage-gate process by refining ideas early and providing insights into their feasibility before major investments. However, successful integration requires careful alignment with existing organizational workflows [12].

Research Proposition 3: How might design thinking and lean startup methods be integrated together in an organization's more established innovation processes?

Integrating design thinking and lean startup into existing innovation frameworks leverages the strengths of both—user-focused problem identification and iterative development. Design thinking is valuable in the early stages, emphasizing deep user understanding and creative ideation. Lean startup complements this by testing hypotheses, experimenting with business models, and refining ideas using MVPs and feedback loops [13]. Organizations can start with design thinking to define user needs, then apply lean startup to prototype and adapt solutions in real-world settings. Agile principles can further refine these innovations, making the process adaptive, risk-aware, and market-responsive.

III. RESEARCH METHODS

This study focuses on the roles of user and stakeholder with regard to the application of design thinking and lean startup methodologies that are used in the design innovation process [15]. To support this endeavour, the study employs digital ethnography, business history, and ethnographic participant observation in the form of an organisational project. This approach provides a way of cross-sectional integration of different observations and perceptions.

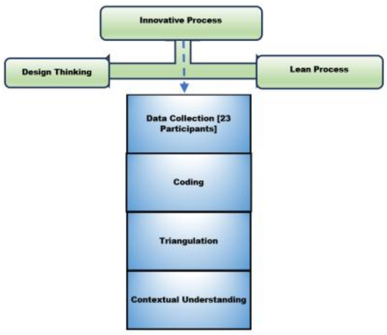

FIG 2. FLOW OF STUDY

This study conducted an exploratory case analysis of an organization's innovation design process, guided by previous research. Over three months, weekly design meetings and three workshops were observed, involving 23 participants. The research team performed real-time coding of data across identified categories. Focusing at the project level—ideal for analyzing innovation tasks—the study provides a detailed methodology for integrating design thinking and lean startup principles. Using a mixed-method qualitative approach, the research offers in-depth insights into innovation practices, emphasizing user and stakeholder involvement.

The study employs digital ethnography, business historiography, and participant observation to explore innovation processes. Digital ethnography helps understand user and stakeholder behaviour in online spaces, while business historiography provides insights from past practices to inform current innovation. Participant observation, through immersion, offers firsthand understanding of organizational innovation.

A qualitative case study approach focuses on a single organization, using weekly design meetings over three months to track innovation developments. This longitudinal method captures evolving challenges and breakthroughs. To deepen insights into design thinking and lean startup methodologies, three prototyping sessions were conducted with 23 participants, encouraging feedback and improvements in the design process.

Real-time coding was applied during sessions to identify emerging themes and adjust the research dynamically. Triangulation enhanced credibility by cross-verifying data from multiple sources, reducing bias.

The research focuses at the project level, aligning well with design thinking and lean startup by examining decision-making and user interaction. Overall, the study integrates various qualitative methods to offer a rich, contextual understanding of how these innovation frameworks function within organizational settings.

IV. RESULT AND DISCUSSION

We propose a high-level framework for applying design thinking and lean startup principles to opportunity development. This framework reflects the evolving innovation process and consists of two main phases, integrating design thinking, lean startup, and agile development [14], [15].

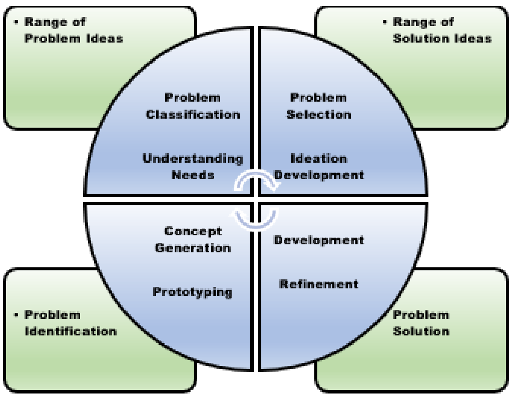

FIG 3.KEY PHASES OF SOFTWARE STARTUPS

Problem Identification involves recognizing and evaluating potential opportunities, often referred to as the "fuzzy front-end." This stage includes assessing user needs, market dynamics, and aligning with business and technological goals. On the other end, the Solution Space focuses on concept development, selection, and engineering efforts geared toward commercialization. Together, these stages form the foundation of the innovation process.

Both design thinking and lean startup methodologies support critical steps such as identifying problems, generating and refining concepts, prototyping, and selecting viable solutions. Ideation is a key phase aimed at generating diverse ideas through techniques like brainstorming, brainwriting, and design heuristics—often facilitated by collaborative tools.

User and stakeholder feedback is vital and is typically gathered through testing initial concepts and prototypes. The minimum viable product (MVP) is central to the lean startup approach, allowing hypothesis testing through simplified versions of products. Prototypes range from storyboards to digital simulations.

Throughout the process, feedback loops guide the refinement of ideas based on feasibility, scope, and user input. Although less structured than SCRUM, the approach aligns with agile development, emphasizing iterative feedback, frequent communication, and collaborative tools, including design sprints.

TABLE 1: RESEARCH PROPOSITION & DESCRIPTION

Research Proposition	Description
RP 1: Integration of Design Thinking in Startup Development Phase	Design thinking, integrated early in an organization's development process, enables problem articulation through user-focused investigations and fosters strong stakeholder relationships that enhance collaboration and information flow.
RP 2: Design Thinking and Lean Startup Integration Process	Design thinking drives innovation by focusing on user insights and problem framing, seamlessly transitioning to lean startup methods for iterative refinement and agile development for a cohesive innovation process.
RP 3: Adoption and Integration Methods	The sequential integration of design thinking, lean startup, and agile methods fosters deeper user insights, builds trust through strong relationships, and enhances collaboration throughout the development process.

Integrating design thinking and lean startup methods into the innovation process has significant theoretical and practical implications. While many organizations still use traditional stage-gate models, methods like design thinking, lean startup, and agile are increasingly being adopted. Previous research suggests that agile and design thinking complement each other due to their iterative nature, and these methods can be applied sequentially across different innovation phases. However, many organizations still treat design thinking as an isolated project, particularly in centralized innovation labs, which complicates the transition of promising ideas to business units for scaling. By integrating these methodologies, organizations can better align concept development, prototyping, and user interactions, fostering regular communication and a deeper understanding with users before formal development begins. Examples like Philips Healthcare's "Cocreate" process illustrate how design thinking-based co-development can drive innovation, with companies like Philips applying design thinking for over 30 years.

V. Conclusion

This article discusses two approaches to innovation that are becoming available to organisations and that show great promise, namely design thinking and lean startup. These are strategies that are used to assist organisations to come up with and test new ideas. Therefore, in this research, we seek to find out how these methods can be incorporated into an organisation's development process. In this paper, we present a conceptual model that focuses on the user level at several points in the opportunity development process. The ability to identify opportunities, prototype, test, and gather early feedback on market potential offers firms a competitive advantage. By pairing design thinking with lean startup methods, organizations can effectively implement these strategies to enhance innovation. The strengths of both methods—focused on customer needs, ideation, and development—work well together in promoting user interaction throughout the process.

Despite the growing body of research and academic publications on these methodologies, questions remain regarding best practices for their implementation. One key question pertains to organizational adoption. For instance, while companies like IBM have successfully integrated design thinking across their operations, the most effective approach remains unclear. Should the implementation be modeled after Six Sigma, with 'design thinking black belts' leading initiatives? Or is it more effective to establish specialized 'S.W.A.T.' teams within the organization to kick-start the adoption process? Additionally, how can these methods be applied to organizations focused on large-scale, complex systems engineering projects? There is a lack of research on how traditional design thinking and Innovative product development (IPD) processes can be adapted for Large-scale Complex Engineered Systems (LaCES), which typically involve large teams over extended periods in highly collaborative environments. LaCES, such as aerospace systems (aircraft, space systems), maritime projects (submarines, aircraft carriers), nuclear power plants, and large-scale infrastructure projects (e.g., water supply systems, transportation networks), require hundreds or even thousands of engineers and scientists working across multiple locations and years to design and complete.

Current research on the intersection of systems thinking and design thinking is mostly theoretical, with studies addressing the roles of systems thinking in design and what makes a designer proficient in systems thinking. Future research, employing both qualitative and quantitative methods, will aim to explore how design thinking and lean startup methods can be integrated into the development processes for complex systems, offering practical insights on how these approaches can improve innovation in large-scale engineering projects.

VI. Acknowledgement

The authors express their gratitude to the Thiagarajar College of Engineering (TCE) for supporting us to carry out this research work. Also, the financial support from TCE under Thiagarajar Research Fellowship scheme (File.no: TRF/Jan-2023/08) is gratefully acknowledged.

Reference

[1] Santisteban, J., Mauricio, D., & Cachay O, "Critical success factors for technology-based startups," *International Journal of Entrepreneurship and Small Business, 42*(4), 397-421, 2021.

[2] Kemell, K. K., Risku, J., Strandjord, K. E., Nguyen-Duc, A., Wang, X., & Abrahamsson P, "Internal software startups–a multiple case study on practices, methods, and success factors," In *2020 46th Euromicro Conference on Software Engineering and Advanced Applications (SEAA)* (pp. 326-333). IEEE, August 2020.

[3] Nguyen-Duc, A., Münch, J., Prikladnicki, R., Wang, X., & Abrahamsson, P, "*Fundamentals of software startup,"* Springer International Publishing, 2020.

[4] Amershi, S., Begel, A., Bird, C., DeLine, R., Gall, H., Kamar, E., ... & Zimmermann, T, "Software engineering for machine learning: A case study," In *2019 IEEE/ACM 41st International Conference on Software Engineering: Software Engineering in Practice (ICSE-SEIP)* (pp. 291-300). IEEE, May 2019.

[5] Bouredja, S., & Bourouaha, A, "Factors of startups success: to do not fail, what should startups do," *Journal of Finance & Corporate Governance*, *6*(2), 63-85, 2022.

[6] Thirupathi, A. N., Alhanai, T., & Ghassemi, M. M. " A machine learning approach to detect early signs of startup success," In *Proceedings of the Second ACM International Conference on AI in Finance*,pp. 1-8, November, 2021.

[7] Razaghzadeh Bidgoli, M., Raeesi Vanani, I., & Goodarzi, M, " Predicting the success of startups using a machine learning approach," *Journal of Innovation and Entrepreneurship*, *13*(1), 80, 2024.

[8] Ross, G., Das, S., Sciro, D., & Raza, H. (2021), "CapitalVX: A machine learning model for startup selection and exit prediction," *The Journal of Finance and Data Science*, *7*, 94-114.

[9] J. A. Gracy, S. Parthasarathy, S. Hirthick and P. Nandhini, "Software Startups Success Prediction: Machine Learning Methods of Comparative Analysis," 2024 First International Conference for Women in Computing (InCoWoCo), Pune, India, 2024, pp. 1-8, doi: 10.1109/InCoWoCo64194.2024.10863014.

[10] de Souza Nascimento, E., Ahmed, I., Oliveira, E., Palheta, M. P., Steinmacher, I., & Conte, T, "Understanding development process of machine learning systems: Challenges and solutions," In *2019 acm/IEEE international symposium on empirical software engineering and measurement (esem)* (pp. 1-6). IEEE, September, 2019.

[11] Parthasarathy, S., & Bagavathilaksmi, R, "Exploring Research Opportunities to Apply Data Mining Techniques in Software Engineering Lifecycle," In *2023 First International Conference on Advances in Electrical, Electronics and Computational Intelligence (ICAEECI)* (pp. 1-5). IEEE, October 2023.

[12] Anitha Gracy, J., Parthasarathy, S., & Sivagurunathan, S, "Navigating the Software Symphony: A Review of Factors and Strategies for Software Development in Startups," *International Journal of Computing and Digital Systems*, *16*(1), 377-390, October 2023.

[13] Pattyn, F, "The Critical Role of Product Managers and Their Responsibilities in Software Startups: A Systematic Literature Review," *American Journal of Engineering and Technology Management*, *9*(4), 2024.

[14] Bousdekis, A., Lepenioti, K., Apostolou, D., & Mentzas, G, " A review of data-driven decision-making methods for industry 4.0 maintenance applications," *Electronics*, *10*(7), 828,2024.

[15] Marion, T., Cannon, D., Reid, T., & McGowan, A. M. (2021). A conceptual model for integrating design thinking and lean startup methods into the innovation process. *Proceedings of the Design Society*, *1*, 31-40.

Rehabilitation of Cool in Tower – A Case Study

Monica D
Department of Civil Engineering,
Thiagarajar College of Engineering,
Madurai, India
Monica.jun12@gmail.com
dbciv@tce.edu

Dr. D. Brindha
Department of Civil Engineering,
Thiagarajar College of Engineering,
Madurai, India
Monica.jun12@gmail.com
dbciv@tce.edu

***Abstract*—The rehabilitation of cooling towers is crucial for maintaining their structural integrity and efficiency. This case study focuses on using micro concreting techniques to restore a cooling tower. Micro concreting, which employs fine aggregates and specialized admixtures, enhances durability and strength, making it suitable for thin-walled structures. The study addresses common issues in aging cooling towers, such as buckling and local failures, by applying micro concrete. It evaluates the construction and testing of a micro concrete model, providing insights into the technique's effectiveness in extending the lifespan and performance of cooling towers. This project assesses the condition of the cooling tower at the CPCL site in Chennai, identifies the causes of structural failures, and selects appropriate repair methods and protection strategies, followed by a post-retrofitting evaluation.**

Keywords*—Rehabilitation, NDT, Micro concreting, Epoxy Coating

I. INTRODUCTION

Concrete construction is generally expected to give trouble free service throughout its intended design life. However, these expectations are not realized in many constructions because of structural deficiency, material deterioration, unanticipated overloading or physical damage. Premature material deterioration can arise from a number of causes the most common being when the constructions specifications are violated or when the facility is exposed to harsher environment than those expected during the planning and design stage. Physical damage can also arise from fire, explosion, as well as from restraint both internal and external against structural movement. Expect in extreme case, most of the structure require restoration to meet its functional requirement by appropriate repair technique.

This project used different techniques along with micro concrete to strength the defective parts of the structure. The success of a repair or rehabilitation project depends on the specific plans designed for it. Concrete Structures: Protection, Repair and Rehabilitation provides guidance on evaluating the condition of the concrete in a structure, relating the condition of the concrete to the underlying cause or causes of that condition, selecting an appropriate repair material and method for any deficiency found, and using the selected materials and methods to repair or rehabilitate the structure. The study examines the challenges and opportunities of sustainable building restoration in Brazil, emphasizing the importance of legislative, technical, and financial factors for promoting sustainable rehabilitation projects [1]. The study explored sustainable techniques in heritage building restoration [2] [3]. This source most likely discusses how important it is to restore and renovate old buildings using traditional materials and techniques in order to maintain their originality and historical accuracy [4]. The researchers stressed the significance of striking a balance between contemporary restoration methods and conservation values [5]. This topic is important because many Asian cities are experiencing rapid urban growth, which makes it challenging to preserve cultural assets and improve living conditions in their historic city centre [6][7]. This resource offers standards and recommendations for restoring old structures while integrating contemporary conveniences and technologies [8]. The case study emphasizes how important it is to restore historic structures using appropriate construction techniques and look into possible other strategies to guarantee their preservation [9]. The guide provides guidance on repointing mortar joints in historic masonry structures, stressing the importance of using the right supplies and techniques to preserve the building's historical authenticity [10]. When evaluating the state of historic buildings without inflicting any harm, non-destructive testing (NDT) techniques are essential. Because there are so many historically valuable buildings, NDT techniques are crucial for managing and conserving these architectural gems [11][12][13]. Non-destructive assessment techniques can be used to conserve old masonry structures and architectural heritage [14]. The study emphasizes how crucial it is to combine field observations with lab testing in order to make informed restoration decisions [15].

II. SCOPE OF STUDY

- Determining the building's current condition.
- Determining the methods for strengthening and repair.
- Creating a program for repairs.
- Establishing the necessary target condition.
- A second examination and check.

III. COOLING TOWER

3.1 Background

The cooling tower at the CPCL plant in Chennai (Manali) has been selected for retrofitting. This structure is an older design, standing up to 15 meters high, and is experiencing damage as it ages. The primary objective of this project is to repair the structure while it is still operational. The flaws and water leaks in the structure are causing deterioration and spalling of the concrete. When concrete spalls, it exposes the reinforcement to air, which can result in severe corrosion. Following a non-destructive test, it was confirmed that the structure is safe and simply needs repair and rehabilitation. It is robust enough to support the loads placed upon it.

3.2 Distress Observed

Due to its age and location in a damp area, the building experienced serious problems with water leaks and reinforcing corrosion. The side walls had developed cracks, which caused leaks. The concrete spalled as a result of the reinforcing corroding.

IV. Rehabilitation Of Cooling Tower

4.1 Site Investigation

The site examination examines the cooling tower's physical state, which is situated in an industrial area. This cooling tower is quite old and constantly in contact with water, which causes it to lose strength. It hasn't been adequately maintained over the years, either. The building is a single structure that is between 15 and 17 meters high.

4.2 Visual Inspection

The most qualitative way to assess a structure's structural soundness and spot common distress signals and the issues that go along with them is to visually inspect it. Even if the structure's outside is badly damaged, the inspection showed that it is still sturdy enough to support the weight and that only retrofitting is necessary. Furthermore, the reinforcement is being exposed to the weather and corroding due to a leak that is happening through created fractures.

4.3 NDT Test

Concrete's in-situ strength and quality can be assessed using non-destructive testing. To evaluate the structure's health, tests like the rebound hammer and soundness tests are performed.

In contrast to a high number, a low value in the rebound hammer test indicates a weak spot in the concrete. Analyzing the sound made when hitting the concrete surface is part of the soundness test. Whereas weak concrete makes a bland sound, good concrete makes a distinct, sharp sound.

4.4 Causes for the Failure

The structure's failure is mostly due to aging and inadequate maintenance. Because of the structure's continuous interaction with water, there are alternating wet and dry spells, which cause cracks to grow. The steel reinforcement corrodes as a result of these fissures and the atmosphere's continued moisture. Concrete eventually spalls as a result of this corrosion, weakening the surface as a whole.

4.5 Suitable Repair Technique

The particular needs and environmental circumstances are taken into consideration when selecting the repair method. The first step should be to chip away the damaged concrete. More shear connectors should be added, and any seriously damaged reinforcement should be replaced. A primer should be applied to the reinforcement to stop corrosion.

The structure must have limited porosity to lower the chance of fracture formation and fast restore its strength because it is in operational state and comes into contact with water. As a result, micro concrete made of polymers is utilized. Additionally, a bonding agent is used to improve the new concrete's adherence to the old concrete.

V. Step by Step Procedure to Carry Out Repair

5.1 General Requirement

Before beginning the work, preliminary safety precautions must be done. For the work to be done correctly, the workers need be given the right instructions and working procedures. The necessary quantity and quality of material should be purchased in advance and kept in a secure location.

Providing sufficient support is crucial to ensuring the building's structural safety, particularly because the structure is still in operational condition. The carefully designed props are intended to temporarily reduce the slab's weight, which is negatively affecting the weak column. A strong solution is guaranteed at this crucial time since each prop is evaluated to sustain an amazing load capacity of 120 kN.

5.3 Chipping of Unsound and Weak Concrete

The deteriorated and fragile concrete should be carefully removed to ensure structural integrity. To minimize vibrations that could compromise the surrounding elements, a power-driven percussion chisel or a pneumatic chisel is employed. Following this process, all debris and waste materials must be thoroughly cleared away to maintain a clean work area and facilitate further construction efforts.

Fig. 3 After chipping

5.4 Cutting Reinforcement Bar

Carefully cut out and remove the highly deteriorated and corroded reinforcing. In order to preserve the integrity of the surrounding structure and avoid additional damage during the removal process, this procedure must be carried out very carefully.

5.5 Inserting New Bar and Shear Key Bar

The surface is carefully drilled using a power drill, creating a precise hole that reaches a minimum depth of 150 mm and extends up to a maximum depth of 200 mm. Once the hole is prepared, the reinforcement bar is expertly positioned and secured using a combination of robust welding and high-strength epoxy to ensure stability and durability. To enhance its longevity and protect against corrosion, the reinforcement bar receives a thorough coating of NITOZIN primer, providing a reliable barrier against the elements.

FIG.4 INSERTING REINFORCEMENT

5.6 Bonding Coat

The bonding coat is to be meticulously applied to the existing concrete surface, ensuring optimal adhesion and durability. We recommend using NITOBOND EP as the bonding agent, as it offers a longer overlay time, providing ample opportunity for adjustments during application.

Its high bond strength ensures a reliable and robust connection to the substrate, while its exceptional formulation serves as an effective barrier, preventing the migration of harmful chloride ions. This combination of attributes makes NITOBOND EP an ideal choice for enhancing the longevity and performance of the concrete structure.

FIG.5 APPLYING BONDING AGENT ON SURFACE

5.7 Micro Concrete

Micro concrete is an advanced polymer-based cementitious material designed specifically for the repair of damaged reinforced concrete elements. Its unique properties make it particularly suitable for applications in areas with restricted access, where traditional repair methods may be difficult due to challenges in material vibration and placement. Remarkably, micro concrete can achieve a compressive strength of up to 60 N/mm², making it a robust choice for structural rehabilitation.

In our testing process, a cube was prepared using a precise mix ratio of 2:1, combining micro concrete powder with 12mm aggregate, and adequate water was added to ensure optimal consistency. The cubes were tested at 12 days of curing, revealing an impressive average strength of 50 N/mm² based on four samples. To further enhance the durability and performance of the micro concrete, a thorough curing process was implemented, allowing the material to fully develop its strength and resilience.

5.8 Post Retrofitting Evaluation

In order to create a cube for the retrofitting examination, pieces of old concrete are creatively combined with a micro concrete mix. After that, this composite cube is put through a thorough testing process to evaluate its performance attributes and structural integrity.

VI. CONCLUSION

From the above study it is noted that with advance techniques for rehabilitation of structure can able to regain its strength higher than that it deserved. By using micro concrete we can able to regain the original strength within the short duration than the construction of new structure and more economical. It also increases the life time of the building.

ACKNOWLEDGMENT

The author express their gratitude to Thiagarajar College of Engineering (TCE) for supporting us to carry out this research work. Also, the financial support from TCE under Thiagarajar Research Fellowship scheme (File.no: TRF/Jul-2023/01) is gratefully acknowledged.

REFERENCES

[1] E. L. Qualharini, L. H. C. Oscar, and M. R. Da Silva, “Rehabilitation of buildings as an alternative to sustainability in Brazilian constructions,” Open Engineering, vol. 9, no. 1, pp. 139–143, 2019, doi: 10.1515/eng-2019-0017.

[2] S. Sandbhor and R. Botre, “A SYSTEMATIC APPROACH TOWARDS RESTORATION OF HERITAGE BUILDINGS-A CASE STUDY,” IJRET: International Journal of Research in Engineering and Technology, [Online]. Available: http://iscarsah. icomos.org/content/principles].

[3] Y. Kantheepan et al., “Rehabilitation of Historical Building-A Case Study.”

[4] S. R. Subramaniam, “A Review on Repair and Rehabilitation of Heritage Buildings,” International Research Journal of Engineering and Technology, 2016, [Online]. Available: www.irjet.net

[5] J. Radnić, D. Matešan, and A. Abaza, “Restoration and Strengthening of Historical Buildings: The Example of Minceta Fortress in Dubrovnik,” Advances in Civil Engineering, vol. 2020, 2020, doi: 10.1155/2020/ 8854397.

[6] U. Department of the Interior National Park Service Technical Preservation Services, “The Secretary of the Interior’s Strandards for the Treatment of Historic Properties With Guidelines For Preserving, Rehabilitating, Restoring & Reconscructing Historic Buildings.”

[7] T. Yee Sing and S. Yoh, “Rehabilitation Methods and Revitalization Strategies in the Old Inner-City Areas of Rapid Growth Cities in Asia,” Urban and Regional Planning Review, vol. 3, no. 0, pp. 1–20, 2016, doi: 10.14398/urpr.3.1.

[8] S. Pescari, L. Budău, and C. B. Vîlceanu, “Rehabilitation and restauration of the main façade of historical masonry building –Romanian National Opera Timisoara,” Case

Studies in Construction Materials, vol. 18, Jul. 2023, DOI: 10.1016/j.cscm.2023.e01838.

[9] C. Natarajan, S.-E. Chen, and M. Syed, "Rehabilitation and Preservation of the St. Lourdes Church, Tiruchirappalli," Journal of Performance of Constructed Facilities, vol. 24, no. 3, pp. 281–288, Jun. 2010, doi: 10.1061/(asce)cf.1943-5509.0000101.

[10] R. C. Mack and J. P. Speweik, "2 PRESERVATION BRIEFS Repointing Mortar Joints in Historic Masonry Buildings."

[11] S. K. Verma, S. S. Bhadauria, and S. Akhtar, "Review of Nondestructive Testing Methods for Condition Monitoring of Concrete Structures," Journal of Construction Engineering, vol. 2013, pp. 1–11, Apr. 2013, DOI: 10.1155/2013/834572.

[12] L. Binda and C. Maierhofer, "Strategies for the assessment of historic masonry structures."

[13] C. W. Wong, "Applications of Non-destructive Tests for Diagnosis of Heritage Buildings: Case Studies from Singapore and Malaysia."

[14] M. E. Kaplan et al., "Non-destructive Evaluation Techniques for Masonry Construction Preservation Architecture Non-destructive evaluation techniques can be of significant value in historic preservation projects."

[15] B. Yildizlar, B. Sayin, and C. Akcay, "A Case Study on the Restoration of A Historical Masonry Building Based on Field Studies and Laboratory Analyses," International Journal of Architectural Heritage, vol. 14, no. 9, pp. 1341–1359, Oct. 2020, DOI: 10.1080/15583058.2019.1607625.

Finite Element Modeling and Analysis of Soft Pneumatic Spinal Cord Wearable Actuator for Ankylosing Spondylitis Patients

S. Meenakshi
Research Scholar,
Department of Electronics and Communication Engineering,
Thiagarajar College of Engineering,
Madurai, India
smeenakshi@student.tce.edu

G. Prabhakar
Assistant Professor, Departmdnt of Electronics and Communication Engineering,
Thiagarajar College of Engineering,
Madurai, India
gpece@tce.edu

***Abstract*—This research presents an initial analysis to aid individuals with Ankylosing Spondylitis (AS) of a soft pneumatic spinal cord wearable assistive device designed. Ankylosing Spondylitis is a very common chronic inflammatory disease affecting the spinal cord, often resulting in progressive stiffness, pain, and kyphotic posture deformities. Pneumatic soft wearable actuator has been proposed and provides a non-invasive and adaptive solution, which provides an improvement in posture. By applying controlled pneumatic pressure to gently correct spinal alignment over time. Finite Element Analysis (FEA) has been conducted to evaluate the deformation, stress distribution, and performance of the wearable actuator under various pressure levels using Finite Element Analysis tool. The safety and efficacy of the device are ensured by this analysis under real-world conditions. Additionally, the system's soft and flexible design minimizes discomfort while promoting improved mobility and posture correction. This novel device offers significant benefits, including injury prevention, enhanced spinal health, and improved quality of life for patients. By addressing a critical gap in assistive technologies for AS, this research gives the way for future advancements in soft robotics for medical and rehabilitative applications.**

Keywords—Ankylosing Spondylitis, Soft Wearable Actuator, Finite Element Analysis

I. Introduction

Ankylosing spondylitis (AS) is a chronic inflammatory disorder affecting the spine and sacroiliac joints, leading to stiffness, pain, and spinal deformities like kyphosis. Management includes NSAIDs, biologics, and physical therapy to alleviate symptoms and prevent disability [1]. Zhu et al. review ankylosing spondylitis, emphasizing its genetic link (HLA-B27), immune dysregulation, and environmental triggers. They outline treatments like NSAIDs, TNF inhibitors, and IL-17 blockers to manage symptoms and slow disease progression [2-5]. Existing assistive devices for Ankylosing Spondylitis (AS) patients may lack effectiveness in addressing pain relief and improving spinal posture. Indian IT professionals, medical professionals, engineering college professors, and weight-lifting workers, who are predisposed to genetic diseases like AS, often suffer severe lower back pain due to prolonged sitting and engaging in tasks like firmware development, R&D activities, and weightlifting [6-8].

A novel solution is needed to integrate soft pneumatic technology, acupressure spikes, and advanced control mechanisms to assist AS patients and alleviate low back pain among these groups affected by both genetic and occupational factors. The proposed Soft Pneumatic Spinal Cord Wearable Assist integrates soft pneumatic actuators with a wide range of bending deformation angles, acupressure spikes, and a learning-based bending deformation control model. This innovative approach targets the challenges faced by AS patients and individuals with low back pain due to occupational factors in India. Objectives include designing and fabricating a wearable soft pneumatic actuator for spinal cord posture correction, integrating acupressure spikes for targeted pressure application, analyzing soft actuators' bending characteristics, and developing a learning-based control model for adaptability.

The research methodology involves designing and fabricating the actuator, analyzing its characteristics through simulation and experiments, and developing a control model using deep neural networks. The expected outcome is the effective alleviation of pain, improved posture, and enhanced quality of life for AS patients and those with low back pain in India. This innovation benefits both patients and healthcare professionals in managing musculoskeletal issues.

II. Problem Statement

Ankylosing Spondylitis (AS), a form of arthritis that primarily affects the spine, poses significant challenges for individuals due to joint inflammation, spinal abnormalities, stiffness, and discomfort in the lower back. These symptoms lead to reduced mobility and a diminished quality of life. While current treatments focus on medication and lifestyle modifications, innovative approaches are needed to alleviate pain and improve mobility without relying solely on painkillers, especially considering the potential for abuse and dependency.

To address these challenges, a soft pneumatic spinal cord wearable assist for AS patients is proposed [1,2]. This assistive device aims to rectify spinal posture, prevent deformities, and provide relief by incorporating soft pneumatic actuators and acupressure therapy targeted at specific lumbar pressure points [5]. However, the development of such a device requires a comprehensive understanding of the bending behavior of soft actuators and the integration of effective control mechanisms to tailor support for individual needs.

In addition to address the needs of AS patients, the research aims to extend its impact to individuals with various spinal problems. Therefore, the creation of a machine learning-based control model is proposed to manage the bending behavior of the soft pneumatic actuators [9-12], offering personalized support and enhancing overall efficacy.

In summary, the problem statement emphasizes the urgent need for innovative solutions to address the challenges faced by individuals with AS and other spinal problems. By leveraging soft pneumatic technology [11-15], acupressure therapy [11,12,15], and machine learning-based control models, the proposed research seeks to improve the quality of life and mobility of affected individuals while minimizing reliance on traditional pain management approaches.

This scenario is clearly shown in figure 1.

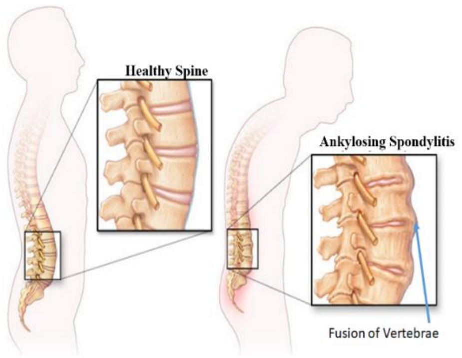

FIG.1. ANKYLOSING SPONDYLITIS

(Image Source: https://www.mayoclinic.org/diseases-conditions/ankylosing-spondylitis/symptoms-causes/syc-20354808)

Recent advancements in soft wearable actuators have demonstrated the potential for self-sensing and adaptive control in rehabilitation robotics. For example, MXene-based conductive composites and embedded liquid-metal sensors have been integrated into soft exosuits and spinal braces for real-time posture correction and force feedback [21–23]. Such approaches motivate the development of pneumatic solutions with embedded proprioceptive capabilities.

III. METHODOLOGY

A. Finite Element Modeling

ANSYS Multiphysics is used for Finite Element Modeling (FEM) to analyze the deformation, stress, and strain of the 3D-designed spinal cord assistive device. The simulation assesses the actuator's mechanical performance under various loading conditions, providing insights into its structural stability, flexibility, and durability. It helps identify critical areas through stress distribution and strain patterns. This analysis ensures the device's reliability, effectiveness, and safety in real-world applications.

The Yeoh hyperelastic model is widely used for characterizing the behavior of materials like rubbers and soft polimers. The second-order Yeoh model has the following strain energy density function:

$$W = C_{10}(I_1 - 3) + C_{20}(I_1 - 3)^2 + \frac{1}{D_1}(J - 1)^2 \qquad (1)$$

where,

W=Strain energy density

C_{10}, C_{20}= Material constants related to the shear behavior

I_1=First invariant of the deformation tensor

J=Determinant of the deformation gradient (for volumetric deformation).

Material Constants $C_{10}\ and\ C_{20}$ are determined experimentally using curve fitting from uniaxial, biaxial, or shear test data. D_1 is related to the bulk modulus (K). For nearly incompressible materials, $D_1$is very small. The simulation in ANSYS was performed using Ecoflex 00-30 silicone rubber as the actuator material, characterized by a second-order Yeoh hyperelastic model. The material constants used were: C_{10}=0.1 MPa C_{20}=0.02 The density of the material was assumed to be 1.07 g/cm³, and Poisson's ratio was set to 0.49 to approximate incompressibility. In the simulation, the bottom layer of the actuator was fixed to replicate a wearable configuration, and a uniform internal pressure (ranging from 5 kPa to 20 kPa) was applied to the inner walls of all chambers. Large deformation effects were enabled to account for nonlinear geometric behavior during inflation.

B. 3D Study Design:

The figure 2 depicts the design and structural components of a Soft Pneumatic Spinal Cord Wearable Actuator designed for Ankylosing Spondylitis (AS) patients. In figure 2.a, the actuator's exterior is shown with a series of pneumatic chambers that enable controlled inflation and deflation, allowing for flexibility in bending, extending, and maintaining posture. Figure 2.b provides a cross-sectional view, revealing internal elements such as a flex sensor that monitors the bending angle and delivers real-time feedback to regulate pneumatic pressure. It also features strategically placed acupressure points that offer therapeutic benefits, including pain relief and enhanced blood circulation. Figure 2.c illustrates a 3D perspective, showcasing the actuator's ability to conform to the spine's natural curvature, while figure 2.d presents a side view, highlighting its slim, lightweight profile for comfortable, discreet wear. This actuator is designed to support spinal alignment, provide dynamic posture correction, and deliver targeted therapeutic effects to improve the quality of life for AS patients.

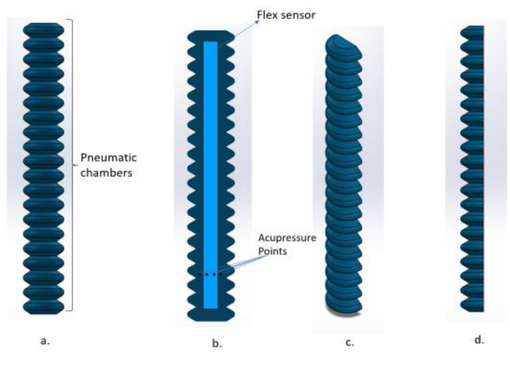

FIG.2. VARIOUS VIEWS OF STUDY DESIGN A. FRONT VIEW B. BACK VIEW

C. Perspective View d. Side View

The study design is designed by using solidworks and it is simple way to create a 3D design. 21 pneumatic chambers Flex sensor in integrated in back side of the pneumatic chamber to trace the bending posture of the human.

D. Proposed Wearable Model

The figure 3 depicts the design of a wearable system featuring a Soft Pneumatic Actuator intended for spinal support. At the top, the Shoulder Belt Lock secures the device around the user's shoulders, ensuring stability and proper positioning. A layer of Stretchable Fabric ensures for flexibility and conforms to the body's shape, enhancing comfort during movement. The core component is the Soft Pneumatic Actuator, which is integrated with a Flex Sensor. By doing continuous monitoring of the spinal curvature and providing real-time feedback to the controller for precise posture adjustments through controlled pneumatic pressure. The actuator is fixed with the stretchable fabric at the bottom with a Hip Belt Lock, offering additional support and keeping the device securely in place. Solenoid Valve used as a final control element in the end of the actuator setup, which allows the airflow to the pneumatic chambers by enabling efficient inflation and deflation of the soft actuator. This compact soft actuator setup allows to improve spinal alignment, support posture correction, and deliver therapeutic benefits for individuals with spinal conditions such as Ankylosing Spondylitis.

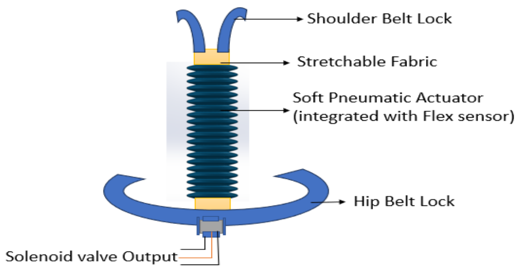

FIG.3. PROPOSED WEARABLE MODEL

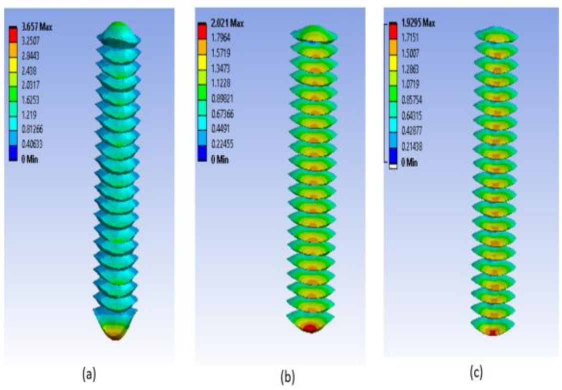

FIG.4. TOTAL DEFORMATION FOR VARIOUS PRESSURE INPUT (A) FOR 20KPA (B) FOR 10KPA (C) FOR 5KPA

IV. RESULTS AND DISCUSSION

Figure 4 illustrates ANSYS simulation, the total deformation of a 21-chamber elastomer spinal cord model under varying pressure inputs (20KPa, 10KPa, and 5KPa). The structural design analysis for the designed 3D model has been considered as large deflection, which expands as pressure increases, showing a significant deformation at higher pressures. As pressure decreases, deformation reduces proportionally, highlighting the material's responsiveness to input variations and the deformation magnitude is indicated in color code form. This study helps in understanding the structural behavior of soft actuators, aiding in optimizing chamber design and material properties for efficient actuation.

V. CONCLUSION AND FUTURE WORK

This study focuses the development of a self-sensing soft actuator-based spinal cord assistive device for individuals affected by Ankylosing Spondylitis. ANSYS simulation has been done for analysing the total deformation at various pressure levels to validate the designed actuator's performance. Future scope of this work will focus on real-time fabrication, control, and experimental validation to further enhance its functionality and practical implementation.

ACKNOWLEDGEMENT

S. Meenakshi thanks Thiagarajar College of Engineering (TCE) for supporting her in this research. Also, the financial support from TCE under the Thiagarajar Research Fellowship scheme (File.no: TRF/Jul-2023/4) is gratefully acknowledged.

REFERENCES

[1] Sieper J, Braun J, Rudwaleit M, et al., Ankylosing spondylitis: an overview Annals of the Rheumatic Diseases 2002;61:iii8-iii18.

[2] Zhu W, He X, Cheng K, Zhang L, Chen D, Wang X, Qiu G, Cao X, Weng X. Ankylosing spondylitis: etiology, pathogenesis, and treatments. Bone Res. 2019 Aug 5;7:22. doi: 10.1038/s41413-019-0057-8. PMID: 31666997; PMCID: PMC6804882.

[3] Akassou A, Bakri Y. Does HLA-B27 Status Influence Ankylosing Spondylitis Phenotype? Clinical Medicine Insights: Arthritis and Musculoskeletal Disorders. 2018;11. doi:10.1177/1179544117751627

[4] Sen R, Goyal A, Hurley JA. Seronegative Spondyloarthropathy. [Updated 2022 Jul 18]. In: StatPearls [Internet]. Treasure Island (FL): StatPearls Publishing; 2022 Jan-. Available from: https://www.ncbi.nlm.nih.gov/books/NBK459356/

[5] Shao, F., Liu, Q., Zhu, Y. et al. Targeting chondrocytes for arresting bony fusion in ankylosing spondylitis. Nat Commun 12, 6540 (2021). https://doi.org/10.1038/s41467-021-26750-6.

[6] https://gokanjo.com/blogs/your-life-relieved/how-can-i-find-acupressure-points-on-my-body

[7] T. Muronosono, T. Nishiyama, S. Kawajiri, T. Imai, K. Arai and T. Kobayashi, "Research on Rheumatoid Arthritis Detection Support System," *2021 IEEE 3rd Global Conference on Life Sciences and Technologies (LifeTech)*, 2021, pp. 122-123, doi: 10.1109/LifeTech52111.2021.9391830.

[8] J. -H. Park, P. R. Stegall, D. P. Roye and S. K. Agrawal, "Robotic Spine Exoskeleton (RoSE): Characterizing the 3-D Stiffness of the Human Torso in the Treatment of Spine Deformity," in IEEE Transactions on Neural Systems and Rehabilitation Engineering, vol. 26, no. 5,

pp. 1026-1035, May 2018, doi: 10.1109/TNSRE. 2018.2821652.

[9] Matthew Chin Heng Chua, Jeong Hoon Lim & Raye Chen Hua Yeow (2019) Design and Characterization of a Soft Robotic Therapeutic Glove for Rheumatoid Arthritis, Assistive Technology, 31:1, 44-52, DOI: 10.1080/10400435.2017.1346000

[10] Leng, J.; Sun, J.; Guan, Q.; Liu, Y. Status of and trends in soft pneumatic robotics. Sci. Sin. Technol. 2020, 50, 897–934.

[11] Lei J, Ge Z, Fan P, Zou W, Jiang T, Dong L. Design and Manufacture of a Flexible Pneumatic Soft Gripper. *Applied Sciences*. 2022; 12(13):6306. https://doi.org/10.3390/app12136306

[12] Ding, L., Niu, L., Su, Y. et al. Dynamic Finite Element Modeling and Simulation of Soft Robots. Chin. J. Mech. Eng. 35, 24 (2022). https://doi.org/10.1186/s10033-022-00701-8

[13] N Koenig, A Howard. Design and use paradigms for Gazebo, an opensource multi-robot simulator. 2004 IEEE/RSJ International Conference on Intelligent Robots and Systems (IROS), Sendai, Japan, 28 Sept.-2 Oct., 2004: 2149–2154.

[14] J Roßmann, M Schluse, M Rast, et al. Simulation technology for soft robotics applications//Soft Robotics: Transferring Theory to Application, Verl A, Albu-Schäfer A, Brock O, et al, Berlin, Heidelberg, 2015: 100–119.

[15] Y Elsayed, A Vincensi, C Lekakou, et al. Finite element analysis and design optimization of a pneumatically actuating silicone module for robotic surgery applications. Soft Robotics, 2014, 1(4): 255–262.

[16] P Polygerinos, Z Wang, J T B Overvelde, et al. Modeling of soft fiber reinforced bending actuators. IEEE Transactions on Robotics, 2015, 31(3): 778–789

[17] E B Joyee, Y Pan. A fully three-dimensional printed inchworm-inspired soft robot with magnetic actuation. Soft Robotics, 2019, 6(3): 333–345.

[18] G. Prabhakar, S. Selvaperumal & P. Nedumal Pugazhenthi (2019) Fuzzy PD Plus I Control-based Adaptive Cruise Control System in Simulation and Real-time Environment, IETE Journal of Research, 65:1, 69-79, DOI: 10.1080/03772063.2017.1407269

[19] G.Prabhakar, S.Selvaperumal, P.Nedumal Pugazhenthi, "Fault Data Injection Attack on Car-Following Model and Mitigation Based on Interval Type2-Fuzzy Logic Controller", IET Cyber Physical Systems: Theory & Applications, Vol. 4(2), June 2019, pp. 128-138.

[20] S. Meenakshi, G. Prabhakar, N. Ayyanar and P. N. Pugazhenthi, "FEM Based Soft Robotic Gripper Design for Seaweed Farming," 2023 International Conference on Energy, Materials and Communication Engineering (ICEMCE), Madurai, India, 2023, pp. 1-5, doi: 10.1109/ICEMCE57940.2023.10434066.

[21] Wang, Y., Guo, T., Tian, Z., et al. (2023). MXenes for soft robotics. *Matter*, 6(9), 2807–2833.

[22] Chen, S., Wang, H. Z., Liu, T. Y., & Liu, J. (2023). Liquid metal smart materials toward soft robotics. *Adv. Intell. Syst.*, 5(8), 2200375.

[23] Liu, H., Chu, H., Yuan, H., et al. (2024). Bioinspired multifunctional self-sensing actuated gradient hydrogel for soft-hard robot remote interaction. *Nano-Micro Letters*, 16(1), 69.

A Novel Edge Caching Framework for Accident Detection in Highways

Michael Valan E M
Department of Information Technology,
Thiagarajar College of Engineering,
Madurai, India
michaelvalan@student.tce.edu

Thiruchadai Pandeeswari S
Assistant Professor, Department of Information Technology,
Thiagarajar College of Engineering,
Madurai, India
eshwarimsp@tce.edu

Kavin Jose J
Department of Information Technology,
Thiagarajar College of Engineering,
Madurai, India
kavinjose@student.tce.edu

Sabarilal A K
Student, Department of Information Technology,
Thiagarajar College of Engineering,
Madurai, India
sabarilal@student.tce.edu

***Abstract*—Real-time accident detection systems are crucial for improving road safety and minimizing response times in transportation networks. Leveraging deep learning models allows for accurate classification of traffic scenarios into accident and non-accident categories. However, challenges arise in handling the large volumes of data from video feeds and ensuring low-latency processing. Traditional cloud-based solutions face bottlenecks due to network congestion and data transfer delays. To address this challenge, a fog based edge caching framework is proposed in this work. The edge caching scheme is utilized to store data closer to the source to reduce reliance on cloud servers, minimize latency, and enhance decision-making speed. The integration of CNN-based classification with edge caching enables efficient and scalable real-time accident detection, supporting smarter traffic management and safer transportation systems. Our experimental results show that the CNN model achieves 91% accuracy, outperforming the Random Forest model (88%). Additionally, CNN exhibits higher precision (0.88 vs. 0.85) and F1-score (0.91 vs. 0.88) for the Non-Accident class, while Random Forest demonstrates better recall for accident detection (0.89 vs. 0.88).**

Keywords—Mobile edge caching, distributed deep learning, proactive, cooperative caching

I. INTRODUCTION

Mobile edge caching (MEC) aims to distribute popular contents closer to mobile users via mobile edge nodes (MENs) to reduce service delay. This project addresses the limitations of traditional cloud-based accident detection systems by integrating a CNN-based machine learning model with edge caching. Conventional systems often rely on reactive resource allocation, leading to increased latency and inefficient performance under high traffic conditions. By utilizing edge caching, our approach processes frequently accessed data closer to the source, significantly reducing latency and enabling faster, real-time accident detection. This proactive method optimizes resource allocation and scalability, enhancing the overall efficiency of the system.

A key aspect of this research is the analysis and identification of optimal deep learning models for real-time accident detection and edge caching optimization. Convolutional Neural Networks (CNNs) will be used for accurate classification of accidents. Data preparation and preprocessing are crucial for the success of the system. The dataset will undergo preprocessing, including noise removal, normalization, and handling of missing frames. In this work, a CNN-based predictive model tailored for real-time accident detection is proposed. The model will be trained with techniques like data augmentation, dropout for regularization, and adaptive learning rate optimization to enhance generalization. It will be evaluated on industry-standard metrics such as Accuracy, Precision, Recall, and F1-Score. Additionally, the model will be aligned with edge caching architecture to ensure efficient data processing, reduce network congestion, and optimize resource utilization, laying the foundation for scalable and responsive accident detection systems in transportation networks.

II. LITERATURE SURVEY

Tian et al. (2019) present an automatic car accident detection system based on Cooperative Vehicle Infrastructure Systems (CVIS), which integrates vehicle sensors and infrastructure elements for reliable accident detection. The system's strength lies in its multi-source data fusion, combining GPS, vehicle speed, and acceleration data. Liyanage et al. (2020) focus on near real-time freeway accident detection using machine learning techniques to analyze traffic data. Their system processes data such as vehicle speed, traffic density, and environmental conditions to detect accidents quickly. Adewopo and Elsayed (2024) propose a deep-learning ensemble model for traffic accident detection in smart city transportation systems. The ensemble combines CNNs, RNNs, and SVMs trained on various data sets, such as traffic conditions, weather, and vehicle behavior. Deng and Wu (2019) investigate a driver drowsiness detection system that uses facial feature analysis for real-time monitoring. The system tracks eye movement, eyelid closure, and head position to detect signs of drowsiness. Edge computing enables local video data processing, reducing latency and the need for cloud processing.

Ahmed et al. (2024) focus on real-time depression monitoring to prevent accidents in smart vehicles. The system uses multimodal data, including facial expressions, voice tone, and physiological signals, to detect signs of depression in drivers. Deep learning models analyze these signals in real-time, providing feedback and intervention without relying on cloud systems. Chavhan et al. (2023) introduce an edge-enabled communication-based trajectory perception system for smart cities. The system uses V2V and V2I communication to predict potential collisions by analyzing the movement patterns of vehicles and pedestrians. From the literature survey carried out, the following observations were made:

- The integration of various data sources (e.g., vehicle sensors, infrastructure elements, traffic data) is crucial for enhancing the accuracy and reliability of accident detection systems.
- Real-time data processing and immediate feedback is essential for accident detection systems to be effective in preventing accidents and minimizing traffic disruptions.
- Use of machine learning and AI techniques, such as deep learning ensembles and supervised learning models, improves the robustness, accuracy, and efficiency of accident detection systems
- Edge computing plays a significant role in reducing latency and enabling real-time processing of data, making it vital for time-sensitive applications like accident detection and prevention.
- Monitoring driver behavior and mental state (e.g., drowsiness, depression) adds an additional layer of safety, complementing traditional accident detection methods.

III. GAP ANALYSIS AND OBJECTIVES

Based on the gaps identified through the literature survey, the following are considered objectives for this work.

- Develop a system capable of real-time detection of traffic accidents using video feeds from highway cameras.
- Implement deep learning models (Convolutional Neural Network and Random Forest) to identify accidents from video data with minimal false positives accurately.
- Utilize edge caching to store and process critical data close to the source, reducing latency and enhancing response times.

TABLE 1. SUMMARY OF LITERATURE SURVEY

Study	Focus	Methods	Key Findings	Strengths	Gaps/Limitations
Tian et al. (2019)	Automatic car accident detection	CVIS, multi-source data fusion (GPS, vehicle speed, acceleration)	Improved accident detection accuracy, reduced latency, suitable for smart cities and ITS	Integration of multi-source data, real-time processing	Limited focus on pedestrian safety
Liyanage et al. (2020)	Near real-time freeway accident detection	Machine learning, traffic data analysis	Quick accident detection, reduced false positives, rapid feedback	Real-time data processing, computational efficiency	Scalability in diverse traffic environments
Adewopo & Elsayed (2024)	Traffic accident detection in smart cities	Deep learning ensemble (CNNs, RNNs, SVMs)	Enhanced robustness and accuracy, reduced false alarms	Handling large-scale traffic data, adaptability to dynamic conditions	Integration with existing infrastructure
Deng & Wu (2019)	Driver-drowsiness detection	Facial feature analysis, edge computing	Real-time monitoring and alerts, reduced latency	Real-time video analysis, local processing	User privacy and data security
Ahmed et al. (2024)	Driver depression monitoring	Multimodal data (facial expressions, voice tone, physiological signals), deep learning	Real-time feedback and intervention, improved driver safety	Behavioral monitoring, real-time processing	Long-term effectiveness and reliability
Chavhan et al. (2023)	Vehicle and pedestrian trajectory perception	V2V, V2I communication, edge computing	Predicting potential collisions, rapid decision-making, enhanced road safety	Scalability, adaptability to urban environments	Limited focus on integration with other systems

IV. SYSTEM MODEL

The architecture of our Real-Time Accident Detection System leverages deep learning models for accident classification, integrated with edge caching to reduce latency and optimize resource usage. The system comprises the following interconnected components:

Data Collection Layer

The Data Collection Layer plays a crucial role in gathering real-time and historical data from various sensors and external sources to detect accidents accurately. It includes data from vehicle cameras, IoT devices, and other sensors that monitor vehicle speed, acceleration, and environmental conditions. The integration of diverse data sources ensures the system can detect accidents across various scenarios, from sudden collisions to abnormal vehicle behaviour.

Prediction Layer

The Prediction Layer employs a Convolutional Neural Network (CNN) to process video frames and classify them as either "Accident" or "Non-Accident." The CNN model is trained using historical accident data, enabling the system to recognize accident patterns and predict the likelihood of accidents in real-time based on current sensor data.

Edge Caching Layer

To reduce latency and improve the efficiency of the system, the Edge Caching Layer stores and processes critical data closer to the source, at the network edge. By caching data locally, the system can perform real-time analysis without needing to communicate with remote cloud servers, thus eliminating delays that could hinder accident detection. .

Action Layer

The Action Layer takes the predictions generated by the CNN model and triggers appropriate actions based on the accident detection results. This can include notifying authorities or emergency services about the incident, activating safety mechanisms such as automatic braking within the vehicle, and sending real-time alerts to traffic control centers.

V. IMPLEMENTATION

The implementation focuses on configuring the system to capture real-time video data, preprocess the frames, and apply machine learning models for accurate accident detection. The process begins with Data Collection Setup, where IP cameras continuously stream video footage of road traffic, and the video feed is sent to a centralized server for processing. Each video frame is extracted using OpenCV at regular intervals (e.g., every second) for analysis. The frames are then preprocessed to normalize lighting conditions, resize the images to a uniform input size, and apply filters to reduce noise and enhance key features.

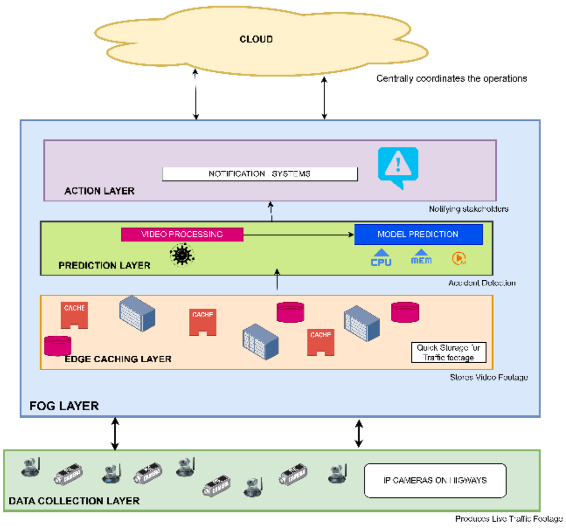

FIG 1. ARCHITECTURE DIAGRAM OF THE PROPOSED SYSTEM

The dataset used for training and evaluating the accident detection system is sourced from Kaggle (http://kaggle.com/datasets/ckay16/accident-detection-from-cctv-footage). It consists of CCTV video footage frames, labeled as accident or non-accident. The Model Training setup involves selecting a Convolutional Neural Network (CNN) model for detecting spatial features in video frames. Performance metrics, such as accuracy, precision, and recall, are calculated on the test set to evaluate the model's effectiveness.

The performance metrics such as accuracy, precision, and recall are computed on the test set to evaluate the CNN and RF models effectiveness and compare them. The model parameters used in both the models are summarized in Table 2 below.

TABLE 2. MODEL PARAMETERS

Parameter	CNN	Random Forest
Learning rate	0.001	N/A
No of epochs	20	N/A
Max Depth	N/A	10
No of Trees	N/A	1000
Batch Size	32	N/A
Image Size	128x128	128x128

VI. RESULTS

The results from the accident detection system show promising performance, with the CNN model achieving an accuracy rate of 91% in detecting accidents from the test dataset. The system effectively identifies both accident and non-accident scenarios. Key performance metrics of the models are presented in Table 3.

The Random Forest (RF) model, utilizing HOG feature extraction, also demonstrates strong performance in accident detection. The RF model achieves an accuracy of 88-90% on the test dataset. While slightly lower than CNN, it remains an effective approach for real-time accident detection with reduced computational complexity. Key performance metrics of Random forest model is presented in Table 4. The confusion matrices of both the models are presented in figure 3 and 4 below.

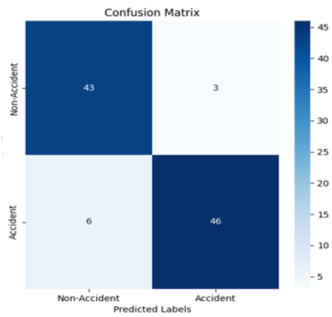

FIG 3. CONFUSION MATRIX – CNN

The CNN model outperforms the Random Forest model across all evaluation metrics, including precision, recall, F1-score, and accuracy.

The comparison of the performance metrics of the CNN and Random forest models are shown in the figure 6 below.

VII. CONCLUSION

This work successfully demonstrated the effectiveness of deep learning models, specifically Convolutional Neural Networks (CNNs), in real-time accident detection using video feeds from IP cameras. By incorporating advanced preprocessing techniques, the system is capable of analyzing traffic scenarios and detecting accidents with high accuracy and minimal latency. In future, the scope of the work may include integrating real-time alerting mechanisms and increasing the system's adaptability to various traffic environments.

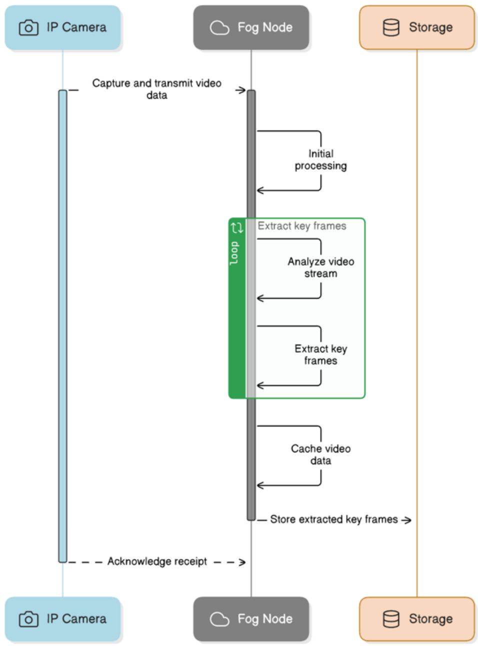

FIG 2. EDGE CACHING WORKFLOW

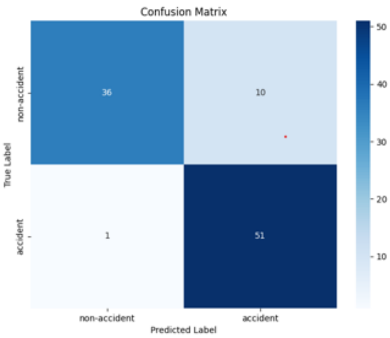

FIG 4. CONFUSION MATRIX – RANDOM FOREST

FIG 5. PREDICTED "ACCIDENT" FOR THE IMAGE USING CNN

TABLE 3. PERFORMANCE METRICS OF CNN

	Precision	Recall	F1-Score	Support
Non-Accident	0.88	0.93	0.91	46
Accident	0.94	0.88	0.91	52
Accuracy			0.91	98
Macro avg	0.91	0.91	0.91	98
Weighted avg	0.91	0.91	0.91	98

TABLE 4. PERFORMANCE METRICS OF RANDOM FOREST

	Precision	Recall	F1-Score	Support
Non-Accident	0.85	0.89	0.87	46
Accident	0.92	0.89	0.90	52
Accuracy			0.88	98
Macro avg	0.89	0.89	0.88	98
Weighted avg	0.89	0.88	0.88	98

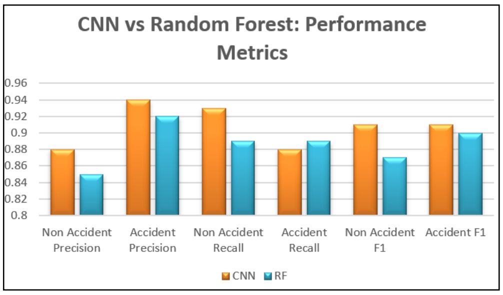

FIG 6. CNN VS RANDOM FOREST – PERFORMANCE METRICS

REFERENCES

[1] Yaqoob, S., Hussain, A., Subhan, F., Pappalardo, G., & Awais, M. (2023). Deep learning based anomaly detection for fog-assisted iovs network. *IEEE Access*, *11*, 19024-19038.

[2] Khan, M. A., Baccour, E., Chkirbene, Z., Erbad, A., Hamila, R., Hamdi, M., & Gabbouj, M. (2022). A survey on mobile edge computing for video streaming: Opportunities and challenges. *IEEE Access*, *10*, 120514-120550.

[3] Thar, K., Tran, N. H., Oo, T. Z., & Hong, C. S. (2018). DeepMEC: Mobile edge caching using deep learning. *IEEE Access*, *6*, 78260-78275.

[4] Tian, Y., Wang, Y., Li, K., & Zhang, D. (2019). Automatic car accident detection based on Cooperative Vehicle Infrastructure Systems (CVIS). *IEEE Transactions on Intelligent Transportation Systems*.

[5] Liyanage, M., Zois, D.-S., & Chelmis, C. (2020). Near real-time freeway accident detection using machine learning techniques. *Transportation Research Part C: Emerging Technologies*.

[6] Adewopo, O., & Elsayed, A. (2024). Deep learning ensemble approach for traffic accident detection in smart city transportation systems. *Journal of Artificial Intelligence Research*.

[7] Deng, J., & Wu, H. (2019). Real-time driver-drowsiness detection system using facial features. *IEEE Transactions on Intelligent Vehicles*.

[8] Ahmed, A., Singh, R., & Gupta, S. (2024). Real-time driver depression monitoring for accident prevention in smart vehicles. *IEEE Access*.

[9] Chavhan, S., Patel, A., & Sharma, R. (2023). Edge-empowered communication-based vehicle and pedestrian trajectory perception system for smart cities. *International Journal of Intelligent Transportation Systems*

Advanced Compression Technique for Low-Latency XR Head-Mounted Displays

Mary James
Department of ECE,
Thiagarajar College of Engineering,
Madurai, India
maryjames1408@gmail.com

Dr. D. Gracia Nirmala Rani
Department of ECE,
Thiagarajar College of Engineering,
Madurai, India
gracia@tce.edu

***Abstract*—The design of architecture for an extended reality (XR) system requires a comprehensive understanding of the different components that make up such a system. The focus is to design architecture for ultra-low-latency head mounted devices for immersive experience in XR systems in VLSI. The aim is to deliver the video content to the users with decreased latency. The data rate should be increased by using pipelining structures. The design of memory unit should be optimized. The compression and decompression algorithms should be optimized. This paper presents the design and implementation of a novel compression algorithm tailored for ultra-low-latency head-mounted devices, utilizing MATLAB for simulation and validation. The algorithm focuses on optimizing data throughput and reducing computational overhead, thereby enhancing real-time interaction in XR environments. Videos were broken into frames. The broken videos were stitched at the receiver end to avoid latency. The algorithm's structure will be discussed and comprehensive performance evaluations will be provided. The results demonstrate significant improvements in latency reduction and data handling efficiency, making this approach a viable solution for next-generation immersive XR applications.**

Keywords—Extended Reality; VLSI; Head Mounted Display (HMD); Immersive experience; low latency, compression

I. INTRODUCTION

Extended reality is the comprehensive term used to represent augmented reality and virtual reality. The need of the hour is to develop a head mounted display with low latency using VLSI technology. The objective of the design is to deliver content on time. The computing capability should be increased. The content selection should predict which tiled videos should be delivered to the user. The latency in data delivery should be reduced. The data collected should be processed immediately and send to the user (XR—user should be merged to the environment. XR facilitates experiential learning by providing interactive and hands-on experiences. From educational simulations to training scenarios in various fields such as medicine, aviation, and engineering, XR enables learners to practice skills and gain practical knowledge in a safe and controlled environment. XR allows users to visualize complex data and scenarios in a more intuitive and interactive manner.

Walsh Hadamard transform [1] is for image compression, filtering and speech processing. The proposed hardware design takes advantage of parallelism inherent in the WHT algorithm to achieve high throughput and low latency. It can be concluded that in the specified design the complexity is high. The analysis and architecture design with VLSI architecture of JPEG XR encoder [2]. The area and the power was decreased because only one hardware is used for the pre-filter in this design. Significant computational and memory resources are required in this implementation. The challenges and considerations when integrating XR and IoT include issues related to network connectivity, data management, privacy, security and so on [3]. The design enhances potential of XR to enhance user experiences by immersing them in virtual environments or overlaying digital content onto the real world. The design in this paper has the features such as high power consumption and high cost. The future work can be done on compatibility in the design and, optimized architecture. The manufacturing process of AR HMDs [4] is explored in detail.

Design of low-power super-resolution architecture for virtual reality wearable devices uses Super resolution (SR) convolutional neural networks (CNNs) technique for the design. SR CNN (FSRCNN) [5] accelerator is implemented on a 28-nm process technology. The design in this paper is able to process up to 214 ultrahigh definition frames/s, while consuming just 0.51 pJ/pixel without compromising the perceptual visual quality, thus achieving a 55% energy reduction and a ×14 times higher throughput rate. Development of an XR simulator for basic life support training [6] uses automated defibrillator cardiac patients in Europe and US. Near-Sensor Distributed DNN Processing for Augmented and Virtual Reality [7]. DNN models on an AR/VR compute platform that consists of an on-sensor processor and an edge processor to minimize energy and latency. This paper analyzes how the AR/VR platform is used to minimize energy configuration changes under the practical design constraints of memory size and silicon area.

Augmented reality and virtual reality displays: emerging technologies and future perspectives [8]. This paper describes the basic structures of AR and VR headsets and also describes the operation principles of various HOEs and lithography-enabled devices. A framework for Extended Reality System development in manufacturing [9] paper describes the XR in manufacturing and extended usage. The paper also describes the software used such as unity 3D, Unreal Engine, Plant simulation from SIEMENS and Robot studio from ABB.

This paper describes the possible health consequences of the prolonged usage [10]. The brightness and contrast of a display should be adjusted to match the external light to decrease eye strain and other symptoms. A Comparative Analysis of Virtual Reality Head-Mounted Display Systems

[11]. Clinical education is an area that especially stands to benefit from VR technology. Virtual Reality Instruction Followed by Enactment Can Increase Procedural Knowledge in a Science Lesson[12]. In this paper, they have examined the efficiency and has found that VR and Enactment has high performance. Exploring Eye Adaptation in Head-Mounted Display for Energy Efficient Smartphone Virtual Reality[13]. The proposed system, Strix, is empowered by a dark adaptation model trained from classic experimental data, a varying trend of perceptual full brightness derived from the dark adaptation model, and a smooth brightness transition scheme balancing energy and experience.

Low Bandwidth HD 1080 @ 60 FPS JPEG XR transform design [14]. This paper has a solution for memory access problem using photo overlap transform. 72 % of memory bandwidth produced. Two macro blocks are described in this design. Tmap is used. Frequency used is 72% lesser compared to conventional methods. Data receiving buffer is used. VERILOG implementation is done in 90nm CMOS technology in CADENCE tool.

Design and implementation of high-performance video processor for head-mounted displays [15]. The paper discusses the key design issue on compact hardware structure for SDRAM access, which is ultimately achieved in a single general SDRAM by data clustering and integration. Both FPGA and ASIC implementations are carried out and the results carefully compared showing that the designed video processor for 3D display could produce well immersing feeling with limited costs in effective decreasing the noise, flicker and crosstalk. VLSI Design of 3D Display Processing Chip for Head Mounted Display[16]. A VLSI design scheme is proposed by using pipeline architecture for 3D display processing chip (HMD100B). Some key techniques including stereo display processing and high precision video scaling based on bicubic interpolation, and their hardware implementations are presented.

Based on the literature survey the XR systems have great potential for improving various aspects of human experiences. The implementation requires addressing technical, user-related, and content-related challenges. Usage of Head mounted displays leads to heavy battery drainage. Techniques must be developed for reducing battery drainage. Long usage of HMD results in blurring of vision and heavy headedness. The optimized design should be such a way that the problems in vision as well as heavy headedness. Easy transmission of data is necessary in future works. Optimization of hardware as well as software designs is necessary. The design development should concentrate on reduced latency. The memory unit for the data transmission as well as storage should be efficient.

II. PROPOSED METHOD

Ultra low latency headsets and displays are to be developed with the key features such as low battery drainage, optimized compression and decompression algorithms for easy transmission of video content. The design will aim increased data rate with pipelining structures. The design will focus on data security as it is necessary to transmit data securely. Here are some key considerations when designing an Ultra Low-Latency Head Mounted Devices for Immersive Experience in XR Systems. The primary goal is to implement optimized algorithms for compression at senders end and decompression at receivers end without losing any data using Verilog HDL in hardware. The algorithms will be implemented using pipelining structures in each step of processing without data loss. The video will be splitted in the senders end and stitched together at the receivers end. Pipelining structures will be implemented for optimization of different components used in XR systems is necessary. Low latency in data transfer and efficient usage of memory will be designed. The design for memory will also be optimized. A high throughput, high memory bandwidth, low computation, low storage and high dynamic features will be added in this architecture using Verilog HDL. Data security is another factor which will be considered in the design. The flowchart gives the workflow of the compression algorithm.

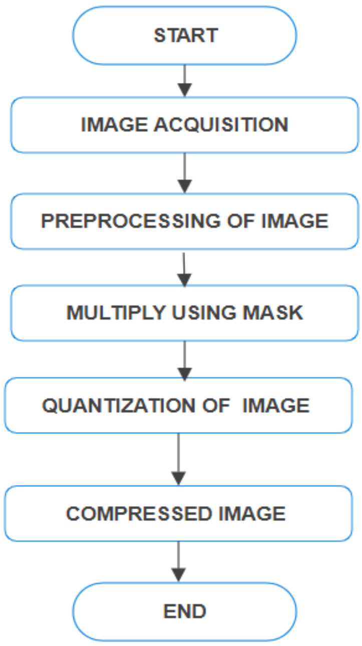

III. RESULTS

The performance of the proposed compression algorithm was evaluated through a series of simulations using MATLAB. The primary metrics for assessment included compression ratio, latency, and image quality. The results demonstrate the effectiveness of the algorithm in achieving ultra low-latency and maintaining high data fidelity, which are crucial for immersive experiences in head-mounted displays (HMDs). Some of the simulation results are given in the images along with compression algorithm.

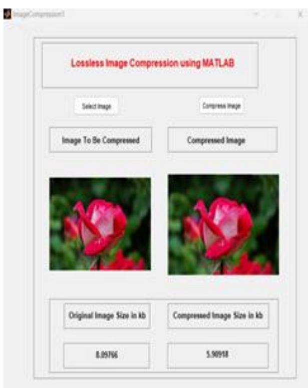

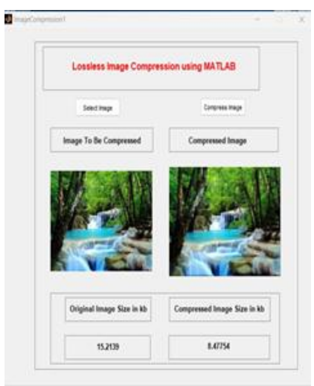

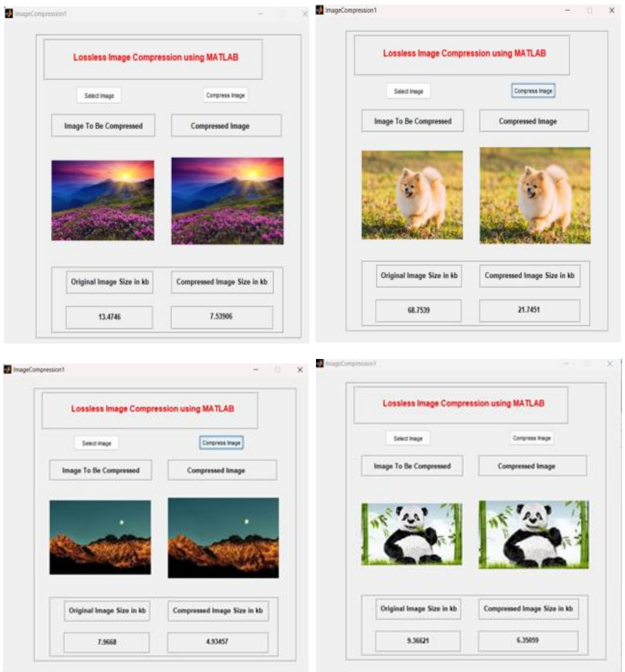

The first consideration is the hardware required for the XR system. This includes the head-mounted display (HMD), tracking devices, controllers, and any other peripherals needed for input/output. The software architecture is the foundation of the XR system. Image compression is one of the factor to be considered for optimization of architecture design for XR systems. Pipelining structures of different components used is XR systems are necessary. In this design, optimization of hardware implementation of XR systems is to be done. Compression of images using encoders will be designed in such a way that the design is optimized. In conclusion, designing an architecture for an XR system requires a holistic approach that considers all the different components that make up the system. The design will be done, by carefully considering each of these factors.

IV. Conclusion and Future Scope

The design of architecture for an extended reality (XR) system requires a comprehensive understanding of the different components that make up such a system. The focus is to design architecture for Ultra Low-Latency Head Mounted Devices for Immersive Experience in XR Systems in VLSI with the given key features. Deliver the video content to the users with decreased latency. Increase the data rate by using pipelining structures. Optimizing the usage of memory unit. Designing optimised compression and decompression algorithms. Ultra low latency XR hardware implementation can be used in various fields such as academics, manufacture, medicine, gaming, entertainment, industries, engineering and so on. The technical requirements for the HMD, including its display resolution, field of view, refresh rate, latency, light weight, and other important factors such as battery drainage. Low latency, increased data rate design would be implemented using pipelining structures. Data compression and decompression algorithms will also be designed with low latency. Long usage of the head mounted display can cause sickness such as nausea, heavy headedness and blurring of vision. The proposed design would result in an optimized hardware implementation of head mounted display.

References

[1] Hafizullah, Shaik, MSS V. Srikrishna Manideep, Vinay Sharma, PallabKumar Nath, Alok Naugarhiya, and Shrish Verma. "An Efficient Hardware Implementation of Walsh Hadamard Transform for JPEG XR." In 2018 15th IEEE India Council International Conference (INDICON), pp. 1-4. IEEE, 2018.

[2] Pan, Chia-Ho, Ching-Yen Chien, Wei-Min Chao, Sheng-Chieh Huang, and Liang-Gee Chen. "Architecture design of full HD JPEG XR encoder for digital photography applications." IEEE Transactions on Consumer Electronics 54, no. 3 (2008): 963-971.

[3] Andrade, Tiago, and Daniel Bastos. "Extended reality in iot scenarios: Concepts, applications and future trends." In 2019 5th Experiment International Conference (exp. at'19), pp. 107-112. IEEE, 2019.

[4] Cheng, Dewen, Qiwei Wang, Yue Liu, Hailong Chen, Dongwei Ni, Ximeng Wang, Cheng Yao et al. "Design and manufacture AR head-mounted displays: A review and outlook." Light: Advanced Manufacturing 2, no. 3 (2021): 350-369.

[5] Spagnolo, Fanny, Pasquale Corsonello, Fabio Frustaci, and Stefania Perri. "Design of a low-power super-resolution architecture for virtual reality wearable devices." IEEE Sensors Journal 23, no. 8 (2023): 9009-9016.

[6] Lee, Dong Keon, Haneul Choi, Sanghoon Jheon, You Hwan Jo, Chang Woo Im, and Song Young Il. "Development of an extended reality simulator for basic life support training." IEEE Journal of Translational Engineering in Health and Medicine 10 (2022): 1-7.

[7] Pinkham, Reid, Andrew Berkovich, and Zhengya Zhang. "Near-sensor distributed DNN processing for augmented and virtual reality." IEEE Journal on Emerging and Selected Topics in Circuits and Systems 11, no. 4 (2021): 663-676.

[8] Xiong, Jianghao, En-Lin Hsiang, Ziqian He, Tao Zhan, and Shin-Tson Wu. "Augmented reality and virtual reality displays: emerging technologies and future perspectives." Light: Science & Applications 10, no. 1 (2021): 1-30.

[9] Gong, Liang, Åsa Fast-Berglund, and Björn Johansson. "A framework for extended reality system development in manufacturing." IEEE Access 9 (2021): 24796-24813.

[10] Vasylevska, Khrystyna, Hyunjin Yoo, Tara Akhavan, and Hannes Kaufmann. "Towards eye-friendly VR: how bright should it be?." In 2019 IEEE Conference on Virtual Reality and 3D User Interfaces (VR), pp. 566-574. IEEE, 2019.

[11] Mehrfard, Arian, Javad Fotouhi, Giacomo Taylor, Tess Forster, Nassir Navab, and Bernhard Fuerst. "A comparative analysis of virtual reality head-mounted display systems." arXiv preprint arXiv: 1912.02913 (2019).

[12] Andreasen, Niels Koch, Sarune Baceviciute, Prajakt Pande, and Guido Makransky. "Virtual reality instruction followed by enactment can increase procedural knowledge in a science lesson." In 2019 IEEE

Conference on Virtual Reality and 3D User Interfaces (VR), pp. 840-841. IEEE, 2019.

[13] Yan, Zhisheng, Chen Song, Feng Lin, and Wenyao Xu. "Exploring eye adaptation in head-mounted display for energy efficient smartphone virtual reality." In Proceedings of the 19th International Workshop on Mobile Computing Systems & Applications, pp. 13-18. 2018.

[14] Hafizullah, Shaik, MSS V. Srikrishna Manideep, Vinay Sharma, PallabKumar Nath, Alok Naugarhiya, and Shrish Verma. "An Efficient Hardware Implementation of Walsh Hadamard Transform for JPEG XR." In 2018 15th IEEE India Council International Conference (INDICON), pp. 1-4. IEEE, 2018.

[15] Fan, Sheng-Wei, Jia-Wai Chen, and Jiun-In Guo. "Low bandwidth HD1080@ 60FPS JPEG-XR transform design." In Proceedings of Technical Program of 2012 VLSI Design, Automation and Test, pp. 1-4. IEEE, 2012.

[16] Zuoxun, Hou, Ge Chenyang, Zhao Wenzhe, Liu Longjun, and Zheng Nanning. "Design and implementation of high-performance video processor for head-mounted displays." In 2011 3DTV Conference: The True Vision-Capture, Transmission and Display of 3D Video (3DTV-CON), pp. 1-4. IEEE, 2011.

[17] Ge, Chenyang, Nanning Zheng, Kuizhi Mei, and Jizhong Zhao. "VLSI design of 3D display processing chip for head-mounted display." In 2009 International IEEE Consumer Electronics Society's Games Innovations Conference, pp. 25-28. IEEE, 2009.

Tandem Perovskite-Silicon Solar Cells: A Review on Advancements and Future Potential

S. Reema Sagitha
Department of Physics,
Thiagarajar College of Engineering,
Madurai, India
reemasagitha@student.tce.edu

M. Nandha Kumar
Department of Physics,
Thiagarajar College of Engineering,
Madurai, India
nandhakumarm@student.tce.edu

V. Aravindan
Department of Physics,
Thiagarajar College of Engineering,
Madurai
Indiavaphy@tce.edu

M. Mahendran
Department of Physics,
Thiagarajar College of Engineering,
Madurai, India
manickam-mahendran@tce.edu

***Abstract*—Tandem perovskite-silicon solar cells have gained as a promising technology to overcome the efficiency constraints of traditional silicon-based solar cells. By combining the advantage of both materials these advanced solar cells offer improved performance and higher energy conversion efficiency The perovskite layer, with its adjustable bandgap and strong light absorption, captures high-energy photons, while the silicon layer utilizes lower-energy photons, ensuring more effective solar energy utilization. A major advantage of this tandem configuration is its ability to achieve high efficiency with affordable. Perovskite materials can be processed at low temperatures using scalable deposition methods, making them suitable for large-scale production. However, certain challenges must be addressed, including stability issues, energy losses at interfaces, and the need for efficient charge transport layers to minimize recombination and enhance carrier extraction. Researchers continue to focus on enhancing their long-term stability to ensure their viability for real-world applications. If these challenges are effectively managed, tandem perovskite-silicon technology could contribute significantly to the future of renewable energy, providing an efficient and economical solution for large-scale solar power generation. This paper explores recent developments in tandem perovskite-silicon solar cells, discussing key improvements, existing challenges, and potential future directions in this rapidly advancing field.**

Keywords—Solar Cell, Photovoltaic, Tandem, Perovskite, Power Conversion Efficiency

I. Introduction

Solar energy has become a key solution to the growing demand for clean and sustainable energy sources, with photovoltaic technology playing a crucial role in harnessing sunlight for electricity generation [1]. Among the different types of solar cells, silicon-based photovoltaics have dominated the industry for decades due to their stability, commercial viability, and well established manufacturing processes [2]. However, conventional silicon solar cells face fundamental efficiency limitations, primarily due to the Shockley-Queisser limit, which restricts the maximum power conversion efficiency of single-junction silicon cells to approximately 29% [3]. The efficiency of solar cells has significantly improved over the years due to advancements in materials, device structures, and fabrication techniques [4]. Initially, silicon –based solar cells, developed in 1950s, had an efficiency of around 6% [5]. Over the decades, extensive research led to the development of more efficient crystalline silicone solar cells, reaching about 26% in laboratory conditions [6]. Meanwhile, thin film solar cells, such as cadmium telluride (CdTe) and copper indium gallium selenide (CIGS), have achieved efficiencies in the range of 20% -23% [7]. Perovskite solar cells, a rapidly emerging technology, have shown remarkable efficiency improvements, growing from about 3% in 2009 to over 25% in recent years [8]. Tandem solar cells, which combine multiple materials to capture a broader spectrum of sunlight, have exceeded 30% efficiency [9]. Theoretical limits, such as the Shockley-Queisser limit for single-junction solar cells, guide researchers toward innovative strategies, including multi-junction and quantum dot based solar cells, which hold the potential to exceed 40% efficiency [10]. The efficiency of solar cells has significantly improved over the years due to advancements in materials, device structures, and fabrication techniques [11]. Silicon solar cells have an indirect bandgap, which makes them less efficient at absorbing light [12]. Because of this, they need a thicker material layer to capture enough sunlight, leading to higher production costs and increased material usage [13]. Despite ongoing advancements, silicon solar cells alone may not be sufficient to meet the ever-growing energy demands efficiently [14].

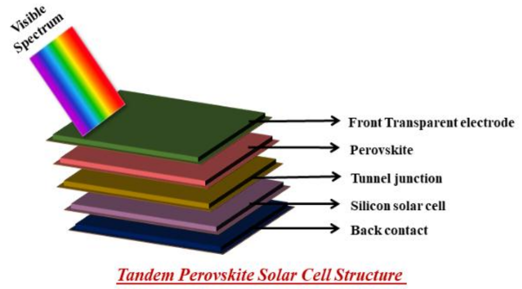

FIG 1.1 TANDEM PEROVSKITE - SILICON SOLAR CELL

To overcome these limitations, researchers have explored alternative photovoltaic materials, with perovskite solar cells (PSCs) emerging as a promising next-generation technology [15]. Perovskites offer advantages such as high optical absorption, low processing costs, and high charge carrier mobility, leading to rapid improvements in power conversion efficiency [8]. Since their initial development, perovskite solar cells have demonstrated remarkable progress, reaching efficiencies comparable to or even exceeding those of silicon-based devices [16]. One promising strategy to improve the efficiency of solar cell is combining perovskite materials with silicon in a tandem structure. Md. Tohidul Islam et al., (2021) explored the potential of $CsSn_{0.5}Ge_{0.5}I_3$ as a lead free top cell material in tandem perovskite-silicon solar cells [17]. Using SCAPS simulations, they compared its performance against traditional MAPb-based tandem devices. Their result demonstrated that $CsSn_{0.5}Ge_{0.5}I_3$ offers a stable, nontoxic, and economically alternative while achieving promising power conversion efficiencies 1. M. V. Dambhare, B. Butey, and S. V. Moharil, J. Phys. Conf. Ser. **1913**, (2021).

This study highlights the potential of lead-free perovskites in overcoming toxicity concerns, making it a valuable reference in the advancement of next-generation tandem solar cells. And Ahmad et al. investigated the design and optimization of four-terminal mechanically stacked and optically coupled silicon-perovskite tandem solar cells. Their study, conducted using SCAPS simulation, focused on improving efficiency by optimizing the thickness and doping concentrations of perovskite layers [18]. The findings revealed that optically coupled configurations exhibited superior performance compared to mechanically stacked designs, demonstrating the potential for achieving higher power conversion efficiency in tandem solar cells. Asghar Asgari et al. investigated the performance enhancement of 4-terminal tandem solar cell by incorporating organic perovskite and silicon materials. Their study focused on optimizing light absorption and energy conversion efficiency and they demonstrated the potential of tandem configurations to exceed the efficiency limitations of conventional single junction solar cells [19]. Emmanuel Akoto et al. explored the integration of $Cs_{0.8}Rb_{0.2}SnI_3$ perovskite with silicon in a two-terminal tandem structure, optimizing various parameters through SCAPS-1D simulations, they demonstrated that careful material tuning and their findings contribute to the ongoing advancements in high efficiency perovskite –silicon tandem solar technology [20]. This integration allows for better utilization of the solar spectrum, leading to enhanced photovoltaic performance [21]. Tandem perovskite-silicon solar cells leverage the advantages of both technologies, with the perovskite top cell capturing high-energy photons and the silicon bottom cell efficiently absorbing lower-energy photons [22]. This structure enables better utilization of the solar spectrum, thereby improved upon the efficiency limits traditional silicon solar cells [23]. Recent advancements in tandem device engineering, including improved interface layers, optimized charge transport materials, and advanced fabrication techniques, have led to power conversion efficiencies exceeding 32% [18]. However, achieving long-term operational stability, scaling up production, and reducing manufacturing costs remain key challenges for commercialization [19]. With continuous advancements in material science, and manufacturing techniques, tandem perovskite-silicon solar cells have the potential to revolutionize the photovoltaic industry by offering high efficiency at competitive costs [24]. Ongoing research efforts are aimed at addressing existing challenges and improving the long term viability of these devices [25]. The progress in this field highlights the importance of continued investment in research and innovation to drive the transition toward sustainable and high-performance photovoltaic solutions.

II. Methodology

SCAPS-1D (Solar Cell Capacitance Simulator of One Dimensional) is a widely used simulation tool for analyzing the electrical and optical behavior of solar cells, particularly perovskite-silicon tandem structures [26]. It was developed by electronics and information system department at university of Gent, Belgium [27]. It helps researchers optimize efficiency by modelling charge transport, recombination, and band alignment while providing key performance metrics like open circuit voltage, short circuit current density, fill factor, power conversion efficiency. The software allows for multi-layer device simulation, defect analysis and doping optimization, making it valuable for photovoltaic research. Different configurations or parameters are tested by modifying the layers and repeating the calculation process [28]. Despite its limitations such as one-dimensional approach and basic optical modelling, SCAPS1D remains preferred tool to it ease of use and fast computation. Future enhancements, including advanced optical and 3D modelling, could further improve its accuracy and applicability in tandem solar cell development.

III. Result and Discussion

Tandem perovskite-silicon solar cells studies emphasize the importance of optimizing material properties to achieve higher power conversion efficiency (PCE). The first paper investigates the $CsSn_{0.5}Ge_{0.5}I_3$ on Silicon tandem device as an alternative to the lead-based $MAPbI_3$ perovskite. Table 3.1 highlights the nontoxicity and stability of the $CsSn_{0.5}Ge_{0.5}I_3$ perovskite, which, despite its slightly lower efficiency (28.53%) compared to $MAPbI_3$ on Si (32.29%), offers a more sustainable solution. In contrast, the second study focuses on HTM free carbon electrode-based perovskite in a four-terminal mechanically stacked and optically coupled silicon-perovskite tandem structure, achieving an efficiency of 28.38% (mechanical) and 29.34% (optical). This study utilizes SCAPS-1D simulation to model and optimize the tandem structures. The first study primarily explores current matching conditions by adjusting the perovskite absorber layer thickness, finding optimal values of 365 nm for $CsSn_{0.5}Ge_{0.5}I_3$ and 225 nm for $MAPbI_3$. It also investigates the impact of defect densities on efficiency and confirms that interfacial defects significantly reduce performance. The second study takes a broader approach, optimizing perovskite thickness (1000-1100 nm) and doping concentration (10^{17} cm^{-3}) to maximize efficiency in a four-terminal configuration. The findings suggest that optically coupled tandem structures outperform mechanically stacked ones due to better spectral utilization. While both studies aim to push tandem solar cell efficiency beyond the Shockley-Queisser limit of single-junction silicon cells (~29%), they take different routes. The $CsSn_{0.5}Ge_{0.5}I_3$ study highlights the trade-off between toxicity and performance, showing that lead-free perovskites can still achieve competitive efficiencies. The four-terminal tandem study demonstrates the advantages of independent cell operation, which allows each sub cell to function optimally without strict current matching constraints. Despite their progress, both studies acknowledge stability and scalability as major challenges. The $CsSn_{0.5}Ge_{0.5}I_3$ study emphasizes the need for further research on Sn-Ge perovskite oxidation resistance, while the four-terminal study points out the cost limitations of optical components in commercial implementation. In the above highlights, the need for improved interface engineering, better encapsulation techniques, and long-term operational stability to make tandem perovskite-silicon solar cells commercially viable. These studies contribute valuable insights into the development of tandem perovskite-silicon solar cells, exploring different materials, architectures, and optimization techniques. While lead-free perovskites offer an environmentally friendly alternative, four-terminal tandems provide a practical pathway to overcoming efficiency. Future research should focus on stability improvements, scalable fabrication methods, and cost reductions to accelerate commercial adoption of these high-efficiency solar technologies. A recent study investigates the performance of 4-terminal tandem solar cells utilizing $Cs_2AgBi_{0.75}Sb_{0.25}Br_6$ as the active layer, focusing on optimizing structural and material properties for improved efficiency. The results indicate that adjusting the active layer thickness to 400 nm ensures optimal light absorption while maintaining efficient charge carrier transport. This balance is crucial for minimizing recombination losses and maximizing power output. The tandem architecture further enhances performance by allowing independent optimization of the top and bottom cells, leading to better energy utilization. This study highlights how proper energy band alignment plays a critical role in efficient charge separation and transport, contributing to higher power conversion efficiency compared to traditional single-junction solar cells. Stability tests suggest that the $Cs_2AgBi_{0.75}Sb_{0.25}Br_6$ demonstrates promising durability, though additional studies are necessary to understand long term degradation effects. A comparative assessment with other tandem solar cell configurations indicates that $Cs_2AgBi_{0.75}Sb_{0.25}Br_6$ offers competitive advantages in efficiency and scalability. The material's potential for cost-effective production makes it a strong candidate for next generation photovoltaic technologies. A lead –free $Cs_{0.8}Rb_{0.2}SnI_3$-Silicon tandem solar cell achieved 29.82% efficiency. Optimization of perovskite thickness, defect density, and doping concentration enhanced performance. Simulation using SCAPS-1D software validated experimental results. Chlorinated ITO front contact improved energy alignment. Tandem cell design enabled better light utilization and charge collection. This study demonstrates a promising approach for high –efficiency, lead-free solar cells. Overall, this study provides valuable insights into material optimization, structural design, and stability considerations, contributing to the ongoing advancement of high-performance tandem solar cells.

IV. Conclusion

The integration of perovskite and silicon in tandem solar cells represents a significant advancement in photovoltaic technology offering higher efficiency compared to single junction silicon cells. By leveraging the superior light absorption of perovskite and the stability of silicon, these devices show great potential for next-generation solar applications. Despite notable progress, challenges related to long-term stability, large scale manufacturing, and material optimization must be addressed. Continued research and innovation will be crucial in making these tandem solar cells commercially viable and widely adopted in the renewable energy sector.

TABLE: 3.1 SHOWS THE OPTIMIZED PARAMETERS OF OPEN CIRCUIT VOLTAGE (VOC), SHORT CIRCUIT CURRENT DENSITY (JSC), FILL FACTOR (FF) AND POWER CONVERSION EFFICIENCY (PCE) REPORTED IN VARIOUS STUDIES.

Tandem Cell Structure	Voc (V)	Jsc (mA/cm2	FF (%)	PCE (%)	References
$MAPbI_3$-C-Si	1.88	19.969	85.99	32.29	[17]
$CsSn_{0.5}Ge_{0.5}I_3$-c-Si	1.72	20.02	83.74	28.53	[17]
$Cs_x (FA_{0.4}MA_{0.6})_{1-x}PbI_{2.8}Br_{0.2}$ – c-Si 4T-Mechanical and 4T-Optical	23.11	1.14	80.52	21.31	[18]
	21.85	1.14	80.37	20.02	[18]
Top perovskite sub-cell ($Cs_2AgBi_{0.75}Sb_{0.25}Br_6$) Bottom Silicon sub-cell	0.98	15.05	58.97	8.72	[19]
	0.68	34.81	83.60	19.83	[19]
$Cs_{1-x}Rb_xSnI_3$-Si	0.79	43.39	85.98	29.82	[20]

V. Acknowledgment

One of the authors, S. Reema Sagitha would like to extend her gratitude to Thiagarajar college of Engineering, Madurai, for granting the "Thiagarajar Research Fellowship". (File No.: TCE/RD/TRF/<<14>> dated 27.09.2024)

References

[1] S. Bhattarai et al., "A detailed review of perovskite solar cells: Introduction, working principle, modelling, fabrication techniques, future challenges," Micro and Nanostructures, vol. 172, no. July, p. 207450, 2022, doi: 10.1016/j.micrna.2022.207450.

[2] N. K. Vishnoi, "A review on perovskite solar cells," Asian J. Multidimens. Res., vol. 10, no. 11, pp. 365–370, 2021, doi: 10.5958/2278-4853.2021.01106.x.

[3] M. Di Sabatino, R. Hendawi, and A. S. Garcia, "Silicon Solar Cells: Trends, Manufacturing Challenges, and AI Perspectives," Crystals, vol. 14, no. 2, 2024, doi: 10.3390/cryst14020167.

[4] A. Tabassum Raisa, M. Shafayet-Ul-Islam, S. Nazmus Sakib, M. Jobayer Hossain, K. Ahmed Rocky, and A. Kowsar, "Progress in multijunction solar cells," pp. 1–17.

[5] K. ElKhamisy, H. Abdelhamid, E. S. M. El-Rabaie, and N. Abdel-Salam, "A Comprehensive Survey of Silicon Thin-film Solar Cell: Challenges and Novel Trends," Plasmonics, vol. 19, no. 1, pp. 1–20, 2024, doi: 10.1007/s11468-023-01905-x.

[6] M. V. Dambhare, B. Butey, and S. V. Moharil, "Solar photovoltaic technology: A review of different types of solar cells and its future trends," J. Phys. Conf. Ser., vol. 1913, no. 1, 2021, doi: 10.1088/1742-6596/1913/1/012053.

[7] V. Paranthaman et al., "Experimental and theoretical insights into enhanced light harvesting in dye-sensitized solar cells via Au@TiO2 core-shell and BaTiO3 nanoparticles," J. Taiwan Inst. Chem. Eng., vol. 165, no. September, p. 105778, 2024, doi: 10.1016/j.jtice. 2024.105778.

[8] R. K. Raji, T. Ramachandran, M. Dhilip, V. Aravindan, J. S. Punitha, and F. Hamed, "Integrating Experimental and Computational Insights: A Dual Approach to Ba2CoWO6 Double Perovskites," Ceramics, vol. 7, no. 4, pp. 2006–2023, 2024, doi: 10.3390/ceramics7040125.

[9] Y. Cheng and L. Ding, "Perovskite/Si tandem solar cells: Fundamentals, advances, challenges, and novel applications," SusMat, vol. 1, no. 3, pp. 324–344, 2021, doi: 10.1002/sus2.25.

[10] F. Schmitz et al., "Improved Hole Extraction and Band Alignment via Interface Modification in Hole Transport Material-Free Ag/Bi Double Perovskite Solar Cells," Sol. RRL, vol. 8, no. 6, 2024, doi: 10.1002/solr.202300965.

[11] P. Sivakumar, P. Peranantham, V. V. S. Kumar, K. Asokan, and Y. L. Jeyachandran, "Structure, composition and photoconductivity analysis of zinc tin phosphide ternary compound nanoparticles synthesized by chemical method," J. Mater. Sci. Mater. Electron., vol. 32, no. 7, pp. 8767–8777, 2021, doi: 10.1007/s10854-021-05548-8.

[12] M. S. Mousa et al., "STUDYING THE EFFECT OF TRANSPORT LAYERS ON ZrS2/MEH-PPV SOLAR CELLS: USING SCAPS-1D SOFTWARE," East Eur. J. Phys., vol. 2024, no. 4, pp. 419–426, 2024, doi: 10.26565/2312-4334-2024-4-49.

[13] F. Hou et al., "Monolithic perovskite/silicon tandem solar cells: A review of the present status and solutions toward commercial application," Nano Energy, vol. 124, no. April 2023, p. 109476, 2024, doi: 10.1016/j.nanoen.2024.109476.

[14] P. Rafieipour, A. Mohandes, M. Moaddeli, and M. Kanani, "Integrating transfer matrix method into SCAPS-1D for addressing optical losses and per-layer optical properties in perovskite/Silicon tandem solar cells," pp. 1–35, 2023, [Online]. Available: https://www.nrel.gov/pv/cell-efficiency.html].

[15] S. Bhattarai et al., "A detailed review of perovskite solar cells: Introduction, working principle, modelling, fabrication techniques, future challenges," Micro and Nanostructures, vol. 172, no. November, p. 207450, 2022, doi: 10.1016/j.micrna.2022.207450.

[16] A. D. K. Kenfack, N. M. Thantsha, and M. Msimanga, "Simulation of Lead-Free Heterojunction CsGeI2Br/CsGeI3-Based Perovskite Solar Cell Using SCAPS-1D," Solar, vol. 3, no. 3, pp. 458–472, 2023, doi: 10.3390/solar3030025.

[17] M. T. Islam et al., "Investigation of CsSn0.5Ge0.5I3-on-Si Tandem Solar Device Utilizing SCAPS Simulation," IEEE Trans. Electron Devices, vol. 68, no. 2, pp. 618–625, 2021, doi: 10.1109/TED.2020.3045383.

[18] E. Raza et al., "Design and optimization of four-terminal mechanically stacked and optically coupled silicon/perovskite tandem solar cells with over 28% efficiency," Heliyon, vol. 9, no. 2, p. e13477, 2023, doi: 10.1016/j.heliyon.2023.e13477.

[19] Z. shokrollahi, M. Piralaee, and A. Asgari, "Performance and optimization study of selected 4-terminal tandem solar cells," Sci. Rep., vol. 14, no. 1, pp. 1–12, 2024, doi: 10.1038/s41598-024-62085-0.

[20] E. Akoto, V. Isahi, V. Odari, C. Maghanga, and F. Nyongesa, "Monolith Cs1-xRbxSnI3 perovskite – silicon 2T tandem solar cell using SCAPS-1D," Results Opt., vol. 12, no. March, p. 100470, 2023, doi: 10.1016/j.rio.2023.100470.

[21] Prem Pratap Singh and Kripa Shanker Singh, "Simulation study of Perovskite/Si Monolithic Multijunction Solar Cell," Int. J. Sci. Res. Mod. Sci. Technol., vol. 3, no. 1, pp. 41–52, 2024, doi: 10.59828/ijsrmst.v3i1.177.

[22] S. Akhil et al., "Review on perovskite silicon tandem solar cells: Status and prospects 2T, 3T and 4T for real world conditions," Mater. Des., vol. 211, p. 110138, 2021, doi: 10.1016/j.matdes.2021.110138.

[23] A. Saidarsan, S. Guruprasad, A. Malik, P. Basumatary, and D. S. Ghosh, "A critical review of unrealistic results in SCAPS-1D simulations: Causes, practical solutions and roadmap ahead," Sol. Energy Mater. Sol. Cells, vol. 279, no. October 2024, p. 113230, 2025, doi: 10.1016/j.solmat.2024.113230.

[24] K. G. Beepat, D. P. Sharma, A. Mahajan, D. Pathak, and V. Kumar, "Simulation of multijunction solar cell interfaces for enhancement of the power conversion efficiency," Discov. Appl. Sci., vol. 6, no. 6, 2024, doi: 10.1007/s42452-024-05930-1.

[25] Y. Chrafih, M. Al-Hattab, A. El Boubekri, K. Rahmani, O. Bajjou, and M. A. Mohamed, "Performance assessment of an eco-friendly tandem solar cell based on double perovskite Cs2AgBiBr6," J. Phys. Chem. Solids, vol. 187, no. September 2023, p. 111815, 2024, doi: 10.1016/j.jpcs.2023.111815.

[26] P. Sahoo, C. Tiwari, S. Kukreti, and A. Dixit, "All oxide lead-free bismuth ferrite perovskite absorber based FTO/ZnO/BiFeO3/Au solar cell with efficiency ∼ 12%: First principle material and macroscopic device simulation studies," J. Alloys Compd., vol. 981, no. December 2023, p. 173599, 2024, doi: 10.1016/j.jallcom.2024.173599.

[27] M. Burgelman, P. Nollet, and S. Degrave, "Modelling polycrystalline semiconductor solar cells," Thin Solid Films, vol. 361, pp. 527–532, 2000, doi: 10.1016/S0040-6090(99)00825-1.

[28] M. Abdelfatah, A. M. El Sayed, W. Ismail, S. Ulrich, V. Sittinger, and A. El-Shaer, "SCAPS simulation of novel inorganic ZrS2/CuO heterojunction solar cells," Sci. Rep., vol. 13, no. 1, pp. 1–14, 2023, doi: 10.1038/s41598-023-31553-4.M. Young, The Technical Writer's Handbook. Mill Valley, CA: University Science, 1989.

Structural and Mechanical Properties of Cubic Phases of ZrO_2 using First Principle Calculations

M. Nandha Kumar
Smart materials Lab
Department of Physics
Thiagarajar College of Engineering
Madurai, Tamil Nadu, India
nandhakumarm@student.edu.in

V. Aravindan
Smart Materials Lab
Department of Physics
Thiagarajar College of Engineering
Madurai, Tamil Nadu, India
vaphy@tce.edu

M. Mahendran
Smart Materials Lab
Department of Physics
Thiagarajar College of Engineering
Madurai, Tamil Nadu, India
manickam-mahendran@tce.edu

***Abstract*—We looked at the structure, electronics, and light properties of ZrO_2 in its cubic forms. We used a VASP to get these results. Our findings showed that the behavior of charges in the material is direction-dependent. We also measured the dielectric functions and got results that matched well with what others have found in experiments. To find the static dielectric constant of ZrO_2, we combined the electronic parts with contributions from optical phonons. This gave us values of 29.5, 26.2, and 21.9 along different directions for the monoclinic phase. These numbers line up well with the experimental data. We found that certain effects, like spin-orbit interaction, are important. They help us get better numbers for the effective mass and give a clearer view of how the dielectric function changes with frequency.**

Keywords—Density Functional Theory; ZrO_2; Optical Study; Semiconductor

I. Introduction

Zirconium dioxide (ZrO_2), commonly referred to as zirconia, is a multifunctional ceramic recognized for its remarkable attributes, such as outstanding mechanical strength, thermal stability, and corrosion resistance [1,2]. While it has traditionally been appreciated for its structural and insulating capabilities, ZrO_2 is gaining considerable interest in optoelectronics due to its distinctive optical and electronic properties [3]. With a wide bandgap generally between 5.5 and 6 eV, it offers transparency in both the visible and ultraviolet (UV) spectrums, making it suitable for numerous optoelectronic applications [4].

The optoelectronic characteristics of ZrO_2 are affected by several factors, including its crystalline phase—monoclinic, tetragonal, or cubic—surface topology, and the incorporation of various metal ions through doping [5,6]. This ability to adjust these variables facilitates the customization of ZrO_2's optical features, including its absorption range and refractive index, as well as its electronic conductivity [7,8]. Doping with elements such as yttrium, cerium, or calcium can significantly improve its conductivity, positioning it for diverse applications in sensors, photodetectors, and optical coatings [9]. Beyond its optical and electrical functionalities, ZrO_2 displays photocatalytic properties when exposed to UV light, making it a promising material for environmental cleanup and energy production, particularly in hydrogen generation [10,11]. Its high refractive index and transparency also render it ideal for advanced coatings and waveguides in photonics. The increasing focus on ZrO_2 in the optoelectronic field highlights its potential in next-generation devices that demand high stability, durability, and flexibility [12,13]. By methodically designing its structural and compositional characteristics, ZrO_2 is poised to play a pivotal role in the advancement of sophisticated optoelectronic technologies.

II. Computational Method

We used the Vienna Ab-initio Simulation Package (VASP) for our computer simulations. It's built on density functional theory (DFT) [14,15]. We looked at how electrons interact with ion cores using a method called projector augmented wave (PAW) potentials. These give us better accuracy compared to the old ultra-soft pseudopotentials. To get the best results for exchange-correlation effects, we tried a few methods [16]. We started with the generalized gradient approximation (GGA-PBE) from Perdew-Burke-Ernzerhof. It works well for the electronic structure but often underestimates band gaps [17,18]. To fix that, we used the (GGA+U) method with a U value of 10 for the d-Zr states. This helped with the band gap problems [19].

We also checked the electronic structure and optical properties using the metaGGA: mBj method [20]. For predictions beyond the band gap, we turned to the modified Becke-Johnson potential (TB-mBJ). Past studies showed this method did well for ZrO2, which made it a good choice for our work on the material's structural, electrical, and optical properties. In this research, we focused on TB-mBJ to predict more than just the band gap [21]. Looked at studies on ZrO_2 that showed this potential matched experiments well. The pseudopotentials we used took into account the valence electrons for zirconium and oxygen [22]. For zirconium, we used [Zr] 5s4d5p, and for oxygen, [He] 2s2p, with core radii of 1.625 and 0.820.

III. Results and discussion

Structural Properties

The ZrO_2 can take on three main forms: monoclinic, tetragonal, and cubic. At room temperature, it's in the monoclinic form. Here, zirconium atoms connect with seven oxygen atoms, creating a complicated 3D structure. When the temperature goes up, ZrO_2 changes to the tetragonal form. In this phase, zirconium still connects with the same number of oxygen atoms, but the shape of the structure changes, making it more stable at high temperatures. If it gets even hotter, ZrO_2 becomes cubic. This form has a simpler structure where each zirconium atom is surrounded by eight oxygen atoms. The crystallographic analysis of zirconium dioxide (ZrO_2) reveals a triclinic structure with a P1 space group (space group number 1), indicating minimal symmetry constraints. The crystal structure of ZrO_2 depicted in Figure 1. The unit cell parameters were determined as a= b=c= 5.14997Å with interaxial angles α, β, and γ all equal to 90°, suggesting a cubic-like arrangement. The calculated unit cell volume is 136.59 Å, and the material exhibits a density of 5.992 Mg/m^3. These structural characteristics confirm the high crystallinity of ZrO_2, aligning with its expected fluorite-type phase. Such structural attributes contribute to its excellent mechanical strength, thermal stability, and suitability for applications in ceramics, catalysis, and solid oxide fuel cells.

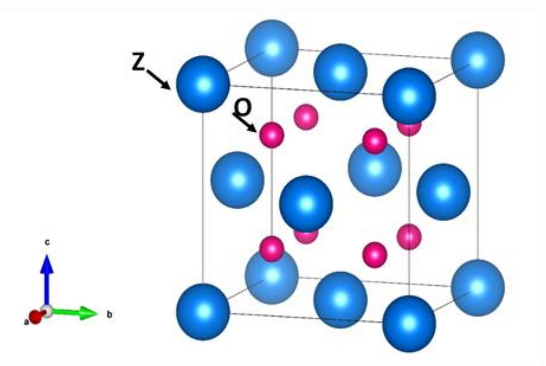

FIG 1: CRYSTALLINE STRUCTURE OF ZrO_2

The X-Ray Diffraction (XRD) of ZrO_2 is shown in Figure 2. The XRD pattern revealed distinct peaks corresponding to the monoclinic and tetragonal phases of ZrO_2. The identified peak positions at 2θ angles matched standard diffraction data for ZrO_2. The major peaks were observed at approximately 28.2°, 31.5°, 34.2°, and 50.1°, which are characteristic of the monoclinic phase. The intensity distribution suggests a high degree of crystallinity. The crystallite size was estimated using the Scherrer equation and found to be in the nanometer range, indicating a well-defined crystalline structure. The XRD analysis of ZrO_2 showed that it has two phases: monoclinic and tetragonal. The strong diffraction peaks mean it's very crystalline. The size of the crystals is in the nanocrystalline range. This makes it good for uses in ceramics, coatings, and catalysis.

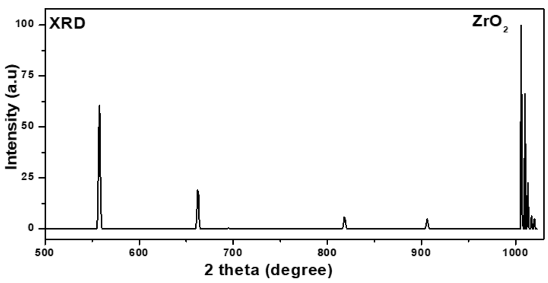

FIG 2 XRD DATA PATTERN OF ZRO2

Optical Properties

Zirconium dioxide (ZrO_2), commonly known as zirconia, is a widely studied material due to its remarkable optical properties and applications in various fields, including optics, electronics, and coatings. Understanding the optical properties of ZrO_2 requires computational techniques that can provide insights into electronic structures and transitions. One of the most effective computational tools for this purpose is the Vienna Ab-initio Simulation Package (VASP), which utilizes density functional theory (DFT) to model complex materials.

The complex dielectric function ε(ω) is expressed as ε(ω) = ε1(ω) + iε2(ω), where ε1(ω) is the real part associated with dispersion, and ε2(ω) corresponds to absorption. The imaginary part ε2(ω) can provide valuable information on the electronic transitions in ZrO_2. Transition energies can be analyzed from the band gap energy obtained from the electronic structure calculations. Optical absorption spectra generated from VASP simulations further elucidate the interaction of ZrO_2 with light. The absorption coefficients derived from the imaginary part of the dielectric function can be correlated with specific wavelengths, determining the transparency and reflectivity of this compound. Generally, ZrO_2 shows significant transparency in the visible range, making it an ideal candidate for applications in optical technologies. In the Figure 3, appears to illustrate an optical absorption spectrum, likely depicting absorbance or transmittance in relation to photon energy (eV). A significant absorption edge is detected around 3.7 eV, indicative of the material's band gap energy. This finding hints at the material's robust absorption capabilities within the ultraviolet spectrum, suggesting potential uses in optoelectronic applications, including UV photodetectors, transparent conductive materials, or solar cells. The pronounced transition at the absorption edge indicates a direct band gap characteristic, which is advantageous for efficient electronic transitions in semiconductor contexts. Further exploration, such as Tauc plot fitting, could yield additional insights into the optical transitions and verify the exact band gap value. Gaining an understanding of the optical characteristics of this material can facilitate the enhancement of its functionality for real-world applications in photonics and energy conversion technologies

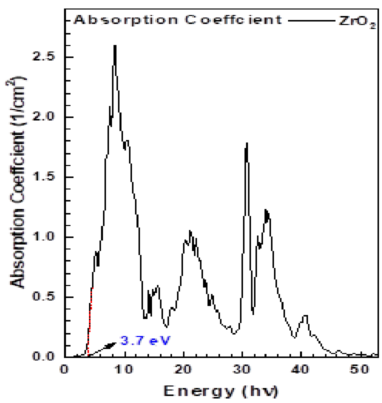

FIG 3. OPTICAL ABSORPTION SPECTRUM OF ZrO_2 USING DFT

Electronic Structure and Calculation Methodology

To analyze the optical properties of ZrO_2, first, a standard crystal structure, typically the cubic phase of zirconia, is optimized using DFT implemented in VASP. The Perdew-Burke-Ernzerhof (PBE) functional is often used for the exchange-correlation potential. The optimization process involves adjusting the lattice parameters and atomic positions to minimize the system's total energy. Once the ground state electronic structure is obtained, the next step involves calculating the complex dielectric function, ε(ω), which provides direct information regarding the optical properties. This function can be derived from the calculated band structure and density of states. The optical susceptibilities can be obtained by a linear response approach, where the response of the electronic system to an external electromagnetic field is evaluated.

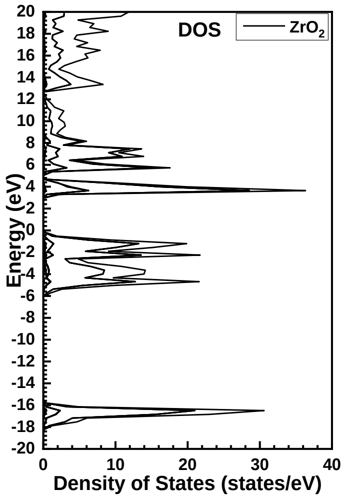

FIG 4 DOS DATA PATTERN OF ZrO_2

The graph displayed in Figure 4, illustrates the density of states (DOS) for zirconium dioxide (ZrO_2), a wide-bandgap material known for its applications in optics, electronics, and catalysis. This DOS plot delineates the distribution of electronic states relative to energy levels, offering valuable insights into the electronic structure of the material. The identification of a bandgap, demonstrated by the gap between the valence and conduction bands, affirms ZrO_2's insulating or semiconducting characteristics. The valence band is primarily made up of oxygen 2p orbitals, while the conduction band features predominantly zirconium 4d states, suggesting notable orbital hybridization. This electronic structure indicates potential uses for ZrO_2 in high-k dielectrics, optical coatings, and semiconductor technology where its stability, transparency, and dielectric attributes are beneficial. Additional computational studies and experimental investigations of the DOS could further elucidate defect states and charge transport dynamics, which are essential for enhancing the performance of ZrO_2-focused electronic and optoelectronic devices

IV. CONCLUSION

The XRD pattern revealed distinct peaks corresponding to the monoclinic and tetragonal phases of ZrO_2. The identified peak positions at 2θ angles matched standard diffraction data for ZrO_2. The major peaks were observed at approximately 28.2°, 31.5°, 34.2°, and 50.1°, which are characteristic of the monoclinic phase. The XRD pattern Computational results from VASP for ZrO2 typically reveal a band gap (~3.7 eV), indicating good semiconducting properties. The optical absorption spectrum demonstrates transitions primarily in the ultraviolet region.

The VASP computational package serves as a powerful tool for investigating the optical properties of ZrO_2. Through DFT calculations, one can successfully determine key optical parameters such as the dielectric function, refractive index, and extinction coefficient. The insights gained from such studies not only enhance the understanding of ZrO_2's optical characteristics but also aid in tailoring its properties for specific applications. Future research may involve exploring the effects of dopants or different phases of zirconia to further refine and expand upon these findings.

V. ACKNOWLEDGMENT

One of the authors, M. Nandha Kumar, would like to thank Thiagarajar College of Engineering, Madurai for providing the Thiagarajar Research Fellowship (TRF) scheme (File.no: TCE/RD/TRF/13 dated 27.09.2024). All authors would like to acknowledge DST-FIST for providing financial support for purchasing VASP Package.

REFERENCES

[1] G.P. Cousland, X.Y. Cui, A.E. Smith, A.P.J. Stampfl, C.M. Stampfl, Mechanical properties of zirconia, doped and undoped yttria-stabilized cubic zirconia from first-principles, J. Phys. Chem. Solids 122 (2018) 51–71. https://doi.org/10.1016/j.jpcs.2018.06.003.

[2] Y. Maithani, J.A. Khan, B.R. Mehta, J.P. Singh, Cubic phase optimization and influence of post-annealing on microstructure, optical, wetting, and nanomechanical properties of zirconia thin films, Ceram. Int. 49 (2023) 1048–1060. https://doi.org/10.1016/j.ceramint.2022.09.080.

[3] J. Zhang, A.R. Oganov, X. Li, M. Mahdi Davari Esfahani, H. Dong, First-principles investigation of Zr-O compounds, their crystal structures, and mechanical properties, J. Appl. Phys. 121 (2017). https://doi.org/10.1063/1.4979913.

[4] Z. Liang, W. Wang, M. Zhang, F. Wu, J.F. Chen, C. Xue, H. Zhao, Structural, mechanical and thermodynamic properties of ZrO2 polymorphs by first-principles calculation, Phys. B Condens. Matter 511 (2017) 10–19. https://doi.org/10.1016/j.physb.2017.01.025.

[5] A. Smirnov, O. Yanushevich, N. Krikheli, Y. Zhukovskaya, M. Soloninkin, N. Nikitin, The Effect of Layer Thickness and Nozzle Diameter in Fused Deposition Modelling Printing on the Flexural Strength of Zirconia Ceramic Samples Produced by a Multistage Manufacturing Process, (2025).

[6] J.W. Du, H.D. Zhang, L. Chen, Y. Kong, Transforming oxidation: The impact of martensitic transition on Zr-O-N coating, Vacuum 231 (2025) 113772. https://doi.org/10.1016/j.vacuum.2024.113772.

[7] E.S.R. Khattab, S.S. Abd El Rehim, W.M.I. Hassan, T.S. El-Shazly, Band Structure Engineering and Optical Properties of Pristine and Doped Monoclinic Zirconia (m-ZrO2): Density Functional Theory Theoretical Prospective, ACS Omega 6 (2021) 30061–30068. https://doi.org/10.1021/acsomega.1c04756.

[8] K. Zhao, W. Huang, P. Deng, R. Zhong, Z. Tan, Y. Hu, J. Li, W. Mao, Mechanical properties, thermal shock resistance and stress evolution of plasma-sprayed 56 wt% Y2O3-stabilized ZrO2 thick thermal barrier coatings, Surf. Coatings Technol. 494 (2024) 131352. https://doi.org/10.1016/j.surfcoat.2024.131352.

[9] Q.J. Liu, Z.T. Liu, L.P. Feng, Elasticity, electronic structure, chemical bonding and optical properties of monoclinic ZrO2 from first-principles, Phys. B Condens. Matter 406 (2011) 345–350. https://doi.org/10.1016/j.physb.2010.10.057.

[10] Y. Wang, X. Li, C. Wang, A Study of the Electronic Structure and Elastic Properties for m-ZrO2 and -Bi2O3

Based on First-Principles Calculations under Ambient Pressure, 76 (2017) 1035–1039. https://doi.org/10.2991/emim-17.2017.206.

[11] X. Song, Y. Ding, J. Zhang, C. Jiang, Z. Liu, C. Lin, W. Zheng, Y. Zeng, Thermophysical and mechanical properties of cubic, tetragonal and monoclinic ZrO2, J. Mater. Res. Technol. 23 (2023) 648–655. https://doi.org/10.1016/j.jmrt.2023.01.040.

[12] J.C. Garcia, L.M.R. Scolfaro, A.T. Lino, V.N. Freire, G.A. Farias, C.C. Silva, H.W.L. Alves, S.C.P. Rodrigues, E.F. Da Silva, Structural, electronic, and optical properties of ZrO2 from ab initio calculations, J. Appl. Phys. 100 (2006). https://doi.org/10.1063/1.2386967.

[13] E. Hevorkian, R. Michalczewski, M. Rucki, D. Sofronov, E. Osuch-Słomka, V. Nerubatskyi, Z. Krzysiak, J.N. Latosińska, Effect of the sintering parameters on the structure and mechanical properties of zirconia-based ceramics, Ceram. Int. 50 (2024) 35226–35235. https://doi.org/10.1016/j.ceramint.2024.06.331.

[14] L. Zhang, G.F. Ji, F. Zhao, Z.Z. Gong, First-principles study of the structural, mechanical and electronic properties of ZnX2O4 (X=Al, Cr and Ga), Chinese Phys. B 20 (2011) 1–7. https://doi.org/10.1088/1674-1056/20/4/047102.

[15] Y. Zhang, J. Zhang, First principles study of structural and thermodynamic properties of zirconia, Mater. Today Proc. 1 (2014) 44–54. https://doi.org/10.1016/j.matpr.2014.09.011.

[16] Y.L. Yang, X.L. Fan, C. Liu, R.X. Ran, First principles study of structural and electronic properties of cubic phase of ZrO2 and HfO2, Phys. B Condens. Matter 434 (2014) 7–13. https://doi.org/10.1016/j.physb.2013.10.037.

[17] F. Saidi, M. Dergal, A. Dendane, N. Ameur, First-Principles Investigation of Structural Stability, Electronic, and Optical Properties of V, Y-Doped, and (V, Y)-Codoped Monoclinic ZrO2, Phys. Chem. Res. 12 (2024) 663–674. https://doi.org/10.22036/pcr.2023.416669.2419.

[18] E. Osei-Agyemang, J.F. Paul, R. Lucas, S. Foucaud, S. Cristol, A.S. Mamede, N. Nuns, A. Addad, Characterizing the ZrC(111)/c-ZrO2(111) Hetero-Ceramic Interface: First Principles DFT and Atomistic Thermodynamic Modeling, Molecules 27 (2022). https://doi.org/10.3390/molecules27092954.

[19] L.X. Lovisa, E.O. Gomes, L. Gracia, A.A.G. Santiago, M.S. Li, J. Andrés, E. Longo, M.R.D. Bomio, F. V. Motta, Integrated experimental and theoretical study on the phase transition and photoluminescent properties of ZrO2:xTb3+ (x=1, 2, 4 and 8 mol %), Mater. Res. Bull. 145 (2022). https://doi.org/10.1016/j.materresbull.2021.111532.

[20] Y. Gao, L. Wang, D. Li, The Surface Modification of ZrO2 Film by Zr/Nb Ion Implantation and First-Principles Calculation, Coatings 13 (2023). https://doi.org/10.3390/coatings13101696.

[21] X.S. Zhao, S.L. Shang, Z.K. Liu, J.Y. Shen, Elastic properties of cubic, tetragonal and monoclinic ZrO2 from first-principles calculations, J. Nucl. Mater. 415 (2011) 13–17. https://doi.org/10.1016/j.jnucmat.2011.05.016.

[22] H. ling ZHOU, L. jun CHEN, X. ling YANG, X. yang LIU, C. SUN, B. feng LUAN, First-principles investigation on structural, thermodynamic, and elastic properties of suboxide Zr3O phase, Trans. Nonferrous Met. Soc. China (English Ed. 34 (2024) 952–965. https://doi.org/10.1016/S1003-6326 (23) 66445-3.

Analysis of the Oxidation Characteristics of Tin Nitride Thin Films Deposited via DC Magnetron Sputtering for Optoelectronic Applications

Poosari Sundararajaperumal
Materials Science Research Laboratory, Department of Physics, Thiagrajar Advanced Research Centre (TARC), Thiagarajar College of Engineering,
Madurai, Tamil Nadu, India
sundaraaa62@gmail.com

Sivakumar Periyasamy
Materials Science Research Laboratory, Department of Physics, Thiagrajar Advanced Research Centre (TARC), Thiagarajar College of Engineering,
Madurai, Tamil Nadu, India
pskphy@tce.edu

Pretika Pandiaraja
Materials Science Research Laboratory, Department of Physics, Thiagrajar Advanced Research Centre (TARC), Thiagarajar College of Engineering,
Madurai-625015, Tamil Nadu, India
Pretika1721@gmail.com

Manickam Mahendran
Smart Material Laboratory, Department of Physics, Thiagarajar College of Engineering, Madurai, Tamil Nadu, India
manickam-mahendran@tce.edu

***Abstract*—Tin Nitride is a promising semiconductor with exceptional optical and electrical properties, rendering it suitable for various photonic and electronic applications. This work employed DC magnetron reactive sputtering to deposit a thin layer of tin nitride onto a glass surface. The duration for applying the layer ranged from 2 to 8 minutes. Initially, the optical and electrical properties of the thin films were analyzed post-fabrication. Subsequently, they were subjected to atmospheric exposure to facilitate spontaneous oxidation. The oxidation process significantly altered the band gap. During a 2-minute deposition, the band gap rose from 2.54 eV to 3.7 eV. During an 8-minute deposition, the energy increased from 1.86 eV to 3.15 eV. The films permitted 90-95% of light transmission in the near-infrared (NIR) spectrum, rendering them suitable for application in electronic devices that utilize light. The electrical characteristics were examined via the four-probe method, revealing a resistivity of 0.32 Ωcm and a sheet resistance of 23 kΩ. The findings indicated that the duration of material application influences the film's width, optical band gap, and electrical conductivity. This work demonstrates that tin nitride coatings may be advantageous for applications including UV radiation detectors and transistors. The films maintain thermal stability and continue to function effectively electrically after 10 days of exposure to air. The results indicate that tin nitride thin films exhibit high transparency in the near-infrared (NIR) region. The study emphasizes the significance of deposition conditions in achieving optimal material properties, which will enhance electronic and protective coatings in the future.**

***Keywords*—Tin Nitride, SnN, Thin film, DC Magnetron sputtering.**

I. INTRODUCTION

Tin nitride has garnered increasing attention in optoelectronics due to its remarkable characteristics and numerous possible uses. Tin nitride thin films possess distinctive optical, electrical, and structural characteristics that render them appropriate for various optoelectronic applications. Scientists have investigated numerous strategies for producing high-quality thin films, including physical vapor deposition, chemical vapor deposition, and sputtering. Using tin nitride thin films in optoelectronics is an important topic. The material has a high refractive index and can be adjusted to get the right bandgap, making it a great option for solar cells, LED lights, and optical waveguides. Tin-doped silicon oxide thin films have been studied for their ability to change refractive properties when exposed to light. This is important for uses in optical data storage and holography [1].

The fabrication of these films has been extensively studied, utilizing processes such as physical vapor deposition, chemical vapor deposition, and sputtering to produce high-quality thin films. Transition metal nitrides are robust refractory substances utilized in various applications due to their exceptional hardness, superior thermal stability, and resistance to oxidation and corrosion. Metal nitride films are extensively utilized in applications necessitating materials with excellent conductivity and resistance to elevated temperatures and oxidative environments. These films are utilized as electrodes in devices such as capacitors and transistors [2]. The combination of physical, mechanical, and chemical qualities yields extensive applications in engineering materials, encompassing overall and wear resistance, as well as various electronic gadgets [3]. Tin is a malleable, ductile, and highly crystalline silvery-white metal. Tin has a melting point of around 232 °C. Tin can be extensively polished and serves as a protective coating for other metals. Sn3N2 is a semiconductor formed from prevalent elements, exhibiting a band gap within the visible spectrum, so positioning it as a viable option for optical and electronic applications. The optical absorbance was assessed at 1.6 eV, and the ionization potential was quantified between 5.9 and 6.0 eV. In polycrystalline thin films of Tin Nitride, the electron concentration was measured at 1018 cm-3, with a Hall mobility of approximately 1 cm2 V-1 s-1 and a minority carrier diffusion length ranging from 50 to 100 nm. The DC magnetron reactive sputtering technique was employed to fabricate the tin nitride films, which were characterized using UV-VIS NIR spectroscopy and four-probe methods [4,5].

The objective of this study is to fabricate tin nitride thin films by DC magnetron reactive sputtering with varying deposition durations, and to analyze the optical and electrical properties of both the tin nitride thin films and the oxidized tin nitride structure following 10 days of exposure to ambient conditions [6].

II. Sample Representation

The sputtering process operates on the idea of momentum transfer between ions in the plasma and atoms on the surface of the target. The target emits atoms, which deposit on the substrates. Microscope slides (76mm×26mm×1mm) used as the substrate. The substrate was cleaned following standard cleaning procedures. The maximum vacuum achieved with the system was 2 x 10-5 mbar. The sputtering and reactive gases were introduced into the chamber via a gas input port controlled by needle valves. A thermocouple was placed in touch with the substrate via a feed through to measure its temperature during film deposition. The nitrogen flow was adjusted to the requisite working pressure (8 x 10-3 mbar), and the dc power supply was turned on to initiate target pre-sputtering, followed by Tin Nitride thin film deposition. Tin Nitride thin films were produced using different deposition times. Deposition time: two minutes and eight minutes [7].

There are several analytical approaches used to characterize tin nitride coatings. The optical behavior of tin nitride thin films was investigated using a V-VIS-NIR spectrometer, while the electrical behavior was investigated using a four-probe approach [8].

III. Results and Discussion

3.1. Stylus Profilometer Technique:

A profilometer was used to measure the tin nitride layers' thickness. Dc magnetron reactive sputtering was used to create tin nitride thin films on a glass substrate with varying deposition times and constant operating pressure. It was discovered that the films' thickness was consistent across the region where the Kapton tape step was used during deposition. which were determined to be 26 and 140 nm, respectively, and about 2 and 8 minutes.

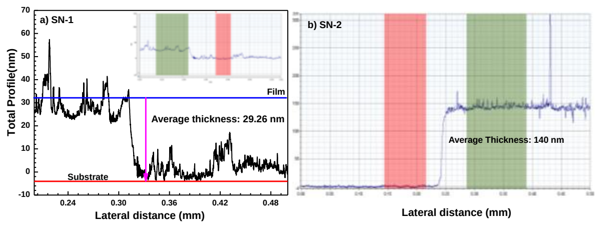

Fig 1. The thickness of the SN-1 and SN-2 samples is approximately 29.26 nm and 140 nm, respectively, as determined by a stylus profilometer

3.2. UV-Vis NIR Spectroscopy:

At the absorption edge of a material, an electron transitions from the highest energy state of the valence band to the lowest energy state of the conduction band. It is referred to as a direct band transition if these transitions occur at the same location in k-space (if the electron and hole crystal momentum is the same). The electron passes through the intermediate state in the event of an indirect band transition, however, and the crystal momentum is transmitted to the crystal lattices. If any semiconducting material has a direct dipole transition from the valence band maximum to the conduction band minimum [9], the likelihood of an electron-hole pair recombining is very high. The outcomes of this semiconductor with an extremely straight band gap are crucial for applications involving lasers and LEDs. Conversely, materials with indirect band gaps, like Si and Ge, are unsuitable for use in optoelectronics. Tin nitride does, in fact, have a direct band gap. The optical band gap of the thin films was determined by applying the relation for direct band transition to the UV-Vis NIR spectroscopy transmission (T%).

$$(\alpha h\nu)^2 = A(h\nu - E_g) \quad (1)$$

here the α is the absorption coefficient, h is the Planck constants, A is a constant and Eg is the band gap of the materials [10].

The transmittance spectra of pristine and oxidized SN-1 and SN-2 thin films are shown in Fig. 2. After 10 days of ambient exposure, the optical transmittance and band gap of Tauc's plot spectra for the incident photon energy on the tin nitride pristine and converted tin oxide-based structure are shown in Fig. 3. The films were made using reactive magnetron sputtering at varying deposition times [11]. The (αhν)2 versus h^0 axis spectrum at (αhν)2 = 0 by extrapolating the solid line to axis. Which interpret the oxidized tin oxide structured films result the higher transmittance percentage 90 – 95 % in NIR region and absorption edge increased in the visible region results the change in band gap from 2.54 eV to 3.7 eV and 1.86 eV to 3.15 eV for 2 min. and 8 min. deposition time respectively. This similar behaviour observed in a reported literature [12].

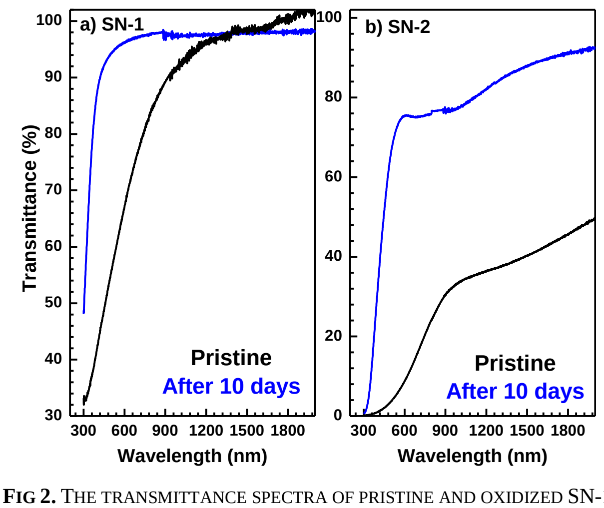

Fig 2. The transmittance spectra of pristine and oxidized SN-1 and SN-2 thin films.

Bandgap

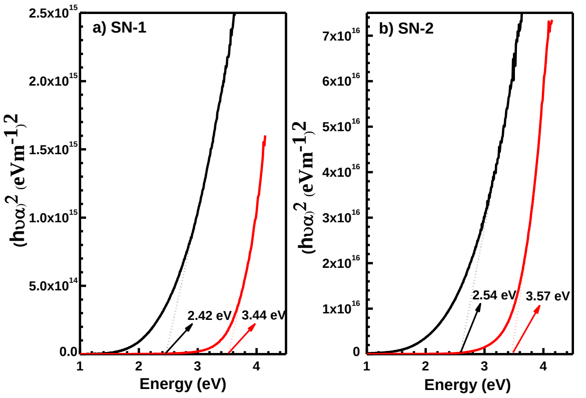

FIG 3. THE TAUC'S PLOT SPECTRA OF PRISTINE AND OXIDIZED SN-1 AND SN-2 THIN FILMS.

Electrical Studies:

In this study, the four-probe method was utilized to test the resistivity and sheet resistance of tin nitride thin films produced by dc magnetron reactive sputtering at room temperature but with variable deposition times. Keithley 2220-30-1, Dual Channel DC The Keithley 2000 Multimeter was used to measure the voltage in the inner probe of the four-probe experimental setup, while a Power Supply was utilized to provide current to the outer probe [13]. The resistivity and sheet resistance are determined using the following relations:

$$\rho_0 = \frac{V}{I} \text{ x } 2\pi s \tag{2}$$

$$\rho = \frac{\rho 0}{G7(\frac{W}{S})} \tag{3}$$

$$G_7\left(\frac{W}{S}\right) = \frac{2S}{W} \log e^2 \tag{4}$$

Where s is the space between the two probes, which is kept at 0.2 cm, eqn. 3 is the correction factor for non-conducting substrates in thin film samples, voltage (V) is measured for the corresponding applied current, and resistivity and sheet resistance values are calculated and shown in table 1.The measured surface sheet resistance values for 8 min deposited tin nitride thin films at ambient temperature using dc reactive magnetron sputtering were equivalent to those reported in the literature [14].

TABLE 1 SHEET RESISTANCE AND RESISTIVITY OF TIN NITRIDE THIN FILM BY FOUR PROBES.

I (A)	V (V)	V/I (Ω)	W (nm)	Resistivity (ρ) (Ωcm)	Sheet Resistance 10^3 Ω
0.001	51.06	5106	140	0.3238	23.128

IV. CONCLUSION

Excellent optical and electrical characteristics are possessed by semiconductor nitrides. In this work, we examined how post-annealing affected the optoelectronic characteristics and thermal stability of various deposition times on a glass substrate. Based on a complementary examination that includes the four-probe method, UV-TRS, stylus profilometer methodology, changes in film thickness, optical characteristics of the energy band gap, and electrical conductivity. It was discovered that the films' thicknesses were approximately 2 and 8 minutes at 26 and 140 nm. The band gap changes from 2.54 eV to 3.7 eV and 1.86 eV to 3.15 eV for 2 and 8 minutes, respectively, as a result of the absorption edge increasing in the visible range. The electrical properties of I= 1 mA, V= 51.06 V, ρ= 0.3238 Ωcm and R= 23.128 kΩ.

V. ACKNOWLEDGMENTS

Thank you to Thiagarajar College of Engineering, Madurai for giving the Thiagarajar Research fellowship (TRF/Jan-2023/03) to the author, P. Sundararajaperumal.

REFERENCES

[1] Ansari, M. Z.; Nandi, D. K.; Janicek, P.; Ansari, S. A.; Ramesh, R.; Cheon, T.; Shong, B.; Kim, S.-H. Low-Temperature Atomic Layer Deposition of Highly Conformal Tin Nitride Thin Films for Energy Storage Devices. ACS Appl. Mater. Interfaces 2019, 11 (46), 43608–43621. https://doi.org/10.1021/acsami.9b15790.

[2] YU, P.; Cardona, M. Fundamentals of Semiconductors: Physics and Materials Properties; Springer Science & Business Media, 2010.

[3] Silicon Nitride and Hydrogenated Silicon Nitride Thin Films: A Review of Fabrication Methods and Applications. https://www.mdpi.com/1996-1944/14/19/5658 (accessed 2025-01-25).

[4] Ansari, M. Z.; Janicek, P.; Nandi, D. K.; Palka, K.; Slang, S.; Kim, D. H.; Cheon, T.; Kim, S.-H. Influence of Post-Annealing on Structural, Optical and Electrical Properties of Tin Nitride Thin Films Prepared by Atomic Layer Deposition. Appl. Surf. Sci. 2021, 538, 147920. https://doi.org/10.1016/j.apsusc.2020.147920.

[5] Mascaretti, L.; Barman, T.; Bricchi, B. R.; Münz, F.; Li Bassi, A.; Kment, Š.; Naldoni, A. Controlling the Plasmonic Properties of Titanium Nitride Thin Films by Radiofrequency Substrate Biasing in Magnetron Sputtering. Appl. Surf. Sci. 2021, 554, 149543. https://doi.org/10.1016/j.apsusc.2021.149543.

[6] Richter, N. A.; Yang, B.; Barnard, J. P.; Niu, T.; Sheng, X.; Shaw, D.; Watanabe, M.; Rane, G.; Krause, U.; Dürrenfeld, P.; Wang, H.; Zhang, X. Significant Texture and Wear Resistance Improvement of TiN Coatings Using Pulsed DC Magnetron Sputtering. Appl. Surf. Sci. 2023, 635, 157709. https://doi.org/10.1016/j.apsusc.2023.157709.

[7] Wang, Z.-D.; Lai, Z.-Q. Preparation and Characterization of Single (200)-Oriented TiN Thin Films Deposited by DC Magnetron Reactive Sputtering. Rare Met. 2022, 41 (4), 1380–1384. https://doi.org/10.1007/s12598-015-0517-2.

[8] Dastan, D.; Shan, K.; Jafari, A.; Gity, F.; Yin, X.-T.; Shi, Z.; Alharbi, N. D.; Reshi, B. A.; Fu, W.; Ţălu, Ş.; Aljerf, L.; Garmestani, H.; Ansari, L. Influence of Nitrogen Concentration on Electrical, Mechanical, and Structural Properties of Tantalum Nitride Thin Films Prepared via DC Magnetron Sputtering. Appl. Phys. A 2022, 128 (5), 400. https://doi.org/10.1007/s00339-022-05501-4.

[9] Yuan, L.-D.; Deng, H.-X.; Li, S.-S.; Wei, S.-H.; Luo, J.-W. Unified Theory of Direct or Indirect Band-Gap Nature of Conventional Semiconductors. Phys. Rev. B

2018, 98 (24), 245203. https://doi.org/10.1103/PhysRevB.98.245203.

[10] Tauc, J. Amorphous and Liquid Semiconductors; Springer Science & Business Media, 2012.

[11] Feng, J. Q.; Chen, J. F. Optical Properties and Zinc Nitride Thin Films Prepared Using Magnetron Reactive Sputtering. Adv. Mater. Res. 2014, 940, 11–15. https://doi.org/10.4028/www.scientific.net/AMR.940.11.

[12] Structural, electrical, and optical characterization of as grown and oxidized zinc nitride thin films | Journal of Applied Physics | AIP Publishing. https://pubs.aip.org/aip/jap/article/120/20/205102/918114 (accessed 2025-01-27).

[13] Smits, F. M. Measurement of Sheet Resistivities with the Four-Point Probe. Bell Syst. Tech. J. 1958, 37 (3), 711–718. https://doi.org/10.1002/j.1538-7305.1958.tb03883.x.

[14] Choi, S.; Kang, J.; Park, J.; Kang, Y.-C. Tin Nitride Thin Films Fabricated by Reactive Radio Frequency Magnetron Sputtering at Various Nitrogen Gas Ratios. Thin Solid Films 2014, 571, 84–89. https://doi.org/10.1016/j.tsf.2014.10.035.

Design of a Hollow- Core Micro structured Optical Fiber Biosensor for Spike RBD Protein Detection

P. Sangeetha
Department of ECE,
Thiagarajar College of Engineering,
Madurai
psatce@tce.edu

N. Ayyanar
Department of ECE,
Thiagarajar College of Engineering,
Madurai
naece@tce.edu

***Abstract*—We present a novel Hollow-Core Micro structured Optical Fibre (HC-MOF) biosensor in this article that was created especially to identify the Spike RBD protein. The suggested sensor detects the refractive index (RI) of the liquid analyte that fills the fibre core by using the photonic bandgap effect, which has a major influence on the location of the transmission peaks. Our suggested HC-MOF biosensor shows a wavelength sensitivity of around 2 nm/mg/ml in our experimental investigations, along with a refractive index (RI) detection range of 1.3420 to 1.3358 for various plasma-to-blood serum ratios. The suggested sensor has enormous potential for detecting liquid analytes and biomolecules, with possible uses in biology, chemistry, and healthcare due to its high sensitivity, user-friendliness, and real-time sensing capacity.**

Keywords—Hollow-core micro structured optical fiber, photonic bandgap, biosensor, sensitivity, Spike RBD Protein.

I. INTRODUCTION

A vital portion of the spike protein found on the surface of coronaviruses like SARS-CoV-2 is called the Spike Receptor-Binding Domain (RBD) Protein. By attaching itself to the host cell receptor, it plays a crucial part in viral entrance [1]. The spike RBD protein is a prime target for vaccines, therapeutic antibodies, and diagnostic biosensors because of its importance in the immunological response to infection. Temperature, pressure, mechanical strain, refractive index, and bio-concentration are just a few of the physical, chemical, and biological characteristics that can be detected in a variety of samples and environments using optical fibres. These sensors provide several advantages over traditional ones, such as improved design, resistance to electromagnetic interference, cost efficiency, built-in remote and distributed sensing capabilities, and outstanding detection sensitivity [2].

A key characteristic of hollow-core micro structured optical fibres (HC-MOFs) is their ability to confine light within a low-index medium using the photonic bandgap effect.

Light is confined and guided within the core of these fibres due to the micro structured cladding, which forms photonic bandgaps that strongly reflect incoming light at specific wavelengths. Present photonic applications of HC-MOFs encompass spectroscopy, thermal imaging, supercontinuum generation, synchronized light-matter interactions, high-power laser delivery, ultrashort pulse compression and lasing, as well as efficient terahertz communication [3].

To detect the Spike RBD Protein, we propose an innovative and reliable HC-MOF biosensor that utilizes a simplified approach for introducing liquid into the fiber's inner core. By exploiting the photonic bandgap effect to analyse the HC-MOF's transmission spectra, we experimentally illustrate its biosensing potential. The initial design of the HC-MOF sensor is based on the finite element method. In our proposed study, varying the analyte concentration resulted in a wavelength shift, which can be utilized to determine the biomolecule levels in the sample [4-6]. At a smaller index difference, the suggested method showed enhanced sensitivity during the index difference analysis. A 43-year-old woman's blood samples, taken before she had the Gam-COVID-Vak (Sputnik V) immunisation, were used for the analysis. Using this technique, serum samples were combined with predetermined concentrations of the Spike RBD, and the effects were tracked.

II. DESIGN OF OPTICAL FIBER

We employed an HC-MOF, that features configurable photonic bandgaps according to the liquid pumped into the fibre core as illustrated in Fig. 1, to develop a sensitive biosensor.

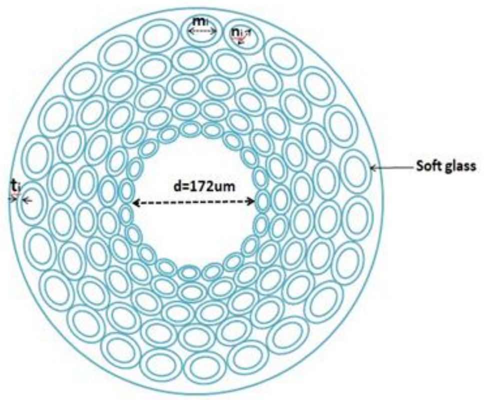

FIG 1 CROSS-SECTIONAL VIEW OF THE PROPOSED HC-MOF FIBER

In order to maintain structural integrity during the drawing process, the suggested fibre is made up of five concentric capillary layers and an outside buffer layer [7]. At 720 nm, a white light source operating in the visible spectrum is linked to the HC-MOF. 172 μm is the core diameter (d). The capillary walls in each layer have the following thicknesses: $t1 = 1.8\mu m$, $t2 = 2.6\mu m$, $t3 = 3.0\mu m$, $t4 = 3.4\mu m$, and $t5 = 4.1\mu m$. Each layer contains soft glass ($n = 1.519$)

with a wavelength of 550 nm. Capillary diameters are represented by m and n, and the values of the five layers are as follows: m1 = 14μm, n1 = 16μm, m2 = 19μm, n2 = 20μm, m3 = 22μm, n3 = 24μm, m4 = 26μm, n4 = 29μm, m5 = 31μm, and n5 = 35μm. Each of the five circular layers of glass tubes contains thirty identical cells, each with a different diameter. The ratio of each tube's inner to outer diameter is 0.85. The addition of an outside buffer layer supports this construction with a bigger diameter cylindrical tube [8].

III. NUMERICAL SIMULATIONS

The effective mode index of the guided modes in the fibre core is found using the finite element technique (FEM) in order to mimic the optical properties of the suggested HC-MOF for sensing applications [9]. Using FEM analysis using COMSOL Multi-Physics software (version 4.3), the electric field distributions of the fundamental guided mode profile in the HC-MOF at a 600 nm excitation wavelength are displayed in Fig. 2. Considering that the fibre structure is the source of all HC-MOF design factors [10]. The boundary surfaces in this simulation are covered with a 7μm perfectly matched layer (PML), which absorbs radiant light and prevents any stray energy from the fibre axis from reflecting. In addition to PML, the scattering boundary condition can be applied to assist reduce the reflected energy. [11–13]. Finally, the model incorporates a fine mesh size to guarantee the precision of the outcomes.

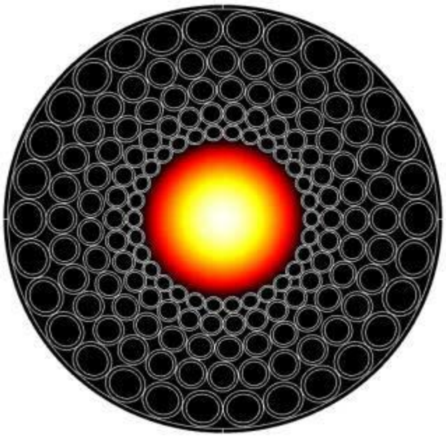

FIG.2 ELECTRIC FIELD PROFILE OF THE FUNDAMENTAL GUIDED MODE IN THE PROPOSED HC-MOF

IV. RESULTS AND DISCUSSION

At the sensor's surface, certain probe ligands are typically affixed to detect the target molecules. Phosphate buffer solution (PBS), a capable viral transport medium, is used for distributing the target molecule over the sensor surface [14]. Several sensor layers' refractive indices (RIs) change as the ligand-analytes becomes immobile. For the obtained serum samples, phosphate buffer solution (PBS) aids in maintaining a steady pH level [15]. The analysis was conducted with serum samples for a 43-year-old woman, before vaccinating with Gam-COVID-Vak (Sputnik V). The procedure involves mixing specific amounts of the Spike RBD with serum samples and calculating the results. The Spike RBD protein was tested at concentrations of 5, 10, and 15 μg/ml, with measurement of refractive indices as depicted in table 1 which can be recorded correspondingly. Control samples were also attached to introduce baselines for the measurements.

TABLE.1 THE REFRACTIVE INDEX (RI) VALUE FOR DIFFERENT CONCENTRATIONS OF SPIKE RBD PROTEIN

S.No.	Solution	RI
1	20 μl SARS-CoV-2 Spike RBD 5 μg/ml + 20 μl serum №1	1,3420
2	20 μl SARS-CoV-2 Spike RBD 10 μg/ml + 20 μl serum №1	1,3422
3	20 μl SARS-CoV-2 Spike RBD 15 μg/ml + 20 μl serum №1	1,3421
4	Control 20 μl PBS+ 20 μl serum №1	1,3358

The proposed SPR sensor's ability for detecting distinct SARS-CoV-2 Spike RBD proteins at varying concentrations before vaccinations are displayed in Fig 3. By calculating the difference between the resonance angles of the Control 20 μl PBS and various concentrations of Spike RBD, the sensitivity for identifying SARS-CoV-2 Spike RBD samples is determined.

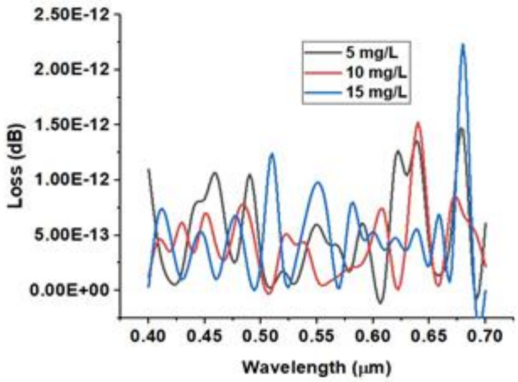

FIG. 3 LOSS(DB) MEASUREMENT AT VARIOUS CONCENTRATIONS

The wavelength sensitivity is a crucial parameter utilized to evaluate the effectiveness of a biosensor [16]. The wavelength sensitivity of the proposed HC-MOF can be easily determined using the following formula,

$$\text{Sensitivity} = \frac{\Delta\lambda}{\Delta C} \text{---------------------------(1)}$$

where ΔC is the difference between the analyte RI of the core filling liquids and Δλ is the difference between the peak wavelengths of the HC-MOF spectra. [17]. By using equation (1), the wavelength sensitivity obtained is 2nm/mg/ml for FEM simulations covering RI detection range from 1.3420 to 1.3358. The variation of resonance wavelength with analyte RI for experiments and simulations is illustrated [18-19]. The resonance wavelength at varying concentrations ranges with 5mg/ml is 0.49μm, 10mg/ml is 0.48μm and for 15mg/ml is 0.47μm is illustrated in fig 4.

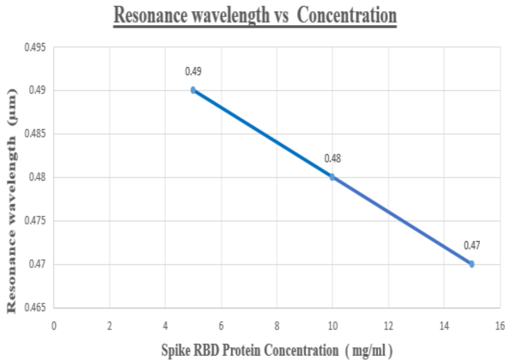

FIG 4: RESONANCE WAVELENGTH OF THE HC-MOF AS A FUNCTION OF ANALYTE RI FOR EXPERIMENTAL STUDIES AND FEM SIMULATIONS.

V. CONCLUSION

The emergence of a hollow-core optical fibre biosensor for Spike RBD protein identification provides a very efficient and sensitive way to detect viruses. Through the utilisation of hollow-core fiber's unique optical properties, this biosensor enhances light-matter interaction, improving response speed and detection accuracy. Optical signal transduction, noise reduction methods, and biorecognition efficiency are some of the elements that affect the sensor's sensitivity. This suggested study achieves a wavelength sensitivity of 2nm/mg/ml. This technique supports early illness identification and trustworthy viral infection surveillance, and it offers promising capabilities for quick and accurate diagnostics in the biomedical and medical domains.

ACKNOWLEDGMENT

N. Ayyanar acknowledges the financial assistance provided by SERB SURE, India, under the State University Research Excellence program (SUR/2022/003424).

REFERENCES

[1] Pandey PS, Raghuwanshi SK, Shadab A, Ansari MT, Tiwari UK, Kumar S. SPR-based biosensing chip for COVID-19 diagnosis - A review. IEEE Sensors Journal. 2022 Jun 14;22(14):13800-10.

[2] Ayyanar, N., Svetlana S. Konnova, Anastasiya A. Zanishevskaya, Pavel A. Lepilin, Andrey A. Shuvalov, Julia S. Skibina, and Fahad A. Alzahrani. "Protein Detection Using Hollow Core Microstructured Optical Fiber." IEEE Sensors Journal (2024).

[3] D. Lopez-Torres, C. Elosua, and F. J. Arregui, "Optical fiber sensors based on microstructured optical fibers to detect gases and volatile organic compounds—A review," Sensors, vol. 20, no. 9, p. 2555,Apr. 2020.

[4] Ayyanar, N., G. Thavasi Raja, Y. S. Skibina, Yashar E. Monfared, A. A. Zanishevskaya, A. A. Shuvalov, and A. Yu Gryaznov. "Hollow-core microstructured optical fiber based refractometer: Numerical simulation and experimental studies." IEEE transactions on nanobioscience 21, no. 2 (2022): 194-198.

[5] J. Bläsi and M. Gerken, "Multiplex optical biosensors based on multi-pinhole interferometry," Biomed. Opt. Exp., vol. 12, no. 7, pp. 4265–4275, 2021.

[6] J. S. Skibina et al., "A chirped photonic-crystal fibre," Nature Photon., vol. 2, no. 11, pp. 679–683, Nov. 2008.

[7] Y. Esfahani Monfared, "Refractive index sensor based on surface plasmon resonance excitation in a D-shaped photonic crystal fiber coated by titanium nitride," Plasmonics, vol. 15, no. 2, pp. 535–542, Apr. 2020.

[8] A. Kumar Paul, A. Krishno Sarkar, A. B. S. Rahman, and A. Khaleque, "Twin core photonic crystal fiber plasmonic refractive index sensor," IEEE Sensors J., vol. 18, no. 14, pp. 5761–5769, Jul. 2018.

[9] J. Sultana et al., "Hollow core inhibited coupled antiresonant terahertz fiber: A numerical and experimental study," IEEE Trans. Terahertz Sci.Technol., vol. 11, no. 3, pp. 245–260, May 2021.

[10] F. Yang, W. Jin, Y. Lin, C. Wang, H. Lut, and Y. Tan, "Hollow-core microstructured optical fiber gas sensors," J. Lightw. Technol., vol. 35,no. 16, pp. 3413–3424, Aug. 15, 2017.

[11] R. F. Cregan *et al.*, "Single-mode photonic band gap guidance of light in air," *Science*, vol. 285, no. 5433, pp. 1537–1539, Sep. 1999.

[12] Y. E. Monfared, "Transient dynamics of stimulated Raman scattering in gas-filled hollow-core photonic crystal fibers," *Adv. Mater. Sci. Eng.*, vol. 2018, Dec. 2018, Art. no. 8951495.

[13] N. Kotsina *et al.*, "Ultrafast molecular spectroscopy using a hollow-core photonic crystal fiber light source," *J. Phys. Chem. Lett.*, vol. 10, no. 4, pp. 715–720, Feb. 2019.

[14] F. Benabid, J. C. Knight, and P. J. Russell, "Particle levitation and guidance in hollow-core photonic crystal fiber," *Opt. Exp.*, vol. 10, no. 21, pp. 1195–1203, 2002.

[15] A.Ermolov, K. F. Mak, M. H. Frosz, J. C. Travers, and P. S. J. Russell, "Supercontinuum generation in the vacuum ultraviolet through dispersive-wave and soliton-plasma interaction in a noble-gasfilled hollow-core photonic crystal fiber," *Phys. Rev. A, Gen. Phys.*, vol. 92, no. 3, Sep. 2015, Art. no. 033821.

[16] G. Humbert *et al.*, "Hollow core photonic crystal fibers for beam delivery," *Opt. Exp.*, vol. 12, no. 8, pp. 1477–1484, 2004.

[17] Y. Y. Wang *et al.*, "Design and fabrication of hollow-core photonic crystal fibers for high-power ultrashort pulse transportation and pulse compression," *Opt. Lett.*, vol. 37, no. 15, pp. 3111–3113, 2012.

[18] H. Pakarzadeh, S. M. Rezaei, and L. Namroodi, "Hollow-core photonic crystal fibers for efficient terahertz transmission," *Opt. Commun.*,vol. 433, pp. 81–88, Feb. 2019.

[19] V. Sharif and H. Pakarzadeh, "Terahertz hollow-core optical fibers for efficient transmission of orbital angular momentum modes," *J. Lightw. Technol.*, vol. 39, no. 13, pp. 4462–4468, Jul. 1, 2021.

Influence of Copper Chloride on the Electrochemical Behaviour of WO_3 Nano Structure Synthesized via Hydrothermal Method

S. Pon Lakshmanan
Department of Physics, (Research Scholar),
Thiagarajar College of Engineering,
Madurai, India.
ponlakshmanan@student.tce.edu

R. Bhuvanesh Kumar
Department of Physics, (Research Scholar),
Thiagarajar College of Engineering,
Madurai, India.
bhuvikumar330@gmal.com

P. Velusamy
Department of Physics, (Assistant Professor),
Thiagarajar College of Engineering,
Madurai, India.
*velusamy.phy@gmail.com

S. Hemapriya
Department of Physics, (Research Scholar),
Thiagarajar College of Engineering,
Madurai, India.
shemapriya@student.tce.edu

Abstract—**In recent decades, researchers have focused on prepared the metallic nanoparticles (NPs) using the Hydro-thermal method, which is a facile, non-toxic, safe, and cost-effective approach. In this study, WO_3 NPs were synthesized via a simple hydrothermal method and characterized using different analytical techniques such as X-ray diffraction (XRD), scanning electron microscopy (SEM), and electrochemical studies. XRD analysis used to find the phase composition and Crystalline size (D), which revealed an average crystallite size of 33 nm. The SEM analysis gave insights into the surface morphology of the prepared WO_3 NPs. Electrochemical studies were performed to evaluate key properties such as energy density, specific capacitance (C_s), over-potential, and resistance. Cyclic voltammetry (CV) studies were performed at different scan rates (mV/s) to assess the electrochemical performance of the WO_3 NPs. The results showed the highest C_s of 131 F/g** and **energy density of 10 Wh/kg, demonstrating their potential for energy storage applications. Additionally, WO_3 NPs exhibited excellent electrocatalytic activity for the hydrogen evolution reaction (HER) and oxygen evolution reaction (OER) in an basic medium, with over - potentials of 280 mV for the HER** and **258 mV for OER at a scan rate of 10 mV/s. This research findings highlight the potential of WO_3 NPs as promising materials for electrocatalytic water splitting and energy depository applications.**

***Keywords**—WO_3, Hydrothermal, Over-potential, SEM, HER Water Splitting.*

I. Introduction

TMOs (Transition metal oxide) have a popular among researchers because they have many uses in physics, chemistry, and materials science. Tungsten trioxide (WO_3) has attracted considerable interest in recent years because of its multifunctional characteristics and broad spectrum of applications in areas such as electrochromism, photocatalysis, and gas sensing and energystorage[1–4]. The researchers follow various method to synthesis WO_3 NPs such as solvothermal method, sol – gel method, template assisted growth, microwave irradiation method, co-precipitation method, green synthesis method, chemical vapour deposition, thermal evaporation and hydrothermal method[5] etc. Among the various synthesis methods for WO_3 preparation, the hydrothermal technique has emerged as a promising approach due to its capability to produce high-quality, well-defined nanostructures with controlled morphology and composition[6–8]. The hydrothermal method offers several advantages are synthesis techniques, including low-temperature processing, uncontaminated of yield, and the ability to control of particle size and shape. This method involves the crystallization of substances from high-temperature aqueous solutions under high vapour pressures, typically carried out in sealed vessels called autoclaves[9]. The hydrothermal synthesis of WO_3 include reaction temperature, pressure, precursor concentration, pH of the solution, and reaction time. By carefully manipulating these variables, researchers can tailor the properties of the resulting WO_3 nanostructures to suit specific applications. This study aims to investigate the optimal conditions for preparing WO_3 nanostructures using the hydrothermal method, with a focus on controlling the surface morphology and crystalline structure of the synthesized material. Additionally, we will explore the effects of various synthesis parameters on the physicochemical properties of the resulting WO_3 nanostructures. This research results are expected to help in future development to improved WO_3-based materials for applications in advanced energy systems, environmental remediation, and sensing technologies[6,9–12]. The last 50 years, energy needs have been the first and foremost problem next to the food we are facing. Researchers have attempted huge approaches, methods and processes to short out these energy needs. Water splitting is nature-friendly processes to generate eenergy[13–15] Various water-splitting methods exist, including photocatalytic, thermocatalytic, electrocatalytic, and biocatalytic processes. Among them, electrocatalytic water splitting stands out as a highly promising technique for generating hydrogen and oxygen while producing no carbon emission[16]. To achieved in the water splitting reaction there are two half reactions to be attempted by the catalyst for HER and OER. The oxygen evolution reaction (OER) is much more difficulty occur than the HER due to Due to its slow reaction, the development of an efficient, affordable, and earth-abundant electrocatalyst for the oxygen evolution reaction (OER) remains a topic of ongoing research [17,18]. The practical, the OER requires higher overpotential than the HER because of its complicated reaction because here involving the tetra-electron process. It is highly preferable to develop a well-designed and cost-effective electrode for long-term stable water splitting process[13,19]. In this present work is synthesis WO_3 NPs using simple hydrothermal method. The prepared WO_3 were characterised by XRD, SEM and a prepared WO_3 NPs were used for electrochemical studies such as cyclic voltammetry (CV), linear sweep voltammetry (LSV) and EIS (electrochemical impedance spectroscopy).

II. MATERIALS AND METHOD

2.1 Chemicals

All the chemicals utilized were of high-purity grade and supplied by Merck. Sodium tungstate dihydrate ($Na_2 WO_4$ $2H_2O$) and Copper chloride dehydrate ($CuCl_2$ $2H_2O$) with a purity of 99.9% was employed as the precursor for synthesizing tungsten trioxide (WO_3) nanoparticles. Concentrated hydrochloric acid (HCl) served as the precipitating agent to achieve the desired morphology of the WO_3 nanoparticles. Double-deionized water was used throughout the process to prevent contamination that could affect the experimental outcomes.

2.2 Synthesis of WO_3 NPs

The precursor solution was prepared by dissolving 0.1M $Na_2 WO_4 2H_2O$ in 60 mL of DI (deionised water) and stirring for 30 min using a magnetic stirrer. Subsequently, 1.0228 g copper chloride was added to the stirring solution. The mixed solution was stirred for half an hour. After that 8 ml of concentrated hydrochloric acid was added to dropwise. The mixture was stirred for half an hour. The stirring transparent solution became paleyellow with a precipitate. Subsequently, the solution is transfer to the autoclave. Then that autoclave kept in a oven at 120 °C for 28 h. Then it slowly cooled. The precipitate was centrifuged thrice with C_2H_6O (ethanol) and Double distilled water. The cleansed precipitate is dry at 80°C for a overnight and annealed at 450°C for 2 h to got the expected WO_3 NPs.

2.3. Preparation of Working electrode

To study the electrochemical measurements of the prepared material, a homogeneous slurry mixture of the active material (WO_3 NPs), 270 µl of ethanol, and 30 µl of Nafion binder was added. Then the homogeneous slurry mixer was sonicated for 1 h. The prepared slurry was coated onto a 1 × 1 cm^2 nickel foam (NF). Subsequently, the coded electrodes were dried with the help of a oven to overnight at 60˚c. Approximately 1 mg/cm^2 active material was coded to the nickel foam. The electrochemical analysis of the prepared WO_3 NPs were studied using a tri-electrode setup. All electrochemical studies, including CV, LSV and EIS was performed using a 3M KOH electrolyte solution at room temperature. The coded NF served as a working electrode, platinum wire was counter electrode and the reference electrode is saturated calomel electrode (SCE). The specific capacitance and energy density were determined by cyclic voltammetry (CV). The HER performance was analysed from a LSV study in saturated 3M potassium hydroxide. The SCE potential is changed to the Reversible hydrogen electrode (RHE) potential using the given equation (1) and (2)

For HER $E_{(RHE)} = E^O_{(SCE)} + E_{(SCE)} + 0.059 \times P^H$ (1)

For OER $E_{(RHE)} = E_{(SCE)} + 0.059 \times P^H - E^O_{(SCE)}$ (2)
(2)

Where '$E_{(RHE)}$' and '$E_{(SCE)}$' is the potential vs. Reversible hydrogen electrode (RHE) and the potential vs. Saturated calomel electrode, respectively. '$E^O_{(SCE)}$' is standard potential vs SCE[13,20]. The impedance analysis spectra (EIS) used to determine the charge-transferred to the electrode–electrolyte interface by applying an AC voltage of 1×10^{-3} V. The frequency range is 100kHz to 0.01Hz.

2.4 Instruments

The synthesized WO_3 NPs were observed to using various analytical techniques, such as XRD measurements using a PANalytical 'X'PERT-PRO XRPD system with Cu-Kα radiation (wavelength = 1.5406 nm). A scans were performed at a rate of 2.0°/minute, covering a 2θ range of 20°– 80° for 20 minute. This technique helps determine the crystalline structure and phase purity of the NPs. The surface morphology of the synthesized materials were examined using a scanning electron microscope (SEM, SU8010). Electrochemical studies were performed by CV, linear sweep voltammetry LSV, and EIS was carried out by FRA-II µAutolab type-III.

III. RESULT AND DISCUSSION

3.1 X-ray diffraction Analysis

From the XRD analysis of the synthesized tungsten trioxide (WO_3) nanoparticles revealed sharp diffraction peaks at 2θ angles of 23.27°, 23.98^0, 24.47^0, 26.88^0, 28.50^0, 33.55^0, 34.15^0, 41.86^0, 50.24^0, and 56.13°. These peaks corresponded to the (002), (020), (200), (120), (112), (-202), (-202), (222), (-114), and (402) crystallographic planes, respectively. The observed diffraction pattern aligns well with the standard data for monoclinic WO_3, as referenced in Standard (JCPDS) File No. 00-043-1035. These distinct peaks confirmed the successful formation of crystalline WO_3 nanoparticles. Figure 1 depict the XRD pattern of synthesized WO_3 NPs. This result is very well matched to earlierfindings[21,22]. The grain size is calculated from the FWHM (full width half maximum) of the central prominent significant peaks using a following Scherer equation,

$$D = \frac{K\lambda}{\beta \, Cos\theta} \quad (3)$$

where'D' is the average size of the ordered (crystalline) domains, 'K' is dimensions less shape factor (0.94), 'λ' is the wavelength of x-ray (λ=1.5406Å) and 'θ' is the Bragg angle.The dislocation density was found using equation (4)

$$\delta = \frac{1}{D^2} \quad (4)$$

Where 'δ' is dislocation density, 'D' is the crystalline size.

The microstrain of the NPs was carried out by using equation (5)

$$\varepsilon = \frac{\beta}{4 \tan \theta} \quad (5)$$

Where 'ε' is the microstrain of the NPs, β is the FWHM of the peak. The specific surface area (SSA) was found to be used in equation (6)

$$SSA = \frac{6\times10^{3}}{D_p\times\rho} \tag{6}$$

TABLE 1 CRYSTALLINE SIZE, MICROSTRAIN AND DISLOCATION DENSITY, AND SPECIFIC SURFACE AREA (SSA)OF SYNTHESISED WO_3NPS.

2θ (°)	FWHM (β)	d - Spacing	D (nm)	ε × 10^{-3}	δ × 10^{14} (lines/m²)	SSA × 10^{10} (m²g⁻¹)
23.2	0.204	3.7690	41.4	0.0005	5.8330	1.990
23.9	0.255	3.6480	33.2	0.0009	9.0373	2.477
24.4	0.307	3.4240	27.6	0.0012	1.3074	2.980
34.1	0.225	2.6230	38.5	0.0001	6.7193	2.136
50.2	0.358	1.8111	25.5	0.0015	1.5269	3.220

This clearly illustrates that WO_3NPs were synthesized using hydrothermal and nanocrystalline methods. In WO_3 NPs, the δ (dislocation density) is inversely related to the grain size. The calculated dislocation density and micro-strain in WO3 NPs were found to be inversely proportional to the grain size. As the grain size increased, the dislocation density and micro-strain decreased. The grain size was inversely proportional to the SSA, as shown in the table. 1. The mean crystalline size of the predominant peaks is 33 nm.

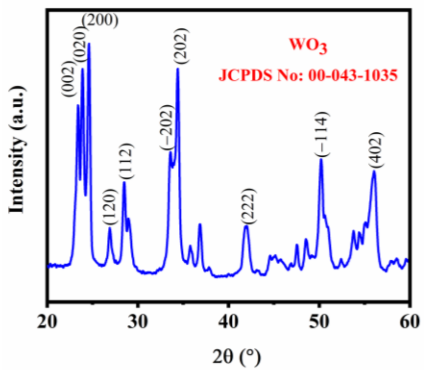

FIG. 1 POWDER XRD PATTERN OF THE SYNTHESIZED WO_3 NPS

3.2 Hall Williamson Plot

Williamson - Hall proposed a technique for clarifying crystalline size and strain broadening by looking at the peak width as a function of 2θ. Here, the W-H plot is plotted with the x-axis is sinθ and the y-axis is βcosθ. A linear fit was obtained from the data. From this linear fit, the crystalline size and strain were filtered from the y-intercept and the slope respectively.[23,24]. The filtered crystalline size is 32 nm and the microstrain was 0.0054. Figure 2 illustrate the a W–H plot.

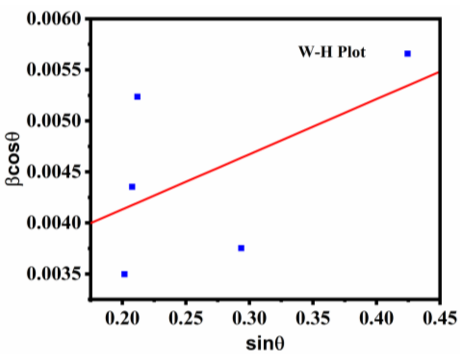

FIG. 2 WILLIAMSON-HALL PLOT OF THE SYNTHESIZED WO_3 NPS

3.3 Scanning electron microscope

The surface morphology of the prepared WO_3 NPs was studied using Scanning Electron Microscope analysis and noted at low and high magnifications, as shown in Fig.3(a). The SEM image shows that the particles are agglomerated surface morphology but its surface is smooth and shape was irregular. All particles were randomly interconnected to another. Its form huge network systems with irregular shapes and pores. At higher magnifications, nanosheet-like structures were observed. The results were compared to earlier literature on its well-matched [24–26]. The SEM images confirmed that the final product comprised many WO_3 NPs clusters. It showed the surface morphology is combination of various shapes, such as cube, square, and rod, observed through low and high magnification resolution. The high-magnification surface morphology image is shown in Fig. 3(b).

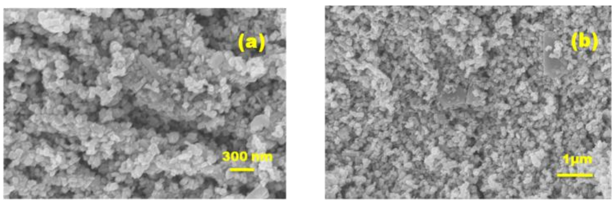

FIG. 3 (A) AND (B) IS HIGH AND LOW-RESOLUTION SEM IMAGES OF SYNTHESIZED WO_3 NPS

3.4 Electrochemical Analysis

The electrochemical characterizations, including CV, LSV and EIS, were conducted using a KOH electrolyte solution of 3M at room temperature in a three-electrode setup with a potentiostat. Cyclic voltammetry (CV) was employed to assess the charge-storage performance of synthesized WO_3 NPs, with measurements recorded at scan rates ranging from 10 mV/s - 60 mV/s with a 0.1 – 0.5 V potential range , as shown in Fig. 4 (a). The thermodynamic and kinetic performance of synthesized tungsten trioxide (WO_3) NPs after heat treatment were analyzed using CV, where a cathodic and anodic current peak appeared at 0.2 V and 0.3 V at the scan rate of 10 mV/s. While increase the scan rates, the anodic and cathodic peak shifted. Anodic peak was shift to higher voltage and cathodic peak shifted to lower voltages, its intimate the increased polarization at higher sweep rates owing to kinetic limitations associated with hydrogen separate through the active working material.[25,26]. CV reveal to 10^{-3} A for the range of current. Its depict to more excellent conductivity and stability of synthesized WO_3 NPs .[27,28].

The C_s (specific capacitance) of the synthesised WO_3 NPs was found to help of the given formula [29],

$$\text{Specific Capacitance: } C_s = \frac{1}{2v \times \Delta m \times \Delta V} \int IdV \quad (7)$$

where 'Cs' is the specific capacitance (F/g), 'v' is the scan rate (V/s), 'Δm' is the mass of the working material, 'ΔV' is the potential difference (V), and 'IdV' is the area of the CV curve respectively. The C_s (specific capacitance) value of the WO_3 NPs found with the help of the above equation. The Energy Density (ED) of the WO_3 NPs shown in Fig. 4(b), can be calculated using the formula[30],

$$\text{Energy Density: } ED = \frac{C_s(\Delta V)^2}{2} (wh/Kg) \quad (8)$$

The calculated specific capacitance (C_s) and Energy Density (ED) values are registered in Table 2.Table 2 C_s (Specific capacitance) and ED (Energy Density) of synthesized WO_3 NPs.

Scan rate	Area (CV)	c_s (F/g)	ED (Wh/Kg)
10	5.25×10^{-4}	131	10.49
20	9.17×10^{-4}	115	9.16
30	1.31×10^{-3}	109	8.739
40	1.69×10^{-3}	106	8.460
50	2.06×10^{-3}	103	8.257
60	2.43×10^{-3}	101	8.098

As increseing the scan rate, the CV cure area also increased. That area is inversely proportional to the specific capacitance and energy density, as Table 2 and Figure 4(b) clearly illustrate. The prepared WO3 NPs have a specific capacitance of 131 (F/g) and an ED (energy density) is 10.49 (Wh/kg) at the scan rate 10 mV/s.

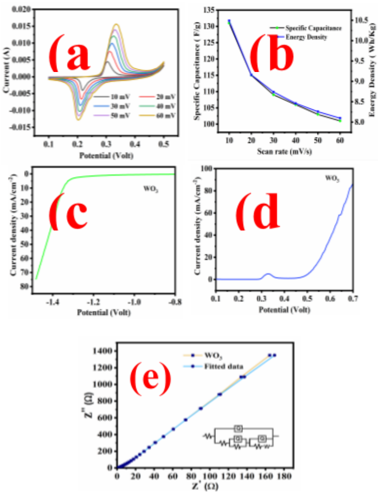

FIG. 4. (A) CYCLIC VOLTAMMETRY GRAPH OF SYNTHESIZED WO_3 NPS, (B) ENERGYDENSITY AND SPECIFIC CAPACITANCE GRAPHOF SYNTHESIZED WO_3 NPS (C) HER GRAPH OF SYNTHESIZED WO_3NPS, (D) OER GRAPH OF SYNTHESIZED WO_3 NPS (E) NYQUIST PLOT OF SYNTHESIZED WO_3NPS.

The electrocatalytic behaviour of the synthesized WO_3 NPs, were study using 3 M KOH as the electrolyte in a three-electrode system, with all electrochemical measurements conducted without iR compensation, as shown in Figure 4. The over-potential, defined as the potential at which the current density reaches 10 mA/cm^{-2} [31,32] was used to assess the catalytic performance of WO_3 NPs for both HER and OER. The recorded current attained **10 mA** for both **HER** and **OER,** but within distinct potential ranges: **−0.8 V to −1.4 V** for **HER** and **0 V to +0.7 V** for **OER**. Figures 4(c) and 4(d) illustrate the HER and OER performances, confirming the capability of WO_3 NPs for efficient water-splitting applications. Table 3 Onset-potential and Over-potential of the synthesized WO_3 NPs.

Electrocatalysis Activity	Scanrate (mV/s)	Current density (mA/cm^2)	Onset-potential (V)	Over-potential (mV)
HER	10	10	-1.347	280
OER	10	10	0.527	258

Table 2 lists the over-potential values at the same current density forthe HER and OER. The over-potential values were compared to those in the literature for HER [32–36] and OER [37–39]. This work obtained better over-potential values for the HER and OER. The HER over-potential of 280 mV suggests that the material Can serve as an electrocatalyst for hydrogen generation in water-splitting applications. Such materials are valuable for **renewable energy technologies**, including **electrolyzers, fuel cells,** and **green hydrogenproduction systems.** Although not as efficient as platinum-based catalysts, materials with moderate over-potentials can be optimized for **cost-effective and scalable hydrogen generation,** particularly in industries that focus on **sustainable energy storage, transportation (hydrogen fuel cells), and chemical synthesis**[40,41]. When the OER over-potential is 258 mV, the material can be an efficient electrocatalyst for applications in metal-air batteries, **renewable energy storage systems,** and **electrolyzers**[42,43]**.** Electrochemical impedance spectroscopy (EIS) was conducted to investigate impedance at the electrode and electrolyte interface for the electrodeposited WO_3. Figure 4(e) illustrates the Nyquist plot of the electrodeposited WO_3 electrodes. The **electrochemical impedance spectroscopy (EIS) spectrum** reveal only smooth, positively sloped curves, without any noticeable semicircles in either the low-frequency or high-frequency regions. In an EIS spectrum, a semicircle typically represents **charge transfer resistance (R_{ct}),** which plays a crucial role in the electrochemical reaction at the electrode surface. A lower **R_{ct}** value indicates enhanced reaction kinetics for the **hydrogen evolution reaction (HER)** leading to better electrocatalytic performance. The absence of a semicircle in the EIS spectrum suggests **minimal charge transfer resistance**, improved ionic mobility in the electrolyte and a capacitive nature. This enhances **charge transfer efficiency and conductivity** making the material suitable for applications in **fuel cells and batteries**. Additionally, the **series resistance (R_s)** observed in the high-frequency region arises primarily from **electrochemical and ionic resistance** within the redox system. When fitted equivalence circuit[44–49]. The R_s values of synthesized WO_3 NPs are 1.715 Ohm (Ω). Their low resistance enables better conductivity, enhancing charge/discharge rates and overall performance.

IV. CONCLUSION

Tungsten oxide nanoparticles **(WO_3 NPs)** were synthesized using a **hydrothermal method,** and their crystallite sizes were determined using the **Scherrer formula**, revealing an average size of **33 nm**, confirming their nanoscale range. The **SEM analysis** showed that the WO_3 NPs exhibit a **clustered structure,** indicating their morphological characteristics. The electrochemical characteristics of the synthesized **WO_3 nanoparticles (NPs)** were analyzed using a **tri-electrode setup**. The WO_3 NPs exhibited a **high charge storage capability**, with a **specific capacitance** of **131 F/g** and an **energy density** of **10.49 Wh/kg,** demonstrating their suitability for **energy storage systems.** Moreover, their **electrocatalytic activity** was evaluated in an **alkaline medium** for both the **hydrogen evolution reaction (HER)** and **oxygen evolution reaction (OER).** The obtained **overpotential values** were **280 mV** for **HER** and **258 mV** for **OER**, indicating their **favorable catalytic performance** at a **scan rate of 10 mV/s.** From **the EIS (**Electrochemical impedance **spectroscopy)** analysis showed a **low resistance of 1.715 Ω**, indicating excellent charge-transfer properties. These results suggest that the synthesized **WO_3 NPs** hold significant potential for applications in **water-splitting technologies andenerg storage**, making them promising materials for renewable energy systems.

V. ACKNOWLEDGEMENT

This research work in financially supported by Thiagarajar Research Fellowship (TRF) scheme - (File.no: TCE/RD/TRF/<<15>> dated 27.09.2024)

REFERENCES

[1] Zheng, H.; Ou, J. Z.; Strano, M. S.; Kaner, R. B.; Mitchell, A.; Kalantar-zadeh, K. Nanostructured Tungsten Oxide – Properties, Synthesis, and Applications. Adv. Funct. Mater.2011, 21 (12), 2175–2196. https://doi.org/10.1002/adfm.201002477.

[2] Low-temperature hydrothermal synthesis of WO3 nanorods and their sensing properties for NO2 - Journal of Materials Chemistry (RSC Publishing). https://pubs.rsc.org/en/content/articlelanding/2012/jm/c2jm30997a/unauth (accessed 2025-01-30).

[3] Palladium nanoparticle deposition onto the WO3 surface through hydrogen reduction of PdCl2: Characterization and gasochromic properties Science Direct. https://www.sciencedirect.com/science/article/abs/pii/S0927024811002030 (accessed 2025-01-30).

[4] Karuppasamy, K. M.; Subrahmanyam, A. The Electrochromic and Photocatalytic Properties of Electron Beam Evaporated Vanadium-Doped Tungsten Oxide Thin Films. Sol. Energy Mater. Sol. Cells2008, 92 (11), 1322–1326.

[5] Aravind, M.; Amalanathan, M.; Aslam, S.; Noor, A. E.; Jini, D.; Majeed, S.; Velusamy, P.; Alothman, A. A.; Alshgari, R. A.; Saleh Mushab, M. S.; Sillanpaa, M. Hydrothermally Synthesized Ag-TiO2 Nanofibers (NFs) for Photocatalytic Dye Degradation and Antibacterial Activity.Chemosphere2023,321,138077.https://doi.org/10.1016/j.chemosphere.2023.138077.

[6] Sarma, R.; Kakati, B. K. Hydrothermal Synthesis of Tungsten Oxide Photo/Electrocatalysts: Precursor-Driven Morphological Tailoring and Electrochemical Performance for Hydrogen Evolution and Oxygen Reduction Reaction Application. Environ. Sci. Pollut. Res.2024. https://doi.org/10.1007/s11356-024-35607-6.

[7] Mozalev, A.; Khatko, V.; Bittencourt, C.; Hassel, A. W.; Gorokh, G.; Llobet, E.; Correig, X. Nanostructured Columnlike Tungsten Oxide Film by Anodizing Al/W/Ti Layers on Si. Chem. Mater.2008, 20 (20), 6482–6493. https://doi.org/10.1021/cm801481z.

[8] Ahmadi, M.; Younesi, R.; Guinel, M. J. Synthesis of Tungsten Oxide Nanoparticles Using a Hydrothermal Method at Ambient Pressure. J. Mater. Res.2014, 29 (13), 1424–1430.

[9] Ogungbesan, S. O.; Ejeromedoghene, O.; Moglie, Y.; Buxaderas, E.; Cui, B.; Adedokun, R. A.; Kalulu, M.; Idowu, M. A.; Díaz, D. D.; Fu, G. Deep Eutectic Solvent Assisted Hydrothermal Synthesis of Photochromic and Nontoxic Tungsten Oxide Nanoparticles. New J. Chem.2024, 48 (35), 15428–15435.

[10] Innovations in WO3 gas sensors: Nanostructure engineering, functionalization, and future perspectives: Heliyon. https://www.cell.com/heliyon/fulltext/S2405-8440(24)03771-X (accessed 2025-01-30).

[11] Hydrothermal Synthesis of WO3•0.33H2O Nanorod Bundles as a Highly Sensitive Cyclohexene Sensor. https://www.mdpi.com/1424-8220/19/5/1257 (accessed 2025-01-30).

[12] Synthesis of SnO2 Nanoparticles via Hydrothermal Method and Their Gas Sensing Applications for Ethylene Detection - ScienceDirect. https://www.sciencedirect.com/science/article/abs/pii/S2214785319317377 (accessed 2025-01-30).

[13] Liu, X. Photoelectrochemical Water Separation and Dye Degradation Catalyzed by g‑C3N4/MoS2 Nanosheets Doped with V2+ Metal Ions Coated on TiO2 Nanorods. 2024. https://doi.org/10.1021/acsanm.3c05151.

[14] Designing Rational and Cheapest SeO2 Electrocatalyst for Long Stable Water Splitting Process | Request PDF. ResearchGate2024. https://doi.org/10.1016/j.jpcs.2020.109544.

[15] Nanostructured Tungsten Oxide – Properties, Synthesis, and Applications - Zheng - 2011 - Advanced Functional Materials - Wiley Online Library. https://advanced.onlinelibrary.wiley.com/doi/abs/10.1002/adfm.201002477 (accessed 2025-01-30).

[16] The influence of activated carbon annealing temperature on sunlight-driven photocatalytic dye degradation and biologica…. http://ouci.dntb.gov.ua/en/works/leRK22E9/ (accessed 2025-01-31).

[17] Modular Design of Noble-Metal-Free Mixed Metal Oxide Electrocatalysts for Complete Water Splitting - Gao - 2019 - Angewandte Chemie International Edition - Wiley Online Library. https://onlinelibrary.wiley.com/doi/abs/10.1002/anie.201900428 (accessed 2025-01-31).

[18] Tan, Y.; Wang, H.; Liu, P.; Shen, Y.; Cheng, C.; Hirata, A.; Fujita, T.; Tang, Z.; Chen, M. Versatile Nanoporous Bimetallic Phosphides towards Electrochemical Water Splitting. Energy Environ. Sci.2016, 9 (7), 2257–2261. https://doi.org/10.1039/C6EE01109H.

[19] Investigate the suitability of g-C3N4 nanosheets ornamented with BiOI nanoflowers for photocatalytic dye degradation and PEC water splitting - ScienceDirect.https://www.sciencedirect.com/science/article/abs/pii/S0045653523002746 (accessed 2025-01-31).

[20] Ghosh, D.; Pradhan, D. Effect of Cooperative Redox Property and Oxygen Vacancies on Bifunctional OER and HER Activities of Solvothermally Synthesized CeO2/CuO Composites. Langmuir ACS J. Surf. Colloids2023, 39 (9), 3358–3370. https://doi.org/10.1021/acs.langmuir.2c03242.

[21] Structural and Optical Studies on WO3/SnO2 and WO3/SnO2/SrO Composites | Journal of Electronic Materials. https://link.springer.com/article/10.1007/s11664-024-11412-2?utm_source=chatgpt.com (accessed 2025-01-31).

[22] Mohamed, F. A.; Salim, E. T.; Hassan, A. I. Monoclinic Tungsten Trioxide (WO3) Thin Films Using Spraying Pyrolysis: Electrical, Structural and Stoichiometric Ratio at Different Molarity. Dig J Nanomater Biostruct2022, 17 (3), 1029–1043.

[23] Theivasanthi, T.; Alagar, M. Electrolytic Synthesis and Characterization of Silver Nanopowder. Nano Biomed. Eng.2012, 4 (2), 58–65. https://doi.org/10.5101/nbe.v4i2.p58-65.

[24] Lakshmanan, S. P.; Jostar, S. T.; Arputhavalli, G. J.; Jebasingh, S.; Josephine, C. M. R. Role of Green Synthesized CuO Nanoparticles of Trigonella Foenum-Graecum L. Leaves and Their Impact on Structural, Optical and Antimicrobial Activity . Int. J. Nanosci. Nanotechnol.2021, 17 (2), 109–121.

[25] Synthesis and characterization of tungsten oxide electrochromic thin films IEEE Conference Publication | IEEE Xplore. https://ieeexplore.ieee.org/abstract/document/8626293/ (accessed 2025-02-05).

[26] Hu, P.; Ma, J.; Wang, T.; Qin, B.; Zhang, C.; Shang, C.; Zhao, J.; Cui, G. NASICON-Structured NaSn2(PO4)3 with Excellent High-Rate Properties as Anode Material for Lithium Ion Batteries. Chem. Mater.2015, 27 (19), 6668–6674. https://doi.org/10.1021/acs.chemmater.5b02471.

[27] Co3O4/WO3/C Nanorods with Porous Structures as High-Performance Electrocatalysts for Water Splitting | ACS Applied Nano Materials. https://pubs.acs.org/doi/abs/10.1021/acsanm.3c05592 (accessed 2025-02-05).

[28] Jafari, F.; Gholivand, M. B. Promoted Oxygen Evolution Reaction Efficiency by Ni3S2/WO3 Nanocomposite Anchored over rGO. Int. J. Hydrog. Energy2023, 48 (9), 3373–3384. https://doi.org/10.1016/j.ijhydene.2022.10.199.

[29] Sainta Jostar, T.; Johnsy Arputhavalli, G.; Palaniyandy, N.; Jebasingh, S.; Alshahrani, M. Y.; Divya, G. S.; Muthu Vijayalakshmi, P. Analyzing the Synergistic Effect of Mg on Mentha Spicata L. Mediated Mn2O3 Nanoparticles for Energy Storage and Bio-Medical Applications. Inorg. Chem.Commun.2025,171,113539. https://doi.org/10.1016/j.inoche.2024.113539.

[30] Analyzing the synergistic effect of Mg on Mentha spicata L. mediated Mn2O3 nanoparticles for energy storage and bio-medical applications - ScienceDirect. https://www.sciencedirect.com/science/article/pii/S1387700324015296 (accessed 2025-02-05).

[31] Hu, G.; Li, J.; Liu, P.; Zhu, X.; Li, X.; Ali, R. N.; Xiang, B. Enhanced Electrocatalytic Activity of WO3@NPRGO Composite in a Hydrogen Evolution Reaction. Appl. Surf. Sci.2019, 463, 275–282. https://doi.org/10.1016/j.apsusc.2018.08.227.

[32] Jiao, Y.; Zheng, Y.; Davey, K.; Qiao, S.-Z. Activity Origin and Catalyst Design Principles for Electrocatalytic Hydrogen Evolution on Heteroatom-Doped Graphene. Nat. Energy2016, 1 (10), 1–9. https://doi.org/10.1038/nenergy.2016.130.

[33] Ma, J.; Ma, Z.; Liu, B.; Wang, S.; Ma, R.; Wang, C. Composition of Ag-WO3 Core-Shell Nanostructures as Efficient Electrocatalysts for Hydrogen Evolution Reaction. J. Solid State Chem. 2019, 271, 246–252. https://doi.org/10.1016/j.jssc.2018.12.020.

[34] (34)WS2–WC–WO3 nano-hollow spheres as an efficient and durable catalyst for hydrogen evolution reaction | Nano Convergence. https://link.springer.com/article/10.1186/s40580-021-00278-3 (accessed 2025-02-06).

[35] Li, Y.; Zhai, X.; Liu, Y.; Wei, H.; Ma, J.; Chen, M.; Liu, X.; Zhang, W.; Wang, G.; Ren, F. WO3-Based Materials as Electrocatalysts for Hydrogen Evolution Reaction. Front. Mater.2020, 7, 105.

[36] Synthesis of hexagonal WO3 nanocrystals with various morphologies and their enhanced electrocatalytic activities toward hydrogen evolution - ScienceDirect. https://www.sciencedirect.com/science/article/abs/pii/S0360319919300138 (accessed 2025-02-09).

[37] (37)Mineo, G.; Scuderi, M.; Bruno, E.; Mirabella, S. Engineering Hexagonal/Monoclinic WO3 Phase Junctions for Improved Electrochemical Hydrogen Evolution Reaction. ACS Appl. Energy Mater. 2022, 5 (8), 9702–9710. https://doi.org/10.1021/acsaem.2c01383..

[38] (38) Diao, J.; Yuan, W.; Qiu, Y.; Cheng, L.; Guo, X. A Hierarchical Oxygen Vacancy-Rich WO3 with “Nanowire-Array-on-Nanosheet-Array” Structure for Highly Efficient Oxygen Evolution Reaction. J. Mater. Chem. A 2019, 7 (12), 6730–6739. https://doi.org/10.1039/C9TA01044K.

[39] (39) Mehboob, A.; Sadiqa, A.; Ahmad, A.; Anwar, A.; Tabassum, S.; Arsalan, M.; Habila, M. A.; Altaf, A. R.; Yao, Y.; El-Naas, M. H. Enhanced Activity of Electrodeposited WO3 Thin Films as Bi-Functional Electrocatalysts for Water Splitting. Results Eng.2024, 23, 102516.

[40] (40) Hydrothermal synthesis of 2D MoS2 nanosheets for electrocatalytic hydrogen evolution reaction - RSC

Advances (RSC Publishing). https://pubs.rsc.org/en/content/articlelanding/2015/ra/c5ra18855e?utm_source=chatgpt.com (accessed 2025-02-06).

[41] (41) Superhydrophilic MoS2–Ni3S2 nanoflake heterostructures grown on 3D Ni foam as an efficient electrocatalyst for overall water splitting | Journal of Materials Science: Materials in Electronics. https://link.springer.com/article/10.1007/s10854-020-03216-x?utm_source=chatgpt.com (accessed 2025-02-06).

[42] (42) Ding, S.; Zhang, Y.; Lou, F.; Aslam, M. K.; Sun, Y.; Li, M.; Duan, J.; Li, Y.; Chen, S. “Uncapped” Metal–Organic Framework (MOF) Dispersions Driven by O2 Plasma towards Superior Oxygen Evolution Electrocatalysis. J. Mater. Chem. A2022, 10 (39), 20813–20818. https://doi.org/10.1039/D2TA05387J.

[43] (43) Frontiers | The current state of transition metal-based electrocatalysts (oxides, alloys, POMs, and MOFs) for oxygen reduction, oxygen evolution, and hydrogen evolution reactions. https://www.frontiersin.org/journals/energy-research/articles/10.3389/fenrg.2024.1373522/full?utm_source=chatgpt.com (accessed 2025-02-06).

[44] (44) Allison, A.; Andreas, H. A. Minimizing the Nyquist-Plot Semi-Circle of Pseudocapacitive Manganese Oxides through Modification of the Oxide-Substrate Interface Resistance. J. Power Sources2019, 426, 93–96.

[45] (45) Uygun, Z. O.; Uygun, H. D. E. A Short Footnote: Circuit Design for Faradaic Impedimetric Sensors and Biosensors. Sens. Actuators B Chem.2014, 202, 448–453.

[46] (46) Fu, L.; Xia, T.; Zheng, Y.; Yang, J.; Wang, A.; Wang, Z. Preparation of WO3-Reduced Graphene Oxide Nanocomposites with Enhanced Photocatalytic Property. Ceram. Int. 2015, 41 (4), 5903–5908. https://doi.org/10.1016/j.ceramint.2015.01.022.

[47] (47) Wondimu, T. H.; Chen, G.-C.; Kabtamu, D. M.; Chen, H.-Y.; Bayeh, A. W.; Huang, H.-C.; Wang, C. H. Highly Efficient and Durable Phosphine Reduced Iron-Doped Tungsten Oxide/Reduced Graphene Oxide Nanocomposites for the Hydrogen Evolution Reaction. Int. J. Hydrog. Energy 2018, 43, 6481–6490. https://doi.org/10.1016/j.ijhydene.2018.02.080.

[48] (48) Chen, J.; Yang, H.; Sang, X.; Su, Z.; Li, D.; Wang, Q. Oxygen Vacancy Rich Tungsten Oxide with Nitrogen Doped Mesoporous Carbon as Matrix for Overall Water Splitting and 4-Nitrophenol Reductive Removal. Solid State Sci.2018, 83, 23–30.

[49] (49) Mehboob, A.; Sadiqa, A.; Ahmad, A.; Anwar, A.; Tabassum, S.; Arsalan, M.; Habila, M. A.; Altaf, A. R.; Yao, Y.; El-Naas, M. H. Enhanced Activity of Electrodeposited WO3 Thin Films as Bi-Functional Electrocatalysts for Water Splitting. Results Eng.2024, 23, 102516.

-

HKUST-1incorporated with AMHT-POM Composite: An Innovative and Sustainable Solution for Removal of Methylene Blue from Water

Madhumathy Parthibana
Department of Chemistry,
Thiagarajar College of Engineering,
Madurai, Tamilnadu.
madhumathyparthiban@gmail.com
madhumathyp@student.tce.edu

Bhaskaran Shankara
Department of Chemistry,
Thiagarajar College of Engineering,
Madurai, Tamilnadu.
bshankardu@gmail.com
bsrchem@tce.edu

***Abstract*—The efficient removal of organic dyes from wastewater has become the necessity for the sustainability of the environment. This study has elaborated the adsorption potential of HKUST-1 incorporated with Ammonium HeptaMolybdate tetrahydrate (HKUST-1incorporated with AMHT) composite for methylene blue (MB) removal. This composite achieved a high adsorption capacity of 99.05 mg/g and a removal efficiency of 98.65%, attributed to strong ionic interactions between MB and the polyoxometalates(POMs). These interactions enhance dye selectivity, making HKUST-1incorporated with AMHT) a promising adsorbent for wastewater treatment.**

***Keywords*—MOFs, Adsorption, HKUST-1, POM, Methylene Blue, MB.**

I. INTRODUCTION

Commercial dyes are used in various industries such as textiles, food processing or cosmetics. This is because commercial dyes possess infinite colour values and are endowed with excellent qualities such as resistance to light, heat, detergents, cleaner and microbial activities. Dyes can be split into two broad categories ionic and non-ionic.[1] Non-ionic dyes are disperse dyes, which are used for specific types of fibres. Cationic (basic) dyes have a positive charge, while anionic dyes, such as direct, acid, and reactive dyes, have a negative charge. Understanding these categories can help us to comprehend how dyes interact with various materials.[2] Among the common/popularly used dyes, compounds like MB[3], MG[4], RhB[5], and MO[6] are prominent industrial pollutants originating from diverse sectors such as textiles[7] cosmetics[8] food[9] and pharmaceutical[10].Many cause harm in a lot of ways such as mutagenic, carcinogenic, or causing birth defects in both animals and humans.[11] Including direct, cationic, acidic, and dispersed dyes, are more likely to form tumours, direct dyes profoundly cause bladder cancer[12]. Their release into industrial sewage poses a direct risk to the environment. The heavily colourized effluents could resist light penetration into the aquatic areas and also could hurt photosynthetic processes. The latter is equally damaging to aquatic life. [13] Even though some of them are not poisonous or overtoxic the bulk release of dyes in water bodies creates BOD and COD[7]. It is been reported that BOD and COD in some mills were found to be 85.35mg/l to 653.75mg/l and 115.66mg/l to 705.25mg/l, respectively[14]. Dye concentrations in textile wastewater have reached 300mg/L on average which includes highly carcinogenic and genotoxic azo dyes[15]In 1993 Koprivanac et al[16] reported that the concentration of a reactive dye effluent was 7000mg/L, this concentration was dangerously high in that period itself. As these enter the food chain this contamination is an alarming issue [9]

From previous works of literature, it can be seen that HKUST-1 is a highly selected material for the adsorption of methylene blue(MB). AHMT-one of the available cheapest molybdenum-oxo clusters characterized as isopolyanion. Polyanions, or polyoxometalate (POM) clusters, are regarded for their uses as electron reservoirs; in medicine, energy applications, sensors, bleaching, etc. Review articles have summarized applications of polyanion that would certainly reflect the same.

II. MATERIALS AND METHODS

A. *Materials*

Copper nitrate trihydrate, 1,3,5-benzene tricarboxylic acid and Ammonium HeptaMolybdatetetrahydrate(AHMT) were purchased from TCI. Methylene blue (MB) and ethanol were purchased from CDH. All the chemicals used in this work received an analytical grade and the solvents were used without further purification.

B. *Methods*

a. *Synthesis of HKUST-1incorporated with POM composite- Solvothermal method*

HKUST-1incorporated with POM (HKUST-1/POM) composite was synthesized by dissolving copper nitrate trihydrateand 1,3,5-benzene tricarboxylic acid separately in ethanol under constant stirring. Both solutions were mixed and stirred at room temperature. Ammonium HeptaMolybdate tetrahydrate(AHMT)POM was added to the MOF precursor and stirred to facilitate thorough integration. Then, the homogeneous mixture was transferred to the Teflon reactor and kept in the oven. After cooling to room temperature the composite was washed thoroughly with ethanol to eliminate the unreacted species from the MOF/POM composite. Further it was driedto get HKUST-1incorporated with POM composite.

b. *Dye adsorption studies*

To optimise the composite's adsorption efficiency, several batch processes on MB were done, including pH effects, different dye concentrations, and various contact times with different adsorbent dosages each flask was allowed to shake in a mechanical shaker for various periods. After shaking, the solutions were centrifuged, and the supernatant solution was analysed using a UV-visible spectrophotometer at a maximum wavelength.

$$Q_e = (C_0 - C_e) \times V/m \qquad (1)$$

Where Qe is the equilibrium adsorption capacity (mg/g), C_0 is the initial concentration (mg/L) and C_e is the final concentration (mg/L).[25]

The removal efficiency is calculated with the formula

$$R\ \% = (C_0 - C_e) / C_0 \times 100\% \qquad (2)$$

R is the removal rate (%), V is the volume of dye solution (L), and m is the weight of the adsorbent (g).

III. Results and Discussion

i. *Characterization of HKUST-1/POM*

The morphology of the composite was characterized by FESEM and PXRD.

a. *FESEM*

The morphology of HKUST-1 is shown in Figure 1. resembles an octahedral structure. The length of each octahedron edge was around 5–20 µm, which was similar to that reported by H. Oliveira.,

b. *PXRD*

HKUST-1 structure was analysed with PXRD, Figure 2. Alsoit was compared with the previosly reported articl tThe diffraction peaks determine the structure's degree of crystallinity. This resultconfirms other works done by researchers such as S. Lin et al.,

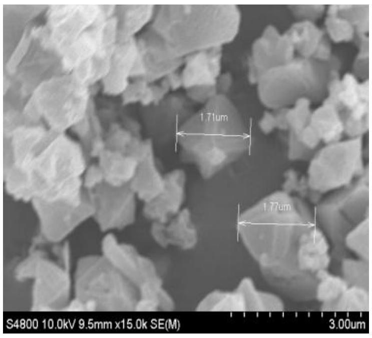

Fig 1. FESEM images of HKUST-1/POM

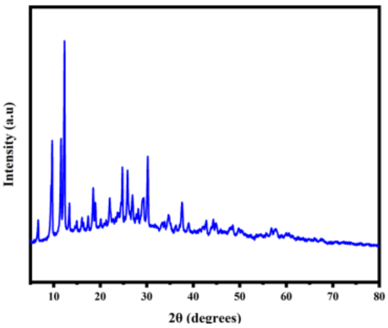

Fig 2. PXRD image of HKUST-1/POM

ii. *Dye adsorption studies:*

The composite was tested for the adsorption of MB with various parameters. The pH of the solution, dye concentration, adsorbent dosage, contact time, temperature and selectiveness of the adsorbent were tested.

iii. *Effect of pH*

To study the effect of pH the dyes were adjusted using 0.1N HCl or 0.1N NaOH solution. The pH range was kept from 2 to 12. 20 mL of dye with any concentration was taken in a conical flask with of the adsorbent. This solution is kept in shaking in a mechanical shaker for 1 hour each. After shaking, the solution was centrifuged.

iv. *Dye concentration*

The effect of dye concentration was studied by keeping the contact time, temperature(RT) and adsorbent dosageconstant. Different dye concentrations ranging from 20 ppm to 100 ppm were taken. The composite was observed to adsorb 100 ppm of MB in 40 minutes of shaking. Also, it can be noted that the adsorption takes place only at acidic pH. Figure 4shows the UV-visible adsorption spectrum of the effect of various dye concentrations.

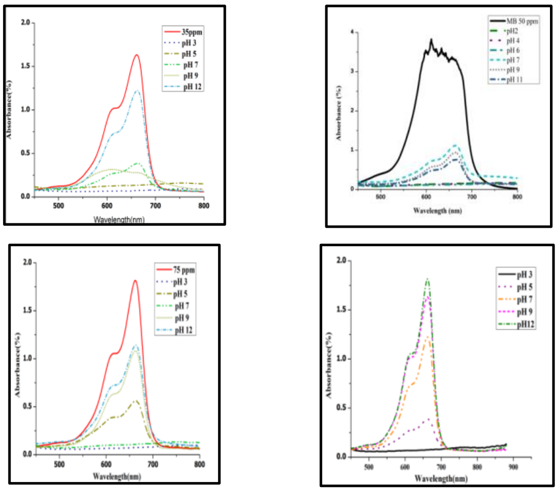

Fig 3. UV-VIS absorbance spectra - Adsorption of MB by HKUST-1/POM towards different concentrations of methylene blue under various pH ranges (a)35 ppm, (b) 50 ppm, (c) 75 ppm (d) 100 ppm

v. *Adsorbent dosage*

The effect of adsorbent dosage was studied at a fixed dye concentration of 100 ppm of 20 mL. Adsorption efficiency was maximized, thus, further increase in suspended solids would not considerably improve adsorption. Likewise, lower adsorbent dosages showed reduced dye removal due to insufficient sites.

vi. *Contact time*

The adsorption behaviour of methylene blue (MB) dye at different time intervals over a total duration of one hour (0 to 60 minutes). It has been shown that there is a continuous increase in the quantity of dye adsorbed with time, which indicates that the HKUST-1incorporated with AMHT composite efficiently removes the dye from the solution.

vii. *Temperature*

The effect of temperature is another critical factor influencing adsorption efficiency, as shown in Figure 7.

The adsorption studies were conducted at room temperature (RT), as well as below and above RT. The results show that the highest adsorption performance was achieved at room temperature. Increasing or decreasing the temperature below RT does not show any significant effect on the adsorption.

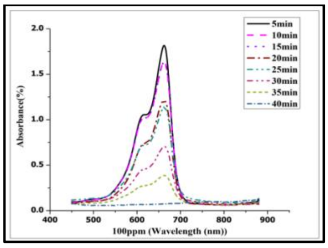

FIG 4. COMPARISON OF UV-VISIBLE SPECTRUM OF ADSORPTION OF 100 PPM OF MB ON 20 MG OF HKUST-1/POM AT DIFFERENT CONTACT TIMES

IV. CONCLUSION

The study showed that the use of the HKUST-1 incorporated with AMHT composite for adsorbing methylene blue from the aqueous solution has an adsorption capacity of 99.05 mg/g, with a removal efficiency of up to 98.65%. This outstanding performance is attributed to strong ionic interactions between methylene blue and polyoxometalates (POMs) in the composite, indicating an enhanced preference for dye molecules. These results revealed that HKUST-1 incorporated with AMHT is a potential and sustainable adsorbent for imaginable environmental remediation applied through wastewater treatment. This might be applicable in addressing organic pollutants, assuring cleaner resources for water and sustainable management of the environment.

V. ACKNOWLEDGMENT

This research was financially supported by the Thiagarajar Research Fellowship (TRF) scheme-dated (27.09.2024)

REFERENCES

[1] D. A. Yaseen and M. Scholz, "Textile dye wastewater characteristics and constituents of synthetic effluents: a critical review," *International Journal of Environmental Science and Technology*, vol. 16, no. 2, pp. 1193–1226, Nov. 2018, doi: 10.1007/s13762-018-2130-z.

[2] G. A. Ismail and H. Sakai, "Review on effect of different type of dyes on advanced oxidation processes (AOPs) for textile color removal," Chemosphere, vol. 291, p. 132906, Nov. 2021, doi: 10.1016/j.chemosphere .2021.132906.

[3] I. Khan *et al.*, "Review on Methylene Blue: Its properties, uses, toxicity and photodegradation," *Water*, vol. 14, no. 2, p. 242, Jan. 2022, doi: 10.3390/ w14020242.

[4] P. O. Oladoye, T. O. Ajiboye, W. C. Wanyonyi, E. O. Omotola, and M. E. Oladipo, "Ozonation, electrochemical, and biological methods for the remediation of malachite green dye wastewaters: A mini review," Sustainable Chemistry for the Environment, vol. 3, p. 100033, Aug. 2023, doi: 10.1016/j.scenv. 2023.100033.

[5] N. Bar and P. Chowdhury, "A brief review on advances in rhodamine B based chromic materials and their prospects," *ACS Applied Electronic Materials*, vol. 4, no. 8, pp. 3749–3771, Jul. 2022, doi: 10.1021/acsaelm. 2c00107.

[6] K. O. Iwuozor, J. O. Ighalo, E. C. Emenike, L. A. Ogunfowora, and C. A. Igwegbe, "Adsorption of methyl orange: A review on adsorbent performance," *Current Research in Green and Sustainable Chemistry*, vol. 4, p. 100179, Jan. 2021, doi: 10.1016/j.crgsc.2021.100179.

[7] M. Berradi*et al.*, "Textile finishing dyes and their impact on aquatic environs," *Heliyon*, vol. 5, no. 11, p. e02711, Nov. 2019, doi: 10.1016/j.heliyon.2019.e02711.

[8] E. Guerra, M. Llompart, and C. Garcia-Jares, "Analysis of Dyes in cosmetics: challenges and recent developments," *Cosmetics*, vol. 5, no. 3, p. 47, Jul. 2018, doi: 10.3390/cosmetics5030047.

[9] N. M. Hosny, I. Gomaa, and M. G. Elmahgary, "Adsorption of polluted dyes from water by transition metal oxides: A review," Applied Surface Science Advances, vol. 15, p. 100395, Mar. 2023, doi: 10.1016/j.envpol.2019.05.072.

[10] Z. U. Zango *et al.*, "Selective adsorption of dyes and pharmaceuticals from water by UiO metal–organic frameworks: A comprehensive review," *Polyhedron*, vol. 210, p. 115515, Oct. 2021, doi: 10.1016/ j.poly.2021.115515.

[11] K. F. Kayani, "Bimetallic metal–organic frameworks (BMOFs) for dye removal: a review," RSC Advances, vol. 14, no. 43, pp. 31777–31796, Jan. 2024, doi: 10.1039/d4ra06626j.

[12] Y. Zhou, J. Lu, Y. Zhou, and Y. Liu, "Recent advances for dyes removal using novel adsorbents: A review," *Environmental Pollution*, vol. 252, pp. 352–365, May 2019, doi: 10.1016/j.envpol.2019.05.072.

[13] L. Young, "Ligninase-catalysed decolorization of synthetic dyes," Water Research, vol. 31, no. 5, pp. 1187–1193, May 1997, doi: 10.1016/s0043-1354(96)00380-6.

[14] N. S. M. Imtiazuddin, N. M. Mumtaz, and N. K. A. Mallick, "Pollutants of wastewater characteristics in textile industries," *Journal of Basic & Applied Sciences*, vol. 8, no. 2, pp. 554–556, Oct. 2012, doi: 10.6000/1927-5129.2012.08.02.47.

[15] A. M. S. Jorge, K. K. Athira, M. B. Alves, R. L. Gardas, and J. F. B. Pereira, "Textile dyes effluents: A current scenario and the use of aqueous biphasic systems for the recovery of dyes," *Journal of Water Process Engineering*, vol. 55, p. 104125, Aug. 2023, doi: 10.1016/j.jwpe.2023.104125.

[16] N. Koprivanac, G. Bosanac, Z. Grabaric, and S. Papic, "Treatment of wastewaters from dye industry," *Environmental Technology*, vol. 14, no. 4, pp. 385–390, Apr. 1993, doi: 10.1080/09593339309385304.

Sustainable Hybrid UiO-66-NH_2 Integrated Mg-Al LDH Composite for Methylene Blue Adsorption

Arumugam Santhana Mariappana
Department of Chemistry,
Thiagarajar College of Engineering,
Madurai, Tamil Nadu
santhoshapsvs@gmail.com
asmntce@tce.edu

Bhaskaran Shankara
Department of Chemistry,
Thiagarajar College of Engineering,
Madurai, Tamil Nadu
bshankardu@gmail.com
bsrchem@tce.edu

***Abstract*—The removal of organic dyes from wastewater is a critical environmental challenge, necessitating the development of highly efficient and sustainable adsorbents. In this study, the hybrid UiO-66-NH2integrated Mg-Al LDH MOFs composite was synthesized and evaluated for its adsorption performance in removing MB from aqueous solutions. The structural and morphological properties of the composite were systematically characterized using, Powder X-ray Diffraction (XRD), Field Emission scanning electron microscopy (FESEM) analyses. The adsorption experiments demonstrated an impressive adsorption capability, highlights the superior performance of the composite. The synergistic effect of the high surface area, abundant active sites and layered structure contributed to enhance the dye uptake through hydrogen bonding and electrostatic interactions. This study establishes UiO-66-NH2integrated Mg-Al LDH MOF composites as a sustainable efficient material for wastewater treatments.**

Keywords—UiO-66-NH2, Metal organic frameworks, Layered Double hydroxide, Methylene blue removal, Wastewater treatment

I. INTRODUCTION

In recent decades, water pollution has emerged as a major global environmental issue, primarily driven by rapid urbanization and industrialization [1]. Industrial effluents often contain persistent and hazardous pollutants such as synthetic dyes, pharmaceuticals, and pesticides [2]. Synthetic dyes, widely used in textiles, paper, paints, leather, and cosmetics, include methylene blue (MB), rhodamine B (RhB), and methyl orange (MO). MB, a commonly used cationic dye, poses significant environmental and health risks, including organ toxicity, carcinogenicity, allergic reactions, and kidney damage [3]. Conventional wastewater treatment methods such as filtration, biological treatment, and chemical precipitation often fail to effectively remove dyes and may generate secondary pollutants [4].Adsorption has emerged as a leading technique for effectively removing dyes due to its facile process, cost-effectiveness,[5]. Traditional adsorbents like zeolites, metal oxides, activated carbons and metal organic frameworks (MOFs) have shown successful steps in dye removal application[6].

MOFs are a class of crystalline, porous coordination polymers known for their high surface area, tunable pore sizes, and structural flexibility, making them attractive candidates for targeted dye adsorption [7,8]. However, their practical application is often limited by poor scalability and low durability in aqueous environments. To address these limitations, recent studies have focused on incorporating two-dimensional (2D) materials into MOF structures [9]. Among these, layered double hydroxides (LDHs) have attracted attention due to their layered structure and interlayer anions, which enhance pollutant capture through electrostatic interactions and surface complexation [10]Hybrid materials that combine MOFs and LDHs offer the potential to synergistically enhance adsorption performance [11]UiO-66-NH_2, a zirconium-based MOFs functionalized with amino groups, exhibits strong electrostatic interactions and hydrogen bonding with dye molecules, making it effective for the adsorption process[12]. Mg-Al-based LDHs contribute chemical stability, anion exchange capacity, and environmental compatibility to the composite[13].

In this study, the facile and advanced UiO-66-NH_2 integrated Mg-Al LDH was synthesized and characterized systematically. The composite is explored for its efficiency in adsorbing MB from aqueous solutions. Further, this study investigates the various parameters influence the adsorption process such as pH, dosage, temperature and contact time. This work aims to evaluate the effectiveness of this adsorbent in wastewater treatment, particularly for real time effluents, while also assessing its potential environmental impacts.

II. EXPERIMENTAL SECTION

a. Synthesis of UIO-66-NH_2 MOF integrated Mg-Al LDH composite

Amine functionalized zirconium MOF (UiO-66-NH_2) was synthesized using previous procedures [14]. Mg-Al layered Double hydroxide were synthesized using co-precipitation method [15]. The pre synthesized UiO-66-NH_2 and Mg-Al LDH ratio were well dispersed in N, N-dimethylformamide and ultra sonicated followed by stirring. The product, UiO-66-NH_2 MOF integrated Mg-Al LDH composite was washed and dried.

b. Adsorption experiments toward MB

The adsorption performance of MB by UiO-66-NH_2/Mg-Al LDH was assessed by adding minimum amount of adsorbent to MB solution. The mixture was shaken at room temperature for an hour, followed by The supernatant was analyzed using a UV-Vis spectrophotometer at 664 nm. The adsorption capacity (Q_e) and removal efficiency (R%) were calculated accordingly.

$$Q_e = (C_0-C_e) \text{ x } V/m \quad (1)$$

$$R\ \% = (C_0-C_e) / C_0 \text{ x } 100\% \quad (2)$$

Where Q_e represents equilibrium adsorption capacity (mg/g), C_0 is the initial concentration (mg/L), C_e is the concentration at equilibrium time (mg/L), R represents removal rate (%), V is the volume of dye(L), and m is the weight of the adsorbent (g).

III. RESULTS AND DISCUSSION

1. Characterization techniques

a. Powder X-ray diffraction analysis

The powdered x-ray diffractogram of the UiO-66-NH_2 integrated Mg-Al LDH reveals prominent peaks corresponding to both the MOF and LDH phase. The peaks corresponding to UiO-66-NH_2 peaks [16] and LDH [17] were aligned with previous reports suggests successful integration of the LDH phase in the MOF framework as shown in Figure 1. Also, in the composite phase the MOF's primary peaks are observed with high intensity clearly suggests the phase purity of the composite at the same time the presence of LDH's prominent peaks indicating the structural integrity and crystallinity of the composite.

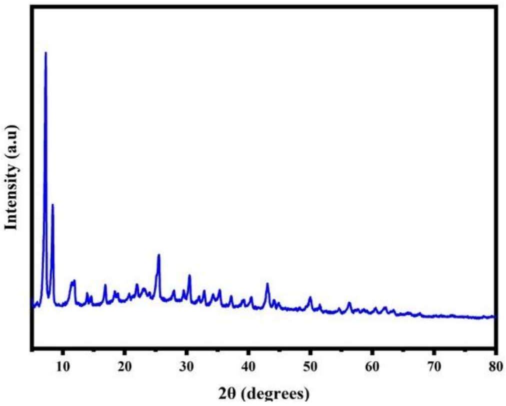

FIG 1. PXRD PATTERN OF UIO-66-NH_2 INTEGRATED MG-AL LDH

b. Field emission scanning electron microscopy

The FESEM images of UiO-66-NH_2 integrated Mg-Al LDH provides distinct morphological structure and surface texture of the composites. Specifically, the UiO-66-NH_2 exhibits its cube like morphology [16] and it can be well integrated with LDH matrix [17], actively enhancing the stability of the composite by forming agglomerated MOF-LDH surface. In agglomerated structures, the particles are cluster together potentially creating larger surface area and porosity which leads to potential adsorption capacity.

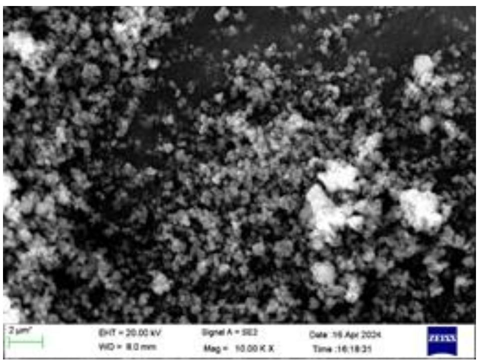

FIG 2. FESEM IMAGES OF UIO-66-NH_2INTEGRATED MG-AL LDH

2. Effects of Different Parameters

The adsorption performance of the UIO-66-NH_2/Mg-Al LDH composite was evaluated under varying pH, adsorbent dosage, temperature, and contact time, as shown in Figure 3(a–d)

a. *Effect of pH*

The pH of the dyes plays a crucial role in the adsorption process. The optimal adsorption capacity was found to be at pH 7 (neutral), where the highest removal efficiency was observed. In acidic conditions, the adsorption capacity is decreased significantly, due to the protonation of the active sites on the composite. Similarly, at the greater pH values, the adsorption efficiency is slightly decreased.

b. *Effect of Adsorbent dosage*

The dosage of the adsorbent was evaluated at a fixed concentration. The adsorption capability was found to be maximized at an adsorbent dosage of 20 mg. Increasing the dosage beyond this point did not significantly enhance the adsorption process. Similarly, lower adsorbent dosages also lead to reducethe dye removal due to insufficient active sites.

c. *Effect of Temperature*

The adsorption studies were conducted at room temperature (RT), as well as below and above RT. The results shows that the highest adsorption performance was achieved at room temperature. Below RT and elevated temperature, the adsorption efficiency decreased due to desorption effects and structural changes.

d. *Effect of contact time*

The adsorption of MB dye was monitored over different contact times, ranging from 0 to 100 minutes. The results demonstrate, the high adsorption capacity observed at the equilibrium time of 60 minutes. Beyond this, the adsorption capacity is started to decreasing, possibly due to the saturation of active sites.

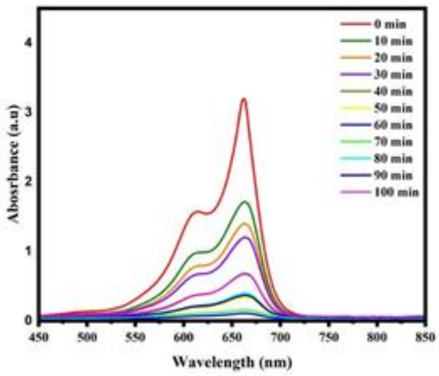

FIG 3. UV-VIS ABSORBANCE SPECTRA - ADSORPTION CAPACITY TOWARDS DIFFERENT CONTACT TIME

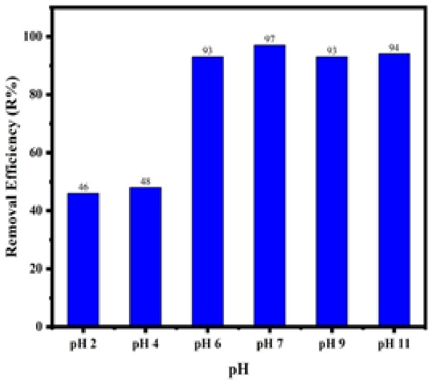

FIG 4. REMOVAL EFFICIENCY AT DIFFERENT AT DIFFERENT PH

IV. CONCLUSION

This study focused on UiO-66-NH_2integrated Mg-Al LDH composite is an efficient adsorbent for the removal of methylene blue with a high adsorption capacity of 98.4 mg. g-1 and removal efficiency of 97.5%. The adsorption process is consistent with the pseudo-second order kinetics, suggests that adsorption is likely chemisorption of the dye onto the MOF/LDH surface due to the strong interaction between dye and MOF/LDH structure. The results show the ability of UiO-66-NH_2 integrated Mg-Al LDH, a facile and sustainable adsorbent for the advanced environmental remediation technologies.

V. ACKNOWLEDGMENT

This research was financially supported by the Science and Engineering Research Board under SERB-SRG grant (Grant No: SRG/2022/001193) and Thiagarajar research Fellowship (TRF) scheme dated 01.03.2025

REFERENCES

[1] S. Dutta, B. Gupta, S. K. Srivastava, and A. K. Gupta, “Recent advances on the removal of dyes from wastewater using various adsorbents: a critical review,” *Materials Advances*, vol. 2, no. 14, pp. 4497–4531, Jan. 2021.

[2] G. Murtaza *et al.*, “Efficient Adsorption of Methylene Blue Using a Hierarchically Structured Metal–Organic Framework Derived from Layered Double Hydroxide,” *ACS Omega*, vol. 9, no. 14, pp. 16334–16345, Mar. 2024.

[3] M. A. M. Salleh, D. K. Mahmoud, W. A. W. A. Karim, and A. Idris, “Cationic and anionic dye adsorption by agricultural solid wastes: A comprehensive review,” *Desalination*, vol. 280, no. 1–3, pp. 1–13, Aug. 2011.

[4] M. A. Qamar *et al.*, “Progress in the development of phyto-based materials for adsorption of dyes from wastewater: A review,” *Materials Today Communications*, vol. 38, p. 108385, Feb. 2024.

[5] J. Zhang, F. Li, and Q. Sun, “Rapid and selective adsorption of cationic dyes by a unique metal-organic framework with decorated pore surface,” *Applied Surface Science*, vol. 440, pp. 1219–1226, Feb. 2018.

[6] A. K. Badawi, M. A. Elkodous, and G. a. M. Ali, “Recent advances in dye and metal ion removal using efficient adsorbents and novel nano-based materials: an overview,” *RSC Advances*, vol. 11, no. 58, pp. 36528–36553, Jan. 2021.

[7] M. J. Uddin, R. E. Ampiaw, and W. Lee, “Adsorptive removal of dyes from wastewater using a metal-organic framework: A review,” *Chemosphere*, vol. 284, p. 131314, Jun. 2021.

[8] Y. Zhou, J. Lu, Y. Zhou, and Y. Liu, “Recent advances for dyes removal using novel adsorbents: A review,” *Environmental Pollution*, vol. 252, pp. 352–365, May 2019.

[9] M. N. Afridi *et al.*, “Progress, challenges, and prospects of MOF-based adsorbents for phosphate recovery from wastewater,” *Journal of Water Process Engineering*, vol. 63, p. 105530, May 2024.

[10] A. Chakraborty and H. Acharya, “ZnAl–LDH/MOF-5 heterostructure nanocomposite for photocatalytic degradation of organic dyes under sunlight irradiation,” *New Journal of Chemistry*, vol. 47, no. 3, pp. 1498–1507, Dec. 2022.

[11] X. Hu, W. Zheng, M. Wu, L. Chen, and S. Chen, “Composites of metal-organic frameworks (MOFs) and LDHs for energy storage and environmental applications: Fundamentals, progress, and perspectives,” *Sustainable Materials and Technologies*, vol. 37, p. e00691, Aug. 2023.

[12] J.-H. Wang, F. Kong, B.-F. Liu, S.-N. Zhuo, N.-Q. Ren, and H.-Y. Ren, “Photogenerated carrier-accelerated 3D mesh-NH2 functionalized Zr-metal organic framework/MgAl-type hydrotalcite composites attacking diclofenac,” *Separation and Purification Technology*, vol. 354, p. 128839, Jul. 2024.

[13] A. Sun *et al.*, “In situ preparation of novel p–n junction photocatalyst MgAl-LDH/(BiO)2CO3 for enhanced photocatalytic degradation of tetracycline,” *Materials Science in Semiconductor Processing*, vol. 150, p. 106939, Jul. 2022.

[14] S. Subudhi, G. Swain, S. P. Tripathy, and K. Parida, “UiO-66-NH2 Metal–Organic Frameworks with Embedded MoS2 Nanoflakes for Visible-Light-Mediated H2 and O2 Evolution,” *Inorganic Chemistry*, vol. 59, no. 14, pp. 9824–9837, Jul. 2020.

[15] T. Baskaran, R. Kumaravel, J. Christopher, and A. Sakthivel, “Silicate anion-stabilized layered magnesium–aluminium hydrotalcite,” *RSC Advances*, vol. 3, no. 37, p. 16392, Jan. 2013.

[16] J. Ren *et al.*, “Construction of efficient g-C3N4/NH2-UiO-66 (Zr) heterojunction photocatalysts for wastewater purification,” *Separation and Purification Technology*, vol. 274, p. 118973, May 2021.

[17] R.-R. Shan *et al.*, “Highly efficient removal of three red dyes by adsorption onto Mg–Al-layered double hydroxide,” *Journal of Industrial and Engineering Chemistry*, vol. 21, pp. 561–568, Mar. 2014.

Advancements and Future Directions in Perishable Food Supply Chain Management: A Literature Review

T. Karthikeyan
Full-time Research Scholar, Mechanical Engineering,
Thiagarajar College of Engineering,
Madurai, India.
karthikeyanthangam007@gmail.com

PL. K. Palaniappan
Professor, Mechanical Engineering,
Thiagarajar College of Engineering,
Madurai, India.
kpal@tce.edu.in

Abstract*—Perishable Food Supply Chain Management, (PFSCM), is inevitable for making sure our food is safe and fresh. It helps to cut down food waste and boosts sustainability [1,3]. This literature review explores recent advancements (2010-2024) in PFSCM, highlighting key trends, methodologies, and future research directions. It mainly focuses on Temperature monitoring in Cold Chain Logistics [19,38], Implementation of Artificial Intelligence (AI) & Internet of Things (IoT) [28,40], Supply Chain Optimization (SCO) and Inventory Management [5,35], Sustainability & Perishable Food Waste [6,33]. Recent findings show that automation, IoT-enabled monitoring [20,29], and AI-driven decision-making [26,39] are becoming bigger players in making PFSCM better. This work focuses on making a summary of the literature on PFSCM, finding the research gap and to propose directions for future research in this ever-growing area. Findings revealed that Data analysis in managing PFSCM uses modern technologies such as radio frequency identification (RFID) [21], internet of Things (IoT), wireless sensors [32], data- driven information technology (IT) systems. Cold chain infrastructure is vital for keeping food safe and fresh [56]. Even though India is one of the top five producers of perishable food, it still faces a lot of issues. Digitization using information and communication technology systems (ICT) is the recent trend in PFCSM and possess a huge scope for future research to adopt new technologies [1]. Future research should use AI for logistics and supply chain management to make supply networks more robust and sustainable [39,51].

Keywords—perishable food supply chain management (PFSCM), sustainable, cold chain logistics.

I. INTRODUCTION

Perishable food supply chain management (PFSCM) seeks to mitigate food risks, reduce waste, and encourage environmental responsibility within the global food supply chain [6,33]. The adoption of the digital technologies such as big data analytics, Artificial Intelligence (AI) and the Internet of Things (IoT) has significantly transformed the management and efficiency of Perishable food supply chain management (PFSCM) [14,28]. New challenges and opportunities in circular supply chains and sustainability have also added to this complexity [9,31]. This paper will review the recent advancements in Perishable food supply chain management (PFSCM) from 2010-2024, focusing on the emerging trends, approaches, and potential areas for future research.

The framework of the paper proposes a series of research questions (RQs) and seeks to answer them.

RQ1. Which factors impact the supply chain for perishable food? and how we manage the supply chain for perishable food? [3,38]

RQ2. What are the modern methods being used for perishable products? [16,39]

RQ3. What are the gaps in research and what areas should we focus on in the future? [32,55]

The next section discusses the existing literature reviews in the area of PFSCM

II. LITERATURE SURVEY

The supply chain for perishable food is changing fast. Modern technology like digital tools and big data is playing a big part in this shift. Experts say that using predictive analytics and AI can help manage inventory better and cut down on food waste [5,26]. Studies show that IoT sensors and block-chain can help trace food in real-time [14,40]. This is key for keeping food safe and meeting regulations. A big focus now is sustainability. People are looking into eco-friendly packaging and ways to share excess food. However, there are still issues [37,43]. It’s tough to make all the digital tools work together and follow regulations. Plus, we haven't fully figured out how to use AI in cold chains or create a common block-chain framework [26,59]. There’s also more to learn about how the circular economy affects food supply. Future research needs to tackle these challenges to build a stronger, smarter, and greener food supply system.

This section of paper explains comprehensive scheme for literature review of PFSCM in three subsections.

Time period: As the momentum of PFSCM research starts from 2010, the periods (2010-2024) are considered for review. The published collected articles are considered for consolidation in perishable food supply chain management.

Selection of database: The articles were collected from SCI Papers (Science Direct, Taylor & Francis, Emerald Insights, Emerald Publishing and Wiley, Sage Publication) for critical review of perishable food supply chain quality.

Material Collection: Major Key terms for perishable food supply chain, cold supply chain, cold chain logistics, food supply chain, modern approaches on Perishable food supply chain management (PFSCM), modern technologies on Perishable food supply chain management (PFSCM).

III. METHODOLOGY

This review looks at research articles from 2010 to 2024. These articles are in top databases like Science Direct, Wiley, Taylor & Francis, and Emerald. This work is focused on key aspects:

- Studies that deliberated problems and solutions in PFSCM [3,6,38].
- Articles that included digital tools like AI and big data analytics [26,28,39].
- Papers that observed sustainability and circular economy practices [9,31,33].

The literature was categorized into key themes to make it a comprehensive analysis. The bibliometric analysis is done with 59 key reference papers and the output is depicted as bibliography as shown in Figure 1.

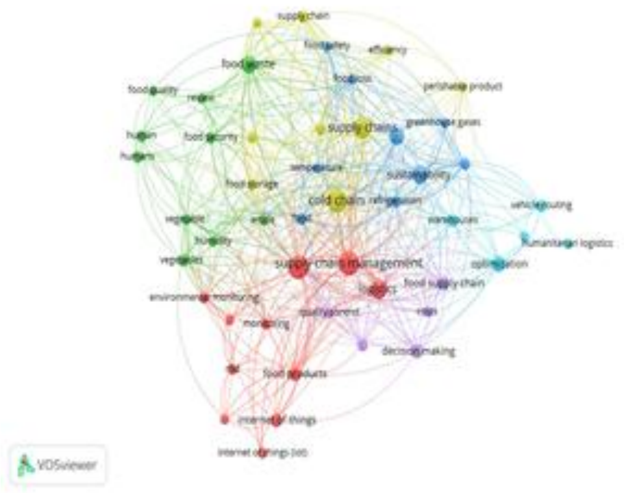

FIG 1: BIBLIOMETRIC ANALYSIS

The methodology is depicted in the flowchart shown in Figure 2.

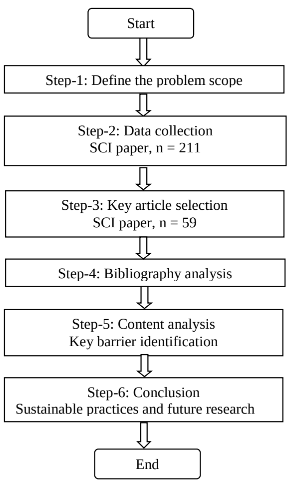

FIG 2: FLOWCHART ON RESEARCH PROCESS

3.1 Major themes in Perishable food supply chain management (PFSCM) research

3.1.1 Temperature Monitoring in Cold Chain Logistics (CCL)

Temperature monitoring is key for keeping food safe and fresh. Use RFID [21,29], wireless sensors [20,32], and other systems to monitor temperatures in real-time and to improve the shelf life of perishable goods is inevitable in Cold Chain Logistics [6,54].

3.1.2 Implementation of Artificial Intelligence (AI) & Internet of Things (IoT)

Modern technologies brought significant changes in the management of perishable food supply chain. Key technologies include:

a. IoT and RFID: Support to track and monitor food in real-time [21].

b. AI and Machine Learning: Improve the ability to predict demand and perform maintenance on equipment [26,39].

c. Blockchain: Make the supply chain more transparent and prevents food fraud [14,48].

3.1.3 Supply Chain Optimization (SCO) and Inventory Management

AI-based optimization models are essential for making the supply chain run better. It helps to control inventory and cut down on food waste by looking at demand patterns and stopping overproduction with AI forecasting models [5,35].

3.1.4 Sustainability & Perishable Food Waste

The idea behind circular supply chains is to reduce food waste and use resources effectively. Innovations like eco-friendly packaging [31,44], sharing of surplus food, and using energy-efficient storage promotes sustainability. Research emphasis that closed-loop systems are becoming more common to improve the sustainability of food logistics [9,33].

3.1.5 Energy Efficiency

New food management systems are designed to reduce food waste and reduce energy consumption. Significance researches are done to explore energy consumption in the sustainable cold chain, cold retention approaches, use of renewable energy [10,47], and Eco-friendly strategies for cold chain logistics [7,19].

3.1.6 Humanitarian Logistics and Food Rescue

Reducing food waste is a big goal in Perishable Food Supply Chain Management (PFSCM). Recent studies show that smart packaging, food redistribution networks [37,43], and AI-driven waste prediction can help make the system more sustainable and efficient [43].

3.1.7 Regulatory Framework and Policy Fabrics in Perishable Logistics

Government rules and regulations are crucial for keeping food safe and sustainable in PFSCM. Various studies have looked at how effective food safety standards [48], global trade laws [42], and compliance systems are at maintaining the integrity of the supply chain [38,58].

TABLE 3.1. IDENTIFICATION OF RESEARCH GAP 2010-2024

Research area	Author (year)	Summary of Literature	Research Gap
Temperature monitoring and Cold Chain Logistics (CCL)	Laniel (2010) Ruiz-Garcia (2010) Kuo (2010) Castro (2012) Jedermann (2017) Mercier (2017 & 2018) Goransson (2018) Ndhara (2018) Mejjaouli (2018) Torres- Sánchez (2020)	Technologies like Radio-frequency identification (RFID, wireless sensors, Multi-Temperature Joint Distribution (MTJD), Tracking, Tracing and Monitoring (TTM), Remote Container Monitoring (RCM), full-time temperature monitoring system, Wi-Fi wireless communication are used for effective cold chain. Management.	Norms for the use of Temperature monitoring techniques for maximizing shelf life of perishable foods is not well established.
Implementation of Artificial Intelligence (AI) & Internet of Things (IoT)	Nakandala (2016) Kong (2016) Bogatai (2017) Kant (2017) Zhang (2017) Verdouw (2018) Pal (2019) Rejeb (2021) Bhutta (2021) Vernier (2021) Baziyad (2022) Liu (2023)	Examine research on perishable logistics using the application of Artificial Intelligence (AI), Internet of things (IoT), and block-chain, Physical Internet (PI), Internet of Perishable Logistics (IoPL), extended material requirements planning (EMRP) model, Wireless Sensor Networks (WSN), Information and communication technologies (ICTs), phase change materials (PCMs) for automation to real-time tracking and predictive analytics is addressed .	Further investigation is required on measures of scalability, risk factors, and cost-effectiveness analysis of AI and IoT-driven cold chain logistics.
Supply Chain Optimization (SCO) and Inventory Management	Aiello (2012) Hertog (2014) Accorsi (2018) Bhatia (2020)	Monte Carlo simulation based optimization model, warehouse management systems, bi-objective integer programming model and integrated model are developed. First expired in first out (FEFO) based inventory management are proposed.	Research needs Artificial Intelligence-based and Supply Chain Optimization (SCO) models focusing on sustainable development goals.
Sustainability & Perishable Food Waste	Sawaya (2017) Spagnol (2018) Begue (2019) Shareef (2020) Kumar (2020) Rossi (2021) Marchi (2022) Chen (2022) Trottet (2022) Du (2023) Sultan (2023)	Emphasis is given for low-temperature environment to maintain the quality and safety of perishable food and reduce food loss and waste (FLW). Integrated interpretive structural modelling–analytic network process (ISM–ANP) decision framework, life cycle assessment (LCA, dielectric barrier discharge plasma (DBD) are used to achieve waste reduction and sustainable food distribution	Deficiencies of research papers on Artificial intelligence-based prophetic/predictive models to reduce food spoilage. Further studies are needed on regulatory fabrics for sustainable practices.
Energy Efficiency	Huang (2017) Behdani (2019) Fan (2021) Maiorino (2021) Marchi (2022)	Explored energy consumption in the sustainable cold chain, cold retention approach, renewable energy, and Eco-friendly strategies for cold chain logistics.	Further studies required on the solar-based and hydrogen powers refrigeration solutions need logistics
Humanitarian Logistics and Food rescue	Philip (2017) Ghadge (2017) Rey (2018) Ferreria (2018) Eisenhandler (2019)	Analyzed food redistribution, food bank optimization, and equitable sharing models for retrieved perishables using Artificial intelligence (AI) and vehicle routing optimization	Essential research of food rescue logistics for real-time integration and last-mile delivery using drone-based food delivery need further exploration.

	Rahidzadeh (2021) Kuhn (2021) Tiwari (2023) Ozarik (2023)		
Regulatory Framework and Policy Fabrics in Perishable Logistics	Mercier (2018) Bremer (2018) Behdani (2019) Chen (2022)	Trade policies, farmer and food safety standards, and global logistics regulations are deliberated.	Needs standardized global policies for perishable goods logistics and the impact of carbon taxation, subsidies, and trade regulations in different regions.

IV. Discussion

Low integration of AI-driven automation within cold chain logistics. Underdeveloped frameworks for implementing IoT technology in perishable food supply chain management (PFSCM). Insufficient research on circular economy models specifically applied to perishable food logistics despite significant advancements, several barriers remain in the field as listed below:

1. Lack of infrastructure and deficiencies such as ineffective cold chain systems, inconsistent electricity supply, insufficient transportation networks and limited internet access in rural areas impede the deployment of IoT and block chain technologies [1, 55].
2. The high upfront cost of IoT sensors, AI software and block chain platforms is unaffordable for small-scale farmers and SMEs [40, 55].
3. Lack of technical expertise and a limited workforce skilled in AI, IoT and block chain technologies [14, 31].
4. Regulatory and policy gaps exist in the absence of standardized protocols for integrating Information and Communication Technologies (ICT) and government incentives for technology adoption [1, 55].
5. Data privacy and security concerns such as mistrust in data-sharing mechanisms and vulnerabilities in block chain IoT networks [14].
6. Cultural and organizational changes are needed to shift from traditional practices to technology-driven processes [40, 55].

V. Conclusion

The importance of digitalization [28], big data analytics [26], and circular supply chains in promoting PFSCM is emphasized in this paper [9,33]. Efficiency is increased by modern technology, yet issues with automation, sustainability, and traceability still exist. In order to increase the resilience of perishable food supply chains, future research should concentrate on integrating AI, block-chain, and policy-driven sustainability frameworks [55,58]. Research on perishable food supply chains can be closely examined. The majority of food waste in developing nations occurs when the product is being harvested, stored, or transported due to poor infrastructure and misaligned processes in the broken supply chain and meager warehousing facilities [33,55].

VI. Future Research Directions

Future studies should concentrate on AI-based smart cold chain management. IoT technology for traceability and transparency establishing industry-wide standards. Development of Policy recommendations for sustainable Perishable food supply chain management (PFSCM) addressing regulatory gaps and promoting environmentally friendly practices. The following is a list of upcoming trends: RFID and WSN-based systems are proposed for data collection and quantification [20,29], while IOT-based monitoring systems are needed for effective supply chain management. Improved project planning, effective risk management strategies, integrated supply chains, IT-enabled hub-based pooled procurements, and multi-level cluster development are needed for effective Perishable food supply chain management PFSCM [45,52]. Future research topics may include alliance of contract farming [5,39], organized retailing and development of cold supply chains through public-private partnerships.

References

[1] Vernier, C., Loeillet, D., Thomopoulos, R. and Macombe, C., 2021. Adoption of ICTs in agri-food logistics: Potential and limitations for supply chain sustainability. Sustainability, 13(12), p.6702.

[2] Chen, C., Feng, Y., Chen, Z., Xia, Y., Zhao, X., Wang, J., Nie, K., Niu, P., Han, J. and Xu, W., 2022. SARS-CoV-2 cold-chain transmission: Characteristics, risks, and strategies. Journal of Medical Virology, 94(8), pp.3540-3547.

[3] Maiorino, A., Petruzziello, F. and Aprea, C., 2021. Refrigerated transport: State of the art, technical issues, innovations and challenges for sustainability. Energies, 14(21), p.7237.

[4] Du, Y., Mi, S., Wang, H., Yang, F., Yu, H., Xie, Y., Guo, Y., Cheng, Y. and Yao, W., 2023. Inactivation mechanism of Alternaria alternata by dielectric barrier discharge plasma and its quality control on fresh wolfberries. Food Control, 148, p.109620.

[5] Kuhn, H., Schubert, D. and Holzapfel, A., 2021. Integrated order batching and vehicle routing operations in grocery retail–a general adaptive large neighborhood search algorithm. European journal of operational research, 294(3), pp.1003-1021.

[6] Chen, Q., Qian, J., Yang, H. and Wu, W., 2022. Sustainable food cold chain logistics: From microenvironmental monitoring to global impact

Comprehensive reviews in food science and food safety, 21(5), pp.4189-4209.

[7] Fan, Y., de Kleuver, C., de Leeuw, S. and Behdani, B., 2021. Trading off cost, emission, and quality in cold chain design: A simulation approach. Computers & Industrial Engineering, 158, p.107442.

[8] Tiwari, K.V. and Sharma, S.K., 2023. An optimization model for vehicle routing problem in last-mile delivery. Expert Systems with Applications, 222, p.119789.

[9] Sultan, F.A., Routroy, S. and Thakur, M., 2023. Understanding fish waste management using bibliometric analysis: A supply chain perspective. Waste Management & Research, 41(3), pp.531-553.

[10] Marchi, B. and Zanoni, S., 2022. Cold chain energy analysis for sustainable food and beverage supply. Sustainability, 14(18), p.11137.

[11] Özarık, S.S., Lurkin, V., Veelenturf, L.P., Van Woensel, T. and Laporte, G., 2023. An adaptive large neighborhood search heuristic for last-mile deliveries under stochastic customer availability and multiple visits. Transportation Research Part B: Methodological, 170, pp.194-220.

[12] Adams, R.M., Evans, C.M. and Peek, L., 2024. Defining, collecting, and sharing perishable disaster data. Disasters, 48(1), p.e12592.

[13] Trottet, A., George, C., Drillet, G. and Lauro, F.M., 2022. Aquaculture in coastal urbanized areas: A comparative review of the challenges posed by Harmful Algal Blooms. Critical Reviews in Environmental Science and Technology, 52(16), pp.2888-2929.

[14] Rejeb, A., Rejeb, K., Simske, S. and Treiblmaier, H., 2021. Blockchain technologies in logistics and supply chain management: a bibliometric review. Logistics, 5(4), p.72.

[15] Rashidzadeh, E., Hadji Molana, S.M., Soltani, R. and Hafezalkotob, A., 2021. Assessing the sustainability of using drone technology for last-mile delivery in a blood supply chain. Journal of Modelling in Management, 16(4), pp.1376-1402.

Carbon-Based MoS_2 Composites as Electrode Materials for Supercapacitors: A Comprehensive Review

S. Hemapriya
Department of Physics,
Thiagarajar College of Engineering,
Madurai, Tamil Nadu, India.
shemapriya@student.tce.edu

P. Velusamy
Department of Physics,
Thiagarajar College of Engineering,
Madurai, Tamil Nadu, India
pvphy@tce.edu

***Abstract*—Dichalcogenides play a crucial role in supercapacitors and are inevitable in this era of electrical and electronic devices. They are well known for their high surface area, excellent electrical conductivity and mechanical flexibility, thermal and chemical stability. Specifically, the transition metal dichalcogenides (MoS_2, WS_2, TiS_2, NbS_2, VS_2, $MoSe_2$, WSe_2, ZrS_2) refer to their unique electrical and catalytical property which plays a vital role in the application of energy storage. Especially Molybdenum disulfide (MoS2) has a layered structure with weak Van der Waals force between the layers. To enhance the electrochemical properties of these materials, cope with the synergistic method. For this method, the preference must revolve around carbon-based materials like Carbon nanotube (CNT), Carbon nanosphere(CNS), Reduced Graphene Oxide(rGO), etc. In this article, a review of the prerogative tendency of carbon materials toward the energy storage system in the presence of MoS_2will be elicited.**

Keywords—Dichalcogenides, Molybdenum disulfide, Carbon-based materials, Energy storage.

I. Introduction

To attain sustainable energy consumption, we need renewable energy storage systems. Considering fossil fuels for this enormous energy requirement situation, the greenhouse effect plays monument damage to the environment. This crisis initiated the development of more capable energy storage devices such as batteries and supercapacitors. From the property of high power density, long cyclic life, quick charge/discharge cycles, and simple mode of operation, the supercapacitors enlarge their attributes in the energy storage field[1]. Discussion about supercapacitors involves the types that make evolution in this field. They are (i) Electric double-layer capacitors (EDLC), (ii) Pseudo capacitors, and (iii) Hybrid capacitors. Generally speaking, the specific capacitance and charge accumulation capacity increase with the specific surface area of carbon. The practical use of EDLC is significantly hampered in several situations where a high energy density is required since specific capacitances derived from carbon materials are typically substantially lower than anticipated[2]. A pseudo capacitor is an electrochemical capacitor that uses redox (faradaic) reactions to store energy. It increases capacitance by including charge transfer reactions at the electrode surface, in contrast to EDLCs. Transition metal oxides (RuO_2 and MnO_2) and conducting polymers (polyaniline and polypyrrole) are common materials. greater energy density than EDLCs because of faradaic charge storage. It offers greater energy density and capacitance than EDLCs, although its charge-discharge speeds are slightly slower. By combining these two, a hybrid was created. This capacitor3 greatly enhanced the supercapacitor's performance. The caliber of the electrode materials used significantly impacts hybrid supercapacitors' functionality. Among the wide variety of possible materials, primarily because of their capacity to promote several redox reactions, which allows them to attain a high specific capacity[4]. Among the various fabrication methods, the template technique has emerged as the most effective for precisely controlling pore size distribution despite its relatively high cost. This approach has significantly advanced supercapacitor performance by highlighting the role of small mesopores and their interconnectivity in rapid charge transport. It also emphasizes the importance of ultra-micropores for efficient charge accumulation[5]. Hybrid supercapacitors' performance heavily depends on the quality of the electrode materials employed. Among various candidates, battery-type electrode materials have gained significant research attention due to their ability to undergo multiple redox reactions, enabling them to deliver high specific capacity. These materials primarily include transition metal-based compounds such as oxides (TMOs), hydroxides, sulfides (TMSs), and selenides (TMSes), which exhibit rich electrochemical activity. Despite their advantages, the practical application of these materials is often hindered by inherent drawbacks, including limited specific capacity, sluggish charge transfer kinetics, and poor electronic conductivity. Additionally, structural instability during prolonged cycling and challenges in achieving high-rate performance further restrict their widespread adoption in energy storage systems[4].Transition metal dichalcogenides (TMDs) are considered promising materials for supercapacitor applications due to their unique structural properties and ease of synthesis. Among them, MoS_2 has garnered significant research interest over the past two decades owing to its graphite-like layered structure and the broad range of molybdenum oxidation states (+2 to +6), contributing to its versatile electrochemical behavior[1]. Transition metal sulfide MoS_2, with its layered structure composed of covalently bonded S–Mo–S sheets separated by weak van der Waals interactions, has gained significant attention due to its diverse potential applications. It has been explored for electrochemical hydrogen storage, solid super lubricants, solid-state secondary lithium battery cathodes, magnesium batteries, and as an industrial catalyst for hydrodesulfurization in crude oil processing[6].Due to their exceptional electrochemical properties, two-dimensional (2D) nanosheets of transition-metal dichalcogenides (TMDs), particularly MoS_2, have demonstrated great potential in various applications, including hydrogen evolution, lithium-ion batteries, solar cells, and supercapacitors when combined with conducting materials. MoS_2 can effectively store charge through pseudocapacitance within a positive potential window, either via a faradaic charge-transfer process at the Mo center (a slower process) or through double-layer formation at the electrode/electrolyte interface due to proton or cation adsorption on the MoS_2 nanosheet (a faster process). These charge storage mechanisms make MoS_2 an auspicious anode material for asymmetric supercapacitors[7]. Various morphologies of MoS_2, including nanospheres, nanotubes, and flower-like structures, have been synthesized. Despite its remarkable properties, MoS_2 faces challenges such as low electrical conductivity and rapid layer restacking due to weak Van der Waals interactions. These limitations can be mitigated by incorporating carbon-based materials into the MoS_2 matrix, which enhances electrical conductivity and improves overall performance[1]. This article discusses combining carbon-based materials with MoS2, such as doping, compounds, and composites.

II. SYNTHESIS

Most researchers employ the bottom-up approach to fabricate these MoS_2 nanostructures and their composites. In particular, three methods have been instrumental in obtaining high-quality nanomaterials: (i) Hydrothermal synthesis, (ii) Chemical Vapor Deposition (CVD), and (iii) Thermal Condensation. Lijian Wang et al. synthesized MoS_2@HCNB (Hollow Carbon Nano Bowl) and HCNB@MoS_2 using two distinct methodologies. In the first case, MoS_2@HCNB was produced through a one-pot Thermal Polymerization process, while for HCNB@MoS_2, the Solvothermal method was adopted to achieve superior results[8]. Tobile N. Y. et al. successfully prepared Spherical MoS_2, Flower-like MoS_2, Carbon Nanospheres, and their composites utilizing the Hydrothermal method[9]. Kemeng Yang et al. synthesized Hollow Carbon Spheres (HCS) via the Thermal Condensation method, followed by the Hydrothermal process for MoS_2@HCS fabrication [10]. Karthi Sekar et al. employed the conventional Hummer's method for Reduced Graphene Oxide (rGO) synthesis, which was further nitrogen-doped. The composite structure, consisting of 3D-MoS_2 nanospheres and N-GQDs anchored with rGO, was synthesized usingthe Hydrothermal technique[11]. Several researchers, including Poe Ei Phyu Win et al., Yongfeng Luo et al., Ming Chen et al., Tian Lv et al., and Honey Gupta et al., adhered to the Hydrothermal method for CNT@MoS_2 composite synthesis [12–16]. Likewise, Liping Zheng et al., Tsung-Wu Lin et al., and Weiwei Liu et al. employed the Hydrothermal approach to fabricate MoS_2@MHCSs (Mesoporous Hollow Carbon Nanospheres)[17–19]. Xingliang Chen et al. utilized the Hydrothermal method to develop Fe_3O_4@C nanospheres and FeS_2@C@MoS_2 composite hybrids[20]. Le-Qing Fan et al. also synthesized MoS_2/C composites using the Hydrothermal process. Meanwhile, Kien-Cuong Pham et al. prepared Graphene Carbon Nanotube (GCNT) hybrids via CVD and deposited MoS_x onto the GCNT/CP structure through Electrodeposition[22]. Pengqian Guo et al. and Devalina Sarmah et al. employed the Self-Assembly method to fabricate MoS_2@NC (Nitrogen-doped Carbon) spheres and MoS_2-rGO/PEDOT nanocomposites, respectivel. Following this, Ke-Jing Huang et al. synthesized MoS_2/MWCNT (Multi-Walled Carbon Nanotube) composites via the Hydrothermal method[25]. V. O. Koroteev et al. developed vertically aligned Multi-Walled Carbon Nanotubes (MWCNTs) using CVD, which were subsequently coated with MoS_2 nanoparticles through the Hydrothermal technique[26]. Similarly, Wei Xiao et al. and M. Murugan et al. synthesized MoS_2@rGO via the Hydrothermal method[27,28]. Jagdees Prasad et al. prepared Graphite Oxide using Staudenmaier's method, followed by the Hydrothermal approach for CNT/MoS_2-rGO nanohybrid synthesis[29]. Hydrothermal synthesis is the most widely employed method for MoS_2 composite fabrication due to its efficiency and scalability.

III. PERFORMANCE

A hydrothermally synthesized MoS_2/carbon (C) nanocomposite utilizing candle soot-derived carbon exhibited a high specific capacitance of 452.7 F/g at 1 A/g in a 3 M KOH electrolyte. The asymmetric supercapacitor (MoS_2/C // C) demonstrated 100% capacitance retention over 10,000 cycles, highlighting its remarkable stability and potential for scalable energy storage applications.Flower-like MoS_2 nanospheres synthesized via a hydrothermal method exhibited a specific capacitance of 122 F/g at 1 A/g in 1 M KCl. The unique morphology, characterized by uniform 300 nm-sized nanospheres, enhances the active surface area and ion diffusion pathways, contributing to improved electrochemical performance.Electrostatically assembled MoS_2-reduced graphene oxide (rGO)/multi-walled carbon nanotube (MWCNT) hybrid fibers demonstrated a volumetric capacitance of 4.8 F/cm³ at 6.3 wt% MoS_2. The composite maintained 3.8 F/cm³ at higher current densities, showcasing its superior electrical conductivity and mechanical flexibility, making it suitable for solid-state and wearable energy storage devices.A template-assisted synthesis method enabled the confined growth of MoS_2 within hollow carbon nano bowls (HCNBs), yielding a specific capacitance of 560 F/g at 0.2 A/g and a volumetric capacitance of 874 F/cm³. The semi-concave structure facilitated enhanced ion diffusion and charge transfer, with an impressive 94.4% retention after 5000 cycles.

Hydrothermally synthesized MoS_2/CNS composites exhibited morphology-dependent performance, with flower-like structures achieving 231 F/g, 26 Wh/kg energy density, and 6443 W/kg power density. In contrast, spherical MoS_2/CNS displayed lower values (108 F/g, 7.4 Wh/kg, and 3700 W/kg), confirming the superior electrochemical properties of flower-like architectures.A complicated template method facilitated the supramolecular assembly of MoS_2 on hollow carbon spheres (HCS), leading to a specific capacitance of 314.5 F/g at 1 A/g with 87% cycle retention after 4000 cycles. The uniform MoS_2 distribution enhanced structural stability and charge storage efficiency.A hydrothermal self-assembled 3D MoS_2-Nitrogen-doped Graphene Quantum Dots (N-GQDs)/rGO composite exhibited a specific capacitance of 416.5 F/g at 1 A/g, with 75.8% retention after 1000 cycles. The MQG structure significantly enhanced ion diffusion and electrical conductivity, making it a potential candidate for high-performance supercapacitors and hydrogen evolution reactions (HER).

Polyelectrolyte-assisted synthesis enabled the formation of CNT@MoS_2/poly(diallyldimethylammonium chloride) (PDDA)/phosphomolybdate (PMo_{12}) nanocomposites, yielding a specific capacitance of 110 F/g at 0.5 A/g, with an energy density of 15.27 Wh/kg and 89% cycle retention over 10,000 cycles—the integration of PMo_{12} enhanced charge storage via multi-electron transfer mechanisms.Encapsulation of MoS_2 within mesoporous hollow carbon spheres resulted in a high specific capacitance of 613.4 F/g at 1 A/g, with a remarkable energy density of 208 Wh/kg at 200 W/kg. This core-shell architecture maximized ion accessibility and electrochemical stability, making it one of the most efficient MoS_2-based composites reported.A hydrothermal MoS_2/CNT composite exhibited a capacitance of 74.05 F/g at 2 A/g, with 80.8% retention after 1000 cycles. The incorporation of CNTs improved the electrical conductivity and mechanical stability of MoS_2, albeit with relatively lower overall capacitance.

MoS2 nanosheets were selectively formed on reduced graphene oxide (rGO) nanosheets, resulting in a hybrid material with abundantly exposed edges. The material exhibited excellent electrochemical properties, including a wide potential window, high Coulombic efficiency, and strong cyclic stability. Alkali-activated functionalized carbon nanotubes (AFCNTs) were combined with nanoflower-like MoS2. The AFCNTs' enhanced surface area (594.7 m^2/g) and functional groups (hydroxyl and carboxylic) improved electron transfer and reduced interfacial resistance. The hybrid showed a high specific capacitance of 516 F/g and an energy density of 71.76 Wh/kg.This ternary nanocomposite exhibited a specific capacitance of 1143.7 F/g at 1 A/g, retaining 73.3% of its capacitance after cycling at higher current densities. It demonstrated remarkable cycling stability with 97.7% retention after 3000 cycles and delivered a specific energy of 33.56 Wh/kg at 450.03 W/kg in a symmetric supercapacitor. By introducing sulfur vacancies into MoS2, this material achieved an ultrahigh particular capacitance of 512 F/g at 1 A/g, with excellent rate performance (342 F/g at 30 A/g) and no decay after 2000 cycles. The composite also demonstrated outstanding energy density (63 Wh/kg) and power density (25.5 kW/kg) in an asymmetrical supercapacitor. This nitrogen-doped, double-layer hollow carbon@MoS2/MoO2 nanosphere exhibited a high specific capacitance (569 F/g) with impressive rate performance (54.8% retention at 20 A/g) and long cycle life (91.4% coulombic efficiency after 5000 cycles). It proved to be an outstanding candidate for supercapacitor electrodes.

This work demonstrates the fabrication of high-energy-density, safer SS-SICs using flake-shaped MoS2/carbon nanotube nanohybrids and optimized sodium-ion ionogel electrolytes. The nanohybrids support short sodium ion migration paths and buffer volume changes during electrochemical reactions. At the same time, the ionogel electrolyte offers improved ionic conductivity, flame-retardant properties, and excellent sodium migration rate. The SS-SICs exhibit a high energy density of 115.7 Wh/kg at 70°C and show excellent durability with 81% capacity retention after 8000 cycles. This study focuses on engineering MoS2 with a multiphase structure (2H and 1T) and edge-rich nanospherical morphology using carbon dots (CDs). The MoS2 nanospheres formed exhibit a large interlayer spacing and enhanced electrical conductivity, contributing to their high specific capacitance (145 F/g), good rate capability, and excellent cyclic stability (90% retention after 2000 cycles). CDs enhance the growth and structural properties of the MoS2, improving its electrochemical performance.

S.No	Name of the Compound	Specific Capacitance ($F\ g^{-1}$)	Power Density ($W\ kg^{-1}$)	Energy Density ($W\ h\ kg^{-1}$)	Cycle & Cycle Retention	Current Density ($A\ g^{-1}$ or $A\ cm^{-3}$)
1	MoS_2/Carbon (C)	452.7	N/A	N/A	94.8% retention after 10,000 cycles	1 A g^{-1}
2	Flower-like MoS_2	122 (at 1 A g^{-1}) / 114 (at 2 mV s^{-1})	N/A	N/A	N/A	1 A g^{-1}
3	MoS_2-rGO/MWCNT (6.3 wt% MoS_2)	4.8 F cm^{-3} (max), 3.8 F cm^{-3} (at 2 A cm^{-3})	N/A	N/A	N/A	0.07 - 2 A cm^{-3}
4	MoS_2@HCNBs	560 F g^{-1} (at 0.2 A g^{-1}) / 874 F cm^{-3}	N/A	N/A	94.4% retention after 5000 cycles	0.2 A g^{-1}
5	f-MoS_2/CNS	231 F g^{-1}	6443	26	N/A	N/A
6	s-MoS_2/CNS	108 F g^{-1}	3700	7.4	N/A	N/A
7	MoS_2@HCS-17	314.5 F g^{-1}	611.6	34	87% retention after 4000 cycles, 93% after 2000 cycles (asymmetric)	1 A g^{-1}
8	3D-MoS_2/N-GQDs/rGO (MQG)	416.5 F g^{-1} (at 1 A g^{-1})	N/A	N/A	75.8% retention after 1000 cycles (at 2 A g^{-1})	1 A g^{-1}
9	CNT@MoS_2/PDDA/PMo_{12}	110 F g^{-1}	152	15.27	89% retention after 10,000 cycles	0.5 A g^{-1}
10	MoS_2@MHCS (Mesoporous Hollow Carbon Spheres)	613.4 F g^{-1} (at 1 A g^{-1}), 358.2 F g^{-1} (at 10 A g^{-1})	10,000	208 (at 200 W kg^{-1}), 82	Excellent cycle performance	1 - 10 A g^{-1}

				(at 10,000 W kg^{-1})		
11	MoS_2/CNT	74.05 F g^{-1} (at 2 A g^{-1})	N/A	N/A	80.8% retention after 1000 cycles	2 A g^{-1}
12	FeS_2@C@MoS_2	1321.4 F g^{-1} (at 2 A g^{-1})	N/A	N/A	81.2% retention after 1000 cycles (at 6 A g^{-1})	2 A g^{-1}
13	MoS_2/C	201.4 F g^{-1} (at 0.2 A g^{-1})	N/A	N/A	High rate capability and long cycle durability	0.2 A g^{-1}
14	MoS_2@NC spheres	1386 mAh g^{-1} (LIBs)	N/A	N/A	330 mAh g^{-1} (after 400 cycles for SIBs)	200 mA g^{-1} (LIBs), 1000 mA g^{-1} (SIBs)
15	MoS_2@HCS (Activated)	458 F g^{-1} (at 1 A g^{-1})	616 W kg^{-1}	13.7 Wh kg^{-1}	86% retention after 1000 cycles at 8 A g^{-1}	1 A g^{-1}
16	MoS_2/MWCNT	452.7 F g^{-1} (at 1 A g^{-1})	N/A	N/A	412.2 F g^{-1} after 1000 cycles	1 A g^{-1}
17	MoS_2/VAMWCNT (Hydrogen-treated)	165 F g^{-1} at 2 mV/s	N/A	N/A	Increased capacitance at low scan rates; reduced capacitance at higher scan rates	Low scan rates (2 mV/s)
18	MoS_2-HCS	334 F g^{-1} at 1 A g^{-1}	N/A	N/A	87% retention after 5000 cycles	1-20 A g^{-1}
19	Stretchable Supercapacitor with MoS_2	13.16 F cm^{-3}	N/A	N/A	98% retention after 10,000 cycles	Stretchability up to 240%
20	MoS_2/RGO Composite Hollow Microspheres	218.1 F g^{-1}	N/A	N/A	91.8% retention after 1000 cycles	1 A g^{-1} (for capacitance); 3 A g^{-1} (for cycling)
21	rGO/MoS_2 Hybrid Material	Not specified	N/A	N/A	Strong cyclic stability	N/A
22	AFCNT and MoS_2 Hybrid Material	516 F g^{-1}	Not specified	71.76 Wh kg^{-1}	Not specified	0.5 A g^{-1}
23	MoS_2-rGO/PEDOTNP Hybrid Nanocomposite	1143.7 F g^{-1}	450.03 W kg^{-1}	33.56 W h kg^{-1}	97.7% after 3000 cycles	1 A g^{-1} to 9 A g^{-1}
24	MoS_2-rGO/PEDOTNP // MoS_2 rGO/PEDOTNP SSC	289.25 F g^{-1}	450.03 W kg^{-1}	33.56 W h kg^{-1}	93.17% after 10,000 cycles	1 A g^{-1} to 20 A g^{-1}
25	MoS_2x@CNTs/ Ni Core/Shell Electrode	512 F g^{-1}	850 W kg^{-1}	63 Wh kg^{-1}	No decay after 2000 cycles	1 A g^{-1} to 30 A g^{-1}
26	NCs@MoS_2/MoO_2 Nanoparticle Composite	569 F g^{-1}	Not mentioned	Not mentioned	81% retention after 5000 cycles	1 A g^{-1} to 20 A g^{-1}

IV. CONCLUSION

In conclusion, the development of advanced MoS2-based materials for energy storage applications has shown promising results in improving the performance of supercapacitors. Integrating MoS2 with carbon nanotubes, optimized electrolytes, and structural modifications, such as multiphase MoS2 and edge-rich nanospherical morphologies, has significantly enhanced conductivity, ionic mobility, and cycle stability. They demonstrated excellent energy density and durability, making them suitable for high-temperature applications. At the same time, the engineered MoS2 nanospheres exhibited high capacitance, good rate capability, and outstanding cyclic stability in aqueous electrolytes. Both approaches highlight the critical role of material design and device configuration.

ACKNOWLEDGEMENT

This research work in financially supported by Thiagarajar Research Fellowship (TRF) scheme – (TCE/RD/TRF/10 dated 27.09. 2024).

REFERENCE

[1] Sangabathula, O.; Potphode, D.; Sharma, C. S. Morphology-Controlled Molybdenum Disulfide/Candle Soot Carbon Composite for High-Performance Supercapacitor. ChemistrySelect2020, 5 (22), 6809–6817. https://doi.org/10.1002/slct.202001443.

[2] A Novel Carbon Electrode Material for Highly Improved EDLC Performance | The Journal of Physical Chemistry B.https://pubs.acs.org/doi/abs/10.1021/jp060110d (accessed 2025-02-09).

[3] Synergetic design of enlarged surface area and pseudo-capacitance for fiber-shaped supercapacitor yarn – Science Direct. https://www.sciencedirect.com/science/article/abs/pii/S221128551930905X (accessed 2025-02-09).

[4] Molaei, M.; Rostami, G. R.; Zardkhoshoui, A. M.; Davarani, S. S. H. In Situ Tellurization Strategy for Crafting Nickel Ditelluride/Cobalt Ditelluride Hierarchical Nanostructures: A Leap Forward in Hybrid Supercapacitor Electrode Materials. J. Colloid Interface Sci.2024, 653, 1683–1693. https://doi.org/10.1016/j.jcis.2023.10.012.

[5] Frackowiak, E. Carbon Materials for Supercapacitor Application. Phys. Chem. Chem. Phys.2007, 9 (15), 1774–1785. https://doi.org/10.1039/B618139M.

[6] Zhou, X.; Xu, B.; Lin, Z.; Shu, D.; Ma, L. Hydrothermal Synthesis of Flower-Like MoS2 Nanospheres for Electrochemical Supercapacitors. J. Nanosci. Nanotechnol.2014, 14 (9), 7250–7254. https://doi.org/10.1166/jnn.2014.8929.

[7] Sun, G.; Zhang, X.; Lin, R.; Yang, J.; Zhang, H.; Chen, P. Hybrid Fibers Made of Molybdenum Disulfide, Reduced Graphene Oxide, and Multi-Walled Carbon Nanotubes for Solid-State, Flexible, Asymmetric Supercapacitors. Angew. Chem.2015, 127 (15), 4734–4739. https://doi.org/10.1002/ange.201411533.

[8] Wang, L.; Liu, F.; Zhao, B.; Ning, Y.; Zhang, L.; Bradley, R.; Wu, W. Carbon Nanobowls Filled with MoS2 Nanosheets as Electrode Materials for Supercapacitors. ACS Appl. Nano Mater.2020, 3 (7), 6448–6459. https://doi.org/10.1021/acsanm.0c00924.

[9] Symmetric pseudocapacitors based on molybdenum disulfide (MoS2)-modified carbon nanospheres: correlating physicochemistry and synergistic interaction on energy storage - Journal of Materials Chemistry A (RSC Publishing). https://pubs.rsc.org/en/content/articlelanding/2016/ta/c6ta00114a (accessed 2025-02-09).

[10] Binder-free preparation of bimetallic oxide vertical nanosheet arrays toward high-rate performance and energy density supercapacitors - Arbaz - 2021 - International Journal of Energy Research - Wiley Online Library.https://onlinelibrary.wiley.com/doi/abs/10.1002/er.6681 (accessed 2025-02-09).

Synthesis of Colloidal TiO_2 Stimulant for the Enhancement of Chlorophyll Content and Plant Yield

Gimna Maria George
Department of Chemistry,
Thiagarajar College of Engineering,
Madurai, India

Pandian Kannan
Department of Soil Science and
Agricultural Chemistry,
Coimbatore, Tamil Nadu

Muniasamy Kottaisamy
Department of Chemistry,
Thiagarajar College of Engineering,
Madurai, India
mmksami10@gmail.com

***Abstract*—Titanium dioxide (TiO_2) nanoparticles have emerged as a promising tool in modern agriculture, capturing significant attention due to their potential to act as nanostimulants that enhance plant growth and productivity. These nanoparticles, with their unique physicochemical properties, have shown the ability to improve photosynthesis, nutrient uptake, and stress tolerance in plants. Their application in agriculture is particularly noteworthy for its potential to reduce reliance on conventional fertilizers, thereby contributing to more sustainable farming practices. This study focuses on investigating the effects of TiO_2 nanostimulants when used as a foliar fertilizer, specifically examining the impact of different concentrations on jasmine plant growth, physiological processes, and overall yield. Foliar application, a method of delivering nutrients directly to the leaves, is considered highly efficient as it enables rapid nutrient absorption and utilization by the plant. The TiO_2nanostimulants enhances physiological activities, such as photosynthetic efficiency, nutrient use efficiency, and stress tolerance.**

***Keywords*—Nanostimulants, Foliar fertilizers, Photocatalytic TiO_2, chlorophyll, nutrients use efficiency.**

I. INTRODUCTION

Modern agriculture is increasingly confronted with a range of complex challenges, including declining soil fertility, the need to meet growing global food demands, and the imperative to adopt environmentally sustainable practices. These challenges are compounded by the overuse of conventional fertilizers and pesticides, which often degrade soil health, pollute water bodies, and contribute to greenhouse gas emissions. To address these issues, nanotechnology has emerged as a promising frontier, offering innovative and sustainable solutions for enhancing crop productivity while minimizing environmental impact. Among the wide array of nanomaterials under investigation, titanium dioxide (TiO_2) nanoparticles stand out due to their unique properties and multifaceted benefits in agricultural applications.

TiO_2 nanoparticles have demonstrated the ability to improve several critical aspects of plant physiology. They can enhance photosynthetic activity by increasing light absorption and energy conversion efficiency in plants. [1] Additionally, these nanoparticles play a vital role in regulating oxidative stress by scavenging reactive oxygen species (ROS), which are often produced under environmental stress conditions such as drought, high temperatures. [2] Furthermore, TiO_2 nanoparticles can improve nutrient uptake efficiency, facilitating better utilization of soil resources and reducing the dependence on traditional chemical fertilizers. [3]

However, despite these benefits, the concentration of TiO_2 nanoparticles applied to plants is a critical determinant of their effectiveness and safety. At optimal concentrations, TiO_2 can act as a beneficial nanostimulant, enhancing plant growth and development. [5] Conversely, excessive concentrations may lead to nanoparticle accumulation, which can induce phytotoxicity, disrupt physiological processes, and potentially harm soil microbial communities. Striking the right balance is, therefore, essential to maximizing the benefits of TiO_2 nanoparticles while minimizing any adverse effects. [5]

This study seeks to evaluate the impact of varying concentrations of TiO_2 nano-stimulants applied as foliar fertilizers on jasmine plants growth and development. By systematically assessing parameters such as photosynthetic efficiency, oxidative stress regulation, nutrient uptake, and overall yield, the research aims to identify an optimal concentration range that ensures maximum efficacy without compromising plant health or environmental safety. The findings from this work will contribute to a deeper understanding of the potential of TiO_2 nanoparticles in agriculture and provide valuable insights into their sustainable application to address pressing challenges in modern farming.

II. MATERIALS AND METHODS

A. *Preparation of TiO_2 Nano-Stimulant*

The TiO_2 nano stimulants foliar fertilizer was synthesized by dissolving the necessary amount of Titanium isopropoxide and citric acid in 100 milliliters of distilled water at a pH of 4-5, followed with stirring and sonicating vigorously until a clear solution was obtained. The solution was then diluted with water to a pH of 6, which caused a white colloid to gradually form. This colloidal solution was diluted with water and ultra-sonicated to create a foliar spray. Then the solutions were sprayed on jasmine plant leaves, and the results were compared to the control.

B. *Field Experiment*

The field's plot was divided into four rows and three columns. The foliar stimulant was not sprayed in the first row

(Control T0). 5% foliar stimulant solution was sprayed in the second row (T1). 10% solution was applied in the third row (T2) and the 20% foliar stimulant was sprayed in the fourth row (T3). As a replication, three columns underwent randomization. The TiO_2 foliar stimulant was sprayed over the Jasmine leaf surface at an interval of seven days, three times after 20 days of planting with a hand sprayer until leaf surfaces were fully wetted.

To assess both yield and flower quality, we focused on crucial parameters such as peduncle length, flower size and flower weight. Ten flowers from all treatments were collected from three replications and the average weight was taken for the comparative studies. The shoot length root length and total biomass of the plants were analyzed. The chlorophyll content was evaluated using UV-visible absorption spectroscopy. For UV spectrum analysis, fresh leaves were carefully harvested from the jasmine plants and then washed thoroughly with distilled water. Then accurately weighed samples were ground in a mortar with acetone as a solvent for extraction [6]. After the extraction and filtration, the resulting sample solution was transferred to a quartz container for spectrometric determination. Absorption values of extracts were taken at 645 and 663 nm and total chlorophyll contents in leaves were determined by using the formula of Arnon [7].

$$\text{Total Chl} = 0.0202 \times A645 + 0.00802 \times A663 \text{ mg/ml}$$

III. Result and Discussion

A. UV-Visible spectrum analysis of stabilizing agent and TiO_2 colloid

Figure 1 displays the transmission spectra of citric acid and citric acid-stabilized TiO_2 colloid, which were measured within the 200–800 nm wavelength range. In comparison to the narrow broadband absorption of citric acid, which ranges from 210 nm to 250 nm, citric acid-stabilized TiO_2 demonstrates an asymmetric broadband absorption that extends from 210nm to 600 nm [8]. This demonstrates the colloidal form of TiO_2 in aqueous media.

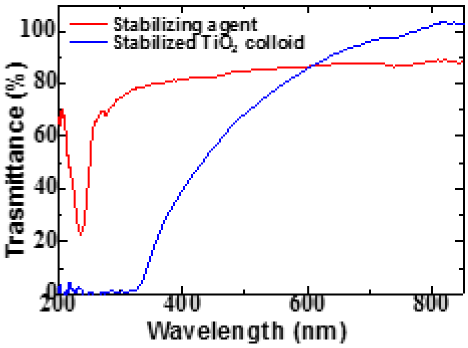

FIG.1. Transmittance spectra of Colloidal TiO_2 in aqueous medium

B. Morphological Analysis of Jasmine Plants

With respect to controlled jasmine plants, those exposed to various concentration of TiO_2 stimulants show significant improvements in shoot length, flower peduncle length, flower weight, and blossoming time. Table 1 shows the comparative study of the morphological characters of control and TiO_2 nano particles sprayed jasmine plants. The results confirmed a remarkable increased in plant growth treated with 10% TiO_2 nanoparticles, as well as a 30% increase in flower weight and a 10% increase in the jasmine plants which treated with 5% TiO_2. The higher concentration shows a decrease in flower yield and quality when compare with the control and other two treatments. Same trend is following in plant growth and biomass too. The foliar application of optimal TiO_2 nanostimulants improves light absorption, increases photosynthesis, and raises photosynthetic efficiency. It also increases nutrient uptake, stimulates metabolic activities, and encourages plant growth and biomass. These nanoparticles can stimulate root and leaf metabolic activities, enhancing water and nutrient absorption.

TABLE 1 Growth and Yield attributes of Jasmine plants under various conditions.

Growth and Yield attributes	T0	T1	T2	T3
Plant fresh weight (g)	57.2	59.8	63.5	56.3
Plant dry weight (g)	21.8	25.9	28.6	22.5
Number of flower buds	10	11	15	8
Peduncle length(cm)	1.2	1.3	1.5	1.2
Total bud length(cm)	2.1	2.2	2.7	2.0
Flower bud weight(g)	0.25	0.27	0.30	0.24
Number of leaves	24	25	27	22
Number of branches	6	6	7	5
Root Volume (cm^3)	8.7	9.1	10	8.6

C. Chlorophyll Content

Chlorophyll is a green, porphyrin-based photosynthetic pigment that uses the photosynthetic process for converting light energy into chemical energy. All green plants contain chloroplasts, which are photochemical active bio membranes and contain the pigment chlorophyll. The amount of chlorophyll in a plant's leaves increases as its photosynthetic activity and plant productivity enhances.

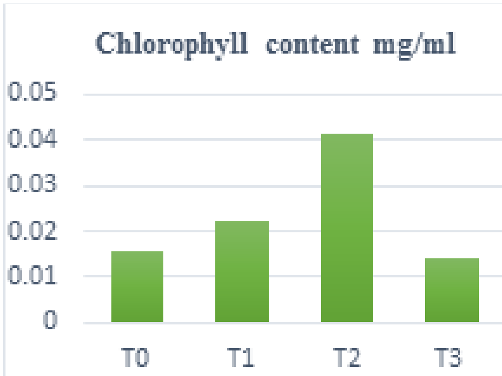

FIG. 2 Total chlorophyll content of Jasmine plants under various conditions

The jasmine plants which treated with 10% of TiO_2 shows a 20% increase in chlorophyll content when compare with the control and other concentrations. The jasmine plants treated with 5% TiO_2shows a 10% increase in chlorophyll content and there is no significant increase in chlorophyll content in control and higher concentration of TiO_2.

IV. Conclusion

Foliar application of optimum concentration (10%) of TiO_2 nanostimulants enhances plant growth, physiological functions, and yield. The photocatalytic activity of TiO_2

enhances crop yield by increasing the chlorophyll content, improving photosynthetic activity, increasing enzyme activity, promoting root growth and nutrient uptake, and protecting it from stress conditions through stable and non-toxicity performance.

References

[1] A. Vatankhah et al., "Plants exposed to titanium dioxide nanoparticles acquired contrasting photosynthetic and morphological strategies depending on the growing light intensity: a case study in radish," Scientific Reports, vol. 13, no. 1, Apr. 2023, doi: 10.1038/s41598-023-32466-y.

[2] S. Lyu, X. Wei, J. Chen, C. Wang, X. Wang, and D. Pan, "Titanium as a beneficial element for crop production," Frontiers in Plant Science, vol. 8, Apr. 2017, doi: 10.3389/fpls.2017.00597.

[3] R. Tighe-Neira et al., "Physiological and agronomical traits effects of titanium dioxide nanoparticles in seedlings of Solanum lycopersicum L," BMC Plant Biology, vol. 24, no. 1, Feb. 2024, doi: 10.1186/s12870-024-04763-9.

[4] G. Gohari et al., "Titanium dioxide nanoparticles (TiO2 NPs) promote growth and ameliorate salinity stress effects on essential oil profile and biochemical attributes of Dracocephalum moldavica," Scientific Reports, vol. 10, no. 1, Jan. 2020, doi: 10.1038/s41598-020-57794-1.

[5] S. Lyu, X. Wei, J. Chen, C. Wang, X. Wang, and D. Pan, "Titanium as a beneficial element for crop production," Frontiers in Plant Science, vol. 8, Apr. 2017, doi: 10.3389/fpls.2017.00597.

[6] D. I. Arnon, "copper enzymes in isolated chloroplasts. Polyphenoloxidase in beta vulgaris," plant physiology, vol. 24, no. 1, pp. 1–15, Jan. 1949, DOI: 10.1104/ pp.24.1.1.

[7] N. D. H. Maibodi, M. Kafi, A. Nikbakht, and F. Rejali, "Effect of foliar applications of humic acid on growth, visual quality, nutrients content and root parameters of perennial ryegrass (Lolium PerenneL.)," Journal of Plant Nutrition, vol. 38, no. 2, pp. 224–236, Jul. 2015, doi: 10.1080/01904167.2014.939759.

[8] H. Yoon et al., "Extraordinary enhancement of UV absorption in TIO2 nanoparticles enabled by Low-Oxidized graphene nanodots," The Journal of Physical Chemistry C, vol. 122, no. 22, pp. 12114–12121, May 2018, doi: 10.1021/acs.jpcc.8b03329.

NiFe MOF-Based Electrocatalysts: A Mini Perspective Review on a Promising Approach for Sustainable Hydrogen Production

Kaviya K
Department of Physics,
Thiagarajar College of Engineering,
Madurai, Tamil Nadu, India.
kaviyak1@student.tce.edu

M. Tamilelakkiya
Department of Physics,
Thiagarajar College of Engineering,
Madurai, Tamil Nadu, India
mtphy@tce.edu

***Abstract*—The increasing demand for clean and sustainable energy has intensified research into efficient electrocatalysts for water splitting. Metal–organic frameworks (MOFs) and their derivatives have emerged as promising materials for electrocatalytic applications due to their high surface area, tunable porosity, and well-defined metal centers. However, their inherent limitations, such as poor electrical conductivity and stability, necessitate rational design strategies to enhance their catalytic efficiency. In this study, we explore the synthesis and electrochemical performance of novel bimetallic MOFs incorporating transition metals such as Ni and Fe for water splitting applications. The structural and electronic properties of these materials are tailored to optimize charge transfer and catalytic activity. A systematic investigation into the hydrogen evolution reaction (HER) and oxygen evolution reaction (OER) mechanisms provides insight into the structure–performance relationship, contributing to the development of cost-effective and durable electrocatalysts. This work not only advances the understanding of MOF-based materials in water splitting but also offers a strategic pathway for their practical implementation in sustainable energy conversion.**

***Keywords*—mof, oer, electrocatalyst.**

I. INTRODUCTION

Fossil fuels, such as coal, oil, and gas, have been the primary energy sources for production and tremendous advancements in quality of life throughout the last century. However, this has resulted in significant greenhouse gas emissions and climate change. The only way to ensure a habitable earth for future generations is to refine our energy system to one that is sustainable and environmentally friendly [1-5]. Furthermore, the development of renewable energy technology has attracted a lot of attention due to the depletion of non renewable resources [6-9]. Since hydrogen has no carbon emissions, high gravimetric energy densities, and is renewable, it is seen as a viable energy source.[10-12] The electrochemical breakdown of water can yield hydrogen, and the oxygen evolution reaction (OER) is the crucial rate-limiting half-cell reaction that requires a high over potential due to the slow kinetics brought on by the high energy barrier for rupturing the O-H bond and creating the O-O bond [12-15].The OER process's kinetic barrier can be successfully surmounted by the electrocatalyst[16,17]. The electrocatalysts for the OER have been precious metal oxides, such as IrO2 and RuO2[18,19]. Unfortunately, their high cost and meager reserves severely hinder their further commercial use [20,21]. Therefore, the creation of strong and effective OER electrocatalysts from Earth-abundant materials is crucial for water electrolysis. As a result, there is a great deal of promise for creating efficient bifunctional electrocatalysts that can accelerate the HER and OER simultaneously. Because of their large specific surface area and rich pore structure, metal-organic frameworks (MOFs) have been generally considered stellar catalysts that aid in the electron/mass-transfer process of water splitting [22,23]. Typically, Metal ions serve as linking elements. The 3D expansion of space is supported by organic ligands. MOF materials find extensive applications in energy storage, separation, and catalysis [24, 25] MOFs are currently a significant topic of study in both organic and inorganic chemistry [26, 27]. High porosities, low densities, large specific surface areas, regular pores, pore sizes that may be adjusted, a variety of topological configurations, and tailoring possibilities are some of its benefits. The choice of organic ligands and synthetic conditions can result in single or mixed pore architectures with a range of pore diameters from micropores to mesoporous. These features promote the proton transfer process of electrocatalytic processes, enhance the dispersion of active components, and offer a large number of active sites.Among them, NiFe-based MOFs have demonstrated exceptional catalytic activity, benefiting from the synergistic interaction between Ni and Fe, which enhances their conductivity and electrochemical performance. Despite these advantages, challenges such as long-term stability, conductivity enhancement, and large-scale synthesis remain unresolved.

This mini perspective review provides an overview of recent advancements in NiFe MOF-based electrocatalysts for water splitting. It highlights their structural advantages, catalytic mechanisms, and challenges while offering insights into potential strategies for improving their performance and industrial feasibility.

II. NIFE MOF AS CATALYST

The study by Asnavandi et al. on NiFe-based metal-organic frameworks (MOFs) for the oxygen evolution reaction (OER) presents a compelling exposition of the profound influence of structural modulation on catalytic efficacy. This investigation underscores the transformative potential of defect engineering, particularly through the introduction of oxygen vacancies via $NaBH_4$ reduction, in augmenting the electrochemical performance of an intrinsically promising catalytic system. By systematically altering the material's structural and electronic attributes, the authors have demonstrated a marked enhancement in both activity and charge transfer kinetics.A salient aspect of this work is the definitive correlation between structural modifications and electrocatalytic performance. The observed decrease in overpotential to 270 mV at 10 mA cm^{-2} constitutes a substantive advancement in catalytic efficiency, indicating a fundamental enhancement in reaction kinetics. The presence of oxygen vacancies is instrumental in lowering the energy barrier for OER intermediates, thereby facilitating more favorable reaction pathways. This phenomenon is further substantiated by the reduction in the Tafel slope to 40 mV dec^{-1}, indicative of highly efficient charge transfer dynamics with minimal energy dissipation. The influence of oxygen vacancies extends beyond the augmentation of intrinsic catalytic activity; their role in modulating electronic conductivity is equally consequential. observed increase in current density to 240 mA cm^{-2} at a relatively low overpotential further corroborates this assertion, underscoring the pivotal role of defect sites in facilitating charge transport and catalytic efficacy. A particularly compelling aspect of this study is the rigorous structural and electronic characterization of the modified catalyst. X-ray diffraction (XRD) analyses reveal an increase in structural disorder, underscoring the significance of amorphous domains in electrocatalysis, as such disordered structures often correlate with a higher density of catalytically active sites. X-ray photoelectron spectroscopy (XPS) and electron paramagnetic resonance (EPR) confirm the modulation of Ni and Fe oxidation states, demonstrating that $NaBH_4$ treatment not only induces surface defects but also fundamentally alters metal-oxygen interactions. The enhanced intensity of oxygen vacancy-associated signals in the O 1s spectrum, coupled with photoluminescence (PL) data indicating suppressed electron-hole recombination, substantiates the role of these vacancies in catalytically beneficial electronic restructuring. [31.]

Sun et al. have presented a significant advancement in the field of electrocatalysis by developing a NiFe-based metal–organic framework (MOF) electrocatalyst directly grown on nickel foam (MIL-53(FeNi)/NF) via a one-step solvothermal method. This approach represents a paradigm shift in the design of high-performance oxygen evolution reaction (OER) catalysts, addressing key challenges such as poor electrical conductivity, weak structural adhesion, and limited long-term stability observed in conventional powder-based electrocatalysts. By leveraging an in situ growth strategy, this study circumvents the inherent drawbacks of binder-assisted catalysts, ensuring strong interfacial contact, enhanced charge transfer, and prolonged durability under electrochemical conditions.A fundamental aspect of this work is the incorporation of Fe into the MIL-53(Ni) framework, which plays a pivotal role in modulating the electronic structure of Ni, thereby optimizing its catalytic activity. The integration of Fe enhances the electrochemically active surface area (ECSA), increases the density of unfilled 3d orbitals in Ni, and improves the adsorption energy of key OER intermediates, thereby facilitating a more efficient reaction pathway. This synergistic interaction is evident in the electrocatalytic performance, where MIL-53(FeNi)/NF achieves an impressively low overpotential of 233 mV at a current density of 50 mA cm^{-2}, a remarkable improvement over conventional Ni-based catalysts. The Tafel slope of 31.3 mV dec^{-1} further underscores the enhanced reaction kinetics, indicating rapid electron transfer and reduced kinetic barriers. Scanning electron microscopy (SEM) reveals a stacked nanosheet morphology that maximizes the exposure of active sites, facilitating efficient mass and charge transport. Beyond initial performance metrics, the long-term stability of MIL-53(FeNi)/NF is a critical parameter that reinforces its potential for practical application. Chronoamperometric studies show that the catalyst maintains its activity over 16,000 seconds, while cyclic voltammetry (CV) cycling tests indicate minimal performance degradation even after 1,000 cycles, highlighting its exceptional structural robustness. Post-OER characterization via SEM and XPS further corroborates the material's stability, as the nanosheet morphology and electronic properties remain largely unaltered after extended electrochemical operation. Theoretical insights derived from density functional theory (DFT) calculations provide a compelling mechanistic understanding of the observed enhancements in catalytic performance. The calculations reveal that Fe incorporation results in an increased density of 3d electrons in Ni, which not only enhances the oxophilicity of Ni sites but also facilitates optimal adsorption of oxygen intermediates, thereby accelerating the OER process. [32].

Salmanion and Najafpour present a comprehensive study that explores how a NiFe-based metal–organic framework (MOF) can serve as a precursor to a highly active oxygen evolution reaction (OER) catalyst under alkaline conditions. The researchers synthesized the MOF by reacting Ni(II) and Fe(III) with benzenedicarboxylic acid, producing a material with a highly ordered, porous, and crystalline structure. This initial porosity is crucial because it facilitates rapid mass transport and exposes a high density of active sites to the electrolyte. However, rather than remaining intact during OER, the MOF undergoes a strategic in-situ transformation. Under the harsh oxidative conditions in a 1 M KOH electrolyte, the organic linkers begin to decompose, triggering a reorganization of the metal centers into a NiFe layered double hydroxide (LDH) phase. This transformation is central to enhancing the OER because the newly formed NiFe LDH stabilizes nickel in a higher oxidation state (Ni(III)), which is more reactive and better suited for water oxidation.

During this transformation, significant electronic and structural modifications occur that further enhance catalytic performance. Electrochemical measurements, particularly linear sweep voltammetry (LSV), reveal a broad anodic peak in the 1.30–1.40 V range (vs. the reversible hydrogen electrode), which is attributed to the oxidation of Ni(II) to Ni(III). This redox transition is a key step in the OER mechanism, as Ni(III) species facilitate the adsorption and activation of water molecules. The presence of iron in the framework plays a synergistic role by subtly shifting the redox potential and stabilizing the Ni(III) centers, effectively lowering the energy barrier for the reaction. Concurrently, the degradation of the MOF introduces a high density of defects and lattice imperfections—such as oxygen vacancies—that serve as additional active sites and enhance electron transfer. The increase in oxygen content, as evidenced by elemental analysis, supports the formation of an oxygen-rich oxide/hydroxide phase, which is inherently more active for catalysis. Scanning electron microscopy (SEM) and energy-dispersive spectroscopy (EDS) provide additional insight into the morphological and elemental changes; SEM images capture the corrosion and formation of layered structures on the catalyst surface, while EDS data indicate a reduction in carbon and an increase in oxygen and nickel content. High-resolution transmission electron microscopy (HRTEM) offers a direct visualization of the nanoscale structure, displaying lattice spacings of approximately 0.21–0.23 nm that correspond to the (012) plane of NiFe LDH. Together, these techniques not only confirm the in-situ transformation from MOF to oxide/hydroxide but also demonstrate that the increased OER activity is directly linked to these structural and electronic modifications. The conversion of the MOF into a defect-rich NiFe oxide/hydroxide phase results in a material that exhibits a higher density of active sites, improved charge transfer, and enhanced stability under prolonged electrochemical operation. The formation of Ni(III) species, stabilized by the synergistic presence of iron, is crucial for accelerating the water oxidation process. Moreover, the introduction of structural defects, which might be considered detrimental in other contexts, actually enhances catalytic activity by providing additional sites for water adsorption and facilitating more efficient electron transfer from the reaction sites to the electrode. This defect engineering, combined with the high porosity inherited from the original MOF, ensures that the catalyst not only operates at lower overpotential but also maintains its performance over extended periods [33].

Zhao et al. have developed a novel approach to enhancing the oxygen evolution reaction (OER) by leveraging the synergistic interaction between nickel (Ni) and iron (Fe) within a metal-organic framework (MOF) matrix. This study demonstrates the ability of Fe to modulate the electronic environment of Ni, thereby optimizing its oxidation states and improving OER kinetics. A key aspect of this work is the role of Fe as an active electronic modulator rather than a passive additive. X-ray photoelectron spectroscopy (XPS) data confirm shifts in binding energy, indicative of electron density redistribution between Ni and Fe. This electronic reconfiguration significantly enhances the catalytic efficiency of NiFe-MOF/NF compared to its monometallic counterpart. The electrochemical performance metrics further highlight the impact of this bimetallic synergy. The NiFe-MOF/NF catalyst exhibits an overpotential of 225 mV at a current density of 50 mA cm^{-2} and 160 mV at 10 mA cm^{-2}, representing a substantial improvement over conventional transition metal-based catalysts. The reduction in Tafel slope further suggests accelerated reaction kinetics, addressing the inherent sluggishness of the OER. Electrochemical impedance spectroscopy (EIS) results reveal a lower charge transfer resistance, indicating improved electron mobility and enhanced catalytic activity. Structural integrity and morphological analysis confirm the stability of the synthesized catalyst. X-ray diffraction (XRD) data reveal a well-defined crystalline structure, while scanning electron microscopy (SEM) and transmission electron microscopy (TEM) images depict a columnar morphology conducive to effective electrolyte interaction. Additionally, the high specific surface area of 663 m^2/g, coupled with a porous architecture, facilitates enhanced electrolyte diffusion and increased exposure of active sites, contributing to sustained catalytic performance. Long-term durability assessments demonstrate the robustness of NiFe-MOF/NF, maintaining catalytic efficiency for over 50 hours at 100 mA cm^{-2} with minimal performance degradation. Post-OER characterization indicates the formation of Ni(Fe)OOH species, confirming the dynamic evolution of the material during the reaction, which further contributes to its stability and efficiency. The comprehensive characterization employed in this study provides a holistic understanding of the catalyst's performance. [34].

Dandan Zhang and colleagues present a compelling study in which they report the one-step hydrothermal synthesis of a rod-shaped bimetallic NiFe metal–organic framework (NiFe-MOF) that demonstrates highly efficient oxygen evolution reaction (OER) catalysis. Their work, underpinned by meticulous experimental design and an array of advanced characterization techniques At the heart of their investigation lies the strategic design of a MOF that not only benefits from the high surface area and ordered porosity typical of these frameworks but also exploits the synergistic interactions between nickel and iron to induce beneficial electronic and structural modifications during catalysis. The rod-like morphology, as revealed by scanning electron microscopy (SEM) and transmission electron microscopy (TEM), is not only aesthetically pleasing but also functionally significant, as it promotes the formation of a highly accessible, high surface-area structure. The mesoporous nature of the material, confirmed by nitrogen adsorption–desorption isotherm measurements (with a surface area of approximately 146.45 $m^2\ g^{-1}$), facilitates efficient electrolyte penetration and ensures that a large number of active sites are available for the catalytic reaction. Such structural features are critical in electrocatalysis, where mass transport limitations and insufficient active site exposure often hinder performance.Beyond the inherent advantages provided by the MOF's morphology and porosity, the incorporation of both nickel and iron into the framework is central to the observed enhancement in OER activity. The bimetallic nature of the NiFe-MOF creates a synergistic effect that is not attainable in monometallic systems. The synergistic interaction between Ni and Fe lowers the energy barrier for these redox transitions, as reflected in the remarkably low Tafel slope of 40.82 mV dec^{-1} observed for the NiFe-MOF—an indicator of favorable reaction kinetics. In contrast, the monometallic analogues (Ni-MOF and Fe-MOF) display significantly higher overpotentials and Tafel slopes, underscoring the importance of the bimetallic composition. Electrochemical measurements further attest to the performance of the catalyst. Linear sweep voltammetry (LSV) reveals that the NiFe-MOF delivers an overpotential of only 264 mV at a current density of 10 mA cm^{-2} in 1 M KOH, which is substantially lower than the overpotentials required by its monometallic counterparts and even lower than that of the commercial RuO_2 benchmark catalyst. These findings are supported by electrochemical impedance spectroscopy (EIS), which shows that the NiFe-MOF exhibits the smallest semicircle in the Nyquist plot among the samples studied.

III. CONCLUSION

NiFe MOF-based electrocatalysts have demonstrated significant potential for efficient electrochemical water splitting, owing to their tunable porosity, high surface area, and diverse compositional flexibility. These materials offer distinct advantages, such as enhanced electron transfer, improved active site exposure, and structural versatility, making them promising candidates for sustainable hydrogen production. However, several challenges remain before their large-scale application can be realized.One of the key challenges is the long-term stability of NiFe MOFs under harsh electrochemical conditions. Structural degradation and dissolution of active metal centers can limit their performance, especially at high current densities and in variable electrolyte environments. Developing robust and durable MOF architectures with enhanced stability in both alkaline and neutral media is crucial for practical applications.

Another major concern is the intrinsic conductivity of MOFs. While coupling with conductive substrates and fabricating ultrathin MOF structures have shown improvements, further advancements are needed to enhance electron transport efficiency. Strategies such as doping with heterometals, incorporating conductive carbon materials, and modifying organic linkers can play a pivotal role in addressing this limitation. Furthermore, understanding the catalytic mechanism of NiFe MOFs remains a critical aspect. In situ/operando characterization techniques, such as synchrotron radiation, infrared spectroscopy, and X-ray diffraction, are essential for identifying the real active species during water splitting. Theoretical modeling and computational studies can further provide insights into the electronic structure and reaction pathways, enabling the rational design of next-generation MOF-based electrocatalysts. To advance the commercialization of NiFe MOFs for hydrogen production, cost-effective and scalable synthesis methods need to be developed. Large-scale fabrication with controlled morphology, precise composition, and environmentally friendly processing is imperative for industrial applications. Additionally, replacing traditional alkaline electrolytes with neutral or seawater-based systems would enhance the feasibility of MOF-based electrocatalysis in real-world scenarios.

In conclusion, while NiFe MOFs have exhibited promising electrocatalytic activity for water splitting, overcoming the challenges related to stability, conductivity, mechanistic understanding, and scalability is essential for their widespread adoption. Continued research efforts in material design, electrochemical engineering, and theoretical investigations will pave the way for the development of high-performance MOF-based electrocatalysts, accelerating the transition toward a sustainable hydrogen economy.

IV. Acknowledgment

This research work in financially supported by Thiagarajar Research Fellowship (TRF) scheme – (TCE/RD/TRF/10 dated 27.09. 2024).

References

[1] G. A. Deluga, J. R. Salge, L. D. Schmidt and X. E. Verykios, Renewable hydrogen from ethanol by autothermal reforming, Science, 2004, 303, 993–997.

[2] M. Ni, D. Y. C. Leung and M. K. H. Leung, A review on reforming bio-ethanol for hydrogen production, Int. J. Hydrogen Energy, 2007, 32, 3238–3247.

[3] M. Ni, D. Y. C. Leung, M. K. H. Leung and K. Sumathy, An overview of hydrogen production from biomass, Fuel Process. Technol., 2006, 87, 461–472.

[4] J. H. Xian, S. S. Li, H. Su, P. S. Liao, S. H. Wang, Y. W. Zhang, W. Q. Yang, J. Yang, Y. M. Sun, Y. L. Jia, Q. L. Liu, Q. H. Liu and G. Q. Li, Electrocatalytic synthesis of essential amino acids from nitric oxide using atomically dispersed Fe on N-doped carbon, Angew. Chem., Int. Ed., 2023, 62(26), e202304007.

[5] J. Xian, S. Li, H. Su, P. Liao, S. Wang, R. Xiang, Y. Zhang, Q. Liu and G. Li, Electrosynthesis of α–amino acids from NO and other NOx species over CoFe alloy–decorated self– standing carbon fiber membranes, Angew. Chem., Int. Ed., 2023, 62(30), e202306726.

[6] S. Y. Tee, K. Y. Win, W. S. Teo, L. D. Koh, S. H. Liu, C. P. Teng and M. Y. Han, Recent progress in energy driven water splitting, Adv. Sci., 2017, 4, 24.

[7] P. Ahmadi, S. H. Torabi, H. Afsaneh, Y. Sadegheih, H. Ganjehsarabi and M. Ashjaee, The effects of driving patterns and PEM fuel cell degradation on the lifecycle assessment of hydrogen fuel cell vehicles, Int. J. Hydrogen Energy, 2020, 45, 3595–3608.

[8] J. P. Jones, G. K. S. Prakash and G. A. Olah, Electrochemical CO2 reduction: recent advances and current trends, Isr. J. Chem., 2014, 54, 1451–1466.

[9] G. Qing, R. Ghazfar, S. T. Jackowski, F. Habibzadeh, M. M. Ashtiani, C. P. Chen, M. R. Smith and T. W. Hamann, Recent advances and challenges of electrocatalytic N2 reduction to ammonia, Chem. Rev., 2020, 120, 5437–5516.

[10] Shi, Y. M.; Zhang, B. Recent advances in transition metal phosphide nanomaterials: Synthesis and applications in hydrogen evolution reaction. Chem. Soc. Rev. 2016, 45, 1529−1541.

[11] Sun, F. C.; Li, Q.; Xue, H. G.; Pang, H. Pristine Transition metal-based metal-organic frameworks for electrocatalysis. ChemElectroChem 2019, 6, 1273−1299.

[12] Morales-Guio, C. G.; Stern, L. A.; Hu, X. L. Nanostructured hydrotreating catalysts for electrochemical hydrogen evolution. Chem. Soc. Rev. 2014, 43, 6555−6569.

[13] Wang, H. F.; Chen, L. Y.; Pang, H.; Kaskel, S.; Xu, Q. MOFderived electrocatalysts for oxygen reduction, oxygen evolution and hydrogen evolution reactions. Chem. Soc. Rev. 2020, 49, 1414−1448.

[14] Tahir, M.; Pan, L.; Idreesd, F.; Zhang, X. W.; Wang, L.; Zou, J. J.; Wang, Z. L. Electrocatalytic oxygen evolution reaction for energy conversion and storage: A comprehensive review. Nano Energy 2017, 37, 136−157.

[15] Liang, Q. N.; Chen, J. M.; Wang, F. L.; Li, Y. W. Transition metal-based metal-organic frameworks for oxygen evolution reaction. Coord. Chem. Rev. 2020, 424, No. 213488.

[16] Y.-C. Zhang, C. Han, J. Gao, L. Pan, J. Wu, X.-D. Zhu and J.-J. Zou, NiCo-Based Electrocatalysts for the Alkaline Oxygen Evolution Reaction: A Review, ACS Catal., 2021, 11, 12485–12509.

[17] K. Zhu, F. Shi, X. Zhu and W. Yang, The roles of oxygen vacancies in electrocatalytic oxygen evolution reaction, Nano Energy, 2020, 73, 104761.

[18] F. Gao, Y. Zhang, Z. Wu, H. You and Y. Du, Universal strategies to multi-dimensional noble-metal-based catalysts for electrocatalysis, Coord. Chem. Rev., 2021, 436, 213825.

[19] L. Han, S. Dong and E. Wang, Transition-Metal (Co, Ni, and Fe)-Based Electrocatalysts for the Water Oxidation Reaction, Adv. Mater., 2016, 28, 9266–9291.

[20] R. Zhang, G. van Straaten, V. di Palma, G. Zafeiropoulos, M. C. M. van de Sanden, W. M. M. Kessels, M. N. Tsampas and M. Creatore, Electrochemical Activation of Atomic Layer-Deposited Cobalt Phosphate Electrocatalysts for Water Oxidation, ACS Catal., 2021, 11, 2774– 2785.

[21] S. A. Chala, M. C. Tsai, B. W. Olbasa, K. Lakshmanan, W. H. Huang, W. N. Su, Y. F. Liao, J. F. Lee, H. Dai and B. J. Hwang, Tuning Dynamically Formed Active Phases and Catalytic Mechanisms of In Situ Electrochemically Activated Layered Double Hydroxide for Oxygen Evolution Reaction, ACS Nano, 2021, 15, 14996–15006.

[22] Furukawa, H.; Cordova, K. E.; O'Keeffe, M.; Yaghi, O. M. The Chemistry and Applications of Metal-Organic Frameworks. Science 2013, 341 (6149), 1230444.

[23] Lin, Y.; Wan, H.; Wu, D.; Chen, G.; Zhang, N.; Liu, X.; Li, J.; Cao, Y.; Qiu, G.; Ma, R. Metal-Organic Framework Hexagonal Nanoplates: Bottom-up Synthesis, Topotactic Transformation, and Efficient Oxygen Evolution Reaction. J. Am. Chem. Soc. 2020, 142 (16), 7317−7321.

[24] A. Bavykina, N. Kolobov, I. S. Khan, J. A. Bau, A. Ramirez and J. Gascon, Metal–Organic Frameworks in Heterogeneous Catalysis: Recent Progress, New Trends, and Future Perspectives, Chem. Rev., 2020, 120, 8468–8535.

[25] R.-L. Peng, J.-L. Li, X.-N. Wang, Y.-M. Zhao, B. Li, B. Y. Xia and H.-C. Zhou, Single-atom implanted two-dimensional MOFs as efficient electrocatalysts for the oxygen evolution reaction, Inorg. Chem. Front., 2020, 7, 4661–4668.

[26] P. Q. Liao, J. Q. Shen and J. P. Zhang, Metal-organic frameworks for electrocatalysis, Coord. Chem. Rev., 2018, 373, 22–48.

[27] S. Yuan, L. Feng, K. C. Wang, J. D. Pang, M. Bosch, C. Lollar, Y. J. Sun, J. S. Qin, X. Y. Yang, P. Zhang, Q. Wang, L. F. Zou, Y. M. Zhang, L. L. Zhang, Y. Fang, J. L. Li and H. C. Zhou, Stable Metal-Organic Frameworks: Design, Synthesis, and Applications, Adv. Mater., 2018, 30, 1704303

[28] G. Gao, D. Wei, L. Li, M. Wei, X. Chen, Y. Yu, G. Yang, G. Zhu, L. Han, J. Jia, Accordion-like Co-MOF derived heterostructured Co/CoP@PNC as highly efficient electrocatalyst for alkaline hydrogen evolution reaction, Int. J. Hydrog. Energy 51 (2024) 1333–1342.

[29] L. Jiao, J.Y.R. Seow, W.S. Skinner, Z.U. Wang, H.L. Jiang, Metal-organic frameworks: Structures and functional applications, Mater. Today 27 (2019) 43–68.

[30] Y.K. Cong, S.S. Huang, Y. Mei, T.T. Li, Metal-organic frameworks-derived selfsupported carbon-based composites for electrocatalytic water splitting, Chem.-Eur. J. 27 (2021) 15866–15888.

[31] Asnavandi, Majid, et al. "Promoting oxygen evolution reactions through introduction of oxygen vacancies to benchmark NiFe–OOH catalysts." *ACS Energy Letters* 3.7 (2018): 1515-1520.

[32] Sun, Fengzhan, et al. "NiFe-based metal–organic framework nanosheets directly supported on nickel foam acting as robust electrodes for electrochemical oxygen evolution reaction." *Advanced Energy Materials* 8.21 (2018): 1800584.

[33] Salmanion, Mahya, and Mohammad Mahdi Najafpour. "Structural changes of a NiFe-based metal-organic framework during the oxygen-evolution reaction under alkaline conditions." *International Journal of Hydrogen Energy* 46.37 (2021): 19245-19253.

[34] Zhao, Tao, et al. "Preparation of a Bimetallic NiFe-MOF on Nickel Foam as a Highly Efficient Electrocatalyst for Oxygen Evolution Reaction." *ChemistrySelect* 6.6 (2021): 1320-1327.

Perspective Review on Terahertz Generation in Organic Nonlinear Optical Crystals

Manoj K.S
Department of Physics,
Thiagarajar College of Engineering,
Madurai, Tamil Nadu, India
ksmanoj@student.tce.edu

M. Tamilelakkiya
Department of Physics,
Thiagarajar College of Engineering,
Madurai, Tamil Nadu, India
mtphy@tce.edu

***Abstract*— Generating Terahertz (THz) radiation has emerged as a critical tool in spectroscopy, imaging, and communication technologies. Organic nonlinear optical (NLO) crystals, with their significant nonlinear coefficients and tuneable properties, have become promising candidates for efficient THz generation. This review synthesizes findings from recent studies on THz generation in organic crystals, including 2-Amino-5-Nitropyridinium Dihydrogen Phosphate (2A5NPDP), 2-Amino-5-Nitrotoluene (MNA), N-benzyl-2-methyl-4-nitroaniline (BNA), and 3-Nitroaniline (mRNA). We discuss these crystals' growth techniques, structural properties, and THz generation efficiency, highlighting their potential for high-intensity THz applications. The review also explores the challenges in crystal growth and the prospects of organic NLO materials in THz technology.**

Keywords*— *NLO, Terahertz, Single Crystal

I. INTRODUCTION

The terahertz (THz) region of the electromagnetic spectrum, lying between microwaves and infrared, has garnered significant attention due to its unique spectroscopy, imaging, and security applications. However, the development of efficient THz sources remains a challenge. Organic nonlinear optical (NLO) crystals, with their high nonlinear coefficients and tuneable properties, have emerged as promising candidates for THz generation. These crystals can efficiently convert near-infrared (NIR) laser pulses into THz radiation through optical rectification, which relies on the crystal's second-order nonlinear susceptibility.Recent studies have focused on optimizing the growth of organic NLO crystals to achieve significant, high-quality single crystals suitable for THz generation. This review examines the growth techniques, structural properties, and THz generation efficiency of several organic NLO crystals, including 2A5NPDP, MNA, BNA, and mRNA. We also discuss the challenges in crystal growth and the potential of these materials for future THz applications.

II. GROWTH TECHNIQUES AND STRUCTURAL PROPERTIES

a) 2-AMINO-5-NITROPYRIDINIUM DIHYDROGEN PHOSPHATE (2A5NPDP)

2A5NPDP is a semi-organic NLO crystal with a large nonlinear coefficient and wide transparency range. The crystal was grown using the modified Sankaranarayanan–Ramasamy (SR) method, allowing unidirectional growth along the c-axis. The modified SR method addresses spurious nucleation and low growth rates, producing high-quality crystals with enhanced optical properties. The crystal exhibits a high laser damage threshold and thermal stability up to 175°C, making it suitable for high-power THz generation.

b) 2-AMINO-5-NITROTOLUENE (MNA)

MNA, known for its sizeable microscopic hyperpolarizability, has been challenging to grow in large single-crystal forms. To produce large MNA crystals, a two-step growth process involving sublimation followed by slow evaporation was developed. The crystals exhibit excellent THz generation properties, particularly when pumped with 1250 nm light, surpassing the performance of its derivative, BNA. The MNA crystals show a broad THz spectrum with high field strengths, making them one of the most efficient yellow THz generators.

c) N-BENZYL-2-METHYL-4-NITROANILINE (BNA)

BNA, a derivative of MNA, was developed to improve crystallization properties. BNA crystals were grown from the melt and cleaved to the desired thickness. When pumped with 800 nm and 1250-1500 nm light, the crystals exhibit a broad THz spectrum. However, the THz generation efficiency of BNA is lower than that of MNA due to its lower molecular density. The crystal's THz refractive index and absorption coefficient were measured, showing minimal absorption features contributing to its smooth THz spectrum.

d) 3-NITROANILINE (M-NA)

m-NA is a well-known organic NLO crystal with a simple molecular structure and significant electro-optic effect. The crystal was grown using a solution method, and its THz generation properties were characterized using a Ti:sapphire laser. The crystal exhibits a moderate THz bandwidth (0.9–2.3 THz), with the largest hyperpolarizability component along the charge transfer axis. The intermolecular hydrogen bonding in m-NA enhances its NLO activity, making it a potential candidate for THz imaging applications.

III. THZ GENERATION EFFICIENCY AND APPLICATIONS

The THz generation efficiency of organic NLO crystals is influenced by crystal thickness, pump wavelength, and phase matching factors. MNA and 2A5NPDP exhibit high THz generation efficiency, with MNA producing THz fields up to 1 MV/cm when pumped with 1250 nm light. While less efficient than MNA, BNA still generates a broad THz spectrum, particularly when pumped with 800 nm light. m-NA, with its moderate THz bandwidth, is suitable for applications requiring lower frequency THz radiation.The

THz generation efficiency of these crystals is also affected by their absorption coefficients and refractive indices. MNA and BNA show minimal absorption in the THz range, contributing to their broad and smooth THz spectra. The phase-matching conditions, which depend on the crystal's refractive index and pump wavelength, are crucial in determining the THz generation efficiency.

IV. CONCLUSION

Organic NLO crystals, such as 2A5NPDP, MNA, BNA, and m-NA, have demonstrated significant potential for efficient THz generation. The development of advanced growth techniques, such as the modified SR method and two-step sublimation-evaporation process, has enabled the production of high-quality single crystals with enhanced optical properties. These crystals exhibit high THz generation efficiency, broad THz spectra, and good thermal stability, making them suitable for various THz applications, including spectroscopy, imaging, and communication.

Future research should focus on further optimizing the growth techniques to produce larger and higher-quality crystals and exploring new organic NLO materials with even higher nonlinear coefficients. Integrating these crystals into practical THz devices will require addressing challenges such as crystal damage thresholds and phase-matching conditions. With continued advancements, organic NLO crystals are poised to play a pivotal role in developing next-generation THz technologies.

V. ACKNOWLEDGEMENT

This research work in financially supported by Thiagarajar Research Fellowship (TRF) scheme – (TCE/RD/TRF/10 dated 27.09. 2024).

REFERENCES

[1] Vediyappan, Sivasubramani, et al. "Evaluation of linear and nonlinear optical properties of D− π–A type 2-amino-5-nitropyridinium dihydrogen phosphate (2A5NPDP) single crystal grown by the modified Sankaranarayanan–ramasamy (SR) method for terahertz generation." *Crystal Growth & Design* 19.12 (2019): 6873-6892.

[2] Palmer, Bruce Wayne H., et al. "Large Crystal Growth and THz Generation Properties of 2-Amino-5-Nitrotoluene (MNA)." *ACS Applied Electronic Materials* 4.9 (2022): 4316-4321.

[3] Krishnakumar, V., and R. Nagalakshmi. "Terahertz generation in 3-nitroaniline single crystals." *Crystal Growth and Design* 8.11 (2008): 3882-3884.

[4] Esaulkov, Mikhail N., et al. "Aminopyridines and 4-nitrophenol cocrystals for terahertz application." *Optics & Laser Technology* 108 (2018): 450-455.

[5] Lasalle, B. Sahaya Infant, et al. "Growth and characterization of piperazine bis (trifluoroacetate) (PTFA) single crystal for terahertz (THz) optoelectronic applications." *Optical Materials* 148 (2024): 114968.

[6] Kim, Pil-Joo, et al. "Highly Efficient Organic THz Generator Pumped at Near-Infrared: Quinolinium Single Crystals." *Advanced Functional Materials* 22.1 (2012): 200-209.

Opto Electrical Studies of TiO_2 Nanoparticles of Chitosan-Polyvinyl Pyrrolidone

Kavitha A
Department of Chemistry,
Thiagarajar College of Engineering,
Madurai
kavithaamunnar@gmail.com

Sunija A.J
Department. of Chemistry,
Thiagarajar College of Engineering,
Madurai
ajschem@tce.edu

***Abstract*— Biopolymers derived from renewable biological sources, have emerged as promising materials in electrical and electronic applications due to their biodegradability, flexibility, and tunable electrical properties. Ionic conductivity is a crucial property of electrolytes that plays a vital role for materials for optoelectronical properties. The electrical properties of film were examined electrical impedance spectroscopy (EIS). The highest ionic conductivity of 2.00×10^{-3} S/cm, was achieved in the 0.1 wt% TiO_2 NPs. The bandgap, absorption of biopolymer were confirmed by UV–Vis spectroscopy. The present results showed the nano particles doped polymer film in suggested for use in electronic application.**

Keywords—*Chitosan, Polyvinyl pyrolidine, TiO_2 NPs, Optical properties, Electrical properties.*

I. INTRODUCTION

The growing demand for sustainable and eco-friendly materials has driven significant advancements in the development of biopolymer-based nanocomposites for electronic, food application, biomedical application. Biopolymers, derived from renewable resources, offer inherent biodegradability and biocompatibility, making them attractive alternatives to conventional synthetic polymers [1]. However, their intrinsic limitations such as relatively low mechanical strength and limited electrical conductivity have restricted their widespread application. Polymers are commonly added to nanofillers which widely used to the energy storage devices to enhancing properties like improved barrier performance, mechanical strength, thermal stability, electrical conductivity, and film forming cabaplity [2]. These attributes make them a promising and innovative alternative for various applications, including packaging and electronics [3]. A wide range of nanofillers has been employed in the fabrication of nanocomposites.

Among these, the integration of Titanium-di-oxide (TiO_2) nanoparticles into biopolymers PolyVinyl Pyrrolidone(PVP) Chitosan (CHI) has gained considerable attention due to unique electrical, and structural properties. Titanium dioxide (TiO_2) as a conductive nano material has applied in the sensors, supercapacitors and electronic chips, photovoltaic cells, sensors[4-6]. One of the most common approaches synthesizing TiO_2 dispersion colloids in different solvents is to include TiO_2 in PVP-CHI [7]. Furthermore, the TiO_2 nanoparticles are more likely to interact in a CHI/PVP matrix because of the presence of –OH- groups in PVP and -NH_2 – PVP-CHI Respectively. The mechanical properties of the CHI matrix were improved by the interaction of TiO_2 via the CHI/TiO_2 composite [8]. Additionally, the use of biopolymers as the matrix material ensures that these advanced materials remain environmentally sustainable and eco-friendly.

II. MATERIALS AND METHODS

A. UV/Vis Spectroscopy

UV/Vis spectroscopy analyzed in the wavelength region from 200–800 nm with a spectrophotometer (OCEAN OPTICS) to analyze the absorbtion of the films and their optical properties.

B. Electrical Impednce spectroscopy

Electrochemical impedance spectroscopy (EIS) is one of the usual methods applied for the analysis of charging and transport phenomena in ion-conducting and conjugated polymers. It examines the conductivity of PVP-CHI-TiO NP biopolymer films. The film was incorporated between two blocking stainless steel electrodes. The impedance spectroscopy data are represented as nyquist plot. In the Nyquist plot, the negative imaginary impedance, -Zi is plotted against the real impedance component, Z [9].

1. Preparation of PVP/Chitosan nanocomposites blended films

A blend matrix of chitosan and polyvinylpyrrolidone (PVP) was prepared using a solution casting method. To prepare the chitosan solution, 1 g of chitosan powder dissolved in 100 ml of deionized water containing 2% acetic acid. The mixture is continuously stirred at 60 °C for 2 hours to obtain a homogeneous, viscous solution. Similarly, the PVP solution is prepared by dissolving 1 g of PVP in 100 ml of deionized water using the same method..

Titanium di oxide nanoparticles (TiO_2NPs) are incorporated 0.075 and 0.1 ratios with continuous stirring to ensure uniform dispersion of TiO_2 NPs within the matrix. The solution were poured into plastic Petri plates and dried in an oven at 40 °C for 5 hours. The films are then cooled at room temperature. The demoulded films are used for various property evalution.

III. RESULT AND DISCUSSION

A. Electrochemical Impedence Spectroscopy:

Electrical impedance spectroscopy is used to evaluate ionic conductivity of the polymer electrolytes. The test was performed using frequency sweep of 1KHz to10 Hz. Fig: 2 shows Nyquist plot of polymer film, where both samples showed a spike in the low-frequency region(10Hz). This spike is associated with charge double layer formation at the interfacial region.[16].Fig:2 also shows that the length of low frequency arc increases with the increase in nano particle concentration. The appearance of the spike signifies the high capacitive impedance, of the films along with a slight semicircle at higher frequencies.[10]

The complete Electrical Equivalent Circuit (EEC) model for the blend electrolytes is depicted (EEC) is also represented Fig:2 [11]. The reduction semicircles is represented for the high addition of nanoparticle content by considering enhanced ionic conductivity. In addition, the plasticizer glycerol to the films significantly contributes to enhancing conductivity by allowing salt dissociation[19].

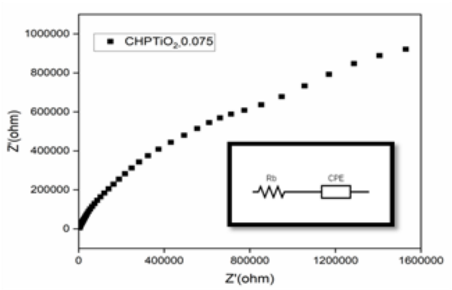

The ionic conductivity of bioplolymer film can be calculated using the following equation:

$\sigma = t\ AR_b\ Scm{-}^1$ ….. equn (1)

where σ is the ionic conductivity, A is the contact area of the sample, t is the thickness, and Rb is the bulk resistance of the polymer membrane.

TABLE 2: IONIC CONDUCTIVITY OF BLEND POLYMER WITH TiO_2 NPS

Composition	σ (Scm−1)	R_b(ohm)
$CHPTiO_2$-0.075	1.37×10^{-3}	65.96
$CHPTiO_2$-0.1	2.00×10^{-3}	46.04

The Table 2 presents the highest recorded ionic conductivity of **2.00×10^{-3} S/cm**, which is attributed to the increased number of charge carriers in the polymer film. In contrast, the lowest ionic conductivity of **1.37×10^{-3} S/cm** is likely due to a reduction in charge carrier mobility. The highest conductivity of **2.00×10^{-3} S/cm** was achieved for a sample with a **0.1 TiO_2 NPs to-polymer matrix ratio** [13]. EIS analysis further confirmed that the sample containing **0.1 TiO_2 NPs** exhibited the best conductivity, reaching **2.00×10^{-3} S/cm** [14]. The ionic conductivity increases by increasing the charge carrier density and ionic mobility of nano particles. Bulk resistance can calculated from the impedence graph (Fig 2).

B. UV-Visible Spectroscopy:

The analysis of the absorption spectrum shows the processes of electron excitation from a lower to a higher energy state. Fig. 3 illustrates the absorption spectrum of polymer matrix (200-800nm). The incorporation of TiO_2 nanoparticles into the PVA-CHI matrix leads to a shift in the absorbtion edge towards lower wavelength, indicating the decreasing the optical band gap[12,13]. The increased band gap energy results in a blueshift (shift to shorter wavelength) in the absorbtion edge of the material. . The absorbtion spectrum in the range of 321 to 293 nm (blue shift) is sharp and intense .The decreasing frequency due to the presence of the TiO_2 NPs and the plastisizer glycerol. The low intense additional peaks contribute from the surface defect in the films [14].

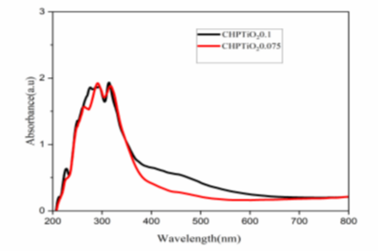

FIG 3: ABSORPTION SPECTRUM OF POLYMER BLENDS

The obtical band hap can calculate following this Equation

Tacue Equation : $\alpha h\nu = B(h\nu - Eg)\ P$……..equn (2)

Where (B) is constant of optical transition (direct or indirect), and the (P) is concerning to the distribution of the density of states.

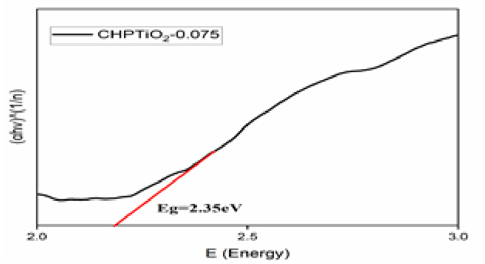

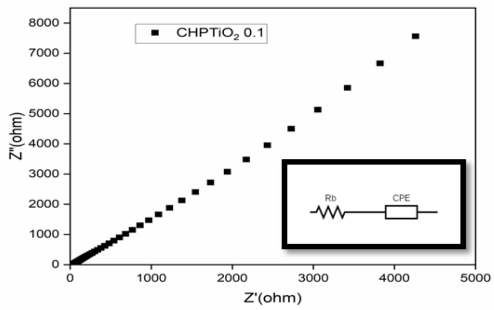

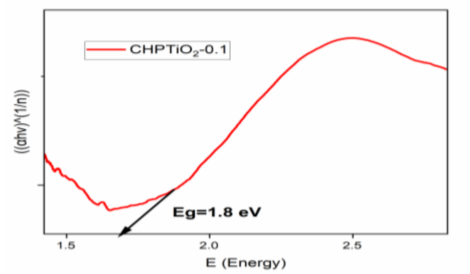

IV. CONCLUSION

The biobased polymer films based on PVA-CHI blend dopped with TiO_2 NPs has been prepared by solution casting method.The UV absorbtion spectrum confirmed the electron excitation from lower energy state to higher energy state and the addition of TiO_2 NPs decresed the bandgap. Electrical impedence analysis shows that increase in TiO_2 NPs concentration and also increase ionic conductivity and the conductance of films obtained from 1.37×10^{-3} to 2.00×10^{-3}

.Thus it can be concluded that the films have possible applications as solid polymer electrolytes in batteries.

V. ACKOWLEDGEMENT

This research work in financially supported by Thiagarajar Research fellowship (TRF) scheme-dated (27.09.2024)

REFERENCE

[1] N. Basavegowda and K.-H. Baek, "Advances in functional biopolymer-based nanocomposites for active food packaging applications," *Polymers*, vol. 13, no. 23, p. 4198, 2021.

[2] N. Olivera, T. B. Rouf, J. C. Bonilla, J. G. Carriazo, N. Dianda, and J. L. Kokini, "Effect of LAPONITE® addition on the mechanical, barrier and surface properties of novel biodegradable kafirin nanocomposite films," *J. Food Eng.*, vol. 245, pp. 24–32, 2019.

[3] M. T. Albdiry and B. F. Yousif, "Toughening of brittle polyester with functionalized halloysite nanocomposites," *Compos. Part B Eng.*, vol. 160, pp. 94–109, 2019.

[4] Y. Lin, S. Hu, and G. Wu, "Structure, dynamics, and mechanical properties of polyimide-grafted silica nanocomposites," *J. Phys. Chem. C*, vol. 123, pp. 6616–6626, 2019.

[5] J. Li, S. Zivanovic, P. M. Davidson, and K. Kit, "Characterization and comparison of chitosan/PVP and chitosan/PEO blend films," *Carbohyd. Polym.*, vol. 79, pp. 786–791, 2010.

[6] W. A. Al-Taa'y, "Optical Properties of Poly (vinyl alcohol) PVA Films Doped with Fe Citrate", Journal of Al-Nahrain University Science, Vol.17, No 4, pp.95-102, (2014)

[7] S. B. Aziz, A. S. F. M. Asnawi, R. T. Abdulwahid, H. O. Ghareeb, S. M. Alshehri, T. Ahamad, J. M. Hadi, and M. F. Z. Kadir, "Design of potassium ion conducting PVA-based polymer electrolyte with improved ion transport properties for EDLC device application," *J. Mater. Res. Technol.*, vol. 13, pp. 933–946, 2021.

[8] H. N. Kwon, S. J. Jang, Y. C. Kang, and K. C. Roh, "The effect of ILs as co-salts in electrolytes for high voltage supercapacitors," *Sci. Rep.*, vol. 9, p. 1180, 2019.

[9] P. Galek, A. Slesinski, K. Fic, and J. Menzel, "Peculiar role of the electrolyte viscosity in the electrochemical capacitor performance," *J. Mater. Chem. A*, vol. 9, pp. 8644–8654, 2021.

[10] P. Arya A. and A. L. Sharma, "Conductivity and dielectric spectroscopy of Na^+ ion conducting blended solid polymer nanocomposites," in *Recent Research Trends in Energy Storage Devices*, Y. Sharma, G. D. Varma, A. Mukhopadhyay, and V. Thangadurai, Eds. Singapore: Springer, 2021.

[11] V. Cyriac, Ismayil, I. M. Noor, K. Mishra, C. Chavan, R. F. Bhajantri, and S. P. Masti, "Ionic conductivity enhancement of PVA: carboxymethyl cellulose poly-blend electrolyte films through the doping of NaI salt," *J. Mater. Sci.*, published online Mar. 7, 2022

[12] D. Harinkhere, N. Karma, K. K. Choudhary, and N. Kaurav, "Structural and optical properties of PPO/PVP blended polymer film," *Mater. Today: Proc.*, vol. 54, no. 3, pp. 620–623, 2022

[13] N. J. Mohammed, Z. S. Rasheed, and A. S. Hassan, "Improvement of optical properties of PVA/TiO_2 and PVA/ZnO nanocomposites,"

Perspective Review of Bismuth Oxysulfide (Bi_2O_2S) in Various Applications and Investigation of its Electrochemical Performance

R. Bhuvanesh Kumar
Department of Physics,
(Research Scholar)
Thiagarajar College of Engineering,
Madurai, India.
rbhuvanesh@student.tce.edu

M. Mahendran
Department of Physics,
(Head & Professor)
Thiagarajar College of Engineering,
Madurai, India.
manickam-mahendran@tce.edu

P. Velusamy
Department of Physics,
(Assistant Professor)
Thiagarajar College of Engineering,
Madurai, India.
velusamy.phy@gmail.com

***Abstract*—Bismuth oxysulfide (Bi_2O_2S) has gained significant attention as a versatile material with a wide range of potential applications in energy storage, photocatalysis, and optoelectronics. Recent studies highlight its unique properties, including a narrow bandgap, high carrier mobility, and excellent photoelectric response, which make it an attractive candidate for these applications. Bi_2O_2S can form heterojunctions with other semiconductors, such as reduced graphene oxide (rGO) and graphitic carbon nitride (g-C_3N_4), further enhancing its performance. These heterojunctions improve the efficiency of energy storage devices, facilitate the photocatalytic degradation of pollutants, and contribute to enhanced near-infrared (NIR) photodetection capabilities. Additionally, recent research into Bi_2O_2S's use in supercapacitors has demonstrated its promising performance, particularly in terms of energy storage and cycling stability. This review consolidates the findings from recent investigations on Bi_2O_2S, providing an in-depth look at its synthesis methods, structural characteristics, and diverse applications. Furthermore, it offers valuable insights into the material's potential for advancing sustainable energy technologies and environmental remediation and we have synthesised and investigated the supercapacitor performance of Bi_2O_2S.**

Keywords—Bismuth oxysulfide, Heterojunction, Photodetection, supercapacitor, photocatalytic degradation

I. INTRODUCTION

Bismuth-based materials have received considerable attention because of their unique electronic and optical properties, making them suitable for a wide range of applications. Among these, bismuth oxysulfide (Bi_2O_2S) stands out due to its layered structure, narrow bandgap (~1.12-1.5 eV), and high carrier mobility. These properties make Bi_2O_2S an excellent candidate for energy storage, photocatalysis, and optoelectronic devices. Recent studies have demonstrated the material's potential in aqueous rechargeable alkaline batteries (ARABs), photocatalytic degradation of antibiotics, and NIR photodetection. This review aims to provide a comprehensive perspective on the synthesis, properties, and applications of Bi_2O_2S, drawing from recent research findings. Functional compounds like Bi_2O_2S are produced by adding oxygen to the chain-like bismuth sulfide of Bi_2S_3. Nanosized Bi2O2S nanoparticles with a direct band gap of 1.12 eV are created using a simple hydrothermal process. However, the poor kinetics and low cycling stability of bi-based materials have significantly limited their use in energy storage applications. Inspired by the unique structural characteristics of two-dimensional (2D) materials, Bi2O2S displays a fast ion diffusion channel and a relatively robust structure.

II. REVIEW

2.1. Energy Storage Applications

Bi_2O_2S has shown promise as an anode material in aqueous rechargeable alkaline batteries (ARABs). Liu et al. (2022) synthesized 2D/2D Bi_2O_2S@rGO nanosheets using a one-step hydrothermal process, achieving a high specific capacity of 250.51 mAh g^{-1} at a current density of 1 A g^{-1}. The full cell, using Bi_2O_2S@rGO as an anode and $(NiCo)_5S_8$ as a cathode, perform a high energy density of 82.91 W h kg^{-1} and good cycling stability, and has capacity retention rate of 92.74% after 5,000 cycles. The improved performance resulted from the synergistic effect of the 2D/2D heterojunction, which enabled rapid ion diffusion and electron transport.

2.2. Photocatalytic Degradation

Bi_2O_2S has also been explored for its photocatalytic properties, particularly in the degradation of organic pollutants. Nadella et al. (2024) investigated the photocatalytic degradation of tetracycline using a Bi_2O_2S/g-C_3N_4 heterojunction. The composite exhibited a degradation rate of 64%, significantly higher than that of g-C_3N_4 and Bi_2O_2S alone. The improved photocatalytic activity was due to the creation of a heterojunction, which enhanced charge separation and minimized electron-hole recombination. The study highlighted the potential of Bi_2O_2S-based composites in environmental remediation, particularly for the degradation of persistent organic pollutants.

2.3. Optoelectronic Applications

In the field of optoelectronics, Bi_2O_2S has demonstrated excellent performance as a NIR photodetector. Chitara et al. (2020) synthesized ultrathin Bi_2O_2S nanosheets via a room-temperature wet-chemical method, achieving a photoresponsivity of 4 A/W and an external quantum efficiency of 630% under 785 nm laser illumination. The material's fast response time (100 ms) and high normalized photocurrent-to-dark-current ratio (1.3×10^{10} per watt) It is a promising candidate for flexible and large-area optoelectronic devices. The study also highlighted the material's air stability, which is crucial for practical applications.

2.4. Superconducting Properties

Zhang et al. (2015) explored the thermal decomposition of Bi_2O_2S to form superconducting $Bi_4O_4S_3$. The study demonstrated that Bi_2O_2S nanocrystals, prepared using a hydrothermal method, exhibited good photoelectric properties under visible light radiant flux. Upon annealing at 500 °C, the material transformed into $Bi_4O_4S_3$, which exhibited a superconducting transition temperature of 4.6 K. This finding opens up new avenues for the synthesis of superconducting materials through thermal decomposition, offering a novel route for the development of high-performance superconductors.

III. SYNTHESIS OF Bi_2O_2S NANOPARTICLE

Bi_2O_2S nanoparticles were made hydrothermally using the previously described technique. In short, 50 mL of deionized H_2O was mixed with 1.7403 g of bismuth (III) nitrate pentahydrate and 0.1542 g of thiourea for 20 minutes, and then 12 g of lithium hydroxide monohydrate was added. After 50 minutes of stirring using sonication, the mixture was moved to a Teflon container and heated to 200 °C for 72 hours. The final product was repeatedly cleaned using ethanol and DD water. The product was Dehydrated in an oven and then heated for four hours at 400 °C under nitrogen gas.

IV. RESULT AND DISCUSSION

4.1 X-ray Diffraction Analysis

XRD analysis of the synthesized Bismuth oxysulfide (Bi_2O_2S) nanoparticles revealed sharp diffraction peaks at 2θ angles of 23.21°, 29.35°, 44.97°, and 49.22°. These peaks corresponded to the (110), (040), (111), (141), and (002) crystallographic planes respectively. The observed diffraction pattern matches with (JCPDS) File No. 00-034-1493. Figure 1 represents the XRD of prepared Bismuth oxysulfide (Bi_2O_2S).

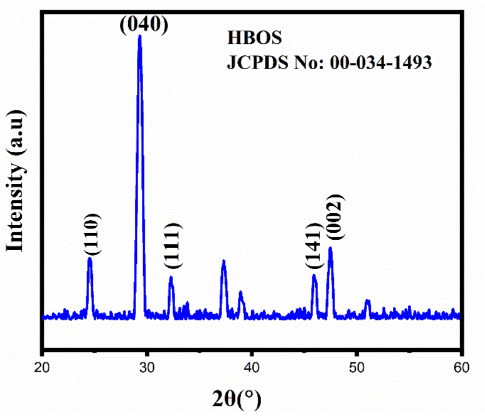

FIG. 1 POWDER XRD PATTERN OF THE SYNTHESIZED BISMUTH OXYSULFIDE (Bi_2O_2S)

The grain size is calculated from the FWHM of the central prominent significant peaks by using the following Scherer equation,

$$D = \frac{K\lambda}{\beta\ Cos\theta} \quad (1)$$

where'*D'* is mean size of ordered (crystalline) domains, *'K'* is dimensions less shape feature (0.94), '*λ*' is the x-ray (λ=1.5406Å), and 'θ' is the Bragg angle.

The dislocation density was found using equation

$$\delta = \frac{1}{D^2} \quad (2)$$

Where 'δ' dislocation density, 'D' is crystalline size.

The microstrain of the NPs was carried out by using equation (3)

$$\varepsilon = \frac{\beta}{4\tan\theta} \quad (3)$$

Where 'ε' is microstrain of the NPs, β is the FWHM of the peak.

TABLE 1 CRYSTALLINE SIZE, MICROSTRAIN AND DISLOCATION DENSITY OF Bi_2O_2S.

2θ (°)	Crystalline Size(D) (nm)	Microstrain(ε) × 10^{-3}	Dislocation Density (δ) × 10^{14} (lines/m^2)
23.21	11.02	0.00010812	8.2205
29.35	24.36	0.0007868	1.6842
44.97	15.83	0.002178	3.9866
49.22	12.13	0.0028430	6.7895

4.2 Electrochemical Studies

The electrochemical investigations were conducted using cyclic voltammetry (CV) in a 3M KOH electrolyte. A three-electrode system was employed, with the working electrode prepared from 1 mg of active material, 370 µL of ethanol, and 30 µL of Nafion, applied to a 1x1 cm area of cleaned nickel foam. A platinum rod served as the counter electrode, while a calomel electrode was utilized as the reference electrode. CV was performed to evaluate the electrochemical performance of the prepared material in the 3M KOH electrolyte at room temperature. Figure 2 illustrates the CV curves of the sample labeled BOS, tested at various scan rates of 10, 20, 30, 40, 50, and 60 mV/s within a fixed potential window of 0 to 0.55 V. The results indicate a larger polygonal area and a higher specific capacitance of 460 F/g at a scan rate of 10 mV/s, suggesting that this material has potential as a supercapacitor and demonstrates good cyclic performance.

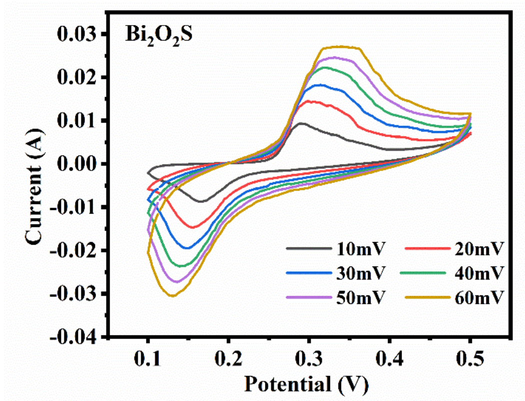

FIG. 2. CYCLIC VOLTAMMETRY GRAPH OF SYNTHESIZED BISMUTH OXYSULFIDE (BOS)

Bismuth oxysulfide (BOS) was later analyzed using the GCD technique to evaluate the performance of the supercapacitor electrode. The following formula was used to calculate the specific capacitance of the electrodes based on their GCD profile:

$$Cs = \frac{I\Delta t}{m\Delta V} \quad (4)$$

Charge/discharge cycles for the electrode were recorded with increasing current densities from 1 to 3 A g−1 in 3 M KOH electrolyte to determine the specific capacitance. Figure 4 displays the GCD profiles. Charge and discharge cycles for the electrode were recorded with increasing current densities from 1 to 3 A g−1 in a 3 M KOH electrolyte to determine the specific capacitance. We have calculated that 1A is 162 gA^{-1}, 2A is 160 gA^{-1}, and 2A is 140 $gA^{-}1$.Figure 3 displays the galvanostatic charge-discharge profiles. An analogous circuit that includes the answer is shown in Fig. 4 inset. The EIS data may be fitted using Q, which stands for Constant Phase Element, and W, which stands for Warburg impedance. The BSO electrode materials have a resistance of around 1.33 Ω, according to the obtained EIS.

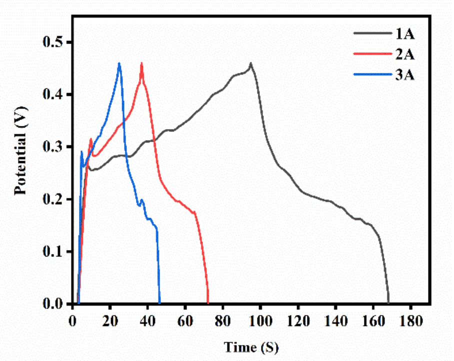

FIG. 3. GCD OF SYNTHESIZED BISMUTH OXYSULFIDE (BOS)

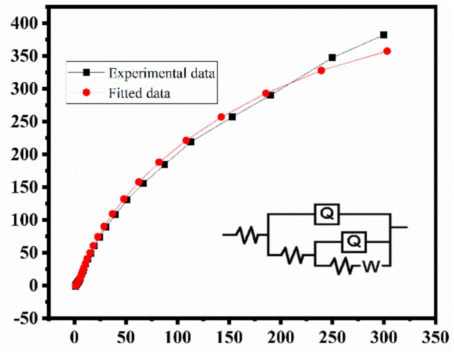

FIG. 4. EIS OF SYNTHESIZED BISMUTH OXYSULFIDE (BOS)

V. CONCLUSION

Bismuth oxysulfide (Bi_2O_2S) has emerged as a multifunctional material with significant potential in energy storage, photocatalysis, and optoelectronics. Its unique properties, such as a narrow bandgap, high carrier mobility, and excellent photoelectric response, make it a promising candidate for various applications. The formation of heterojunctions with materials like rGO and g-C_3N_4 has further enhanced its performance, enabling high energy density in batteries, efficient photocatalytic degradation of pollutants, and high-performance NIR photodetection. Additionally, the thermal decomposition of Bi_2O_2S to form superconducting $Bi_4O_4S_3$ highlights its potential in the development of new superconducting materials. Future research should focus on optimizing the synthesis methods, exploring new heterojunction combinations, and scaling up the production of Bi_2O_2S-based devices for practical applications. With continued advancements, Bi_2O_2S is poised to play a crucial role in the development of sustainable energy and environmental technologies. Through XRD we conform the material at Nano scale and Bi_2O_2S shows higher specific capacity and good cyclic stability and so it is suitable for supercapacitor application

VI. ACKNOWLEDGEMENT

This research work in financially supported by Thiagarajar Research Fellowship (TRF) scheme - (File.no: TCE/RD/TRF/<<11>> dated 28.02.2025)

REFERENCES

[1] Liu, Y.-L., et al. (2022). Bi_2O_2S nanosheets anchored on reduced graphene oxides as superior anodes for aqueous rechargeable alkaline batteries. *Electrochimica Acta*, 427, 140833.

[2] Nadella, S., et al. (2024). Photocatalytic degradation of antibiotic tetracycline by 2D Bi_2O_2S/g-C_3N_4 heterojunction under visible irradiation. *AIP Conference Proceedings*, 3170, 040009.

[3] Chitara, B., et al. (2020). Ultrathin Bi_2O_2S nanosheets near-infrared photodetectors. *Nanoscale*.

[4] Zhang, X., et al. (2015). Thermal decomposition of bismuth oxysulfide from photoelectric Bi_2O_2S to superconducting $Bi_4O_4S_3$. *ACS Applied Materials & Interfaces*, 7(7), 4442-4448.

[5] K. Fic, A. Platek, J. Piwek, E. Frackowiak, Sustainable materials for electrochemical capacitors, Mater. Today 21 (4) (2018) 437–454.

[6] N.M. Shinde, Q.X. Xia, J.M. Yun, R.S. Mane, K.H. Kim, Polycrystalline and mesoporous 3-D Bi2O3 nanostructured negatrodes for high-energy and power-asymmetric supercapacitors: superfast room-temperature direct wet chemical growth, ACS Appl. Mater. Interfaces 10 (13) (2018) 11037–11047

[7] D.-H. Nam, K.-S. Choi, Bismuth as a new chloride-storage electrode enabling the construction of a practical high capacity desalination battery, J. Am. Chem. Soc. 139 (32) (2017) 11055–11063.

[8] A. Rabenau, The role of hydrothermal synthesis in preparative chemistry, Angew. Chem. 97 (1985) 1017–1032.

[9] W. Luo, Z. Li, T. Yu, Z. Zou, Effects of surface electrochemical pretreatment on the photoelectrochemical performance of Mo-doped BiVO4, J. Phys. Chem. C 116 (2012) 5076–5081.

Synthesis and Investigation of SnO_2 and $SnFeO_2$ Nanoparticles for Improved Photocatalytic Activity and Antibacterial Performances

M. Deepika
Department of Physics,
Thiagarajar College of Engineering,
Madurai, India
deepikaam@student.tce.edu

S. Karthickprabhu
Department of Physics,
Thiagarajar College of Engineering,
Madurai, India
physics.karthickprabhu@gmail.com

***Abstract*—Nanotechnology has emerged as a revolutionary field with applications environmental science, and materials engineering. The synthesis of nanoparticles has gained significant attention due to their unique physicochemical properties, tunable optical properties, including high surface area, and enhanced reactivity. Among various nanomaterials, tin dioxide (SnO_2) and its doped derivatives have been extensively studied for their potential in antibacterial and photocatalysis applications. In this study, pure SnO_2 and $SnFeO_2$ nanoparticles were synthesized using the Sol-Gel method and characterized by XRD, SEM, EDAX, UV-Vis spectroscopy, photocatalytic activity, and antibacterial activity. XRD analysis confirmed the tetragonal crystal structure and the grain sizes calculated for SnO_2 and $SnFeO_2$ were 3.6652 nm and 3.8230 nm indicating an increase in grain size upon Fe doping. The microstrain values were determined as 2.096×10^{-3} and 1.975×10^{-3}, showing a decrease with doping. SEM images revealed a particle size of approximately 200 nm, while EDAX confirmed the presence of Sn, O, and Fe ions. UV-Vis spectroscopy shows a reduction in bandgap energy upon Fe doping. $SnFeO_2$ exhibited superior photocatalytic performance in the degradation of Malachite Green dye under visible light exposure. Additionally, both SnO_2 and $SnFeO_2$ nanoparticles effectively inhibited the growth of *Staphylococcus aureus*, demonstrating their potential as antibacterial agents.**

Keywords—Nanotechnology, Sol-gel method, Antibacterial, Photocatalytic, Dye Degradation.

I. Introduction

Nanotechnology is the science of designing, producing, and using structures and devices having one or more dimensions of about 100 millionth of a millimeter (100 nanometers) or less. Nanotechnology is the manipulation of matter on an atomic, molecular, and supramolecular scale. Nanotechnology referred to the particular technological goal of precisely manipulating atoms and molecules for fabrication of macro scale products [1,2]. The most important requirement for the nanotechnology definition is that the nano-structure has special properties that are exclusively due to its nanoscale proportions [3,4]. The design, characterization, production, and application of structures, devices, and systems by controlled manipulation of size and shape at the nanometer scale (atomic, molecular, and macromolecular scale) that produces structures, devices, and systems with at least one novel/superior characteristic or property [5,6,7]. The main types of nanostructure materials based on the dimensions of their structural elements are: zero-dimensional (0D), one-dimensional (1D), two-dimensional (2D) and three-dimensional (3D) nanomaterials. They can also be arranged by methods based on equilibrium or near equilibrium thermodynamics such as methods of self-organization and self-assembly (sometimes also called bio-mimetic processes) [8]. Using these methods, synthesized materials can be arranged into useful shapes so that finally the material can be applied to a certain application [9]. A reduction in the size of nano-sized particles increases the particle surface area. Additional chemical molecules may attach to this surface, enhancing the reactivity and increasing toxic effects. Small nanoparticles have more pathological and destructive power on the lungs due to the larger surface area, greater tendency to conjugate and energy sustainability [10]. High surface charge densities may cause higher cytotoxic effects than those with low charge densities. High surface charges react more intensely with cell membranes, creating additional damage to the cell. High surface charge densities may cause higher cytotoxic effects than those with low charge densities [11,12]. High surface charges react more intensely with cell membranes, creating additional damage to the cell. T. Preethi et. al synthesized $SnFeO_2$ nanoparticles using hydrothermal method. It shows the decrease of PL emission peak intensity with Fe doping revealed the generation of singly charged oxygen vacancies. The antibacterial behavior of Fe-SnO_2 NPs against Escherichia coli is examined by using the colony count method, and the inhibition rate was found to be 49, 65, 70, and 78% for pure, 0.01, 0.03, and 0.05M Fe-SnO_2 NPs, respectively [13]. Masoumeh Ghalkhani et. al synthesized $SnFeO_2$ nanoparticles using hydrothermal method. Obtained results indicated the effective role of the employed dopant. Best response in terms of the current enhancement, overvoltage reduction, and reversibility improvement of the L-Dopa oxidation reaction under experimental conditions was obtained by modified electrode with Fe doped SnO_2 nanoparticles [14].

In this present work, pure SnO_2 and $SnFeO_2$ was synthesized by sol-gel method. While doping the Fe to pure SnO_2 will increase the grain size and decrease in the microstrain. And it shows the better antibacterial activity which used for the paramedical industry.

II. SYNTHESIS OF SnO_2 AND $SnFeO_2$ NP

A. Methodology

Pure SnO_2 nanoparticles have been prepared by Sol-gel method. At first 0.05 molar solution of Stannous chloride was prepared by dissolving in 200ml of deionized water. After 10 minutes of stirring, Ammonium hydroxide was added drop by drop into the solution. The solution was stirred for 45 minutes and white precipitate was obtained. The excess water was removed from the obtained solution and dried in a room temperature for 5 days. Then it grained for 1 hour and then the obtained powder was kept in muffle furnace in 500°C for 2 hours. After that, the obtained powder was again grained for 1 hour to obtain a fine powder. The obtained powder was used for further measurements and analysis. Similar, process was used for the 1% of $SnFeO_2$ particle was prepared.

B. Characterization techniques:

The sample was characterized using various analytical instruments, including powder X-ray diffraction (PANalytical-XPERT PRO, Netherlands) measurement using CuKα radiation was employed to characterize the synthesized material.

$$D = \frac{k\lambda}{\beta \cos \theta}$$

Where,

D = Crystalline grain size

β = FWHM of the observed peak

λ = Wave length of the X-ray diffraction

θ = Angle of diffraction

$$\varepsilon = \frac{\beta}{4 \tan \theta}$$

Where, ε = Strain

β = FWHM of the observed peak

θ = Angle of diffraction

The morphological behavior and elemental analysis were done using SEM analyzer (JEOL-JSM.6400 with acceleration voltage of 5 kV). UV analysis of the samples was done at "Kalasaligam Academy for Research and Education, Krishnankoil ", in the wavelength range of 200 to 2000nm. The solvent use was deionized water. Antibacterial study of the sample was done at " V.V.Vanniaperumal College for Women, Virudhunagar" by using the bacteria *Staphylococcus*.

III. RESULT AND DISCUSSION

The crystal structure of undoped SnO_2 and Fe-doped SnO_2 recorded by powder X-ray diffraction (XRD) (λ = 1.5418 A˚), at scanning speed of 2°/min from 20° to 80°. The XRD features appeared at 2θ = 33.54°, 37.62°, 51.47°, 54.65° and 61.60° which were due to the diffractions of (101), (200), (211), (220)and (310) planes of the tetragonal rutile shape of SnO_2 crystal with standard JCPDS data card No. 880287. Average grain sizes of the samples were determined by using Scherer's equation on (101),(200),(211),(220)and (310) diffraction peak. The grain sizes were estimated to be 3.6652 nm and 3.8230 nm for SnO_2 and Fe doped SnO_2, respectively [15,16].While dopping value the grain was increased.

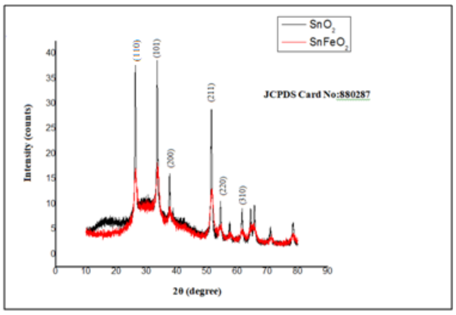

FIG:1 XRD PROFILE OF SnO_2 AND FE-DOPED SnO_2.

TABLE: 1 GRAIN SIZE AND STRAIN VALUE FOR SnO_2 AND $SnFeO_2$ FROM XRD DATA.

Sample	2θ (degree)	FWHM (10^{-3})	Grain size (nm)	Strain (10^{-3})
SnO_2	33.540	0.357	4.06812	1.1846
	51.479	0.444	3.47684	3.3214
	37.627	0.374	3.92790	2.2243
	61.605	0.462	3.50414	2.4976
	54.659	0.440	3.44912	1.2544
$FeSnO_2$	33.771	0.348	4.10553	1.4751
	51.576	0.357	4.03276	1.3311
	37.574	0.378	3.84446	2.5594
	61.678	0.456	3.38624	3.2379
	54.698	0.388	3.74645	1.2738

Figure shows the SEM image of the SnO_2 and $SnFeO_2$. The surface information near the surface of SnO_2 and $SnFeO_2$ (200 nm) were examined by using SEM. The image shows crystals of different sizes with smooth surfaces.

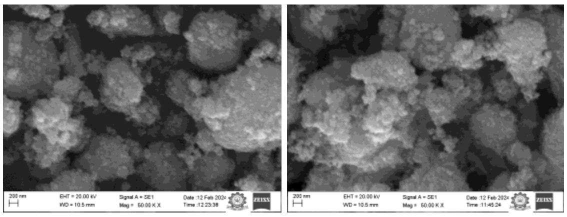

FIG:2 SEM IMAGES FOR SnO_2 AND $SnFeO_2$.

The EDS analysis of SnO_2 and SnFeO2was taken in order to find the elemental composition of The EDS spectrum of the sample was shown in figure 2 from the study of EDS, it is inferred that the concentration of manganese is found [17]. EDAX result for SnO_2 and Fe doped SnO_2 was shown in Table 2 and 3 .

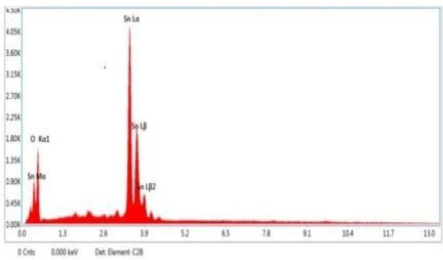

FIG:3 EDAX SPECTRUM FOR SnO_2 .

TABLE:2 PARAMETERS OF SnO_2 FROM EDAX.

Element	Weight %	Atomic %	Error %	Kratio
O K	13.5	53.7	9.2	0.0574
SnL	86.5	46.3	2.1	0.8264

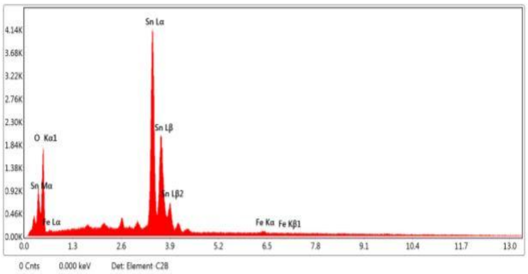

FIG: 4 EDAX SPECTRUM FOR SNFEO2.

TABLE:3 PARAMETERS OF $SnFeO_2$ FROM EDAX.

Element	Weight %	Atomic %	Error %	Kratio
O K	14.4	55.1	9.1	0.0619
SnL	84.1	43.3	2.1	0.7998
FeK	1.5	1.6	24.5	0.0145

The UV spectrums are shown in the figure:4.6 for SnO_2 and Fe doped SnO_2 respectively.

From the UV plot, the energy band gap is measured with the help of Tauc relation,

$\alpha h\nu = A(h\nu - Eg)n$

The graph is plotted between ($h\nu$) vs $(\alpha h\nu)^2$

Where,

α = Absorption coefficient,

h = Plank constant,

A = Optical constant,

ν = Frequency,

Eg = Energy band gap.

The extrapolation of the linear region of the curve towards the x-axis meets the energy axis in the case of SnO_2 and for the $SnFeO_2$ the values are decreasing from respectively. The results from UV analysis are tabulated in table 4. It shows that the band gap value has decreased after doping [18,19].

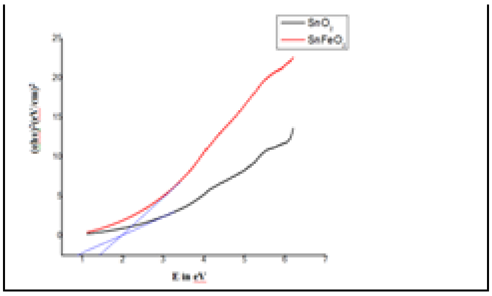

FIG:5 SHOWS THE BANDGAP OF SnO_2 AND $SnFeO_2$

TABLE 4 DETERMINATION BAND GAP FROM UV FOR SnO_2 AND $SnFeO_2$.

SAMPLE	BANDGAP(ev)
SnO_2	0.9
$SnFeO_2$	1.5

The photocatalytic degradation of Malachite green dye molecule using SnFeO2its are performed at room temperature under UV light at a wavelength of 617 nm. The least peak was noticed at 617 nm indicates the decreased level of Malachite green dye molecule with increasing UV exposure time that denotes the degradation of dye molecule at UV-irradiation. This shows 96 % of the degradation rate of dye molecule using $SnFeO_2$ within 80 min is due to excitation of semiconductor by UV-light to produce free radicals in the degradation of dye in which the excited electrons move from the valence band to the conduction band and generates high energy electron-hole pairs which transfer to adsorbed species on semiconductor results heterogeneous photo catalysis. The photocatalytic activity was done within 1.20 hrs and the Malachite green dye (0.2 L) was degraded successfully. Moreover, we have observed $SnFeO_2$ as an efficient photocatalytic adaptive nanoparticles [20,21,22].

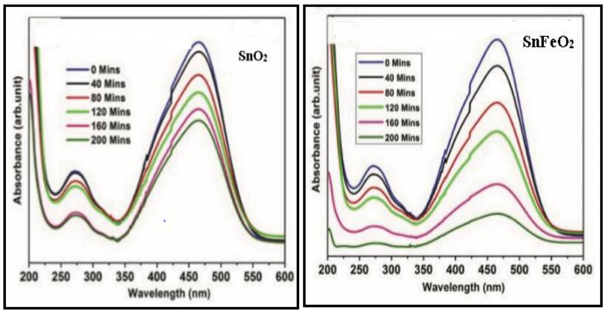

FIG 6 PHOTOCATALYTIC DEGRADATION OF SnO_2 AND $SnFeO_2$USING MALACHITE GREEN DYE.

Based on the impartial of a generation of novel antibiotics, the antibacterial activity was supported in contradiction of microbes and G+ (Staphylococcus aureus) bacteria for enlightening the efficacy of killing of bacteria [23,24,25]. Figure 6 reveals SnO_2 and $SnFeO_2$ against Staphylococcus aureus bacteria, respectively, and its displays the upgraded antibacterial action besides the target cultures and exposed nearly related that the typical antibiotics towards all the bacterial strains. It inhibits the antibacterial activity for both SnO_2 and SnFeO2nanoparticles. The enhanced antibacterial action of $SnFeO_2$ is conservative allied to the Fe ions, and SnO_2 NPs would effectually decorate on the microbial cell walls. Similarly, the microbe which is abundant transferences of a negative charge, while the metal oxide transferrals a positive charge, and these stocks electromagnetic desirability amid the metals and fourth the microbe summits to oxidative dynamic and finally bacteria will be dead [26,27,28] Additionally, this study will pave the way toward a green approach for producing metallic oxide nanoparticles and their use in many industries, such as agriculture and biomedicine [29,30] .

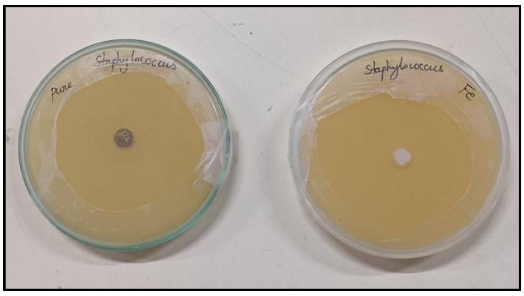

FIG 7 SHOWS A SnO_2 AND $SnFeO_2$ AGAINST THE BACTERIA STAPHYLOCOCCUS AUREUS.

TABLE 5 DETERMINATION OF ZONE INHIBITION FROM ANTIBACTERIAL ACTIVITY.

S.No	Name of the organisms	SnO_2 and $SnFeO_2$	zone of (mm) inhibition	Sensitive/ resistance
1	Staphylococcus	Amoxillin	20	Sensitive
		Tetracycline	11	Sensitive

IV. CONCLUSION

Pure SnO_2 and $SnFeO_2$ nanoparticle was prepared by Sol-Gel method and characterized by XRD, SEM, EDAX, UV-Spectroscopy, Photocatalytic Activity and Antibacterial Activity.When the preparation of SnO_2 and $SnFeO_2$ ammonium hydroxide was taken as the precursor solution. XRD pattern of SnO_2 and SnFeO2 nanoparticle was compared with JCPDS card no.880287 which confrimed the tetragonal structure of the crystal. The grain size was calculated using Debye Scherrer formula and found to be 3.6652 nm and 3.8230 nm for SnO_2 and Fe doped SnO_2, respectively. While doping the grain size was increased. The strain was calculated by using $\epsilon= \beta/4\tan\theta$ and found to be 2.096×10^{-3} and 1.975×10^{-3}.While doping the strain was decreased.A surface morphology was observed in synthesized samples from SEM images. From the SEM image the particle Size is around 200nm.The presence of Sn,O_2, and Fe ions was identified by EDAX analysis. Moreover, the bandgap energy was calculated through UV-Vis Spectroscopy, the optical belonging to enhanced significantly and reduction in bandgap was observed. The better photocatalyst was found to be $SnFeO_2$ for the Malachite green dye degradation process under visible light exposure. From the antibacterial activity for both SnO_2 and $SnFeO_2$ nanoparticles it inhibits the growth of Staphylococcus aureus bacteria and shows the promising potential of the synthesized nanoparticles as antibacterial agent.

V. ACKNOWLEDGMENT

This research work in financially supported by Thiagarajar Research Fellowship (TRF) scheme – (File no: TCE/RD/TRF/<<11>> dated 28.02.2025)

REFERENCES

[1] http://crno.orgm/whatis.htm

[2] http://eng.thesaurus.rusnano.com/wiki/article1371

[3] http://www.slideshare.net/tavirsir/xray-diffraction-technique

[4] http://science.howstuffworks.com/scanning-electron-microscope.htm

[5] http://www.princeton.edu/~achaney/tmve/wiki100k/docs/Ultraviolet_visible-spectroscopy.html

[6] https://www.sciencedirect.com/topics/chemistry/photocatalytic-activity

[7] https://www.sciencedirect.com/topics/pharmacology-toxicology-and-pharmaceutical-science/antibacterial-activity

[8] https://www.vedantu.com/chemistry/tin-oxide

[9] https://pubchem.ncbi.nlm.nih.gov/compound/FerricChloride#:~:text=Ferric%20chloride%20is%20an%20orange,to%20aluminum%20and%20most%20metals.

[10] https://www.turito.com/blog/chemistry/ferric-chloride

[11] Masoumeh Ghalkhani, Bahram Hosseini nia, Javad Beheshtian, Azam Anaraki Firooz Synthesis of undoped and Fe nanoparticles doped SnO_2 nanostructure: study of structural, optical and electrocatalytic properties. CROSSMARK publisher, 2021.

[12] Masoumeh Ghalkhani,Bahram Hosseini nia,Javad Beheshtian Azam Anaraki Firooz. Synthesis of undoped and Fe nanoparticles doped SnO2 nanostructure: study of structural, optical and electrocatalytic properties

[13] T.Preethi, K.Senthil, M.P.Pachamuthu ,R.Balakrishnaraja ,B Sundaravel,N.Geetha,and Stefano Bellucci . Effect of Fe Doping on Photocatalytic Dye-Degradation and Antibacterial Activity of SnO2 Nanoparticles.

[14] K.Sujatha, T.Seethalakshmi, A.P.Sudha and O.L. Shanmugasundaram. Photoluminescence properties of pure, Fe-doped and surfactant-assisted Fe-doped tin-oxide nanoparticles

[15] Ren L, Chong J, Loya A, et al. Determination of Cu 2+ ions release rate from antimicrobial copper bearing stainless steel by joint analysis using ICP-OES and XPS. Mater Technol [Internet]. 2015;30:B86–B89.

[16] Nune KC, Somani MC, Spencer CT, et al. Cellular response of Staphylococcus aureus to nanostructured metallic biomedical devices: surface binding and mechanism of disruption of colonization. Mater Technol [Internet]. 2017;32:22

[17] Rana S, Rawat J, Sorensson MM, et al. Antimicrobial function of Nd3+-doped anatase titania-coated nickel ferrite composite nanoparticles: A biomaterial system. Acta Biomater [Internet]. 2006;2:421–432.

[18] Y.Tanaka, H.Sakai, T.Tsuke, Y.Uesugi, Y.Sakai and K.Nakamura, "influence of coil current modulation on TiO nanoparticles synthesis using pulse modulated irradiation thermal plasma"519 (2011) 7100.

[19] K.S. Walton, R.Q. Snurr, "Applicability of the BET method for determining surface areas of microporous metal− organic frameworks, J. Am. Chem. Soc. 129 (27) (2007) 8552–8556.

[20] T.G. Glover, G.W. Peterson, B.J. Schindler, D. Britt, O. Yaghi, MOF-74 building unit has a direct impact on toxic gas adsorption, Chem. Eng. Sci. 66 (2) (2011) 163–170.

[21] M. Thommes, K.A. Cychosz, Physical adsorption characterization of nanoporous materials: progress and challenges, Adsorption 20 (2–3) (2014) 233–250.

[22] K.S. Walton, R.Q. Snurr, "Applicability of the BET method for determining surface areas of microporous metal− organic frameworks, J. Am. Chem. Soc. 129 (27) (2007) 8552–8556.

[23] T.G. Glover, G.W. Peterson, B.J. Schindler, D. Britt, O. Yaghi, MOF-74 building unit has a direct impact on

toxic gas adsorption, Chem. Eng. Sci. 66 (2) (2011) 163–170. [58] M. Thommes, K.A. Cychosz, Physical adsorption characterization of nanoporous materials: progress and challenges, Adsorption 20 (2–3) (2014) 233–250.

[24] D. Banerjee, H. Wang, B.J. Deibert, J. Li, Chapter 4: alkaline earth metal-based metal-organic frameworks: synthesis, properties and applications, in: S. Kaskel (Ed.), The Chemistry of Metal-Organic Frameworks: Synthesis, Characterization, and Applications, John Wiley & Sons, Hoboken, New Jersey, United States, 2016, pp. 73–99.

[25] D. Britt, H. Furukawa, B. Wang, T.G. Glover, O.M. Yaghi, Highly efficient separation of carbon dioxide by a metal-organic framework replete with open metal sites, Proc. Natl. Acad. Sci. Unit. States Am. 106 (49) (2009) 20637–20640. [17] M. Lopez, P. Canepa, T. Thonhauser, NMR study of small molecule adsorption in MOF-74-Mg, J. Chem. Phys. 138 (15) (2013) 154704.

[26] I. Ahmed, S.H. Jhung, Composites of metal-organic frameworks: preparation and application in adsorption, Mater. Today 17 (3) (2014) 136–146. [27] X.-W. Liu, T.-J. Sun, J.-L. Hu, S.-D. Wang, Composites of metal-organic frameworks and carbon-based materials: preparations, functionalities and applications, J. Mater. Chem. 4 (10) (2016) 3584–3616.

[27] Y. Liu, Z.U. Wang, H.C. Zhou, "Recent advances in carbon dioxide capture with metal-organic frameworks, Greenhouse Gases: Sci. Technol. 2 (4) (2012) 239–259.

[28] C. Petit, B. Levasseur, B. Mendoza, T.J. Bandosz, Reactive adsorption of acidic gases on MOF/graphite oxide composites, Microporous Mesoporous Mater. 154 (2012) 107–112.

[29] Y. Zhao, Y. Cao, Q. Zhong, CO2 capture on metal-organic framework and graphene oxide composite using a high-pressure static adsorption apparatus, Journal Of Clean Energy Technologies 2 (1) (2014) 34–37. [23] C. Petit, B. Mendoza, T.J. Bandosz, Reactive adsorption of ammonia on Cu-based MOF/graphene composites, Langmuir 26 (19) (2010) 15302–15309.

[30] C. Petit, B. Mendoza, T.J. Bandosz, Hydrogen sulfide adsorption on MOFs and MOF/graphite oxide composites, Chem Phys Chem 11 (17) (2010) 3678–3684.

Synthesis and Characterization of Cerium-Doped $CuNi_2O_4$ as a Potential Electrode for Enhanced Pseudo Capacitive Energy Storage

K. Aruna Devi
Department of Physics,
Thiagarajar College of Engineering,
Madurai, Tamil Nadu, India
arunadevik@student.tce.edu

S. Karthickprabhu
Department of Physics,
Thiagarajar College of Engineering,
Madurai, Tamil Nadu, India
physics. karthick@gmail.com

M. Mahendran
Department of Physics,
Thiagarajar College of Engineering,
Madurai, Tamil Nadu, India
manickam-mahendran@tce.edu

***Abstract*—Traditional energy storage technologies are increasingly required to meet rigorous performance standards, including rapid charge and discharge rates, high energy and power density, compact design, and lightweight attributes. These demands are primarily boosted by the fast-paced innovations within the electronics industry and the growing applications in electric vehicles, which call for higher efficient energy solutions. In this research, we focused on synthesizing cerium-doped $CuNi_2O_4$ using a facile solid-state reaction technique. To ensure the purity of the phases and to analyse the microstructural features of the synthesized materials, structural characterization techniques like XRD, FT-IR, SEM, and EDX. The electrochemical evaluation, mainly through cyclic voltammetry, revealed significant pseudocapacitive behaviour featuring distinct redox peaks. These findings indicate that the materials possess exceptional capacitive performance and stability. Additionally, galvanostatic charge-discharge experiments demonstrated a remarkable specific capacitance, showcasing the materials' efficiency at different current densities. Our findings, encouraged by thorough structural and electrochemical analyses, suggest that both $CuNi_2O_4$ and cerium-doped $CuNi_2O_4$ hold great promise as innovative materials for energy storage applications, paving the way for enhanced performance in future energy storage devices.**

Keywords—Binary Metal Oxide; $CuNi_2O_4$; Solid state reaction method; Pseudocapacitor.

I. INTRODUCTION

The rapid development of modern electronic gadgets has created a great need for simple and creative ways to efficient energy storage systems. The global reliance on electronic gadgets necessitates substantial study into developing low-cos tand highly efficient energy storage technology [1]. Battery is the most often utilized electrical energy storage technology. Battery is the favored technology for many applications.due to its ability to store Massive amounts of energy in a little space and weigh, while also providing adequate power levels. The storage surface and cycle life of most batteries have been an issueHowever, individuals have persisted in utilizing them due to the lack of alternatives until the advent of supercapacitors as a substitute [2]. Supercapacitors are perfect for uses where a high power density is needed, and quick charging, such as emergency actuators in airplanes, hybrid electric vehicles, photography flashes, electric screwdrivers, gondolas, and other high-power devices. Supercapacitors have also helped to stabilize power supplies and voltage in a variety of industries where load fluctuation is a significant issue. Flexible supercapacitors are used in wearable and portable electronics, allowing for twisting and folding [3].

Supercapacitors can be divided into three groups. These include hybrid capacitors, electrical double layer capacitors, and pseudocapacitors. The EDLC improves energy density and specific capacitance by storing charge at the interface between the electrode material and electrolyte ions. On the other hand, hybrid supercapacitors integrate both methods of charge storage. Electrochemical double layer capacitors (EDLC) are being investigated using graphene, activated carbon, graphene oxide, and carbonaceous compounds as materials. Potential materials for EDLC and psedocapactors include conducting polymers, transition metal oxides, and metal oxide composites [4].

Numerous study teams have looked at the electrochemical measurements of transition metal oxides. Spinel metal oxides, designated as MNi2O4, M represents Co, Ni, Mn, Cu, Zn are a kind of binary/ternary metal oxide that are cost-effective, abundant in nature, and have unique features. Cerium doped CuNi2O4 is a superior chemical and thermal stability, in addition to its supercapacitor properties [5,6]. Dopant ions alter the spinel lattice's cation distribution, affecting the structural and electrical characteristics of the samples. Few reports exist regarding Cerium substitution ferrite nanoparticles. K.Elayakumar et al [7]. In this paper, reported the $CuCe_xFe_{2-x}O_4$ (x = 0.01, 0.03, and 0.05) spinel ferrites with Ce^{3+} doping were produced using a sol-gel method at room temperature and investigated how Ce3+ ions affect the structural, optical, microstructure, and magnetic properties of nano-samples.

This study used a solid state reaction technique to synthesized a novel Cerium doped CuNi2O4 ($CuNi_{2-x}Ce_xO_4$(x = 0.01, 0.03, and 0.05)) electrode material for Pseudocapacitor application. The analysis of X-ray diffraction (XRD), Fourier transform infrared spectroscopy (FTIR), and scanning electron microscopy (SEM) were used to analyse the surface morphology, structure, With the composition of elements of the prepared materials have been examined. Additionally, galvanostatic charging/discharging (GCD), electrochemical impedance spectroscopy (EIS), and cyclic voltammetry (CV) have been utilized to investigate the capacitive electrochemical behaviour of Cerium copper nickel oxide (CeCuNi2O4) electrodes in a 1 M KOH electrolyte. The synthesized materials have demonstrated cycling stability and a remarkable specific capacitance (Csp).

II. EXPERIMENTAL METHOD

A. Materials

A variety of resources were used in the study, such as Cerous nitrate ($CeN_3O_9.H_2O$) was purchased from sd fine-chem limited with 99 percent purity, Cupric nitrate ($(Cu(NO)_2.3H_2O)$), which was acquired from Loba Chemical with 99 percent purity, Nickel nitrate ($(Ni(NO_3)2.3H_2O)$), which was acquired from Himedia Labs with 99 percent purity, KOH from Thermo Scientific India, N-methyl 2-pyrrolidone (NMP), It was acquired from Loba Chemical with 98 percent purity, Nice Chemicals' Activated Carbon, and Sigma Aldrich's Polyvinylidene difluoride (PVDF).

B. Preparation of Ce doped CuNi2O4

The Samples of $CuNi_{2-x}Ce_xO_4$ (x = 0.01, 0.03, and 0.05) were made using the method of a solid state reaction. This procedure used an agate mortar and pestle to grind the stoichiometric proportions of Cerous nitrate, Cupric nitrate, and Nickel nitrate. Then, the mixture was warmed at 400° C for four hours in air to eliminate the nitrate. To obtain Ce doped $CuNi_2O_4$ powders, the resultant powder was once more crushed and calcined for eight hours at 800 °C.

C. Electrode preparation

The active electrodes were created using nickel foil and a slurry mixture of $CuNi_2O_4$ material, PVDF as a binder, and AC in an 80:10:10 ratio, respectively. After using a few drops of Nmethyl-2-pyrrolidone as a solvent, the active material-based modified electrode was left to dry overnight at 80 °C for later usage. When the electrode material is created, its Csp derived from the GCD investigation and CV analysis as [8]

$$C_{sp} = \int I\, dv/m \times \Delta v \qquad (1)$$

$$C_{sp} = I \times \nabla t/m \times \nabla v \qquad (2)$$

where, "m" stands for the mass of the electrode material, "V" for the working potential, and "S" for the scan rate (mV/S) and "I" represent current, which are dependent on the sweep voltage (V). The electrochemical performances of electrodes modified with a $CuNi_2O_4$ working electrode have been investigated using methods including CV, GCD, and EIS.In a three-electrode test setup using an AUTOLAB electrochemical workstation, the reference electrode was Calomel, and the counter electrode was Pt. The electrochemical characteristics of the collected samples were then examined.

D. Material Characterization

Using an X-ray diffractometer (SSD160 1D detector with D8 advanced ECO XRD systems) to measure Cu Kα radiation (λ=1.5406 Å), the structural characteristics and crystallinity of the $CuNi_2O_4$ sample were examined within the scan angle range of 10° to 60°. Fourier-transform infrared spectroscopy (FTIR) was performed using a Shimadzu IR Trace-100 spectrometer to determine the chemical structure and functional groups of the materials. The morphology and average particle size (SEM) of the sample were examined using a scanning electron microscope. The chemical composition was assessed by energy dispersive X-ray analysis using the ZEISSEVO 18 and a BRUKER X-Flash 6130 spectrometer. Using an AUTOLAB electrochemical workstation, prepared samples were put through electrochemical tests such cyclic voltammetry (CV), galvanostatic charge-discharge (GCD), and electrochemical impedance spectroscopy (EIS).

III. RESULT AND DISCUSSIONS

A. X-ray Diffraction Analysis

Figure 1 shows XRD patterns of spinel $CuNi_{2-x}Ce_xO_4$ samples that are consistent with $CuNi_2O_4$ standard values (JCPDS file: 47-1049) [9]. The diffraction peaks corresponding to the (002), (111), (112), and (200) lattice planes resulted in the cubic structure of $CuNi_2O_4$.

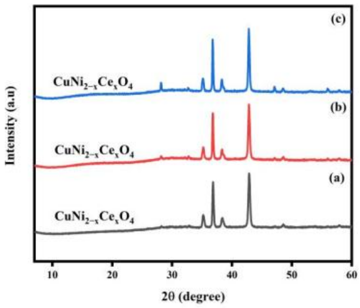

FIG 1. (A-C) XRD PATTERN OF CE DOPED $CuNi_2O_4$, (A) XRD PATTERN OF $CuNi_{1.99}Ce_{0.01}O_4$, (B) XRD PATTERN OF $CuNi_{1.97}Ce_{0.03}O_4$ AND (C)XRD PATTERN OF $CuNi_{1.95}Ce_{0.05}O_4$

This suggests that Ce ions have fully penetrated the spinel $CuNi_2O_4$ structure in the Ce doped CuNi2O4 samples. As Ce concentrations in $CuNi_{2-x}Ce_xO_4$ lattice increases, the XRD peaks are progressively moving toward the direction of the larger 2θ value. XRD pattern of $CuNi_{1.97}Ce_{0.03}O_4$ and (c)XRD pattern of $CuNi_{1.95}Ce_{0.05}O_4$ Figure 1 shows an expanded view of the (3 1 1) and (2 2 2) peaks to provide a unique perspective on the XRD peak shifting. Using the Scherrer formula (equation 3), [10]

$$D = {}^{0.9\lambda}/_{\beta\cos\theta} \qquad (3)$$

The crystallite size of $CuNi_{2-x}Ce_xO_4$ samples was assessed using the (3 1 1) plane. The measured values for $CuNi_{2-x}Ce_xO_4$ with x = 0.01, 0.03, and 0.5 samples by approximately 22.36 nm, 23.5 and 25.53 nm.

B. FTIR Spectroscopy analysis

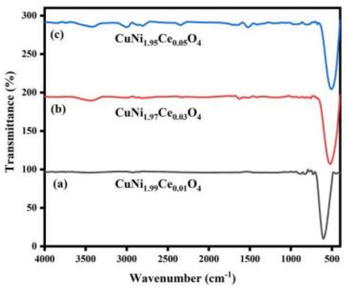

FIG 2. (A-C) FTIR SPECTRA OF CE DOPED $CuNi_2O_4$, (A) FTIR SPECTRA OF $CuNi_{1.99}Ce_{0.01}O_4$, (B) FTIR SPECTRA OF $CuNi_{1.97}Ce_{0.03}O_4$ AND (C) FTIR SPECTRA OF $CuNi_{1.95}Ce_{0.05}O_4$

Utilizing Fourier Transform Infrared Spectroscopy (FT-IR) data, the functional group between 4000 cm-1 and 400 cm-1 was investigated. The FTIR spectra of $CuNi_{1.99}Ce_{0.01}O_4$,

$CuNi_{1.98}Ce_{0.02}O_4$ and $CuNi_{1.95}Ce_{0.05}O_4$ are displayed in figure 2. Four distinct peaks were seen in the FTIR spectrum at 538.14 cm^{-1}, 705 cm^{-1}, 742 cm^{-1}, and 875 cm^{-1}. Based on the FTIR results, a peak at wave number 538.14 cm^{-1} was identified in the fingerprint region of $CuNi_2O_4$, which is caused by Cu-O and Ni-O bond vibration. The peaks at 742 cm^{-1} and 705 cm^{-1} represent water molecules in the atmosphere coupled with Cu. However, the peak was noted at 875 cm^{-1}. The existence of C-H symmetric stretching and antisymmetric stretching modes in both samples were confirmed by a doublet band in the region of 2800-2930 cm^{-1}, indicating organic compounds. Due to, Cu and Ni stretching. Overall, these findings show the desired spinel-structure Ce doped $CuNi_2O_4$ compound.

C. Scanning Electron Microscopy Analysis

The surface morphology of the nanoparticles was investigated using scanning electron microscopy (SEM) techniques [11]. SEM images of $CuNi_2O_4$ samples with varying levels of cerium doping are displayed in Figure 3 (a,b). The image shows that Ce doped $CuNi_2O_4$ were produced at the nanoscale and The SEM images revealed well-grown particles and grouped particles.

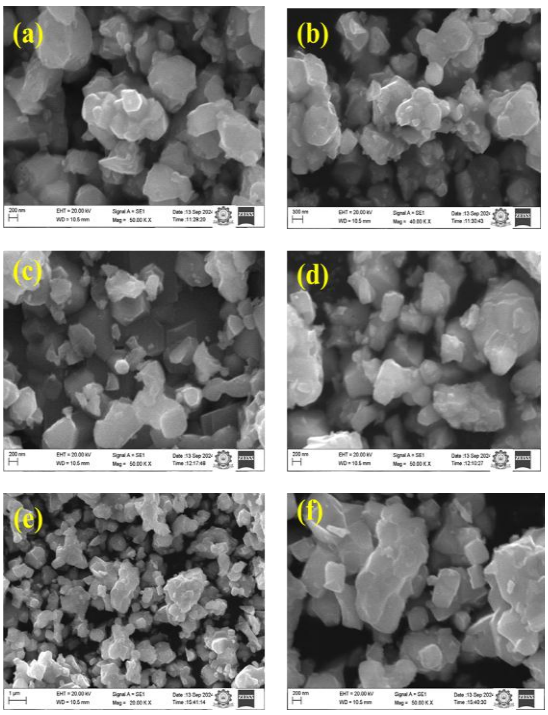

FIG 3. (A-F) SEM IMAGES OF CE DOPED $CuNi_2O_4$, (A) SEM IMAGES OF $CuNi_{1.99}Ce_{0.01}O_4$, (B) SEM IMAGES OF $CuNi_{1.97}Ce_{0.03}O_4$ AND (C) SEM IMAGES OF $CuNi_{1.95}Ce_{0.05}O_4$

D. Cyclic Voltammetry

The electrochemical characteristics of produced $CuNi_{2-x}Ce_xO_4$ (x = 0.01, 0.03, 0.05) in 1M KOH were examined using cyclic voltammetry measurements. Figures 4 (a), (b)and (c) show cyclic voltammogram curves for cerium doped $CuNi_2O_4$ nanoparticles, with scan rate ranging from 5 to 100 mV/s. The capacitance formula is calculated using the formula 1. At a scan rate of 5 mV/s, the specific capacitance values for the $CuNi_{1.99}Ce_{0.01}O_4$, $CuNi_{1.97}Ce_{0.03}O_4$ and $CuNi_{1.95}Ce_{0.05}O_4$ electrodes were determined from the CV curves to be 834.66 F/g, 179.2 F/g and 1066 F/g, respectively.

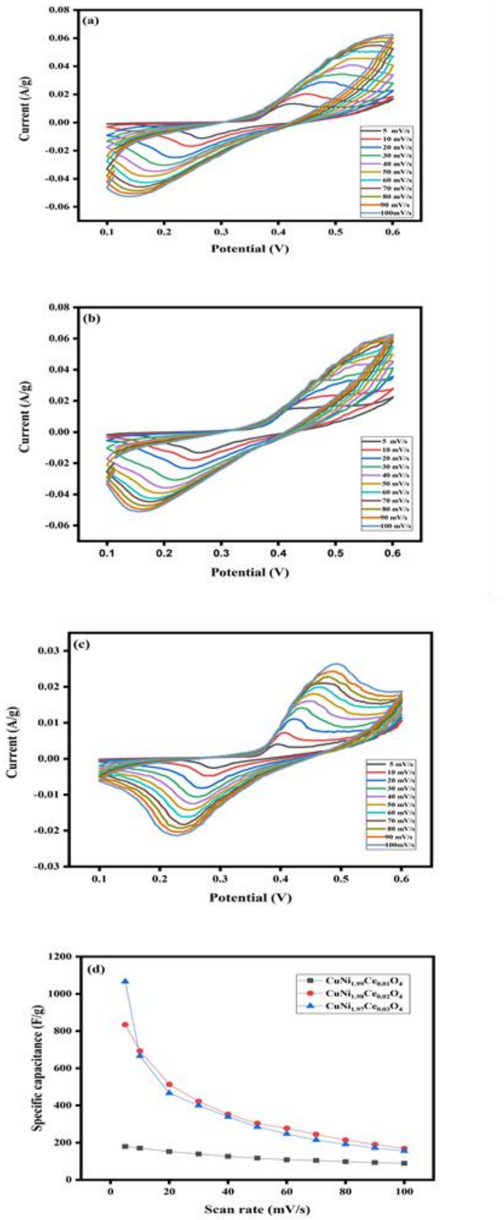

FIG 4. (A-D) CV CURVE FOR CE DOPED $CuNi_2O_4$, (A) CV CURVE FOR $CuNi_{1.99}Ce_{0.01}O_4$, (B) CV CURVE OF $CuNi_{1.98}Ce_{0.02}O_4$, (C) CV CURVE OF $CuNi_{1.97}Ce_{0.03}O_4$, (D) SPECIFIC CAPACITANCE VS SCAN RATE OF CE DOPED $CuNi_2O_4$

The electrode $CuNi_{1.95}Ce_{0.05}O_4$ has lower capacitance values than the $CuNi_{1.97}Ce_{0.03}O_4$ electrodes. It shown that the $CuNi_{1.97}Ce_{0.03}O_4$ electrode's area (I(V)dV) of the CV curve was significantly larger than the $CuNi_{1.97}Ce_{0.05}O_4$ electrode's, increasing the specific capacitance [12]. According to the specific capacitance Vs. scan rate plot obeyed the well-established electrochemical fact that, as the scan rate increased, the specific capacitance for both nanoparticles decreased because, at higher scan rates, ionic diffusion occurs only on the outer surfaces rather than on the inner and outer surfaces, lowering the specific capacitance shows the figure 4 (d).

E. Galvanostatic charge-discharge

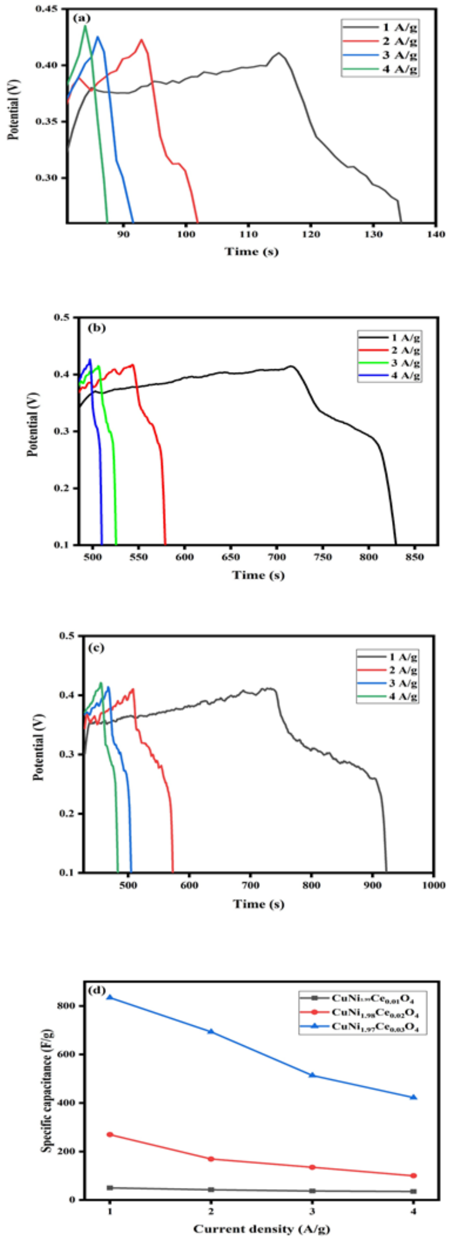

FIG 5. (A-D) GCD CURVE OF CE DOPED $CuNi_2O_4$, (A) GCD CURVE OF $CuNi_{1.99}Ce_{0.01}O_4$, (B) GCD CURVE OF $CuNi_{1.97}Ce_{0.03}O_4$, (C) GCD CURVE OF $CuNi_{1.95}Ce_{0.05}O_4$, (D) SPECIFIC CAPACITANCE VS CURRENT DENSITY OF CE DOPED $CuNi_2O_4$

Figures 5 (a), (b) and (c) show the galvanostatic charge-discharge comparison of $CuNi_{1.99}Ce_{0.01}O_4$, $CuNi_{1.97}Ce_{0.03}O_4$ and $CuNi_{1.95}Ce_{0.53}O_4$ at current densities of 1A g^{-1} to 4 A g^{-1}. The charge-discharge curve is triangular, indicating high reversibility and capacitance at various ratios [13]. $CuNi_{1.97}Ce_{0.03}O_4$ has a higher specific capacitance than $CuNi_{1.95}Ce_{0.05}O_4$ and $CuNi_{1.99}Ce_{0.01}O_4$ at lower current density compared to 1 to 4.A g^{-1}. These findings suggest that the Ce doped $CuNi_2O_4$ is suited for charging and discharging at low current density. The value of specific capacitance for $CuNi_{1.99}Ce_{0.01}O_4$, $CuNi_{1.97}Ce_{0.03}O_4$ and $CuNi_{1.95}Ce_{0.05}O_4$ is 269.75, 438.04 and 49.84 F g^{-1} at current densities of 1,2,3, and 4 A g^{-1}, resulting in the best charging and discharging performance. Figure 5 (d) displays the current density vs specific capacitance. From this figure comparison of $CuNi_{1.99}Ce_{0.01}O_4$, $CuNi_{1.97}Ce_{0.03}O_4$ and $CuNi_{1.95}Ce_{0.05}O_4$ at different current density of 1 to 4 A/g.

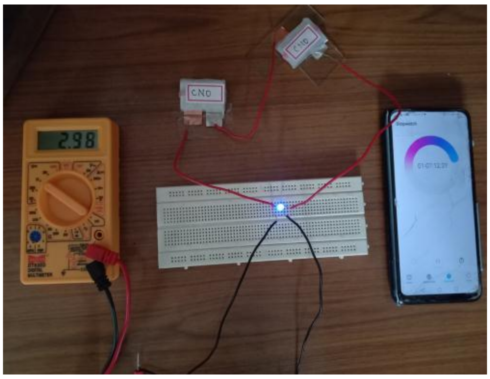

FIG 6 TWO DEVICES IN SERIES ILLUMINATING BLUE LEDS.

Figure 6 shows the fabricated ASC adding two device in series light up blue LEDs for more then 1 hours with holding 2.98V

IV. CONCLUSION

Cerium doped $CuNi_2O_4$ nanoparticles were prepared using the solid-state technique. Structural analysis (XRD) verified the cubic spinel structure. The doped samples had an average particle size of 22.36 nm, 23.5 nm, and 25.53 nm. SEM images revealed clusters of nanoparticles. Three bands were visible in the FTIR spectra below 1000 cm-1 indicating Ce doped $CuNi_2O_4$ group vibrations. For $CuNi_{1.99}Ce_{0.01}O_4$, $CuNi_{1.97}Ce_{0.03}$O4 and $CuNi_{1.95}Ce_{0.05}O_4$, cyclic voltammetry showed specific capacitance values of 834.66 F/g, 1066 F/g and 179.2 F/g at a scan rate of 5 mV/s. Galvanostatic charge discharge revealed specific capacitance values of 269.75 F/g 49.84 F/g, and 438.04 F/g at a Current density of 1 A/g for $CuNi_{1.99}Ce_{0.01}O_4$, $CuNi_{1.97}Ce_{0.03}O_4$ and $CuNi_{1.95}Ce_{0.05}O_4$, Two devices connected in series shine blue LED for more than 1 hour, making them suitable for supercapacitor applications.

V. ACKNOWLEDGMENT

This research work in financially supported by thiagarajar research fellowship (trf) scheme - (file.no: Tce/rd/trf/<<9>> dated 27.09.2024)

REFERENCES

[1] B. Carmel Jeeva Mary, J. Judith Vijaya, Radhika R. Nair, A. Mustafa, P. Stephen Selvamani, B. Saravanakumar, M. Bououdina, and L. John Kennedy, Reduced Graphene Oxide-Tailored $CuFe_2O_4$ Nanoparticles as an Electrode Material for High-Performance Supercapacitors, Hindawi Journal of Nanomaterials Volume 2022, Article ID 9861440, 15 pages. https://doi.org/10.1155/2022/9861440.

[2] P. Ramadevi, F. Kous , A. Sangeetha, M. Stalin Mano Gibson, Ra. Shanmugavadivu, Structural and electrochemical investigation on pure and nickel doped cobalt ferrite nanoparticles for supercapacitor application, 2214-7853/ 2020 Elsevier Ltd, https://doi.org/10.1016/j.matpr.2020.04.050

[3] Waseem Raza, Ghulam Nabi, Asim Shahzad, Nafisa Malik, Nadeem Raza, Electrochemical Performance of Lanthanum Cerium Ferrite Nanoparticles for

Supercapacitor Applications, Journal of Materials Science: Materials in Electronics on February 20th, 2021, https://doi.org/10.21203/rs.3.rs-160990/v1.

[4] Qian Liu, Zhuang Wang, Jie Liu, Zhe Lu, Dipan Xuan, Fenqiang Luo, Dr. Shuirong Li, Dr. Yueyuan Ye, Dr. Duo Wang, Dr. Dechao Wang, Prof. Zhifeng Zheng, One-Dimensional Spinel Transition Bimetallic Oxide Composite Carbon Nanofibers (CoFe2O4@CNFs) for Asymmetric Supercapacitors, https://doi.org/10.1002/celc.202100998.

[5] Sara Khorshidian, Dr. Behrooz Vaseghi, Dr. Ghasem Rezaei, Dr. David Jenkins, Dr. Niroj Kumar, Arunima Rajan, Synthesis of Ultra-fine Co1-(x+y)NixZnyFe2O4 Ferrite Nanoparticles: Customizing Magnetic Properties, https://doi.org/10.1002/slct.202004461.

[6] K. Elayakumara,b , A. Manikandanc,□ , A. Dineshd , K. Thanrasud , K. Kanmani Rajad , R. Thilak Kumara,e , Y. Slimanif , S.K. Jaganathang,h,i , A. Baykalj, Enhanced magnetic property and antibacterial biomedical activity of Ce^{3+} doped CuFe2O4 spinel nanoparticles synthesized by sol-gel method, *Journal of Magnetism and Magnetic Materials 478 (2019) 140–147,* https://doi.org/10.1016/j.jmmm.2019.01.108.

[7] Chen Zhang, Aijuan Xie , Wanqi Zhang, Jianing Chang, Chenyang Liu, Linyang Gu, Xiaoxiao Duo, Fei Pan, Shiping Luo, $CuMn_2O_4$ spinel anchored on graphenenanosheets as a novel electrode material for supercapacitor, *Journal of Energy Storage 34 (2021) 102181,* https://doi.org/10.1016/j.est.2020.102181.

[8] Javad Gholami and Majid Arvand, Controlled synthesis of a hierarchical $CuNi_2O_4$@SnS nanocauliflower-like structure on rGO as a positive electrode material foran asymmetric supercapacitor, DOI: 10.1039/d1nj01508g.

[9] A. Baykal, S. Guner, H. Gungunes, K.M. Batoo, Md. Amir, A. Manikandan, Magneto optical properties and hyperfine interactions of Cr3+ ion substituted copper ferrite nanoparticles, J. Inorg. Organomet. Polym. 28 (2018) 2533–2544.

[10] S. Asiri, M. Sertkol, H. Güngüneş, M. Amir, A. Manikandan, İ. Ercan, A. Baykal, The temperature effect on magnetic properties of NiFe2O4 nanoparticles, J. Inorg. Organomet. Polym. 28 (2018) 1587–1597.

[11] Packiaraj, P. Devendran, K.S. Venkatesh, S.A. Bahadur, A. Manikandan, N. Nallamuthu, Electrochemical investigations of magnetic Co3O4 nanoparticles as an active electrode for supercapacitor applications, J. Supercond. Nov. Magn. https://doi.org/10.1007/s10948-018-4963-6.

[12] Muhammad Saeed, Asim Mansh, Muhammad Hamayun, Aziz Ahmad, Atta Ulhaq, Muhammad Ashfaq, Corrigendum to: Green Synthesis of CoFe2O4 and Investigation of its Catalytic Efficiency for Degradation of Dyes in Aqueous Medium, Zeitschrift fur Physikalische Chemie 232 (2018) 359–371, https://doi.org/10.1515/zpch-2017-9065.

[13] Md. Amir, H. Gungunes, Y. Slimani, N. Tashkandi, H.S. El Sayed, F. Aldakheel, M. Sertkol, H. Sozeri, A. Manikandan, I. Ercan, A. Baykal, Mössbauer studies and magnetic properties of cubic CuFe2O4 nanoparticles, J. Supercond. Nov. Magn. (2018), https://doi.org/10.1007/s10948-018-4733-5.

[14] B. Carmel Jeeva Mary, J. Judith Vijaya, Radhika R. Nair, A. Mustafa, P. Stephen Selvamani, B. Saravanakumar, M. Bououdina, and L. John Kennedy, Reduced Graphene Oxide-Tailored $CuFe_2O_4$ Nanoparticles as an Electrode Material for High-Performance Supercapacitors, Hindawi Journal of Nanomaterials Volume 2022, Article ID 9861440, 15 pages. https://doi.org/10.1155 /2022/9861440.

Hybrid Organic Silica-Lithium/Zinc Polymeric Surface Coating on Al 7075: Corrosion Behavior under Saline condition

Ajay P
Department of Chemistry,
Thiagarajar College of Engineering,
Madurai, Tamil Nadu

Velkannan V
Department of Chemistry,
Thiagarajar College of Engineering,
Madurai, Tamil Nadu
velkannan@gmail.com

Arun Kumar S
Department of Mechanical Engineering,
Thiagarajar College of Engineering,
Madurai, Tamil Nadu

Kottaisamy M
Department of Chemistry,
Thiagarajar College of Engineering,
Madurai, Tamil Nadu

***Abstract*—Hybrid organic polymer coating based on ((3-glycidoxypropyl) trimethoxysilane) GPTMS, Tetraethyl orthosilicate (TEOS), nano colloidal Silicon dioxide (SiO_2) with Lithium or Zinc based coating was used to prevent the Aluminum 7075 metal Surface from corrosion. The corrosion preventing efficiency of the modified hybrid polymer film coating under 3.5% NaCl medium was investigated through Electrochemical Corrosion analysis (open circuit potential (OCP), electrochemical impedance spectroscopy (EIS) and TAFEL polarization). All the coating specimens show higher resistance and lower corrosion current density (Icorr) with lower corrosion rate. Uniformed distribution of metals on the polymeric thin film structure forming the passive layer on metal surface which prevent further metal corrosion. Lithium added system (TGSL) has lower corrosion rate of 1.421mpy, 85% lower than uncoated Al 7075.**

Keywords*—Hybrid Organic Polymer Coating, Aluminum 7075, Corrosion Prevention, Impedance spectroscopy, Tafel plot, Pin on-disc.

I. INTRODUCTION

Aluminum 7075, a high-strength alloy widely used in aerospace and marine applications, remains highly susceptible to localized corrosion in chloride-rich marine environments, leading to premature structural failure. The face center structure has high ductility at room temperature and a lower melting point (660°C), which makes aluminum easy to machine.[1]. The wide usage of Al7075 depends on its mechanical properties and surface properties, especially corrosion resistance[2]. Higher costs, expensive equipment requirements, and unfriendly environments are disadvantages of these methods. A productive thin coating on the metal surface can enormously prevent metal deterioration. Researchers are exploring various materials to prevent metal corrosion, and sol-gel processed coating shows their potential against corrosion resistance [3]. Traditional corrosion protection methods, such as chromate-based coatings, are increasingly restricted due to environmental and health concerns, necessitating the development of eco-friendly and high-performance alternatives. Recent advances in hybrid organic-inorganic coatings have demonstrated potential by combining the flexibility of polymers with the durability of inorganic matrices. For instance, silane-based coatings, including (3-glycidoxypropyl) trimethoxysilane (GPTMS) and tetraethyl orthosilicate (TEOS), have gained attention for their ability to form dense, cross-linked networks that enhance barrier properties and adhesion to metal substrates. Incorporating nano-colloidal silicon dioxide (SiO_2) further improves mechanical strength and corrosion resistance by reducing porosity and crack propagation. Recent studies highlight the synergistic effects of hybrid systems with metal ions (e.g., Zn^{2+}, Li^{+}), which inhibit active corrosion through passivation and self-healing mechanisms. Building on these advancements, this work develops a novel bi-functionalized GPTMS/TEOS hybrid coating reinforced with nano-SiO_2 and lithium/zinc-based inhibitors, aiming to achieve long-term protection for Aluminum 7075 in aggressive marine conditions. The design leverages recent insights into multifunctional silane matrices[4], [5], [6], [7] and nanoparticle-enhanced barrier coatings addressing critical gaps in marine applications' durable, non-toxic and anti-corrosion technologies[8], [9], [10].

In this work, organic hybrid polymeric coating based on modified silicon surface coating to prevent aluminum 7075 was developed using a bi-functionalized trimethoxysilane material ((3-glycidoxypropyl) trimethoxysilane) GPTMS, the organic ethyl ester of orthosilicic acid commonly known as Tetraethyl orthosilicate (TEOS), nano colloidal Silicon dioxide (SiO_2) with Lithium or Zinc based coating was used to prevent the Aluminum 7075 metal corrosion under marine environment.

II. EXPERIMENTAL SECTION

A. *Materials*

All the chemicals are obtained from Sigma-Aldrich and used without any further purification.

B. *Preparation of Hybrid Sol-gel coatings*

A hybrid colloidal solution was prepared from the hydrolysis of TEOS and GPTMS at equimolar concentrations with isopropyl alcohol to prevent the quick gelation of the solution; the mixture was stirred at 500 rpm for 1 hr to form a clear, homogeneous mixture. This solution is named TG.

On the other hand, the pyrogenic silica powder was sonicated in ethanol for 30 min., then 10% colloidal silica solution was added to the hydrolyzed TEOS and GPTMS solution and stirred for 2 h. Named TGS. The pH of the solution mixture was maintained at 8-9 pH using Liq. Ammonia solution to get fine spherical Si formations. The prepared colloidal silica solution was composited with zinc or lithium metal using 5% metal nitrate salt solutions named TGSZ and TGSL.

The cleaned aluminum coupons were coated with synthesized TG, TGS, TGSZ, and TGSL hybrid solutions. An ethanol solution was used to reduce the viscosity of the colloidal solutions. Dip coating techniques were employed for coating with a 1-min immersion time. Then, it was initially dried at ambient conditions for solvent evaporation and then dried at 80°C for 3h to get stable film formation.

C. *Characterization techniques*

The prepared hybrid colloidal silica-based solution coatings' corrosion inhibition and wear resistance properties were investigated through electrochemical corrosion analysis using the CHI660A electrochemical workstation. These corrosion analyses include Open circuit potential (OCP), Electrochemical impedance spectroscopy (EIS), and Potential dynamic polarization (Tafel). A three-electrode cell setup was carried out for the corrosion analysis, which included Platinum wire as the counter, a saturated calomel electrode as the reference, and an aluminum strip as the working electrode; 3.5% NaCl solution was used to mimic the marine environment.

III. RESULT AND DISCUSSION

A. *Electrochemical Impedance Spectroscopy (EIS)*

The corrosion resistance of the silicone hybrid coatings was determined through electrochemical impedance spectroscopy (EIS). The EIS spectra were recorded in the frequency range of 10^5 to 10^{-1} Hz with 0.005V amplitude. The frequency regions were separated into higher (10^5-10^3 Hz), mid (10^2-10^0 Hz), and lower (10^0- 10^{-1} Hz) regions. The initial voltage was gained through Open circuit potential (OCP) measurement. A potential difference in the coated materials was observed without current flow.Fig.1(a) shows the obtained OCP spectra. Aminimal magnitude at alternating current was observed in OCP (~0.05V). The faradic relationship between the electrical resistivity and double layered capacitance was measured in EIS spectra Fig.1(b) Nyquist plot of the coated and uncoated Al7075 specimens under 3.5% NaCl saline condition. Bare and coated Al metal shows depressed semicircle formation. The diameter of the semi-circle reveals the charge transfer resistance of the materials. The entire sol-gel coated specimen shows higher charge transfer resistance than bare Al. Among them, lithium composited material (TGSL) has a higher charge transfer resistance of 16731 Ωcm^2 while bare Al has 2040 Ωcm^2 resistance, 85.64% more resistance than Bare Al. Fig.1(c and d) shows the Bode modules and phase angle plot of the bare and coated Al. In Fig.1(c) bode spectra, all the specimens show a horizontal spectrum with increased |Z| resistance modules towards the lower frequency regions. Fig.1(d) shows the phase angle plot of all the specimens. All coated samples have a single higher Phase angle (θmax) value than bare Al, clearly indicating the capacitive behavior of the coating materials.[11] EC LAB software optimized the Fitting curvature with the randles circuit Fig 2(a & b)All the Fitted faradic values are in the Table 1.

B. Potential Dynamic Polarization

The corrosion prevention behavior of the bare Al and coated materials are examined through potential dynamic polarization, also known as the tafel plot.Fig.2(c). Shows the obtained tafel plot of the bare and coated Al. The relationship between the applied potential and current flow. The focal potential point represents the corrosion current density (Icorr), corrosion potential (Ecorr) and the polarization resistance (LPR), anodic curve (βa), cathodic curve (βc), corrosion current and corrosion efficiency (IE%) was tabulated in Table 2.[12], [13] bare Al shows corrosion current density of 17.59 μA cm^{-2}. In contrast, all the coated material shows lower Icorr values of TG 11.76 μA cm^{-2}, TGS 9.113 μA cm^{-2}, TGSZ 2.781 μA cm^{-2}, and TGSL has 2.096 μA cm^{-2} of corrosion current density. The zinc and lithium-adding materials show significantly reduced Icorr values, which are 84.18 and 88.01% more efficient than bare Al. From that, TEOS and silica-based protective coating proved to have a corrosion prevention capacity against saline conditions by decreasing the corrosion rate. (Table 2)

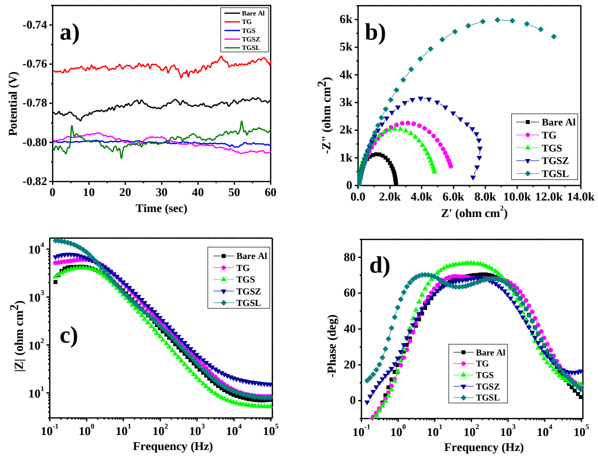

FIG.1 (A) OCP PLOT, (B) NYQUIST PLOT, (C) BODE PLOT, AND (D) PHASE ANGLE PLOT OF BARE AND COATED AL 7075 IN 3.5% NACL MEDIUM.

TABLE 1. EIS RESULT OF BARE AND COATED AL 7075 IN 3.5% NACL SOLUTION.

Sample	Rs (Ω cm^2)	CPE ($\Omega^{-1}s^ncm^{-2}$)	Rc (Ω cm^2)	CPE_{dl} ($\Omega^{-1}s^ncm^{-2}$)	Rct (Ω cm^2)	χ^2	IE%
Bare Al	8.295	26.27	-	-	2402	0.87	-
TG	8.412	22.96	301.9	0.123	5668	0.80	57.6
TGS	12.51	13.28	406.8	19.33	5196	0.31	53.7
TGSZ	12.98	17.0	857.4	36.02	8485	0.42	71.6
TGSL	6.95	32.76	771	75.84	16731	0.13	85.6

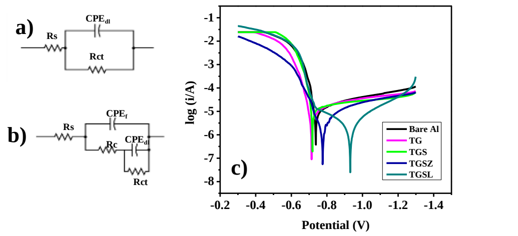

FIG.2 (A & B) RANDELS EQUIVALENT CIRCUIT AND (C) TAFEL PLOT BARE AND COATED AL 7075 IN 3.5% NACL MEDIUM

Corrosion medium, which was clearly observed in Fig.4 (e). Also, corrosion residual growth between the destroyed films was observed.

TABLE 2. POTENTIAL DYNAMIC POLARIZATION RESULTS OF BARE AND COATED AL 7075 IN 3.5% NACL SOLUTION

Sample	Ecorr (mV/SCE)	Icorr (μA cm^{-2})	β_c (mV/dec)	β_a(mV/dec)	LPR (Ω cm^2)	Corrosion rate (mpy)	IE%
Bare Al	-0.720	17.58	1.872	16.562	1044.7	14.51	-
TG	-0.739	11.76	3.001	13.264	1505.3	11.42	33.1
TGS	-0.715	9.113	3.13	17.183	2349.3	5.858	48.16
TGSZ	-0.777	2.781	4.80	14.729	8004	1.788	84.18
TGSL	-0.932	2.096	5.764	11.246	13307	1.421	88.01

IV. CONCLUSION

The silicon-modified hybrid organic surface coating material, a combination of organic siloxane material TEOS combined with bifunctional organosilane 3-methoxy modified silica polymer composited with nano colloidal silica coating synthesized through a simple sol-gel process than it was lubricated with lithium/zinc metal additives was presented in this work and the corrosion prevention behavior under marine environment was investigated through EIS and tafel polarization studies. All the hybrid organic silica coating materials exhibits excellent resistance with lower corrosion current density, among them lithium added coating system shows more lower resistance of 16731Ω cm^{-1} with lower corrosion rate of 1.421 mpy which is 88% more efficient then the bare Al 7075. The surprising results from lithium may due to uniformed distribution of the lithium materials throughout the polymeric thin film structure forming the passive layer on metal surface which prevent further metal corrosion. The surface morphology of coatings and corroded metal surfaces were observed through SEM analysis.

V. ACKNOWLEDGMENT

The author AJAY P extends their due thanks to the Thiagarajar College of Engineering Management, Madurai, India, for their extensive research facilities and the financial backing from Thiagarajar Research Fellowship (TRF) scheme (File. no: TCE/RD/TRF/2023/07 dated September 01, 2023) is gratefully acknowledged. We thank Mr. B. Anand Viswanath, Mr. P. Raghul and Dr. P. Ram Kumar from the Department of Chemistry, TCE, Madurai, for their support regarding this effort.

Author's contribution: AP: Conceptualization, Methodology, Investigation, software, Validation, Characterization, Writing-original draft; VV: Resources, investigation, validation, supervision, Review, and editing; AKS: Validation, review and editing; KM: Conceptualization, Methodology, Resources, Validation, review and editing.

Conflict of interest: The authors affirm that there is no conflict of interest to declare, given that all sources of information used have been appropriately cited and attributed

REFERENCES

[1] M. C. Santos, A. R. Machado, W. F. Sales, M. A. S. Barrozo, and E. O. Ezugwu, "Machining of aluminum alloys: a review," Int J Adv Manuf Technol, vol. 86, no. 9–12, pp. 3067–3080, Oct. 2016, doi: 10.1007/s00170-016-8431-9.

[2] W. J. Van Ooij et al., "Corrosion protection properties of organofunctional silanes—an overview," Tsinghua Science and technology, vol. 10, no. 6, pp. 639–664, 2005, Accessed: Feb. 16, 2025. [Online]. Available: https://ieeexplore.ieee.org/abstract/document/6075842

[3] M. I. Bashir et al., "Enhanced surface properties of aluminum by PVD-TiN coating combined with cathodic cage plasma nitriding," Surface and Coatings Technology, vol. 327, pp. 59–65, 2017, Accessed: Feb. 16, 2025.

[4] M. Mirzaee et al., "Amino-silane co-functionalized h-BN nanofibers with anti-corrosive function for epoxy coating," Reactive and Functional Polymers, vol. 174, p. 105244, 2022, Accessed: Feb. 16, 2025.

[5] N. Huang, Y. Wang, Y. Zhang, L. Liu, N. Yuan, and J. Ding, "Multifunctional coating on magnesium alloy: Superhydrophobic, self-healing, anti-corrosion and wear-resistant," Surface and Coatings Technology, vol. 463, p. 129539, 2023, Accessed: Feb. 16, 2025.

[6] Q. Qiu et al., "Silane-functionalized polyionenes-coated cotton fabrics with potent antimicrobial and antiviral activities," Biomaterials, vol. 284, p. 121470, 2022, Accessed: Feb. 16, 2025.

[7] S. Nayak, R. K. Nayak, and I. Panigrahi, "Effect of nano-fillers on low-velocity impact properties of synthetic and natural fibre reinforced polymer composites- a review," Advances in Materials and Processing Technologies, vol. 8, no. 3, pp. 2963–2986, Jul. 2022, doi: 10.1080/2374068X.2021.1945293.

[8] W. Yang, H. Liu, and H. Wang, "Experimental study on mechanical properties of basalt fiber reinforced nano-SiO2 concrete after high temperature," Frontiers in Materials, vol. 11, p. 1415144, 2024

[9] X. Li, F. Wang, X. Cai, S. Meng, and L. Wang, "Dual Nanoparticles Synergistically Reinforce Polyurethane/Epoxy Grouting Material with High Mechanical

[10] E. B. Caldona, D. W. Smith, and D. O. Wipf, "Surface electroanalytical approaches to organic polymeric coatings," Polymer International, vol. 70, no. 7, pp. 927–937, Jul. 2021.

[11] P. Ajay, V. Velkannan, P. R. Kumar, and M. Kottaisamy, "Enhancing corrosion resistance of mild steel with a hybrid surface coating: Film-forming zinc titanate/oleic acid composites," Ceramics International, vol. 51, no. 1, pp. 751–763, 2025.

Advancing Microplastic Detection and Classification: Integration of Electrochemical Impedance Spectroscopy and Machine Learning for Real-Time Marine Pollution Monitoring

K. Ramani
Department of Computer Application,
Thiagarajar College of Engineering,
Madurai, Tamil Nadu, India
ramanik@student.tce.edu

Mrs, T. Mutharasi
Department of Computer Application,
Thiagarajar College of Engineering,
Madurai, Tamil Nadu, India
tmica@tce.edu

Drs. S. Vijayalaksmi
Department of Computer Application,
Thiagarajar College of Engineering,
Madurai, Tamil Nadu, India
svlcse@tce.edu

Udaya Sowmya K
Department of Computer Application,
Thiagarajar College of Engineering,
Madurai, Tamil Nadu, India
udayasowmya@student.tce.edu

***Abstract*—Microplastic pollution is an escalating environmental issue with serious implications for marine ecosystems and public health. Traditional detection techniques like Raman and FTIR spectroscopy, while chemically accurate, lack scalability and real-time capability. This paper proposes an integrated approach using Electrochemical Impedance Spectroscopy (EIS) and Machine Learning (ML) for accurate, real-time microplastic classification. Using impedance-based features and models like SVM, KNN, and PCA, our system achieves up to 95% accuracy, offering a cost-effective solution for pollution monitoring and recycling infrastructure**.

Keywords—Microplastics, Electrochemical Impedance Spectroscopy, Machine Learning, Real-time Monitoring, Environmental Sensors.

I. INTRODUCTION

Microplastics (MPs), defined as plastic particles <5 mm in size, have emerged as a critical global pollutant. Their persistence in marine ecosystems, potential to enter food chains, and chemical reactivity make their monitoring essential. Current detection methods such as FTIR and Raman Spectroscopy are accurate but costly, lab-dependent, and require lengthy preprocessing.

Electrochemical Impedance Spectroscopy (EIS) provides a promising alternative by detecting shifts in electrical impedance caused by MPs in water. However, interpreting EIS data manually is complex. Hence, combining EIS with Machine Learning (ML) offers a novel, automated detection mechanism.

This paper proposes an integrated EIS-ML framework for real-time microplastic classification, aiming to enable scalable, field-deployable detection systems.

II. LITERATURE REVIEW

1. Flow-Through Quantification of Microplastics Using Impedance Spectroscopy

Colson & Michel (2021) [1] demonstrated electrochemical impedance spectroscopy (EIS) as a rapid, real-time method for detecting microplastics in aquatic environments. Unlike traditional methods, EIS enables direct quantification of particles without extensive preprocessing, achieving a recovery rate of ≥90% for microplastics in the 300–1000 µm size range**.**

2. Microplastic Identification Using Spectroscopy and Machine Learning

Sarmiento et al. (2024) [2] integrated machine learning with EIS to enhance microplastic detection. Using AI models like SVM, K-NN, and PCA, they improved classification accuracy for PET microparticles. Their study showed the potential of EIS combined with AI for real-time, scalable microplastic monitoring, although challenges such as data standardization remain**.**

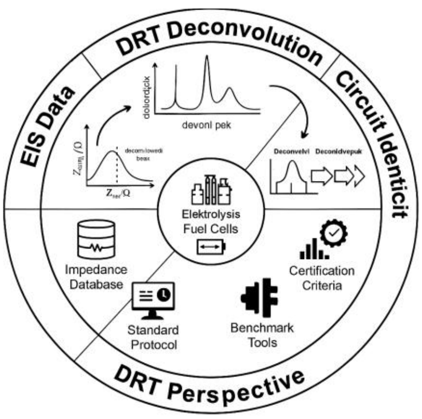

3. Measuring Microplastic Concentrations in Water by Electrical Impedance Spectroscopy.

Gomes et al. (2024) [3] developed a submersible EIS sensor for quantifying microplastics in water. They measured impedance across a wide frequency range (100 Hz to 40 MHz), achieving an error margin of less than 3%. The study confirmed EIS as a sensitive and reliable method, with pH levels affecting detection sensitivity.

4. Advancements in Microplastic Detection Using Electrochemical Sensors.

Zhao et al. (2023) [4] explored the use of electrochemical sensors for detecting microplastics in marine environments. Their research found that integrating EIS with other electrochemical techniques significantly improved detection limits, offering a promising approach for monitoring microplastic pollution in real-time.

5. Real-Time Detection of Microplastics in Aquatic Systems Using AI and Sensors.

Martínez et al. (2023) [5] combined AI-driven EIS with portable sensor devices for real-time microplastic detection in rivers. Their results demonstrated the system's ability to distinguish different microplastic types effectively, highlighting the feasibility of using such systems for widespread environmental monitoring.

III. METHODOLOGY

A. Microplastic Sample Preparation

Water samples were collected from local rivers known for varying water quality levels. A filtration system with appropriate mesh size was used to remove large particulate matter and organic debris. The samples were treated with hydrogen peroxide (H_2O_2) to digest any remaining biological matter, leaving behind only inorganic substances. MPs were sorted into polyethylene (PE), polyethylene terephthalate (PET), and polyvinyl chloride (PVC), with further validation from FTIR scans confirming the chemical identity of each type.

B. Sample Collection and Processing:

Samples were collected from various points of the river using grab sampling techniques. Each sample underwent filtration through a 0.5 mm mesh, and organic matter was removed by digesting with concentrated hydrogen peroxide (H_2O_2). MPs were separated by density in a salt solution, categorized into PE, PET, and PVC based on their densities. FTIR spectrometry confirmed their chemical composition, ensuring accurate categorization for impedance profiling.

C. EIS Data Acquisition

Impedance Data Acquisition Electrochemical Impedance Spectroscopy (EIS) was used to capture the dielectric properties of each microplastic type. A custom-designed sensor recorded impedance across a frequency range from 100 Hz to 40 MHz, enabling detailed analysis of electrical properties. Each microplastic type (PE, PET, PVC) exhibited a distinct impedance signature, influenced by their dielectric constants, conductivity, and polymer composition.

D. Feature Extraction and Normalization:

Key features were extracted from the raw EIS data, including real and imaginary impedance, phase angle, and frequency response slopes. These features provide insights into the MPs' electronic properties and their physical characteristics. All features were normalized using min-max scaling to improve model generalization, reducing bias from feature scale variations.

E. ML Model Training: Machine Learning Training

Three machine learning models were tested: Support Vector Machine (SVM) with an RBF kernel, K-Nearest Neighbor (K-NN) with K=3, and Principal Component Analysis (PCA)-based classifiers. The models were trained on 80% of the dataset and validated on the remaining 20%. SVM was chosen for its effectiveness in high-dimensional spaces, while K-NN used proximity for classification. PCA reduced dimensionality and improved classifier efficiency by focusing on key components.

F. Deployment Setup: Real-Time Deployment Setup

The machine learning models were integrated into a Raspberry Pi-based embedded system, interfacing with the custom EIS sensor to process impedance data in real time. The processed data was sent to a web-based dashboard for monitoring and logging. The dashboard displayed real-time classification results and additional data visualizations, enabling efficient monitoring of microplastic pollution for environmental analysis.

This elaboration adds depth to each of the methodology steps, highlighting the rationale behind each approach and emphasizing how they contribute to the overall research.

IV. RESULTS AND DISCUSSION

A. Detection Accuracy and System Performance

The EIS-based system achieved approximately 95% classification accuracy for microplastics sized between 300–1000 µm, with SVM outperforming K-NN and PCA. False positive rates were below 5%, affirming its reliability. However, accuracy decreased for particles <300 µm, highlighting a need for sensor resolution enhancement.

B. Real-Time Monitoring and Sensor Design

A submersible EIS sensor operating across 100 Hz – 40 MHz was developed to detect PE, PVC, PET, and PS microplastics in flowing water. The system supports real-time detection, wireless data transmission, and long-term deployment. Unlike FTIR or Raman methods, it requires no sample preprocessing, reducing lab workload and costs.

C. Machine Learning Integration

Integration of ML models (SVM, K-NN, PCA) helped classify microplastics from biological/inorganic materials with improved precision. These models adapt to variations in size and type, though standardization of training data and real-world adaptability remain key challenges.

D. Differentiation from Biological Interference

Microplastics were effectively differentiated from algae and organic matter (>90% accuracy) using impedance differences. However, biofilm presence occasionally altered readings. Further optimization of frequency range and signal processing is necessary to mitigate this issue in natural samples.

E. Comparison with Traditional Methods

Compared to FTIR and Raman spectroscopy, EIS offers faster, cheaper, and non-invasive screening, though it lacks polymer-specific identification. Hence, it works best as a pre-screening tool, potentially coupled with traditional methods for deeper analysis.

F. Limitations and Challenges

Key limitations include:

- Low sensitivity for particles <300 μm
- Environmental interference (e.g., turbidity, salinity)
- Lack of polymer-specific data Addressing these requires better sensor calibration, hybrid detection systems, and advanced ML integration.

V. FUTURE WORK

A. Advanced ML Algorithms

To improve adaptability and classification, future efforts should explore deep learning models like CNNs and transformers, along with few-shot and transfer learning for better generalization with limited training data.

B. Hybrid Detection Approaches

Combining EIS with FTIR, Raman, or hyperspectral imaging can improve specificity and provide molecular composition data. This hybrid setup can enhance microplastic identification and quantification, especially in complex environmental samples.

VI. CONCLUSION

The proposed EIS-ML framework demonstrates strong potential for real-time microplastic monitoring. It offers a scalable, low-cost alternative to lab-based detection. Future enhancements will include integration with deep learning (CNN), deployment via IoT nodes, and real-world testing in varied aquatic conditions.

REFERENCES

[1] B. C. Colson and A. P. M. Michel, 'Flow-through quantification of microplastics using impedance spectroscopy,' ACS Sensors, 2021.

[2] J. Sarmiento et al., 'Microplastic identification using impedance spectroscopy and ML,' Environ. Sci. Technol., 2024.

[3] D. Gomes et al., 'Measuring microplastic concentrations using EIS,' Water, vol. 16, 2024.

[4] A. J. Bard et al., Electrochemical Methods, 3rd ed., Wiley, 2022.

[5] M. E. Orazem and B. Tribollet, 'A tutorial on EIS,' ChemTexts, vol. 6, 2020.

[6] T. Müller and D. Klotz, "Review on the distribution of relaxation times approach for electrochemical impedance spectroscopy," *Electrochimica Acta*, vol. 354, p. 136618, 2020.

[7] H. Schichlein, A. Müller, M. Voigts, A. Krüger, and V. Hackbarth, "Impedance analysis of fuel cells and electrolyzers: Equivalent circuit modeling and DRT," *J. Power Sources*, vol. 113, no. 1, pp. 80–91, 2002.

[8] M. Schoenleber, D. Klotz, and E. Ivers-Tiffée, "A methodology for the deconvolution of electrochemical impedance spectra using the DRT," *Electrochimica Acta*, vol. 131, pp. 20–27, 2014.

[9] E. Barsoukov and J. R. Macdonald, *Impedance Spectroscopy: Theory, Experiment, and Applications*, 2nd ed. Hoboken, NJ, USA: Wiley, 2005.

[10] . Lasia, *Electrochemical Impedance Spectroscopy and its Applications*. Cham, Switzerland: Springer, 2014.

[11] S. Song, Y. Wang, C. Wang, Y. Chen, and X. Zhang, "Recent progress in EIS-based diagnosis for lithium-ion batteries," *J. Energy Chem.*, vol. 27, no. 1, pp. 1–13, 2019

[12] F. Ciucci, "Modeling electrochemical impedance spectroscopy with physics-informed neural networks," *ACS Energy Lett.*, vol. 5, no. 9, pp. 3039–3047, 2020

[13] U. Bertocci, H. O. B. Ayed, and A. Lasia, "Automated DRT deconvolution using regularization and Bayesian techniques," *Electrochem. Commun.*, vol. 124, p. 106947, 2021.

[14] L. Buteau and J. R. Dahn, "Automated fitting of over 100,000 electrochemical impedance spectra with an inverse model neural network," *J. Electrochem. Soc.*, vol. 166, no. 10, pp. A2121–A2126, 2019.

[15] J. Schaeffer, M. Koerver, and W. G. Zeier, "Machine learning-based classification of equivalent circuit models for EIS data analysis,"

[16] R. Xiong, Y. Qiao, X. Liu, and H. He, "A semi-supervised deep learning approach for battery capacity degradation estimation based on electrochemical impedance spectroscopy," *J. Energy Chem.*, vol. 74, pp. 514–524, 2023.

[17] J. Li, Y. Wang, Y. Liu, and B. Han, "Interpretable state-of-health estimation of lithium-ion batteries using deep learning on EIS data," *Energies*, vol. 18, no. 6, p. 1385, Mar. 2023.

[18] D. Parsons, T. Nguyen, and M. Pecht, "Early cycle classification and remaining useful life prediction of lithium-ion batteries using EIS and machine learning," *arXiv preprint arXiv:2408.03469*

[19] M. Chen, S. Zhang, and Q. Wang, "State-of-charge prediction for electric vehicle lithium-ion batteries using EIS and machine learning," *Energy*, vol. 227, p. 120483, Mar. 2021.

A Machine Learning Approach for Real-Time Estimation of Sodium Aerosol Concentration

Muthukumar. G
Indira Gandhi Centre for Atomic Research,
Kalpakkam, Tamil Nadu
muthuganeshece@gmail.com

Avinash Kumar Acharya
Indira Gandhi Centre for Atomic Research,
Kalpakkam, Tamil Nadu
avinashaacharya.hit@gmail.com

***Abstract*—Sodium is used as a coolant in sodium-cooled fast breeder reactors and the detection of sodium combustion aerosols is crucial for ensuring safe handling during fire events. This paper presents a feasibility study for the accurate estimation of sodium aerosol concentration with light detection and ranging (LiDAR) sensor data using machine learning approaches, eliminating the need for offline chemical analysis. Experimental data is collected from multiple controlled sodium combustion experiments. The LiDAR system captures real-time depth images, which are pre-processed and transformed into statistical representations for analysis, and mapped to the corresponding concentration data collected using ion chromatography analysis. A robust machine learning pipeline is developed, incorporating data pre-processing, data augmentation, feature engineering, and model evaluation. Various traditional machine learning models are applied, and performance comparisons are conducted. The results indicate that tree-based models, particularly Random Forest, outperform other approaches, achieving a mean absolute percentage error of 1% and a root mean squared error of approximately 5 mg/m^3. Feature importance analysis reveals that certain parameters such as Points Range and Mean Range contribute significantly to the prediction accuracy. Residual analysis validates the independence of predictions, with minimal high-error data points. The study concludes that the proposed machine learning framework can be effectively employed for the estimation of sodium aerosol concentration using LiDAR data, with future work aimed at leveraging deep learning techniques and deploying the system for real-time monitoring.**

***Keywords*—LiDAR, Machine Learning, Random Forest, Sodium Aerosols**

I. Introduction

Sodium is used as a coolant in the fast breeder reactors, where its efficient heat transfer properties contribute to reactor safety and performance. However, in the event of a sodium fire, sodium combustion aerosols—tiny particles in the micro meter (µm) range—are generated through spray and pool combustion processes. Accurate and real time measurement of sodium aerosol concentration is crucial for ensuring safe handling and mitigation of sodium fire incidents within reactor buildings. Presently, the concentration of sodium aerosol is measured by conventional chemical techniques like ion chromatography, Gravimetric analysis [16] etc. The offline methods are very accurate but time-consuming and inappropriate for real-time monitoring. To address this limitation, this paper proposes a novel approach that leverages machine learning algorithms for the accurate estimation of sodium aerosol concentration with LiDAR data, eliminating the dependence on offline chemical analysis.

LiDAR operates by emitting monochromatic laser pulses that reflect off surfaces and return to the receiver [1]. The system records the time of flight for each pulse to determine distances, forming a detailed point cloud representation of the environment [4]. The Ouster 3D LiDAR system, operating at a wavelength of 0.865 µm, enables mapping of sodium aerosol concentration based on light scattering principles.

Multiple experiments were conducted using LiDAR under controlled conditions with known sodium aerosol concentrations. The LiDAR system captures real-time depth images, which are pre-processed and transformed into statistical representations for analysis, and mapped to the corresponding concentration data collected using ion chromatography analysis.

Various traditional machine learning algorithms are explored in this study, with a focus on identifying the most suitable algorithm for the accurate estimation of sodium aerosol concentration. The results of this analysis contribute to the development of non-invasive, real-time monitoring techniques for aerosol measurement in the industrial environment.

The following sections of this paper are organized as follows Section 2 presents the experimental framework, detailing the experimental setup and procedure. Section 3 outlines the methodology, including data processing and machine learning approaches. Section 4 provides a comprehensive analysis of the results, and Section 5 discusses future work and conclusions.

II. Experimental Framework

The design of the experimental setup, the experimental steps and the collection of online sensor data and offline measurements from the experiments are discussed in this section.

A. *Experimental Setup*

An enclosed volume of 150-liter leak tight chamber consists of a heater, half inch sampling line for sodium aerosol measurement, a Perspex viewing port for optical analysis using LiDAR, sodium loading window and feed through for electrical connections as shown in Fig. 1. Sodium aerosols are generated by burning a known quantity of solid sodium using an electrical heater. The pool temperature is measured using K-type thermocouples. The aerosol concentration is sampled using filter paper sampling method through the sampling line for offline chemical analysis. The distribution of the aerosols within the chamber is continuously monitored and recorded using Ouster LiDAR sensor as shown in Fig. 1

FIG. 1. EXPERIMENTAL SETUP FOR AEROSOL MEASUREMENT USING LIDAR

LiDAR Data Acquisition: The specifications of the ouster LiDAR sensor is shown in Table I. The acquisition of data is performed with Ouster Studio application.

TABLE I: SPECIFICATIONS OF OUSTER LIDAR

Model Name	**OS1-32**
Laser Wavelength	865nm
Laser Power	< 1mW
Horizontal Resolution	512, 1024, 2048 Channels
Vertical Resolution	32 Channels
Vertical FOV	45 degree
Points per second	655360 at 10 Hz
Precision	±0.7 – 5 cm

The LiDAR data were recorded in PCAP and JSON format [1, 2, 3]. PCAP file stores raw data packets transmitted by the LiDAR sensor, including depth image information that represents three-dimensional point cloud data. The JSON file contains metadata, such as configuration parameters, sensor position, and environmental conditions.

B. Experimental Procedure

To establish a baseline, the initial background samples of the chamber without aerosols were captured using the LiDAR sensor and continuously recorded for post-processing. Data acquisition was performed at a rate of 10 frames per second and covering an angular range of 140° to 220° to minimize interference from external elements within the experimental facility. The sodium aerosol generation process was initiated by preheating a tray inside the chamber. Once the desired temperature was reached, 2 grams of sodium was placed on the tray, leading to combustion and aerosol formation. To quantify the aerosol concentration, Ion Chromatography (IC) was employed, as it enables precise measurement of sodium aerosol concentration at ppb levels. The resulting sodium aerosol was collected using the filter paper sampling method. A filter paper with a pore size of 0.45 µm was placed inside a holder, which was connected to the sampling port. A vacuum pump, coupled with a rotameter, was used to maintain a constant sample suction rate of 15 L/min, for the collection of aerosols on the filter paper over an one minute duration. Sampling was performed at 2-minute intervals. Post-sampling, the filter paper was weighed before and after aerosol collection to determine mass deposition. Subsequently, the filter paper was placed in 10 mL of water inside a polypropylene bottle. The resulting solution was then subjected to IC analysis for quantitative measurement of sodium aerosol concentration.

C. Experiemental Results

Three experiments were conducted following the same procedure, maintaining consistent environmental conditions and experimental configurations across all trials to ensure repeatability.

The Ouster LiDAR system provides The measurement parameters such as Signal Photon Strength, Range, Ambient Photon Strength, and Reflectivity for analyzing the characteristics of detected particles [3].

1) *Signal Photon Strength:* This parameter represents the intensity of the returned laser pulse detected by the sensor. Higher values indicate a stronger reflection, which can be attributed to either a highly reflective surface or a shorter distance between the sensor and the target [2].
2) *Range:* The range measurement refers to the distance between the LiDAR sensor and the target within its field of view, determined using the time-of-flight principle [2].
3) *Ambient Photon Strength:* This parameter quantifies the natural environmental illumination in field of view of the sensor using Near-Infrared (NIR) light [2].
4) *Reflectivity:* The reflectivity of a target is derived by adjusting the signal photon strength based on the measured range and the sensor's sensitivity at that distance [2].

The results of ion chromatography is expressed in mg per m^3 and measured concentration for each sample in each experiment is illustrated in the Fig. 2.

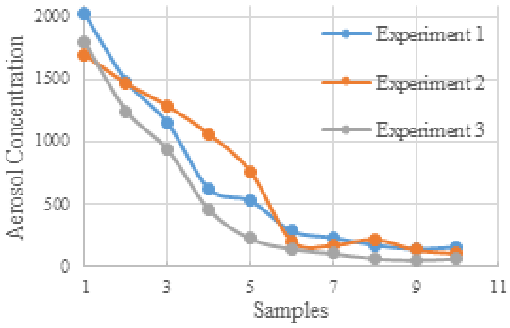

FIG. 2. RESULTS OF ION CHROMATOGRAPHY FOR EACH EXPERIMENTS

III. METHODOLOGY

This section presents the complete machine learning pipeline, encompassing data collection, transformation, augmentation, and the fusion of online and offline experimental results. It outlines the methodologies applied at each stage, focusing on the data preparation and the implementation of traditional machine learning algorithms. The flow chart of the proposed machine learning approach for the prediction of sodium aerosol concentration is shown in Fig. 3.

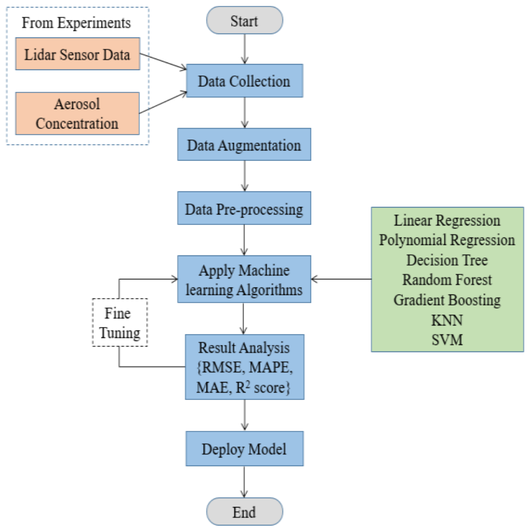

FIG. 3. FLOW CHART OF PROPOSED MACHINE LEARNING APPROACH

A. *Data Collection*

Each experiment includes LiDAR data recordings of three distinct phases: Background, Aerosol Generation, and Aerosol Settling, as shown in Fig. 4.

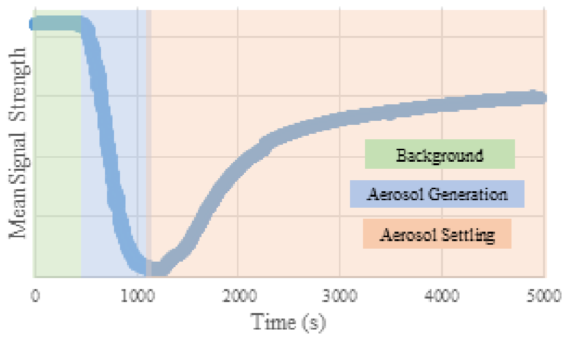

FIG. 4. TEMPORAL VARIATION OF MEAN SIGNAL STRENGTH DURING EACH PHASE OF THE EXPERIMENT

1) *Background*: This phase represents the initial conditions inside the chamber before the experiment begins, characterized by the absence of aerosol. It serves as a baseline reference for comparison with subsequent stages.

2) *Aerosol Generation:* This phase begins when sodium combustion is initiated, resulting in mild fire and highly nonlinear aerosol generation, making it unsuitable for aerosol sampling. Instead, LiDAR data collection focuses on capturing real-time distribution of aerosol.

3) *Aerosol Settling:* This phase occurs after the completion of sodium combustion, when no additional aerosol is generated. The settling of aerosol is a gradual process, making it an ideal stage for offline sampling. During this phase, filter-based sampling of aerosol is performed.

B. *Data Preparation*

Since the offline sampling is not performed during the Generation phase, the LiDAR data captured in this phase is excluded for further analysis.

1) *Data Pre Processing:* As the LiDAR sensor is configured to capture data within a focused 80° horizontal field of view, resulting in sparse pixel distribution in the captured frames. For computational efficiency, out-of-range pixels are truncated, and the total effective range of pixels is calculated using the following equation:

$$Eff\ Pixels = \frac{Effective\ Field\ of\ View}{Total\ Field\ of\ View} \times Total\ pixels$$

$$*\ Total\ Pixels\ =\ 2048$$
$$*\ Total\ Field\ of\ View\ =\ 360°$$
$$*\ Effective\ Field\ of\ View\ =\ 80°$$

Applying this reduction to each parameter reducing the frame size from 32 × 2048 to 32 × 470 pixels, preserving only the relevant data points.

2) *Statistical Feature Extraction:* For traditional machine learning algorithms the high dimensional LiDAR frames for each parameter is transformed into a statistical representation that provide a comprehensive summary of the spatial variations in the captured aerosol data. The statistical features include central tendency measures such as mean and median, distribution metrics like first quartile (Q1), third quartile (Q3), minimum, and maximum, as well as higher-order statistics such as skewness and kurtosis.

3) *Background Data Subtraction:* The Background data represents the initial LiDAR measurements captured in the absence of sodium aerosols. However, slight variations in the background values across different experiments lead to inconsistent parameter ranges. Therefore, a background correction procedure is applied to each LiDAR parameter. This involves scaling of the statistically estimated parameter values with respect to the corresponding background values for each experiment. By performing this correction, variations due to sensor drift, environmental factors, or initial baseline differences are minimized.

C. *Data Augmentation*

Since the aerosol concentration measured using IC is at discrete time intervals, it is quadratically interpolated to align with each corresponding LiDAR data sample. To prevent data leakage into the concentration values, the interpolation is performed without incorporating any real-time sensor data, ensuring unbiased estimation. This procedure is systematically applied across all experimental datasets, resulting in a dataset suitable for further analysis and model development.

D. *Data Analysis*

Fig. 5 illustrates the variation of each statistical parameter during the Aerosol Settling phase for one of the experiments. The graph represents the variation of amplitude over time for each statistical parameter. Since concentration samples from chemical analysis are obtained only during the aerosol settling phase, further analysis is restricted to this phase. For consistency, each plot in Fig. 5 begins from the aerosol settling phase, as indicated in Fig. 4.

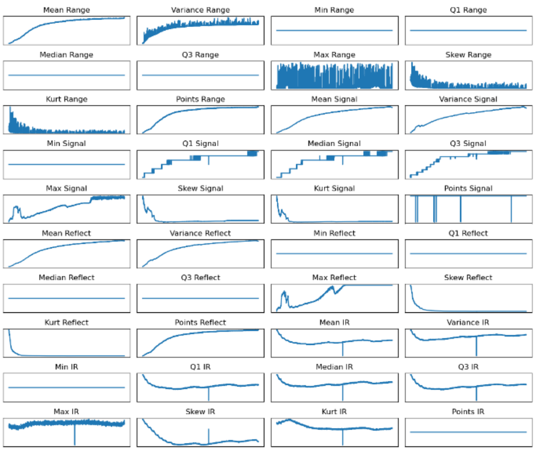

FIG. 5. TEMPORAL VARIATION OF STATISTICALLY REPRESENTED LIDAR PARAMETERS IN THE AEROSOL SETTLING PHASE

It is observed that certain parameters, such as Min Range, Q1 Range, and Median Range, exhibit no significant variation and can be excluded from further analysis due to their lack of statistical relevance. In addition to that an anomaly data point is observed across all parameters of the ambient photon data.

Correlation with Target: Among the significant features, most exhibit strong positive or negative correlations with the target variable. However, certain features, such as Points Signal and Max Range, show minimal or no correlation, indicating their insignificance for predictive modeling. These weakly correlated features can be excluded to enhance model efficiency and reduce redundancy.

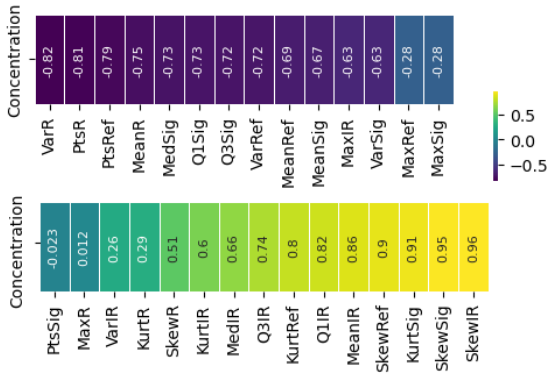

E. *Feature Engineering*

The dataset can be further optimized by applying a feature transformation. The implementation of customized feature engineering approaches can significantly improve the model's performance.

1) *Outlier Analysis:* Some significant outliers are observed in all the parameter of Ambient Photon data. Since machine learning algorithms are sensitive to outliers, it is imputed with mean value of neighbourhood samples

2) *Scaling:* Robust scaling is applied due to the presence of severe outliers in the LiDAR data. Traditional scaling methods, such as standardization, are highly sensitive to extreme values, which can distort the feature distribution. Instead, robust scaling normalizes the data by centering it around the median and scaling it using the interquartile range (IQR).

F. *Machine Learning Models*

This section provides an overview of the supervised machine learning techniques employed to evaluate and compare various performance metrics for the prediction of aerosol concentration.

1) *Linear Regression (LR):* LR is a linear model, which provides a linear relationship between the single dependent variable and multiple independent variables. It is commonly used as a baseline model for regression problems due to its simplicity [12].

2) *Polynomial Regression (PR):* PR is an extension of linear regression that captures nonlinear relationships by incorporating polynomial degrees of the independent variables. PR models with higher-degree increase the risk of overfitting, making them less generalizable

3) *Decision Trees (DTs):* DT is a non-parametric tree based model and its primary objective is to predict the target variable by deriving decision rules from the given data features [10, 11]. It is easy to interpret but prone to overfitting.

4) *Random Forest (RF):* RF is an ensemble learning method that combines multiple decision trees using bootstrap aggregation (bagging) technique. The inherent randomness in RF arises from training multiple decision trees on randomly sampled subsets of the dataset [7, 8]. In comparison to other traditional algorithms RF demonstrates superior robustness and reliability.

5) *Gradient Boosting (GB): GB* is an iterative ensemble method that builds decision trees sequentially, correcting errors of previous trees by minimizing a loss function [9]. It is highly effective for structured data.

6) *K Nearest Neighbors (kNN):* KNN works by predicting a value based on the weighted average of the **k** nearest data points. The 'k', distance calculation, and selected features affect its accuracy [13].

7) *Support Vector Machine (SVM):* SVM generates hyper-planes by optimizing the margin of separation around the separating hyper-planes. Kernel functions (linear and non-linear) are utilized to optimize the distance between the hyper-planes [5, 6].

G. *Performance Evaluation Metrics:*

Mean Absolute Error (MAE) is a commonly employed evaluation metric that measures the average magnitude of absolute errors in a predictive model. It is defined as:

$$MAE = \frac{1}{n}\sum_{i=1}^{n}|y_i - \hat{y}_i| \quad (1)$$

where yi represents the actual values, y^i\y-hat represents the predicted values, and n is the total number of observations.

Root Mean Square Error (RMSE) Eq. (2), assigns equal penalties to both underestimations and overestimations by measuring the square root of the average squared differences between predicted and actual values [14].

$$\mathrm{RMSD} = \sqrt{\frac{1}{n}\sum_{i=1}^{n}(X_i - x_0)^2}. \quad (2)$$

Eq. (3) is R² Score, which is also widely used as an evaluation metric for the regression tasks. It represents the proportion of variance in the target variable that can be explained by the independent variables in the model [14]. It is defined as:

$$R^2 = 1 - \frac{SS_{\text{res}}}{SS_{\text{tot}}} \tag{3}$$

where SSres is the sum of squared residuals and SStot is the total sum of squares. An R² value of 1 indicates a perfect fit, while a value of 0 suggests that the model performs no better than a mean-based prediction.

MAPE (Mean Absolute Percentage Error) is a metric that calculates the average percentage difference between the actual and predicted values. It expresses errors as a percentage, and it is explained by Eq. (4)

$$MAPE = \frac{1}{n}\sum_{i=1}^{n}\left|\frac{y_i - \hat{y}_i}{y_i}\right| \times 100 \tag{4}$$

IV. Results And Discussions

The dataset consists of approximately 10,000 data points, which is split into training (70%) and test (30%) sets. Each machine learning algorithm is fine-tuned, and their performances are compared in this section

A. *Performance Analysis:*

The performance of the conventional regression algorithms on the training and test sets are shown in Table II and Table III respectively.

LR captures the variance in the data, but it performs poorly in terms of MAE and RMSE. This suggests that the dataset exhibits nonlinear relationships, which cannot be well represented by a simple linear model. Thus, LR serves as a baseline model but is not suitable for production use. A polynomial regression model with degree 2 demonstrates a significant improvement over LR, confirming the nonlinear nature of the dataset. However, polynomial models may still be limited in handling complex feature interactions. Decision Trees, being highly flexible, fit the training data perfectly but suffer from overfitting on the test set. RF is employed as an ensemble approach, it effectively reduces overfitting and provides superior predictive performance compared to all other models. Unlike RF, GB does not significantly enhance prediction accuracy. This could indicate that boosting does not provide additional benefits in this dataset, possibly due to limited variance reduction or insufficient weak learners contributing to performance gains. SVM with linear kernel and KNN models exhibit suboptimal performance, lagging behind tree-based methods. The nature of the dataset, including high-dimensional statistical transformations and complex patterns, might not be well captured by these approaches.

In conclusion, RF emerges as the best-performing model, effectively handling non-linearity while reducing overfitting. Hence, it is the most reliable choice for sodium aerosol concentration prediction.

TABLE II: PERFORMANCE ON TEST SET

Model	MAE	RMSE	R^2	MAPE
LR	47.88	63.18	0.97	0.39
PR	9.42	14.94	0.99	0.07
DT	3.06	8.19	0.99	0.01
RF	**1.99**	**4.9**	**0.99**	**0.01**
GBDT	8.97	13.32	0.99	0.06
K-NN	11.4	40.45	0.98	0.07
SVM	63.73	95.28	0.93	0.44

TABLE III: PERFORMANCE ON TRAINING SET

Model	MAE	RMSE	R^2	MAPE
LR	48.60	63.84	0.97	0.40
PR	8.40	12.38	0.99	0.07
DT	0.0	0.0	1.0	0.00
RF	**0.72**	**1.91**	**0.99**	**0.01**
GBDT	7.75	11.21	0.99	0.06
K-NN	9.79	34.22	0.99	0.06
SVM	65.72	100.30	0.93	0.44

B. *Variables Influencing the Estimation*

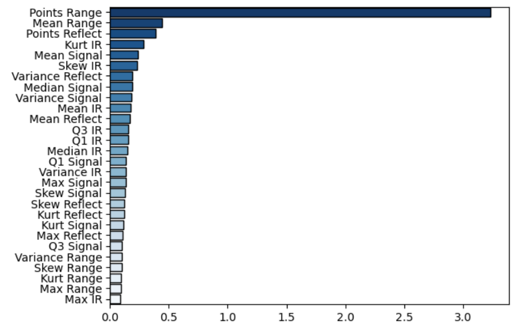

FIG. 6. FEATURE IMPORTANCE RANKING FROM RANDOM FOREST

The Fig. 6 presents the feature importance ranking obtained using a Random Forest model. As expected, Points Range, Mean Range, and Points Reflectivity contribute to more than 90% of the overall influence on the prediction. The other features exhibit significantly lower contributions, indicating their minimal impact on the model's predictions. Though many features exhibit minimal significance, feature selection was not performed, as it led to a slight reduction in the model's performance.

C. *Residual Plot Analysis*

A residual plot is a graphical representation of the differences between actual and predicted values (residuals) vs predicted values across the test set. Ideally, residuals should be randomly distributed around zero. The residual plot shown in Fig.7 does not exhibit any obvious patterns, indicating the independence of residuals, which is a desirable property for a well-fitted model. However, the predictions show a slight overestimation in the lower concentration range compared to the higher concentration range. It is due to the severe non linearity in the sensor data at lower concentration range. A few data points with large errors are observed, and these points have been highlighted.

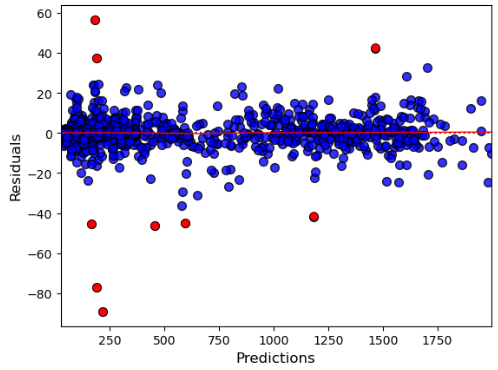

FIG. 7. RESIDUAL PLOT

V. FUTURE WORK AND CONCLUSION

Future work will focus on leveraging deep learning approaches to consider the full dataset without dimensionality reduction through statistical transformations. A Convolutional Neural Network (CNN) will be employed for feature extraction, followed by temporal-based algorithms to capture dynamic aerosol behaviour more effectively. In order to enhance the generalizability of the model, experiments will be extended to chambers of varying dimensions and different sodium quantities. The proposed methodology will be integrated into a hardware system for real-time sodium aerosol monitoring.

In this study, an extensive analysis was conducted on experimental LiDAR data to develop a predictive model for sodium aerosol concentration measurement. The data underwent pre-processing, statistical transformation, and augmentation to enhance its usability. Exploratory data analysis provided insights into feature significance, interdependencies, and correlations with sodium aerosol concentration. Feature engineering techniques were applied to handle outliers, followed by robust scaling to ensure model stability. The performance of various traditional machine learning algorithms was evaluated, with tree-based models outperforming others. While a simple Decision Tree model demonstrated high accuracy, it was prone to overfitting. In contrast, the Random Forest model emerged as the best-performing algorithm, achieving a MAPE of 1% and a RMSE of approximately 5 mg/m^3. The results highlight the effectiveness of Random Forest in providing accurate and reliable predictions for real-time sodium aerosol concentration measurement.

REFERENCES

[1] Syed Saad ul Hassan: “Analysis of LIDAR Data”, Published in Research Gate, 2022

[2] Ouster Sensor Documentation: Introduction to Ouster Sensor LiDAR

[3] M. V. Okunsky, N. V. Nesterova: “Velodyne LIDAR method for sensor data decoding”, IOP Conference Series. Materials Science and Engineering , 516(1), [5 p.], 2019

[4] Tao Yang, You Li, Yassine Ruichek: “Performance Modeling a Near-Infrared ToF LiDAR Under Fog: A Data-Driven Approach”, IEEE Transactions on Intelligent Transportation Systems, Vol. 23, Issue 8, 2022

[5] W.S. Noble: "What is a support vector machine?", Nat. Biotechnol., pp. 1565-1567, 24 (12) (2006),

[6] A.L. Oliveira: "Estimation of software project effort with support vector regression", Neurocomputing, 69 (13–15) (2006), pp. 1749-1753

[7] I. Reis, D. Baron, S. Shahaf: "Probabilistic random forest: A machine learning algorithm for noisy data sets", Astron. J., 157 (1) (2018), p. 16

[8] Y. Liu, Y. Wang, J. Zhang: "New Machine Learning Algorithm: Random Forest", Springer, (2012)

[9] J.H. Friedman: "Greedy function approximation: a gradient boosting machine", Ann. Stat. (2001), pp. 1189-1232

[10] Y.Y. Song, L. Ying: "Decision tree methods: applications for classification and prediction", Shanghai Arch. Psychiatry, 27 (2) (2015), p. 130

[11] L. Rokach, O. Maimon: "Decision trees:, Data Mining and Knowledge Discovery Handbook, Springer (2005), pp. 165-192

[12] A. Schneider, G. Hommel, M. Blettner: "Linear regression analysis: part 14 of a series on evaluation of scientific publications", Dtsch. Ärzteblatt Int., 107 (44) (2010), p. 776

[13] Z. Zhang: "Introduction to machine learning: k-nearest neighbors", Ann. Transl. Med., 4 (11) (2023)

[14] Muthukumar G, Jyosna Philip: “CNN-LSTM Hybrid Deep Learning Model for Remaining Useful Life Estimation”, Published in International Journal For Innovative Research In Multidisciplinary Field, 2024

[15] Ganesh N, Amitava Choudhury, Prasun Dutta, Kanak Kalita, Paolo Barsocchi: Random Forest Regression-Based Machine Learning Model for Accurate Estimation of Fluid Flow in Curved Pipes, Processes, 9(11):2095, 2021

[16] Kihong Park, David B. Kittelson, Peter H. McMurry: A closure study of aerosol mass concentration measurements: comparison of values obtained with filters and by direct measurements of mass distributions, Atmospheric Environment, Volume 37, Issues 9–10, Pages 1223-1230, 2003

First National Research Conclave 2025 on Sustainability: Advancing towards a Resilient Future

OUR SPONSORS

Assistance to Professional Bodies & Seminar / Symposia Scheme – Anusandhan National Research Foundation (ANRF)

The Science and Technology Professional Bodies and Academies of Science and Engineering play a vital role in fostering collaboration and knowledge-sharing within the scientific community. Through the organization of technical meetings, seminars, conferences, and workshops, these bodies help create a cohesive research ecosystem. In addition, they contribute significantly to the dissemination of scientific knowledge by publishing journals, technical bulletins, conference proceedings, and other literature that document current research and innovation.These events serve as important platforms for scientists and technologists to stay updated with the latest developments in their respective fields. More importantly, they enable networking and sustained engagement among researchers, institutions, and industry professionals, beyond the duration of the event itself. Recognizing the importance of these initiatives, the **Anusandhan National Research Foundation (ANRF)** provides **partial financial support** on a **selective basis** for organizing such events—both at national and international levels. Eligible organizations include academic institutions, research laboratories, professional societies, and other non-profit entities engaged in promoting scientific research and development.The primary focus of this scheme is to:

- Encourage active participation of **young scientists and early-career professionals**.
- Provide limited support for pre-event operational expenses such as publicity materials, brochures, and announcements.

We are pleased to share that an amount of **₹1,50,000/-** has been sanctioned to us under this scheme to support the organization of TCE Research Conclave 2025. The financial assistance will help us in achieving the following objectives:

1. **To bring together experts, researchers, industry professionals, and students** to promote interdisciplinary collaboration and knowledge exchange.
2. **To showcase breakthrough research and innovations** in areas such as climate resilience, green technologies, renewable energy, sustainable agriculture, smart urban solutions, and circular economy models.
3. **To engage in critical discussions** on pressing issues like climate adaptation, energy transitions, waste management, and social equity, aimed at developing comprehensive and sustainable solutions.
4. **To facilitate strategic partnerships** among academia, industry, policymakers, and funding agencies to accelerate the deployment of sustainable technologies and practices.
5. **To provide a dynamic platform** for students and early-career researchers to enhance their learning through keynote lectures, technical sessions, and hands-on workshops.

FIRST NATIONAL RESEARCH CONCLAVE 2025 ON SUSTAINABILITY: ADVANCING TOWARDS A RESILIENT FUTURE

OUR SPONSORS

FIRST NATIONAL RESEARCH CONCLAVE 2025 ON SUSTAINABILITY: ADVANCING TOWARDS A RESILIENT FUTURE

OUR SPONSORS

quantanics

Quantanics Techserv Pvt Ltd
"Digitize Your Lifestyle"
No.207/49 A, VOC Nagar, North Street, PP Chavadi,
Madurai - 625016, India.
+91-90887940111
support@quantanics.in
https://www.quantanics.in

Blockchain, Internet of Things (IoT), ETAP, Robotics & Automation, Artificial Intelligence (AI), Extended Reality (XR), Big Data, Industrial 3D Module Development

DrillBit

Plagiarism Detection Software

Affordable Anti - Plagiarism Software - A Make India Initiative

#361/1, 2nd Floor, End Main Road, 7th Block,
Nagarbhavi 2nd stage,
Bangalore - 560072 -
+91 9840353157
https://www.drillbitplagiarism.com

FIRST NATIONAL RESEARCH CONCLAVE 2025 ON SUSTAINABILITY: ADVANCING TOWARDS A RESILIENT FUTURE

OUR SPONSORS

Website:
www.knimbus.com
Head Office:Unit No. 408 B, 4th Floor,D-2, Southern Park,
Saket District Centre,
New Delhi – 110017, India

Software distribution and training support services for Bentley Systems software products across India.

Email: sales@techappsconsulting.in
www.techappsconsulting.in

Our Sponsors

Thiagarajar College of Engineering (TCE)

Established in 1957, TCE is a Government-Aided Autonomous Institution affiliated with Anna University, Chennai. Accredited by NBA and NAAC (A++ Grade, CGPA 3.56), TCE excels in technical education with Competency-Based Curriculum, Outcome-Based Education, and the CDIO framework. A leader in digital learning, TCE introduced MOOCs in 2021 and the Thiagarajar Research Fellowship (TRF) for PhD scholars. In 2024, it received a Platinum Certificate in the 5S Audit for campus sustainability.

First National Research Conclave on Sustainability @TCE

The First National Research Conclave on Sustainability: Advancing Towards a Resilient Future (May 16-17, 2025) unites thought leaders, researchers, and scholars to explore solutions to global challenges. Featuring keynote addresses, panel discussions, and research presentations in areas like renewable energy, smart cities, and waste management, the conclave fosters collaboration for a sustainable future.

This book presents the event proceedings, including keynote summaries, program details, and selected research papers.

https://www.tce.edu/rctce2025

978-93-342-3695-8